PROCEEDINGS OF THE TENTH INTERNATIONAL SYMPOSIUM ON ARTIFICAL LIFE AND ROBOTICS

(AROB 10th '05)

Feb. 4–Feb. 6, 2005
B-Con Plaza, Beppu, Oita, JAPAN

Supported by Air Force Office of Scientific Research,
Asian Office of Aerospace Research and Development
(AFOSR/AOARD)

Editors : Masanori Sugisaka and Hiroshi Tanaka
ISBN4-9900462-5-0

The Tenth International Symposium on Artificial Life and Robotics 2005(AROB 10th ’05), B-con Plaza, Beppu, Oita, Japan, February 4-6, 2005

Program of The Tenth International Symposium on

ARTIFICIAL LIFE AND ROBOTICS
(AROB 10th ’05)

February 4-6, 2005
B-Con Plaza, Beppu, Oita, Japan

Editors: Masanori Sugisaka and Hiroshi Tanaka

The Tenth International Symposium on Artificial Life and Robotics 2005(AROB 10th ’05),
B-con Plaza, Beppu, Oita, Japan, February 4-6, 2005

THE TENTH INTERNATIONAL SYMPOSIUM ON ARTIFICIAL LIFE AND ROBOTICS

(AROB 10th '05)

ORGANIZED BY

Organizing Committee of International Symposium on Artificial Life and Robotics
(Department of Electrical and Electronic Engineering, Oita University, Japan)

OPERATED BY

Santa Fe Institute (SFI, USA)
The Society of Instrument and Control Engineers (SICE, Japan)
The Robotics Society of Japan (RSJ, Japan)
The Institute of Electrical Engineers of Japan (IEEJ, Japan)
Institute of Control, Automation and Systems Engineers (ICASE, Korea)
Chinese Association for Artificial Intelligence (CAAI, China)

CO-OPERATED BY

The Institute of Systems, Control and Information Engineers (ISCIE)
The Institute of Electronics, Information and Communication Engineers (IEICE)
The Institute of Electrical and Electronics Engineers, Inc.(IEEE Japan Council)
Japan Robot Association (JARA)

SPONSORED BY

Air Force Office of Scientific Research, Asian Office of Aerospace Research and Development (AFOSR/AOARD)
Mitsubishi Electric Corporation Advanced Technology R&D Center
Oita Gas Co., Ltd.
STK Technology Co., Ltd.
Sanwa Shurui Co., Ltd.
Yatsushika Brewery Co., Ltd.

SUPPORTED BY

Kyushu Bureau of Economy, Trade and Industry, Ministry of Economy, Trade and Industry
Oita Prefecture
Oita City
Beppu City
The Federation of the Chamber of Commerce and Industry in Oita Prefecture
The Oita Prefectural Organization of the Industrial Groups
Kyodo News
JIJI Press
Oita Godo Shimbunsya
The Asahi shimbun Co.
The Mainichi Newspapers Co.
THE YOMIURI SHIMBUN
The Nishinippon Newspaper Co.

The NIKKAN KOGYO SHIMBUM. LTD.
Nihon Keizai Shimbun, Inc.
NHK Oita Station
Oita Broadcasting System
Television Oita System
Oita Asahi Broadcasting Co., Ltd.
Oita System Control Research Society

ADVISORY COMMITTE CHAIRMAN

F. Harashima (Tokyo Denki University, Japan)

GENERAL CHAIRMAN

M. Sugisaka (Oita University, Japan)

CO-GENERAL CHAIRMAN (PROGRAM)

H. Tanaka (Tokyo Medical & Dental University, Japan)

CO-CHAIRMAN

J.L. Casti (Santa Fe Institute, USA)

ADVISORY COMMITTEE

F. Harashima (Tokyo Denki University, Japan)
H. Kimura (The University of Tokyo, Japan)
T. Fukuda (Nagoya University, Japan)
S. Ueno (Kyoto University, Japan)
M. Tomizuka(University of California at Berkeley, USA)
T.J. Lyons(Asian Office of Aerospace Research & Development, USA)

INTERNATIONAL ORGANIZING COMMITTEE

K. Aihara (The University of Tokyo, Japan)
W. B.Arthur (Santa Fe Institute, USA)
W. Banzhaf (University of Dortmund, Germany)
C. Barrett (Los Alamos National Laboratory, USA)
M. Bedau (Reed College, USA)
Z. Bubnicki (Wroclaw University of Technology, Poland)
J.L. Casti (Santa Fe Institute, USA)
H.S. Cho (KAIST, Korea)
J.M. Epstein (The Brookings Institution, USA)
T. Fukuda (Nagoya University, Japan)
H. Hashimoto (The University of Tokyo, Japan)
D. J.G.James (Coventry University, UK)
S. Kauffman (Santa Fe Institute, USA)
K.Kosuge(Tohoku University, Japan)
K.Kyuma(Mitsubishi Electric Corporation, Advanced Technology
R&D Center, Japan)
C.G. Langton (Santa Fe Institute, USA)
M.H. Lee (Pusan National University, Korea)

J.J. Lee (KAIST, Korea)
M. Nakamura (Saga University, Japan)
G. Obinata (Nagoya University, Japan)
S. Rasmussen (Santa Fe Institute, USA)
T.S. Ray (University of Oklahoma, USA)
P. Sapaty (National Academy of Science of Ukraine, Ukraine)
M. Sugisaka (Oita University, Japan) (Chairman)
H. Tanaka (Tokyo Medical & Dental University, Japan)
C. Taylor (University of California-Los Angeles, USA)
K. Tsuchiya (Kyoto University, Japan)
G. Wang (Tsinghua University, China)
W.R. Wells (University of Nevada-Las Vegas, USA)
Y.G. Zhang (Academia Sinica, China)

INTERNATIONAL PROGRAM COMMITTEE

K. Abe (Tohoku University, Japan)
K. Aihara (The University of Tokyo, Japan) (Co-chairman)
T. Arita (Nagoya University, Japan)
H. Asama (The University of Tokyo, Japan)
M. Bedau (Reed College, USA)
R. Belew (University of California-San Diego, USA)
Z. Bubnicki (Wroclaw University of Technology, Poland)
T. Christaller (Fraunhofer Institute for Autonomous intelligent Systems-AiS)
C.S. Han (Hanyang University, Korea)
I. Harvey (University of Sussex, UK)
H. Hashimoto (The University of Tokyo, Japan)(Co-chairman)
K. Hirasawa (Waseda University, Japan)
H. Hirayama (Asahikawa Medical College, Japan)
N. Honma (Tohoku University, Japan)
T. Ikegami (The University of Tokyo, Japan)
H. Inooka (Tohoku University, Japan)
K. Ito (Tokyo Institute of Technology, Japan)
T. Ishimatsu (Nagasaki University, Japan)
T. Iwamoto (Mitsubishi Electric Corporation, Advanced
Technology R&D Center, Japan)
J. Johnson (The Open University, UK)
Y. Kakazu (Hokkaido University, Japan)
M. Kaneko (Hiroshima University, Japan)
O. Katai (Kyoto University, Japan)
S. Kawaji (Kumamoto University, Japan)
S. Kawata (Tokyo Metropolitan University, Japan)
S. Kitamura (Kobe University, Japan)
T. Kitazoe (University of Miyazaki, Japan)
S. Kumagai (Osaka University, Japan)
J. M.Lee (Pusan National University, Korea)
C. G.Looney (University of Nevada-Reno, USA)
H.H. Lund (University of Southern Denmark, Denmark)
M. Minami (Fukui University, Japan)
H. Miyagi (The University of Ryukyus, Japan)
T. Nagashima (Muroran Institute of Technology, Japan)
M. Nakamura (Saga University, Japan)
R. Nakatsu (KWANSEI GAKUIN University, Japan)
S. Omatu (Osaka Prefecture University, Japan)

M. Okamoto (Kyushu University, Japan)
M. Osano (Aizu University, Japan)
R. Pfeifer (University of Zurich-Irchel, Switzerland)
T.S. Ray (University of Oklahoma, USA) (Co- chairman)
T. Sawaragi (Kyoto University, Japan)
T. Shibata (AIST, Japan)
K. Shimohara (ATR, Japan)
M. Sugisaka (Oita University, Japan)
H. Tanaka (Tokyo Medical & Dental University, Japan) (Chairman)
M. Tanaka-Yamawaki (Tottori University, Japan)
N. Tosa (ATR, Japan)
K. Ueda (The University of Tokyo, Japan)
K. Uosaki (Osaka University, Japan)
H. Wakamatsu (Tokyo Medical & Dental University, Japan)
K. Watanabe (Saga University, Japan)
M. Yano (Tohoku University, Japan)

LOCAL ARRANGEMENT COMMITTEE

X. Feng (University of Singapore, Singapore)
A. Loukianov (Baikal State University of Economy & Law, Russia)
M. Rizon (Northern Malaysia University College of Engineering, Malaysia)
M. Sugisaka (Oita University, Japan) (Chairman)
Y. Suzuki (Tokyo Medical & Dental University, Japan)
J. Wang (Oita University, Japan)
X. Fan (Oita University, Japan)
X. Wang (Tokushima University, Japan)
F. Dai (Matsue National College of Technology, Japan)
M. Ito (Konan University, Japan)

HISTORY

This symposium was founded in 1996 by the support of Science and International Affairs Bureau, Ministry of Education, Culture, Sports Science and Technology, Japanese Government. Since then, this symposium has been held every year at B-Con Plaza, Beppu, Oita, Japan except in Oita, Japan (AROB 5th ’00) and in Tokyo, Japan (AROB 6th ’01). The tenth symposium will be held on 4-6 February, 2005, at B-Con Plaza, Beppu, Oita, Japan. This symposium invites you all to discuss development of new technologies concerning Artificial Life and Robotics based on simulation and hardware in the twenty first century.

OBJECTIVE

The objective of this symposium is the development of new technologies for artificial life and robotics which have been recently born in Japan and are expected to be applied in various fields. This symposium will discuss new results in the field of artificial life and robotics.

TOPICS

Artificial brain research
Artificial intelligence
Artificial life

Artificial living
Artificial mind research
Bioinformatics chaos
Brain science
Cognitive science evolutionary computations
Complexity
Computer graphics
DNA computing
Fuzzy control
Genetic algorithms
Human-machine cooperative systems
Human-welfare robotics
Innovative computations
Intelligent control and modeling
Micromachines
Micro-robot world cup soccer tournament
Mobile vehicles
Molecular biology
Multi-agent systems
Nano-biology
Nano-robotics
Neural networks
Neurocomputers
Neurocomputing technologies and its application for hardware
Pattern recognition
Robotics
Robust virtual engineering
Virtual reality

COPYRIGHTS

Accepted papers will be published in the proceeding of AROB and some of high quality papers in the proceeding will be requested to re-submit their papers for the consideration of publication in an international journal ARTIFICIAL LIFE AND ROBOTICS (Springer) and APPLIED MATHEMATICS AND COMPUTATION (North-Holland). All correspondence related to the symposium should be addressed to AROB Secretariat.

Dept. of Electrical and Electronic Engineering,
Oita University
700 Dannoharu, Oita 870-1192, JAPAN
TEL：+81-97-554-7841, FAX：+81-97-554-7818
E-MAIL arobsecr@cc.oita-u.ac.jp
Home Page http://arob.cc.oita-u.ac.jp/

MESSAGES

Fumio Harashima
Chairman of Advisory Committee
(President, Tokyo Denki University)

Fumio Farashima
Advisory Committee Chairman of AROB

The science and technology(S&T) on Artificial Life and Robotics is newly born recently. This new S&T provides human being with happiness. Research is heart and desire of human being and the S&T is going toward clarifying human mind and heart. Artificial Life and Robotics provides us with a strong tool to achieve our objective.

I would like to congratulate researchers who work in the fields on Artificial Life and Robotics.

Masanori Sugisaka
General Chairman
(Professor, Oita University)

Masanori Sugisaka
General Chairman of AROB

It is my great honor to invite you all to the Tenth International Symposium on Artificial Life and Robotics (AROB 10th ’05).

The symposiums from the first (February 18-20, 1996) to the ninth (January 28-30, 2004) were organized by Oita University under the sponsorship of the Science and Technology Policy Bureau, the Ministry of Education, Science, Sports, and Culture (Monkasho), Japanese Government and Air Force Office of Scientific Research, Asian Office of Aerospace Research and Development (AFOSR/AOARD), USA and co-operated by Santa Fe Institute (USA), SICE, RSJ, IEEJ, ICASE, CAAI, ISCIE, IEICE, IEEE (Japan Council), and JARA.

I would like to express my sincere thanks to Monkasho, AFOSR/AOARD and scientific societies for their repeated support.

This Tenth symposium is sponsored by AFOSR/AOARD and Japanese companies (Mitsubishi Electric Corporation Advanced Technology R&D Center, Oita Gas Co. Ltd., STK Technology Co. Ltd, Sanwa Shurui Co. Ltd., Yatsushika Brewery Co. Ltd. And others. I would like to express special thanks for AFOSR/AOARD and the companies stated above.

The symposium invites you to discuss the development of new technologies in the 21st century concerning Artificial Life and Robotics, based on simulation and hardware.

We hope that AROB 10th ’05 will facilitate the establishment of an international joint research institute on Artificial Life and Robotics in future. I hope that you will obtain fruitful results from exchange of ideas between researchers during the symposium.

Hiroshi Tanaka
Program Chairman
(Professor, Tokyo Medical and Dental University)

Hiroshi Tanaka
Program Chairman of AROB

On behalf of the program committee, it is truly my great honor to invite you all to the Tenth International Symposium on Artificial Life and Robotics (AROB 10th ’05). This symposium is made possible owing to the cooperation of Oita University and Santa Fe Institute. We are also debt to Japanese academic associations such as SICE, RSJ, and several private companies. I would like to express my sincere thanks to all of those who make this symposium possible.

As is needless to say, the complex systems or Alife approach now attracts wide interests as a new paradigm of science and engineering. Take an example in the field of bioscience. The accomplishment of HGP (Human Genome Project) and subsequent post-genomic comphrensive “Omics dat” such as transcriptome, proteome and metabolome,brings about vast amount of bio-information. However, as a plenty of omics data becomes available, it becomes sincerely recognized that the framework by which these omics data can be understood to make a whole picture of life is critically necessary, thus, in the post-genomic era , the complex systems or Alife approach is now actually expected to be an efficient methodology to integrate this vast amount of bio-data.

This example shows the complex system approach is very promising and becomes widely accepted as a paradigm of next generation of science and engineering. We hope this symposium becomes a forum for exchange of the ideas of the attendants from various fields who are interested in the future possibility of complex systems approach.

I am looking forward to meeting you in Beppu, Oita.

John Casti
Co-Chairman
(Professor, Technical University of Vienna)

John L. Casti
Co-Chairman of AROB

Since its inception by Masanori Sugisaka in 1996, the annual AROB meeting has become probably the single most important event on the calendar of Asian workers in the fields of artificial life and robotics. It has been a distinct pleasure and privilege for researchers from the Santa Fe Institute community to actively contribute to this AROB "phenomenon" from the very beginning. Starting with the "father" of artificial life, Chris Langton, who delivered a plenary talk at the first AROB meeting, SFI researchers Tom Ray, Steen Rasmussen, Josh Epstein, Brian Arthur and others have ensured an ongoing SFI presence at every one of the nine previous meetings.

Everyone in the SFI community congratulates Masanori Sugisaka on making the AROB meeting just a bit better each year. This is strong testimony to his untiring efforts to promote the field of A-Life through not only the meeting itself, but by helping to form networks of researchers around the world by means of the journal, *Artificial Life and Robotics*. It is a pleasure to acknowledge these efforts and to wish Masanori another decade or more of success in the AROB field.

Plenary talker:

Prof. Kazuyuki Aihara

PT Complexity Modeling and its Applications

Kazuyuki Aihara
Institue of Industrial Science
University of Tokyo
4-6-1 Komaba, Meguro-ku, Tokyo 153-8505, Japan

The brain is a typical example of a complex system with much complexity and many functions. In this plenary talk, I will review our study on creating an artificial brain with chaotic dynamics, or a chaotic brain. I will also discuss importance of several bifaces in modelling complex systems, namely generality / universality & individuality / specialty, abstracted & detailed, and stability & instability.

Special session talkers for artificial life and robotics

Dr. Harriet H. Natsuyama

SS-1 THE WORK OF SUEO UENO, ROBERT KALABA, AND RICHARD BELLMAN

Harriet H. Natsuyama
Los Angeles, CA 90066, hhnatsu@yahoo.com

Abstract: This paper recalls the critical developments of three exceptional individuals in the fields of nonlinear analysis, systems modeling, computational solution of initial value problems, system identification and optimal control

Prof. Yang-gang Zhang

SS-2 Machinery Cognition and Artificial Intelligent

Y.G. Zhang[1] and M. Sugisaka[2]
Institute of Systems Science, Academia Sinica, Beijing China, 100080
yzhang@iss.ac.cn
The Dept. of Electrical and Electronic Engineering, Oita University, Oita, Japan, 870-1192 msugi@ee.u-oita.edu.jp

Abstract: In this paper authors show some heuristic thinking first, and then proposed an engineering definition of artificial intelligence in artificial brain that is the abilities to obtain knowledge, to use knowledge and to operate knowledge. There are still two open important problems: one is the expression of knowledge for this goal and the other is how to construct the integration up operation and detailed down operation.

Keywords: Artificial Intelligence, Creating intelligence, Knowledge, Cognition, Evolution of intelligence.

Prof. Henrik Hautop Lund

SS-3 ATRON Hardware Modules for Self-reconfigurable Robotics

Henrik Hautop Lund, Richard Beck, Lars Dalgaard
Maersk Mc-Kinney Moller Institute for Production Technology
University of Southern Denmark, Campusvej 55, 5230 Odense M., Denmark
hhl@mip.sdu.dk beck@mip.sdu.dk dalgaard@mip.sdu.dk
www.adaptronics.dk

Abstract: We exploit a holistic behavioural and morphological adaptation in the design of new artefacts, and exemplify the potential of the new design principle through the construction of robotic systems that can change morphology. Here we present the ATRON design in which the modules are individually simple, attach through physical connections, and perform 3D motions by collective actions. We produced 100 ATRON modules, and performed both simulation and real world experiments. In this paper, we report on the ATRON hardware design and investigations related to the verification of the suitability of the ATRON module design for self-reconfigurable robotics.

The Tenth International Symposium on ARTIFICIAL LIFE AND ROBOTICS (AROB 10th '05)

Opening Ceremony

Chair: J.Johnson (Open University, UK)

February 4 (Friday)

Room D: 10:20-10:40

Welcome Addresses

1. General Chairman of AROB	M. Sugisaka (Oita University, RIKEN, Japan)
2. Advisory Committee Chairman	F. Harashima (Tokyo Denki University, Japan)
3. President of SOFT, President of IEEE Nanotechnology Council	T. Fukuda (Nagoya University, Japan)
4. Program Chairman of AROB	H. Tanaka (Tokyo Medical and Dental University, Japan)

TIME TABLE

	RoomA	RoomB	RoomC	RoomD
2/3(Thu.) 8:00				
13:00	Registration (Registration Desk)			
17:30	Welcome Party (at Beppu Kamenoi Hotel 10th Floor)			
2/4(Fri.) 8:00	Registration (Registration Desk)			
8:40	GS6(4) Chair H.Tanaka	GS7(4) Chair Y.G. Zhang	IS4(4) Chair H.Yanagimoto	
10:00	Coffee Break			
10:20				Opening Ceremony
10:40				Plenary Talk PT K. Aihara Chair J.J. Lee
11:40	Lunch			
12:40	GS11(6) Chair H. Umeo	GS14(4) Chair M.Okamoto will end at 14:00	GS15(6) Chair X.Wang	
14:40	Coffee Break			
14:50	GS21(6) Chair S.M. Chen will end at 16:50	IS8(5) Chair J.J.Lee will end at 16:30	GS17(4) Chair K.Ohnishi will end at 16:10	
16:50	GS5(3) Chair M.Oswald will end at 17:50	IS5(4) Chair H.Suzuki will end at 17:50	GS12(4) Chair K.B. Sim will end at 17:30	
18:10				

GS: General Session IS: Invited Session

GS1 Artificial Intelligence
GS2 Artificial Life-I
GS3 Artificial Life-Ⅱ
GS4 Artificial Living
GS5 Bioinformatics
GS6 Complexity
GS7 Cognitive Science
GS8 Computer Graphics
GS9 Evolutionary Computations-I
GS10 Evolutionary Computations -Ⅱ
GS11 Fuzzy Control
GS12 Genetic Algorithms-I
GS13 Genetic Algorithms-Ⅱ
GS14 Intelligent Control and Modeling-I
GS15 Intelligent Control and Modeling-Ⅱ
GS16 Micro-Robot World Cup-Soccer Tournament
GS17 Molecular Biology
GS18 Mobile Vehicles-I
GS19 Mobile Vehicles-Ⅱ
GS20 Neural Networks-I
GS21 Neural Networks-Ⅱ
GS22 Robotics-I
GS23 Robotics-Ⅱ
GS24 Robotics-Ⅲ
GS25 Image Processing
IS1 Soft Robotics
IS2 Computer Vision and Mobile Robot
IS3 Intelligent Pattern Classification
IS4 Intelligent Information Retrieval
IS5 Analysis and Implementation of Nonlinear Models
IS6 Hyper Human Technology
IS7 Biomimetic Machines and Robots
IS8 Robot Sensing and Control
IS9 Robot Control and Application
IS10 Human and Agents: Social Interaction and Organization (1)
IS11 Human and Agents: Social Interaction and Organization (2)
IS12 BIO MEDICAL field

	RoomA	RoomB	RoomC	RoomD
2/5(Sat.) 8:00	Registration (Registration Desk)			
8:40	GS18(5) Chair J. Wang	GS4(5) Chair T.Arita	GS20(5) Chair A.Buller	
10:20	Coffee Break			
10:30				Special Session Y.G. Zhang, H.Lund H.H.Natsuyama Chair Y.Yin
11:30	Lunch			
12:30	IS1(4) Chair T.Yamamoto	GS9(4) Chair K. Uosaki	IS10(4) Chair K.Shimohara	
13:50	Coffee Break			
14:00	GS19(4) Chair K.Sugawara will end at 15:20	GS10(5) Chair H. Kawamura will end at 15:40	IS11(4) Chair K.Shimohara will end at 15:20	
15:20	GS1(7) Chair P. Sapaty will end at 17:40.		GS13(4) Chair J. Johnson will end at 16:40.	
15:40		GS25(7) Chair S. Ishikawa will end at 18:00.		
16:40			IS12(3) Chair T.Ishimatsu will end at 17:40.	
18:10	AROB Award Ceremony (Chair: K. Watanabe) Banquet (Hotel Shiragiku)			
20:30				

GS: General Session IS: Invited Session

GS1 Artificial Intelligence
GS2 Artificial Life-I
GS3 Artificial Life-Ⅱ
GS4 Artificial Living
GS5 Bioinformatics
GS6 Complexity
GS7 Cognitive Science
GS8 Computer Graphics
GS9 Evolutionary Computations-I
GS10 Evolutionary Computations -Ⅱ
GS11 Fuzzy Control
GS12 Genetic Algorithms-I
GS13 Genetic Algorithms-Ⅱ
GS14 Intelligent Control and Modeling-I
GS15 Intelligent Control and Modeling-Ⅱ
GS16 Micro-Robot World Cup-Soccer Tournament
GS17 Molecular Biology
GS18 Mobile Vehicles-I
GS19 Mobile Vehicles-Ⅱ
GS20 Neural Networks-I
GS21 Neural Networks-Ⅱ
GS22 Robotics-I
GS23 Robotics-Ⅱ
GS24 Robotics-Ⅲ
GS25 Image Processing
IS1 Soft Robotics
IS2 Computer Vision and Mobile Robot
IS3 Intelligent Pattern Classification
IS4 Intelligent Information Retrieval
IS5 Analysis and Implementation of Nonlinear Models
IS6 Hyper Human Technology
IS7 Biomimetic Machines and Robots
IS8 Robot Sensing and Control
IS9 Robot Control and Application
IS10 Human and Agents: Social Interaction and Organization (1)
IS11 Human and Agents: Social Interaction and Organization (2)
IS12 BIO MEDICAL field

	RoomA	RoomB	RoomC	RoomD
2/6(Sun.) 8:00	Registration (Registration Desk)			
8:40	IS9(5) Chair S.H. Han	IS2(5) Chair M.Kono	GS22(5) Chair K. Nakano	
10:20	Coffee Break			
10:40	IS7(5) Chair K. Watanabe	GS2(5) Chair M. Osano	GS23(4) Chair J.M. Lee will end at 12:00	
12:20	Lunch			
13:20	IS6 (5) Chair M. Kaneko will end at 15:00.	GS3(5) Chair N. Mirenkov will end at 15:00.	GS24(6) Chair S.Sagara will end at 15:20.	
15:00	GS8(4) Chair M. Yokota will end at 16:20.	IS3(4) Chair S. Omatu will end at 16:20.		
15:20			GS16(3) Chair J. Nishii will end at 16:20.	
16:20	Farewell Party (Room A)			
17:20				

GS: General Session IS: Invited Session

GS1 Artificial Intelligence
GS2 Artificial Life-I
GS3 Artificial Life-Ⅱ
GS4 Artificial Living
GS5 Bioinformatics
GS6 Complexity
GS7 Cognitive Science
GS8 Computer Graphics
GS9 Evolutionary Computations-I
GS10 Evolutionary Computations -Ⅱ
GS11 Fuzzy Control
GS12 Genetic Algorithms-I
GS13 Genetic Algorithms-Ⅱ
GS14 Intelligent Control and Modeling-I
GS15 Intelligent Control and Modeling-Ⅱ
GS16 Micro-Robot World Cup-Soccer Tournament
GS17 Molecular Biology
GS18 Mobile Vehicles-I
GS19 Mobile Vehicles-Ⅱ
GS20 Neural Networks-I
GS21 Neural Networks-Ⅱ
GS22 Robotics-I
GS23 Robotics-Ⅱ
GS24 Robotics-Ⅲ
GS25 Image Processing
IS1 Soft Robotics
IS2 Computer Vision and Mobile Robot
IS3 Intelligent Pattern Classification
IS4 Intelligent Information Retrieval
IS5 Analysis and Implementation of Nonlinear Models
IS6 Hyper Human Technology
IS7 Biomimetic Machines and Robots
IS8 Robot Sensing and Control
IS9 Robot Control and Application
IS10 Human and Agents: Social Interaction and Organization (1)
IS11 Human and Agents: Social Interaction and Organization (2)
IS12 BIO MEDICAL field

TECHNICAL PAPER INDEX

February 4 (Friday)

Room D

10:40~11:40 Plenary Talk
Chair J.J. Lee (KAIST, Korea)

PT *Complexity modeling and its applications*
K. Aihara (University of Tokyo, Japan)

February 5 (Saturday)

10:30~11:30 Special Session on Artificial Life and Robotics
Chair Y. Yin (The Beijing University of Science and Technology, China)

SS-1 *The work of Sueo Ueno, Robert Kalaba, and Richard Bellman*
H.H. Natsuyama

SS-2 *Machinery cognition and artificial intelligent*
Y.G. Zhang (Academia Sinica, China)
M. Sugisaka (Oita University, Japan)

SS-3 *ATRON hardware modules for self-reconfigurable robotics*
H.H. Lund, R. Beck, L. Dalgaard (University of Southern Denmark, Denmark)

February 4 (Friday)

8:00~ Registration

Room A

8:40~10:00 GS6 Complexity
Chair: H. Tanaka (Tokyo medical & Dental University)

GS6-1 *An investigation into state-change complexities in synchronization algorithms for cellular automata*
K. Matsumoto, H. Umeo (Osaka Electro-Communication University, Japan)

GS6-2 *State-efficient implementations of synchronization algorithms for two-dimensional cellular automata*
H. Umeo, M. Teraoka, M. Hisaoka,M. Maeda (Osaka Electro-Communication University, Japan)

GS6-3 *A Study of the basic concept of information in a complex system*
Y. Kinouchi, T. Komiyama (Tokyo University of Information Sciences, Japan)

GS6-4 *Qualitative analysis of self-organizing multi agent interaction with entropy and mutual information*
K. Nishikawa, H. Kawamura, M. Yamamoto, A. Ohuchi (Hokkaido University, Japan)

12:40~14:40 GS11 Fuzzy Control
Chair: H. Umeo (Osaka Electro-Communication University, Japan)

GS11-1 *Development of the fuzzy control for a GPS-located airship*
M. Sugisaka (Oita University, Japan)
F. Dai, Y. Fujihara, T. Kamoika (Matsue National College of Technology, Japan)

GS11-2 *Fuzzy information retrieval based on weighted power-mean averaging operators*
W-S Hong, S-M Chen (National Taiwan University of Science and Technology, Taiwan)
S-J Chen (Ching-Yun University, Taiwan)

GS11-3 *Temperature prediction based on genetic simulated annealing techniques and high-order fuzzy time series*
L-W Lee (National Taiwan University of Science and Technology, Taiwan)
L-H Wang (Chihlee Institute of Technology, Taiwan)
S-M Chen (National Taiwan University of Science and Technology, Taiwan)

GS11-4 *Design of a fuzzy expert system for electric vehicle speed control*
M. Sugisaka, Z. Mbaitiga (Oita University, Japan)

GS11-5 *A harness line color recognition method based on fuzzy similarity measure*
Y-T. Kim, H. Bae, Y-I. Kim, S. Kim (Pusan National University, Korea)

GS11-6 *An EPS system control for fuzzy logic in HILS system*

M.K. Lee, J.Y. Choi, S.K. Ha, M.H. Lee (Pusan National University, Korea)

14:50~16:50 GS21 Neural Networks-Ⅱ
Chair: S-M. Chen (National Taiwan University of Science and Technology, Taiwan)

GS21-1 *Applying FIFO-Queue ACO algorithm to broadcast problem of wireless Sensor Networks*
J. Katsuki, T. Isokawa, N. Kamiura, N. Matsui (University of Hyogo, Japan)

GS21-2 *Predicting selection of artificial network by cluster coefficient*
S. Yoshimura, S. Yoshii (Hokkaido University, Japan)

GS21-3 *Evolution of development and heterochrony in artificial neural networks*
A. Matos, R. Suzuki, T. Arita (Nagoya University, Japan)

GS21-4 *Multi-procedure ozone concentration prediction using fuzzy clustering and DPNN*
S-P Cheon, S-T Lee, S. Kim (Pusan National University, Korea)

GS21-5 *A model of emergence of reward expectancy neurons using reinforcement learning and neural network*
S. Ishii (Oita University, Japan)
M. Shidara (National Institute of Advanced Industrial Science and Technology)
K. Shibata (Oita University, Japan)

GS21-6 *Shape-recognition using randomly selected pixel-pair neurons*
V. Rose, J. Johnson (Open University, Uk)

16:50~17:50 GS5 Bioinformatics
Chair: M. Oswald (Vienna University of Technology, Austria)

GS5-1 *Information-theoretic approach to embodied category learning*
G. Gomez (University of Zurich, Austria)
M. Lungarella (Tokyo University, Japan)
D. Tarapore (Indian Institute of Technology)

GS5-2 *On the diversity of HIV using cellular automata approach*
H. Ueda, Y. Iwaya, T. Abe, T. Kinoshita (Tohoku University, Japan)

GS5-3 *Construction and strategy of a soccer team by the agent using immune concept*
N. Kogawa, M. Obayashi, A. Maeda, K. Kobayashi, T. Kuremoto (Yamaguchi University, Japan)

Room B

8:40~10:00 GS7 Cognitive Science
Chair: Y.G. Zhang (Academia Sinica, China)

GS7-1 *Transforming information to Knowledge and intelligence*
Y.X. Zhong (University of Post and Telecommunication, China)

GS7-2 *Establishment of sound-correspondence laws of word-initial consonants between*

Finnish/Uralic and Malayo-Polynesian/ Proto-Austronesian languages: Towards making comparative analysis of word-initial consonant frequencies
K. Ohnishi, S. Akiyama,Y. Murayama, M. Goda (Niigata University, Japan)

GS7-3 *Effect of action selection on the emergence of one-way communication using Q-learning*
M. Nakanishi, K. Shibata (Oita University, Japan)

GS7-4 *Design of a robust adaptive controller for a class of uncertain nonlinear systems with time-delay input*
T-M-H. Nguyen, T-N. Dinh, T-N. Nguyen, V-T.Tran (Center for Automation Technology-CAT, Vietnam)

12:40~14:00 GS14 Intelligent Control and Modeling- Ⅰ
Chair: M. Okamoto (Kyushu University, Japan)

GS14-1 *Solving Constrained Motion Problems Using the GI Method*
Y. Y. Fan (University of California, U.S.A.)

GS14-2 *Moving robot path search including obstacles by GA using quadrant idea*
H. Yamamoto, E. Marui (Gifu University, Japan)

GS14-3 *Design of novel adaptive routing by mimicking enzymic feedback control mechanism in the cell*
T. Kawauchi (Kyushu University, Japan)
M. Hirakawa (Fukuoka International University, Japan)
M. Okamoto (Kyushu University, Japan)

GS14-4 *Agent based plant allocation and transfer routing of products in case of emergency*
S. AlSehaim, M. Konishi (Okayama University, Japan)
K. Nose (Osaka Sangyo University, Japan)

14:50~16:30 IS8 Robot Sensing and Control
Chair: J.J. Lee (Korea Advanced Institute of Science and Technology, Korea)
J.M. Lee (Pusan National University, Korea)

IS8-1 *The hybrid SOF-PID controller for the control of a MIMO biped robot*
T-Y Choi, S-Y Park, Ju-Jang Lee (Korea Advanced Institute of Science and Technology, Korea)

IS8-2 *Strategy of cooperative behaviors for distributed autonomous robotic systems*
H-U Yoon, S-H Whang, D-W Kim, K-B Sim (Chung-Ang University, Korea)

IS8-3 *Development of the tactile sensor system using fiber Bragg grating sensors*
J.S. Heo, Jung Ju Lee (Korea Advanced Institute of Science and Technology, Korea)

IS8-4 *A distributed precedence queue mechanism to assign efficient bandwidth in CAN networks*
H.S. Choi, J.M. Lee (Pusan National University, Korea)

IS8-5 *Adaptive occupancy grid mapping with clusters*

B.G. Jang, T.Y. Choi, Ju-Jang Lee (Korea Advanced Institute of Science & Technology, Korea)

16:30~17:50 IS5 Analysis and Implementation of Nonlinear Models
Chair: H.Suzuki (University of Tokyo,Japan)
Co-Chair: S. Horai (University of Tokyo,Japan)

IS5-1 *MOSFET implementation of class I^* neurons coupled by gap junctions*
T. Takemoto (Tokyo University, Japan)
T. Kohno (Aihara Complexity Modeling Project, ERATO, JST, Japan)
K. Aihara, H. Suzuki (Tokyo University, Japan)

IS5-2 *Parameter tuning of a MOSFET-based nerve membrane*
T. Kohno (Aihara Complexity Modeling Project, ERATO, JST, Japan)
K. Aihara, H. Suzuki (Tokyo University, Japan)

IS5-3 *Wayland test, noise, and surrogate*
Y. Hirata (Tokyo University, Japan)
S. Horai (Aihara Complexity Modeling Project, ERATO, JST, Japan)
K. Aihara, H. Suzuki (Tokyo University, Japan)

IS5-4 *Analysis of bifurcation and optimal response on the evolution of cooperation*
Y-H Otake, K. Aihara, H. Suzuki (Tokyo University, Japan)

Room C

8:40~10:00 IS4 Intelligent Information Retrieval
Chair: H.Yanagimoto (Osaka Prefecture University, Japan)

IS4-1 *Information filtering using probabilistic model*
H. Yanagimoto, S. Omatu (Osaka Prefecture University, Japan)

IS4-2 *Modification of user profile using the genetic algorithm*
H. Yanagimoto, S. Omatu (Osaka Prefecture University, Japan)

IS4-3 *Information filtering using SVD and ICA*
T. Yokoi, H. Yanagimoto, S. Omatu (Osaka Prefecture University, Japan)

IS4-4 *Improvement of information filtering using topic selection*
T. Yokoi, H. Yanagimoto, S. Omatu (Osaka Prefecture University, Japan)

12:40~14:40 GS15 Intelligent Control and Modeling-Ⅱ
Chair: X. Wang(Tokushima University, Japan)

GS15-1 *Decision method of reference input time interval and sampling time interval that considered contour control performance in software servo system*
S. Satou, M. Nakamura, S. Goto (Saga University, Japan)
N. Egashira (Kurume Institute of Technology, Japan)
N. Kyura (Kinki University, Japan)

GS15-2 *An automatic decoupling control system for ship harbor maneuvers and its robustness evaluation*
M-D Le (VINASHIN, Vietnam)
A-T Dang (SHIPSOFT JSC., Vietnam)

GS15-3 *CPU resource double auction system with an anonymous protocol*
T. Matsumoto, H. Kawamura, A. Ohuchi (Hokkaido University, Japan)

GS15-4 *Issues and applications of robot control using internet*
M. Sugisaka, H. Desa (Oita University, Japan)

GS15-5 *Hard / soft switching particle filters for efficient real-time visual tracking*
T. Bando, T. Shibata, K. Doya, S. Ishii (Nara Institute of Science and Technology, Japan)

GS15-6 *Robotics and the Q-analysis of behaviour*
I. Pejman, J. Johnson, L.Rapanotti (The Open University, UK)

14:50~16:10 GS17 Molecular Biology
Chair: K. Ohnishi (Niigata University, Japan)

GS17-1 *Nanoparticles as biosensors components*―*a brief review*
T. Kubik (Wroclaw University of Technology, Poland)
M. Sugisaka (Oita University, Japan)

GS17-2 *P systems with dynamic channels transporting membrane vesicles*
R. Freund, M. Oswald (Vienna University of Technology, Austria)

GS17-3 *Design of soccer-ball-shape DNA molecules and preliminary experiments in vitro*
Y. Kita (Hokkaido University, Japan)
A. Kameda, (CREST, Japan Science and Technology Agency, Japan)
M. Yamamoto, A. Ohuchi (CREST, Hokkaido University, Japan)

GS17-4 *Amoebic ability to arrive at signal sources in obstacle-rich space*
S. I. Nishimura, M. Sasai (Nagoya University, Japan)

16:10~17:30 GS12 Genetic Algorithms-Ⅰ
Chair: K-B. Sim (Chung-Ang University)

GS12-1 *The analysis for the movement characteristics of the flying object with genetic algorithms*
R. Goto, Y. Sato (Hosei University, Japan)

GS12-2 *Proposal of serially and dynamically separating genetic algorithm and its application to optimization of robot control systems*
K. Nakayama (Kyoto University, Japan)
H. Matsui (Mie University, Japan)
K. Shimohara (ATR Network Informatics Laboratories, Japan)
O. Katai (Kyoto University, Japan)

GS12-3 *Proposal of genetic operations reducing the evaluator workload to the voice quality conversion using interactive GA*
T. Nishizono, S. Noami, Y. Sato (Hosei University, Japan)

GS12-4 *Fitness modification in genetic algorithms for function optimization problems*
T. Yoshida, T. Nakashima, H. Ishibuchi (Osaka Prefecture University, Japan)

February 5 (Saturday)

8:00~ Registration

Room A

8:40~10:20 GS18 Mobile Vehicles-I
Chair: J. Wang (Oita University, Japan)

GS18-1 *A Controller design method for an articulated vehicle employing self-organizing relationship(SOR) network*
T. Koga, K. Horio, T. Yamakawa (Kyushu Institute of Technology, Japan)

GS18-2 *Automatic control of an electric vehicle using visual information*
K. Tokuda, M. Sugisaka, Z. Mbaitiga (Oita University, Japan)

GS18-3 *Mobile sensor device in intelligent space*
H. Isu, T. Sasaki, H. Hashimoto (Tokyo University, Japan)

GS18-4 *Real-time path planning for senor-based mobile robot based on probabilistic roadmap method*
Z. Li, X. Chen (Fudan University, China)

GS18-5 *Gesture clustering and imitative behavior generation for partner robots*
Y. Nojima (Osaka Prefecture University, Japan)
N. Kubota (Tokyo Metropolitan University, Japan)
F. Kojima (Kobe University, Japan)

12:30~13:50 IS1 Soft Robotics
Chair: T. Yamamoto (University of Ryukyus, Japan)
Co-Chair: H. Kinjo (University of Ryukyus, Japan)

IS1-1 *Improvement of the real-coded genetic algorithms for optimization problems*
H. Kinjo, H. Nakanishi, T. Yamamoto (University of the Ryukyus, Japan)
D.S. Chau (Hanoi Agricultural University, Vietnam)

IS1-2 *Enhanced performance for multi- variable optimization problems by use of GAs with recessive gene structure*
E. Muhando, H. Kinjo, T. Yamamoto (University of the Ryukyus, Japan)

IS1-3 *Identification of time series signals using dynamical neural network with GA-based training*
K. Nakazono (University of the Ryukyus, Japan)
K. Ohnishi (Keio University, Japan)
H. Kinjo, (University of the Ryukyus, Japan)

IS1-4 *Spontaneous speciation by GA for division of labor in two-agent systems*
N. Oshiro, K. Kurata, T. Yamamoto (University of the Ryukyus, Japan)

14:00~15:20 GS19 Mobile Vehicles-Ⅱ
Chair: K. Sugawara (Tohoku Gakuin University, Japan)

GS19-1 *How to make a mobile robot move more reliably?*
J. Wang, M. Sugisaka (Oita University, Japan)

GS19-2 *PID orbit motion controller for indoor blimp robot*
H. Kadota, H. Kawamura, M. Yamamoto (Hokkaido University, Japan)
T. Takaya (RICOH SYSTEM KAIHATU COMPANY, LTD.)
A. Ohuchi (Hokkaido University, Japan)

GS19-3 *Automated moving objects detection with an on-board camera for avoidance of car accident*
S. Sunahara, Y. Tsuboi, O. Ono (Meiji University, Japan)

GS19-4 *Improving odometry accuracy for a car using tire radii measurements*
H.C. Lee, C.S. Kim, K-S Hong, M.H. Lee (Pusan National University, Japan)

15:20~17:40 GS1 Artificial Intelligence
Chair: P. Sapaty (Aizu University, Japan)

GS1-1 *Learning algorithms and uncertain variables in knowledge-based pattern recognition*
Z. Bunicki (Wroclaw University, Poland)

GS1-2 *Association rule mining using genetic network programming*
K. Shimada, K. Hirasawa, T. Furutsuki (Waseda University, Japan)

GS1-3 *Evolution of metaparameters for efficient real time learning*
G.. Capi (Fukuoka Institute of Technology, Japan)
M. Yokota (Fukuoka Institute of Technology, Japan)
K. Doya (CREST, Japan Science and Technology Agency, Japan)

GS1-4 *A reinforcement learning scheme of adaptive flocking behavior*
M. Tomimasu, H. Nishimura, K. Morihiro, T. Isokawa, N. Matsui (University of Hyogo, Japan)

GS1-5 *Learning control of manipulator with a free joint*
T. Goto, H. Lee (Tohoku University, Japan)
K. Abe (Tohoku University, Japan)
H. Kamaya (Hachinohe National College of Technology, Japan)

GS1-6 *Evolutionary simulations based on a robotic approach to emotion*
T. Kato, T. Arita (Nagoya University, Japan)

GS1-7 *Models of individuals for constructive approach of dynamic view of language and society*
T. Hashimoto, T. Sato, A. Masumi (Japan Advanced Institute of Science and Technology, Japan)

Room B

8:40~10:20 GS4 Artificial Living
Chair: T. Arita (Nagoya University, Japan)

GS4-1 *Interactive musical editing system for supporting human error and offering personal preferences for an automatic piano-preference database for crescendo and decrescendo-*
E. Hayashi, Y. Takamatsu (Kyushu Institute of Technology, Japan)

GS4-2 *The role of population structure in language evolution*
Y. Lee, T.C. Collier, E.P. Stabler, C.E. Taylor (University of California, Los Angeles, U.S.A.)

GS4-3 *Truth table language for generating self-replicating systems*
H. Harada, Y. Toquenaga (Tsukuba University, Japan)

GS4-4 *Effectiveness of emerged pheromone communication in an ant foraging model*
Y. Nakamichi, T. Arita (Nagoya University, Japan)

GS4-5 *Foraging behavior of ant-like Robots with virtual pheromone*
K. Sugawara, T. Kazama (Tohoku Gakuin University, Japan)

12:30~13:50 GS9 Evolutionary Computations-I
Chair: K. Uosaki (Osaka University, Japan)

GS9-1 *DNA computing approach to evolutional reasoning algorithm by using restriction Enzyme*
Y. Tsuboi, I. Zuwairie, O. Ono (Meiji University, Japan)

GS9-2 *A model for coevolution*
K. Makino (Tokyo Institute of Technology, Japan)
K. Nakano (Tokyo University of Technology, Japan)

GS9-3 *Simultaneous state and parameter estimation of nonlinear models by evolution strategies based particle filters*
K. Uosaki, T. Hatanaka (Osaka University, Japan)

GS9-4 *Evaluating a solution of tour planning problem based on the partially exhaustive exploration Monte Carlo method*
M. Onodera, H. Kawamura, A. Ohuchi (Hokkaido University, Japan)

14:00~15:40 GS10 Evolutionary Computations-Ⅱ
Chair: H. Kawamura (Hokkaido University, Japan)

GS10-1 *A comprehensive evaluation of the methods for evolving a cooperative team*
Y. Suzuki, T. Arita (Graduate School of Information Science, Nagoya University)

GS10-2 *A fast algorithm in finding communities of book network*
S. Wang, C. Zhang (Tsinghua University, China)

GS10-3 *Autonomous evolutionary machine vision systems*
J.H. Johnson, V. Rose (Open University, United Kingdom)

GS10-4 *Real-time adaptive maintenance for performance improvement on daily-use computer*
S. Hirose, S.Yoshii (Hokkaido University, Japan)

GS10-5 *Swarm search for fast face detection with neural networks*
X. Fan, M. Sugisaka (Oita University, Japan)

15:40 ~18:00 GS25 Image Processing
Chair: S. Ishikawa (Kyushu Institute of Technology, Japan)

GS25-1 *An optimal capturing trajectory planning for a moving object*
B-S. Choi, J-M. Lee (Pusan National University, Korea)

GS25-2 *Proposing a passive biometric system for robotic vision*
M.M. Rahman, S. Ishikawa (Kyushu Institute of Technology, Japan)

GS25-3 *Human motion recovery by mobile stereoscopic cameras*
J.K. Tan, I. Yamaguchi, S. Ishikawa (Kyushu Institute of Technology, Japan)
T. Naito, M. Yokota (Kyushu Dental College, Japan)

GS25-4 *A high-speed human motion recovery based on back projection*
M. Uchinoumi, J.K. Tan, S. Ishikawa (Kyushu Institute of Technology, Japan)
T. Naito, M. Yokota (Kyushu Dental College, Japan)

GS25-5 *Auto-correlation probabilistic relaxation matching method*
X. Wang (The University of Tokushima, Japan)
M. Sugisaka (Oita University, Japan)
J. Wang (Hebei University of Science & Technology, China)

GS25-6 *Segmentation and object recognition for robot bin picking systems*
R. Nagarajan, (Universiti Malaysia Sabah, Malaysia)
Y. Sazali (Northern Malaysia University College of Engineering, Malaysia)
P. Pandiyan (Universiti Malaysia Sabah, Malaysia)
C. R. Hema (Universiti Malaysia Sabah, Malaysia)
A. Shamsudin (Universiti Teknologi Malaysia, Malaysia)
K. Marzuki (Universiti Teknologi Malaysia, Malaysia)
M. Rizon (Northern Malaysia University College of Engineering, Malaysia)

GS25-7 *Stereo camera based artificial vision for blind through hearing*
G. Balakrishnan, G. Sainarayanan, R. Nagarajan (Universiti Malaysia Sabah, Malaysia)

Y. Sazali, M. Rizon (Northern Malaysia University College of Engineering, Malaysia)

Room C

8:40~10:20 GS20 Neural Networks- Ⅰ
Chair: A.Buller (ATR Network Infomatics Laboratories, Japan)

GS20-1 *Improving the tuning capability of the adjusting neural network*
Y. Sugita (Hitachi,Ltd. Hitachi Research Laboratory, Japan)
K. Hirasawa (Waseda University, Japan)

GS20-2 *Fault diagnosis for electro-mechanical control system by neural networks*
T. Torigoe, M. Konishi, J.Imai, T. Nishi (Okayama University, Japan)

GS20-3 *Image processing for GIS applications supported by the use of artificial neural networks*
T. Kubik, W. Paluszynski (Wroclaw University of Technology, Poland)
A. Iwaniak, P. Tymkow (Agricultural University of Wroclaw, Poland)

GS20-4 *A supervised learning rule adjusting input-output pulse timing for pulsed neural network*
M. Motoki, S. Koakutsu, H. Hirata (Chiba University, Japan)

GS20-5 *Remarks on tracking method of neural network weight change for learning type neural network direct controller*
T. Yamada (Ibaraki University)

12:30~13:50 IS10 Artificial Human and Agents: Social Interaction and Organization (1)
Chair: K. Shimohara (Kyoto University, ATR Network Laboratories, Japan)
Co-Chair: H. Fujii

IS10-1 *Sociable and affective artificial cohabitant*
N. Matsumoto and A. Tokosumi (Tokyo Institute of Technology, Japan)

IS10-2 *Child-robot interaction mediated by building blocks: From field observation in a public space*
M. Goan, H. Fujii, M. Okada (ATR Network Informatics Laboratories, Japan)

IS10-3 *Social influence of overheard communication by life-like agents to a user*
S.V. Suzuki (DCISS, IGSSE, Tokyo Institute of Technology, Japan)
S. Yamada (National Institute of Informatics, Japan)

IS10-4 *Do complementarities exist in agent interactions?*
M. Lee, M. Goan, M. Okada (ATR Network Informatics Laboratories, Japan)

14:00~15:20 IS11 Artificial Human and Agents: Social Interaction and Organization (2)
Chair: K. Shimohara (Kyoto University, ATR Network Laboratories, Japan)
Co-Chair: M. Goan (ATR Network Informatics Laboratories, Japan)

IS11-1 *Multi user learning agent based on social interaction*
D. Katagami, H. Ohmura, Y. Yasumura, K. Nitta (CISS, IGSSE, Tokyo Institute of Technology, Japan)

IS11-2 *Can robots get "membership" through social interaction?*
H. Fujii, M. Okada (ATR Network Informatics Laboratories, Japan)

IS11-3 *Minimal design for human-agent communication*
N. Matsumoto, H. Fujii, M. Okada (ATR Network Informatics Laboratories, Japan)

IS11-4 *Development of a speech-driven embodied laser pointer with a visualized response equivalent to nodding*
H. Nagai, T. Watanabe, M. Yamamoto (Okayama Prefectural University, Japan)

15:20 ~16:40 GS13 Genetic Algorithms-Ⅱ
Chair: J. Johnson (Open University, UK)

GS13-1 *Data mining using genetic network programming*
T. Fukuda, K. Shimada, K. Hirasawa, T.Furuzuki (Waseda University, Japan)

GS13-2 *Performance comparison between fuzzy rules and interval rules in rule-base classification systems*
S. Namba, Y. Nojima, H. Ishibuchi (Osaka Prefecture University, Japan)

GS13-3 *Design of an augmented automatic choosing control with the weighted automatic choosing functions using Hamiltonian and genetic algorithm*
T. Nawata (Kumamoto National College of Technology, Japan)
H. Takata (Kagoshima University, Japan)

GS13-4 *Evolution and niche construction in NKES fitness landscape*
R. Suzuki, T. Arita (Nagoya University, Japan)

16:40 ~17:40 IS12 Bio Medical Field
Chair: T. Ishimatsu (Nagasaki University, Japan)

IS12-1 *Development of pointing device to use vision for people with disability*
M. Kubo, M. Tanaka, S. Moromugi, Y. Shimomoto, Y. Ohgiya, T. Ishimatsu (Nagasaki University, Japan)

IS12-2 *Monitoring system of body movements for bedridden elderly*
R-S. Dong, M. Tanaka, M. Ushijima, T. Ishimatsu (Nagasaki University, Japan)

IS12-3 *Development of a training machine for elderly people with muscle activity sensor*
S-J. Yoon, S-H. Kim, M. Tanaka, S. Moromugi, Y. Ohgiya, N. Matsuzaka, T. Ishimatsu (Nagasaki University, Japan)

February 6 (Sunday)

8:00~ Registration

Room A

8:40~10:20 IS9 Robot Control and Application
Chair: S.H. Han (Kyungnam University, Korea)

IS9-1 *Real time implementation of visual servoing control for SCARA robot with eight joints*
D-Y. Jung, H-R. Kim, S-H. Han (Kyungnam University, Korea)

IS9-2 *Tolerance of permanent magnet Biased bidirectional magnetic bearings and its robotic application*
Y- T. Kim, U-J. Na (Kyungnam University, Korea)

IS9-3 *Detecting method of friction force on linear actuators of a parallel manipulator based on the gravitational force*
H-B. Shin, S-H. Lee (Kyungnam University, Korea)

IS9-4 *Real time control of feature based visual tracking for dual-arm robot*
J-S. Kim, H-R. Kim, S-H. Han (Kyungnam University, Korea)

IS9-5 *Calibration and control experiments on redundant legs of a Stewart platform based machine tool*
W-S. Lee, H-S. Kim (Kyungnam University, Korea)

10:40~12:20 IS7 Biomimetic Machines and Robots
Chair: K. Watanabe (Saga University, Japan)
Co-Chair: K. Izumi (Saga University, Japan)

IS7-1 *A view-based navigation system for autonomous robots*
C. Pathirana, K. Watanabe, K. Izumi (Saga University, Japan)

IS7-2 *Intelligent vision system for dynamic environments*
C. Pathirana, K. Watanabe, K. Izumi (Saga University, Japan)
A. Hewawasam, L. Udawatta (University of Moratuwa, Sri Lanka)

IS7-3 *Human interaction with binocular vision robots in ubiquitous environment*
J.C. Balasuriya, K. Watanabe, K. Izumi (Saga University, Japan)

IS7-4 *Fuzzy coach player method with shared environmental data*
K. Izumi, K. Watanabe, Y. Tamano, A. Oshima (Saga University, Japan)

IS7-5 *Cost function analysis of optimizing fuzzy energy regions in control of underactuated manipulators*
K. Izumi, K. Ichida, K. Watanabe, (Saga University, Japan)

13:20~15:00 IS6 Hyper Human Technology
Chair: M. Kaneko (Hiroshima University, Japan)

IS6-1 *Dynamic preshaping based design of capturing robot driven by wire*

S. Nishio, M. Higashimori, M. Kaneko (Hiroshima University, Japan)

IS6-2 *Design of tracing type jumping robots*
M. Harada, M. Higashimori, I. Ishii, M. Kaneko (Hiroshima University, Japan)

IS6-3 *Development of a laparoscopic surgery training system and preliminary experiments*
H. Masugami, T. Kawahara, H. Egi, M. Yoshimitsu, M. Okajima, M. Kaneko (Hiroshima University, Japan)

IS6-4 *Toward a real time force measurement by vision*
T. Mizoi, I. Ishii, M. Kaneko (Hiroshima University, Japan)

IS6-5 *Non-contact impedance sensing*
T. Kawahara, K. Tokuda, M. Kaneko (Hiroshima University, Japan)

15:00~16:20 GS8 Computer Graphics
Chair: M.Yokota (Fukuoka Institute of Technology, Japan)

GS8-1 *Optimization of camera positions for taking all indoor sceneries by GA*
Y. Tominari, T. Nakagawa, K. Yamamori, I. Yoshihara (University of Miyazaki, Japan)
H. Takeda (Office of Strategic Planning Systems Development Laboratory Hitachi,Ltd.)

GS8-2 *Real time structure preserving image noise reduction for computer vision on embedded platforms*
W. Nistico, U. Schwiegelshohn, M. Hebbel, I. Dahm (University of Dortmund, Germany)

GS8-3 *Model-less visual servoing using modified simplex optimization*
H. Inooka, K. Hashimoto (Tohoku University, Japan)
J. Gangloff, M. de Mathelin (Louis Pasteur Strasbourg University, France)
K. Miura (Tohoku University, Japan)

GS8-4 *Impulsive noise reduction using M-transform and wavelet with applications to AFM signals*
H. Harada, S.K. Jeon, H. Kashiwagi (Kumamoto University, Japan)

Room B

8:40~10:20 IS2 Computer Vision and Mobile Robot
Chair: M. Kono (University of Miyazaki, Japan)
Co-Chair: M. Yokomichi (University of Miyazaki, Japan)

IS2-1 *Indication of object spatial position by finger pointing*
M. Hirasawa, M. Oshima (Tokyo University of Marine Science and Technology, Japan)

IS2-2 *Accepting powers of four-dimensional alternating turing machines with only universal states*
Y. Nakama, M. Sakamoto, M. Saito, S. Taniguchi, (University of Miyazaki, Japan)
T. Ito (Ube Natinal College of Technology, Japan)
K. Inoue (Yamaguchi University, Japan)
H. Furutani S. Katayama (University of Miyazaki, Japan)

IS2-3 *Some properties of four-dimensional multicounter automata*
M. Saito, M. Sakamoto, Y. Nakama (University of Miyazaki, Japan)
T. Ito (Ube Natinal College of Technology, Japan)
K. Inoue (Yamaguchi University, Japan)
H. Furutani[1], S. Katayama (University of Miyazaki, Japan)

IS2-4 *Simulation study for intelligent wheelchair vehicle with ultrasonic and infrared sensors*
K. Kamimura, T. Kai, M. Yokomichi (University of Miyazaki, Japan)
T. Kitazoe (The Inter National University of Kagoshima, Japan)

IS2-5 *Object recognition using a self-organizing map for an autonomous mobile robot*
M. Tabuse, H. Kaneko (Kyoto Prefectural University, Japan)

10:40~12:20 GS2 Artificial Life-Ⅰ
Chair: M. Osano (Aizu University, Japan)

GS2-1 *Grasping the distributed entirety*
P. Sapaty (National Academy of Science, Ukraine)
M. Sugisaka (Oita University, Japan)
N. Mirenkov, M. Osano (University of Aizu)
R. Finkelstein (Robotic Technology Inc., U.S.A)

GS2-2 *Motion control of biped robot bending the knees*
K. Umezaki, M. Sugisaka (Oita University, Japan)

GS2-3 *Acquisition of common symbols with development of cooperative behaviors*
Y. Hashizume, J. Nishii (Yamaguchi University, Japan)

GS2-4 *A hierarchical learning model for basic locomotor patterns*
T. Hioki, J. Nishii (Yamaguchi University, Japan)

GS2-5 *Artificial life-based search technique on the solution of singular configurations concerning screw parameters in helicoidal robots*
I. Juarez-Campos (Universidad Michoacana, Mexico)

13:20~15:00 GS3 Artificial Life-Ⅱ
Chair: N. Mirenkov (Aizu University, Japan)

GS3-1 *Human-following robot using the particle filter in ISpace with distributed vision senosrs*
T-S. Jin, K. Morioka, H. Hashimoto (University of Tokyo, Japan)

GS3-2 *On vector autoregressive model for action of human arm's*
K. Tomizawa (Tokyo Denki University, Japan), K. Oura (Kokushikan University, Japan)
I. Hanazaki (Tokyo Denki University, Japan)

GS3-3 *Outwit game -- a dynamical systems game for market dynamics*
M. Konno, T. Hashimoto (Advanced Institute of Science and Technology (JAIST), Japan)

GS3-4 *Artificial ecosystem on the resource-conservative tierra structure*
S. Matsuzaki (Aizu University, Japan)
H. Suzuki (ATR Human Information Science Labs., Japan)
M. Osano (Aizu University, Japan)

GS3-5 *Rule ecology dynamics for studying dynamical and interactional nature of social institutions*
T. Hashimoto (Japan Advanced Institute of Science and Technology, Japan)
M. Nishibe (Hokkaido University, Japan)

15:00~16:20 IS3 Intelligent Pattern Classification
Chair: S. Omatu (Osaka Prefecture University, Japan)

IS3-1 *Image compression for bill money by neural networks*
S. Omatu, K. Kibi (Osaka Prefecture University, Japan)
M. Teranishi (Nara University of Education, Japan)
T. Kosaka (Glory Ltd, Japan)

IS3-2 *Intelligent classification of bill money*
S. Omatu (Osaka Prefecture University, Japan)
T. Kosaka (Glory Ltd., Japan)

IS3-3 *An image segmentation method using the histograms and the human characteristics of HSI color space for a scene image*
S. Ito, M. Yoshioka, S. Omatu (Osaka Prefecture University, Japan)
K. Kita, K. Kugo (Noritsu Koki Co. Ltd., Japan)

IS3-4 *An image recognition method by rough classification for a scene image*
S. Ito, M. Yoshioka, S. Omatu (Osaka Prefecture University, Japan)
K. Kita, K. Kugo (Noritsu Koki Co. Ltd., Japan)

Room C

8:40~10:20 GS22 Robotics-Ⅰ
Chair: K. Nakano (The University of Electro-communications, Japan)

GS22-1 *Development of the autonomous driving personal robot "The visual processing system for autonomous driving"*
T. Umeno, E. Hayashi (Kyushu Institute of Technology, Japan)

GS22-2 *Development of a system for self-driving by an autonomous robot*
E. Hayashi, K. Ikeda (Kyushu Institute of Techonology, Japan)

GS22-3 *Research about ZMP of biped walking robot*
K. Imamura, M. Sugisaka (Oita University, JAPAN)

GS22-4 *Verification of trajectory generation of bipedal walking robot*
N. Masuda, M. Sugisaka (Oita University, Japan)

GS22-5 *Run control of the mobile robot using visual information*
T. Hashizume, M. Sugisaka (Oita University, Japan)

10:40~12:00 GS23 Robotics-Ⅱ
Chair: J.M. Lee (Pusan National University, Korea)

GS23-1 *Digital RAC for underwater vehicle-manipulator systems considering singular configuration*
S. Sagara, M. Tamura, T. Yatoh, K. Shibuya (Kyushu Institute of Technology, Japan)

GS23-2 *Modeling of pneunatic artificial muscle actuator*
H. Zhao, M. Sugisaka (Oita University, Japan)
D. Yu (Zhengzhou University, China)

GS23-3 *Secure cooperation in a distributed robot system using active RFIDs*
M. Obayashi (Tokyo Metropolitan Industrial Technology Research Institute, Japan)
H. Nishiyama, F. Mizoguchi (Tokyo University of Science, Japan)

GS23-4 *A soccer robot control design based on the immune system*
J. Ito, K. Sakurama, K. Nakano (The University of Electro-Communications, Japan)

13:20~15:20 GS24 Robotics-Ⅲ
Chair: S. Sagara (Kyushu Institute of Techonology, Japan)

GS24-1 *Robot's behavior driven by internal tensions regulated by pulsed para-neural networks*
J. Li, (University of Science and Technology, China)
A. Buller, J. Liu (ATR Network Informatics Labs., Japan)

GS24-2 *Robotic-control blocks (RCB) for research and education*
A. Stefanski, A. Buller (ATR Network Informatics Labs., Japan)

GS24-3 *Human-robot communication through a mind model based on the mental image Directed Semantic Theory*
M. Yokota (Fukuoka Institute of Technology, Japan)
M. Shiraishi (Fukuoka University of Education, Japan)
G. Capi (Fukuoka Institute of Technology, Japan)

GS24-4 *The case for radical epigenetic robotics*
A.I. Kovacs, H. Ueno (The Graduate University for Advanced Studies, National Institute of Informatics, Japan)

GS24-5 *Development of a robotic surgical manipulator for minimally invasive surgery system*
H-S. Song, J-H. Jung, Jung Ju. Lee (Korea Advanced Institute of Science and Technology, Korea)

GS24-6 *Identification of nonlinear mechatronic servo motor system having backlash*
Y. Toyozawa (FANUC Corp., Japan)
H. Harada, H. Kashiwagi (Kumamoto University, Japan)

15:20~16:20 GS16 Micro-Robot World Cup-Soccer Tournament
Chair: J. Nishii (Yamaguchi University, Japan)

GS16-1 *Cooperative behavior acquisition for multiple autonomous mobile robots*

K.Nakano, M. Obayashi, K. Kobayashi, T. Kuremoto (Yamaguchi University, Japan)

GS16-2 *Multi-agent learning mechanism based on diversity of rules: from the view point of LCS*
H.Inoue (Kyoto University, ATR Network Informatics Laboratories, Japan)
Y.L. Suematsu (Kyoto University, ATR Network Informatics Laboratories, Japan)
K. Takadama (Science, Tokyo Institute of Technology ATR Network Informatics Laboratories, Japan)
K. Shimohara (Kyoto University, ATR Network Informatics Laboratories Japan)
O. Katai (Kyoto University, Japan)

GS16-3 *Gradual emergence of communication in multi-agent environment*
S. Tensho(Nara Institute of Science and Technology, Japan)
S. Maekawa (National Institute of Information and Communications Technology, Japan)
J. Yoshimoto (Okinawa Institute of Science and Technology, Japan)
T. Shibata, S. Ishii (Nara Institute of Science and Technology, Japan)

The Tenth International Symposium on Artificial Life and Robotics 2005(AROB 10th '05),
B-con Plaza, Beppu, Oita, Japan, February 4-6, 2005

Complexity Modelling and its Applications

Kazuyuki Aihara
Institute of Industrial Science, University of Tokyo
4-6-1 Komaba, Meguro-ku, Tokyo153-8505, Japan
and
Aihara Complexity Modelling Project, ERATO, JST
45-18 Oyama-cho, Shibuya-ku, Tokyo 151-0065, Japan
aihara@sat.t.u-tokyo.ac.jp

Abstract

In this plenary talk, I review our study on creating an artificial brain with chaotic dynamics and its possible applications.

keywords: Complexity, Chaos, Mathematical Modelling, Neural Networks, Combinatorial Optimization

Recent progress in nonlinear systems analysis has made possible mathematical modelling of complex phenomena not only in natural systems but also in engineering systems [1, 2]. Among various complex systems in this real world, the brain is a typical example of a complex system with much complexity and many superior functions. In this plenary talk, I review our study on creating an artificial brain with chaotic dynamics, or a chaotic brain [3].

Biological neurons are highly nonlinear and dynamical devices. For example, we can observe chaotic responses and different bifurcations in nonlinear dynamics of nerve membranes both experimentally with squid giant axons and numerically with nerve equations [4]. The chaotic properties of nerve membranes have provided a clue of making a chaotic brain composed of chaotic neural networks with spatio-temporal chaos, which are derived based on the experimentally observed neuronal chaos and described by coupled bimodal maps [5]. Moreover, the chaotic brain has possible applications to biologically inspired computation like combinatorial optimization such as traveling salesman problems and quadratic assignment problems [6, 7] and hardware implementation with analog electronic circuits [8, 9].

Finally, I discuss importance of several bifaces in modelling complex systems, namely generality / universality & individuality / specialty, abstracted & detailed, and stability & instability.

References

[1] T. Miyano, S. Kimoto, H. Shibuta, K. Nakashima, Y. Ikenaga, and K. Aihara: "Time Series Analysis and Prediction on Complex Dynamical Behavior Observed in a Blast Furnace," *Physica D*, Vol.135, pp.305–330 (2000).

[2] K. Mitsubori and K. Aihara: "Delayed-feedback Control of Chaotic Roll Motion of a Flooded Ship in Waves," *Proceedings of the Royal Society of London, Series A*, Vol.458, pp.2801–2813 (2002).

[3] K. Aihara: "Chaos Engineering and its Application to Parallel Distributed Processing with Chaotic Neural Networks," *Proceedings of the IEEE*, Vol.90, No.5, pp.919–930 (2002).

[4] K. Aihara, G. Matsumoto, and Y. Ikegaya: "Periodic and Non–Periodic Responses of a Periodically Forced Hodgkin–Huxley Oscillator," *Journal of Theoretical Biology*, Vol.109, pp.249–269 (1984).

[5] K. Aihara, T. Takabe, and M. Toyoda: "Chaotic Neural Networks", *Physics Letters A*, Vol.144, No.6/7, pp.333–340 (1990).

[6] L. Chen and K. Aihara: "Strange Attractors in Chaotic Neural Networks," *IEEE Trans. CAS–I*, Vol.47, No.10, pp.1455–1468 (2000).

[7] M. Hasegawa, T. Ikeguchi and K. Aihara: "Combination of Chaotic Neurodynamics with the 2-opt Algorithm to Solve Traveling Salesman Problems", *Physical Review Letters*, Vol.79, No.12, pp.2344–2347 (1997).

[8] Y. Horio, K. Aihara and O. Yamamoto: "Neuron–Synapse IC Chip-Set for Large-Scale Chaotic Neural Networks," *IEEE Trans. Neural Networks*, Vol.14, No.5, pp.1393–1404 (2003).

[9] T. Kohno and K. Aihara: "A MOSFET-based Model of a Class 2 Nerve Membrane," *IEEE Trans. Neural Networks* (in press).

THE WORK OF

SUEO UENO, ROBERT KALABA, AND RICHARD BELLMAN

Harriet H. Natsuyama
Los Angeles, CA 90066
hhnatsu@yahoo.com

Abstract

This paper recalls the critical developments of three exceptional individuals in the fields of nonlinear analysis, systems modeling, computational solution of initial value problems, system identification and optimal control.

1 Introduction

This paper was suggested by Masanori Sugisaka who initiated the AROB symposia ten years ago and who attributes their success to the inspiration and contributions of three giants: Sueo Ueno, Robert Kalaba, and Richard Bellman. They are special for their great talents, productivity and personalities. I am privileged to have worked with them since the early 1960s.

2 Decades of Research

My relationship with these three giants of modern analysis and computing is very special to me. It goes back to the early days of the Rand Corporation, the quasi-governmental think tank in Santa Monica. In the decade of the 1950s, after their World War II efforts had ceased, many of the top scientists from Los Alamos National Laboratories joined the exciting new work at Rand.

John von Neumann developed the general-purpose digital computer (as opposed to special purpose military computers) in the basement and it was fondly called the Johnniac. Programmers used machine language to code paper tapes. The field of computer science had yet to be named, and the mathematicians using these computers called themselves numerical analysts.

When I joined Rand in 1961, IBM had introduced their mainframe computers and I learned Fortran by reading the manual written by McCracken. Fresh out of graduate school with a masters degree in physics, I had been hired to assist Bob Kalaba and Dick Bellman in their computational experiments.

Dick Bellman had already introduced the principle of optimality and the concept of dynamic programming for nonlinear optimization problems. Some numerical examples had been worked out and more computations were needed. Dynamic programming, I learned during my later years, applies to life as well as manmade systems

Bob Kalaba had created the technique called quasilinearization to solve nonlinear two-point boundary value problems, such as those that arise when solving Euler equations from the calculus of variations. One of the first problems that we attacked together was that of orbit determination. Remember this was going on during the early days of the space program. We formulated the problem of estimating the orbit of a moving body whose angular position has been observed at various instants of time. In other words, a complete set of initial conditions would be sought such that the theoretical orbit explained the observations in a least squares sense. This is a multipoint boundary value problem.

We extended Bob's quasilinearization to handle the multiple conditions. We were delighted to see that solutions converged quadratically and we could determine the missing initial conditions even when the initial estimates were rather crude. We also introduced noise into the measurements and it still worked. Then we tried estimating the unknown mass of the moving object, letting its dynamical equation be that the time derivative of mass is zero and requiring that its initial condition be determined along with the other initial conditions for the equations of motion. This experiment was successful also. The results were published in the Proceedings of the National Academy of Sciences, and there were many, many requests from aerospace companies for reprints of this paper.

A couple of years later, Sueo Ueno from Kyoto University arrived at Rand. This distinguished astrophysicist had been in correspondence with Dick Bellman for a number of years. Dick wanted to learn more about the multiple scattering of radiation through slabs of finite thickness. Dick saw that there was a resemblance with the problems of neutron transport which he had dealt with at Los Alamos with Milt Wing using the new method of invariant imbedding. But the physical aspects seemed more complex. He wanted Prof. Ueno to spend some time at Rand so they could apply invariant imbedding to radiative transfer.

Prof. Ueno, during these correspondences, was spending a year with Jacqueline Lenoble and other French scientists in Paris, with side trips to visit Ida Busbridge in Cambridge, Ambarzumian in Leningrad, and Sobolev in Moscow. Then he had to return to Kyoto University for another year before he could go abroad again. Thus it was that he arrived in Santa Monica after I had been there for a while.

Prof. Ueno taught us the physical principles of multiple scattering so that we could "count photons" for invariant imbedding and derive initial value problems for the Riccati equations of reflection functions. We, or rather it was I, who wrote the Fortran programs for large systems of ordinary differential equations with initial conditions. When we integrated these equations using fourth-order Runge-Kutta, the solutions agreed with those previously published for very thin or very thick slabs. Furthermore, we obtained solutions for all thicknesses between zero and effectively infinity. We saw reflection functions that no one else had seen before!

This research program in which I was involved led to Prof. Ueno becoming my advisor for the doctoral degree in *uchu butsuri* in the Department of Astrophysics of Kyoto University. In particular I investigated and demonstrated various techniques for solving inverse problems of atmospheric physics as system identification problems.

While the approach of invariant imbedding was regarded by Bob and Dick as dynamic programming without the optimization, it led to a nonlinear filter, a powerful extension of the Kalman filter. This filter was developed in collaboration with R. Sridhar, and further developed by M. Sugisaka. Indeed, Prof. Sugisaka was introduced to this nonlinear filter by Sueo Ueno, and that is how we came to meet each other and how I spent three delightful months in his department at Oita University in the fall of 1995.

In subsequent years, I had the opportunity to spend time on various occasions with Prof. Ueno and learn about his life and his work. By this time, he had retired from Kyoto University and Kanazawa Institute of Technology, and he was head of information systems at Kyoto Computer Gakuin. We produced the Springer book on terrestrial radiative transfer with Alan Wang. I compiled Prof. Ueno's collected works and deposited them in the new library of Kyoto University where they are available for researchers and students alike. Prof. Ueno lives quietly in Yokohama.

In the late sixties both Dick and Bob left Rand to become professors at the University of Southern California. Dick, who established a program in biomathematics, passed away in 1984.

Robert Kalaba held a joint appointment at the University of Southern California in the departments of economics and biomedical engineering. There, he prepared a new generation of students and was well-loved by students and staff alike. Bob passed away at the end of September, 2004. Dr. Yueyue Fan, the last of Bob's doctoral students, and I are in the process of organizing Bob's papers so that a library can be established in his memory at USC.

3 Summary

Richard Bellman, Robert Kalaba, and Sueo Ueno – to these pioneers we owe great thanks. And I thank you for your interest in continuing these explorations.

4. Bibliography

Richard E. Bellman: see ***Memorial Tributes,*** National Academy of Engineering, Vol. 3, pp 22-29, 1989, and ***The Bellman Continuum***, Robert S. Roth (ed.), World Scientific Pub. Co., 1986.

Robert E. Kalaba: see the special issue, ***Applied Mathematics and Computation***, Vol. 45, n. 2, September 1991.

Sueo Ueno: see the special issue, ***Applied Mathematics and Computation***, Vol. 116, n. 1-2, November 2000, and ***Terrestrial Radiative Transfer: Modeling, Computation, and Data Analysis,*** H. H. Natsuyama, S. Ueno, A.P. Wang, Springer-Verlag Telos, 1998.

Machinery Cognition and Artificial Intelligent

Y.G. Zhang
Institute of Systems Science, Academia Sinica, Beijing China, 100080
yzhang@iss.ac.cn

M. Sugisaka
The Dept. of Electrical and Electronic Engineering, Oita University, Oita, Japan, 870-
msugi@ee.u-oita.edu.jp

ABSTRACT In this paper authors show some heuristic thinking first, and then proposed an engineering definition of artificial intelligence in artificial brain that is the abilities to obtain knowledge, to use knowledge and to operate knowledge. There are still two open important problems: one is the expression of knowledge for this goal and the other is how to construct the integration up operation and detailed down operation.

Keywords: Artificial Intelligence, Creating intelligence, Knowledge, cognition, Evolution of intelligence.

I. Introduction

Animal Brain's basic function is to process the information received from the sensing organs build in the body. That means it could process the visual sensing information, auditory sensing information and others simultaneously, which include tactual, gustatory and olfactory information. However, the observations results from the wolf boy told us that although the wolf boy has human's sensing organs and human's brain, but he has only the intelligence level of wolf. The reason is that his "mother" is a wolf but not human's mother. His ability to cognize the world surrounded him is kept in the level of wolf. So, the appearance of intelligence is not only depends on the physical device—Brain, but also mother's teaching and communication with the "society" surrounded him.

If we want to create a machine which possesses certain intelligence, the machine has to have two functions, one is to cognize the outer world by perceptron equipped on its "body", the other is to accept the teaching and communication from "mother" (or "teacher") and the other members in the "society" surrounded it. In animal world mammal mother teaches their child how to find food and avoid enemy by her body language and very simple primitive natural language (different voice).

Usually, the results of cognition are the understanding outer world. It must be expressed as memory of something, this king memory is different from the process in computer. For biological individuals, usually the memory in brain is a gradual process to accept and strength a cognized result. Once it is be memorized and understood, it is formed a scheme in which possesses certain structure. The knowledge we talked in this paper can be expressed as a relation of several schemes, and this relation is with fixed pattern. So far, we did not see this kind of knowledge warehouse. If we want to implement a true artificial intelligence based on knowledge using some equipments and machine or computer, machinery cognition must be needed. Following this introduction we will explain and describe more deep thinking.

II. Emerge multiple -modal information

Now many achievements about computer vision and computer hearing appeared and new equipments related them have been developed very fast. The problem is how to emerge this kind of information as the result of machinery cognition.

2.1 Scheme

General speaking, the computer vision and

[1] This work is supported by Chinese Natural Science Foundation, Number # 60275016

hearing are different type of information, vision is image information and hearing is sonic information, processing methods of them are different. When mother shoes baby an apple in her hand it give baby a **impression** that consist of a moving pictures and mother's voice or language, baby memories the both components together simultaneously in his/her brain, though they are input from different path. This impression is on a concrete subject or thing with their attributes, sometimes the impression is on an action with dynamic atributtes. We say all these presentative impressions as a **scheme**, they are the basic components of memories.

To express a scheme in computer we need a unit, in which store a presentative impression which may be a subject image plus a noun sound, or an action moving picture plus a verb sound. Of course, for real biological individual this unit (the scheme) not only includes visional and hearing information, but also includes tactual, gustatory and olfactory information. However, to implement machinery cognition we limit our attention into the computer vision and computer hearing. Once we build up this kind of unit in computer we should build up the relations between units and to form knowledge.

2.2 From scheme to knowledge

Scheme is essentially some primitive knowledge due to it has incomplete structure of knowledge comparison with human knowledge structure, even if for a human child. Scheme is only a fragment of knowledge discussed in this paper and it is not the final result of cognition. In this paper we try to discuss the knowledge with certain structure and similar to human's knowledge, or the evolutionary configuration of knowledge. In fact, we could observe the process of mother teaching baby language and you could find that "mother" use natural language to make a link of schemes stored in baby's brain. Natural language is the link between scheme and human baby knowledge. At beginning the human baby could know mother's face, the taste of mother's milk, some toys and mother's sound, and then they try to understand some very simple repetitive worlds. The baby gradually learned them and could repeat them. Thus baby got some schemes and obtained primitive knowledge about the surrounded world. Later they could understand some simple sentence; they start to get complete knowledge.

So, we say that the natural language is the key from scheme to presentative knowledge.

2.3 Structure of presentative knowledge

From the above we could try to explain the structure of presentative knowledge. First, the schemes are divided into several groups according to the noun, verb, adjective, and adverb and so on. The relations are defined according to grammar. The relations are grouped as several layers, such that "fragment", "very simple", "simple", "usual", "complex", "very complex", etc. any relation in those groups will combine some schemes, this combination is very similar to the structure of a sentence but it is not a sentence. A combination corresponds a mapping between the semantic of combination and a real scene or subject. So, the knowledge expression is to define those rules grouped schemes as different layers.

Examples of the relations:
"fragment":
(Food--Noun scheme);
(Eating--Action scheme);
(Color—Adjective scheme).
"very simple":
(Eating) + (food).
"usual":
(Look) + (at) + (here).

The people in different countries speak various languages, and the grammar is different. The rules defined groups of relation layers is really different, however, if the mapping between the semantic and the scene or subject is the same we could say that it means the same knowledge.

If using several combination to construct a bigger combination, it is similar to a paragraph consists of several sentences in a article. At this time the mapping is a composite of mapping. Note, the structure of knowledge must can be extended in the same manner. So, the knowledge in a human brain is definitely not isolated, it is similar to an article or a tree, it has fractal property.

2.4 Knowledge warehouse

The result of machinery cognition is to combine with the schemes as the presentative knowledge. So, we expect a special storage form in computer, in which there are "units" to save schemes simultaneously formed by using of machinery visual and sonic perceptron; in which there are defined rules to construct knowledge; also, the real knowledge--mapping to obtained.

This kind of knowledge warehouse must be parallel operation. The storage of scheme may be not very difficult, but the retrieve of scheme may be more difficult.

III. Knowledge's emergence

Machinery perceptrons are not enough if we want to create an Artificial Brain. Naturally, it concern the question that what is knowledge stored in computer? How dose the knowledge is emerged from the information cognized by computer vision and computer hearing? The first question has been discussed previously. The second question concerns with a very difficult field that the creation of intelligence or knowledge emergence.

In fact, knowledge emergence is a process to operate knowledge. It contains two operations; one is the **detail down** process. This operation make the obtained knowledge has more detailed contents. On the other hand, baby can find the common attributes between some similar schemes himself or by mother's teaching, for example, baby learned "apple", "strawberry", "pear" and know all these are eatable and a new scheme "fruit" was established. This is also a process to operate knowledge; we say it as an **integrated up** process. This process maybe cause knowledge emergence. Both processes are to make the relation and mapping between schemes and subject (or scene) more complicated. Knowledge emergence will make all knowledge has the free-scale structure

A lot of cognitive and psychological study experiments for children's intelligence tell us how they cognize outside environment and obtain knowledge, these are very important. Here we want to emphasize mother's role. At beginning period of babyhood they just could see some objects surrounding them and could hear the voice from mother mainly. Mother's voice and gesture language make baby establish a mapping gradually. This mapping is the process to establish a structure to fit attributes of scheme Of course, not only vision and hearing. This mapping will store in baby's brain. When this mapping was established firmly, the baby had obtained knowledge.

IV. Intelligence on artificial brain

To study machinery cognition is try to investigate the new ways creating artificial intelligence. Once artificial brain is mounted computer vision and hearing the machinery cognition will be basic component. We cannot expect artificial brain has the same intelligence like human being's, however, our research focus on the creation of intelligence using artificial brain. We could hope that to do some experiments on it. What kind intelligence could appear on artificial brain? We limit the definition here as the following:

"Intelligence" is the abilities that to obtain knowledge, to use knowledge and to operate knowledge.

Based on our analysis here we want to promote the study of knowledge based artificial brain. We propose the key techniques on the research as the following:

a. Knowledge expression;
b. Knowledge warehouse;
c. Knowledge emergence and operation.

After these key techniques were implemented, we could play as "mother" to teach and train the artificial brain gradually. The human being's intelligence is evolutionary result with the evolutionary process of human being's natural language. So, artificial intelligence mounted on artificial brain should be evolutionary either.

REFERENCES

[1] Zhang,Y.G. and Sugisaka,M., "Might we train an artificial brain as a baby? ", The Proceedings of the seventh international symposium on artificial life and robotics (AROB'02), pp.92-97, Beppu, Japan,2002
[2] Zhang, Y.G. and Sugisaka. M., "KANSEI Technology and Artificial Brain", (invited talk) The Proceedings of International Symposium on KANSEI technology, Muroran Institute of Technology, Hokkaido, Japan, October 5-6, 2001
[3] Zhang, Y.G., Sugisaka, M. and Wu, X.Q., "Bottom-up Way To Development of Multi-Cellular Digital Organization", **Journal** of Artificial Life and Robotics, Springer(Tokyo), No. 3, Vol.5, 2001.
[4] Zhang, Y.G. and Sugisaka, M., "Trainable Artificial brain (TAB)", The Proceedings of International Symposium of Knowledge and Systems Science (KSS), Dalian, China, September, 2001
[5] Zhang, Y.G., "Zhang, Y.G. and Sugisaka, M, "A mode to create artificial intelligence—From knowledge to intelligence", The proceedings of The nineth international symposium on artificial life and robotics (AROB'04), pp. I-28-31, Beppu, Japan, 2004

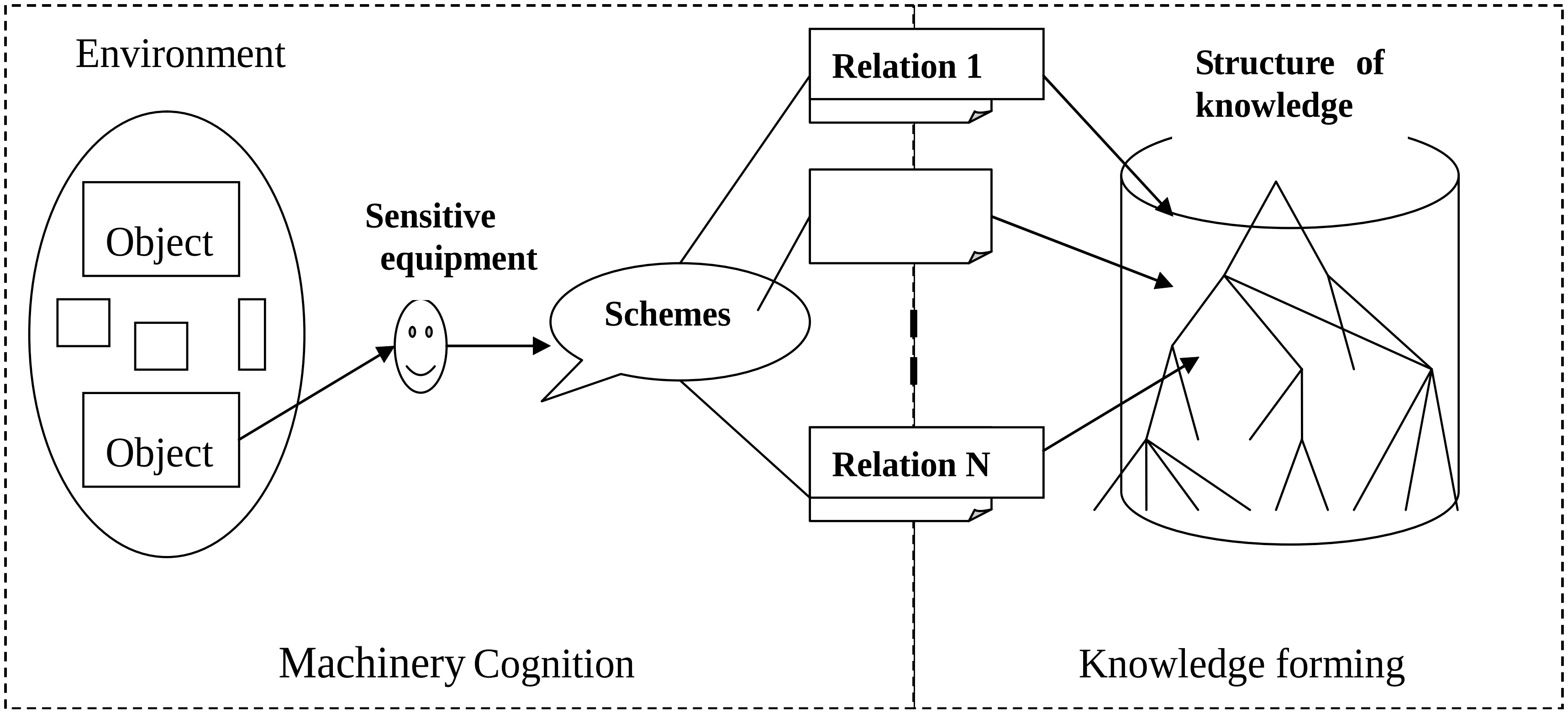
Environment
Object
Object
Sensitive equipment
Schemes
Relation 1
Relation N
Structure of knowledge
Machinery Cognition
Knowledge forming

ATRON Hardware Modules for Self-reconfigurable Robotics

Henrik Hautop Lund, Richard Beck, Lars Dalgaard

Maersk Mc-Kinney Moller Institute for Production Technology
University of Southern Denmark, Campusvej 55, 5230 Odense M., Denmark

hhl@mip.sdu.dk beck@mip.sdu.dk dalgaard@mip.sdu.dk
www.adaptronics.dk

Abstract
We exploit a holistic behavioural and morphological adaptation in the design of new artefacts, and exemplify the potential of the new design principle through the construction of robotic systems that can change morphology. Here we present the ATRON design in which the modules are individually simple, attach through physical connections, and perform 3D motions by collective actions. We produced 100 ATRON modules, and performed both simulation and real world experiments. In this paper, we report on the ATRON hardware design and investigations related to the verification of the suitability of the ATRON module design for self-reconfigurable robotics.

Introduction

One of the main objectives of our work is to provide an architecture made up of simple building blocks, simple connections, and simple interactions, in order to allow end-users of our approach to design new artefacts in an easy manner. Indeed, the ATRON modules are simple building blocks that can be viewed as simple "cells" or "atoms" in a larger system composed of numerous of these individually simple building blocks. Ultimately, the design should allow a suitable way of performing self-reconfiguration by limiting the motion constraints in the system of building blocks as much as possible.

The connector mechanism of self-reconfigurable robots is known to be difficult to design because of the many constraints on the connector mechanism. Therefore, this problem was addressed with highest priority, since 3D motion in a terrestrial scenario demands attachment of modules to each other.

The methodology for choosing the right design for the connectors was to extract inspiration from the biological designs and to perform an extensive comparison of state-of-the-art, and afterwards make several design, realization and evaluation cycles for developing the final, mechanical solution for the modules. The biological designs pointed us towards a minimal design of "cells" that each should be very simple, but provide extensive possibilities for self-design and self-repair when combined in huge numbers. The survey of the state-of-the-art [1] told us that such a system based on these considerations would be novel. Related work includes the CONRO [2] and the M-TRAN [3] self-reconfigurable robotic systems. Other approaches include the Telecubes [5], the PolyBots [6] and the Crystalline [7]. Based on the inspiration from cell biology, we wanted to design a module to be simple and provide simple ways of avoiding many of the motion constraints known from other systems.

Figure 1. ATRON modules for self-reconfigurable robotics.

Module Design

The ATRON modules are placed in a surface-centred cubic lattice structure that corresponds to the titanium atoms in the CuTi3 crystal lattice. The basic idea behind the ATRON modules is to have two half cells joint together by a rotation mechanism. On each half cell, there are two female and two actuated male connectors, by which a module can connect to the neighbouring modules. A major advantage for reaching the objective of producing many modules is that the ATRON modules are designed to be homogenous. Also, an ATRON module can switch or rotate either rotation axis 180°, maintaining the same global function of the module. Further, the shape allows one module to move to an adjacent hole in an otherwise fully packed structure (without colliding with other modules). So the module design seems to fulfill our objectives. Indeed, the design was guided by the considerations on how to reduce control complexity of self-reconfiguration by an appropriate module design. However, the design that meets these objectives demands strong and reliable point-to-point connectors, which also is achieved in the ATRON module with the novel, mechanical connectors, which are fast, strong and reliable.

A module may communicate with neighbouring modules through IR communication. When placed in the surface-centred cubic lattice structure, the modules can move in this structure to self-reconfigure into different overall arrangements or movements.

Figure 2. The first, second, and third (final) hardware prototype of the ATRON modules.

If a first ATRON module is attached to a second neighbouring module and detached on other connection points, the second neighbouring module may move the first ATRON module by turning around equator with the rotation mechanism. Hence, the first ATRON module may be moved to another position in the lattice structure where it may attach itself to another module in the structure and, for instance, detach itself from the second ATRON module that transported it to the new position.

As illustrated above, the reconfiguration of the overall system becomes a process of transitions in the lattice structure. Simulations (e.g. [xx, xx]) showed that, if we can perform the individual transitions in the hardware implementation in a reliable manner, numerous distributed control possibilities exist and will lead to self-reconfigurable and mobile systems. Hence, the module design and tests described below were guided by this demand.

Mechanical Design

The mechanical design was guided by the demand for strong point-to-point connectors in modules being able to lift another two modules and being placed in the surface-centred cubic lattice structure.

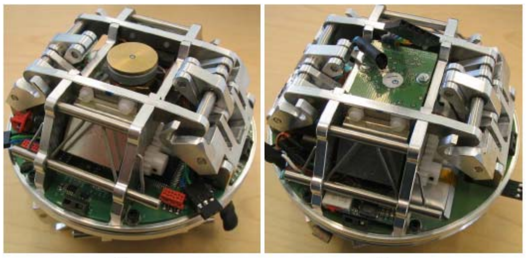

a) b)

Figure 3. An ATRON module: a) Northern hemisphere, b) southern hemisphere.

Connectors

Based on the knowledge gained from the survey of state-of-the-art, three alternative connector designs were developed and considered. The first was based on a screw for holding two connected modules together. The second connector design was based on a pushing block, while the third is based on a triangular configuration of hooks, with a large base line for good rigidity. The screw mechanism was used in the first prototype, but shown not to be robust. Therefore, this design was abandoned. The remaining two approaches originated from the same idea and conformed to the same overall constraints. They differed in several mechanical aspects, the major differences between them being in the mechanical parts, which physically connect two neighbouring modules and in the rotation mechanism coupling the two hemispheres of the ATRON module. The two alternative connector designs were tested using two different hardware prototypes, and both connector prototypes performed comparably on most criteria, but the hook-based design was found to be most robust. The pushing-block design had a "weak" direction in which it sometimes would lock due to friction forces. For this reason the hook-based design was selected for the final design of the ATRON modules for the terrestrial scenario.

Active Connector

The push mechanism in the active male connectors is designed in such a way that a lead screw is used to transmit rotation to linear movement, and both lead screws and motors are installed in the same frame as the passive female connector parts. Figure 4 right illustrates the female frame parts where the motor and lead screw are installed. The push mechanism has been designed so that it is self-locking and very stiff, thereby ensuring that the connection between modules is always stable. The remaining parts of the active male connector mechanism are illustrated in figure 4 left.

The new teflon coated lead screw used in the actuation mechanism of the active male connectors has reduced the required torque from the connector motor, such that the connection time could be reduced to two seconds (the better efficiency compared to earlier prototypes made it possible to achieve the same force using a thread with greater pitch).

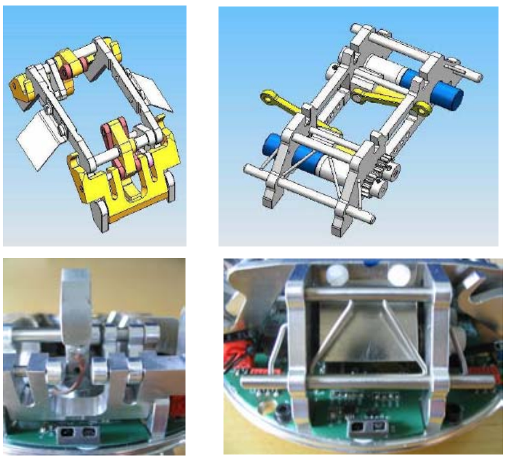

Figure 4. Left: Male hook that may transfer positive voltage. Right: An electrical isolated plate behind the female connector allows the male hook to touch the plate and power-share.

Centre Arrangement

A 1-stage planet gear in the centre of the module reduces the load requirements of the industrial gearbox with a factor of 118/10. Therefore the size of the gearbox is reduced compared to earlier prototypes, such that the centre motor and gearbox are fully contained in the northern hemisphere of the module.

Also, the identical frames used in the northern and southern hemispheres only differ in their centre part.

Slip Ring

To facilitate the ATRON module with intra-module power and signal distribution over equator, a slipring combined with carbon shoes has been installed in the module. The slipring is shown in figure 4b, where the inner five rings are used for electrical signals. The specialized slipring has been gold plated to ensure stable electrical connections. Furthermore the reflection abilities for the optical encoders are enhanced using a black diffuse background for better contrast (the outer fields are for the optical encoder). The encoders and carbon shoes are illustrated in figure 5a.

a) b)

Figure 5. Centre arrangement with gears and slip ring for transferring power and data between the two half spheres of the ATRON module. a) northern hemisphere, b) southern hemisphere.

Rotational Lock

The mechanism to drive the rotation of the module consists of the 1-stage planet gear, and the industrial planet gearbox and is thus not a self-locking transmission. The module has therefore been equipped with a solenoid that can drive a bar into rotational lock holes placed in both the northern and southern centre plates. The holes are positioned, such that the rotation can be locked in 90° intervals.

Wheel

The centre plates are made circular to aid manufacturing but also to add "wheel functionality" to the module. One of the centre plates is equipped with a O-ring (see figure 1). The O-ring acts as a tire, and a module can therefore be used as a wheel when placed in an upright position. This facilitates the creation of wheeling organisms.

Shell

The plastic shell illustrated in figure 1 has been designed to protect the electric and mechanical parts of the module and to ease the visual distinction and orientation of each module in a given structure. The shell has been produced in four different colors, which extends the visual distinction. Since the shell also gives a module a surface the infra-red proximity detection is made more stable and reliable. The shell also gives the ATRON module a more compact look.

Electronics Design

Every ATRON module has, besides its five main actuators, a solenoid actuator, a tilt sensor for measuring its two tilt angles with respect to the horizontal plane, eight Light Emitting Diodes (LEDs) useful for easy readout, a solenoid controlled plug for keeping the rotational angle between the two hemispheres at strict 90° intervals and an encoder disc placed perpendicular to the centre axis for measuring both the absolute rotational angle and relative rotational angle (for velocity calculations).

For neighbouring modules to inter-communicate, each connector is equipped with an infra red (IR) light transmitter and receiver allowing a wireless communication channel to be established between two modules. The IR diodes are also used for simple distance measurements.

Each ATRON module also contains two rechargeable Lithium-Ion Polymer batteries wired to enable power-sharing among connected ATRON modules. Power-sharing is necessary to power compensate the more motion active modules with power from the more motion passive modules. This is implemented through the connectors such that a mechanical connection between two ATRON modules also results in an electrical connection between the modules. A consequence of this is that re-charging the batteries of an ATRON module can be done even if it is placed within a structure formed by several ATRON modules.

To be able to electronically control all these hardware components several printed circuit boards (PCB) were constructed. On the Northern Hemisphere an ATmega8 (henceforth denoted *North-AT8*) microcontroller from ATMEL is responsible for reading the tilt sensor, controlling the centre motor in conjunction with the encoder disc, toggling the solenoid plug and opening and closing the two actuated male connectors.

The North-AT8 is also connected to an ATmega128 (henceforth denoted *North-AT128*) through the I^2C-bus. The North-AT128 is responsible for controlling the IR communication to and from the Northern Hemisphere but its main task is to function as the main coordinator of the components of the entire module (i.e. the main part of the *ATRONcontroller*).

On the Southern Hemisphere an ATmega8 (henceforth denoted *South-AT8*) is used for implementing the power control of the ATRON module. That is, charging the battery and making sure that a correct internal voltage levels is kept no matter the voltage level of connected modules or external power supply.

The South-AT8 is also connected to an ATmega128 (henceforth denoted *South-AT128*) through the I^2C-bus which is responsible for controlling the IR communication to and from the Southern Hemisphere and also for opening and closing the two actuated male connectors.

The two ATmega128 run at a clock frequency of 16 MHz and the two ATmega8 at 1 MHz.

The Northern and Southern Hemispheres are electrically connected through the rotational centre axis through a gold plated *slipring* (see above) with which carbon shoes maintain electrical contact also during rotation. The communication between the two hemispheres is conducted through a RS485 network of which the North-AT128 and the South-AT128 are the only nodes. The encoder disc for measuring the rotational angel is also placed on the slipring but is read optically. Figure 6 shows a block diagram of the electronic components in an ATRON module to which unit numbers in the following refer.

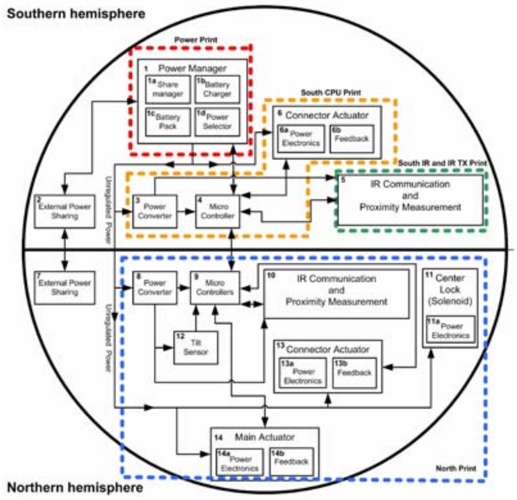

Figure 6. Overview of the electronic components in an ATRON module.

Tilt Sensor Interface

The Tilt Sensor Interface produces two DC voltage levels to the *North-128* proportional to the level of tilt (±90 degrees) in the planar x and y axis.

Connector Motor Interface

The connector actuator (figure 6, Unit 6 and Unit 13) is used for actuating the two male, active parts of a connection mechanism in each hemisphere. The actuator is a single DC motor rotating the arms until a firm connection is achieved.

Power electronics

The power electronics (Unit 6a and Unit 13a) used for controlling the DC motor is a fullbridge H-bridge build from an integrated circuit A3966.

Feedback

The only feedback from the actuators (Unit 6b and Unit 13b) that gives important information on the actuation is the power consumed by the motors. This is monitored through shunt resistors and when the current consumption reaches its highest level the arms are either fully extended or retracted and the motors are therefore stalled. This information is used to disable the motors to avoid overloading.

Centre Motor Interface

The Centre Motor Interface (Unit 14 called Main Actuator) consists of a brushless AC motor controlled by a dedicated driver circuit generating the necessary control signals (ASIC5660) and delivering the necessary power (L6234).

The torque delivered to the motor is controlled from the *North-AT8* which generates a PWM signal to the ASIC5660 with a duty-cycle proportional to the desired torque. Two output pins from the *North-AT8* controls the rotational direction and brake status (on/off), respectively.

Encoder Interface

The Encoder Interface implements the optical reader of the three outer rings of the slipring (see Figure 5b). The outermost ring has 108 "slots" which are read optically by two infrared readers (see Figure 5a) phase shifted 90° with respect to each other. This means that in one rotational direction one signal lags the other and if the rotational direction is changed it will instead lead the other. By feeding these signals to a D type Flip-Flop using one signal as clock and the other as data, the output will be either high or low depending on the rotational direction. This information along with the "clock" is read by the *North-AT8*.

The other two rings on the slipring implement a 2-bit gray-code (meaning only one bit changes at a time) allowing detection of 90° intervals when a transition occurs. This is used for accurate positioning of the rotational angle and is also read by the *North-AT8*.

Solenoid Interface

The Solenoid Interface (Unit 11) delivers power to the solenoid that drives the metal bar for the rotational lock mechanism. The solenoid is controlled by the *North-AT8*.

IR Interface

Unit 5 and Unit 10 are responsible for the IR communication and proximity measurement. Each hemisphere has four IR send-receive pairs (channels) able to communicate via the IrDA protocol at 9600 Baud or they can be used for proximity measurements. However, only one channel can be used at a time for either communication or for proximity measurement on each hemisphere.

The communication part is implemented using an IrDA physical-layer controller (MCP2120) that interfaces directly to the RS232 serial port of the *North-AT128* and *South-AT128* and the channel to use is selected by IO-pins.

The proximity measurement is implemented mostly in, but it relies on the ability of changing the strength of the light emitted thus a power control circuit was implemented by low-pass filtering a microcontroller generated PWM signal.

RS485 Interface

The RS485 Interface is implemented using two RS485 line-drivers connected through the slipring. One line-driver is connected to the RS232 serial interface of the *North-AT128* and the other similarly to the *South-AT128*.

LED Interface

The LED Interface consists of 8 LEDs which can be toggled on/off by the *North-AT128*.

Power Interface

The power management unit (Unit 1) is mainly responsible for supplying the ATRON module with power based on the current state of the batteries, the unregulated power and the current energy consumption. In addition, if the power manager detects that the voltage on the unregulated power supply meets a certain criterion it knows that the ATRON module is connected to a recharger and informs the battery charger that it may start charging the batteries. The power management unit is supported by four subparts each of which is described below:

Sharemanager

The Sharemanager (Unit 1a) pays attention to the modules battery supply and compares it to the voltage on the unregulated power supply and decides if it is safe to share power with other ATRON modules. The Sharemanager can choose how much current to deliver to the bus and, if necessary, entirely turn off the sharing.

Charger

The charging unit (Unit 1b) maintains all aspects of the actual charging of the battery pack and is ordered to start or stop charging by the power manager. Since the batteries are coupled and thus charged in series it is essential that the voltage difference between the two batteries is kept very low to avoid that the battery with the lowest potential drains the other.

This prevents proper charging and could potentially lead to battery malfunction. To account for this a voltage divider has been placed across one of the batteries and the voltage is measured by an AD-converter and compared to the series voltage also measured. This allows the power circuit to detect a skew voltage level and to react by preventing battery charging (however, we have also implemented a manual disconnect of the voltage divider when the module is inactive).

Battery pack

The batteries (Unit 1c) powering a single module consists of two series coupled Ion-Lithium Polymer batteries which can be charged to a maximum level of 4.2V each, giving a total of 8.4V maximum. Experiments on their operational time (before recharging is necessary) were conducted (see below) and the conclusion was that the batteries could sustain about 150 minutes at medium current load (300 mA).

Power Selector

The power selector (Unit 1d) monitors the voltage drop across the batteries and the voltage on the unregulated power supply. The highest is selected and used for supply. This ensures that a module will consume power from the source with the highest energy supply at any time.

Power converter

The unregulated power supplied from the Power Manager (Unit 1) in the Southern Hemisphere is passed through to the Northern Hemisphere. The Power Electronics (Unit 6a, Unit 11a, Unit 13a and Unit 14a) is directly connected to the unregulated power.

In each hemisphere the unregulated power is down converted to 5V by the power converter units (Unit 3 and Unit 8). The 5V from the power converters is needed to drive the basic electronic components and the micro controllers.

Module Tests

In order to test the mechanical and electronical design of the ATRON module, we performed a number of simple tests before going to the larger experiments related to self-reconfiguration and self-repair. These simple tests are reported below.

Battery Discharge Test

In order to test the operational time of an ATRON module with fully charged batteries, a burnout test of a module was performed. The code executed was a repetitious open-close sequence of the male connectors on the Northern Hemisphere. Current measurements during the test showed that the current used was somewhere between 200-400mA which is about half the maximum level. It was estimated that this level is a good representation of an average working condition.

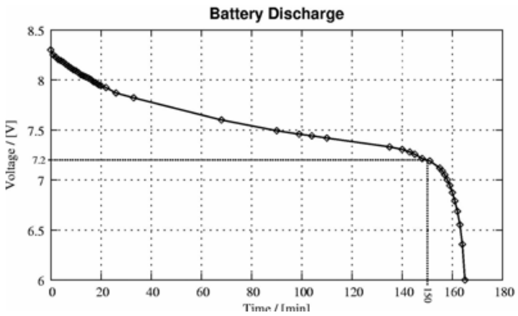

Figure 7. The battery discharge curve during burn-out test.

Figure 7 shows the voltage over the two series coupled batteries as the experiment progressed. It is noted that the starting level was 8.3V and after about 150 min. the voltage level had dropped to about 7.2V. From here it drops rapidly to about 6.0V in only 15 min. This discharge curve is consistent with the supplied data sheet for the batteries which also states that the battery voltage of any one battery must not fall below 3V where it may suffer damage.

From these information it can be concluded that 7.2V across the batteries is a good and safe choice for indicating that the batteries urgently need recharging. Furthermore the test showed that about 150 min. of operational time can be expected on fully charged batteries, which is acceptable.

Mechanical Deformation Test

A mechanical test has been performed, to measure the vertical deformation of a module structure due to slackness, elasticity and inaccuracies in the manufactured components and the angular tilt of the ball bearings. Figure 8 shows the setup used for the test where the red line illustrates a horizontal laser beam. The points **A** and **B** indicate where the deformation was measured.

A laser was placed on a table on the left side on the picture (not shown). The laser beam was levelled out horizontally by a mirror fixed to the steel bar seen on the right side of the picture and was adjusted such that the reflected beam was returned to the same horizontal level as its origin. After this the mirror was replaced by the module structure as shown in the picture such that the laser beam met the topmost point of the module attached to the steel bar (denoted **A** in the picture). A piece of card board was fixed at the topmost point on the leftmost module and the laser dot was marked at point **B** and the vertical displacement (the deformation) was measured to be 3.1mm. This value is surprisingly low but underlines the fact that the mechanical contruction is very stiff.

According to the manufacturer of the bearing the maximum angular tilt of the bearing is 0.0009 radians which result in a maximum vertical deformation due to the bearing of 0.42*mm*. Since our measurement shows a total deformation of 3.1mm, the remaining 2.68mm are therefore due to slackness, inaccuracies and elasticity in the components.

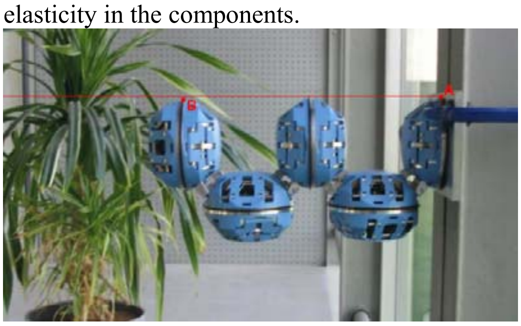

Figure 8. The setup for the mechanical deformation test.

Power Sharing Test

This test verifies that the modules are able to share power through their power sharing facilities. Figure 9 shows 4 pictures dumped form a video which illustrate a successful power sharing test.

Module **A** in figure 9 a) is a half passive module fixed to metal plate, and its power sharing circuit is externally connected to a power supply. Module **B** is switched off and is therefore supplied through its connection with module **A**. Module **C** is switched off.

In figure 9 a) Module **B** has started a connection to module **C**. In b) an electrical connection of the power sharing circuit has been established and the LEDs are turned on (marked with a circle). In c) the mechanical connection has completed and the two connectors in the upper hemisphere of module **C** is being actuated. In d) the connectors are fully extended.

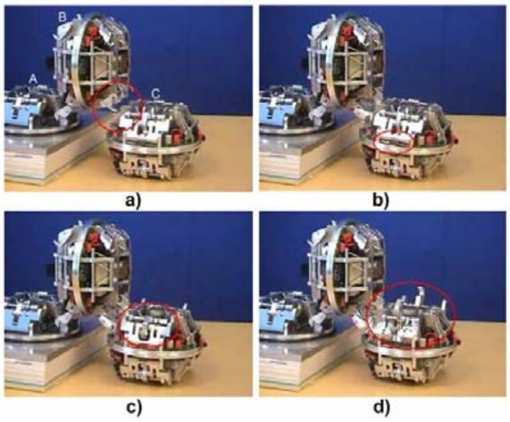

Figure 9. The setup for the power sharing test.

Rotation Test

In Figure 10 a setup for testing the rotational load abilities of an ATRON module is shown. The four pictures are screenshots from a video where the battery powered module **B** continuously rotates the two passive modules **C** and **D**. To obtain a stable platform, module **B** is connected to module **A** which is a half passive module fixed to metal plate.

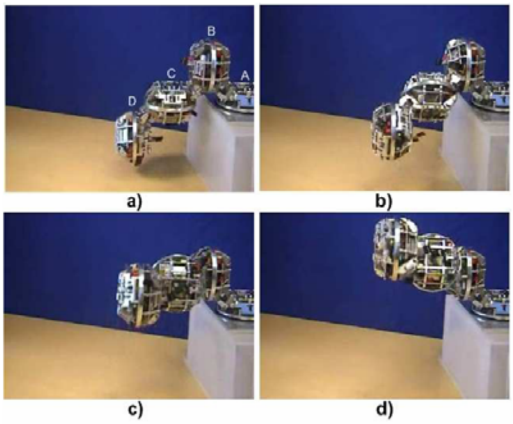

Figure 10. The setup for the rotation test.

In Figure 10 *a)* the initial position is shown. The rotation is initiated with an angular velocity of approximately 0.8 rad/s. In *b)* the modules have been rotated about 45° in counterclockwise direction and are approaching the 90° position *c)* where the inertial load is greatest.

Here the rotation is stopped and the solenoid lock is activated holding the modules in place for 3 sec. Hereafter the lock is released and the rotation continues as seen in *d)* pausing at the 180°, 270°, 360°, and 90° positions.

One of our initial design criteria for an ATRON module's rotational load abilities was that it should be able to smoothly rotate two other modules in a configuration as seen on Figure 10. This criterion was required to allow the overall system to have the necessary degrees-of-freedom to build complex structures and to limit motion constraints, and has now been verified to hold for the physical platform.

Misalignment Test

The purpose of this test is to show the ATRON module's abilities to connect to misaligned modules. Figure 11 shows 4 pictures of a successful connection between an active module and a passive misaligned module. In a) the active module has started the connection process. In b) the passive module is pulled towards the active module. In c) the passive module is twisted into its right lattice position.

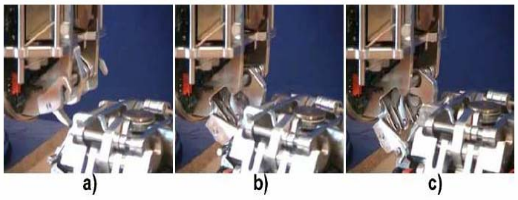

Figure 11. The setup for the misalignment test.

The misalignment corrections guides are illustrated in figure 12. The construction allows misalignment corrections of ± 5.7mm in the x direction, and at least ± 3.0mm in the y direction.

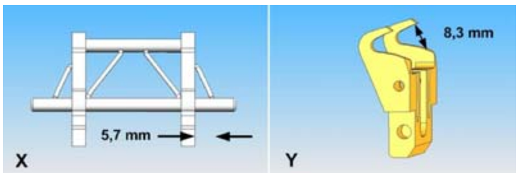

Figure 12. CAD drawings illustrating the possible misalignment corrections. (Left) The female frame part with guides, which allow misalignment corrections of ± 5.7mm in the x direction. (Right) The lower active male arm, which allows misalignment corrections of at least ± 3.0mm in the y direction.

Conclusion

We developed the ATRON design as simple building blocks with simple connections for simple interactions, in order to provide a design suitable for performing self-reconfiguration and for future miniaturization. Of great importance is the connector mechanism that is strong, fast and reliable despite being a point-to-point connector. Tests showed that the modules connect even when misaligned in the three dimensions, that a module can lift another two modules, that on-board batteries provide energy for approximately 150 minutes, and that power sharing between modules may be possible with the design outlined in this paper. We therefore believe the design to be suitable for self-reconfiguration and self-repair experiments (e.g. [8]), and will show such in future work with the 100 ATRON modules that we have produced now.

Acknowledgements

This work is partly funded by the EU FET project HYDRA, and the Self-assembling Robotic Artefacts project sponsored by the Danish Technical Science Council. C. Ryberg, D. Kyrping, D. Brandt, D. Christensen, E. Østergaard, J. Hallam, K. Støy, K. Kassow, L. Paramonov have contributed to the ATRON.

References

[1] E. Østergaard. Ph.D. dissertation, University of Southern Denmark, December 2004.

[2] W.-M. Shen and P. Will. Docking in self-reconfigurable robots. In *Proceedings IEEE/RSJ Intl. Conf. on Intelligent Robots and Systems (IROS)*, pp 1049–1054, 2001.

[3] S. Murata, E. Yoshida, K. Tomita, H. Kurokawa, A. Kamimura, and S. Kokaji. Hardware design of modular robotic system. In *Proceeding of Intl. Conf. on Intelligent Robots and Systems (IROS)*, pp 2210–2217, 2000.

[5] J.W. Suh, S.B. Homans, and M. Yim. Telecubes: mechanical design of a module for self-reconfigurable robotics. In *Proceedings on the IEEE Intl. Conf. on Robotics and Automation (ICRA)*, pp 4095–4101, 2002.

[6] Craig Eldershaw, Mark Yim, David Duff, Kimon Roufas, and Ying Zhang. Modular self-reconfigurable robots. In *Robotics for future land warfare seminar and workshop*. Defence Science Technology Organisation, Adelaine, 2002.

[7] D. Rus and M. Vona. A physical implementation of the crystalline robot. In *Proceedings of IEEE Intl. Conf. on Robotics & Automation (ICRA)*, pp 1726–1733, 2000.

[8] E. Østergaard and H. H. Lund. Distributed cluster walk for the ATRON self-reconfigurable robot. In *Proceedings of the The 8th Conference on Intelligent Autonomous Systems (IAS-8)*, pp. 291– 298, 2004.

The Tenth International Symposium on Artificial Life and Robotics 2005(AROB 10th '05),
B-con Plaza, Beppu, Oita, Japan, February 4-6, 2005

Improvement of Real-coded Genetic Algorithms for Optimization Problems

Hiroshi Kinjo, Hiroki Nakanishi and Tetsuhiko Yamamoto
kinjo,hiroki,yamamoto@mibai.tec.u-ryukyu.ac.jp
Faculty of Engineering, University of the Ryukyus
Nishihara, Okinawa 903-0213, Japan

Duong Sam Chau
Faculty of Electric Mechanics
Hanoi Agricultural University
Gialam, Hanoi, Vietnam

Abstract

Genetic algorithms (GAs) are widely used in solving optimization problems. In this paper, we present a crossover method used in real-coded GAs for multivariable optimization problems. A well-known crossover operator of real-coded GAs is the blend crossover (BLX). The BLX has a range parameter that determines the offspring production range. The search performance of the GA depends on the value of the range parameter. However, determination of the range parameter is sometimes difficult. In this paper, we propose a crossover operator for real-coded GAs that is a close-to-parent offspring. The crossover is based on the idea that offspring should be close to their parents. In order to improve the evolution performance, we applied a mutation operator to the real-coded GA. Simulation shows that the use of a close-to-parent crossover with the mutation operator effectively improves search performance.

Keywords: Real-coded GA, Crossover method, Close-to-parent offspring, Optimization problem.

1 Introduction

Recently, genetic algorithms (GAs) have been applied widely and effectively in various fields [1]-[3]. The most useful property of GAs is their ability to solve search and optimization problems with very little required information about the problems. The performance of GAs depends, to a great extent, on the performance of the crossover operator used. The crossover operation is performed upon the selected chromosome. The crossover operates on two chromosomes at a time and generates offspring by combining the features of both chromosomes. A chromosome is usually a binary bit string, but not necessarily. There are several different variants of basic GAs. It is possible to use real-coded (or floating-point) genes and actually, several methods have been presented that use real-coded genes [4]. The crossover operators of the real-coded GA called the blend crossover (BLX-α). The BLX has a range parameter that determines the production ranges of the offspring. The evolution performance of GAs is dependent on the value of the range parameter. Selection the range parameter is determined by trial and error. However, the determination of the range parameter is sometimes difficult.

The BLX is an offspring production method using a random number of uniform distributions based on the intervals of two parents and a range parameter. That is, the method is not based on the parents them selves but on the intervals between parents. We consider that offspring production should be based on the parents them selves. Based on the above-mentioned idea, in this paper, we present a new method, i.e., a close-to-parent crossover. Furthermore we applied a mutation operator to the crossover system to improve the search performance for optimization problems.

In section 2, we describe the close-to-parent offspring production method. In section 3, we describe the search performance of the crossover for three two-variable functions. In section 4, we describe the evolution performance for a neural network training problem. In section 5, we conclude this paper.

2 Close-to-parent offspring

Figure 1 (a) shows, a conventional crossover, the BLX. In the figure, offspring are produced using random values on a uniform distribution in the range of $[p_1 - \alpha I, p_2 + \alpha I]$, where p_1 and p_2 are the real values of the parents and α is the range parameter. α determines the search area of the offspring.

Figure 1(b) shows, the proposed crossover, that is, the close-to-parent offspring (CPO). CPO also has a range parameter α that determines the offspring production range based on each parent. For producing offspring using CPO, two individuals are produced using random values that have uniform distributions in

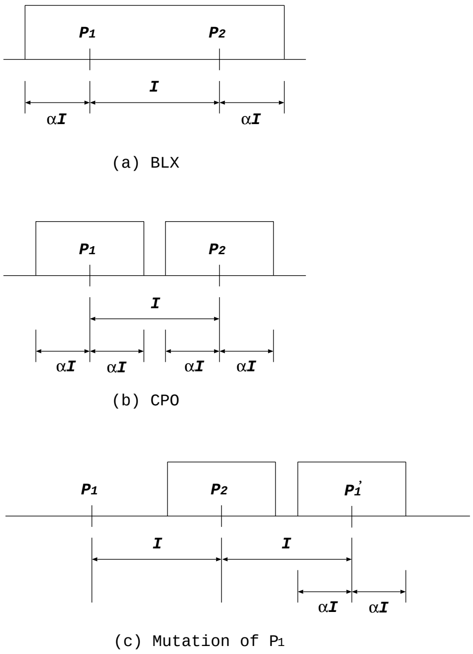

Fig. 1 Offspring production methods

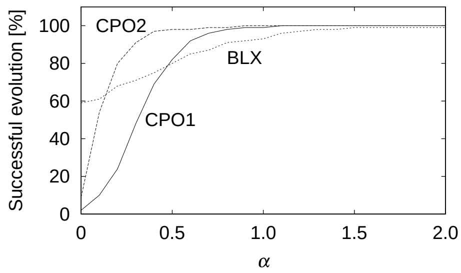

Fig. 2 Evolution performance of Sphere function

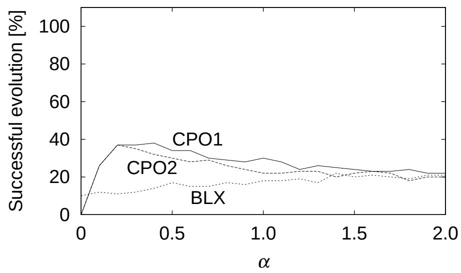

Fig. 3 Evolution performance for Rosenbrock function

the ranges of $[p_1 - \alpha I,\, p_1 + \alpha I]$ and $[p_2 - \alpha I,\, p_2 + \alpha I]$.

Figure 1 (c) shows a mutation of the CPO. In the figure, p'_1 denotes the center of the range of the mutation of parent p_1. The range of the offspring applied to the mutation is $[p'_1 - \alpha I,\, p'_1 + \alpha I]$.

3 Two-variable optimization problem

In this section we investigate the search performance of the proposed method for optimization problems for three two-variable functions: Sphere function, Rosenbrock function, and Rastrigin function [5].

The search performance is measured using successful evolution rates obtained from the minimum values of the functions in the GA.

In this test, we use the following GA parameters: population size is $N_p = 100$ and generation number is limited to 300. The produced offspring is 60% of the population N_p. The parents selection is the roulette wheel selection.

The sphere function, which is the simplest case in this test, is described by the following equation.

$$f(x, y) = x^2 + y^2, \quad x, y \in [-1.5, 1.5] \tag{1}$$

The minimum value of this function is 0.0 and occurs when $(x, y) = (0, 0)$.

Figure 2 shows the evolution performance of the Sphere function. In the figure, the CPO1 line shows the result of the cross-to-parent offspring and the CPO2 line shows the results of CPO with mutation, where the mutation rate is 20 %. We define a successful evolution as that having a minimum value of the function $f(x, y) < 0.001$. The lines of successful rate in the figure show the mean value of 1000 trials. We can see that the range of α in CPO2 which has a good performance is wider than that in BLX.

Figure 3 shows the evolution performance for the Rosenbrock function. The Rosenbrock function is described by the following equation.

$$f(x, y) = 100(x - y^2)^2 + (y - 1)^2, \quad x, y \in [-0.25, 1.25] \tag{2}$$

The minimum value of this function is 0.0 and occurs when $(x, y) = (0, 0)$. We can see that the rate of successful evolution of CPO1 is approximately two times better than that of BLX at $\alpha = 0.3$. From the figure, the result of CPO2, i.e., with the mutation operator, is poor compared with the result obtained when mutation operator is not used. In this case the mutation does not have a good effect on search performance.

Figure 4 shows the evolution performance for the Rastrigin function. The Rastrigin function, which is the most complicated function in this research, is described by the following equation.

$$\begin{aligned} f(x, y) = 20 &+ \{x^2 - 10\cos(2\pi x)\} \\ &+ \{y^2 - 10\cos(2\pi y)\}, \quad x, y \in [-0.25, 1.25] \end{aligned} \tag{3}$$

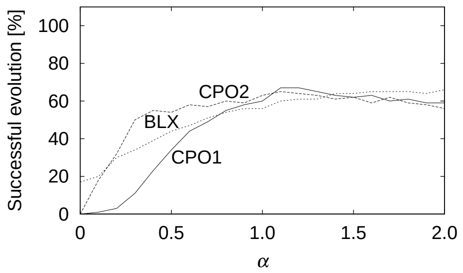

Fig. 4 Evolution performance for Rastrigin function

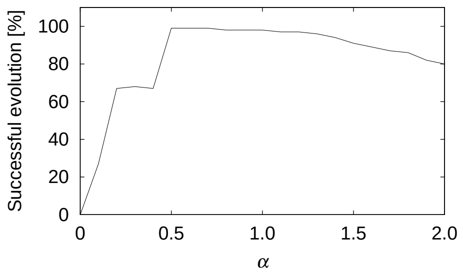

Fig. 5 Evolution performance for Rastrigin function using CPO with sign mutation

The minimum value of this function is 0.0 and occurs when $(x, y) = (0, 0)$. We can observe that the COP2 has a better search performance than BLX and CPO1. In the case of the Rastrigin function, it is difficult to search the solution because the surface of the function is in the shape of valleys and peaks [5]. We considered that a mutation more effective and severer than the range mutation described in Fig. 1 (c) is required. Figure 5 shows a result of CPO with a sign mutation. The sign mutation means a change in the sign of the real value of the offspring. This figure shows the result when the mutation rate is 20 %. We can see that CPO with a sign mutation has a better evolution performance than the previous results of the three methods shown in Fig. 4.

4 Neural network training problem

This section presents simulation results of neural network training problems. The training of neural network is known as a nonlinear multivariable optimization problem.

In order to obtain results comparable to those of the BLX, We should select the well-known exclusive-or (XOR) problem.

In this test, we use GAs for training a XOR network. For clearer results, we examine the XOR net-

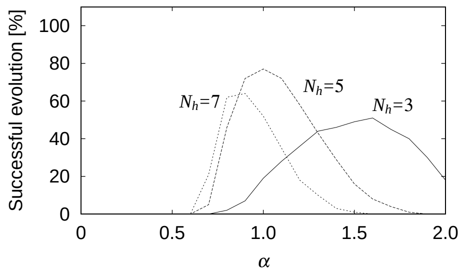

(a) BLX

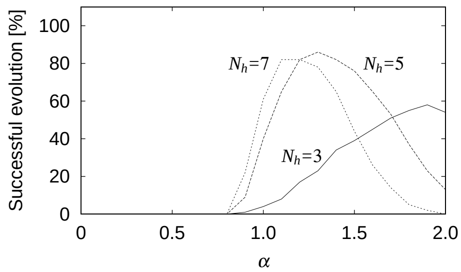

(b) CPO1

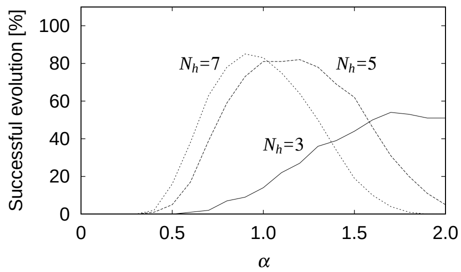

(c) CPO2

Fig. 6 Evolution performance for neural network ($N_p = 25$)

works for various population sizes of GAs: $N_p = 25, N_p = 50$ and $N_p = 100$. In each case of N_p, we also change the number of neurons in the hidden layer of the network: $N_h = 3, N_h = 5$ and $N_h = 7$. The performance results of the XOR network training are shown in Figs. 6-8; in this training we use GAs with crossover operators: BLX, CPO1 and CPO2. We can see that, in all of the cases, CPO achieved better performances than BLX could. Moreover, in CPO, the range of α, which has a good performance, is significantly wider than that in BLX. That is, CPO could obtain good results several times better than those of BLX. We can also observe that the addition of mutation effects the good results of the neural network training problem.

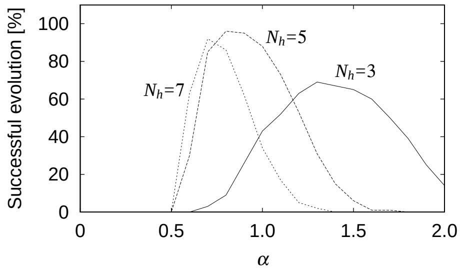

(a) BLX

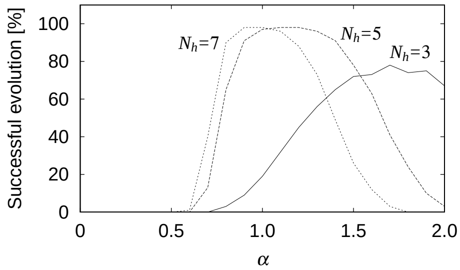

(b) CPO1

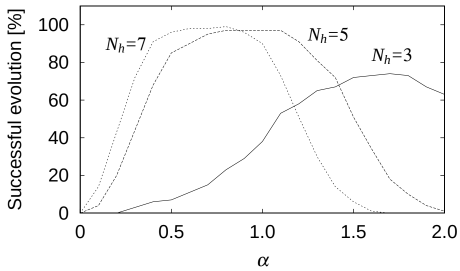

(c) CPO2

Fig. 7 Evolution performance for neural network ($N_p = 50$)

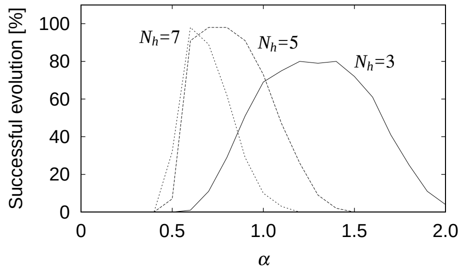

(a) BLX

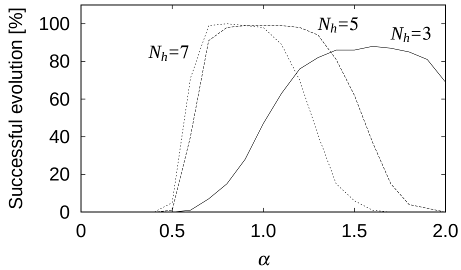

(b) CPO1

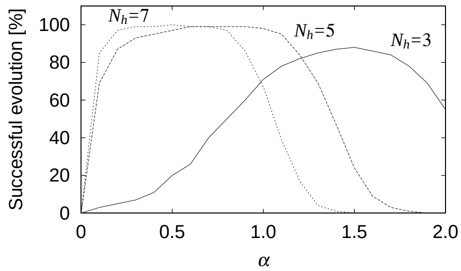

(c) CPO2

Fig. 8 Evolution performance for neural network ($N_p = 100$)

5 Summary

Improving crossover operator in GAs is an area of active research for developing GAs. In this paper, we presented a new method of improving real-coded GAs by examining new search spaces of the crossover operator. The simulations show that GAs can achieve a good performance by changing search spaces to generate two close-to-parent offspring.

References

[1] D. E. Goldberg, *Genetic Algorithms in Search, Optimization & Machine Learning*, Addison-Wesley, 1989.

[2] L. Davis, *Hand Book of Genetic Algorithms*, Van Nostrand Reinhold, 1991.

[3] M. Gen and R. Cheng, *Genetic Algorithm and Engineering Design*, Wiley-Interscience, 1997.

[4] L. J. Eshelman and J. D. Schaffer, "Real-Coded Genetic Algorithms and Interval-Schemata" *Foundations of Genetic Algorithms 2*, Edited by L. Darrell Whitley, Morgan Kaufmann Publishers, 1993.

[5] H. Okamura, K. Kitasuka and T. Dohi, "Performance Evaluation of Genetic Algorithms Based on Markovian Analysis - Evaluation by Relaxation Time and Application to Real-Coded Genetic Algorithms," Transactions of the ISCIE, Vol. 16, No. 7, pp. 303-312, 2003. (in Japanese)

The Tenth International Symposium on Artificial Life and Robotics 2005(AROB 10th '05),
B-con Plaza, Beppu, Oita, Japan, February 4-6, 2005

Enhanced Performance for Multi-variable Optimization Problems by Use of GAs with Recessive Gene Structure

MUHANDO Endusa
muhando@mibai.tec.u-ryukyu.ac.jp

KINJO Hiroshi
kinjo@tec.u-ryukyu.ac.jp

YAMAMOTO Tetsuhiko
yamamoto@tec.u-ryukyu.ac.jp

Mechanical Systems Engineering
University of the Ryukyus
Senbaru 1, Nishihara, Okinawa. 903-0213 JAPAN

Abstract

In this paper we propose a dual gene system using the recessive gene model, RGM, to solve difficult multi-variable optimization problems. Genetic algorithms (GAs) are widely applied to many optimization problems and usually suffer loss of diversity, leading to evolutionary stagnation. The dual gene system is exploited to maintain diversity, significantly boost evolutionary computation precision and avoid stagnation. We show by computer simulations that RGM has a higher search efficiency in multi-variable optimization functions. Further, RGM performs better on small populations than the single, dominant gene approach for the same computational cost.

Keywords: Recessive gene, Multi-modal function, Multi-variable optimization, Computational cost.

1 Introduction

Evolutionary computation in optimization relies on processes loosely based on natural selection, cross-over and mutation, that are repeatedly applied to a population of binary strings which represent potential solutions. Most GAs experience problems of convergence due to loss in diversity [1]. There is need to devise ways of avoiding the mechanism of evolutionary stagnation.

We used the basic information on Mendelian genetics to illustrate that a recessive characteristic might significantly affect a closed population [2]. In observing living organisms, characteristics of the offspring do not always resemble those of parents. A dual gene system exists whereby some alleles are dominant hence always expressed, while some are recessive, that is, only expressed under certain conditions. However, the individual preserves the recessive gene, which is sent to the next generation, thus maintaining the diversity of the characteristics of the living organism. RGM utilizes both dominant and recessive genes in the cross-over and mutation operations in the mating phase of the GA. To confirm the efficiency of the scheme we applied RGM to two multi-variable optimization problems.

The structure of this paper is as follows: in Section 2 we present the RGM and in Section 3 we describe the test functions. Simulation results are detailed in Section 4 and a discussion makes up section 5. Finally, we draw some general conclusions in Section 6.

2 Recessive Gene Model, RGM

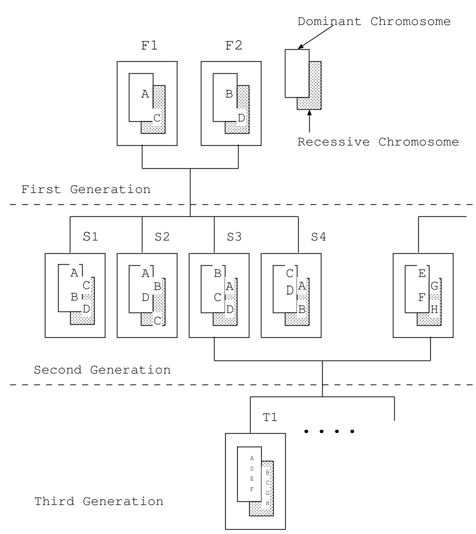

Figure 1: Schematic of the Recessive Gene Model

Figure 1 shows the structure of the double gene system. In usual GA systems only the dominant genes appear, hence in the first generation of two individuals F_1 and F_2, only the dominant characteristics A and B appear, respectively. In the second generation, each of the individuals S_1, S_2, S_3 and S_4 will display two chromosomes: 1 dominant and 1 recessive. As an example, F_1 and F_2 will produce two offspring, $S3$ and its complement, $S3'$, in the second filial generation simultaneously. Offspring $S3$ will have the chromosomes BC (dominant) and AD (recessive), while $S3'$, has CB and DA as dominant and recessive, respectively.

P is the probability that a recessive chromosome is selected to be a dominant chromosome in the next generation. In the special cases of $P = 0\%$ and $P = 100\%$ then the offspring will be S_1 and S_4 respectively. The essence of the dual gene system is to provide a larger variety of offspring for the search.

3 Problem Formulation

Our two test functions were Easom's and Schaffer's F6, from the classical benchmark similar to those defined by Kenneth De Jong [3], [4], [5].

3.1 The Easom Unimodal Function

For this function the global minimum has a small area relative to the search space; the function was inverted for minimization, and takes the form:

$$f(x,y) = -\cos(x)\cos(y)\mathrm{e}^{-((x-\pi)+(y-\pi))}$$

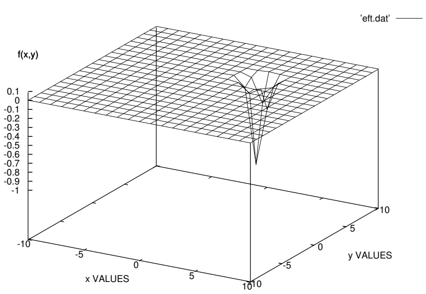

Figure 2: Easom function in 3-D

Figure 2 shows a 3-D depiction of the Easom function. The analytical global minimum of the Easom function is -1 when $(x, y) = (\pi, \pi)$.

3.2 Schaffer's F6 Multi-modal Function

This parametric optimization problem is multimodal, represented by the equation:

$$f(x,y) = 0.5 + \frac{\sin^2(\sqrt{x^2+y^2}) - 0.5}{1+0.001(x^2+y^2)^2}.$$

The function is a two-parameter "ripple", like the waves in a pond caused by a pebble.

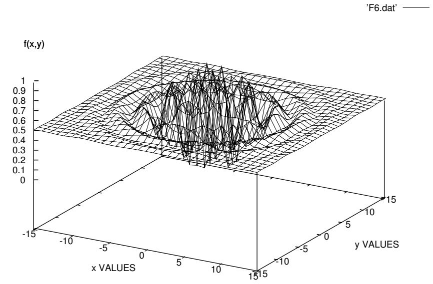

Figure 3: Schaffer's F6 function in 3-D

Figure 3 shows Schaffer's F6 function; the centermost ring represents the circular global optimum.

Table 1: Analytical results for Schaffer's F6

Optima	r	$f(x,y)$
Global	$\frac{\pi}{2}$	0.996989
1st local	$\frac{3\pi}{2}$	0.838081
2nd local	$\frac{5\pi}{2}$	0.606185
3rd local	$\frac{7\pi}{2}$	0.532483

Table 1 gives the analytical values for the various maxima. For each set of values at the various optima, the relation $r = \sqrt{x^2+y^2}$ exists.

4 Simulation Results

4.1 GA Parameters

A random generation of (x, y) values in Euclidean space was used in the GA search for both functions.

Table 2: Constant parameters

Binary bit length, B	16
Selection pressure, parents P_p	0.5
Selection pressure, children P_c	0.6
Selection method	Roulette wheel
Crossover	2-point

Table 2 shows the constant parameters in the GA search. The sample size, N, was kept at 50 for most of the simulations.

Table 3: Variables

Percentage of recessive gene, $P\%$	$0 < P < 100$
Rate of mutation, $M\%$	$0 < M < 100$
No. of generations, G	$0 < G < 100$
Sampling population, N	$20 < N < 100$

Table 3 shows the variables utilized in the GA search.

4.2 Searching performance results for the Easom function

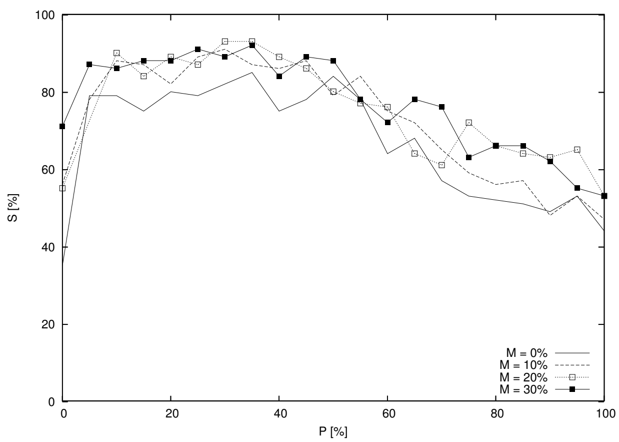

Figure 4: Recessive gene performance for the Easom function.

Figure 4 shows the searching performance for the Easom function. In the case of $P = 0\%$, only using dominant chromosomes, success rate is lower than for for the case of the recessive gene, when $P \neq 0\%$; however, when P is too large the search is not very efficient. Mutation plays a significant role in the search. It is seen that in the absence of mutation, for the case $M = 0\%$, then the search improves with P. Search space was in the whole region, (x, y) = [-10,10].

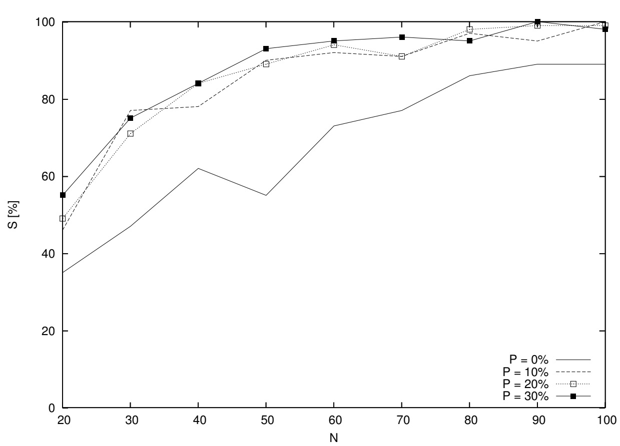

Figure 5: Effect of varying sampling population on performance for the Easom function. ($M = 20\%$).

From Figure 5 we can observe that though the search performance improves with increase in the population size, the recessive gene performs better at low populations than for the case where $P = 0\%$.

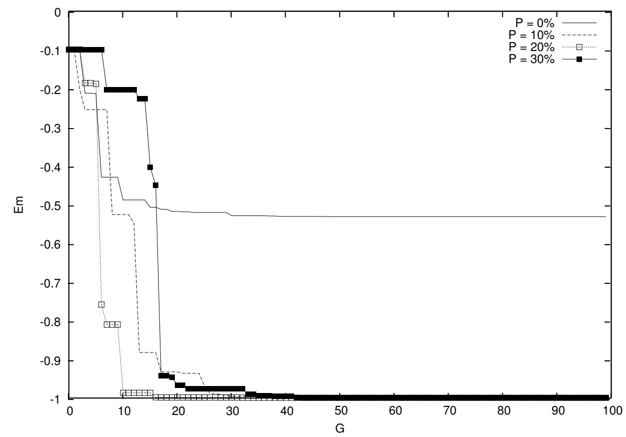

Figure 6: Effect of generations and recessive gene on efficiency for the Easom function. ($M = 20\%$).

Figure 6 shows the mean of the best values of the function on 100 trials per generation. It gives a strong indication of the advantage of the recessive gene in this unimodal search, where the attainment of the best mean value, E_m, of the function is faster when $P \neq 0\%$ and there is stagnation when $P = 0\%$. For the Easom function, rate of convergence to solution is fastest when $P = 20\%$.

4.3 Searching performance results for Schaffer's F6 function

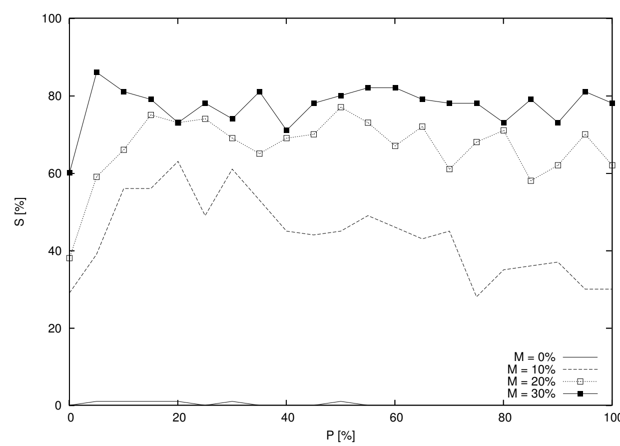

Figure 7: Recessive gene performance, Schaffer's F6.

Figure 7 shows that success in search for the global optimum is best when $P \neq 0\%$. Mutation is essential in this multimodal search, as there is practically no search when $M = 0\%$. Mutation enhances the search by offering diversity among the population. Search for the global optimum was investigated from an initial sampling in the range [11,13] of the global search space [-15,15] for (x, y) values.

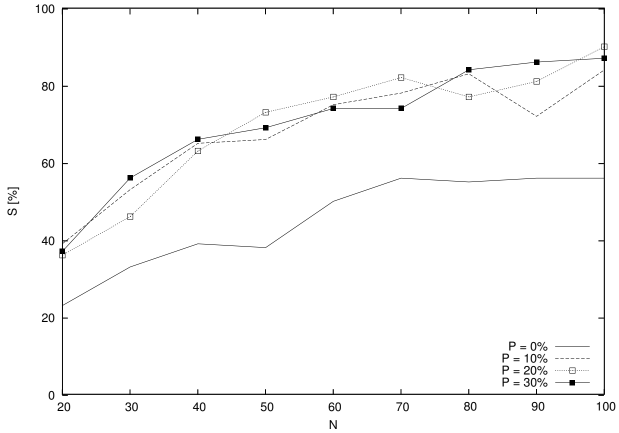

Figure 8: Effect of varying sampling population on performance for Schaffer's F6 function. ($M = 20\%$).

Figure 8 shows that though increasing N greatly improves the search, RGM performs relatively well with small population when $P \neq 0\%$ and it is inadequate when $P = 0\%$.

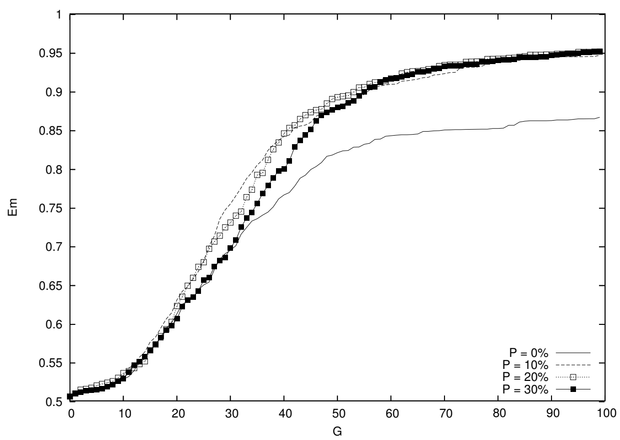

Figure 9: Effect of generations and recessive gene on efficiency for Schaffer's F6 function. ($M = 20\%$).

Figure 9 indicates the advantage of using the recessive gene as convergence is influenced by P; for $P = 0\%$ there is stagnation at some local optima.

5 Discussion

Using RGM, we compared the performance of the GA driven by a gradually increasing recessive gene to the dominant case. Figures 4 and 7 are the basis of our research; for the Easom function the success rate is lower when using only dominant chromosomes than for $P \neq 0\%$. However the search performance is degraded when P is too large. It can be inferred that for the unimodal search the recessive gene performs the function of mutation. For the Schaffer's F6, search improves with P; mutation is integral to the evolution as there is practically no success for $M = 0\%$.

Figures 5 and 8 show that for the respective functions, though N greatly influences the search, there is inferior evolutionary success for $P = 0\%$. GA efficiency is enhanced by a large N, though this requires more memory and takes longer to converge. Since computational cost, C_c, in terms of time and memory, is in direct proportion to N, then C_c for $N = 100$ should be twice the C_c for $N = 50$. It can be seen from Figures 5 and 8 that performance is superior for the case $P \neq 0\%$, $N = 50$ than for $P = 0\%$, $N = 100$.

Figures 6 and 9, for Easom and Schaffer's F6 respectively, show that the rate of convergence is high for $P \neq 0\%$ and that there is stagnation when $P = 0\%$.

Maintaining diversity in the GA search ensures high efficiency yet avoids quick convergence and stagnation. RGM ensures accurate convergence at low N and this is desirable for memory storage during computations. However, RGM may be computationally expensive.

6 Conclusions

In this paper, we have shown that RGM avoids stagnation due to diversity, works very well at low sampling populations and that the recessive gene performs the function of mutation. Further, performance with recessive chromosomes is superior to the purely dominant chromosomes case. We believe the management of the computational cost could be further improved.

References

[1] D. E. Goldberg: GAs in Search, Optimization & Machine Learning, Addison-Wesley (1989)

[2] Holland H. John: Adaptation in Natural and Artificial Systems: An Introductory Analysis with Applications to Biology, Control and AI, MIT Press (1995)

[3] De Jong, K. A., 1975: An Analysis of the Behaviour of a Class of Genetic Adaptive Systems. Dept. of Computer and Comms., Univ. of Michigan, Ann Arbor.

[4] Shaffer J., Caruana R., Eshelman L.: A study of control parameters affecting online performance of GAs for function optimization. *Proceedings of the 3rd Int'l Conference on GAs*. Morgan Kaufman Publishers. 1989

[5] Xavier Hue: GAs for Optimization: Background and Applications. EPCC, Univ. of Edinburgh, (Feb 1997).

The Tenth International Symposium on Artificial Life and Robotics 2005(AROB 10th '05),
B-con Plaza, Beppu, Oita, Japan, February 4-6, 2005

Identification of Time Series Signals Using Dynamical Neural Network with GA-based Training

Kunihiko Nakazono
University of the Ryukyus
Senbaru 1, Nishihara, Okinawa. 903–0213
nakazono@tec.u-ryukyu.ac.jp

Kouhei Ohnishi
Keio University
Hiyoshi 3–14–1, Yokohama. 222–8522
ohnishi@sd.keio.ac.jp

Hiroshi Kinjo
University of the Ryukyus
Senbaru 1, Nishihara, Okinawa. 903–0213
kinjo@tec.u-ryukyu.ac.jp

Abstract

In this paper, we propose a dynamical neural network (DNN) having the properties of inertia, viscosity, and stiffness and its training algorithm based on a genetic algorithm (GA). In a previous study, we proposed a modified training algorithm for the DNN based on error backpropagation method. However, in the former method it was necessary to determine the values of the DNN parameters by trial and error. In the proposed DNN, the GA is designed to train not only the connecting weights but also the parameters of the DNN. Simulation results show that the DNN trained by GA obtains good training performance for time series patterns generated from unknown system.

1 Introduction

Recently, recurrent neural networks and spiking neural networks have attracted more research interest than layered neural networks having static mapping capability [1, 2, 3, 4]. The recurrent neural network is a possible candidate for improving the system dynamics because it incorporates a feedback structure in the neuron unit and takes time delayed inputs into consideration. Research on spiking neural networks is also ongoing. Spiking neural networks treat spike trains and process the signals based on spike pulses. However, the network structure in recurrent neural networks and spiking neural networks is complex compared to that in layered neural networks with a training algorithm.

Here, we propose a dynamical neural network (DNN) that realizes a dynamical property and has a network structure with the properties of inertia, viscosity, and stiffness without time delayed input elements. In a previous study, the proposed DNN was constructed with a training algorithm that used error backpropagation method [5]. However, that algorithm modified only the connecting weights and the property parameters for the DNN had to be determined by trial and error. We design a GA-based training [6] both the connecting weights and the parameters of the DNN.

The validity of the proposed DNN was verified by identifying periodic functions such as a simple one-period sine waveform and several periodic sine waveforms [7]. In this paper, it is verified by identifying the time series signals of linear system and nonlinear system. Simulation results show that the proposed DNN provides higher performance than the conventional neural network.

2 Structure of DNN

In this paper, a DNN is configured using a neuron having the properties of inertia, viscosity, and stiffness. In this neuron model, we assume the image output from neuron possesses the properties of inertia, viscosity, and stiffness, and that the output is propagated in the next neuron. The proposed DNN is composed of three hierarchy layers and the proposed neuron adopts a hidden layer and an output layer. The structure of the DNN is shown in Figure 1.

The equations for the DNN are expressed as follows.

$$y_i = u_i, \quad (i = 1, 2, \cdots, N_I) \tag{1}$$

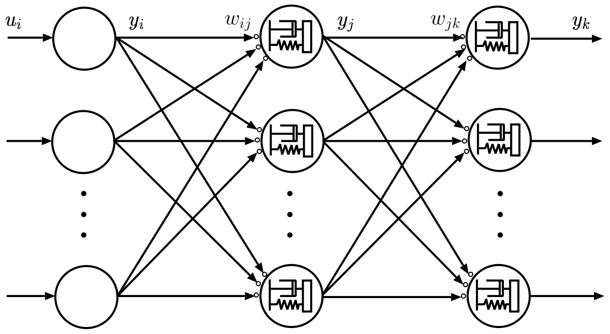

Figure 1: Structure of DNN

$$y_j = K_j f_j(net_j) + D_j \dot{f}_j(net_j) + M_j \ddot{f}_j(net_j) \quad (2)$$

$$net_j = \sum_{i=1}^{N_I} w_{ij} y_i, \quad (j = 1, 2, \cdots, N_J) \quad (3)$$

$$y_k = K_k f_k(net_k) + D_k \dot{f}_k(net_k) + M_k \ddot{f}_k(net_k) \quad (4)$$

$$net_k = \sum_{j=1}^{N_J} w_{jk} y_j, \quad (k = 1, 2, \cdots, N_K) \quad (5)$$

Here, u_i shows input value to the DNN, and y_i, y_j, and y_k show output values in input, hidden, and output layers, respectively. The Connecting weight from unit i in input layer to unit j in hidden layer is denoted by w_{ij}. Similarly, w_{jk} is a connecting weight from unit j in hidden layer to unit k in output layer. The total sum of products of the connecting weight and the output value is denoted by net. M_j, D_j, and K_j are the property parameters of inertia, viscosity, and stiffness, respectively. N_I, N_J, and N_K are the number of neurons in input, hidden, and output layers, respectively. The threshold function uses a sigmoid function in the range of $[-1, 1]$.

3 Training algorithm based on GA

The DNN is trained using a GA in an off-line process. Figure 2 shows the flowchart of the evolution process in the DNN. The evolution algorithm for the DNN is as follows.

STEP1: Produce the initial DNNs at random. The connecting weights w_{ij} and w_{jk} in the range of $[-1, 1]$ and the property parameters M_j, D_j, K_j, M_k, D_k, and K_k of DNNs in the range of $[0, 10]$ are transformed to the chromosome. The genetic code is transformed to the binary code (16 bit).

STEP2: Sum all of the fitnesses for the DNNs.

STEP3: Select the parent DNNs by means of roulette wheel parent selection.

STEP4: Perform a crossover operation for the chromosome to produce new DNNs.

STEP5: Perform a mutation operation for some additional new DNNs.

STEP6: Sum all of the fitnesses for the DNNs including the new DNNs. Go back to STEP2 until the evolution process arrives at generation 10,000.

Further information regarding the parameters of the GA is shown in Table 1.

During the GA-based training process, an error function E is used to evaluate the performance of each

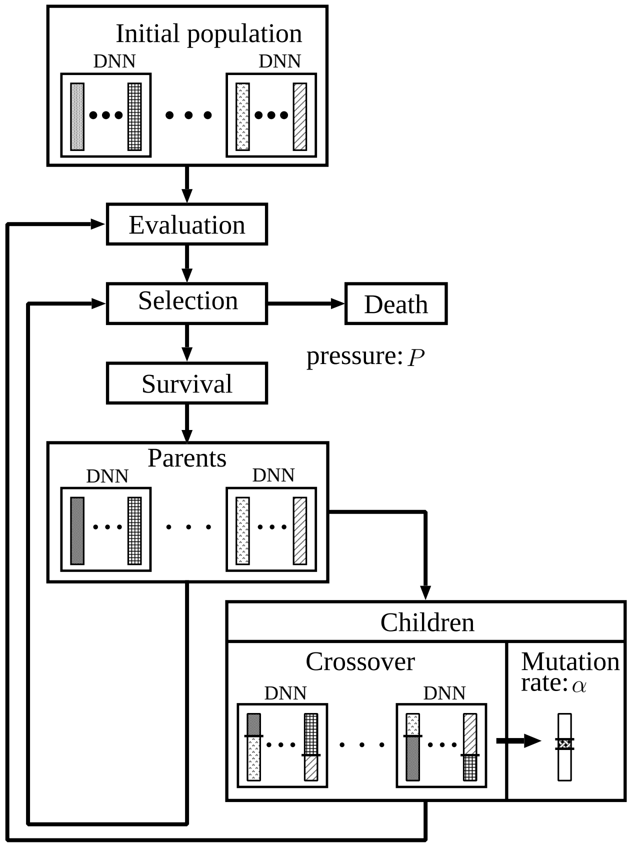

Figure 2: Flowchart of GA-based training

Table 1: Simulation parameters of GA

Initial DNNs	400 individuals
Selection	Roulette wheel parent selection $P = 0.6$
Crossover	One-point crossover
Mutation	Bit mutation $\alpha = 0.10$
Final generation	10,000

DNN. The error function E is described by the following equation as

$$E = \frac{1}{2}\sum_k e(t)^2 = \frac{1}{2}\sum_k (d(t) - y(t))^2 \qquad (6)$$

where $d(t)$ is the desired signal. The fitness of DNN is expressed in terms of the inverse of the error function E. The connecting weights and property parameters of the DNN are modified in order to maximize the fitness function determined by the error function in Equation (6).

4 Numerical simulation

The effectiveness of the proposed DNN is verified by numerical simulation in order to identify time series signal. The method by which a time series signal from an unknown system can be identified is shown in Figure 3. The DNN is structured to have a single input

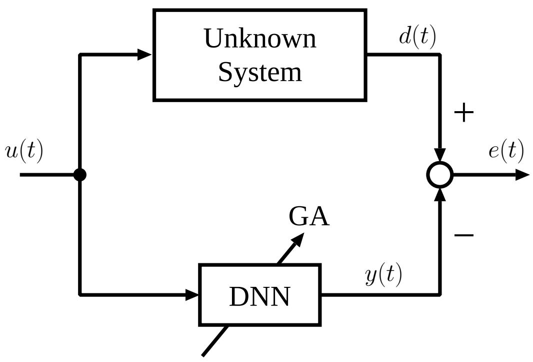

Figure 3: System identification of time series signal

and single output (SISO). The input signal $u(t)$ of the DNN and the unknown system is a random number of normal distribution (mean 0.5 and variance 0.5). The desired signal, namely the training data $d(t)$, is the output signal of the unknown system.

In numerical simulation, the validity of the proposed DNN is verified by identifying the unknown system such as linear system expressed in Equation (7) and nonlinear system expressed in Equation (8).

- Simulation 1 (linear system)

$$d(t) = 0.1d(t-1)+0.2d(t-2)+0.3u(t)+0.4u(t-1) \quad (7)$$

- Simulation 2 (nonlinear system)

$$d(t) = 0.1d(t-1) + 0.2d(t-2) + \sin\left(\frac{\pi u(t)}{4}\right) \quad (8)$$

4.1 Evolution process

In GA simulation, we set the GA parameters shown in Table 1 and the number of neurons in hidden layer is 12 units. The input signal $u(t)$ uses 1,000 sampling data. In simulation 1 and simulation 2, the evolution processes of the best DNN with the GA-based training are shown in Figure 4.

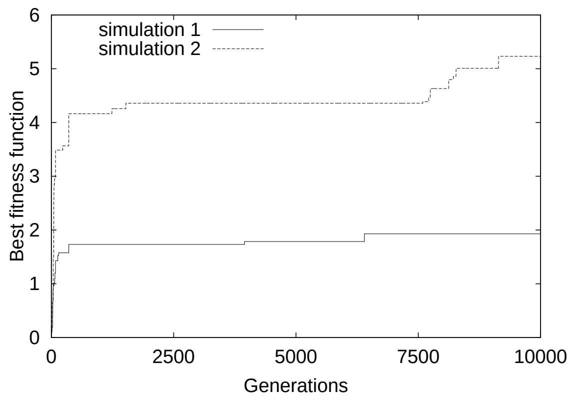

Figure 4: Evolution process

It is observed that either of the evolution processes provide performance to some extent. The fitness values increase gradually and the evolutions almost stagnate at generation 7,000 in simulation 1 and at generation 9,000 in simulation 2, respectively.

4.2 Simulation 1 (linear system)

The result of the regenerating signal using the trained DNN is shown in Figure 5. The figure shows the regenerating signal in range of $[100, 200]$.

The output of the DNN deviated negligibly from the desired signal, but the DNN could not cope with a quick transition.

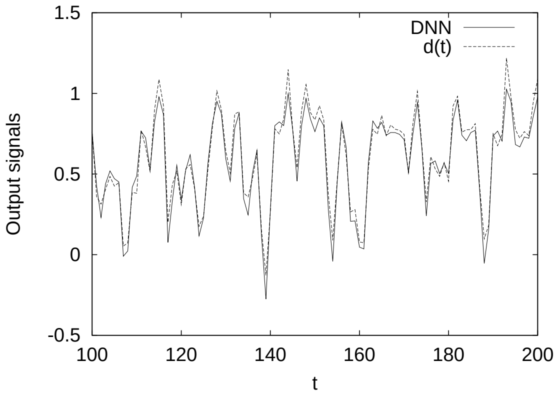

Figure 5: Regenerated result (simulation 1)

4.3 Simulation 2 (nonlinear system)

The result of the regenerating signal using the trained DNN is shown in Figure 6. The figure shows the regenerating signals in range of $[100, 200]$.

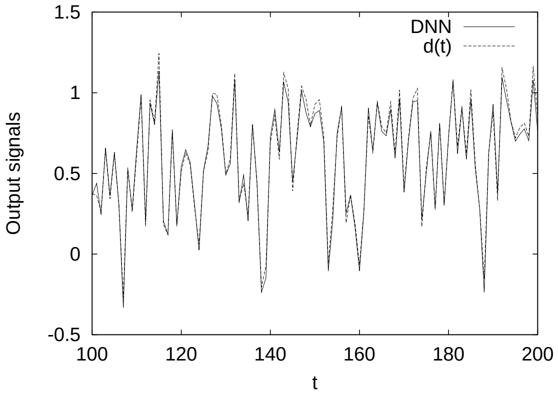

Figure 6: Regenerated result (simulation 2)

The output $y(t)$ of the best DNN deviated negligibly from the desired signal $d(t)$. The DNN trained by GA obtained good training performance for time series signal generated from the output of the nonlinear system.

5 Conclusion

In this paper, the proposed DNN, exhibiting the effectiveness of dynamical neuron with properties of inertia, viscosity, and stiffness, was configured. The training algorithm adopt the GA-based training method. Simulation results showed that the DNN trained by the GA realized good training performance for time series signals generated from either of unknown systems with linearity and nonlinearity.

In future work, we will try to identify a unknown system with strong nonlinearity.

References

[1] D. E. Rumelhart, J. L. McClelland, and the PDP Research Group (1989), Parallel Distributed Processing, *The MIT Press.*

[2] R. J. Williams and D. Zipser (1989), A Learning Algorithm for Continually Running Fully Recurrent Neural Networks, *Neural Computation*, 1, No.2, pp.270–280.

[3] H. Kinjo, K. Nakazono, and T. Yamamoto (1997), Pattern Recognition for Time Series Signals Using Recurrent Neural Networks by Genetic Algorithms (in Japanese), *Trans. of ISCIE*, Vol. 10, No. 6, pp.304–314.

[4] W. Mass and C. M. Bishop (1999), Pulsed Neural Networks, pp. 16-53, *MIT Press.*

[5] K. Nakazono, K. Ohnishi, H. Kinjo, and T. Yamamoto (2003), Identification of Periodic Function Using Dynamical Neural Network, *AROB 8th '03*, Vol.2, pp. 633–636.

[6] Edited by L. Davis (1991), Handbook of Genetic Algorithms, *Van Nostrand Reinhold.*

[7] K. Nakazono, K. Ohnishi, and H. Kinjo (2004), System Identification Using Dynamical Neural Network with GA-based Training, *AROB 9th '04*, Vol.1, pp. 75–78.

The Tenth International Symposium on Artificial Life and Robotics 2005(AROB 10th '05),
B-con Plaza, Beppu, Oita, Japan, February 4-6, 2005

Spontaneous speciation by GA for division of labor in two-agent systems

Naoki Oshiro, Koji Kurata and Tetsuhiko Yamamoto
Faculty of Engineering, University of the Ryukyus,
1 Senbaru, Nishihara, Okinawa. 903–0213
oshiro@mibai.tec.u-ryukyu.ac.jp

Abstract

In this paper, we propose a framework of genetic algorithm in which division of labor among the agents emerges. The agents in the system spontaneously develop different charactaristics to cooperate effectively to achive a task and speciate to different species. We assume the agents recieve input to specify the task and can observe each other. We apply the framework to a mechanical system. The task is designed simple and essential to elucidate the effectiveness of the algorithm.

Key Words: spontaneous speciation, coevolution, multi-agent system, genetic algorithm

1 Introduction

There are many researchs about multi-agent system to solve complex problem like n-Traveling Salesman Problem (nTSP)[1], and Genetic Algorithm (GA)[3] with speciation is an important and effective idea for organiging cooperative sharing of a task by agents. Speciation is also an important aspect in evolutional biology. There are also researchs to build a virtual ecosystem with GA-like framework[2].

In this paper, we apply this framework to a mechanical system. We assume two agents cooperating for a task (Figure 1). Each agent A_i receives external input x and generates its outputs y_i and z_i, generally. z_i is the action of the agent, and y_i is the signal to be observed by the other agent. y_i can be identical to z_i or a part of z_i. We assume rather a poor ability for the agents, so that the task is too difficult and two agents must cooperate. For better performance each of the cooperative pair must play a different role. This formulation will give rise to the division of labor. We want to make this division emerge spontaneously. For this purpose, we assume every agents have a same structure, learning mechanism and live in a same environment.

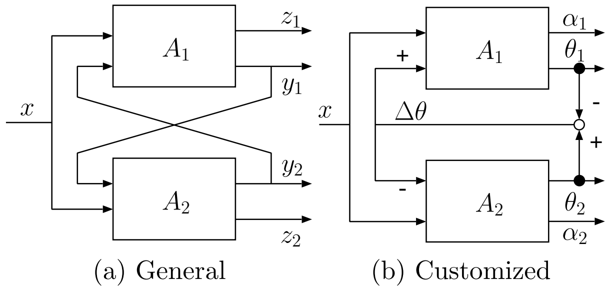

Figure 1: Information flow between two agents. (a) General framework. Each agent receives external input x and part of the other agent's output y_i. To achive given tasks, the agents use these information appropriately. (b) Customized framework for our task. Each agent can obtain the difference $\Delta\theta$ between its angle and its coleage's. Agents change their location θ_1, θ_2 only once using this information.

The task adopted in this paper is "disk moving problem", which is simple and essential to test the framework.

2 Disk moving problem

We assume two agents set on a disk in two dimensional space (Figure 2). Initially, the agents are located on the edge of the disk randomly and recieve input x to specify one of two target motions to be caused, "rotation" or "translation". Then they observe the relative angle between them. Based on the observation each of them moves along the circumference to the final position, where the two agents apply force simultaneously in the directions determined by x to cause rotation or translation.

Each agent has two state variables the angle representing the position of the agent on the edge of the disk θ_i and force angle α_i measured counterclockwise from the direction of center of the disk. $\bar{\boldsymbol{f}}_1$, $\bar{\boldsymbol{f}}_2$ are the impulsive force applied by the agents. The forces are assumed to have a fixed absolute value f ($|\bar{\boldsymbol{f}}_1| = |\bar{\boldsymbol{f}}_2| = f$). The forces give two kind of velocities to the disk. One is the angular velocity $\omega = \frac{2f}{MR}(\sin\theta_1 + \sin\theta_2)$, where R, M are radius and mass of the disk. The other is the translation velocity $\boldsymbol{v} = \frac{1}{M}(\bar{\boldsymbol{f}}_1 + \bar{\boldsymbol{f}}_2)$.

Each agent has four parameters $\{a_i, b_i, c_i, d_i\}$ to determine its final position and force angle. These parameters will be coded binary and used as chromosomes for GA. Movement from the initial position θ_i^{init} to the final position θ_i^{fin} is determined by parameters a_i and b_i:

$$\begin{cases} \theta_1^{\text{fin}} := \theta_1^{\text{init}} + a_1(\theta_2^{\text{init}} - \theta_1^{\text{init}}) + b_1, \\ \theta_2^{\text{fin}} := \theta_2^{\text{init}} + a_2(\theta_1^{\text{init}} - \theta_2^{\text{init}}) + b_2. \end{cases} \tag{1}$$

Here we assumed the agents can observe only the relative angle between them, and the positional change is determined by the observation (Figure 1 (b)). After this, each agent apply impulsive force in direction α_i, which is determined as

$$\alpha_i = xc_i + d_i, \tag{2}$$

where x is motion specification ($x = 1$ is for "rotation" and $x = -1$ for "translation" of the disk). Then the rotational and translational velocities of the disk are obtained as described before and are used for evaluating the fitness function of the agents.

It will be easily understood that the agents cannot achive the task with a same behavior, so they must emerge their different characteristics to play different roles. It means division of labor between the agents.

3 Learning method

Let us consider a population of agents with a chromosome $\{a_i, b_i, c_i, d_i\}$ which are coded binary. These parameters range over the following intervals: $a_i \in [-1, 1]$, $b_i, c_i, d_i \in [-\pi, \pi)$. We initialize all agents by assigning random values to all the parameters. We evaluate every two combination of different agents A_i, A_j, $(i \neq j)$. These two agents are set on the edge of the disk randomly and input $x = \pm 1$ is given. Then rotational velocity ω and translational velocity $\boldsymbol{v}$ is calculated as described before. The quality $F_{i,j}$ of the resulting motion is evaluated as:

$$F_{i,j} = x(\omega^2 - |\boldsymbol{v}|^2). \tag{3}$$

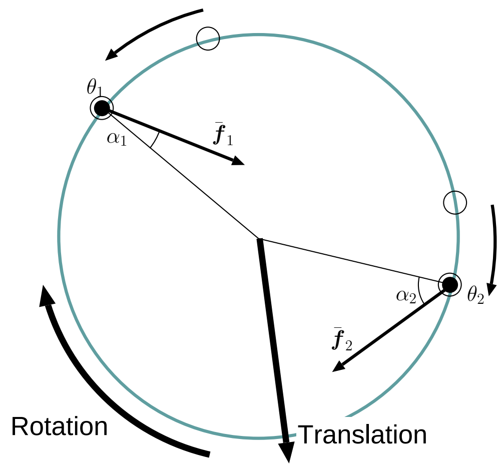

Figure 2: Action of two agents on a disk. Agents have two state variables, location angle θ_i, force angle α_i. To generate rotational or translational velocities effectively.

For this evaluation function $|\omega|$ must be maximized (minimized) and $|\boldsymbol{v}|$ minimized (maximized) when $x = 1$ ($x = -1$). This evaluation process is repeated several times with $x = 1$ and with $x = -1$ same number of times to obtain the averaged evaluation $\bar{F}_{i,j}$, which is used for evaluation of the pair of agents.

After testing all combination of agents, we define the fitness function of agent i as follows:

$$F_i = \max_j\{\bar{F}_{i,j}\}, \tag{4}$$

which is the average quality of the motion given by agent i with its best partner.

After all combination are tested, we apply the standard genetic algorithm to the population of agents. The agents, namely, is sorted according to the fitness values F_i and inferior half of the population are deleted. From the superior half of the population a pair of agents are randomly chosen for mating and two new agents are generated from the pair with crossover operation and mutation (see Figure 3). New agents are generated until the deleted population is recovered.

4 Simulation results

We set the absolute value of impulsive force $f = 1$ and moment of inertia $I = 1$ ($M = 1, R = 2$). Thus, the maximum value of two kinds of velocities are $|\omega| = 2$ and $|\boldsymbol{v}| = 2$, and the maximum evaluation value is $F_i = 4\ (= \omega_{\max}^2 = |\boldsymbol{v}|_{\max}^2)$.

In our GA, we set the parameters as follows: number of the units is 40, bit length of binary expression of

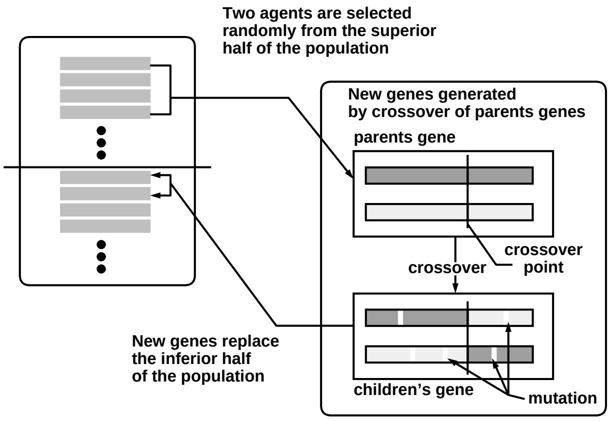

Figure 3: Genetic algorithm of parameters of the agents

each parameter is 28, mutation rate is 5%, and maximum generation is 100. Simulation results are depicted in Figures 4, 5 showing agents' behavior on the disk. An arrow in the figure corresponds to an agent. Root of the arrow represents the value (angle) of parameter b_i and the direction of the arrow represents the force angle α_i. Figure 6 shows the distribution change of (a) b_i and (b) α_i. Values of b_i clearly splits to two values with difference π corresponding to two different types necessary for effective operation.

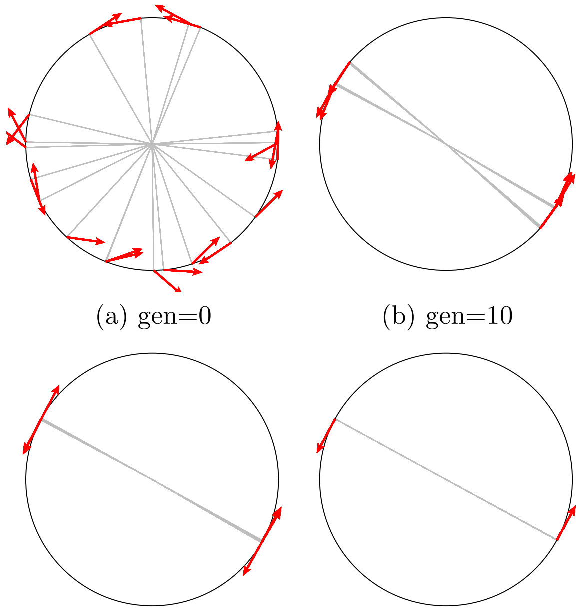

(a) gen=0 (b) gen=10 (c) gen=30 (d) gen=100

Figure 4: Position shifts b_i and force directions α_i of the agents generated in the simulation ($x = 1$, generation $0 \sim 100$).

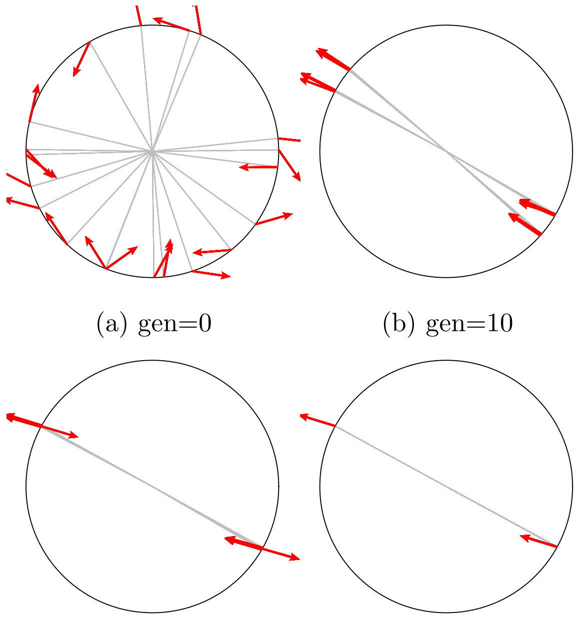

(a) gen=0 (b) gen=10 (c) gen=30 (d) gen=100

Figure 5: Position shifts b_i and force directions α_i of the agents generated in the simulation ($x = -1$, generation $0 \sim 100$).

5 Discussion

In optimal condition for disk rotation ($x = 1$), two agents are located at opposite positions on the disk edge ($\theta_1 - \theta_2 = (2n + 1)\pi$). If the final positions of the agents satisfy this condition, we can obtain the following equation from Equation (1)

$$\begin{aligned}\theta_1^{\mathrm{fin}} - \theta_2^{\mathrm{fin}} &= (\theta_1^{\mathrm{init}} - \theta_2^{\mathrm{init}})(1 - a_1 - a_2) + b_1 - b_2 \\ &= (2n - 1)\pi. \end{aligned} \tag{5}$$

To make this hold regardless of the random initial positions θ_1^{init} and θ_2^{init} the following condition is necessary and sufficient: $a_1 + a_2 = 1$ and $b_1 - b_2 = (2n + 1)\pi$. There are infinitely many solutions for these conditions also. Different values are obtained in each GA simulations. The optimal force angles for rotation ($x = 1$) are $\alpha_1 = \alpha_2 = \pm\pi/2$ (Figure 4 (d)), and the optimal force angles for translation ($x = -1$) must satisfy $\alpha_1 - \alpha_2 = (2n+1)\pi$ (Figure 5 (d)). There are infinitely many solutions for these conditions also. Different values are obtained in each GA simulations.

For disk translation ($x = -1$) only there is another solution in which two agents are located at a same

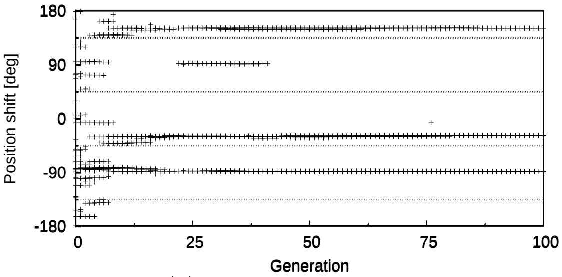

(a) Position shifts b_i

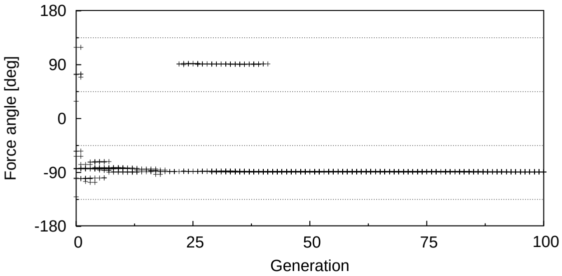

(b) Force angles $\alpha_i(= c_i + d_i)$

Figure 6: Evolution of parameters.

position and a force direction angle for both is π, but this placement is not effective for rotation. Therefore, the placement did not appear in our simulation.

Figure 4 (c) shows that in the early stage of evolution the force angles almost converged to $-\pi/2$, and then the other optimal force angle $\pi/2$ appeared and the two optimal force angles coexisted for a while, but $\pi/2$ disappeared before the 50th generation. This shows the excellent ability of this scheme to search for other optimal solutions. The ability partially comes from the definition of fitness function as the maximum of pairwise evaluations (Equation (4)). An alternative for it is the average of all the pairwise evaluations. This definition, however, might not give the scheme such ability because of the following reason. Suppose a new optimal pair of agents appear, they will not obtain higher fitness value because they cannot cooperate properly with the majority of the agents and average performance will be poor. Thus, they will be eliminated soon.

6 Conclusion

In this paper, we proposed the framework of genetic algorithm to give rise to spontaneous cooperation by division of labor. We apply this method to a simple mechanical problem of disk motion by two agents on the disk. Simulation results show emergence of optimal division of labor by the two agents.

References

[1] Toma, N., Endo, S., Yamada, K., (1998). Immune algorithms for nTSP, Bulltin of the faculty of engineering university of the ryukyus. (in Japanese)

[2] Clement, R., (2003). Multi-Agent Simulations of Evolution and Speciation in Cichlid Fish, *15th European Simulation Symposium and Exhibition ESS2003*. Delft, Holland.

[3] Edited by Davis, L., (1991). Handbook of Genetic Algorithms, *Van Nostrand Reinhold*

The Tenth International Symposium on Artificial Life and Robotics 2005(AROB 10th '05),
B-con Plaza, Beppu, Oita, Japan, February 4-6, 2005

Indication of Object Spatial Position by Finger Pointing

Masato HIRASAWA
Graduate of Mercantile Marine
Tokyo University of
Marine Science and Technology

Masaki OSHIMA
Faculty of Marine Technology
Tokyo University of
Marine Science and Technology

Tokyo-to Koto-ku Etchujima 2-1-6 〒135-8533

***Key Words*: Spatial Coordinate, Finger Pointing, Conversation, Indication**

Abstract

Human often communicate with each other by gesture for natural communication. The target of this study is to provide a technology that enables to communicate with robot by finger indication in natural way.

In order to set the direction of finger to one, at least two spatial coordinates are required on the finger. In this research, spatial coordinate is acquired using stereo method. This spatial straight line is called "Finger indication vector".

The finger area is extracted by skin color and shape feature of hand. From the area of the extracted finger, the portion of the tip of a finger and the root of a finger are made into the corresponding points.

Plane information is calculated by normal vector. And the object is pointed out by connecting intersection of finger indicated vector and object plane, and finger.

The result of experiment is shown finger indication vector run out in the portion without feature in object plane. It is shown in 3-dimensional space that the finger indication vector and object plane crossed. Even if this technique does not put on special equipment, it can presume the direction of finger, and subject is able to experiment it in free state.

1. Introduction

In order to support life and work of human, the robot that coexists with people have developed [1],[2]. Human must understand with each other for coexistence in everyday life. Human often communicate by "Hearing", "Looking", "Speaking". Study for human and robot talking communication have been done by language such as character and sound [3][4]. As oppose to this, the technology to communicate with robots have been developed by non-language such as gesture [5][6]. In order to communicate in natural, human often communicate with each other by gesture. For example, when speaker wants to take the object in the position which speaker left, he says "Please take that object to me" while it points out [7]. The system which holds a conference as if people who are present in a mutually different place meet with a same place is proposed. One of the factor reproducing presence, it is made important that enables to point out by finger through a screen. In order to communicate in natural, this also shows that finger pointing is important. It relates to this, the research which teaches objective fields and the position of the peak using the laser pointer [8], and the research which detects the gazing point from a look [9] have accomplished.

Even if it dose not use special device, if it is human, it is possible by directing the target object with finger to aim at communication. The target of this research is to provide a technology that enables to communicate with robot by finger pointing in natural way. In order to know spatial position between finger and object, hand and object are horizontally taken using stereo camera. Spatial coordinate of finger and object are acquired based on stereo photos and indication direction is appointed. And, in order to confirm validity, the experiment that directed object is made to answer computer is conducted.

2. Decision of Finger Indication Vector

2.1 Finger Indication Vector

Indication direction is conducted by attached spatial straight line on finger. In order to set the direction of finger to one, at least two spatial coordinates are required on the finger. In this research, spatial coordinate is acquired by stereo method. The direction of finger is presumed by applying straight line on these spatial coordinates. Straight line vector is calculated by formula (1). This is called "Finger Indication Vector" in this research.

$$\vec{r} = \vec{b} + t \cdot \vec{a} \qquad (1)$$

However, $\vec{a}$ and $\vec{b}$ are expressed "Finger Indication Vector", and t is expressed real number.

2.2 Acquisition of hand area

After moving object is extracted by inter-frame difference, each extracted areas are done labeling, and small areas are removed as noise. Skin color area is extracted from left-behind area and it is considered that recognized as hand area. Inter-frame difference tends to be influenced of noise, even if indoor environment. It is caused incorrect detection by sunlight and fluorescent light. If it thinks that density pattern of picture does not change, incorrect detection can be reduced by making luminosity value normalization like formula (2).

$$f_i^{'}(x,y) = \frac{f_i(x,y)}{\sqrt{\sum_{x,y}\{\overline{f_i(x,y)} - f_i(x,y)\}^2}} * k \qquad (2)$$

However $f(x,y)$ is expressed luminosity, $\overline{f(x,y)}$ is expressed average, and k is expressed real number.

Color information is changed Hue by formula (3), and skin color area is extracted. However R,G,B and $C_{\max}, C_{\min}$ are expressed color information and value of maximum or minimum into R,G,B, respectively, and H is expressed value of Hue.

$$H = \begin{cases} if \quad G = C_{\max} \\ (B-R)/(C_{\max} - C_{\min}) * 60 + 120 \end{cases}$$

$$H = \begin{cases} if \quad B = C_{\max} \\ (R-G)/(C_{\max} - C_{\min}) * 60 + 120 \end{cases} \qquad (3)$$

$$H = \begin{cases} if \quad R = C_{\max} \quad B > G \\ (G-B)/(C_{\max} - C_{\min}) * 60 + 360 \end{cases}$$

$$H = \begin{cases} if \quad R = C_{\max} \quad G > B \\ (G-B)/(C_{\max} - C_{\min}) * 60 \end{cases}$$

2.3 Determination of finger direction

The flow chart of algorithm, which determines finger direction, is shown in Fig.2. The direction of hand (horizontal or vertical) is determined by form of the rectangle of the extracted hand area. If it is in the tendency for the hand to be horizontally suitable, it scans vertically, and the number of pixels of the pixel value 255 is recorded an account for the every sequence. By the middle of scan, the boundary line of finger and back of hand is made the portion which count value changed a lot. If the hand is vertically suitable, the scanning direction is changed and it processes similarly. If difference of vertically direction and horizontally direction are not clear, it corresponds scanning aslant.

2.4 Determination of spatial coordinate on finger

Fig.1 The shape of hand

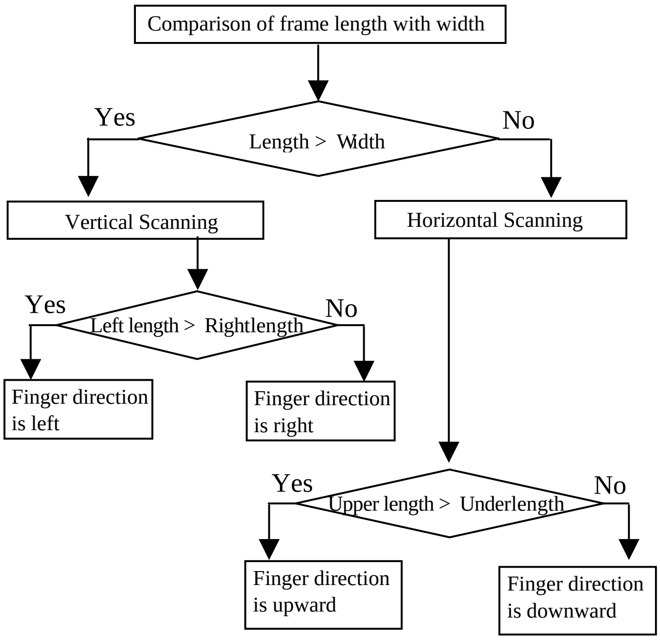

Fig.2 The flowchart of algorism

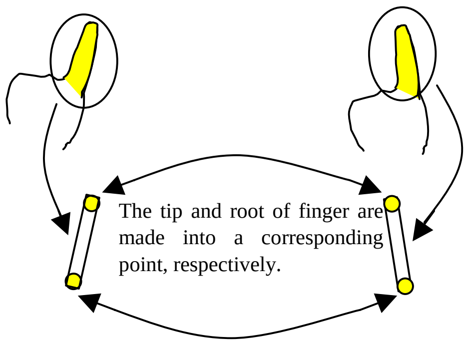

Fig.3 Extraction of correspondence points

In order to determinate direction of finger indication vector, two spatial coordinates are search on the finger. Since it calculates by stereo method, corresponding points have to be searched in the picture on either side. From the area of the extracted finger, the portion of the tip of a finger and the root of a finger are made into the corresponding points, respectively, as depicted by Fig.3. Formula (1) is calculated by searched two spatial coordinates.

Cameras are used the lens of the same characteristic and arranged it in the same height. Starting point of

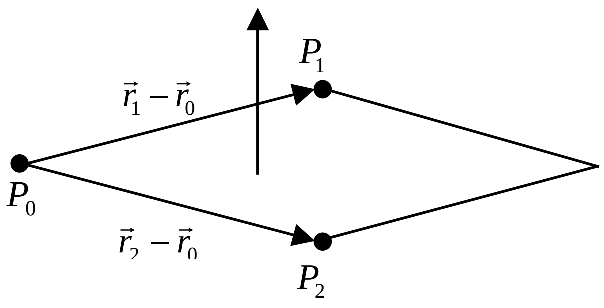

Fig.4 The Normal

spatial coordinate is taken as the position of lens on the left-hand side of a stereo camera.

3. Detection of object position

By the experiment, which searches intersection with an object plane, it shows validity of finger indication vector searched section 2. Although the plane information is able to search for also by method by reference [10], this paper presumes plane information by searching for the three spatial coordinates, which exists on the same plane (Fig.4). First, plane equation is expressed formula (4). ρ_0 is expressed normal and can calculate it like formula (5). Normal ρ is able to calculate by substituting one of value $\vec{r}_1, \vec{r}_2$ or $\vec{r}_3$. Here it is necessary to search for three spatial coordinates, which exist on the same plane. Then three feature points, such as objective edges, are extracted on the same plane. Next, three spatial points are acquired by taking correspondence between the pictures obtained from the camera on either side. Formula (6) is drawn from formula (1) and (4), coefficient can be calculated. Intersection $\vec{r}$ can be obtained by substituting for formula (1) the value calculated here. The object is pointed out by connection finger indicated vector and intersection $\vec{r}$.

$$\vec{r} \cdot \rho_0 = \rho \tag{4}$$

$$\rho_0 = \frac{(\vec{r}_2 - \vec{r}_0) \times (\vec{r}_1 - \vec{r}_0)}{\left|(\vec{r}_2 - \vec{r}_0) \times (\vec{r}_1 - \vec{r}_0)\right|} \tag{5}$$

$$t = \frac{\rho - \rho_0 \cdot \vec{b}}{\rho_0 \cdot \vec{a}} \tag{6}$$

4. The experiment

4.1 The environment of experiment

In order to discover object, the experiment about finger pointing is conclude. The picture photo by the stereo camera (3DC-2000Z SONY) is send to computer through a picture edit machine (Accom-WSD-2Xtreem NGC) , and result is outputted. An experiment is conducted so that the hand and object are taken under complicated background. Objective spatial position is acquired beforehand and memorized. The target object is premised on not changing position frequency as if home electronics. But, if a position changes, moving area is extracted and memory is updated.

4.2 Evaluation of finger pointing

The experiment for confirming the accuracy of a finger indication vector is conducted by comparing actual spatial angle with the direction of vector calculated from reproduced spatial coordinates. In the experiment, a laser pointer is fixed to a tripod and a gazing board is installed in the position 1m away from the tripod. The actual angle is determined by attaching gazing points to the interval of 5 degrees vertically, attaching to the interval of 10 agrees horizontally, and irradiating each gazing points by laser point. This state is photoed and direction vector is calculated by formula (7) and (8). Here, (X_1, Y_1, Z_1), (X_2, Y_2, Z_2) expresses there produced spatial coordinates. The graph which compared actual measurements with calculation values is shown in Fig.5.6. An actual measurement is shown in vertical axis and a calculation value is shown in horizontal axis. The graph expresses comparison with the straight line of ideal which the error of angle is 0 ° , and the straight line obtained by experiment. Moreover, the error of finger pointing of the 1[m] beyond, 5[m] beyond, and each 10[m] beyond which the error of angle of an angle brings about, is shown in Table1 and 2.

$$\vartheta = \tan^{-1}\left(\frac{X_2 - X_1}{Z_2 - Z_1}\right) \tag{7}$$ （Vertically）

$$\vartheta = \tan^{-1}\left(\frac{Y_2 - Y_1}{Z_2 - Z_1}\right) \tag{8}$$ （Horizontal）

4.3 The result of finger pointing

The result of experiment is shown in the Fig.7 and 8. Each experiment shows the result by projecting the spatial vector obtained by the formula (1) on plane coordinate. After extracting also for an intersection spatially, it is produced on plane coordinates. In this figure, finger indication vector run out in the portion without feature in object plane. It is shown in 3-dimensional space that the finger indication vector and object plane crossed. The desirable method for state that

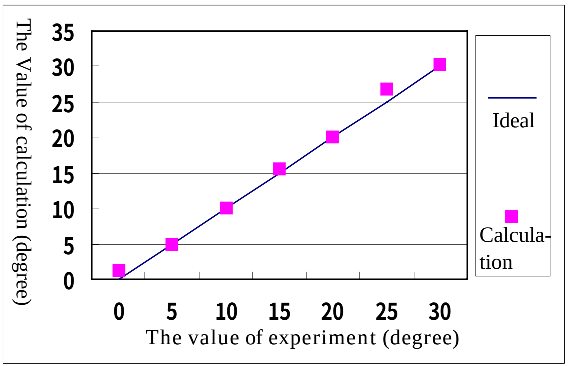

Fig.5 Calculation value and actual measurement of vertical

Table.1 Digital data of Fig.6

Actual measurement (degree)	Calculation value (degree)	Angle error (degree)	The point error of 1m beyond (mm)	The point error of 5m beyond (mm)
0	1.23	1.23	21.54	107.70
5	4.97	-0.03	-0.52	-2.62
10	9.98	-0.02	-0.38	-1.92
15	15.61	0.61	10.68	53.41
20	20.07	0.07	1.19	5.93
25	26.89	1.89	33.07	165.34
30	30.39	0.39	6.86	34.30

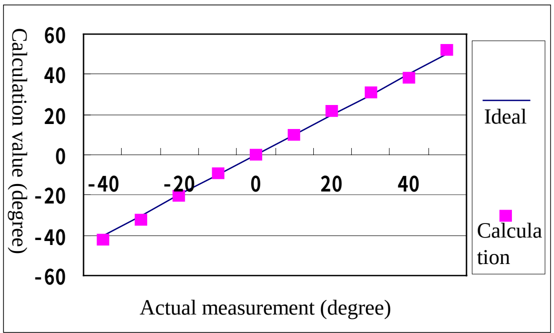

Fig.6 Calculation value and actual measurement of horizontal

Table.2 Digital data of Fig.7

Actual measurement (degree)	Calculation value (degree)	Angle error (degree)	The point error Of beyond (mm)	5m 先のポイント誤差 (mm)
-40	-42.34	-2.34	-40.86	-204.32
-30	-32.42	-2.42	-42.25	-211.22
-20	-20.21	-0.21	-3.68	-18.41
-10	-9.26	0.74	12.90	64.49
0	-0.06	-0.06	-1.01	-5.062
10	9.70	-0.31	-5.32	-26.62
20	21.89	1.89	32.91	164.56
30	31.28	1.28	22.29	111.46
40	38.53	-1.47	-25.68	-128.40
50	52.03	2.03	35.46	177.31

Fig.7 Example of pointing (TV)

Fig.8 Example of pointing (Display)

object is directed being shown is giving definition as a polyhedron using a solid modeler, and judging the interaction with the finger indication vector and object plane. Here, since it is simple, only a certain field on object is taught, only the spread range is defined, and it is considered that the object is directed only within the intersection within the limit of it.

5. Conclusion

In this report, finger indication is recognized from the picture obtained by the stereo camera, and object is directed. Even if this technique does not put on special equipment, it can presume the direction of finger, and subject is able to experiment it in free state. Position error and angle error is a maximum of 211 [mm] and 2.42 degree, respectively in the distance of 5[m] around. As a result, if it is a size like home electronics, the objective position is able to be taught. It is necessary to raise pointing accuracy so that it can presume, even if it is the small object that distance left from now on. Whether the finger is correctly suitable in the direction of objective influences evaluation greatly. As a subject, the rough instruction of "being around here generally" is also construction of a system by which information is transmitted.

Reference

[1] T.Takahashi, S.Nakanishi, Y.Kuno and Y.Shirai:" Helping

Computer Vision by Verbal and Nonverbal Communication", International Conference on Pattern Recognition, Vol.2, pp.1216-1218, 1998

[2] C.Breazeal and B.Scassellati: "How to build robots that make friends and influence people", Proc. IEEE/RSJ International. Conference. Intelligent Robots and Systems, 1999

[3] K.Shobaki, J.P.Hosom and R.A.Cole: "The OGI Kid's speech corpus and recognize" Proc. ICSLP2000, Vol.4, pp.258-261, 2000

[4] K.Ohtsuki, T.Matsuoka, S.Matsunaga and S.Furui: "Topic extraction based on continuous speech recognition in broadcast news speech", IEICE Trans. Inf. & Syst., Vol.E85-D, no.7, pp1145-1152, July, 2002

[5] V.I.Pavlovic, R.Sharma and T.S.Huang: "Visual Interpretation of Hand Gestures for Human-Computer Interaction: A Review", *IEEE Trans.Pattern Analysis and Machine Intelligence*, Vol.19, No.7, pp.677-695, 1997, 7

[6] A.Pentland: "Looking at People: Sensing for Ubiquitous and Wearable Computing", *IEEE Trans.Pattern Analysis and Machine Intelligence*, Vol.22, No.1, pp.107-119, 2000, 1

[7] O. Morikawa and T. Maesako: "HyperMirror :Toward Pleasant-to-use Video Mediated Communication System", CSCW'98, pp.149-158, 1998

[8] T.Hasegawa and S.Kameyama: "Geometric Modeling of Manipulation Environment with Interactive Teaching and Automated Accuracy Improvement", 20th Int. Symp. on Industrial Robots, pp.419-426, 1989

[9] Jacob. R: "What you look at is what you get: Eye movement-based interaction techniques", Proc. ACM CHI'90 Human Factors in Computing System Conference, pp.11-18, 1990

[10] Y. Kawai, Y. Ueshiba, T. Yoshimi and M. Oshima: "Reconstruction of 3D Objects by Integration of Multiple Range Data", ICPR(International Conference on Pattern Recognition), Hague, The Netherlands, pp.154-157, 1982, 9

The Tenth International Symposium on Artificial Life and Robotics 2005(AROB 10th '05),
B-con Plaza, Beppu, Oita, Japan, February 4-6, 2005

Accepting Powers of Four-Dimensional Alternating Turing Machines with Only Universal States

Youichirou NAKAMA[1], Makoto SAKAMOTO[1], Makoto SAITO[1], Shinya TANIGUCHI[1], Takao ITO[2], Katsushi INOUE[3], Hiroshi FURUTANI[1] and Susumu KATAYAMA[1]

[1]Dept. of Computer Science and Systems Engineering, Miyazaki University, Miyazaki 889-2192, JAPAN
[2]Dept. of Business Administration, Ube National College of Technology, Ube 755-8555, JAPAN
[3]Dept. of Computer Science and Systems Engineering, Yamaguchi University, Ube 755-8611, JAPAN

Abstract

During the past about forty years, many types of two- or three-dimensional automata have been proposed and investigated the properties of them as the computational model of pattern processing. On the other hand, recently, due to the advances in many application areas such as computer animation, motion image processing, and so on, the study of three-dimensional pattern processing with the time axis has been of crucial importance. Thus, we think that it is very useful for analyzing computation of three-dimensional pattern processing with the time axis to explicate the properties of four-dimensional automata. In this paper, we deal with four-dimensional alternating Turing machines, and investigate several accepting powers of four-dimensional alternating Turing machines which each sidelength of each input tape is equivalent.

KeyWords : alternation, configuration, four-dimensional input tape, space bound, Turing machine.

1 Introduction and Preliminaries

Blum et al. first proposed two-dimensional automata, and investigated their pattern recognition abilities in 1967 [1]. Since then, many researchers in this field have been investigating a lot of properties about automata on two- or three-dimensional tapes. In 1976, Chandra et al. introduced the concept of 'alternation'as a theoretical model of parallel computation [2]. After that, Inoue et al. introduced two-dimensional alternating Turing machines as a generalization of two-dimensional nondeterministic Turing machines and as a mechanism to model parallel computation [5]. Moreover, Sakamoto et al. presented three-dimensional alternating Turing machines in [7].

On the other hand, recently, due to the advances in many application areas such as computer animation, motion image processing, and so forth, it has become increasingly apparent that the study of four-dimensional pattern processing, i.e., three-dimensional automata with the time axis should be of crucial importance. Thus, we think that it is very useful for analyzing computation of four-dimensional pattern processing to explicate the properties of four-dimensional automata. From this viewpoint, we introduced some four-dimensional automata[6, 8].

In this paper, we continue the investigations about four-dimensional alternating Turing machines [6], and mainly investigate fundamental properties of four-dimensional alternating Turing machines with only universal states which each sidelength of each input tape is equivalent.

Let Σ be a finite set of symbols. A *four-dimensional input tape* over Σ is a four-dimensional rectangular array of elements of Σ. The set of all the four-dimensional input tapes over Σ is denoted by $\Sigma^{(4)}$. Given an input tape $x \in \Sigma^{(4)}$, for each $j(1 \leq j \leq 4)$, we let $l_j(x)$ be the length of x along the jth axis. The set of all $x \in \Sigma^{(4)}$ with $l_1(x) = m_1$, $l_2(x) = m_2$, $l_3(x) = m_3$, and $l_4(x) = m_4$ is denoted by $\Sigma^{(m_1,m_2,m_3,m_4)}$. If $1 \leq i_j \leq l_j(x)$ for each $j(1 \leq j \leq 4)$, let $x(i_1, i_2, i_3, i_4)$ denote the symbol in x with coordinates (i_1, i_2, i_3, i_4). Furthermore, we define $x[(i_1, i_2, i_3, i_4), (i'_1, i'_2, i'_3, i'_4)]$, when $1 \leq i_j \leq i'_j \leq l_j(x)$ for each integer $j(1 \leq j \leq 4)$, as the four-dimensional input tape y satisfying the following:

(i) for each $j(1 \leq j \leq 4)$, $l_j(y) = i'_j - i_j + 1$;

(ii) for each r_1, r_2, r_3, r_4 $(1 \leq r_1 \leq l_1(y), 1 \leq r_2 \leq l_2(y), 1 \leq r_3 \leq l_3(y), 1 \leq r_4 \leq l_4(y))$, $y(r_1, r_2, r_3, r_4) = x(r_1 + i_1 - 1, r_2 + i_2 - 1, r_3 + i_3 - 1, r_4 + i_4 - 1)$.

As usual, a four-dimensional input tape x over Σ is surrounded by the boundary symbols #'s ($\# \notin \Sigma$). Furthermore, four-dimensional tape is the sequence of three-dimensional rectangular arrays along the time axis. By $Cube_x(i)$ $(i \geq 1)$, we denote the ith three-dimensional rectanglar array along the time axis in $x \in \Sigma^{(4)}$ which each sidelength is equivalent.

We now recall the definition of a *four-dimensional alternating Turing machine* (4-ATM), which can be considered as an alternating version of a four-dimensional Turing machine (4-TM) [8].

4-ATM M is defined by the 7-tuple

$$M = (Q, q_0, U, F, \Sigma, \Gamma, \delta), \text{ where}$$

(1) Q is a finite set of *states*;

(2) $q_0 \in Q$ is the *initial state*;

(3) $U \subseteq Q$ is the set of *universal states*;

(4) $F \subseteq Q$ is the set of *accepting states*;

(5) Σ is a finite input alphabet ($\# \notin \Sigma$ is the *boundary symbol*);

(6) Γ is a finite *storage-tape alphabet* ($B \in \Gamma$ is the *blank symbol*), and

(7) $\delta \subseteq (Q \times (\Sigma \cup \{\#\}) \times \Gamma) \times (Q \times (\Gamma - \{B\}) \times$ {east, west, south, north, up, down, future, past, no move} $\times$ {right, left, no move}) is the *next-move relation*.

A state q in $Q - U$ is said to be *existential*. As shown in Fig. 1, the machine M has a read-only four-dimensional input tape with boundary symbols #'s and one semi-infinite storage tape, initially blank. Of course, M has a finite control, an input head, and a storage-tape head. A *position* is assigned to each cell of the read-only input tape and to each cell of the storage tape, as shown in Fig. 1. The *step* of M is similar to that of a two- or three-dimensional Turing machine [3–5, 7], except that the input head of M can move in eight directions. We say that M *accepts* the tape x if it eventually enters an accepting state. Note that the machine cannot write the blank symbol. If the input head falls off the input tape, or if the storage head falls off the storage tape (by moving left), then the machine M can make no further move.

A *seven-way four-dimensional alternating Turing machine* (SV4-ATM) is a 4-ATM whose input head can move in seven directions – east, west, south, north, up, down, or future, and an alternating version of a seven-way four-dimensional Turing machine (SV4-TM).

Let $L(m)$: $\mathbf{N} \rightarrow \mathbf{R}$ be a function with one variable m, where $\mathbf{N}$ is the set of all positive integers and $\mathbf{R}$ is the set of all nonnegative real numbers. With each 4-ATM (or SV4-ATM) M we associate a space complexity function $SPACE$ that takes configurations to

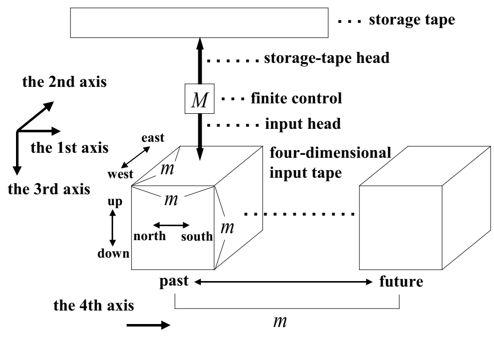

Fig. 1: Four-dimensional alternating Turing machine.

natural numbers. That is, for each configuration $c = (x, (i_1, i_2, i_3, i_4), (q, \alpha, j))$, let $SPACE(c) = |\alpha|$. M is said to be $L(m)$ *space-bounded* if for each $m \geq 1$ and for each x with $l_1(x) = l_2(x) = l_3(x) = l_4(x) = m$, if x is accepted by M, then there is an accepting computation tree of M on input x such that for each node v of the tree, $SPACE(L(v)) \leq \lceil L(m) \rceil$[1]. We denote an $L(m)$ space-bounded 4-ATM (SV4-ATM) by 4-ATM $(L(m))$ [SV4-ATM $(L(m))$].

A 4-$ATM(0)$ [SV4-$ATM(0)$] is called a four-dimensional alternating finite automaton (seven-way four-dimensional alternating finite automaton), which can be considered as an alternating version of a four-dimensional finite automaton (4-FA) (seven-way four-dimensional finite automaton (SV4-FA)), and is denoted by 4-AFA (SV4-AFA).

In order to distinguish among determinism, nondeterminism, and alternation, we denote a deterministic 3-TM [nondeterministic four-dimensional Turing machine (4-TM), deterministic seven-way four-dimensional Turing machine (SV4-TM), nondeterministic SV4-TM, deterministic 4-TM $(L(m))$, nondeterministic 4-TM $(L(m))$, deterministic SV4-TM $(L(m))$, nondeterministic SV4-TM $(L(m))$, deterministic 4-FA, nondeterministic 4-FA, deterministic SV4-FA, nondeterministic SV4-FA] by 4-DTM [4-NTM, SV4-DTM, SV4-NTM, 4-DTM $(L(m))$, 4-NTM $(L(m))$, SV4-DTM $(L(m))$, SV4-NTM $(L(m))$, 4-DFA, 4-NFA, SV4-DFA, SV4-NFA].

Let M be an automaton on a three-dimensional tape. We denote by $T(M)$ the set of all three-dimensional tapes accepted by M. As usual, for each $X \in \{D, N, A\}$, we denote, for example, by £[3-XTM] the class of sets of all the four-dimensional tapes accepted by 4-XTM's. That is, £[4-XTM] = $\{T \mid T = T(M)$ for some 4-XTM $M\}$. £[SV4-

[1] $\lceil r \rceil$ means the smallest integer greater than or equal to r.

XTM], $\pounds[4\text{-}XTM\ (L(m))]$, $\pounds[SV4\text{-}XTM\ (L(m))]$, $\pounds[4\text{-}XFA]$, and $\pounds[SV4\text{-}XFA]$ also have analogous meanings.

2 Accepting Powers of $SV4$-UTM's

We denote by $SV4$-UTM ($SV4$-UFA) an $SV4$-ATM ($SV4$-AFA) which has only universal states. For any function L: $\mathbf{N} \to \mathbf{R}$, we denote by $SV4$-UTM $(L(m))$ an $L(m)$ space-bounded $SV4$-UTM, and let $\pounds[SV4\text{-}UTM(L(m))] = \{T \mid T = T(M)$ for some $SV4$-UTM $(L(m))$ $M\}$. $\pounds[SV4\text{-}UFA]$ is defined in a similar way.

In this section, we investigate the relationship between the accepting powers of $SV4$-UTM's and $SV4$-ATM's ($SV4$-NTM's or $SV4$-DTM's).

The following lemma says that there exists a set accepted by an $SV4$-NFA, but not accepted by any $SV4$-UTM $(L(m))$ for any L such that $L(m) = o(m^3)$.

Lemma 2.1. *Let* $T_1 = \{x \in \{0,\ 1\}^{(4)} \mid \exists\ m \geq 2\ [l_1(x) = l_2(x) = l_3(x) = l_4(x) = m]\ \&\ Cube_x(1) = Cube_x(2)\}$. *Then*

(1) $\overline{T}_1 \in \pounds[SV4\text{-}NFA]$,[2] *and*

(2) $\overline{T}_1 \notin \pounds[SV4\text{-}UTM\ (L(m))]$ *for any* L: $\mathbf{N} \to \mathbf{R}$ *such that* $L(m) = o(m^3)$.

Proof: The set $\overline{T}_1$ is accepted by an $SV4$-NFA which, given an input $x \in \{0,\ 1\}^{(4)}$, simply checks by using nondeterministical states that $Cube_x(1) \neq Cube_x(2)$. It is obvious that part (1) of the lemma holds. Here, we only prove (2). Suppose that there exists an $SV4$-UTM $(L(m))$ M accepting $\overline{T}_1$, where $L(m) = o(m^3)$. Let s and r be the numbers of states (of the finite control) and storage tape symbols of M, respectively. For each $m \geq 3$, let

$$\begin{aligned} V(m) = \{x \in \{0,\ 1\}^{(4)} \mid l_1(x) = l_2(x) = l_3(x) = l_4(x) \\ = m\ \&\ Cube_x(1) = Cube_x(2) \\ \&\ x\ [(1,\ 1,\ 1,\ 3),\ (m,\ m,\ m,\ m)] \in \{0\}^{(4)}\}. \end{aligned}$$

For each x in $V(m)$, let $S(x)$ and $C(x)$ be sets of semi-configurations of M defined as follows:

$S(x) = \{((i_1,\ i_2,\ i_3,\ 2),\ (q,\ \alpha,\ j)) \mid$ there exists a computation path of M on x, $I_M(x) \vdash_M^* (x,\ ((i_1,\ i_2,\ i_3,\ 1),\ (q',\ \alpha',\ j'))) \vdash_M (x,\ ((i_1,\ i_2,\ i_3,\ 2),\ (q,\ \alpha,\ j)))$ (that is, $(x,\ ((i_1,\ i_2,\ i_3,\ 2),\ (q,\ \alpha,\ j)))$ is a configuration of M just after the input head reached $Cube_x(2))\}$,

$C(x) = \{\sigma \in S(x) \mid$ when, starting with the configuration $(x,\ \sigma)$, M proceeds to read the segment $Cube_x(2)$, there exists a sequence of steps of M in which M never enters an accepting state$\}$.

(Note that, for each x in $V(m)$, $C(x)$ is not empty since x is not in $\overline{T}_1$, and so not accepted by M.) Then the following proposition must hold.

Proposition 2.1. *For any two different tapes* x, y *in* $V(m)$, $C(x) \cap C(y) = \phi$.

[**Proof:** This proposition can be proved by the well-known technique [7]. □]

Proof of Lemma 2.1(*continued*) **:** Clearly, $|V(m)| = 2^{m^3}$ and $p(m) \leq s(m+2)^3 L(m) r^{L(m)}$, where $p(m)$ denotes the number of possible semi-configurations of M just after the input head reached the second plane of tapes in $V(m)$. Since $L(m) = o(m^3)$, we have $|V(m)| > p(m)$ for large m. Therefore, it follows that for large m there must be two different tapes x, y in $V(m)$ such that $C(x) \cap C(y) \neq \phi$. This contradicts Proposition 2.1 and completes the proof of (2). □

We need the following three lemmas. The proof of the following lemmas is omitted here since it is similar to that of Lemma 2.1.

Lemma 2.2. *Let* $T_2 = \{x \in \{0,\ 1\}^{(4)} \mid \exists\ m \geq 1\ [l_1(x) = l_2(x) = l_3(x) = l_4(x) = 2m\ \&\ x\ [(1,\ 1,\ 1,\ 1),\ (2m,\ 2m,\ 2m,\ m)] = x\ [(1,\ 1,\ 1,\ m+1),\ (2m,\ 2m,\ 2m,\ 2m)]]\}$. *Then*

(1) $\overline{T}_2 \in \pounds[SV4\text{-}NTM\ (\log m)]$, *and*

(2) $\overline{T}_2 \notin \pounds[SV4\text{-}UTM\ (L(m))]$ *for any* L: $\mathbf{N} \to \mathbf{R}$ *such that* $L(m) = o(m^4)$.

Lemma 2.3. *Let* T_2 *be the set described in Lemma* 2.1. *Then*

(1) $T_1 \in \pounds[SV4\text{-}UFA]$, *and*

(2) $T_1 \notin \pounds[SV4\text{-}NTM\ (L(m))]$ *for any* L: $\mathbf{N} \to \mathbf{R}$ *such that* $L(m) = o(m^3)$.

Lemma 2.4. *Let* T_2 *be the set described in Lemma* 2.2. *Then*

(1) $T_2 \in \pounds[SV4\text{-}UTM\ (\log m)]$, *and*

(2) $T_2 \notin \pounds[SV4\text{-}NTM\ (L(m))]$ *for any* L: $\mathbf{N} \to \mathbf{R}$ *such that* $L(m) = o(m^4)$.

From Lemmas 2.1–2.4, we can get

Theorem 2.1. *Let* L: $\mathbf{N} \to \mathbf{R}$ *be a function such that* (i) $L(m) = o(m^2)$, *or* (ii) $L(m) \geq \log m$ $(m \geq 1)$ *and* $L(m) = o(m^4)$. *Then*

(1) $\pounds[SV4\text{-}UTM\ (L(m))] \subsetneq \pounds[SV4\text{-}ATM\ (L(m))]$,

[2]If $T \subseteq \Sigma^{(4)}$, then define $\overline{T} = \Sigma^{(4)} - T$.

(2) $\pounds[SV4\text{-}UTM\ (L(m))]$ *is incomparable with* $\pounds[SV4\text{-}NTM\ (L(m))]$, *and*

(3) $\pounds[SV4\text{-}DTM\ (L(m))] \subsetneq \pounds[SV4\text{-}UTM\ (L(m))]$.

Corollary 2.1. (1) $\pounds[SV4\text{-}UFA] \subsetneq \pounds[SV4\text{-}AFA]$. (2) $\pounds[SV4\text{-}UFA]$ *is incomparable with* $\pounds[SV4\text{-}NFA]$. (3) $\pounds[SV4\text{-}DFA] \subsetneq \pounds[SV4\text{-}UFA]$.

It is natural to ask how much space is necessary and sufficient for $SV4\text{-}DTM$'s and $SV4\text{-}NTM$'s to simulate $SV4\text{-}UFA$'s. The following theorem answers this question.

THEOREM 2.2. (1) $\pounds[SV4\text{-}UFA] \subsetneq \pounds[SV4\text{-}DTM\ (m^3)]$. (2) m^3 *space is necessary and sufficient for* $SV4\text{-}DTM$'s *and* $SV4\text{-}NTM$'s *to simulate* $SV4\text{-}UFA$'s.

Moreover, by using a technique similar to that in the proof of Theorem 3.2 in [2], we can get the following theorem.

THEOREM 2.3. m^4 *space is necessary and sufficient for* $SV4\text{-}DTM$'s *to simulate* $SV4\text{-}AFA$'s *and* $4\text{-}AFA$'s.

3 Accepting Powers of 4-UTM's

We denote by $4\text{-}UTM$ ($4\text{-}UFA$) a $4\text{-}ATM$ ($4\text{-}AFA$) which has only universal states. For any function L: $\mathbf{N} \to \mathbf{R}$, we denote by $4\text{-}UTM\ (L(m))$ an $L(m)$ space-bounded $4\text{-}UTM$, and let $\pounds[4\text{-}UTM\ (L(m))] = \{T \mid T = T(M)$ for some $4\text{-}UTM\ (L(m))\ M\}$. $\pounds[4\text{-}UFA]$ is defined in a similar way. This section first investigates a relationship between the accepting powers of $4\text{-}UTM$'s and $4\text{-}ATM$'s ($4\text{-}NTM$'s or $4\text{-}DTM$'s).

From Lemma 5.2 in [7], we can get the following results.

Theorem 3.1. *Let* L: $\mathbf{N} \to \mathbf{R}$ *be a function such that* $L(m) = o(\log m)$. *Then,* $\pounds[4\text{-}DTM\ (L(m))] \subsetneq \pounds[4\text{-}UTM\ (L(m))] \subsetneq \pounds[4\text{-}ATM\ (L(m))]$.

Corollary 3.1. $\pounds[4\text{-}DFA] \subsetneq \pounds[4\text{-}UFA] \subsetneq \pounds[4\text{-}AFA]$.

We then investigate relationships between the accepting powers of eight-way and seven-way four-dimensional machines. By using the same way as in the proof of Theorems 2.1–2.3, we can get the following results.

Theorem 3.2. *Let* L: $\mathbf{N} \to \mathbf{R}$ *be a function such that* (i) $L(m)^3 = o(m^3)$, *or* (ii) $L(m) \geq \log m$ $(m \geq 1)$ and $L(m) = o(m^4)$. *Then,* $\pounds[SV4\text{-}UTM\ (L(m))] \subsetneq \pounds[4\text{-}UTM\ (L(m))]$.

Corollary 3.2. $\pounds[SV4\text{-}UFA] \subsetneq \pounds[4\text{-}UFA]$.

Theorem 3.3. (1) $\pounds[4\text{-}UFA] \subsetneq \pounds[SV4\text{-}DTM\ (m^4)]$, *and* (2) m^4 *space is necessary and sufficient for* $SV4\text{-}DTM$'s *to simulate* $4\text{-}UFA$'s.

4 Conclusion

In this paper, we investigated the accepting powers of four-dimensional alternating Turing machines with only universal states which each sidelength of each input tape is equivalent.

Let T_c be the set of all the four-dimensional connected tapes. If T_c is accepted by four-dimensional alternating Turing machines with only universal states, it will be interesting to investigate how much space is necessary and sufficient for four-dimensional alternating Turing machines with only universal states to accept T_c.

References

[1] M. Blum et al., *IEEE Symposium on Switching and Automata Theory* :155-160(1967).

[2] A. K. Chandra et al., *J. ACM* 28(1):114-133 (1981).

[3] J. E. Hopcroft et al., *J. Assoc. Comput. Mach.* 16:168-177 (1969).

[4] J. E. Hopcroft et al., *Introduction to Automata Theory, Languages, and Computation*, Addison-Wesley, Reading, MA, (1979).

[5] K. Inoue et al., *Theoret. Comput. Sci.* 27:61-83 (1983).

[6] H. Okabe et al., *Proc. 7th Words Multiconf. on SCI* :241-246 (2003).

[7] M. Sakamoto et al., *Inform. Sci.* 72:225-249 (1993).

[8] M. Sakamoto et al., *WSEAS Trans. on Computers*, Issue 5, Vol. 3 :1651-1656 (2004).

[9] H. Taniguchi et al., *Inform. Sci.* 26:65-85 (1982).

The Tenth International Symposium on Artificial Life and Robotics 2005(AROB 10th '05),
B-con Plaza, Beppu, Oita, Japan, February 4-6, 2005

Some Properties of Four-Dimensional Multicounter Automata

Makoto SAITO[1], Makoto SAKAMOTO[1], Youichirou NAKAMA[1], Takao ITO[2], Katsushi INOUE[3], Hiroshi FURUTANI[1] and Susumu KATAYAMA[1]

[1] Dept. of Computer Science and Systems Engineering, University of Miyazaki, Miyazaki 889-2192, JAPAN
[2] Dept. of Business Administration, Ube National College of Technology, Ube 755-8555, JAPAN
[3] Dept. of Computer Science and Systems Engineering, Yamaguchi University, Ube 755-8611, JAPAN

Abstract

Recently, due to the advances in many application areas such as computer animation, motion image processing, and so forth, it has become increasingly apparent that the study of four-dimensional pattern processing has been of crucial importance. Thus, we think that the research of four-dimansional automata as a computational model of four-dimensional pattern processing has also been meaningful. This paper introduces four-dimensional multicounter automata, and investigates some their properties. We show the differences between the accepting powers of seven-way and eight-way four-dimensional multicounter automata, and between the accepting powers of deterministic and nondeterministic seven-way four-dimensional multicounter automata.

Key Words **:** computational complexity, four-dimensional automaton, multicounter, nondeterminism.

1 Introduction and Preliminaries

Inoue et al. [5] introduced a two-dimensional multicounter automaton and investigated its basic properties. Szepietowski also investigated some of its properties [10]. A two-dimensional k-counter automaton M is a two-dimensional finite automaton [1] that has k counters. The action of M is similar to that of the one-dimensional off-line k-counter machine [3], except that the input head of M can move up, down, right, or left on a two-dimensional input tape. In [7], Sakamoto et al. introduced multicounter automata on three-dimensional input tapes.

By the way, during the past about forty years, several automata on two- or three-dimensional tapes have been proposed and many properties of them have been obtained [6,8]. On the other hand, recently, due to the advances in computer animation, motion image processing, and so on, the study of four-dimensional information processing has been of great importance. Thus, we think that the study of four-dimensional automata has been meaningful as the computational model of four-dimensional information processing [9].

In this paper, we introduce and investigate about eight-way four-dimensional multicounter automata as new four-dimensional computational models. An eight-way four-dimensional k-counter automaton (4-kCA), which consists of a finite control, k counters, a read-only four-dimensional input tape, k counter heads, and an input head which can move in eight directions — north, east, south, west, up, down, future or past. In general, when we must think about the algorithm of four-dimensional pattern processing by using the restricted computational resources, if the algorithm is fine in spite of its restricted computational resources, it will be valued highly. It is the same with automata theory. So we next introduce and investigate a seven-way four-dimensional k-counter automaton ($SV4$-kCA) which is a restricted type of 4-kCA. $SV4$-kCA is a 4-kCA whose input head can move in seven directions — north, east, south, west, up, down, or future. In this paper, we let each sidelength of each input tape of these automata be equivalent in order to increase the theoretical interest.

Let Σ be a finite set of symbols. *A four-dimensional tape* over Σ is a four-dimensional rectangular array of elements of Σ. The set of all the four-dimensional tapes over Σ is denoted by $\Sigma^{(4)}$.

Given a tape $x \in \Sigma^{(4)}$, for each $j (1 \leq j \leq 4)$, we let $l_j(x)$ be the length of x along the jth axis. The set of all $x \in \Sigma^{(4)}$ with $l_1(x) = m_1,\ l_2(x) = m_2,\ l_3(x) = m_3$, and $l_4(x) = m_4$ is denoted by $\Sigma^{(m_1,m_2,m_3,m_4)}$. When $1 \leq j_i \leq l_j(x)$ for each $j(1 \leq j \leq 4)$, let $x(i_1, i_2, i_3, i_4)$ denote the symbol in x with coordinates (i_1, i_2, i_3, i_4). Furthermore, we define

$$x[(i_1, i_2, i_3, i_4), (i'_1, i'_2, i'_3, i'_4)],$$

when $1 \leq i_j \leq i'_j \leq l_j(x)$ for each integer $j(1 \leq j \leq 4)$, as the four-dimensional tape y satisfying the following (i) and (ii) :

(i) for each $j(1 \leq j \leq 4)$, $l_j(y) = i'_j - i_j + 1$;

(ii) for each r_1, r_2, r_3, r_4 $(1 \leq r_1 \leq l_1(y), 1 \leq r_2 \leq l_2(y), 1 \leq r_3 \leq l_3(y), 1 \leq r_4 \leq l_4(y))$, $y(r_1, r_2, r_3, r_4) = x(r_1 + i_1 - 1, r_2 + i_2 - 1, r_3 + i_3 - 1, r_4 + i_4 - 1)$.

Four-dimensional tape is the sequence of three-dimensional rectangular arrays along the time axis. By $Cube_x(i)$ $(i \leq 1)$, we denote the ith three-dimensional rectangular array along the time axis in a tape $x \in \Sigma^{(4)}$ which each sidelength is equivalent.

We now introduce a seven- or eight-way four-dimensional multicounter automaton. An *eight-way four-dimensional k-counter automaton* (4-kCA) M, $k \geq 1$, has a read-only four-dimensional input tape surrounded by *boundary symbols* $\sharp$'s and k *counters*. (Of course, M has a *finite control*, an *input head*, and k *counter heads*.) The action of M is similar to that of the two- or three-dimensional multicounter automaton [5, 7, 10], except that the input head of M can move in eight directions — east, west, south, north, up, down, future, or past. That is, when an input tape $x \in \Sigma^{(4)}$ (where Σ is the set of input symbols of M and the boundary symbol $\sharp$'s is not in Σ) is presented to M, M determines the next state of the finite control, the move direction (east, west, south, north, up, down, future, past, or no move) of the input head, and the move direction (right, left, or no move) of each counter head, depending on the present state of the finite control, the symbol read by the input head, and whether or not the contents of each counter is zero (i.e., whether or not each counter head is on the bottom symbol Z_0 of the counter). If the input head falls off the tape x with boundary symbols, M can make no further move. M starts in its initial state, with the input head on position (1,1,1,1) of the tape x, and with the contents of each counter zero (i.e., with each counter on the bottom symbol Z_0 of the counter). We say that M *accepts* the tape x if M eventually halts in a specified state (accepting state) on the bottom boundary symbol $\sharp$ of the input. We denote by $T(M)$ the set of all the four-dimensional tapes accepted by M. A *seven-way four-dimensional k-counter automaton* ($SV4$-kCA) is a 4-kCA whose input head can move in seven directions — east, west, south, north, up, down, or future (see Fig.1).

Let $L(m) : \mathbf{N} \mapsto \mathbf{N}$ (where $\mathbf{N}$ is the set of all the positive integers) be a function with one variable m. A 4-kCA ($SV4$-kCA) M is said to be $L(m)$ *counter-bounded* if for each $m \geq 1$ and each input tape x (accepted by M) with $l_1(x) = l_2(x) = l_3(x) = l_4(x) = m$, the length of each counter of M is bounded by $L(m)$. As usual, we define nondeterministic and deterministic 4-kCA's ($SV4$-kCA's). By $N4$-$kCA(L(m))$ (respectively, $D4$-$kCA(L(m))$, $NSV4$-$kCA(L(m))$, and $DSV4$-$kCA(L(m))$), we denote a nondeterministic 4-kCA (respectively, deterministic 4-kCA, nondeterministic $SV4$-kCA, and deterministic $SV4$-kCA) whose each sidelength of each input tape is equivalent and which is $L(m)$ counter-bounded. Let $\mathcal{L}[N4\text{-}kCA(L(m))] = \{T \mid T = T(M)$ *for some* $N4\text{-}kCA(L(m))$ $M\}$. $\mathcal{L}[N4\text{-}kCA(L(m))]$, $\mathcal{L}[NSV4\text{-}kCA(L(m))]$, and $\mathcal{L}[DSV4\text{-}kCA(L(m))]$ have similar meanings.

We briefly recall *seven-way four-dimensional Turing machines* [9]. A seven-way four-dimensional Turing machine M has a read-only four-dimensional input tape with boundary symbols $\sharp's$ and one semiinfinite *storage tape*. (Of course, M has a *finite control*, an *input head*, and a *storage-tape head*.) The action of M is similar to that of the two- or three-dimensional Turing machine [6,8] which has a read-only input tape with boundary symbols $\sharp's$ and one semiinfinite storage tape, except that the input head of M can move in seven directions — east, west, south, north, up, down, or future. M starts in its initial state, with the input head on position $(1,1,1,1)$ of an input tape x, and with all the cells of the storage tape blank. We say that M *accepts* the tape x if M eventually halts in an accepting state. Let $L(m) : \mathbf{N} \mapsto \mathbf{N}$ be a function with one variable m. By $NSV4\text{-}TM(L(m))$ ($DSV4\text{-}TM(L(m))$) we denote a nondeterministic (deterministic) seven-way four-dimensional Turing machine whose each side-length of each input tape is equivalent and which does not scan more than $L(m)$ cells on the storage tape for any input tape x (accepted by M) with $l_1(x) = l_2(x) = l_3(x) = l_4(x) = m$. Let $\mathcal{L}[NSV4\text{-}TM(L(m))]$ ($\mathcal{L}[DSV4\text{-}TM(L(m))]$) denote the class of sets accepted by $NSV4\text{-}TM(L(m))$'s ($DSV4\text{-}TM(L(M))$'s).

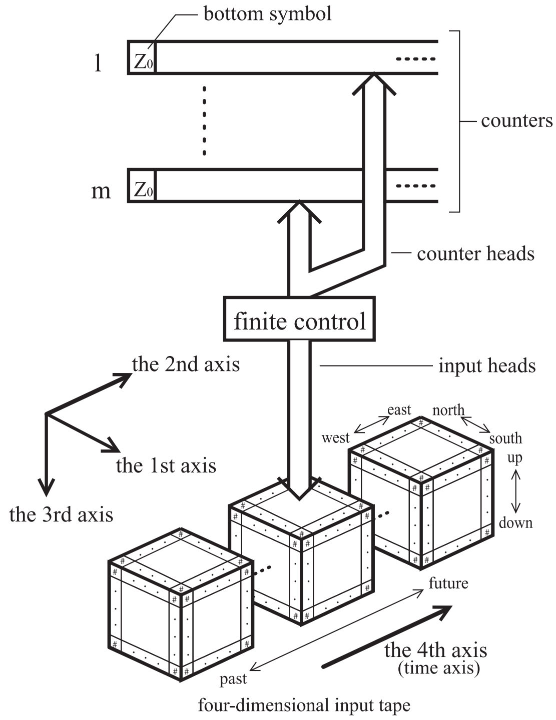

Fig. 1: Four-dimensional k-counter automaton.

We denote a nondeterministic (deterministic) four-dimensional finite automaton by $N4$-FA ($D4$-FA). A seven-way $N4$-FA (seven-way $D4$-FA) is an $N4$-FA ($D4$-FA) whose input tape head can move in seven directions — east, west, south, north, up, down, or future. By $N4$-FA ($D4$-FA, $NSV4$-FA, $DSV4$-FA) we denote an $N4$-FA ($D4$-FA, seven-way $N4$-FA, seven-way $D4$-FA) whose each sidelength of each input tape is equivalent [9]. For example, let $\mathcal{L}[D4\text{-}FA]$ denote the class of sets accepted by $D4$-FA's. As is easily seen, it follows that for any constant k, $\mathcal{L}[D4\text{-}FA] = \mathcal{L}[D4\text{-}1CA(k)]$, $\mathcal{L}[DSV4\text{-}FA] = \mathcal{L}[DSV4\text{-}1CA(k)]$, and so on.

We conclude this section by giving a relationship between seven-way four-dimensional multicounter automata and seven-way four-dimensional Turing machines, which will be used in the latter sections.

[Theorem 1.1]

(1) $\bigcup_{1\le k<\infty} \mathcal{L}[XSV4\text{-}kCA(L(m))] \subseteq \mathcal{L}[XSV4\text{-}TM(\log L(m))]$ *for any* $L(m) : \mathbf{N} \mapsto \mathbf{N}$ *and any* $X \in \{D, N\}$,

(2) $\bigcup_{1\le k<\infty} \mathcal{L}[XSV4\text{-}kCA(m)] = \mathcal{L}[XSV4\text{-}TM(\log m)]$ *for any* $X \in \{D, N\}$.

(**Proof**) (1) : Let M be an $XSV4\text{-}kCA(L(m))$. The set $T(M)$ is also accepted by the $XSV4\text{-}TM(\log L(m))$ which divides the storage tape into k tracks and makes each track play a role of the corresponding counter of M.

(2) : From (1), $\bigcup_{1\le k<\infty} \mathcal{L}\ [XSV4\text{-}kCA(m)] \subseteq \mathcal{L}[XSV4\text{-}TM(\log m)]$. It is well known that any $\log m$ tape-bounded one-dimensional off-line Turing machine can be simulated by a one-dimensional two-way multihead finite automaton [4]. By using the same argument as in the proof of this fact, we can easily show that any $XSV4\text{-}TM(\log m)$ can be simulated by an $XSV4\text{-}kCA(m)$ for some $k \ge 1$. Thus $\mathcal{L}[XSV4\text{-}TM(\log m)] \subseteq \bigcup_{1\le k<\infty} \mathcal{L}[XSV4\text{-}kCA(m)]$. □

2 Seven-Way versus Eight-Way

In this section, we investigate the difference between the accepting powers of counter-bounded eight-way and seven-way four-dimensional multicounter automata.

We need the following two lemmas.

[Lemma 2.1] *Let* $T_1 = \{x \in \{0,1\}^{(4)} \mid \exists m \ge 2\ [\ l_1(x) = l_2(x) = l_3(x) = l_4(x) = m]\ \&\ Cube_x(1) = Cube_x(2)\}$, *and let* $L_1(m) : \boldsymbol{N} \mapsto \mathbf{N}$ *be a function such that* $\lim_{m\to\infty} [(\log L_1(m))/m^3] = 0$. *Then,*

(1) $T_1 \in \mathcal{L}[D4\text{-}FA]$, *and*

(2) $T_1 \notin \bigcup_{1\le k<\infty} \mathcal{L}[NSV4\text{-}kCA(L_1(m))]$.

(**proof**) The proof of (1) is omitted here, since it is obvious. We now prove (2). Suppose that there is an $NSV4\text{-}TM(L_1'(m))$ M accepting T_1, where $L_1'(m) : \mathbf{N} \mapsto \mathbf{N}$ is a function such that $\lim_{m\to\infty} [L_1'(m)/m^3] = 0$. For each $m \ge 3$, let

$$V(m) = \{x \in T_1 \mid l_1(x) = l_2(x) = l_3(x) = l_4(x) = m \ \&\ x[(1,1,1,3),(m,m,m,m)] \in \{0\}^{(4)}\}.$$

Clearly, each tape in $V(m)$ is accepted by M. For any (seven-way) four-dimensional Turing machine M, we define the *configuration* of M to be a combination of the (1) state of the finite control, (2) position of the input head within the input tape, (3) position of the storage-tape head within the nonblank portion of the storage tape, and (4) contents of the storage tape. For each $x \in V(m)$, let $conf(x)$ be the set of configurations of M just after the point, in the accepting computations on x, where the input head left the first cube of x. Then the following proposition must hold.

[Proposition 2.1] *For any two different tapes* $x, y \in V(m)$,

$$conf(x) \cap conf(y) = \phi \ (\textit{empty set}).$$

(**Proof**) Suppose that $conf(x) \cap conf(y) \ne \phi$ and $\sigma \in conf(x) \cap conf(y)$. It is obvious that if, starting with this configuration σ, the input head proceeds to read the $[(1,1,1,2),(m,m,m,m)]$-segment of x, then M could enter an accepting state. Therefore, by assumption, it follows that the tape $z[\ l_1(z) = l_2(z) = l_3(z) = l_4(z) = m]$ satisfying the following two conditions must be also accepted by M: (i) $z[(1,1,1,1),(m,m,m,1)] = y[(1,1,1,1),(m,m,m,1)]$; (ii) $z[(1,1,1,2),(m,m,m,m)] = x[(1,1,1,2),(m,m,m,m)]$. This contradicts the fact that z is not in T_1. □

(**Proof of Lemma 2.1** (*continued*)) Clearly, $|V(m)| = 2^{m^3}$, where for any set S, $|S|$ denotes the number of elements of S. Let $c(m)$ be the number of possible configurations of M just after the input head left the first cube of tapes in $V(m)$. Then

$$c(m) \le s(m+2)^3 L_1'(m) t^{L_1'(m)}.$$

(The factor s is the number of possible states of finite control, $(m+2)^3$ is the number of possible positions of the input head, $L_1'(m)$ is the number of possible positions of the storage-tape head, t is the number of storage-tape symbols, and $t^{L_1'(m)}$ is the number of possible contents of the nonblank portion of storage tape.) Since $\lim_{m\to\infty} [L_1'(m)/m^3] = 0$, we have

$$|V(m)| > c(m) \text{ for large } m.$$

Therefore, it follows that for large m there must be different tapes $x, y \in V(m)$ such that $conf(x) \cap conf(y) \ne \phi$. This contradicts Proposition 2.1, and thus T_1 is not in $\mathcal{L}[NSV4\text{-}TM(L_1'(m))]$, where $L_1'(m) : \mathbf{N} \mapsto \mathbf{N}$ is a function such that $\lim_{m\to\infty} [L_1'(m)/m^3] = 0$. From this result and from the condition that $\lim_{m\to\infty} [(\log L_1(m))/m^3] = 0$, it follows that T_1 is not in $\mathcal{L}[NSV4\text{-}TM(\log L_1(m))]$. Part (2) of the lemma follows from this fact and Theorem 1.1 (1). □

[Lemma 2.2] *Let* $T_2 = \{x \in \{0,1\}^{(4)} \mid \exists m \ge 1\ [\ l_1(x) = l_2(x) = l_3(x) = l_4(x) = 2m\ \ \&\ \ x[(1,1,1,1),(2m,2m,2m,m)] = x[(1,1,1,m+1),(2m,2m,2m,2m)]$ (*that is, the top and bottom halves of* x *are identical*)]}, *and let* $L_2(m) : \mathbf{N} \mapsto \mathbf{N}$ *be a function such that* $\lim_{m\to\infty}[(\log L_2(m))/m^4] = 0$. *Then,*

(1) $T_2 \in \mathcal{L}[D4\text{-}1CA(m)]$, *and*

(2) $T_2 \notin \bigcup_{1\le k<\infty} \mathcal{L}[NSV4\text{-}kCA(L_2(m))]$.

(Proof) The proof of Part (1) is omitted here, since it is obvious. Part (2) is given by using the same technique as in the proof of Lemma 2.1 (2). □

From Lemmas 2.1 and 2.2, we can get the following theorem.

[Theorem 2.1] (1) *Let* $L(m) : \mathbf{N} \mapsto \mathbf{N}$ *be a function such that* $\lim_{m\to\infty}[(\log L(m))/m^3] = 0$. *Then,* $\mathcal{L}[D4\text{-}FA] - \bigcup_{1\le k<\infty} \mathcal{L}[NSV4\text{-}kCA(L(m))] \ne \phi$. (2) *Let* $L'(m) : \mathbf{N} \mapsto \mathbf{N}$ *be a function such that* $\lim_{m\to\infty}[(\log L'(m))/m^4] = 0$. *then,* $\mathcal{L}[D4\text{-}1CA(m)] - \bigcup_{1\le k<\infty} \mathcal{L}[NSV4\text{-}kCA(L'(m))] \ne \phi$.

3 Nondeterminism versus Determinism

In this section, we investigate the difference between the accepting powers of counter-bounded deterministic and nondeterministic seven-way four-dimensional multicounter automata.

We need the following two lemmas. The proof of the following lemmas is omitted here since it is similar to that of Lemma 2.1.

[Lemma 3.1] *Let* $T_3 = \{x \in \{0,1\}^{(4)} \mid \exists m \ge 2\ [\, l_1(x) = l_2(x) = l_3(x) = l_4(x) = m] \ \&\ Cube_x(1) \ne Cube_x(2)\}$, *and* $L_1(m) : \mathbf{N} \mapsto \mathbf{N}$ *be a function such that* $\lim_{m\to\infty}[(\log L_1(m))/m^3] = 0$. *Then,*

(1) $T_3 \in \mathcal{L}[NSV4\text{-}FA]$, *and*

(2) $T_3 \notin \bigcup_{1\le k<\infty} \mathcal{L}[DSV4\text{-}kCA(L_1(m))]$.

[Lemma 3.2] *Let* $T_4 = \{x \in \{0,1\}^{(4)} \mid \exists m \ge 2\ [\, l_1(x) = l_2(x) = l_3(x) = l_4(x) = 2m \ \&\ x[(1,1,1,1),(2m,2m,2m,m)] \ne x[(1,1,1,m+1),(2m,2m,2m,2m)]]\}$, *and let* $L_2(m) : \mathbf{N} \mapsto \mathbf{N}$ *be a function such that* $\lim_{m\to\infty}[(\log L_2(m))/m^4] = 0$. *Then,*

(1) $T_4 \in \mathcal{L}[NSV4\text{-}1CA(m)]$, *and*

(2) $T_4 \notin \bigcup_{1\le k<\infty} \mathcal{L}[DSV4\text{-}kCA(L_2(m))]$.

From Lemmas 3.1 and 3.2, we can get the following theorem.

[Theorem 3.1] (1) *Let* $L(m) : \mathbf{N} \mapsto \mathbf{N}$ *be a function such that* $\lim_{m\to\infty}[(\log L(m))/m^3] = 0$. *Then,* $\mathcal{L}[NSV4\text{-}FA] - \bigcup_{1\le k<\infty} \mathcal{L}[DSV4\text{-}kCA(L(m))] \ne \phi$. (2) *Let* $L'(m) : \mathbf{N} \mapsto \mathbf{N}$ *be a function such that* $\lim_{m\to\infty}[(\log L'(m))/m^4] = 0$. *Then,* $\mathcal{L}[NSV4\text{-}1CA(m)] - \bigcup_{1\le k<\infty} \mathcal{L}[DSV4\text{-}kCA(L'(m))] \ne \phi$.

4 Conclusion

In this paper, we introduced four-dimensional multicounter automata, and we investigated the accepting powers of counter-bounded seven-way and eight-way four-dimensional multicounter automata. Then, we investigated a relationship between determinism and nondeterminism. In these subjects, we stated only for four-dimensional input tape which each sidelength is equivalent.

It will be also interesting to investigate the accepting powers of 'alternating' four-dimensional multicounter automata (see [2] for the concept of 'alternation').

References

[1] M.Blum et al., Automata on a two-dimensional tape, *in IEEE Symposium of Switching and Automata Theory*, pp. 155–160 (1967).

[2] A.K.Chandra et al., Alternation, *J.ACM*, Vol. 28, No. 1 pp. 114–133 (1981).

[3] S.A.Greibach, Remarks on the complexity of nondeterministic counter languages, *Theoretical Computer Science*, Vol. 1, pp. 269–288 (1976).

[4] J.Hartmanis, On non-determinancy in simple computing devices, *Acta Informatica*, Vol. 1, pp. 336–344 (1972).

[5] K.Inoue et al., Three-way two-dimensional multicounter automata, *Information Sciences*, Vol. 19, pp. 1–20 (1979).

[6] K.Inoue et al., A survey of two-dimensional automata Theory, *Information Sciences*, Vol. 55, pp. 99–121 (1991).

[7] M.Sakamoto et al., Three-dimensional Multicounter Automata, *in Proceedings of the 6th International Workshops on Parallel Image Processing and Analysis*, pp. 267–280 (1999).

[8] M.Sakamoto, Three-Dimensional Alternating Turing Machines, *Ph.D. Thesis, Yamaguchi Univ.* (1999).

[9] M.Sakamoto et al., A note on Four-dimensional Finite automata, *WSEAS Trans. on Computers*, Issue 5, Vol. 3, pp. 1651–1656 (2004).

[10] A.Szepietowski, On three-way two-dimensional multicounter automata, *Information Sciences*, Vol. 55, pp. 35–47 (1991).

The Tenth International Symposium on Artificial Life and Robotics 2005(AROB 10th '05),
B-con Plaza, Beppu, Oita, Japan, February 4-6, 2005

Simulation Study for Intelligent Wheelchair Vehicle with Ultrasonic and Infrared Sensors

Kouichi Kamimura*, Takahiro Kai*, Masahiro Yokomichi* and Tetsuro Kitazoe**
* Faculty of Engineering, University of Miyazaki **International University of Kagoshima
Gakuen Kibanadai Nishi 1-1, Miyazaki City, Japan, 889-2192
kai@cs.miyazaki-u.ac.jp

Abstract

In this paper, we propose wheelchair navigation system with infrared sensors and ultrasonic sensors to aid senior people and the handicapped to drive a wheelchair. We consider neural network to connect input sensor signals and output wheel speed. To get nice wheelchair controller, we constructed wheelchair simulator and applied G.A. for synaptic couplings in the neural networks. We investigated that a wheelchair controlled by this system ran safely and comfortably.

1 Introduction

Recently, many people have been researching autonomous mobile robots extensively. The purpose of these researches is to build the robots that are able to run safely in unknown or dynamically changing environments. In order to perceive the surrounding environments, robots mount many kinds of sensors, e.g., infrared sensors, ultrasonic range sensors and CCD cameras.

There is a growing demand for more safe and comfortable wheelchairs as mobile aids, as the population of senior people has been increasing. There are two research issues with these wheelchairs. One is autonomous (or semi-autonomous) and safe navigation, such as avoiding obstacles, wall following, going to a goal using various sensors [1,2]. The other is to develop human interfaces for easy operation [3,4].

In this paper, we aim to build an autonomous wheelchair robot so as to reduce navigation efforts of a handicapped person as far as possible. We use wide ranged ultrasonic sensors in front of wheelchair to detect obstacles and sharp ranged infrared sensors mounted on both sides of wheelchair to measure a distance to a wall.

The most major problem to construct the best robot is to make a realistic simulation of a robot. We use Webots by *Cyberbotics*[3] which is an excellent software to take account of noises in real world and to enable us to build any shape of mobile robot easily. We focus the task in the present paper to the navigation going along a right side wall by using front and right side sensors. If we are successful to get a task of going along a right side wall, then we can easily extend it to the task of going along a left side wall. If a robot can move along any side of a wall or can proceed straight, it will be possible to build a robot to go from one place to a destination, following an ordinary corridor in a building. We connected input sensors and output wheels by neural networks and developed G.A for the wheelchair simulator in a rather complicated test course to obtain the best robot. The simulation result was applied to the real wheelchair navigation in a corridor inside our building and eventually we had a smoothly moving nice wheelchair robot.

2 Outline of Wheelchair system

Fig. 1: *Wheelchair system*

The wheelchair system in our research is composed of a commercial electric wheelchair (Matsunaga MD-100), a desktop PC (CPU:PentiumIV 2.66GHz, OS:Linux), infrared sensors (GP2D12) and ultrasonic sensors (BTE054) as shown in Fig.1 The wheelchair has the maximum speed of 4.5 [km/h]. The infrared sensors are mounted on the side of the wheelchair and the ultrasonic sensors are mounted on the front. The PC processes infrared and ultrasonic sensor input values and controls wheel motors of the robot.

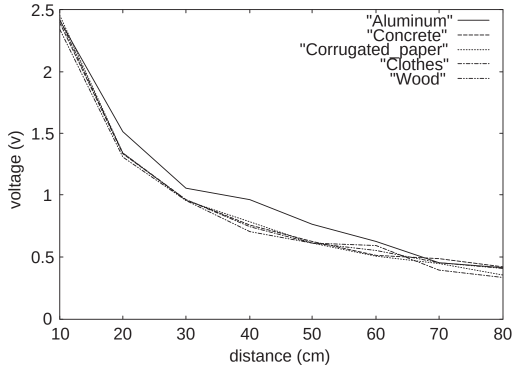

Fig. 2: *Distance-Voltage graph of an infrared sensor*

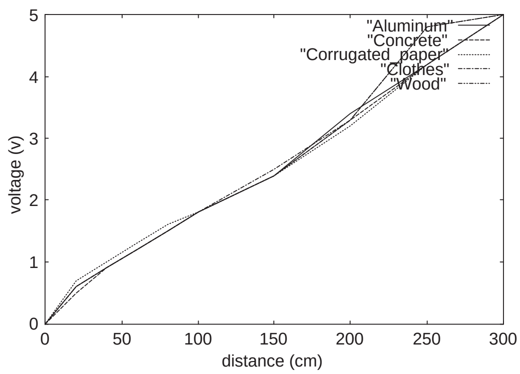

Fig. 3: *Distance-Voltage graph of an ultrasonic sensor*

The infrared and ultrasonic sensors output a distance to an object in voltage. Fig.2 shows distance - voltage graph for several kinds of objects. We find that the maximum detection ranges of the infrared and ultrasonic sensors are about 80 cm and 300cm, respectively. They have almost simulator response to the different objects as shown in Fig.2 and Fig.3.

3 Control methods

We consider control methods of a wheelchair so that a wheelchair runs along a right-hand side wall. We mount infrared and ultrasonic sensors on the wheelchair as shown in Fig.4. Since the ultrasonic sensors cover wide range of angle, three ultrasonic sensors($X01, X02, X03$) are installed on the front to detect front obstacles. Since the infrared sensors have narrow range sensing angle, four infrared sensors $X1, X2, X3, X4$ are installed on left and right sides to measure the distance to a wall. Since we do not use left side sensors $X3, X4$ for our present task of going along a right side wall, we can easily extend our task to go along a left side wall by using $X3, X4$. The ultrasonic sensors ($X01, X02, X03$) which detect an obstacle or a wall in the front direction are normalized in the range 0∼1.0 by defining

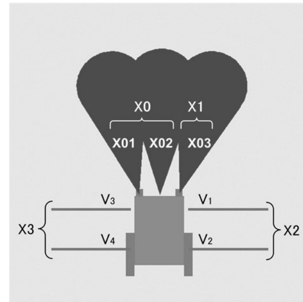

Fig. 4: *Sensor configurations for wheelchair robot*

$$X01 = \alpha_{ultra\_s}/V01, \quad X02 = \alpha_{ultra\_s}/V02 \quad (1)$$
$$X03 = \alpha_{ultra\_s}/V03$$
$$\alpha_{ultra\_s} = 75.0 \quad (2)$$

where $V01$ is the output voltage of the sensor and α_{ultra_s} is a normalization constant. To reduce variables, we take the mean value of $X01$, $X02$ as

$$X0 = (X01 + X02)/2.0 \quad (3)$$
$$X1 = X03$$

Side infrared sensor values are denoted by

$$X2 = (V_1 + V_2)/2V_{infra\_s} \quad (4)$$
$$X3 = (V_3 + V_4)/2V_{infra\_s}$$

To normalize Xi to take 0∼1.0, we choose

$$V_{infra\_s} = 2.78 \quad (5)$$

The control system of the wheelchair consists of neural networks shown in Fig.5. To train the synaptic couplings by means of genetic algorithms, we investigated robot movement in a computer simulation model. A difficult problem in computer simulations is how to simulate the real world with respect to noises. *Webots ver.4.0.24 by Cyberbotics*[5], is an excellent software tool that takes account of uncertainties assumed to exist in the real world. Noises of ±10% and ±10% are randomly added to the amplitude of the sensor value, and the amplitude of the motor speed, respectively.

Another difficulty in computer simulation is how to build a simulator to imitate the real object as far as possible. The webots software package is composed of VRML coding and any parts of an object are easily replaced or modified. As a typical example, we take a rectangular area with concave spaces surrounded by a wall as shown in Fig.6, in which wheelchair webots is required to follow the wall counterclockwise. It must keep a safe and short distance from the wall on the right, and enters wide spaces and narrow spaces.

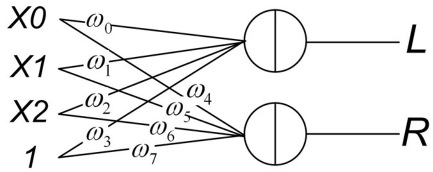

Fig. 5: *Neural Network to control left and right wheel*

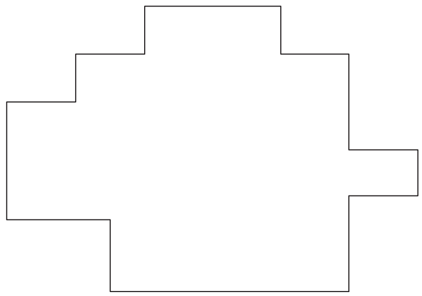

Fig. 6: *Test course for simulator wheelchair robot*

4 Evolutionary Adaptation

To train robot control systems, we perform adaptation under a computer simulation model of a robot and its environment. As shown in Fig.5, the data $X0, X1, X2$ output from the sensors are fed to the neural networks with self-training ability. The synaptic couplings are then revised by genetic algorithms. The control signals to the right wheel and left wheel, L and R are given by

$$L = F(\omega_0 X0 + \omega_1 X1 + \omega_2 X2 + \omega_3) \quad (6)$$
$$R = F(\omega_4 X0 + \omega_5 X1 + \omega_6 X2 + \omega_7) \quad (7)$$
$$F(x) = \tanh(x) \quad (8)$$

where L and R are normalized as $-1.0 \leq L, R \leq 1.0$. We define mean voltage V_m and differnce voltage V_d supplied to the wheel motors so as to control wheel speeds as

$$V_m = V_{max} \cdot (L + R)/2.0 \quad (9)$$
$$V_d = V'_{max} \cdot (L - R)/2.0 \quad (10)$$

where $V_{max} = 1.12volt$, $V'_{max} = 1.0volt$. A given voltage V_m, V_d determine left and right wheel speeds v_L, v_R. The functional relations between these variables are decided by moving our actual wheelchair. We obtained the best fit functions experimentally and denote them as

$$v_R = f_R(V_m, V_d) \quad (11)$$
$$v_L = f_L(V_m, V_d) \quad (12)$$

$\omega_0 \sim \omega_7$ are synaptic couplings, as shown in Fig.5, connecting data from sensors with the control of the right or left motors. We determine ω_i by using the genetic algorithms. The algorithms for obtaining the best genes are as follows:

1) Make N_1 robots with randomly generated synaptic couplings and left them run in the area shown in Fig.6 for certain period.

2) Make new N_2 robots from the old N_1 robots by using genetic algorithms in which the synaptic couplings of new robots are generated by real-coded genetic algorithms, in which α of $BLX - \alpha$[5] is set to 0.5. Then let them run for the same period as in step 1.

3) Make new N_3 robots from the old N_1 robots by using mutation.

4) Measure all the robots $N_1 + N_2 + N_3$ by using a given evaluation function, and choose N_1 robots with the highest scores. If the total score of the N_1 robots exceeds a given threshold, stop the loop; otherwise go to step 2.

5 Experimental results and conclusion

We performed simulation in the fairly complicated test course shown in Fig.6. The evaluation function in genetic algorithms is given as

$$g = \left(\frac{\sum^{STEP} speed}{STEP} \right) \cdot \left(\frac{\sum^{STEP} X2}{STEP} \right) \cdot \left(1 + \sum^{STEP} X3 \right)^{-1} \cdot \left(1 + \sum^{STEP} collision \right)^{-1} \quad (13)$$

Each term in Eq.(13) evaluates the robot performance from different points of view, ①measuring wheelchair robot's speed, ②going along a right side wall, ③movements without obstacles on the left side, and ④avoiding collision against a wall. The evaluation function g has a high value if a robot fallows a wall without colliding with anything and if it moves forward as far as possible. We take $N_1 = 10, N_2 = 4, N_3 = 11, speed = (v_R + v_L)/2v_{max}$, and $v_{max} = 0.88[m/s], STEP = 400$.

As a result of evolutionary adaptation after 400 generations, the coupling values of the best 10 robots became to have almost the same value which are shown in Table.1 together with the fitness value. Table.2 shows the behaviors of the best robot at the typical places shown in Fig.7. The trace of the robot in the test course is also shown in Fig.7.

Table 1: *The coupling values of the best robot after 400 generations.*

ω_0	ω_1	ω_2	ω_3	ω_4	ω_5	ω_6	ω_7	fitness
-5.24	-4.09	-0.23	1.59	1.77	1.05	0.73	0.05	9011.29

Table 2: *Typical behaviors of the best robot in Table.1*

	$X0$	$X1$	$X2$	L	R	v_L	v_R	
A	0.04	0.04	0.25	0.82	0.34	2.80	1.83	Turn right
B	0.24	0.21	0.25	-0.52	0.71	-0.13	1.18	Turn left
C	0.04	0.19	0.29	0.49	0.49	1.90	1.93	Go straight

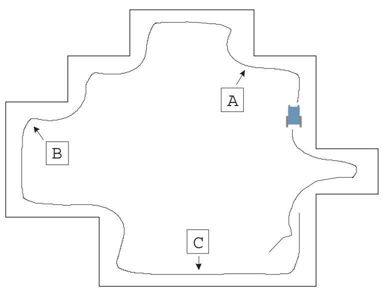

Fig. 7: *Result of test course simulation*

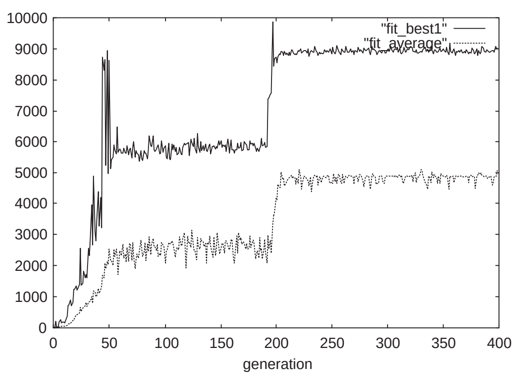

Fig. 8: *Evaluation function in GA*

The evaluation function for the best robot and their average value among robots are given in Fig.8 against generation development.

We made simulation experiments of wheelchair navigation on the second floor in the north building of the faculty of engineering, University of Miyazaki as shown in Fig.9. The robot moved smoothly as the trace is shown by a solid line in Fig.9. We conclude that our two step strategies, test course simulation and its application to real mapped course led to a successful result.

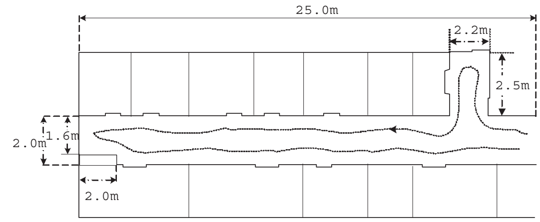

Fig. 9: *Course of the corridor inside our building and trace of the best robot*

References

[1] T.kitazoe, M.Tabuse, T.Uemura, S.kitazato, T.shinchi, Wheelchair Navigation System with Infrared Sensors, Proc. of The Eighth International Symposium On Artificial Life And Robotics, p.p. 102-105

[2] Webots User Guid release 4.0.25 (2004).

[3] *webots* Package version 4.0.24. Mobile robot simulator. The World Wide Web at `http://www.cyberbotics.com`

[4] M.Tabuse, T.shinchi, A.Todaka, and T.kitazoe, Evolutionaly Robot with Competitive-Cooperative Neural Network, IPSJ Journal, Vol.44 No.10, pp.2530-2513, 2003.

[5] Eshelman, L.J. and Schaffer, J.D, Real-Coded Genetic Algorithms and Interval-Schemata, Foundations of Genetic Algorithms 2, pp.187-202 (1993).

[6] D.P. Miller, M.G. Slack, "Design and Testing of a Low-Cost Robotic Wheelchair Prototype", Autonomous Robotics, 2, pp.77-88, 1995.

[7] T. Gomi, A.Griffith, "Developing Intelligent Wheelchairs for the Handicapped", Assistive Technology and Artificial Intelligence, Lecture Notes in AI, 1458, pp.150-178, Springer, 1998.

[8] Y. Matsumoto, T. Ino, T. Ogasawara, "Development of Intelligent Wheelchair System with Face and Gaze Based Interface", Int. Workshop on Robot and Human Interactive Communication, pp.262-267, 2001.

[9] S. Nakanishi, Y. Kuno, N. Shimada, Y. Shirai, "Robotic Wheelchair Based on Observations of Both User and Environment", Int. Conf. on Intelligent Robotics and Systems, pp912-917, 1999.

The Tenth International Symposium on Artificial Life and Robotics 2005(AROB 10th '05),
B-con Plaza, Beppu, Oita, Japan, February 4-6, 2005

Object Recognition Using a Self-Organizing Map for an Autonomous Mobile Robot

Masayoshi Tabuse Haruna Kaneko
Department of Environmental Information, Kyoto Prefectural University, Kyoto, 606-8522, Japan
tabuse@kpu.ac.jp

Abstract

In this research, we propose a control system by using the self-organizing map, a neural network and the genetic algorithm. The control system autonomously extracts visual information and decides behaviors. We investigate that a mobile robot controlled by this system performs a given task very well.

Key words: object recognition, Self-organizing map, neural network, mobile robot

1 Introduction

Recently, many people have been researching autonomous robots extensively. One purpose of this research is to build the robots that are able to behave in unknown or dynamically changing environments. In the case of a robot with visual sensors, most of methods are that useful information is extracted using image processing and robot behaviors are decided based on this information. However, appropriate image processing methods are generally constructed by a designer who has a good knowledge of tasks, so that autonomy and flexibility of a robot may be reduced [1]. Therefore we propose a control system in which a robot autonomously extracts visual information and decides behaviors.

In this system, we use a CCD camera as a visual sensor. Images obtained from the camera inputs Kohonen's self-organizing map [2], which classifies images, and a robot recognizes objects in the environment. A behavior decision part consists of a neural network and parameters of the neural network are chosen so that the robot accomplishes a given task by using a genetic algorithm [3]. We examine this system using a miniature robot Khepera with a CCD camera. A task is that the robot moves in a field, finds a coloring block and carries it to a same coloring area. We investigate that Kohonen's self-organizing map classifies a floor, a wall, coloring blocks and coloring areas and that the robot accomplishes the task very well.

2 Outline of the System

2.1 A mobile Robot

We use a miniature mobile robot Khepera II in our experiments as shown in Figure 1. This robot is 70mm in diameter and has two independent wheels and eight infrared proximity sensors (six in front and two in rear). We attach a gripper to this robot so that it grips a small block. Furthermore, we place a small CCD camera (KEYENCE CK-200) on the gripper to capture images.

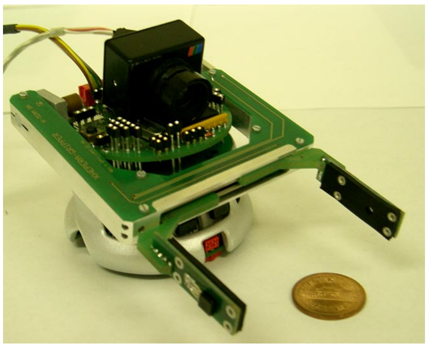

Figure 1: A mobile robot Khepera II

2.2 Control System

The control system consists of Kohonen's self-organizing map (SOM) and a two-layer neural network (NN). Kohonen's self-organizing map classifies images and the neural network control each wheel and a gripper. A CCD camera mounted on Khepera captures front images. These images are inputted into SOM. The output data from SOM are fed to a two-layer neural network. Weights of the neural network are determined using the genetic algorithms so that

Khepera performs appropriate behaviors. The outline of control system is shown in Figure 2.

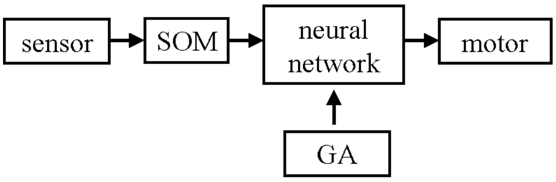

Figure 2.: The outline of control system

2.3 SOM

The self-organizing map (SOM) is a neural network of unsupervised learning proposed by T. Kohonen in the early 1980s. The goal is to discover some underlying structure of the data. SOM consists of two layer structures. One is an input layer and the other is an output layer, which is usually represented by 2 dimensional grid. The network is fully connected, i.e., all nodes in input layer are connected to all nodes in output layer, as shown in Figure 3.

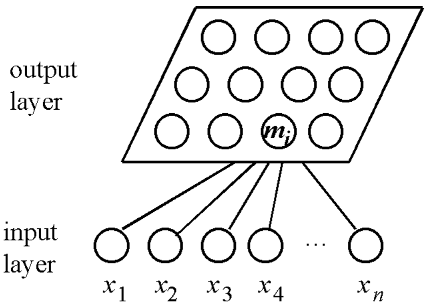

Figure 3: SOM

The learning algorithm for *n* dimensional input vectors is as follows:

(1) Properly choose a reference vector of i-th output node

$$\vec{m}_i = (m_{i1}, m_{i2}, \ldots, m_{in}),\ i = 1,2,\ldots,M,$$

connected with *n* input nodes, where *M* is the number of output nodes.

(2) An input vector $\vec{x} = (x_1, x_2, \ldots, x_n)$ is compared with all the reference vectors $\vec{m}_i$. The best-matching output node where the reference vector is most similar to the input vector in some metric (e.g. Euclidean) is identified. This best matching node is called the winner. The winner node *c* is determined by

$$c = \arg\min_i \|\vec{x} - \vec{m}_i\|.$$

(3) The reference vectors of the winner and its neighboring nodes on the grid are changed towards the input vector according to the following equation:

$$\vec{m}_i(t+1) = \vec{m}_i(t) + h_{ci}(t)[\vec{x}(t) - \vec{m}_i(t)],$$

$$h_{ci}(t) = \alpha(t) \cdot \exp\left(-\frac{\|\vec{r}_c - \vec{r}_i\|^2}{2\sigma^2(t)}\right),$$

where t=0,1,2,… is a discrete learning time, $h_{ci}(t)$ is a neighborhood function, $\alpha(t)$ is a learning rate, $\sigma(t)$ is a decreasing function which defines a radius of neighborhood and $\vec{r}_c$ and $\vec{r}_i$ are coordinate vectors of the winner node *c* and the neighborhood node *i* on the grid, respectively.

(4) Repeat processes (2) and (3).

According to this algorithm, the network organizes itself and a self-organizing map for input vectors is built. This map classifies input vectors. In Figure 5 we show a self-organizing map obtained in our experiments. Light and shade of the map represent similarity of reference vectors. Light color means that reference vectors of both sizes are similar. Thus we guess that a robot with our control system recognizes objects without appropriate image processing methods constructed by a designer.

2.4 Neural network and genetic algorithm

A two-layer neural network controls left and right wheels and a gripper according to output data of SOM as input data. We think that a neural network is good controller because it outputs continuous signals for various input data. Usually, learning methods of the neural network are supervised learning. In supervised learning, we must have knowledge of correct outputs of the neural network for any input data. However, in dynamical changing environments, we suppose that it is impossible to teach correct outputs in any cases. Therefore, We use the genetic algorithm to find appropriate weights of the network to perform a given task.

3 Experiments

3.1 Experimental Environment

Figure 3 shows the environment in our experiments. The color of a floor and a wall is white and we set red, blue and green blocks and the same coloring areas on the floor. A task is that Khepera carries a block to the same coloring area.

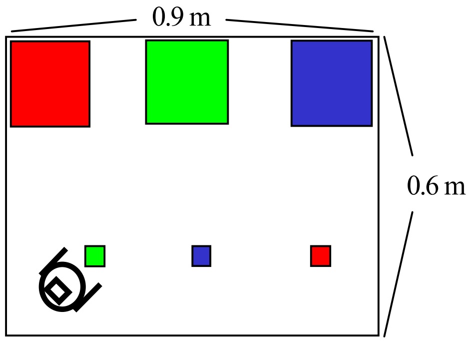

Figure 3: Experimental environment

3.2 Learning methods

First we capture total 190 sample images of a block, a coloring area, a wall and a floor using a CCD camera mounted on Khepera. Each image is 320×240 pixels, but to reduce the dimension of input data and to obtain a image of the nearest object, we use only the lower half of the image after dividing into tiles (tile size : 20×20) and averaging in each tile. A capture image and its lower half average image are shown in Figure 4. Then $16 \times 6 = 96$ dimensional images are the input data of SOM. SOM consists of 96 nodes in input layer and 6×8 nodes in output layer, and SOM classifies input data using the learning algorithm. Figure 5 shows a self-organizing map for 190 sample images. Images of a coloring block, a floor or a wall and a red area are classified in the left upper side, in the center and in the lower side of this map, respectively. The number on the map represents a sample image number.

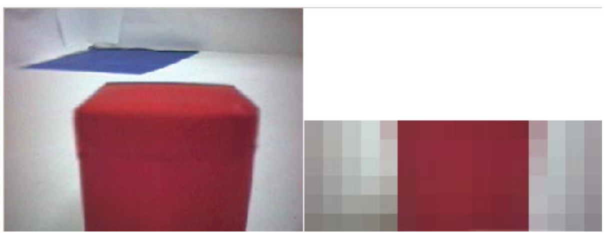

Figure 4: A example of a capture image and its lower half average image

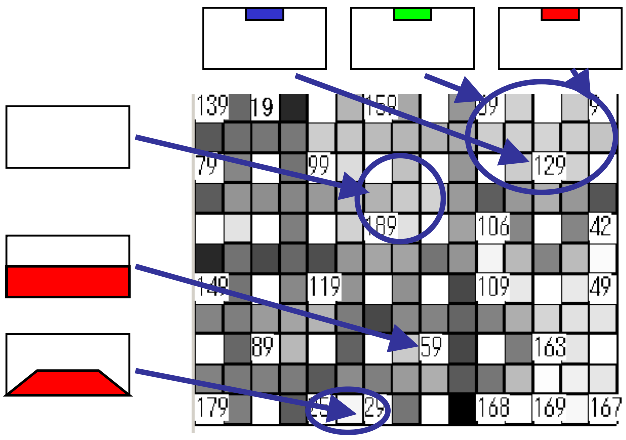

Figure 5: SOM of our experiments

Next we determine weights of the neural network to perform a given task using the genetic algorithm in computer simulation. The neural network consists of two layers, as shown in Figure 6. Input data are 48 dimensional data from SOM and 3 internal states of Khepera. Internal states denote that Khepera is gripping a block, i.e.,

$$\text{internal state} = \begin{cases} (0,0,0) & \text{for gripping no block} \\ (1,0,0) & \text{for gripping a red block} \\ (0,1,0) & \text{for gripping a green block} \\ (0,0,1) & \text{for gripping a blue block} \end{cases}$$

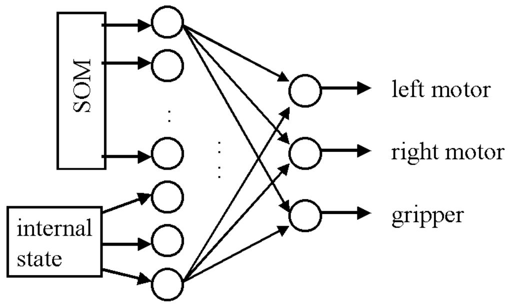

Figure 6: The neural network

In this research, we investigate object recognition by using SOM. Therefore, we consider that learning behaviors of Khepera are finding a block, approaching a block, carrying a block to a same coloring area and outputting signals of gripping and placing a block to the gripper. The behaviors of gripping and placing a block are constructed by hand so that if the signal to the gripper indicates gripping a block and infrared sensors detect a object in front, Khepera grips a block and that if the signal indicates placing a block, Khepera places a block.

In the genetic algorithm we set that the population has 50 individuals, it runs for 2000 generations and individuals run 200 steps for each generation. Each individual has a chromosome, which represents weight of the neural network in a real number. At each generation, individuals with high fitness are selected and produce descendants using crossovers and mutations of their chromosomes. The fitness function is given by

$$fitness = \begin{cases} 1000 & \text{for gripping a block} \\ 1000 & \text{for placing a block} \\ & \text{on the same coloring area} \\ -500 & \text{for going back or rotating} \\ & \text{in a free space} \\ 10 & \text{for capturing a block} \\ -100 & \text{for missing a block} \end{cases}$$

After 2000 generations, we select an individual with highest fitness, decide weights of the neural network and investigate Khepera's behaviors with the control system.

3.3 Result

The mobile robot Khepera moves around in the field and finds a coloring block. Then the robot approaches the block, and grips and carries it and places it on a same coloring area. Thus we find that Kohonen's self-organizing map classifies a floor, a wall, coloring blocks and coloring areas and that the robot accomplishes the task very well. Figure 7 and 8 show scenes of gripping and placing a block, respectively.

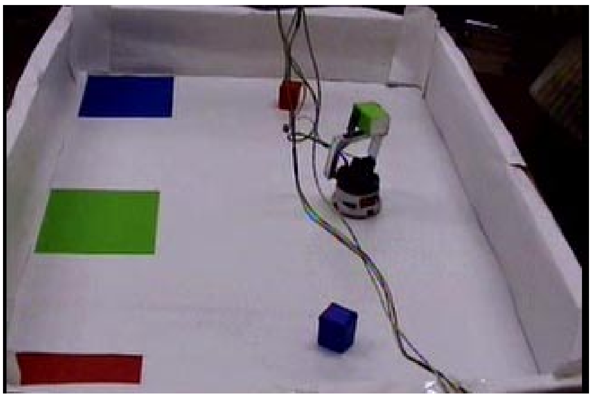

Figure 7: Griping a block

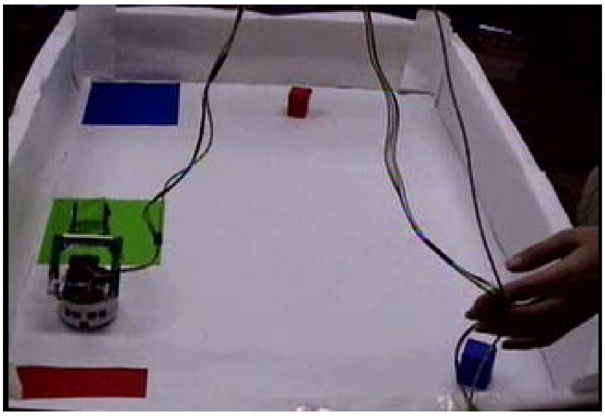

Figure 8: Placement of a block on the same color area

4 Conclusion

We have presented the control system for an autonomous mobile robot using a combination of Kohonen's self-organizing map and neural network. In this system, the robot autonomously extracts visual information and recognizes objects in the environment. Thus the robot finds a colored block, grips and carries it and places it on a same colored area.

In our experiments, we use a map of 6×8 in SOM. If the size of a map is larger, SOM may classify visual images more precisely. However, for a larger size of a map it requires more time to find proper weights of neural network, so that we will find a proper size of a map.

As the future works, we will consider a control system in which a robot recognizes a shape of objects and construct a robust system in dynamically changing environments.

References

[1] K. Shibata, M. Iida, "Acquisition of box pushing by direct-vision-based reinforcement learning", SICE 2003 Annual Conference, pp.2322- 2327, 2003.

[2] T. Kohonen, "Self-Organizing Maps", Springer-Verlag, 1995.

[3] S. Nolfi, D. Floreano, "Evolutionary Robotics; The Biology, Intelligence, and Technology of Self-Organizing Machines", MIT Press, 2000.

The Tenth International Symposium on Artificial Life and Robotics 2005(AROB 10th '05),
B-con Plaza, Beppu, Oita, Japan, February 4-6, 2005

Image Compression for Bill Money by Neural Networks

Sigeru Omatu Kenji Kibi Masaru Teranisi Toshihisa Kosaka
Computer and Systems Sciences Graduate School of Engineering
Osaka Prefecture University
Sakai, Osaka, 599-8531 Japan
omatu@cs.osakafu-u.ac.jp

Abstract

We propose an image compression method using Self-Organizing feature Map (SOM) for various kinds of bill money images which have been obtained by receiving the light reflected from the bill through a specific frequency band filter for the specific frequency incident light. The reason why such an image is required is to detect the false bill. Incident light for every 15 angstrom has been emitted toward the bill and the reflected light has been measured by using the filter with 15 angstrom wave length. The image size is 1,024x1, 024pixls. Therefore, huge numbers of images are obtained. In this paper we will extract images with specific important features among those images by using the SOM clustering.
Keywords: SOM, Feature extraction, Bill Money data, Clustering Algorithm

1 Introduction

Recently, the rapid progress of electronic copying technology, there have many color printing machines which can print out almost the same quality of the original pictures. Although the technology has offered many advantages for users in printing field, there have appeared some disadvantages such as printing the false bills.

In order to recognize the bills correctly, we need more additional information about the bills. One of them is to check the spectral property of the bill. In this case, there are many images corresponding to the various frequency bands of the filter of the sensing devices as well as those of the emitted light frequencies.

In this paper, we consider the data compression methods of those various images of the bills which have been obtained by sensing the reflected images by using specific frequency band-pass filters to the specific emitted light for the various frequencies. The technique used here is Self-Organizing Feature Map technique which has been developed by Kohonen [1] and the bill is 10,000 Bolivar in Venezuela. We use 145 images with 1,024x1,024 pixels and 256 resolution levels. Five patterns of the emitted lights and twenty nine patterns for the sensing filter bands have been used in this experiment. The aim is to find the specific images among 5x29 images which keep the representative features to detect the false bills.

2 Image Data for Data Compression

The date used here are images with 1,024x1,024 pixels of 10,000 Bolivar bill in Venezuela which are obteined as the reflected light image through specific spectral band-pass filters for preassigned lights with several frequency bands. The data used here are shown in Table 1.

From now on we denote the image data as X-number such as A-01 to show the image with emitted light A and receiving filter frequency band number 01. The original image data of 10,000 Bolivar bill which has whole spectral data without no spectral band-pass filter is shown in Fig.1. Here, the fram in the picture is the study area and in this part there are many secret symbols which will appear if we emit a special light with specific spectral bannd and observe the refrected light through a filter with specific spectral band. Therefore, we can obtain various types of images which have been observed throughband-pass filters for various emitted lights. Some of them are shown in Fig.2. In oder to keep the secret, we cannot show the real values and we use the symbols, A,b,...E

Table 1: The image data used here.

Image size	1,024x1,024 pixels
Intensity	256
Emitted light frequency	5 patterns(A-E)
Received filter band	29 patterns(01-29)

The Tenth International Symposium on Artificial Life and Robotics 2005(AROB 10th '05),
B-con Plaza, Beppu, Oita, Japan, February 4-6, 2005

for different emitted lights and use numbers 01 to 29. In this paper, we will propose a data compression method among those image data using the SOM of competitive neural networks which can cluster the image data such that the similar images can be clustered autonomously.

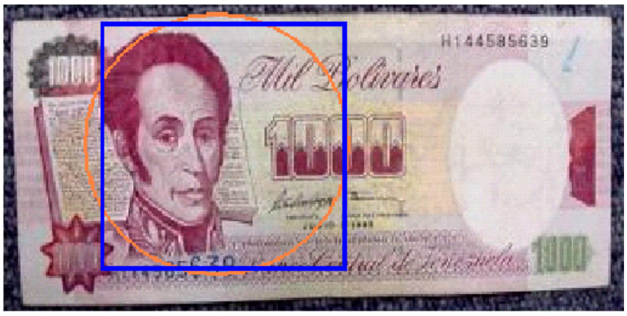

Figure 1: An example of images for data compression.

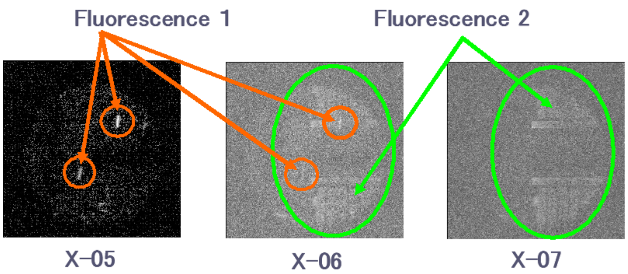

Figure 2: Examples of an fluorescence images.

3 The Data Processing Method

In this section, we will explain the proposed method by using the SOM. The observed images are low power reflected lights and sensitive to the temperature and humidity in the sensing environment. Thus, they includevaruious noises, especially, pepper and solt noises. Therefore, we apply median filter to original data to delete the noise. An example of noisy image and the noise removed data is shown in Fig.4. Comparing these images, we can see how much noise is included in the present image and the effect of the median filtering operation.

To make the comparison data, we will subtract the pixel values of the one image from the corresponding pixel values of the neighbouring next image. From these values we can see how much difference occurred by changing the filter band. If the difference values attain the maximum and the decrease, the image corresponding the maximum value difference is the typical image to be stored. But the maximum values are not reflect the precise measure for the image change. Thus, we store some neighbouring images and from those images we find the suitable representative image by using the SOM. The Som structure is shown in Fig.5.

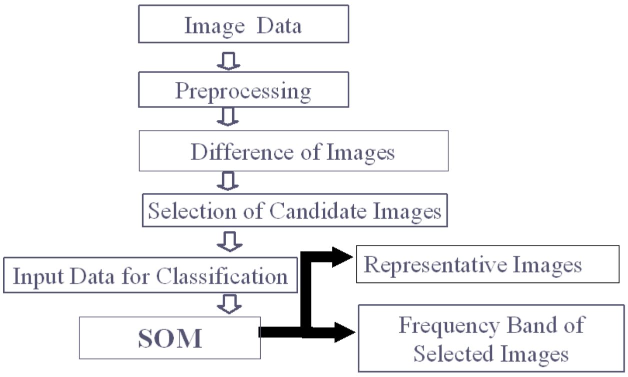

Figure 3: Flow of the proposed method.

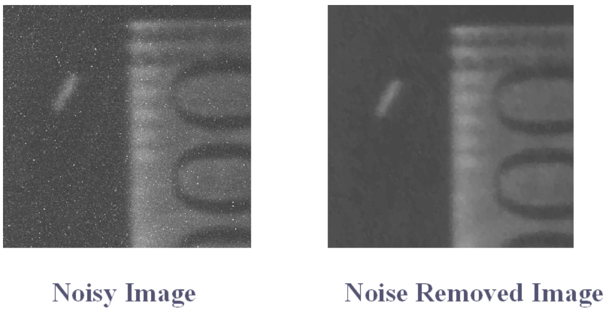

Figure 4: Noisy image and noise removed image.

The compressed input data for the SOM are given by projection to vertical and holizontal axes as hown in Fig.6. Using this technique we can rduce the image data size from 1,024x1,024 to 2,048 as shown in Table 1. Thus, for emitted light A we have obtained 29 images recived 29 filter bands. Some of the images is illustrated in Figs.7 and 8. Therefore, the object is to find the typical image data among those many data and store the specific features for the representative image.

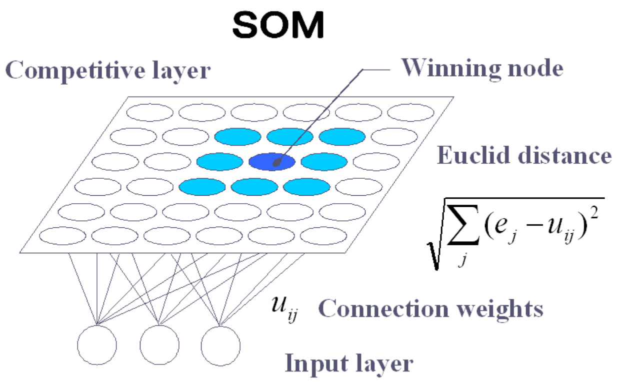

Figure 5: SOM structure for classification.

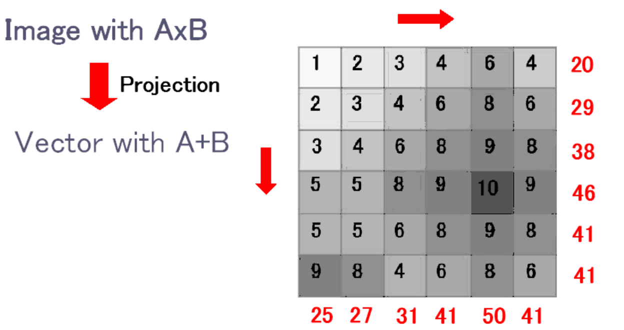

Figure 6: Data compression by projection to vertical and horizontalaxes.

3.1 Classification Results by SOM

3.2 Classification Results by SOM

Using the proposed method we can get the representative images which has been extracted by deleting the similar images from the observed images. By taking the difference of grey levels by pixel to pixel between the successive two images, we could reduce the number of images from 145 to 22 among which there are four different patterns as shown in Fig.9. Those four patterns include A-01,14(for Pattern 1), B-01,02,26, C-01,05,28(for Pattern 2), D-01,04,19,28(for Pattern

Table 2: Parameters of SOM.

Parameters	Values
Number of nodes	5x5
Total learning time	1,000
Learning rate	0.8
Initial distance of neighborhood	3

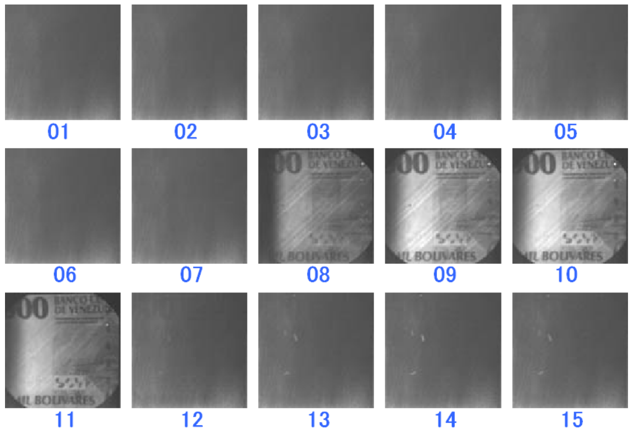

Figure 7: An example of rceived images from 01-15 for emitted light A.

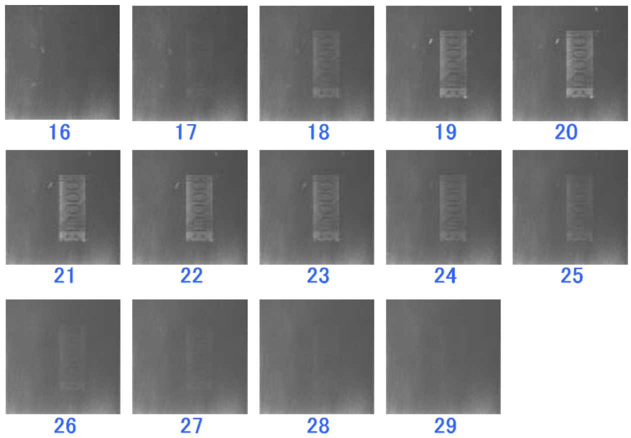

Figure 8: An example of rceived images from 16-29 for emitted light A.

3), and E-01,05,08,26(for Pattern 4). Pattern 1 shows the background image, Patterns 2 and 3 show the central part without and with slanting lines, and Pattern 4 shows the dashed symbols near 10,000. These images correspond to the images selected by our inspection.

Figure 10 shows the classification results among the classified patterns stated above by using the SOM. The number of input data for the SOM is 2,048 and the number of the competitive layer is 5x5. The initial value of the neighborhood distance is 3, the learning rate is 0.8, and the total learning time is 1,000 as shown in Table 2.

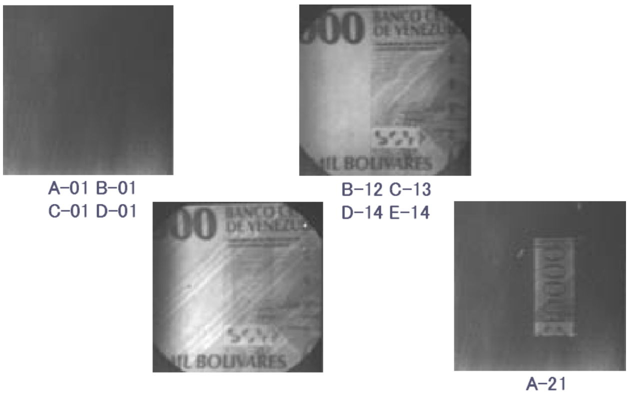

Figure 9: Representative images.

4 Conclusion

In this paper, we have proposed a new method to select representative images among huge image data by using the SOM. To reduce the number of images we have used the difference method in the first and then applied the SOM to four pattern classes to find the specific features. The results obtained here show the effectiveness for image data compression.

References

[1] T. Kohonen, "Self-Organizing Maps", Springer-Verlag, 1997.

[2] R. Palaniappan, P. Raveendran, and S. Omatu,Improved Moment Invariants for Invariant Image Representation, World Scientific, 2000.

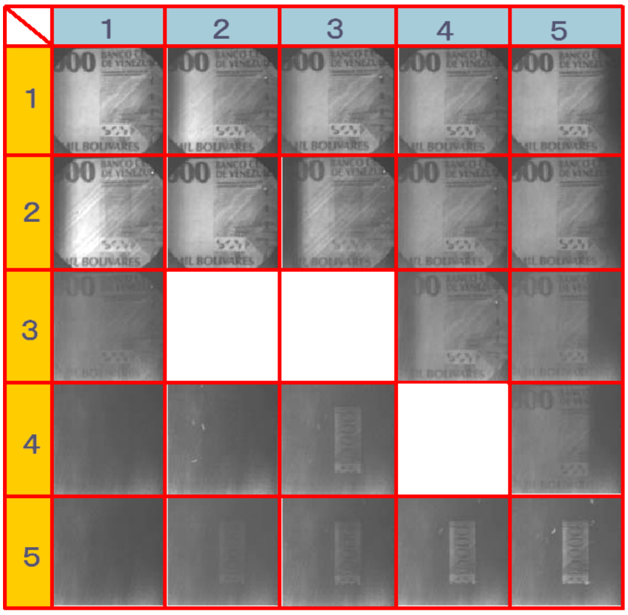

Figure 10: Classification results by the proposed method.

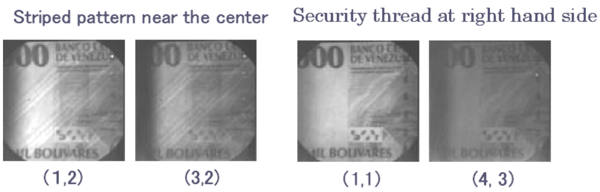

Figure 11: An example of specific feature of the representative image.

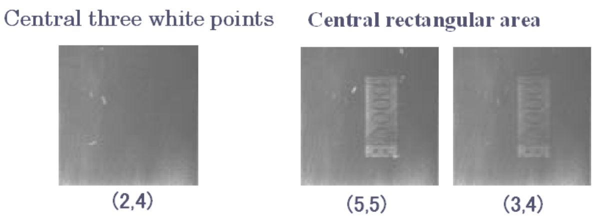

Figure 12: Feature extracted from the representative image.

The Tenth International Symposium on Artificial Life and Robotics 2005(AROB 10th '05),
B-con Plaza, Beppu, Oita, Japan, February 4-6, 2005

Intelligent Classification of Bill Money

Sigeru Omatu+ and Toshihisa Kosaka++
+Osaka Prefecture University, Sakai, Osaka 599-8531, Japan
omatu@cs.osakafu-u.ac.jp
++ Glory TD Himeji, Hyougo 670-8567 Japan

ABATRACT

For the pattern classification problems the neuro-pattern recognition which is the pattern recognition based on the neural network approach has been paid an attention since it can classify various patterns like human beings. In this paper, we adopt the learning vector quantization (LVQ) method to classify the various money. The reasons to use the LVQ are that it can process the unsupervised classification and treat many input data with small computational burdens. We will construct the LVQ network to classify the Italian Liras. Compared with a conventional pattern matching technique, which has been adopted as a classification method, the proposed method has shown excellent classification results.

1. INTRODUCTION

Bill money classification by transaction machines has been important to make progress the office automation [1]. Since sizes of bills are different according to kinds of bills, the measurement data of bills include various variations. Human being can classify the bills correctly even if they are suffered from those variations such as rotation and shift. But usual pattern recognition using a conventional transaction machine cannot give us the correct classification result under such cases since the basic method is a pattern matching principle. Furthermore, the conventional pattern matching method requires many template patterns for many kinds of bills, which takes much time and needs much experience [1].

Recently, neural networks which are based on the biological mechanism of human brain have been focussed since they have intelligent pattern recognition ability [2]. In this paper, we will apply the neural network approach to classify the bill money under various conditions by using transaction machines. The learning vector quatization (LVQ) has been used to classify the bills since it can treat high dimensional input and has simple learning structure [3]. The LVQ network adopted here has 64x15 units in the input layer and many units at the output layer. The bills are Italian Liras of 8 kinds, 1,000, 2,000, 5,000, 10,000, 50,000 (new), 50,000 (old), 100,000 (new), 100,000 (old) Liras with four directions A,B,C, and D where A and B mean the normal direction and the upside down direction and C and D mean the reverse version of A and B. The simulation results show that the proposed method can produce the excellent classification results.

2. COMPETITIVE NEURAL NETWORKS

We will explain the competitive neural networks that are used to classify the bill money. The structure of a LVQ competitive network is shown in Fig. 1. The input for the LVQ is bill money data where an original image consists of 128x64 pixels and the input data to the network is compressed as 64x15 pixels to decrease the computational load. The output of the network consists of the Italian Liras of 8 kinds, 1,000, 2,000, 5,000, 10,000, 50,000 (new), 50,000 (old), 100,000 (new), 100,000 (old) Liras with four directions A,B,C, and D where A and B mean the normal direction and the upside down direction and C and D mean the reverse version of A and B.

In the input layer the original bill money data are applied and all the units at the input layer are connected to all the neurons at the output layer with connection weight W_{ij}. W_{ij} denotes the connection weight from the unit j in the input layer to unit i in the output layer. The output layer will output only one neuron which is called winner neuron. The winner neuron is selected as the neuron with the minimum distance between an input vector and its connection weight vector. The connection weights W_{ij} are set by the random number at the beginning. Here, we set the mean vector of the cluster plus small random number. Then the following learning algorithm of the

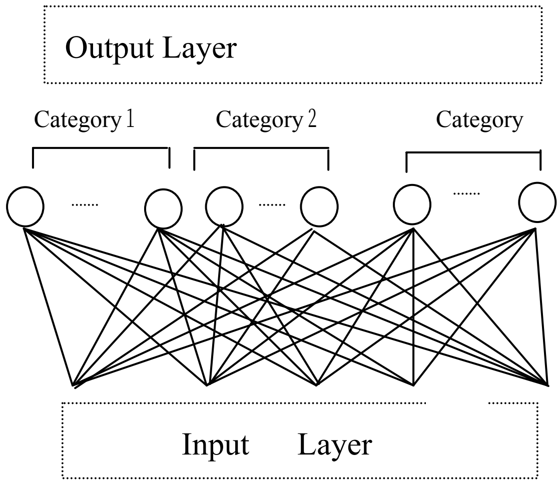

Fig. 1. Structure of the LVQ networks.

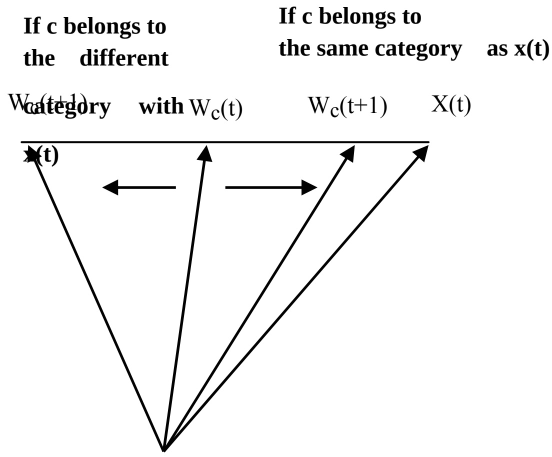

Fig.2. Principle of the LVQ algorithm where the right hand side shows the same category case of **x**(t) and Category c and the left hand side denotes the different category case.

connection weight vector is used.

LVQ algorithm

Step 1. Find the unit c at the output layer which has the minimum distance from the input data **x** (t)

$$\|\mathbf{x}(t)-\mathbf{W}_c\| = \min_i \|\mathbf{x}(t)-\mathbf{W}_i\|$$

where $\|\ \|$ denotes the Euclidean norm and t denotes the iteration time.

Step 2. If the input **x** (t) belongs to Category c, then

$$\mathbf{w}_c(t+1) = \mathbf{w}_c(t) + \alpha(t)(\mathbf{x}(t)-\mathbf{w}_c(t))$$

$$\mathbf{w}_i(t+1) = \mathbf{w}_i(t)\ ,\quad i \neq c$$

and if the input **x** (t) belongs to the other Category j ($j \neq c$), then

$$\mathbf{w}_c(t+1) = \mathbf{w}_c(t) - \alpha(t)(\mathbf{x}(t)-\mathbf{w}_c(t))$$

$$\mathbf{w}_i(t+1) = \mathbf{w}_i(t)\ ,\quad i \neq c$$

where $\alpha(t)$ is a positive function and denotes learning rate.

In the usual LVQ $\alpha(t)$ is given by

$$\alpha(t) = \alpha_0(1-\frac{t}{T})$$

where ($0<\alpha_0<1$) is a positive and T is a total number of learning iterations.

The above algorithm for selection of new weight vector $W_c(t+1)$ can be explained graphically as shown in Fig. 2 .

In the above LVQ algorithm, the learning rate $\alpha(t)$ plays an important role for convergence. To adjust the parameter, Kohonen has proposed an optimization method without proof as follows:

$$\alpha_c(t) = \frac{\alpha_c(t-1)}{1+s(t-1)\alpha_c(t-1)}$$

where s(t) =1 if **x**(t) belongs to the same Category c and s(t)=-1 if **x**(t) does not belong to the same Category c. Here, $\alpha_c(t)$ denotes the learning rate for the pattern of Category C. In what follows, we will prove the above relation. From the learning rule of the LVQ, we have

$$\mathbf{w}_c(t+1) = \mathbf{w}_c(t) + s(t)\alpha_c(t)(\mathbf{x}(t)-\mathbf{w}_c(t))$$
$$= (1-s(t))\alpha_c(t)\mathbf{w}_c(t) + s(t)\alpha_c(t)\mathbf{x}(t)$$

and

$$\mathbf{w}_c(t) = \mathbf{w}_c(t-1) + s(t-1)\alpha_c(t-1)$$
$$(\mathbf{x}(t-1) - \mathbf{w}_c(t-1))$$
$$= (1-s(t-1))\alpha_c(t-1)\mathbf{w}_c(t-1)$$
$$+ s(t-1)\alpha_c(t-1)\mathbf{x}(t-1)$$

Substituting the latter equation the former one, we have

$$\mathbf{w}_c(t+1) = (1-s(t)\alpha_c(t))(1-s(t-1)\alpha_c(t-1))\mathbf{w}_c(t-1)$$
$$+ s(t)\alpha_c(t)\mathbf{x}(t) \ + s(t-1)\alpha_c(t-1)(1-s(t)\alpha_c(t))\mathbf{x}(t-1).$$

We assume that the optimal rate adjusts the effect of x(t) and x(t-1) equally within the absolute value, that is,

$$\alpha_c(t) = (1-s(t)\alpha_c(t))\alpha_c(t-1)\ .$$

Then we have

$$\alpha_c(t) = \frac{\alpha_c(t-1)}{1+s(t-1)\alpha_c(t-1)}\ .$$

From the above equation, we can see that the value of $\alpha_c(t)$ become larger than 1 when s(t-1)= - 1, which may make the learning algorithm unstable. Thus, we must fix the $\alpha_c(t)$ to a boundary value α_0 when it becomes larger than 1.

$$\alpha_c(t+1)=\alpha_0 \quad \text{if} \quad \alpha_c(t+1)>1\,.$$

Using the above OLVQ1 algorithm, we will classify the Italian bills in the following section.

3. PREPROCESSING ALGORITHM

The images obtained by transaction machine, there are variations such as rotation or shift. Therefore, we must adjust the images such that the variations may be reduced as much as possible by using the preprocessing. The flow char of the preprocessing procedure is illustrated in Figure 3. In this figure, the original image with 128x64 pixels are observed at the transaction machine in which rotation and shit are included. After correction of these effects, we select a suitable aria which show the bill image and compressed as the image with 64x15 pixels to the neural networks. Although the neural network of the LVQ type could process any order of the dimension of the input data, the small size is better to achieve the fast convergence result. Thus, we have selected the above size of the image.

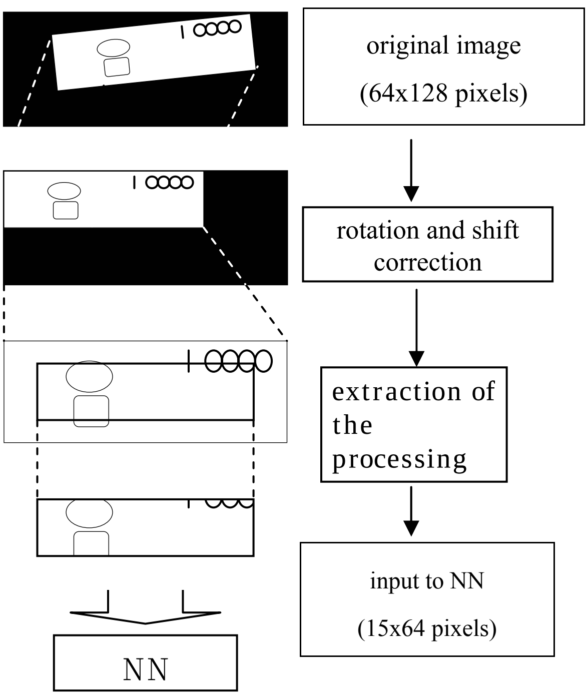

Fig. 3. Preprocessing algorithm.

4. ITALIAN LIRA CLASSIFICATION

The bills used here are Italian liras, which have 8 kinds such as 1,000 Liras, 2,000 Liras, 5,000 Liras, 10,000 Liras, new 50,000 Liras, old 50,000 Liras, new 100,000 Liras, and old 100,000 liras. Those Lira bills are used at the input of the transaction machine where

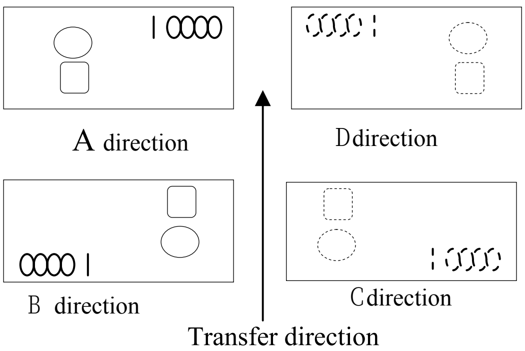

Fig. 4. Four directions of bill money.

(a) A direction of 1,000Lira

(b) B direction of 1,000 Lira

(c) C direction of 1,000 Lira

(d) D direction of 1,000 Lira

Fig.5. Image of four directions of 1,000 Lira.

four directions such as A, B, C, and D appear since normal direction, reverse direction, and their upside down directions occur at the input as shown in Fig.4.

The typical images of 1,000 Lira for four directions are shown in Fig.5. Thus, thirty-two bill images are one set of the classification pattern of the experiment. Total number of data sets is 30 and 10 data sets are used for training of the network and the remaining 20 data sets are used to test the network. In order to reduce the misclassification, we have set the threshold value d_θ such that if $d_c > d_\theta$, unit c is not fired. This means that if the minimum distance is not less than d_θ, the input data is not classified. The parameters of the neural network used here are as follows:

- Number of units in the input layer=960
- Number of units in the output layer in the initial state=32 where every 50 iterations the number has been adjusted.
- Total learning timeT=150
- $\alpha_i(0) = 0.5,\ i = 1, \cdots M$
- Initial values of the weight vectors=mean vectors for training patterns
- $d_\theta = \min_c (m_c + 4.5\sigma_c)$

After training the neural network, 20 data sets are tested how well the LVQ network could work. Table 1 denotes the recognition rate in the beginning (t=0), which means the result by the conventional pattern matching method. Table 2 shows the number of not fired numbers at t=0. Tables 3 and 4 show those values at t=160. We can see the improvement by learning. Table 5 shows the number of the neuron units at t=160 which are determined by increasing them.

Table 1. Recognition rate (%) at t=0.

		Directions			
		A	B	C	D
Italian Liras	1,000	100	100	100	100
	2,000	100	100	100	100
	5,000	100	100	100	100
	10,000	100	100	100	100
	50,000(new)	100	100	100	100
	50,000(old)	85	100	80	95
	100,000(new)	100	100	90	100
	100,000(old)	100	100	95	90

Table 2. Not fired rate (%) at t=0.

		Directions			
		A	B	C	D
Italian Liras	1,000	20	15	15	10
	2,000	5	10	25	25
	5,000	15	20	5	0
	10,000	10	10	10	5
	50,000(new)	5	0	20	5
	50,000(old)	0	0	0	0
	100,000(new)	0	0	0	0
	100,000(old)	0	5	0	0

Table 3. Recognition rate (%) at t=160.

		Directions			
		A	B	C	D
Italian Liras	1,000	100	100	100	100
	2,000	100	100	100	100
	5,000	100	100	100	100
	10,000	100	100	100	100
	50,000(new)	100	100	100	100
	50,000(old)	100	100	95	95
	100,000(new)	100	100	90	100
	100,000(old)	100	100	95	90

Table 4. Not fired rate (%) at t=160.

		Directions			
		A	B	C	D
Italian Liras	1,000	5	0	5	0
	2,000	0	10	25	25
	5,000	15	20	5	0
	10,000	10	0	0	5
	50,000(new)	5	0	0	0
	50,000(old)	0	5	0	0
	100,000(new)	0	0	0	0
	100,000(old)	0	5	0	0

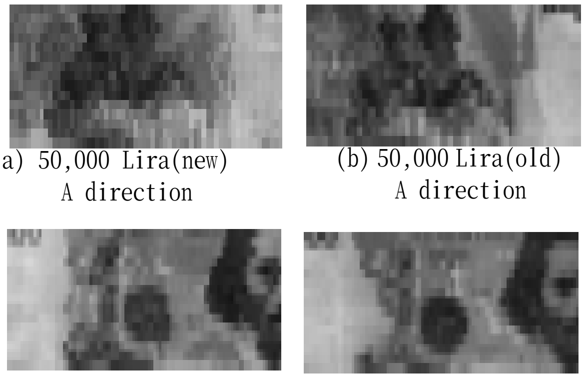

(a) 50,000 Lira(new) A direction
(b) 50,000 Lira(old) A direction
(c) 50,000 Lira(new) D direction
(d) 50,000 Lira(old) D direction

Fig. 6. New and old 50,000 Liras.

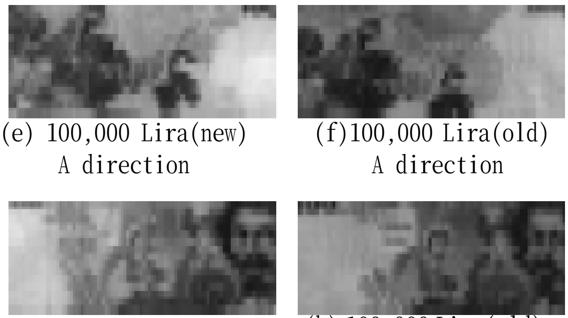

(e) 100,000 Lira(new) A direction
(f)100,000 Lira(old) A direction
(g) 100,000 Lira(new) D direction
(h) 100,000 Lira(old) D direction

Fig.7. New and old 100,000 Liras.

From the original image data we can see that the difference between 50,000 Lira old and new is slight and the difference between old and new100, 000 Liras as shown in Figs. 6 and 7. Therefore, it is rather difficult to recognize them so perfectly. But in this case the misclassification like old and new bills within the same values is not serious. Thus, we have regarded this misclassification as the correct one. Furthermore, we have introduced the threshold value to prevent from making the misclassification. Thus, even if the minimum distance criterion results in the correct classification, we have decided these bells are unknown. Without threshold constraints, we could obtain 100% classification rate.

Table 5. Number of units after learning.

		Directions			
		A	B	C	D
Italian Liras	1,000	2	2	2	2
	2,000	2	1	1	1
	5,000	1	1	1	1
	10,000	1	2	2	1
	50,000(new)	2	1	1	1
	50,000(old)	2	1	3	1
	100,000(new)	1	1	1	1
	100,000(old)	1	1	1	1

6. CONCLUSIONS

We have proposed a new classification method of Italian Liras by using the OLVQ1 algorithm. The experimental results show the effectiveness of the proposed algorithm compared with the conventional pattern matching method.

REFERENCES

[1] S. Fukuda, T. Kosaka, and S. Omatu: Bill Money Classification of Japanese Yen Using Time Series Data, Trans. Of IEE of Japan, Vol.115-C, No.3, pp.354-360, 9995(in Japanese).

[2] J. Dayhoff: Neural Network Architectures: An Introduction, International Thompson Computer Press, New York, 1990.

[3] T. Kohonen: Self-Organizing Maps, Springer, Berlin, 1995.

The Tenth International Symposium on Artificial Life and Robotics 2005(AROB 10th '05),
B-con Plaza, Beppu, Oita, Japan, February 4-6, 2005

An Image Segmentation Method Using the Histograms and the Human Characteristics of HSI Color Space for a Scene Image

Seiji Ito
Computer and Systems Science
Osaka Prefecture University
1-1 Gakuencho Sakai-City
Osaka 599-8531 Japan
seiji@sig.cs.osakafu-u.ac.jp

Michifumi Yoshioka
Computer and Systems Science
Osaka Prefecture University
1-1 Gakuencho Sakai-City
Osaka 599-8531 Japan
yoshioka@cs.osakafu-u.ac.jp

Sigeru Omatu
Computer and Systems Science
Osaka Prefecture University
1-1 Gakuencho Sakai-City
Osaka 599-8531 Japan
omatu@cs.osakafu-u.ac.jp

Kouji Kita
Noritsu Koki Co., LTD.
579-1 Umehara, Wakayama-City
Wakayama, 640-8550, Japan
k-kita@nkc.noritsu.co.jp

Kouichi Kugo
Noritsu Koki Co., LTD.
579-1 Umehara, Wakayama-City
Wakayama, 640-8550, Japan
k-kugo@nkc.noritsu.co.jp

Abstract

An image segmentation is an important subject for an image recognition. In this paper, we propose a new image segmentation method for scene images. The proposed segmentation method classifies images into several segments without using the Euclidian distance. We calculate the histograms of the image for each component of HSI color space, and obtain three results of the image segmentation from each histogram. We consider the achromatic colors to decrease the number of regions. We compare the results of the proposed and the k-means methods for the effectiveness of the proposed method.

Keywords: Scene image, Image segmentation, HSI color space, Achromatic color

1 Introduction

An image recognition is one of the most important techniques in robotics and image retrieval. However, the image recognition technique is not complete and is in study phase. An image segmentation is a very important subject for the image recognition.

The k-means method[1] is one of the most well-known clustering methods. However, the number of clusters and the initial values must be decided in the method. The k-means application[2],[3] and the ISODATA[4],[5] have been proposed in order to overcome the problems. The Euclidian distance have been applied by the traditional methods in order to represent a difference between colors. The Euclidean distance does not always correspond to the difference between colors in human eyes. In the [7], HSI color space is divided into 9 regions by thresholds previously. Images are segmented by the 9 regions. However the thresholds differ from image to image.

We propose a new image segmentation method for scene images. The proposed method segments images without using the Euclidian distance.

2 The problems of the conventional methods

The problems of the conventional methods[1]-[6] are shown in the follows.

1. The parameters optimization
2. The Euclidian distance

At first, we discuss the parameters. In the case of the k-means method, the most important parameter is the number of clusters. It is difficult to decide the number of clusters in our study. Setting of the initial value is also one of the papameter problems. Though, [5] has overcome the parameter problems, the number of parameters has increased.

Next, we discuss the Euclidian distance. The Euclidian distance is very useful, since we can translate multi-dimensional points into one-dimension. Therefore, it is also used as the indicator of a difference between colors in the image processing. The

Fig. 1: An example of the Euclidian distance problem

Euclidean distance does not always correspond to a difference between colors by human eyes. For example, we give three colors whose RGB values are (92,172,203), (143,196,217) and (100,148,153) as Fig.1. The Euclidian distances between (92,172,203) and (143,196,217) and between (92,172,203) and (100,148,153) are 58.1 and 56.0, respectively. In the human visual sence, however, the distance between (92,172,203) and (143,196,217) is shoter than the distance between (92,172,203) and (100,148,153). Therefore, it is not effective that the Euclidian distance is applied to the difference of colors.

3 The proposed method

We propose the new image segmentation method to overcome the problem. The proposed method segments images without using the Euclidian distance. The process of the proposed method is as follows. At first, we transform image information from RGB to HSI (hue, saturation and intensity), since HSI color space is close to a human visual sense and the components of HSI are the high independent components. Human pays attention to not only a pixel but also pixels around it, when he sees an image. To reflect the human characteristics, the moving average method is used. We calculate the histograms of the image for each component, and obtain three results of the image segmentation from each histogram. The clustering is to decide the boundaries among the classes on the histograms. The boundary is decided by maximizing between-class variance. In the proposed method, the boundaries are decided at a valley between peaks in a waveform of a histogram. One or more boundaries are obtained by iterating the same process until a maximum value of between-class variance is less than a threshold. The final segmentation result is obtained by the AND operation from three clustering results. However, the simple AND operation may result in many regions, since the simple AND operation does not consider the achromatic colors. In our research, we obtain the final segmentation results by AND operation with the consideration of the achromatic colors, which have low intensity or low saturation values. In the former, only the result of the intensity is reflected to the final result. In the later, the results of the intensity and saturation are reflected to the final result. We describe the details of the processes in follows.

Fig. 2: An original image

3.1 The moving average method

Human pays attention to not only a pixel but also pixels around it, when he sees an image. For example, when a target pixel color differs from colors of pixels around it, human understands it as a noise. To reflect the human characteristics, the moving average method is used. The moving average is the method that a value of a pixel (i,j) is converted into an average value of pixels around it. In this paper, the filter size of the method is defined as 5×5. The value of target pixel using the method is defined as $g(i,j)$, which is given by

$$g(i,j) = \sum_{k=-2}^{2} \sum_{l=-2}^{2} \frac{1}{5 \times 5} f(i+k, j+l) \qquad (1)$$

where, f(i,j) is the value of target pixel in the original image. In this paper, although the method is used for the intensity and the saturation values, the method is not used for the hue. Figure 3 shows the histograms of Fig.2, and Fig.4 shows the histograms using the moving average method. From the figures, it is found that noises are removed by the moving average method.

3.2 The clustering processing

The clustering method in this paper is to decide the boundaries among the classes on the histograms. A boundary is decided by maximizing between-class

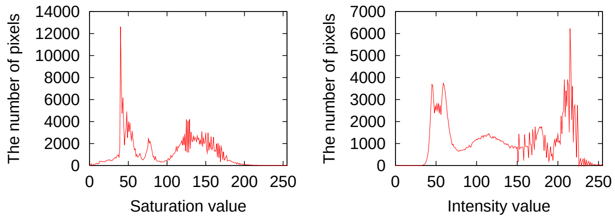

(a) Saturation (b) Intensity

Fig. 3: Histograms of Fig.2

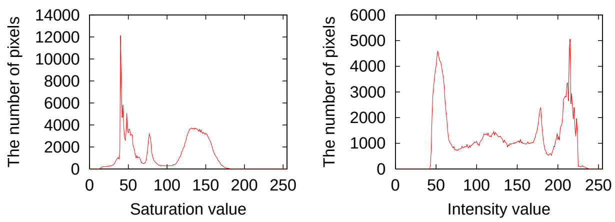

(a) Saturation (b) Intensity

Fig. 4: Histograms using the moving average method

variance. In the proposed method, the boundaries are decided at a valley between peaks in a waveform of a histogram. One or more boundaries are obtained by iterating the same process until a maximum value of between-class variance becomes less than a threshold. The between-class variance when a histogram is devided into two classes at a boundary i is given by

$$\sigma_B(i) = \omega_1(i)\omega_2(i)(M_1(i) - M_2(i))^2 \tag{2}$$

where, ω_1 and ω_2 mean the number of pixels in class 1 or 2 respectively, and M_1 and M_2 mean averages in class 1 or 2 respectively. Therefore, the boundary is given as

$$t = \arg\max_i \sigma_B(i) \tag{3}$$

The process is iterated until $\sigma_B(i)$ becomes a smaller value than a threshold.

3.3 The AND operetion

The final segmentation result is obtained by the AND operation from three clustering results. Figure 5 shows an example of the AND operation. However, the simple AND operation may result in many regions obtained, since the simple AND operation does not consider the achromatic colors. In this paper, we obtain the final segmentation results by AND operation with considering the achromatic colors. The regions of the achromatic colors are defined as the follows.

1. The region including low saturation pixels
2. The region including low intensity pixels

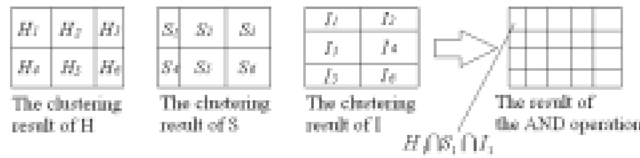

Fig. 5: An example of the AND operation

The reason of the (1) which is mentioned above is that the achromatic color is not vivid simply. However, the (1) does not cover all the achromatic colors. For example, the color whose RGB value is (0,0,1) does not satisfy the (1) despite being an achromatic color clearly. The calculating formula of the saturation in this paper is given by

$$S = \frac{\max(r,g,b) - \min(r,g,b)}{\max(r,g,b)} \tag{4}$$

Therefore, the saturation of the color is 1. The achromatic color condition is not only (1) but also (2).

The process of the AND operation with considering the achromatic colors is discribed in the follows. First, we check if a region satisfies (2). If so, the results of the saturation and the hue are not reflected to the final region. If not, we check if a region satisfies (1). If so, the results of the intensity and the saturation are reflected to the final region. If not, we use the all results to the final region. In this paper, the (1)'s condition is the region including even one pixel whose saturation is less than 25, and the (2)'s condition is the region including even one pixel whose intensity is less than 50.

4 Computer simulation

In order to effectiveness of the proposed method, we simulate the proposed and the k-means (Method 1, Method 2) methods by several scene images. The parameters at end conditions and the number of clusters in the simulation of Fig.2 are shown in Table 1.

In the Method 1, the Euclidian distance between a center of a cluster $(\bar{H}, \bar{S}, \bar{I})$ and a point (H, S, I) is

Table 1: The end conditions of the clustering and the number of clusters

	H	S	I
Threshold	1000	490	450
The number of clusters	2	2	4

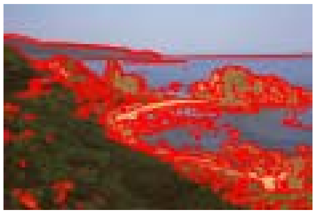

(a) The proposed method

(b) k-means（Method 1）

(c) k-means（Method 2）

Fig. 6: The image segmentation results of Fig.2

given as

$$D = \left\{ \left(\frac{1 - \cos(\bar{H} - H)}{2} \right)^2 + (\bar{S} - S)^2 + (\bar{I} - I)^2 \right\}^{\frac{1}{2}} \tag{5}$$

In the Method 2, we compare the clustering method of this paper with the k-means method. The distances are given as

$$\begin{aligned} D_H &= |\bar{H} - H| \quad (\text{if} \quad D_H > \pi, \text{then} \quad D_H = 2\pi - D_H) \\ D_S &= |\bar{S} - S| \\ D_I &= |\bar{I} - I| \end{aligned} \tag{6}$$

The image segmentation results using each method are shown in Fig.6.

We compare the results of the proposed method and Method 1. The result of the proposed method is better than the result of Method 1 clearly. For example, in Method 1 the sea and the sky are the same region, and in the proposed method the sea and the sky are different regions. As the results of comparing the proposed method with Method 2, the proposed is similar to Method 2. However, the proposed method is more convenient than Method 2, since we must set the number of clusters in Method 2.

5 Conclusion

We have proposed the new image segmentation method. We have solve the problems of the parameters and the Euclidian distance using the proposed method, and have been reflected the characters of human visual sense. In order to show the effectiveness of the proposed method, we have segmented the several scene images. As the result of the simulation, We can show the proposed method.

In future work we will propose a image recognition method using the image segmentation method.

References

[1] S. Z. Selim and M. A. Ismail, "K-means-Type Algorithm," *IEEE Trans. on Pattern Analysis and Machine Intelligence*, 6-1 (1984) pp.81–87.

[2] N. W. Campbell, W. P. J. Mackeown, B. T. Thomas and T. Troscianko, "Interpreting Image Databases by Region Classification," *Pattern Recognition (Special Edition on Image Databases)*, 30-4 (1997) pp.555–563.

[3] S. Sakaida, Y. Shishikui, Y. Tanaka and I. Yuyama: "An Image Segmentation Method by the Region Integration Using the Initial Dependence of the K-Means Algorithm", *IEICE TRANS.*, Vol.J81-D-II, No.2, (1998) pp.311–322. (in Japanese)

[4] G.H. Ball and D.I. Hall: "Some Fundamental Concepts and Synthesis Procedures for Pattern Recognition Preprocessors," *Proc. Int'l Conf. Microwaves, Circuit Theory, and Information Theory,* (1964) pp. 281-297.

[5] K. Takahashi and K. Abe: "Color Image Segmentation Using ISODATA Clustering Algorithm", *IEICE TRANS.*, Vol.J82-D-II No.4, (1999) pp.751–762. (in Japanese)

[6] S. Ito, S. Omatu, "Keywords Specification for Images Using Sandglass-Type Neural Networks," *IJCIA*, Vol.4 No.2 (2004) pp.143–152.

[7] J. Cheng, Y. Chen, H. Lu and X. Zeng, "A Spatial Weighted Color Histogram for Image Retrieval," *IEICE TRANS. INF. & SYST.*, Vol.E87-D No.1 (2004) pp.246–249.

The Tenth International Symposium on Artificial Life and Robotics 2005(AROB 10th '05),
B-con Plaza, Beppu, Oita, Japan, February 4-6, 2005

An image recognition method by rough classification for a scene image

Seiji Ito
Computer and Systems Science
Osaka Prefecture University
1-1 Gakuencho Sakai-City
Osaka 599-8531 Japan
seiji@sig.cs.osakafu-u.ac.jp

Michifumi Yoshioka
Computer and Systems Science
Osaka Prefecture University
1-1 Gakuencho Sakai-City
Osaka 599-8531 Japan
yoshioka@cs.osakafu-u.ac.jp

Sigeru Omatu
Computer and Systems Science
Osaka Prefecture University
1-1 Gakuencho Sakai-City
Osaka 599-8531 Japan
omatu@cs.osakafu-u.ac.jp

Kouji Kita
Noritsu Koki Co., LTD.
579-1 Umehara, Wakayama-City
Wakayama, 640-8550, Japan
k-kita@nkc.noritsu.co.jp

Kouichi Kugo
Noritsu Koki Co., LTD.
579-1 Umehara, Wakayama-City
Wakayama, 640-8550, Japan
k-kugo@nkc.noritsu.co.jp

Abstract

We have analyzed the regions of scene images for the image recognition. At first, the segmentation method which we have proposed classifies images into several segments without using the Euclidian distance. We need several features to recognize regions, but they are different between chromatic and achromatic colors. Regions are divided into three categories (black, achromatic, chromatic). In this paper, we focus on the achromatic category, the several features of the regions in the achromatic category are calcurated and plotted.
Keywords: Scene image, Image recognition, Image segmentation, Chromatic color, Achromatic color

1 Introduction

Recently, enormous image data exist on the world wide web by the rapid development of the Internet. Therefore, it is difficult to obtain only requested images on the web. There have been several methods for the image search. They are classified into three kinds; keyword search, similarity-based image retrieval, and browsing search. In the keyword search method, requested images are retrieved by using a database such as Google searching system which is constructed by images and keywords. Using the searching method, only requested images are not always obtained, since they are based on the file name searching. In the similarity-based image retrieval method, requested images are drawn by selection of sample images [1],[2],[5],[6]. However, users have taken many tasks for selecting or drawing a requested image. The browsing search method is an interactive method. The method takes much time to search images. Therefore, we focus on searching the keyword from an image. Once the database is constructed, the system enables us to search images by keywords which are desired by users. Some extraction methods [3],[4] by using location information have been proposed. Since they depend on specific images, it is difficult to construct a database.

In this paper, we propose a method to extract keywords from images automatically. The method enables us to add the keywords to the database. The object images in this paper are only scene images. The images are segmented into some regions in order to specify a keyword for the region of the image by the method which we have proposed. In this paper, we propose the region recognition method by using the image segmentation method which we proposed. In the proposed method of image segmentation, an achromatic color is considered. Since, features of colors are different between chromatic and achromatic colors. Therefore, we classify roughly regions into the chromatic and achromatic colors.

2 The image segmentation method

We segment the images for the region recognition. The conventional methods[7]-[11] have been proposed, but they have used the Euclidian distance. We have

(a) An original image (b) The image segmentation result

Fig. 1: An image segmentation result by the proposed method

proposed the new image segmentation method. The proposed method segments images without using the Euclidian distance, since the Euclidean distance does not always correspond to the difference between colors in human eyes. The process of the proposed method is as follows.

At first, we transform image information from RGB to HSI (hue, saturation and intensity), since HSI color space is close to a human visual sense and the components of HSI are the high independent components. Human pays attention to not only a pixel but also pixels around it, when he sees an image. To reflect the human characteristics, the moving average method is used. We calculate the histograms of the image for each component, and obtain three results of the image segmentation from each histogram. The clustering is to decide the boundaries among the classes on the histograms. The boundary is decided by maximizing between-class variance. The method is that a boundary is decided at a valley between peaks in a waveform of a histogram. One or more boundaries are obtained by iterating the same process until a maximum value of between-class variance is less than a threshold. The final segmentation result is obtained by the AND operation from three clustering results. However, the simple AND operation may result in many regions obtained, since the simple AND operation does not consider the achromatic colors. In our research, we obtain the final segmentation results by AND operation with the consideration of the achromatic colors. The achromatic colors have low intensity or low saturation values. In the former, only the result of the intensity is reflected to the final result. In the later, the results of the intensity and saturation are reflected to the final result. A result of the image segmentaiton method is shown in Fig.1

3 Features distribution of the regions

The regions which are obtained by using the image segmentation method are recognized. We need several features to recognize regions, but these are different between chromatic and achromatic colors. As regions are divided into the black, achromatic and chromatic categories in the image segmentation phase, we divide regions into three categories in the recognition phase.

In this paper, we recognize the regions in chromatic category. The main regions in the category are "Cloud", "Sky" and "Snow". In the category, the effective color feature is only intensity. The average and the standard deviation of the regions are calculated, and distributions of the features are checked. The energy and the homogeneity which are obtained from gray-level co-occurrence matrix are also calculated and checked. $P(i,j|d,\theta)$ denotes the (i,j)th element of a co-occurence matrix, where d is a distance, θ is an angle. The energy $E(d,\theta)$ and the homogeneity $H(d,\theta)$ are given as follows.

$$E(d,\theta) = \sqrt{\sum_i \sum_j P^2(i,j|d,\theta)} \quad (1)$$

$$H(d,\theta) = \sum_i \sum_j \frac{P(i,j|d,\theta)}{1+(i-j)^2} \quad (2)$$

The results are shown in Fig.3.

From Fig.3, The average is effective for recognizing the regions. However the standard deviation and the features from the gray level co-occurrence matrix are not effective. From Fig.2(b), it is found that the value of intensity is different among the regions. Therefore, the average is effective. However, the reason why the standard deviation is not different among the regions is that the differences between the average of the region and the value of intensity are not large. The reason why the texture features are not different among the region is the same as above.

4 Conclusion

In this paper, we have analyzed the features of the regions for the image recognition. At first, regions have been obtained by using the image segmentation method which we had proposed. The regions have been divided into three categories. The features of regions in the achromatic category have been calculated and plotted. From the results, we must obtain new features.

(a)Regions of the black category

(b)Regions of the achromatic category

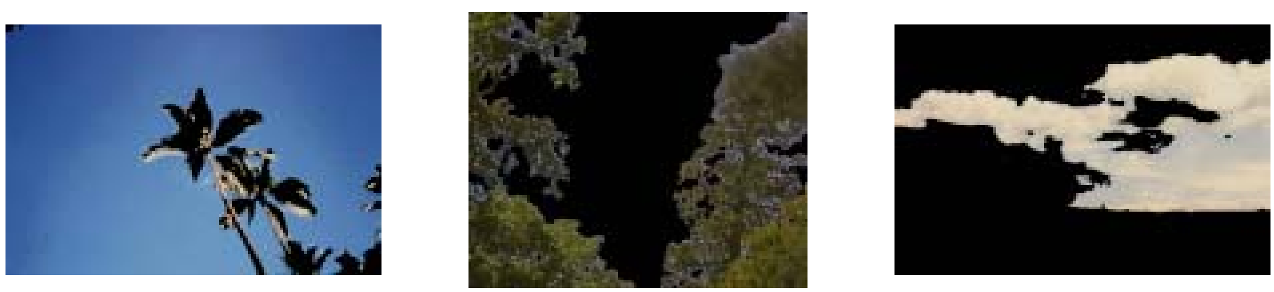

(c)Regions of the chromatic category

Fig. 2: Regions examples of the three categories

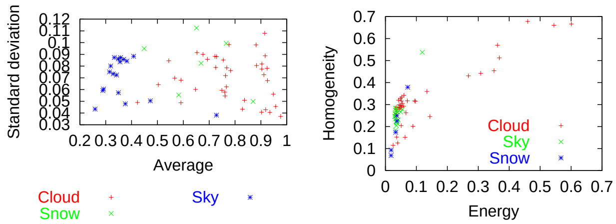

(a) Average and standard deviation

(b) Energy and homogeneity

Fig. 3: The distributions of the features

References

[1] M. Mukunoki, M. Minoh and K. Ikeda, A Retrieval Method of Outdoor Scenes Using Object Sketch and an Automatic Index Generation Method, *IEICE Trans.*, Vol.J79-D-II, No.6 (1996) pp.1025–1033. (in Japanese)

[2] Wei Ren Maneesha, Image Retrieval Using Spatial Context "http://citeseer.nj.nec.com/535521.html"

[3] H. Iyatomi and M. Hagiwara, "Scenery Image Recognition and Interpretation using Fuzzy Inference Neural Networks," *Pattern Recognition*, Vol.35, No.8 (2002) pp.1793-1806.

[4] A. Yamamura and M. Hagiwara, "Recognition of Scenery Images considering Positional Relation using Fuzzy Inference Neural Networks," *IEE Japan Trans.*, Vol.122-C (2002) pp.506–511.

[5] J. Cheng, Y. Chen, H. Lu, and X. Zeng, A Spatial Weighted Color Histogram for Image Retrieval, *IEICE Trans. Information & Systems*, Vol.E-87D, No.1 (2003) pp.246–249.

[6] X. Zeng, Y. Chen, Z. Nakao, J. Chen and H. Lu, Image Retrieval based on Independent Components of Color Histgrams, *Proc. Knowledge-Based Intelligent Information and Engineering Systems*, Oxford, UK, September 2003, pp.1435–1442.

[7] S. Z. Selim and M. A. Ismail, "K-means-Type Algorithm," *IEEE Trans. on Pattern Analysis and Machine Intelligence*, Vol.6, No.1 (1984) pp.81–87.

[8] S. Sakaida, Y. Shishikui, Y. Tanaka and I. Yuyama: "An Image Segmentation Method by the Region Integration Using the Initial Dependence of the K-Means Algorithm", *IEICE TRANS.*, Vol.J81-D-II, No.2, (1998) pp.311–322. (in Japanese)

[9] G.H. Ball and D.I. Hall: "Some Fundamental Concepts and Synthesis Procedures for Pattern Recognition Preprocessors," *Proc. Int'l Conf. Microwaves, Circuit Theory, and Information Theory,* (1964) pp.281-297.

[10] K. Takahashi and K. Abe: "Color Image Segmentation Using ISODATA Clustering Algorithm", *IEICE TRANS.*, Vol.J82-D-II No.4, (1999) pp.751–762. (in Japanese)

[11] S. Ito, S. Omatu, "Keywords Specification for Images Using Sandglass-Type Neural Networks," *IJCIA*, Vol.4 No.2 (2004) pp.143–152.

The Tenth International Symposium on Artificial Life and Robotics 2005(AROB 10th '05),
B-con Plaza, Beppu, Oita, Japan, February 4-6, 2005

Information filtering using probabilistic model

Hidekazu Yanagimoto
Department of Computer and Systems Sciences
Osaka Prefecture University
1-1, Gakuencho, Sakai
Osaka 599-8531, Japan

Sigeru Omatu
Department of Computer and Systems Sciences
Osaka Prefecture University
1-1, Gakuencho, Sakai
Osaka, 599-8531, Japan

({hidekazu, omatu}@cs.osakafu-u.ac.jp)

Abstract

We propose an information filtering system based on a probablistic model. We have an assumption that a document is generated according to a probability distribution and regard a document as a sample drawn according to the distribution. In this paper, we adopt multinomial distribution and represent a document as probabilitiy which has random values as words in the document. When an information filtering system selects information, it uses a similarity between a user profile and a document. Since our proposed sytem is constructed under the probalistic model, the similarity is defined using Kullback-Leibler divergence. To create the user profile, we must optimize the Kullback-Leibler divergence. Since Kullback-Leibler divergence is non-linear function, we use a genetic algorithm to optimize it. We carry out experiments and confirm effectiveness of the propsed method.

Keyword: Information Filtering, Genetic Algorithm, Kullback Leibler Divergence

1 Introduction

Users can have access to vast store of information through the Internet recently, as the Internet becomes widespread. When they search information they desire with search engines, they get a lot of search results and hardly find ones they desire truly. To cope with this situation, many researchers have paid attention to developing information filtering systems. The information filtering systems automatically select information depending on user's interests (user profile). To select information correctly, the systems must create the user profile which represents user's interests exactly.

Many researchers pay attention to studying a probablistic model of documents. This model is different from vector space model (VSM) which is used in many information retirieval systems. In the VSM, documents are described as vectors using term frequency and document frequency. On the other hand, doucments are described as a probability distribution in the probabilistic model. This causes improving information filtering systems.

In this paper, we propose an information filtering system based on a probablistic model. A similarity between a user profile and a document is defined using Kullback-Leibler divergence (KL divergence). The KL divergence is a measure which represents a similarity between two probability distributions. Since the KL divergence is non-linear, a GA explores the user profile. Since our aim is to improve an information filtering system, we discuss effectiveness of a proposed mnethod in the viewpoint of selection ability.

2 Previous work

An information filtering system selects information depending on user's interests. Hence, it is important for the system to keep user's interests (user profile) exactly. To make the user profile, information retrieval techniques, pattern recognition and machine learning are used.

To deal with documents on computers, VSM and relevance feedback are reported by Salton et al[1]. In the VSM all documents are represented as vectors and a distance between documents is defined using an inner produce between the documents. To clear up user's interest in the VSM, relevance feedback is used.

A probabilistic approache is reported to enrich a document vector[3]. In this approache, we assume documents are generated from an unknow distribution. Hence, our aim is to identify the unknown disribution. In the probabilistic model, the distribution is regarded as a binomial distribution or a multinomial distribution.

A GA is an algorithm which simulates biological evolution and is proposed by Holland[2]. The GA is often applied to combinational optimization problems and can optimize a non-linear function.

3 Methodology

In this section we explain key concepts of a proposed mnethod. They are a probablistic model, a similarity using Kullback-Leibler divergence and a GA.

3.1 Probabilistic Model

In a probabilistic model it is assumed that that a document is generated from an unknown probability distribution. Hence, a main aim is to identify the unknown distribution from sample documents. In probabilistic information retrieval, the unknow distribution is restrictive. For example, we assume that the distribution is a binomial distribution or a multinomial distribution. In this paper, we adopt the assumption that the distirbution is a multinomial distribution.

The multinomial distribution is represented below.

$$Pr(X_1 = n_1, \cdots, X_k = n_k) = \frac{n!}{\prod_{i=1}^{k} n_i!} \prod_{i=1}^{k} p_i^{n_i} \quad (1)$$

where X_i is a random variable, p_i is a probability of the ith random variable X_i, n_i is a frequency of X_i and n is a sum of n_i. Since a document is generated from the multinomial distribution in this paper, we estimate p_i in Equation(1) using a maximum likelihood estimate method. THe maximum likelihood estimate is calculated below.

$$p_i = \frac{n_i}{n} \quad (2)$$

We estimate one multinomial distribution from one document and consider the distribution represents the document. We define a user profile as a probability distribution, too . However, we do not assume that the user profile is any probability distribution.

3.2 Similarity using Kullback-Leibler divergence

As noted above, we express a probabilistic model and represented a document as a multinomial distribution. To use the probabilistic model in information filtering, we must define a distance between a user profile and a document. Since the distance denote a similarity between the user profile and the document, we propose Kullback- Leibler divergence (KL divegence) to calculate the distance. The KL divergence is a divergence to compare two probability distributions and is defined as below.

$$Div(p_k||q_k) = \sum_{k=1}^{n} q_k \; log \frac{q_k}{q_k} \quad (3)$$

where q_k and p_k are probabilities of kth word in probability distributions of q and p. The KL divergence does not become negative. If two distributions is same, KL divergence is 0.

As the user profile represents user's interest, it is close to the document vector of an interesting document and far from the one of an uninteresting document. Recommending documents according to user's interest, our proposed mnethod selects documents depending on the similarity calculated between a user profile and a document.

3.3 Genetic Algorithm

We make a user profile using a GA since to make the user profile is to find the vector which maximizes the similarity between a gene and an interesting document vector and minimizes the similarity between a gene and an uninteresting document vector. In the GA, a gene represents the user profile and is a real valued vector.

To carry out a GA, a fitness function must be defined. The fitness function is

$$F_k = \sum_{D_i \in I} Div(gene_k||doc_i) - \sum_{D_j \in U} Div(gene_k||doc_j) \quad (4)$$

where $Div(gene_k||doc_i)$ is the KL divergence between a document vector for D_i and the kth gene, I is a set of interesting documents and U is a set of uninteresting documents.

Our crossover is unimodal normal distribution crossover (UNDX) proposed by Ono et al [4]. The UNDX is one of crossover techniques implemented for a real-coded GA and explores a search space depending on a distribution of genes. Pseudocode for the GA is shown in Figuer 1.

4 Experiment

In this section, we describe a test collection, simulation setting and results.

Given initial genes at random. For $t = 0, \cdots, T$:
·Select two genes as parents.
·For $n = 0, \cdots, N$
·Produce two child genes using UNDX.

$$\mathbf{C}_1 = \mathbf{m} + z_1\mathbf{e}_1 + \sum_{k=2}^{n} z_k\mathbf{e}_k$$
$$\mathbf{C}_2 = \mathbf{m} - z_1\mathbf{e}_1 - \sum_{k=2}^{n} z_k\mathbf{e}_k$$
$$\mathbf{m} = \frac{(\mathbf{P}_1+\mathbf{P}_2)}{2}$$
$$z_1 \sim N(0, \sigma_1^2),\ z_k \sim N(0, \sigma_2^2)$$
$$\sigma_1 = \alpha d_1,\ \sigma_2 = \frac{\beta d_s}{\sqrt{n}}$$
$$\mathbf{e}_1 = \frac{(\mathbf{P}_1-\mathbf{P}_2)}{|\mathbf{P}_1-\mathbf{P}_2|},\ \mathbf{e}_i \perp e_j (i \neq j)$$

·Select two genes as survivors from all child genes.

Figure 1: The GA algorithm.

4.1 Data

To evaluate a proposed method, we use NTCIR2 test collection which consists of many evaluated documents. In the NTCIR2, many tasks, for example queries on information retrieval, homesickness syndroand and singular point, are prepared. In each task, a document has a label which denotes whether it is relevant or not.

In this experiment, we regard relevant documents as interesting documents and make a user profile. We pick up 14 tasks which have more than 20 relevant documents and use them as experiment tasks. Since a GA is a probabilistic optimizing method, we carry out 10 trials per one task. Traning documents consist of 100 documents drawn at random from all documents and test data consist of the other documents. Each trial uses different training data and test data. In Table 1, we show the number of all documents, all relevant documents and average relevant documents in one trial.

4.2 Simulation and Result

To discuss our proposed mnethod, we compare it with relevance feedback. The relevance feedback is used in the VSM and uses an innar product as a similarity between a user profile and a document. The similarity calculated with an inner product is defined below.

$$sim_i = profile \cdot doc_i \quad (5)$$

where sim_i is a similarity between a user profile and the ith document, doc_i is a document vector of the ith document Doc_i and $\cdot$ denotes an inner product. The document vector is calculated using tf·idf in the relevance feedback. In a comparative experiment, traning data is the same data as in our proposed mnethod.

Table 1: The tasks used in the experiment.

Task No.	all	relevant	relevant/trial
108	371	64	19.0
109	453	21	3.9
110	624	34	5.0
111	540	40	7.2
114	616	20	3.1
115	931	94	9.6
119	387	20	4.6
121	501	63	11.4
126	279	22	6.8
132	210	22	11.2
138	253	24	10.6
139	386	142	39.0
140	309	23	7.7
147	591	80	13.1

Table 2: The Parameters of GA.

population	Generations	Crossover	α	β
5000	50000	20	0.5	0.35

The relevance feedback is defined below.

$$profile = a \sum_{D_i \in I} doc_i - b \sum_{D_j \in U} doc_j \quad (6)$$

where both a and b are arbitrary positive numbers. We decide both a and b using leave-one-out.

Since our proposed mnethod uses a GA, the parameters of the GA for two methods are shown in Table 2. The GA needs more population and generationsto explore wide search space.

In Table 3, 11-point average precision is shown. The 11-point average precision is calculated with 11 precision on 11 recall levels.

4.3 Discussion

In Table 3, we realize that our proposed mnethod is superior to relevance feedback in 9 tasks. However, in the other 5 tasks, relevance feedback is superior to the proposed mnethod. We discuss this 5 tasks in detail especially.

Since a genetic algorithm is probabilistic method, the proposed mnethod depends on various conditions (initial genes, generation of child genes and selection). Hence, we discuss a difference of 11-point average precision using t-test. The t-test is a statistical method to consider whether this difference is significant. In

Table 3: The 11-point average precision.

Task No.	KL divergence($\hat{\mu}_{KL}$)	cosine($\hat{\mu}_{COS}$)
108	0.342	0.282
109	0.189	0.100
110	0.170	0.076
111	0.164	0.188
114	0.152	0.085
115	0.261	0.169
119	0.174	0.087
121	0.390	0.281
126	0.112	0.287
132	0.206	0.208
138	0.609	0.641
139	0.807	0.772
140	0.207	0.192
147	0.357	0.376

Table 4: The result of t-test.

Task No.	t
108	2.937
109	2.329
110	3.599
111	$\underline{1.198}$
114	1.942
115	3.809
119	2.667
121	2.765
126	$\underline{3.547}$
132	$\underline{0.064}$
138	$\underline{0.664}$
139	2.020
140	0.430
147	$\underline{0.530}$

this case a null hypothesis H_0 is $\mu_{KL} = \mu_{COS}$ where μ_{KL} is an expectation of 11-point average precision for the proposing method and μ_{COS} is an expectation of 11-point average precision for the relevance feedback. First, the difference of the 11-point average precisions is transformed with next formula in each task.

$$t = \frac{\hat{\mu}_{KL} - \hat{\mu}_{COS}}{s\sqrt{\frac{1}{n_{KL}} + \frac{1}{n_{COS}}}} \tag{7}$$

where s is standard deviation of 11-point average precisions for all trials, n_{KL} is the number of 11-point average precision for the proposing method ($n_{KL} = 10$) and n_{COS} is the number of 11-point average precision for the relevance feedback ($n_{COS} = 10$). Since we adopt the level of significance of 5% in this t-test, t becomes 2.101. When t is more than 2.101, the null hypothesis H_0 is rejected. In table 4, we show the result of t-test. When a value of relevance feedback is bigger, the t is underlined.

In Table 4, we find that in 6 tasks the proposed mnethod is superior to the relevance feedback in the view of t-test and in one task inferior.

5 Conclusion

In this paper, we proposed information filtering using a probabilistic model. We introduced a multinomial distribution to express documents and KL divergence to calculate a similarity between a user profile and a document. We confirmed that the proposed mnethod is superior to relevance feedback in some tasks with significance test.

We will apply this proposed mnethod to other situations and evaluate the proposed mnethod in detail.

Acknowledgements

This study is supported by Grants-in-Aid for Scientific Research. We would like to thank MEXT for the supports.

References

[1] G. Salton and M. McGill(1983), Introduction to Modern Information Retrieval, McGrwa-Hill Book Company, New York

[2] C. D. Manning and H. Schutze(1999), Foundation of Statistical Natural Language Processing, MIT Press.

[3] J. H. Holland(1962), Outline for a Logical Theory of Adaptive Systems, Journal of the Association for Computing Machinery, vol.3, pp.297–314.

[4] I. Ono and S. Kobayashi(1997), A Real-coded Genetic Algorithm for Function Optimization Using Unimodal Normal Distribution Crossover, Proceedings of 7th International Conference on Genetic Algorithms, pp.246–253

The Tenth International Symposium on Artificial Life and Robotics 2005(AROB 10th '05),
B-con Plaza, Beppu, Oita, Japan, February 4-6, 2005

Modification of user profile using the genetic algorithm

Hidekazu Yanagimoto
Department of Computer and Systems Sciences
Osaka Prefecture University
1-1, Gakuencho, Sakai
Osaka 599-8531, Japan

Sigeru Omatu
Department of Computer and Systems Sciences
Osaka Prefecture University
1-1, Gakuencho, Sakai
Osaka, 599-8531, Japan

({hidekazu, omatu}@cs.osakafu-u.ac.jp)

Abstract

We propose a method which modifies a user profile (user's interests) using a genetic algorithm (GA). In information filtering, a method which constructs linear function using cosine distance, for example relevance feedback is often used. This discriminant linear function represents a hyperplain in vector space model (VSM). We focus on the classification hyperplane in the VSM and discuss a selection method of the most optimal hyperplane. Our aim is to make a selection criterion based on the above discussion. To decide the hyperplain which satisfies the criterion, we explore search space using a GA. Finally we describe experiments to evaluate a proposed method and discuss effectiveness of it.

Information filtering, Genetic Algorithm

1 Introduction

Users can have access to vast store of information through the Internet recently, as the Internet becomes widespread. When they search information they desire with search engines, they get a lot of search results and hardly find ones they desire. To cope with this situation, many researchers have paid attention to developing information filtering systems. The information filtering systems automatically select information depending on user's interests (user profile). To select information correctly, the systems must keep appropriate user's interests.

In this paper, we propose a method which modifies a user profile using a genetic algorithm (GA). To make the user profile is to decide a hyperplain in vector space model (SVM). There are many hyperplains which can separate training data according to their labels. Hence, we introduce a new criterion which can select many documents correctly and maximize a distance between the hyperplain and each training data. We use the GA to make the user profile which satisfies the criterion.

To evaluate our proposed method, we carry out an expriment and discuss effectiveness of the criterion in the view of selection ability.

2 Previous work

The proposing system consists of an information filtering and a GA to create user profile. We describe related works in detail.

An information filtering system is a system which selects information depending on user's interests. A content-based filtering system[1] chooses information analyzing a content of information. The content-based filtering system generally selects texts. A social filtering system[2] is a system which selects information using the relationship between a user and an information creator. Since social information is used without analyzing a content of information, the systems can be expanded to a systems which deal with non-text data. A collaborative filtering system[3] is a system which selects information depending on ratings voted by many other users. The system calculates a similarity among users and recommends information which other users who have the same interests are interested in. The system is applied to texts, graphical data, music and so on.

A GA is an algorithm which simulates biological evolution and is proposed by Holland[4]. The GA is often applied to combinational optimization problems. NewT[5] is an information filtering system using a GA.

3 Methodology

In this section, we explain key concepts of a proposed method. They are a problem setting, VSM and a GA.

3.1 Problem setting

We consider a linear discriminant function without a threshold and training data without noise in a classification problem. Then the discriminant function represents a hyperplain and weights of the discriminant function represents a normal vector. The normal vectors form a hypersphere in VSM. The normal vectors which can select training data are correctly included in a part of the hypersphere. Hence, to decide the optimal discriminant function, we must select one of the normal vectors included in the part of hypersphere using a criterion.

We introduce a criterion to select one of discriminant functions which select training data correctly. Using the criterion, we focus on the nearest trainig data from the hyperplain and select the hyperplain maximizing a distance between the hyperplain and the training data. To make discriminant function (user profile), this criterion is applied to a fitness function of a GA.

3.2 Vector Space Model

In VSM, documents written with natural language is represented as vectors to deal with them on computers. The vector is called a document vector below. An element of the document vector denotes a word included in a document and is calculated by TF-IDF.

$$w^i_j = tf^i_j \; log\frac{N}{df_j} \tag{1}$$

where w^i_j is a weight of the jth term T_j in ith document Doc_i, tf^i_j is a term frequency of T_j in Doc_i, df_j is a document frequency of T_j and N is the total number of documents.

In the VSM, a similarity between two documents can be defined by a distance between them. The distance is generally calculated by an inner product.

$$sim_i = profile \cdot doc_i \tag{2}$$

where sim_i is a similarity between a user profile and a document, doc_i is a document vector of the ith document Doc_i and $\cdot$ denotes an inner product.

In this paper, a user profile, which represents user's interest, is the same vector as a document vector. As the user profile represents user's interest, it is close to document vectors of interesting documents and far from ones of an uninteresting documents. Recommending documents according to user's interest, our proposed method selects a document depending on the similarity between the user profile and the document.

3.3 Genetic Algorithm

We make a user profile using a GA since to make the user profile is to find a vector which maximizes a similarity between a gene and an interesting document vector and minimizes a similarity between a gene and an uninteresting document vector. In the GA, a gene represents the user profile and is a real valued vector.

To carry out a GA, a fitness function must be defined. The fitness function is

$$F_k = |D_c| + \min_{D_i \in I} sim_i - \min_{D_i \in U} sim_i \tag{3}$$

where $|\cdot|$ is the number of elements in a set, D_c is a set of documents selected correctly, I is a set of interesting documents and U is a set of uninteresting documents. The first term in Equation 3 denotes ability to select documents correctly, the other terms denote distances between a hyperplain and a document. This fitness function denotes that the fitness value becomes a maximum value when a gene selects documents according to their ratings.

Our crossover is unimodal normal distribution crossover (UNDX) proposed by Ono et al [6]. The UNDX is one of crossover techniques implemented for a real-coded GA and explores a search space depending on a distribution of genes. Pseudocode for the GA is shown in Figure 1.

Given initial genes at random. For $t = 0, \cdots, T$:
- ·Select two genes as parents.
- ·For $n = 0, \cdots, N$
  - ·Produce two child genes using UNDX.
    - $\mathbf{C}_1 = \mathbf{m} + z_1\mathbf{e}_1 + \sum_{k=2}^{n} z_k\mathbf{e}_k$
    - $\mathbf{C}_2 = \mathbf{m} - z_1\mathbf{e}_1 - \sum_{k=2}^{n} z_k\mathbf{e}_k$
    - $\mathbf{m} = \frac{(\mathbf{P}_1+\mathbf{P}_2)}{2}$
    - $z_1 \sim N(0, \sigma_1^2)$, $z_k \sim N(0, \sigma_2^2)$
    - $\sigma_1 = \alpha d_1$, $\sigma_2 = \frac{\beta d_s}{\sqrt{n}}$
    - $\mathbf{e}_1 = \frac{(\mathbf{P}_1-\mathbf{P}_2)}{|\mathbf{P}_1-\mathbf{P}_2|}$, $\mathbf{e}_i \perp e_j (i \neq j)$
- ·Select two genes as survivors from all child genes.

Figure 1: The GA algorithm.

Table 1: The tasks used in the experiment.

Task No.	all	relevant	relevant/trial
108	371	64	16.1
109	453	21	3.8
110	624	34	6.3
111	540	40	7.5
114	616	20	3.1
115	931	94	9.3
119	387	20	4.9
121	501	63	11.9
126	279	22	7.7
132	210	22	10.5
138	253	24	9.0
139	386	142	36.7
140	309	23	6.6
147	591	80	14.6

4 Experiment

4.1 Data

To evaluate a proposed method, we use NTCIR2 test collection which consists of many evaluated documents. In the NTCIR2, many tasks, for example queries on information retrieval, homesickness syndroand and singular point, are prepared. In each task, a document has a label which denotes whether it is relevant or not.

In this experiment, we regard relevant documents as interesting documents and make a user profile. We pick up 14 tasks which have more than 20 relevant documents and use them as experiment tasks. Since a GA is probabilistic optimizing method, we carry out 10 trials per one task. Traning documents consist of 100 documents drawn at random from all documents and test data consist of the other documents. Each trial uses different training data and test data. In Table 1, we show the number of all documents, all relevant documents and average relevant documents in one trial.

4.2 Simulation and Result

To discuss our proposed method, we compare it with relevance feedback. The relevance feedback is used in the VSM and uses an innar product as a similarity between a user profile and a document. The relevance feedback is defined below.

$$profile = a \sum_{D_i \in I} doc_i - b \sum_{D_j \in U} doc_j \qquad (4)$$

Table 2: The Parameters of GA.

population	Generations	Crossover	α	β
5000	50000	20	0.5	0.35

Table 3: The 11-point average precision.

Task No.	GA($\hat{\mu}_{GA}$)	cosine($\hat{\mu}_{COS}$)
108	0.283	0.287
109	0.235	0.126
110	0.121	0.065
111	0.166	0.188
114	0.157	0.120
115	0.225	0.174
119	0.254	0.084
121	0.300	0.313
126	0.257	0.290
132	0.240	0.176
138	0.737	0.592
139	0.618	0.760
140	0.309	0.246
147	0.336	0.339

where both a and b are arbitrary positive numbers. We decide both a and b using leave-one-out.

Since our proposed method uses a GA, the parameters of theGA for two methods are shown in Table 2. The GA needs more population and generations than usual to explore wide search space.

In Table 3, 11-point average precision is shown. The 11-point average precision is calculated with 11 precision on 11 recall levels.

4.3 Discussion

In Table 3, we realize that our proposed method is superior to relevance feedback in 8 tasks. However, in the other 6 tasks, relevance feedback is superior to the proposed method. We discuss this 6 tasks in detail especially.

Since a genetic algorithm is probabilistic method, the proposed method depends on various conditions (initial genes, generation of child genes and selection). Hence, we discuss a difference of 11-point average precision using t-test. The t-test is a statistical method to consider whether this difference is significant or not. In this case a null hypothesis H_0 is $\mu_{GA} = \mu_{COS}$ where μ_{GA} is an expectation of 11-point average precision for the proposing method and μ_{COS} is an expectation of 11-point average precision for the relevance feedback. First, the difference of the 11-point average precisions

Table 4: The result of t-test.

Task No.	t
108	0.208
109	2.627
110	2.545
111	1.008
114	1.088
115	2.443
119	3.176
121	0.684
126	0.883
132	1.724
138	2.703
139	3.463
140	1.418
147	0.096

is transformed with next formula in each task.

$$t = \frac{\hat{\mu}_{GA} - \hat{\mu}_{COS}}{s\sqrt{\frac{1}{n_{GA}} + \frac{1}{n_{COS}}}} \qquad (5)$$

where s is standard deviation of all 11-point average precisions for all trials, n_{GA} is the number of 11-point average precision for the proposing method ($n_{GA} = 10$) and n_{COS} is the number of 11-point average precision for the relevance feedback ($n_{COS} = 10$). Since we adopt the level of significance of 5% in this t-test, t becomes 2.101. When t is more than 2.101, the null hypothesis H_0 is rejected. In table 4 we show the result of t-test. When a value of relevance feedback is bigger, the t is underlined.

In Table 4, we find that in 5 tasks the proposed method is superior to the relevance feedback in the view of t-test and in one task inferior.

5 Conclusion

In this paper, we proposed information filtering using a GA. We introduced a new criterion which regards a distance between a discriminant hyperplain and training data. We confirmed that the proposed method was superior to relevance feedback in some tasks with significance test.

We will apply this proposed method to other situations and evaluate the proposed method in detail.

Acknowledgements

This study is supported by Grants-in-Aid for Scientific Research. We would like to thank MEXT for the supports.

References

[1] T. W. Malone, K. R. Grant and F. A. Turback(1987), The Information Lens: As Intelligent System for Information Sharing in Organizations, Proceedings of ACM CHI'86, pp.1–8.

[2] P. Maes(1994), Agents that Reduces Work and Information Overload, Communication of ACM, Vol. 37, No. 7, pp.30–40

[3] J. A. Konstan, B. N. Miller, D.Maltz, J. L. Herlocker, L. R. Gordon and J. Riedl(1997), GroupLens: Applying Collaborative Filtering to Usenet News, Communications of the ACM, Vol. 40, No. 3, pp.77–87.

[4] J. H. Holland(1962), Outline for a Logical Theory of Adaptive Systems , Journal of the Association for Computing Machinery, vol.3, pp.297–314.

[5] B. Sheth and P. Maes(1993), Evolving Agents for Personalized Information Filtering, Proceedings of the Conference on Artificial Intelligence Application, Vol. 9, pp.345-352.

[6] I. Ono and S. Kobayashi(1997), A Real-coded Genetic Algorithm for Function Optimization Using Unimodal Normal Distribution Crossover, Proceedings of 7th International Conference on Genetic Algorithms, pp.246–253

The Tenth International Symposium on Artificial Life and Robotics 2005(AROB 10th '05),
B-con Plaza, Beppu, Oita, Japan, February 4-6, 2005

Information Filtering Using SVD and ICA

Takeru Yokoi
Computer and Systems Science
Osaka Prefecture University
1-1 Gakuencho Sakai-City
Osaka 599-8531
takeru@sig.cs.osakafu-u.ac.jp

Hidekazu Yanagimoto
Computer and Systems Science
Osaka Prefecture University
1-1 Gakuencho Sakai-City
Osaka 599-8531
hidekazu@cs.osakafu-u.ac.jp

Sigeru Omatu
Computer and Systems Science
Osaka Prefecture University
1-1 Gakuencho Sakai-City
Osaka 599-8531
omatu@cs.osakafu-u.ac.jp

Abstract

We propose an information filtering system using Singular Value Decomposition(SVD) and Independent Component Analysis (ICA). The number of the independent components to estimate increases as the number of documents increases. Therefore, ICA requires much calculation amount according to it. When ICA is applied to documents, it is considerd that topics included in the documents are obtaied. However, it is difficult to clearly recognize the meaning of topics obtained by ICA. To solve these problem, before applying ICA, we transform the documents with SVD. Using SVD, we expects accuracy of the topic extraction becomes better and effects a user profile well. Then, in our proposed method, we map the document vectors into topic space. We create the user profile from transformed documents with Genetic Algorithm. Finally, we recommend documents by the user profile and evaluate accuracy by 11-point average precision. We carry out an experiment to confirm advantage of the poposed method.

Keywords: Independent Component Analysis, Singular Value Decomposition, Information Filtering System, User Profile

1 Introduction

As information technologies have been advanced, a plenty of information are served in the Internet. It has been difficult to find what we demand from large amount of information by existing retrieval systems since we cannot express our query exactly. A lot of researchers pay attention to developing information retrieval systems which automatically select the information depending on our interests.

The information retrieval systems with user's interests have been studied. For example, there are ranking methods that sort information depending on the user's interests and filtering systems which select the information depending on the user's interests. It is reported the method such as Latent Semantic Analysis(LSA)[1]. LSA is the method which chooses axes to focuse on the variance and cuts off noise. In LSA, Singular Value Decompositon(SVD) is often used to search the axes.

We search the axes from the viewpoint of independence instead of variance. Independent Component Analysis(ICA) is the method to find the axes depending on the independene. ICA is recently used for signal processing, image processing and so on. It has been already reported that we can obtain topics included in the documents on applying ICA to documents[2][3]. We use the topics for transformation of document vectors and improve recommendation accuracy of documents.

However, it is difficult to clearly understand meaning of some topics obtained by ICA. This is why input documents includes some noise. Hence, we use SVD to cut off the noise. It is reported to use SVD before applying ICA, for the accuracy of topic extraction to become better[4].

In this paper, we combine denoising by SVD and topic extraction by ICA to improve the user profile. Then we map the document vectors into the space which consists of the topics and construct the user profile with the transformed document vectors by GA. Finally, to confirm the proposed method, we carry out an experiment on test collection (NTCIR2[5]). In addition, we discuss about the topics obtaind by this algorithm.

2 Our proposed method

In this chapter, we explain a user profile, ICA and SVD.

2.1 User Profile

A document vector is a row vector whose elements are weights of words in a document. When the number of words is n and the weight for the ith word is w_i, the document vector x is denoted as

$$x = [\mathbf{w}_1 \quad \mathbf{w}_2 \quad \cdots \quad \mathbf{w}_n]^T \tag{1}$$

where $[\cdot]^T$ means transportation.

A user profile is also denoted by a row vector whose elements are weights of words like a document vector. In the user profile, interesting words need to have large weights and uninteresting ones need to have small weights. We construct the user profile using Genetic Algorithm(GA). In order to create a user profile which fulfills the conditions mentioned above, the fitness function of GA is defined as

$$f = \sum_i \alpha_i G^T D_i \tag{2}$$

where G means a gene, D_i means a document and α_i is a coefficient for each document.

2.2 Abstract of SVD

SVD is a method to look for an axis of large variance. It is reported that when SVD is applied to documents, we can analysis the word cooccurrence[1].

Now, we assume that m document vectors denoted as $x_1, x_2, \cdots, x_m$ and a document vector matrix X is denoted by equation(3).

$$X = [\mathbf{x}_1 \quad \mathbf{x}_2 \quad \cdots \quad \mathbf{x}_m]^T \tag{3}$$

Then SVD decomposes X into the equation(4), using two orthogonal matrices U, V and one diagonal matrix Σ.

$$X = U\Sigma V^T \tag{4}$$

The row vectors of U are called singular vectors and orthogonal bases of X. In this paper, we select k singular vectors with a large singular value to remove noise. In addition, k is determined by the rate of contribution. U_k represents these k singular vectors. The input matrix X is changed into X_k as follows using U_k.

$$X_k = U_k^T X \tag{5}$$

2.3 Extraction of Topics Using ICA

In signal processing, ICA extracts independent signals from some mixed signals. When ICA is applied to speech processing, observed variables are time series data recorded by microphones and independent variables are source signals. On the other hand, when ICA is applied to documents, the inputs of microphones correspond to document vectors.

Now m independent components are denoted as $s_1, s_2, \cdots, s_m$ and independent component matrix S are denoted by equation(6).

$$S = [\mathbf{s}_1 \quad \mathbf{s}_2 \quad \cdots \quad \mathbf{s}_n]^T \tag{6}$$

At that time, X_k, which is mensioned previous section, is assumed to follow a formula(7).

$$X_k = AS. \tag{7}$$

Here, A is an m k full rank mixing matrix. In addition, we assume $m \geq k$. If A is known, we can obtain the generalized inverse matrix $A^\dagger$ of A easily. However, $A^\dagger$ cannot be generally found because the mixing matrix A is unknown.

The purpose of ICA is to estimate a topic matrix S with only observed variables X_k under the condition where under the condition where mixing matrix A is unknown. In the other word, ICA finds a restored signal matrix Y which is statistically independent using the restored matrix W in the following equation.

$$Y = WX_k. \tag{8}$$

In addition, by the property of evaluation criteria, a magnitude and an order of the restored signals have not been determined uniquely.

Fast ICA[6] is one of ICA solution algorithms. This paper uses Fast ICA to find the independent components. The update criteria by hyperbolic tangent to find the independent components is equation(9).

$$\begin{aligned} w^+ &= E[Yg(w^TY)] - E[g'(w^TY)]w \\ g(u) &= tanh(u) \end{aligned} \tag{9}$$

In this paper, A which is inverse matrix of W is used as a feature axis showing a topic included in the documents. In fact, the topic is denoted by equation(10) since space conversion by U_k is performed before applying ICA.

$$Topic = U_k A \tag{10}$$

A Document vectors $\mathbf{x_i}$ is mapped to the space constructed by topics and represented with the topics. Here, we construct a user profile with $\hat{X}$ represented by topics in equation(11).

$$\hat{X} = Topic * X^T. \tag{11}$$

3 Experiment and result

3.1 Experiment environment and procedure

The data for an experiment are the 625 documents concerning with information retrieval from test collection NTCIR2. These documents have already been evaluated whether each document is relevant or not. In the documents, there are 34 relevant documents.

Each document is represented as a vector with vector space model[7]. As a methodology to represent a document with a vector, at first, we apply morphological analysis tool ChaSen[8] to documents and extract nouns. After that, we remove stop words and high frequency words thorough all documents. We set the threshold of frequency with 20 documents. With the above process, we get 5,948 words and the dimension of document vector is 5,948. Using tf-idf, these words are weighted.

We apply SVD to 625 document vectors and pick up axes until these contribution ratio is 0.8. Then we obtain 409 unique vectors. The input document vectors are changed with these vectors and we apply ICA to them. After that, we converted input documents with topics obtained by ICA.

We use GA for construction of a user profile in cross validation. We provide 625 documents into 5 subsets which include 125 documents. The number of relevant documents and non-relevance ones included in each subset is showed in Table 1. We put 3 subsets together as training data for the construction of the user profile and set the others with evaluate data. Hence, we carry out experiments on 10 patterns of training data.

In GA, each element of individual is expressed with 5 bit. To make the ratio of relevant documents and non-relevance ones set to 1:1, the coefficient α_i in the equation(2) is defined as

$$\alpha_i \quad = \quad \begin{cases} +1 & Di : Relevant \\ -N_I/N_J & Di : Non-relevance \end{cases}$$

where N_I means the number of relevant documents and N_J means the number of non-relevance documents. Other parameters of GA are shown in Table 2 and we use two point crossover. In addition we construct the user profile at 5 times and the average of 5 times results since the GA is a probabilistic approach.

Table 1: The Input Data.

@@@@	all	set1	set2	set3	set4	set5
relevant	34	7	13	5	3	6
non-relevance	591	118	112	120	122	119

Table 2: The Parameter of GA

@@@@	Generation	Cross Over	Mutation
Only GA	10000	1	0.005
ICA+GA	10000	1	0.05
SVD+ICA+GA	10000	1	0.05

Finally, we recommend evaluation documents depending on the user profile and evaluate accuracy of recommendation with 11-point average precision ratio. The recommended documents are determined depending on the similarity S_i between the user profile and the ith document vector D_i. Similarity S_i is defined as

$$S_i \quad = \quad U^T D_i \tag{12}$$

where U means user profile.

We summarize the experiment in the following steps.

Step1 Make document vectors with vector space model.

Step2 Apply SVD to document vectors and convert the space of input documents with unique vectors.

Step3 Apply ICA to converted documents.

Step4 Return the space of A with unique vectors and it is defined topics.

Step5 Transform the input documents with topics.

Step6 Construct the user profile with Genetic Algorithm.

Step7 Recommend documents and evaluate the user profile with 11-point average precision ratio.

Moreover, we construct the user profile with other 2 methods to confirm the advantage of the proposed method, which are construction of the user profile using only GA with original documents and ICA and GA without SVD. The parameters of GA used in these comparable experiments are shown in Table 2.

3.2 Results

In this section, we show the result of the evaluation experiment. Figure 1 shows recall precision curves and Table 3 shows 11-point average precision ratios. In addition, Table 4 shows the feature axes. Table 4 shows the some words sorted by absolute of word weights.

Figure 1: Imputation Precision with GA.

Table 3: 11-points Average Precision Ratio

	Original	ICA	ICA+SVD
0	0.160	0.322	0.331
0.1	0.133	0.218	0.294
0.2	0.126	0.139	0.219
0.3	0.121	0.115	0.171
0.4	0.118	0.099	0.145
0.5	0.116	0.096	0.133
0.6	0.112	0.089	0.124
0.7	0.108	0.082	0.113
0.8	0.106	0.075	0.103
0.9	0.101	0.070	0.087
1	0.098	0.067	0.076
Average	0.118	0.125	0.163

4 Discussion

From the Figure 1, the precision ratio of ICA version becomes better than original version. This is the reason why the concretization of topics contributes the improvement of precision ratio. The proposed method which uses SVD also left much better result than only ICA at low recall ratio especially. In addition, comparing the result from the viewpoints of 11-points average ratio in Table 3, the proposed method left good average precison. According to this, it can be said the proposed method has realized the totally improvement. This is because the accuracy of the topic used for conversion went up, which is shown in Table 4. Seeing Table 4, we can estimate the topics clealy. It is considered that Axis1 means "Cross Language Retrieval" and Axis2 means "Processor Array".

5 Conclusion

In this paper, we proposed the method of improving the accuracy of the user profile by detection of correct topic. Then, we confirmed the advantage of information filtering accuracy. Consequently, it checked that a user profile became good by improvement of topic detection.

Table 4: Example of Feature Axes

Axis1	Axis2
Language crossing	Array
Information access	Processor array
Use field	Processor
List stage	Mapping
Document selection	Physical array
Translation display	Routing
Real use	Size
Technical know-how	Failure processor
International exchange	Logic array
Gate	Mapping algorithm

References

[1] Deerwester.S, Dumais.T, Landauer.T, Furnas.W, Harshman.A, "Indexing by Latent Semantic Analysis", *Journal of the Society for Information Science* Vol.41, No.6, pp.391–497.

[2] Ata Kabán and Mark Girolami, "Topic Separation and Keyword Identification in Document Collections : A Projection Approach", Technical Report available in http://cis.paisley.au.ck/reseach/reports/index.html.

[3] T.Kolenda and L.K.Hansen, "Independent Components in Text", Advances in Independent Component Analysis, Springer-Verlag, 2000.

[4] Masafumi Hamamoto, Hiroyuki Kitagawa, Jia-Yu PAN and Christos Faloutsos, "Topic Detection from Text Data Using Independent Component Analysis", DEWS2004 3-B-04

[5] "NTCIR2", NII-NACSIS Test Collection for IR System, http://research.nii.ac.jp/ntcir/index-en.html.

[6] Aapo Hyvārinen, Erkki Oja, "Independent component analysis: A tutorial", Neural Network, Vol. 13, pp. 411–430, 2000.

[7] G.Salton, M.J.McGill, "Introduction to Modern Information Retrieval", McGraw-Hill Book Company, 1983.

[8] Y.Matsumoto, "Japanese Morphological Analysis System:CHASEN", Information Science Technical Report NAIST-IS-TR97007, Nara Institute of Science Technology,1997.

The Tenth International Symposium on Artificial Life and Robotics 2005(AROB 10th '05),
B-con Plaza, Beppu, Oita, Japan, February 4-6, 2005

Improvement of Information Filtering Using Topic Selection

Takeru Yokoi
Computer and Systems Science
Osaka Prefecture University
1-1 Gakuencho Sakai-City
Osaka 599-8531
takeru@sig.cs.osakafu-u.ac.jp

Hidekazu Yanagimoto
Computer and Systems Science
Osaka Prefecture University
1-1 Gakuencho Sakai-City
Osaka 599-8531
hidekazu@cs.osakafu-u.ac.jp

Sigeru Omatu
Computer and Systems Science
Osaka Prefecture University
1-1 Gakuencho Sakai-City
Osaka 599-8531
omatu@cs.osakafu-u.ac.jp

Abstract

We propose an information filtering system using Independent Component Analysis (ICA). A document-word matrix is generally sparse and has ambiguity of synonyms. To solve this problem, we propose a method to use document vectors represented by independent components generated by ICA. The independent component is considered as a topic. Concretely speaking, we map the document vectors into topic space. Since some independent components are useless for recommendation, we select necessary components from all independent components by Maximum Distance Algorithm. We create a user profile from transformed documents with Relevance Feedback. Finally, we recommend documents by the user profile and evaluate accuracy of the user profile by 11-point average precision. We carry out an experiment to confirm the advantage of the poposed method.

Keywords: Independent Component Analysis, Information Filtering System, User Profile, Maximum Distance Algorithm

1 Introduction

As information technologies have been advanced, a plenty of information are served in the Internet. It has been difficult to find what we demand from large amount of information by existing retrieval systems since we cannot express our guery correctly. A lot of researchers pay attention to developing information retrieval systems which automatically select the information depending on our interests.

The information retrieval systems with user's interests have been studied. For example, there are ranking methods that sort information depending on the user's interests and filtering systems which select the information depending on the user's interests. Since documents usually have noise which worsens accuracy of information filtering, it is a promising method to cut off the noise from documents. It is reported that the method such as LSA[1], which transforms document space, is effective in denoising. The LSA focuses on variance of documents and cuts off the components of low variance for denoising.

We take account of independence of topics included in documents and introduce Independent Component Analysis (ICA) to obtain the topics. ICA is recently used for signal processing, image processing and so on. It has been already reported that the independent components mean topics included in the documents in applying ICA to documents[2][3]. We use the independent components for transformation of document vectors and improve recommendation accuracy of documents.

However, some components obtained by ICA are unnecessary components(noise) for the object of information filtering. Though it is important to remove the noise, there is no criterion to select the independent components. Hence, to focus on the similarity of topics, we use Maximum Distance Algorithm (MDA)[4] which is often used in the field of pattern recognition. This algorithm is applied to classifying the independent components and extracting the useful components for document recommendation. Then we map the document vectors into the space which consists of the selected topics and construct a user profile with the transformed document vectors by relevance feedback(RFB)[5]. Finally, to confirm the proposed method, we carry out an experiment on test collection (NTCIR2[6]).

2 Our proposed method

In this chapter, we explain a user profile, ICA and MDA.

2.1 User Profile

A document vector is a row vector whose elements are weights of words in a document. When the number of words is n and the weight for the ith word is w_i, the document vector d is denoted as

$$d = [\mathbf{w}_1 \quad \mathbf{w}_2 \quad \cdots \quad \mathbf{w}_n]^T \tag{1}$$

where $[\cdot]^T$ means transportation.

A user profile is also denoted by a row vector whose elements are weights of words like a document vector. Interesting words have large weights and uninteresting ones have small weights. We construct the user profile using RFB. The update fomula of RFB is denoted as

$$U = a\sum_i D_i - b\sum_j D_j \tag{2}$$

where U means a user profile, D_i means an interesting document, D_j means an uninteresting document. Both a and b are arbitary positive numbers. When we construct the user profile with documents, the weight of the word included in the interesting document increases.

2.2 Abstract of ICA and Space Transformation

In signal processing, ICA extracts independent signals from some mixed signals. When ICA is applied to speech processing, observed variables are time series data recorded by microphones and independent variables are source signals. On the other hand, when ICA is applied to documents, the inputs of microphones correspond to document vectors and the independent components are equivalent to independent topics included in the documents.

Now, we assume that m document vectors denoted as $x_1, x_2, \cdots, x_m$ are described with the combination of n unknown topics denoted as $s_1, s_2, \cdots, s_n$. Each topic vector is statistically independent and its mean is 0.

A document vector matrix X and a topic vector matrix S are denoted by equation(3).

$$\begin{aligned} X &= [\mathbf{x}_1 \quad \mathbf{x}_2 \quad \cdots \quad \mathbf{x}_m]^T \\ S &= [\mathbf{s}_1 \quad \mathbf{s}_2 \quad \cdots \quad \mathbf{s}_n]^T \end{aligned} \tag{3}$$

At that time, we assume X is linear combination of topic vectors.

$$X = AS \tag{4}$$

Here, A is an m n full rank mixing matrix. In addition, if the number of document is larger than that of topic, the solutions are unspecified. Thus, we assume $m \geq n$. If A is known, we can obtain the generalized inverse matrix $A^\dagger$ of A easily. However, $A^\dagger$ cannot be generally found because the mixing matrix A is unknown.

The purpose of ICA is to estimate a topic matrix S with only observed variables X under the condition where each topic is independent. In other words, ICA finds a restored signal matrix Y which is statistically independent using the restored matrix W in the following equation.

$$Y = WX \tag{5}$$

In addition, by the property of evaluation criteria, a magnitude and an order of the restored signals have not been determined uniquely.

Fast ICA[7] is one of ICA solution algorithms. This paper uses Fast ICA to find the independent components. The update criteria by hyperbolic tangent to find the independent components is equation(6).

$$\begin{aligned} w^+ &= E[Yg(w^TY)] - E[g'(w^TY)]w \\ g(u) &= tanh(u) \end{aligned} \tag{6}$$

The independent components Y obtained by ICA mean topics included in the documents. In this paper, document vectors $\mathbf{x_i}$ is mapped to the space constructed by the topics and represented with the topics. Here, we construct a user profile with $\hat{X}$ represented by topics in equation(7).

$$\hat{X} = YX^T \tag{7}$$

2.3 Abstract of MDA

Some topics obtained by ICA are unnecessary topics for information filtering which worsen accuracy of information filtering. For instance, a document about GIS system includes topics such as city plan and information retrieval. Considering with land-use plan, the topic of information retrieval is regarded as noise. In this paper, to remove those topics, we apply MDA, which does not have to decide the number of classes, to categorize similar topics and select topics.

MDA is stated in the follow steps.

Step1 Set the threshold ratio r which denotes the distance between the farthest clusters.

Step2 Set topic y_1 as cluster center Z_1.

Step3 Calculate $D_i = \min_j(y_i, Z_j)$ for $y_2, y_3, \cdots, y_n$. $D(y_i, Z_j)$ is defined as equation(8).

$$D(y_i, Zj) = \sqrt{(y_i - \bar{Z}_j)^T(y_i - \bar{Z}_j)} \tag{8}$$

Step4 Calculate $l = \max_i D_i$ and set the element of l with y_k.

Step5 If $l/MAX > r$, where $MAX = max(Z_i, Z_j)$ means the distance between the farthest classes, make new class whose center Z_{j+1} is y_k and return Step3. Otherwise, go to Step6.

Step6 Output all classes.

After classification, we extract all components of a class which has the most components. The components in the class are considered as specific topics on a theme. In other words, this selection method means to extract the detail components for a main topic.

3 Experiment and result

3.1 Experiment environment and procedure

The data for an experiment are the 625 documents concerning with information retrieval from test collection NTCIR2. These documents have already been evaluated whether each document is relevant or not. In the documents, there are 34 relevant documents.

Each document is represented as a vector with vector space model[8]. As a methodology to represent a document with a vector, at first, we apply morphological analysis tool ChaSen[9] to documents and extract nouns. After that, we remove stop words and high frequency words thorough all documents. We set the threshold of frequency with 20 documents. With the above process, we get 5,948 words and the dimension of document vector is 5,948. Using tf-idf, these words are weighted.

We apply ICA to 625 document vectors and obtain 623 independent components. The number of topics is less than the numbers of documents since some documents are dependent. Next we normalize the 623 independent components and remove the unnecessary components with MDA. It has been already mentioned in Section2.3 how to select the useful components. In consequence, we select 324 topics. After that, we converted input documents with the components selected by MDA.

We use RFB for construction of a user profile in cross validation. We provide 625 documents into 5 subsets which include 125 documents. The number of relevant documents and non-relevant ones included in each subset is showed in Table 1. We put 3 subsets together as training data for the construction of the user profile and set the others with evaluate data. Hence, we carry out experiments on 10 patterns of training data.

In RFB, to make the ratio of relevant documents and non-relevant ones set to 1:1, the coefficients, a and b, in the equation(2) are defined as

$$\begin{aligned} a &= +1 \\ b &= -N_i/N_j \end{aligned} \tag{9}$$

where N_i means the number of relevant documents and N_j means the number of non-relevant documents.

Finally, we recommend documents depending on the user profile and evaluate accuracy of recommendation with 11-point average precision ratio. The recommended documents are determined depending on the similarity S_i between the user profile and the ith document vector D_i. Similarity S_i is defined as

$$S_i = U^T D_i. \tag{10}$$

We summarize the experiment in the following steps.

Step1 Make document vectors with vector space model.

Step2 Apply ICA to document vectors

Step3 Classify the independent components with MDA and remove unnecessary components.

Step4 Transform the input documents.

Step5 Construct the user profile with RFB.

Step6 Recommend documents and evaluate the user profile with 11-point average precision ratio.

Moreover, we construct the user profile with other two methods to confirm the advantage of the proposed method, which are construction of the user profile using only RFB with original documents and ICA and RFB without topic selection.

3.2 Results

In this section, we show the result of the experiment. Figure 1 shows recall precision curves and Table 2 shows 11-point average precision ratios.

Table 1: The Input Data.

@@@@	all	set1	set2	set3	set4	set5
relevant	34	7	13	5	3	6
non-relevant	591	118	112	120	122	119

Figure 1: Imputation Precision with RFB.

Table 2: 11-points Average Precision Ratio.

	Original	ICA	Euclid
0	0.458	0.463	0.638
0.1	0.420	0.432	0.535
0.2	0.325	0.368	0.525
0.3	0.301	0.346	0.459
0.4	0.270	0.320	0.381
0.5	0.257	0.288	0.325
0.6	0.238	0.237	0.250
0.7	0.152	0.198	0.165
0.8	0.095	0.160	0.122
0.9	0.080	0.103	0.106
1	0.248	0.085	0.092
Average	0.248	0.273	0.327

4 Discussion

From the Figure 1, the precision ratio of ICA version becomes better than one of original version. This is the reason why the concretization of topics contributes the improvement of precision ratio. The proposed method which selects topics with MDA also left much better result than only ICA. Especially, the improvement is clear at low recall ratio points. We cannot clearly recognize some precision ratios at high recall ratio points to become better in Figure 1. Therefore, comparing the result from the viewpoints of 11-points average ratio in Table 2, it is clearly found that the proposed method can improve the precision ratio. This is because the unnecessary components for information filtering are removed with selecting components.

5 Conclusion

In this paper, we proposed a new method to select necessary topics for information filtering using the MDA and confirmed the advantage of the proposed method. This gives that the accuracy of information filtering can be improved with removing unncecessary topics.

Since we deal with the one topic data in this experiment, we will have to extend the data including multiple topic in future.

References

[1] Deerwester.S, Dumais.T, Landauer.T, Furnas.W, Harshman.A, "Indexing by Latent Semantic Analysis", *Journal of the Society for Information Science* Vol.41, No.6, pp.391–497.

[2] Ata Kabán and Mark Girolami, "Topic Separation and Keyword Identification in Document Collections : A Projection Approach", Technical Report available in http://cis.paisley.au.ck/reseach/reports/index.html.

[3] T.Kolenda and L.K.Hansen, "Independent Components in Text", Advances in Independent Component Analysis, Springer-Verlag, 2000.

[4] Tou,J.T. and Gonzalez,R.C., "Pattern Recognition Principles", Addison-Wesley, Reading, MA. 1974.

[5] J.Rocchio, "Relevance feedback in information retrieval" , The SMART Retrieval System Experiments in Automatic Document Processing, pp. 313–323,1971

[6] "NTCIR2", NII-NACSIS Test Collection for IR System, http://research.nii.ac.jp/ntcir/index-en.html.

[7] Aapo Hyvārinen, Erkki Oja, "Independent component analysis: A tutorial", Neural Network, Vol. 13, pp. 411–430, 2000.

[8] G.Salton, M.J.McGill, "Introduction to Modern Information Retrieval", McGraw-Hill Book Company, 1983.

[9] Y.Matsumoto, "Japanese Morphological Analysis System:CHASEN", Information Science Technical Report NAIST-IS-TR97007, Nara Institute of Science Technology,1997.

The Tenth International Symposium on Artificial Life and Robotics 2005(AROB 10th '05),
B-con Plaza, Beppu, Oita, Japan, February 4-6, 2005

MOSFET Implementation of Class I* Neurons Coupled by Gap Junctions

Takashi Takemoto*, Takashi Kohno† and Kazuyuki Aihara† ‡
*Complexity Science and Engineering Frontier Science, The University of Tokyo.
† Aihara Complexity Modelling Project, ERATO, JST.
‡ Institute of Industrial Science, The University of Tokyo.

Abstract

This paper proposes a class I* neuron circuit coupled by gap junctions (GJs) consisting of enhancement-type MOSFETs. Some neurons that belong to a subclass of class I, when coupled by GJs, exhibit extensive spatio-temporal chaos in some parameter regions. This subclass is called class I* and characterized by a phase plane structure called a narrow channel. In the proposed circuit, one can metamorphose the model continuously - class I*, class I without a narrow channel, and even to class II - by changing the value of the resistance. The circuitry is compatible with standard CMOS semiconductor processes. Hence it can be implemented in an analog very-large-scale integrated circuit (aVLSI) and the construction of a relatively large network is possible. We show PSPICE simulation results for a circuit implementeted with discrete elements. A GJ-coupled network consisting of twenty such neurons is shown to reveal itinerant dynamics similar to class I* GJ-couple systems.

1 Introduction

Neuromorphic hardware has been studied extensively, and various circuitries have been proposed to emulate biological neurons [1]. Some studies implement conductance-based models [3] such as the Hodgkin-Huxley (HH) model and others implement phenomenological models [4] such as the integrate-and-fire (I&F) model. The I&F neuron is very simple and more popular for studies of large network dynamics, but biological neurons have more complex electrical dynamics. On the other hand, the HH model describes in detail the electrical dynamics of biological neurons. It is difficult to analyze mathematically because this model includes four-dimensional nonlinear differential equations.

As Hodgkin pointed out, there are two classes of neurons: class I and class II [5]. When a strong enough sustained current is applied, neurons fire repetitively. The firing frequency of class I neurons at the onset is asymptotically zero, whereas that of class II neurons is nonzero. It is well known that saddle-node bifurcation produces class I excitability, and the subcritical Hopf bifurcation class II. These bifurcations can be generated in two-dimensional systems. Thus, we adopt two-dimensional reduction models of neurons so that the temporal evolution of the variables can be visualized in the phase plane.

Recent physiological data indicate the massive presence of gap junctions (GJs) among the interneurons in the neocortex [6] [7]. They raise a serious question about the role of interneurons for neural coding and the dynamics of system levels for inhibitory neurons electronically coupled by GJs. Fujii et al. claimed that some neurons that belong to a subclass of class I, when coupled by GJs, can exhibit extensive spatio-temporal chaos in some parameter regions [8]. This subclass is characterized by a phase plane structure called a narrow channel. They named these neurons class I*. They show perfectly regular firings when isolated, so this chaotic behavior is an emergent property of coupled systems.

In this paper, we propose a class I* silicon neuron circuit, that has a simple phase plane structure. In the following section we briefly summarize the class I* neuron models. In Section 3 we describe the characteristics of the silicon neuron circuitry and PSPICE simulation results for a circuitry implemented with discrete elements. Finally in Section 4 we make concluding remarks.

2 Class I* Neuron Models

The two-dimensional reduction models of a single cell are written as [10]

$$\begin{cases} \tau_V \dfrac{dV}{dt} = F(V,R) + I \\ \tau_R \dfrac{dR}{dt} = G(V,R) \end{cases}, \tag{1}$$

where V represents the membrane potential, R is the conductance parameter of the ion channels, and I is the stimulus current. In two-dimensional reduction models, dynamic behavior can be characterized in the two nullclines corresponding to the two variables. In many case, the class I neurons have U-shaped R-nullclines, while the class II neurons have inclined I-shaped R-nullclines. Most neurons have inverted-N-shaped V-nullclines.

The essential nonlinearity of class I* is characterized by (1) the presense of a narrow channel, (2) the presence of an unstable spiral, and (3) the presence of orbits (with positive measure) reentering into the channel. It is not difficult to construct class I* models. The neuron models with inverted-N-shaped V-nullclines and U-shaped R-nullclines can be turned into class I* by adjusting the parameters.

3 The Silicon Neuron

In this section, we describe the characteristics of the proposed circuits and present PSPICE simulation results with discrete elements (NEC $\mu PA602$ and $\mu PA603$). These two devices are a complementary pair. The supply voltages are $V_{DD} = 5.0$ V and $V_{SS} = -5.0$ V.

3.1 Circuit Operation and Characteristics

Tne neuron circuit mainly consists of three blocks (see Fig. 1): inverted-N-shaped nonlinear resistance, U-shaped nonlinear resistance, and V-I converter.

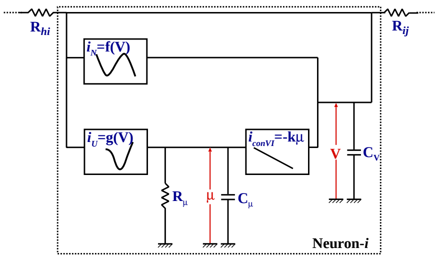

Figure 1: Block diagram of class I* neuron circuits.

The circuit equations of this silicon neuron are

$$\begin{cases} C_V \dfrac{dV}{dt} = f(V) - k\mu \\ C_\mu \dfrac{d\mu}{dt} = g(V) - \dfrac{\mu}{R_\mu} \end{cases}, \tag{2}$$

where C_V is the membrane capacitance, V represents the membrane potential, k is the ratio of V-I converter, μ is the channel conductance variables, C_μ represents the time constant of μ, R_μ is the constant resistance, $f(V)$ is the inverted-N-shaped-nonlinear resistance, and $g(V)$ is the U-shaped nonlinear resistance.

Fig. 2 shows a schematic of the V-I converter. The source-follower M31-M32 produces $V'_{IN} \simeq V_{IN} + V_{DD} - V_{conVI}$, where V_{IN} is the input voltage and V_{conVI} is a constant bias voltage. The feedback M33-M34 has the effect of suppressing the nonlinearity of the input/output (IO) characteristics. Hence the output current of this circuit may be expressed as $I_{conVI} \simeq -kV'_{IN} + \Delta I$, where k is the ratio of the V-I converter. This ratio can be altered by R_{conVI}.

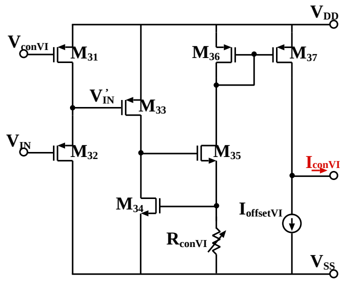

Figure 2: Schematic of the V-I converter.

Fig. 3 shows the IO characteristics of the V-I converter. This circuit is very simple and has good linearity.

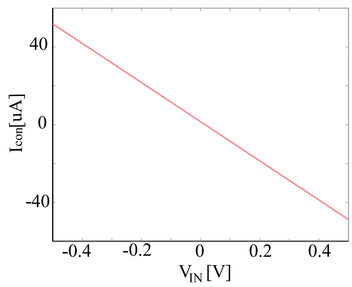

Figure 3: IO Characteristics of V-I converter. V_{conVI} =2.8 V, R_{conVI} =10 kΩ, $I_{offsetVI}$ =0.24 mA.

The inverted-N-shaped nonlinear resistance is schematically shown in Fig. 4. This circuit consists of a differential pair M1-M2 and a V-I converter M5-M9. The output current of this circuit may be expressed as $I_N = I_{diffN} + I_{conN}$, where I_{diffN} is the output current of the differential pair and I_{conN} is the output current of the V-I converter respectively.

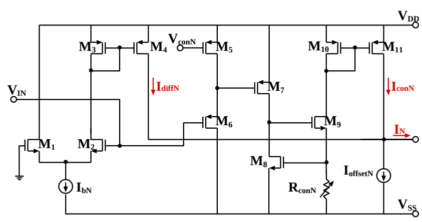

Figure 4: Schematic of inverted-N-shaped circuit.

Fig. 5 shows the I-V characteristics of this circuit. These characteristics represent the V-nullcline of the silicon neuron.

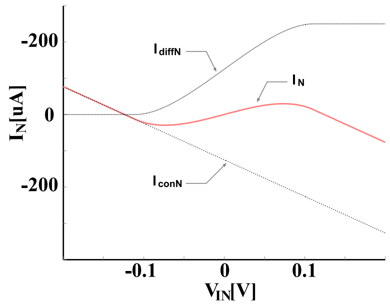

Figure 5: I-V characteristics of inverted-N-shaped nonlinear resistance. I_{bN} =0.25 mA, V_{conN} =2.8 V, R_{conN} =1 kΩ, $I_{offsetN}$ =2.54 mA.

A schematic of the U-shaped nonlinear resistance is shown in Fig. 6. This circuit consists of an improved anti-bump circuit M12-M19 and the V-I converter M22-M26. The differential pair M12-M15 is used to shift the input voltage V_{IN} by a constant voltage V_{bump}. The original anti-bump circuit [2] takes two input voltages, V_1 and V_2, and generates three output currents. The two outside currents, I_1 and I_2, are a measure of the dissimilarity betweeen the two inputs; the center current I_{mid} is the measure of the similarity. Hence this circuit has Gaussian-like I-V characteristics. In the proposed circuit, V_2 is connected to GND, and the amplitude of V_1 can be altered by the resistance R_{bump} to adjust the left slope of the Gaussian curve. The output current of this circuit may be expressed as $I_U = I_{bump} - I_{conU}$, where I_{bump} is the output current of the improved anti-bump circuit and I_{conU} is the output current of the V-I converter. The I-V characteristics of this circuit represent the μ-nullcline of the silicon neuron.

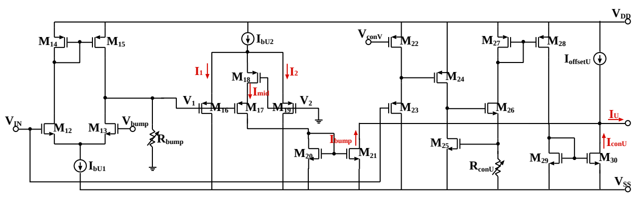

Figure 6: Schematic of U-shaped nonlinear resistance.

3.2 Behavior of The Single Neuron

The phase plane structure of the silicon neuron is shown in Fig. 7. By changing the value of R_{bump}, we can metamorpose the model continuously: class I*, class I without a narrow channel, and class II.

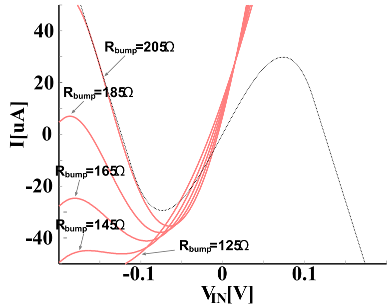

Figure 7: Nullcline of the proposed silicon neuron. The dashed line is μ-nullcline and the solid line is V-nullcline. I_{bN} =0.25 mA, V_{conN} =2.8 V, R_{conN} =1 kΩ, $I_{offsetN}$ =2.54 mA, I_{bU1} =0.9 mA, V_{bump} =5 mV, I_{bU2} =4 mA, V_{conU} =2.8 V, R_{conU} =4 kΩ and $I_{offsetU}$ =1.35 mA.

Fig. 8 shows the membrane potential V of the silicon neuron for the phase plane structure in Fig. 7. The single silicon neuron shows perfectly regular firings.

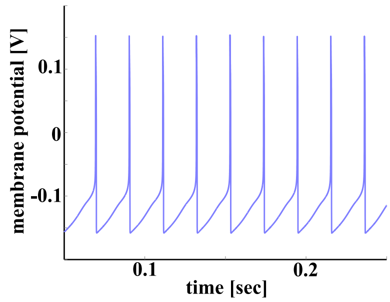

Figure 8: Time course of the membrane potential of the proposed silicon neuron. C_V =10 nF, C_μ =100 nF, R_μ =10 kΩ, $k \simeq$0.1 mS and R_{bump} =205 Ω

3.3 Itinerant Dynamics in Class I* GJ-Coupled Systems

The currents induced by GJs are [9]

$$
\begin{aligned}
J_i &= \frac{1}{R_{GJ}} \sum_{nb_i} (V_{nb_i} - V_i) \\
&= g_{GJ} \sum_{nb_i} (V_{nb_i} - V_i), (nb_i \in coupledneigborcell),
\end{aligned} \tag{3}
$$

where g_{GJ} is a coupling constant, which is assumed to be identical for all connections in this simulation. The neurons at the boundaries connect only to the inner neurons.

Fig. 9 shows the time series of the GJ-coupled network that consists of twenty of the proposed circuits.

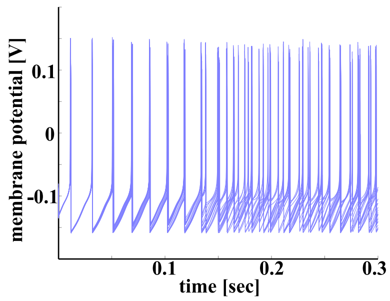

Figure 9: Time series of the GJ-coupled network consisting of twenty of the silicon neurons. R_{GJ} =10 kΩ.

At time t=0, there is a slight variation in the charges of the capacitors (C_V, C_μ) of the neurons. This system has been shown to exhibit chaotic dynamics as time elapses. Note that each neuron shows perfectly regular firings when isolated. Hence this chaotic behavior is an emergent property of coupled systems.

4 Concluding Remarks

We have proposed a class I* silicon neuron circuitry with a simple phase plane structure. We combined inverted-N-shaped and U-shaped nullclines to reproduce the narrow channel structure. Differential pair circuitries, bump circuitries, and linear resistances were employed to implement these nullclines. Their I-V characteristics can be easily altered by external voltages and resistances. The varieties of I-V characteristics allow the proposed circuit to behave as a class I*, class I, or class II neuron. We have also shown PSPICE simulation results for a circuit implemented with discrete elements. A GJ-coupled network consisting of twenty neurons was shown to generate itinerant dynamics similar to class I* GJ-coupled systems in the work of Fujii et al. Moreover, this circuitry is compatible with standard CMOS semiconductor processes. Hence it can be implemented in an analog very-large-scale integrated circuit (aVLSI) and the construction of relatively large networks is possible as well.

Acknowledgements

This study is partially supported by the Superrobust Computation Project in 21st Century COE Program on Information Science and Technology Strategic Core from the Ministry of Education, Culture, Sports, Science, and Technology, the Japanese Government.

References

[1] M. Mahowald and R. Douglas, "A Silicon Neuron", *Nature*, Vol. 354, pp. 515-518, 19/26 Dec. 1991.

[2] T. Delbruck, "Bump Circuits for computing similarity and dissimilarity of analog voltages", *IJCNN*, pp. I-472-479, 1991.

[3] Simoni MF., Cymbalyuk GS., Sorensen ME., Calabrese RL. and DeWeerth SP., "A Multiconductance Silicon Neuron With Biologically Matched Dynamics", *IEEE Trans Biomed Eng.*, Vol. 51(2) pp. 342-54, Feb. 2004.

[4] G. Indiveri, "A low-power adaptive integrate-andfire neuron circuit",*In ISCAS 2003. The 2003 IEEE International Symposium on Circuits and Systems, 2003. IEEE* , 2003.

[5] Hodgkin A.L., "The local electric changes associated with repetitive action in a non-medullated axon", *J. Physiology*, Vol. 107, pp. 165-181, 1948.

[6] Galarreta M. and Hestrin S., "A network of fast-spiking cells in the neocortex connected by electrical synapses", *Nature*, Vol. 402, pp. 72-75, 1999.

[7] Gibson JR, Beierlein M and Connors BW, "Two networks of electrically coupled inhibitory neurons in neocortex", *Nature*, Vol. 402, pp. 75-79, 1999.

[8] H. Fujii and I. Tsuda, "Itinerant dynamics of class I* neurons coupled by gap junctions", *COMPUTATIONAL NEUROSCIENCE: CORTICAL DYNAMICS LECTURE NOTES IN COMPUTER SCIENCE*, Vol. 3146, pp. 140-160, 2004.

[9] N. Schweighofer, K. Doya and M. Kawato, "Electrophysiological Properties of Inferior Olieve Neurons: A Compartment model", *J. Neurophysiol.*, Vol. 82 pp. 804-817, 1999.

[10] Rinzel J., "Excitation dynamics: insights from simplified membrane models", *Fed. Proc.*, Vol. 44, pp. 2944-2946, 1985.

The Tenth International Symposium on Artificial Life and Robotics 2005(AROB 10th '05),
B-con Plaza, Beppu, Oita, Japan, February 4-6, 2005

Parameter tuning of a MOSFET-based nerve membrane

Takashi Kohno* and Kazuyuki Aihara*†
* Aihara Complexity Modelling Project, ERATO, JST., Shibuya-ku, Tokyo, 151-0064
† Institute of Industrial Science, The University of Tokyo, Meguro-ku, Tokyo, 153-8505

Abstract

Two major principles for silicon neuron implementations are the phenomenological and the conductance-based ones. The former reproduces some properties perceived by the designers and does not claim mechanism consistency. The latter reproduces the dynamics of the ion channels on the nerve membranes. It makes the silicon neurons more similar to biological ones, but the implementations tend to be complicated because it attempts to replicate the detailed dynamics of the biological components. In the previous work [1], we proposed a new principle based upon phase plane analyses. It reproduces the mathematical structures of biological neurons, which makes the silicon neurons simple and faithful. In this paper, we show how Class 1 and Class 2 nerve membranes are realized by parameter tuning based on simple phase plane analyses with an illustrative MOSFET-based nerve membrane.

1 Introduction

Neural systems process massive and various incoming information flexibly, appropriately, and in real time. One of the purposes of studies on silicon neurons is to implement artificial systems that inherit these exquisite properties, and another is to produce some devices to interface between electrical circuits and living nerve systems [2]. There are two major types of silicon neuron design principles. One is the phenomenological implementation, which aims to reproduces some phenomena of biological neurons. Integrate-and-fire silicon neurons are good examples [3], which reproduce the integration property of spatiotemporal inputs and the threshold property of generating action potentials. Circuitries can be simple in these implementations but some properties that are not regarded may be lost. The other is the conductance-based implementation, which aims to reproduce some or all mechanisms in biological neurons faithfully. Most phenomena of biological neurons can be inherited in these implementations but circuitries tend to be complex. It is impossible to reproduce those mechanisms completely.

In the previous work [1][4], we proposed a design methodology that allows us to implement simple and biologically realistic silicon nerve membranes. It is based upon phase plane analyses that have been utilized to reveal the mathematical structures behind the properties of biological neurons. These properties can be given to simple silicon neurons by constructing the mathematical structures similar to that of biological neurons with silicon-friendly functions.

One of the well-known properties of biological neurons is oscillation against sustained input currents. Hodgkin [5] found in his biophysical experiments of stimulating various nerve membranes with sustained currents that some membranes start oscillating with an arbitrary low frequency when the currents exceed thresholds and others with non-zero frequency. He named the former Class 1 and the latter Class 2. Masuda and Aihara [6] indicated that these differences in excitation mechanisms may play a key role in neural coding. Bifurcation analysis studies on biological neuron models have revealed the mathematical structure behind the Class 1 and 2 excitabilities [7][8]. Typical bifurcations that lead to Class 1 excitability are a saddle-node on an invariant circle bifurcation and a saddle loop homoclinic orbit bifurcation. It is well known that Class 2 excitability can be produced by a Hopf bifurcation.

In this paper, we show how to tune the mathematical structure of silicon nerve membranes to make them reveal Class 1 or Class 2 excitabilities, utilizing a simple MOSFET-based nerve membrane as an example.

2 MOSFET-based nerve membrane

The design principle we proposed in the previous work [1] replicates the mathematical structures lying behind the properties of biological neurons with some 'MOSFET-friendly' functions. One of the simplest silicon nerve membrane models based upon the generalized Hodgkin-Huxley equations can be described as follows:

$$C_y\frac{dy}{dt} = -\frac{y}{R_y} + \frac{\beta_m}{2}m^2 - \frac{\beta_n}{2}n^2 + a + I_{stim}, \quad (1)$$

$$\frac{dm}{dt} = \frac{f_m(y) - m}{T_m}, \quad (2)$$

$$\frac{dn}{dt} = \frac{f_n(y) - n}{T_n}, \quad (3)$$

where y represents membrane potential, m is a faster conductance variable, n is a slower conductance variable, C_y is membrane capacity, R_y is a constant resistance, a is a constant, I_{stim} is a stimulus current input, β_m and β_n are the transconductance coefficients of the MOSFETs for the ion channel current corresponding to m and n, respectively, and T_m and T_n are the time constants for m and n, respectively. Ordinarily we make T_m an order of magnitude smaller than T_n because the faster conductance corresponds to the sodium channel activation variable in the Hodgkin-Huxley equations and the slower one to the potassium channel activation variable. If we use the V-I characteristic curves of differential pairs (see appendix B for $x = m$ and n) as the sigmoidal functions $f_m(y)$ and $f_n(y)$, this system can be implemented with a very simple MOSFET circuitry [4].

Because the time scale for m is sufficiently smaller than that for n, we can reduce the faster conductance m by assuming it relaxes to $f_m(y)$ instantaneously. This reduction gives the slower subsystem that allows us to trace the system's behavior on the time scale of a whole generation of an action potential on a phase plane. The system equations are as follows:

$$C_y\frac{dy}{dt} = -\frac{y}{R_y} + \frac{\beta_m}{2}f_m^2(y) - \frac{\beta_n}{2}n^2 + a + I_{stim}, \quad (4)$$

$$\frac{dn}{dt} = \frac{f_n(y) - n}{T_n}. \quad (5)$$

Thus the y-nullcline and the n-nullcline are:

$$n = \sqrt{\frac{2}{\beta_n}\left(\frac{\beta_m}{2}f_m^2(y) - \frac{y}{R_y} + a + I_{stim}\right)}, \quad (6)$$

$$n = f_n(y), \quad (7)$$

respectively. A typical relation between the two nullclines is shown in Fig. 1. The conditions that they have to satisfy for the system to inherit the fundamental properties of the biological neurons are discussed in [1].

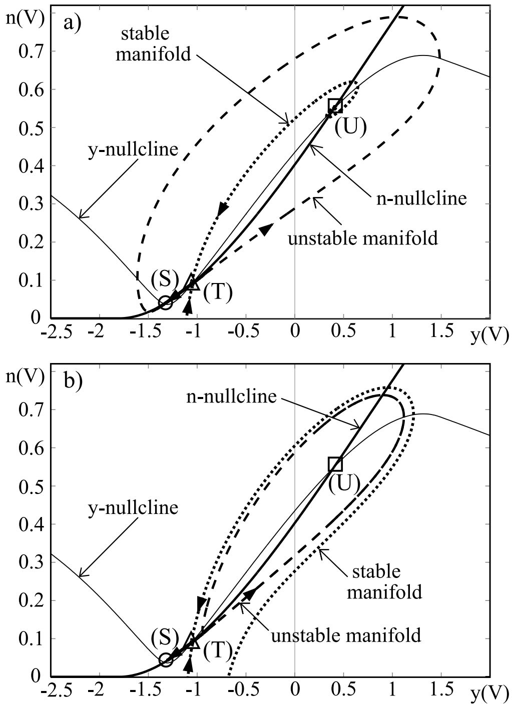

Figure 1: Typical phase planes of the slower subsystem. (S) is a stable equilibrium (the rest state). (T) is a saddle and (U) is an unstable equilibrium. a) The system is near a saddle-node on an invariant circle bifurcation. The parameters are shown in appendix A. b) The system is near a saddle loop homoclinic orbit bifurcation. The right segment of the unstable manifold of (T) wraps around a stable limit cycle around (U). The parameters are as in a) except C_y =0.0140(mF).

3 Parameter tuning for Class 1 and Class 2 excitabilities

3.1 Bifurcations of the rest state

The increase in the stimulus current transforms the phase space structure and destabilizes the rest state in our illustrative silicon nerve membrane like in most biological ones, which induces the repetitive firing. As described in the introduction, it is well known that Class 1 excitability is observed if the rest state loses stability via a saddle-node bifurcation or a saddle loop homoclinic orbit bifurcation, and the Class 2 excitability via a Hopf bifurcation [7][8]. These are the most major scenarios of repetitive firings. The phase plane structure near a saddle-node on an invariant circle bifurcation is shown in Fig. 1a). In this case, the stable equilibrium point (S) and the saddle point (T) approach each other as the y-nullcline (eq. (6)) moves up in response to the increase in stimulus current I_{stim}. The smaller segment of the unstable manifold of (T) vanishes when (S) merges with (T), and the other segment of the unstable manifold turns to a stable limit cycle when they disappear. This limit cycle passes near the narrow channel between the y- and n-nullclines around the vanished saddle point, where the velocity is very slow. By narrowing this channel, we can delay the period of the limit cycle arbitrarily up to infinity when the channel width becomes zero. Figure 1b) shows the phase plane structure near a saddle loop homoclinic orbit bifurcation. In this case the right unstable manifold of (T) gets closer to the upper stable manifold as the y-nullcline moves up, until it merges with the upper segment of the stable manifold and becomes a closed homoclinic orbit. Then a stable limit cycle is born around (U), which passes near the saddle point where the velocity is very slow. In contrast to above two scenarios, the saddle point (T) has no role in the Hopf bifurcation. The rest state loses stability singularly, and the system moves to a stable limit cycle around it if one exists. Because the system jumps to a limit cycle, the repetitive firing begins abruptly with a certain non-zero frequency.

3.2 Tuning the bifurcations

As described in the above subsection, the stability of the rest state plays a key role in neural excitabilities. The local linearization method tells how it depends on the parameters. The necessary and sufficient conditions for an equilibrium point to be stable are:

$$\lambda_1 + \lambda_2 < 0 \Leftrightarrow \eta'(y_0) < \frac{C_y}{n_0 \beta_n T_n}, \qquad (8)$$

$$\lambda_1 \cdot \lambda_2 > 0 \Leftrightarrow \eta'(y_0) < f_n'(y_0), \qquad (9)$$

where λ_1 and λ_2 are the eigenvalues of the Jacobian matrix in equations (4)-(5), (n_0, y_0) denotes an equilibrium point, $'$ denotes $\frac{d}{dy}$, and $\eta(y)$ is the right side of eq. (6). These conditions indicate that at a stable equilibrium point the y-nullcline should cross the n-nullcline from over to under and the gradient of the y-nullcline should keep smaller than a certain value. Thus the stabilities of the equilibrium points can be configured as in Fig. 1 if we place the leftmost crosspoint of the y-nullcline and the n-nullcline where the gradient of the y-nullcline is sufficiently small and the rightmost one where it is sufficiently large. Of course we must tune C_y and T_n properly so that $\frac{C_y}{n_0 \beta_n T_n}$ is between these two gradients. In this situation, (S)

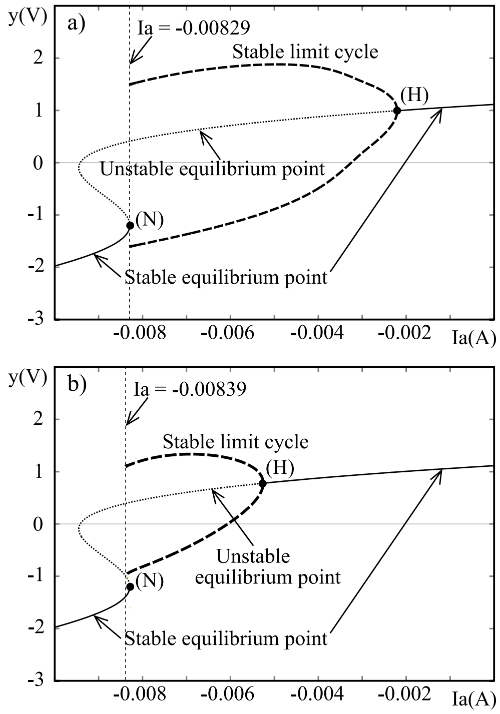

Figure 2: The bifurcation diagrams for a) a saddle-node on invariant circle bifurcation and b) a saddle loop homoclinic orbit bifurcation. (N) represents the point where the stable and saddle points merge and (H) the point where the stable limit cycle emerges. a) The limit cycle vanishes at I_a =-0.00829(A) where (N) exists. The parameters are as in Fig. 1 a) except I_a is swept. b) The limit cycle vanishes at I_a =-0.00839(A). The parameters are as in Fig. 1 b) except I_a is swept.

and (T) get closer as the y-nullcline moves up and (S) loses stability when they merge because condition (9) is no longer satisfied. This is the common scenario for Class 1 excitability. If the rightmost side of condition (8) is smaller than $f_n'(y)$ at the point where (S) and (T) merge, (S) loses stability singularly via the Hopf bifurcation before merging with (T). This is the basic scenario for Class 2 excitability. To obtain a Class 2 nerve membrane that generates action potentials of a reasonable size and keeps firing repetitively for a reasonably wide range of stimulus current, the y-nullcline should be shifted right to make (T) and (U) disappear or, at least, to make (S) and (T) further aprat than in Fig. 1. Class 2 excitability in our silicon nerve membrane is discussed in [1].

The local stability analysis does not tell which of the two scenarios appears. The bifurcation diagrams for these scenarios are shown in Fig. 2. Let us trace

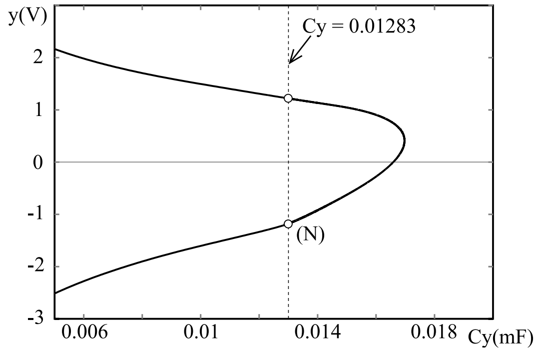

Figure 3: The bifurcation diagram of the limit cycle along C_y. Parameters are as in appendix A except $I_a = -0.00829$(A) and C_y is swept. The vertical axis represents the upper and lower limits of the limit cycle. The white circles at C_y =0.01283(mF) represent the limit cycle is unstable around it.

them from right to left. In both cases, the limit cycle that emerges via the Hopf bifurcation continues with its amplitude increasing. If the amplitude is sufficiently large at the point where the pair of stable and saddle points emerges ((N) in Fig. 2, where $I_a =$ -0.00829(A)), the orbit of the limit cycle gets 'trapped' and vanishes; otherwise it persists until it merges with the unstable manifold of the saddle point.

The amplitude of the limit cycle can be controlled by C_y, which works as a time scale factor. It gets smaller as C_y becomes larger because the velocity of the system in the y direction decreases. In Fig. 3, we show the bifurcation diagram of the limit cycle for an I_a value just near the point (N) in Fig. 2. The limit cycle is stable except when the limit cycle passes at the point (N) ($C_y \simeq 0.01283$(mF) in Fig. 3). Thus, we obtain the saddle-node on invariant circle bifurcation if C_y is below 0.01283 (mF) and the other one if it is above.

4 Conclusions

We have shown how Class 1 and Class 2 excitabilities are obtained with a MOSFET-based nerve membrane. Once the phase plane structure is configured properly by tuning the parameters that affect the forms of the nullclines, we can easily realize the desired neural excitability by tuning C_y and T_n. We have shown that the two types of Class 1 excitabilities can be selected only by tuning C_y. Because the ratio of the time scales of y and n affects the amplitude of the limit cycle, T_n can also be tuned. This paper indicates that our illustrative MOSFET-based nerve membrane can function as a Class 1 or Class 2 nerve membrane according to the proposed parameter tuning.

References

[1] T. Kohno and K. Aihara, "Design of Neuromorphic Hardware Based upon Mathematical Methods," *Proc. SBRN 2004*, 3470, 2004.

[2] M. Simoni, G. Cymbalyuk, M. Sorensen, et al., "A Multiconductance Silicon Neuron With Biologically Matched Dynamics," *IEEE Trans. Biomed. Eng.*, Vol. 51, No. 2, pp. 342-354, Feb., 2004.

[3] D. Rubin, E. Chicca, and G. Indiveri, "Characterizing the firing properties of an adaptive analog VLSI neuron," *Proc. Bio-ADIT 2004, Lausanne*, pp. 314-327, 2004.

[4] Takashi Kohno and Kazuyuki Aihara, "A MOSFET-based model of a Class 2 Nerve membrane," *Submitted to IEEE Trans. Neural Networks.*

[5] A. L. Hodgkin, "The local electric changes associated with repetitive action in a non-medullated axon," *J. Physiol.*, Vol. 107, pp. 165-181, 1948.

[6] Naoki Masuda and Kazuyuki Aihara, "Band-pass filtering properties of interspike interval encoding with Morris-Lecar neurons," *Proc. SBRN 2004*, 3611, 2004.

[7] J. Rinzel and B. Ermentrout, *"Analysis of Neural Excitability and Oscillations," in "Methods in Neural Modeling", ed. C. Koch and I. Segev*, pp. 251-291, MIT Press, 1998.

[8] E. M. Izhikevich, "Neural Excitability, Spiking, and Bursting," *International Journal of Bifurcation and Chaos*, Vol. 10, pp. 1171-1266, 2000.

Appendix

A Parameters:

Parameter	Value	Parameter	Value
β_m	0.0406 (A/V^2)	β_n	0.0799 (A/V^2)
δ_m	-0.5200 (V)	δ_n	0.8000 (V)
ϵ_m	2.000 (V)	ϵ_n	2.600 (V)
$\bar{m}$	1.300 (V)	$\bar{n}$	1.400 (V)
T_m	0.1300 (ms)	T_n	1.500 (ms)
C_y	0.0100 (mF)	R_y	200 (Ω)
a	0 (A)	I_A	-0.00834 (A)

B Characteristics of differential pairs:

$$f_x(y) \equiv \begin{cases} \bar{x} \quad when \quad y > \delta_x + \epsilon_x, \\ \frac{\bar{x}}{2}\{1 + \frac{1}{\epsilon_x^2}(y-\delta_x)\sqrt{2\epsilon_x^2 - (y-\delta_x)^2}\} \\ \quad when \quad \delta_x - \epsilon_x \le y \le \delta_x + \epsilon_x, \\ 0 \quad when \quad y < \delta_x - \epsilon_x, \end{cases}$$

The Tenth International Symposium on Artificial Life and Robotics 2005(AROB 10th '05),
B-con Plaza, Beppu, Oita, Japan, February 4-6, 2005

Wayland test, noise, and surrogates

Yoshito Hirata[1,*], Shunsuke Horai[2], Hideyuki Suzuki[1], and Kazuyuki Aihara[3,1,2]
[1]Department of Mathematical Informatics, The University of Tokyo,
7-3-1 Hongo, Bunkyo-ku, Tokyo 113-8656, Japan
[2] Aihara Complexity Modelling Project, ERATO, JST,
45-18 Oyama, Shibuya-ku, Tokyo 151-0065, Japan
[3] Institute of Industrial Science, The University of Tokyo,
4-6-1 Komaba, Meguro-ku, Tokyo, 153-8505, Japan
* yoshito@sat.t.u-tokyo.ac.jp

15 October 2004

Abstract

We show analytically and numerically that Wayland test can exceed one when a time series is contaminated with observational noise. Therefore, the test is not suitable for detecting the determinism from noisy experimental data. We also report a weird phenomenon: When the Wayland test is applied to random shuffle surrogates, they could show more "determinism" than the original data.

1 Introduction

Nonlinear time series analysis has been intensively investigated for the last two decades. One of the main aims is to give evidence that a given time series is generated from deterministic chaos. There are some key features of deterministic chaos. One of them is determinism. For detecting the determinism from time series, there are several methods proposed [1, 2]. Among them, a simple and easy-to-use one is Wayland test [2]. In the original paper, it was shown using examples that the statistic becomes close to 0 when a time series is deterministic, and it becomes about 1 when it is not.

In this paper, we report that the statistic of the Wayland test can be greater than 1 if a time series, generated by a deterministic system, is contaminated with observational noise. In Section 2, we introduce the Wayland test [2]. In Section 3, we argue analytically that the statistic of the Wayland test increases if the level of observational noise increases. In Section 4, we demonstrate the above analysis using some numerical examples. When the Wayland statistic is used in surrogate tests, a weird thing happens; randomly shuffled surrogates could exhibit more determinism than the original data. We report an example of this phenomenon in Section 5. We conclude the paper in Section 6.

2 Wayland test

In this section, we summarize a method proposed by Wayland *et al.* [2] for detecting the determinism in a time series. Suppose that a scalar time series $\{s_t\}_{t=1}^N$ is given. Let τ be the time lag, and m, the embedding dimension. Then we form delay coordinates x_t by $(s_t, s_{t-\tau}, \cdots, s_{t-(m-1)\tau})^T$. We call $\{x_t\}_{t=(m-1)\tau+1}^N$ the experimental attractor.

Choose the number l of integers between $(m-1)\tau+1$ and $N-1$. Call this set of integers T. For x_t of $t \in T$, find the number k of nearest neighbors from the experimental attractor. We label the i-th nearest neighbor for x_t as $x_{n_i(t)}$. For notational convenience, we define $n_0(t) = t$. For each $x_{n_i(t)}$, we look at its image $x_{n_i(t)+1}$ and take the translation vector,

$$v_i(t) = x_{n_i(t)+1} - x_{n_i(t)}. \tag{1}$$

To quantify this notion, let

$$v(t) = \frac{1}{k+1}\sum_{i=0}^{k} v_i(t). \tag{2}$$

This $v(t)$ shows the average of the translation vectors $v_i(t)$. Using it, we define the translation error $e(t)$ as

$$e(t) = \frac{1}{k+1}\sum_{i=0}^{k} \frac{\|v_i(t) - v(t)\|^2}{\|v(t)\|^2}. \tag{3}$$

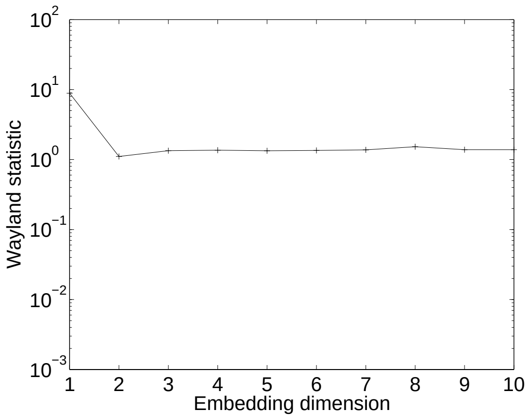

Figure 1: The result of the Wayland test, applied to a scalar time series of the Lorenz model.

The translation error $e(t)$ shows the fractional spread in the displacements of $x_{n_i(t)}$ relative to the average displacement $v(t)$.

We find the median of $e(t)$ over T, and declare it as the test statistic for the determinism. Wayland *et al.* showed using examples that the test statistic is close to 0 if a time series is deterministic and the test statistic is about 1 if a time series is random.

We applied the Wayland test to a time series generated by the Lorenz model [3]. The Lorenz model is defined as

$$\left\{\begin{array}{lcl} \frac{dx}{dt} & = & -ax+ay \\ \frac{dy}{dt} & = & -xz+bx-y \\ \frac{dz}{dt} & = & xy-cz, \end{array}\right. \tag{4}$$

where $(a,b,c)=(10,28,8/3)$. We integrated the equation using ode45 of MATLAB. During integrating, we observed x-coordinate every 0.01 unit time and obtained a scalar time series of length 1000. Then we added to the data observational noise, which follows the Gaussian distribution $N(0,(0.05\sigma_o)^2)$ of the mean 0 and standard deviation $0.05\sigma_o$, where σ_o is the standard deviation of the original clean data.

The result is shown in Fig. 1. We used the parameters $\tau=16$, $k=4$, and $l=100$. As the statistic exceeds 1 for all the tested dimensions, the time series should be interpreted as not deterministic. Although the Lorenz model itself is deterministic, the Wayland test did not detect its determinism from the noisy time series.

We remark that Wayland *et al.* [2] defined $\{s_t\}_{t=1}^N$ deterministic if x_t can be accurately modeled as the iteration of some continuous function. Therefore, according to this definition, the noisy time series tested here is not deterministic.

3 Analytical reasoning that Wayland statistic can be bigger than one

Why does the statistic of the Wayland test exceed 1? We argue in this section that there is a scaling law between the Wayland statistic and the level of observation noise.

Suppose that $\{y_t\}_{t=1}^N$ is a clean deterministic scalar time series and that $\{y_t\}_{t=1}^N$ is contaminated by observational noise $\{\eta_t\}_{t=1}^N$. Therefore, now the observed time series $\{s_t\}_{t=1}^N$ has the relation $s_t=y_t+\eta_t$ for each t. We assume that for each t, the noise η_t follows the Gaussian distribution $N(0,\sigma^2)$ of mean 0 and standard deviation σ.

Let

$$\tilde{v}_i(t)=\begin{pmatrix} y_{n_i(t)+1}-y_{n_i(t)} \\ y_{n_i(t)+1-\tau}-y_{n_i(t)-\tau} \\ \vdots \\ y_{n_i(t)+1-(m-1)\tau}-y_{n_i(t)-(m-1)\tau} \end{pmatrix}, \tag{5}$$

$$\tilde{v}(t)=\frac{1}{k+1}\sum_{i=0}^{k}\tilde{v}_i(t). \tag{6}$$

Then

$$v_i(t)=\tilde{v}_i(t)+\begin{pmatrix} \eta_{n_i(t)+1}-\eta_{n_i(t)} \\ \eta_{n_i(t)+1-\tau}-\eta_{n_i(t)-\tau} \\ \vdots \\ \eta_{n_i(t)+1-(m-1)\tau}-\eta_{n_i(t)-(m-1)\tau} \end{pmatrix}. \tag{7}$$

Hence, the average translation $v(t)$ is written as

$$\tilde{v}(t)+\begin{pmatrix} \frac{\sum_{i=0}^{k}(\eta_{n_i(t)+1}-\eta_{n_i(t)})}{k+1} \\ \frac{\sum_{i=0}^{k}(\eta_{n_i(t)+1-\tau}-\eta_{n_i(t)-\tau})}{k+1} \\ \vdots \\ \frac{\sum_{i=0}^{k}(\eta_{n_i(t)+1-(m-1)\tau}-\eta_{n_i(t)-(m-1)\tau})}{k+1} \end{pmatrix} \tag{8}$$

Assume that each $n_i(t)$ is far from the others in time. Then, for each j, the sum $\sum_{i=0}^{k}(\eta_{n_i(t)+1-j\tau}-\eta_{n_i(t)-j\tau})$ follows Gaussian distribution $N(0,2(k+1)\sigma^2)$. Therefore $\frac{1}{k+1}\sum_{i=0}^{k}(\eta_{n_i(t)+1-j\tau}-\eta_{n_i(t)-j\tau})$ follows $N(0,\frac{2\sigma^2}{k+1})$. Because $2\sigma^2/(k+1)$ is small if k is big, we approximate it as

$$\frac{1}{k+1}\sum_{i=0}^{k}(\eta_{n_i(t)+1-j\tau}-\eta_{n_i(t)-j\tau})\approx 0. \tag{9}$$

As a result, we have $v(t)\approx\tilde{v}(t)$.

Next we calculate $e(t)$. From its definition, we have

$$\begin{aligned} & e(t) \\ = & \frac{1}{k+1}\sum_{i=0}^{k}\frac{\|v_i(t)-v(t)\|^2}{\|v(t)\|^2} \\ = & \frac{1}{(k+1)\|v(t)\|^2}\sum_{i=0}^{k}\sum_{j=0}^{m-1}\left[([\tilde{v}_i(t)]_j-[v(t)]_j)^2\right. \\ & +2(\eta_{n_i(t)+1-j\tau}-\eta_{n_i(t)-j\tau})([\tilde{v}_i(t)]_j-[v(t)]_j) \\ & \left.+(\eta_{n_i(t)+1-j\tau}-\eta_{n_i(t)-j\tau})^2\right]. \end{aligned}$$

Taking the mean of $e(t)$ over all η_t's, we have

$$E[e(t)] = \frac{\sum_{i=0}^{k}(\|\tilde{v}_i(t)-v(t)\|^2+2m\sigma^2)}{(k+1)\|v(t)\|^2}.$$

Letting

$$\tilde{e}(t)=\frac{1}{k+1}\sum_{i=0}^{k}\frac{\|\tilde{v}_i(t)-\tilde{v}(t)\|^2}{\|\tilde{v}(t)\|^2}, \quad (10)$$

we obtain

$$E[e(t)] \approx \tilde{e}(t)+\frac{2m\sigma^2}{\|v(t)\|^2}. \quad (11)$$

The quantity $\tilde{e}(t)$ can be different from the statistic we obtain from a clean time series as the selected nearest neighbors can be different because of the observation noise. However, if the noise level is moderate, the selected points are still the neighbors of x_t, and the value of $\tilde{e}(t)$ is close to the one we obtain from a clean time series. Hence, we regard that $\tilde{e}(t)$ is approximately equal to the statistic we obtain from a clean time series as far as the noise level is moderate.

As $\frac{m}{\|v(t)\|^2} > 0$, the average of $e(t)$ will increase if the variation of the noise increases.

4 Numerical examples

To verify the formula in Eq. (11) numerically, we used a time series generated from the Hénon map [5]. The Hénon map is defined as $(u_{t+1}, v_{t+1}) = (1-a{u_t}^2+bv_t, u_t)$ where $(a, b) = (1.4, 0.3)$. We observed u_t and obtained a scalar time series of length 1000.

We tested the formula with several noise levels: $\sigma = 0, 0.01\sigma_o, 0.02\sigma_o, \cdots, 0.25\sigma_o$ where σ_o is the standard deviation of the original time series. For each noise level, we generated 100 realizations of noisy data and found the Wayland statistic for each of them. For calculating the Wayland statistic, we used $m = 2$, $\tau = 1$, $k = 4$ and $l = 100$. The result is shown in Fig. 2. We

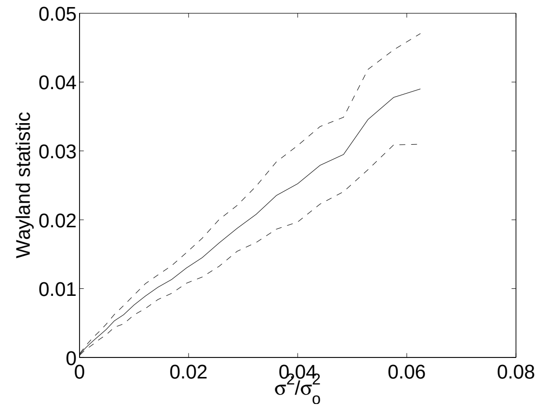

Figure 2: The relation between the Wayland statistic and the noise level σ in the example of the Hénon map. The solid line is the mean, the broken lines are the mean $\pm$ the standard deviation of 100 realizations.

observed the linear relationship between the Wayland statistic and σ^2, which was expected from Eq. (11).

We also tested this relation using the data of the Lorenz model. We observed the x-coordinate of the Lorenz model every 0.01 unit time and obtained a time series of length 1000. The tested noise levels σ are $0, 0.01\sigma_o, 0.02\sigma_o, \cdots, 1\sigma_0$ where σ_o is the standard deviation of the original clean time series. For finding the Wayland statistic, we used $m = 3$, $\tau = 16$, $k = 4$ and $l = 100$. The lag τ was chosen such that τ gives the first minimum of the mutual information [4]. The result is shown in Fig. 3. In this example, we also observed the linear relationship between the Wayland statistic and σ^2 when σ^2 is small. When the noise level is high, the average of the Wayland statistic is greater than one.

5 Wayland statistic and surrogates

When the Wayland statistic is used for a time series contaminated by observation noise with surrogate data analysis, we might observe a strange phenomenon: randomly shuffled surrogates show more "determinism" than the original time series.

We applied surrogate data analysis to the time series of the Lorenz model which is contaminated with 5% observation noise. The result is shown in Fig. 4. We observed that in most embedding dimensions, the Wayland statistic for the original time series is greater than the maximum of 39 randomly shuffled surrogates.

The following two reasons explain the phenomenon: When applied to a surrogate, or a dataset without any

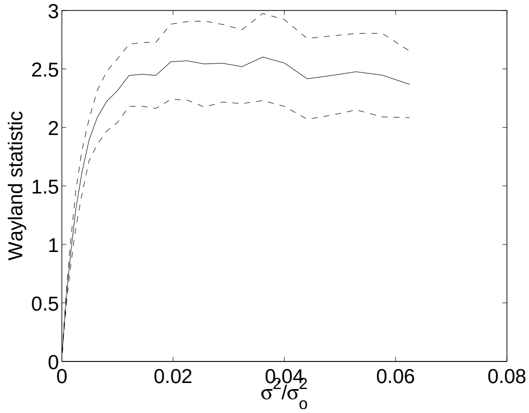

Figure 3: The relation between the Wayland statistic and the noise level σ of the observation noise, in the example of the Lorenz model. The solid line is the mean, the broken lines are the mean $\pm$ the standard deviation of 100 realizations.

temporal correlation, the Wayland statistic tends to be close to 1 [2]. However, because of the scaling law between the Wayland statistic and the noise level, the original data, or a dataset contaminated by observational noise, can yield a value greater than 1.

6 Conclusion

We showed that Wayland test is not appropriate for the test of the determinism in noisy experimental data because the statistic of the test can be greater than 1 even if there is a deterministic law behind the dynamics of a time series. The reason is that there is a scaling law between the statistic of the Wayland test and the level of observational noise. Although the original paper contains the analysis of observational noise, the result is too optimistic to be applied to noisy experimental data.

Because of the scaling law, when the statistic of the Wayland test is used for the test statistic of a surrogate data test, randomly shuffled surrogates can demonstrate more determinism than the original time series.

Acknowledgment

This study was supported by Industrial Technology Research Grant Program in 2003 from New Energy and Industrial Technology Development Organization (NEDO) of Japan.

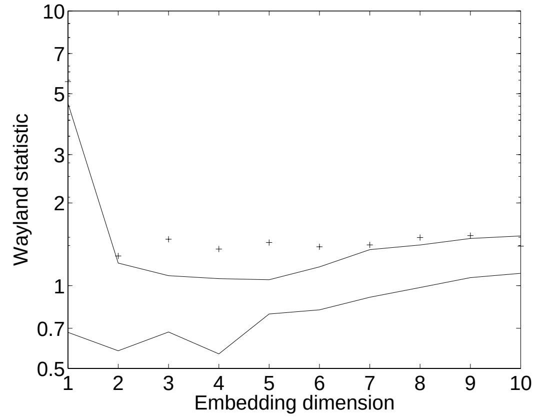

Figure 4: The result of surrogate data analysis on the data of the Lorenz model, contaminated with 5% observational noise. We generated 39 randomly shuffled surrogates from the original time series. For each embedding dimension, the sign + shows the value of the Wayland statistic obtained for the original noisy data, and the solid lines show the minimum and maximum of the Wayland statistic obtained from 39 surrogates.

References

[1] D. T. Kaplan and L. Glass, "Direct test for determinism in a time series," *Phys. Rev. Lett.*, vol.68, pp.427–430, 1992; D. T. Kaplan and L. Glass, "Coarse-grained embeddings of time series: random walks, Gaussian random processes, and deterministic chaos," *Physica D*, vol.64 pp.431–454, 1993; J. Bhattacharya and P. P. Kanjilal, "On the detection of determinism in a time series," *Physica D*, vol.132, pp.100–110, 1999; S. Horai, T. Yamada, and K. Aihara, "Determinism analysis with iso-directional recurrence plots," *T. IEE Japan*, vol.122, pp.141–147, 2002 (in Japanese).

[2] R. Wayland, D. Bromley, D. Dickett, and A. Passamante, "Recognizing determinism in a time series," *Phys. Rev. Lett.*, vol.70, pp.580–582, 1993.

[3] E. N. Lorenz, "Deterministic non-periodic flow," *J. Atmos. Sci.*, vol.20, pp.130–141, 1963.

[4] A. M. Fraser and H. L. Swinney, "Independent coordinates for strange attractors from mutual information," *Phys. Rev. A*, vol.33, pp.1134–1140, 1986.

[5] M. Hénon, "A two-dimensional mapping with a strange attractor," *Commun. Math. Phys.*, vol. 50, pp.69–77, 1976.

The Tenth International Symposium on Artificial Life and Robotics 2005(AROB 10th '05),
B-con Plaza, Beppu, Oita, Japan, February 4-6, 2005

Analysis of bifurcation and optimal response on the evolution of cooperation

Yo-Hey Otake
Graduate School of Frontier Sciences
The University of Tokyo
4-6-1 Komaba, Meguro-ku, Tokyo 153-8505, Japan
yoheyo@sat.t.u-tokyo.ac.jp

Kazuyuki Aihara
Institute of Industrial Science
The University of Tokyo
4-6-1 Komaba, Meguro-ku, Tokyo 153-8505, Japan
and Aihara Complexity Modelling Project, ERATO, JST
45-18 Oyama-cho, Shibuya-ku, Tokyo 151-0065, Japan
aihara@sat.t.u-tokyo.ac.jp

Abstract

A variety of strategies are needed to maintain cooperative behavior. Such strategy diversity in replication arises from various circumstances; for example, mutation in replication, noise, mistakes and moods. In this paper, we deal with the iterated prisoner's dilemma game, which has been widely used to study the evolution of cooperation. We approach the question of how cooperation evolves from the standpoint of dynamical systems and also analyze the evolution in terms of optimal response. Through these analyses, we have confirmed that strategy variation is important for the evolution of cooperation. In addition, we show that this approach is more useful than previous approaches because use of dynamical systems theory allows us to express a transient process dynamically.
Keywords: evolutionary game dynamics, replicator equation, cooperative behavior, iterated prisoner's dilemma, bifurcation analysis, optimal response.

1 Introduction

1.1 Evolutionary game theory

An aim of sociology and economics is to understand how cooperative behavior is maintained. It is important for research on behavior to look at the sustainability of such phenomena as well as their initial causes.

For this purpose, Maynard Smith applied game theory to ecological situations[1], which is known as evolutionary game theory. The main concept of this approach is that an evolutionarily stable strategy can be achieved. This concept of stability enables us to discuss sustainability.

Evolutionary game theory is now widely applied to many fields such as behavioral biology, ecology and economics.

1.2 Need for dynamic analysis

Most evolutionary researches on cooperation have emphasized an invasion condition of cooperative behavior in a population characterized by selfish behavior. To make up for the insufficiency of this approach, we need mathematical tools for analyzing dynamic processes as well as static states. Therefore, we have used nonlinear dynamical systems analysis to analyze the global behavior of evolutionary dynamics in the phase space of a strategy set.

1.3 Analysis of mutation in the evolution

Past researches have not accounted for all properties of evolution. Our goal is thus to consider situations containing various evolutionary factors, especially effects of mutation.

Through consideration of mutation, we examine effects of diversity on the evolution of cooperation. For this analysis, we emphasize the importance of dynamical systems, especially through bifurcation analysis.

2 Theory and methods

First, we introduce the game used to model the situations we consider, namely the prisoner's dilemma game, and prepare a strategy set for playing the game. After that, we introduce tools for the analysis. We describe the replicator equation and the form of mutation.

2.1 The Iterated Prisoner's Dilemma game

The iterated prisoner's dilemma (IPD)[1] is the most widely used model for the evolution of cooperation. Axelrod held a competition to study IPD strategy through a computer simulation [2]. This competition showed that a "tit-for-tat" (TFT) strategy was the most advantageous. A player using this strategy cooperates in the first interaction and then in subsequent interactions repeats (imitates) what the opponent did in the immediately preceding interaction.

On the other hand, the evolutionarily stable strategy (ESS) [1] in a finite IPD is the "always defect" (AllD) strategy. A violation of AllD, which is equivalent to destabilization of the ESS, is necessary for the evolution of cooperation. The evolution of cooperation in such cases can arise from various conditions (for example, groupings or spatial structures).

2.2 Strategy set

We must consider a class of various types of strategy ranging from selfish behavior to cooperative behavior. Thus, we prepared a strategy set (Table 1) like those used elsewhere [3, 4, 5].

strategy	explanation
TFT	Tit for tat
E1	Tit for tat and defect in the last interaction
E2	Tit for tat and defect in last two interactions
⋮	⋮
Ek	AllD (The number of interactions is k)

Table 1: Strategy set

TFT represents cooperative behavior (not being the first to defect) and AllD represents selfish behavior. This strategy set is filled from cooperation to defection.

[1]A payoff matrix for the prisoner's dilemma game (PD) is shown below.

		Opponent	
		Cooperation	Defection
Self	Cooperation	R	S
	Defection	T	P

S < P < R < T and T + S < 2R. This situation leads to the self's conflict and dilemma: if each of two players chooses the behavior maximizing self payoff, it brings about the situation minimizing the sum of the payoffs. Through iteration of the PD, the tendency towards cooperation increases.

2.3 Evolutionary game dynamics: the replicator equation

The fundamental law of evolutionary game theory is described by the replicator equation [6], and the evolutionary path can be understood as the dynamics on the phase space spanned by the frequency of each strategy.

We consider a replicator map of the following form:

$$x_i(t+1) = F_i(\vec{x}(t)) = \frac{x_i(t)w_i(\vec{x}(t))}{\sum_{j=1}^{N} x_j(t)w_j(\vec{x}(t))}, \quad (1)$$

where the variable x_i denotes the frequency of strategy i, which fitness, $w_i(\vec{x})$, is a function of the distribution of the population given by the vector $\vec{x} = (x_1, \cdots, x_n)$. The denominator, $\sum_{j=1}^{N} x_j(t)w_j(\vec{x}(t))$, ensures that $\sum_{j=1}^{N} x_j(t) = 1$. This map describes frequency-dependent selection. The evolutionary game theory assumes that Darwinian fitness is determined by the payoff matrix of a game (e.g., the IPD).

If the number of iterations of an IPD is finite and fixed[2], this map is deterministic and has no stochasticity.

We carried out numerical simulations based on this map. Similar analyses of population dynamics based on game theory have been done in [7].

2.4 Mutation

The elements of the evolution are as follows:

- Heredity
- Selection
- Mutation.

The replicator system mentioned above does not allow mutation, then we introduce the effect of mutation.

In this work, we discuss the replicator-mutator map of the following form [8, 9, 10]:

$$x_i(t+1) = F_i(\vec{x}(t)) = \frac{\sum_{j=1}^{N} x_j(t)w_j(\vec{x}(t))q_{ji}}{\sum_{j=1}^{N} x_j(t)w_j(\vec{x}(t))}, \quad (2)$$

where each setting is the same as for the replicator map (1). The probability that replication of strategy j gives rise to strategy i is given by q_{ji}. These quantities define the mutation matrix (a Markov matrix). This map describes both frequency-dependent selection and

[2]As in previous studies [3, 4, 5].

mutation.

Here, we consider a mutation matrix (Markov matrix) with uniform mutation[3] of the following form:

$$(q_{ji}) = \begin{cases} 1-(N-1)\epsilon & (j=i) \\ \epsilon & (j \neq i) \end{cases} . \qquad (3)$$

We consider the population dynamics of this model and analyze the stability and bifurcations of this system.

3 Results

In this section, we analyze the effects of mutation. First, we show time series obtained by numerical simulation with several mutation rates. After that, we show a bifurcation diagram and discuss its bifurcation structure. The number of strategies is N and the number of iterations of the IPD is k (N=k+1).

3.1 No mutation: the replicator equation

Previous studies [3, 4, 5] considered the case of no mutation. No mutation is equivalent to the mutation matrix being an identity matrix, namely $\epsilon = 0$ in Equation (3).

A numerical simulation result of the equation is shown in Figure 1.

The orbit in the simulation resembles a heteroclinic cycle, and approaches each of the corners on the k-dimensional simplex.

The sojourn time in each strategy exponentially increases. Various researchers have discussed the possibility that because the evolution of non-cooperative strategies cause the waste of much time, cooperation can evolve.

[3]We can also consider other types of formalization of the mutation matrix. A simple model is

$$(q_{ji}) = \begin{cases} 1-2\epsilon & (j=i) & (1-\epsilon \text{ if } j=1 \text{ or } N) \\ \epsilon & (j=i-1,i+1) & \end{cases} .$$

A strategy easily mutates into a similar strategy on the phenotype, but cannot mutate into a radically different strategy. The distance on the phenotype is strictly determined by the distance on the genotype. In this model, mutation will similarly affect the evolution of cooperation, but various dynamics would not be able to arise.

3.2 Slight mutation

Next, we investigated effects of mutation.

While the orbit property is the same as in the case of no mutation, the population dynamics are drastically changed even by a slight mutation.

A numerical simulation result of evolutionary dynamics with a slight mutation is shown in Figure 2.

If there is a slight mutation, the sojourn time in each strategy except the final one (AllD) is constant. Therefore, the evolution time of non-cooperative behavior is linear and selfish behavior evolves in actual time. Since the models used in previous studies cannot tolerate even a small amount of mutation, we consider them insufficient for interpreting the evolution of cooperation.

3.3 Greater mutation

Since there are reasons other than those considered in previous studies that can account for the evolution of cooperation, we look at the conditions affecting the evolution.

One factor that helps explain the evolution of cooperation is effective mutation.

We make the variation of strategy wider. In addition, the population dynamics change drastically depending on the mutation rate. In this instance, moreover, the orbit property differs from those in the cases of no mutation and a slight mutation.

A numerical simulation result of the evolutionary dynamics with a fairly weak mutation is shown in Figure 3.

For any initial condition, the dynamics fall into this quasi-periodic orbit. Thus, non-cooperative behavior cannot evolve. The result of evolution is periodic change of behavior.

3.4 Bifurcation analysis

We measure the level of cooperation in the population as a function of the mutation parameter ϵ. This is the level of cooperation after sufficient time has passed and the influence of the initial conditions is negligible. The bifurcation diagram is shown in Figure 4.

A mutation threshold exists and the dynamics of this system drastically change with changing the value of ϵ. The period of the limit cycle also continuously changes.

This system contains a saddle-node bifurcation on an invariant circle and a Neimark-Sacker bifurcation [11].

4 Discussion

We assert that mutation may play an important role in the evolution of cooperation, because population dynamics are drastically changed by mutation in replication. Here, we discuss the bifurcation at this change.

4.1 Comparison with recent research

Recent research based on dynamic programming suggested similar outcomes [12]. Therefore, we compare a dynamical systems technique to an analysis of optimal response and discuss the similarities and differences between the former research and our own.

The earlier research on the evolution of cooperation through analysis of optimal response has two limitations. First, a limited situation was assumed where most of the population adopted one strategy and other strategies were distributed among the population according to a distribution of a given variance. If a state is a mixture of strategies, it is difficult to analyze. Second, the response could only be examined for certain static situations, and dynamic processes could not be accommodated. McNamara et al. [12] demonstrated the importance of mutation (variation) from this viewpoint.

To determine whether cooperative behavior is sustainable, we need to describe the time evolution of behavior. An approach based on a dynamical system allows the expression of various states like mixtures of strategies and transient processes. The resulting abundance of information makes this a more fruitful approach. This is important for studying the evolution of cooperation [13].

The advantage of the approach with a dynamical system is that it allows us to examine not only the direction of evolution but also the time evolution of the frequencies of the strategies and transient processes. This is what makes the dynamical system approach so effective.

4.2 Consideration as game theory

In this paper, we have dealt with a finitely iterated prisoner 's dilemma game; that is, we have discussed the situation where the period of interaction is fixed and known. This is a difficult problem in the sense that it is difficult for cooperative behavior to evolve.

In biological and economic situations, the period of interaction may be known to everyone. In this case, cooperative behavior is maintained. Nevertheless, it is difficult for cooperation to evolve theoretically because of backward induction reasoning, and few theoretical approaches have allowed the evolution of cooperation.

When the period of interaction is fixed and known, previous studies have shown that it is difficult for cooperation to evolve because of backward induction reasoning [3, 4, 5]. Backward induction is powerful premise, leading some to consider theoretical research on the evolution of cooperation to be impossible. The few studies that supported the evolution of cooperation [3, 4, 5, 14] used models that did not contain all properties of evolution. Therefore, we wanted to consider situations involving various evolutionary factors, especially the effect of mutation.

Our goal is to bridge the gap between the theoretical and empirical researches. In this paper, we sought to do this by incorporating the role of mutation. By considering mutation, we found a remarkable phenomenon: mutation can promote the evolution of cooperation. This phenomenon arises from a bifurcation of the equation solution.

5 Conclusion

We have examined the factors affecting the evolution of cooperation in a finitely IPD. Players cooperate in a situation where the interaction term is finite and known. This evolution is supported by mutation. Our research indicates that mutation plays an important role in the evolution of cooperation. Moreover, through a comparison with another approach, we have confirmed the effectiveness of applying dynamical systems theory to the evolution of behavior.

Acknowledgements

We would like to thank Koh Hashimoto, Joe Yuichiro Wakano (The University of Tokyo) and Hisashi Ohtsuki (Kyushu University) for their fruitful suggestions and comments.

References

[1] J. Maynard Smith, *Evolution and the Theory of Games*, Cambridge University Press: Cambridge, 1982.

[2] R. Axelrod, *The Evolution of Cooperation*, Basic books: New York, 1984.

[3] J. H. Nachbar, "Evolution in the finitely repeated prisoner's dilemma," *J. Econ. Behav. Organ.*, vol.19, pp.307–326, 1992.

[4] R. Schuessler, "The gradual decline of cooperation: endgame effects in evolutionary game theory," *Theory Decis.*, vol.26, pp.133–155, 1989.

[5] T. Shimizu, "Evolution of cooperation in the finitely repeated Prisoner's Dilemma (in Japanese)," *Koudoukeiryougaku*, vol.24, pp.101–111, 1997.

[6] P. D. Taylor & L. B. Jonker, "Evolutionary stable strategies and game dynamics," *Math. Biosci.*, vol.40, pp.145–156, 1978.

[7] E. C. Zeeman, "Population dynamics from game theory," In: *Global theory of dynamical systems.* Springer Lecture Notes in Mathematics, vol.819, pp.471–497, 1978.

[8] J. Hofbauer & K. Sigmund, *Evolutionary Games and Population Dynamics*, Cambridge University Press: Cambridge, 1998.

[9] K. M. Page & M. A. Nowak, "Unifying Evolutionary Dynamics," *J. Theor. Biol.*, vol.219, pp.93–98, 2002.

[10] N. L. Komarova, "Replicator-mutator equation, universality property and population dynamics of learning," *J. Theor. Biol.*, vol.230, pp.227–239, 2004.

[11] Y. A. Kuznetsov, *Elements of Applied Bifurcation Theory* (2nd ed.), Springer Verlag: New York, 1998.

[12] J. H. McNamara, Z. Barta & A. I. Houston, "Variation in behaviour promotes cooperation in the Prisoner's Dilemma game," *Nature*, vol.428, pp.745–748, 2004.

[13] M. A. Nowak & K. Sigmund, "Chaos and the evolution of cooperation," *Proc. Natl. Acad. Sci. USA*, vol.90, pp.5091–5094, 1993.

[14] M. A. Nowak & K. Sigmund, "Invasion dynamics of the finitely repeated prisoner's dilemma," *Games Econ. Behav.*, vol.11, pp.364–390, 1995.

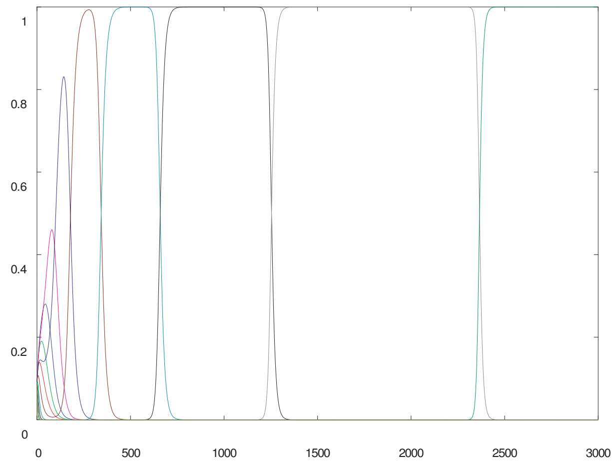

Figure 1: Population dynamics without mutation (k = 10, $\epsilon = 0$). The horizontal axis is time (generation) and the vertical axis is the population frequency of each strategy.

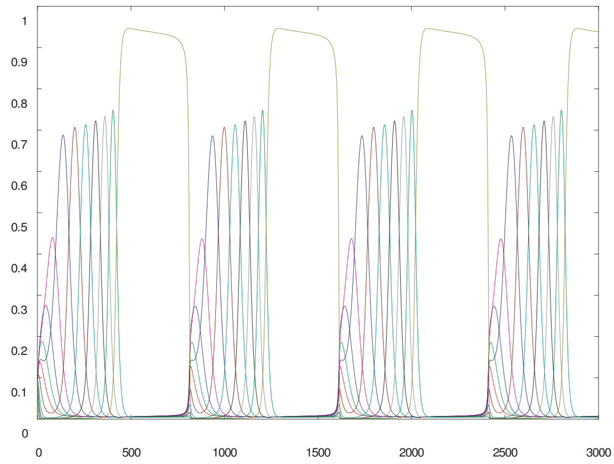

Figure 3: Population dynamics with a weak mutation (k = 10, $\epsilon = 3.5 \times 10^{-4}$). The horizontal axis is time (generation) and the vertical axis is the population frequency of each strategy.

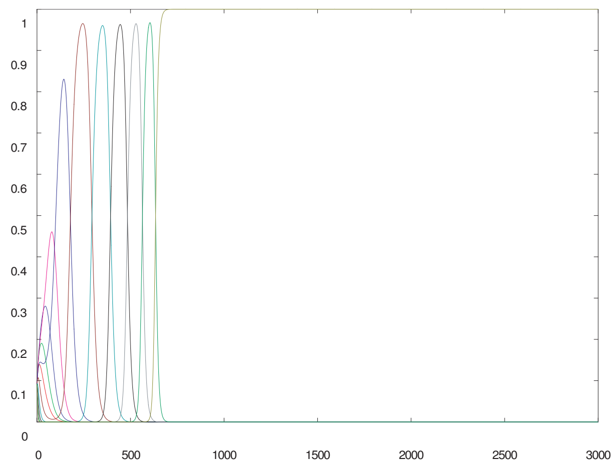

Figure 2: Population dynamics with a slight mutation (k = 10, $\epsilon = 1.0 \times 10^{-6}$). The horizontal axis is time (generation) and the vertical axis is the population frequency of each strategy.

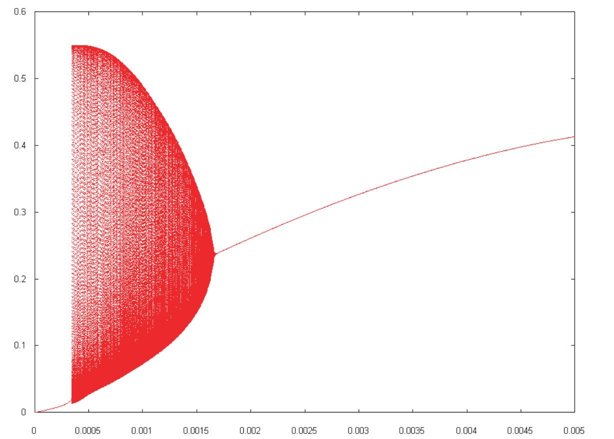

Figure 4: Bifurcation diagram: The horizontal axis is the mutation rate (the bifurcation parameter) and the vertical axis is the frequency of cooperative behavior after sufficient time has passed.

The Tenth International Symposium on Artificial Life and Robotics 2005(AROB 10th '05),
B-con Plaza, Beppu, Oita, Japan, February 4-6, 2005

Dynamic Preshaping Based Design of Capturing Robot Driven by Wire

Shoichi NISHIO , Mitsuru HIGASHIMORI , and Makoto KANEKO

Graduate School of Engineering, Hiroshima University, Higashi-Hiroshima 739-8527, JAPAN

Abstract

This paper discusses the design of wire drive capturing robots based on dynamic preshaping. As the speed of a robot hand increases, dynamic eflects become dominant. In order to successfully catch an object by a high speed capturing robot, it is important to consider mass distribution, wiring, and joint spring when designing the robot. After explaining the design procedure by considering those mechanical parameters, experiments as well as simulations are shown to verify the basic idea.

1 Introduction

While a number of robots have been developed so far, we are particularly interested in high speed robots that can capture a moving object quickly. As the first trial of such a high speed robot, we have designed and developed the 100G capturing robot[1] that can catch a flying object in the air within the motion time of 50[msec]. Fig.1 shows an experimental result where the 100G capturing robot is capturing a ball by the gripper. Due to such a high speed, we cannot follow by our eyes what is really happening during the capturing motion. Therefore, we can not see directly why the robot fails in catching the object while it looks like that the gripper successfully reaches the target object position. After precise analysis utilizing a high speed camera with the frame rate of 1[msec], we found that the preshape of the gripper is not appropriate, especially for the final stage of catching motion. Considering the finger link posture during the high speed capturing motion, it is impossible to neglect inertia force applied to the finger links. Therefore, the preshaping issue under such a high speed condition results in an optimum design problem to determine the joint torque distribution with considering the effects of dynamics. The goal of this work is to provide a design procedure on preshaping issue for a high speed capturing robot.

Reducing mass of the robot is really important for achieving a high acceleration. In such sense, wire drive robots are good candidates for reducing mass of both arm and gripper, since we can install all actuators at the base. We suppose a robot where all joints are controlled by a single wire. A feature of such robots is that the torque distribution is determined by both the size of pulley in each joint and the way of wiring. By focusing on such a wire drive robot, we define that the dynamic preshaping problem is to produce a joint torque set so that all links make contact with an object. We explore the geometrical issue where the design for wiring is precisely discussed. After explaining the design procedure for achieving the reference posture under high speed condition by considering mechanical parameters of the robot, experiments as well as simulations are shown to verify the basic idea.

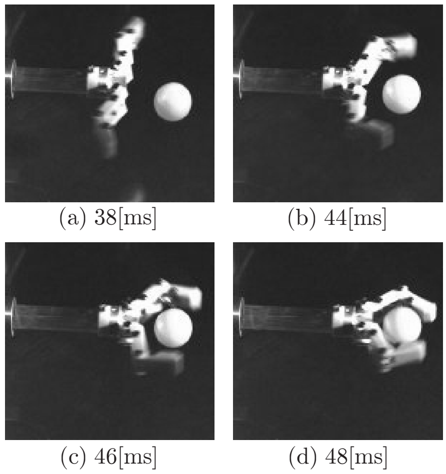

Fig. 1: A two-fingered robot hand for capturing an object.

2 Related Works

There have been a couple of works discussing preshaping issues so far[3]–[8]. Bard and Troccaz[3] have discussed an automatic preshaping for a dexterous hand from a single description of objects, where the object model is automatically extracted from a low-level visual data and a system for preshaping a planar two-fingered hand with four joints grasping planar ob-

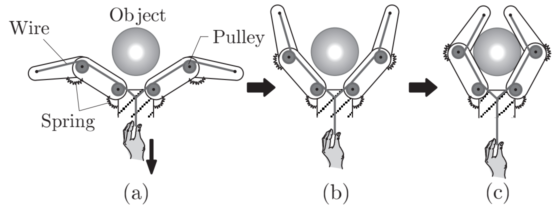

Fig. 2: Basic mechanism of a high speed capturing robot driven by a single wire.

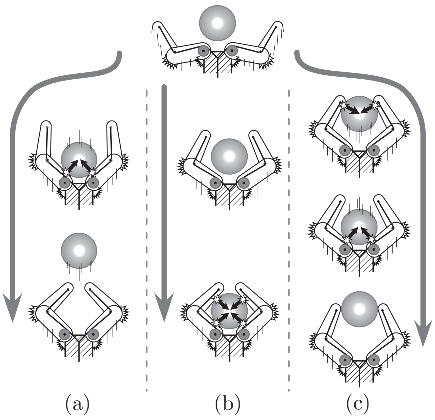

Fig. 3: Various behaviors of object when finger links make contact with it.

jects is described. Kang and Ikeuchi[4] have proposed an automatic robot instruction for recognizing a grasp from observation. Hong and Slotine[5] have proposed a catching algorithm by which they succeeded in real time catching free-flying spherical balls being tossed from random locations. The postures of the robot hand and arm at the moment of capturing are planned by the information obtained by vision. Nakamura et. al. [6] have challenged the reactive grasp of a three-fingered robot hand by using a learning method, where the preshaping is planned by integrating 48 kinds of sensor signals and 29 primitive behaviors. As far as we know, our paper is the first work discussing dynamic preshaping.

3 Problem Formulation

3.1 Robot Hand Driven by a Single Wire

Suppose a typical robot hand where each actuator is placed at each joint. In such a case, the whole weight of the robot increases and the motion of the robot becomes slow as a result. In order to decrease the weight, the wire drive method where all actuators are arranged at the base of the robot and the torque driving each joint is transmitted through wire, has been utilized[1][2]. Consider a multi-linked robot hand where all joints are controlled by a single wire, as shown in Fig.2. Now we focus on only open-close motion of fingers. The motions of the arm are ignored. Since all joints of the robot are driven by the tension of one control wire[1], the distribution of drive torque for each joint is determined by the wiring, i.e., pulley position and radius. In addition, a spring is attached to each joint to keep the initial link posture when wire tension is zero. This spring produces a resistant force for the joint torque coming from wire tension.

3.2 Reference Posture

Suppose a capturing robot trying to capture an object, as shown in Fig.3, where (a) and (c) are examples of failure in catching an object, and (b) is an example of successful catching, respectively. From the geometrical point of view, it is more likely that the simultaneous contact between links and the object leads to a successful catching. Based on this consideration, we define the reference posture of finger links as shown in Fig.3(b), and this is given by following.

Reference Posture: The reference posture is given by the grasping form where all links make contact with an object, and is expressed by the joint angular vector $\boldsymbol{\theta}_r \in \mathcal{R}^{\,{}_{s=1}^{U} N_s \times 1}$, where U and N_s denote the number of fingers and the number of joints (= the number of links) of the s-th finger, respectively.

3.3 Dynamic Preshaping Problem

In this work, we suppose that capturing motions by robot hands can be regarded as realizing the given reference posture $\boldsymbol{\theta}_r$. We define the dynamic preshaping problem as follwing.

Dynamic Preshaping Problem: By giving the reference joint angle $\boldsymbol{\theta}_r$, determine the mechanical parameters (pulley radius, pulley position, spring constant, and mass of finger link), so that the following condition is satisfied.

$$\Delta t_{\theta_r} = \max \left| t_{\theta_{sir}} \quad t_{\theta_{sjr}} \right| < \varepsilon \qquad (1)$$
$$(s = 1, \ldots, U,\ i = 1, \ldots, N_s,\ j = 1, \ldots, N_s)$$

where $t_{\theta_{sir}}$ denotes the time when the i-th joint of the s-th finger reaches the reference angle and ε is a small positive value.

The Tenth International Symposium on Artificial Life and Robotics 2005(AROB 10th '05),
B-con Plaza, Beppu, Oita, Japan, February 4-6, 2005

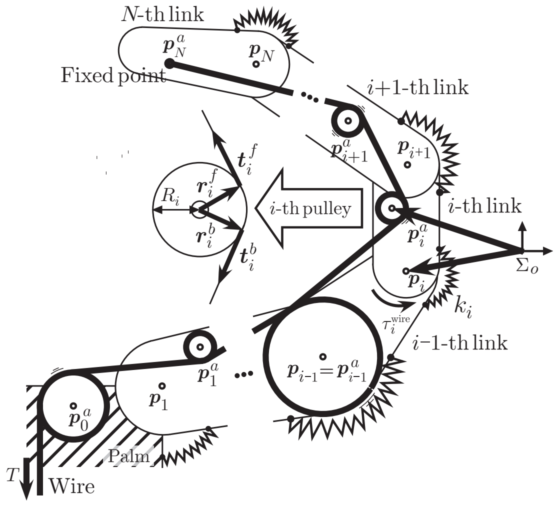

Fig. 4: A 2D finger model driven by a single wire.

4 Mechanical Analysis

4.1 Wiring

Suppose a 2D finger is driven by a single wire as shown in Fig.4, where $\boldsymbol{p}_i$, $\boldsymbol{p}_i^a$, and $\boldsymbol{p}_N^{fix} \in \mathcal{R}^{2\times 1}$ are the position vectors expressing the i-th joint position, the i-th pulley position at inner link, and the wire fixing point at the N-th link, respectively, and all pulleys can be freely rotated around their axes. $\boldsymbol{p}_0^a$ is the position vector expressing the pulley position at the palm, and whole link system is fixed with the base at $\boldsymbol{p}_1$. Let $\boldsymbol{t}_i^f \in \mathcal{R}^{2\times 1}$ and $\boldsymbol{t}_i^b \in \mathcal{R}^{2\times 1}$ be the tension vectors before and after the i-th pulley, respetively, as shown Fig.4. Supposing that there is no friction around each pulley axis, we have $\|\boldsymbol{t}_i^b\| = \|\boldsymbol{t}_i^f\| = T$ where T is the wire tension. Also, let $\boldsymbol{r}_i^f \in \mathcal{R}^{2\times 1}$ and $\boldsymbol{r}_i^b \in \mathcal{R}^{2\times 1}$ be the vectors denoting the positions where the wire tensions are given. Under the above preparation, we have the following relationship.

$$\boldsymbol{t}_i^f = \boldsymbol{t}_{i+1}^b \tag{2}$$

$$\boldsymbol{r}_i^b \otimes \boldsymbol{t}_i^b = \boldsymbol{r}_i^f \otimes \boldsymbol{t}_i^f \tag{3}$$

where $\otimes$ denotes the operator providing $x_1y_2 \quad x_2y_1$ for two vectors $\boldsymbol{x} = [x_1, x_2]^{\mathrm{T}}$ and $\boldsymbol{y} = [y_1, y_2]^{\mathrm{T}}$. By letting $\boldsymbol{d}_i^{i+1} \in \mathcal{R}^{2\times 1}$ express the vector from the wire release point of the i-th pulley to that of the $i+1$-th pulley, we get

$$\boldsymbol{p}_{i+1}^a = \boldsymbol{p}_i^a + \boldsymbol{r}_i^f + \boldsymbol{d}_i^{i+1} \quad \boldsymbol{r}_{i+1}^b \tag{4}$$

By multiplying $\otimes \boldsymbol{t}_{i+1}^b$ by right side to each term on eq.(4) and considering $\boldsymbol{d}_i^{i+1} \otimes \boldsymbol{t}_{i+1}^b = 0$, we obtain the following equation:

$$(\boldsymbol{p}_{i+1}^a \quad \boldsymbol{p}_i^a) \otimes \boldsymbol{t}_{i+1}^b = (\boldsymbol{r}_i^f \quad \boldsymbol{r}_{i+1}^b) \otimes \boldsymbol{t}_{i+1}^b \tag{5}$$

The torque around the i-th joint is given by the following form:

$$\tau_i^{\text{wire}} = (\boldsymbol{p}_i^a \quad \boldsymbol{p}_i) \otimes \boldsymbol{t}_i^b + (\boldsymbol{p}_i^a \quad \boldsymbol{p}_{i+1}) \otimes \boldsymbol{t}_i^f \tag{6}$$

From eqs.(2), (3), (5), and (6), τ_i^{wire} can be rewritten with $\boldsymbol{r}_i^b$ by the following form.

$$\tau_i^{\text{wire}} = T R_i^{vp} \tag{7}$$

where

$$\begin{aligned} R_i^{vp} = {} & (\boldsymbol{p}_i^a \quad \boldsymbol{p}_i + \boldsymbol{r}_i^b) \otimes \boldsymbol{e}_i^b \\ & (\boldsymbol{p}_{i+1}^a \quad \boldsymbol{p}_{i+1} + \boldsymbol{r}_{i+1}^b) \otimes \boldsymbol{e}_{i+1}^b \end{aligned} \tag{8}$$

Let $\boldsymbol{e}_i^b (= \boldsymbol{t}_i^b / T) \in \mathcal{R}^{2\times 1}$ be the unit vector expressing the direction of tension. Eq.(7) means that the torque produced by a wire can be expressed by the multiplying the wire tension with the radius of virtual pulley. We would note that the radius of such a virtual pulley varies depending upon the link posture.

The above discussions provide us with the relationship between the torque and the wire tension in the following form:

$$\boldsymbol{\tau}^{\text{wire}} = T\,[\boldsymbol{A} + \boldsymbol{B}]\,\boldsymbol{e}^b \tag{9}$$

where

$$\boldsymbol{\tau}^{\text{wire}} = \left[\tau_1^{\text{wire}}, \quad , \tau_N^{\text{wire}}\right]^{\mathrm{T}} \in \mathcal{R}^{N\times 1} \tag{10}$$

$$\boldsymbol{A} = \begin{bmatrix} [\boldsymbol{q}_1\otimes] & [\boldsymbol{q}_2\otimes] & & \boldsymbol{0} \\ & & \ddots & \\ & & [\boldsymbol{q}_{N\ 1}\otimes] & [\boldsymbol{q}_N\otimes] \\ \boldsymbol{0} & & & [\boldsymbol{q}_N\otimes] \end{bmatrix} \in \mathcal{R}^{N\times 2N} \tag{11}$$

$$\boldsymbol{q}_i = \boldsymbol{p}_i^a \quad \boldsymbol{p}_i \in \mathcal{R}^{2\times 1} \tag{12}$$

$$\boldsymbol{B} = \begin{bmatrix} [\boldsymbol{r}_1^b\otimes] & [\boldsymbol{r}_2^b\otimes] & & \boldsymbol{0} \\ & & \ddots & \\ & & [\boldsymbol{r}_{N\ 1}^b\otimes] & [\boldsymbol{r}_N^b\otimes] \\ \boldsymbol{0} & & & [\boldsymbol{r}_N^b\otimes] \end{bmatrix} \in \mathcal{R}^{N\times 2N} \tag{13}$$

$$\boldsymbol{e}^b = \left[\boldsymbol{e}_1^{b\,\mathrm{T}}, \quad , \boldsymbol{e}_N^{b\,\mathrm{T}}\right]^{\mathrm{T}} \in \mathcal{R}^{2N\times 1} \tag{14}$$

where $[\boldsymbol{x}\otimes]$ means $[\ \ x_2, x_1] \in \mathcal{R}^{1\times 2}$ for a vector $\boldsymbol{x} = [x_1, x_2]^{\mathrm{T}}$. $\boldsymbol{A}\boldsymbol{e}^b$ and $\boldsymbol{B}\boldsymbol{e}^b$ express the torque components controlled by the position of pulley and by both the radius of pulley and the way of wiring, respectively.

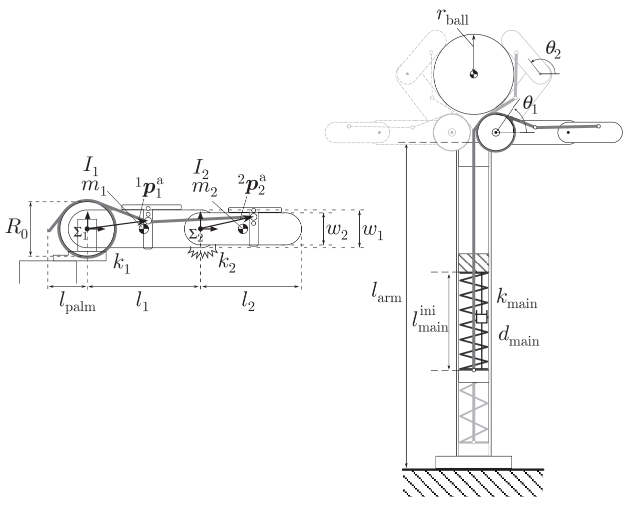

Fig. 5: Finger model for determining parameters.

Table 1: Mechanical parameters used for simulation.

l_1	length of the 1st link	60.0[mm]
l_2	length of the 2nd link	45.0[mm]
m_1	mass of the 1st link	55.0[g]
m_2	mass of the 2nd link	30.0[g]
I_1	moment of inertia of the 1st link	27.6[kgmm^2]
I_2	moment of inertia of the 2nd link	7.1[kgmm^2]
w_1	width of the 1st link	20.0[mm]
w_2	width of the 2nd link	17.0[mm]
l_{palm}	position of the 1st joint	10.0[mm]
l_{arm}	length of arm	260.0[mm]
$l^{\mathrm{ini}}_{\mathrm{main}}$	initial length of main spring	70.0[mm]
k_{main}	spring constant of main spring	0.60[N/mm]
d_{main}	damping coe cient of main spring	0.01[Ns/mm]
$l_{k_{\mathrm{main}}}$	natural length of main spring	180.0[mm]
r_{ball}	radius of object	32.5[mm]
θ^{ini}_1	initial angle of the 1st joint	0.0[rad]
θ^{ini}_2	initial angle of the 2nd joint	0.0[rad]
k_1	spring constant of the 1st joint	90.0[Nmm/rad]
k_2	spring constant of the 2nd joint	120.0[Nmm/rad]
R_0	radius of base pulley	15.0[mm]
R_1	radius of pulley on the 1st link	0.01[mm]

4.2 Joint Compliance

Let us now consider the effect of spring distribution among joints, where k_i is the i-th joint spring constant as shown in Fig.4. Each joint spring plays an important role for controlling the finger link posture when the fingers approach an object. We have the following relationship between the joint torque and spring constant.

$$\boldsymbol{\tau}^{\mathrm{spring}} = \quad \boldsymbol{Q}\boldsymbol{k} \tag{15}$$

where

$$\boldsymbol{\tau}^{\mathrm{spring}} = \left[\tau^{\mathrm{spring}}_1, \cdots, \tau^{\mathrm{spring}}_N\right]^{\mathrm{T}} \in \mathcal{R}^{N\times 1} \tag{16}$$

$$\boldsymbol{Q} = \begin{bmatrix} \theta_1 \;\; \theta_1-\theta_2 & & & \boldsymbol{0} \\ & \ddots & & \\ & & \theta_i-\theta_{i-1} \;\; \theta_i-\theta_{i+1} & \\ & & & \ddots \\ \boldsymbol{0} & & & \theta_N-\theta_{N-1} \end{bmatrix} \in \mathcal{R}^{N\times N} \tag{17}$$

$$\boldsymbol{k} = [k_1, \cdots, k_N]^{\mathrm{T}} \in \mathcal{R}^{N\times 1} \tag{18}$$

4.3 Equation of Motion

The equation of motion of the finger link system can be modeled by the following,

$$\boldsymbol{M}(\boldsymbol{\theta})\ddot{\boldsymbol{\theta}} + \boldsymbol{h}(\dot{\boldsymbol{\theta}}, \boldsymbol{\theta}) = \boldsymbol{\tau}^{\mathrm{wire}} + \boldsymbol{\tau}^{\mathrm{spring}} \tag{19}$$

where $\boldsymbol{M}(\boldsymbol{\theta}) \in \mathcal{R}^{N\times N}$ and $\boldsymbol{h}(\dot{\boldsymbol{\theta}}, \boldsymbol{\theta}) \in \mathcal{R}^{Ns\times 1}$ are the inertia matrix and velocity related torque vector, respectively. From eqs.(9) and (15), eq.(19) can be rewritten in the following form:

$$\boldsymbol{M}(\boldsymbol{\theta})\ddot{\boldsymbol{\theta}} + \boldsymbol{h}(\dot{\boldsymbol{\theta}}, \boldsymbol{\theta}) = T\left[\boldsymbol{A}(\boldsymbol{\theta}) + \boldsymbol{B}(\boldsymbol{\theta})\right]\boldsymbol{e}^b(\boldsymbol{\theta}) \quad \boldsymbol{Q}(\boldsymbol{\theta})\boldsymbol{k} \tag{20}$$

5 Dynamic Preshaping

5.1 Parameter Determination

Since the equation of motion given by eq.(20) is highly nonlinear, it is really difficult to formulate an algorithm for solving the dynamic preshaping problem. Through the analysis of wiring, we learnt that each joint torque is very sensitive to the pulley position and even negative torque can be generated according to the location, while it is hard to achieve such a characteristic by changing either spring constant or mass distribution. Based on these considerations, let us now replace the problem obtaining the mechanical parameters for realizing $\boldsymbol{\theta}_r$ by the following optimization problem.

Minimize

$$Z = \Delta t_{\boldsymbol{\theta}_r}$$

Subject to

$$ {}^i\boldsymbol{p}^{a\min}_i \quad {}^i\boldsymbol{p}^{a}_i \quad {}^i\boldsymbol{p}^{a\max}_i \qquad (i = 1, \ldots, N)$$
$$\boldsymbol{M}(\boldsymbol{\theta})\ddot{\boldsymbol{\theta}} + \boldsymbol{h}(\dot{\boldsymbol{\theta}}, \boldsymbol{\theta}) = T\left[\boldsymbol{A}(\boldsymbol{\theta}) + \boldsymbol{B}(\boldsymbol{\theta})\right]\boldsymbol{e}^b(\boldsymbol{\theta}) \quad \boldsymbol{Q}(\boldsymbol{\theta})\boldsymbol{k}$$

where ${}^i\boldsymbol{p}^{a\min}_i$ and ${}^i\boldsymbol{p}^{a\max}_i \in \mathcal{R}^{2\times 1}$ are the minimum and the maximum limitations of the pulley position, respectively. Now, the evaluation function Z is corresponding to eq.(1).

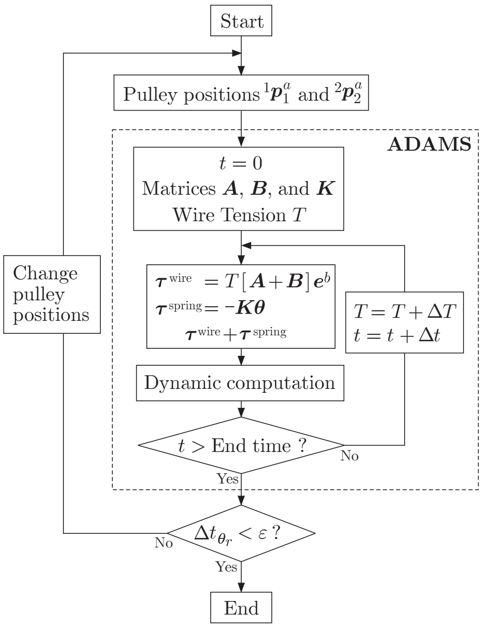

Fig. 6: Flow chart for computing the pulley positions.

5.2 Simulations

In order to obtain the pulley position satisfying the condition expressed by eq.(1), we repeat computation until it converges. Consider a two-fingered hand and a sphere object as shown in Fig.5. All parameters except for $^1\boldsymbol{p}_1^a$ and $^2\boldsymbol{p}_2^a$ are given by Table.1. We also suppose that one tip of the wire is fixed at the one side of the spring implemented in the arm and the other tip of wire is fixed at the second finger link. We assume that the wire tension T is generated by the following equation.

$$T = k_{\text{wire}}\Delta l_{\text{wire}} \quad d_{\text{wire}}\Delta \dot{l}_{\text{wire}} \tag{21}$$

where k_{wire}, d_{wire}, and Δl_{wire} are virtual stiffness, damping coefficient, and the amount of stretch, respectively. Now, we give $k_{\text{wire}} = 1.0 \times 10^6$[N/mm] and $d_{\text{wire}} = 1.0 \times 10\ ^2$[Ns/mm]. We also suppose that the friction between each finger link and the object is given by $\mu = 0.0$. The dynamic simulator ADAMS (Mechanical Dynamics, Inc.) is utilized for computing finger motion for a given set of parameters. Fig.6 shows the flow chart for computing the pulley positions $^1\boldsymbol{p}_1^a$ and $^2\boldsymbol{p}_2^a$ in Fig.5 for achieving the reference finger posture at the instance of contact. Fig.7 shows two simulation results where (a) and (b) are $\varepsilon = 13$[ms] and $\varepsilon = 0.4$[ms], respectively. In case of $\varepsilon = 13$[ms], we obtain the optimum pulley positions $^1\boldsymbol{p}_1^a = [32.0, 2.0]^{\text{T}}$[mm] and $^2\boldsymbol{p}_2^a = [25.0, 2.5]^{\text{T}}$[mm].

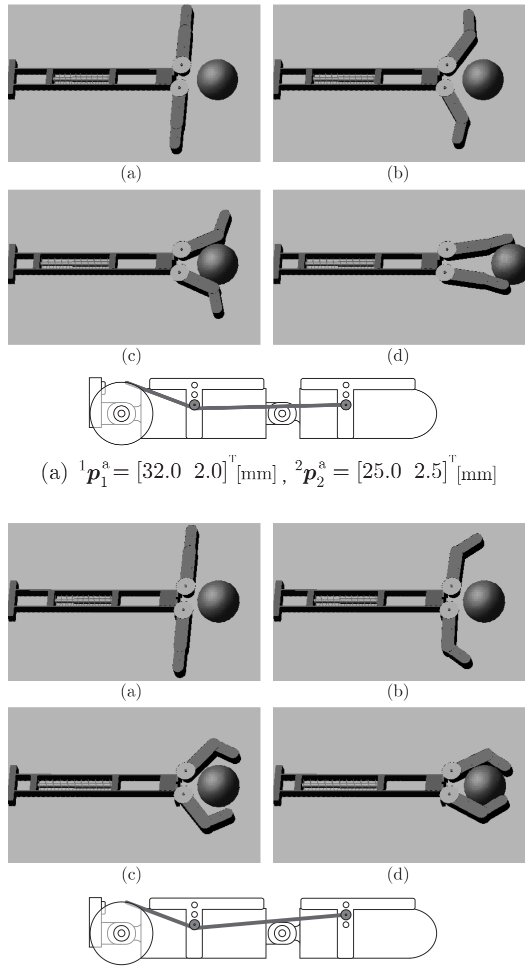

Fig. 7: Simulation results for two different sets of pulley position.

As shown in Fig.7(a), the first link makes contact with the object earlier than the second one and the object is finally pushed away. This result suggests that $\varepsilon = 13$[ms] is not small enough. In case of $\varepsilon = 0.4$[ms], we obtain $^1\boldsymbol{p}_1^a = [32.0, 2.0]^{\text{T}}$[mm] and $^2\boldsymbol{p}_2^a = [25.0, 6.5]^{\text{T}}$[mm] after convergence. In this case, all links make contact with the object with in 1[ms]. As shown in Fig.7(b), the robot can capture the object successfully while it includes a small oscillational motion.

6 Experiments

We designed and developed an experiment system for confirming the simulation results, where we can change the wiring route by changing the pulley posi-

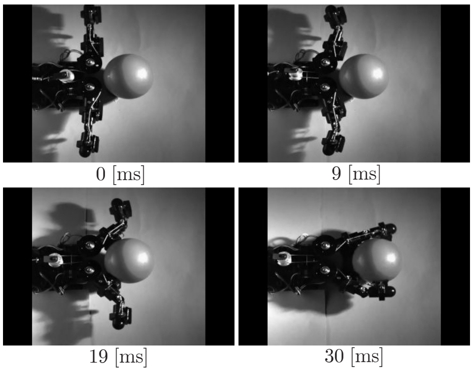

(a) ${}^1\boldsymbol{p}_1^{\mathrm{a}} = [32.0\ \ 2.0]^{\mathrm{T}}$[mm] , ${}^2\boldsymbol{p}_2^{\mathrm{a}} = [25.0\ \ 2.5]^{\mathrm{T}}$[mm]

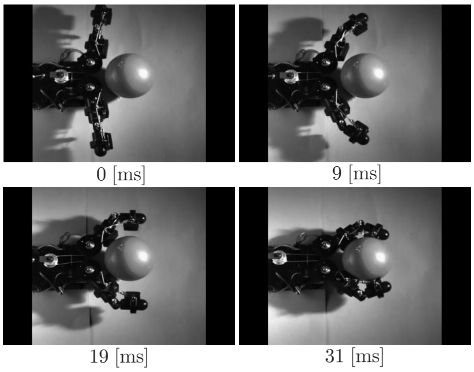

(b) ${}^1\boldsymbol{p}_1^{\mathrm{a}} = [32.0\ \ 2.0]^{\mathrm{T}}$[mm] , ${}^2\boldsymbol{p}_2^{\mathrm{a}} = [25.0\ \ 6.5]^{\mathrm{T}}$[mm]

Fig. 8: Experimental results for two different sets of pulley position.

tion and the pulley size, the joint spring constant, and the mass distribution of the links, respectively. The tension of the wire is generated by the elastic energy of the spring mounted in the arm. Mechanical parameters except for the pulley positions are given by Table.1 where parameter explanation is given in Fig.5. We observe the change of the link posture by shifting the pulley positions along the simulation results. Fig.8 shows a series of photo taken by a high-speed camera with 1 [ms/frame], where the hand is taking action for capturing a sphere object. The hand as shown in Fig.8(a) and (b) are designed under the pulley position as shown in Fig.7(a) and (b), respectively. While the first link makes contact with the object earlier than the second one in Fig.8(a), all links almost make contact with the object simultaneously in Fig.8(b). From Fig.8, we can see that the behaviors of finger links in the simulation and experiment nicely coincide. Therefore, the validity of the optimum parameters obtained by the simulation are supported by experiments.

7 Concluding Remarks

We discussed the design of capturing robot driven by a wire from the viewpoint of dynamic preshaping. The main results are summarized as follows;

(1) Dynamic preshaping is important, especially just before finger links make contact with the object. We choose the preshape so that all links make contact with the object simultaneously.

(2) The mechanical parameters which influences joint drive torque were considered and the relationship between the wire tension and the joint torque distribution was introduced precisely.

(3) The design procedure for achieving the reference posture under dynamic condition was explained. A couple of simulations were executed to obtain the optimum parameter and the validity is confirmed experimentally.

This work was supported by CREST of JST (Japan Science and Technology). We are very thankful for the support.

References

[1] M. Kaneko, R. Takenaka, M. Higashimori A. Namiki and M. Ishikawa: "The 100G Capturing Robot –Too Fast to See–," IEEE/ASME Trans. on Mechatronics, vol.8, no.1, pp.37-44, 2003.

[2] S. Hirose and Y. Umetani: "Soft Gripper," Proc. of ISIR, pp.112–127, 1983.

[3] C. Bard and J. Troccaz: "Automatic Preshaping for a Dexterous Hand from a Single Description of Objects," IEEE Proc. of Int. Workshop Intelligent Robots and Systems, pp.865–872, 1990.

[4] S. B. Kang and K. Ikeuchi: "Toward Automatic Robot Instruction from Perception–Recognizing a Grasp from Observation," IEEE Trans. on Robotics and Automation, vol.9, pp.432–443, Aug, 1993.

[5] W. Hong and J.E. Slotine: "Experiments in Hand-Eye Coordination Using Active Vision," Proc. of the 4th Int. Symp. of Experimental Robotics, pp.130–139, 1995.

[6] Y. Nakamura, T. Yamazaki and N. Mizushima: "Motion Synthesis, Learning and Abstraction through Parameterized Smooth Map from Sensors to Behaviors," Proc. of the Int. Symp. of Robotics Research, pp.69–80, 1998.

[7] L. Deman, A. Konno and M. Uchiyama: "Flexible Manipulator Trajectory Learning Control with Input Preshaping Method," Proc. of the 38th SICE Annual Conf. Int., pp.967–972, 1999.

[8] A. Namiki and M. Ishikawa: "Optimal Grasping Using Visual and Tactile Feedback," IEEE Proc. Int. Conf. on Multisensor Fusion and Integration for Intelligent Systems, pp.584–596, 1996.

The Tenth International Symposium on Artificial Life and Robotics 2005(AROB 10th '05),
B-con Plaza, Beppu, Oita, Japan, February 4-6, 2005

Design of Tracing Type Jumping Robots

Manabu HARADA , Mitsuru HIGASHIMORI , Idaku ISHII , and Makoto KANEKO
Graduate School of Engineering, Hiroshima University, Higashi-Hiroshima, JAPAN

Abstract

This paper discusses a leg design for a tracing type jumping robot driven by an actuator with an extremely high output/weight. We found that there is a close relationship between the jump ratio(= h/l) and the leg length. Through analysis and simulation, we found that there exists the optimum design speci cation where the jump motion becomes maximum. After explaining an design orientation by considering joint torque and mechanical parameters, experiments are shown to verify the basic idea.

Keywords—**Jumping Robot, Motor Based Actuation, Jump Ratio**

1 Introduction

There have been many works discussing legged robots. Legged robots can be classified into two groups; static based locomotion where the center of gravity is always ensured within the support polygon constructed by the supporting legs, and dynamic based locomotion where the center of gravity is allowed to be away from the support polygon. Jumping robot can be categorized into the latter one. While various jumping robots have been proposed so far, accumulated energy using either spring or pneumatic actuator is utilized for most of them. This is because there have been no powerful actuator ensuring an enough jump height. With the increase of actuation technique, it has become possible to see the chance that a motor based robot can jump since the effect to gravitational force is reduced. For a given actuator, how much size is appropriate for achieving a jump? How to design a robot for achieving the maximum jump height?

To answer these questions, we consider a simple model where the robot is composed of one actuator and two legs, as shown in Fig.1. The open-close motion of both legs is controlled by one actuator. As a result, this robot realizes the jumping motion by tracing the surface of the ground by both tips of leg. For such a simple model, we obtain the analytical result of the jumping height ratio defined by the height normalized by the leg length. Although the result is available only under a couple of limited assumptions, it includes really useful information for determining the specification of a jumping robot.

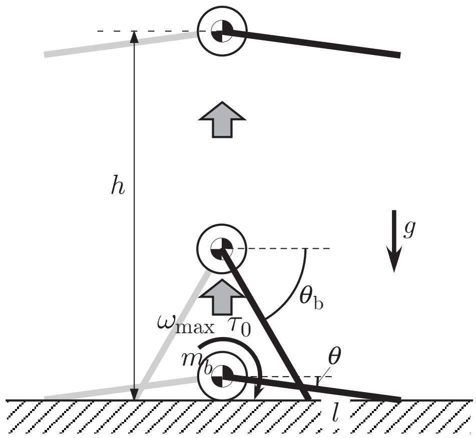

Fig. 1: Model for tracing type jumping robot.

Through above analysis, we show an interesting observation is that there exists the optimum design where the jump ratio becomes maximum. For a given specification of actuator, we explain how to determine the robot specification leading to the optimum design. Along the proposed approach, we design a jumping robot which can achieve the maximum jump ratio. Finally, We develop the jumping robot with optimum design and show that experiments strongly support our design. Nice qualitative coincidences are observed between analysis and experiments.

2 Related Works

While there are many works discussing walking machine[1][2], most of them supposed that at least one leg makes contact on the ground. On the other hand, there exists a phase where all legs are away from the ground in jumping robots[3]. Raibert et al.[4] have developed one-legged hopping machine driven by a pneumatic actuator. Okubo et al.[5][6] have proposed a jumping machine with small output actuator where they utilized self-energizing spring system. The jump ratio which we utilize as the index of evaluation can be regarded as "Jumping height index" proposed in [5] by replacing the maximum distance that body can move with the leg length. Tsukagoshi et al.[7] have developed the jumping & rolling inspector as a rescue robot and discussed the control of the jumping height and energy saving by using a pneumatic actuator. Arikawa and Mita[8] have developed the design of multi-DOF jumping robot. They have discussed planning parameters of robot motions for achieving jumping and somersault.

3 Design of Jumping Robots

3.1 Model for Analysis

Let us consider the two-legged model as shown in Fig.1, where h, l, m_b, τ_0, $\omega_{\max}$, and g are the maximum height of jump, the length of leg, mass of body, torque of actuator, the maximum angular velocity of actuator, and the gravitational acceleration, respectively. We suppose that the actuator operates with constant torque τ_0 with respect to angular velocity. While a regular DC servo motor has a decreasing characteristics with respect to angular velocity, there are a couple of AC servo motors approximately supporting this characteristics by supplying current depending upon the angular velocity. We also suppose that the actuator has the limitation of angular velocity with its maximum value of $\omega_{\max}$ and each leg is controlled by a single motor. We ignore the effect of the friction between the tip of leg and the ground, since we regard it as a secondary factor for reducing the jumping height.

In this work, we utilize jump ratio J_c to evaluate the height of jump as follows;

$$J_c = \frac{h}{l} \tag{1}$$

Physical meaning of J_c is that it expresses the maximum height which the robot can jump in units of its leg length.

3.2 Optimum Design on Leg Length

We now consider an extremely simple model as shown in Fig.1, where we assume that two rigid links without mass are connected to an actuator with the mass of m_b and the robot motion is symmetry with respect to the z-axis. Suppose that the robot is jumping as shown in Fig.1 where the link angle is θ with respect to the horizontal line. Let the joint torque τ_0 is given until $\theta > \theta_b$.

The work where the torque executes during $0 \quad \theta \quad \theta_b$ is given as follows;

$$W = \int_0^{2\theta_b} \tau_0 d\theta \tag{2}$$

$$= 2\tau_0\theta_b \tag{3}$$

Since W is fully transmitted to the potential energy when the robot reaches the highest position by jumping

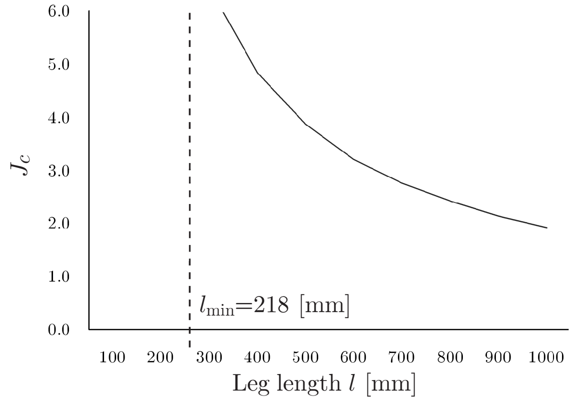

Fig. 2: Relationship among l, $l_{\lim}$, and J_c.

motion, we can obtain the jump ratio with the function of τ_0 as follows;

$$J_c = \frac{2\theta_b\tau_0}{m_b g l} \tag{4}$$

Eq.(4) is the closed form solution exhibiting the relationship between J_c and mechanical parameters, where both legs maintain contact with the ground during $0 \quad \theta \quad \theta_b$. Now, we would note that the leg cannot rotate with more than $\omega_{\max}$. The above constraint for angular velocity leads to the following inequality.

$$\dot{\theta}_{\max} \quad \omega_{\max} \tag{5}$$

The maximum angular velocity of joint $\dot{\theta}_{\max}$ is achieved at the moment of $\theta = \theta_b$ and the energy balance at this moment is given as follows;

$$\frac{1}{2}\left(\dot{\theta}_{\max} l \cos\theta_b\right)^2 + m_b g l \sin\theta_b = 2\tau_0\theta_b \tag{6}$$

From eq.(6), we can obtain $\dot{\theta}_{\max}$ as follows;

$$\dot{\theta}_{\max} = \dot{\theta}\Big|_{\theta=\theta_b} \tag{7}$$

$$= \frac{1}{l\cos\theta_b}\sqrt{2\left(\frac{2\tau_0\theta_b}{m_b} \quad g l \sin\theta_b\right)} \tag{8}$$

Now, we would focus on the leg length from the viewpoint of the design for robots. Substituting eq.(8) into ineq.(5) yields,

$$l \geq l_{\lim} \tag{9}$$

where

$$l_{\lim} = \frac{q + \sqrt{q^2 + 4 m_b \tau_0 \theta_b p^2}}{m_b p^2} \tag{10}$$

$$p = \omega_{\max}\cos\theta_b \tag{11}$$

$$q = m_b g \sin\theta_b \tag{12}$$

Table 1: Specification of the lightweight high-speed motor

motor type	AC
max torque [Nm]	1.71
max speed [r/min]	300
time response to a step input [msec]	30
weight [g]	59.6

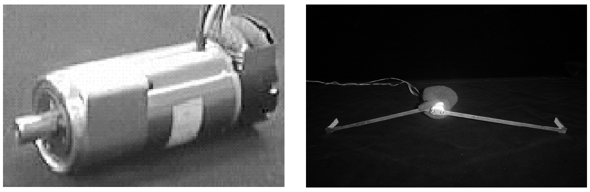

(a) (b)

Fig. 3: The lightweight high-speed motor and the developed jumping robot.

In the case where $l < l_{\mathrm{lim}}$, eq.(4) is not guaranteed since each tip of the leg cannot trace the ground and is away from it. Fig.2 shows the relationship among l, l_{lim}, and J_c. While we can suppose that jump ratio decrease less than the that of eq.(4), we would note that l_{lim} may be the optimum leg length when the specification of actuator is given.

4 Experiments

Table.1 shows the specification of the lightweight powerful motor (Harmonic Drive Systems, Inc.)[9][10]. This motor has the maximum torque of 1.71[Nm], the maximum rotational speed of 300[r/min] and the mass of 59.6[g]. Fig.3(a) and (b) show an overview of the motor and a photo of the developed robot, respectively. Fig.4 shows an overview of the developed robot where one leg is connected to the axis of the motor and the other one is fixed to the outer case of the motor.

Fig.5 shows the map showing experimental results with respect to l. The circles shown in Fig.5 are points obtained by experiments. For reference, the results obtained by eq.(4) and eq.(10) are also provided in Fig.5, where $\theta_b = 0.5$. A really interesting observation is that we can find the maximum jump ratio between $l = 200$[mm] and 300[mm] for analysis, which supports the idea of this work. Fig.6 and Fig.7 show series of photos during a jump motion of the robot with the leg length of 100[mm] and 200[mm], respectively. The robot with the length of 200[mm] achieved a big jump with 550 [mm] with $J_c = 2.75$.

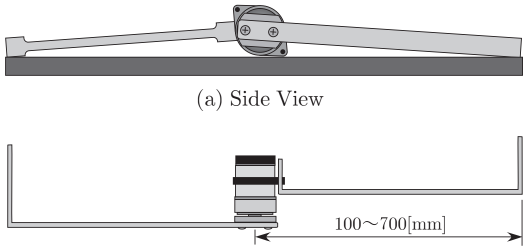

(a) Side View

(b) Top View

Fig. 4: An overview of the developed robot.

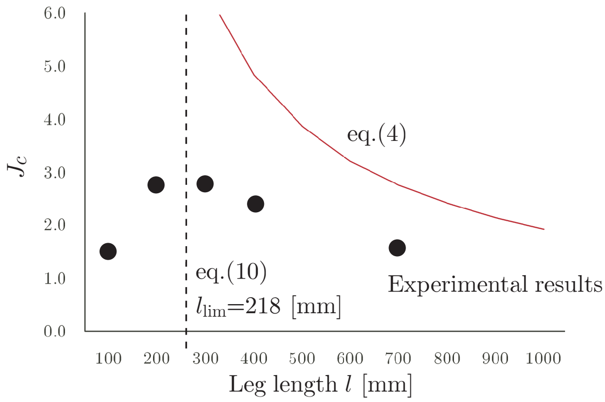

Fig. 5: Experimental results.

5 Concluding Remarks

We discussed the design of tracing type jumping robots by focusing on the leg length. The main results are as follows:

(1) Jump ratio was chosen as the evaluation index for designing a jumping robot.
(2) We obtained the relationship between the jump ratio and the leg length by using a simple model.
(3) It was shown experimentally that there exists the optimum design point leading to the maximum jump ratio.

One of features for using motors for a jumping robot is that we can expect the capability of grasping as well as jumping. Fig.8 shows an example where the robot is capturing an object suspended in air after jumping up. We believe that a kind of dexterity can be anticipated through an AC motor based jumping robot.

This work is supported by CREST of Japan Science and Technology (JST). We are very thankful for the support. Also, we would like to express sincere thanks for Mr. Masahiro Yuya for his experiments.

References

[1] T. Frank: "Dynamic study of a four-bar linkage walking machine leg", *M.S. thesis, Ohio State University*, pp.133,

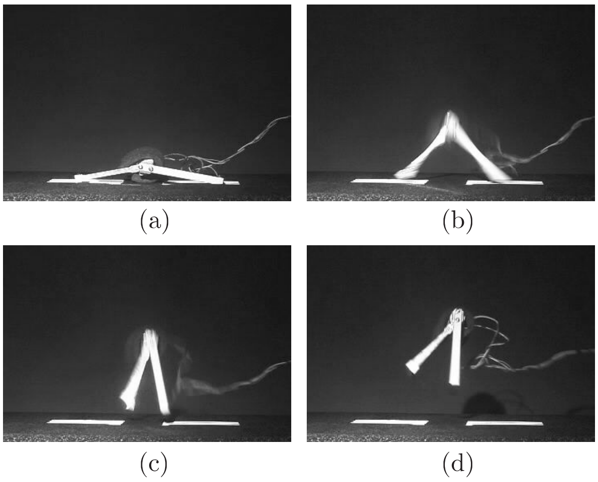

Fig. 6: A series of photos during a jumping motion(l = 100[mm]).

1973.

[2] S. Hirose and Y. Umetani: "The basic considerations on energetic efficiencies of walking vehicles", *Trans. Soc. Instrument Countr. Engineers(In Japanese)*, vol.15, no.7, pp.928–933, 1979.

[3] E. Nakano and H. Okubo: "Jumping Machines", *Journal of RSJ (in Japanese)*, vol.11, no.3, pp.342–347, 1993.

[4] M. H. Raibert, H. B. Brown, Jr, and M. Chepponis: "Ezperiments in Balance with a 3D One-Legged Hopping Machine", *The Int. Journal of Robotics Research*, vol.3, no.2, pp.75–92, 1984.

[5] H. Okubo, E. Nakano, and H. Kimura: "Design of Jumping Machine using Spring and Actuators", *Journal of RSJ (in Japanese)*, vol.10, no.7, pp.948–954, 1992.

[6] H. Okubo, M. Handa, and E. Nakano: "Design of a Jumping Machine using Self-energizing Spring — Jumping by Small Actuators—", *Journal of RSJ (in Japanese)*, vol.16, no.5, pp.633–639, 1998.

[7] H. Tsukagoshi, Y. Mori, M. Sasaki, T. Tanaka, and A. Kitagawa: "Development of Jumping & Rolling Inspector to Improve the Debris Traverse Ability", *Journal of Robotics and Mechatronics*, vol.15, no.5, pp.482–490, 2003.

[8] K. Arikawa and T. Mita: "Design of Multi-DOF Jumping Robot", *IEEE Proc. of Int. Conf. on Robotics and Automation*, pp.3992–3997, 2002.

[9] A. Namiki, Y. Imai, M. Ishikawa, and M. Kaneko: "Development of a High-speed Multifingerd Hand System and Its Application to Catching", *In Proc. of IEEE/RSJ Int. Conf. on Intelligent Robots and Systems*, pp.2666–2669, 2003.

[10] http://www.hds.co.jp/HDS_hp_english/english/index.html

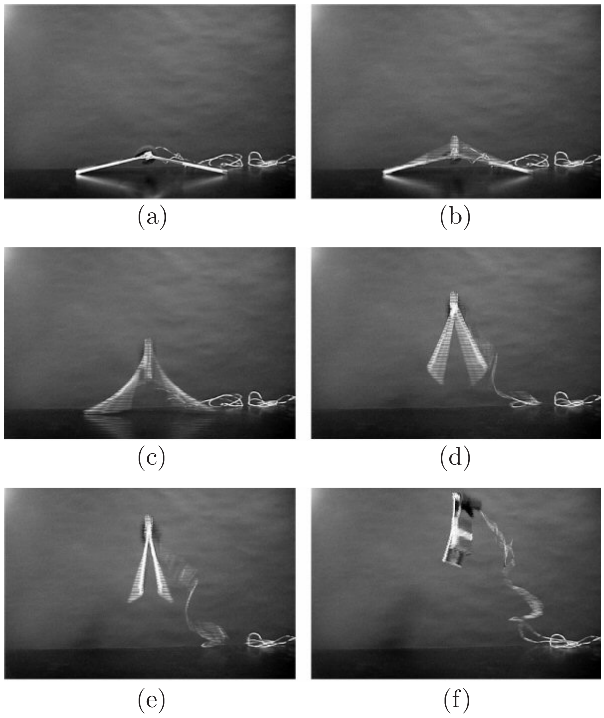

Fig. 7: A series of photos during a jumping motion(l = 200[mm]).

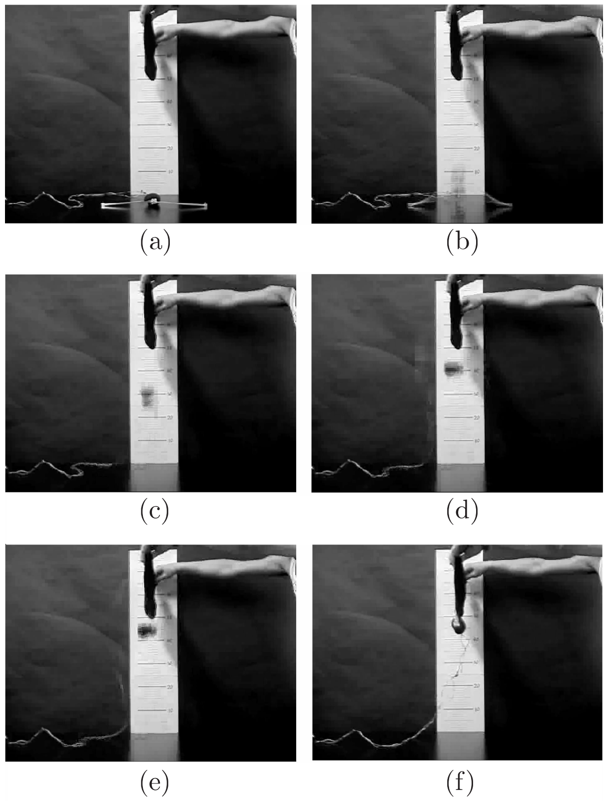

Fig. 8: A series of photos during a jumping and grasping motion.

The Tenth International Symposium on Artificial Life and Robotics 2005(AROB 10th '05),
B-con Plaza, Beppu, Oita, Japan, February 4-6, 2005

Development of a Laparoscopic Surgery Training System and Preliminary Experiments

Hirokazu MASUGAMI*, Tomohiro KAWAHARA*, Hiroyuki EGI**
Masanori YOSHIMITSU**, Masazumi OKAJIMA** and Makoto KANEKO*
*Graduate School of Engineering, Hiroshima University
**Graduate School of Biomedical Science, Hiroshima University
masugami@hfl.hiroshima-u.ac.jp

Abstract

This paper discusses the direction dependent dexterity of surgeons in laparoscopic surgery. In laparoscopic surgery, a surgeon can observe the concerned tissue only through a 2D display and is obliged to convert the image from 2D to 3D in his (or her) brain. In this report, we examine the effect of 2D or 3D visual information on the manipulation dexterity by utilizing the newly developed evaluation system.

1 Introduction

Laparoscopic surgery is a well established method in modern medicine. In laparoscopic surgery, a surgeon inserts forceps and a scope into the abdomen through small holes, so no large cuts are necessary as in open surgery. It is a method in minimal invasive surgery. It was well examined scientifically that it does not affect a life prognosis, and has a similar rate of cures for malignant diseases[1][2][3].

On the other hand, many reports in operation mistakes by laparoscopic surgery are seen in the news in recent years. In order to prevent such operation mistakes, the education to surgery residents is necessary. In laparoscopic surgery, as shown in Fig.1, surgeons have to operate forceps, looking at a monitor, without seeing the affected part directly, and have to convert the image from 2D to 3D in their brain.

The purpose of this study is quantifying the direction dependent dexterity of surgeons in laparoscopic surgery. In this paper, we analyze how a surgeon obtains a distance feeling for the depth direction while converting the 2D display image to a 3D space. Then, we show that the image conversion capability to 3D can be considered as an element to judge a surgeon's skill.

2 Related research

There are many reports that evaluate laparoscopic surgical skills. Although Kopta[4] presented methods to evaluate surgical skills, they are not widely accepted. Martin[5] and others made an evaluation system called Objective Structured Assessment of Technical Skill (OSATS), which gained consensus for the first time based on its excellent objectivity. Moreover, Rosser, et al.[6][7][8][9] claimed what makes laparoscopic surgery difficult is the limitation of the

Fig.1: Overview of Laparoscopic Surgery

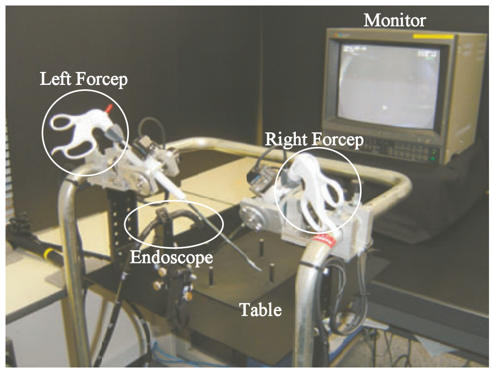

Fig.2: Overview of the Developed System

spatial information due to the 2D display, and supported their claim by monitoring the learning effect by change of performance time. Most of these reports evaluated the improvements in reaching the training goal, which had not been necessarily quantitive. However, recently, the tip position of forceps is measured, and thus the number of test methods using quantitive analysis about the operation increases. Cuschieri, et al. developed the Advanced Dundee Endoscopic Psychomotor Tester (ADEPT) which acquires the forceps tip position information by using an encoder[10][11]. Darzi, et al. developed the Imperial College Surgical Assessment Device (ICSAD) which acquires the forceps tip position information by using an electromagnetic field, and utilizes it effectively to improve laparoscopic skills[12][13][14]. Sokollik, et al. considered the tip speed profile from the forceps tip position data by the ultrasonic sensor[15]. Also, there are simulators that perform the analysis and evaluation of the

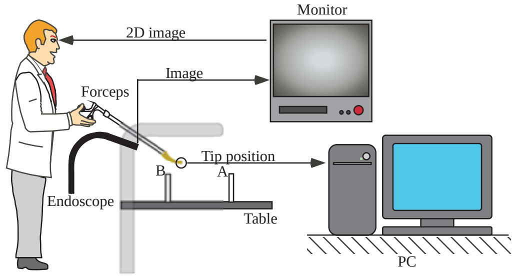

Fig.3: System Architecture

position information by vision sensors[16] and others that use a virtual reality to simulate an actually undergoing operation[17].

Here, the image conversion capability from 2D to 3D is considered as one of the necessary skills in laparoscopic surgery. We focus on the distinction between the vertical movement and the front-and-back direction movement, as it is regarded as being very difficult.

3 Materials

3.1 The feature of the developed device

Fig.2 and Fig.3 show the experiment device and the system architecture. As can be seen from Fig.2, the endoscope is installed in front of a table and the 2D image is shown on the monitor. A gimbals mechanism is used in this system to grasp the forceps. Two encoders are attached to the two rotational axes. In addition, we fixed a scale seal (LBP = 0.1[mm]) on the stem part of forceps, in order to be able to acquire the displacement of the length. Then, we used the heat shrink tube to secure the seal on the stem. Furthermore, the opinion of surgeons was taken into account. In order to reproduce the load felt in an actual operation, we used a spring mechanism that enables to adjust rotation friction of the gimbals. Furthermore, in order to prevent the candidate to look at the subject directly, instead of the monitor during an experiment, we manufactured a cover made of a black plastic plate. Fig.3 shows the information flow of this system by arrows.

3.2 The forceps tip position detection method

We can measure the two rotation angle parameters and one distance parameter by using three encoders. As shown in Fig.4, by measuring the three parameters l, θ and ϕ, the relative position coordinates $x = l \cdot \sin\phi$, $y = l \cdot \cos\phi \cdot \sin\theta$ and $z = -l \cdot \sin\phi \cdot \cos\theta$ of the gimbal central point can be calculated.

3.3 Position detection accuracy

We acquired the position data for both tips by putting the tip of the forceps on pre-defined 14 points on the table that were separated by 50[mm]. Then, we investigated the deviation from the true value when acquiring position information for the 14 points of the two tips 10 times. As shown in Fig.5(a), the maximum error was 6.20[mm], the average error was 2.54[mm], and standard deviation 1.28[mm].

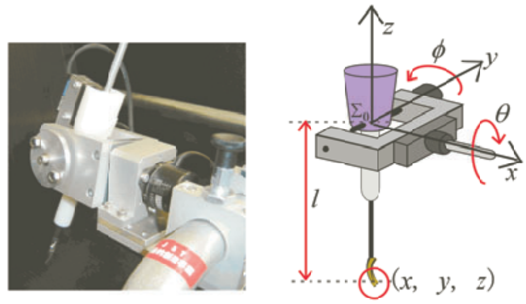

Fig.4: Coordiate System

Then, we considered the error due to alignment, and corrected it by the method shown in the following paragraph. As a result, the maximum error was 3.23[mm], the average error was 0.92[mm], and standard deviation 0.62[mm] after the correction as shown in Fig.5(b). Thus the position accuracy was greatly improved. The circles of Fig.5 shows the average error before and after compensation, respectively.

3.4 Compensation method

In a first step of the compensation method of the system, the three points v_{t1}, v_{t2} and v_{t3} were chosen as calibration points and their true x-y-z values are known. Next, using v_{t1} as a reference point, the position data on the remaining points v_{t2} and v_{t3} is acquired by the parameter from each encoder of the system and the equations $x = l \cdot \sin\phi$, $y = l \cdot \cos\phi \cdot \sin\theta$, $z = -l \cdot \sin\phi \cdot \cos\theta$. Then, the deviations Δv_2, Δv_3 of the acquired values v_2, v_3 from the true values v_{t2}, v_{t3} were derived from the equations:

$$\begin{aligned} v_{t1} &= v_1 && (1) \\ v_{t2} &= v_2 + \Delta v_2 && (2) \\ v_{t3} &= v_3 + \Delta v_3. && (3) \end{aligned}$$

As is commonly known, the arbitrary positions in the 3D space can be expressed as follows by using the three position vectors:

$$v = Vk \tag{4}$$

where $V = [v_1\ v_2\ v_3]$ and $k = [k_1\ k_2\ k_3]^T$.

That is, if v and $V = [v_1\ v_2\ v_3]$ are known, equation (4) can be changed into

$$k = V^{-1}v \tag{5}$$

in order to obtain $k = [k_1\ k_2\ k_3]^T$.

Therefore, $k = [k_1\ k_2\ k_3]^T$ can be found, if v_{t1}, v_{t2}, v_{t3}, v_1, v_2 and v_3 are known beforehand. Also, the true value $\hat{v}_t$ can presume as follows,

$$\hat{v}_t = v_{t1}k_1 + v_{t2}k_2 + v_{t3}k_3 \tag{6}$$

using equations (1), (2) and (3), equation (6) can be changed into

$$\hat{v}_t = v_1k_1 + (v_2 + \Delta v_2)k_2 + (v_3 + \Delta v_3)k_3. \tag{7}$$

With equation (4), we finally obtain

$$\hat{v}_t = v + \Delta v_2k_2 + \Delta v_3k_3. \tag{8}$$

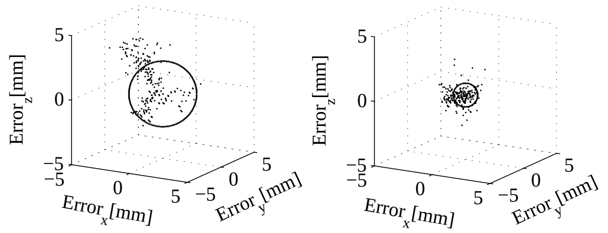

(a)Before Compensation (b)After Compensation

Fig.5: Position Errors before/after Compensation

4 Preliminary Experiment

4.1 Purpose

This chapter shows that the human characteristic when only on carrying out 3D movements of the forceps relying the information from a 2D display. It is shown that the difference in skill of an amateur and a surgeon is appearant in this setup.

4.2 Methods

In the experiment point A and point B on the table in Fig.3 are 150[mm] apart. The subject was asked to move the forceps tip from point A to point B and back again to point A. The tip position information was acquired during the whole movement.

4.3 Definition of the target point attainment

The attainment times $t_i (i = 1, 2)$ to the intermediate point B and the ending point A are taken when the forceps tip stays with in a distance of $d_g = 3$[mm] from target point for $t_g = 0.3$[s]. They are defined as follows:

$$t_i = \inf \left\{ t_n \;\middle|\; \begin{array}{c} \|p_i - p(t)\| < d_g, \\ t_n - t_g \le t \le t_n \end{array} \right\}. \qquad (9)$$

Here, $p(t)$ is the forceps tip position vector after t[s] from start, and $p_i (i = 1, 2)$ is a target position vector, respectively. Also, $t_1 < t_2$.

4.4 Results

The experimental results of an amateur and an expert are shown in Fig.6 and Fig.7. They show the tip trajectory in the xy plain (top view) and in the yz plain (side view) in the experiment done by an amateur (Fig.6) and by an expert (Fig.7). Here, looking at both top views, deviation from the ideal trajectory in the side direction is very small. Looking at both side views respectively, a large difference in the deviation in the hight direction of the expert's and amateur's forceps tips trajectory can be seen.

4.5 Discussion

That the different deviations discussed the last paragraph are due to the shortage of the information by a 2D display. A motion in the actual vertical direction and a motion of the front-and-back direction cause a both vertical movement on a monitor, while a motion in the side direction on a monitor corresponds

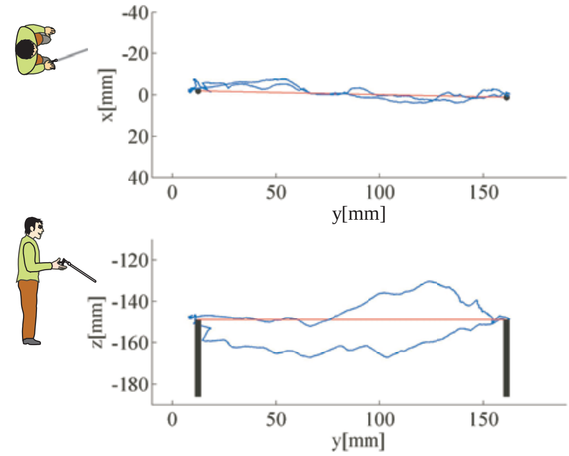

Fig.6: Tip Trajectory of an Amateur

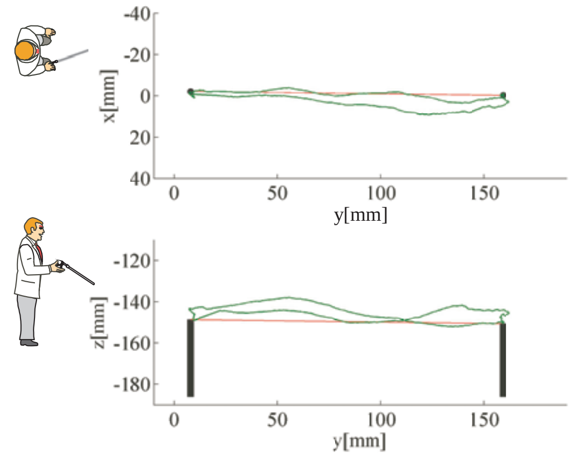

Fig.7: Tip Trajectory of an Expert

to the actual side motion. Therefore, a subject considers the correction of the deviation in the vertical direction difficult, while the correction of the deviation in the side direction is considered comparably easy.

5 Direction dependent dexterity

5.1 Integration according to direction ingredient

In case of the experiment shown in the preceding chapter, it is characteristic deviation of the vertical direction was large, compared to the deviation of the side direction was very small. Here, the deviation in the side direction and the deviation in the vertical direction are integrated over the move distance according to the ingredient. Then, the result of the amateur's tip movement seen from Fig.6, the deviation integration value A_x of the side direction is $A_x = 616.27$[mm^2], and the deviation integration value A_z of the vertical direction is $A_z = 2934.37$[mm^2]. The result of the expert's tip movement seen from Fig.7 is $A_x = 954.99$[mm^2], $A_z = 1347.27$[mm^2].

5.2 Direction dependence line

We express the relation m between the deviation integration value A_x of this side direction and the deviation integration value A_z of the vertical direction as follows.

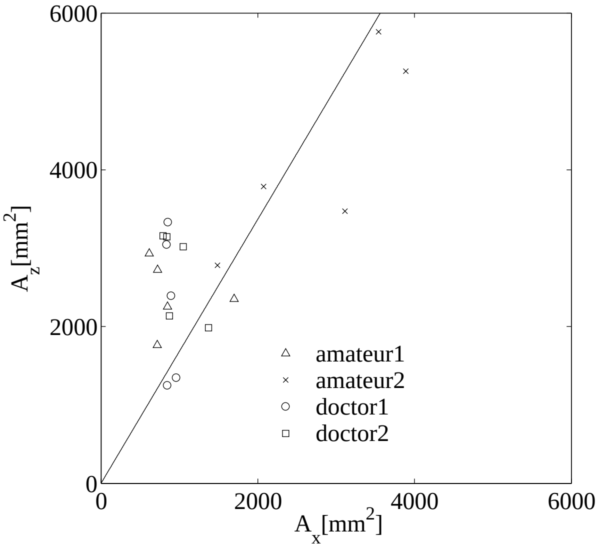

Fig.8: Direction Dependence Line

$$m = \frac{A_z}{A_x}. \tag{10}$$

In order to verify the tendency of a direction dependence in two or more experiment results, we consider the graph which sets the horizontal axis to A_x, the vertical axis to A_z and the inclination to m. Each point in Fig.8 is the result of one of 5 experiments carried out by two amateurs and two experts, respectively. The straight line in the graph marks the direction dependence m obtained by using the least-squares method in the data for these 20 data points. The inclination of the straight line is $m = 1.95$.

Moreover, as can be seen from the graph, it turns out that each point $m > 1$. Thus, the correction of the deviation in the vertical direction is again observed to be more difficult due to the lack of information from the 2D display.

6 Conclusion

In this report, we introduced an equipment for evaluating a doctor's skill in laparoscopic surgery, and described the forceps tip position data acquisition method, and its accuracy. Also, we found that obtaining the distance feeling of the depth direction is very difficult, due to the conversion of information from a 2D display to 3D that the surgeon has to perform in laparoscopic surgery, and conducted the basic experiments. As a result, distinction of the vertical direction and the front-and-back direction from 2D display is difficult. Thus, the direction dependence might be one parameter that shows a surgeon's skill. Furthermore, we defined the characteristics of human operation in endoscopic condition by the direction dependence, and considered its tendency by the results of a preliminary experiments.

In the next step, we will consider the know-how of experts to use one forceps to help to judge the position of the other forceps in the 3D conversion.

Finally, we would express our sincere thanks to Dr. Roland Kempf for his valuable comments.

References

[1] H. Hasegawa, Y. Kabeshima, et al: "Randomized controlled trial of laparoscopic versus open colectomy for advanced colorectal cancer," *Surg Endosc*, vol.17, no.4, pp636-640,2003.

[2] Clinical Outcomes of Surgical Therapy Study Group: "A Comparison of laparoscopic Assisted and Open Colectomy for Colon Cancer," *N Engl J Med*, vol.350, no.20, pp2050-2059,2004.

[3] R. Gonzalez, C. D. Smith, et al: "Laparoscopic vs open resection for the treatment of diverticular disease," *Surg Endosc*, vol.18, no.2, pp276-280,2004.

[4] J. A. Kopta: "An approach to the evaluation of operative skills," Surgery, vol.70, no.2, pp297- 303,1971.

[5] J. A. Martin, G. Regehr, R. Reznick, et al: "Objective structured assessment of technical skill (OSATS) for surgical residents," *Br. J. Surg*, vol.84, no.2, pp273- 278,1997.

[6] J. Rosser, L. Rosser, R. Savalgi: "Skill acquisition and assessment for laparoscopic surgery," *Arch Surg*, vol.132, no.2, pp200- 204,1997.

[7] J. Rosser, L. Rosser, R. Savalgi: "Objective evaluation of a laparoscopic surgical skill program for residents and senior surgeons," *Arch Surg*, vol.133, no.6, pp657- 661,1998.

[8] D. Risucci, J. Rosser, et al: "Experience and visual perception in resident acquisition of laparoscopic skills," *Curr Surg*, vol.57, no.4, pp368- 372,2000.

[9] D. Risucci, J. Rosser, et al: "Surgeon-specific factors in the acquisition of laparoscopic surgical skills," *Am J Surg*, vol.181, no.4, pp289- 293,2001.

[10] A. I. Macmillan, A. Cuschieri: "Assessment of Innate Ability and Skills for Endoscopic Manipulations by the Advanced Dundee Endoscopic Psychomotor Tester: Predictive and Concurrent Validity," *Am J Surg*, vol.177, no.3, pp274-277,1999.

[11] N. K. Francis, G. B. Hanna, A. Cuschieri: "Reliability of the Advanced Dundee Endoscopic Psychomotor Tester for Bimanual Tasks," *Arch Surg*, vol.136, no.1, pp40- 43,2001.

[12] K. Moorthy, Y. Munz, A. Darzi, et al: "Motion analysis in the training and assessment of minimally invasive surgery," Taylor & Francis Health Sciences, vol.12, no.3-4, pp137-142,2003.

[13] K. Moorthy, Y. Munz, A. Darzi, et al: "Objective assessment of technical skills in surgery," *BMJ*, vol.327, no.7422, pp1032-1037,2003.

[14] K. Moorthy, Y. Munz, A. Darzi, et al: "Validity and reliability of a virtual reality upper gastrointestinal simulator and cross validation using structured assessment of individual performance with video playback," *Surg Endosc*, vol.18, no.2, pp328-333,2004.

[15] C. Sokollik, J. Gross, G. Buess: "New model for skills assessment and training progress in minimally invasive surgery," *Surg Endosc*, vol.18, no.2, pp495-500,2004.

[16] Haptica: ProMIS, http://www.haptica.com/.

[17] Reachin: Reachin Laparoscopic Trainer 2.0, http://www.reachin.se/.

[18] G. B. Hanna, A. Cuschieri: "Optimal port locations for endoscopic intracorporeal knotting," *Surg Endosc*, vol.11, no.4, pp397-401,1997.

[19] G. B. Hanna, A. Cuschieri: "Influence of the optical axis-to-target view angle on endoscopic task performance," *Surg Endosc*, vol.13, no.4, pp371-375,1999.

[20] G. B. Hanna, A. Cuschieri, et al: "Influence of Two-dimensional and Three-dimensional Imaging on Endoscopic Bowel Suturing," *World J. Surg*, vol.24, no.4, pp444-449,2000.

[21] G. B. Hanna, A. Cuschieri, et al: "Effect of the angle between the optical axis of the endoscope and the instruments' plane on monitor image and surgical performance," *Surg Endosc*, vol.18, no.1, pp111-114,2003.

The Tenth International Symposium on Artificial Life and Robotics 2005(AROB 10th '05),
B-con Plaza, Beppu, Oita, Japan, February 4-6, 2005

Toward a Real Time Force Measurement by Vision

Toshiyuki MIZOI, Idaku ISHII and Makoto KANEKO
Graduate School of Engineering, Hiroshima University
mizoi@hfl.hiroshima-u.ac.jp

Abstract

This paper discusses the way for estimating a contact force by high speed vision with a frame rate of 2[kHz]. We particularly focus on the estimation of a contact force through the deformation of a flexible beam. We show the basic working principle of the contact force estimation. We developed the experimental system for confirming the basic idea. By utilizing the system, we executed several experiments where the dynamics effects appear.

1 Introduction

The strain gauge is the most commonly used contact force sensor. The reasons why this sensor is widely used are that it has a very simple structure and keeps a high frequency response. However, there are couple of situations where it is hard to use it. For example, under a strong magnetic field, such as the case of fMRI(functional Magnetic Resonance Imaging). In such a case, there are alternative force sensors, such as a hand dynamometer using water pressure [1] or a force sensor by using an optical fiber where the loss of the light quantity depends upon how large the bending angle is [2]. Another case where it is hard to utilize a strain gauge would be a micro hand which can achieve a simple manipulation of a microscopic object, as shown in Fig.1, where two chopsticks like micro gripper is grasping a target object. For the force sensing in such a micro hand under the microscope [3], the displacement of an elastic beam by using a vision sensor is measured for estimating an equivalent contact force. Up to now, it has been restricted to force measurement only of a quasi-static condition because the response of processing speed of camera was as low as 30[Hz].

In this research, we propose the method which estimates the contact force in real time by measuring the displacement of an elastic deformation under dynamic condition using an online high speed vision system with a frame rate of 1[kHz] in the standard window.

Let us consider the case of a micro hand, as shown in Fig.1. The micro hand consists of a support beam and an action beam. As a simplified model for the micro hand, we regard it as a single beam, as shown in Fig.2. We consider the problem of estimating a periodic external force which acts at the tip of the beam. This paper is organized as follows. We refer to the related works in Chapter 2. A problem setup is performed in Chapter 3. In Chapter 4, after deriving a basic formula about the relation between the displacement of beam and contact force, we introduce a nondimensional parameter R which expresses the ratio of inertia force and the static bending force. We further show a method how to estimate the contact force. In Chapter 5, we verify the basic working principle of the introduced method by comparing the conventional approaches.

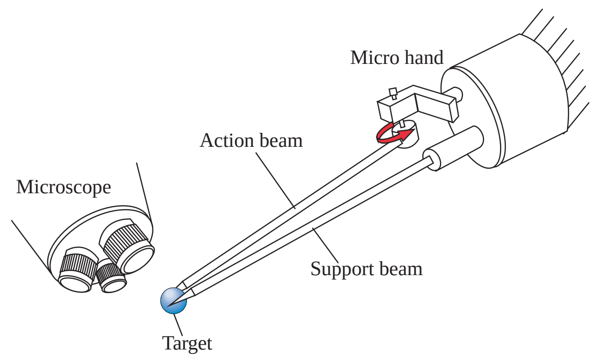

Fig.1: A view of micro hand

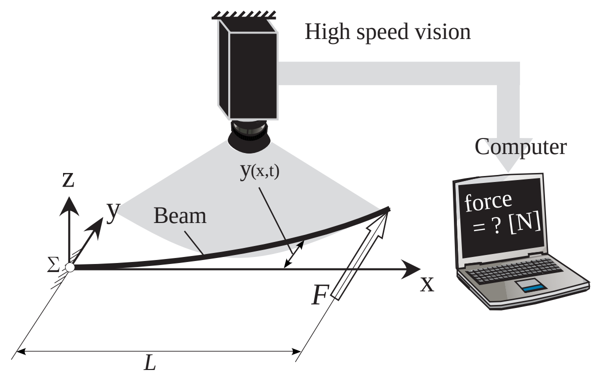

Fig.2: Conceptual image of vision based force sensing

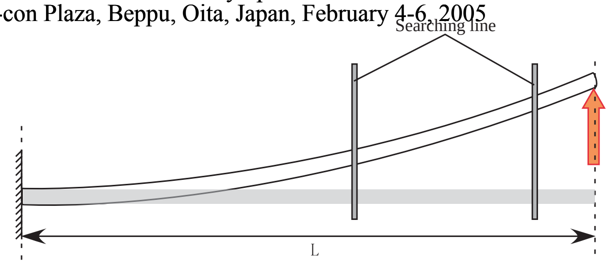

Fig.3: Explanation of searching line

2 Related works

There have been a couple of works where contact force is estimated by vision. Kaneko and others have proposed a system [4, 5] consisting an elastic beam and a vision sensor. They showed that both contact force and contact point can be estimated by measuring the displacement on two points of the beam. However, their system was limited to quasi-static condition where the change of motion is slow enough to ensure that any dynamic effect can be neglected.

As for vision sensors, Ishii and others developed the Mm(Mega-pixel and milli-second)Vision[6, 7]. The MmVision includes an intelligent pixel selection software which is able to find the center of gravity of an object with the frame rate of 1[kHz] in the standard window. However, within our knowledge, there has been no work discussing the dynamic based contact force estimation by utilizing an online high speed vision.

3 Problem setup

We suppose a beam whose shape in steady state is a straight line. Also let μ, E, I, and L be the mass per unit length, young's modulus, area moment of inertia, and the length of beam, respectively. We set the coordinate system as shown in Fig.2. The main assumption in this work are as follows.

Assumption 1: Attenuation of vibration by the viscosity of the beam can be neglected.

Assumption 2: The displacement of the beam is assumed to be so small, such that the movement of the contact point in the x-direction can be neglected, i.e. $y(L,t)/L < 0.1$.

Assumption 3: The movement of the beam is limited to planar motion.

Assumption 4: A periodic external force $F(L,t)$ excites the beam.

Assumption 5: Other frequency modes except the external force frequency can be neglected.

Under the above assumptions, we consider the simplified model shown in Fig.3, where we search for the center-of-gravity of the beam only along the shown searching lines. We treat the following problem.

Problem setup:
Suppose that an unknown periodic external force $F(L,t)$ is applied to the free end of the beam. Under this condition, answer the following questions:

(1)How many searching lines are necessary and are sufficient to determine the shape of the beam?

(2)How can we estimate the periodic external force?

4 Principle of estimation

4.1 General solution of bending equation

We consider the bending vibration of a beam for a given external force, as shown in Fig.3. The equation of motion of a small part of the beam can be expressed by the following equation [8].

$$EI\frac{\partial^4 y}{\partial x^4} + \mu\frac{\partial^2 y}{\partial t^2} = f(x,t); \tag{1}$$

$$f(x,t) = \begin{cases} 0 & (0 \le x < L) \\ F(L,t) & (x = L). \end{cases} \tag{2}$$

Let us now define f_s and f_d as follows,

$$f(x,t) = f_s + f_d \tag{3}$$

$$f_s = EI\frac{\partial^4 y}{\partial x^4} \tag{4}$$

$$f_d = \mu\frac{\partial^2 y}{\partial t^2} \tag{5}$$

where f_s and f_d correspond to the forces generated by static bending and inertia forces, respectively. Supposing that the beam is under harmonic vibration, we can obtain the general solution by using the method of separation of variables

$$y(x,t) = Y(x)\cdot(A\cos\omega_t + B\sin\omega_t), \tag{6}$$

where

$$\begin{aligned} Y(x) &= C_1\cos(\frac{\alpha x}{L}) + C_2\sin(\frac{\alpha x}{L}) \\ &+ C_3\cosh(\frac{\alpha x}{L}) + C_4\sinh(\frac{\alpha x}{L}); \end{aligned} \tag{7}$$

$$\alpha^4 = \mu L^4\omega^2/EI. \tag{8}$$

4.2 Introduction of nondimensional parameter R

When the periodic external force ($F_0\sin\omega t$) is applied at the tip of the beam, f_s and f_d can be approximated as follows:

$$f_s \simeq EI\frac{y_{max}}{L^4}, \tag{9}$$

$$f_d \simeq \mu y_{max}\omega^2. \tag{10}$$

Let us now, define the nondimensional parameter R as follows,

$$R = \frac{\mu L^4 \omega^2}{EI} \tag{11}$$

where R expresses the ratio of inertia force and static bending force. As R increasess, the inertia force also increases. Note that R exactly coincides with α^4 in Eq.(8).

4.3 Force estimation under quasi-static condition

In a quasi-static case, we can neglect the inertia force. By setting $f_d = 0$ in Eq.(3), the contact force $F(L,t)$ is given by

$$F(L,t) = \frac{3EI}{L^3} y(L,t). \tag{12}$$

4.4 Force estimation under dynamic condition

We suppose that the periodic external force $(F_0 \sin \omega t)$ is applied at the end of the beam. At the fixed end $(x = 0)$, the displacement and the bending angle are zero, i.e.

$$Y(0) = 0,$$
$$Y'(0) = 0.$$

At the free end $(x = L)$, the bending moment is zero and the shearing force has the same value as the periodic external force. i.e.

$$Y''(L) = 0,$$
$$EI \cdot Y'''(L) \cdot (A \cos \omega t + B \sin \omega t) = -F_0 \sin \omega t.$$

We can determine all coefficients of eq.(7) under the above boundary conditions and obtain the contact force at the time $t = t_p$ is given by

$$F(L, t_p) = y(x_v, t_p)\{\frac{2EI\alpha^3(1 + \cos\alpha \cosh\alpha)}{L^3}\}$$
$$/\{(\sin\alpha + \sinh\alpha)(\cos\frac{\alpha x_v}{L} - \cosh\frac{\alpha x_v}{L}) -$$
$$(\cos\alpha + \cosh\alpha)(\sin\frac{\alpha x_v}{L} - \sinh\frac{\alpha x_v}{L})\}. \tag{13}$$

Applying the theorem of L'Hopital to eq.(13), we have the following relationship

$$\lim_{\alpha \to 0} F = \frac{3EI}{L^3} y. \tag{14}$$

Eq.(14) coincides with eq.(12). Finally, the answers to the problem setup in Chapter 3 are

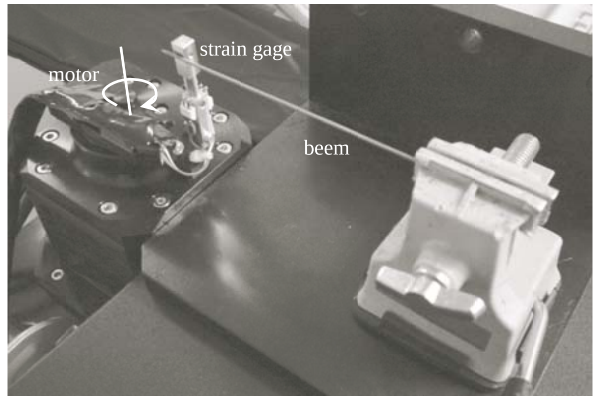

Fig.4: Experimental system

(1)One searching line is necessary and sufficient to determine the shape of the beam.

(2)We can estimate the periodic external force by eq.(13).

5 Experiment

5.1 The experiment method

The experimental setup is shown in Fig.4. The beam used in the experiment has the diameter of 1[mm] and the length of 110[mm]. Fig.5 shows the geometrical relationship between the beam and the force sensor stick. An arm is fixed to the axis of the motor. On the other end of the arm, the force sensor stick to which the strain gauge is attached, is fixed perpendicular to the arm. This arm is vibrated by

$$y = y_0 + y_1 \sin \omega t,$$

where $y_0 \geq y_1$. The displacement of the beam is measured at a particular point by the vision sensor. In this experiment, we use the MmVision (Photron) as a vision sensor, which can take frames with a resolution of 1024×1280 pixels and with the frame rate of 1[kHz] in standard window. In order to simplify the measurement, we use a white beam so that we can easily distinguish from the background. Fig.6 shows the way for measuring a point on the beam schematically. While the vision sensor has 1024×1280 pixels, we set the window of 1024×512 pixels as shown in Fig.6. Within the window, we focus only on one searching line with 1×512 pixels for detecting the displacement of the beam at one particular point $(x = x_v)$. To search the center-of-gravity of the beam, we binarize the picture by setting up the threshold value against the 8 bit gray scale. As the beam moves by an external force, the center-of-gravity of the beam in the searching line also changes. In this experiment, x_v is fixed to the

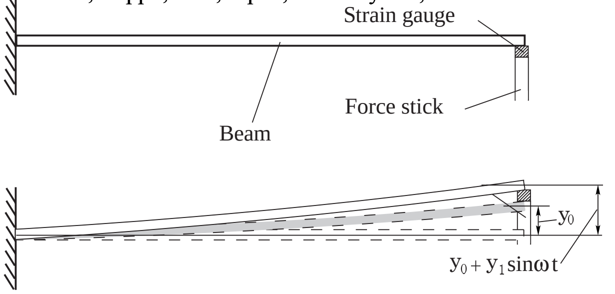

Fig.5: The geometrical relationship between the beam and strain gauge

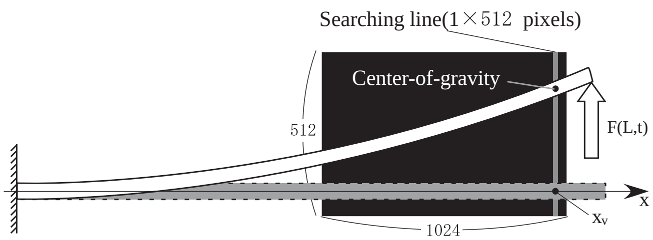

Fig.6: Explanation of searching line

distance 2[cm] from the tip of the beam. By measuring the center-of-gravity of the beam in the searching line, we obtain the displacement of the beam $y(x_v, t_p)$. The contact force is computed by using eq.(13).

5.2 Experimental results

Fig.7 shows the experimental results for R = 0.0001, 0.0021, 0.15, and 0.21, respectively. Fig.8 shows the experimental results for $R = 0.15$ and 0.21 with a scale change with respect to time. Each figure shows the force measured with the strain gauge, the force estimated by the introduced method, and the force estimated by the static method (eq.(12)). When R is small, these figures show that the force estimated by all methods nicely agree with the measurement by strain gauge. As R increases, the force estimated by static method differ from two other methods, while both the introduced method and strain gauge based one still keep a nice coincidence.

6 Conclusion

This paper proposed an approach for estimating the contact force between a flexible beam and an environment by a high speed vision. The proposed approach made it possible to estimate the contact force by using just one searching line. The approach enabled us to estimate the contact force with the sampling rate of 2[kHz]. We confirmed that the approach could successfully estimate the contact force.

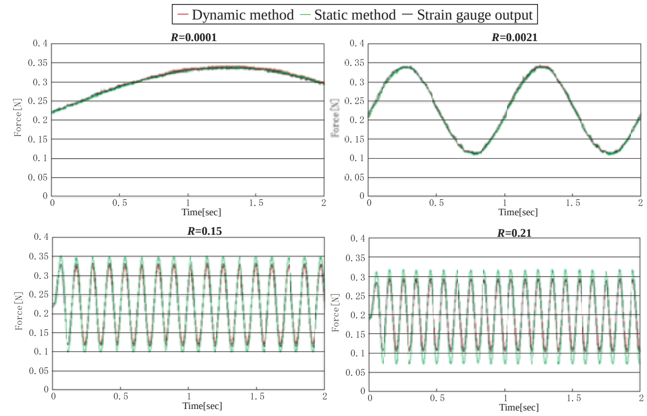

Fig.7: Experimental results (2[seconds])

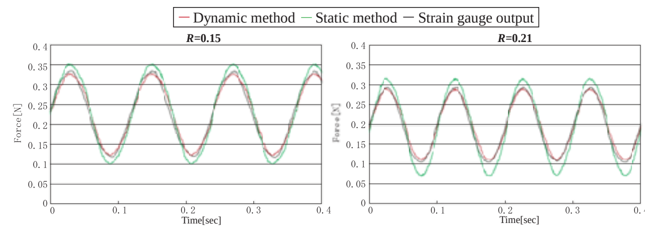

Fig.8: Experimental results (0.4[seconds])

References

[1] J. Z. Liu *et al.* : " Simultaneous measurement of human joint force, surface electromyograms, and functional MRI-measured brain activation", *Neuroscience Methods*, Vol. 101, pp. 49-57 2000.

[2] N. Takahashi, M. Tada, J. Ueda, Y. Matsumoto, and T. Ogasawara : " An optical 6-axis force sensor for brain function analysis using fMRI", *Proceedings of the IEEE International Conference on Sensors*, 2003.

[3] T. Arai, T. Tanigawa, and R. Larsonneur : " Mechanism design and motion control of finger module for micro hand", *Journal of the Robotics Society of Japan*, Vol. 15, No. 3, pp. 402-407 1997.

[4] M. Kaneko, N. Kanayama, and T. Tsuji : " Vision based active antenna", *Proc. of the 1996 IEEE Int. Conf. on Robotics and Automation*, pp.2555–2560, 1996.

[5] M. Kaneko, N. Kanayama, and T. Tsuji : " Vision based active antenna — basic considerations on two-points detecting method", *Proc. of the 1996 IEEE/RSJ Int. Conf. on Intelligent Robots and Systems.*

[6] I. Ishii *et al.* : " High speed mega-pixel vision with intelligent scanning", *Proc. The 20th Annual Conf. of the Robotics Society of Japan*, 3A15, 2002.

[7] I. Ishii *et al.* : " Development of MmVision(Mega-pixel and milli-second vision) camera head", *Proc. of the 10th Symposium on Sensing via Image Information*, pp.185–188, 2004.

[8] K. Yasuda : " Modal analysis and dynamic design", CORONA PUBLISHING CO., LTD., 1993.

The Tenth International Symposium on Artificial Life and Robotics 2005(AROB 10th '05),
B-con Plaza, Beppu, Oita, Japan, February 4-6, 2005

Non-Contact Impedance Sensing

T. Kawahara, K. Tokuda and M. Kaneko

Graduate School of Engineering
Hiroshima University
4-1, Kagamiyama 1-Chome, Higashi-Hiroshima 739-8527

Abstract

This paper discusses the non-contact impedance sensing that can measure the mass, viscosity and stiffness of environment. The developed sensor is composed of a laser displacement sensor and air force supply nozzle. We applied the developed sensor to fruits to confirm the possibility for measuring their surface impedance.

1 Introduction

There are various needs for measuring the mechanical impedance (mass, viscosity, stiffness) of environment, such as medical examination of a cancer tissue, medical examination of eye pressure, estimation of human skin age, judgment of the best time for eating fruits or meats, and evaluation of the degree of completeness of compliant material in industrial products. While various approaches have been proposed for answering these issues, most of them are based on the direct contact method [1]−[3], where the pushing force is actively given by a force probe. By the relationship between the applied force and the displacement, we can compute the impedance parameters. These approaches, however, cause several inherent issues due to the direct contact between the probe and the environment, for example, imparting damages to environment, receiving damage of the sensing probe itself, and sanitary issue especially for both foods and human beauty care.

To cope with these issues, non-contact approaches have been proposed recently and their effectiveness has been reported. As for a non-contact method, Shinoda and others [4], have first proposed the non-contact impedance sensor by utilizing air pressure actuated by an acoustic speaker, and showed the capability of measuring impedance parameters through the non-contact approach. One of most popular examples as a non-contact impedance sensor is perhaps the eye pressure measuring system [5] where air pressure is given to the eye from the front direction and the displacement of eye surface is measured by an infrared LED sensor with an inclination angle with respect to the front direction.

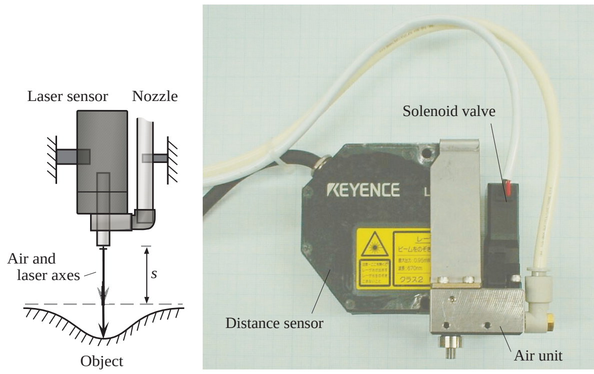

Fig. 1: An overview of the developed sensor

We discuss the non-contact impedance sensing capable of estimating the local impedance parameters without any contact. In this paper, we show the overview of the whole system including the non-contact impedance sensor[6]. As an example of application, we applied this sensor for measuring the degree of ripeness for pear. We show that impedance parameters for the pear are measured with reasonable estimation.

2 Non-Contact Impedance Sensing

2.1 Design of the Developed Sensor

Fig. 1 shows the basic design of the developed sensor unit and its overview, respectively. The sensor unit is composed of a laser distance sensor and an air supply adaptor, where s denotes the distance between the nozzle and the surface to be measured. The key idea is that the hole of air supply adaptor is so designed that the longitudinal axis perfectly coincides with the sensing axis of the laser sensor. To achieve this tuning up easily, we attach a sliding mechanism for the air supply adaptor, which helps us to change the position with observing the laser spot. The air supply system is equipped with a high speed solenoid valve which is the key element of the sensor toward a high speed sensing. The valve can operate with the maximum switching frequency of 500[Hz] under the supply pressure of 0.05[MPa] through 0.25[MPa]. It is composed of only three mechanical components and enables us to impart a force to the environment with high response with respect to time. Such a high response allows us to estimate the impedance parameters with high quality as well as high speed. Toward a field test, we would note that since the width of air flow becomes large as s increases. This will bring both the weakness of pushing force to the environment and the low resolution of local impedance parameters in test surface. We should design the hole of the air nozzle small enough for ensuring a high resolution in surface and keep a sufficiently short s for avoiding a weak force to the environment. Another remark should be also given to the following point. Even though the axis of nozzle coincides with that of the laser sensor, it is not guaranteed that the axis of actual air flow coincides with the nozzle axis. This is because the air is supplied to the sensor unit from the side wall and largely bent with a right angle within the sensor unit. The appropriateness of design can be confirmed only through experiments.

2.2 How to Operate the Sensor

Fig. 2 shows the overview of the whole system including the non-contact impedance sensor. The system includes a compressor for producing high pressurized air source, an accumulator for keeping pressurized air, a control driver for sending the switching signal to the sensor, and a PC for collecting measured signals from the sensor as well as for sending a command signal to the driver. The command signal is produced by two parameters;

$$f_{req} = \frac{1}{\tau_{on} + \tau_{off}}, \ (0 < f_{req} \leqq 500[\mathrm{Hz}]) \quad (1)$$

$$\alpha = \frac{\tau_{on}}{\tau_{on} + \tau_{off}}, \ (0 < \alpha \leqq 1) \quad (2)$$

where f_{req}, α, τ_{on}, and τ_{off} are the switching frequency for the valve, the duty factor for the valuve, ON time of time period, and OFF time of time period, respectively. By changing f_{req} and α, we can produce various force patterns for each frequency.

2.3 How to Sensing Impedance

The flowchart for estimating impedance is shown in Fig. 3(a).

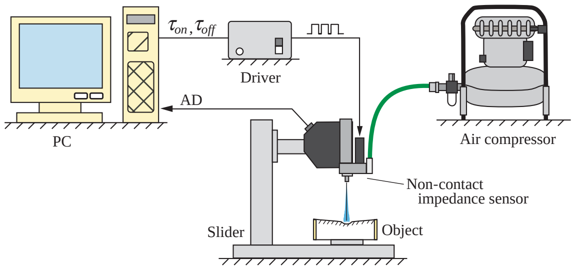

Fig. 2: Experimental system

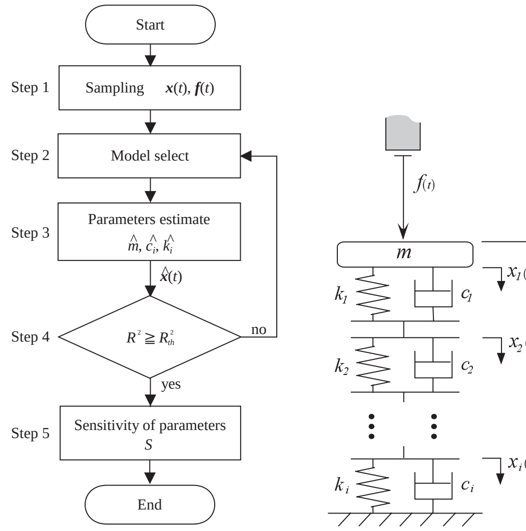

(a) Sensing flowchart (b) Impedance model

Fig. 3: Procedure for estimating impedance parameter

Step1 Measurement of the force and displacement data set:
Air force is sprayed on object and the displacement data set $\boldsymbol{x}(t) = [x_1, x_2, \cdots, x_n]^T$ is obtained. At the same time, the air force data set $\boldsymbol{f}(t) = [f_1, f_2, \cdots, f_n]^T$ is also obtained, where f_j is given step-wisely.

Step2 Select of the impedance model:
Since the behavior differs greatly from objects, the impedance model has to be carefully chosen. By considering that it generally becomes the complicated model due to the coupled spring effect, it is given by a multi-element impedance model as shown in Fig. 3(b), where m, c_i and k_i are the mass, the i-th damper, and the i-th spring, respectively.

Step3 Estimation of the model parameter:
The estimated parameters of selected model is determined by the ordinary least square method using $\boldsymbol{f}(t)$ and $\boldsymbol{x}(t)$.

The Tenth International Symposium on Artificial Life and Robotics 2005(AROB 10th '05),
B-con Plaza, Beppu, Oita, Japan, February 4-6, 2005

Step4 Evaluation of the selected model:
The response of displacement can be reproduced by using the estimated value $\hat{m}, \hat{c}_i$ and $\hat{k}_i$. By comparing the reproduced displacement $\hat{\boldsymbol{x}}(t) = [\hat{x}_1, \hat{x}_2, \cdots, \hat{x}_n]^T$ and the actual $\boldsymbol{x}(t)$ we can evaluate how nicely the impedance are estimated. By applying the coefficient of determination R^2, we can obtain the evaluation of the degree of approximation as follows[7];

$$R^2 = 1 - \frac{\displaystyle\sum_{j=1}^{n} |\hat{x}_j - x_j|^2}{\displaystyle\sum_{j=1}^{n} |x_j - \bar{x}|^2} \qquad (0 \leqq R^2 \leqq 1) \qquad (3)$$

where $\bar{x}$ is the average value of x_j. We can say that the degree of approximation of the reproduced waveform is good, when R^2 is close to 1. If $R^2 \geqq R^2_{th}$, we progress to Step5 by regarding that the model utilized is reasonably good where R^2_{th} is the threshold value. Re-selection of a model is required when $R^2 < R^2_{th}$. We return to Step2 when $R^2 < R^2_{th}$.

Step5 Sensitivity evaluation of estimated parameters:
By Step4, We can check whether the estimated parameters are reasonable or not. However, even if R^2 becomes a large value, it is not guaranteed that the estimated parameters nicely coincide with actual ones. In order to check this, we define the sensitivity of parameter by the following[8]:

$$S = \frac{p}{g}\frac{\delta g}{\delta p} \qquad (4)$$

where g is the function of p. The sensitivity for each parameter obtained by Step3 is examined. We would note that if S is sufficiently small, the reliability of parameter estimation is not guaranteed.

3 Experiments

3.1 Air Flow Characteristics

Fig. 4 shows experimental results where Fig. 4(a), (b) and (c) are the step responses of the air jet under α=0.5, f=2.5[Hz] and s=10[mm], the air flow patterns under α=1.0 and s=10[mm], and the pushing force with respect to s under α=1, respectively. From Fig. 4(a), we can confirm that the step-up response is roughly 1[msec] while the step-down response is roughly 2[msec]. We would note that the origin of the horizontal axis in Fig. 4(b) coincides with the laser sensor axis. From Fig. 4(b), we can see a symmetry shape of the flow pattern with respect to the laser sensor axis. Now, let us define w by the width of the air pressure distribution with more than 80% of the maximum pressure. From Fig. 4(b), we can also see w=2.5[mm] for the diameter of nozzle of 2[mm], which means that the width of air flow is not big enough under s=10[mm]. In Fig. 4(c), circles and triangles show the pushing force to the environment and w, respectively. Fig. 4(c) says that the total force keeps almost constant with respect to s, while w increases gradually with respect to s. In other words, although the area affected by the air jet increases with respect to s, the pushing force does not change largely. This is because the force obtained by the integration of local pressure distribution is determined by the change of the total momentum of the air flow. The reason why the force decreases when s becomes small is that the pressurized air is difficult to come out from the nozzle due to a large flow resistance when the nozzle hole is close to the environment.

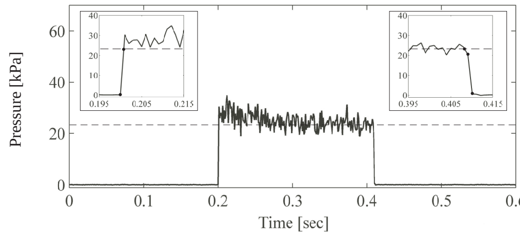

(a) Step response

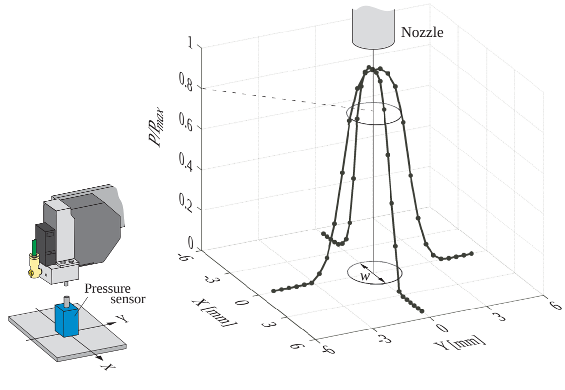

(b) Pressure distribution

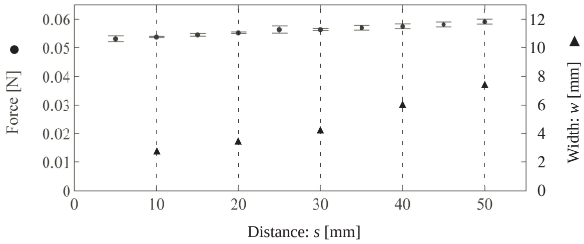

(c) Force with respect to distance

Fig. 4: Characteristics of air flow

3.2 Application to Fruit

As an example of application, we applied the developed sensor to estimate impedance parameters for pear. Fig. 5 shows the experimental result for pear. We apply stepwise air jet for 200[msec] for the surface of pear and measure the displacement of the surface. The real line in the figure shows the displacement. Although the displacement of a pear is only 60[μm], we can measure such a tiny displacement. Let us suppose that we apply a force for a linear four elements model ($i = 2$ and $m = 0$ in Fig. 3(b)). We can describe the equation of motion for the model as follows:

$$b_2\ddot{x}(t) + b_1\dot{x}(t) + b_0x(t) = a_1\dot{f}(t) + f(t) \qquad (5)$$

$$\left(\begin{array}{ll} b_2 = \frac{c_1c_2}{k_1+k_2}, & b_1 = \frac{c_1k_2+c_2k_1}{k_1+k_2} \\ b_0 = \frac{k_1k_2}{k_1+k_2}, & a_1 = \frac{c_1+c_2}{k_1+k_2} \end{array} \right)$$

This model is conventionally well known that it approximates the action of viscoelasticity, such as food and human skin. By using this model, we estimate $\hat{k}_1$, $\hat{k}_2$, $\hat{c}_1$, and $\hat{c}_2$, as indicated in Fig. 5. The displacement reproduced by these parameters is also expressed with the dashed line in Fig. 5. In this case, R^2 is higher than the given $R^2_{th}(= 0.950)$. Fig. 6 shows the computed sensitivity S between 100[msec] and 300[msec] in Fig. 5. From these results, $|S|_{k_1}$ is even larger than $|S|_{k_2}$, $|S|_{c_1}$ and $|S|_{c_2}$. Furthermore, we pay our attention to a time history of the sensitivity of $|S|_{c_1}$. Fig. 6 means that the parameter c_1 contributes to the response at the initial phase, for example up to 20[msec]. From the viewpoint of good estimation of c_1, we should choose the time interval in the range of 20[msec]. On the other hand, we need an appropriate time interval for obtaining sufficient number of data for estimation. There exists a compromise time interval for satisfying both requirements. We have done this experiment every two days for five pears. Fig. 7 shows the change of $\hat{k}_1$ of the pear. Through this experiment, we observe how stiffness changes every two days. In six days after we start this experiment, stiffness is changes as shown in Fig. 7. We found that the taste becomes good after six days we start this experiment. We can say this surface stiffness provides us with a good hint for judging the time for eating.

4 Concluding Remarks

We discussed the developed non-contact impedance sensor capable of estimating the local impedance parameters without any contact. We precisely explained the sensing method. As an application example, we took pear and showed that impedance parameters can be nicely evaluated by utilizing the four-elements impedance model.

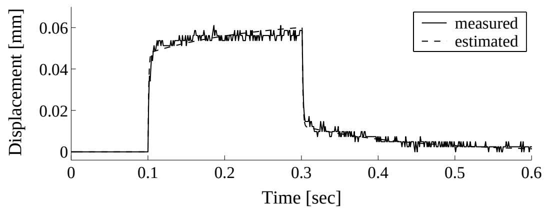

$\hat{k}_1 = 3800$[N/m], $\hat{k}_2 = 11100$[N/m], $\hat{c}_1 = 3.68$[Ns/m], $\hat{c}_2 = 1550$[Ns/m]

Fig. 5: Application to pear ($R^2 = 0.993$)

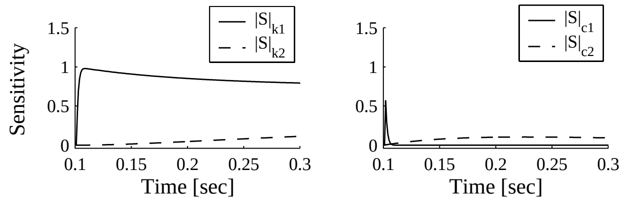

Fig. 6: Sensitivity of the eatimated parameters

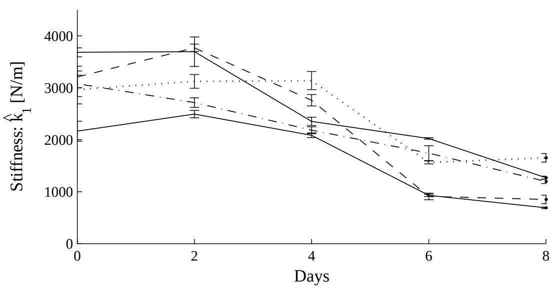

Fig. 7: Time history of stiffness of pear

References

[1] S. Omata and Y. Terunuma, "New tactile sensor like the human hand and its applications", *Sensors and Actuators A*, Vol.35, pp.9–15, 1992.

[2] Y. Yoshitoshi and M. Nagasaka, "Viscoelasetic Properties of Edematous Skin", *Japanese Heart Journal*, Vol.3, No.3, pp.220–230, 1962.

[3] H. Oka and T. Irie, "Mechanical impedance of layered tissue", *Medical Progress through Technology*, Vol.21, pp.1–4, 1997.

[4] H. Shinoda and H. Yamasaki, "Noncontact sensing of surface hardness", *J. of SICE*, Vol.27, No.7, pp.749–754, 1991.

[5] TOPCON MEDICAL SYSTEMS, INC., Non-contact tonometer, *http://www.topcon.com/medical.html.*

[6] M. Kaneko and T. Kawahara, "Co-axis type non-contact impedance sensor", *In Proc. of the IEEE Int. Conf. on Robotics and Automation*, pp.709–714, 2004.

[7] B. W. Bolch and C. J. Huang, Development of the multivariate analysis, Morikita Publishing Company, pp.133–139, 1976.

[8] K. Nonami, H. Nishimura, A foundation for the control theory, Tokyo Denki University Press, pp.94–95, 1998.

The Tenth International Symposium on Artificial Life and Robotics 2005(AROB 10th '05),
B-con Plaza, Beppu, Oita, Japan, February 4-6, 2005

A View-Based Navigation System for Autonomous Robots

Chandima Pathirana
Dept. of Advanced Systems Control Eng.
Graduate School of Science and Eng.
Saga University
1-Honjomachi, Saga 840-8502, Japan

Keigo Watanabe, Kiyotaka Izumi
Dept. of Advanced Systems Control Eng.
Graduate School of Science and Eng.
Saga University
1-Honjomachi, Saga 840-8502, Japan

Abstract

We present a purely vision-based scheme for learning a topological representation of an open environment. The system represents selected places by local views of the surrounding scene, and finds traversable paths between them. The set of recorded views and their connections are combined into a graph model of the environment. To navigate between views connected in the graph, we employ a homing strategy inspired by findings of insect ethology. In robot experiments, complex visual exploration and navigation tasks can thus be performed without using metric information.

1 Introduction

To survive in unpredictable and sometimes hostile environments animals have developed powerful strategies to find back to their shelter or to a previously visited food source. Successful navigation behaviour can already be achieved using simple reactive mechanisms such as association of landmarks with movements [1] or tracking of environmental features [2]. However, for complex navigation tasks extending beyond the current sensory horizon, some form of spatial representation is necessary. Higher vertebrates appear to construct representations—sometimes referred to as *cognitive maps*—which encode spatial relations between relevant locations in their environment [3, 4].

Under certain conditions, such maps can be acquired visually without any metric information. Humans, for instance, are able to navigate in unknown environments after presentation of sequences of connected views [5]. This has led to the concept of a view graph as a minimum representation required to explain experimentally observed navigation competences [7]. A view graph is defined as a topological representation consisting of local views and their spatial relations. Depending on the task, these relations can be, e.g., movement decisions connecting the views, or mere adjacencies.

Motivated by the findings of vertebrate ethology, researchers have started to investigate topological representations for robot navigation. These systems rely primarily on local sonar patterns for the identification of places, in combination with metric knowledge derived from compasses or wheel encoders. Bachelder and Waxman [8] have reported results on a vision-based topological system which uses a neural control architecture and object recognition techniques for landmark detection. In their current implementation, however, the system has to rely on artificially illuminated landmarks and a pre-programmed path during exploration of the environment. For maze-like environments, Schölkopf and Mallot [7] have shown that learning a graph of views and movement decisions is sufficient to generate various forms of navigation behavior known from rodents. The scheme has subsequently been implemented in a mobile robot [7].

The purpose of the present study is to extend the view graph approach from the mazes of [7] to open environments. In doing so, we present a navigation system that uses purely topological information based on visual input. By focusing on just one type of information we want to make the contribution of topological knowledge explicit.

2 Learning View Graphs

2.1 Discrete Representation of Continuous Space

In view-based navigation tasks, visual information is used to guide an agent through space. The reason why this is feasible at all, is the fact that there is a continuous mapping between position space (x- and y-coordinates, possibly supplemented by gaze directions) and the space of all possible views: for each spatial position, a certain view is perceived, and this view changes continuously as the observer moves around in space. Unfortunately, this mapping can be singular, because identical views can occur at different spatial locations, i.e., there is no guarantee for the existence of a global coordinate system on the manifold of all possible views. In principle, this problem can be dealt with using context information: In points with identical views, we can use views from nearby spatial positions to disambiguate between them.

It is sufficient to store views which allow the description of relevant paths. This leads to a less detailed representation of the view manifold, namely by a graph consisting of representative views and connections between them.

Since open environments do not impose a structure on the view graph, we have to select a set of views which are representative for the manifold (in the following referred to as snapshots), and to find connections between them. Since the connecting paths between the snapshots are not explicitly coded in the view graph, we have to provide a homing method which allows us to find connected views from a given start view.

In the following sections, we introduce a system that is able to solve these tasks. The vertices of the acquired view graph are panoramic views of the environment, and their edges are connections between views that can be traversed using a visual homing procedure. This homing procedure allows the system to approach a location from any direction such that the graph edges denote mere adjacency relations without any directional labelling. The resulting view graph does not contain any explicit metric information.

2.2 A Minimal System for Learning a View Graph

The overall architecture of the system is shown in Fig. 1. Here, we discuss the basic building blocks, the details are described in the following sections.

2.2.1 *View Classifier*

As we mentioned above, a crucial component of any graph learning scheme is the selection of vertices. The graph vertices have to be distinguishable, because otherwise the representation could not be used for finding a specific location. Since we confine our system to use only visual information, we must guarantee that the recorded views are sufficiently distinct. This can be performed by a classifier which detects whether the incoming views can be distinguished from the already stored vertices of the view graph. If this condition is

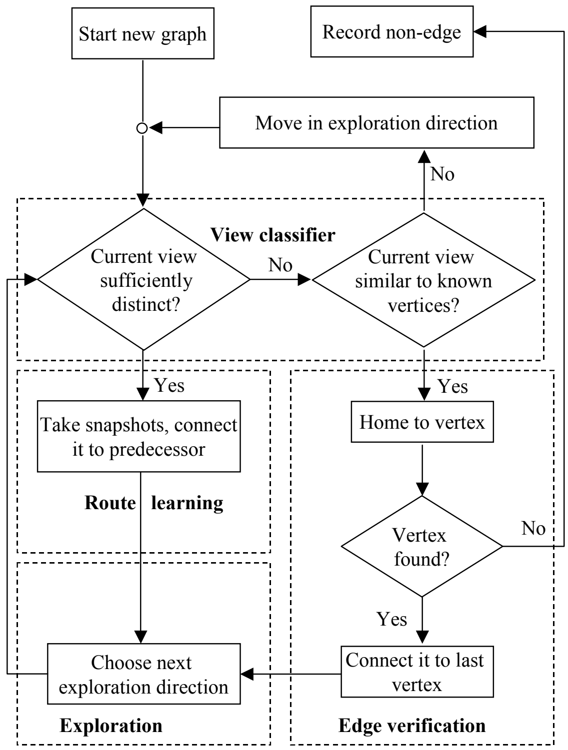

Figure 1: Block diagram of the graph learning algorithm

fulfilled, the system takes a new snapshot and adds it to the graph. The classifier is described in Section 2.3.

2.2.2 *Route Learning*

In this system, a new snapshot is automatically connected to the previously recorded vertex of the view graph. Thus, the system records chains of snapshots, or routes. These routes can be used to find a way back to the start position by homing to each intermediate snapshot in inverted order. We describe the homing procedure in Section 2.4. The area from which a specific snapshot can be reached by the homing procedure is called its catchment area. The view classifier has to make sure that every snapshot can be reached from its neighbour, i.e., all vertices of the view graph have to be in the catchment areas of their adjacent vertices.

2.2.3 *Choice of Exploration Direction*

When the system has taken a new snapshot, a new exploration direction must be chosen. This choice primarily affects the exploration strategy of this system, because it determines how thoroughly an area is explored and how fast the explored area grows. In Section 2.5, we describe several local exploration strategies used in this system.

2.2.4 *Edge Verification*

The route learning procedure described above has no way of forming new edges to previously visited views, i.e., the resulting graphs will be mere chains. By adding the following behaviour we can obtain nontrivial graphs: during exploration, the system constantly checks whether the current view becomes similar to the already recorded snapshots. This again is a view classification task which can be solved by the same classifier as used for the selection of the snapshots (see Section 2.3). In a second step, the system checks whether the detected snapshot is not yet connected to the vertex from which the current exploration step started. Whenever these conditions hold, the system tries to home to the snapshot. If successful, an edge connecting the two vertices is included, and the exploration continues from the detected snapshot. In cases where the robot gets lost or bumps into obstacles, the system reports a "non-edge" between both vertices thus preventing the failed action from being repeated. Before starting to home, the verification procedure always checks whether a "non-edge" for this action has already been recorded. After a failed verification, we start a newgraph, which will typically get connected to the old one in due course by the edge verification procedure.

If an already connected view is encountered during an exploration step, the system homes to it as well(not shown in Fig. 1). This procedure does not produce additional knowledge, but has the effect that edges intersecting previously stored edges are less likely to be recorded.

2.2.5 *Arbitration and Obstacle Avoidance*

Since the focus of this work is on navigation, any sophisticated obstacle avoidance systems are not necessarily employed into this system. During exploration, kind of simple sensors like infrared sensors can be used for the presence of nearby objects. If obstacles were detected at distances larger than 1 cm, the robot is made to turn away without slowing down. Smaller distances can be interpreted as collisions causing the robot to back up and turn away from the obstacle. Both behaviors and the graph learning system of Fig. 1 are combined into a subsumption architecture where the collision-induced escape behavior had highest, the graph learning procedure lowest priority.

The robot is not allowed to take snapshots as long as the obstacle avoidance system is active. The resulting graph structure tends to concentrate in the open space between obstacles. This feature makes the navigation system more effective, because the visual input changes very rapidly near objects. Exploration of these areas would require a large number of snapshots which, in complex natural environments, would ultimately lead to a fractal graph structure near objects.

2.3 View Classifier

Ideally, the set of snapshots taken to represent the view manifold should satisfy three criteria: first, the views should be distinguishable. In purely graph-based maps, this is the only way to guarantee that specific vertices can be navigated to. This can be achieved by incorporating only distinct views into the graph. Second, a large proportion of the view manifold should be covered with a small number of vertices to keep processing requirements small. Third, the spatial distance of neighbouring views should be small enough to allow reliable homing between them.

As we confine this system to use only visual input, the selection of the snapshots must be based on the current view and the stored snapshots. The above criteria can be satisfied by measuring the degree of similarity between views: dissimilar views are distinguishable by definition while being distant on the view manifold, and similar views often are spatially close.

Clearly, a threshold of classifier can also be used to detect whether the current view becomes similar to one of the already recorded snapshots. If the image distance to a snapshot falls below the threshold, the robot starts its edge verification procedure (as stated in Section 2.2) and tries to home to the snapshot. In this system, we use the same classifier for both tasks. A suitable threshold can be determined experimentally.

2.4 Navigating Between Places: View-Based Homing

In order to travel between the vertices of the view-graph, we need a visual homing method. Since the location of a vertex is only encoded in the recorded view, we have to deduce the driving direction from a comparison of the current view to the goal view. After the robot has moved away from the goal, the images of the surrounding landmarks in the current view are displaced from their former image positions in the goal view. If the robot moves so as to reduce these displacements, it will finally find back to the goal where current view and snapshot match. The displacement field has a focus of contraction in the goal direction. Driving into the direction of this focus most quickly reduces the image displacements.

A number of experiments have shown that invertebrates such as bees or ants are able to pinpoint a location defined by an array of nearby landmarks. Apparently, these insects search for their goal at places where the retinal image forms the best match to a memorized snapshot. Cartwright and Collett [9] have put forward the hypothesis that bees might be able to actively extract the goal direction by a homing mechanism as described above.

2.5 Local Exploration Strategies for Graph Learning

The exploration strategies used by this system have been motivated by the principle of maximizing knowledge gain [6]. As we have not formalized any notion of knowledge, this principle was used as a qualitative guideline. In this context, knowledge gain is possible, for instance, through the recording of new edges and new snapshots. In the following, we describe several exploration strategies, which concern primarily the choice of the next direction to explore after a snapshot has been taken, or after an existing vertex has been reached (as discussed in Section 2.2).

2.5.1 *Exploration Direction During Route Learning*

The simplest conceivable rule is to choose a random direction and then to go straight until the next snapshot is taken. The resulting Brownian motion pattern has the advantage that eventually every accessible point of the environment will be explored without the danger that the exploring agent is caught in an infinite loop. Good results can also be achieved if one uses a fixed turning angle. Using smaller angles, distant areas are reached faster, whereas angles closer to lead to a more thorough exploration of the local neighbourhood.

2.5.2 *Exploration of the Largest Open Angle*

This navigation scheme is designed such that all vertices of the view graph remain in the catchment areas of their respective neighbours. This property can be used to choose the next exploration direction, if a vertex has already more than one edge: the system determines the directions to all neighbouring vertices using the homing procedure, and directs the next exploration step to the largest open angle between them. Alternatively, one could use information about neighbouring vertices, such as their connectivity or similarity. For example, exploring areas where neighbouring views are connected to each other would be more likely to lead to possibly undesired edge intersections.

3 Summary

This paper has presented the view graph learning method that can be used for view based navigation system of autonomous robots. This method is expected to incorporate into a real robotic system which is expected to work only on visual inputs.

References

[1] R. Wehner, B. Michel, and P. Antonsen, "Visual navigation in insects: Coupling of egocentric and geocentric information," *J. Exp. Biol.*, vol. 199, pp. 129–140, 1996.

[2] T. S. Collett, "Insect navigation en route to the goal: Multiple strategies for the use of landmarks," *J. Exp. Biol.*, vol. 199, pp. 227–235, 1996.

[3] J. O'Keefe and L. Nadel, *The Hippocampus as a Cognitive Map*, Clarendon Press: Oxford, 1978.

[4] R. Gallistel, *The Organization of Learning*, MIT Press: Cambridge, MA, 1990.

[5] M. J . O'Neill, "Evaluation of a conceptual model of architectural legibility," *Environment and Behavior*, vol. 23, pp. 259–284, 1991.

[6] S. Thrun, "Exploration in active learning," in *The Handbook of Brain Theory and Neural Networks*, M.A.Arbib(Ed.), MIT Press, pp. 381–384, 1995.

[7] B. Schölkopf and H. A. Mallot, "View-based cognitive mapping and path planning," *Adaptive Behavior*, vol. 3, pp. 311–348, 1995.

[8] I. A. Bachelder and A. M. Waxman, "A view-based neurocomputational system for relational mapmaking and navigation in visual environments," *Robotics and Autonomous Systems*, vol. 16, pp. 267–289, 1995.

[9] B. A. Cartwright and T. S. Collett, "Landmark learning in bees," *J. Comp. Physiol. A*, vol. 151, pp. 521–543, 1983.

The Tenth International Symposium on Artificial Life and Robotics 2005(AROB 10th '05),
B-con Plaza, Beppu, Oita, Japan, February 4-6, 2005

Intelligent Vision System for Dynamic Environments

Chandima Pathirana, Keigo Watanabe, Kiyotaka Izumi (Saga University, Japan)
H.Y. Aruna Hewawasam, and Lanka Udawatta (University of Moratuwa, Sri Lanka)
E-mail: dpchandima@yahoo.com;{watanabe,izumi}@me.saga-u.ac.jp;lanka@ieee.org

Abstract

This paper describes an intelligent vision system that absorbs useful information from its environment and draws useful conclusions. This system can give the instructions to locate vacant seats that are currently occupying in a cinema theater. Extraction of useful information without viewing or exposing inside details of an environment through an active vision system is proposed. Reasoning based conclusions are drawn for optimum searching. The effectiveness of the proposed method is demonstrated using an experiment.

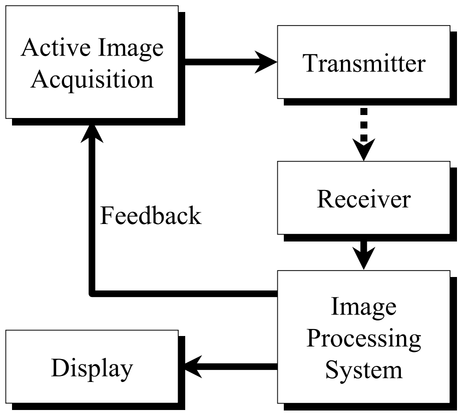

Figure 1: Intelligent vision system architecture

1 Introduction

Computer vision is a new and rapidly growing field, currently focusing on building intelligent systems. It basically processes active image data captured by a vision system and draws intelligent conclusions. Much accurate timely information could be obtained without human involvements. In practice, this would also save time, avoid the occurrence of any disturbances and enhance the security. As an example, in a multi storey building, required information of a particular floor that is used for common seating could be displayed at other floors (see **Fig. 1**). In a parking, registration numbers and the entering time of the vehicles could be recorded. Camera system would be used to obtain a view of that particular environment and the desired data is transmitted to the location where the data is processed in order to display the useful information. Finally, all these disciplines are needed for building advanced intelligent systems [1].

Image processing plays a great role in this research field [2] backed by artificial intelligent techniques [3] in order to build these intelligent vision systems. Combining visual model acquisition and agent control system was presented for visual space robot task specification, planning and control [4]. In [5], an evolutionary based approach was described to develop an active vision system for dynamic feature selection with simple neural control system.

In the present example, the system first detects objects or humans on the seats using a wide-angle image and analyzes them for conclusions. Image data is continuously transmitting from the environment and analyzing for vacant seats using image-processing techniques. Reasoning based conclusions are drawn for the users entering into the environment for optimum seat searching. The recognition algorithm with image processing tools will be used in order to analyze video images. The experimental results show the feasibility of the system. The rest of the paper is organized as follows: system features and methodology are described in Section 2 and Section 3, respectively. In Section 4, analysis used for identification is presented. Then, some experimental results are given in Section 5. Finally, concluding remarks is given in Section 6.

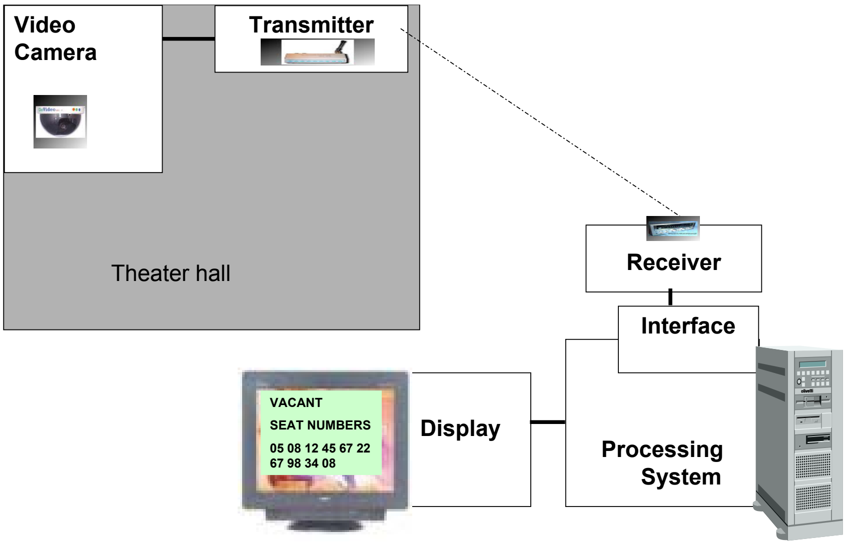

Figure 2: System architecture for the experiment

2 System Overview

In this illustration, we use a cinema theater hall, which should be arranged in such a way that a clearly distinguishable mark should be stick on each chair and seat locations should be unchanged after setting up the system. Once the system is set up, seat locations should be unchanged and if seat locations are going to be changed the system should be set up again before using the system. If it is going to change, simple recognition mechanism can be employed in order to apply this technique. The video camera should be fixed at a correct elevation to get the plan view of the theater hall. Install and configure the transmitter receiver camera system. Focus the camera, adjust the position and correct the lighting level if required by previewing the video stream. Basically, the system used for the experiment is similar to the system in **Fig. 2**. Follow the set of instructions that comes with image acquisition device. Setup typically involves:

- Installing the frame grabber board in your computer.
- Installing any software drivers required by the device.
- Connecting a camera to a connector on the frame grabber board.
- Verifying that the camera is working properly by running the application software that came with the camera and viewing a live video stream

The device ID is a number that the adaptor assigns to uniquely identify each image acquisition device with which it can communicate. The video format specifies the image resolution (width and height) and other aspects of the video stream. However, before starting, you might want to see a preview of the video stream to make sure that the image is satisfactory. For example, you might want to change the position of the camera, change the lighting, correct the focus, or make some other change to your image acquisition setup.

3 Methodology

We develop this algorithm to setup the system explained in Section 2:

1. Read the color image frame acquired from image acquisition device.

2. Convert color image to an intensity image.
3. Resize intensity image so that the image matrix could be viewed.
4. Suppress light structures connected to image border
5. Convert clear border image to a binary image
6. Create sub matrices M_i and $\hat{M}_i$ (explained later in Section 4)
7. Process and determine whether the seats are vacant or not
8. Display the results

Note here that once the system is set up, seat locations should be unchanged and if seat locations are going to be changed, the system should be set up again before using the system.

4 Image Analysis

The video camera should be fixed at a correct elevation to get the plan view of the theater hall. Install and configure the transmitter receiver camera system. Focus the camera, adjust the position and correct the lighting level if required by previewing the video stream. When nobody is seated in the hall, a color image frame is acquired and converted to an intensity image and then processed in order to set up the system as below. Consider intensity image matrix $f(x, y)$ of dimension $m \times n$

$$f = \begin{bmatrix} f(0,0) & f(0,1) & \dots & f(0,n-1) \\ f(1,0) & f(1,1) & \dots & f(1,n-1) \\ & & \vdots & \\ f(m-1,0) & f(m-1,1) & \dots & f(m-1,n-1) \end{bmatrix}$$

Here $f(x, y)$ was subjected to reduce overall intensity level and to suppress structures that are lighter than their surroundings and that are connected to the image border and converted to a binary matrix A.

Next, consider matrix M_i such that

$$\begin{aligned} M_i &\subset A \\ M_i &\subset \hat{M}_i, \end{aligned}$$

where $i = 1, 2, ..., S$. Here, i is the seat number and S is the total number of seats detected by the camera.

Sub matrix $\hat{M}_i$ should be selected from matrix A such that its center element or elements should align with the center element relevant to the mark on seat i. Dimension of $\hat{M}_i$ should be as large as possible subjected to the criteria that all the elements should cover the mark area and some more space beyond the mark too.

Then the matrix $\hat{M}_i$ should be selected in a way that $M_i \subset \hat{M}_i$ and dimensions of $\hat{M}_i$ should be $(m + p) \times (n + p)$, where p is an integer. Center element of M_i and $\hat{M}_i$ should be aligned with each other.

Then use the following criteria to determine whether the seat is vacant or not

$$\begin{aligned} &\text{IF} \quad \sum_{j=1}^{m}\sum_{k=1}^{n} m_{jk} = mn \\ &\text{AND} \quad \sum_{j=1}^{m+p}\sum_{k=1}^{n+p} \hat{M}_{ij} \neq (n+p)(m+p) \\ &\text{THEN} \quad \text{Seat is Vacant} \end{aligned} \tag{1}$$

5 Results

Figure 3 shows the resulting images according to the algorithm explained in the previous sections. Use of three marks on the seat instead of one mark enhanced the reliability. As shown in **Fig. 4(a)** when the seat is occupied by a person all three marks will be covered and when there is an object placed on the chair such as a bag may not cover all three marks. Use of remarkable color mark with a fine thick edge as shown in **Fig. 4(b)** and suitable lighting conditions enhanced the system.

6 Conclusions

The system has detected objects or humans on the seats using a wide-angle image and analyzed them for conclusions. Image data was continuously transmitting from the environment and analyzing for vacant seats using image-processing techniques. The reasoning based conclusions were drawn for the users entering into the environment for optimum seat searching

The system can be further developed and generalized for other applications. In a multi storey building,

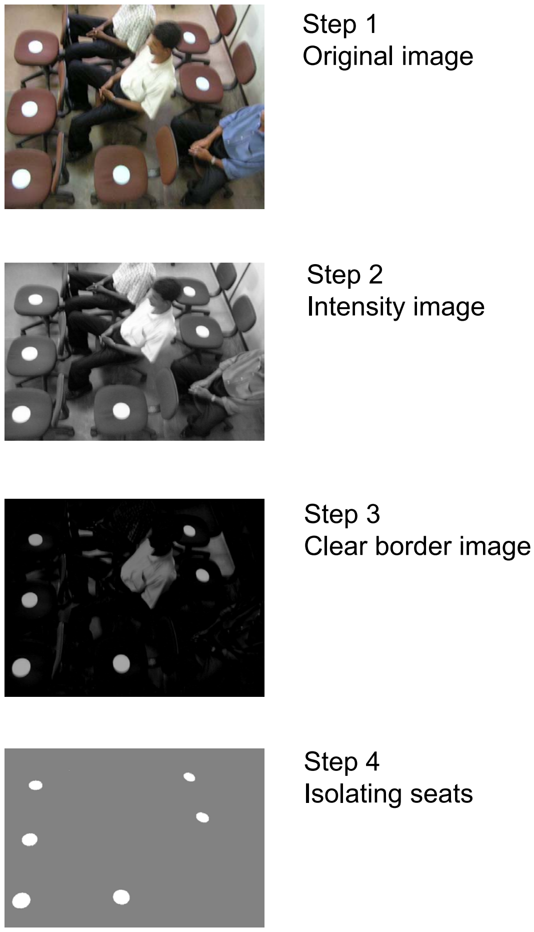

Figure 3: Image processing steps

required information of a particular floor that is used for common seating could be displayed at other floors. In a vehicle park, the registration number and the entering time of the vehicles could be recorded.

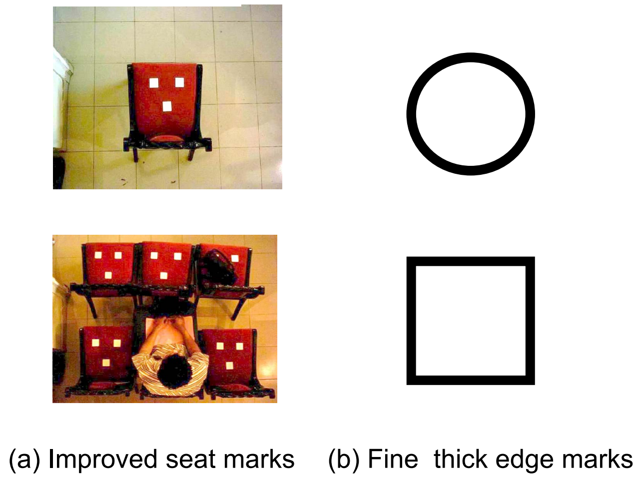

Figure 4: Improving the accuracy

References

[1] J. Nakanishi, T. Fukuda, and D. E. Koditschek, "A Brachiating Robot Controller," *IEEE Trans. on Robotics and Automation,* vol. 16, pp. 109–123, 2000.

[2] R.C. Gonzalez and R.E. Woods, *Digital Image Processing*, Boston, MA, Addison-Wesley Longman Publishing Inc., 1992.

[3] S. Russell and P. Norvig, *Artificial Intelligence: A Modern Approach*, New-Delhi, India, Prentice Hall, 2003.

[4] M. Jagersand and R. Nelson, "On-line Estimation of Visual-Motor Models using Active Vision," in *Proc. ARPA Image Understanding Workshop*, 1996.

[5] D. Marocco and D. Floreano, "Active Vision and Feature Selection in Evolutionary Behavioral Systems," in *Proc. of the Seventh International Conference on Simulation of Adaptive Behavior on From Animals to Animats* , pp. 247–255, 2002.

[6] S.Y. Huang, C.W. Mao, and K.S. Cheng, "A Codeword-Based Approach to Diagnose the Thermal Imaging of Printed CircuitBoards," in *Knowledge-Based Intelligent Information Engineering Systems Allied Technologies, Volume 69*, N. Baba, L.C. Jain and R.J. Howlett, Eds., The Netherlands: IOS Press, 2001, pp. 663–668.

The Tenth International Symposium on Artificial Life and Robotics 2005(AROB 10th '05),
B-con Plaza, Beppu, Oita, Japan, February 4-6, 2005

Human Interaction with Binocular Vision Robots in Ubiquitous Environment

Janaka Chaminda Balasuriya Keigo Watanabe Kiyotaka Izumi
Department of Advanced Systems Control Engineering
Graduate School of Science and Engineering
Saga University, 1-Honjomachi, Saga 840-8502, Japan

Abstract

Human interactive robotics is a fast developing area today. There are many aspects to be fulfilled for a robot to be more similar to human behavior. For example, a robot with a binocular vision head needs to recognize various gestures of the humans in order to respond to them accordingly. It is also necessary to have a sense of environmental changes, especially if interaction is being made while in motion. This is achieved with the help of an overhead monitoring system. Making the robot be "ubiquitous" will be possible by manipulating Bluetooth Wireless Technology. In order to apprehend the demand of more human like intelligent system, this research project is planned to search for new solutions for better achievement.

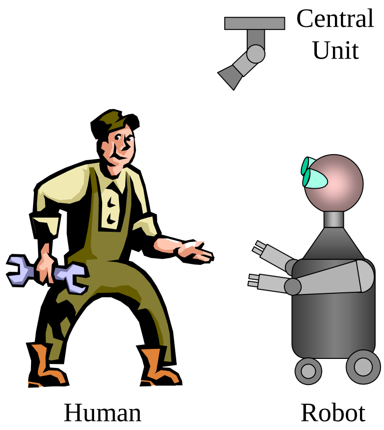

Figure 1: Human interaction

1 Introduction

For few years, research is going on to assist people by finding new robotic solutions. In the near future there may be robots in everywhere as our partners. These "ubiquitous" or present everywhere robots are human interactive not only to voice commands but also to human gestures as well (see Figure 1). In conversation, humans are capable of getting sense of other activities going around themselves. These include static / dynamic environment, environmental conditions, other sounds and noises in the vicinity, etc. But unfortunately there are human limitations as well. For an example, they are incapable of presenting themselves in anytime, anywhere or anyway. These may be due to human limitations or due to some natural disasters like fire, earthquakes, etc. However, it is useful to have a companion, who can represent a human. This may include basic things like; watching, listening, understanding, communicating as well as many other things. An attempt to build such a human interactive intelligent system is shown in Figure 1.

2 Binocular Vision

Humans are capable of getting a vision in breadth, width and depth, i.e. three-dimensional view. This has gained humans lot of features of characterizing the object in concern. In humans, the brain gets images from both (bi) eyes (ocular) at the same time and combines those two images into one, to make vision. The images that the brain gets from the eyes are however slightly different from each other and this small difference is used to work out how far away an object is. This is called the depth perception. It also helps to work out how quickly an object is moving towards or away from a person. This is the movement perception [1]. In order to interact effectively with humans, Ubiquitous robots require such information. Some examples are, to recognize a particular object or person (as a requested by third party interactor), to clearly identify face impressions / body gestures (while in conversation), to guidance in motion, etc.

2.1 Object Tracking

In order to do any of the above tasks, the primary objective is to obtain a clear view of the object. This requires continuous gazing at the right place at the right time. In other words, it is required to focus the lenses of the vision system according to the position changes of an object, especially if it is moving. As these trajectories of motion are not always simple as straight lines, the tracking mechanism becomes complicated and advanced. For a binocular vision system, both eyes (or cameras) should be focused separately over the object under consideration continuously.

2.2 Fuzzy Logic System

Matlab simulation results of one such tracking program written using fuzzy reasoning, is given in Figure 2. Once received the position of the object, relative distance to it from the current focal point is calculated. This is taken as 'Distance Error (DE)'. In addition to above, considering the motion of the object and the robot; rate of change of distance error (RateChangDE) is calculated. Obtaining these two values, will serve as the inputs to the Fuzzy Logic system, resulting in controlling the focal length of the lens (FocusLens). Rules such as; If DistanceError is positive big and RateChangDE is positive big then FocusLens is positive big, If DistanceError is negative small and RateChangDE is negative small then FocusLens is negative small, etc. are used. Here, for simplicity, a straight-line motion has been considered. But in realistic situation, the trajectories of motion will be much more complex. An adaptive neuro-fuzzy system will be much useful.

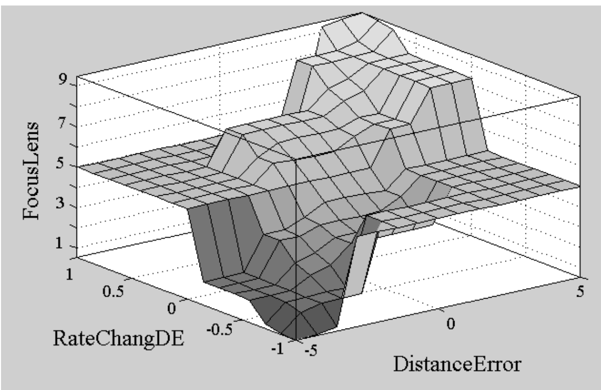

Figure 2: Fuzzy object tracking

2.3 Vision Function

On the other hand, if we consider the trends in modern communication techniques, video teleconferencing over the Internet provides an arguably more realistic interface into a remote space; but it is more of an enhancement to existing telephone communication technology rather than a new form of communication. With video conferencing, the participants find themselves fixed, staring almost all the time through the gaze of an immovable camera atop of someone's computer monitor. As actions and people pass across the camera's field of view, the observers are helpless to pan and track them or follow them into another room. In essence, here, it still lacks mobility and autonomy. The observers cannot control what they see or hear. Even if there are cameras in every room and the ability to switch between them is provided, the experience would still lack the spatial continuity of a walk around a building.

It will always be better to deliver a more realistic perception of physical embodiment of the user within the remote space being explored. Such system must immerse the user in the remote world by providing continuity of motion and control. These would provide the user the visual cues necessary to stitch together the entire visual experience into a coherent picture of a building and its occupants. It will be much advantageous and also be thoroughly appreciated if the user is provided with the necessary means of communication and interaction with the remote world and its real inhabitants using this new system. Furthermore, as Paulos et al. [2, 3] and Schulz et al. [4] have planned in their research, such a system can be further developed to give access to any user in the Internet with standard software running on currently existing computer architecture.

3 Localization and Target Tracking

Ubiquitous robots, finding its own path by means of visuals, sounds or any other method, have many problems due to the limitations of the sensory elements. Robots with binocular vision system have many advantages in this regard; but there are some limitations such as reduction in visible area [5] once the cameras are focused to obtain a closer view of an object as shown in Figure 3. This gets worse when there are moving objects in the surrounding area. There may be possible collisions due to blank angles and hence necessity of a continuous environmental awareness system arises.

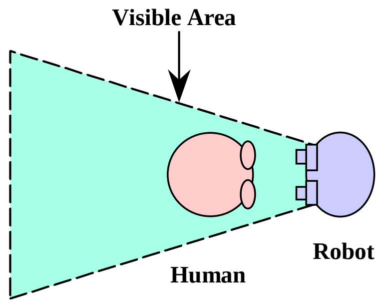

Figure 3: Limitation of visibility

There are platforms that estimate relevant quantities in the vicinity formed by combining information from multiple distributed sensors. For an example, robots in a team estimate their relative configuration by combining the angular measurements obtained from all of the ominidirectional images and performing triangulation operation as described by Spletzer et al. [6]. There are other variants such as the system proposed by Gurinaldo et al. [7] for controlling the perceptual process of two cooperative non holonomic mobile robots by formalism called perceptual anchoring. Their system enhances the awareness of the system by employing an anchor based active gaze control strategy to control the perceptual effort according to what is important at a given time. But such a system is of little use or not adequate for the robots whose main intention is to interact with humans. The situation gets critical, when such robots require to interact with a human while in motion. To place other robot units in the vicinity just to obtain an idea of the surrounding will be redundant and expensive. According to Splitzer et al. [6], questions of the quality and of how informative the gathered data are also arise, because they are obtained from individual robot units (sensors). In addition, there may be other issues like how the robot units (sensors) should be deployed in order to maximize the quality of the estimates returned by the team, because the robot platforms are mobile.

On the other hand, a different set of questions arises when one considers the problem of integrating information from a number of fixed distributed sensors such as cameras. Cost associated with transmitting and processing data, sensors that should be used to form an estimation for a given time, coordination among the sensors, automatically relating events among each other, sensor geometry, effects due to characteristic differences, etc. are some of the problems to be solved. In multiple video streams generated by multiple distributed cameras, finding correspondence is the key issue as observed in Lee et al. [8]. Hence a newer, simpler yet versatile localization and tracking system is required.

3.1 Networking

It should be possible to recruit such ubiquitous robots covering a large area. Hence to combine information gathered by one robot as well as to seek information / instruction, effective and convenient communication medium is required. In other words, these robots, while in motion, should be able to interconnect easily to a computer network as shown in Figure 4. Here the central unit with overhead camera monitors the environment continuously. Shapes of the various objects, positions at time to time, direction of motion, velocities, etc. are observed. These data is distributed among the ubiquitous robots in the surrounding area. In addition to the above, the central unit gathers the information send by these robots and sends to the respective recipients.

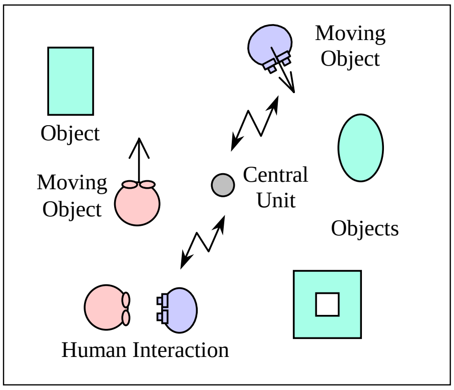

Figure 4: Interconnection of robots

3.2 Bluetooth Technology

In order to achieve the above mentioned communication, Bluetooth wireless technology, which facilitates an electronic equipment to make its own connections without wires, cables or any direct human intervention, will be very useful [9]. This type of a system will facilitate connection and synchronization; it will control the other electronic devices such as computers, printers, cell phones, PDA, televisions, alarm systems and telephone systems. These are the equipment developed by more than 1200 companies worldwide who represent the Bluetooth Special Interest Group including the giant leaders in the Electronic / Computer Industry like Ericson, IBM, Intel, Nokia, Toshiba, 3COM, Microsoft, Motorola, etc. [10]. All of these communications can take place in an ad hoc manner, without being aware and totally automatically. This gives the robots the freedom of appearing anywhere, any time and in any way very effectively.

4 Summary

It is difficult to design a human like robot in a ubiquitous environment that caters for interaction of any kind at the first instance. This research project tries to tackle such difficulties by manipulating some of the effective systems in a more realistic way. The approach is focused on the designing of a more human like robot while allowing services of many other systems at the same time. Here it tries to manipulate the services, capabilities and advantages of other existing systems as they are without any changes or with minimum alterations if required. But more complex interaction, will alternatively complicate the interface in return. This may make obtaining the so called 'Ubiquitous' more difficult. In the first instance, interaction may not provide the full facilities and functionalities such as two humans in conversation or in manipulating a task. But more general approach now will be available for a greater diversity of interactions to be managed in a later stage.

References

[1] T. Brown, *Stereoscopic phenomena of light and sight: A Guide to the Practice of Stereoscopic Photography and its Relations to Binocular Vision*, Reel Three-D Enterprises Publications, 1994.

[2] E. Paulos and J. Canny, "Space browsers: A tool for ubiquitous tele-embodiment," in *Proc. of International Conference on Computer Graphics and Interactive Techniques (SIGGRAPH)*, Digital Bayou 1996.

http://www.siggraph.org/conferences/siggraph96/core/conference/bayou/26.html

[3] E. Paulos and J. Canny, "Delivering real reality to the world wide web via telerobotics," in *Proc. of IEEE International Conference on Robotics and Automation*, vol. 2, 22–28 April 1996, pp. 1694 – 1699, 1996.

[4] D. Schulz, W. Burgard, A. B. Cremers, D. Fox, and S. Thrun, "Web interfaces for mobile robots in public places," *IEEE Robotics and Automation Magazine*, vol. 7, no. 1, pp. 48–56, March 2000.

[5] D. J. Coomb, "Real time gaze holding in binocular robot vision," *Technical Report, University of Rochester*, Dept. of Computer Science, 1992.

[6] J. Spletzer and C. J. Taylor, "Sensor planning and control in a dynamic environment," in *Proc. of IEEE International Conference on Robotics and Automation (ICRA '02)*, vol. 1, pp. 676–681, May 2002.

[7] S. A. Gurinaldo, K. Watanabe, and K. Izumi, "Enhancing awareness in cooperative robots through perceptual anchoring," in *Proc. of the 9th International Symposium on Artificial Life and Robotics (AROB)*, vol. 2, pp. 523–526, January 2004.

[8] L. Lee, R. Romano, and G. Stein, "Monitoring activities from multiple video streams: Establishing a common coordinate frame," *IEEE Trans. on Pattern Analysis and Machine Intelligence*, vol. 22, no. 8, pp. 758–767, Aug. 2000.

[9] M. Miller, *Discovering Bluetooth*, Sybex Inc. Publications, 2001.

[10] B. R. Miller and C. Bisdikian, *Bluetooth Revealed: The Insider's Guide to an Open Specification for Global Wireless Communication*, 2nd Edition, Prentice Hall, 2001.

[11] C. Stauffer and W. E. L. Grimson, "Learning patterns of activity using real-time tracking," *IEEE Trans. on Pattern Analysis and Machine Intelligence*, vol. 22, no. 8, pp. 747–757, Aug. 2000.

[12] T. B. Sheridan, *Telerobotics, Automation and Human Supervisory Control*, MIT Press, 1992.

[13] H. Monson, "Bluetooth Technology and Implications," *System Optimization Information Article*, December 14, 1999.

(http://www.sysopt.com/articles/bluetooth/)

[14] http://www.bluetooth.com/news/dex.asp?A=2&PID=1192

[15] http://www.open.ac.uk/oubs-future/Millennium/ 636.htm

The Tenth International Symposium on Artificial Life and Robotics 2005(AROB 10th '05),
B-con Plaza, Beppu, Oita, Japan, February 4-6, 2005

Fuzzy Coach Player Method with Shared Environmental Data

Kiyotaka Izumi, Keigo Watanabe, Yuya Tamano, and Ayumu Oshima
Dept. of Advanced Systems Control Engineering,
Graduate School of Science and Engineering, Saga University,
1-Honjomachi, Saga 840-8502, Japan

Abstract

In recent years, voice is used as an interface between human and robot or computer. An interface between human and robot, based on a fuzzy coach player method, is discussed in this paper. The concept of a coach player method comes from the training of athlete with his/her coach. In general, the coach teaches a skill for the athlete by speech with fuzziness. Therefore, authors propose a fuzzy coach player method so as to reflect a fuzzy voice command. Some simple examples are shown by experiments on a robot manipulator.

1 Introduction

In general, speech or voice is used as a major communication method between humans. Now, we are considering with teaching using voice for robots, because the communication by voice has several advantages. As for the advantages that one uses voice to an interface, it is easily pointed out that 1) there are few burdens to users because we need not necessarily remember the special knowledge and operations on input devices such as keyboards and mouse; 2) it is an available interface to the man who has a handicap in hand and foot, old people, and the man whose both hands are closed by some manual operation; and 3) since it is a sociable interface ordinarily utilized by human beings, we can have an attached heart to a controlled object.

From the above backgrounds, attention has gathered also in the research of a robot control by voice commands [1]~[4]. However, in the conventional research of a robot control by voice, it is difficult to apply for an actual task, because a user has to command by voice repeatedly with observing carefully the robot motion. In other words, a user provides many voice commands to the robot to perform an actual task.

In this paper, in order to achieve a cooperating between human and robot, we construct a voice interface with a fuzzy coach player method using shared environmental data. The effectiveness of the present method is illustrated through some simple experiments.

2 Fuzzy Coach Player Method

In order to smoothly realize a cooperative operation or work between a human and a robot, some intelligent exchanges need to be found between them. In particular, when a human issues "an operation command" through a natural spoken-language command to a robot, an ambiguous (or fuzzy) expression is always contained in the human conversation. Through the exchange of the knowledge of a human and a robot, especially through operator's voice commands and the observation of robot behaviors, a series of actions in which an operator makes a robot realize a desired behavior or motion is similar to the relation between a coach and a player who are doing the coaching of skill acquisition and performance improvement.

In this case, the following three points should be noted:

1. *Intention understanding* : A player incorporates the "command" well according to his performance state and posture, and reflects it on acquiring of skill or improving of performance, in spite of containing ambiguous expressions in an advice to the player by the coach voice.

2. *Evaluation of the player by the coach* : On the other hand, from the aspect of a coach, the coach judges subjectively whether performance, as the image which the coach has, and skill acquisition have been attained by the player, and decides whether to issue the following improvement command.

3. *Improvement of the motion skill by the player itself*: The player itself does not only blindly response to the spoken-language command from a coach; rather he usually improves his performance etc. so that the former effort (or action) result is employed more efficiently. Furthermore, he has an ability of accumulating the knowledge that can realize a more efficient performance by him, using sometimes reading of coach intent from a simple voice command.

2.1 Constructing a fuzzy coach player model

2.1.1 Interpretation of "fuzzy indication" from a coach

The voice indication of a coach is based on his experiences and consists of action (verb) plus action modification (adverb) or repetition of action.

2.1.2 Subjective evaluation of a coach

After giving a voice indication, a confirmation (through a direct observation or indirect observation) is performed on the motion of a player and the subjective evaluation based on the past experience of a coach is performed to the motion of the player. For example, an index of degree-of-satisfaction of the coach is introduced.

2.1.3 Improvement commands after evaluation

If the player motion is satisfactory based on the coach data-base, then any further improvement commands are not given to the motion. Otherwise, a further improvement command should be provided.

2.1.4 Introduction of a sub-coach

We consider the introduction of a virtual sub-coach who can support the role of a coach and reduce the load of the coach, by using a data-base composed of various intelligent information that could be acquired from the indirect vision through any display and camera and the voice uttered from the coach, i.e., using a set of sequential data composed of the subjective evaluation and the improvement command to the player. After the sub-coach obtains the behavior and intelligence of the coach by any way, the sub-coach (i.e., computer) and the coach (i.e., operator) control a robot in a cooperative manner.

2.1.5 Autonomous action modification of player

If there exist multiple commands of action modification from the coach, or repetition of the same commands, then it may be need to set a function that can suddenly increase or decrease the amount of the action modification, which is normally based on the current state of the player. Namely, by predicting the irritation of the coach, we need to make a function that can cope with a more action modification than the usual increment (or reduction) for the next step.

2.2 Representation of a relationship between the coach voice indication and the operation input

In the framework of a conventional robot control, it needs to control the joint position and velocity of the robot (or the end-effector position and orientation) using the joint input torques, or to control the velocity of the end-effector position and orientation using the joint input velocities.

On the contrary, in the fuzzy coach player system, it needs to find the followings: For example, the control inputs for a manipulator consist of motion indication commands that are very vague and are composed of a verb and adverb (or multiple adverbs, or adverb phrase), such as "move more quickly," "move to the right more slowly," "lower an elbow more and move," "move as it is," etc., which are different from the conventional input torques that are taken within a real-number region.

Therefore, let the input sequence of a fuzzy human voice indication from a microphone at time k be $v(k) \in \mathcal{V}$, and the $v(k)$ passed through a speech recognizer is assumed to be split into the language variable $v_a(k) \in \mathcal{V}$, which is not necessary for the action indication, the verb $v_b(k) \in \mathcal{V}$, and the adverb (or adverb phrase) $v_{ab}(k) \in \mathcal{V}$,

$$v(k) = v_a(k) + v_b(k) + v_{ab}(k)$$

where $\mathcal{V}$ denotes the voice space that is a time-series of signal or character level. A fuzzy NN is used to generate a desired velocity command $\boldsymbol{u}(k) \in \Re^m$ (or torque command $\boldsymbol{\tau}(k) \in \Re^m$) to the robot, from the effective action indication language variables $v_b(k)$ and $v_{ab}(k)$.

For example, we consider the method of changing multiple action FNNs. In this method, an action i is selected and switched out of N action modules, according to the consistence with the current pseudo sentence such as

$$\boldsymbol{u}(k) = \sum_{i=1}^{N} \phi_i(v_b(k), v_{ab}(k)) FNN_i(s_i(k), v_{ab}(k))$$

where $FNN_i(\cdot) : \Re \times \Re \mapsto \Re^m$ and it is assumed that

$$\phi_i = \begin{cases} 1 & \text{if } \{v_b(k), v_{ab}(k)\} \text{ is consistent with } i\text{-th action} \\ 0 & \text{otherwise} \end{cases}$$

Note here that if there exists no inconsistence between the action and the action modification languages in the voice command uttered from a coach, then the above judgment of $\phi_i(k)$ can be implemented by only using the information of $v_b(k)$.

2.3 Observation of robot state

Considering the general dynamical model of a robot, it follows that

$$\boldsymbol{f}(\ddot{\boldsymbol{q}}(t), \boldsymbol{q}(t), \boldsymbol{q}(t)) = \boldsymbol{\tau}(t)$$

where $\boldsymbol{q}(t) \in \Re^n$ is the generalized coordinate vector and $\boldsymbol{f}(\cdot) : \Re^n \times \Re^n \times \Re^n \mapsto \Re^m$ is a vector-valued function representing the robot dynamics. Instead of measuring the joint angles and velocities as the robot states, the coach (i.e., operator) generally observes the velocity of the end-effector or the elbow that is the overall and ambiguous information for the state and orientation of the robot. Therefore, it is assumed that

$$\boldsymbol{z}_h(k) = M_d(\dot{\boldsymbol{q}}(k), \boldsymbol{q}(k))$$

for the observation of the robot state through direct human eyes and

$$\boldsymbol{z}_{id}(k) = M_{id}(\dot{\boldsymbol{q}}(k), \boldsymbol{q}(k))$$

for the displayed information of the robot, respectively, where $\boldsymbol{z}_h(k), \boldsymbol{z}_{id}(k) \in \Re^p$ and $M_d(\cdot), M_{id}(\cdot) : \Re^n \times \Re^n \mapsto \Re^p$. Moreover, the observation through human eyes for the displayed information is assumed to be

$$\boldsymbol{z}_{hd}(k) = M_{hd}(\dot{\boldsymbol{q}}(k), \boldsymbol{q}(k))$$

where $\boldsymbol{z}_{hd}(k) \in \Re^p$ and $M_{hd}(\cdot) : \Re^n \times \Re^n \mapsto \Re^p$.

For example, if we focus on the motions of the end-effector and the elbow for a robot manipulator with seven-degrees-of-freedom, then we can set $p = 6$ and $\boldsymbol{z}_h(t) = [\boldsymbol{z}_{htip}^T \quad \boldsymbol{z}_{helb}^T]^T$, where the first three-dimensional vector $\boldsymbol{z}_{htip} = [z_{1htip} \quad z_{2htip} \quad z_{3htip}]^T$ denotes each subjective and fuzzy (interpretation) variable for the position, velocity and orientation of the end-effector (e.g., the position is almost good; the velocity is a little late; and the orientation is generally good) and the latter three-dimensional vector $\boldsymbol{z}_{helb} = [z_{1helb} \quad z_{2helb} \quad z_{3helb}]^T$ similarly denotes the information of the elbow. In addition, observation vectors $\boldsymbol{z}_{id}(t)$ and $\boldsymbol{z}_{hd}(t)$ are defined similarly.

2.4 Generation of voice commands for the next step operation through a human subjective evaluation

After observing the fuzzy position, velocity and orientation of the robot end-effector and elbow through direct eyes or display, and evaluating such a motion with the subjective criterion of the coach, the voice command $v(t)$ for the next step operation is assumed to be generated by

$$v(k) = BF(\boldsymbol{z}_h(k)) \text{ or } v(k) = BF(\boldsymbol{z}_{hd}(k))$$

where $BF(\cdot) : \Re^p \mapsto \mathcal{V}$ is a criterion, for realizing a desired robot motion, in which the coach (or human) has been assumed to have it in advance.

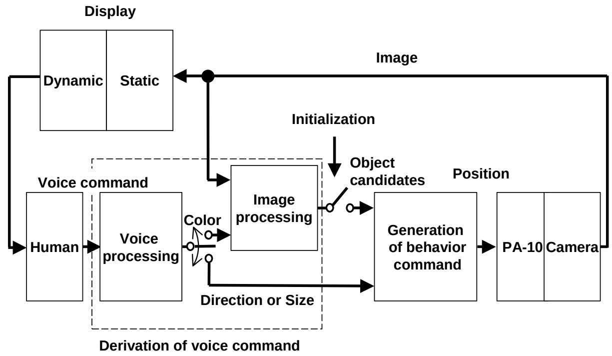

Figure 1: Example of fuzzy coach-player model with shared environmental data

3 Example of Fuzzy Coach Player System

The construction of proposed voice interface with vision is shown in Fig. 1. The proposed system is constructed with the derivation part of object candidates and the generation part of behavior command. At first, a user command by voice is given for object's color at first. The environmental data is initialized with each geometric center of object candidates and the commanded color. The initial object is determined as the object which has minimum distance between the initial position of manipulator's tip and the geometric center of the object. Next, if a user command is given for direction, then the derivation part of object candidates outputs the commanded direction to the generation part of behavior command. Finally, the generation part of behavior command provides the reference point of the manipulator's tip in the world coordinate depending on direction command and the environmental data.

The derivation part of object candidates is constructed with the voice processing part and the image processing part. The voice processing part is constructed with the voice recognition process, the morphology analysis and the pattern matching. The image processing creates the environmental data for the generation part of behavior command. The image process is carried out at initial stage or at changing the color of the object. The derivation part of object candidates outputs the command or the environmental data.

Derivation part of behavioral command provides a reference point of the manipulator using all geometric centers of object candidates and the voice command related to the direction or size. A user observes the working environment by this image in which the left image is a movie in the current working environment and the right image is the static image when the system was started. As shown in Fig. 2, when a user commands "red", right image shows +

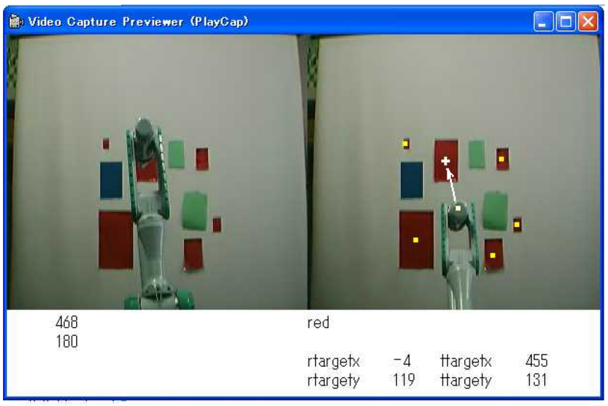

Figure 2: Initial movement with voice command "red"

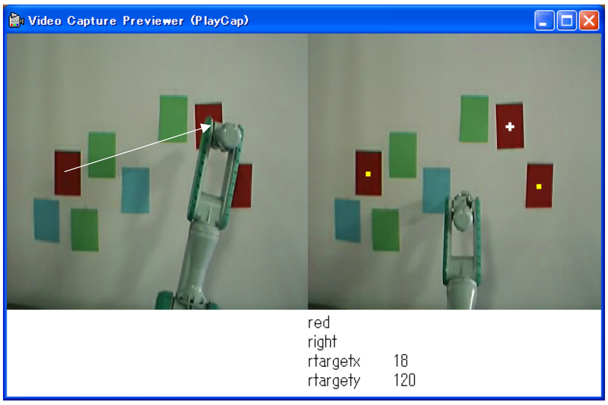

Figure 3: Result of voice command "move right"

or □ on each geometric center of red colored objects, where + means the target object, whereas □ means the red colored objects except for the target object. A user can observe the command and the position of the target object at the image coordinate through the bottom area of the image. It is found from Fig. 2 that the manipulator moves to the target object. The user confirms the desired object from + position in the right image and the displayed data at the bottom area as shown in Fig. 2. Next, when the user commands "move to left", the target object is changed, and the robot move to the left side target. When the user commands "move to up and small object", it is found from Fig. 3 that the user can perform the same fact as stated in Fig. 2. Finally, the user commands "move to smaller object" after completing the Fig. 3. The user selects a new target object on the manipulator's way to the former target object. The user can check the change of the target object in the right image and the movement of the manipulator in the left movie, as shown in Fig. 4.

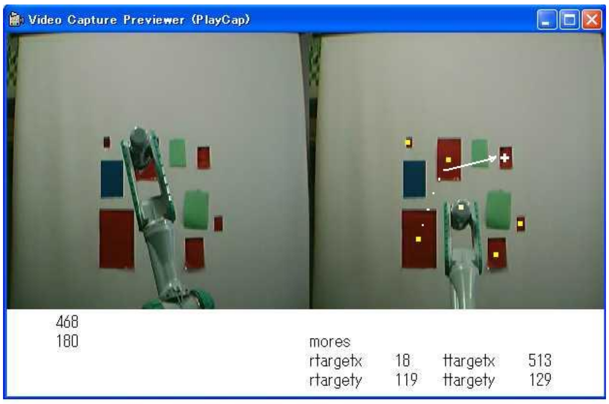

Figure 4: Result of voice command "a little small"

4 Conclusions

The concept of a fuzzy coach player method is discussed to smoothly realize a cooperative operation or work between a human and a robot, some intelligent exchanges need to be found between them. The environmental data is shared with image view to understand easy a robot movement. Simple experiment is carried out, so that it was easy to change the robot movement by voice command at any time.

References

[1] K. Komiya, K. Moita, K. Kakegawa, and K. Kurosu, "Guidance of a Wheelchair by Voice," *Proc. of IECON'2000*, pp. 102–107, 2000.

[2] K. Pulasinghe, K. Watanabe, K. Kiguchi, and K. Izumi, "A Novel Modular Fuzzy Neural Controller Driven by Natural Language Commands," *Proc. of the 40th SICE Annual Conference (SICE2001), Int. Session Papers*, 312C-4, 2001.

[3] K. Pulasinghe, K. Watanabe, K. Kiguchi and K. Izumi, "Modular Fuzzy Neural Controller Driven by Voice Commands," *Proc. of ICCAS2001*, pp. 194–197, 2001.

[4] C.T. Lin and M.C. Kan, "Adaptive Fuzzy Command Acquisition with Reinforcement Learning," *IEEE Trans. on Fuzzy Systems*, Vol. 6, No. 1, pp. 102–121, 1998.

Cost Function Analysis of Optimizing Fuzzy Energy Regions in Control of Underactuated Manipulators

Kiyotaka Izumi, Keisuke Ichida, and Keigo Watanabe
Dept. of Advanced Systems Control Engineering,
Graduate School of Science and Engineering, Saga University,
1-Honjomachi, Saga 840-8502, Japan

Abstract

Underactuated manipulators have to be controlled by following a restricted way that the number of actuators is less than the number of generalized coordinates, because they have some passive joints.

In this paper, we propose a logic based switching mechanism using fuzzy energy region. Boundary curves to separate an energy region into some energy subregions are constructed by fuzzy reasoning. Therefore, fuzzy related parameters are optimized by genetic algorithm (GA). The present method is applied to an underactuated system with drift term such as an 2-DOF planar manipulator which has only one active joint. The effectiveness of the present method is illustrated with some simulations.

1 Introduction

Control of underactuated manipulators is an attractive research theme in robotics because of complex behaviors and difficulty of control [1, 2, 3]. Since underactuated manipulators have some passive joints, their energy efficiency can be better than full actuated manipulators.

As a control method for underactuated systems, authors have already proposed a switching control, in which some partly stable controllers were designed by computed torque method and the switching low was obtained as the index of controller directly by fuzzy reasoning [4]. The switching control is proposed to design simply a control low without any complex variable transformation for underactuated manipulators. The switching low is a key-point to obtain sufficient results in this method. A logic based switching method using energy regions [5] is also proposed for a nonholonomic system without drift term.

In this paper, we propose a logic based switching mechanism using fuzzy energy region. Boundary curves to separate an energy region into some energy subregions are constructed by fuzzy reasoning. Fuzzy related parameters and control gains of the partly stable controllers are optimized by genetic algorithm (GA). We prepare some cost functions of GA. The present method is applied to an underactuated system with drift term such as an 2-DOF planar manipulator which has only one active joint. The effectiveness of the present method is illustrated with some simulations.

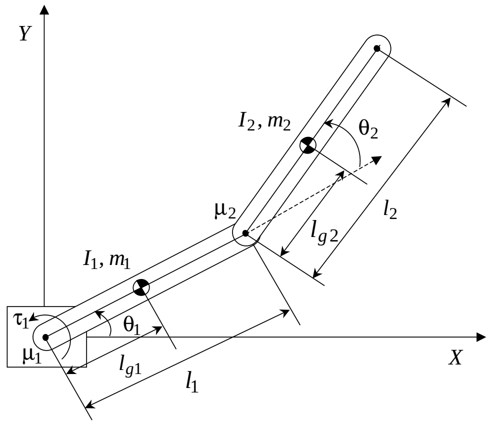

Figure 1: Model of 2-link underactuated manipulator

2 Underactuated Manipulator

Figure 1 shows a two-link underactuated manipulator, in which the second joint is constructed of a passive joint. Here, τ_1 denotes the applying torque of 1st joint, θ_i denotes the angle of ith link, m_i denotes the mass of ith link, l_{gi} denotes the distance from the joint to the center of mass of ith link, I_i denotes the moment of inertia of ith link, and μ_i denotes the coefficient of viscous friction. The dynamical model of the underactuated manipulator is given as follows:

$$M(\boldsymbol{\theta})\ddot{\boldsymbol{\theta}} + \boldsymbol{h}\left(\boldsymbol{\theta},\ \dot{\boldsymbol{\theta}}\right) = \boldsymbol{\tau} \qquad (1)$$

where

$$\begin{aligned} \boldsymbol{\theta} &= [\theta_1\ \ \theta_2]^T \\ \boldsymbol{\tau} &= [\tau_1\ \ 0]^T \end{aligned}$$

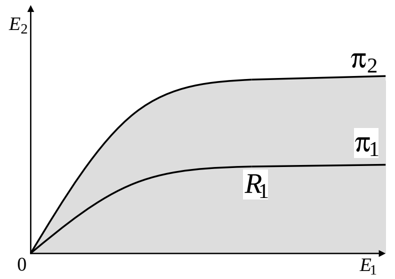

(a)

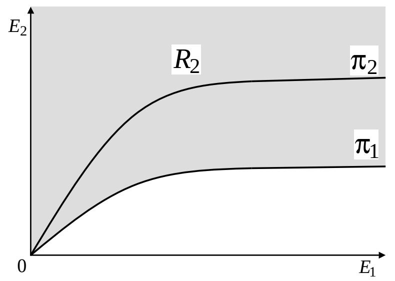

(b)

Figure 2: Subregions of energy

$$
\begin{aligned}
M(\boldsymbol{\theta}) &= \begin{bmatrix} M_{11}(\boldsymbol{\theta}) & M_{12}(\boldsymbol{\theta}) \\ M_{12}(\boldsymbol{\theta}) & M_{22}(\boldsymbol{\theta}) \end{bmatrix} \\
M_{11}(\boldsymbol{\theta}) &= (m_1 l_{g2}^2 + m_2 l_1^2 + I_1) + (m_2 l_{g2}^2 + I_2) \\
&\quad + 2 m_2 l_1 l_{g2} \cos\theta_2 \\
M_{12}(\boldsymbol{\theta}) &= (m_2 l_{g2}^2 + I_2) + m_2 l_1 l_{g2} \cos\theta_2 \\
M_{22}(\boldsymbol{\theta}) &= m_2 l_{g2}^2 + I_2 \\
\boldsymbol{h}\left(\boldsymbol{\theta},\, \dot{\boldsymbol{\theta}}\right) &= \left[h_1\left(\boldsymbol{\theta},\, \dot{\boldsymbol{\theta}}\right)\ h_2\left(\boldsymbol{\theta},\, \dot{\boldsymbol{\theta}}\right)\right]^T \\
h_1\left(\boldsymbol{\theta},\, \dot{\boldsymbol{\theta}}\right) &= -(m_2 l_1 l_{g2})(2\dot{\theta}_1\dot{\theta}_2 + \dot{\theta}_2^2)\sin\theta_2 + \mu_1\dot{\theta}_1 \\
h_2\left(\boldsymbol{\theta},\, \dot{\boldsymbol{\theta}}\right) &= m_2 l_1 l_{g2}\dot{\theta}_1^2 \sin\theta_2 + \mu_2\dot{\theta}_2
\end{aligned}
$$

3 Fuzzy Region Based Switching Control

3.1 Partly stable controller

Equation (1) can be described by

$$
\begin{aligned}
\ddot{\theta}_1 &= -\frac{M_{22}(\boldsymbol{\theta})}{D} h_1\left(\boldsymbol{\theta},\, \dot{\boldsymbol{\theta}}\right) + \frac{M_{12}(\boldsymbol{\theta})}{D} h_2\left(\boldsymbol{\theta},\, \dot{\boldsymbol{\theta}}\right) \\
&\quad + \frac{M_{22}(\boldsymbol{\theta})}{D}\tau_1 \qquad (2) \\
\ddot{\theta}_2 &= \frac{M_{12}(\boldsymbol{\theta})}{D} h_1\left(\boldsymbol{\theta},\, \dot{\boldsymbol{\theta}}\right) - \frac{M_{11}(\boldsymbol{\theta})}{D} h_2\left(\boldsymbol{\theta},\, \dot{\boldsymbol{\theta}}\right)
\end{aligned}
$$

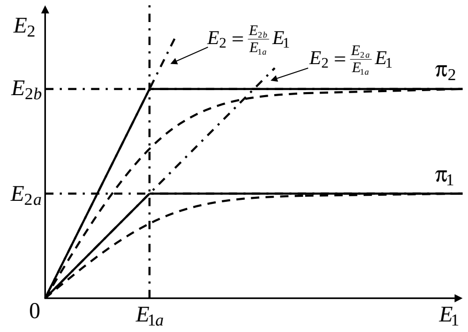

Figure 3: Approximation of regions for a logical switching

$$
-\frac{M_{12}(\boldsymbol{\theta})}{D}\tau_1 \qquad (3)
$$

where

$$
D = M_{11}(\boldsymbol{\theta}) M_{22}(\boldsymbol{\theta}) - M_{12}^2(\boldsymbol{\theta})
$$

Here, it is found that we can design partly stable controllers for link 1 and link 2 using the computed torque method. The controller 1 to stabilize the link 1 is given by

$$
\begin{aligned}
\tau_1 &= \frac{D}{M_{22}(\boldsymbol{\theta})}\left(\ddot{\theta}_1^* + \frac{M_{22}(\boldsymbol{\theta})}{D} h_1\left(\boldsymbol{\theta},\, \dot{\boldsymbol{\theta}}\right)\right. \\
&\quad \left. - \frac{M_{12}(\boldsymbol{\theta})}{D} h_2\left(\boldsymbol{\theta},\, \dot{\boldsymbol{\theta}}\right)\right) \qquad (4) \\
\ddot{\theta}_1^* &= \ddot{\theta}_{d1} + K_{v1}\left(\dot{\theta}_{d1} - \dot{\theta}_1\right) + K_{p1}(\theta_{d1} - \theta_1)
\end{aligned}
$$

and the controller 2 to stabilize the link 2 is given by

$$
\begin{aligned}
\tau_1 &= -\frac{D}{M_{12}(\boldsymbol{\theta})}\left(\ddot{\theta}_2^* - \frac{M_{12}(\boldsymbol{\theta})}{D} h_1\left(\boldsymbol{\theta},\, \dot{\boldsymbol{\theta}}\right)\right. \\
&\quad \left. + \frac{M_{11}(\boldsymbol{\theta})}{D} h_2\left(\boldsymbol{\theta},\, \dot{\boldsymbol{\theta}}\right)\right) \qquad (5) \\
\ddot{\theta}_2^* &= \ddot{\theta}_{d2} + K_{v2}\left(\dot{\theta}_{d2} - \dot{\theta}_2\right) + K_{p2}(\theta_{d2} - \theta_2)
\end{aligned}
$$

where the desired vector of $\boldsymbol{\theta}$ is defined as $\boldsymbol{\theta}_d = [\theta_{d1}\ \ \theta_{d2}]^T$, in which the proportional gain of the controller i is K_{pi} and the derivative gain of the controller i is K_{vi}.

3.2 Logic based switching method

Energy of each link is defined by

$$
E_i \triangleq e_i^2 + \dot{e}_i^2, \quad i = 1,\ 2 \qquad (6)
$$

with

$$
\begin{aligned}
e_i &= \theta_{di} - \theta_i \\
\dot{e}_i &= \dot{\theta}_{di} - \dot{\theta}_i
\end{aligned}
$$

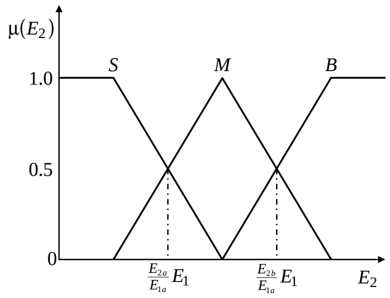

Figure 4: Membership functions for $E_1 \leq E_{1a}$

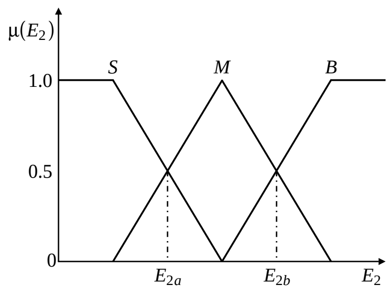

Figure 5: Membership functions for $E_1 > E_{1a}$

Energy plane is composed of E_i as shown in Fig. 2. In Fig. 2, π_i is a boundary curve which determines the subregion of energy to use a partly stable controller, and is plotted by an exponential curve. The region R_i with gray shadow is the subregion to which the controller i is applied.

3.3 Fuzzy energy region method

If a boundary curve comprises an exponential function, we can suitably design it with the amplitude and the time constant of a step-response. It is difficult to design such parameters of the function in advance, because we can't theoretically analyze them depending on the switching control. Therefore, we propose a fuzzy energy region based switching control method. At first, boundary curves are approximated by several straight-lines as shown in Fig. 3. After these approximations, fuzzy sets for E_2 can be defined for $E_1 \leq E_{1a}$ and $E_1 > E_{1a}$ cases as shown in Fig. 4 and Fig. 5. E_{1a}, E_{2a} and E_{2b} are design parameters of fuzzy sets. In order to realize ideal energy responses, fuzzy rules are given as follows:

Rule 1	:	If $E_2 = S$	Then $s_1 = 1$	
Rule 2	:	If $E_2 = M$	and $\phi_{t-1} = 1$	Then $s_2 = 1$
Rule 3	:	If $E_2 = M$	and $\phi_{t-1} = 2$	Then $s_3 = 2$
Rule 4	:	If $E_2 = B$	Then $s_4 = 2$	

Table 1: GA operations and methods

GA operations	Method
Selection for crossover	Tournament strategy with 3 individuals
Crossover	Uniform crossover with probability 0.6
Probability of mutation	1/96
Alternation	Elite strategy with 10 individuals

Table 2: Setting parameters of simulations

Conditions	Setting value
Simulation time	30 [s]
Sampling interval	0.01 [s]
Mass of each link	$m_1 = 0.582$ [kg], $m_2 = 0.079$ [kg]
Length of each link	$l_1 = 0.4$ [m], $l_2 = 0.22$ [m]
Distance between center of gravity and each joint	$l_{g1} = 0.2$ [m] $l_{g2} = 0.11$ [m]
Coefficient of viscous friction of each joint	$\mu_1 = 0$ [Ns/m^2] $\mu_2 = 0.02$ [Ns/m^2]
Desired state vector	$[0\ 0\ 0\ 0]^T$
1st initial state vector	$[0\ \pi/4\ 0\ 0]^T$
2nd initial state vector	$[\pi\ \pi/6\ 0\ 0]^T$

Note that, a parameter ϕ_{t-1} which means the index of controller for one-step delay, is introduced, because one-step delayed controller must be retained in the overlapped energy region according to ideal energy response. s_i is the index of controller that must be used in the fuzzy rule i.

The advantage of the present method is to set design parameters roughly, comparing to the logic based switching method, because the boundary curves have fuzziness to use the present fuzzy reasoning.

4 Optimizing Fuzzy Energy Regions by GA

The present method has the same difficulty to design parameters in advance as the logic based switching method. Here, we discuss about the design parameters of fuzzy rules using GA. These parameters are E_{1a}, E_{2a}, E_{2b}, K_{p1}, K_{v1}, K_{p2} and K_{v2}. Each parameter is encoded by 32 [bit], then the size of an individual is 224 [bit]. The searching domain of E_{1a}, E_{2a} and E_{2b} is set from 0.1 to 15. The searching domain of K_{pi} and K_{vi}, $i = 1, 2$ is set from 0.01 to 100. Each parameter is decoded using gray code. The size of a population is 100. The maximum number of generations is 1000. GA operations used here are shown in Table 1.

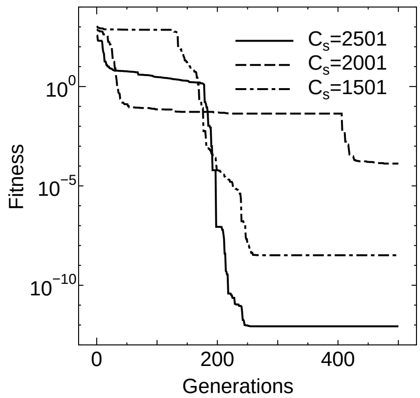

Figure 6: Optimizing history of cost functions

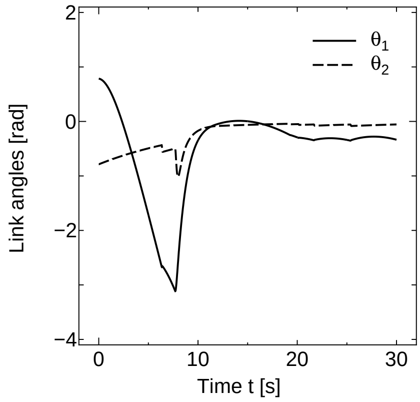

Figure 7: Simulation result with untrained initial value

Table 3: Obtained design parameters of fuzzy energy region method

	C_s = 2501	C_s = 2001	C_s = 1501
E_{1a}	11.5097	12.6989	14.0461
E_{2a}	0.2906	0.2978	1.0417
E_{2b}	12.4336	14.9812	8.1119
K_{p1}	10.5593	5.2048	10.4885
K_{v1}	11.5647	5.7413	11.0411
K_{p2}	5.2400	2.6096	24.2865
K_{v2}	56.3331	50.7481	4.0119

A cost function is given by

$$f_c = \sum_{i=1}^{2} \sum_{j=C_s}^{3000} \sum_{k=1}^{2} E_k(j) \tag{7}$$

where i is the index of simulation trials, j is the index of discrete times, k is the index of energy of each link and C_s is the starting index of discrete time to evaluate the response of an underactuated manipulator. Simulation conditions to train fuzzy parameters are shown in Table 2. Note that, the fitness function is not evaluated during a transition segment due to the dynamic characteristics of an underactuated system.

Training history in cost function is shown in Fig. 6. It is found from Fig. 6 that the case of $C_s = 2501$ is smaller than other cases. Obtained parameters are shown in Table 3. The obtained parameters in the case of $C_s = 2501$ are applied to the cases of untrained initial state vectors such as $\boldsymbol{\theta}(0) = [\pi/4 \ \ -\pi/4 \ 0 \ 0]^T$. Response of link angles is shown by Fig. 7. The small steady state error is found in θ_1 from Fig. 7. Differential gain of partly stable controllers is high, so that a response has such error.

5 Conclusions

We have proposed a logic based switching method using fuzzy energy region, in which fuzzy design parameters and gains of partly stable controllers were trained by genetic algorithm. A cost function was tried to use in optimizing parameters. Obtained differential gains are a little bit high, so that a simulation result using untrained initial states has a steady state error. However, each link converges near the desired value.

References

[1] Y. Nakamura, T. Suzuki, and M. Koinuma, "Nonlinear behavior and control of a nonholonomic free-joint manipulator," *IEEE Trans. on Robotics and Automation*, vol. 13, no.6, pp. 853–862, 1997.

[2] H. Arai, K. Tanie, and N. Shiroma, "Nonholonomic control of a three-DOF planar underactuated manipulator," *IEEE Trans. on Robotics and Automation*, vol. 14, no. 5, pp. 681–695, 1998.

[3] I. Fantoni, R. Lozano, and M. W. Spong, "Energy based control of the pendubot," *IEEE Trans. on Automatic Control*, vol. 45, no. 4, pp. 725–729, 2000.

[4] L. Udawatta, K. Watanabe, K. Izumi, and K. Kiguchi, "Control of underactuated manipulators using fuzzy logic based switching controller," *J. of Intelligent and Robotic Systems*, vol. 38, pp. 155–173, 2003.

[5] J. P. Hespanha and A. S. Morse, "Stabilization of nonholonomic integrators via logic-based switching," *Automatica*, vol. 35, pp. 385–393, 1999.

The Hybrid SOF-PID Controller for a MIMO Biped Robot

Tae-Yong Choi and So-Yeon Park and Ju-Jang Lee
Electrical Engineering and Computer Science
Korea Advanced Institute of Science and Technology(KAIST)
373-1, Guseong-dong, Yuseong-gu, Daejeon, 305-701, Korea
ermzace@odyssey.kaist.ac.kr, arashi@odyssey.kaist.ac.kr, jjlee@ee.kaist.ac.kr

Abstract

The application of the hybrid Self-Organizing Fuzzy PID controller to a multi input multi output nonlinear biped robot is studied in this paper. The SOF-PID controller was initially studied by H. B. Kazemian on his papers, [1], [2] and etc. Actually his SOF-PID controller has limits. The supervisory of the SOF-PID controller can adjust only a kinds of parameters. So, In here the hybrid SOF-PID controller are introduced to tune some kinds of parameters and tested on a MIMO biped robot. In experiment the hybrid SOF-PID controller shows better performances than the SOF-PID.

Keywords : *self-organizing fuzzy, biped, pid controller.*

1 Introduction

Over the past few decades many industrial processes have been controlled using PID. Despite of extensive use of PID in conventional control problems, its performance in industrial application is limited. For instance in case of step input problem, it can't show the best performance. For fast response you must suffer bad overshoot property. Even if you succeeded in tuning PID gain to show fine overshoot and ripple you must have some steady state error. In this reason a few replacement algorithm were appeared but It is not necessary to discard an existing controller such as conventional PID, which works well and is already in operation with proper performance even if it is not best. Supervisory controller which can adopt the conventional PID controller is enough and can be good solution.

Kazemian studied the SOF-PID to adjust PID controller which is applied to complex nonlinear system and showed fine performances[1],[2],[3]. He tuned only proportional gains. For other gains of differential gains and Integral gains he used Ziegler-Nichols tuning method because only one kind of parameters, proportional gains, can be tuned using his method. So in here I will suggest the hybrid SOF-PID to adjust all three kinds of PID gains. Though the hybrid SOF-PID can tune all of three PID gains, in experiments actually proportional gains and differential gains are tuned because PD controller is enough to control nonlinear MIMO robot.

Section 2 describes the structure of SOF-PID controller suggested by Kazemian. Section 3 describes the structure of Hybrid SOF-PID controller. Section 4 explains the experimental results of MIMO Biped robot's trajectory following and compares the results with the SOF-PID. Finally Section 5 discusses and concludes the contribution of this work.

2 Basic structure of the SOF-PID controller

The block diagram of Fig.1 shows the basic structure of the SOF-PID controller. This diagram shows the SOF at a supervisory level readjusting the PID gains at an actuator level. An error from the actuator level is fed into the supervisory level to enable the SOF to analyse the process output. There is also an input from the PID controller block to the history of past states block via the PID input section to continuously fuzzify the values of the PID gains. Finally the SOF adjust the PID gains during operation and feeds the results from the output section block into the actuator block. Detail of the SOF block is followed.

- error input section : error and error change are defined as (1), (2) for each.

$$error(e_i) = setpoint(s_i) - system\ output(po_i) \quad (1)$$

$$error\ change(ce_i) = error(e_{i-1}) - error(e_i) \quad (2)$$

  where i is sampling instant. The fuzzification of the error and error change are also done in this block.

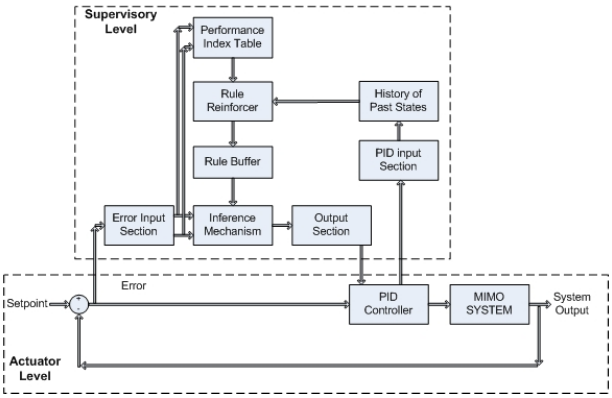

Figure 1: The SOF-PID Controller

- PID input section : The PID gains are fuzzified in this section

- Performance index table : The performance index table is designed as such that if no errors are happened, then no action is taken and the PID gain correction value P is equal to zero. If errors are happened. then PID gain correction P is chosen. Using the equations (1)and (2) a set of thirteen linguistic rules are produced, Table1, and from this a performance index table is obtained.

1. If E is NL and CE is NL or NM or NS then P is ZO.
2. If E is NL and CE is ZO or PS or PM or PL then P is NL.
3. If E is NM and CE is NL or NM or NS then P is ZO.
4. If E is NM and CE is ZO or PS or PM or PL then P is NM.
5. If E is NS and CE is NL or NM or NS then P is ZO.
6. If E is NS and CE is ZO or PS or PM or PL then P is NS.
7. If E is ZO and CE is NL or NM or NS or ZO or PS or PM or PL then P is ZO.
8. If E is PS and CE is NB or NM or NS or ZO then P is PS.
9. If E is PS and CE is PS or PM or PL then P is ZO.
10. If E is PM and CE is NB or NM or NS or ZO then P is PM.
11. If E is PM and CE is PS or PM or PL then P is ZO.
12. If E is PL and CE is NB or NM or NS or ZO then P is PL.
13. If E is PL and CE is PS or PM or PL then P is ZO.

Table 1: Linguistic rules of The SOF-PIDC

NL : -3 or -2.5, NM : -2 or -1.5, NS : -1 or -0.5
ZO : 0, PS : 0.5 or 1, PM : 1.5 or 2, PL : 2.5 or 3

- History of past states : A storage for the fuzzfied values of PID gains. These past states could be retrieved on the basis of first-in and first-out.

- Rule reinforcer : This block update the existing rules and to create new ones. If the PID gain correction P is zero from the performance index table, then no rule modification are taken. If P is not zero, then the rule modification is required for sampling instant i the following equations.

$$K_{Pl}(reinforcer) = K_{Pl-n[i]} + P \tag{3}$$

where i is the sampling instant, n represents number of samples before the present sample, and l is number of links or robot parameters. $K_{Pl-n[i]}$ is the fuzzified proportional PID gain from the history of past states block.

- rule base : The rule base contains all the appropriate PID gains to be used in the supervisory controller block. The rules are the exact control rule strategy which have been obtained from the learning section of the master controller.

- Inference mechanism : From this block output is produced by combining the e_i, ce_i and the rules from rule base block. Implication function and defuzzification take place in here.

- output section : The output section provides a non fuzzy input signal to be fed into the PID controller. In here the fuzzy signal is dequantised and descaled.

$$K_{P(after-apps)} = K_{P(before-apps)} + U_{Pi} \times K_1 \tag{4}$$
$$K_{D(after-apps)} = K_{D(before-apps)} + U_{Di} \times K_2 \tag{5}$$
$$K_{I(after-apps)} = K_{I(before-apps)} + U_{Ii} \times K_3 \tag{6}$$

where K_P, K_I, K_D represent the PID gains. The left is prior to changes by the supervisory level and the right is after the change taken place. K_1, K_2, K_3 are the descaled coefficients. U_{Pi}, U_{Di}, U_{Ii} are the output from supervisory controller block.

3 The structure of the hybrid SOF-PID controller

Basic structure of the hybrid SOF-PID controller is same as the SOF-PID controller except the hybrid structure to provide another PID gains, differential gains. In the previous work only proportional gains are provided by the SOF and U_{Di}, U_{Ii} is directly valued by Ziegler-Nichols tuning method : $U_{Di} = 2U_{Pi}/To, U_{Ii} = U_{Pi} \times To/8$, where To is the oscillation period. In the hybrid SOF-PID controller U_{Di} are also provided by the hybrid SOF with relation to U_{Pi}. I aimed to control a MIMO biped robot system and the PD controller is enough to control a biped robot. In this reason integral parameters aren't considered.

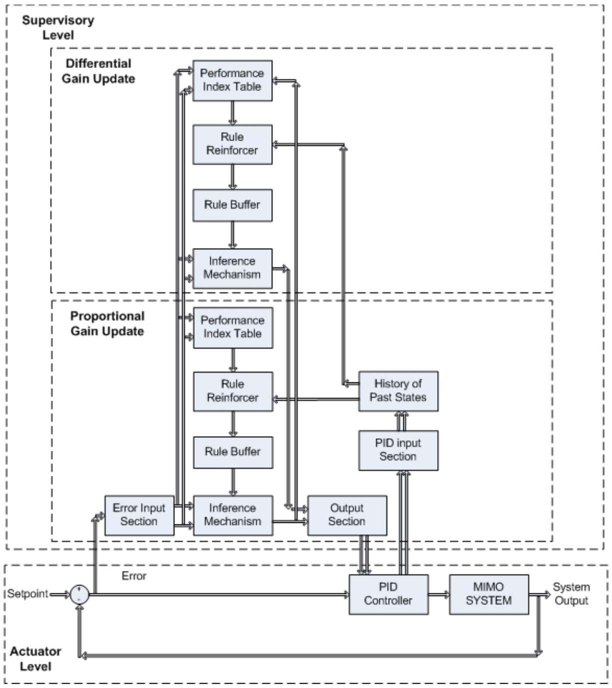

Figure 2: The Hybrid SOF-PID Controller

The detailed block diagram is shown in Fig2. The differential gain update part is for differential parameters of PID control. The different with proportional gain update part is that U_{Pi} is used to readjust U_{Di}. Linguistic rule is shown, Table2. The proposed controller aims to be used on on-line but the hybrid SOF-PID controller needs more computing power than the SOF-PID of previous works. In experiments sampling time is set to more longer than the SOF-PID to reduce computing time.

4 Experiment

A five linked biped robot simulator are used to test The hybrid SOF-PID cotroller and SOF-PID controller. Robot kinematics are used to control robot. Robot joint values are described like Fig3.

α : torso angle
$\Delta\beta = \beta_R - \beta_(L)$: difference of the thigh angles
$\gamma_(L)$: left leg knee angle
$\gamma_(R)$: right leg knee angle

For four joint values, errors are compared between the SOF-PID controller and the hybrid SOF-PID controller in Fig.4,5,6 and 7. It shows that roughly the hybrid SOF-PID controller is better than the SOF-PID controller.

1. If E is NL and CE is NL or NM or NS and Upi is NL or NM or NS then D is ZO.
2. If E is NL and CE is NL or NM or NS and Upi is ZO or PS or PM or PL then D is ZO.
3. If E is NL and CE is ZO or PS or PM or PL and Upi is NL or NM or NS then D is NL.
4. If E is NL and CE is ZO or PS or PM or PL and Upi is ZO or PS or PM or PL then D is NL.
5. If E is NM and CE is NL or NM or NS and Upi is NL or NM or NS then D is ZO.
6. If E is NM and CE is NL or NM or NS and Upi is ZO or PS or PM or PL then D is ZO.
7. If E is NM and CE is ZO or PS or PM or PL and Upi is NL or NM or NS then D is NM.
8. If E is NM and CE is ZO or PS or PM or PL and Upi is ZO or PS or PM or PL then D is NM.
9. If E is NS and CE is NL or NM or NS and Upi is NL or NM or NS then D is ZO.
10. If E is NS and CE is NL or NM or NS and Upi is ZO or PS or PM or PL then D is ZO.
11. If E is NS and CE is ZO or PS or PM or PL and Upi is NL or NM or NS then D is NS.
12. If E is NS and CE is ZO or PS or PM or PL and Upi is ZO or PS or PM or PL then D is NS.
13. If E is ZO and CE is NL or NM or NS or ZO or PS or PM or PL and Upi is NL or NM or NS or ZO or PS or PM or PL then D is ZO.
14. If E is PS and CE is NB or NM or NS or ZO and Upi is NL or NM or NS then D is PS.
15. If E is PS and CE is NB or NM or NS or ZO and Upi is ZO or PS or PM or PL then D is PS.
16. If E is PS and CE is PS or PM or PL and Upi is NL or NM or NS then D is ZO.
17. If E is PS and CE is PS or PM or PL and Upi is ZO or PS or PM or PL then D is ZO.
18. If E is PM and CE is NB or NM or NS or ZO and Upi is NL or NM or NS then D is PM.
19. If E is PM and CE is NB or NM or NS or ZO and Upi is ZO or PS or PM or PL then D is PM.
20. If E is PM and CE is PS or PM or PL and Upi is NL or NM or NS then D is ZO.
21. If E is PM and CE is PS or PM or PL and Upi is ZO or PS or PM or PL then D is ZO.
22. If E is PL and CE is NB or NM or NS or ZO and Upi is NL or NM or NS then D is PL.
23. If E is PL and CE is NB or NM or NS or ZO and Upi is ZO or PS or PM or PL then D is PL.
24. If E is PL and CE is PS or PM or PL and Upi is NL or NM or NS then D is ZO.
25. If E is PL and CE is PS or PM or PL and Upi is ZO or PS or PM or PL then D is ZO.

NL, NM, NS, ZO, PS, PM, PL : same as value in Table 1.

Table 2: Linguistic rules of The Hybrid SOF-PIDC

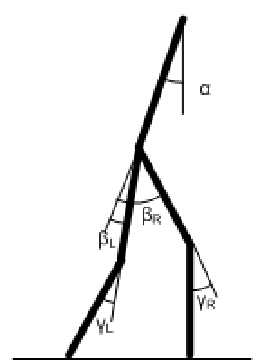

Figure 3: A MIMO Biped Robot

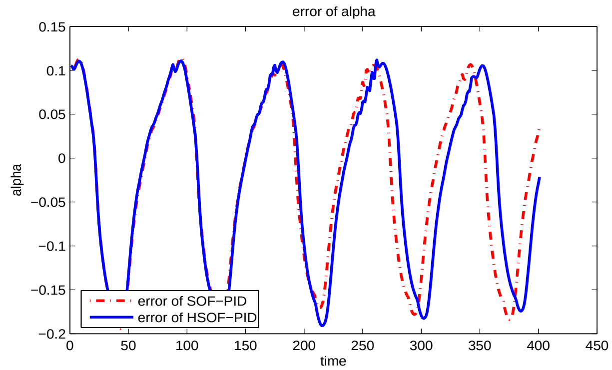

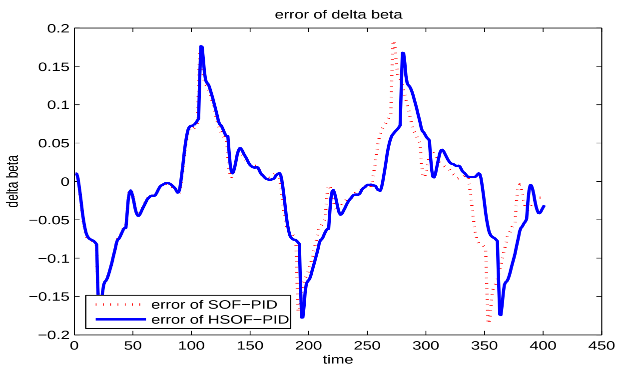

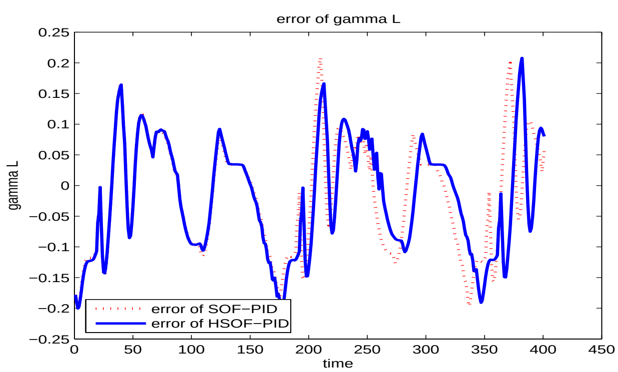

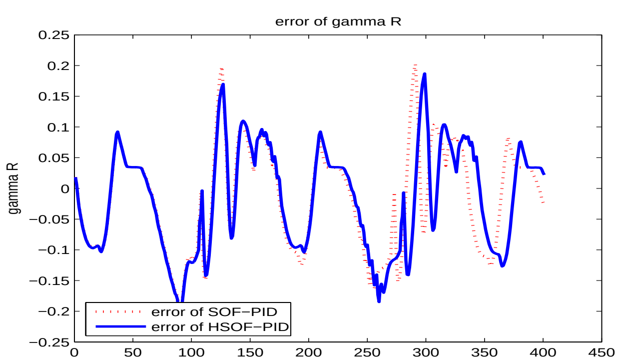

Figure 4: Error of α

Figure 5: Error of $\Delta\beta$

Figure 6: Error of left γ

Figure 7: Error of right γ

5 Conclusion

Both of the hybrid SOF-PID and the SOF-PID controller are tested on a MIMO biped robot simulator. In experiment the hybrid SOF-PID controller shows more smaller error than the SOF-PID as operating time goes. In effect to adjust conventional PID controller the hybrid SOF-PID can be a good solution than the SOF-PID.

The hybrid SOF-PID controller have some drawbacks. First, it need more computing power than the the SOF-PID to apply on on-line control problems. If all three PID gains are tuned computing power will be serious problem. Second it is difficult to construct performance index table without help of experienced human.

References

[1] H. B. Kazemian, "The SOF-PID Controller for the Control of a MIMO Robot Arm," *IEEE Trans. Fuzzy Syst.*,Vol. 10, pp. 523-532, Aug 2002.

[2] H. B. Kazemian, "Comparative study of a learning fuzzy PID controller and a self-tuning controller," *ISA Transactions*,Vol. 40, pp. 245-253, 2001.

[3] H. B. Kazemian, "The self organizing fuzzy PID controller," *Proc. IEEE World Congr. Computational Intelligent, Anchorage, AK*, May 1998, pp. 319-324.

[4] R. K. Mudi and N. R. Pal, "A robust self-tuning scheme for PI- and PD-type fuzzy controllers," *IEEE Trans. Fuzzy Syst.*,Vol. 7, pp. 2-16, Feb 1999.

[5] Franck Plestan, "Stable Walking of a 7-DOF Biped Robot," *IEEE Trans. Robotics and Automation.*,Vol. 19, pp. 653-668, Aug 2003.

[6] Zhe Tang, "Trajectory Planning for smooth Transition of a Biped Robot," *Proc. IEEE International Conf. Robotics and Automation, Taiped, Taiwan*,Sep 2003, pp. 2455-2460.

[7] Daiki Ito, "An Approach to Generation of Smooth Walking Pattern for Biped Robot," *AMC, Maribor, Slovenia*, 2002, pp. 98-103.

[8] T. Furuta, "Design and construction of a series of compact humanoid robots and development of biped walk control strategies," *Robotics and Autonomous Systems*,Vol. 37, pp. 81-100, 2001.

[9] G. F. Franklin and J. D. Powell, em Digital Control of Dynamic Systems., Addison-Wesley, 1990.

Strategy of Cooperative Behaviors for Distributed Autonomous Robotic Systems

Han-Ul Yoon, Se-Hee Whang, Dae-Wook Kim, and Kwee-Bo Sim

School of Electrical and Electronics Engineering
Chung-Ang University
221 Heukseok-Dong, Dongjak-Gu, Seoul, 156-756 Korea
e-mail: huyoon@wm.cau.ac.kr, kbsim@cau.ac.kr

Abstract

In this paper, we present the strategy of distributed autonomous robotic systems (DARS) for cooperative behaviors. The DARS are the systems which consist of multiple autonomous robotic agents into which required function is distributed. For building of DARS, the agents can recognize the environment where they are located, communicate each other, and generate some rules to act by themselves. In the paper, we introduce our DARS robot to perform cooperative behavior which is the task of our research – the pursuit competition with one-fugitive robot versus multi-detective robot. The paper also presents the area-based decision making algorithm to determine the direction of the robot maneuver.

Keywords: DARS, camera vision, sensor, motor, bluetooth communication, main MCU, area-based decision making algorithm, fugitive and detective robot

1. Introduction

Nowadays, the robots replace the human working in the fields of rescue a life at highly destroyed building by fire or gas contaminated place, getting some information in the deep sea or the space, and watching the weather condition at the extremely cold area like the Antarctica. Especially, we need to penetrate multiple robots to get more trustful and robust information data from hardly accessible area, such an ant's nest under the ground. In this case multiple robots send the data by cooperation and communication each other and make a decision to act by themselves.

Distributed autonomous robotic systems (DARS) have been focused by many researchers as a new way to control the multi-agents more flexibly and robustly. The DARS are the systems being organized by multiple autonomous robotic agents into which required function is distributed. The most unique and important feature of DARS is that each system is a distributed system composed of multiple agents (robots) [1]. According to this feature, the subject of DARS can be various widely. DARS are now applied to multi-robot behavior, distributed control, coordinated control, and cooperative operation, etc.

Typical mobile robot systems consist of robot body (frame), vision system, sensor system, drive (motor) system, communication system, and main controllers. There are many ways, which depends on the main task of robot and which part of robot will be specially intellectualized, to apply these systems efficiently [2]. For cooperative works, the Khepera can be the role model of design. It consists of a main processor (Motorola 68331), driven by two d.c. motors, and has eight infra-red proximity sensors around its body (55mm diameter, and 30mm height) [3]. This robot still being used for in many fields like fuzzy control, wall following, obstacle avoidance. We take similar appearance with Khepera or RoboSot (one model of the soccer robots) for our robot.

In this paper, we organize DARS to perform the pursuit competition with one-fugitive robot versus multi-detective robot. The paper introduce about our robot system and its functional block component in chapter 2. We present the task of our DARS, the area-based decision making algorithm, and experimental results in chapter 3. The paper concludes the subject and issues future works in chapter4.

2. The Autonomous Robot for DARS

Our robot system consists of four sub-parts and a main micro-controller part. The sub-parts are camera vision, sensor, motor, and bluetooth communication, respectively. Each sub-part has its own controller to perform a unique function more efficiently. The main micro-controller part controls four sub-parts to avoid process collision and performs decision making by the data of its sub-parts.

2.1. Camera vision

The camera, which we use for the robot, is Movicam II made by Kyosera. The Movicam II is the CCD camera being used for SKY cellular phone. Its size is 30×47×29 mm (width × height × thick) and weight is 12g approximately. A frame consists of header, image data, and end maker. Fig. 1 shows camera appearance and the data components of a frame in detail.

When clock is applied to the clock-port (port # 2), it starts to send the data at rising clock from the header to the end maker bit by bit. The data-out port (port # 1) of camera is attached to DSP (Digital Signal Processor) TMS320LF-2407A which is programmed to perform signal processing. The size of image data is rather bigger to wait the end of pro-

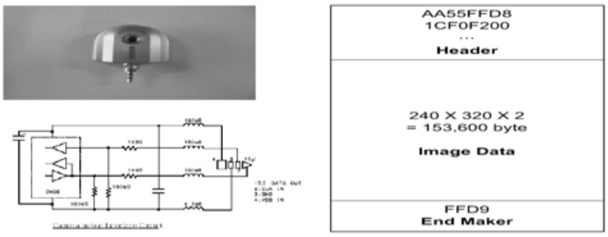

Figure 1. Camera and the data component of a frame

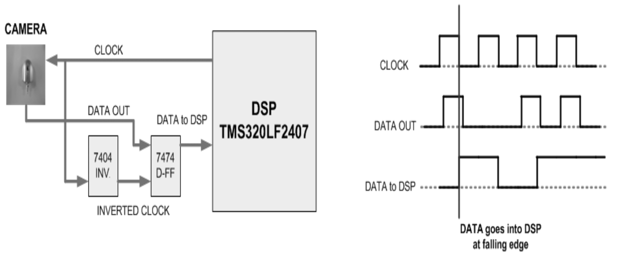

Figure 2. The connection between camera and DSP (left), the data transfer timing (right).

cess with whole image(153,600 byte). Accordingly, we optimize the program to cramp the image data within 25,000 byte. The connection between DSP and camera is showed in Fig. 2(left). The data transfer is presented in Fig. 2(right).

2.2. Sensor

The robot has six of infra-red (IR) sensor pairs (emitter/detector) to measure the distance around itself. The emitter is Kodenshi EL-1kl3, high-power GaAs IR mounted in durable, hermetically sealed TO-18 metal package. The detector is ST-1kla, high-sensitivity NPN silicon phototransistors mounted in durable, and the package is same with the emitter's. The six IR sensors are placed with 60 degree angle of each other, so they can cover whole 360 degree.

We chose the emitter, which has narrow beam angle (about 17°), to avoid interference. The detector, however, has almost 50° beam angle, therefore it can detect most of IR reflection by the object. The appearance is showed in Fig. 3 (left). The arrangement, the area where can be covered by the six of sensor pairs, and the block diagram are depicted in Fig. 3 (right).

2.3. Motor

As driving part, we use NMB PG25L-024 stepping motor. Its characteristics are drive voltage-12V, drive method 2-2 phase, and 0.495° step angle, etc. Fig. 4(left) shows torque-

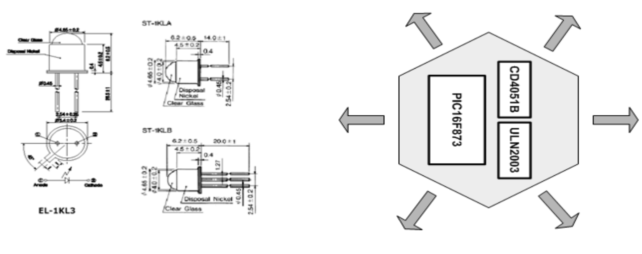

Figure 3. El-1ka3 and ST-1kla (left), sensor block diagram (right).

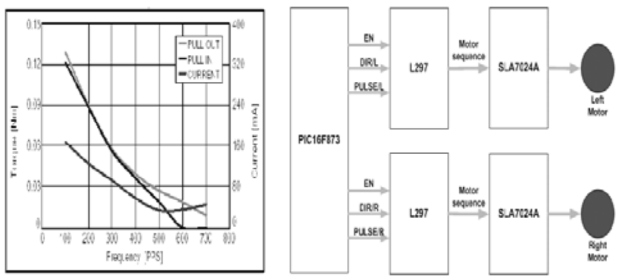

Figure 4. Torque characteristic (left), motor block diagram (right).

Table 1. The relationship of signals and actions.

Signals	Actions
0x00	Forward
0x01	Rotate 60° clockwise
0x02	Rotate 120° clockwise
0x03	Turn around (rotate 180°)
0x04	Rotate 60° counter clockwise
0x05	Rotate 120° counter clockwise

frequency-current characteristic curve. By the figure, the maximum self-operating frequency is 600 pps. We assemble the driver with L297 and SLA7024A combination to control two motors. Fig. 4(right) and Table 1 present the block diagram and the signals associated actions pair of robot by decision making.

2.4. Bluetooth communication

Blutooth communication was developed to use for mobile device, which includes battery source, with the motto 'low -cost,' 'low-power,' and 'compact.' For these characteristics, bluetooth regard as very suitable for wireless communication system [4].

Bluetooth fundamentally organizes its network with 1 master to 7 slave architecture. The PicoNet is the net which consists of one master and multiple slaves. The ScatterNet is the net organized by PicoNets. Fig. 5 depicts the concept of PicoNet and ScatterNet.

In DARS, there is no pre-defined classification like master and slave. All agent robots should be distributed individually. We'd like to apply, however, the concept of master/slave only for communication. The detective robots need to communicate each other only when they catch the fugitive robot in their vision. Therefore it can be said that "We are still in the DARS."

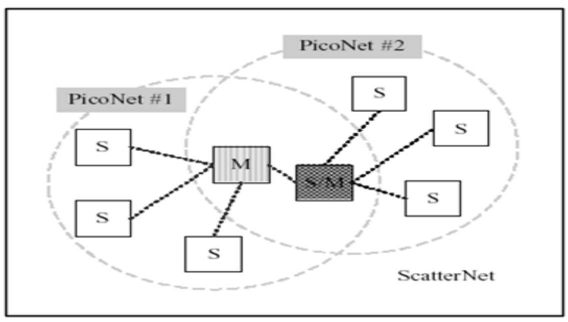

Figure 5. The PicoNet and the ScatterNet diagram.

2.5. Main Controller

We design the system as every sub-part has its own controller. Therefore, main controller has little overhead. The function of the main controller is control the UART Tx/Rx communication between main controller and sub-controller. It also generates the rules of next action, change moving direction or camera vision on/off or send the data to other robot, by the sub-parts' data. Fig. 6 is the block diagram of whole robot system connected with main controller and the appearance of our robot.

3. Cooperative Behavior Example of DARS

In DARS, the best role model for cooperative behavior is the ants' cooperation. When the ants find a food which is much bigger than an ant itself, they get around by the food and start to cooperation. Similarly, the robot cooperation means operating multiple robots cooperatively. Therefore, the communication between robots is essential.

In our system, the fugitive robot must run away from the pursuit of multiple detective robots. To perform their own task (i.e. escaping and tracking), both the fugitive and the detective robot recognize the surrounding by their sensors, and generate the rule by recognizing the situation. In this chapter we discuss with two issues – the distance measurement and the area-based decision making to generate rules and change direction, and show the experimental results.

3.1. Distance measurement

The robots must know its situation by measuring the distance around itself. In Fig. 7, dashed line presents the distance-A/D converting value curve. It is expected to have inversely proportional form rather than linear or hyperbola. The approximation of this fomula is

$$Distance = \frac{\alpha}{A/D\ conv.\ value} + offset \qquad (1)$$

We set the coefficient $\alpha = 580$ and *offset* = 7 by experiential result. The solid line presents its approximated value curve in Fig. 7.

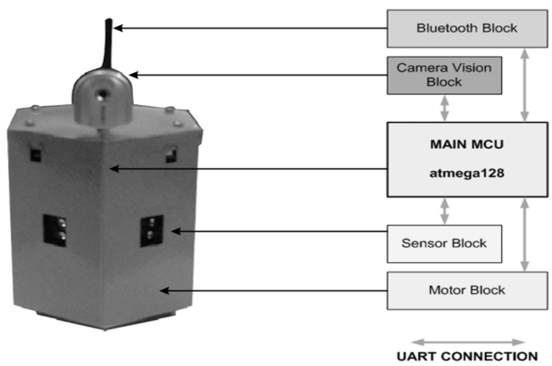

Figure 6. The robot and main MCU with 4 sub-parts connection.

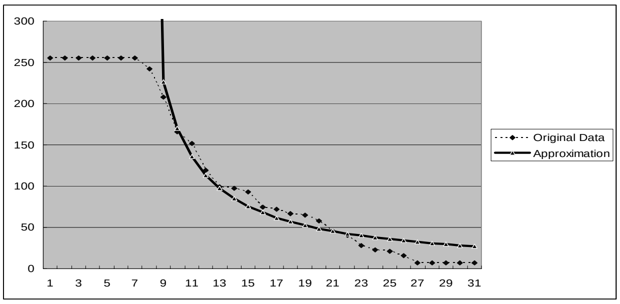

Figure 7. Distance to A/D conv. value curve by equation (1).

3.2. Area-based decision algorithm

To change the direction of running, we can consider two algorithms – the distance-based and the area-based algorithm.

In the distance-based decision algorithm, the fugitive robot considers the direction which a sensor returns the longest distance as the safest direction. Thus, the robot takes the following steps to determine the next direction.

- The robot gets 6 of A/D conv. value from detect sensor.
- The robot decides the direction which returns the longest distance as safe way without any obstacles.
- The robot changes the direction.

In the area-base decision algorithm, however, the robot follows these steps,

- The robot gets 6 A/D conv. value from detect sensor.
- The robot calculates the 6 areas with each A/D conv. value from detect sensor.

  $Area = \frac{1}{2}\overrightarrow{s_1} \times \overrightarrow{s_2} \sin 60°$, where $\overrightarrow{s_1}, \overrightarrow{s_2}$ are the distance measured by sensor 1 and 2.
- The robot decides the direction which returns the widest area as safe way.
- The robot changes the direction.

In brief, we can generate the rule of fugitive robot's behavior with this simple concept,

"Change your direction to where you can guarantee more wide space."

The rule of the detective robots can be define easily by adding one more condition to above,

"If you get the fugitive in your camera, try to occupy more wide area in the fugitive's plane."

This is the basic concept of area-based decision making. The concept is similar with the behavior-based decision making but is different to change the direction by the area [5]. Fig. 8 shows the difference between the distance-based and the area-based decision making by example.

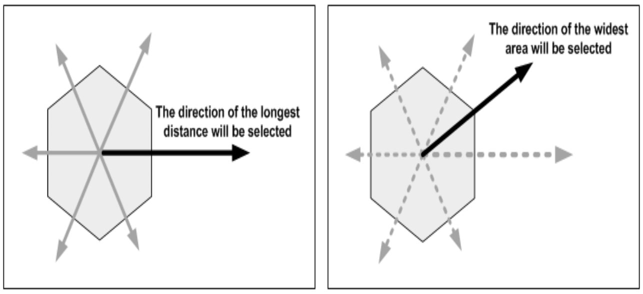

Figure 8. The different results, with the same sensor values, by the distance-based (left) and the area-based (right) decision making.

3.3. Experiments

We experiment two different situations with our robots. The results are shown in this chapter.

First, we release the robot on the hallway where no obstacle but walls. Fig. 9 shows the pictures of the robot on running. We tested the robot's running by 50 trials. The robot succeeded 43 times out of 50 trials, but 7 times failed. The reason of fails was the robot took the turnaround (turn 180°) decision continuously, even if both its front and back space are freely empty. To clear this problem, we modified area- calculating function by the multiplying of weight, $\boldsymbol{w}_{front}$ = 1.2, to the calculation of front area.

Second, we try for the robot to explore the hallway where three obstacles are located. Fig. 10 depicts the robot's running in the second situation. The result shows the robot found the next direction more easily when it is surrounded by other obstacles. At the 1st and the 3rd turns, however, the robot has many other choices to avoid the 1st and the 3rd obstacle. It is the main reason that the malfunction (i.e. back to the 1st obstacle when tries to avoid the 3rd) occurs several times. By the reason, the robot succeeded its task 31 times out of 50 trials.

Figure 9. The robot is running in the hallway.

Figure 10. The robot is running through the 3 obstacles.

4. Conclusions and Future Works

In this paper, we introduced the hardware specification of the robot and architecture of our DARS. We also proposed the area-based decision making algorithm and presented the two experimental results with the robots in the two different situations. The result shows us that the area-based decision making can be a new way for the obstacle avoidance.

The future works would be to complete the implementtation of the detective robots and to find out appropriate and efficient way to pursue the fugitive robot more concretely in DARS.

Acknowledgement

This research was supported by the Brain-tech 21 from Ministry of Science and Technology of Korea.

References

[1] H. Asama, T. Fukuda, T. Arai, et al, Distributed autonomous robotic systems, Springer-Verlag, 1994.

[2] J. H. Kim, H. S. Sim, S. H. Kim, et al, Robot soccer engineering, Dooyang, 2003.

[3] S. H. Lian, "Fuzzy logic control of an obstacle avoidance robot," *Proc. of the Fifth IEEE International Conference on Fuzzy Systems*, vol. 1, pp.26-30, 1996.

[4] S. H. Whang, K. B. Sim, I. C. Jeong, et al, "Design of efficient strategies for distributed multi-agent robot soccer system," *FIRA Robot Congress*, pp. 1-5, 2004.

[5] W. Ashley, S. Balch, and T. Balch, "Value-based observation with robot teams (VBORT) using probabilistic techniques," *Proc. of ICAR 2003*, vol. 1, pp. 1-8, 2003.

The Tenth International Symposium on Artificial Life and Robotics 2005(AROB 10th '05),
B-con Plaza, Beppu, Oita, Japan, February 4-6, 2005

Development of the Tactile Sensor System Using Fiber Bragg Grating Sensors

Jin-Seok Heo
Dept. of Mechanical Engineering
Korea Advanced Institute of Science and Technology,
Daejon, Korea 305-701
dandyheo3070@kaist.ac.kr

Jung-Ju Lee
Dept. of Mechanical Engineering
Korea Advanced Institute of Science and Technology,
Daejon, Korea 305-701
leejungju@mail.kaist.ac.kr

Abstract

This paper shows the development of flexible force sensor using the fiber Bragg grating. This force sensor consists of a Bragg grating fiber and flexible silicone rubber. This sensor does not have special structure to maximize the deflection or elongation, but have good sensitivity and very flexible characteristics. In addition, this sensor has the immunity to the electro magnetic field and can be multiplexed easily, which is inherited from the characteristics of fiber Bragg grating sensor. In the future, this sensor can be utilized the tactile sensor system minimizing the sensor size and developing the fabrication method.

1. Introduction

Many force sensors based on the strain gages, until now, have been used mainly to monitor the durability of bridges, buildings from the view point of safety, and control some material test machines and industry robots, and so on. However, recently, as some system is now small and need high sensitivity and accuracy, a new force sensor with small size and high sensitivity, not some conventional load cells, has been required to control small force accurately. On the other hand, MEMS shows the possibility of development of micro force sensor similar to the pressure sensor. Especially, some researchers have tried to develop tactile sensor combined small force sensors for intelligent robotics, teleoperational manipulators and haptic interfaces. These tactile sensors can detect normal forces on the taxel for gripping force control and generating tactile images for object recognition. However, in addition to acquiring tactile images and normal forces, detecting tangential forces is also critical. The fabrication process of sensor is very simple. This paper shows the development of three component force sensor based on the fiber optic sensors Until now, a few tactile sensors on behalf of the human skin have been developed compared with the other kinds of sensors, such as, image sensors and sound sensors. Because the tactile sensors have some requirements to adapt the practical engineering field, such as humanoid robot system and telerobotic system and so on. These sensors must have the flexibility and must have a good spatial resolution mimicking the human skin. Some researchers tried to make the tactile sensors using the MEMS(Micro Electric-Mechanical System) technology. Although these sensors have a good spatial resolution and sensitivity, they are not flexible and don't have sufficient durability[1-4]. In this paper, we will show the flexible optical fiber force sensor which can be the basis of the tactile sensor. This force sensor has very simple structure

2. The Structure of the Flexible FBG Sensor

2.1 The Principle of the FBG sensor

Fiber Bragg grating (FBG) sensors based on wavelength-division multiplexing (WDM) technology are attracting considerable research interest and appear to be ideally suitable for structural health monitoring of smart structure[5]. FBG sensors are easily multiplexed and have many advantages such as linear response and absolute measurement. As the spectral response of the FBG sensor signal renders the measurement free from intensity fluctuations, it guarantees reproducible measurements despite optical losses due to bending or connectors. The basic principle of a fiber Bragg grating (FBG)-based sensor system lies in the monitoring of the wavelength shift of the returned Bragg-signal, as a function of the measurand (e.g. strain, temperature and force). The Bragg wavelength is related to the refractive index of the material and the grating pitch. Sensor systems involving such gratings usually work by injecting light from a spectrally broadband source into the fiber, with the result that the grating reflects a narrow spectral component at the Bragg wavelength, or in transmission this component is missing from the observed spectrum. Fig.1 shows this simply and schematically. The intensity of the reflected optical signal is a function of the Bragg grating wavelength that relates to the applied strain on the fiber Bragg grating. Therefore, the dynamic strain can be derived from the intensity change measurement as function of the wavelength of the reflected optical signal. The operation of a FBG is based on a periodic, refractive index change that is produced in the core of an optical fiber by exposure to an intense UV interference pattern. This grating structure results in the reflection of the light at a specific narrow band wavelength, called Bragg wavelength. The Bragg condition is given by

$$\lambda_B = 2n_e\Lambda \quad (1)$$

where λ_B is the Bragg wavelength of the FBG, n_e is the effective index of the fiber core, and Λ is the grating period. The shift of the Bragg wavelength due to strain and temperature can be expressed as

$$\Delta\lambda_B = \lambda_B\left[\left(\alpha_f + \xi_f\right)\Delta T + \left(1 - p_e\right)\Delta\varepsilon\right] \quad (2)$$

$$p_e = \left(\frac{n^2}{2}\right)\left[p_{12} - \nu\left(p_{11} - p_{12}\right)\right] \quad (3)$$

where α_f is the coefficient of the thermal expansion (CTE), ξ_f is the thermo-optical coefficient, and p_e is the strain-optical coefficient of the optical fiber. The value of p_e =0.22[7] was measured experimentally and used for this study. If there is no temperature change, we can measure the strain from the wavelength shift as

$$\varepsilon = \frac{1}{\left(1 - p_e\right)}\frac{\Delta\lambda_B}{\lambda_B} \quad (4)$$

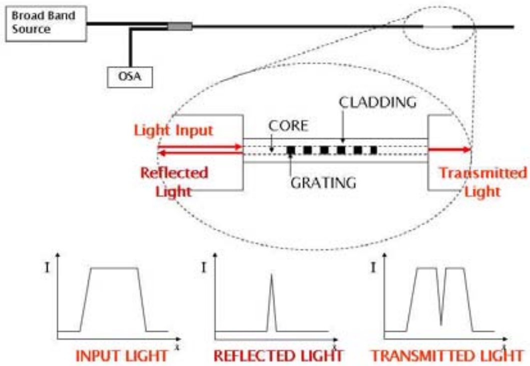

Fig.1 FBG sensor encoding operation

2.2 The Structure of Flexible FBG Force Sensors

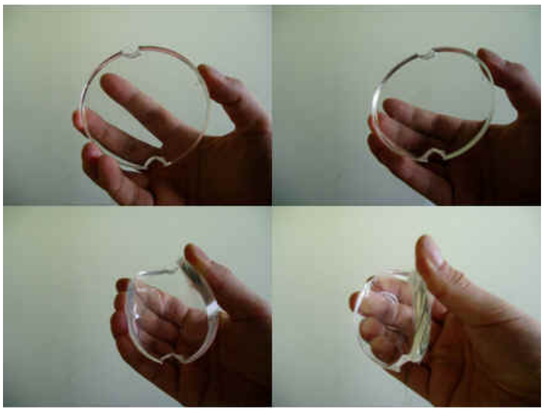

Fig.2 Prototype flexible FBG sensor

The sensor has the simple structure which is composed of FBG and silicone rubber (DC184 Dow corning Co. Ltd). The fabrication process of this sensor is easier than that of diaphragm type sensor. The FBG sensor with the length of 10mm is embedded in the silicone rubber.

Once the external force is applied on the silicone rubber, the fiber Bragg grating in the silicone rubber is deformed. The deformation of fiber Bragg gratings is induced on the change of the Bragg wavelength. Therefore, this sensor can detect the fore through the change of Bragg wavelength. Fig.2 shows the flexible characteristics of the prototype sensor.

3 Design of the Flexible FBG force sensor

3.1 FEM Analysis of Silicone rubber

We simulated the deformation of the silicone rubber to verify the resolution of the sensor. ABAQUS 6.3 was used and the 2-dimensional element model was applied to the silicone rubber. As the model is symmetric, the half geometric model was used. And the fixed condition on the all directions was applied on the base of the model. And the force (1~10N) was applied through the rigid ball with the diameter of 3mm to simulate the real experimental condition.

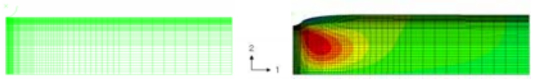

Fig. 3 Finite Element Model and FEA (Finite Element Analysis) of DC 184

The optical fiber was excluded from the FEM model. Because the optical fiber have the very small diameter (250μm) compared with the whole size of the sensor. That is, the sensor model have only the silicone rubber and we assumed the deformation of the silicone rubber should be the deformation of the optical fiber. As the deformation of the silicone rubber is very small, we used the general elastic solver to verify the deformation[6]. The elastic modulus of the silicone rubber is 9.2MPa and the Poission's ratio is 0.49.

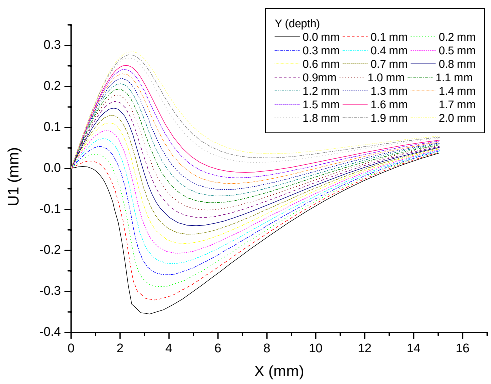

Fig. 4 U1 distribution of DC184 according to the depth (Load: 10N)

Fig. 4 shows the deformation of the U1 direction (the axial direction of the optical fiber). If the optical fiber is located on the surface of the silicone rubber, positive deformation is induced by the transverse load. As the optical fiber is deeper inside, the positive deformation is appeared. And the positive deformation is in the whole optical fiber above the 1.5mm deep inside the silicone rubber.

3.2 Determination of the Depth of FBG sensors

Using the results of the FEA, the efficient depth of the optical fiber can be determined. The large deformation is occurred in 1~4mm depth. And the output signal, the change of the Bragg wavelength can be easily influenced in 1~4mm depth. If the optical fiber is located on the surface of the silicone rubber, the output is most efficient, but the fiber can be easily broken because of the brittle characteristics of the optical fiber. Fig. 5 shows that the positive and concentrated deformation was occurred in the 2mm depth of the silicone rubber. Therefore, the 2mm depth was determined as the prototype flexible force sensor.

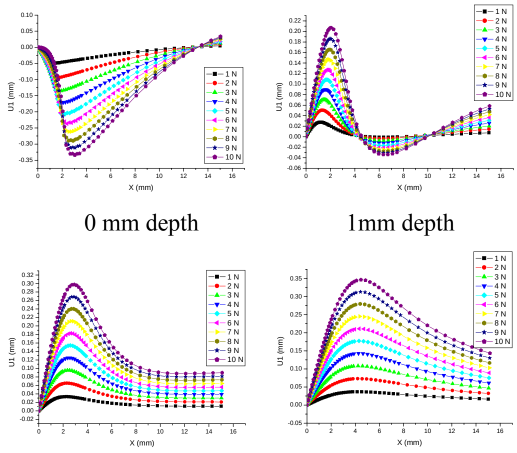

0 mm depth 1mm depth

2 mm depth 4mm depth

Fig. 5 U1 distribution of DC184 according to the load

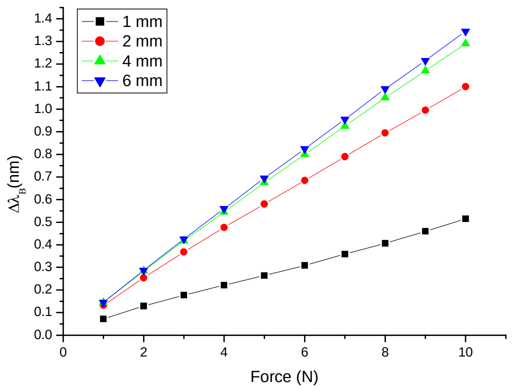

Fig. 6 Bragg wavelength shift analysis using FEM

Using the equation (4) and the results of FEA, we can calculate the change of Bragg wavelength. The photoelastic constant of the used optical fiber is 0.22[7]. Fig 6 shows the calculated the change of Bragg wavelength according to the applied force. The fiber Bragg grating sensor located in the 2mm depth has the about $1.0\times10^{-3}\,nm/gf$ sensitivity.

4. Experimental Results

4.1 Experimental Equipment

Fig. 7 shows the experimental setup. The broadband light source having the 1527~1602nm wavelength is incident in the optical fiber and the light is separated by the 2 by 1 coupler. The separated light is transmitted in the Bragg grating. And the reflected light is experienced the applied load is send the optical spectrum analyzer (OSA). Therefore we can know the applied force through the Bragg wavelength change of the reflected light. And the applied load is measured by the load cell like Fig.7.

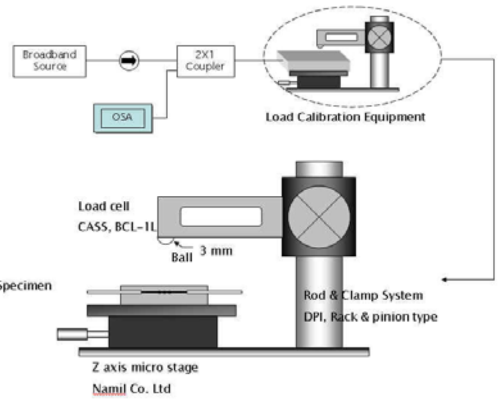

Fig. 7 Experimental setup

4.2 Evaluation of flexible FBG force sensors

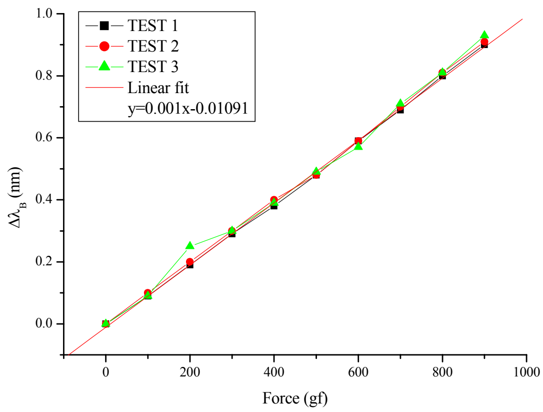

Fig. 8 Shifted wavelength according to the applied force of flexible FBG force sensor (depth 2mm)

Three flexible fiber Bragg grating force sensors were fabricated and tested in the same environment. Three sensors have the same sensitivity, about $1.0 \times 10^{-3} nm/gf$ which is the same resolution of the simulated results. This means that the 1.0nm Bragg wavelength was changed by the applied force, 1000gf. As OSA can detect the 0.01nm wavelength, these sensors can detect at least 10gf (0.1N).

5. Conclusion

In this paper, the flexible fiber Bragg grating force sensor was introduced and verified. The experimental results mated the simulated results by the FEA. The sensors are very flexible and can detect the absolute strain. And these sensors can attach the arbitrary surface. This characteristic is suitable to the artificial skin and the tactile sensors. The resolution of theses sensors is about 10gf (0.1N) and will be improved by the ability of the OSA or interrogation system of the fiber Bragg grating. Now these sensors cannot have the good spatial resolution to adapt the tactile sensors. In the future, the length of the FBG with the 1~5mm, the sensors can be minimized, that is, the spatial resolution of the sensor would be improved.

Acknowledgement

This research (paper) was performed for the Intelligent Robotics Development Program, one of the 21st Century Frontier R&D Programs funded by the Ministry of Science and Technology of Korea.

Reference

[1] Mei, T., Li, W.J., Ge, Y., Chen, Y., Ni, L. and Chan, M.H., "An integrated MEMS three dimensional tactile sensor with large force range", Sensors and Actuators (A), Vol. 80, pp155-162, 2000
[2] Wang, L. and Beebe, D.J., "A silicon shear force sensor: development and characterization", Sensors and Actuators (A), Vol. 84, pp33-44, 2000
[3] Kim, J. H., Kang, D. I., Park, Y. K., "Research Trends on the Development of Micro Force Sensor and Its Application", J. of KSPE, Vol. 19, No. 3, pp. 7~12, 2002
[4] Yoon, M. J., Yu, K. H., Jeong, G. Y., Lee, S. C., Kwon, T. G., "Development of a Distributed Flexible Tactile Sensor System", J. of KSPE, Vol. 19, No. 1, pp. 212~218, 2002
[5] Kenaeth O. Hill and Gerald Meltz, "Fiber Bragg grating technology: fundamentals and overview", Journal of Lightwave Technology, Vol. 15, No.8, August 1997
[6] Yang, L.M., Shim, V.P.W., Lim, C.T., "A visco-hyperelastic approach to modeling the constitutive behavior of rubber.", International Journal of Impact Engineering Vol. 24, pp545~560, 2000
[7] Udd, E., "Fiber optic smart structure", John Willey and Sons, 1995

The Tenth International Symposium on Artificial Life and Robotics 2005(AROB 10th '05),
B-con Plaza, Beppu, Oita, Japan, February 4-6, 2005

A Distributed Precedence Queue Mechanism to Assign Efficient Bandwidth in CAN Networks

Ho-Seek Choi, Jang-Myung Lee

Department of Electronics Engineering, Pusan National University
San 30 Jangjeon-dong Kumjeong-ku, Busan, 609-735, Korea
chs_chs@hanmail.net, jmlee@pusan.ac.kr

Abstract

This paper presents a distributed precedence queue mechanism to resolve unexpected transmission delay of a lower priority transaction in a CAN based system, which keeps a fixed priority in data transactions. The mechanism is implemented in the upper sub-layer of the data link layer (DLL), which is fully compatible with the original medium access control layer protocol of CAN. Thus the mechanism can be implemented dynamically while the data transactions are going on without any hardware modification. The CAN protocol was originally developed to be used in the automotive industry and it was recently applied for a broader class of automated factories. Even though CAN is able to satisfy most of real-time requirements found in automated environments, it is not to enforce either a fair subdivision of the network bandwidth among the stations or a satisfactory distribution of the access delays in message transmissions. The proposed solution provides a superset of the CAN logical link layer control, which can coexist with the older CAN applications. Through the real experiments, effectiveness of the proposed mechanism is verified.

1. Introduction

The controller area network protocol (CAN) was developed to solve complex cable problems and reliability reduction in automotive [1,2]. This availability was built network of high reliability applied various industry environment [3,4,5].

Unlike the IEEE 802.3 standard-access-technique-based CSMA/CD protocol[6], CAN's medium-access control mechanism ensures that when collision occurs a non-destructive contention-based arbitration is initiated that stops all of the transmitting stations except the one which is sending the frame having the highest priority. The frames that are transmitted are not addressed to a specific destination, but they are considered as global objects, each of which is associated with a network-wide unique identifier. CAN allocates absolutely priority to messages or objects transmitted in a network using ID. This mechanism is a good method to manage collisions in network.

If a network is overloaded, the data transmission quantity is rapidly decreased to increase data transmission collision. If this state is continuous, a network may be groggy and the state of non-transmission may continue over a long period of time. This paper presents a mechanism that can create a fair transmission chance and can reduce delay time [7,8,9] using a distributed precedence queue, and assigning a precedence queue to relatively low priority and objects having similar transmission purposes when a network is overloaded, and which can compensate a maximum tolerance delay time and to remove ineffectiveness for an identifier assigned statically into an overload condition [10].

This precedence queue is not assigned statically but assigned dynamically According to transmission quantity, so that the transmission efficiency can be optimized in network. And each queue can independently assign transmission sequences of data of a relative priority.

So, this paper can contribute to the mechanism that can transmit data within a constant time to adjust its priority dynamically based on an extended CAN protocol when a low priority object delays transmission because of an overload in a network.

Identifier is assigned statically in the CAN protocol, the two requirements of a fair transmission chance and delay time, can not be satisfied because this solve collision problem by a static identifier. In this paper it is shown that the problem can be solved collision by the filtering of input frames according to the identifier of each object and by redefining the identifier in the identifier field. By redefinition of the distributed precedence queue (DPQ) to use the identifier field of the extended CAN, each object can be transmitted according to a fair transmission sequence and can thus satisfy the maximum tolerance delay time.

2. CAN Analysis

2.1 A basic CAN protocol

The CAN is based on a CSMA/CD channel access technique. It uses a priority modification mechanism for transmitted-received messages to resolve collisions in a network. The CAN protocol adopts a layered architecture that is based on the OSI reference model, even though it is not fully OSI compliant, and the architecture is composed of three layers the factory automation environment.

1. The Application Layer
   ; Support to access on a Network
2. The Data Link Layer
   ; Connection physical address to the upper-low layer
3. The Physical Layer
   ; Transmission bit stream to physical medium

This paper resolves the transmission delay time problem using the data link layer and the only LLC sub-layer between the MAC (Medium Access Control) and the LLC (Logical Link Control) of the data link layer.

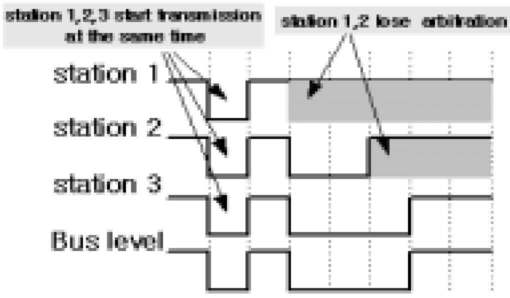

Fig 1. CAN arbitration phase

3. A Distributed Precedence Queue Mechanism (DPQ)

The CAN implicitly assigns to each object exchanged in the network a priority that corresponds to the identifier of the object itself. Even though this mechanism enforces a deterministic arbitration that is able to resolve any conflict that occurs when several nodes start transmitting at the same time, it is clearly unfair. If many nodes are connected in the network, nodes that are of low priority rank can continuously lose a transmission opportunity. That is, if high priority objects transmit continuously, finally a low priority object can miss an important message which is relatively unimportant compared to that of a high priority object.

Accordingly, a mechanism that uses a relative priority according to the consideration of low priority nodes is necessary although the CAN implicitly assigns a priority. Fair behavior, which for example enforces a round-robin policy among different stations, has to be guaranteed to all the objects exchanged at a given priority level.

In this paper, it is shown that this kind of behavior can be obtained by slightly modifying the frame acceptance filtering function of the LLC sub-layer. In particular, only the significance of the identifier field in the transmitted frame has to be modified in some way. The resulting arbitration mechanism is able to enforce a round-robin policy among the stations that want to transmit a message on the bus, and provides two levels of priority for the frame transmission services. Little or nothing has to be changed at the MAC level; and in this way it is possible to reuse the same electronics components developed for the implementation of the standard CAN protocol.

3.1 DPQ principle

The basic idea of this CAN fairness control mechanism that is to insert into a global queue all of the nodes that want to transmit over the shared medium. For Node C, of which transmission is continuously delayed as shown in Fig 1, a queue is created to transmit Node C and the other nodes that transmit with C. So, several queues can be partially made in this research, two queue were used.

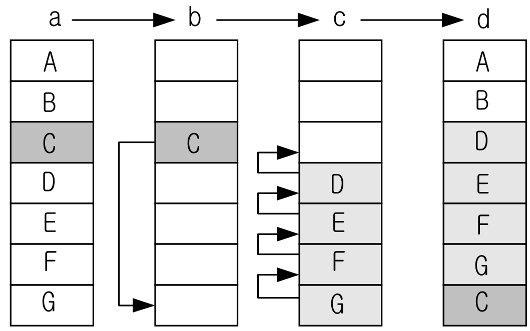

Fig 2. Generation of a precedence queue in DPQ mechanism

This distributed precedence queue protocol provides the opportunity to create precedence queues for all nodes in a network. And, in the case that several precedence queues exist, each precedence queue assigned a priority so that they can be implemented independently.

The DPQ mode ID, which is stored in the 11 bit standard ID field shown in the Fig 4, indicates the precedence queue order of each node. Whenever a node carries out a transmission, it moves to the end of the queue, thus lowering its precedence to the minimum. All of the nodes following the transmitting node advance by one position in the queue, occupying the space that has just been created. Using this round-robin policy, collisions among messages are avoided.

The queue is not stored in some specific location. Instead, it is distributed among all the nodes in the network. Each node is responsible for storing and updating. That is, if the maximum permission delay time is reached, it creates a precedence queue, and then it has to dynamically change priorities to transmit preferentially with other nodes. And a precedence queue has to be dissolved when is completed an urgent task.

We suppose a network that is composed of Nodes A to G as shown in Fig 2. If Node C builds up a queue, the ID that is entered into the data frame queue can transmit and designate to 7 by lower 7 byte. At this time, it will be designated precedence priority to higher byte. Then, each node filters to enter itself into the queue, and it assigns its queue. After Node C transmits a message, it will go to the last position in the queue. And the other nodes will move up one position by order. And the remaining nodes that to be transmitted are designated using the upper 1 byte as shown in Fig 3; their queues will be dissolved or maintained using the upper 1 byte, as shown the Fig 3 after all transmissions are completed.

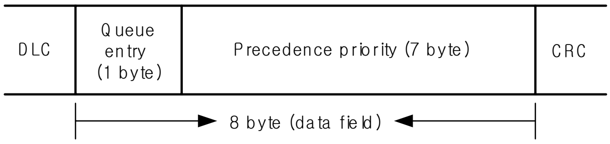

Fig 3. Structure of a data field for DPQ

3.2 DPQ Realization Method

The DPQ mechanism can be implemented without any modifications to the basic format of CAN frames. It uses an identifier field to designate the priority queue. Because the length of the conventional identifier field defined in the CAN standard is too small, the CAN extended format can be adopted.

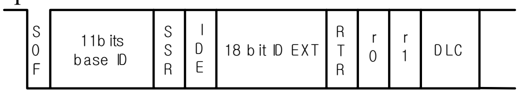

Fig 4. Format of the header of extended CAN frames

The DPQ uses the first 11 bits of the identifier field for its control information, whereas the remaining lower order 18 bits (ID ext.) are used to dynamically store the effective identifier of the an exchanged object (EID).

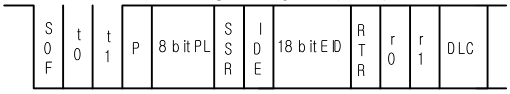

Fig 5. Format of the header of DPQ frames

The first two bits (t0, t1) must be set at the logical value of zero as shown in Fig 5. Then, the protocol is divided by a standard CAN communication and DPQ mechanism. So, DPQ always has a higher priority than a CAN mechanism, and they can exist in this same space.

The priority bit P specifies whether the frame has to be transmitted as a high priority frame (P=0) or as a low priority frame (p=1). When T1 and P are used, the priority can be assigned a maximum 4 queues.

The next 8 bits represent the precedence level of the frame. Namely, these 8 bits show the transmission queue order. The DPQ, which was used in this research, uses t0, t1, and then distinguishes the standard CAN mechanism, and sets each queue using P, and concludes the precedence in the queue using 8 bits.

4. System Architecture and Experiments

To verify the usefulness of the mechanism presented in this paper, actuator ECU that are used in throttle-body controllers of vehicles and portable inspection equipment ECU that can set sensor limit values and can diagnosis vehicle problems, established the basic nodes.

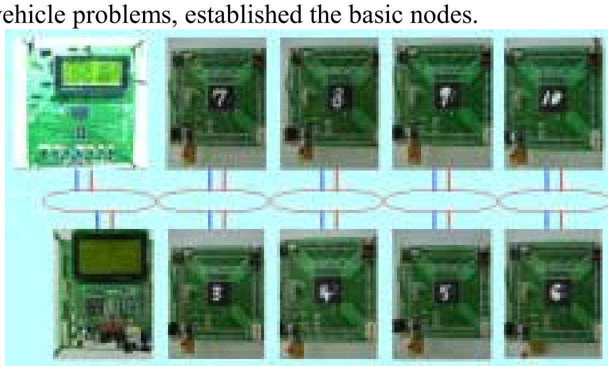

Fig 6. Total system organization

The total system consisted of additional virtual ECU of 10 nodes used in many parts of the vehicles as inhalation fuel ECU, lighting ECU, side-mirror ECU, and exhaust port ECU.

Each node used TMS320LF2407 with the CAN module and PCA82C251 with the CAN transceiver. Each node was set to a 250 Kbps transmission time.

The transmission period for the total 10 nodes was set to two states, 10ms and 2ms. When the transmission period was 10 ms, Collisions did not often occur. But when it was 2 ms, collisions often occurred. The transmission message priority was arranged as Node 1 (portable ECU) and node 2 (main ECU) for each transmission period and this priority decreased gradually. When the transmission period was 2 ms, Node 8,9,10 suffered a long transmission delay because of message collision on the bus, and the DPQ mode was applied to resolve this problem at Node 8,9,10.

Table 1. Identification Definition (ID)

node	standard CAN	DPQ
PORTABLE	11 1 0000 0001	11 1 0000 0001
MAIN ECU	11 1 0000 0010	11 1 0000 0010
3	11 1 0000 0011	11 1 0000 0011
4	11 1 0000 0100	11 1 0000 0100
5	11 1 0000 0101	11 1 0000 0101
6	11 1 0000 0110	11 1 0000 0110
7	11 1 0000 0111	11 1 0000 0111
8	11 1 0000 1000	00 1 1111 1101
9	11 1 0000 1001	00 1 1111 1110
10	11 1 0000 1010	00 1 1111 1111

5. Result and Analysis

Fig 7 shows the transmission delay time of the Node 1. From 1 to 50, the X axis values show the transmission delay time when the transmission period was 10 ms. And from 51 to 100, the values show the transmission delay time when the transmission period was 2 ms. And from 101 to 150, the values show the transmission delay time when the DPQ mode was applied.

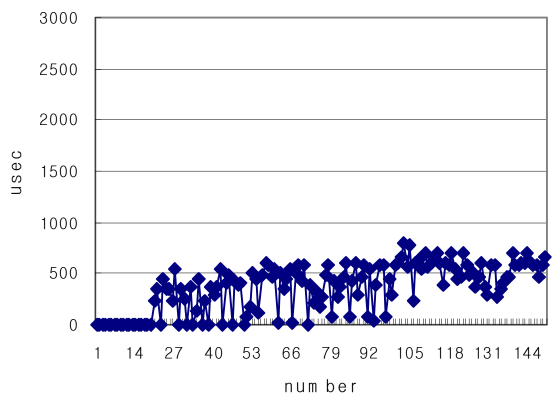

Fig 7. Transmission delay time of node 1

From the Fig 7 results, we know that Node 1 increased the delay time more when the transmission period was 2 ms than when the transmission period was 10 ms. And additional delay time occurred for Node 8, 9 and 10 in DPQ mode.

As shown in Fig 8, in the case of Node 8, the state which a transmission period is 2ms, a longer delay time occurred for low priority nodes than other nodes. To overcome this problem, we can verify that a transmission chance was guaranteed and the delay time was advanced outstandingly, when the DPQ mode was applied instead of changing the priority permanently, as shown in Fig 9.

In case of experiment 2 shown in the Fig 11, the graph shows a transmission delay time. From 1 to 50, the X axis values show a transmission delay time for the highest priority Node 1 when the transmission period was 2 ms. And from 51 to 100, the values are shown for that when the node number was 10. From 101 to 150, the values are shown for when the DPQ mode was applied.

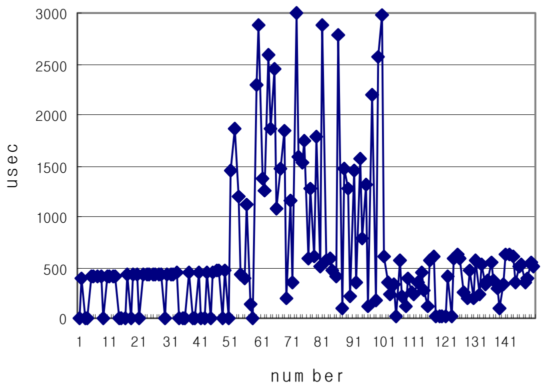

Fig 8. Transmission delay time of node 8

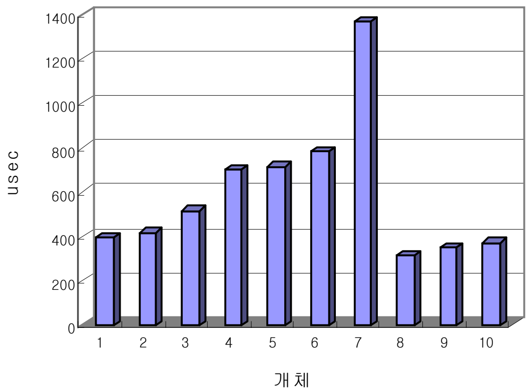

Fig 9. Average transmission delay time of DPQ mode

6. Conclusion

This study applied the DPQ mechanism to correct the ineffectiveness occurring according to a fixed priority mechanism and to arbitrate collisions in a network using a standard CAN protocol. The proposed mechanism established the availability through an experiment of two different states.

The experiment showed that a transmission of a low priority node does not exceed the maximum tolerance delay time using the DPQ mode, despite frequently occurring collisions in transmission and the rapid transmission of each node.

But, in the case of the DPQ mode being applied to high priority object, the effectiveness was lower than that of a standard CAN application. In future research, algorithms will be developed to efficiently manage the time delay of each object, applying the DPQ mechanism dynamically. And it will be shown how these algorithms can be applied conveniently for compatibility with other CAN applications.

Acknowledgments

This work was supported (in part) by the Ministry of Science & Technology, Korea, under the Region Research Center University (RRCU).

References

[1] International Standard Organization, "Road - vehicles Interchange of digital information - Controller area network for high-speed communication" *ISO 11898*, November, 1993.

[2] International Standard Organization, "Road - vehicles Interchange of digital information - Controller area network for high-speed communication" Draft Amendment, *ISO 11898*:1993/DAM 1, February, 1994.

[3] CAN in AUTOMATION International Users and Manufacturers Group e. V. "CAN Application Layer (CAL)", CiA/DS201-CiA/DS205, CiA/DS207.

[4] Jin W. Park, Dong K. No, Jae H. Park, Hwa R. Hur, Jang M. Lee, "Implementation of a Mobile Robot with Distributed Control Structure using CAN" Autumn Combination Conference . pp 251-255.1999.

[5] Sung S. Hong, "A distributed real time control systems," CASE Technical Special: Real-Time Control System (3), *ICASE*, 1, 1998.

[6] IEEE Standards for Local Area Networks, "Carrier Sense Multiple Access with Collision Detection (CSMA/CD) Access Method and Physical Layer Specifications", *ANSI/IEEE Std 802.3*- ISO/DIS 8802/3, 1985.

[7] K. Tindell and A. Burns and A. Wellings, "Calculating Controller Area Network (CAN) Message Response Times", *in Proc. 1994 IFAC Workshop on Distributed Computer Control Systems*, Toledo, Spain, September, 1994.

[8] K. Tindell and A. Burns, "Guaranteeing Message Latencies on Control Area Network (CAN)", *in Proc. 1 st International CAN Conference*, Mainz, Germany, September, 1994.

[9] K. Tendell, A. Burns and A. Wellings, "Analysis of Hard Real-Time Communications", *Report YCS 222, Department of Computer Science*, University of York , to appear in Real-Time Systems, 1994.

[10] "SDS-Smart distributed system specification" *Hineysell Inc.*, Micro Switch Division, Phoenix, AZ, GS 052-103/104/1-5/106/107/108.

Adaptive Occupancy Grid Mapping With Clusters

Byoung-Gi Jang and Tae-Yong Choi and Ju-Jang Lee
Electrical Engineering and Computer Science
Korea Advanced Institute of Science and Technology(KAIST)
373-1, Guseong-dong, Yuseong-gu, Daejeon, 305-701, Korea
ee185zzang@kaist.ac.kr, ermzace@odyssey.kaist.ac.kr, jjlee@ee.kaist.ac.kr

Abstract

In this paper, we describe an algorithm for acquiring occupancy grid maps with mobile robots. The standard occupancy grid mapping developed by Elfes and Moravec in the mid-Eighties decomposes the high-dimensional mapping problem into many one-dimensional estimation problems which are then tackled independently. Because of the independencies between neighboring grid cells, it often generates maps that are inconsistent with the sensor data. To overcome it, we propose the cluster which is a set of cells. The cells in the clusters are tackled dependently with another occupancy grid mapping with EM algorithm. The occupancy grid mapping with EM algorithm yields more consistent maps, especially in the cluster. As we use mapping algorithm adaptively with clusters according to the sensor measurements, our mapping algorithm is faster and more accurate than the previous mapping algorithms.

Keywords : occupancy grid, mobile robotics, mapping, Bayes rule, cluster

1 Introduction

Robotic mapping has been a highly active research area in robotics and AI for a few decades. Robotic mapping addresses the problem of acquiring spatial models of physical environments through mobile robots. There are a number of mapping algorithms. However, the occupancy grid mapping is more popular than others, since it has the reputation of being extremely robust and easy to implement. Once mapped through occupancy grid mapping, they enable various key functions necessary for mobile robot navigation, such as localization, path planning, collision avoidance, and people finding.

Occupancy maps have been built using various sensors, such as sonar sensor, laser range finders, and stereo vision, etc. However, all these sensors are subject to errors often referred to as measurement noise. In addition, sonar sensors cover an entire cone in space and form a single sonar measurement it is impossible to say where in the cone the object is. The sonar sensors are also sensitivity to the angle of an object surface relative to the sensor and the reflective properties of the surface. The above properties of sensors make a mapping problem be difficult and lead inconsistent map.

The occupancy grid mapping resolves such problems by generating probabilistic maps. As the name suggests, occupancy grid maps are represented by girds. Namely, they decompose the high-dimensional mapping problem into many one-dimensional estimation problems which are then tackled independently. Because of the independency of neighboring cells, they often generate maps that are inconsistent with the data, particularly in cluttered environments.

To overcome it, we define the cluster which is a set of cells. The cluster is the region that has the high probability to be inconsistent with the sensor data when the standard occupancy grid mapping is used. Existing occupancy grid mapping algorithms do the task with the emphasis on individual cells. However, our approach maps with the emphasis on clusters. As making the cluster and choosing the optimal mapping algorithm according to the sensor measurements, maps generated by our approach more accurate than ones generated by the previous occupancy grid mapping algorithm. Our mapping algorithm is also as fast as the standard occupancy grid mapping algorithm.

2 Standard Occupancy Grid Mapping

The Standard occupancy grid mapping approach (Elfes, 1989; Moravec, 1988)[2][3] constitutes two algorithms mainly. First, it decomposes a multidimensional (typically 2D or 3D) tessellation of space into many independent cells. Second, each cell calculates a probabilistic estimate of its state. To calculate this estimate, techniques such as Bayesian reasoning are then employed on the grid cell level. And each cell is tackled independently.

Let m be the occupancy grid map. The grid cell has the index $\langle x, y\rangle$ to store a probabilistic occupancy, which is $m_{x,y}$. Occupancy grid maps are estimated from sensor measurements. Let $z_1, \cdots, z_T$ denote the measurements from time 1 through time T. The measurement is composed of a sonar scan and the robot pose at which the measurement was taken. The robot pose which is assumed to be known is xy coordinates of the robot and heading direction. Each measurement carries information about the occupancy of many gird cells. Thus, the problem addressed by occupancy grid mapping is the problem of determining the probability of occupancy of each grid cell $m_{x,y}$ given the measurements $z_1, \cdots, z_T$.

$$p(m_{x,y} \mid z_1, \cdots, z_T) \tag{1}$$

For computational reasons, it is common practice to calculate the *log-odds* instead of estimating the above posterior. The *log-odds* is defined as follows.

$$l^T_{x,y} = \log \frac{p(m_{x,y} \mid z_1, \cdots, z_T)}{1 - p(m_{x,y} \mid z_1, \cdots, z_T)} \tag{2}$$

The assumption in standard occupancy grid mapping is the static world and conditional independence given knowledge of each individual grid cell $m_{x,y}$. Two assumptions and Bayes rule allow us to simplify the posterior to following:

$$\begin{aligned} p(m_{x,y} \mid z_1, \cdots, z_t) \\ = \frac{p(m_{x,y} \mid z_t)p(z_t)p(m_{x,y} \mid z_1, \cdots, z_{t-1})}{p(m_{x,y})p(z_t \mid z_1, \cdots, z_{t-1})} \end{aligned} \tag{3}$$

Let $\overline{m}_{x,y}$ be freeness of the grid cell. The probability of the freeness of grid cell can be calculated as same way.

$$\begin{aligned} p(\overline{m}_{x,y} \mid z_1, \cdots, z_t) \\ = \frac{p(\overline{m}_{x,y} \mid z_t)p(z_t)p(\overline{m}_{x,y} \mid z_1, \cdots, z_{t-1})}{p(\overline{m}_{x,y})p(z_t \mid z_1, \cdots, z_{t-1})} \end{aligned} \tag{4}$$

By dividing (3) by (4) and adapting logarithm, the desired *log-odds* is expressed as follow:

$$l^t_{x,y} = \log \frac{p(m_{x,y} \mid z_t)}{1 - p(m_{x,y} \mid z_t)} + \log \frac{1 - p(m_{x,y})}{p(m_{x,y})} + l^{t-1}_{x,y} \tag{5}$$

Finally, the desired posterior occupancy probability $p(m_{x,y}|z_1, \cdots, z_T)$ can be recovered from the log-odds representation of the map.

Standard occupancy grid mapping does not take the occupancy of neighboring cells into account. It makes the crucial independence assumption that the occupancy of a cell can be predicted regardless of a cell's neighbors. Herein lies a major problem of the standard occupancy approach. This leads to incorrect map.

3 Adaptive Occupancy Grid Mapping With Clusters

This section presents an algorithm to improve the problems of the previous occupancy grid mapping. A key idea is adapting the cluster which is a set of cells. The cells in the cluster mean that they have the high probability to be inconsistent with the sensor data when the standard occupancy grid mapping is used. Unlike existing occupancy grid mapping algorithm, our approach does the mapping with the emphasis on the clusters. One cluster doesn't affect the others, since the cluster is independent each other. The occupancy of the cells in the cluster is calculated with the occupancy grid mapping proposed by Thrun in 2003[1]. Using Expectation Maximization algorithm, in short EM, the alternative mapping algorithm solves the mapping problem as maintaining the dependencies between neighboring cells. Hence, it leads to the more accurate maps than the standard occupancy grid mapping in the cluster. The clusters are made with the neural networks[4][5][6] which is a powerful tool in pattern recognition.

To make the cluster, we use the neighboring sensor measurements which are the input of neural networks.

$$P = [p_1, \cdots, p_R] \tag{6}$$

R is the number of the sensor measurements used. The output of neural networks, y, is $'1'$ if the region swept by the sensors is cluttered or erroneous place. Otherwise y is $'0'$. That is, if y is $'1'$, we assemble the cells in that region and make a new cluster.

The occupancy of cells out of cluster is calculated with the standard occupancy grid mapping algorithm explained in section 2. The binary occupancy of cells in the cluster is calculated with the alternative occupancy grid mapping proposed by Thrun.

Let K_i the number of obstacles in the sensor cone of the i-th measurement. Let $D_t = \{d_{t,1}, \cdots, d_{t,K_t}\}$ denote the distances to these obstacles and ordered in increasing order. To describe the multiple causes of a sensor measurement z_i, the new variables, called correspondence variables, are defined as follow:

$$c_t = \{c_{t,*}, c_{t,0}, c_{t,1}, \cdots, c_{t,K_t}\} \quad (7)$$

Each of these variables corresponds to exactly one cause of the measurement z_t. If $c_{t,k}$ is 1 for $1 \leq k \leq K_t$, the measurement is caused by the k-th obstacle. If $c_{t,0}$ is 1, none of the obstacles were detected and the sensor returns a max-range reading. The random variable $c_{t,*}$ corresponds to the case where a measurement was purely random. The log-likelihood of all data and correspondences is written as follows:

$$\log p(Z, C|m) = \sum_t \log p(z_t, c_t|m) \quad (8)$$

Here Z denotes the set of all measurements and C is the set of all correspondences c_t for all data. Not calculating the probability of the correspondence variables but Maximization the likelihood of the data is important, since the probability of correspondence variables is unobservable. This is achieved by maximizing the expected log-likelihood $E[\log p(Z, C|m)|Z, m]$, where the expectation is taken over the correspondence variables C. The expected log-likelihood can be obtained as follows:

$$\begin{aligned} & E[\log p(Z, C|m)|Z, m] \\ & \quad = \sum_t [E[\log p(c_t)|z_t, m] + \log \frac{1}{\sqrt{2\pi\sigma^2}} \\ & \quad -\frac{1}{2}[E[c_{t,*}|z_t, m] \log \frac{z_{max}^2}{2\pi\sigma^2} \\ & \quad +E[c_{t,0}|z_t, m] \frac{(z_t - z_{max})^2}{\sigma^2} \\ & \quad +\sum_{k=1}^{K_t} E[c_{t,k}|z_t, m] \frac{(z_t - d_{t,k})^2}{\sigma^2}]] \end{aligned} \quad (9)$$

Maximizing the above expected log-likelihood is the final goal. To do this, *expectation maximization algorithm*, EM algorithm, is used. The EM algorithm is one such elaborate technique. The EM algorithm is a general method of finding the maximum-likelihood estimate of the parameters of an underlying distribution form a given data set when the data is incomplete or has missing values.

As the above way, we choose the optimal mapping algorithm according to the sensor measurements, namely clusters. Hence, maps generated by our approach are faster and more accurate than ones generated by the previous occupancy grid mapping algorithm.

4 Simulation

In order to test our approach, we applied our approach to learning grid maps using simulated data. Our main finding are that the maps generated our approach are more accurate and the approach has less time than the previous occupancy grid mapping algorithm, such as the standard occupancy grid mapping algorithm and the alternative occupancy grid mapping algorithm with EM.

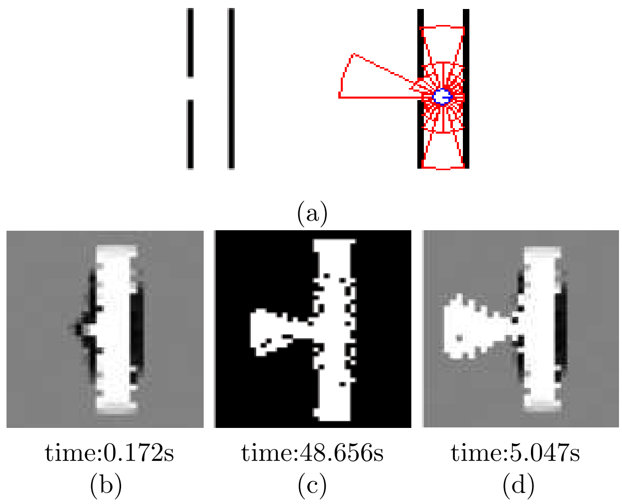

Figure 1: Narrow open door without error

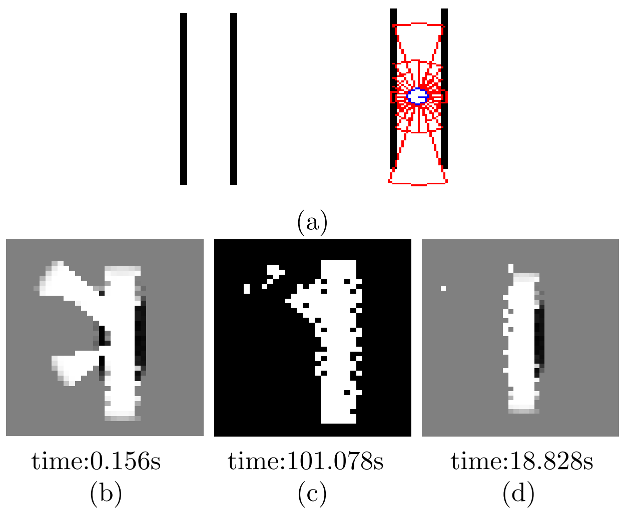

Figure 2: Corridor with error

The sensor measurements are gathered in a corridor while driving by an open door. The mobile robot is equipped with a circular array of 24 sonar sensors.

Figure 1(a) shows a narrow open door as a first example. The width of the door is two times wider than the width of mobile robot. Hence, the mobile robot can pass through the door, but it may be difficult to control. Figure 1(b) shows the result of the standard occupancy grid mapping algorithm. In the standard occupancy grid mapping, a narrow open door is not detected, but other places are similar to Figure 1(a). Figure 1(c) is obtained by the alternative occupancy grid mapping with EM. In Figure 1(b), the door is detected, but it takes much time to calculate. In Figure 1(d) generated by our approach, the door is detected and it takes less time than the occupancy grid mapping with EM. Figure 2 shows the result of corridor with the error measurements. Figure 2(a) is a simulated environment. As Figure 2(b) shows map of the standard occupancy grid mapping, map is incorrect because of the sensor error. In Figure 2(c), the alternative occupancy grid mapping detect incorrectly in one place though it is better than (b). Unlike Figure 2(b) and Figure 2(c), Figure 2(d) shows an accurate map. As Figure 2(d) is generated by our approach, the map is similar to the environment(a). Because of clusters, our approach is more accurate than the occupancy grid mapping with EM in erroneous place. Our approach takes also less time than others.

As a result, because our approach maps with the emphasis on the clusters, maps generated with adaptive occupancy grid mapping algorithm, more accurate and faster than the others.

5 Conclusion

In this paper, the adaptive occupancy grid mapping algorithm is proposed. Unlike existing occupancy grid mapping algorithm, our approach relies on the clusters. The clusters are the region that have the high probability to be inconsistent with the sensor data. Neural networks is used to make a cluster. According to the cluster, we use optimal occupancy grid mapping algorithm. As seeing in simulation result, we can map more accurate and faster than the previous occupancy grid mapping.

References

[1] Thrun, S, "Learning Occupancy Grid Maps with Forward Sensor Models," *Autonomous Robots*,Vol. 15, pp. 111-127, 2003.

[2] A. Elfes, "Using Occupancy Grids for Mobile Robot Perception and Navigation," *IEEE Computer*,Vol. 22, pp. 46-57, 1989.

[3] H.P Moravec, "Sensor Fusion in Certainty Grids for Mobile Robots," *IEEE Computer*,Vol. 22, pp. 46-57, 1989.

[4] L, Fausett, "Fundamentals of Neural Netwoks: Architectures, Algorithms, and Application," Prentice-Hall, 1994.

[5] Riedmiller, M, "A Direct Adaptive Method for Faster Backpropagation Learning: The RPROP Algorithm," *IEEE Neural Network*,Vol. 1, pp. 586-591, 1993.

[6] C.H Kim, "Feature Extration Method for A Robot Map Using Neural Networks," *AROB*, Vol. 1, pp. 256-258, 2002.

The Tenth International Symposium on Artificial Life and Robotics 2005(AROB 10th '05),
B-con Plaza, Beppu, Oita, Japan, February 4-6, 2005

Real Time Implementation of Visual Servoing Control of SCARA Robot with Eight Joints

Dong Yean Jung, Hong Rae Kim

Dept. of Mechanical Design, Graduate School,
Kyungnam University,
Masan, Gyeongnam, 631-701, Korea

Sung Hyun Han

School of Mechanical and Automation Eng.,
Kyungnam University,
Masan, Gyeongnam, 631-701, Korea

Abstract

Visual servoing is the fusion of results from many elemental areas including high-speed image processing, kinematics, dynamics, control theory, and real-time computing. It has much in common with research into active vision and structure from motion, but is quite different from the often described use of vision in hierarchical task-level robot control systems. We present a new approach to visual feedback control using image-based visual servoing with the stereo vision in this paper. In order to control the position and orientation of a robot with respect to an object, a new technique is proposed using a binocular stereo vision. The stereo vision enables us to calculate an exact image Jacobian not only at around a desired location but also at the other locations. The suggested technique can guide a robot manipulator to the desired location without giving such priori knowledge as the relative distance to the desired location or the model of an object even if the initial positioning error is large. This paper describes a model of stereo vision and how to generate feedback commands. The performance of the proposed visual servoing system is illustrated by the simulation and experimental results and compared with the case of conventional method for dual-arm robot made in Samsung Electronics Co., Ltd..

1 Introduction

Many of the control and vision problems are similar to those encountered by active vision researchers who are building " robotic heads" . However the task in visual servoing is to control a robot to manipulate its environment using vision as opposed to just observing the environment.

There are mainly two ways to put the visual feedback into practice. One is called look-and-move and the other is visual servoing. Visual servoing is the fusion of results from many elemental areas including high-speed image processing, kinematics, dynamics, control theory, and real-time computing. It has much in common with research into active vision and structure from motion, but is quite different from the often described use of vision in hierarchical task-level robot control systems. The former is the method which transforms the position and orientation of an object obtained by a visual sensor into those in the world frame fixed to an environment and guides the arm of the manipulator to a desired location in the world frame.[1,2] In this method, precise calibration of a manipulator and camera system is needed. On the contrary, visual servoing uses the Jacobian matrix which relates the displacement of an image feature to the displacement of a camera motion and performs a closed-loop control regarding the feature as a scale of the state. Therefore, we can construct a servo system based only on the image and can have a robust control against the calibration error because there is no need to calculate the corresponding location in the world frame.[2,3,4] A hand eye system is often used in visual feedback and there are two ways of arranging the system. One is placing a camera and a manipulator separately; the other is placing the camera at the end-tip of the manipulator. The former motion strategy of the manipulator becomes more complicated than the latter. In the latter, it is easy to control the manipulator using a visual information because the camera is mounted on the manipulator end-tip. In this paper, we deal with the latter method. In the conventional works, some researches have presented methods to control the manipulator position with respect to the object or to track the feature points on an object using a hand eye system as the application of visual servoing.[3,4] These methods maintain or accomplish a desired relative position between the camera and the object by monitoring feature points on the object from the camera.[5,6]

However, these have been all done by the hand eye system with monocular visions and it is necessary to compensate for the loss of information because the original three-dimensional information of the scene is reduced to two-dimension information on the image. For instance, we must add an information of the three-dimension distance between the feature point and the camera in advance or use a model of object stored in the memory. Besides, a problem that the manipulator position fails to converge to a desired value arises depending on the way of selecting feature points or when the initial positioning error is not small. It is because some elements of the image Jacobian cannot be computed with only the information of the image and substituting approximate values at the desired location for them may result in large errors at the other locations.[7]

This paper presents a method to solve this problem by using a binocular stereo vision. The use of stereo vision can lead to an exact image Jacobian not only at around a desired location but also at the other locations. The suggested technique places a robot manipulator to the desired location without giving such priori knowledge as the relative distance to the desired location or the model of an object even if the initial positioning error is large.

This paper deals with modeling of stereo vision and how to generate feedback commands. The performance of the proposed visual servoing system was evaluated by the simulations and experiments and obtained results were compared with the conventional case for a SCARA type dual-arm robot.

2 Visual Servo System

Visual servo systems typically use one of two camera configurations: end-effector mounted, or fixed in the workspace.

The first, often called an eye-in-hand configuration, has the camera mounted on the robot's end-effector. Here, there exists a known, often constant, relationship between the pose of the camera(s) and the pose of the end-effector.

We define the frame of a hand-eye system with the stereo vision and use a standard model of the stereo camera whose optical axes are set parallel each other and perpendicular to the baseline. The focal points of two cameras are apart at distance d on the baseline and the origin of the camera frame Σ_c is located at the center of these cameras.

An image plane is orthogonal to the optical axis and apart at distance f from the focal point of a camera and the origins of frame of the left and right images, Σ_l and Σ_r, are located at the intersecting point of the two optical axes and the image planes. The origin of the world frame Σ_w is located at a certain point in the world. Now let ${}^l p=({}^l x, {}^l y)$ and ${}^r p=({}^r x, {}^r y)$ be the projections onto the left and right images of a point p in the environment, which is expressed as ${}^c p=({}^c x\ {}^c y\ {}^c z)^T$ in the camera frame. Then the following equation is obtained (see Fig. 1).

$$\begin{aligned} {}^l x\ {}^c z &= f\,({}^c x + 0.5d) \\ {}^r x\ {}^c z &= f\,({}^c x - 0.5d) \\ {}^l y\ {}^c z &= f\ {}^c y \\ {}^r y\ {}^c z &= f\ {}^c y \end{aligned} \tag{1}$$

Suppose that the stereo correspondence of feature points between the left and right images are found. In the visual servoing, we need to know the precise relation between the moving velocity of camera and the velocity of feature points in the image, because we generate a feedback command of the manipulator based on the velocity of feature points in the image.

This relation can be expressed in a matrix form which is called the image Jacobian. Let us consider n feature points $p_k\,(k=1,\cdots,n)$ on the object and the coordinates in the left and right images are ${}^l p_k({}^l x_k, {}^l y_k)$ and ${}^r p_k({}^r x_k, {}^r y_k)$, respectively. Also define the current location of the feature points in the image ${}^I p$ as

$${}^I p = ({}^l x_1\ {}^r x_1\ {}^l y_1\ {}^r y_1\ \cdots\ {}^l x_n\ {}^r x_n\ {}^l y_n\ {}^r y_n)^T \tag{2}$$

where each element is expressed with respect to the virtual image frame Σ_p.

First, to make it simple, let us consider a case when the number of the feature points is one. The relation between the velocity of feature point in image ${}^I \dot{p}$ and the velocity of camera frame ${}^c \dot{p}$ is given as

$${}^I \dot{p} = {}^I J_c\ {}^c \dot{p} \tag{3}$$

where ${}^I J_c$ is the Jacobian matrix which relates the two frames. Now let the translational velocity components of camera be σ_x, σ_y and σ_z and the rotational velocity components be w_x, w_y, w_z then we can express the camera velocity V as

$$\begin{aligned} V &= [\sigma_x\ \sigma_y\ \sigma_z\ w_x\ w_y\ w_z]^T \\ &= [{}^c v\ {}^c w_c]^T \end{aligned} \tag{4}$$

Then the velocity of the feature point seen from the camera frame ${}^c \dot{p}$ can be written

$$\begin{aligned} {}^c \dot{p} &= \frac{d\ {}^c p}{dt} \\ &= \frac{d}{dt}\ {}^c R_w\,({}^w p - {}^w p_c) \\ &= {}^c R_w \{-{}^w w_c \times ({}^W p - {}^w p_c)\} + {}^c R_w ({}^W \dot{p} - {}^w \dot{p}_c) \end{aligned} \tag{5}$$

Where ${}^c R_w$ is the rotation matrix from the camera frame to the world frame and ${}^w p_c$ is the location of the origin of the camera frame written in the world frame. As the object is assumed to be fixed into the world frame, ${}^w \dot{p}=0$. The relation between ${}^c \dot{p}$ and V is

$$\begin{aligned} {}^c \dot{p} &= {}^c R_w \{-{}^w w_c \times ({}^w p - {}^w p_c)\} - {}^c R_w\ {}^w \dot{p}_c \\ &= -{}^c w_c \times {}^c p - {}^c \dot{p}_c \\ &= \begin{bmatrix} -w_y\ {}^c z + w_z\ {}^c y - v_x \\ -w_z\ {}^c x + w_x\ {}^c z - v_y \\ -w_x\ {}^c y + w_y\ {}^c x - v_z \end{bmatrix} \end{aligned} \tag{6}$$

Therefore, substituting Eq. (6) into Eq. (3), we have the following equation.

$$\begin{aligned} {}^{I}\dot{p} &= {}^{I}J_{c}\,{}^{c}\dot{p} \\ &= JV \end{aligned} \tag{7}$$

In Eq. (7) matrix J which expresses the relation between velocity ${}^{I}\dot{p}$ of the feature point in the image and moving velocity V of the camera is called the image jacobian.

From the model of the stereo vision Eq. (1), the following equation can be obtained.

$$2\,{}^{c}x(\,{}^{l}x - {}^{r}x) = d\,(\,{}^{l}x + {}^{r}x) \tag{8}$$

$${}^{c}y(\,{}^{l}x - {}^{r}x) = {}^{l}y d = {}^{r}y d \tag{9}$$

$${}^{c}z(\,{}^{l}x - {}^{r}x) = f\,d \tag{10}$$

Above discussion is based on the case of one feature point. In practical situation, however, the visual servoing is realized by using plural feature points. When we use n feature points, image Jacobian $J_1,\cdots,J_n$ are given from the coordinates of feature points in the image. By combining them, we express the image Jacobian (J_{im}) as

$$J_{im} = [\,J_1 \cdots\cdots J_n\,]^T \tag{11}$$

Then, it is possible to express the relation of the moving velocity of the camera and the velocity of the feature points even in the case of plural feature points, that is,

$${}^{I}\dot{p} = J_{im}V \tag{12}$$

where we suppose that the stereo and temporal correspondence of the feature points are found.

In the case of the monocular, the image Jacobian J has the following form.

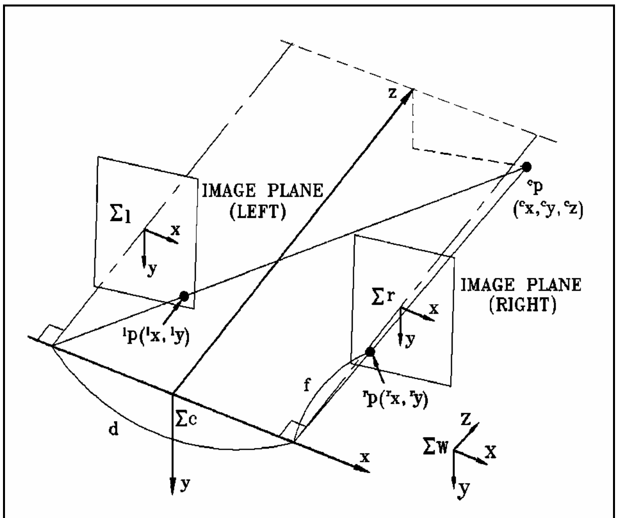

Fig. 1 The coordinates system of vision model

$$J = f\begin{bmatrix} -\dfrac{1}{{}^{c}x} & 0 & \dfrac{{}^{c}x}{{}^{c}x^2} & \dfrac{{}^{c}x{}^{c}y}{{}^{c}z} & -\left(1+\dfrac{{}^{c}x^2}{{}^{c}x^2}\right) & \dfrac{{}^{c}y}{{}^{c}z} \\ 0 & -\dfrac{1}{{}^{c}x} & \dfrac{{}^{c}y}{{}^{c}x^2} & 1+\dfrac{{}^{c}y^2}{{}^{c}z_2} & -\dfrac{{}^{c}x{}^{c}y}{{}^{c}x^2} & -\dfrac{{}^{c}x}{{}^{c}z} \end{bmatrix} \tag{13}$$

The x, y and z axes of the coordinate frames are shown in Fig. 1.

We now introduce the positional vector of the feature point in the image of monocular vision using the symbol ${}^{m}P = ({}^{m}x,\ {}^{m}y)$. This is the projection of the point expressed as ${}^{c}P = ({}^{c}x\ {}^{c}y\ {}^{c}z)^T$ in the camera frame into the image frame of the monocular vision, and has the following relation.

$${}^{m}x = f\ {}^{c}x\ {}^{c}z^{-1} \tag{14-a}$$

$${}^{m}y = f\ {}^{c}y\ {}^{c}z^{-1} \tag{14-b}$$

Substituting Eq.s (14-a) and (14-b) into Eq. (13) yields another expression of the image Jacobian for the monocular vision.

$$J = f\begin{bmatrix} -\dfrac{1}{{}^{c}z} & 0 & \dfrac{{}^{m}x}{{}^{c}x} & \dfrac{{}^{m}x{}^{m}y}{f} & -\dfrac{{}^{m}x^2+f^2}{f^2} & {}^{m}y \\ 0 & -\dfrac{f}{{}^{c}x} & \dfrac{{}^{m}y}{{}^{c}x} & 1+\dfrac{{}^{m}y^2+f^2}{f^2} & -\dfrac{{}^{m}x{}^{m}y}{f} & -{}^{m}x \end{bmatrix} \tag{15}$$

A disparity which corresponds to the depth of the feature point, is included in J in the case of the stereo vision, but s-term expressed in the camera frame ${}^{c}z$ is included in J in the case of the monocular vision.

In the visual servoing, the manipulator is controlled so that the feature points in the image reach their respective desired locations.

We define an error function between the current location of the feature points in image ${}^{I}p$ and the desired location ${}^{I}p_d$ as

$$E = Q({}^{I}p - {}^{I}p_d) \tag{16}$$

where Q is a matrix which stabilizes the system. Then the feedback law is defined as following equation

$$V = -G\ E \tag{17}$$

where G corresponds to a feedback gain.

To realize the visual servoing, we must choose Q so that convergence is satisfied with the error system can be satisfied with

$$\begin{aligned} \dot{E} &= \frac{\partial E}{\partial t} = Q\frac{\partial^{I}\dot{p}}{\partial t} = Q^{I}\dot{P} \\ &= QJ_{im}V = -GQJ_{im}E \end{aligned} \tag{18}$$

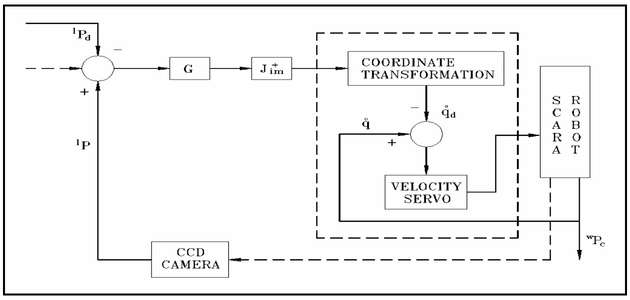

Fig. 2 Block diagram of visual feedback system.

We use pseudo-inverse matrix of the image Jacobian J_{im} for Q to make $Q J_{im}$ positive and not to make an input extremely large, that is,

$$Q = J_{im}^{+} = (J_{im}^{T} J_{im})^{-1} J_{im}^{T} \qquad (19)$$

Therefore, the feedback command is given as

$$V = -G J_{im}^{+} ({}^{I}p - {}^{I}p_d) \qquad (20)$$

Fig. 2 shows a block diagram of the control scheme described by Eq. (20). Note that the feedback command u is sent to the robot controller and both the transformation of u to the desired velocity of each joint angle $\dot{q}_d$ and its velocity servo are accomplished in the robot controller as show in Fig. 2.
Furthermore, as J_{im} is a $4n \times 6$ matrix and pseudo-inverse matrix J_{im}^{+} is a $6 \times 4n$ matrix, a feedback command Eq. (20) of 6 degrees of freedom is obtained.

3 Experiments

We have compared the visual servoing using the monocular vision with that using the stereo vision by the experiment. Fig. 3 represents the experimental equipment set-up. In Fig. 3 two DSP vision boards were used, which had been made Samsung Electronics Company in Korea based-on the TMS320C31 chips.
In the experiment, feature points of an object are the four corners of a square whose side dimension is $300\,mm$. In the same condition, we used four feature points even in the stereo vision. Parameters used the focal length, $f = 16\,mm$, baseline $d = 130\,mm$, sampling time of $50\,m\sec$, gain $\lambda = 1$, desired location ${}^{c}P_d = (100\ 100\ 500)^T\,mm$, desired orientation in Euler angle $(\phi, \theta, \psi) = (0, 0, 0)\,rad$, initial error $(-50, -50, -50)^T\ mm$ in the translation and $(\phi, \theta, \psi) = (20, 20, 20)\,rad$ in the orientation.

We select the four corners of a rectangle whose size is $200 \times 200\,mm$ as the feature points and set the translational error as $(-150\ -150\ -450)\,mm$ and the other values are the same as before.

The error between the desired location and the current location of the feature points in cases of the monocular and stereo visions are shown in Fig. 4.
Next, we will show the results for the change of the way to choose the feature points and set the initial error image.

In Fig. 4, we can see that the result diverges in the case of the monocular vision, but converges in the case of the stereo vision. This is because the image Jacobian is fixed at the desired location in case of the monocular vision. Therefore, a correct feedback command can not be generated when the initial error is large. On the other hand, the image Jacobian can be updated at every in the case of the stereo vision, thus it is possible to generate a correct feedback command which assures the stability visual servoing.

In experiments, we used a SCARA type dual-arm robot made in Korea with a stereo camera attached to the end tip of the arm. The feature points are three circular planes of $20\,mm$ radius on three corners of a equilateral triangle, one side $87\,mm$ and are placed on the board. Precise calibration had not been done for the stereo camera attached to the end-tips.

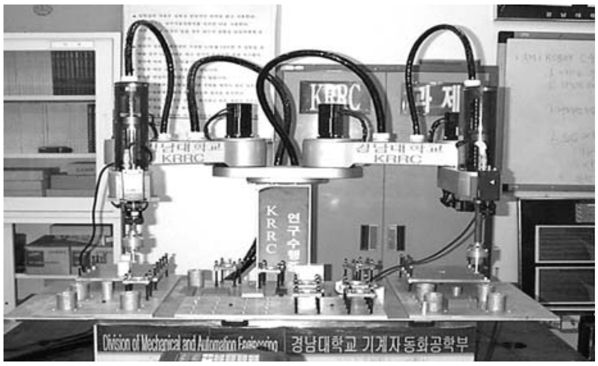

Fig. 3 The experimental equipment set-up.

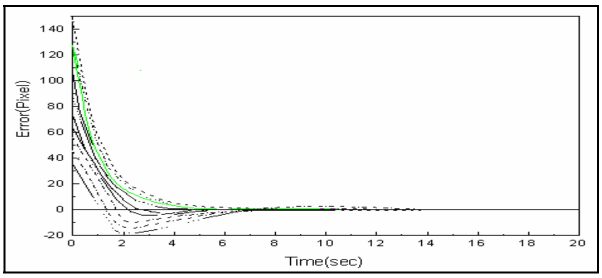

(a) Monocular

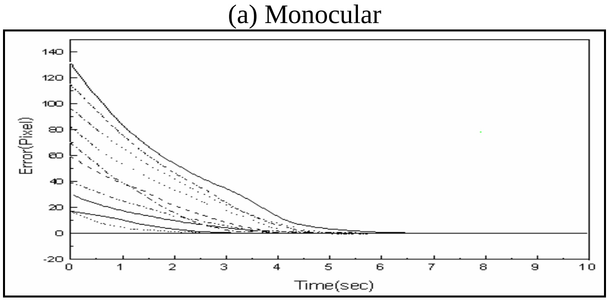

(b) Stereo

Fig. 4 Positional error in x and y axes in the case of the stereo and monocular vision.

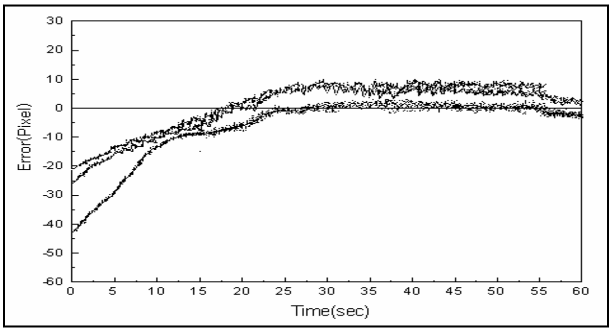

(a) Left image

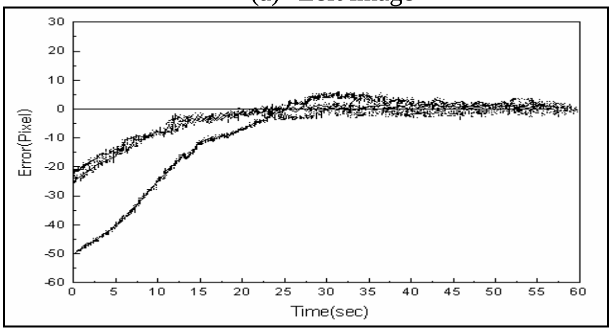

(b) Right image

Fig. 5 Position error in x and y axes.

Two stereo images were taken and transformed to the binary images in the real time and in parallel by two image input devices and the coordinate of the gravitational center of each feature point was calculated in parallel by two transporters. We gave the stereo correspondence of the feature point in the first sampling. However, the stereo and temporal correspondence of the feature points in the succeeding sampling were found automatically by searching a nearby area where there were the feature points in the previous sampling frame. The coordinates of the feature points were sent to a transporter for motion control and it calculated a feedback command for the robot. The result was sent to the robot controller by using RS-232C, and the robot was controlled by a velocity servo system in the controller.

The sampling period of visual servoing was about $50m\sec$. Details were $16m\sec$ for taking a stereo images, about $1m\sec$ for calculating the coordinates of the feature points, $3m\sec$ for calculating feedback command, about $16m\sec$ for communicating with the robot controller. If we send a feedback input to the robot controller without using RS-232C, the faster visual servoing can be realized.

The desired location was $(0,0,500)^T mm$ and the desired orientation in Euler angle, $(\phi,\theta,\psi)=(0,0,0)$ degree and the initial error was $(50,50,50)^T mm$ for translation. The other parameters were the same as in the simulation. The error of current and desired location of the feature points are shown in Fig. 5. From these experimental results, we can see that the manipulator converges toward a desired location even if the calibration is not precise.

4 Conclusion

We proposed a new technique of visual servoing with the stereo vision to control the position and orientation of an assembling robot with respect to an object. The method overcomes the several problems associated with the visual servoing with the monocular vision. By using the stereo vision, the image Jacobian can be calculated at any position. So neither shape information nor desired distance of the target object is required. Also the stability of visual servoing is assured even when the initial error is very large. We have shown the effectiveness of this method by simulation and experiments.

To use this visual servoing in practical tasks, there still exist many problems such as the number of feature points to reduce noise or the quantization error and the way to choose feature points. Nevertheless, this method overcomes the several problems in visual servoing with the monocular vision.

Acknowledgements

This research was supported by the **N**ew **U**niversity for **R**egional **I**nnovation program of the Ministry of Education & Human Resources Development (NURI MECHANO 21).

References

[1] Hashimoto, K., Edbine, T., and Kimura, H., "Dynamic visual feedback control for a hand-eye manipulator". *In Proceedings of the IEEE/RSJ International Conference on Intelligent Robots and Systems*, pp. 1863-1868, 1992.

[2] Bernard, E., Francois, C., and Patrick, R., "Anew approach to visual servoing in robotics". *IEEE Transactions on Robotics and Automation*, pp. 313-326, 1992.

[3] Weiss, L. E., Sanderson, A. C., and Neuman, C. P., "Dynamic sensor-based control of robots with visual feedback". *IEEE Journal of Robotics and Automation*, pp. 404-417, 1987.

[4] G. Hager, S. Hutchinson, and P. I. Corke. "A tutorial on visual servo control". *IEEE Trans. Robotics & Automation*, Vol. 12, No. 5, pp. 651-670, 1996.

[5] V. Sundareswaran, P. Bouthemy, and F. Chaumette. "Exploiting image motion for active vision in a visual servoing framework". *International Journal of Robotics Research*. Vol. 15, No. 6, pp. 629-645, 1996.

[6] Allen, P. K., Toshimi, B., Timcenko, A., "Real Time Visual Servoing". *In Proceeding of the IEEE International Conference on Robotics and Automation*, pp. 851-856, 1991.

[7] Hashimoto, K., Kimoto, T. Edbine, T., and Kimura, H., "Manipulator control with image-based visual servo". *In Proceedings of IEEE International Conference on Robotics and Automation*, pp. 2267-2272, 1991.

The Tenth International Symposium on Artificial Life and Robotics 2005(AROB 10th '05),
B-con Plaza, Beppu, Oita, Japan, February 4-6, 2005

Tolerance of Permanent Magnet Biased Bidirectional Magnetic Bearings and Its Robotic Applications

Yong Tae Kim

Dept. of Mechanical Design, Graduate School,
Kyungnam University,
Masan, Gyeongnam, 631-701, Korea

Uhn Joo Na

School of Mechanical and Automation Eng.,
Kyungnam University,
Masan, Gyeongnam, 631-701, Korea

Abstract

A fault tolerant scheme of a bi-directional magnetic bearing is presented. The bearing continues to function normally even though one coil among four radial coils and one coil of two axial coils fail. The dynamic properties and load capacity remain unchanged for the suggested fault tolerant control scheme. A one-dimensional circuit that represents the bi-directional bearing is utilized to obtain the optimal bearing parameters such as the radial pole face area, number of coil turns, and permanent magnet size. The results identify advantages of the fault tolerant scheme and bi-directional bearing improvements relative to conventional magnetic suspension. Bidirectional magnetic bearings find applications in robotic joints.

1 Introduction

Magnetic bearings find greater use in high speed, high performance, applications such as gas turbines, energy storage flywheels, and pumps since they have many advantages over conventional fluid film or rolling element bearings, such as lower friction losses, lubrication free, temperature extremes, no wear, quiet, high speed operations, actively adjustable stiffness and damping, and dynamic force isolation. Unlike heteropolar bearings, homopolar magnetic bearings have a unique biasing scheme that directs the bias flux flow into the active pole plane where it energizes the working air gaps, and then returns through the dead pole plane and the shaft sleeve. Some of the results on modeling, design, and control of homopolar magnetic bearings are shown in literature. Meeks [1] utilized a permanent magnet biased homopolar magnetic bearing to provide smaller, lighter, and power-efficient operation. Fault-tolerance of the magnetic bearing system is of great concern for highly critical applications of turbomachinery since a failure of any one control components may lead to the complete system failure. Much research has been devoted to fault-tolerant heteropolar magnetic bearings. Maslen and Meeker [2] introduced a fault-tolerant 8-pole magnetic bearing actuator with independently controlled currents and experimentally verified it in [3]. Flux coupling in heteropolar magnetic bearings allows the remaining coils to produce force resultants identical to the unfailed bearing, if the remaining coil currents are properly redistributed. Na and Palazzolo [4, 5] also investigated the optimized realization of fault-tolerant magnetic bearing actuators, so that fault-tolerant control can be realized for an 8-pole bearing for up to 5 coils failed. This paper introduces a fault-tolerant 4-active-pole permanent magnet biased, bi-directional magnetic bearing such that the bearing can preserve the same decoupled magnetic forces identical to the unfailed bearing even after any one coil out of 4 coils fails.

2 Magnetic Circuit Analysis

Figure 1 shows a schematic drawing of a permanent magnet biased combo bearing. Four independent coils are wound on each radial pole to supply control fluxes. A pair of coils supplies axial control fluxes.

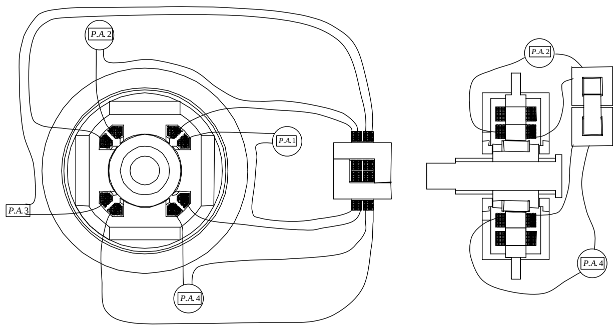

Fig. 1 Schematic of a Bidirectional Magnetic Bearing

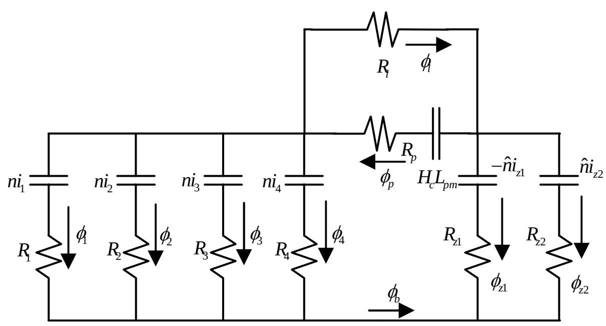

Fig. 2 Circuit for a Bidirectional Bearing

The permanent magnets are represented as the source H_cL_{pm} and the total permanent magnet reluctance R_p.

The coercive force and the length of the permanent magnet are H_c and L_{pm}, respectively. The reluctance in air gap j of the active pole plane is;

$$R_j = \frac{g_j}{\mu_0 a_0} \tag{1}$$

where

$$g_j = g_0 - x\cos\theta_j - y\sin\theta_j \tag{2}$$

The parameters μ_0, a_0, and g_0 represent the permeability of air, the pole face area of the active pole, and nominal air gap, respectively, and x and y are the journal displacements. The axial air gap reluctances are described as;

$$R_{zj} = \frac{g_{zj}}{\mu_0 a_{z0}} \tag{3}$$

where

$$g_{z1} = g_{z0} - z \ , \ \ g_{z2} = g_{z0} + z \tag{4}$$

and where a_{z0} and g_{z0} are the axial pole face area and the nominal axial gap, respectively, and z is the rotor displacement along the axial direction. Applying Ampere's law and Gauss's law to the radial magnetic circuit leads to a matrix equation.

$$\begin{bmatrix} R_1 & -R_2 & 0 & 0 \\ 0 & R_2 & -R_3 & 0 \\ 0 & 0 & R_3 & -R_4 \\ 1 & 1 & 1 & 1+\dfrac{R_4}{R_R} \end{bmatrix} \begin{bmatrix} \phi_1 \\ \phi_2 \\ \phi_3 \\ \phi_4 \end{bmatrix} = \begin{bmatrix} 0 \\ 0 \\ 0 \\ \dfrac{H_c L_{pm}}{\tilde{R}_R} \end{bmatrix} + \begin{bmatrix} 0 & 0 \\ 0 & 0 \\ 0 & 0 \\ \dfrac{-R_{z2}\tilde{n}}{R_R(R_{z1}+R_{z2})} & \dfrac{R_{z1}\tilde{n}}{R_R(R_{z1}+R_{z2})} \end{bmatrix} \begin{bmatrix} i_{z1} \\ i_{z2} \end{bmatrix} + \begin{bmatrix} n & -n & 0 & 0 \\ 0 & n & -n & 0 \\ 0 & 0 & n & -n \\ 0 & 0 & 0 & \dfrac{n}{R_R} \end{bmatrix} \begin{bmatrix} i_1 \\ i_2 \\ i_3 \\ i_4 \end{bmatrix} \tag{5}$$

where

$$R_R = \frac{R_p R_l}{R_p + R_l} + \frac{R_{z1} R_{z2}}{R_{z1} + R_{z2}} \quad \tilde{R}_R = R_p + \frac{R_{z1} R_{z2}}{R_{z1} + R_{z2}}\left(1 + \frac{R_p}{R_l}\right)$$

and ϕ_j, i_j, i_{zj}, n, and $\tilde{n}$ are fluxes, currents through j-th pole, axial currents, the number of radial coil turns, and the number of axial coil turns, respectively. Equation (5) is rewritten in vector form as;

$$R\Phi = H + H_z I_z + NI \tag{6}$$

The flux densities in the gaps are reduced by flux leakage, fringing, and saturation of magnetic material. The flux density vector is then;

$$B = \varsigma A^{-1}\Phi \tag{7}$$

where

$$A = diag([a_0, a_0, a_0, a_0])$$

The parameter ς represents flux fringing factor, and can be empirically estimated. Magnetic forces developed in the radial pole plane are described as;

$$F_\varphi = -B^T \frac{\partial D}{\partial \varphi} B \tag{8}$$

where the air gap energy matrix is;

$$D = diag(g_j a_0 / (2\mu_0)) \tag{9}$$

and where φ is either x or y. Applying Ampere's law and Gauss's law to the axial magnetic circuit leads to a matrix equation.

$$\begin{bmatrix} R_{z1} & -R_{z2} \\ 1+\dfrac{R_{z1}}{R_A} & 1 \end{bmatrix} \begin{bmatrix} \phi_{z1} \\ \phi_{z2} \end{bmatrix} = \begin{bmatrix} 0 \\ \dfrac{-R_l H_c L_{pm}}{R_A(R_p+R_l)} - \dfrac{H_{eq}}{R_A} \end{bmatrix} + \begin{bmatrix} -\tilde{n} & -\tilde{n} \\ \dfrac{-\tilde{n}}{R_A} & 0 \end{bmatrix} \begin{bmatrix} i_{z1} \\ i_{z2} \end{bmatrix} \tag{10}$$

where

$$R_A = \frac{R_p R_l}{R_p + R_l} + R_{eq} \quad , \quad R_{eq} = \frac{1}{\dfrac{1}{R_1} + \dfrac{1}{R_2} + \dfrac{1}{R_3} + \dfrac{1}{R_4}} \quad ,$$

$$H_{eq} = \frac{\dfrac{ni_1}{R_1} + \dfrac{ni_2}{R_2} + \dfrac{ni_3}{R_3} + \dfrac{ni_4}{R_4}}{\dfrac{1}{R_1} + \dfrac{1}{R_2} + \dfrac{1}{R_3} + \dfrac{1}{R_4}}$$

Equation (10) can be rewritten in vector form as;

$$R_z \Phi_z = \tilde{H} + H_{xy} I + \tilde{N} I_z \tag{11}$$

where

$$H_{xy} = \begin{bmatrix} 0 & 0 & 0 & 0 \\ h_1 & h_2 & h_3 & h_4 \end{bmatrix}, \ h_i = \frac{\dfrac{n}{R_i}}{R_A\left(\dfrac{1}{R_1} + \dfrac{1}{R_2} + \dfrac{1}{R_3} + \dfrac{1}{R_4}\right)}$$

The flux density vector is then;

$$B_z = \varsigma_z A_z^{-1} \Phi_z \tag{12}$$

where

$$A_z = diag([a_{z0}, a_{z0}])$$

The parameter ς_z represents the flux fringing factor in the axial air gaps. Magnetic forces developed in the axial pole plane are described as;

$$F_z = -B_z^T \frac{\partial D_z}{\partial z} B_z \tag{13}$$

where the air gap energy matrix is;

$$D_z = diag([g_{z1}a_{z0}/(2\mu_0), g_{z2}a_{z0}/(2\mu_0)]) \tag{14}$$

3 Fault Tolerant Control

The currents distributed to the radial poles are generally expressed as a distribution matrix T and control voltage vector v. The current vector is;

$$I = T\,v \tag{15}$$

where

$$T = \lfloor T_x \; T_y \rfloor, \; v = \begin{bmatrix} v_x \\ v_y \end{bmatrix},$$
$$T_x = \begin{bmatrix} t_{x1} & t_{x2} & t_{x3} & t_{x4} \end{bmatrix}^T,$$
$$T_y = \begin{bmatrix} t_{y1} & t_{y2} & t_{y3} & t_{y4} \end{bmatrix}^T,$$

and v_x and v_y are x and y control voltages, respectively. For example, the current distribution scheme for unfailed radial poles is;

$$\tilde{T} = \begin{bmatrix} 1 & 0 \\ 0 & 1 \\ -1 & 0 \\ 0 & -1 \end{bmatrix} \tag{16}$$

The currents distributed to the axial plane are expressed as;

$$I_z = T_z v_z \tag{17}$$

where $T_z = \begin{bmatrix} t_{z1} \\ t_{z2} \end{bmatrix}$, and v_z is z control voltage. For example, the current distribution scheme for unfailed axial poles is;

$$\tilde{T}_z = \begin{bmatrix} 1 \\ 1 \end{bmatrix} \tag{18}$$

The remaining three currents, if one coil fails, are redistributed such that the same opposing poles, C-core like, control fluxes still can be realized. The calculated distribution matrix for the 4th coil failed operation is;

$$T_4 = \begin{bmatrix} 1 & 1 \\ 0 & 2 \\ -1 & 1 \\ 0 & 0 \end{bmatrix} \tag{19}$$

The nonlinear magnetic forces of F_x, F_y, and F_z can be linearized about equilibrium positions and the control voltages by using Taylor series expansion. The linearized magnetic forces are;

$$\begin{bmatrix} F_x \\ F_y \\ F_z \end{bmatrix} = -\begin{bmatrix} k_{pxx} & k_{pxy} & k_{pxz} \\ k_{pyx} & k_{pyy} & k_{pyz} \\ k_{pzx} & k_{pzy} & k_{pzz} \end{bmatrix}\begin{bmatrix} x \\ y \\ z \end{bmatrix} + \begin{bmatrix} k_{vxx} & k_{vxy} & k_{vxz} \\ k_{vyx} & k_{vyy} & k_{vyz} \\ k_{vzx} & k_{vzy} & k_{vzz} \end{bmatrix}\begin{bmatrix} v_x \\ v_y \\ v_z \end{bmatrix} \tag{20}$$

or

$$F = -K_p Z + K_v V \tag{21}$$

The flux coupling between the axial and radial planes can be determined by the cross coupled stiffness properties of Eq. (20). The linearized magnetic forces calculated at the equilibrium points (x_0 = 2 mils, y_0 = -1 mils, z_0 = 3 mils, v_{x0} = 0.5 volts, v_{y0} = 0.3 volts, v_{z0} = 1 volts) after the 4-th radial coil and an axial coil failed operation are;

$$K_p = \begin{bmatrix} -939484.13 & -16547.43 & -10407.28 \\ 3011.03 & -968484.90 & 9227.66 \\ -13725.16 & 10856.53 & -2699194.87 \end{bmatrix},$$
$$K_v = \begin{bmatrix} 82.55 & 2.64 & 1.64 \\ 0.28 & 81.09 & -1.32 \\ 0.32 & 12.08 & 179.82 \end{bmatrix}$$

The fault-tolerant control scheme can be easily implemented in a physical controller (DSP). The controller consists of two independent parts, which are a feedback voltage control law and an adaptive current distribution mechanism. Though any control algorithm for magnetic bearing systems appearing in the literature can be utilized with the fault tolerant scheme, for sake of illustration, a simple PD feedback control law is used to stabilize the system.

$$v_{c\varphi} = K_p \varphi + K_d \dot{\varphi} \tag{22}$$
$$\varphi \in (x,\, y)$$

While the feedback control law remains unaltered during the failure the appropriate current distribution matrix T can be continuously updated using an adaptive current distribution mechanism. Failure status vectors and the corresponding distribution matrices for the 5 possible states including an unfailed vector can be tabulated in a reference table and stored in the DSP controller as a part of searching algorithm. The distribution matrix corresponding to the failure vector is implemented in the controller. By prior experience this series of actions for failure detection, searching for T, and replacement by the new T can be implemented in one loop time of a fast (> 15K sec^{-1}) DSP controller. Any one coil out of 4 coils is free to fail while bearing properties such as the load capacity and stiffness remain invariant, if $\tilde{T}$ is replaced by T_1, T_2, T_3, and T_4 shortly after failure.

4 Conclusion

A fault tolerant current distribution scheme is developed for a bi-directional, permanent magnet biased, homopolar magnetic bearing. The bearing preserves the same magnetic forces before and after failure even though one coil among four radial coils and one coil of two axial coils fail. A one-dimensional circuit that represents the bi-directional bearing is analyzed to obtain the optimal bearing parameters such as the radial pole face area, number of coil turns, and permanent magnet size. The results show advantages of the fault tolerant scheme and bi-directional bearing improvements relative to conventional magnetic suspension. Fault tolerance of the magnetic bearing actuator can be achieved at the expense of additional hardware requirements and reduction of overall bearing load capacity.

These bidirectional magnetic bearings with fault tolerant capability can be used as robot joints. Since magnetic bearing supported robot arms can avoid oil lubrication and dust generation, they can be used for robots in clean environment, in vacuum chambers, or in space. They also have some more advantages over conventional robot joints such as frictionless manipulation, force control, force sensing, active vibration control.

Acknowledgements

This research was supported by the **N**ew **U**niversity for **R**egional **I**nnovation program of the Ministry of Education & Human Resources Development (NURI MECHANO 21).

References

[1] C.R. Meeks, E. DiRusso, G.V. Brown, "Development of a Compact, Light Weight Magnetic Bearing," AIAA Paper No. AIAA-90-2483 (1990)

[2] E. H. Maslen and D. C. Meeker, "Fault Tolerance of Magnetic Bearings by Generalized Bias Current Linearization," *Magnetics – Transactions of the IEEE,* **31**, 2304 – 2314 (1995)

[3] E. H. Maslen, C. K. Sortore, G. T. Gillies, R. D. Williams, S. J. Fedigan, and R. J. Aimone, "A Fault Tolerant Magnetic Bearings," *Journal of Engineering for Gas Turbines and Power – Transactions of the ASME* **121**, 504-508 (1999)

[4] U. J. Na and A. B. Palazzolo, "Optimized Realization of Fault-Tolerant Heteropolar Magnetic Bearings for Active Vibration Control," *Journal of Vibration and Acoustics – Transactions of the ASME* **121**, 504-508 (2000)

[5] U. J. Na and A. B. Palazzolo, "Fault Tolerance of Magnetic Bearings with Material Path Reluctances and Fringing Factors," *Magnetics – Transactions of the IEEE* **36**, 3939 – 3946 (2001)

Detecting Method of Friction Force on Linear Actuators of a Parallel Manipulator Based on the Gravitational Force

Haeng Bong Shin

Dept. of Mechanical Design, Graduate School,
Kyungnam University,
Masan, Gyeongnam, 631-701, Korea

Se Han Lee

School of Mechanical and Automation Eng.,
Kyungnam University,
Masan, Gyeongnam, 631-701, Korea

Abstract

Parallel manipulators have been used to a variety of applications, including the motion simulators and mechanism for precise machining. A Stewart-Gough type parallel manipulator is composed of six linear joints, which have wider contact areas than revolute ones, so linear joints are more affected by frictional force. First, the reference trajectories are computed from the model of the parallel manipulator assuming that it is subject to only the gravitational force and no friction exists. In the actual operation where friction exists, the control inputs, which correspond to the friction forces, are obtained by forcing the actual joint variables to follow these trajectories by proper control. It is shown that control performance can be improved when the friction compensation based on this information is added to the controller for position control of the moving plate of a parallel manipulator.

1. Introduction

Recently, there are carried out so many parallel manipulator applications for machining machine, motion simulator [1,2] and so on. In particular, a conventional Stewart-Gough type parallel manipulator has a good rigidity ration over the weight since it uses mainly linear actuators where bending effect does not apply. In addition, the errors from each actuator are not accumulated and distributed since the actuators are arranged in parallel with closed loop form. Thanks to the characteristics, there is introduced the parallel manipulator to applications of handling tool and carriage in the machining machine which requires high rigidity.

Generally, on the contrary to the merits above, there is a deficit of small workspace since the actuators have limited stroke and are arranged in parallel with closed loop form and they can interfere with themselves. In addition, in case of the conventional Stewart-Gough platform, there is significant friction force on each actuator. A linear type actuator has wider contacting surface than a revolute one and has more friction problem. Meanwhile, ball-screw device for converting rotation to translation motion may have an intentional pre-stress because pre-stress can eliminate backlash and any other mechanical alignment error. The pre-stress can cause more friction problem. In particular, the conventional Stewart-Gough platform has 6 identical actuators, and the actuators are required to be as more identical as possible. However, it is impossible that they are all identical perfectly. Friction force on each actuator is expected to be detected and is compensated for better control performance.

As a method for detecting friction force, when a constant force is applied to the destination, the resultant acceleration can tell us how much friction force is. That is hard to be performed due to a calibration problem because it is hard to apply an exactly scaled force to the destination. The gravitational force can be a candidate for that because the gravitational force can be easily assumed as constant force. Actually, the gravitational force is most likely a constant and even free cost.

If the gravitational force is applied to an ideal parallel manipulator without any friction effect, the end-effector of the parallel manipulator falls down freely according to the Newton's law. Actually, the end-effector falls down slowly than expected or even stops with the friction force on each actuator. When the actuators are controlled in order to make the end-effector follow the ideal free fall trajectory, the control input for the actuators can be assumed as the efforts for compensating the friction force. For better tracking performance, the control efforts corresponding to actuator's position can be stored and recalled for controlling the end-effector to follow an arbitrary trajectory.

In this study, Chapter 2 describes characteristics of a conventional Stewart-Gough platform, Chapter 3 describes a method for detecting friction force, Chapter 4 shows the validity of the method with experimental results, Chapter 5 makes conclusions finally.

2. Stewart-Gough parallel manipulator

Stewart-Gough has two plates, moving plate (end-effector) and fixed plate that are connected with 6 linear actuators in parallel. The end-effector has 6 dof (degree of freedoms) with 3 dof of position and 3 dot of orientation [4]. A parallel manipulator like the

Stewart-Gough platform, has opposite characteristics to the a serial one that inverse kinematics for the parallel is easier than that for a serial one, forward kinematics of the parallel one is more difficult than that of a serial one and does not even have analytical solutions. In addition, it is possible to perform accurate control since the actuation structure is closed form and the error on each actuator is distributed and it is also to obtain high rigidity over lightweight since the actuators run stress and tensional direction without bending. Meanwhile the end-effector workspace is limited since the actuator's stroke is limited and has closed form structure.

Meanwhile as a parallel manipulator uses a linear type actuator and the contacting surface of the linear type actuator becomes wider than a revolute type actuator, friction force effect of the parallel manipulator is significantly increasing. In addition, ball-screw device for converting rotation to translation motion may have an intentional pre-stress because pre-stress can eliminate backlash and any other mechanical error. The pre-stress can cause more friction problem. As a result, the parallel manipulator falls down slowly or even is fixed due to the friction force without any actuation force.

Figure 1 shows a conventional Stewart-Gough platform built in the study. As an experimental setup, the Stewart-Gough platform uses a ball-screw device at which a high pre-stress (75kgf) is applied. Due to the friction force, the end-effector of the parallel manipulator is fixed. It is well known that friction force is a negative factor for control performance. If the friction force can be detected exactly and compensated, the control performance will be improved.

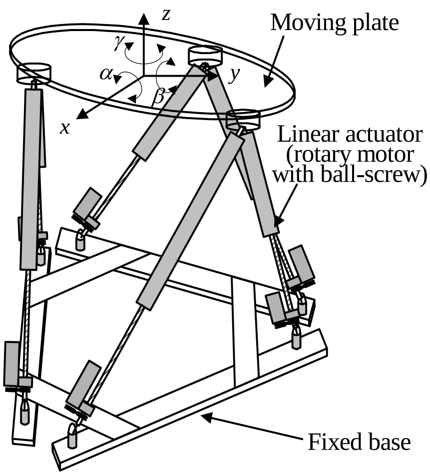

Fig. 1 Stewart-Gough type parallel manipulator.

3. Friction force detection using gravitational force

As a method for detecting friction force on a manipulator, when and external force magnitude applied to a manipulator is increasing, a force corresponding to the moment at where the manipulator begins to move can be assumed a friction force on the manipulator. This method is very simple, however, it is most likely impossible to generate force exactly and it is required additional equipment for generating force. In this study, the gravitational force that always exists everywhere manipulator and even free cost will be used for detecting friction force.

Dynamic equations for a multi-degree manipulator are described as a non-linear form equation as following

$$\mathbf{J}(\mathbf{q})\ddot{\mathbf{q}} + \mathbf{N}(\mathbf{q},\dot{\mathbf{q}}) + \mathbf{G}(\mathbf{q}) = \boldsymbol{\tau} \tag{1}$$

where $\mathbf{q}\in R^n$ denotes joint variables on the manipulator (n stands for the numbers of the joints), $\mathbf{J}(\mathbf{q})$ denotes moment of inertia, $\mathbf{N}(\mathbf{q},\dot{\mathbf{q}})$ denotes non-linear term corresponding to centripetal and Coliolis force, $\mathbf{G}(\mathbf{q})$ denotes gravitational force term, and $\boldsymbol{\tau}$ denotes external torques. The gravitational force term $\mathbf{G}(\mathbf{q})$ in (1) is dependent on the configurations, $\mathbf{q}$ and is independent of initial velocity or acceleration. If there is no external force, $\boldsymbol{\tau} = \mathbf{0}$, (1) becomes

$$\mathbf{J}(\mathbf{q})\ddot{\mathbf{q}} + \mathbf{N}(\mathbf{q},\dot{\mathbf{q}}) = -\mathbf{G}(\mathbf{q}) \neq 0 \tag{2}$$

Only the gravitational force in (2) is applied to the manipulator. In case of a serial manipulator with a revolute type actuator that has less friction force than parallel one, the end-effector of the serial one falls down slowly along the gravitational direction since the friction force cancels some part of the gravitational force. If there is no friction force on each actuator, the end-effector falls down freely. By solving (2), the joint variable, $\mathbf{q}_g$ corresponding to the free fall trajectory can be obtained.

Here is considering a case with friction force. If the friction force is bigger than the external one, the friction force is the same as the applied external force and the external force is canceled exactly. As described above, friction force on the parallel manipulator is relatively large and the external force (gravitational force in this case) fades away due to the friction force. As a result, (2) becomes

$$\mathbf{J}(\mathbf{q})\ddot{\mathbf{q}} + \mathbf{N}(\mathbf{q},\dot{\mathbf{q}}) = -\mathbf{G}(\mathbf{q}) + \mathbf{F}_{\text{friction}}(\dot{\mathbf{q}}/|\dot{\mathbf{q}}|) \neq 0 \tag{3}$$

where $\mathbf{F}_{\text{friction}}(\dot{\mathbf{q}}/|\dot{\mathbf{q}}|)$ denotes friction force acting opposite direction of the manipulator.

As if there is controlled the manipulator following the free fall trajectory, the control efforts to each actuator are the same as friction force on each actuator. The control input $\mathbf{u}$ is carefully adjusted in order for the joint variable $\mathbf{q}$ to follow the pre-computed trajectory $\mathbf{q}_g$.

$$\begin{aligned}&\mathbf{J}(\mathbf{q_g})\ddot{\mathbf{q}}_\mathbf{g} + \mathbf{N}(\mathbf{q_g},\dot{\mathbf{q}}_\mathbf{g})\dot{\mathbf{q}}_\mathbf{g}\\ &\quad = -\mathbf{G}(\mathbf{q_g}) + \mathbf{F}_{\text{friction}}(\dot{\mathbf{q}}_\mathbf{g}/|\dot{\mathbf{q}}_g|) + \mathbf{u}\end{aligned} \tag{4}$$

By letting the left side of (2) be the left one of (4), the following is satisfied

$$\mathbf{F}_{\text{friction}}(\dot{\mathbf{q}}_\mathbf{g}/|\dot{\mathbf{q}}_\mathbf{g}|) + \mathbf{u} = 0 \tag{5}$$

As (5) shows that the control input, $\mathbf{u}$, cancels the friction force, $\mathbf{F}_{\text{friction}}(\dot{\mathbf{q}}/|\dot{\mathbf{q}}|)$, the control input will be corresponding to the friction force. A friction force $\mathbf{F}_{\text{friction}}(\mathbf{q})$ corresponding to joint variable $\mathbf{q}$ can be obtained. Base on that friction force, the friction force can be added into control effort as following and better control performance is expected.

$$\mathbf{u}_{\text{enhanced}} = \mathbf{u}_{\text{nominal}} + \mathbf{F}_{\text{friction}}(\mathbf{q}) \tag{6}$$

4. Experiments

A Stewart-Gough platform is constructed for the study. It consists of 6 linear actuators with 400W class BLDC (BrushLess DC) motor and ball-screw device. Detail specifications are on the following Table 1, and the experimental setup is shown in Fig. 2. A computation burden for the controlling the parallel manipulator is very significant. The controller consists of 2 parts, high level and low level controller. The high level controller, PC takes role of kinematics computation while the low level controller, TMS320C31 DSP takes role of controlling each actuator.

Table 1 Workspace of the developed parallel manipulator.

Items	Ranges
Pay Load	200kg
X-translation	±0.2m
Y-translation	±0.2m
Z-translation	±0.1m
Roll	$\pm 25^o$
Pitch	$\pm 25^o$
Yaw	$\pm 30^o$

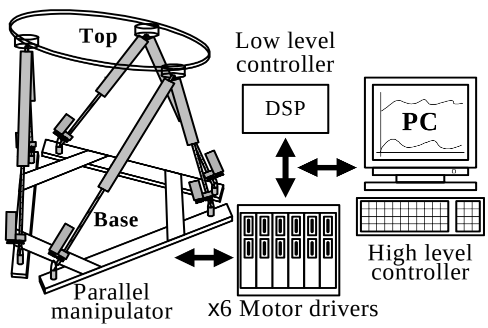

Fig. 2 Schematic of experimental setup.

4.1 Friction force detection

Before performing the experiments, inverse dynamics of the parallel manipulator is computed under external force condition of gravitational force. As the external force is applied vertically to the parallel manipulator and the configuration of the manipulator is symmetric, every trajectory of each actuator is the same. For that reason, only one trajectory of the actuator and vertical trajectory of the end-effector are shown in Fig. 3.

Each actuator connected to the real parallel manipulator is controlled to follow the pre-computed free fall trajectory and the control efforts are shown in Fig. 4. They are corresponding to forces overcoming the friction forces. There are shown friction forces of 250 N average. They show that the biggest friction is on 3rd actuator and the smallest one is on 4th actuator.

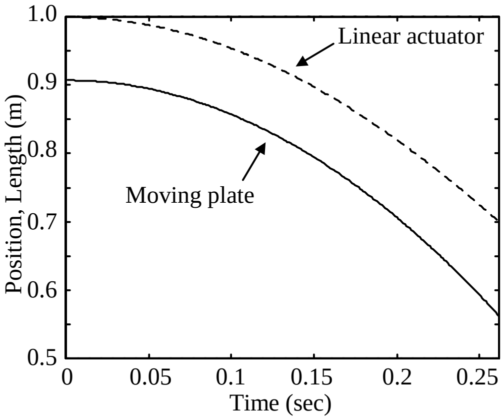

Fig. 3 Trajectories of linear actuator and moving plate under gravitational force alone.

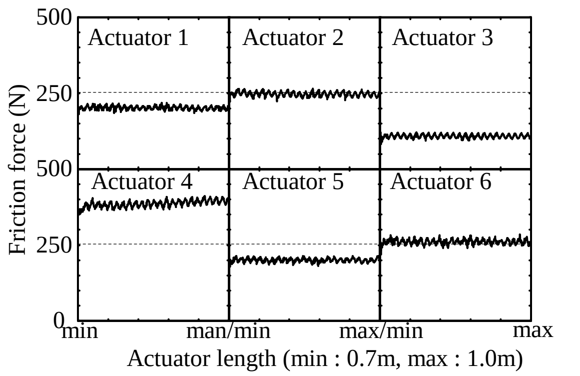

Fig. 4 Control efforts of six linear actuators which follow the ideal trajectories.

As a result of detecting the friction force of the parallel manipulator, the resultant shows that the friction force on each actuator is different with each other though the configuration of the parallel manipulator is symmetric. The reason is that all the parts for the parallel manipulator is not ideally uniform and fabricated. If the same gain is applied to the each controller without considering each actuator's property, it is hard to expect to obtain uniform control performance.

4.2 Friction compensation

In order to check the validity of the detected friction force, the friction force profiles are applied to the controller. There is introduced a simple PID controller for showing potential of the friction force compensation.

$$\mathbf{u} = \mathbf{K}_P(\mathbf{q}_{\text{ref}} - \mathbf{q}) + \mathbf{K}_I \int (\mathbf{q}_{\text{ref}} - \mathbf{q})dt + \mathbf{K}_D(\dot{\mathbf{q}}_{\text{ref}} - \dot{\mathbf{q}}) \tag{7}$$

where $\mathbf{K}_P, \mathbf{K}_I, \mathbf{K}_D, \mathbf{q}_{\text{ref}}$ denotes proportional gains, integral gains for compensating the gravity, derivative gains, and reference trajectory respectively. The detected friction force is added into the control effort finally shown in (6).

Figure 5 shows 2 cases; one is that only feedback controller takes role of compensating property of each actuator (assuming that mechanical property and friction force on each actuator is the same), the other is that pre-computed friction force is added into the control input. In order for all 6 actuators to move simultaneously, a circular trajectory is introduced for reference trajectory. Figure 5 shows that the tracking performance for friction compensation with feedforwarding pre-computed friction force to the control input along the joint variable **q**, is better than that for no friction compensation. In case of no friction compensation, the reason for the irregular tracking pattern is that each error on the actuator is represented in end-effector non-linearly due to the non-linear kinematics of the manipulator.

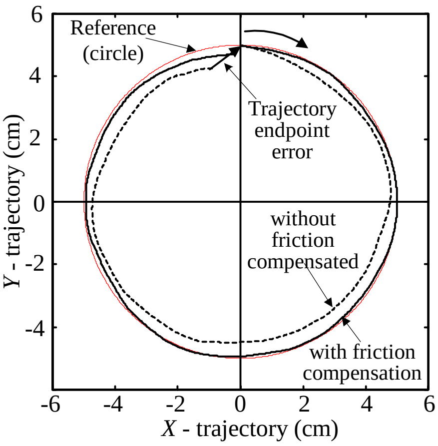

Fig. 5 Tracking performance of the moving plate following reference circular trajectory during the PID control without and with friction compensation.

Figure 6 shows control inputs of both cases. Though the outlines of both cases are similar to each other, in case of friction compensation, the control input difference between max. and min. is decreasing little bit. The reason is expected that the integral part increases the control input to overcome the friction force.

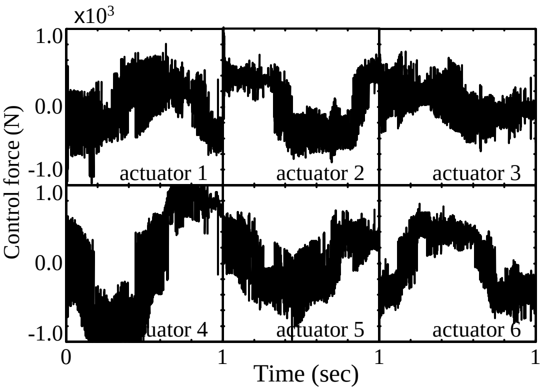

(a)

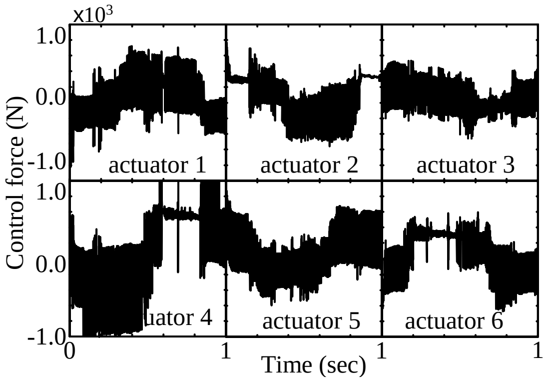

(b)

Fig. 6 Control inputs for (a) the controller without friction compensation, and (b) the controller with friction compensation.

5. Conclusions

There is introduced a friction force detection scheme for a parallel manipulator in this study. This scheme uses the gravitational force for free cost and makes the compensation algorithm be only a part of control algorithm without any additional equipment. Because the scheme is included in the controller as a part of algorithm, the friction detection scheme can be carried out at every initial action or at any time for the request. The possibility to carry out the friction detection at every initializing becomes a very significant merit when the friction force is always subject to change according to environmental temperature, humidity, and operating conditions.

By performing experiment of friction compensation with the detected friction force, the validity of the friction detection method is presented. Since the friction compensation method can be implemented into main controller with feedforward form, it does not require additional complicated computation burden.

Acknowledgements

This research was supported by the **N**ew **U**niversity for **R**egional **I**nnovation program of the Ministry of Education & Human Resources Development (NURI MECHANO 21).

References

[1] G. Lebret, K. Liu, and F. L. Lewis, "Dynamic Analysis and Control of a Stewart Platform Manipulator," *J. of Robotic Systems*, 10(5), pp.629-655, 1993.

[2] S. Chae, C. Chung, H. Yang, Y. Choi, and S. Lee, "Adaptive Control of a 6 DOF Stewart Platform Based Machine Tool," MOVIC '98, vol. 2, pp.461-466, 1998

[3] L. W. Tsai, *Robot Analysis: The Mechanics of Serial and Parallel Manipulator*, John Wiley and Sons, 1999.

[4] D. Stewart, "A platform with six degrees of freedom," Proc. Inst. Mech. Engr., 180(1), pp.371 – 386, 1965.

[5] M. W. Spong, M. Vidyasagar, *Robot Dynamics and Control*, John Wiley and Sons, 1989.

Real Time Control of Feature Based Visual Tracking for Dual-Arm Robot

Jong Soo Kim, Hong Rae Kim

Dept. of Mechanical Design, Graduate School,
Kyungnam University,
Masan, Gyeongnam, 631-701, Korea

Sung Hyun Han

Division of Mechanical and Automation Eng.,
Kyungnam University,
Masan, Gyeongnam, 631-701, Korea

Abstract

This paper presents how it is effective to use many features for improving the speed and the accuracy of the visual servo systems. Some rank conditions which relate the image Jacobian and the control performance are derived. It is also proven that the accuracy is improved by increasing the number of features. Effectiveness of the redundant features is evaluated by the smallest singular value of the image Jacobian which is closely related to the accuracy with respect to the world coordinate system. Usefulness of the redundant features is verified by the real time experiments on a Dual-Arm Robot manipulator made in Samsung Electronic Co. Ltd..

1 Introduction

Recently, robots can perform assembly and material handling jobs with speed and precision yet, compared to human workers robots, are hampered by their lack of sensory perception. To address this deficiency considerable research into force, tactile and visual perception has been conducted over the past two decades.

Visual servoing is the fusion of result from many elemental areas including high-speed image processing, kinematics, dynamics, control theory, and real-time computing. It has much in common with research into active vision and structure from motion, but is quite different from the often described use of vision in hierarchical task-level robot control systems. Many of the control and vision problems are similar to those encountered by active vision researchers who are building robotic heads. However the task in visual servoing is to control a robot to cope with its environment using vision as opposed to just observing the environment.

Most visual servoing problems can be considered as nonlinear control problems with the gray level of each two dimensional pixel array being an observation. The difficulty of the problem is the size and the nonlinearity. The size of the observation is larger than ten thousand and they have nonlinear interaction with each other. A few researches based on the stochastic models of the two-dimension observation are found, but most visual servoing schemes uses the features of the image as the observation. To manipulate objects with complex shapes, it is important to deal with complex features such as spheres and cylinders. However, the time extracting complex features will become too long based on limited hardware. Accordingly, visual servoing scheme which utilizes many features effectively is required. Furthermore exploiting the information carefully from the features will give robust and accurate control performance [4], [5], [6].

Sanderson et al. proposed a feature-based approach and defined the Jacobian of ideal inverse interpretation which was considered as the infinitesimal change of the relative position and orientation between the camera and the object in the environment.

Newman et al. proposed an adaptive control law based on a single input single output model and a feature selection criterion were proposed [10], [11], [12]. The criterion addressed the choice of which feature should be used to control each actuator, where the number of selected features is equal to the number of the actuator. Feddema et al. [3], [4], [5], [6] also studied the selection method of the features to make the Jacobian good condition. Real time experiment of gasket tracking showed that the proper selection of features is necessary to minimize the effect of image noise.

Papanikolopoulos et al. [5], [6], [7] experimentally examined many control algorithms including Proportional-Plus- Integral, pole assignment and linear quadratic gaussian. Some adaptive control schemes were also examined in [8]. These approaches do not consider to use the redundant features which are defined as the features whose number is more than the degrees of freedom of the robot manipulator.

Chaumette el al. [8] and Espiau el al. [9] derived the interaction matrix, and introduced the concept of task function. Chaumette [2] extended the task function approach to the complex features. Jang and Bien [10] mathematically defined the “feature”, and derived the feature Jacobian matrix. The authors [12] derived the image Jacobian, and used its generalized inverse and PD control to generate the hand trajectory. These schemes are based on the generalized inverse of the Jacobian. Redundant features can be used. However, the parameters to improve the control performance are very limited and the controllability of the redundant features are not discussed.

The authors proposed a linearized dynamic model of the visual servo system and linear quadratic control scheme for redundant features [11], [13].

The controllability problem was discussed but the performance improvement by utilizing the redundant features was not presented.

This paper presents how the control performance of the feature-based visual servoing system is improved by utilizing redundant features. Effectiveness of the redundant features is evaluated by the smallest singular value of the image Jacobian which is closely related to the accuracy in the world coordinate system. Usefulness of the redundant features is verified by the real time control experiments. To illustrate the accuracy of the redundant visual servo system, real time experiments on the Dual-Arm robot with eight joints are carried out. Translation and rotation step response with three, four and five features are examined in this experiment.

2 System Modeling and Formullation

The object image moves with the joint angle to the object image, which is composed of the kinematic model and the camera model as shown in Fig.1. Suppose that a camera is mounted on the robot hand and the object does not move. The kinematic model is a map from the joint angle to a position of the camera. Since the camera is on the robot hand, the camera position is uniquely defined by the joint angle θ based on the kinematic structure of the robot. The camera model is a map from the position of the camera to the camera to the image of the object.

The object image is generated by the perspective of the relative position between the camera and the object. The perspective projection is a map between two different representations of the position of the object, i.e., the representations in the camera coordinate system $[XYZ]^T$ and in the image plane $[xy]^T$.

The perspective projection with f being the focal length of the lens is given by

$$[x \quad y]^T = [X \quad Y]^T (f / z) \tag{1}$$

Suppose that there are n feature points, namely $p_i = [X_i Y_i Z_i]^T \quad (i = 1,....,n)$, on an object and the corresponding positions in the image plane are $\xi_i = [x_i y_i]^T \quad (i = 1,....,n)$. Assume that the shape and the size of the object are known and constant (i.e., the object is a rigid body). Then ξ_i for $i = 1,....,n$ become functions of the joint angle θ. Let us define a $2n$ dimensional feature vector by $\xi \cong [\xi_1^T \cdots \xi_n^T]^T$. Then the system model for n feature points is defined by the map $\psi : \mathbf{R}^m \to \mathbf{R}^{2n}$ from the joint angle θ to the feature vector ξ as follows:

$$\psi(\theta) \cong \xi \tag{2}$$

where m is the number of the joints of the robot.

Since the task must be carried out in the nonsingular region of the robot, the nonsingular region is called the operation region $\mathrm{M}_\theta \subset \mathbf{R}^m$. We restrict the robot motion in the operation region. Thus the robot Jacobian J robot is invertible in the working area. It is useful to introduce the feature manifold M, which is defined by

$$\mathrm{M} = \{\xi \in \mathbf{R}^{2n} : \xi = \psi(\theta), \theta \in \mathrm{M}_\theta\} \tag{3}$$

The features on the feature manifold is called the admissible features. If the features are admissible, then the robot Jacobian is invertible by definition. In equation (3), θ represents joint angle.

Differentiation of the system model yields

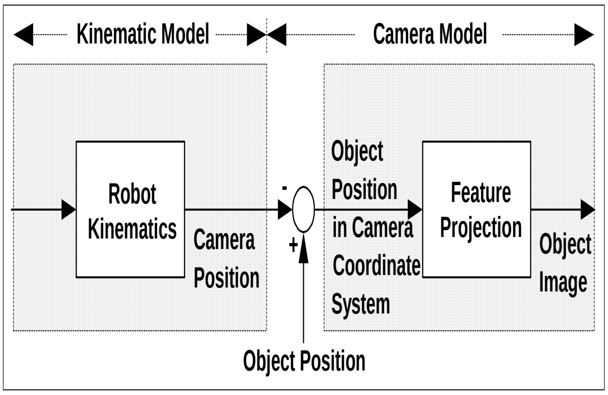

Fig. 1 System Modeling

$$\dot{\xi} = J\,\dot{\theta} \tag{4}$$

where the $2n \times m$ matrix J is defined by

$$J \cong \begin{bmatrix} J_{im}^{(1)} \\ \vdots \\ J_{im}^{(n)} \end{bmatrix} {}^c J_{ARM} \tag{5}$$

The matrix $J_{im}^{(i)}$ is given by [14], [12]

$$J_{im}^{(i)} \cong \begin{bmatrix} -\dfrac{f}{z_i} & 0 & \dfrac{x_i}{Z_i} & \dfrac{x_i y_i}{f} & -\dfrac{x_i^2 + f^2}{f} & y_i \\ 0 & -\dfrac{f}{z_i} & \dfrac{y_i}{Z_i} & \dfrac{y_i^2 + f^2}{f} & \dfrac{x_i y_i}{f} & -x_i \end{bmatrix} \tag{6}$$

and called the image Jacobian [12]. ${}^c J_{ARM}$ is the robot Jacobian expressed in the camera coordinate system. Since the vector ${}^c J_{ARM}\,\dot{\theta} \in \mathbf{R}^6$ is the linear and angular velocities of the camera expressed in the camera coordinate system, $J_{im}^{(i)}$ becomes the infinitesimal change of the position of the camera. Moreover, $J(i) \cong J_{im}^{(i)}\,{}^c J_{ARM}$ becomes the infinitesimal change of the features according to the infinitesimal change of the joint angles.

The degenerated features are the features for which the extended image Jacobian is not full rank. The degenerate features should be avoided because the

The Tenth International Symposium on Artificial Life and Robotics 2005(AROB 10th '05),
B-con Plaza, Beppu, Oita, Japan, February 4-6, 2005

inverse map (the map from ξ to θ) becomes singular. Thus, when the number of joints is m,

$$rank\ J(\theta) = m \qquad \forall \theta \in \mathrm{M}_\theta \tag{7}$$

is required for all admissible features. To satisfy this condition $n \geq m/2$ is an obvious necessary condition, but it is not sufficient for some cases.

For example, consider a general six degree of freedom $(m = 6)$. In this case, $n \geq 3$ is necessary. If $n = 3$, $rank\, J \langle 6$ the camera lies on the cylinder(Fig. 2) which includes the three points and the axis of which is perpendicular to the plane containing these points. For any attitude of the camera, J is singular. Thus $n = 3$ is not sufficient and $n \geq 4$ is desirable. For the case of $n = 4$, we have the following theorem.

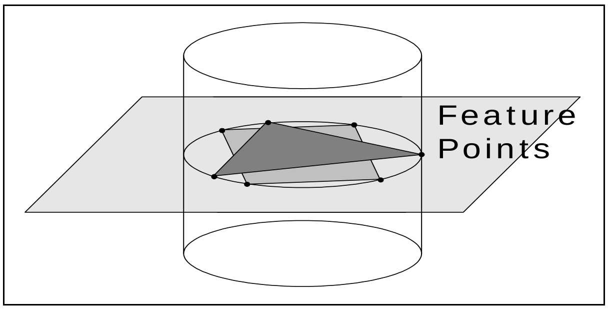

Fig. 2 Singular Cylinder

Theorem 1: Suppose that there are four points on a plane and the corresponding feature vector is admissible. Then the extended image Jacobian is full rank if any three feature points out of them are not collinear in the image plane.

Proof : Let the plane on which the four points exist be $Z = pX + qY + r$. Then Z_i satisfies $Z_i = pX_i + qY_i + r$ for $i = 1, \cdots, 4$. Substituting (1) into this yields

$$\frac{f}{Z_i} = \frac{f - px_i - qy_i}{r} \tag{8}$$

And substituting this into (6) yields

$$J_{im}^{(i)} = M_i N \tag{9}$$

where M_i and N are defined by

$$M_i = \begin{bmatrix} f & 0 & x_i & y_i & 0 & 0 & x_i^2/f & x_i y_i/f \\ 0 & f & 0 & 0 & x_i & y_i & x_i y_i/f & y_i^2/f \end{bmatrix},$$
$$N = \frac{1}{r}\begin{bmatrix} -1 & 0 & 0 & 0 & -r & 0 \\ 0 & -1 & 0 & r & 0 & 0 \\ p & 0 & 1 & 0 & 0 & 0 \\ q & 0 & 0 & 0 & 0 & r \\ 0 & p & 0 & 0 & 0 & -r \\ 0 & q & 1 & 0 & 0 & 0 \\ 0 & 0 & -p & 0 & -r & 0 \\ 0 & 0 & -q & r & 0 & 0 \end{bmatrix} \tag{10}$$

Then we obtain $J = MN\,{}^cJ_{ARM}$, where $M = \left[M_1^T\ M_2^T\ M_3^T\ M_4^T\right]^T$. It is straightforward to see that

$$\det M = \begin{vmatrix} 1 & x_1 & y_1 \\ 1 & x_2 & y_2 \\ 1 & x_3 & y_3 \end{vmatrix} \bullet \begin{vmatrix} 1 & x_2 & y_2 \\ 1 & x_3 & y_3 \\ 1 & x_4 & y_4 \end{vmatrix} \bullet \begin{vmatrix} 1 & x_3 & y_3 \\ 1 & x_4 & y_4 \\ 1 & x_1 & y_1 \end{vmatrix} \bullet \begin{vmatrix} 1 & x_4 & y_4 \\ 1 & x_1 & y_1 \\ 1 & x_2 & y_2 \end{vmatrix} \tag{11}$$

Thus M is invertible because any three feature points are not collinear. On the other hand, if $p^2 + q^2 \neq 0$, the first six rows of N is linearly independent. If $p = q = 0$, the first four and the last two rows are linearly independent. Thus rank $N = 6$. finally, since all features are admissible, ${}^cJ_{ARM}$ is invertible. Therefore, the extended image Jacobian J is full rank.

3 Analysis of Visual Servoing

For evaluating the performance of the feature-based visual servo system, it is useful to discuss the ratio of the joint angle error to the feature vector. The following theorem shows that increasing the number of the feature point is an effective way to improve the performance.

Let the joint error be $\Delta\theta = \theta - \theta_d$ and the feature error be $\Delta\xi = \xi - \xi_d$. Define the worst joint/feature error ratio ER, called sensitivity, as follows:

$$ER = \sup_{|\Delta\xi \neq 0} \frac{\|\Delta\theta\|}{\|\Delta\xi\|} = \frac{1}{\beta_{\min}(J)} \tag{12}$$

where $\beta_{\min}(J)$ is the minimum singular value of J. Then the sensitivity ER decreases strictly by increasing the number of non-degenerated features on the object.

Let J_n be the image Jacobian for n feature points and J_{n+1} be the image Jacobian obtained by adding an extra feature point to the already existing feature points.

Then we have

$$J_{n+1} = \begin{bmatrix} J_n \\ J^{(n+1)} \end{bmatrix} \tag{13}$$

where $J^{(n+1)}$ is the $2 \times m$ image Jacobian corresponding to the newly added feature point. It is straightforward to see that

$$\beta_{\min}(J_n) \leq \beta_{\min}(J_{n+1}) \tag{14}$$

The equal sign holds only if each row of $J^{(n+1)}$ is linearly dependent to J_n, i.e., only if J_{n+1} is not full rank. Since we assumed that the features are not degenerated, the equal sing should be dropped. Thus adding extra feature points strictly increases the minimum singular value.

This theorem says that we can reduce the joint angle error by increasing the number of feature points.

Linearizing the model (2) with the feature vector being the state vector yields an uncontrollable model because ξ can not move arbitrarily in $\mathbf{R}^{2n}$ [13]. A simple way to avoid this problem is to map $\xi \in \mathrm{M}$ onto the tangent space of M by using the following transformation.

$$z = J_d^T(\xi - \xi_d) \tag{15}$$

where $J_d = J(\theta_d)$ is the image Jacobian at the desired point[16]. Note that z and θ are one-to-one in the neighborhood of θ_d. The dynamics of the feature error on the tangent space of the manifold M is given by

$$\dot{z} = J_d^T J(\theta)\dot{\theta} \tag{16}$$

Thus, for a simple continuous time control law $\dot{\theta} = -Kz$ with a positive definite constant matrix K yields an asymptotic stability if $J_d^T J(\theta)$ is positive definite. It is shown that this condition is satisfied fairly large region about θ_d [13].

4 Experiments and Discussion

As shown in Fig.3, the objects are white boards with three, four and five black marks. Three points are arranged to make a regular triangle with edge length 120mm. Four points are on corners of a square with edge length 120mm. All marks are on a plane except the one of five points at the center of the square, which has height 60mm. Dual-Arm robot holds the objects and a camera(Fig.4). The world coordinate system $\omega_X - \omega_Y - \omega_Z$ is at the base of the Dual-Arm robot. A nominal camera position is almost in front of the plane on which the marks exist. To avoid the singular cylinder(Fig.2) the optical axis and the normal axis of the object plane are not aligned. The distance is about 1000mm. The features are the x and y coordinates of the center of the image of each mark. Computing their minimum singular values at the reference position gives

$$\begin{aligned} \beta_{\min} &= (J_3) = 0.35\,, \\ \beta_{\min} &= (J_4) = 0.65\,, \\ \beta_{\min} &= (J_5) = 3.60 \end{aligned} \tag{17}$$

Thus accuracy of the position control of the camera in the 3D work space will be improved by using 5 features. We carried out many step tests to this observation.

The first experiment is a step motion in vertical axis. The object is moved upward for 120mm (i.e., in ω_Z direction). The camera is controlled to keep the features at the initial positions. Thus the initial values and the reference values are the same. The object motion is considered as a disturbance for the plots of the features in the image plane. On the other hand, the object motion becomes the step change of the reference position for the plots of the camera motion in the world coordinate system. Since Dual-Arm robot has only 6 degrees of freedom, the orientation of the object changed slightly. Thus, the reference orientation is [2.8, 0, -1.8] degrees expressed in the Euler angles, say p, η, ϕ.

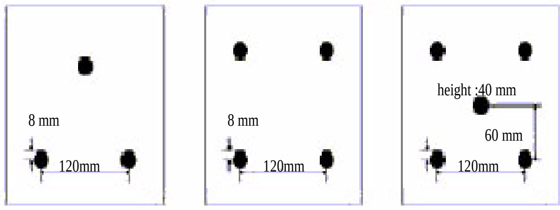

Fig. 3 Configuration of Feature Points

Fig. 4 Experimental Setup

Table 1. Specification of Dual Arm Robot

Content		Unit	Spec.	Remark
Workspace	1st Arm	deg	180	
	2nd Arm	deg	450	
	Z Axis	mm	150	
	R Axis	deg	±180	
Maximum Reach		mm	(350+ 260)	
Payload		Kg	2.5	High-speed
Max. Resultant Vel.		m/sec	5.4	1,2 Axis
Position Repeatability	Plane	mm	0.05	1,2 Axis
	Z Axis	mm	0.02	
	M Axis	deg	0.05	
Weight		Kg	200	
Coincident Control Axis No.		EA	8Axis (4+ 4)	

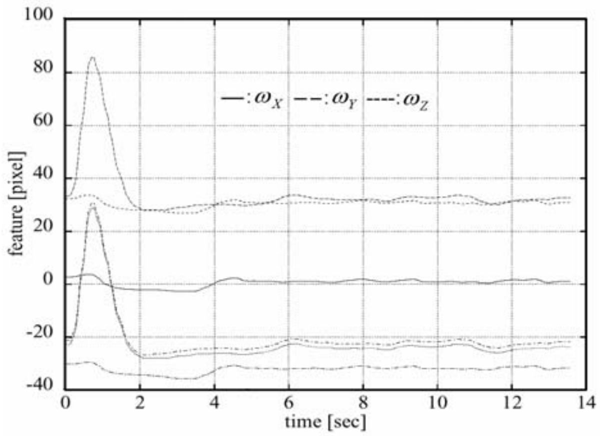

Fig. 5 Response in Image Plane for 3 Points (Vertical Step)

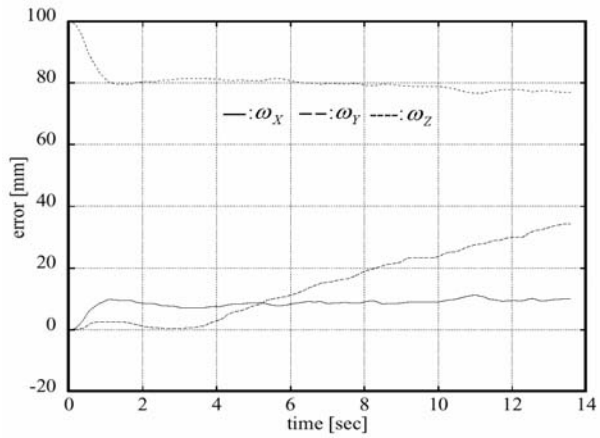

Fig. 8 Error in 3D for 3 Points (Vertical Stop)

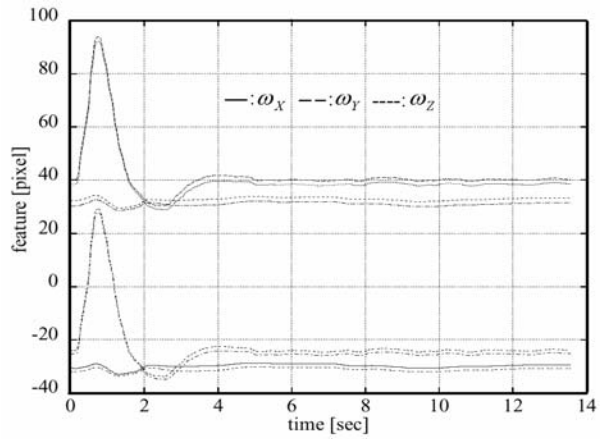

Fig. 6 Response in Image Plane for 4 Points (Vertical Step)

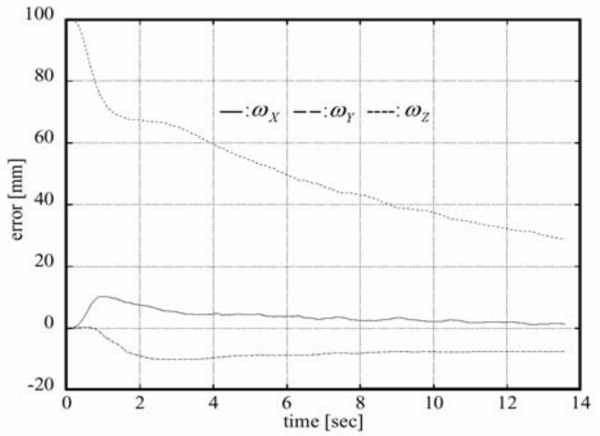

Fig. 9 Error in 3D for 4 Points (Vertical Step)

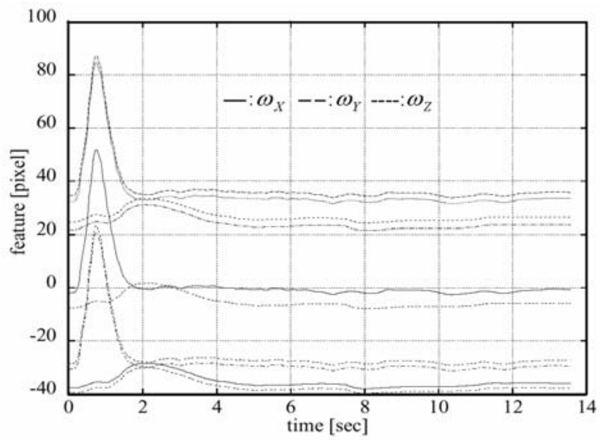

Fig. 7 Response in Image Plane for 5 Points (Vertical Step)

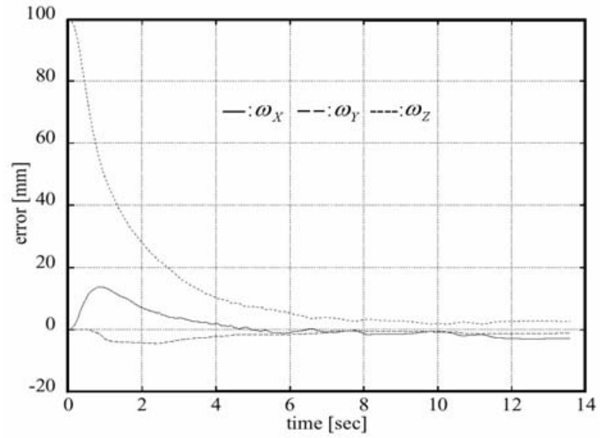

Fig. 10 Error in 3D for 5 Points (Vertical Stop)

Fig. 5 has six curves which show the x and y coordinates of the three feature points in the image plane. The horizontal axis is the time. The curves disturbed largely are the y coordinates and the others are the x coordinates. They are almost stabilized in two seconds. Fig.7 depicts the image coordinates of five points. All responses in the image plane are similar to each other.

The plots in Fig.8 depicts the position errors of the camera for three feature points (measured in the world coordinate system). The error in ω_Y direction is diverging. However, as shown in Fig.9, the response of the camera position with four feature points is stabilized. It is sluggish, and it takes more than 20 seconds to stabilize the disturbance. Fig.10 is the response with five feature points. It is improved very much for both speed and accuracy. The steady state errors are smaller than 5mm for all directions

5 Conclusion

In this paper, it has been presented how the control performance of the feature-based visual servo system is improved by utilizing redundant features. Effectiveness of the redundant features is evaluated by the smallest singular value of the image Jacobian which is closely related to the accuracy in the world coordinate system. It shows that the accuracy of the camera position control in the world coordinate system was increased by utilizing redundant features. Real time experiments on dual-arm-robot were carried out to evaluate the improvement of the accuracy and speed by utilizing the redundant features. The results verifies that the minimum singular value of the extended image Jacobian plays an important role for performance improvement of the feature-based visual servoing.

Acknowledgements

This research was supported by the **N**ew **U**niversity for **R**egional **I**nnovation program of the Ministry of Education & Human Resources Development (NURI MECHANO 21).

References

[1] K. Hashimoto et al.,1991, " Image-based dynamic visual servo for a hand-eye manipulator," in *MTNS-91*, Kobe, Japan, pp. 609~614.

[2] Sung Hyun Han, Man Hyung Lee, Hideki Hashimoto, 2000, "Image-Based Servoing Control of a SCARA Robot" *KSME International Journal*, Vol. 14, No. 7, pp. 782~788.

[3] P. K. Allen, A. Timccnko, B. Yoshimi, and P. Michelman, 1993, "Automated tracking and grasping of a moving object with a robotic hand-eye system," *IEEE Trans. Robotics and Automation*, vol. 9, no. 2, pp. 152~165.

[4] K. Hashimoto, T. Ebine, and K. Kimura, 1996," Visual servoing with hand-eye manipulator— optimal control approach," *IEEE Trans. on Robotics and Automation*, vol. 12, no. 5, pp. 766~774.

[5] K. Hashimoto. T. Ebine, K. Sakamoto, and H. Kimura, 1993, " Full 3D visual tracking with nonlinear model-based control," in *American Control Conference*, San Francisco, Calif., pp. 3180~3184.

[6] L. E. Weiss, A. C. Sanderson, and C. P. Newman, 1987, "Dynamic sensor-based control of robots with visual feedback," *IEEE J. Robotics and Automation*, vol. RA-3, no. 5, pp. 404~417.

[7] J. T. Feddema and O. R. Michell, 1989, " Vision guided servoing with feature-based trajectory generation," *IEEE Trans. Robotics and Automation*, vol. 5, no.5, pp. 691~ 700.

[8] K. Hashimoto et al., 1991," Manipulator control and with image-based visual servo," in *IEEE Int. Conf. Robotics and Automation*, Sacramento, Calif., pp. 2267~ 2272.

[9] W. Jand and Z. Bien, 1991," Feature-based visual servoing of an eye-in-hand robot with improved tracking performance," in *IEEE Int. Conf. Robotics and Automation*, Sacramento, Calif., pp. 2254~2260.

[10] B. Espiau, F. Chaumette, and P. Rives, 1992," A new approach to visual servoing in robotics," *IEEE Trans. Robotics and Automation*, vol. 8, no. 3, pp. 313~ 326.

[11] F. Chaumette, 1994, " Visual servoing using image features defined upon geometrical primitives," in *Proc. 33rd Conf. Decision and Control*, Lake Buena Vista, Florida, pp. 3782~3787.

[12] J. T. Feddema, C. S. G. Lee, and O. R. Michell, 1987, " Automatic selection of image features for visual servoing of a robot manipulator," in *IEEE Int. Conf. Robotics and Automation*, Scottsdale, Ariz, pp. 832~837.

[13] N. Papanikolopoulos and P. K. Khosla, 1993, " Adaptive robotic visual tracking: theory and experiments," *IEEE Trans. Automatic Control*, vol. 38, no. 3, pp. 429~445.

[14] N. Papaniklolpoulos, P. K. Khosla, and T. Kanade, 1991, " Vision and control techniques for robotic visual tracking," in *IEEE Int. Conf. Robotics and Automation*, Sacramento, Calif., pp. 857~864.

[15] F. Chaumette, P. Rives, and B. Espiau, 1991, " Positioning of a robot with respect to an object, tracking it and estimating its velocity by visual servoing," in *IEEE Int. Conf. Robotics and Automation*, Sacramento, Calif., pp. 2248~2253.

[16] H. Longuet-Higgins and K. Prazdny, 1984, " The interpretation of a moving retinal image," *Proc. Royal Soc. London Ser. B*, vol. 208, pp. 385~397.

The Tenth International Symposium on Artificial Life and Robotics 2005(AROB 10th '05),
B-con Plaza, Beppu, Oita, Japan, February 4-6, 2005

Calibration and Control Experiments on Redundant Legs of a Stewart Platform based Machine Tool

Woo Song Lee

Dept. of Mechanical Design, Graduate School,
Kyungnam University,
Masan, Gyeongnam, 631-701, Korea

Han Sung Kim

School of Mechanical and Automation Eng.,
Kyungnam University,
Masan, Gyeongnam, 631-701, Korea

Abstract

In recent robotics research, a parallel-kinematic manipulator has been increasingly studied for possible use as a machine tool due to the advantages of high stiffness and accuracy over serial-kinematic manipulators. In general, a spatial parallel manipulator has some limitations for increasing the stiffness only with six actuators. In order to further increase the stiffness of a machine tool, the method to add more than one additional actuator may be considered, although it may cause some more cost and restrict the workspace to some extent. In this paper, a prototype Stewart platform based machine tool with two redundant legs is demonstrated. The passive force controller for the redundant legs is suggested and the kinematic calibration of the redundant legs is performed. Finally, cutting experiment result is presented to show the effectiveness of the redundant actuation method.

1 Introduction

It has been well recognized that the Gough-Stewart type parallel manipulator, or referred to here shortly as the Stewart platform, has some advantages over serial-type manipulators in view of positioning accuracy and stiffness [1]. Among all the possible applications, the Stewart platform interests many researchers especially in using it as a machine tool. In designing and evaluating a machine tool, stiffness may be one of the most important factors to be considered, since the stiffness directly affects accuracy in machining applications. Although a parallel manipulator is usually stiffer than a serial manipulator, it is made up of several serial chains. For example, a Stewart platform consists of 6 serial chains, which can be modeled as 6 linear springs connecting base to moving platform. If there are limitations to increase the stiffness of each serial chain, the remaining way to further increase the Cartesian stiffness is to add more serial chains, i.e., springs in parallel.

With this regards, the redundant actuation method to add more than one additional serial chain is suggested. In general, the stiffness of a Stewart platform along the X- and Y-axes is smaller that that along the Z-axis. Therefore, in this work, two redundant legs are placed on the XY plane, in order to further increase the stiffness along the X- and Y-axes; One (7^{th} leg) is mounted along the X-axis and the other (8^{th} leg) is along the Y-axis as shown in Figs. 1 and 2.

Since the six legs of a Stewart platform fully define the position and orientation of the end-effector, the lengths of the two redundant legs cannot be arbitrarily determined. When there exist some kinematic errors in the redundant legs, the legs need to have some compliance not to break the system. To give some compliance to the redundant legs and to make the redundant legs act like linear spring, a passive force control method is developed. In order to reduce undesired internal forces between the redundant legs and the Stewart platform, the initial lengths of the springs should be accurately determined. For that purpose, the kinematic calibration method of using constrained optimization is suggested. The experiment result of the calibration shows that the suggested algorithm is more robust to measurement noises that the previous ones [2-5].

This paper is organized as follows: First, a prototype Stewart platform based machine tool with two redundant legs is demonstrated. The passive force controller for the redundant legs is suggested and the kinematic calibration of the redundant legs is performed. Finally, cutting experiment result is presented to verify the effectiveness of the redundant actuation method.

2 System Configuration

The overall system of the Stewart platform based machine tool system with two redundant legs is shown in Fig. 1. The kinematic parameters of the manipulator are as follows (refer to Fig. 2 and [6]):

$r_b = 400$, $r_m = 150$,

$l_{i,\min} = 801$, $\Delta l_i = 364$, for $i = 1,2,\ldots,6$

where r_b and r_m denote the radii of the base and moving platforms, respectively, $l_{i,\min}$ and Δl_i denote the minimum length and stroke of a leg, and the unit of length is millimeter. The locations of the spherical joints of the machine tool with respect to each coordinate system can be expressed by

$$\boldsymbol{b}_i = r_b[\cos\Lambda_i, \sin\Lambda_i, 0]^T$$
$$\boldsymbol{M}_i = r_m[\cos\lambda_i, \sin\lambda_i, 0]^T, \text{ for } i = 1,2,\ldots,6$$

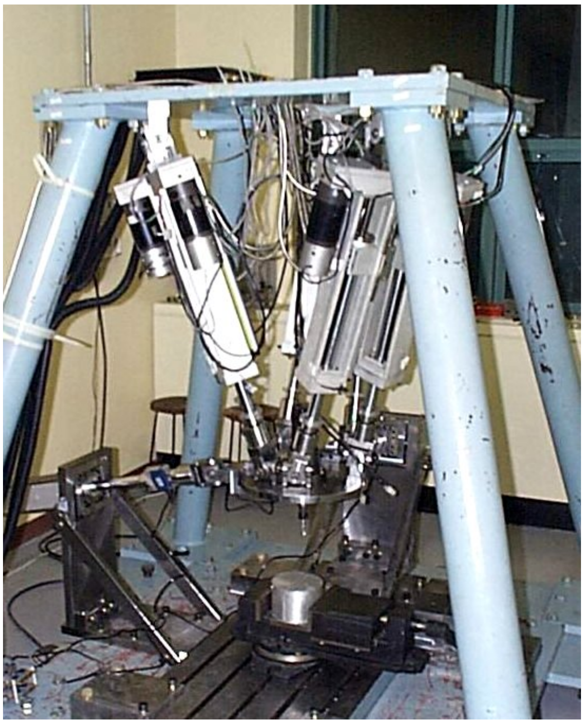

Fig. 1 Prototype Stewart platform based machine tool with two redundant actuators.

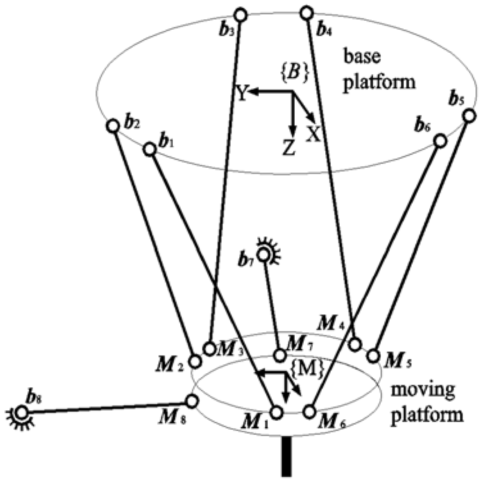

Fig. 2 Kinematic configuration of the manipulator.

where $\Lambda = [60^\circ - \phi_b, 60^\circ + \phi_b, 180^\circ - \phi_b, 180^\circ + \phi_b, -60^\circ - \phi_b, -60^\circ + \phi_b]$, $\lambda = [\phi_m, 120^\circ - \phi_m, 120^\circ + \phi_m, -120^\circ - \phi_m, -120^\circ + \phi_m, -\phi_m]$, $\phi_b = 10^\circ$ and $\phi_m = 16^\circ$.

The minimum length and stroke of a redundant actuator are given by

$$l_{i,\min} = 291,\ \Delta l_i = 364,\ \text{for}\ i = 7,8\ .$$

The locations of the spherical joints of the redundant actuators with respect to each coordinate system are given by

$$\boldsymbol{b}_7 = [-725, 0, 985]^T,\ \boldsymbol{b}_8 = [0, 725, 1045]^T$$

$$\boldsymbol{M}_7 = [-255, 0, 62]^T,\ \boldsymbol{M}_8 = [-255\sin 10^\circ, 255\cos 10^\circ, 62]^T$$

3 Passive Force Control

Since the six legs of the Stewart platform fully define the position and orientation of the end-effector, the lengths of the two redundant legs cannot be arbitrarily determined. If all the kinematic parameter values were perfectly known, the lengths of the redundant legs can be simply determined by the inverse kinematics. However, since it is almost impossible to know the exact kinematic parameter values, the redundant legs must have some compliance, otherwise, the manipulator may not move or very large internal forces may be generated, which could break some parts.

For better stability, the following passive force controller is suggested, which can provide two virtual linear springs to the moving platform in cutting as shown in Fig. 3. Therefore, the static and dynamic errors of the moving platform due to cutting force may be reduced. In this work, the passive force controller with the trajectory estimator is suggested by

$$\text{Control Law: } f = k_p(\hat{x} - x) - k_d\dot{x} \qquad (1)$$

$$\text{Trajectory Estimator: } \hat{x} = x_d + \frac{1}{k_f} f_s \qquad (2)$$

where x_d and x denote respectively desired and actual positions and $\dot{x}$ is the derivative of actual position with respect to time. f_s is the measured force from the load cell mounted at the end of a redundant leg. $\hat{x}$ is the estimated trajectory based on the information of the force sensor. k_p and k_d are the proportional and derivative gains, respectively, and k_f corresponds to the stiffness of a redundant leg. The block diagram of the suggested passive controller is shown in Fig. 4. The reason for using the trajectory estimator instead of the traditional stiffness controller is that the back-drivable force of redundant actuators is relatively large.

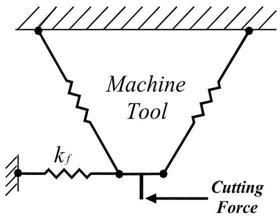

Fig. 3 Planar representation of the passive force controllers.

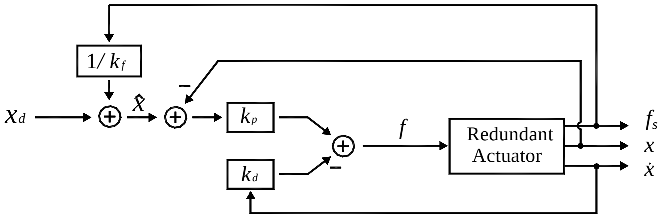

Fig. 4 Block diagram of the suggested passive force controller.

4 Kinematic Calibration

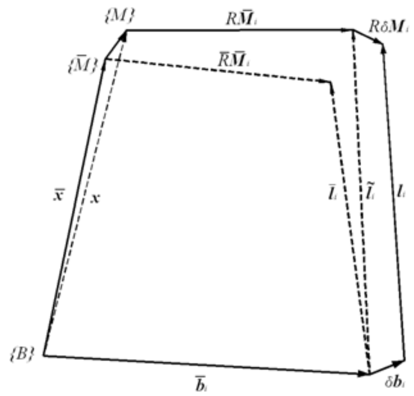

Fig. 5 Kinematic error model.

4.1 Kinematic Error Model

In Fig. 5, the outer vector loop represents the actual model to be estimated through calibration, and the inner vector loop indicates the nominal model based on the CAD data. The actual leg length and position vectors of the spherical joints can be written as

$$l_i = \bar{l}_i + \delta l_i\,,\ \boldsymbol{M}_i = \bar{\boldsymbol{M}}_i + \delta \boldsymbol{M}_i\,,\ \boldsymbol{b}_i = \bar{\boldsymbol{b}}_i + \delta \boldsymbol{b}_i \tag{3}$$

where the kinematic parameters for a nominal model are expressed with an upper bar. δl_i , $\delta \boldsymbol{M}_i$ and $\delta \boldsymbol{b}_i$ are the kinematic errors of a leg length and locations of spherical joints at the moving and base plates, which will be estimated by the kinematic calibration.

Using the vector loop in Fig. 5, an actual leg can be expressed by

$$\boldsymbol{l}_i = \tilde{\boldsymbol{l}}_i + R\,\delta \boldsymbol{M}_i - \delta \boldsymbol{b}_i \tag{4}$$

where $\tilde{\boldsymbol{l}}_i$ is defined as a virtual leg by [6-8]

$$\tilde{\boldsymbol{l}}_i = \boldsymbol{x} + R\bar{\boldsymbol{M}}_i - \bar{\boldsymbol{b}}_i \tag{5}$$

where $\boldsymbol{x}$ and R denote the actual position vector and rotation matrix of the end-effector. The quadratic form of Eq. (4) can be written as the following:

$$\begin{aligned} l_i^2 &= (\bar{l}_i + \delta l_i)^2 = \tilde{l}_i^{\,2} + \|\delta \boldsymbol{M}_i\|^2 + \|\delta \boldsymbol{b}_i\|^2 \\ &\quad + 2(\tilde{\boldsymbol{l}}_i^T R\,\delta \boldsymbol{M}_i - \tilde{\boldsymbol{l}}_i^T \delta \boldsymbol{b}_i - \delta \boldsymbol{M}_i^T R\,\delta \boldsymbol{b}_i) \end{aligned} \tag{6}$$

4.2 Kinematic Calibration Method

When there exist some measurement errors not to be negligible, the calibrated kinematic values may be updated to an undesirable direction. Although the exact information about the kinematic errors cannot be known without the well-organized calibration method, the bounds of the kinematic errors may be estimated. When the updated kinematic parameters will go to an unexpected point due to measurement noises, it may be required or useful to impose the inequality constraints on the kinematic errors. Furthermore, even in absence of noise in the measurement, the previous calibration algorithms may lead to up to 20 different values for the kinematic parameter [5]. With this regards, the optimization with inequality constraints is suggested for the kinematic calibration. The constrained optimization problem for the kinematic calibration can be stated as follows: [8]

$$\begin{aligned} &\text{Minimize} \quad : H = \sum_{k=1}^{m} F_k^{\,2} \\ &\text{Subject to} \quad : |\delta l_i| \le e_l\,, \|\delta \boldsymbol{M}_i\| \le e_m\,, \|\delta \boldsymbol{b}_i\| \le e_b \end{aligned} \tag{7}$$

where the subscript $k = 1, \ldots, m$ denotes the number of each measurement, the bounds of kinematic parameter errors can be obtained from the information on tolerances of parts and assembling errors, and the objective function is given by

$$\begin{aligned} F_k &\equiv (\bar{l}_i + \delta l_i)^2 - \tilde{l}_{i,k}^{\,2} - \|\delta \boldsymbol{M}_i\|^2 - \|\delta \boldsymbol{b}_i\|^2 \\ &\quad - 2(\tilde{\boldsymbol{l}}_i^T R_k \delta \boldsymbol{M}_i - \tilde{\boldsymbol{l}}_i^T \delta \boldsymbol{b}_i - \delta \boldsymbol{M}_i^T R_k \delta \boldsymbol{b}_i) \end{aligned} \tag{8}$$

4.3 Experiment Results

In this section, the effectiveness of the constrained optimization is verified through the calibration experiments on two redundant actuators of the Stewart platform in Fig. 1. Since the proposed passive force controller for redundant legs is basically based on a position control, the accurate kinematic information becomes one of the most important factors in control. Since the lengths of six non-redundant legs are given, the position and orientation of the end-effector can be obtained from the forward kinematics, which will be used for the measurement positions and orientations in the calibration of redundant legs.

In order to show the effectiveness of the proposed constrained optimization method, the results from the unconstrained and constrained optimization methods have been compared. The bounds of the kinematic errors are assumed as

$$|\delta l_{7,8}| < 0.05\,,\ \|\delta \boldsymbol{b}_{7,8}\| < 50\,,\ \|\delta \boldsymbol{M}_{7,8}\| < 1\ [\text{mm}]\,.$$

It is noted that the bounds of the constraints are based on the information about tolerances of parts and assembling errors. It can be seen that the kinematic errors from the constrained optimization are obtained within the ranges of constraints.

In Fig. 6, the errors between the measured and the calculated lengths before and after calibration are plotted at the sixteen measured points. From these plots, it can be said that the proposed calibration algorithm using constrained optimization is more effective than the previous algorithm using unconstrained optimization. The length errors from the constrained optimization are within ± 1 mm.

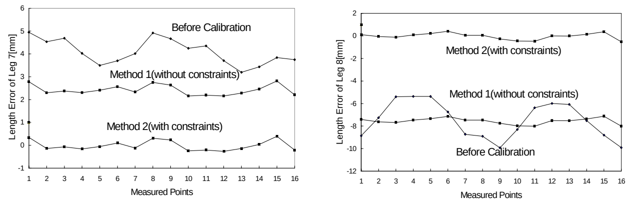

Fig. 6 Calibration results of the redundant legs.

5 Cutting Experiment

In order to show the effectiveness of the redundant actuation scheme, the dynamic errors in cutting have been measured both for the non-redundant and redundant cases. Some of the cutting conditions for the machining experiment are as follows:

Tool: flat end-mill with 2 flutes and $\phi 10$ [mm],
Feedrate: 30 [mm/min],
Spindle speed: 2000 [rpm],
Material: Al 2024,
Measurement device: resolution with 1[μm].

The cutting direction is along the X-axis, and using the linear encoder, the dynamic error in the cutting operation is measured along the X- and Y-axes for both non-redundant and redundant cases as shown in Fig. 7. In Fig. 8(a) and (c), the dynamic errors along the X- and Y-axes are plotted when no redundant legs are used. In Fig. 8(b) and (d), the dynamic errors are plotted when redundant legs are used. From Fig. 8, it can be seen that the dynamic error along the Y-axis, i.e., perpendicular to the cutting direction is larger than that along the X-axis, i.e., the cutting direction. For the cutting experiment with 2mm depth, the maximum dynamic error along the Y-axis is reduced about from 120 μm (without redundant actuation) to 60 μm (with redundant actuation). However, it is noticed that the static error in the redundant case is much larger than that in the non-redundant case. The major source of relatively large static error in the redundant case is the inaccurate kinematic information.

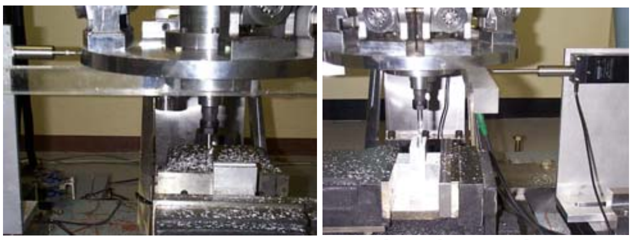

Fig. 7 Dynamic error measurement along the X- and Y-axes.

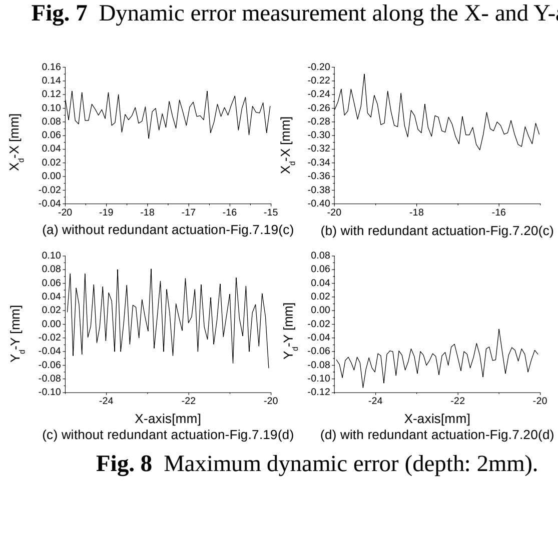

Fig. 8 Maximum dynamic error (depth: 2mm).

6 Conclusions

The prototype Stewart platform based machine tool with two redundant legs is developed. For the redundant legs, the passive force controller is suggested, which provides virtual linear springs to the cutting tool so as to increase the stiffness along the X- and Y-axes and to reduce the dynamic error in cutting. The kinematic calibration method of using constrained optimization is suggested, which is robust to measuring noise. The calibration experiment on the two redundant legs shows that the constrained optimization method provides more reasonable solution than the unconstrained one. Using the updated kinematic parameters of the redundant legs and the suggested controller, the cutting experiment is performed. It shows that the redundant actuation scheme can increase the overall stiffness and reduce the dynamic error. However, it may yield larger static error if the kinematic calibration is not perfect. In the further works, we will focus on reducing the static error.

Acknowledgements

This research was supported by the **N**ew **U**niversity for **R**egional **I**nnovation program of the Ministry of Education & Human Resources Development (NURI MECHANO 21).

References

[1] A. J. Wavering, "Parallel Kinematic Machine Research at NIST: Past, Present, and Future," *Parallel Kinematic Machines*, pp. 17-32, Milano, Italy, June, 1999.
[2] H. Zhuang and Z. S. Roth, "Method for Kinematic Calibration of Stewart Platforms," *Journal of Robotics Systems*, vol. 10, no. 3, pp. 391-405, 1993.
[3] Z. J. Geng and L. S. Haynes, "An Effective Kinematic Calibration Method for Stewart Platforms, " *ISRAM*, pp. 87-92, 1994.
[4] T. Roppenen and T. Arai, "Accuracy Analysis of a Modified Stewart Platform Manipulator," *IEEE International Conference on Robotics and Automation*, pp. 521-525, Nagoya, Aichi, Japan, 1995.
[5] C. Innocenti, "Algorithms for Kinematic Calibration of Fully-Parallel Manipulator," In J.-P. Merlet B. Ravani(eds.), *Computational Kinematics*, pp. 241-250, 1995.
[6] H. S. Kim, *Design and Control of a Stewart Platform based Machine Tool*, Ph. D. Thesis, Yonsei Univ., Korea, 2000.
[7] H. S. Kim and Y. J. Choi, "The Kinematic Error Bound Analysis of the Stewart Platform," *Journal of Robotic Systems*, vol.17, no.1 pp. 63-73, 2000.
[8] H. S. Kim, B. J. Kim and Y. J. Choi, "Kinematic Calibration for Redundant Legs of a Stewart Platform," *Proceedings of the 32nd International Symposium on Robotics*, Seoul, Korea, 19-21 Apr., 2001.

A sociable and affective artificial cohabitant

Naoko Matsumoto & Akifumi Tokosumi
Department of Value and Decision Science
Tokyo Institute of Technology
2-12-1 Ookayama, Meguro-ku, Tokyo Japan
{matsun, akt}@valdes.titech.ac.jp

Abstract

In this paper, we summarize our previous research concerning human-artifact relations conducted over the past few years from an interdisciplinary perspective encompassing cognitive science, psychology, and human-robot interfacing. Based on our findings, we discuss the cognitive significance of a newly-emerging sociable and affective artificial cohabitant.

Keywords: attachment, affective artifact, toy doll, cohabitant, social interactions

1 Introduction

Why do people feel strong affection toward artificial things such as toy dolls, robots, some characters? Japan is seeing a craze for talking toy dolls. We have investigated this form of human-artifact relation over the past few years from an interdisciplinary perspective encompassing cognitive science, psychology, and human-robot interfacing. In this paper, we summarize our findings obtained through analyses on the texts of fan letters sent to the toy company by the users of Primopuel (produced by BANDAI. Co., Ltd), a talking toy doll. The purpose of this paper is to discuss the cognitive significance of a newly-emerging sociable and affective artificial cohabitant.

2 The craze for an artificial cohabitant

Primopuel (Figure 1), produced by BANDAI. Co., Ltd., is very popular in Japan among middle-aged people. Primopuel has touch sensors, a sound sensor, a temperature sensor, and a calendar system, and a talking function (250-280 expressions) (e.g. " *I love you.* " " *Good morning.* " " *How 's your life?* "). The voice of a 5-year-old boy was adopted as the voice for the toy. Utterance selection is controlled based on an easy learning system according to user actions. The popularity of the toy doll is evident in the fact that more than one million units have been sold over the last five years in Japan alone.

Figure 1. Primopuel

3 Fan letters as data

The research methodology we have adopted is to analyze the texts of fan letters sent to the toy company by Primopuel users. We analyzed 51 fan letters mailed to the company and 271 electronic mail messages submitted to the manufacturer 's web site. In order to determine the underlying cognitive states of the users from the textual data, we categorized propositions in the texts according to a classification system ([8]), which has a number of sub-categories, such as ' descriptions of the toy as an artifact ', ' personifying descriptions of the toy ', ' user actions toward the toy as an artifact ', ' user attachment behaviors ', and ' user actions toward others mediated by the toy '.

4 Characteristics of the toy and users

In this section, we briefly present some of research results and outline our views concerning (i) the characteristics of affective artifacts and (ii) the characteristics of user states experienced by users who regard to the toy as a cohabitant artifact.

4.1 Toy story

4.1.1 Affective cohabitant

Perception of the toy as a cohabitant is a key in evoking user attachment. We suggest three factors that prompt users to regard the toy as a cohabitant; namely, (a) inferable states, (b) reactions, and (c) time sharing. First, approximately 85 % of the propositions in which users describe what they find attractive about the toy mention the toy 's utterances (53 out of 63 propositions) rather that its appearance ([8]). For instance, " *He (= the toy) says ' Good night ' to me and I feel all warm inside* " or " *He asked me to make a scarf, so I made one for him.* " Users clearly make inferences about the toy 's state from its utterances and regard it as a cohabitant. Second, the results of factor analysis indicate that the toy 's reactions to user behavior evoke in the users strong affection toward the toy. Third, factor analysis indicates that caring behavior and time-sharing with the toy also evoke user affection ([5]).

4.1.2 Sociable cohabitant

An interesting characteristic of affective toys is their sociable function. We have found that the toy 's character facilitates social behavior, which, in turn, strengthens user affection ([5]). This finding prompts us to regard the toy as being a ' sociable and affective ' artificial cohabitant.

4.2 Fan story

4.2.1 Perceiving the toy as cohabitant artifact

Users regard the toy as a cohabitant artifact, toward which they can experience strong affection. Counting expressions related to Primopuel, we found 34 (66.7 %) letters and 67 (24.7 %) e-mails including such expressions. Users described Primopuel as either a toy (toy, stuffed toy, toy doll) or as a cohabitant (family including grandchildren, child, brother, partner, roommate, friend, idol, pet). Even within a single letter, it is possible to observe mixed cognition towards the toy. Figure 2 presents a breakdown of users according to their perception of the toy (as toy only, as cohabitant only, or as both toy and cohabitant).

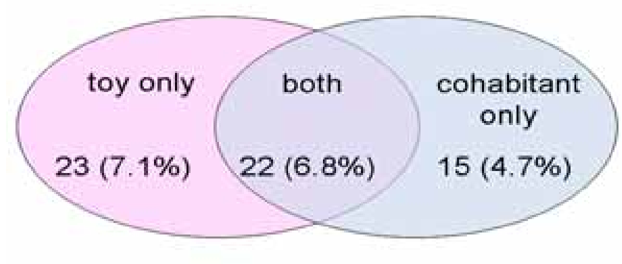

N=322 (51 letters and 271 e-mails)
Figure 2. Users recognition about what the toy is

Another issue examined is whether the toy is regarded as an artifact or whether it is personified in any way? We extracted descriptions that are relevant to this issue. While 1,130 propositions (36.1 %) indicate the user regarding the toy as an artifact (e.g. " *I changed the batteries* "), 809 propositions (25.8 %) suggest that the user are personifying the toy (e.g. "*He (= toy) seems to sleep well*"). These results lead us to the conclusion that perception of the artifact as a cohabitant is an underlying cognitive state of users who experience strong affection for the artifact.

4.2.2 Attachment behaviors effect

We have collected a total of 292 propositions that indicate attachment behaviors, where there is a clear relationship between positive emotions/evaluations and actions, such as " *this toy is so cute, I showed it to my friend* " and " *this is really lovely, so I will buy another one.* " More concretely, attachment behaviors include naming ("*I named him Tatsu*"), conversation (" *I talk with him* "), inferring the toy 's state (" *He seems to be cold* "), social actions (" *She proudly shows her Primopuel to her friend* "), negative actions toward the toy (" *I ignore him..* "), and being together (" *I took him for a drive* "). We have hypothesized that attachment behaviors function in strengthening attachment emotions ([6]). This has been confirmed by the results of factor analysis (e.g. User descriptions like " *I ignore him (= toy) for a while, and then he seemed to get angry. The way he gets angry is very lovely, I can 't resist it,* " indicate that attachment behaviors strengthen attachment emotions.) ([5]). There is also an age difference in terms of self-cognition. While young people more often evaluate the toy positively (young (0-39): 21.1 %, middle-aged (40-): 10.4 %), middle-aged people more frequently describe their attachment behavior (young: 10.7 %, middle-aged: 34.3

%). Although young people tend to just describe attachment emotions, such as " *it 's very cute*, " middle-aged people also mention causes and attachment behaviors, such as " *it 's very cute, especially its face, which makes me want to hold him tightly.* " This indicates that middle-aged people demonstrate greater meta-self-recognition concerning their emotion states and actions toward the toy rather than young people.

4.2.3 Life-state improvements

The positive physical and mental states of users are often attributed to the toy, with 8.9 % of the descriptions indicate positive changes in life state (e.g. " *talking with the toy makes me relax,* " " *The toy gives me warmth, energy, and vitality* " " *Primopuel makes my life enjoyable* ") ([8]). Moreover, it was found that users believe the toy enhances interaction with family members and/or with friends, as evidence by 16.4 % of the letters and 10.7 % of the e-mails. (e.g. " *I give Primopuel to my neighbors as a present to let them know just how cute he it* "). One of five factors extracted in our factor analysis, ' social action triggered attachment, ' relates to how attachment emotions can facilitate social behavior ([5]). This is consistent with our cognitive Socially-supported Emotion Model (SEM) ([7], [8]). In addition, we have observed that middle-aged people more frequently experience shifts in their interactions with others (22.4 %) than young people (14.4 %) ([7]). Another finding is that descriptions of negative user life states before obtaining the toy are correlated with their sense of improved well-being (e.g. " *I have lived alone since my husband passed away. I felt a keen sadness in this house. Since getting the toy, I can say ' Good night ' in bed, and often smile.* ") ([5]). Taking these results together, clearly the users with high meta-self-recognition can experience state improvements due to the affective artifact.

5 Sociable and affective artificial cohabitant

In this section, we discuss the newly-emerging sociable and affective artifact cohabitant and our cognitive model SEM based on our findings described in Section 4.

5.1 A newly-emerging artifact

People with attachment emotions, that is, people who have a strong positive affection toward something are able to perceive themselves more positively. This positive self-recognition can, in turn, lead these people to have a sense of well-being in their physical/mental states. Improved physical/mental states can facilitate social actions. Extending Norman 's claim that attractive things work better as a heuristic of problem solving ([9]), our findings indicate that ' attractive things can heighten one 's sense of positive self-awareness. ' Moreover, our results not only support previous research that shows that attachment fosters emotional communication skills in human babies and higher cognitive skills ([1]), but they also highlight the effects in facilitating social behavior.

This artifact which evokes human affection may be seen as a new kind of sociable and affective artificial cohabitant, because users both regard it as a cohabitant and believe that it enhances their social actions. This kind of sociable and affective artificial cohabitant is now emerging in our daily lives, particularly in situations where people lack rich social interaction, such as elderly people living alone, single workers, being an only child, in the nuclear family, and computerholics, for individuals who have sufficient meta-self recognition.

5.2 Socially-supported Emotional Model (SEM)

Our results indicate that one factor that strengthens user affection for the cohabitant artifact is its social effects. That is, both attachment emotions and social interaction are mutually strengthened each other. This notion is consistent with the cognitive Socially-supported Emotional Model (SEM) of emotional transmission that we have developed ([7], [8]); people strengthen their attachment to the toy by interacting or communicating with other people who also have attachment to the cohabitant artifact. As Kitayama ([3]) claims subjective well-being is dependent upon the cultural constructions of emotion, which is similar to the notion of socially-transmitted emotions that is incorporated within SEM.

5.3 Future work

Our research, which has investigated the craze for a talking toy doll, has certain advantages from analyzing fan letters in obtaining insights into the daily psychological states of the users of the toy. It would not be possible to gain such insights within the experimental setting. We can extract the underlying cognitive states relating to the natural relationships between the user and the toy. However, further investigation is required employing other research methods, such as interviews and questionnaires. Moreover, this craze is very limited in being restricted to within Japan and in involving a particular talking toy doll, which points to the need to conduct comparative studies with other forms of artifacts. It is hoped, however, that our research can contribute to a better understanding of human-artifact relationships involving strong human affection.

6 Summary

In this paper, we have identified a newly-emerging sociable and affective artificial cohabitant in our daily lives. This kind of artificial cohabitant may play a role in enriching daily life through improving physical/mental health and enhancing social interaction.

Acknowledgements

The work presented here is part of the 21st Century COE Program " Framework for Systematization and Application of Large-scale Knowledge Resources " and financially supported by the " Japanese Ministry of Education, Culture, Sports, Science and Technology " within the " 21st Century COE (Center of Excellence) Program " framework. We are greatly indebted to Professor Furui for his continuous support. We would also like to thank Dr. Terry Joyce and Yoko Hirai for their helpful comments.

References

[1] Greenspan S. I., Shanker S. G. (2004), *The first idea: How symbols, language and intelligence evoked from our primate ancestors to modern humans.* Da Capo Press.

[2] Haga Y. (2002), Contemporary toy business and tomorrow of robot toy (In Japanese). *Journal of the Robotics Society of Japan*, 20(7):683-686.

[3] Kitayama, S., Markus, H. R., Kurokawa, M. (2000), Culture, emotion, and well-being: Good feelings in Japan and the United States. *Cognition and Emotion*, 14:93-124.

[4] Libin E., Libin A. (2002), Robotherapy: Definition, assessment, and case study. *Proceedings of the Eighth International Confrence on Virtual Systems and Multimedia, Creative Digital Culture*, pp.906-915.

[5] Matsumoto N., Tokosumi A. (Submitted), Sense of well-being based on empathy for cohabitant character.

[6] Matsumoto N., Tokosumi A., Hirai Y. (2004a), Affection for cohabitant toy dolls. *Computer Animation and Virtual World*, 15(3-4):339-346.

[7] Matsumoto N., Tokosumi A. (2004b), Comparison of affection for toy dolls between middle aged people and young people (In Japanese). *Proceedings of the 4th Conference of the Toys for Well-Being Association*, Sibuya, Tokyo, Japan, July 4, 2004, pp. 13-15.

[8] Matsumoto N., Hirai Y., Tokosumi A. (2003), Toy doll as a cohabitant artifact (In Japanese). *Cognitive Studies*,10(3):383-400.

[9] Norman D. (2002), Emotion and design: Attractive things work better. *ACM Interactions* July-August:36-42.

The Tenth International Symposium on Artificial Life and Robotics 2005(AROB 10th '05),
B-con Plaza, Beppu, Oita, Japan, February 4-6, 2005

Child-robot interaction mediated by building blocks: From field observation in a public space

Miki GOAN, Hiroyuki FUJII and Michio OKADA

ATR Network Informatics Laboratories
Department of Ecological Communications
2-2-2 Hikaridai, "Keihanna Science City", Kyoto 619-0288, Japan
Phone: +81-774-95-2626 Facsimile: +81-774-95-2653
goamik@atr.jp

Keywords: **field observation, communication, robot, children**

Abstract

This study attempts to describe children's behaviors from the viewpoint of microscopic adjustment of actions when they encounter an oddly shaped robot, called 'Muu.' We investigated this through field observation at a workshop in a children's museum. Various aged children and their parents participated in the workshop together. They were instructed by an experimenter to play with building blocks while talking with Muu. As a result, it was found that the children and the robot could establish rich communications with each other not when the children evaluated Muu's behavior but when Muu evaluated the children's works. This indicates that the robot could become an 'other' that might interact with children mediated by the building blocks, whereas many children and parents treated it as a 'toy', just as the building blocks where considered merely 'objects' during interaction.

1. Introduction

How do children behave toward robots, especially a robot that asks to communicate with them? Do they gather around the robot because of its novelty but then soon lose interest? Or would such a robot become an object to which the children attached themselves? This study investigates how a robot should be put to practical use in a social organization from the viewpoint of systems engineering and also considers the development processes in human communications.

A developmental psychologist, L. S. Vygotsky attempted to investigate children's mental processes experimentally. In that study, the researcher intensively confused the subjects (children) in their communications and left them alone in a situation without a parent's support, which they usually received. Then the children became upset and struggled to understand the meanings of the things in front of them by themselves. Vygotsky revealed from this experiment that children have faint but ceaseless mental activity, which is normally buried in the parent's supports[1]. He called their development of such activities 'The Zone of Proximal Development. [2]' Harold Garfinkel, who was originator of Ethnomethodology, implemented a series of 'breaching experiments' in order to find a method to construct 'seen but unnoticed' reality in daily life[3]. This attempt disrupted the general ideas held in daily life by artificially making a situation that betrays 'background expectancies' such as rules or social common sense, which are not explicitly visible because they are naturally and tacitly shared by people.

A communication robot sometimes confuses our natural human communications, since it looks neither mechanical nor the same as a human. The authors intend to clarify the process of development in human communications by investigating the behaviors of children and their parents in front of the robot, which is the very research theme of Vygotsky and Garfinkel. The communication robot 'Muu' used in this study has restricted capability in its functions so as to construct meanings of things through communications with others (humans). The authors call this type of design method the 'minimal design of relationship.'

2. Method

2.1 Observation conditions

This experiment was implemented in the field at a workshop in a children's museum, 'Kids Plaza OSAKA,' for three days in June 2004. This paper reports the results of a two-day observation period under the same experimental conditions.

2.2 Participants

A child and his/her attendants (usually parents of the child) were regarded as a team for this experiment. Teams participated in the experiment by interacting with Muu in order of their arrival. The total number of participants was 69: 30 teams from 42 children and 27 attendants. The children's ages varied from two to twelve.

2.3 Experimental setup

The experimental setup was located within the facility and surrounded by partition walls. The setup is composed of a low table, 120 cm square, on which Muu and a basket full of toy blocks were placed.

In this study, the behaviors of Muu are regulated as follows.

Linguistic behavior: The Wizard of Oz method was used. That is, Muu was controlled to speak the appropriate words, selected from 150 prepared words, according to the interaction with the subject. The subjects were not informed of this fact. They seemed to guess that Muu autonomously and spontaneously spoke by itself. The contents of its speech were divided into different categories: One is concerned with toy blocks, for example, "Pile on a red block, please." Another involves evaluation of the child's work, for example, "It's cool, isn't it?" Another category is for compliments or chiming in, for instance, "I see."

Non-linguistic behavior: Muu was controlled to generate some slight rolling and pitching motion of its body and to move about 20 cm forward and backward. Muu was also controlled to move its body corresponding to the expressions, "Hello," "Good bye," and so on.

2.4 Observation procedure

Observation was implemented in the following way.

(1) Let the children who want to interact with Muu stand in a line in order of arrival.
(2) Induce the first child in the line and his/her attendants to enter the test field, ask his/her name, and tell him/her while pointing at Muu "This is Muu. It seems he wants to ask of you to build up the toy blocks while speaking with him. Will you help him to build up the toy blocks? Please ask him 'Say, what?' if you cannot clearly hear Muu's words."
(3) Recede to the side and begin to observe the interactions among the child, attendant, and robot. The time period for one interaction session was limited to about 5 minutes. Two video cameras captured the experiments, with the agreement of the participants. One camera was installed to the right-front of the subjects and the other was set to the left-rear of the subjects to record an elevated view of the experimental field.

2.5 Analysis

In this study, the situation of talking with the robot confused most children and attendants. However, a few cases showed rich and natural human-robot communication. This section focuses on three typical cases of 'good' communication. In order to distinguish between the former cases and the latter ones, the Conversation Analysis method was used as a qualitative evaluation for the in-depth study of behavior in context. An ethological analysis method was also exploited in handling the video recordings of the children's play: gaze and timing of movements were incorporated in an index of social interaction.

3. Results and Discussions

This study focuses on the interactions of children aged more than 5 years (23 teams). This policy is supported by the fact that only the participant teams that include children aged over 5 years showed spontaneous speech directed toward Muu. Accordingly, this age is regarded as the threshold for children to begin interacting with others independently of their parents, in spite of being under the influence of parents.

3.1 Most observed interaction cases

In the type of interactions most often observed, the children built with the toy blocks to temporarily satisfy Muu's requests. In these cases, they seemed to have no clear of what they should build. After once following Muu's requests, the children piled on the toy blocks in their own way without taking notice of Muu. Most attendants ordered the children to speak to Muu when they were independently playing with the toy blocks. If the children still did not speak to Muu, the parents induced them to speak about themselves to Muu by saying words such as "Ask him how old he is." Due to the limitation in Muu's capacity of speaking words (150 words), inappropriate responses from Muu to participants' words were sometimes observed. For example, when the child received the same words from Muu as in a previous situation, he/she pointed out that fact by saying in amazement "Hey, you said the same words before." On the other hand, when Muu made adequate responses, the parents complimented Muu with such expressions as, "You are cool", "You are so cute", "You must be so wise", and so on.

3.2 Rich and natural communication cases

In three cases, the subjects had such a clear concept of their work that it was easily observable, and these were obviously different from most other cases observed. Furthermore, in these three cases, natural communications were observed between the subjects and Muu. These three cases are described in detail below.

3.2.1 Case 1: Subject A (aged 6) and her father

In this case, it was observed that subject A began speaking spontaneously. Although she would not talk to Muu at the beginning of the experiment, through the encouraging advice and interventions of her father, she started communicating. The difference from most cases is that, in case 1, the father built with the toy blocks in himself and induced his daughter to join to build them, without compelling her to speak to the robot. At the beginning of the interaction with Muu, subject A noticed that Muu was slightly moving; however, she did not spontaneously speak to Muu, but just repeatedly glanced at Muu. On the other hand, her father himself began to build with the toy blocks, and informed her of what Muu had said, for example, "He said feels so cool!" as if interpreting Muu's words whenever Muu used the evaluating words for their works. Subject A repeated Muu's words such as "Feels so cool!" loud enough to let her father and Muu hear the words. In the meantime, her father suggested that she built the blocks closer to Muu, saying "Closer is better for Muu." Subject A accepted the suggestion. Subject A and her father began to build with the blocks closer to Muu's eye. Meanwhile, Muu said the evaluating words for their work, "That's cool!" Subject A guessed that her work was highly evaluated, however, her father insisted that the evaluation was for his work, not for hers. Then, subject A looked at Muu for a while, read Muu's expression, and finally was convinced that her father's claim was right. After that, she gave up using ambiguous words that might be taken the words for both her father and Muu. Instead, she began to frequently direct words to Muu asking for an evaluation of her father's work, such as "How do you feel about this one?" and "How about this?" (**Fig. 2**).

3.2.1 Case 2: Subject B (aged 7) and his father

Subject B accomplished two-person interaction with Muu beside his father but without permitting his father's intervention, in contrast to the case of subject A, who began to spontaneously speak to Muu with the support of her father. The interaction in this case continued in a style characterized by the subject piling on the blocks one by one while asking about Muu's intentions. For example, his question to Muu at the beginning, "Hey! Which block should I use first?" typically shows this style. Gazing at Muu, conducting conversation, and piling on the blocks are repeated in order. Subject B asked questions while looking at Muu, and he received some responses from Muu (**Fig. 3**). If he could not hear Muu's words, he again asked Muu with the word "Eh?" while gazing at it. When he guessed Muu's words, he turned his eyes to the basket of blocks, found the block that Muu pointed out, and placed it in the way Muu commanded. After that, he again looked at Muu and asked what to do next. This case of interaction continued by repeating the steps of communication and piling on blocks. In this case, the utterances of subject B and Muu never overlapped, as if they were making a certain communication rhythm; this was quite different from most other observed interactions. Interestingly, his father's utterance sometimes overlapped Muu's. Subject B made replies only to Muu's words, not to his father's. However, he did not ignore his father's intention. For example, when he was asked to pile on a red block, he looked up at his father. This behavior is unprecedented among his behaviors, in which he gazed at only Muu or the toy blocks. At that time, their work of toy blocks was piled so high that if they continued to pile on the blocks as instructed by Muu, it might fall down. This implies that the subject had to find a new way to overcome the situation. After that, subject B began to tell his intentions or suggestions to Muu, for example, "How about this way?" The concept of subject B was consistent from the start to the end, which was that he decided to build the work that Muu intended on behalf of Muu. He paid attention to Muu's intention and carefully piled on the blocks one by one. This behavior was not observed in the other subjects. The role of his father was to keep his eyes on his son and to give suggestions when his son had some trouble with the work. As in case 1, the father's words were directed toward the concept of the work, such as how to build with the blocks, and not toward compelling his son to speak to Muu or to evaluate Muu's behavior such as "This robot is cool" or "This one is smart!".

3.2.1 Case 3: Subject C (aged 11)

In this case, it was observed that subject C came to clarify the concept of the work by referring to Muu's evaluation during interactions. This subject had the habit of talking to himself very loudly, as if addressing Muu. At the beginning of the interactions, he repeated mumbled expressions like "I can't guess", "I've no idea" and so on, which expressed that he had no idea about the concept of the work. Then, he received a comment from Muu, "You are such a funny guy, aren't you?" After a moment, he muttered, "He said I am so funny, or something like that," and began to laugh. When he received the comment from Muu "A poor hand!", he burst into laughter and broke the work down into many pieces, saying "A poor hand! Come on! What are you talking about?". After the accident, subject C silently continued to build up the blocks. During the construction, although he received several comments from Muu such as "I see" and "That's cool," he made nearly no reply, except for rare giggling. The shape of the toy-block work was gradually tuned, and at nearly the end of the given time, it became clear that subject C intended to make a toy-block robot (**Fig. 4**). At that time, Muu spoke something but it was lost in the surrounding noise. Then he promptly asked Muu in a loud voice, "Eh? What?"; Subject C seemed eager to know Muu's evaluation of his work.

4. Conclusions

It was clarified that children and the communication robot 'Muu' were able to establish rich and natural communication with each other not when children evaluated Muu's behavior but when Muu evaluated the children's works. In order to retrieve an appropriate evaluation, it was necessary for the children to produce an utterance in any way and to provide a trigger for Muu to converse, for example, by talking to themselves in a distinct tone, repeating Muu's words, and so on. The role of the communicative children's parents was to arouse their children's interests in their work, to induce them to begin speaking voluntarily, and to construct communications or conversations toward accomplishing results. As future study, we are planning to provide an environment for human-robot interactions from a global viewpoint, ranging from the development of the system to a method for teaching subjects. Such an environment will produce more substantial results and build upon the knowledge obtained in this study.

References

[1] Takagi K (2001), The way of Vygotsky (in Japanese) . Kaneko Shobo, Tokyo.
[2] Vygotsky LS (1978), Mind in society: The development of higher psychological processes. Harvard Univ. Press, Cambridge.
[3] Garfinkel H (1964). Studies in the routine grounds of everyday activities. Social Problems, 11: 225-250.

Fig. 1: Experimental setup

Fig. 2: Case 1 "How about this?"

Fig. 3: Case 2 "Build with this block? This way?"

Fig. 4: Case 3 A toy-block robot under construction

The Tenth International Symposium on Artificial Life and Robotics 2005(AROB 10th '05),
B-con Plaza, Beppu, Oita, Japan, February 4-6, 2005

Social influence of overheard communication by life-like agents to a user

Satoshi V. Suzuki
CISS, IGSSE
Tokyo Institute of Technology
R1–42 4259 Nagatsuta, Midori-ku
Yokohama 226–8502 Japan

Seiji Yamada
National Institute of Informatics
2–1–2 Hitotsubashi Chiyoda
Tokyo 101–8430 Japan

Abstract

It is important to investigate influence of novel information technology, such as life-like agents, toward receivers of the information since some studies reveal that such novel technology can "persuade" people, in other words, they have strong power to change people's attitude and behavior. In this study, considering social influence of life-like agents' embodied expression, to a user, the influence of overheard communication (OC) by life-like agents toward online shopping Web site users was examined, since the OC by people often changes attitude of receivers. An experiment to compare the effect of OC by two life-like agents (a persuader agent and a persuadee agent) with regular communication (RC) by one persuader agent were conducted. The result of this experiment implied that even the OC by life-like agents could promote Web site users' online shopping purchase likelihood more than the RC by them. Moreover, attractiveness toward a persuader agent evaluated by participants was positively correlated with their purchase likelihood. This result suggests a new direction of studies of social influence from life-like agents, especially from a viewpoint of embodied expression of life-like agents, such as presence, gaze, appearance, and so on.

Keywords Life-like agents, embodied expression, overheard communication, social response to communication technologies, social influence

1 Introduction

Recently, there is much argument regarding influence of social interaction between users and communication technology as the communication technology prevails into our everyday life. Among such technology, a life-like agent (embodied conversational agent) has a possibility to interact with a user using embodied expression, and appeared in application softwares for presentation, Web navigation, and so on [4]. In particular, a life-like agent has potential to change a user's attitude. A life-like agent technology can be one of "interactive computing systems designed to change people's attitudes and behaviors" [5] with its many modalities. In this study, we approach life-like agent technology from the framework of life-like agents as social actors [6] applying the theories established in persuasion studies [10].

In this article, first we review the studies of social response toward life-like agents, and clarify the problem in the studies of inter-agent interaction. Second, the behavior rule called overheard communication is introduced and applied to inter-agent interaction. Then, through results of a psychological experiment, the influence and potential of overheard communication by life-like agents is discussed.

2 Related Works

2.1 Persuasion by Life-like Agents

Some studies of life-like agents as "social persuaders" already exist, however, there is still no study which focuses on the social influence of existence of inter-agent interaction. For example, André et al. [1] claimed the effect of inter-agent interaction in implementation of online car dealer agent system, but they did not argue how effective inter-agent interaction was. Moreover, Takeuchi and Katagiri [7] insisted that authorizing a life-like agent by other agent could grab a user's attention stronger than non-authorizing situation. Their study compared two inter-agent interaction styles, not existence of inter-agent interaction and absence of inter-agent interaction, and they did not mention the social influence by inter-agent interaction. Therefore, the influence of existence of inter-agent interaction toward a user's attitude change was investigated in this study.

2.2 Influence of Gaze by a Life-like Agent

Among embodied expression by a life-like agent, where the agent gaze plays a very important role in human-agent interaction. As people pay attention to someone's eyes when interacting with him/her [2], the agent's "eyes" imply social meanings toward the user [6]. Although Reeves and Nass [6] claimed that the agent should gaze the user in front of a display since it would be the "etiquette" which the agent should obey, especially if there is inter-agent interaction, it is natural that two or more agents talk with gazing at each other. For these reasons, the influence of the agent's direction of gaze to distinguish to whom the agent talk was considered.

3 Overheard Communication by Life-like Agents

Suppose you hear the reputation of a movie in which you are not so much interesting in these two situations:

1. Your friend directly told to you that the movie was very interesting and you *must* watch it.

2. You overheard that someone told to another one that the movie was very interesting and he/she *must* watch it.

In some cases, the message from your friend may seem intrusive since your friend *directly* told you such an imposing message in situation 1. On the contrary, in situation 2, you may have interests in the movie because you did not receive someone's message directly and the message did not seem so intrusive. The persuasion style shown in situation 2, that a persuader tell another one the message, without telling the "true" persuadee, is known as *overheard communication* (OC) in persuasion studies [9, 10]. In this study, the persuasion style that a persuader directly tell the persuadee the message, represented in situation 1, is called *regular communication* (RC). Moreover, a life-like agent which behaves as a persuader is called a *persuader agent*, and a *persuadee agent* represents a life-like agent persuaded by a persuader agent in the situation of OC by life-like agents.

Considering the influence of human-agent interaction and inter-agent interaction, and the effect of OC-style persuasive communication, we implemented OC by life-like agents in the following manner:

- Let both the persuader agent and the persuadee agent appear on the screen, because users will perceive that two distinguishable social actors exist and each of them behave at their own thought.

- The persuader agent always tell the persuadee agent a message, because users will perceive the message of the persuader agent with distinguishing whom the persuader agent tell the message by where the persuader agent gazes.

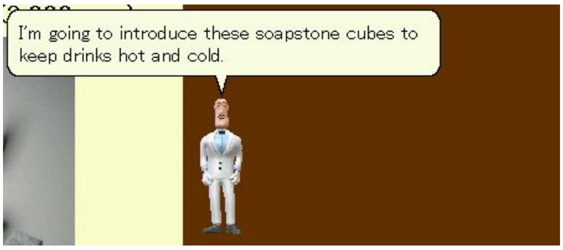

Figure 1: Explanation of characteristics of an item in RC condition

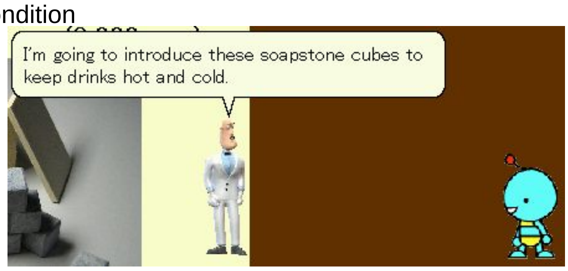

Figure 2: Explanation of characteristics of an item in OC condition

4 Psychological Experiment

4.1 Experimental Design and Prediction

In this study, we suppose two conditions for the psychological experiment. When a persuader agent explains characteristics of items, in the RC condition, it gazes toward a user in front of the screen; on the other hand, it gazes toward a persuadee agent in the OC condition. Considering the argument above, the OC by two life-like agents should promote a user's attitude change more than the RC by a life-like agent. Additionally, the OC by a persuader agent should emphasize its attractiveness which it provides more than the RC by it. Then, considering these hypotheses above, the following predictions should be determined:

P1 Participants in the OC condition will evaluate the purchase likelihood of items higher than those in the RC condition.

P2 Participants in the OC condition will evaluate the persuader agent's attractiveness which it provides higher than those in the RC condition.

4.2 Procedure

Valid experimental data were collected from 24 Japanese participants (19 males and 5 females). The participants consisted of undergraduate students, graduate students, and office workers. Their age ranged from 19 to 29.

They were randomly assigned to either RC condition or OC condition. Each condition contained equal participants.

Participants are asked to look at the explanation of items by a persuader agent on an online shopping WWW site with a note PC. In the RC condition, the persuader agent introduced items directly gazing at participants (Figure 1); in the OC condition, a persuadee agent appeared on the screen and the persuader agent introduced items gazing at the persuadee agent (Figure 2). The same item explanation phrases by the persuader agent were used in both condition. To preserve natural conversation context, the persuadee agent gave short responses to the persuader agent for each item explanation phrase in the OC condition. As introduction of each item ended, participants answered how much he/she want to purchase this item by a 10-point scale. The evaluation of purchase likelihood for the items which the participants had already possessed were omitted for analysis. The price of the items was considered so that the participant could afford to buy the item if he/she wanted it.

For all participants, the agent "James[1]" played a role of the persuader, and the agent "Cosmy[2]" played a role of the persuadee. These agents did not change their roles among participants. When participants finished the evaluation of purchase likelihood for 15 items, they answered the questionnaire about attractiveness of the persuader agent. The attractiveness was evaluated on a 10-point scale for four adjectives: kind, friendly, useful, and likable. After reporting the impression of this experiment, participants were debriefed, thanked for their participation, and dismissed. It took around 30 minutes to finish the experiment for each participant.

4.3 Result of Experiment

Mean and standard deviation values of all variables in this experiment were shown in Table 1.

First of all, the mean value of purchase likelihood scores in OC condition was significantly higher than that of RC condition. Since the difference of variance between these two variables was significant ($F(11,11) = 4.124$, two-tailed $p < .05$), Welch test was applied to confirming the significant difference between the mean values of them. As a result, the significant difference between them observed ($t(16.04) = 2.984$, two-tailed $p < .01$, $ES = 1.166$). Thus, the result supported the prediction **P1**.

However, there was no significant difference between the two condition in the score regarding impression toward the persuader agent. Despite the attractiveness score in the OC condition exceeded that in the RC condition, according to the result of two-tailed t-tests, significant difference between the two conditions did not appear in the score, as shown in Table 1. Then, the prediction **P2** was rejected by the result. Nevertheless, between the score of attractiveness and the score of purchase likelihood for each participant, there was a significant positive correlation. The values of Pearson's product-moment correlation coefficient and the significance test of these values proved there were significant correlations between the two scores for each condition (in RC condition, $r = .505$, $t(10) = 1.851$, two-tailed $p < .10$, and in OC condition, $r = .615$, $t(10) = 2.463$, two-tailed $p < .05$).

5 Discussion and Future Works

The result shown in section 4.3 suggested that the OC induced a user's purchase likelihood of products on online shopping Web site more than the RC. This result implied that life-like agents could play a role of a clerk and another customer virtually. One reason why the OC by life-like agents influenced user's attitude is because the persuader agent gazed at the persuadee agent when explaining feature of items and never gazed at the user. Therefore, the gaze of the persuader agent could be perceived as a important embodied expression to participants. In fact, one participant in OC condition reported: "It is good to see the conversation between two agents from the viewpoint of a stranger, since it may feel annoying if one agent directly talks to me." Another reason is because the persuadee agent existed on the screen. Thus, the existence of the persuadee agent could serve as a criterion for participants to consider whether they should buy the items or not. There were two participants who answered that he/she took the behavior of the persuadee agent into consideration. This fact suggests that the influence of the existence of the persuadee agent could not be ignored.

As for the impression of a persuader agent, there was no significant difference between the OC condition and the RC condition in three scores of impression. However, the scores of attractiveness is significantly correlated with the scores of purchase likelihood. This result indicated the influence of physical appearance of a persuader agent because we used the persuader agent with same appearance in both the RC condition and the OC condition. Fogg [5] argued physical appearance of life-like agents as a important factor of persuasion of a user by life-like agents, and some participants answered that the persuader agents used in this experiment looked "too strong" or "not so cute." However, participants' evaluation of attractiveness of the persuader agent was affected to their purchase likelihood both in the RC condition and in the OC condition.

[1]This agent is available at `http://www.cantoche.com/english/gallery/msagent.htm`.

[2]This agent is available at `http://www2.mic.atr.co.jp/agent/`.

Table 1: Mean (standard deviation in parentheses) values of measured variables for each condition and results of statistical tests

	RC cond. ($n = 12$)	OC cond. ($n = 12$)	t-value (d.f. = 22)	Effect Size (ES)
Purchase likelihood scores	4.127 (1.348)	5.421 (0.664)	$2.984^{**\star}$	1.166
Impression of the persuader agent	5.729 (1.760)	6.521 (1.694)	1.123	0.439

* For the significant difference of variances between the two conditions, the t-value by Welch test was shown here (d.f. = 16.04). **: $p < .01$

In the OC by life-like agents, the persuader agent's gaze was functioned in the experiment. However, there are still few studies which focus on the function of a body of a life-like agent [8]. Thus, the influence of embodied expression triggered by the appearance and behavior of life-like agents is not clear so far. This influence should not only apply to human-agent interaction, but to human-robot interaction. If we hope that technology pervade many aspects of our life, we should emphasize the social aspect of human-agent interaction.

Besides, we did not mention the interactivity between a user and agents. First, this study does not consider the influence of the difference of a reaction by a persuadee agent since we focus on the existence of inter-agent interaction. Some persuasion studies reveal that the negative reaction of others toward a persuader gave people negative impression (for example, Axsom et al. [3]). The valence of reaction of a persuadee agent can influence the decision of users, and should be considered in future works.

In this study, we discussed the influence and potential of overheard communication by life-like agents. Particularly, it is pointed out that embodied expression, especially existence of the persuadee agent and the direction of the persuader agent's gaze, played an important role in the overheard communication by life-like agents. From the stance of social influence of the embodied expression of life-like agents to a user, the way to utilize life-like agents for the voluntary attitude change of users should be explored in the future.

References

[1] André E, Rist T, van Mulken S, Klesen M, Baldes S (2000), The automated design of believable dialogues for animated presentation teams. In: Cassell J, Sullivan J, Prevost S, Churchill E (eds), Embodied Conversational Agents, The MIT Press, Cambridge, MA, pp. 220–255

[2] Argyle M, Cook M (1976), Gaze and Mutual Gaze. Cambridge University Press, New York

[3] Axsom D, Yates S, Chaiken S (1987), Audience response as a heuristic cue in persuasion. Journal of Personality and Social Psychology, 53(1):30–40

[4] Cassell J, Sullivan J, Prevost S, Churchill E (eds) (2000), Embodied Conversational Agents, The MIT Press, Cambridge, MA, pp. 220–255

[5] Fogg BJ (2003), Persuasive Technology: Using Computers to Change What We Think and Do. Morgan Kaufmann Publishers, San Francisco, CA

[6] Reeves B, Nass C (1996), The Media Equation: How people treat computers, television, and new media like real people and places. Cambridge University Press, New York

[7] Takeuchi Y, Katagiri Y (2002), Social dynamics in Web page through inter-agent interaction. Transactions of the Japanese Society for Artificial Intelligence, 17(4):439–448

[8] Takeuchi Y, Watanabe K, Katagiri Y (2004), Social identification of embodied interactive agent. In: Proceedings of the 13th International Workshop on Robot and Human Interactive Communication (ROMAN-2004), Kurashiki, Japan

[9] Walster E, Festinger L (1962), The effectiveness of "overheard" persuasive communications. Journal of Abnormal and Social Psychology, 65(6):395–402

[10] Zimbardo PG, Leippe MR (1991) The Psychology of Attitude Change and Social Influence. McGraw-Hill, New York

The Tenth International Symposium on Artificial Life and Robotics 2005(AROB 10th '05),
B-con Plaza, Beppu, Oita, Japan, February 4-6, 2005

Do Complementarities Exist in Agent Interactions?

Mingyi Lee
ATR Network Informatics Labs
2-2-2 Hikaridai, Keihanna Science City
Kyoto 619-0288, Japan

Miki Goan
The Same as Left

Michio Okada
The Same as Left

Abstract

In social interactions and communications, agents are required to coordinate their own activity patterns to maintain and continue dynamic balanced interactions. These activity patterns consist of dynamically the balanced changes in distance, postures, and positions of agents. There is a clear tendency for social interactions to apply such particular motion changes to exclude irrelevant patterns.

But how these activity patterns correlate with each other and the mechanisms they use in interaction remain a mystery. We use the concepts of action system theory from ecological psychology to formulate these activity patterns and study the complementarity of behavior coordination in agent interactions.

We simulated behavior coordination of agents for the argument of our formulation and found that agents in interaction could correlate their activity patterns complementarily when they orient themselves each other. These initial findins are expected to provide us new possibilities for the analysis of human-robot interaction.

1 Introduction

In the interactional activities of animate objects, many macro and micro actions compose entire behaviors. Macro actions involve smooth, habitual or periodic movements. On the other hand, micro actions include erratic and atypical movements, for example, hesitation. Accordingly, a behavior composed of macro or micro actions exhibits its own order or disorder of activity patterns. To date, a wide variety research in behavior generation and coordination suggests that behaviors in interaction have some coordinative structures(synergetics). For example, these include skillful bodily movements[1][2][3].

Meanwhile, we wonder whether behaviors in social interaction also have such synergetics. From the standpoint of relational design, we want to study behaviors in social interaction to find the coordination mechanism of behavioral changes.

In this paper, by using concepts from ecological psychology, we first formulated environmental and interactional factors for behavior generation. Next, we simulated behavior coordination of agents for the argument of our formulation and found that there is a probability of complementarity between activity patterns of agents in interaction. We believe the results of this work will provide new possibilities for the analysis of human-robot interaction.

2 Relational Design of Behavior

2.1 Relational Properties for Activities

We use the concepts of ecological psychology to discuss behavior generation and coordination. In ecological psychology, behavior is regulated by *affordances* as relational properties of the agent-environment system[4][5][6]. We formulate *affordances* as environmental and interactional factors to study or design agent-environment systems that regulate behavior. In general, a behavior in interaction would involve two kinds of activity: exploratory and performatory activity[4].

Exploratory activity, i.e. the scanning for and use of information, typically does not require the expenditure of a significant amount of force to alter the substances or surfaces of the environment. Adjustments of this activity are typically embodied in low-energy and low-impact movements. In performatory activity, an agent(actor) does use a significant amount of force to alter the substances and surfaces of its environment. For example, it is one thing to see or to smell a piece of food, but it is quite another thing to obtain it and eat it.

We presuppose that the physical properties relating an agent's perception and action are nearly invariant within a period of time. X is defined as the set of environmental states available for perception and action,

The Tenth International Symposium on Artificial Life and Robotics 2005(AROB 10th '05),
B-con Plaza, Beppu, Oita, Japan, February 4-6, 2005

and S is the set of perceptional states, and A is the set of actions. Let $T(x, a|x \in X, a \in A) = x' \in X$ denote the state transition function and $O(x|x \in X) = s \in S$ denote the perceptional function.

First, if an agent involved in exploratory activity reliably finds or chooses a certain equivalence relation R^e of environmental perception, then S with A will be partitioned into several equivalence classes S_i with A_i^e under R^e, as follows:

$$S = \sum_{i \in M} S_i, \quad A = \bigcup_{i \in M} A_i^e \tag{1}$$

with $S/R^e = \{S_i | \exists u, v \in S_i, uR^e v\}$, $A_i^e = \{a^e \in A | \exists s = O(x \in X) \in S_i, O(T(x, a^e) \in X) \in S/R^e\}$. In this case, S/R^e is called the quotient set of S by R^e, and A_i^e is the set of *perceptional actions* a^e.

Second, if an agent involved in performatory activity reliably finds a certain equivalence relation R^p of actions in the environment, then X with A will be partitioned under R^p, as follows:

$$X = \sum_{j \in N} X_j, \quad A = \bigcup_{j \in N} A_j^p \tag{2}$$

with $X/R^p = \{X_j | \exists u', v' \in X_j, u' R^p v'\}$, $A_j^p = \{a^p \in A | \exists x \in X_j, T(x, a^p) \in X/R^p\}$. In turn, X/R^p is called the quotient set of X by R^p, and A_j^p is the set of *direct actions* a^p. Then, an agent would extract factors from two kinds of relational property *affordances* to regulate both activities. We can describe these two kinds of *affordances* as follows:

$$Af_i^e = S_i \times A_i^e, \quad Af_j^p = X_j \times A_j^p \tag{3}$$

where $i \in M, 0 < M \leq |S| \leq |X|$ and $j \in N, 0 < N \leq |X|$. In addition, the role of equivalence relation R^e or R^p is used here to brush against and aside *affordances*, or, more precisely, to abstract and eliminate changes in the layout of affordances for perception and behavior cycles.

2.2 Triggers for Behavior Coordination

Each activity takes advantage of each corresponding relational property Af_i^e, Af_j^p to generate behavior, since these properties provide templates for the activity patterns in behavior (see Fig.1). If the next set A_{ij}^{ep}, in which several elements of A_i^e and A_j^p can satisfy within the same given period,

$$A_{ij}^{ep} = \{\tilde{a} \in A | \exists s = O(\exists x \in X_j) \in S_i, \underline{O(T(x, \tilde{a}) \in X/R^p) \in S/R^e}\} \tag{4}$$

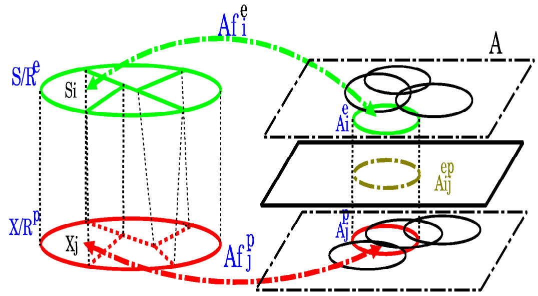

Figure 1: Relational properties *affordances* Af^e, Af^p are respectively for exploratory and performatory activity.

is $A_{ij}^{ep} \subseteq A_i^e \cup A_j^p$, $A_{ij}^{ep} \cap A_i^e \neq \emptyset$, $A_{ij}^{ep} \cap A_j^p \neq \emptyset$, then both activities would be synchronous or identifiable. In this period, a particular behavior that nests exploratory and performatory activity can share A_{ij}^{ep}.

In contrast, the underlined part of eq.(4) can also be modified as below:

1. $O(T(x, a) \in X/R^p) \notin S/R^e$
2. $O(T(x, a) \notin X/R^p) \in S/R^e$
3. $O(T(x, a) \notin X/R^p) \notin S/R^e$

These three cases would provide possibilities for changes in the intentionalities of the behavior. In the first case, a recognized action involves an undistinguishable perceptional state. That is, it needs another suitable equivalence relation, $R^{e'}$, on perceptional states S to distinguish and identify that undistinguishable perceptional state as another kind of perceptional state. In the second case, an unrecognized action involves a distinguishable perceptional state. It needs another suitable equivalence relation, $R^{p'}$, on environmental states X to identify one's own current capacity for direct actions. In a third case, an unrecognized action involves an undistinguishable perceptional state. It needs suitable equivalence relations $R^{e'}$ and $R^{p'}$. In these cases, another suitable exploratory or performatory activity is, or both is required to follow the adjacent behavior. However, the effort to find the suitable one is sometimes successful and sometimes not. In addition, we assume that changes in these cases would promote the breakup or reorganization of behavior.

Furthermore, if an agent has abundant equivalence relations for exploratory or performatory activity, then it is possible that suitable activities would form the

The Tenth International Symposium on Artificial Life and Robotics 2005(AROB 10th '05),
B-con Plaza, Beppu, Oita, Japan, February 4-6, 2005

coordinative behavior as the dynamic equilibrium process or state. In addition, we assume that the activity patterns of a number of agents in interaction might be complementary if they could share identifiable equivalence relations.

3 Agent-Environment Interaction

3.1 Preparations

We designed identifiable equivalence relations to implement agents in the verification of complementarity between the activity patterns of agents in interaction. We prepared a mobile agent and an experimental environment to analyze the interaction of agents in the environment. The agent as an actor has two wheels to move itself and six distance sensors to detect changes in distances between itself and its surroundings as an informational flow. A radio emitter and a receiver were installed to emit or receive signals in an area of a certain diameter. The designed environment provides the agent a limited range of movement (see Fig.2).

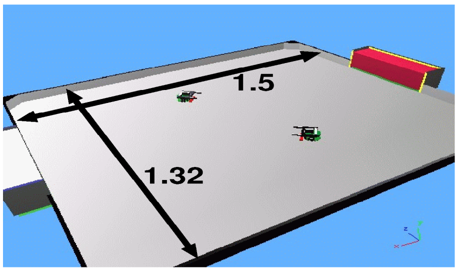

Figure 2: The experimental environment.

3.2 Mutual Interaction among Agents

Two agents have different but constant moving velocity. They both use the same equivalence relation R^{e_1} to distinguish the perceptional states existing when an object is moving in their surroundings, this is done by using the distance sensors. Their other equivalence relation R^{e_2} is used to distinguish perceptional states existing when a signal is produced; this is done by using the radio emitter and receiver.

These equivalence relations could be designed by using the differences of time-series data from the sensory equipment. In addition, the state that affords the informational flow could be defined as the ideal state for the agent. The design criterion to judge an unsuitable state becomes effective, for example, when an agent is surrounded by something. We use these conditions to implement the learning algorithm in an agent in order to generate the variational equivalence relation R^p and regulate action patterns by R^p. In this case, we use the Q-learning method, one of the reinforcement learning methods, not for its usual purpose (i.e. to reach the goal) but for possible behavioral coordination. The following is the update rule of the learned action-value function in Q-learning:

$$Q(s_t, a_t) \leftarrow (1-\alpha)Q(s_t, a_t) + \alpha(E_t + \gamma max_{b \in A} Q(s_{t+\Delta}, b))$$

where Q, E denote the action value and the state value, t is the number of steps, factors $\alpha, \gamma \in [0, 1)$. We assume that the action values correspond to the variational equivalence relation R^p to regulate actions.

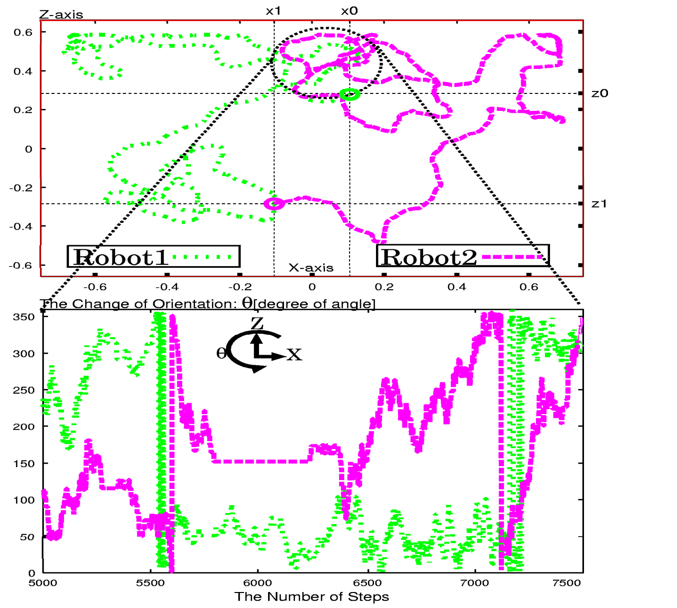

Figure 3: Changes of the trajectory and orientation of agents in interaction. The starting points (x_0, z_0), (x_1, z_1) are respectively for each agent.

In the experiment, the behaviors of two agents in a common environment apparently exhibited irregular and disorganized patterns (see Fig.3). However, Fig.4(a) shows that changes in the orientation of the two agents are in particular branched patterns. Significantly, when they have mutual interaction between 5000 and 7000 steps, they orient their positions and postures to each other. Moreover it appears that their activity patterns in interaction gather in the embodied actions set $A_{ijk}^{e_1 p e_2}$ (see Fig.4(b),(c)). The dashed circles in Fig.4(b) and (c) also show that mutual interaction among the two agents, or coordination of their behavior, are complementary. That is, we could hypothesize

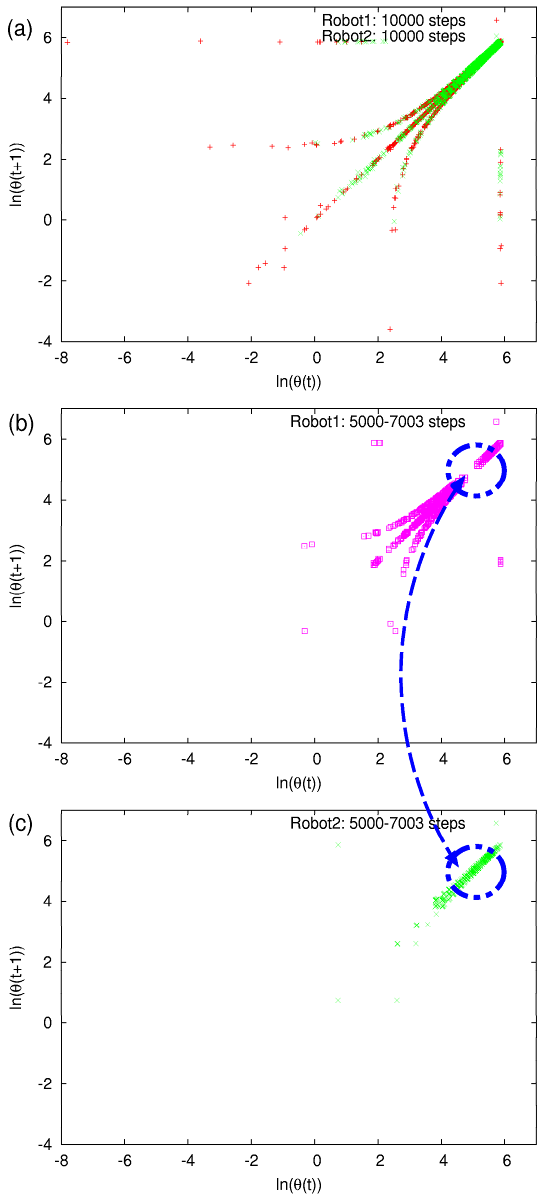

Figure 4: The phase space of $\theta(t), \theta(t+1)$ and t is the number of steps. (a) Changes in orientations of agents during 10^4 steps, show sort of spatio-temporal patterns. (b)(c) Changes in orientations of each agent between 5000 and 7003 steps. Dashed circles in (b), (c) exhibit mutual interaction among agents are complementary.

that if multiple actors use the same homogeneous informational flows, then their mutual interaction can emerge and have dynamic complementarity.

4 Conclusion

This paper presents formulas of relational properties as environmental and interactional factors for activities, based on concepts from ecological psychology. We used these formulated properties to study behavior processes. As a result, complementarity between activities was found to be one property for developing interaction. However, the work reported here needs to be followed up by further research, such as a comprehensive analysis of human-robot interaction.

Acknowledgements

This work is supported in part by the Ministry of Public Management, Home Affairs, Posts and Telecommunications Strategic Information and Communication R&D Promotion Scheme, in Japan. The authors would like to thank the ECS members of ATR Network Informatics Laboratories in Japan.

References

[1] N. Bernstein, "On dexterity and its development" the japanese edition, Kanekoshobo Press, 2003.

[2] T. Fujinami and T. Yamamoto and M. Abe, "Synchronisation and Differentiation found in skillful bodily movements", *The 18th Annual Conference of the Japanese Society for Artificial Intelligence 2004*, 3D1-04, 2004.

[3] K. Yamane and Y. Nakamura, "Pin-and-Drag Synergetic Interface for Choreography of Hman Figures", *Journal of the Robotics Society of Japan*, Vol.20, No.3, pp.335-343 2002.

[4] E.S. Reed, "*Encountering the World - Toward an Ecological Psychology*", (Oxford University Press., 1996).

[5] T.A. Stoffregen, "Affordances as properties of the animal-environment system", *Ecological Psychology*, 15(2), 2003, 115-134.

[6] E.C. Goldfield, "Development of infant action systems and exploratory activity: a tribute to Edward S.Reed", *Ecological Psychology*, 12(4), 2000, 303-318.

The Tenth International Symposium on Artificial Life and Robotics 2005(AROB 10th '05),
B-con Plaza, Beppu, Oita, Japan, February 4-6, 2005

Multi User Learning Agent based on Social Interaction

D. Katagami
IGSSE
Tokyo Institute of Technology
Yokohama, 226-8502

H. Ohmura
Advanced System Development Center
Yamaha Corporation
Shizuoka, 438-0192

Y. Yasumura
Factory of Engineering
Kobe University
Kobe, 657-8501

K. Nitta
IGSSE
Tokyo Institute of Technology
Yokohama, 226-8502

Abstract

In this paper, we propose Multi User Learning Agent(MULA) to interact with various types of people effectively towards realization of Social Interaction. MULA is equipped with two learning functions for Social Inteaction. One is direct learning function using individualization of the user parameters, and another is indirect learning function using past experience and the similarity between each users. MULA adopts an extended classifier system which uses a classifier strength and a user profile for each people. Each person's classifier strength is enhanced by the interaction with the person and the past experience with similar type of people. We verified the effect of MULA by experimenting in interaction with six participants using a pet-type robot AIBO.

1 Introduction

In recent years, research of HAI (Human-Agent Interaction)[1] aiming at forming communication between an agent, such as a robot, and human is capturing the spotlight. However, the present HAI research is in the stage of a designing one-to-one adaptations between human and an agent, and the methodology with two or more users is not established. In this research, we aim at realizing a social interaction performed by the social learning which learns from interaction with two or more users using a constructive approach. Social Intearction is realized by two learning functions. One is direct learning function using individualization of user parameters, and another is indirect learning function using past ecperience and the similarity between each users. In particular, indirect learning uses experience with other users for the target user. We think it is one form of social learning to realize the suitable action from experience with two or more users to the current user. We named an agent equipped with Social Interaction as Multi User Learning Agent (MULA). MULA adopts an extended classifier system which uses a classifier strength and a user profile for each people. We veryfied MULA in experiments of a user's preference prediction task in a real world.

2 Implementation of MULA

2.1 A learning based on past experience

A target here is to realize an adaptation to the current user by using experience with another users. Then, we realized MULA which incorporated past experience using the function explained based on the model-based reinforcement learning (Dyna-Q algorithm [2]). In this paper, we define changing the action by the influence of the others as "social".

[Direct learning by individualization of user parameters]
Although the technique [3] of preparing knowledge and the rule set for each environment is common, the problem of efficiency, such as a problem of a memory and dignity attachment of the knowledge, occurs. Then, we adopt the approach individually prepared for every user about how to use knowledge (user parameters) instead of using two or more rule sets.

[Indirect learning using past experience]
Since it corresponds to two or more users, it is important to use past experience well. Here, the similarity between users is used like *collaborative filtering*. Especially this may become the indicator for the next interaction in a stage with little experience with a current user.

2.2 Social leraning using a interaction with users

In order to realize above two functions we propose MULA architecture (Fig. 1) and it's learning algorithm (Fig. 2).

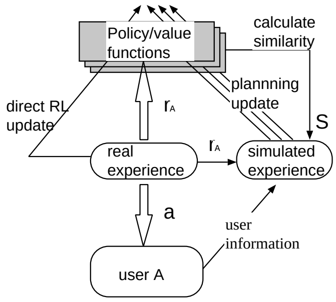

Figure 1: MULA architecture

Initialize $p(s,a,i)$ and $Model(s,a,i)$ for all s,a,i
Do forever
  user identification $i \in I$
  simple Q-learning
  $UserProfileR_i(s,a,i) \leftarrow r_i$
  for $j = 0$ *to* $j = n$ *do*
    Similarity $S_{ij} \leftarrow UserProfile\ R_i,\ R_j$
    $q(s,a,j) \leftarrow q(s,a,j) +$
      $\alpha S_{ij}(|r_i + \gamma max_{a'} q(s',a',i) - q(s,a,i)|)$

Figure 2: MULA algorithm

MULA specifies a user first. MULA updates directly individual user parameters of the user (it considers as User A temporarily) using simple Q-learning from an interaction (MULA receives remuneration r_A to act output a_A to certain state s_A) with the user. It is actual experience. Next, MULA calculates the similarity S_{AX} of $UserProfile$ between user A and another users X using users' information. MULA updates each $UserProfile$ and individual variables of all users indirectly using the interactive information $s_A, a_A, and\ r_A$ and this similarity with user A. It is indirectly experience.

2.3 The outline of the system

Fig.3 shows the outline figure of the system proposed by this research. This system has adopted XCS[4] as a fundamental learning mechanism, which is one of most useful classifier systems. XCS uses new three parameters instead of strength of classifier system for each classifier.

prediction$p$**:** prediction of classifier.

$$p_t = p_{t-1} + \alpha(|r_{t-1} + \gamma max_{a'} p_{t-1}(s',a') - p_{t-1}|) \quad (1)$$

prediction errorε**:** An error between prediction p and actual measurement.

Fitness$F$**:** It adopts as an evaluation value of the rule creation by GA.

[individual variables]
This system prepares the variables of a classifier (a prediction value p, a prediction error ε, and the degree of adaptation F), without preparing a new rule set for every user. We call it an individual prediction value, an individual prediction error, and an individual fitness, respectively. Moreover, we prepared **the individual evaluation value** R which records evaluation of the past interaction. Each classifier has an individual evaluation value, for each user. When positive evaluation is received, the value increases, and when negative evaluation is received, it decreases. We call these values **individual variables**.

[The procedure of the system]
MULA updates individual evaluation value R based on evaluation of a user's interaction, and the similarity is calculated by it each time. MULA updates individual variables $p,\ \varepsilon,\ and\ F$ other than an individual evaluation value R like the usual XCS does. However, in individual prediction value p, although individual prediction value p_A is directly updated according to the similarity between user A and other users. All of other users' individual prediction values p_X are also updated indirectly. The method how MULA learns the individual prediction value p of a classifier is updated by the interaction with users is explained in Fig.3.

(1) MULA acquires sensor information S_A (1001) by interacting with user A.

(2) MULA generates Match Set $[M]$ from sensor information. And the action a chosen from an action selection method is outputted.

(3) MULA gets evaluation for the action from user A, and updates prediction value p and other individual variables directly.

(4) MULA calculates all of the similarities S_{AX} from user A's updated profile $\mathbf{R}_A$ and other users' profiles $\mathbf{R}_X$.

(5) MULA updates all other users' inidividual prediction values p_X using the similarities S_{AX} indirectly.

We will explain about $UserProfile$, calculation of the similarity in (5) and indirect update of individual prediction in (6) as follows.

[User profile]
We regard the vector containing the individual evaluation value R which is an individual variable as **user**

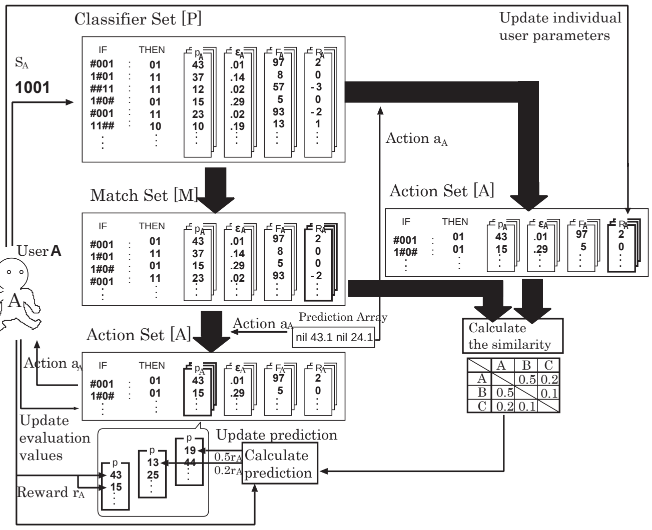

Figure 3: MULA based on XCS

profile. Therefore, the number of the individual evaluation values R in the profile to user A is the same as the number of classifiers (rules) which this system has. This system uses user profiles of two users by calculation of the similarity in the following subsection.

[Calculation of the similarity]
We adopt the vector space method as one of the simplest methods of calculating the similarity. Corresponding to the output action, this system makes the information of user's preference to an individual evaluation value, and acquires it for every classifier. The similarity S between user A and user B is then computed by the vector of individual evaluation value $\mathbf{R}_i$ and $\mathbf{R}_j$ in the following formulas from the user profile of each user which is used as the ingredient of the vector. $\mathbf{f}$ and $\mathbf{g}$ are two vectors (user profiles) to compare.

$$S(\mathbf{R}_i, \mathbf{R}_j) = \frac{(\mathbf{R}_i, \mathbf{R}_j)}{||\mathbf{R}_i||||\mathbf{R}_j||} = \frac{\sum_{m=1}^{K} R_i^m R_j^m}{\sqrt{\sum_{m=1}^{K}(R_i^m)^2}\sqrt{\sum_{m=1}^{K}(R_j^m)^2}} \quad (2)$$

[Indirect update of individual prediction value]
MULA introduces a social element into the update of individual prediction value p of each classifier. It is explained how to update this individual precidiction by interaction between human and MULA as follows.

Other users' individual prediction values p^j are updated by the following formulas according to the similarity S_{ij}. Here, p_j^t is a prediction value in step t to user j. α is a coefficient. r_j^t is the reward from human j in step t. r_max is maximum reward. Where $(S \leq 0)$, it decides r_i, r_{max} as criteria initial value $p_i^{t=0}$ in order to be able to reinforce the inverse direction. In this paper, we simply deal with single-step task in the experiment. Therefore update formula in Fig. 2 can express formulas below. Here, the formulas update users' individual prediction value indirectly by experience with user i.

$$p_j^t = \begin{cases} p_j^{t-1} + \alpha S_{ij}(r_i^{t-1} - p_i^{t-1}) \ (S > 0) \\ p_j^{t-1} - \alpha S_{ij}(r_{max} - r_i^{t-1} - p_i^{t-1}) \ (S \leq 0) \end{cases} \quad (3)$$

3 Experiments

3.1 Purpose of experiment and settings

We investigate MULA's efficiency in experiments of a user's preference prediction. In order to investigate the agent's effect intelligibly, we verified based on the following points.

- MULA predicts a user's preference individually using past experience with users and their user profiles. We verify correlation between a user's true preference and a prediction value using past experience of a user and a user profile.
- The interaction (for example, evaluation and taste) from human is always not optimal. And it is changeable. We investigate changes of the similarity.

In this experiments, we introduced MULA into pet-type robot SONY AIBO. All experiments are conducted in the following procedure based on the interaction between a user and AIBO.

(1) A subject pushes the button of AIBO and AIBO outputs an action.

(2) The subject gives one evaluation from two kinds, "praise($r = 100$)" or "scold($r = 0$)", by preference to the action of AIBO. It returns to (1).

The above procedure is considered as *one procedure of an interaction*. In this experiment, the initial values of update parameters are $\alpha = 0.2$, $r_{max} = 100$, $p^{t=0} = 50$, $R^{t=0} = 0$, $S^{t=0} = 0$.

We prepared 5 kinds of actions (e.g. "bark","dance","greeting") of agent, and 3 kinds of situation ("back button","head button","jaw button"). According to Fig. 3, all user profiles are created by classifier set selected by the same act, the similarity S_{AX} is created from them, and a suitable act is predicted to the state.

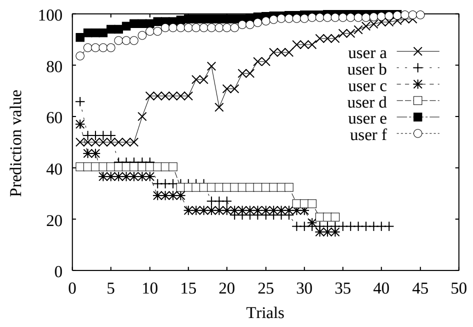

Figure 4: Changes of individual prediction values

Six subjects (a-f) participate in the experiments. The experiments divided into two phase. All subjects perform a profile creation phase first. They enter an evaluation phase in order. In an evaluation phase, a subject is influenced by the subjects who performed this phase before. For example, the 6th subject is influenced by five previous subjects.

3.2 Experimental results and discussions

Fig. 4 shows changes of individual prediction in evaluation phase. The prediction value of user e and f is large compared with the initial value $p^{t=0} = 50$, and direction of convergence "praise($r = 100$)" is in agreement, and you can see learning is promoted. In order to check the efficiency of learning, the prediction value of each action of user from b to f was investigated. The action which prediction was successful and accelerated learning was 74% and the action which prediction was not successful was 9%. The correlation coefficient of user's actual preference and a prediction value is 0.73 on the whole. Therefore, MULA has been predicted the suitable action to a user's preference.

Moreover, the similarity is always changing with the interaction between users and MULA dynamically. According to the past experience between users, the similarity will change dynamically and it will be convergenced to the fixed value in the situation of change of the similarity between users (Fig. 5). Thus, MULA calculates the optimal prediction value for the moment according to the calculated similarity for every trial. Therefore, finally exact anticipation like this experimental result was completed.

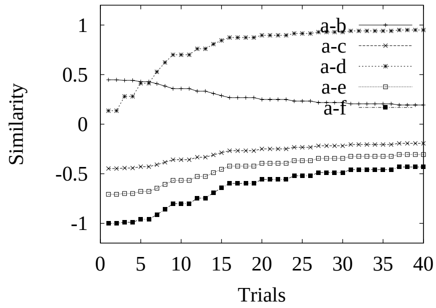

Figure 5: The changes of the similarity between user a and the others

4 Conclusion

In this paper, we attempted to realize social interaction by constructing MULA which performs social learning from an interaction with two or more users. Two learning functions realized social learning. One is direct learning function using individualization of user parameters, and another is indirect learning function using past ecperience and the similarity between each users. Especially indirect learning uses experience with other users for the target user. We think it is one form of social learning to realize the suitable action from experience with two or more users to a current user. By the experiment in real environment, we verified that MULA can respond to dynamic change of users' preference, and perform efficient learning.

References

[1] S. Yamada, T. Yamaguchi : Mutual Learning of Mind Reading between a Human and a Life-like Agent, The Fifth Pacific Rim International Workshop on Multi-Agents, pp.138–150, 2002.

[2] R. S. Sutton: Integrated Architectures for Learning, Planning, and Reacting Based on Approximating Dynamic Programming, Proc. of the 7th International Conference on Machine Learning, pp.216-224, 1990.

[3] R. Parr and S. Russel: Reinforcement Learning with Hierarchies of Machines, Advances in Neural Information Processing Systems 10, pp.1043-1049, 1998.

[4] S. W. Wilson : Classifier Fitness Based on Accuracy, Evolutionary Computation, 3(2), pp.149-175, 1995.

Can robots get "membership" through social interaction?

Hiroyuki FUJII and Michio OKADA
Department of Ecological Communications,
Network Informatics Laboratories, ATR
Hikaridai 2-2-2, "Keihanna Science City", Kyoto
fujii_h@atr.jp

Abstract

To investigate how robots behave as social entities, we analyzed the interaction of humans and "Muu," an embodied artificial entity, to find the salient patterns of behavior that distinguish the robot from humans in the course of interaction. Through exploratory observation, we found the manner of repetition and the address mismatch to be such salient patterns. We discussed how the social display of such patterns as "marked" features plays a very important role in mutual interaction.

Keywords: human-robot communication, social entity, quasi-interpersonal behavior

1 Introduction

Communication robots are expected to becocme a novel social entities that can interact socially with humans. For a communication robot to become an adequate participant in social interaction, it needs not only to implement the mechanism for the skill or ability of communication individually, but also to acquire "membership" in a community in the course of social interaction with other social entities.

Our research is based on the notion of categorizing the social membership of an artificial entity according to the degree of difference between the quasi-interpersonal behavior of humans interacting with the artificial entity and the natural interpersonal behavior of humans interacting with other humans. Humans tend to interact with a robot (or a computer or an animal) in nearly the same manner as they do with the other humans. Such behavior is referred to as quasi-interpersonal behavior.

We analyzed the interaction of humans and "Muu," a communication robot, to find the salient patterns of behavior that distinguish the robot from human in the course of interaction. Consequently, we explored how these salient patterns in interaction are linked to the categorized "membership" in a community.

2 Quasi-interpersonal behavior in human-robot interaction

Chatting or playing is a form social interaction, and, under limited conditions, we can perform this "social" interaction with robots. Humans tend to interact with an object (robot, car, computer, or animal) in nearly the same manner as with other humans. Such behavior is referred to as " quasi-interpersonal behavior" (cf. Yamamoto (1994)[8] , and Takeuchi (1995)[7]).

A series of research using the "Media Equation [6]" paradigm showed that humans considered computers to have social existence along with personality, despite knowing that the computer is merely a machine that certainly does not have a personality. However, the behaviors in interaction sequences with artificial entities have many features that are different from the interaction behaviors among humans. The authors believe that these differences are linked to the definition of the social entities of robots. To define the social aspects of robots, it is necessary to identify the characteristic patterns of interaction sequences that let us distinguish whether an interaction partner is a robot or another human.

In this research, we try to describe such characteristic patterns by analyzing the social interaction between humans and "Muu."

3 Analysis of Interaction between Humans and "Muu"

In the authors' research group, the "Muu project," we have attempted to observe the social interactions between humans and "Muu" in various domains. The communication robot "Muu" was developed for research on social interaction (Fig. 1). Muu was designed for human-robot communication mediated by social display such as contingent utterances, orienta-

Figure 1: Muu : Embodied Artificial Creature

Figure 2: Interaction with “Muu” observed at Kids plaza Osaka

tions of the body, and mutual coordination of body arrangement. Muu has a big fish-like eye, and his rounded body is covered with soft urethane rubber. Muu's shape and behaviors are based on Lorentz's “baby schema,” which was assumed to elicit the empathetic attitudes of participants.

In this paper, for analysis, we focused on the situation of participants playing with building blocks while talking with Muu.

Experimental Settings This experiment was implemented in the field at a workshop in a children's museum, ‘Kids Plaza OSAKA,’ for three days in June 2004 (Fig. 2). In the experimental session, Muu was presented to the participants as behaving autonomously and spontaneously. The utterances made by Muu were selected from 150 prepared sentences by a hidden operator (Wizard of Oz [4] method). These 150 sentences were synthesized by CHATR (speech synthesizer system [1]) for use in the situation of playing with building blocks with children (greetings, operations of blocks, color of blocks, evaluations). One session was about 5 minutes. Every interaction session was video recorded, with the agreement of the participants. As long as the behavior of a participant followed the context of playing with building blocks according to the instructions of the experimenter, Muu could behave appropriately, to some extent, by using suitable timing and contents to initiate, continue, and finish an intaractive session.

4 Analysis

From observing the participants' behaviors at the event, it was clear that the adults acted in a more awkward manner with Muu than did the children. To clarify the pattern of such quasi-interpersonal behavior, we focus here on an interaction session between an adult female and Muu. In that session, the participant seemed to be able to play with the building blocks while talking with Muu for about five minutes. For closer analysis, that session was decomposed into a sequence of pairs of robot-human utterances. This session consists of 32 pairs of robot-human uttarances. Then, an observer (one of the authors) identified the points at which some kind of “trouble” was assumed to occur if that behavior were actually carried out within common human-human social interaction. The identified instances were found in six cases. These cases were sorted into two categories, named “Manner of repetition” and “Address mismatch”.

4.1 Manner of Repetition

Case 1 to 4 were included in a category named “manner of repetition.” These are the cases in which the contingent responses of the participant with Muu (Fig. 3 b) were out of the normal manner (Fig. 3 a).

Case 1: Reply without adequate interval In about one fourth of the Muu-human uttarance pairs (9/32), the start timing of the human's uttarance followed the utterance of Muu too early. In these sequences, the intervals of two uttarances were 0.1 seconds or less. Commonly, the interval of two utterances is distributed around 0.7 seconds (cf. Nagaoka et al., 2002 [5]). These replies of insufficient interval length indicate that these behaviors were pre-fixed and not conducted in a manner of mutual coodination.

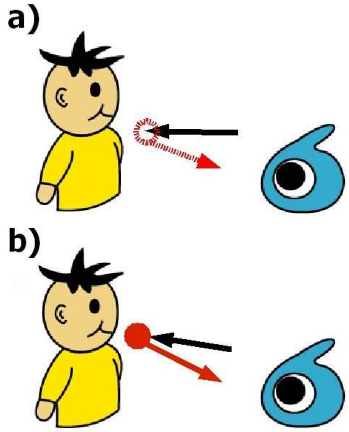

Figure 3: Manner of Repetition

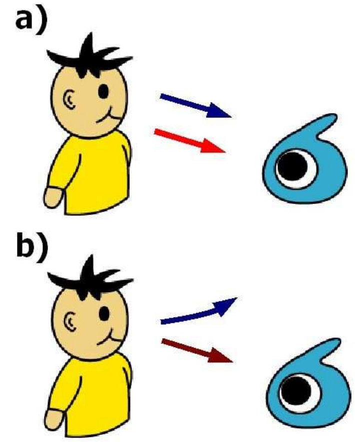

Figure 4: Address Mismatch

Case 2: Repetition without modification Many times (7/32) the participant simply repeated the preceding uttarance of Muu. In the common human-human interaction, simple repetition (like a parrot) is a "marked" pattern. This pattern is sometimes considered as a display of teasing, so it could be a source of "trouble" in the interaction. These simple repetitions usually make continuation of utterance sequences difficult. The frequent occurrence of simple repetition showed that Muu was a social entity that couldn't recognize possible source of trouble in the course of social interaction, and such a lack of ability in interaction could be exposed in public.

Case 3: Ignoring overlap Overlapping of the utterances of Muu and the human occurred two times, but both times the participant continued her utterance and did not seem to care about having been interrupted. These patterns also means that these behaviors were pre-fixed and not conducted in a manner of mutual coodination.

Case 4: Ignoring no-responce of Muu The participant sometimes mentioned "Lion" or "Table" built by the blocks, but these utterances did not seem to require a response from Muu. She didn't display an attitude of concern about the non-response of Muu. Rather she seemed to ignore the non-responce of Muu, and these patterns showed that Muu was a social entity that wasn't able to respond such spontaneous topics in social interaction.

4.2 Address Mismatch

Case 5 and 6 were included in a category named "Address mismatch (Fig. 4)."

These are the cases where the direction of gaze or focusing differed (Fig. 4 b) from the object predicted from the flow of utterance sequences (Fig. 4 a).

Case 5:Gaze Aversion while replying The participant sometimes responded or talked to Muu without changing the direction of her face or gaze. In a face-to-face situation, a speaker usually orients his/her face or gaze to the listener, or at least moves the direction of gaze. This pattern of behaviors showed that Muu was a social entity who didn't have the ability to care about the orientation of the face or gaze of the speaker in a face-to-face situation, and the deficiency could be exposed in public.

Case 6:Seeking other person The participant sometimes sought out another person when she seemed unable to hear the uttarance of Muu. This pattern of behaviors showed that Muu was a social entity that didn't have the responsibility for its own utterances, and the deficiency could be exposed in public.

5 General Discussion

5.1 Display for "marked" pattern

Our analysis showed that the awkward patterns in the observed session of human-robot interaction to be pre-fixed and not conducted in a manner of mutual coodination. These cases suggested that Muu behave as a social existence that was unworthy of mutual interaction. These cases also suggested that Muu as a social existence was incapable of using the normal manners of mutual interaction.

The "manner of repetition" and "address mismatch" are "salient" or "marked" patterns in social interaction, awareness of such patterns is definitely an important aspect of social entities in social interaction. These results suggested that for mutual interaction, communication robots have to be aware of such "marked" patterns in the couse of interaction and have to display this awareness in approriate situations.

5.2 "Robots" from the viewpoint of "Membership Category Devices"

How to define a social entity in social interaction is not only a problem involving the ability of each individual. From the viewpoint of a socio-cultual approach, a social entity is also defined in social interaction by its "membership" in the community. In the socio-cultural context that we commonly use in mutual interaction, the "membership categorization device" functions as a "label" that has various attribute [2]. The fact that the participants could interact in some way with the robot in their first meeting with it at the event suggested that the "robot" could be categorized as having some kind of "membership" in the surrounding society. Peoples can use some kind of implicit schema of how to interact with the "robot" in human-robot interaction.

It is necessary to create not only a mechanism for social interaction but also the "common sense" of the robot to evolve a social entity that can participate in mutual interaction with humans, to become a social and cultural partner of people.

Acknowledgements

The research reported here was supported in part by a contract with the National Institute of Information and Communications Technology entitled, 'Research on Human Communication.'

References

[1] CHATR URL:http://www.red.atr.jp/soft_page/chatr.html

[2] Gerfinkel,H.: Studies in Ethnomethodology; Prentice-Hall(1967)

[3] Goan, M., Fujii, H., and Okada, M., The first contact of children and robots: From the field observation in a public space, In Proceedings of Human Interface Symposium 2004, pp.503-508 (2004)

[4] Kelley, J.F.: An interactive design methodology for user-friendly natural language office information applications; ACM Transactions on Office Information Systems, Vol.2, issue 1, pp. 26-41, (1984).

[5] Nagaoka, C., Draguna, M., Komori, M., and Nakamura, T., The Influence of Switching Pauses on Interpersonal Perception in Dialogues, In Proceedings of Human Interface Symposium 2002, (2002).

[6] Reeves,B., Nass,C.: The Media Equation; Cambridge University Press, (1996).

[7] Takeuchi, S., About "Interpersonal behavior," Cognitive studies, **Vol.2**, No.4, pp.103-107, (1995).

[8] Yamamoto, Y, "Interpersonal behavior" Cognitive Studies, **Vol.1**, No.2, pp.95-99, (1994).

The Tenth International Symposium on Artificial Life and Robotics 2005(AROB 10th '05),
B-con Plaza, Beppu, Oita, Japan, February 4-6, 2005

Minimal Design for Human-agent Communication

Nobuyoshi MATSUMOTO, Hiroyuki FUJII, Michio OKADA

Department of Ecological Communications,
ATR Network Informatics Laboratories
2-2-2 Hikaridai,
"Keihanna ScienceCity," Kyoto, 619-0288 JAPAN
nobu@atr.jp

Keywords: **minimal design, quasi-interpersonal behavior**

Abstract

Robots have been anticipated to become both workers and partners of humans from the earliest period on their history. Thus, robots should become artificial entities that can potentially socially interact with human beings in social communities. Recent advances in technology have added various functions to robots: Development of actuators and grippers show us infinite possibilities for factory automation, and robots can now walk movements and performance very smoothly. All of these functions have been developed as solutions to robots moves and performance However, there are many remaining problems in communication between robots and humans. These unsolved problems can be clarified by adopting the idea of subtractive methods.

In this paper, we consider minimal design of the robots from the viewpoint of designing communication. By minimal design, we mean eliminating the non-essential portions and keeping only the most fundamental functions. We expect that due to the simple and clean design of minimally designed objects, humans can interact with these robots without becoming bored too quickly. Because humans have "a natural dislike for the absence of reasoning" nature, artificial entities built according to the minimal design principles have the ability to extract the human drive to relate with others. We propose a method of designing a robot that has "character" and is situated in a social context from the viewpoint of minimal design.

1. Introduction

The goal of robot research is not to manufacture mechanical humans. What we are interested in is communication between robots and humans. Communication between robots and humans cannot replace communication among people. Without using a Turing test to determine whether they are communicating with a robot or a human, humans would communicate with a robot based on the assumption that a robot is a machine. The behavior in such communication is called quasi-interpersonal behavior. People are always looking for non-human things subconsciously and it could be said that communication is an exchange of incomplete information with others. People often complement such incomplete information automatically. In designing a communication robot, it is also important to arouse such abilities in humans who communicate with robots. However, robots to date have been designed only to feature improved functions, without a strong focus on communication between robots and humans.

"Life-likeness" can also be found on television, in video games, etc. People can get a feeling of "life-likeness" from other people, even non-living objects, so describing a robot as life-like is quite feasible. However, which may be why humans and robots cannot maintain smooth communication. This problem cannot be overcome via the methodology of building robots as copies of living organisms.

A good communication robot cannot be designed by the present method of only enriching the functions of a robot. By such a method, the problem of lost "life-likeness" mentioned above is unconquerable, In order to realize interaction with people over a long period, it is also an important condition that a robot 's appearance should be attractive to humans. Norman who argued what is difficult to use in the book "The Psychology of Everyday Things," classified the elements of a design into instinctive design, behavioral design and introspective design in a recent work "Emotional Design." The ease of use referred in Norman's previous work was intended only for behavioral design. Norman claimed that balance between instinctive design in connection with appearance, and introspective design in connection with meanings of appearance, and an action-design, is important. Moreover, he claimed that not only ease of use but also the attractive features of a design, could satisfy people.

In this paper, in order to design a continuous-communication robot different to conventional robot research, we claim that subtraction design and minimal design, in which subtraction is systematically performed based on a certain intention, are important. In minimal design, not to abbreviate elements but to clarify the interface in communication, the design should be completed after distinguishing what is essential. In addition, we propose a minimal design to clarify what the interfaces in communication are, such as the type of action or a situational setup, not only abbreviation as a design.

2. Communication Design

Communication is exchanging incomplete information with others. Communication robots to date have been intended to deal with problems of how to resolve incompleteness of information. Communication is not enriched by large quantities of information, but should be designed to clarify intentions or messages that contain insufficient information. It is difficult to simulate communication, since there is so much background information necessary to realize communication and that information is uncontrollable in engineering, making it difficult to make a simulation that includes it.

2.1. Additional design

To contrast the minimal design proposed in this paper, we call the main guiding principle of robot design the "additional design" here. In the design of a conventional communication robot, transfer equipment and a structure for voice dialogs are added to a fixed-position, industrial type factory robots. Although there are robots that depend on wheels as a simple form of transfer equipment, bipedal robots have also received much research attention in recent years. Robot researchers believed that their purpose was attained by enriching the functions of the robot. However, even if the number of functions increases and each function approaches that of a living thing, in comparison with a dog or a cat which are actually alive, people will lose interest

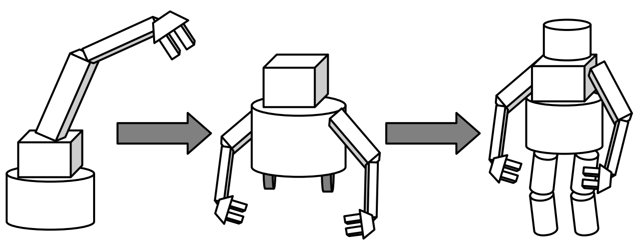

examples of design by addition

2.2. Subtractive design

A design with function curtailment will be called "subtraction design" as opposed to the methodology of function addition. As a robot designed by functional addition becomes more like a living thing that really exists, ironically the difference between the robot and the living thing becomes even clearer. Such a problem could be avoided by a design peculiar to the robot, not by copying the figure of a living thing. A clear policy is needed to determine how far a design would be reduced.

3. Benefit of Minimal Design

We discussed, design by subtraction in the preceding section. In this section, we will discuss minimal design, which is we called the directional simplification of subtraction design. In order to emphasize the main point of communication, it is better to omit non-essential design elements. Which design elements to omit are determined by goal setting. A minimally designed robot is not complete in itself. It is designed for communication with others, initiating interest in communication in a human. A minimal design targets the principle design of communication.

3.1. Designing derivative form of robots

Once the principle design elements are found, they will facilitate in designing a derivative form of a robot based on principle design. A design problem is solves by the calculation of elements, and such calculations comprise with exaggerations, omissions, and other modifications. They will help in the design of future personalized robots.

4. Expression technique

The design of a robot is considered with the design of living organisms in mind. The expression methods for living things can be a good reference for minimal design. Character designs in comics, cartoons and video games are particularly inspired by nature. We also have much to learn from the representation techniques of performing arts. For example, Noh-play, a Japanese traditional performing art has no stage props, only big drawings of a pine tree.

4.1. Expression technique in comics

The expression technique in comics provides useful information for minimal design. In comics, non-realistic descriptions, grossly exaggerated and with bold omissions are often used. Character design in comics uses a lot of symbols and metaphors for living things, comics the characters are drawn vividly. They are expressed by character form, speech, body movements, and others in various communication channels, Characters have strong features. A communication robot must also be designed like a comic character, having strong features.

4.2. Expression technique in Noh Play

The expression technique in Japanese Noh plays also provides useful information for minimal design. Noh mask for the lead actor, which is called Onna-Men(woman's mask) wears an empty expression. The mask is not complete in itself, It takes meaning from actor's movements.

A robot with a cute face, like that of a stuffed toy, softens the user's heart as its first impression, though this feeling does not last long. Such a prepared pretty face is unusable for long-term communication design. Instead of preparing a pretty face, we suggest designing robot movement to express the robot's feelings. If the robot laughs, it will actually show it is pleased. If it takes five seconds, however, it may show an artificial smile. Feelings can be expressed by actions.

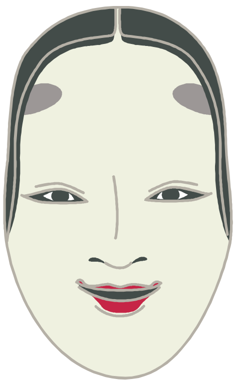

Noh mask(Onna men)

5. *in situ* Design

In minimal design, a robot is designed in accompaniment with a situation and the user's preference,; communication depends on the situation. A message can have various meanings in a given situation; non-verbal expressions also affect communication. However, even if communication is successful the first time in a controlled environment like an experimental laboratory, there is no guarantee that the second time will be successful. We expect there to be many further problems in classrooms, patients' rooms, or in homes.

A robot must be designed not to fit various environments, but to tune in to the relationship between itself and a user. In a classroom, it may be more important for a robot not to break even if it drops from a desk than to climb one flight of stairs. It would also be important that it could talk in small voice in a patients' room. A user may also wish to take a bath together with a communication robot.

Summary

Until recent times, robots were merely tools for production. Now, however people have certain expectations to robots as partners in communication, and recently many communication robots have appeared. Many of such robots are designed on the same principle as factory robots: the idea of design by addition. Also many robots have been created to imitate the figures of living things, as mechanical animals. Although such robots resemble living things differences do stand out.

In this paper, we proposed a technique called "minimal design." Minimal design is a design primarily for maintaining communication. Also, we showed the significance of designing a robot with relation to the user and the situation. In minimal design, in order to emphasize an important design element, the non-essentials are omitted.

Although a minimal-design communication robot is dissimilar to animals, it still recalls animal characteristics in some ways. Since they are not physically similar to animals, users don't expect too much. In addition, we suggested a useful way for robots to express feelings similarly to characters in comics and a Noh plays.

Minimal design does not express sharp disagreement with improvements in elemental technology of robotics. Technology can be used for making superior communication robots with minimal design way. Though minimal design, a communication robot that never causes boredom can become possible.

Acknowledgements

The research reported here was supported in part by a contract with the National Institute of Information and Communications Technology entitled, 'Research on Human Communication'.

References

[1]Norman D. A., The Design of Everyday Things, Perseus Books Group, 2002.
[2]Norman D. A., Emotional Design ; Why we love (or hate) everyday things, BASIC BOOKS, 2004.
[3]Reeves B. Clifford N., The Media Equation, CSLI publication, 1996.
[4]Ekuan, K. The aesthetics of Japanese lunchbox, MIT Press, 1998.
[5]Fushimi, K., Anno, M., Nakamura, G., Bi no kikagaku (Aesthetic of geometry), Chuo koron, 1979.

The Tenth International Symposium on Artificial Life and Robotics 2005(AROB 10th '05),
B-con Plaza, Beppu, Oita, Japan, February 4-6, 2005

Development of a Speech-Driven Embodied Laser Pointer with a Visualized Response Equivalent to Nodding

Hiroyuki Nagai*1, Tomio Watanabe*1,*2 and Michiya Yamamoto*1
*1 Okayama Prefectural University
111 Kuboki, Soja, Okayama, 719-1197, Japan
*2 CREST of Japan Science and Technology Agency (JST)

Abstract

InterActor is the speech-driven embodied entrainment character for activating human interaction and communication by embodied rhythms between speech and body motions such as nodding in human face-to-face conversation. In this paper, a new speech-driven embodied laser pointer InterPointer is developed for supporting embodied interaction and communication for both a lecturer and audiences. InterPointer is a pointing device in which the beam pattern is changed from a point to an oval with a visualized response equivalent to nodding in the same timing as InterActor to speech input.

1 Introduction

According to the rapid progress of information and communication technology, it has become possible easily to communicate with distant people in everyday life. In human face-to-face communication, not only verbal message but also nonverbal behavior such as nodding and body motions are rhythmically related and mutually synchronized between talkers [1]. It is to be desired that people can share embodied rhythm by the entrainment between human speech and nonverbal actions and motions in remote communication.

We have developed the speech-driven embodied interactive actor called InterActor which has both functions of speaker and listener by generating expressive actions and motions coherently related to speech input. We demonstrated that the system can be effective for supporting human interaction and communication between remote talkers [2].

It is difficult for a lecturer on the platform to see audiences' reaction because they are separated in a conference room, and they are not entrained. Therefore, it is difficult for the lecturer to present the lecture like face-to-face communication. It is expected to support interactive communication by introducing the synchrony of embodied rhythms.

In this paper, a new speech-driven embodied laser pointer InterPointer is developed for supporting embodied interaction and communication in a lecture. InterPointer is a pointing device in which the beam pattern is changed from a point to an oval with a visualized response equivalent to nodding in the same timing as InterActor to speech input.

2 Development of a speech-driven embodied laser pointer

2.1 Concept of InterPointer

Figure 1 shows the concept of a speech-driven embodied laser pointer "InterPointer". InterPointer is the system for supporting interaction with lecturer and audiences through visualized response equivalent to nodding of listener on the basis of speaker's speech. Even if audiences' reaction cannot be seen and it is hard to talk on the platform, a lecturer can make presentation with ease by using InterPointer that can feed back a typical nodding reaction. Audiences can also

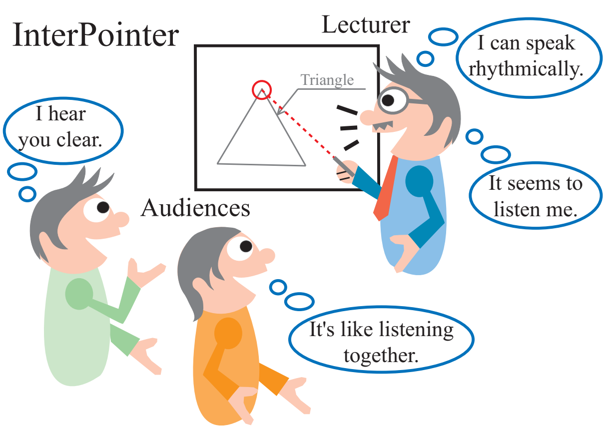

Figure 1: Concept of InterPointer.

The Tenth International Symposium on Artificial Life and Robotics 2005(AROB 10th '05),
B-con Plaza, Beppu, Oita, Japan, February 4-6, 2005

enjoy good presentation, because they can share embodied rhythm with the lecturer and feel a sense of togetherness by seeing InterPointer's nodding reaction.

2.2 Outline of InterPointer

Figure 2 shows the outline of InterPointer. InterPointer utilizes the change of beam patterns of a laser pointer LP-2000 (CABIN) for the visualization of nodding. LP-2000 can generate four kinds of beam patterns by laser light reflection in the mirror which is vibrated by two electromagnetic vibrators (Figure 3). At the same time, slight vibration arises at the timing of pattern generation.

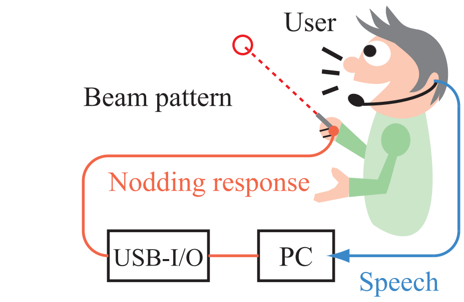

Figure 2: Outline of InterPointer.

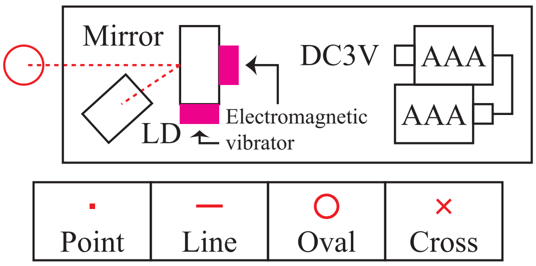

Figure 3: Outline of LP-2000.

Users can feel the nodding response of listener by change of beam patterns. Response time of a nodding was set to 200 ms. InterPointer is controlled by the USB-I/O from PC equipped with the microphone input and the USB connector. Table 1 shows beam patterns of InterPointer.

2.3 Development of InterPointer

Figure 4 shows InterPointer. InterPointer has installed the microcomputer PIC16FL84A (MICROCHIP) which can set up input and output for pattern generation. The microcomputer PIC16FL84A was connected to the button input part and it generated pattern switch signals. InterPointer had a connector in order to connect an USB-I/O cable and to receive a nodding signal from PC.

Table 1: Beam patterns of InterPointer.

	USB-I/O cable is not connected.		Nodding response		
			OFF	ON	
Pattern	·	—	·	·	—
	○	×		○	×

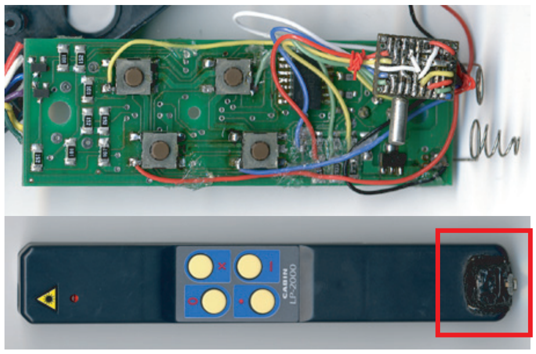

Figure 4: InterPointer.

Original cable called USB-I/O cable was developed to connect USB with InterPointer as shown in Figure 5. USB-IO was built in the USB-I/O cable. The control chip of USB-I/O (Morphy Planning) was a CY7C63001A-PC (Cypress Semiconductor). It supported USB 1.1 (Low-speed, 1.5 Mbps) and was bus-powered.

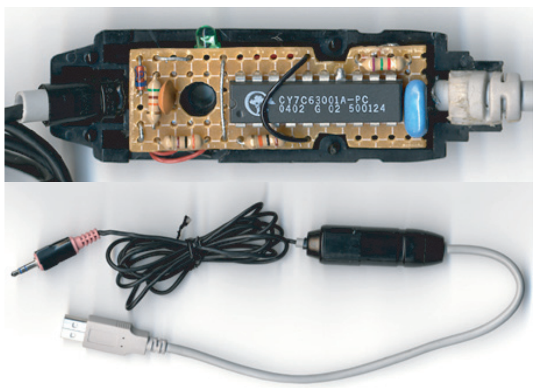

Figure 5: USB-I/O cable of InterPointer.

2.4 Listener's interaction model

InterPointer is the laser pointer that can change beam patterns in the equivalent timing to listeners nodding, which is one of the typical patterns of non-verbal interaction, and it plays an important role in smooth interaction in human communication. As for the prediction model of nodding on human face-to-face communication, the MA (Moving-Average) model which estimated the nodding $y(i)$ as the weighted sum of the binary speech signal $x(i)$ in each video frame of 1/30 second was introduced as follows [3].

$$\hat{y}(i) = \sum_{j=1}^{J} a(j)\, x(i-j) + w(i) \qquad (1)$$

$a(j)$: linear prediction coefficient, $w(i)$: noise

3 Evaluation of the system

3.1 Experimental method

The effectiveness of the InterPointer system was examined by sensory evaluation. Figure 6 shows the experimental setup of the system. One of paired subjects was a lecturer who makes a presentation in front of a screen, and the other was an audience for the presentation. The following four modes from (a) to (d) were put to paired comparison in the experiment.

(a) Point (the beam pattern was a point, and doesn't change during the experiment)
(b) Oval (the beam pattern was an oval, and doesn't change during the experiment)
(c) Model (the beam pattern changes from Point to Oval in the nodding timing by MA-model and returns to Point after 200 ms)
(d) Exponential (the beam pattern changes from Point to Oval in the timing of exponential distribution and returns to Point after 200 ms)

The subjects were instructed to experience a presentation and choose better mode out of randomly selected two modes from (a) to (d). The exponential distribution was generated as follows.

$$T = -3\ln(1-\lambda), \;\; \lambda = [0,1] = (0.1 \sim 0.9) \qquad (2)$$

The average of exponential distribution was set at 3 seconds which denotes the mean nodding interval.

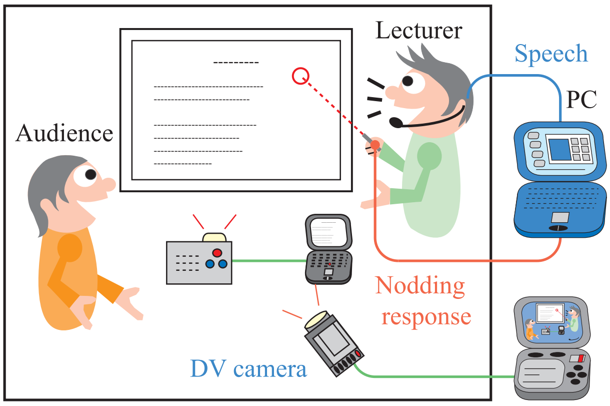

Figure 6: Experimental setup of InterPointer.

The experiment was examined in the following steps :

Steps 1 ; Subjects tried InterPointer, so that they can get used to the system.

Steps 2 ; They were instructed to divide into a lecturer and an audience to perform paired comparison by one-minute use for each mode.

Steps 3 ; A lecturer and an audience swapped roles in the same way.

Figure 7 shows the experimental scene of InterPointer and Figure 8 shows the example of change of beam pattern (200 ms). The contents of slides were the formulas of area, such as a triangle and a trapezoid, as subjects can explain easily and straightforwardly. The experiment was examined by 10 pairs of 20 Japanese students. The outline of a system was not explained to subjects beforehand.

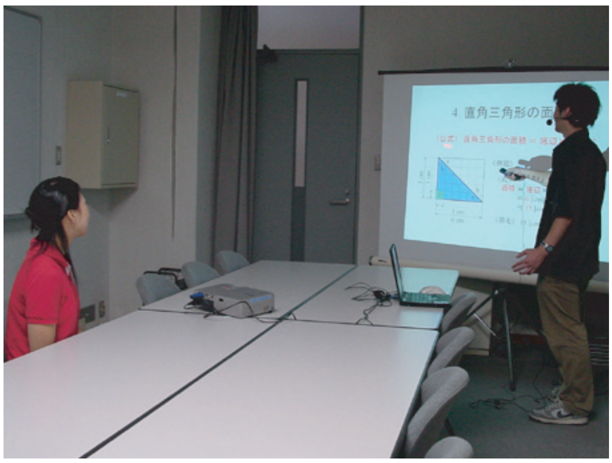

Figure 7: Experimental scene of InterPointer.

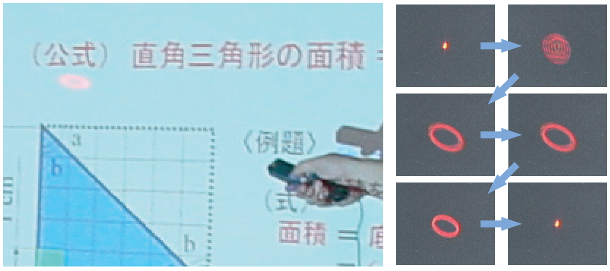

Figure 8: Example of change of beam pattern (200 ms).

3.2 Experimental result

Table 2 shows the result of paired comparison for the lecturer and audience. The number in the table shows that of subjects who preferred the line mode to the row mode. Namely, this number is the number of the subjects who answered that it was more desirable in the mode of each line. The Bradley-Terry model was assumed to evaluate the preference of mode by InterPointer quantitatively, defined as follows [4].

$$P_{ij} = \frac{\pi_i}{\pi_i + \pi_j} \tag{3}$$

$$\sum_i \pi_i = const.(= 30) \tag{4}$$

π_i : intensity of i,
P_{ij} : probability of judgment that i is better than j

Here, π_i shows the intensity of preference of mode by InterPointer. The model enables to determine the preference based on the paired comparison. The Bradley-Terry model assumed by using the result of paired comparison is also shown in Table 2. To approve the matching of the model, the goodness-of-fit test and likelihood rate test were applied to this Bradley-Terry model. As a result, the model was not rejected and π was validated.

By the result of paired comparison, the proposed model was highest. This indicates that the change from Point to Oval by InterPointer is preferred to Point by both lecturer and audiences. Much affirmative opinions for InterPointer were also seen by the comments after the experiment.

Table 2: Result of paired comparison of InterPointer.

IP	(a)	(b)	(c)	(d)	Σ	π
(a)		23	21	23	67	8.54
(b)	17		12	8	37	3.87
(c)	19	28		24	71	9.48
(d)	17	32	16		65	8.11

(a) · (Point) (c) · →○ (Model)
(b) ○ (Oval) (d) · →○ (Exponential)

4 Conclusion

In this paper, a new speech-driven embodied laser pointer was proposed, and the prototype of the system InterPointer was developed for supporting embodied interaction and communication for both a lecturer and audiences. The effectiveness of InterPointer was demonstrated by sensory evaluation.

Acknowledgements

This work under our project E-COSMIC has been supported by CREST (Core Research for Evolutional Science and Technology) of JST (Japan Science and Technology Agency).

References

[1] N. Kobayashi, T. Ishii, T. Watanabe, "Quantitative Evaluation of Infant Behavior and Mother-Infant Interaction", *Early Development and Parenting*, pp. 23-31, 1992.

[2] T. Watanabe, "E-COSMIC: Embodied Communication System for Mind Connection", *Proceedings of the 13th IEEE International Workshop on Robot and Human Interactive Communication (RO-MAN 2004)*, pp. 1-6, 2004.

[3] T. Watanabe, M. Okubo, M. Nakashige, R. Danbara, "InterActor: Speech-Driven Embodied Interactive Actor", *International Journal of Human-Computer Interaction*, Vol. 17, No 1, pp. 43-60, 2004.

[4] R. A. Bradley and M. E. Terry, "Rank analysis of incomplete block designs", *Biometrika*, Vol. 39, pp. 324-345, 1952.

Development of Pointing Device to Use Vision for People with Disability

Masakazu Kubo*, Motohiro Tanaka*, Shunji Moromugi*, Youichi Shimomoto*,
Yasuhiko Ohgiya* and Takakazu Ishimatsu*

* Graduate School of Science and Technology, Nagasaki University, Nagasaki, Japan
Tel :+ 81-95-819-2508; Fax :+81-95-819-2508; E-mail: ishi@net.nagasaki-u.ac.jp

Abstract

Persons suffering from ALS disease present symptoms of muscular deteriorations. Muscular deteriorations often impede communicating actions like uttering voice or pushing buttons. In order to support their communication, a device to use vision is proposed. This device can be settled apart from the bed of the patient. This means the device do not interfere with the nursing care. This device is developed for ALS patients who have ability to move his head intentionally. The head movement is measured by an original compact vision system. Corresponding to the head movement, the computer mouse on the computer display is moved. This device enables fast input operations. This device is applied to ALS patients. Applicability of this input device is confirmed.

1. Introduction

Everybody should be able to enjoy his independent life. However, patients suffering from ALS (Amyotrophic Lateral Sclerosis) are difficult to live independent lives. They need intensive cares by care-workers. As a typical symptom of ALS patients their muscular functions deteriorate rapidly. In two or three years after the onset of the disease, patients are obliged to use artificial respirators since even the breathing action becomes difficult. Once they start to use the artificial respirator, uttering voice becomes impossible. In such a physical situation, they are usually confined to bed and possible physical actions are limited to slight movements of head, fingers, lips or eyes. Therefore, their relationships with society are extremely limited. However, recent development of computer technology and network technology brought great benefits to those peoples.

Using the computer and network system, they can communicate and talk with others in far places even if they are confined to bed. Computer systems to support their communication are already commercialized. But difficulties remain at input devices for them. Considering the deteriorated muscular ability, some input devices for ALS patients were developed. Those input deices are categorized as a stand type and a wearable type [1]. The stand type devices include touch switches, laser sensors and vision sensors. These devices are usually attached to the bed or table and used to detect some body movements. The wearable type devices introduce sensors like acceleration, angle, strain and EMG (Electromyogram) sensors that are attached to the patient's body. These sensors measure physical movement or condition of the patient body and input signal is activated based on the data measured.

Input devices to use a vision system have distinguished advantages over the other devices that the devices can be applied to ALS patients in a variety of ways [2], [3]. The vision device can be settled apart from the bed. This means care workers can be free from annoying sensors, wires and mechanical parts around the bed. Furthermore, the device can be applied to detect various body movements like lips, fingers, eyebrow as well as eyeball. It is also important to note that the vision devices have a supreme feature to reject miss-operation by introducing tactful image processing. Vision techniques only to process images of eyeball were already reported since eyeball movement remains possible even if the physical situations of ALS patients become serious [2], [3], [4].

In this paper an input device to use vision for ALS patients are proposed. An image processing technique is introduced to extract intentional slight body movements.

This input device corresponds to a two-dimensional pointing device [5]. This input device requires the operator's remaining ability to move his or her head two-dimensionally. The input device measures the two-dimensional head movement of the operator. The operator is requested to wear an LED mark on his forehead. The raster coordinates of the LED mark are obtained by an image processing board. The board is compactly composed of one FPGA chip and one chip CPU.

This input device is incorporated into the computer system to support communication of the patient. In order to test the applicability, this communication system is applied to ALS patients. Test results revealed the feasibility of the system.

2. Configuration of Communication Device

Proposed communication systems are composed of a computer, a remote controller and an input device as shown Fig.1. In the computer communication software developed for the people with disability is installed. And a remote controller is composed of an infrared light remote controller. As an input device composed of a camera and an image processing board is employed. The input device is used to detect the body movement of the user. By processing the sequential image of the body, intentional movement of the body is extracted. Once the intentional movement is detected, the control signal is transferred to the personal computer.

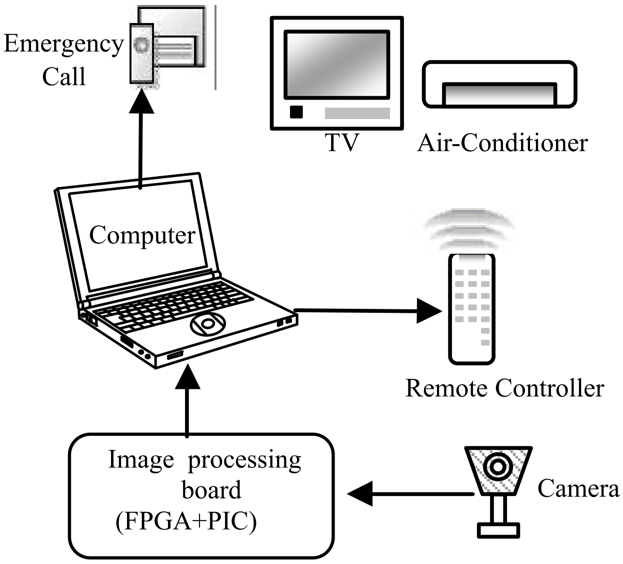

Fig. 1 Configuration of communication device

This system is applied able to detect variety of body movements like lips, eyes, and fingers. Considering the application to ALS patient with capability to move his head two-dimensionally, an efficient input device is recommended. In Fig.2, a proposed pointing device is shown where a LED light reflector is attached to the forehead of the operator. A compact image processing board detects the raster coordinates of the LED light in the image. The image processing board is composed of one FPGA (Altera EPM9320ALC84-10) and one CPU chips (PIC16F876: Microchip Co. Ltd.). The logic circuit implemented on one FPGA chip executes the real time image processing.

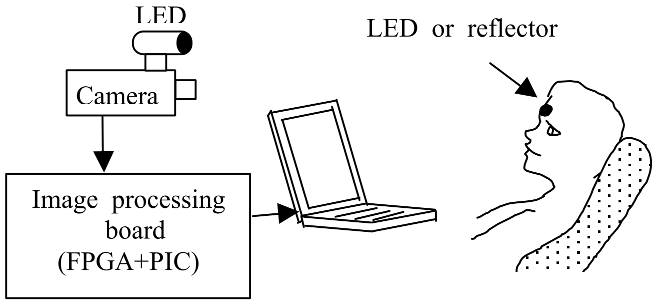

Fig.2 Pointing device to use vision

Immediately after the movement is detected, the communication software in the computer responds. The communication software has two main functions to write texts and to control various home electric appliances. Using these functions, the user can call family members at home, talk with them and enjoy TV programs he wants.

3. Detection of Head Movement

At every frame the image processing board detects raster coordinates of the brightest pixel in the image. Firstly every image is converted to binary one by considering the maximal brightness obtained in the preceding image. An example of resultant binary image is shown in Fig.3. The proposed image processing board detects the leftmost and the rightmost horizontal coordinates of the bright cluster as U_L and U_R. Similarly, the top and the bottom vertical coordinates V_T and V_B of the bright cluster are detected.

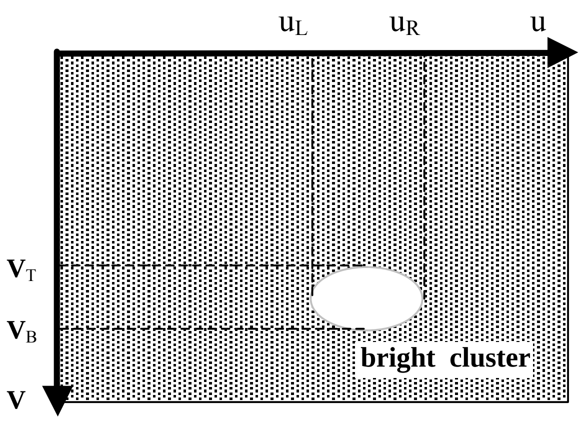

Fig.3 Image of bright cluster

Fig.4 shows the block diagram of the logic circuit to perform the real-time image processing. From the video signal, the Sync. Signal generator extracts horizontal synchronous signals H and vertical synchronous signals V.

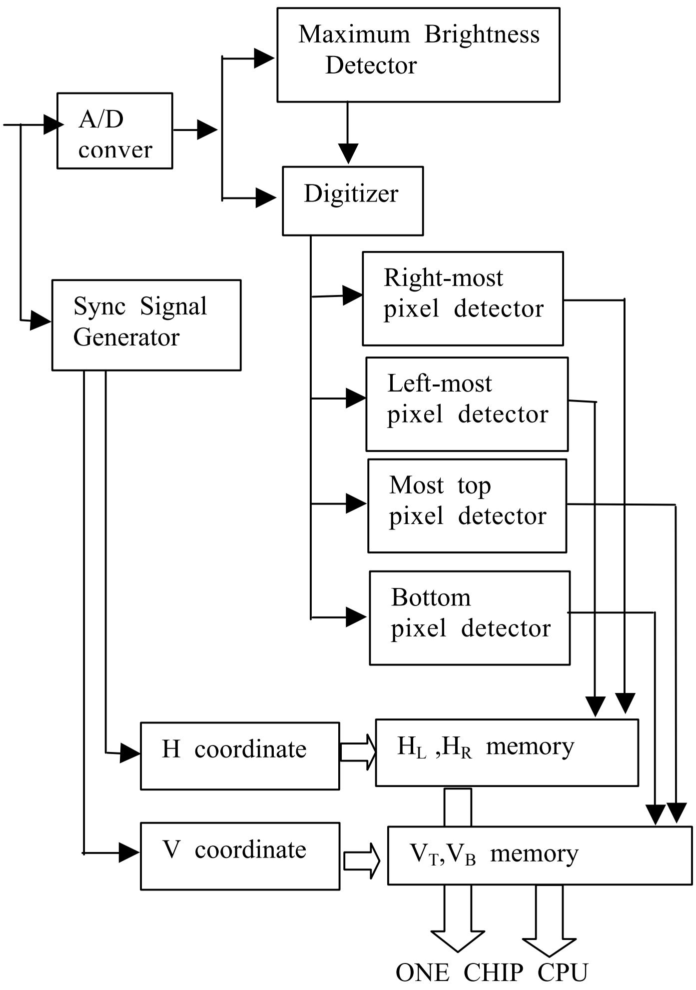

Fig.4 Block diagram of image processing

Using these H and V signals, horizontal coordinate (H coordinate) and vertical coordinate (V coordinate) of every pixel can be determined.

At the maximum brightness detector the video signal is converted to 8-bit digital data and the brightest pixel in the image is extracted. At Digitizer the video signal converted to binary one based on the threshold level. From the binary image, the value U_L, U_R, V_T and V_B in Fig.3 are obtained. An image of the target LED is shown in Fig.5.

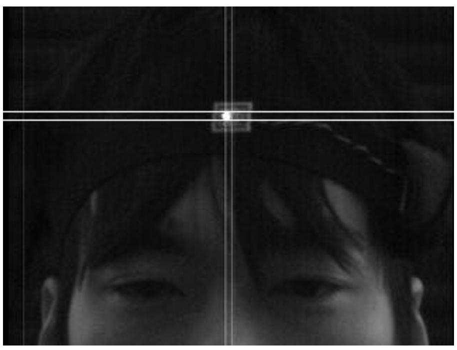

Fig.5 Image of target LED

The data are transferred to one chip CPU. The one-chip CPU checks the size of the rectangular. Once the size is allowable, the central coordinates of the bright cluster are transferred to the computer. The computer uses the raster coordinates of LED light as the positioning data of the computer mouse.

4. Evaluation of Pointing Accuracy and Field Test

Pointing accuracy of the input device explained in section 3 was evaluated by healthy examinees without any physical disability. The data obtained by the pointing device were used to locate the mouse pointer on the computer display in proportion to the head movement. A camera (CCD sensor with 570H×480V resolution) was settled 200cm apart from the examinee. The examinee was requested to move his head so that the mouse pointer traced the rectangular shape in the computer display. One example of the test result is shown in Fig.6. The examinee moved his head 4cm in the horizontal direction and 3 cm in the vertical direction. The positioning error in the computer display

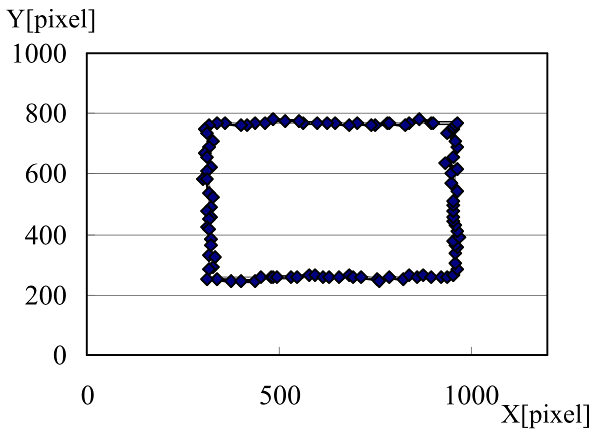

Fig.6 Tracing test along rectangular

was less than 10 pixels, which corresponds to about one percent in the horizontal and vertical direction on the display. Five examinees tried to trace the rectangular on the computer display. The positioning accuracy was less than 10 pixels. The required time was shown in Table 1.

Table 1 Time required to trace rectangular

User No.	1	2	3	4	5
Time Required	26 sec	36 sec	53 sec	38 sec	54 sec

The pointing device was applied to write a text. A computer display of the communication software is shown in Fig.7. In the lower half of this display many buttons were arranged. To each button one character or one function was allocated. Moving the computer mouse onto the target button and keeping it on the target button for a pre-specified interval ? T the desired character is selected.

By selecting the desired characters sequentially, desired text could be completed as shown in the upper half of the display.

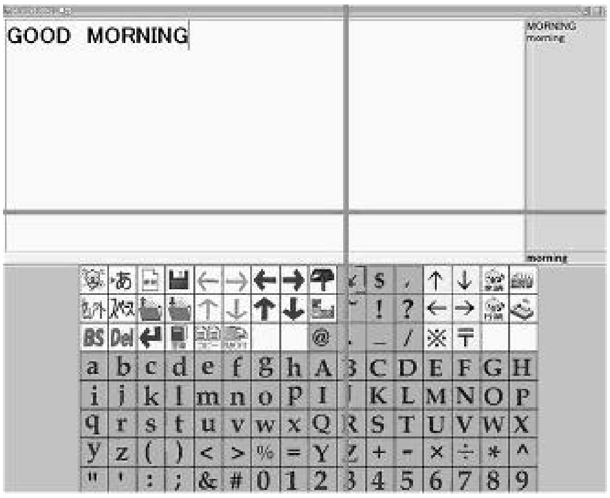

Fig.7 Computer display of communication system

Using this communication system, examinees wrote the text "GOOD MORNING" under two values of ? T. Table 2 shows time required to write the text. For ? T=0.5sec, all examinees finished to write the text "GOOD MORNING" in 30 seconds. This means one character takes around 2.5 second to select. For ? T=1.0sec, around 40 seconds are required. The speed was compared with that of conventional communication system to use a touch sensor. Conventional system always required more than three minutes.

Table 2 Time required to write "GOOD MORNING"

User No.	1	2	3	4	5
Trial 1 ΔT =0.5 s	26	28	22	29	26
Trial 2 ΔT =1.0 s	34	39	33	43	35

Fig.8 shows a prototype of the proposed image processor board, where one FPGA, one PIC (one chip CPU) and one A/D converter chips are mounted. This one PIC communicates with the computer via serial communication line.

This system was applied to an ALS patient who was difficult to move his hands. He succeeded to operate the communication system effectively using proposed input device as shown in Fig.9.

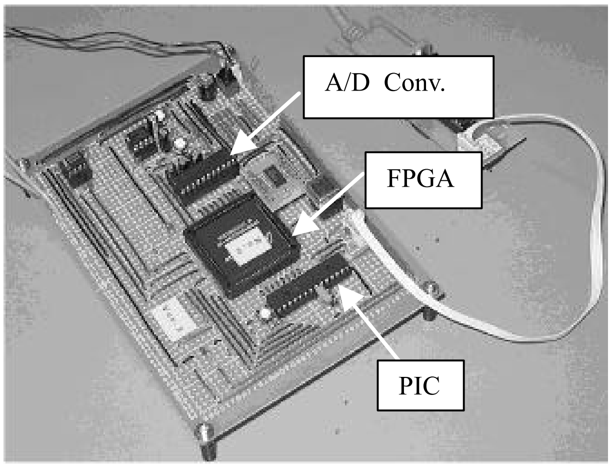

Fig.8 Image processing board

Fig.9 Operation by two-dimensional input device

5. Conclusions

A vision sensor is proposed as an effective input device of a communication system. Different from the conventional devices like a touch sensor and a push button, the proposed vision sensor could extract operator's intentional movement with enough accuracy rejecting disturbing body movements. A distinct feature of this technique is that vision sensor is used as a two-dimensional pointing device. This device enabled fast operations of the communication system. Communication systems to employ this vision device were applied to ALS patients. The patients successfully could communicate with their families and operate electric devices by using the communication device.

In this paper we focused on the simple and robust algorithm to use vision sensor for the ALS patients. Considering various symptoms of the ALS patients, also other algorithms need to be developed based on the remaining ability of the ALS patient.

References

[1] Y.Fukuda, M.Tanaka, S. Moromugi and T. Ishimatsu, A Communication device for disabled slight movement capabilities, International Journal of HWRS, vol.4, No.4, December, pp.7-12, 2003.

[2] T. Ochiai, T. Ishimatsu, Computer Input device for handicapped using vision sensor, in Proc.3rd Int. symposium on artificial life and robotics Vol.2, pp.634-637, 1997.

[3] O.Takami, T.Ishimatsu, and T.Shimomachi, Development of the environmental control system by using eyeball movements, Proceeding of the Asian Control Conference, pp.715-718, July 27-30, 1994.

[4] O.Takami, K.Morimoto, T.Ochiai, and T. Ishimatsu, Computer Interface to use head and eyeball movement for handicapped people, 1995 IEEE International Conference of System, Man and Cybernetics, Vancouver, Canada, October 22-25, 1995.

[5] H.Kawamura, N.Dohi, T.Oshima, “Experimental Production of Light Mouse using PSD sensor”, Proc. of 5th Rehabilitation Engineering, Tokyo, Japan, 21-24 August, 1990, pp.233-236

The Tenth International Symposium on Artificial Life and Robotics 2005(AROB 10th '05),
B-con Plaza, Beppu, Oita, Japan, February 4-6, 2005

Monitoring System of Body Movements for Bedridden Elderly

Rue Shao Dong*, Motohiro Tanaka*, Miki Ushijima*, Takakazu Ishimatsu*

*Department of Mechanical System Engineering, Nagasaki University, Nagasaki, Japan

Tel: +81-95-819-2508; Fax: +81-95-819-2508; E-mail ishi@net.nagasaki-u.ac.jp

Abstract: In this paper we propose a system to detect physical behavior of the elderly under bedridden status. This system is used to prevent those elderly from falling down and being wounded. Basic idea of our approach is to measure the body movements of the elderly using the acceleration sensor. Based on the data measured, dangerous actions of the elderly are extracted and warning signals to the caseworkers are generated via wireless signals. A feature of the system is that the senor part is compactly assembled as a wearable unit. Another feature of the system is that the system adopts a simplified wireless network system. Due to the network capability the system can monitor physical movements of multi-patients. Applicability of the system is now being examined at hospitals.

Keywords: dementia patient, monitoring system, vital sign, warning signal, wireless signal

1. INTRODUCTION

Increase of the aged people is becoming a serious social problem. In the care house for the elderly only a few care workers are working for many aged people. Typically in the nighttime care workers are too busy to deal with various kinds of tasks, since only two or three care workers are staying at night. Many of the care workers are doing their best but are too tired. One serious problem at care-houses is the injury of the aged caused by slipping and falling down on the floor. Once they broke their legs and feet, it is not easy for them to recover sooner. Typically in the case of dementia patient, they easily forget and neglect the request not to leave the bed alone by the caregiver. One simple answer to protect such cases is to fasten the patient onto the bed. But such kind of treatment means neglecting the human right of the patient. Touch sensors and pressure sensor is proposed to detect the escape or wake up motions of patient from the bed. But what required by the care workers is some technique to detect body movements of the patient and forecast occurrence of the risky actions of the patients. Of course, forecasting the risky actions with reliability is not easy matters. But smart care workers say every elderly represents individual physical behaviors. They also says an alert signal can be generated before the risky event occurs by preparing individual criterion for each elderly. Already some related researches are achieved, where techniques to measure vital sighs, like sleeping stages, heartbeat, respiration and snore [1], [2], [3], [4]. Image processing is also one technique to measure such sighs, but the technique is not preferred because of the violation of the privacy. Furthermore, the image processing costs a lot [5].

In this paper a monitoring system is proposed which measures body movements of the bedridden patient. The data measured is used to evaluate the current physical status of the patient and the possibility of risky actions. Considering practical application, the wearble sensor unit is compactly achieved employing a two-dimensional acceleration sensor, a one-chip computer and a wireless communication module. Due to the introduction of the simplified wireless network system, the system is applicable to the multi-user condition. The proposed system can recognize some kinds of physical movements like deep sleeping, a light sleeping, walking, standing up, slipping, falling down and jumping up. Furthermore, based on the criterion about the time sequences of these physical movement actions, the sensor sends an alert signal to care workers. The care workers considering the features of the physical behavior determine the criterion. The proposed system is now under examination at hospitals.

2. SYSTEM CINFIGURATION

A system configuration is shown in Fig.1 where patients are wearing sensor units on their chest. On the sensor unit, an acceleration sensor (ADXL202: Analog Device Co. Ltd.), a one-chip CPU (PIC16F84A) and a wireless communication module (iTRX315: itec Co.Ltd.) are implemented in a compact body as shown in Fig.2. The acceleration sensor detects two-dimensional acceleration. Of course, since the sensor detects the acceleration caused by the gravity, the sensor gives information about the posture of the sensor. Therefore, if a patient wears the sensor on his chest, the physical behavior or posture of the patient can be readily detected by the data obtained. A compact wireless communication module on every sensor unit enables to communicate with the master computer. Furthermore, by introducing an original communication protocol, every unit can communicate with each other. In each sensor unit, individual criterion is implemented considering the each patient's situation. Based on the each criterion, the one-chip computer recognized the risky condition of the patient. Once the one-chip computer recognizes the situation of the patient is dangerous, it sends the risky condition to the master computer. It should be noticed that the sensor unit could detect extraordinary body movements like gastric spasm or spasmodic asthma as well.

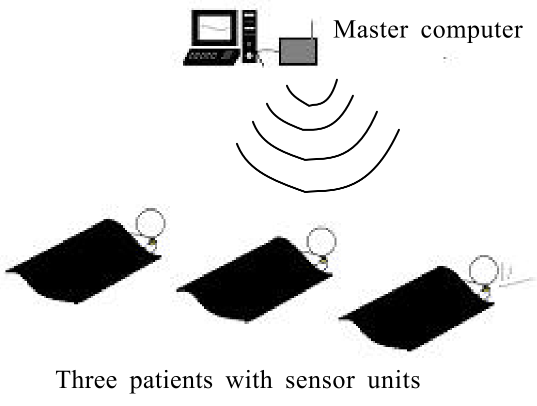

Fig.1 System configuration

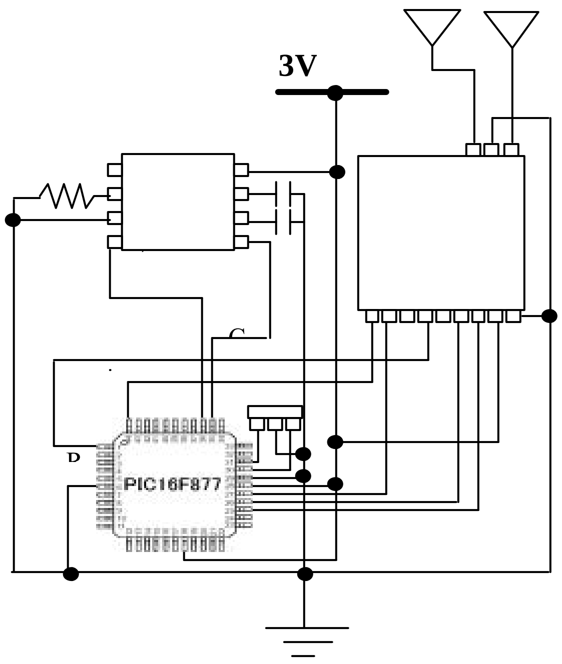

Fig.2 Electric circuit for sensor unit

2. NETWORK SYTEM

In the proposed system an original network protocol is introduced. The basic idea of the protocol is that every communication module communicates with each other synchronizing with the base synchronous signal emitted by the master computer. A feature of our protocol is that even if a sensor unit cannot detect the base synchronous signal emitted by the master computer, another sensor unit that can detect the base synchronous signal acts as an auxiliary master computer. This feature provides us a great benefit under the situation that only low power communication system is available.

Suppose the base synchronous signal can be detected in the range of sensor unit 1 to 5 as shown in Fig.3. And sensor unit 6 is out of the range. As everyone notice the master computer can recognize that sensor units 1 to 5 are in the accessible range and the sensor unit 6 is out of the range. In this situation, the master computer asks every sensor unit if some unit can access the sensor unit 6. After that, each sensor unit tries to communicate with sensor unit 6 sequentially. If one of the sensor units is able to communicate with the sensor unit 6, the sensor acts as an auxiliary master computer for the sensor unit 6. Thereafter, the sensor unit can communicate with the master computer via the auxiliary master computer. This means that even if the maximum accessible range of the communication module is less than 10 meters, by introducing relaying sensor units the accessible range can be expanded as far as we like. Therefore, our proposed system can be applicable to a hospital or nursing facilities even if only low power wireless communication is available. This feature is important since in most of medical facilities only low power wireless communication is allowed. Suppose this network system is realized in a nursing facility. Using this network features, we can detect the position of the patient in the facilities or detect the absence of the patient.

In the sensor unit consumption of the electricity needs to be suppressed since the compact battery is indispensable for comfortable wearable sensor unit. Therefore, the protocol of the communication was determined.

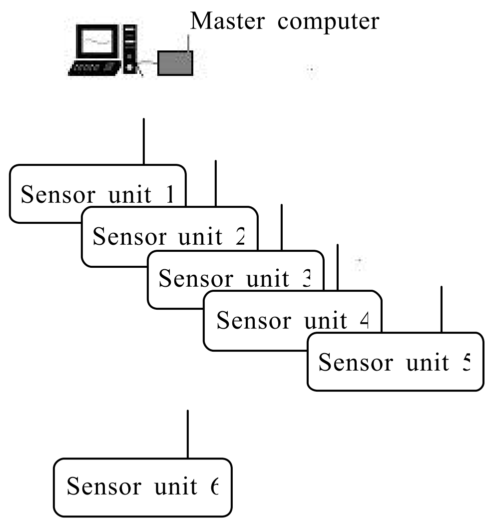

Fig.3 Sensor units and master computer

3. EXPERIMENT

Every components of the sensor unit could be realized in a compact body as shown in Fig.4. The reachable range of each wireless transmitter was around 10m.

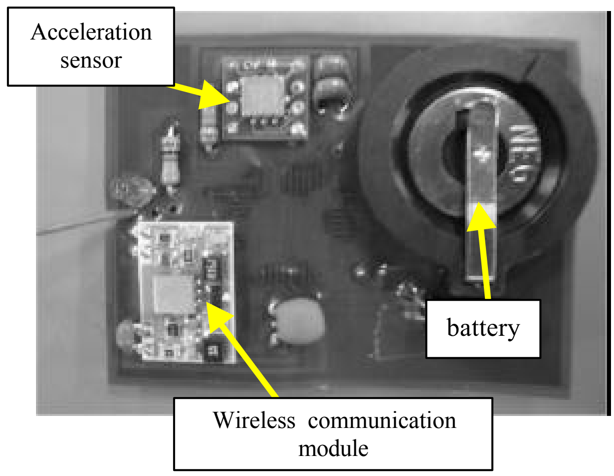

Fig.4 Arrangement of components in the sensor unit

This sensor is attached to an examinee to check the feasibility to recognize current status of body movements. An examinee wearing the sensor on his chest is requested to (1) lie on the bed, (2) roll over, (3) wake up and (4) walk around the bed. During the above body movements, the sensor measured the acceleration. Fig.5 shows the acceleration data toward the foot direction of the examinee. Fig.6 shows the acceleration data toward the leftward of the examinee.

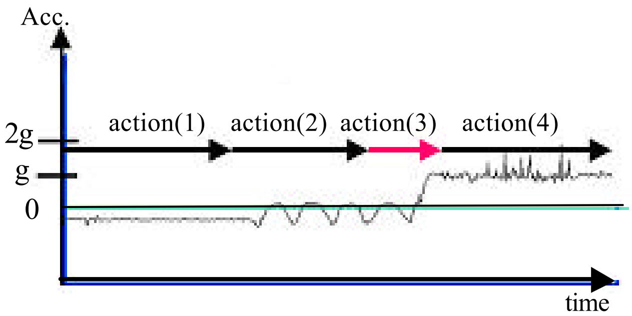

Fig.5 Sensor signal toward foot direction

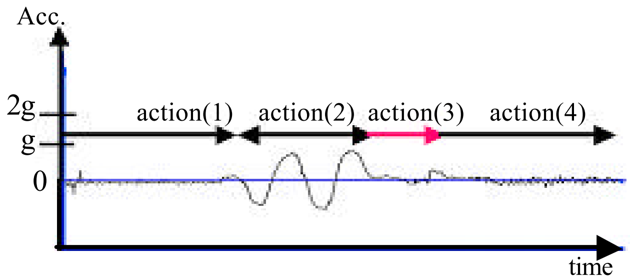

Fig.6 Sensor signal toward leftward

Corresponding actions are shown in Fig.7. During t
he period of the action (1), where the examinee
lies on the bed, the acceleration toward foot directi
on was negative. This means the sensor unit on the
chest inclined slightly upward. During the period o
f the action (2), the examinee repeated roll over tw
ice from rightward and leftward. During the period
of the action (3), because of wake up action the ac
celeration toward the foot direction increased till
around 1.0g. During the period of walking around t
he acceleration toward the foot direction fluctuated
around 1.0g.

4. ALGORITHM TO RECOGNIZE BODY STATUS

Denote the acceleration toward the foot direction as A_F, and the acceleration toward the leftward as A_L. From the data obtained in section 3, a simple criterion to recognize current body status becomes as follows.

(Status 1: Lying on the bed) when A_F is around zero.

(Status2: Rolling over) when A_F is around zero and A_L is fluctuating.

(Status3: Waking up) when A_F is increasing up to 1.0g.

(Status4: Walking) when A_F is fluctuating around 1.0g.

In order to prevent the bedridden elderly from falling down and being wounded, another criterion to determine degrees of risk can be proposed as follows.

(3rd degree: risky level) when impulsive behaviors of the acceleration is detected.

(2nd degree: nearly risky) when frequent fluctuations of the acceleration are detected.

(1st degree: slightly risky:) when different pattern of the time sequences of the acceleration fluctuations are detected.

Fig.7 Sequences of actions

The above criterion comes from one idea that before the risky action occurs some specified body movements' occur.

The criterion should be determined based on the behavior of the elderly.

5. DISCUSSIONS

We built a prototype composed of one master computer and three sensor units. At every one second the master computer checked accessibility of three sensor units. And at every one second, every sensor unit responded that the sensor unit was accessible with the current body status. In case one sensor unit was not accessible by the master computer, the accessible sensor unit acted as an auxiliary master computer. In case that one sensor is not accessible with any other sensor unit and the master computer, the master computer could recognize the situation.

4. CONCLUSIONS

We developed a monitoring system of physical behavior of the elderly under bedridden condition. The sensor can be effectively applicable to suppress the number of the accidents caused by the slipping and falling down on the floor. The system can be readily connected to the Internet system. Due to the developing ability of Internet, our system can be expanded to more advanced system like remote care of the patients in the far place. Furthermore, patients could be cared safely in the care house even if the caseworkers are busy.

We are now testing a prototype system at hospitals in Nagasaki city. The results of the test will be demonstrated sooner.

REFERENCES

[1] T. Togawa, Home health monitoring, J.Med. Dent. Sci, 45, 151-160, 1998.

[2] B.W.Carlson,et al., Evaluation of a Non-Invasive Respiratory Monitoring system for sleeping subject, Physiol.Meas., 20, 53-63, 1999.

[3] H.Andoh, et.al., Network Health Monitoring System in the Sleep, Proc. SICE Annual Conf.in Sapporo, 1421-1424,2004.

[4] K.WEatanabe,et.al., Estimation of Sleep Stage Based on Heart Rate Fluctuation and Body Movement, Proc. SICE Annual Conf.in Sapporo, 2153-2156,2004.

[5] R. Satoh, et al., Non-contact sensor to detect movement of dementia patient, ICCAS, 2001.

Development of a training machine for elderly people with muscle activity sensor

Sung Jae Yoon*, Seok-Hwan Kim*, Motohiro Tanaka*, Shunji Moromugi*,
Yasuhiko Ohgiya*, Nobuou Matsuzaka** and Takakazu Ishimatsu*

*Department of Mechanical Systems Engineering, Nagasaki University, Nagasaki, Japan
(Tel : +81-95-819-2508; E-mail: ishi@net.nagasaki-u.ac.jp)
**Department of Physical therapy, Nagasaki University, Nagasaki, Japan Engineering, Japan

Abstract

An advanced training machine that can adjust load according to muscle activity is proposed for elderly people. The training machine allows users to have a safe and effective training through exercise close to ordinal motion appears in daily life such as stretching or stooping motion. The activation level of user's muscle is real timely monitored by a muscle activity sensor during the exercise and the training load is adjusted based on the data measured. The training load is exerted and continuously controlled by actuation of an electronic motor.

Keywords: **M**achine training, Elderly people, Preventive approach, Load control, Muscle activity sensor

1. INTRODUCTION

The welfare issues accompanying by the aging of society are highly concerned in most of the advanced countries. It is strongly hoped that the government provides adequate care and accommodation to people when they become old. However, it is extremely difficult to support all the people perfectly because each aged person needs different care. In addition to the fact, it costs huge and needs many hands to achieve it. Under this situation in Japan, that is one of the most aged society, the government started to focus on the approach to reduce the number of aged people who need nursing care more than to offer perfect caring system for them. The government promotes aged people to maintain enough strength to keep their independent life and allocate budgets for activities to promote the preventive approach against becoming bedridden status. The importance of the preventive approach is currently being recognized among other aging countries as well.

As one of the effective preventive approaches the physical training using machines is recommended. It is reported that the constant physical training is highly effective for aged people to maintain their strength and quality of life. Some care center introduced machine training in their program. However, there are several problems. One is that those machines are designed for sports training not for training of elderly people therefore users cannot use the machines comfortably in some cases. The other is that the exercise required in the machine training is too hard for those aged people. That could be a reason to keep aged people away from the machine training. The third is that too much machine training might cause damage in user's body, therefore it is hard to ensure the safety in the training because aged the people's body is somewhat weakened. Thus the training machine that is designed for elderly people is needed. It should be enough safe and comfortable to use for aged people and also have high adaptability for wide range of the size and ability of aged people.

In this paper we propose a training machine for the elderly people. The machine is developed by introducing power assisting technology.

2. FEATURES OF THE TRAINING MACHINE PROPOSED

An advanced training machine is proposed for keeping elderly people healthy and energetic so that they can keep living an independent life. The training machine let user to work on an exercise to maintain/recover physical abilities to support their body against the gravity. We focus on the leg strength because the ability to support their body or to stand up by themselves is very important both for aged people to keep their quality of life high and for care worker's to care their patients with less energy. This training machine has three major futures as follows.

1) Leg pressing exercise

Usually sports training machines are designed to develop specific muscles through a simple exercise such as knee flexion, elbow extension and twist of main body. It is effective for sports players to shape their body as they desire. However, for elderly people, those machines are not always comfortable because the purpose of the training is different from that of athletes. It is not for strengthening their muscles to compete against other players but maintaining or recovering their physical function to do everyday movements such as stretching or stooping of leg. The training machine proposed in this study is specially designed for aged people to train stretching and stooping ability. By using this training machine users can enforce their strength of both legs through leg pressing exercise. In addition to the physical training effect, it also works for recovering sense of body motion or strong desire to support their own body by themselves.

2) Adjust load with electronic actuator

Training load is generated by weights in the case of most of conventional training machine. Users select preferable load level before the exercise and train under the constant load through the exercise. The proposed training machine uses an electronic actuator. Therefore the training load can be continuously adjusted during the exercise.

3) Feed back of muscle activity on load control

In the elderly training safety issue needs to be considered carefully more than the case of sports training. Different from the sound body of young athletes elderly people's body is generally remarkably weakened. The proposed system monitors the activation level of user's muscles and output force of the leg. It is possible to select optimum load simultaneously and achieve effective and safe training for elderly people.

3. MECHANICAL SYSTEM CONFIGURATION

Figure 1 shows the proposed system. The system is composed of a moving seat, an electronic actuator, step force sensor, muscle stiffness sensor to detect user's muscle activation level, and a PC & FPGA based controller.

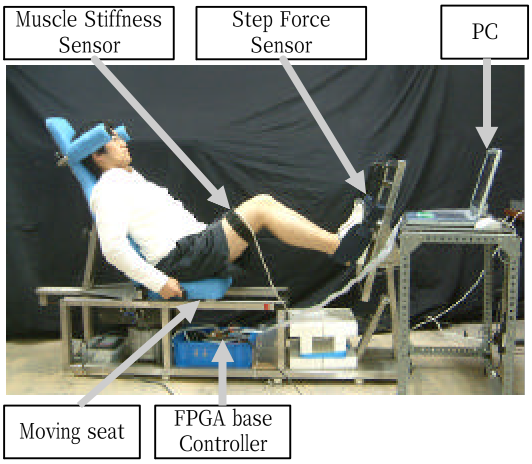

Figure 1 Overview of the system

3.1 Moving Seat

While the target of the custom sports training machine is to support user to strengthen his muscle, the target of the proposed training machine system is to support user to maintain his physical ability. In this point, the moving seat is designed to provide user to stretch and to stoop with easy due to the electronic actuator. Basically user's weight is supported by moving seat so that user can exercise without exerting all his weight to leg. So, by just setting the reference load according to one's physical ability, user can enjoy exercise with the proposed system.

Figure 2 shows two status of the system. During the stretching motion, user has to stretch his leg against the pre-defined load generated by the actuator. And during the stooping motion, user does not have to strengthen his leg, just enjoys stooping motion against a light pre-defined load actuated by the motor.

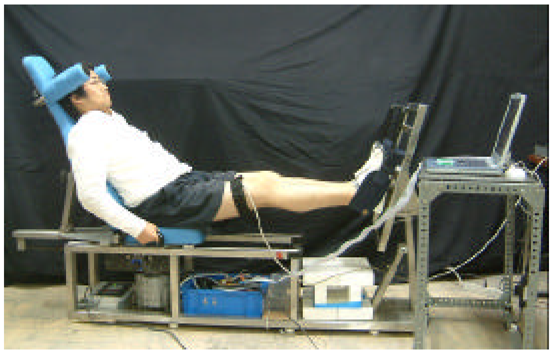

(a) Stretch

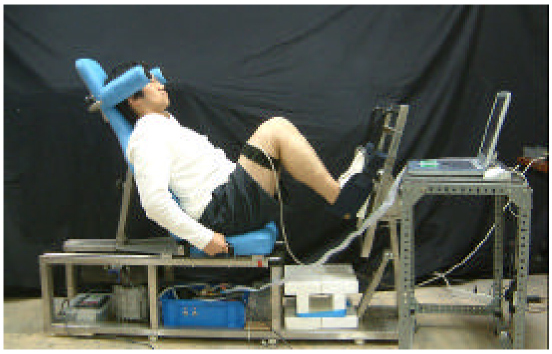

(b) Stoop

Figure 2 Two states of leg pressing exercise

Table 1 Major specification of motor

Model	Honda DDW 2020 L size
Voltage	24 V
No load Maximum rpm	65 rpm
Rated rpm	40 rpm
Rated torque	52 Nm

3.2 Human Machine Interface

Figure 3 Muscle Stiffness Sensor

To detect user intentions of stretching, stooping and controlling the speed, the proposed system adapts two kinds of sensors, one is a stepping force sensor and the other is a muscle stiffness sensor. The step force sensor is used to detect the force between stepping force to the foot plate and the load that is generated by an electronic actuator. With this sensor, the proposed system controls the load on the foot plate in real time base. Figure 3 shows the muscle stiffness sensor. The muscle stiffness sensor is attached to thigh and detects muscle activity as stiffness parameter that shows high similarity with EMG sensor. It is developed as man-machine interface for the power-assisting system. It was confirmed that there was high correlation between the data obtained from this muscle stiffness sensor and the activity level of the muscle through author's studies. Figure 4 shows change of stiffness parameter according to muscle activity change. The detail of this muscle stiffness sensor is described in [1]-[3]. One advantage of this sensor is that it is easy to put on/off from the body. The other advantage is its high robustness on measurement against the disturbing contacting force from outside. By using this sensor user can work on the training comfortably and safely with this training machine.

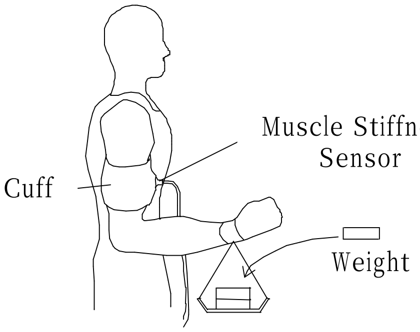

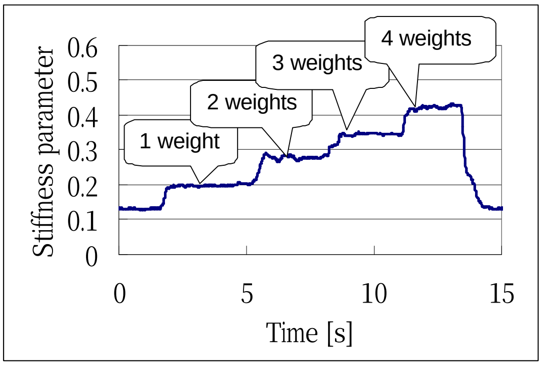

Figure 4. Stiffness parameter versus Muscle activation

3.5 PC & FPGA based Controller

As the controller, PC and FPGA (Flexibly Programmable Gate Allay) based control circuit are adapted. PC interfaces with the user to set up the target load and notices the present state to user. FPGA based control circuit is used to archive position data, muscle stiffness parameter, and stepping force signal through A/D converter, and send control command to the actuator through D/A converter. Figure 5 shows the configuration of the control system.

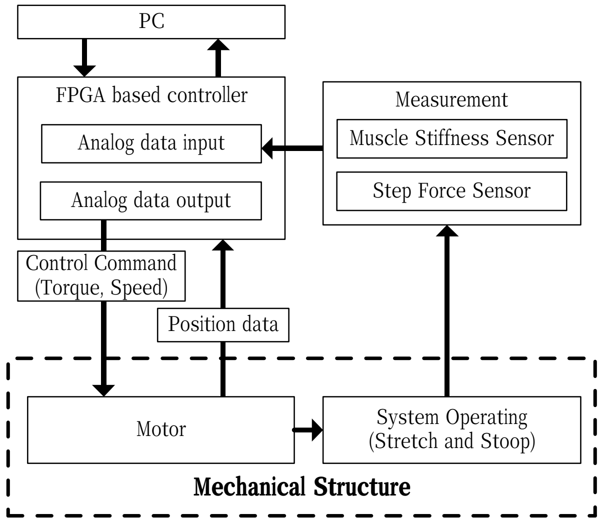

Figure 5 Configuration of a control system

Figure 6 shows the computer screen that is used to set up the reference force and moving distance based on each user, and displays present state during the training. With this program, each user's training data can be classified and analyzed for the better management.

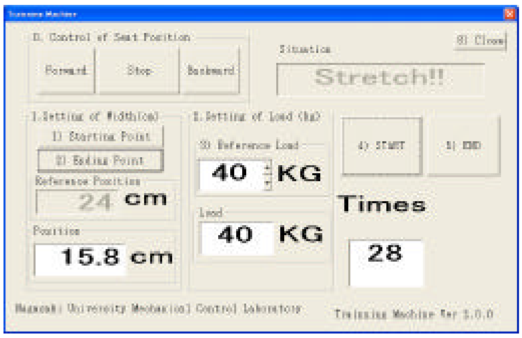

Figure 6 Interface display

4. EXPERIMENT

Experiment is conducted to verify the effectiveness of the proposed training machine system. In this experiment, muscle stiffness sensor is used to detect muscle activity and to trigger stretching or stooping motion. During the training, even if the stepping force is changed, the load to leg is controlled to maintain the reference value. Four kinds of load are tested to evaluate the controllability of the proposed system and its HMI.

Because the proposed training machine adapted the electronic actuator, it can impose load to both stretching and stooping motion. But in this experiment, the load is imposed to only stretching motion, and the actuator executes stooping motion automatically, so that user can enjoy the leg pressing exercise.

Through the experiment, it can be verified whether the system can control the load to leg, the stepping force, in real-time base. Muscle stiffness sensor can be used as human-machine interface that detects muscle activity.

4.1 Control algorithm

Simple control algorithm is adapted for the proposed training machine system as followed:

In real-time base, the error between the stepping force and the reference force is calculated by equation (1).

$$\Delta F = F_{STEP} - F_{REF} \qquad (1)$$

where F_{STEP} is the stepping force measured by step force sensor, and F_{REF} is the reference force.

And, based on the error (ΔF), the control force F_M is calculated by Equation (2).

$$\Delta F > 0, \quad F_{M1} = F_{M0} - C \qquad (2\text{-}1)$$

$$\Delta F < 0, \quad F_{M1} = F_{M0} + C \qquad (2\text{-}2)$$

$$\Delta F = 0, \quad F_{M1} = F_{M0} \qquad (2\text{-}3)$$

where F_{M0}, F_{M1} are the previous and present control forces to the foot plate, and C is the control offset. Based on the error (ΔF), C is also chosen by equation (3).

If $|\Delta F| \geq 5, \quad C = 5 \qquad (3\text{-}1)$

If $|\Delta F| < 5, \quad C = 1 \qquad (3\text{-}2)$

4.2 Result

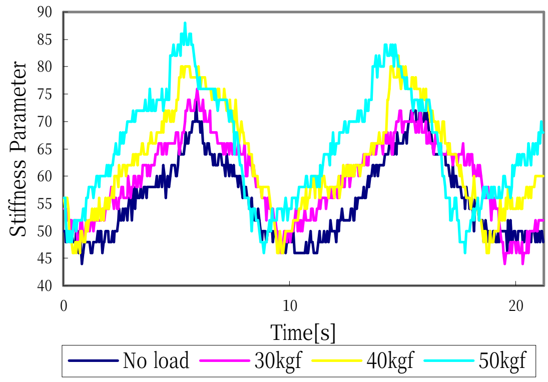

Figure 7. Stiffness change during leg pressing motion under four kinds of load [0, 30kgf, 40kgf, 50kgf]

When the posture of leg changes, correlated muscle makes change in their activity. Figure 7 shows that even there is no load on the leg, stiffness parameter changes during the leg pressing motion (stretching and stooping). And it also shows that stiffness parameter increases according to the increase of the load. It means that muscle stiffness sensor can be used as HMI for the power-assisting devices.

In Figure 8, each (a), (b), and(c) shows graphs of stiffness parameter, stepping force, position data, and reference value at each load 30kgf, 40kgf, and 50kgf. In each case, it is demonstrated that the system succeeds in controlling the stepping force to the reference value.

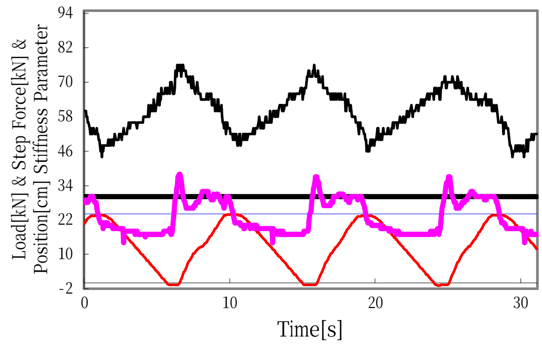

(a) 30kgf

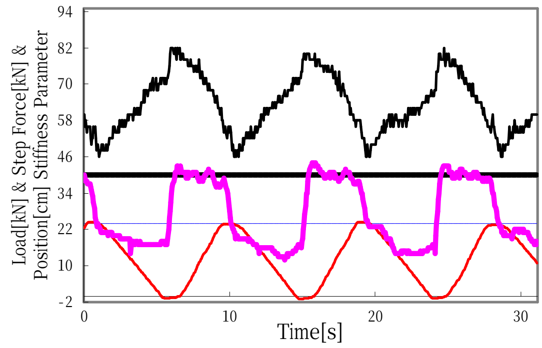

(b) 40kgf

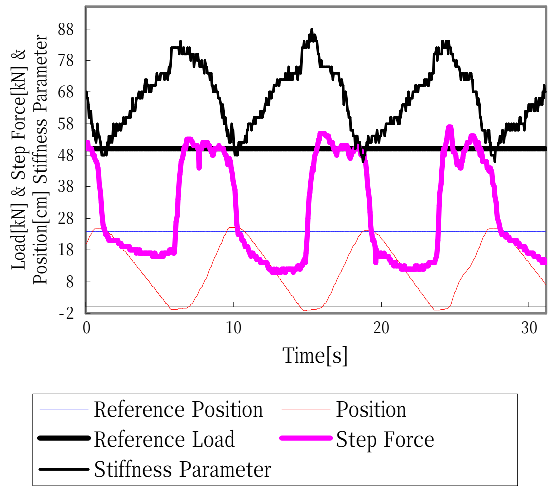

(c) 50kgf

Figure 8. Experiment data of leg pressing motion

5. CONCLUSION

A new type of training machine is proposed that can help elderly people maintaining their health. A feature of the machine is that a muscle stiffness sensor is incorporated to monitor the muscle status and control the reference load of the training. Through the experiment using a prototype, it is demonstrated that the training load of this machine can be controlled based on both the stepping force and the muscle activity. It is expected that this training machine provides effective and safe training opportunities for elderly people and be a great help for preventive approach against serious situation of aging society by reducing people who needs daily care.

REFERENCES

[1] S. Moromugi, K. Izumi, T. Yoshimochi, T. Ishimatsu, T. Tanaka and M.Q. Feng, "Device for Assisting Grasping Function," Proc. 17th Korea Automatic Control Conference, International Conference on Control, Automation and Systems, Muju, Korea, pp.1250-1254, Oct., 2002.

[2] S. Moromugi, Y. Koujina, S. Ariki, A. Okamoto, T. Tanaka, M. Q. Feng and T. Ishimatsu, "Muscle Stiffness Sensor to control assisting device for disabled," Proc. 8th International Symposium on Artificial Life and Robotics, Oita, Japan, pp.459-462, Jan., 2003.

[3] S. Moromugi, A. Okamoto, S. H. Kim, H. Tanaka, T. Ishi matsu and Y. Koujina, "Device for Assisting Grasping Fu nction(2nd Report: Maneuverability Evaluation)," Proc. 18th Korea Automatic Control Conference, International Conference on Control, Automation and Systems, Gyeon gju, Korea, pp.2665-2669, Oct., 2003.

Learning Algorithms and Uncertain Variables in Knowledge-Based Pattern Recognition*

Z.Bubnicki
Institute of Control and Systems Engineering, Wroclaw University of Technology
Wyb. Wyspianskiego 27, 50-370 Wroclaw, POLAND
e-mail: zdzislaw.bubnicki@pwr.wroc.pl

Abstract

The paper is concerned with a class of intelligent recognition systems described by a relational knowledge representation with unknown parameters. The main idea consists in the combination of two approaches: application of uncertain variables and a learning process with *step by step* knowledge updating. The recursive recognition algorithm with a modification of a current expert's knowledge at each step is presented. An example illustrates the presented approach.

Keywords: uncertain variables, uncertain systems, learning systems, knowledge-based systems, recognition, intelligent systems

1 Introduction

The paper is concerned with a class of intelligent recognition systems described by a relational knowledge representation with unknown parameters. For decision making in such systems two different approaches have been proposed and developed [1,2]:

1. The application of uncertain variables described by certainty distributions given by an expert.
2. The application of a learning process consisting in *step by step* knowledge validation and updating.

The purpose of this paper is to present a new idea based on the combination of these two approaches. At each step of the learning process an expert's knowledge is modified according to the current result of the learning. Such an idea has been applied to uncertain decision systems [3]. The application to pattern recognition requires to take into account a specification of this problem. The uncertain variable is described by a certainty distribution given by an expert and characterizing his/her opinion on approximate values of the variable. In the description of the uncertain variable $\bar{x}$ we introduce a certainty distribution $h(x) = v(\bar{x} \cong x)$ where $\bar{x} \cong x$ means that "$\bar{x}$ is approximately equal to *x*" and v is a certainty index given by an expert. We introduce also a soft property $\bar{x} \,\tilde{\in}\, D$ which means that "$\bar{x}$ approximately belongs to the set *D*" or "an approximate value of $\bar{x}$ belongs to *D*", with the certainty index

$$v(\bar{x} \,\tilde{\in}\, D) = \max_{x \in D} h(x). \tag{1}$$

The details concerning the uncertain variables and their applications may be found in [4,5] and in books [1,2].

2 Recognition problem based on uncertain variables

Let an object to be recognized or classified be characterized by a vector of features $u \in U$ which may be measured, and the index of a class j to which the objects belongs; $j \in \{1,2,...,M\} \stackrel{\Delta}{=} J$. The set of the objects may be described by a *relational knowledge representation* $R(u, j; x_j)$ where $x_j \in X_j$ is a vector of unknown parameters which is assumed to be a value of an uncertain variable $\bar{x}_j$ described by a certainty distribution $h_{xj}(x_j)$ given by an expert for all $j \in J$ .. The relation R is reduced to the sequence of sets

$$D_u(j; x_j) = \{u \in U : (u, j) \in R(u, j; x_j)\}, \; j \in \overline{1, M} . \tag{2}$$

Now we can formulate the recognition problem consisting in the determination of a class j maximizing the certainty index that j belongs to the set of all possible classes for the given u

$$D_j(x_1,..., x_M) = \{ j \in J : u \in D_u(j; x_j)\} .$$

Optimal recognition problem [2]: For the given $D_u(j; x_j)$, $h_{xj}(x_j)$ $(i \in \overline{1, M})$ and u (the result of measurement) one should find j^* maximizing

$$v[\, j \,\tilde{\in}\, D_j(\bar{x}_1,..., \bar{x}_M)] \stackrel{\Delta}{=} v(j).$$

Using (1) and (2) we obtain

* This work was supported by Polish State Committee for Scientific Research under Grant No. 4 T11C 001 22

$$v(j) = v[u \mathrel{\tilde{\in}} D_u(j;\bar{x}_j)] = v[\bar{x}_j \mathrel{\tilde{\in}} D_{xj}(j)] = \max_{x_j \in D_{xj}(j)} h_{xj}(x_j) \tag{3}$$

where $D_{xj}(j) = \{x_j \in X_j : u \in D_u(j; x_j)\}$. (4)

To find j^* it is necessary to determine $v(j)$ according to (3) and to maximize it with respect to j. Such a way may be applied under the assumption that $\bar{x}_j$ and $\bar{x}_i$ are independent uncertain variables for $i \neq j$.

3 Learning process

Assume now the parameter x_j has the value $x_j = c_j$ and c_j is unknown. Assume also that we can use the learning sequence $(u_1, j_1), (u_2, j_2), \ldots, (u_n, j_n)$ where j_i is the result of the correct classification given by a trainer. Let us denote by $\bar{u}_{ji}$ the subsequence of u_i for which $j_i = j$, by $\hat{u}_{ji}$ the subsequence for which $j_i \neq j$, and introduce the following sets in X_j:

$$\overline{D}_{xj}(n) = \{x_j \in X_j : \text{each } \bar{u}_{ji} \in D_u(j; x_j)\}, \tag{5}$$

$$\hat{D}_{xj}(n) = \{x_j \in X_j : \text{each } \hat{u}_{ji} \in U - D_u(j; x_j)\}. \tag{6}$$

The set

$$\overline{D}_{xj}(n) \cap \hat{D}_{xj}(n) \stackrel{\Delta}{=} \Delta_{xj}(n)$$

may be proposed as the estimation of c_j [2]. The determination of $\Delta_{xj}(n)$ may be presented in the form of the following *recursive algorithm* for the fixed j:

If $j_n = j$ $(u_n = \bar{u}_{jn})$

1. **Knowledge validation** for $u_n = \bar{u}_{jn}$. Prove if

$$\bigwedge_{x_j \in \overline{D}_{xj}(n-1)} [u_n \in D_u(j; x_j)].$$

If yes then $\overline{D}_{xj}(n) = \overline{D}_{xj}(n-1)$. If not then one should determine new $\overline{D}_{xj}(n)$, i.e. update the knowledge.

2. **Knowledge updating** for $u_n = \bar{u}_{jn}$

$$\overline{D}_{xj}(n) = \{x_j \in \overline{D}_{xj}(n-1) : u_n \in D_u(j; x_j)\}.$$

If $j_n \neq j$ $(u_n = \hat{u}_{jn})$

3. **Knowledge validation** for $u_n = \hat{u}_{jn}$. Prove if

$$\bigwedge_{x_j \in \hat{D}_{xj}(n-1)} [u_n \in U - D_u(j; x_j)].$$

If yes then $\hat{D}_{xj}(n) = \overline{D}_{xj}(n-1)$. If not then one should determine new $\hat{D}_{xj}(n)$, i.e. update the knowledge.

4. **Knowledge updating** for $u_n = \hat{u}_{jn}$

$$\hat{D}_{xj}(n) = \{x_j \in \hat{D}_{xj}(n-1) : u_n = U - D_u(j; x_j)\}.$$

Put $\overline{D}_{xj}(n) = \overline{D}_{xj}(n-1)$ and $\Delta_{xj}(n) = \overline{D}_{xj}(n) \cap \hat{D}_{xj}(n)$. Without an *a priori* knowledge on x_j (considered in the next section), the result of the estimation may be used in the following way: Values x_{jn} are chosen randomly from $\Delta_{xj}(n)$ and put into $D_u(j; x_j)$ in place of x_j. Then $D_u(j; x_{jn})$ are used to determine j_n^* in a way described in the previous section.

4 Learning system based on current expert's knowledge

At the *n*-th step, the result of the learning process in the form of a set $\Delta_{xj}(n)$ may be used to present an expert's knowledge in the form of a certainty distribution $h_{jn}(x_j)$ such that $h_{jn}(x_j) = 0$ for every $x_j \notin \Delta_{xj}(n)$. Thus, the expert formulates his / her current knowledge, using his / her experience and the current result of the learning process based on the knowledge of the external trainer. In particular, $h_{jn}(x_j) = h(x_j, b_{jn})$, i.e. the form of the certainty distribution is fixed, but the parameter b_{jn} (in general, b_{jn} is a vector of parameters) is currently adjusted. For example, if in one-dimensional case $\Delta_{xj}(n) = [x_{j\min,n}, x_{j\max,n}]$ and $h_{jn}(x_j)$ has a parabolic form presented in Fig. 1, then $b_{jn} = (d_{jn}, a_{jn})$ and

$$d_{jn} = \frac{x_{j\min,n} + x_{j\max,n}}{2}, \quad a_{jn} = \frac{x_{j\max,n} - x_{j\min,n}}{2}.$$

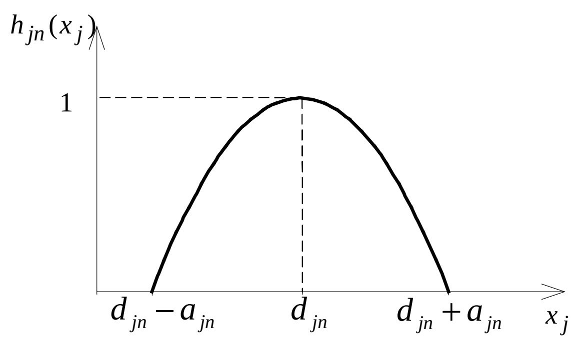

Fig. 1

For $h_{jn}(x_j)$ the next result of the recognition j_n^* may be determined in the way presented in Sec 2, i.e.

$$j_n^* = \arg\max_{j \in J} v_n(j) \tag{7}$$

where $v_n(j)$ is determined by (3) with $h_{jn}(x_j)$ instead of $h_{xj}(x_j)$ and u_n instead of *u*. In general, as a result of the maximization (7) one may obtain a set of the classes $D_{jn} \in J$. For $h_j(x_j, b_{jn})$ we obtain the fixed form of the function $v(j, b_{jn})$:

$$v_n(j) = \max_{x_j \in D_{xj}(x_j)} h_j(x_j, b_{jn}) \stackrel{\Delta}{=} v(j, b_{jn})$$

and consequently, the fixed form of the final result, i.e. $j_n^* = j(b_{jn})$ or the set of the classes $D_{j,n+1} = D_j(b_{jn})$. The same approach may be presented in the case of C-uncertain variables, with v_c instead of v (see [3]).

The block scheme of the learning recognition system under consideration is presented in Fig. 2 where G is a generator of random variables for the random choosing of j_n^* from *D*. The blocks in the figure illustrate parts of the computer recognition system or parts of the program which may be used for computer simulations.

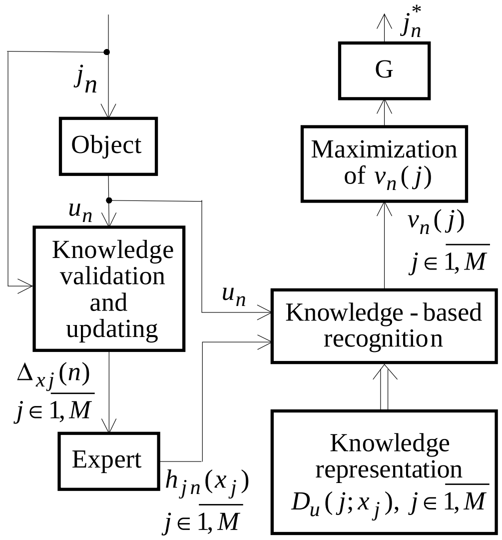

Fig. 2

5 Example

Let the sets $D_u(j; x_j)$ be described by the inequalities

$$x_j \le u^T u \le 2x_j, \quad j = 1,2,..., M.$$

Assume that the parameter x_j has the value $x_j = c_j > 0$ and c_j is unknown. It is easy to note that the sets $\overline{D}_{xj}(n)$ in (5) and $\hat{D}_{xj}(n)$ in (6) have now the forms of the following intervals:

$$\overline{D}_{xj}(n) = [\frac{1}{2}\max_i \overline{u}_{ji}^T \overline{u}_{ji}, \ \min_i \overline{u}_{ji}^T \overline{u}_{ji}],$$

$$\hat{D}_{xj}(n) = (a_{jn}, \frac{1}{2} b_{jn})$$

where a_{jn} is the maximum value $\hat{u}_{ji}^T \hat{u}_{ji}$ less than $\min_i \overline{u}_i^T u_i$, and b_{jn} is the minimum value $\hat{u}_{ji}^T \hat{u}_{ji}$ greater than $\max_i \overline{u}_i^T u_i$. The estimation of c_j has the form $\Delta_{xj}(n) = \overline{D}_{xj}(n) \cap \hat{D}_{xj}(n)$ and may be determined by a recursive algorithm presented in Sec. 3. Assume that the certainty distributions $h_{jn}(x_j)$ has a parabolic form presented in Fig. 1. In this case the sets (4) for the given $u^T u$ are described by the inequality

$$\frac{1}{2} u^T u \le x_j \le u^T u \ .$$

Applying (3), one obtains $v_n(j)$ as a function of d_{jn} illustrated in Fig. 3 for $a_{jn} = 1$:

$$v_n(j) = \begin{cases} 0 & \text{for } d_{jn} \le \frac{1}{2} u^T u - a_{jn} \\ -(\frac{1}{2} u^T u - d_{jn})^2 + a_{jn} & \text{for } \frac{1}{2} u^T u - a_{jn} \le d_{jn} \le \frac{1}{2} u^T u \\ 1 & \text{for } \frac{1}{2} u^T u \le d_{jn} \le u^T u \\ -(u^T u - d_{jn})^2 + a_{jn} & \text{for } u^T u \le d_{jn} \le u^T u + a_{jn} \\ 0 & \text{for } d_{jn} \ge u^T u + a_{jn} \ . \end{cases} \tag{8}$$

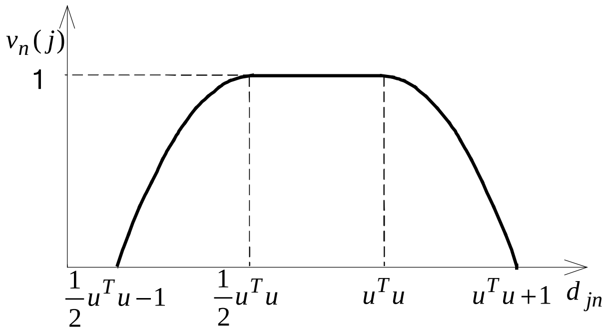

Fig 3.

For example, for $M = 3$, $u^T u = 5$, $d_{1n} = 2$, $d_{2n} = 5.2$, $d_{3n} = 6$ we obtain $v_n(1) = 0.75$, $v_n(2) = 0.96$ and $v_n(3) = 0$. Then $j_n^* = 2$, which means that for $u^T u = 5$ the certainty index that $j_n = 2$ belongs to the set of the possible classes has the maximum value equal to 0.96.

The recognition algorithm in the learning system is as follows:

1. Determine $x_{j,\min,n}$ and $x_{j,\max,n}$ using the estimation algorithm with the knowledge updating
2. Find d_{jn}, a_{jn} using the formulas in Sec.4
3. Determine $v_n(j)$ using (8) with $u = u_n$.
4. Find j_n^* maximizing $v_n(j)$.

6 Conclusions

For a class of the recognition systems under consideration, at each step of the learning process it is possible to use the current expert's knowledge based on uncertain variables. Numerical examples and simulations show that the using of the expert's knowledge during the learning process may improve the quality of the decisions. On the other hand, the algorithm is more complicated and requires using the correct classifications given by a trainer. The presented approach may be extended to other cases of uncertain recognition systems, for which the applications of uncertain variables and the learning algorithms were elaborated separately, especially for systems with three level uncertainty and for complex systems with a distributed knowledge [6,7,8,9].

References

[1] Bubnicki Z (2002), Uncertain logics, variables and systems. Springer-Verlag, Berlin, London, N. York

[2] Bubnicki Z (2004), Analysis and decision making in uncertain systems. Springer-Verlag, Berlin, London, N. York

[3] Bubnicki Z (2004), Application of uncertain variables to learning process in knowledge-based decision systems. Proceedings of the 9th International Symposium on Artificial Life and Robotics, Oita, Japan, Jan 28-30, 2004, Vol. 2, pp. 396-399

[4] Bubnicki Z (2001), Uncertain variables and their applications for a class of uncertain systems. International Journal of Systems Science 5:651-659

[5] Bubnicki Z (2001), Uncertain variables and their application to decision making. IEEE Trans. on SMC, Part A: Systems and Humans 6:587-596

[6] Bubnicki Z (2002), Application of uncertain variables to decision making in a class of distributed computer systems. Proceedings of 17th IFIP World Computer Congress, Montreal, Canada, Aug 25-30, 2002, Kluwer Academic Publishers, Norwell, MA, Vol. "Intelligent Information Processing", pp. 261-264

[7] Bubnicki Z (2004), Application of uncertain variables and learning algorithms in a class of distributed knowledge systems. Proceedings of 18th IFIP World Computer Congress, Toulouse, France, Aug 22-27, 2004, Vol. "The Symposium on Professional Practice in AI", pp. 111-120

[8] Bubnicki Z (2004), Uncertain variables and systems – new problems and results. Artificial Intelligence and Soft Computing – ICAISC 2004. Lecture Notes in Artificial Intelligence. Springer Verlag, Berlin, Vol. 3070, pp. 17-29

[9] Bubnicki Z (2005), Uncertain variables and their applications in knowledge-based decision systems. International Journal of Intelligent Systems (in press)

The Tenth International Symposium on Artificial Life and Robotics 2005(AROB 10th '05),
B-con Plaza, Beppu, Oita, Japan, February 4-6, 2005

Association Rule Mining Using Genetic Network Programming

Kaoru Shimada
Graduate School of Information,
Production and Systems,
Waseda University, Japan

Kotaro Hirasawa
Graduate School of Information
Production and Systems,
Waseda University, Japan

Takayuki Furutsuki
Graduate School of Information
Production and Systems,
Waseda University, Japan

Abstract

A method of association rule mining using Genetic Network Programming (GNP) is proposed to improve the performance of rule extraction. The proposed system can evolve itself by an evolutionary method and measures the significance of the association via the chi-squared test using GNP. In this paper, we describe the algorithms capable of finding the important association rules and present some experimental results. GNP examines the attribute values of database tuples using judgement nodes and calculates the measurements of association rules using processing nodes. The proposed method measures the significance of associations via the chi-squared test for correlation used in classical statistics, where GNP evolves itself using it as a part of the fitness value. Accordingly, the algorithms can extract the important association rules efficiently. Extracted association rules are stored in a pool all together through generations in order to find new important rules. Therefore, the proposed method is fundamentally different from all other evolutionary methods in its evolutionary way.

Keywords

Evolutionary Computation, Genetic Network Programming, Data Mining, Association Rule

1 Introduction

Association rule mining is the discovery of association relationships or correlations among a set of attributes in a database [1]. Association rule in the form of ' If X then Y ' is interpreted as ' database tuples satisfying that X (antecedent) are likely to satisfy Y (consequent) '. Association rules are widely used in marketing, decision making, and business management. Agrawal et al. have built a support-confidence framework for mining association rules from databases [2]. This model measures the uncertainty of an association rule with two factors: support and confidence. However, the measure is not adequate for modeling all uncertainties of association rules. For instance, the measurement does not provide a test for capturing the correlation of two itemsets. In order to improve this framework, some measurements on the support and confidence of association rules, such as chi-squared test model have been recently proposed by Brin et al [3]. The chi-squared test method measures the significance of associations via the chi-squared test for correlation used in classical statistics. However, it is difficult to use in case that the number of items included in association rules is increased.

Genetic Network Programming (GNP) [4, 5, 6] is a kind of evolutionary methods, which evolves arbitrary directed graph programs and includes judgement nodes and processing nodes in the network. GNP is useful because it can form not only the optimal structure effectively, but it also avoid the premature convergence. In this paper, we describe the algorithms capable of finding the important association rules using GNP to improve the performance of rule extraction. Attributes (items) in database correspond to judgement nodes in GNP, respectively. We are able to represent the connection of nodes as association rules and nodes are reused and shared with some other association rules because of GNP 's feature. This method measures the support, confidence and significance of associations via the chi-squared test for correlation used in classical statistics using GNP. GNP evolves itself by an evolutionary method using chi-squared values as a part of the fitness value. Using genetic operation of GNP, we are able to obtain candidates of important association rules. Accordingly, the algorithms can extract the important association rules efficiently. In addition, extracted association rules are stored all together through generations and GNP evolves in order to find new interesting rules. Therefore, the method is fundamentally different from all other evolutionary algorithms.

2 Genetic Network Programming

In this section, the outline of Genetic Network Programming (GNP) [4, 5, 6] is explained. GNP is one of the evolutionary optimization techniques, which uses network structures as solutions. The basic structure of GNP is shown in Fig.1. GNP is composed of two kind of nodes: judgement node and processing node. Judgement nodes correspond nearly to elementary functions of Genetic Programming (GP). Judgement nodes are the set of J_1, J_2,..., J_m, which work as *if-then* type decision making functions. On the other hand, processing nodes are the set of P_1, P_2,..., P_n, which work as some kind of action/processing functions. The practical roles of these nodes are predefined and stored in the library by supervisors. Once GNP is booted up, the execution starts from Start node, then the next node to be executed is determined according to the connection from the current activated node.

The genotype expression of GNP node is shown in Fig.2. This describes the gene of node i, then the set of these genes represents the genotype of GNP individuals. NT_i describes the node type, $NT_i = 0$ when the node i is judgement node, $NT_i = 1$ when the node i is processing node. ID_i is an identification number, for example, $NT_i = 0$ and $ID_i = 1$ mean node i is J_1. C_{i1}, C_{i2},..., denote the nodes which are connected from node i firstly, secondly,..., and so on depending on the arguments of node i. d_i and d_{ij} are the delay time. They are the time required to execute the processing of node i and delay time from node i to node C_{ij}, respectively. All programs in a population have the same number of nodes, and the nodes with the same node number have the same function, respectively. The following genetic operators are used in GNP. Mutation operator affects one individual. All the connections of each node are changed randomly by mutation rate of P_m. Crossover operator affects two parent individuals. All the connections of the uniformly selected corresponding nodes in two parents are swapped each other by crossover rate P_c. GNP evolves the fixed number of nodes and these operators only change the connections among the nodes.

3 Association Rules

The following is a formal statement of the problem of mining association rules [1, 2] . Let $I = \{i_1, i_2, \ldots, i_l\}$ be a set of literals, called items or attributes. Let D be a set of transactions, where each

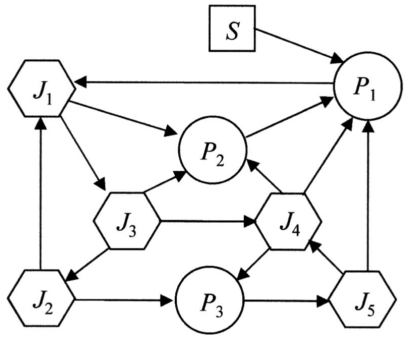

Figure 1: The basic structure of GNP individual

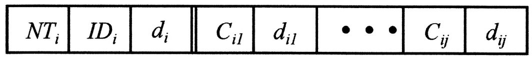

Figure 2: Gene structure of GNP (node i)

transaction T is a set of items such that $T \subseteq I$. Associated with each transaction is a unique identifier, called TID. We say that a transaction T contains X, a set of some items in I, if $X \subseteq T$. An association rule is an implication of the form $X \Rightarrow Y$, where $X \subset I$, $Y \subset I$, and $X \cap Y = \emptyset$. X is called the antecedent and Y is called the consequent of the rule. In general, a set of items is called an itemset. Each itemset has an associated measure of statistical significance called *support*. If the fraction of transactions in D containing X equals s, then we say that $support(X) = s$. The rule $X \Rightarrow Y$ has a measure of its strength called *confidence* defined as the ratio of $support(X \cup Y)/support(X)$. An example is shown below using Table 1. Let item universe be $I = \{A, B, C, D\}$ and transaction universe be $TID = \{1, 2, 3, 4\}$. In order to extend our research not only to market baskets problems but also to others, we indicate the items of the transaction by a 1 as shown in Table 1. In Table 1, itemset $\{A, C\}$ occurs in two transactions of $TID = 1$ and $TID = 3$. So, its frequency is 2, therefore, its support, that is, $support((A = 1) \wedge (C = 1))$ becomes 0.5. Itemset $\{A, C, D\}$ occurs in the transaction of $TID = 3$. Its frequency is 1, and its support, i.e., $support((A = 1) \wedge (C = 1) \wedge (D = 1))$ becomes 0.25. Therefore, $support((A = 1) \wedge (C = 1) \Rightarrow (D = 1)) = 0.25$, and $confidence((A{=}1) \wedge (C{=}1) \Rightarrow (D{=}1)) = 0.5$.

Table 1: An example of database

TID	A	B	C	D
1	1	0	1	0
2	0	1	1	1
3	1	1	1	1
4	0	1	0	1

The Tenth International Symposium on Artificial Life and Robotics 2005(AROB 10th '05),
B-con Plaza, Beppu, Oita, Japan, February 4-6, 2005

Calculation of χ^2 value of the rule $X \Rightarrow Y$ is described as follows [3]. Let $support(X) = x$, $support(Y) = y$, $support(X \wedge Y) = z$ and the number of database tuples equals N. If events X and Y are independent then $support(X \wedge Y) = xy$. Table 2 is the contingency of X and Y : the upper parts are expectation values under the assumption of independence, and the lower parts are observational. Now, let E denote the value of expectation value under the assumption of independence and O the value of observational. Then the chi-squared statistic is defined as follows:

$$\chi^2 = \sum_{AllCells} \frac{(O-E)^2}{E} \tag{1}$$

We calculate χ^2 using x, y, z and N of Table 2.

$$\chi^2 = \frac{N(z-xy)^2}{xy(1-x)(1-y)} \tag{2}$$

This has 1 degree of freedom. If it is higher than a cutoff value (3.84 at the 95% significance level, or 6.63 at the 99% significance level), we reject the independence assumption.

Table 2: The contingency of X and Y

	Y	$\neg Y$	$\sum_{row}$
X	Nxy Nz	$N(x-xy)$ $N(x-z)$	Nx
$\neg X$	$N(y-xy)$ $N(y-z)$	$N(1-x-y+xy)$ $N(1-x-y+z)$	$N(1-x)$
$\sum_{col}$	Ny	$N(1-y)$	N

4 Association Rule Mining Using GNP

In this section, a method of association rule mining using GNP is proposed. Let A_i, B_i be attributes (items) in a database and its value is 1 or 0. The method extracts the association rule as follows:
$(A_j = 1) \wedge \cdots \wedge (A_k = 1) \Rightarrow (B_m = 1) \wedge \cdots \wedge (B_n = 1)$ (briefly, $A_j \wedge \cdots \wedge A_k \Rightarrow B_m \wedge \cdots \wedge B_n$).

4.1 GNP for Association Rule Mining

Attributes in the database correspond to judgement nodes in GNP, respectively. We are able to represent the connection of nodes as association rules. GNP examines the attribute values of database tuples using judgement nodes and calculates the measurements of association rules using processing nodes. The measurements include *support* and *confidence*. Judgement node determines the next node by a judgement result (Yes/No). Fig.3 shows a basic structure of GNP. P_1 is a processing node and is a starting point of association rules. Each Processing node have an inherent numeric order (P_1, P_2,..., P_n) and basically are connected from a judgement node. Yes-side of judgement node is connected to another judgement node. Judgement nodes can be reused and shared with some other association rules because of GNP 's feature. No-side of judgement node is connected to the next numbered processing node. We now demonstrate this using an example. In Table 1, the tuple $TID = 1$ satisfies $A = 1$ and $B \neq 1$, therefore the moving is from P_1 to P_2 in Fig. 3. If the examination of the connection from the stating point P_n is ended, then GNP examines $TID = 2$ likewise. Thus, all tuples in database will be examined. The total number of tuples moving to Yes-side at each judgement nodes are calculated for every processing node, which is a starting point for calculating association rules. All GNP individuals are searched parallel at the same time. If Yes-side connection of judgement nodes continue and the number of their judgement nodes becomes a cutoff value (maximum number of attributes in extracted association rules), then Yes-side connection is transferred to the next processing node obligatorily.

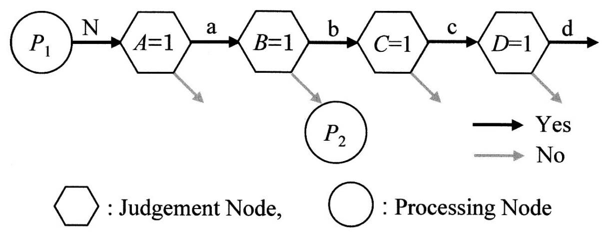

Figure 3: GNP for association rule mining

4.2 Extraction of Association Rules

In Fig.3, N is the number of total tuples, and a, b, c and d are the numbers of tuples moving to Yes-side at each Judgement node. Table 3 shows the measurements of association rules. The proposed method measures the significance of associations via the chi-squared test for correlation used in classical statistics. For example, if we change the connection of P_1 node from '$A = 1$' node to '$B = 1$' node (judgement node) in Fig.3, then we are able to calculate the support of B, $B \wedge C$ and $B \wedge C \wedge D$ in the next examination. As a result, we obtain chi-squared statistics and repeat this like a chain operation. We can define important association rules as the rules which satisfy the following:

$$\chi^2 > 6.63 \tag{3}$$

$$support \geq sup_{min} \tag{4}$$

sup_{min} is the threshold minimal support given by supervisors. The extracted important association rules are stored in a pool all together through generations in order to find new important rules. When an important rule is extracted, the overlap of the attributes is checked and it is also checked whether an important rule is new or not. If the rule is new, it is stored in the pool with its *support*, *confidence* and χ^2. Therefore, the method is fundamentally different from all other evolutionary algorithms.

Table 3: Association rules

association rules	support	confidence
$A \Rightarrow B$	b/N	b/a
$A \Rightarrow B \wedge C$	c/N	c/a
$A \Rightarrow B \wedge C \wedge D$	d/N	d/a
$A \wedge B \Rightarrow C$	c/N	c/b
$A \wedge B \Rightarrow C \wedge D$	d/N	d/b
$A \wedge B \wedge C \Rightarrow D$	d/N	d/c

4.3 Genetic Operators

Fitness evaluation function of GNP is defined as

$$F = \sum_{i \in I} \{ {\chi_i}^2 + 10(n(i_{ante}) - 1) + 10(n(i_{con}) - 1) + \alpha_{i_{new}} \} \quad (5)$$

The components are as follows:
I : a set of the number of important association rules which satisfy (3) and (4) in a GNP (individual)
$n(i_{ante})$: the number of attributes at the antecedent of rule i. $n(i_{con})$: the number of attributes at the consequent of rule i. ${\chi_i}^2$: chi-squared value of rule i.
$\alpha_{i_{new}}$: additional constant defined as

$$\alpha_{i_{new}} = \begin{cases} \alpha_{new} & (i \text{ is new}) \\ 0 & (i \text{ has been extracted already}) \end{cases} \quad (6)$$

At each generation, individuals are replaced with new ones by selection and reproduction rules. Each individual is ranked by fitness evaluation value and selected by ranking. New individuals are generated by crossover and mutation. These operators are executed at a part of judgement nodes and a part of processing nodes of GNP genes, respectively. We demonstrate the rule concretely using the case of 120 individuals at each generation. The individuals are ranked by fitness values and the top 40 individuals are selected. They are reproduced three times and three genetic operators are executed to them as follows:
Crossover : crossover we used is the uniform crossover, and it is executed between two parents and generates two offspring. Each judgement node is selected as a crossover node with the probability of P_c. Two parents exchange the genes of the corresponding crossover nodes. 40 individuals are divided into 20 pairs of parents and replaced with new 40 individuals.
Mutation-1 : Mutation-1 operator affects one individual. The connection of each judgement node is changed randomly by mutation rate of P_{m1}. Top 40 individuals reproduce new 40 individuals by Mutation1.
Mutation-2 : Mutation-2 operator also affects one individual. The connection is changed to barter the judgement nodes. For example, in Fig.3, if '$B = 1$' node is bartered with '$D = 1$' node in position, then we examine $A \Rightarrow D$, $A \wedge D \Rightarrow C$, $A \wedge D \wedge C \Rightarrow B$ and so on. Mutation-2 is executed using the rate of P_{m2} at each judgement node. New 40 individuals are reproduced by Mutation2. Table 4 shows samples of P_c, P_{m1} and P_{m2}. All the connections of processing nodes are changed randomly in order to extract rules efficiently.

Table 4: Conditions of crossover and mutation

	GNP-M	GNP-L
Crossover Probability (P_c)	15/78	10/78
Mutation-1 Probability (P_{m1})	25/78	15/78
Mutation-2 Probability (P_{m2})	16/78	12/78

(Note: 78 corresponds to the number of Judgement nodes)

5 Simulation Results

We have performed experiments and estimated the performance of our algorithms. All the experiments were run on synthetic data. The synthetic database includes 26 attributes (A_j, $j = 1, 2, \ldots, 26$). The number of tuples are 200, $support(A_j = 1) = 0.7$ ($j = 1, 2, \ldots, 5$) and $support(A_j = 1) = 0.5$ ($j = 6, 7, \ldots, 26$). Evaluation is studied in the case of
free consequent (Simulation 1)
fixed consequent (Simulation 2)
in order to analyze the performance of rule extraction. In simulations, the population size is 120. The number of processing nodes is 10, and 26 different kind of judgement nodes ('$A_j = 1$', $j = 1, 2, \ldots, 26$) are used, each by three. We use (3), (4), (5) and (6) ($\alpha_{new} = 150$). Table 4 shows the two conditions of crossover and mutation. In addition, we consider the Random GNP model, which does not evolve but repeats random initialization every generation.

5.1 Simulation1

We have performed two experiments as follows:
1) $sup_{min} = 0.2$, $n(i_{ante}) \leq 5$, $n(i_{con}) \leq 5$

Table 5: Number of association rules of free consequent in the pool (Simulation 1)

		25^{th} generation			100^{th} generation			1000^{th} generation		
		GNP-M	GNP-L	Random	GNP-M	GNP-L	Random	GNP-M	GNP-L	Random
$sup_{min} = 0.2$	Max	748	741	616	905	903	808	922	922	922
	Ave	714.8	708.3	604.3	898.9	868.6	794.4	921.9	921.3	922.0
	Min	658	678	593	889	833	781	921	920	922
$sup_{min} = 0.1$	Max	97	131	57	1000	1305	181	4821	3696	1323
6 or more	Ave	55.3	68.8	31.8	300.5	918.5	136.1	2834.5	3029.2	1213.6
attributes	Min	20	36	20	148	549	111	1568	1121	1139

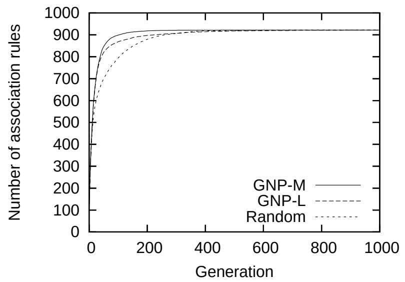

Figure 4: Number of association rules of free consequent ($sup_{min} = 0.2$)

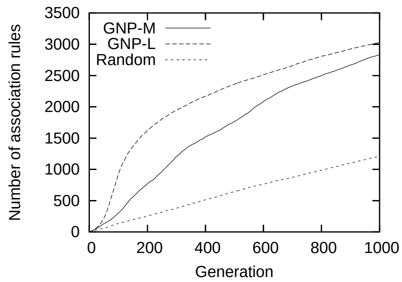

Figure 5: Number of association rules of free consequent ($sup_{min} = 0.1$, 6 or more attributes)

2) $sup_{min} = 0.1$, $n(i_{ante}) + n(i_{con}) \geq 6$, $n(i_{ante}) \leq 5$, $n(i_{con}) \leq 5$

The number of changing the connections of processing nodes is 5. Table 5, Fig.4 and Fig.5 show the number of important association rules in the pool. The system can extract the important association rules in the database effectively. Each figure shows the mean value over ten simulations. Fig.6 and Fig.7 show fitness curve. Fig.8 and Fig.9 are the results of the number of association rules at each generation. These show the different important association rules in 120 individuals at each generation. GNP-M suits the extraction of the rules including 3-5 attributes, while GNP-L will be convenient for 5-7 attributes rules. The results show that our method works effectively by its fitness curve and the number of extracted rules at each generation. It is found that the proposed evolutionary method is effective in association rule mining. In addition, it is also found that we can set a condition to extract rules, for instance, the number of attributes in the rules.

5.2 Simulation2

We have performed experiments with one specific consequent attribute (A_{26}) supposing $sup_{min} = 0.05$ and $n(i_{ante}) \leq 8$. (such as $A_1 \wedge A_2 \wedge A_3 \wedge A_4 \wedge A_5 \Rightarrow A_{26}$ will be extracted.) As we suppose that the $support(A_{26} = 1) = 0.5$, the method is fairly simplified. Each judgement node examines the '$A_{26} = 1$'. For example, in Fig.3, the number of tuples 'b' indicates $support((A = 1) \wedge (B = 1))$, and GNP calculates $support((A = 1) \wedge (B = 1) \wedge (A_{26} = 1))$ at the same time, because $support(A_{26} = 1)$ is known. Then we can obtain the measurements of the rule $A \wedge B \Rightarrow A_{26}$. Experiments is performed by $P_c = 15/75$, $P_{m1} = 25/75$, $P_{m2} = 16/75$. (judgement node '$A_{26} = 1$' is not used.) Fig.10 shows the number of important association rules. Especially, Fig.11 shows the number of rules satisfying $n(i_{ante}) \geq 7$. The results also show that our method works effectively. It is also found that the system can extract the interesting rules easily, which are made up of 7 or more antecedent attributes.

6 Conclusions

In this paper, a new method of association rule mining using Genetic Network Programming (GNP) has been proposed. The proposed system can evolve itself by an evolutionary method and measures the significance of associations via the chi-squared value. An efficient algorithm for identifying association rules of importance was designed. We have performed experiments and estimated the performance of our algorithms. The results showed that our method extracts the important association rules in the database effectively. In addition, it is found that we can set a condition to extract rules, for instance, the number of attributes in the rules. In a future, we plan to extend the proposed method to the one applicable to large databases.

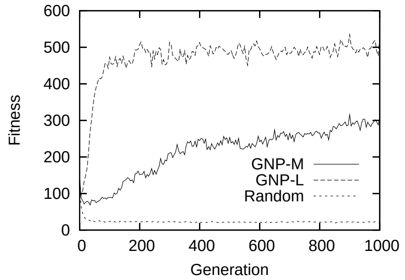

Figure 6: Fitness curves of free consequent ($sup_{min} = 0.2$)

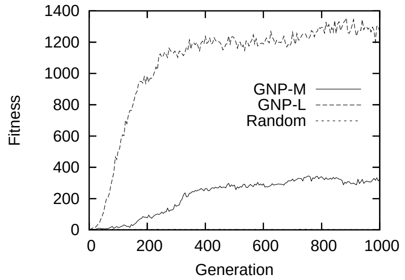

Figure 7: Fitness curves of free consequent ($sup_{min} = 0.1$, 6 or more attributes)

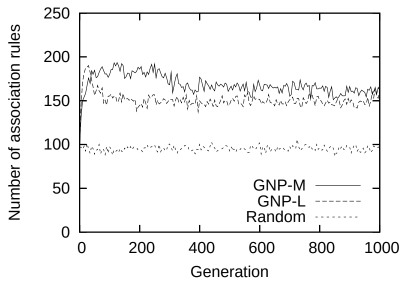

Figure 8: Number of association rules of free consequent ($sup_{min} = 0.2$)

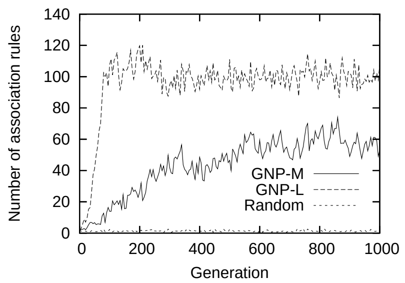

Figure 9: Number of association rules of free consequent ($sup_{min} = 0.1$, 6 or more attributes)

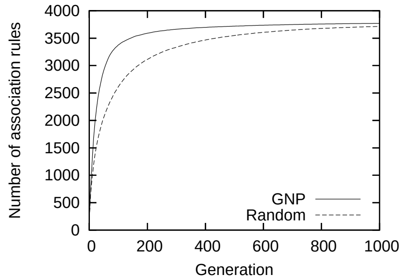

Figure 10: Number of association rules of fixed consequent ($sup_{min} = 0.05$)

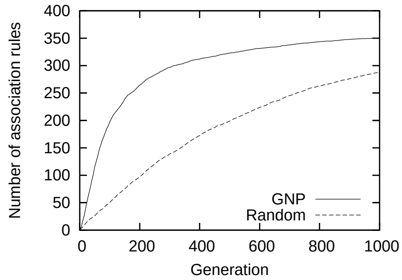

Figure 11: Number of association rules of fixed consequent ($sup_{min} = 0.05$, 7 or more attributes)

References

[1] C. Zhang , S. Zhang , Association Rule Mining: models and algorithms , Springer (2002)

[2] R. Agrawal, R. Srikant : "Fast Algorithms for Mining Association Rules ", *Proc. of the 20th VLDB Conf.* Santiago , Chile, pp.487-499 (1994)

[3] S. Brin, R. Motwani, and C. Silverstein. "Beyond market baskets : generalizing association rules to correlations " *In Proc. of ACM SIGMOD*, pp.265-276 (1997)

[4] H. Katagiri, K. Hirasawa, and J. Hu : "Genetic network programming - application to intelligent agents -", *In Proc. of IEEE International Conf. on Syst. , Man and Cybernetics*, pp.3829-3834 (2000)

[5] H. Katagiri, K. Hirasawa, J. Hu and J. Murata: "Network Structure Oriented Evolutionary Model - Genetic Network Programming", *in Proc. of Genetic and Evolutionary Computation Conference*, pp.219-226 (2001)

[6] K. Hirasawa, M. Okubo, H. Katagiri, J. Hu and J. Murata: "Comparison between Genetic Network Programming (GNP) and Genetic Programming (GP)", *in Proc. of Congress of Evolutionary Computation*, pp.1276-1282 (2001)

The Tenth International Symposium on Artificial Life and Robotics 2005(AROB 10th '05),
B-con Plaza, Beppu, Oita, Japan, February 4-6, 2005

Evolution of Metaparameters for Efficient Real Time Learning

Genci Capi[1], Masao Yokota[1] and Kenji Doya[2]

[1]Faculty of Information Engineering
Fukuoka Institute of Technology
3-30-1 Wajiro-Higashi, Higashi-ku, Fukuoka, 811-0195, Japan

[2] CREST, Japan Science and Technology Agency (JST)
ATR, Computational Neuroscience Laboratories
"Keihanna Science City", Kyoto, 619-0288, Japan

capi@fit.ac.jp

Abstract
In this paper, we propose a new method based on evolutionary computation for setting the metaparameters of reinforcement learning in order to match the demands of the task and reduce the learning time. The basic idea is to encode the metaparameters of the reinforcement learning algorithm as the agent's genes, and to take the metaparameters of best-performing agents in the next generation. We considered a complex task where the Cyber Rodent robot has to survive and increase its energy level. The results show that appropriate settings of metaparameters found by evolution have a great effect on the learning time and are strongly dependent on each other.

KEY WORDS
Actor-critic Reinforcement Learning, Genetic Algorithm, metaparameters.

1. Introduction

Reinforcement learning (RL) ([1], [2],[3], [4]) provides a sound framework for autonomous agents to acquire adaptive behaviors based on reward feedback. The theory of RL has been successfully applied to a variety of dynamic optimization problems, such as game programs ([5]), and resource allocation.

In RL, the learning capabilities are strongly dependant on a number of parameters, such as learning rate, the degree of exploration, and the time scale of evaluation. The appropriate settings of metaparameters depend on the environmental dynamics, the goal of the task, and the time allowed for learning. The permissible ranges of such metaparameters are dependant on particular tasks and environments, making it necessary for a human expert to tune them usually by trial and error. But tuning multiple metaparameters is quite difficult due to their mutual dependency, e.g., if one changes the noise size, one should also change the learning rate. In addition hand tuning of metaparameters is in a marked contrast with learning in animals, which can adjust themselves to unpredicted environments without any help from a supervisor.

The specific questions we ask in this study are: 1) whether GA can successfully find appropriate metaparameters subject to mutual dependency and 2) how the metaparameters and initial weight connections effect the learning time. In our method, the basic idea is to encode the metaparameters of the RL algorithm as the agent's genes, and to take the metaparameters of best-performing agents in the next generation.

In order to answer these questions, we considered a surviving behavior for the Cyber Rodent (CR) robot ([11]), which is a two wheeled robot with a wide-angle camera. The robot must recharge itself by capturing active battery packs distributed on the environment. In order to see the effect of metaparameters and initial weight connections on learning time we considered learning with: 1) arbitrarily selected metaparameters and random initial weight connections; 2) evolved initial weight connections and arbitrarily selected metaparameters; 3) evolved metaparameters and random initial weight connections; 4) evolved metaparameters and initial weight connections.

Results show that appropriate settings of meta-parameters can be found by evolution. The learning time is significantly reduced when the agent learned using the optimized metaparameters and the initial weight connections.

Fig. 1. Cyber Rodent robot.

2. Cyber Rodent Robot

The CR robot is a two-wheel-driven mobile robot as shown in Fig. 1. The CR is 250 mm long and weights 1.7 kg. The CR is equipped with:

- Omni-directional C-MOS camera.
- IR range sensor.
- Seven IR proximity sensors.
- 3-axis acceleration sensor.
- 2-axis gyro sensor.
- Red, green and blue LED for visual signaling.
- Audio speaker and two microphones for acoustic communication.
- Infrared port to communicate with a nearby agent.
- Wireless LAN card and USB port to communicate with the host computer.

3. Task and Environment

In the second environment, the CR robot has to survive and increase its energy level. The environment has 8 battery packs, as shown in Fig. 2. The positions of battery packs are considered fixed in the environment and the CR robot is initially placed in a random position and orientation.

The agent can recharge its own battery by capturing active battery packs, which are indicated by red LED color. After the robot captures the battery pack, it can recharge its own battery for a determined period of time (charging time), then the battery pack becomes inactive and its LED color changes to green. The battery becomes active again after the reactivation time. Therefore, in this environment the following parameters can vary:

- The number of battery packs;
- The reactivation time;
- The energy received by capturing the battery pack (by changing the charging time);
- The energy consumed by the agent for 1m motion.

Based on the energy level and the distance to the nearest active battery pack, the agent can select among three actions: 1) capture the active battery pack; 2) search for a battery pack or 3) wait until a battery pack becomes active. In the simulated environment, the batteries have a long reactivation time. In addition, the energy consumed for 1m motion is low. Therefore, the best policy is to capture any visible battery pack (the nearest when there are more than one). When there is no visible active battery pack, the agent must search in the environment.

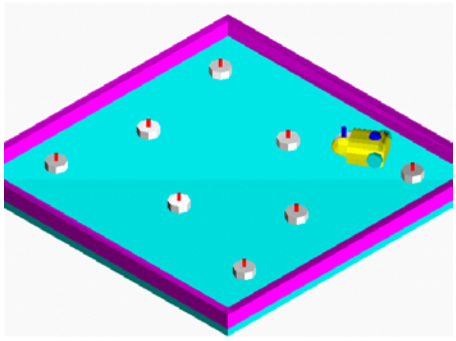

Fig. 2. Environment.

4. Actor-Critic RL

We applied an actor-critic RL. The agent can selects among three actions: 1) Capture the active battery pack; 2) Search for an active battery pack; 3) Wait for a determined period of time. The wait behavior is interrupted if a battery becomes active or after a pre-determined period of time. Both networks receive as input a constant bias input, the CR battery level and the distance to the nearest active battery pack (both normalized between 0 and 1).

4.1 The Critic

The critic has a single output cell, whose firing rate is calculated as follows:

$$O_c = \sum_{i=1}^{3} b_i x_i + \sum_{i=1}^{m} c_i y_i \qquad (1)$$

where m is the number of hidden neurons,

$$y_i = g\left(\sum_{j=1}^{3} a_{ij} x_j\right), \quad g(s) = \frac{1}{1+e^{-s}}.$$

The TD error is calculated as follows:

$$\hat{r}[t+1] = \begin{cases} 0 \text{ if the start state} \\ \mathrm{r}[\mathrm{t}+1] + \gamma^{\mathrm{k}} v[t] \text{ otherwise} \end{cases}, \quad (2)$$

using the reward

$$r_{t+1} = (En\_level_{t+1} - En\_level_t)/50.$$

TD reduces the error by changing the weights, as follows:

$$b_i[t+1] = b_i[t] + \rho_1 \hat{r}[t+1] x_i[t]$$
$$c_i[t+1] = c_i[t] + \rho_1 \hat{r}[t+1] y_i[t] \quad (3)$$
$$a_{ij}[t+1] = a_{ij}[t] + \rho_2 \hat{r}[t+1] y_i[t](1 - y_i[t]) \operatorname{sgn}(c_i[t]) x_j[t],$$

where ρ_1, ρ_2 are the learning rates.

4.2 The actor

The agent can select one of three actions and so the actor make use of three action cells, p_j, $j=1,2,3$. The captured behavior is considered pre-learned ([6]). When the search behavior is activated, the agent rotates 10 degrees clockwise. The agent does not move when the wait behaviour becomes active. The output of action neurons is calculated as follows:

$$z_i = g(\sum_{j=1}^{3} d_{ij} x_j), \quad (4)$$

$$p_i = g(\sum_{i=1}^{3} e_{ij} x_i + \sum_{i=1}^{n} f_{ij} z_i), \quad (5)$$

where $g(s) = \dfrac{1}{1+\exp^{-s}}$ and n is the number of hidden neurons

A winner-take-all rule prevents the actor from performing two actions at the same time. The action is selected based on the softmax method as follows:

$$P(a, s_t) = \frac{e^{p_i(a,s)/\tau}}{\sum_{i=1}^{3} (e^{p_i(a,s)/\tau})}, \quad (6)$$

where τ is the temperature of the algorithm.

Table 1. GA functions and parameters.

Function Name	Parameters
Arithmetic Crossover	2
Heuristic Crossover	[2 3]
Simple Crossover	2
Uniform Mutation	4
Non-Uniform Mutation	[4 GNmax 3]
Multi-Non-Uniform Mutation	[6 GNmax 3]
Boundary Mutation	4
Normalized Geometric Selection	0.08

The actor weights are adapted as follows:

$$e_i[t+1] = e_i[t] + \alpha_1 \hat{r}[t+1](q[t] - p[t]) x_i[t]$$
$$f_i[t+1] = f_i[t] + \alpha_1 \hat{r}[t+1](q[t] - p[t]) z_i[t] \quad (7)$$
$$d_{ij}[t+1] = d_{ij}[t] + \alpha_2 \hat{r}[t+1] z_i[t](1 - z_i[t])$$
$$\operatorname{sgn}(f_i[t])(q[t] - p[t]) x_j[t]$$

5. Evolution of Metaparameters

In our implementation, a real-value GA was employed in conjunction with the selection, mutation and crossover operators (Table 1).

The fitness function in the surviving behavior is considered as follows:

$$Fitness = \begin{cases} \dfrac{CR_{life}}{learn\_t} & \text{if aget dies} \\ En_{level} + 1 & \text{if agent survives} \\ En_{\max} + \dfrac{learn\_t}{CR_{life}} & \text{battery fully recharged} \end{cases}$$

where CR_{life} is the CR life in seconds, *max_learning_time* is the maximum learning time, En_{level} is the level of energy if the agent survives but the battery is not fully recharged and En_{max} is the maximum level of energy. The maximum learning time is 7200 s. The value of En_{max} is 1 and En_{level} varies between 0 and 1. Based on this fitness function the agents that can not survive get a better fitness if they live longer. The agents that survive get a better fitness if the energy level at the end of maximum learning time is higher. The agents that learned to fully recharge their battery faster get the highest fitness value.

In order to see the effect of metaparameters and initial weight connections on learning time, we considered the following cases: (a) Evolution of meta-parameters, initial weight connection of actor and critic networks, and the number of hidden neurons; (b) Evolution of meta-parameters with randomly initialized weight connections; (c) Evolution of initial weight connections with arbitrary selected meta-parameters; (d) Learning with arbitrary selected meta-parameters and randomly initialized weight connections.

6. Results

In order to determine the energy level after each action, we measured the battery level of CR when the robot moves with a nearly constant velocity of 0.3m/s. The collected data are shown in Fig. 3. The graph shows that there is a nonlinear relationship between time and energy level. Therefore, we used the virtual life time to determine the energy level after each action. Except capturing the battery pack, the search and wait actions increased the virtual life time.

First, learning took place with arbitrarily selected metaparameters (Table 2) and random initial weight connections. The agent continued learning for nearly 5500s until the battery was fully recharged (Figure 4). Then, using the same metaparameters and neural structure, we evolved the initial weight connections. Initially, 100 individuals are created and the evolution terminated after 20 generations. Figure 4 shows that learning time is reduced.

When the metaparameters are evolved and initial weight connections are randomly selected, the learning time is significantly reduced (Figure 4). This result is important because it shows that metaparameters has larger effect on learning time compared to initial weight connections. The searching interval and GA results, when both metaparameters and initial weight connections are optimized by GA, are shown in Table 3. The critic and actor networks have 1 and 3 hidden neurons, respectively. The initial value of weight connections are very near with their respective values after learning. In addition, the optimized value of cooling factor is low. Therefore, the agent starts to exploit the environment and make greedy actions soon after the learning starts, recharging its own battery in a very short time.

Table 2. Values of metaparameters

Parameters	Values
Initial Weights	Randomly between [-0.5 0.5]
$\rho_1, \rho_2, \alpha_1, \alpha_2$	0.2; 0.1; 0.8; 0.3
τ_0	10
γ	0.9

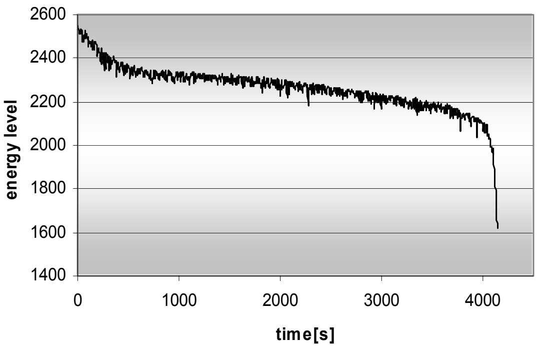

Fig. 3. Battery level during CR motion.

Table 3. Searching space and GA results.

Optimized parameters	Searching interval	Results
Initial Weights	[-1 1]	
$\rho_1, \rho_2, \alpha_1, \alpha_2$	[0 1]	0.9210; 0.3022; 0.9256; 0.6310
τ_0	[1 10]	5.3718
γ	[0 1]	0.794

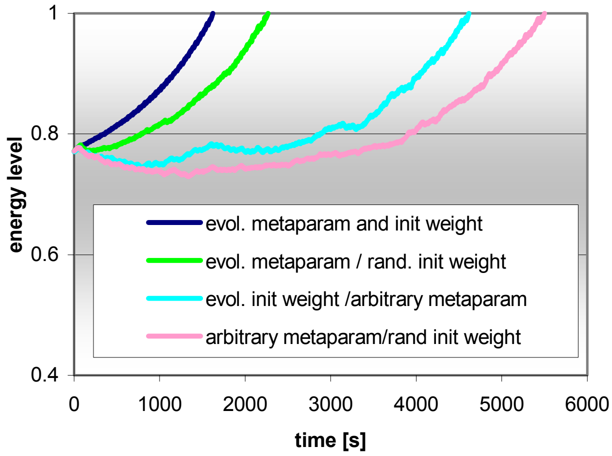

Fig. 4. Energy level of the best agent for different combinations of learning and evolution.

7. Conclusion

In this paper, we presented a method to optimize the metaparameters in RL based on evolutionary approach. Based on the simulations and experimental results we conclude:

- Evolutionary algorithms can be successfully applied to determine the optimal values of metaparameters.
- Meaparameters play important role on the agent learned policy.
- Optimized metaparameters can significantly reduce the learning time.

In the future, we are interesting to see if evolution can also be applied to shape the reward function used during the learning process.

References:

[1] Barto AG(1995), Reinforcement learning. In M. A. Arbib (Ed.), The handbook of brain theory and neural networks, (pp. 804–809). Cambridge, MA: MIT Press.
[2] Doya K (2000), Reinforcement learning in continuous time and space. Neural Computation, 12:215–245.
[3] Doya K, Kimura H, Kawato M (2001), Computational approaches to neural mechanism of learning and control. IEEE Control Systems Magazine, 21(4):42–54.
[4] Sutton RS, Barto AG (1998), Reinforcement learning. Cambridge, MA, MIT Press.
[5] Tesauro G (1994), TD-Gammon, a self teaching backgammon program, achieves master-level play. Neural Computation, 6:215–219.
[6] Capi G, Uchibe E, Doya K (2002). Selection of neural Architecture and the environment Complexity. Advanced Intelligence, Vol. 6, pp. 311-317, Editors: K. Murase and T. Asakura.

The Tenth International Symposium on Artificial Life and Robotics 2005(AROB 10th '05),
B-con Plaza, Beppu, Oita, Japan, February 4-6, 2005

A Reinforcement Learning Scheme of Adaptive Flocking Behavior

Masahito Tomimasu[1], Koichiro Morihiro[2,1], Haruhiko Nishimura[3], Teijiro Isokawa[1], and Nobuyuki Matsui[1]
[1] University of Hyogo, 2167 Shosha, Himeji, 671-2201, JAPAN
E-mail: tomimasu@comp.eng.himeji-tech.ac.jp,{isokawa,matsui}@eng.u-hyogo.ac.jp
[2] Hyogo University of Teacher Education, 942-1, Yashiro, 673-1494, JAPAN
E-mail: mori@info.hyogo-u.ac.jp
[3] University of Hyogo, 1-3-3 Higashikawasaki-cho, Chuo-ku, Kobe, 650-0044, JAPAN
E-mail: haru@ai.u-hyogo.ac.jp

Abstract

Flocking by birds, herding by land animals, or schooling by fishes is well-known collective behavior in nature. Many previous observations suggest that there are no leaders who control the behavior of the group. Several models have been proposed for describing the flocking behavior (we call the aggregate motions only as flocking from now on). In these models, a rule is given to each of individuals a priori for their interactions in reductive and rigid manner. Instead of this, we propose a new framework for self-organized flocking of agents by reinforcement learning. It will become important to introduce a learning scheme for making collective behavior in artificial autonomous distributed systems. The behavior of agents is demonstrated and evaluated through computer simulations and it is shown that the flocking behavior of agents emerges as a result of learning.

1 Introduction

Bird-flocking or fish-schooling is well-known collective behavior in nature. Many previous observations suggest that there are no leaders to control the behavior of the group; rather it emerges from the local interactions among individuals in the group. Several models have been proposed for describing the flocking behavior. In these models, a rule is given to each of individuals a priori for their interactions[1][2][3]. This reductive and rigid approach is plausible for modeling flocks of biological organisms, for they seem to inherit the ability of making a flock. However what is more, it will become important to introduce a learning scheme for making collective behavior. In a design of artificial autonomous distributed system, fixed interactive relationships among agents (individuals) lose the robustness against nonstationary environments. It is necessary for agents to be able to adjust their parameters of the ways of interactions. Some learning framework to form individual interaction will be of importance. In addition to securing the robustness of system, this framework will give a possibility to design systems easier, because it determines the local interactions of agents adaptively as a certain function of the system.

In this paper, we propose an adaptive scheme for self-organized making flock of agents. Each of agents is trained in its perceptual internal space by Q-learning, which is a typical reinforcement learning algorithm[4][5][6]. The behavior of agents is demonstrated and evaluated through computer simulations.

2 Reinforcement Learning

2.1 Q-learning

Machine learning that gives a computer system an ability to learn has been developed and used in various situations. A lot of learning algorithms and methods are proposed for the system to acquire step-by-step the desired function. Reinforcement learning is originated in experimental studies of learning in psychology. Almost all reinforcement learning algorithms are based on estimating value functions. The system gets only an evaluative scalar feedback of a value function from its environment, not an instructive one as in supervised learning. Q-learning is known as the best-understood reinforcement learning algorithm. The value function in Q-learning consists of values decided from a state and an action, which is called Q-value. In Q-learning, proceedings on learning consist of acquiring a state(s_t), deciding an action(a_t), receiving a reward(r) from an environment, and updating Q-value($Q(s_t, a_t)$). Q-value is updated by the equation written as follows:

$$Q(s_{t+1}, a_{t+1}) = Q(s_t, a_t) + \alpha[r + \gamma \max_{a' \in A(s')} Q(s', a') - Q(s_t, a_t)] \quad (1)$$

where A denotes a set of actions, α is the learning rate($0 < \alpha \leq 1$), γ is the discount rate($0 \leq \gamma \leq 1$).

2.2 Action Choice Generator

In the reinforcement learning, many kinds of exploration policies have been proposed as a process of trial and error such as ϵ-greedy, softmax, and weighted roulette action selection. Here, we adopt softmax action selection, and the rule is given as follows:

$$p(a|s) = \frac{\exp\{Q(s,a)/T\}}{\sum_{a_i \in A} \exp\{Q(s,a_i)/T\}} \quad (2)$$

where T is a positive parameter called the temperature. High temperatures cause the actions to be all (nearly) equi-probable, and low temperatures cause a greater difference in selection probability for actions that differ in their value estimates.

3 Model and Method

In this section, we introduce a scheme of perceptual internal space as the Q-value coordinates in the situation that an agent perceives (finds) another one among the others.

3.1 Perceptual Internal Space for Each Agent

We employ a configuration where N agents that can move to any direction are placed in a two-dimensional field. The agents act in discrete time, and their velocities are 1 body-length(1 BL). At each time-step an agent (agent i) finds other agent (agent j) among N-1 agents. In the perceptual internal space, the state s_t of $Q(s_t, a_t)$ for the agent i is definded as [R], the maximum integer not surpassing the Euclidean distance from agent i to agent j, R. As the action a_t of $Q(s_t, a_t)$ four kinds of action patterns (a_1, a_2, a_3, a_4) are taken as follows, shown in Fig.1.

a_1 : Attraction to agent j
a_2 : Parallel positive orientation to agent j
$(\mathbf{m_a} \cdot (\mathbf{m_i} + \mathbf{m_j}) \geq 0)$
a_3 : Parallel negative orientation to agent j
$(\mathbf{m_a} \cdot (\mathbf{m_i} + \mathbf{m_j}) < 0)$
a_4 : Repulsion to agent j

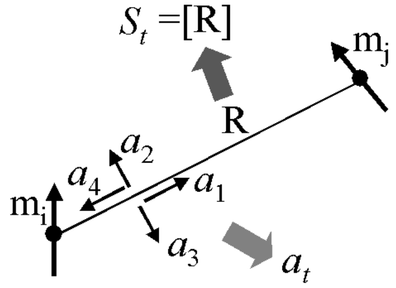

Figure 1: Constitution of perceptual internal space for each agent

where $\mathbf{m_a}$ is the directional vector of a_t, $\mathbf{m_i}$ and $\mathbf{m_j}$ are the velocity vectors of agent i and agent j, respectively, with $|\mathbf{m_a}|=|\mathbf{m_i}|=|\mathbf{m_j}|=1$(BL). Agent i moves according to $\mathbf{m_i}$ at each time-step, and $\mathbf{m_i}$ is updated by

$$\mathbf{m_i} \leftarrow \frac{(1-\kappa)\mathbf{m_i} + \kappa\mathbf{m_a}}{|(1-\kappa)\mathbf{m_i} + \kappa\mathbf{m_a}|} \quad (3)$$

where κ is a positive parameter($0 \leq \kappa \leq 1$).

3.2 Learning Method for Each Agent

In our proposed model, we prepare the reward for (s_t, a_t) of each agent as shown in Table 1, where R_1,R_2, and R_3 have the relationship of $R_1 < R_2 < R_3$.

Table 1: Reward r preparation for the selected action a_t in the state s_t=[R]

s_t	0 <[R]≤ R_1		R_1 <[R]≤ R_2		R_2 <[R]≤ R_3	
a_t	a_4	a_1,a_2,a_3	a_2	a_1,a_3,a_4	a_1	a_2,a_3,a_4
r	1	-1	1	-1	1	-1

The learning of the agents proceeds according to a positive or negative reward. In case [R]>R_3, agent i cannot perceive agent j, and then receives no reward and choose an action from the four action patterns(a_1, a_2, a_3, a_4) randomly. In case 0 <[R]≤R_3, agent i can perceive another agent with the probability in proportion to $R^{-\beta}$, where β is a positive parameter. This means that the smaller R value is, the easier the agent at that position is selected.

4 Simulations and Results

To demonstrate our proposed scheme in computer simulations, we take the following experimental conditions : α = 0.1, γ = 0.7 in Eq.(1), T = 0.5(under

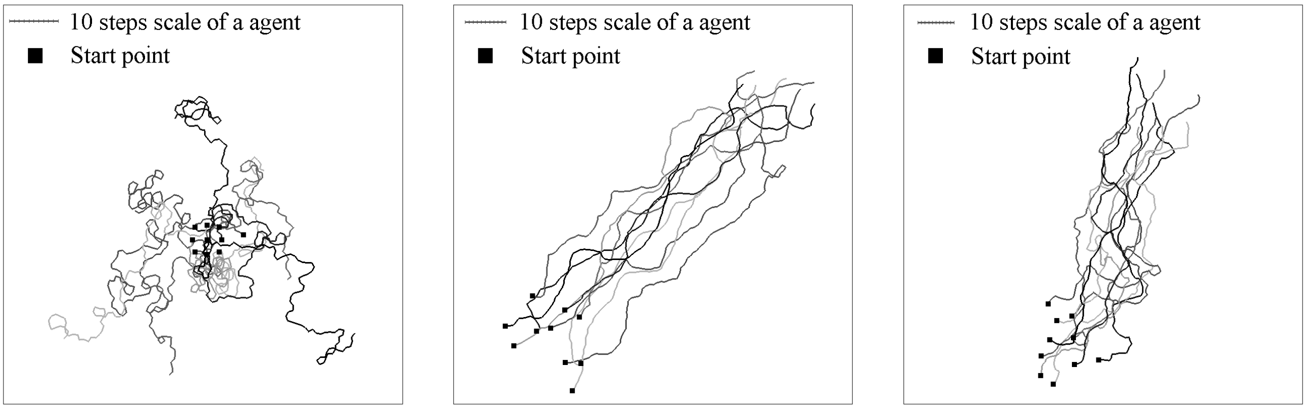

(a) Under learning, in the range 0 – 100 steps

(b) Under learning, in the range 4900 – 5000 steps

(c) After learning, in the range 500 – 600 steps

Figure 2: The trajectories of agents under and after learning in the case of $N = 10$, and $(R_1, R_2, R_3) = (4, 20, 50)$

learning) in Eq.(2), $\kappa = 0.5$ in Eq.(3), and $\beta = 0.5$ for the distance dependence of $R^{-\beta}$. The total number of trials is set to 5000 time-step through all simulations. Under these conditions we check whether agents make a flock for the parameters N and (R_1, R_2, R_3).

4.1 N=10 with $(R_1, R_2, R_3) = (4, 20, 50)$ Case

We simulated our model in the case of the number of agents N=10, and R_1=4(BL), R_2=20(BL) and R_3=50(BL). Figures 2(a),(b), and(c) show the trajectories in the range 0 – 100 steps, 4900 – 5000 steps under learning, and in the range 500 – 600 steps after learning. In Fig.2(a) each of the agents changes its direction very often, but it keeps the direction for long time-step with the others in Figs.2(b) and (c). This indicates that the learning succeeded in flocking. In order to evaluate how the agents make flocking behavior quantitatively, we introduce a measure $|\mathbf{M}|$ of the uniformity in direction :

$$|\mathbf{M}| = \frac{1}{N}\left|\sum_{i=1}^{N}\mathbf{m_i}\right| \tag{4}$$

The value of $|\mathbf{M}|$ becomes closer to 1 when the directions of agents increase their correspondence. Figure 3 shows the time-step dependence of $|\mathbf{M}|$ in this case. The transition of $|\mathbf{M}|$ evolves good except for the fluctuation owing to the exploration effect in every time-step. To remove these large variations we further take the average of 100 events by repeating the above simulation with various random series in exploration. As a result, Fig.4 is obtained in which the value of $|\mathbf{M}|$ increases up to near 0.9.

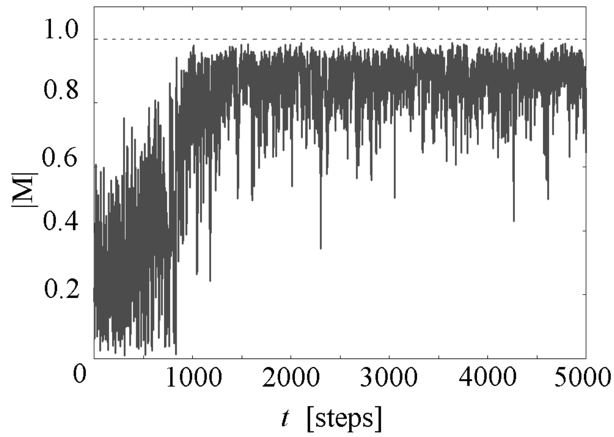

Figure 3: The time-step dependence of $|\mathbf{M}|$ (Eq.(4)) for the case in Fig.2

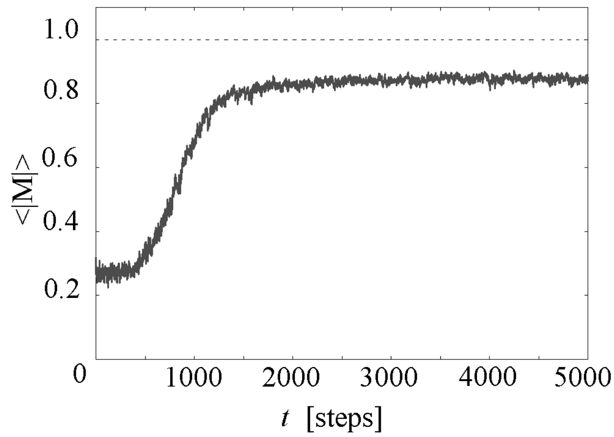

Figure 4: The step-time dependence of the averaged $|\mathbf{M}|$ in 100 events of Fig.3 case

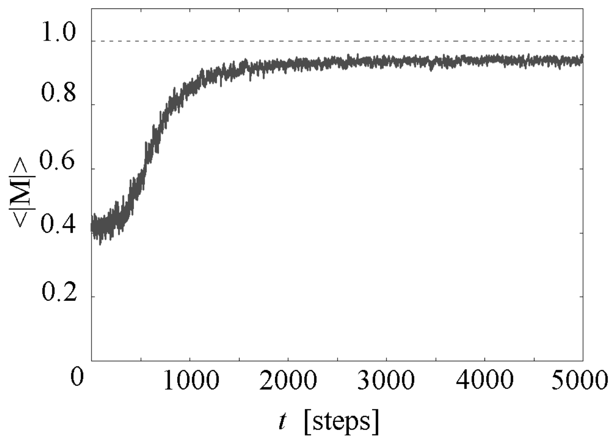

(a) 4 agents case

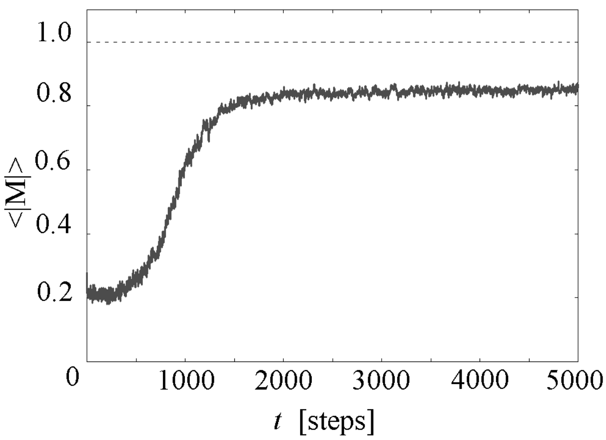

(b) 16 agents case

Figure 5: The time-step dependence of the averaged $|\mathbf{M}|$ in 100 events in the cases of N=4 and 16

4.2 N=4, 16 with (R_1,R_2,R_3)=(4,20,50) Cases

We simulated our model in the cases of 4 and 16 agents with (R_1,R_2,R_3) = $(4, 20, 50)$. Figures 5(a) and (b) show the transition of averaged $|\mathbf{M}|$ in 100 events respectively. It is found that the performances are good in both cases depending a little on the number of agents.

4.3 N=10 with Individual (R_1,R_2,R_3) Case

The case of 10 agents with (R_1,R_2,R_3) = (3,16,40), (3,17,45), (4,19,47), (4,18,48), (4,20,50), (4,21,51), (4,22,52), (5,25,45), (5,23,53), (6,25,55) was furthermore simulated. From Fig.6 the performance is as well as the case with common (R_1,R_2,R_3) in section 4.1.

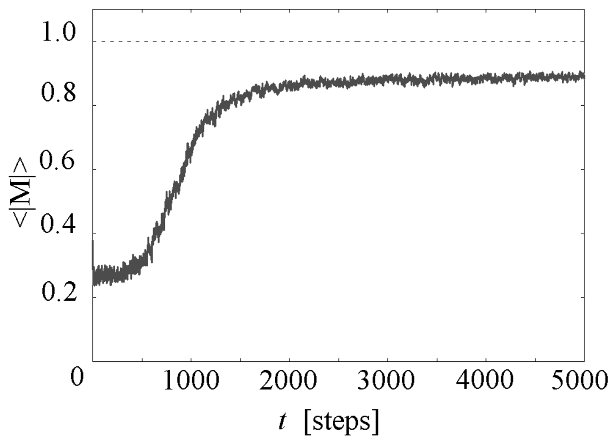

Figure 6: The time-step dependence of the averaged $|\mathbf{M}|$ in 100 events in the case of N=10 with individual (R_1,R_2,R_3)

5 Conclusion

We proposed a scheme for autonomously making flock of agents by reinforcement Q-learning and could show the flocking behavior of agents emerges as a result of learning in simulations. In order to confirm whether our scheme is effective under various environments, we proceed further investigations on various parameters and on introducing different kind of agents such as predators.

References

[1] I. Aoki, "A Simulation Study on the Schooling Mechanism in Fish, " *Bulletin of the Japanese Society of Scientific Fisheries*, Vol.48, No.8, pp.1081-1088, 1982.

[2] C. W. Reynolds, "Flocks, herds, and schools: A distributed behavioral model, " *Comp. Graph*, Vol.21, No.4, pp.25-34, 1987.

[3] A. Huth and C. Wissel, "The Simulation of the Movement of Fish Schools, " *J. theor. Biol*, Vol.156, pp.365-385, 1992.

[4] R. S. Sutton and A. G. Barto, Reinforcement Learning, Cambridge, The MIT press, 1982.

[5] L. P. Kaelbling, M. L. Littman and A. W. Moore, "Reinforcement Learning : A Survey, " *Journal of Artificial Intelligence Research*, Vol.4, pp.237-285, 1996.

[6] C. J. C. H. Watkins and P. Dayan, "Q-learning, " *Machine Learning*, Vol.8, pp.279-292, 1992.

The Tenth International Symposium on Artificial Life and Robotics 2005(AROB 10th '05),
B-con Plaza, Beppu, Oita, Japan, February 4-6, 2005

Learning Control of Manipulator with a Free Joint

T.Goto, H.Lee, K.Abe
Dept. of Elec. & Comm. Eng.
School of Eng.,Tohoku Univ.
Sendai, Aoba05. 980-8579

Hiroyuki Kamaya
Dept. of Elec. Eng.
Hachinohe National College of Technology
Hachinohe. 039-1192

Abstract

In this paper, reinforcement learning approach to motion control of 2-link planer underactuated manipulator is described. This manipulator has one passive joint and is difficult to control. The experiments of learning to control this manipulator by RL and human are executed. Using the experimental results, the associations between RL and human learning are considered.

1 introduction

Reinforcement learning (RL) is a general framework for describing learning problems in which an autonomous agent learns strategies for interacting with its environment[1]. RL has been applied to many research areas. Motion learning is one of such areas. For the robot, in order to adapt to a dynamic environment, motion learning is one of key issues. Therefore, many algorithms for motion learning have been intensively discussed for years[2]. Many control objects are tested in *acrobot*, inverted pendulum, walking robot etc., and most of these tasks are nonlinear. They have some equilibrium points which can be stabilized by continuous feedback control. In these cases, by using the information of these equilibrium points as prior knowledge, more distinguished motion learning algorithms can be designed, e.g. a hierarchical RL algorithm composed of linear controllers and an adequate reward function[2]. However, there are several typical nonlinear systems which are not able to apply such hierarchical algorithms. 2-link planer under-actuated manipulator (2PUAM) is one of those systems. This system has been widely studied by control engineers[3]. But only a few researches have been done from view point of learning. On design of RL algorithm for 2PUAM, setting of the reward is difficult, and in addition, the state space is multidimensional and continuous. Therefore, the approximation of value function is needed to solve the local optimal problem.

On the other hand, some researchers have applied the cognitive and learning capability of human to complex control systems. Even though, a human operator fails to control complex system in the beginning, but after enough training, he, she can find a way to control it satisfactory. It is apparent that he, she does not use a mathematical model. This fact shows that human can find a satisfactory control law by a trial-and-error without the knowledge of the mathematical model to control object. For example, it is reported that the joint angle control of 2PUAM can be achieved by human operator[4]. This indicates the capability of learning the behavior which can not be achieved by using continuous feedback.

In order to solve such difficult control object, realization of RL algorithm reproducing human abilities is desirable. Therefore, the investigation of human learning mechanism from the perspective of RL is basically necessary. In this paper, a 2PUAM is selected as the learning problem. And learning experiments by RL and human are tested. In the RL experiment, Q-learning is implemented. For the experiment of human manual control, a 2PUAM simulator is developed. It includes a policy evaluation module. This module automatically approximates the Q-value function according to the action series of human. By using these experimental results, the comparison between RL agent and human learning is described.

2 Model of manipulator

In this paper, a 2PUAM is used for the learning task. It has only one active joint and one passive joint, and neither gravity nor friction torque acts on it. It is one of the simplest forms of underactuated manipulators. The equation of motion of the manipulator is:

$$\mathbf{M}_{11}(\theta)\ddot{\theta_1} + \mathbf{M}_{12}(\theta)\ddot{\theta_2} + \mathbf{c}_1(\theta, \dot{\theta}) = \tilde{\tau}, \tag{1}$$

$$\mathbf{M}_{21}(\theta)\ddot{\theta_1} + \mathbf{M}_{22}(\theta)\ddot{\theta_2} + \mathbf{c}_2(\theta, \dot{\theta}) = 0, \tag{2}$$

where θ_1 and θ_2 are angle of each joint, $\mathbf{M}$ is inertia matrix, $\mathbf{c}$ denotes centrifugal term, and right sides of boss Eq. (1), (2) are the input torque. Therefore Eq. (2) means the dynamic constraint caused by the zero torque at the passive joint. This manipulator has two main characteristics. The first is that the inertia matrix includes the passive joint angle θ_2 as usual[3], then, Eq. (2) is nonintegrable. It is called second-order nonhoronomic constraint. The second principal characteristic is that this manipulator is not bound by gravity or friction, i.e., arbitrary angle become equilibrium points. However, it is not controllable by a continuous feedback. To stabilize an equilibrium point, this manipulator must be controlled by discontinuous or time variant feedback control.

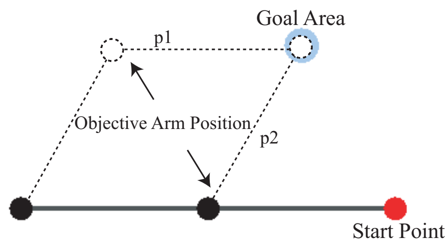

Figure 1: Environment of Learning.

2.1 Environment of Learning

In learning the task of 2PUAM called "manipulator task", the actuator installed in active joint is regarded as an agent. As shown in Fig. 1, by selecting an input torque, $\tau \in (-0.1, 0, 0.1)$ the RL agent or the subjects must drive the end effector to the goal area and bring to halt or keep between $\pm 1 (degree/s)$ angular velocity. Because of the 2PUAM's mechanism, it would be two objective positions, the upper position p_1 and the lower p_2.

3 Reinforcement Learning

At each time step $t (\in 0, 1, 2, \ldots)$, the agent observes its environmental state, $s_t \in S$ and selects an action, $a_t \in A(s_t)$. As a consequence of the action, the agent receives a scalar reinforcement signal, referred reward, $r_t \in R$. One time step later, the agent observes a new state, s_{t+1}.The aim of the agent is to maximize the expected discounted reward $E\{\sum_{t=0}^{\infty} \gamma^t r_t\}$, where γ is the discount factor. In this paper, Sarsa(λ)[5] is employed to learn estimates of optimal Q-value functions that map state-action pairs (s, a) to optimal return on the action taken in the current state.

3.1 Function Approximation

In motion learning such as manipulator, continuous state variables are dealt with. Thus, tile coding is employed[1] here. In tile coding, the receptive fields of the features are grouped into exhaustive partitions of input space. Each partition is called a tiling, and each element of the partition is called a tile. When the agent observes its environmental state s, and selects an action a, the Q-value function is calculated as

$$\mathrm{Q}(s, a) = \sum_{i,j} q_i(j, a) \phi_i^s(j) \tag{3}$$

where $i (i = 1, 2, \ldots, m)$ is the number of tiling, $j (j = 1, 2, \ldots, n)$ is the number of tile. q is the parameter vector of each tiling and ϕ is binary feature vector. If the state is inside the tile of each tiling, the corresponding feature has the value 1, otherwise the feature is 0.

3.2 Sarsa(λ)

In Sarsa(λ), on experiencing transition $< s, a, r, s', a' >$, the following updates are performed in order:

$$\eta_i(j, \bar{a}) = \begin{cases} \phi_i^s(j) & \text{for } \bar{a} = a \\ 0 & \text{for } \bar{a} \neq a \end{cases} \tag{4}$$

$$\delta = r + \gamma \mathrm{Q}(s', a') - \mathrm{Q}(s, a) \tag{5}$$

for all i and j

$$q_i(j, \bar{a}) \leftarrow q_i(j, \bar{a}) + \alpha \delta \eta_i(j, \bar{a}), \tag{6}$$
$$\eta_i(j, \bar{a}) \leftarrow \gamma \lambda \eta_i(j, \bar{a}), \tag{7}$$

where $\alpha (0 < \alpha \leq 1)$ is the learning rate, $\gamma (0 \leq \gamma \leq 1)$ is the discount factor, η is the replacing eligibility trace function, and $\lambda (0 \leq \lambda \leq 1)$ eligibility factor.

During learning, at time step t, the agent will select an action according to some strategies. In the experiments of this paper, Max-Boltzmann distribution[6] rule is employd. In Max-Boltzmann distribution, an action with maximal Q value is chosen with probability p_{max}, and an action according to the Boltzmann distribution is chosen with probability $(1 - p_{max})$. The probability of selecting action a_i in state s is

$$\mathrm{Prob}(a_i \mid s) = \frac{e^{\frac{\mathrm{Q}(s, a_i)}{T}}}{\sum_k e^{\frac{\mathrm{Q}(s, a_k)}{T}}} \tag{8}$$

where temperature T adjusts the degree of randomness of action selection.

3.3 Learning Parameters

In manipulator task, the observable parameters of the agent are the angles and angular velocities of the joints, θ_1, θ_2, $\dot{\theta}_1$, and $\dot{\theta}_2$. Thus, the state space in this task is a bounded rectangular region in four dimensions. In this environment, the state space is divided into $21\times21\times11\times11$ tiles, and 10 tilings are used. The remaining parameter of tile coding and Sarsa(λ) algorithm are $\alpha = 0.1/m$, $\lambda = 0.9$, $\tau = 0.1$, and $Q_0 = 0$. The parameter of Max-Boltzmann, p_{max} is linearly increased from 0.9 to 1.0. The constant physical parameters are; the mass of the arms, $m_1 = m_2 = 1.0$; the length, $l_1 = l_2 = 0.2$; the length from joint to the center of each arm, $r_1 = r_2 = 0.1$. The time step $t = 0.03$. The action is chosen after every one time step. A trial ends whether 10000 steps are elapsed, or the goal is reached.

4 Manual Control Experiment

Experiment of manual control is conducted with the cooperation of 5 subjects. They have no knowledge about the dynamic response. they observe the manipulator's states from visual data, and input torque $\tau \in (-0.1, 0, 0.1)$ given by a joystick. The time limit is set at 2000 steps, and the number of trial is set at 20 trials a day. The subjects do the same task for a week. In this experiment, the Q-value is recorded according to Sarsa(λ). The other details of this experiment are roughly same as RL's.

5 Experimental Results

5.1 RL Experiment

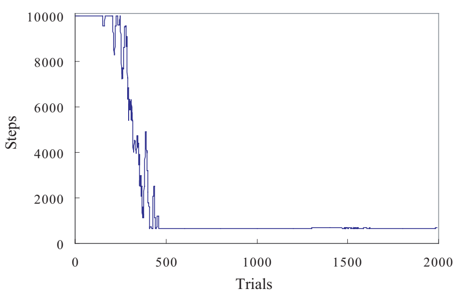

Figure 2: Result of learning by Tile Coding Sarsa(λ).

The result of RL experiment is shown in Figs. 2 and 3. In Fig. 2, the number of steps indicates how long the agent takes to achieve the goal. It is clear from Fig. 2 that the steps required to achieve the goal is reduced

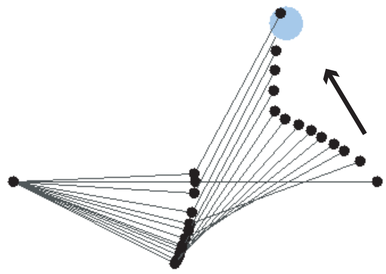

Figure 3: Motion of 2PUAM.

and converged. This result shows that it is possible to learn manipurator task by using RL algorithm. Fig. 3 shows the best trajectory acquired by RL agent. First, the agent inputs the torque crock wise (CW) in order to make angle of free joint θ_2 take the value at which the arm forms in lower objective position p_2. Then the agent manages to keep the value θ_2, and drives the end effector to the goal area with low speed.

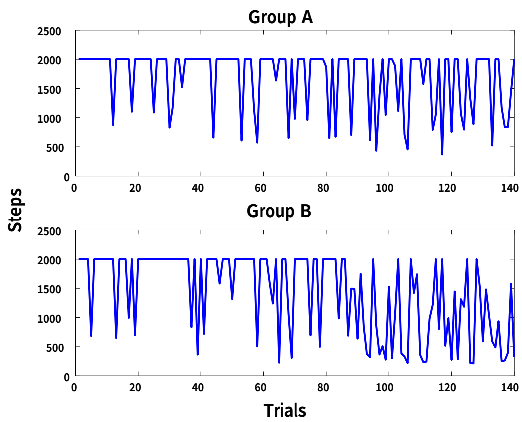

Figure 4: Result of learning by Subjects

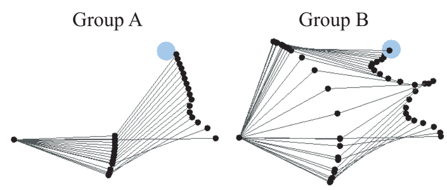

Figure 5: Motions of 2PUAM controled by Subjects.

5.2 Manual Control Experiment

From the result of Manual Control Experiment , the learning pattern of subjects is divided into Group A and Group B. Fig. 4 shows the typical learning curve

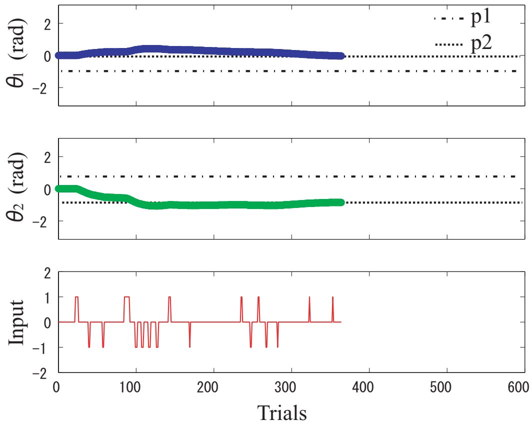

Figure 6: Input and Trajectory(Group A).

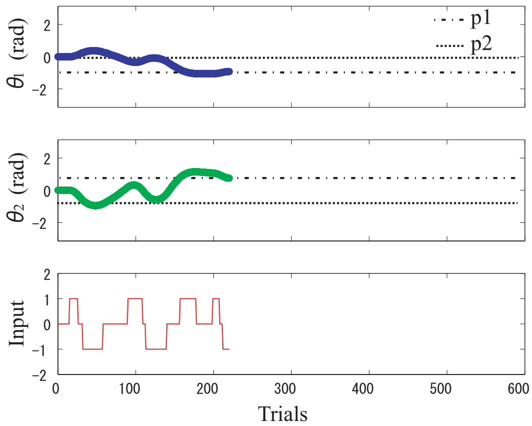

Figure 7: Input and Trajectory(Group B).

of each group. As shown in Fig. 4, each group first achieve the goal within a day. However, the failures and required steps of Group B are notably reduced from 60 to 80 trials.

Fig. 5 shows the best trajectories, and Fig. 6, Fig. 7 show the time series of each joint angle and input torque. It is clear from Fig. 5 that Group A 's is very similar to RL 's. That of Group B is also same as Group A at the beginning. However, at the end, Group B changed their policy and achieve the goal much faster than Group A.

5.3 Discussions

As the result of these experiments, some noticeable points of human learning in 2PUAM environment are found. The first is that, after once the subjects find a trajectory to the goal, such as the left side of Fig. 5, all subjects try to trace the same trajectory and achieve the goal faster by increasing input. It partly makes them possible to shorten the time passing through the trajectory. However, because of 2PUAM's mechanical property, it is impossible to slow down the angular velocity of second joint near the end of this trajectory. Therefore it causes the failure of the first approach. In this case, Group B searches another way to the goal in a way of changing the objective position, e.g., from p_2 to p_1. Therefore, the failure of Group B temporarily increases during 20 to 40 trials. In an alternating succession of such approach, they are enable to find the better trajectory like the right side of Fig. 5. In this trajectory, it is possible to decelerate each joint speed near the goal. Hence, it is thought that Group B come to achieve the goal much faster.

6 Summary

In this paper, RL approach for motion control of 2PUAM was proposed. And the associations between RL and human learning were investigated. As the result, some noticeable characteristics about human learning process were found. In particular, it was realized that the structure of human learning in 2PUAM has two processes. One is finding the trajectory to the goal, and another is shortening the time of passing through the found trajectory.

As future works, we aim to apply these characteristics into the machine learning process.

References

[1] R. S. Sutton and A. G. Barto, Reinforcement Learning: An Introduction, MIT Press, (1998).

[2] J. Yoshimoto, S. Ishii, M. Sato, Application of reinforcement learning based on on-line EM algorithm to balancing of acrobot, Systems and Computers in Japan, 32Vol. 5, 12-20, (2001).

[3] G. Oriolo and Y. Nakamura, Free-Joint Manipulators: Motion Control under Second-Order Nonholonomic Constraints, Proc. of IROS'91, 1248-1253, (1991).

[4] M. Yagai, T. Ishihara, H. Inooka, Manual Control of the Positioning of Two-link Arm with a Free Joint, SICE Tohoku chapter workshops, 206-1, (2002)(in Japanese).

[5] G. A. Rummery and M. Niranjan, On-line Q-learning using Connectionist Systems, Technical Report CUED/F-INFENG/TR 166, Engineering Department, Cambridge University, (1994).

[6] M. Wiering and J. Schmidhuber, HQ-learning, Adaptive Behavior, 6-2, 219-246, (1997).

Evolutionary Simulations based on a Robotic Approach to Emotion

Tomoko KATO Takaya ARITA
Graduate School of Information Science, Nagoya University
Furo-cho, Chikusa-ku, Nagoya 464-8601, Japan
E-mail: tomo@create.human.nagoya-u.ac.jp, arita@nagoya-u.jp

Abstract

This paper reports on the current state of our efforts to synthesize emotion in robots from a selectionist perspective in order to explore the origin and the adaptations of emotion and to realize efficient robotic systems. We have defined a minimal model of emotion in robots based on a behavioristic theory on human emotions, and have shown by conducting a robotic experiment that human beings can identify a set of basic emotions in robots. In this paper, we conduct evolutionary simulations based on the definition of emotions to verify the evolutionary adaptivity with the scenario of the origin and the evolution of human emotions in mind. The simulations show that robots are evolved to move effectively in the environments with various physical conditions by changing their emotions corresponding to the type of the condition they encounter.

Keywords: Emotion in robots, Artificial life, Behavior modulation, Evolutionary psychology

1 Introduction

The function of emotion has been studied by many researchers. Typical explanations are based on flexibility of behavior response to reinforcing signals, communications which transmit the internal states, or social bonding between individuals, which could increase fitness in the context of evolution. We believe that the possession of emotion is an adaptive "trait" also to robots, which is parallel with a selectionist view that emotion in humans is the product of adaptive evolution. The first purpose of our study is to explore the origin and the adaptations of emotion by synthesizing an emotion system "as it could be" in robots (Fig. 1). The second purpose is to realize an efficient robotic system in which robots perform tasks flexibly and effectively by using their emotional system. Although there is a possibility that our emotion system is rapidly becoming obsolete as our life environment has changed at a much faster rate than evolution, the emotion system in robots can be optimized according to given tasks by evolutionary algorithms.

We have already proposed a minimal model of emotion in robots, which is based on Dietrich Doerner's theory on human emotions described in Section 2. Also, we have shown by conducting a robotic experiment with 1000 human subjects that human beings can identify a set of basic emotions in robots synthesized based on the definition [1].

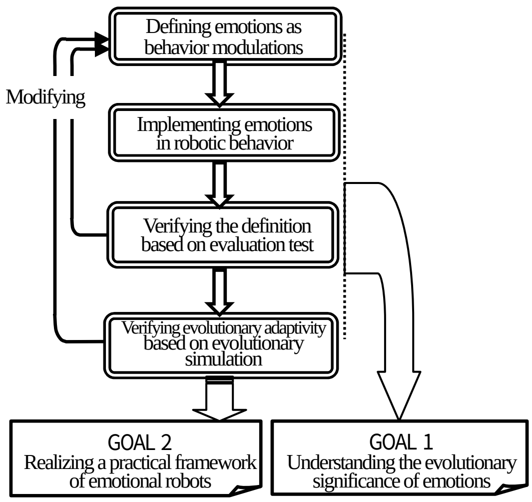

Fig. 1 Study scheme.

Based on these, this paper conducts evolutionary simulations to verify the evolutionary adaptivity with the scenario of the origin and the evolution of human emotions in mind. Each robot moves with the emotion based on 4 modulator values (activation, externality, precision and focus) from the start point to the goal point in the environments with various physical conditions like hazard, poorly-lit and so on. The fitness function is defined as the time for completing the task. In the first experiments, each individual contains modulator values directly in its genome, and is evolved in an environment with one type of conditions. In the next experiments, each robot has a simple neural network in which input is the type of conditions of the area and output is modulator values. Each individual contains the synaptic weights. Robots are evolved to move effectively by changing their emotions corresponding to the type of the area they encounter in the environment.

2 Emotions as Behavior Modulations

Our model of emotion in robots is based on the Dietrich Doerner's theory on human emotions. His claim is, in short, that emotions are seen as behavior modulations [2][3][4]. The theory identifies four different modulators that describe goal-directed behavior at any given time, activation, externality, precision and focus.

a) **Activation** indicates the amount of nonspecific activation that is involved while pursuing a goal. It has the extremes of hypoactivation (a lack of energy) and hyperactivation (a surplus of energy).

b) **Externality** indicates the proportion of time spent in external activity. It has the extremes of introversion (devoted mainly to information processing) and extroversion (devoted mainly to action).

c) **Precision** indicates how much care or precision a goal is pursued with. it has the extremes of imprecision and precision.

d) **Focus** indicates the amount of attention that is allocated to the current task rather than to the surveillance of the background. It has the extremes of broadened senses and of narrowed senses.

Following analogy [5] might help our understanding of emotions as behavior modulations. For example, a television can be adjusted for brightness, contrast and so on. These adjustments determine a "behavior modulation" for the television such as how bright, how much contrast and so on. The point here is they are all independent of the TV program actually showing. Similarly, human behavior can be modulated by emotions as behavior modulations. The volume control and so on in televisions correspond to activation, externality, precision, and focus in the emotion systems. Fig.2 shows a simple overview of this concept. Emotion system modulates behavior selected by another system (behavior generator). Each modulation pattern is associated with a particular emotion as shown in Tab. 1.

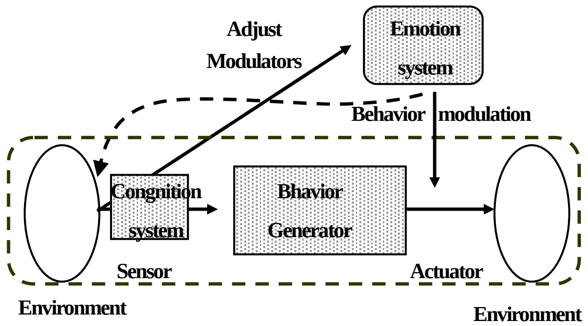

Fig. 2 An overview of the concept of behavior modulations.

We have defined following four modulators to synthesize emotional behaviors in the robot used in the simulations.

Tab. 1 Modulation patterns of six emotions [4].

	Modulation pattern in terms of modulators			
Emotion	Activation	Externality	Precision	Focus
None	0.50	0.50	0.50	0.50
Anger	1.00	1.00	0.00	1.00
Anxiety	1.00	0.00	1.00	1.00
Contentment	0.25	0.25	0.75	0.00
Excitement	0.75	0.75	0.25	0.00
Sadness	0.00	0.00	1.00	1.00

a) **Activation** indicates how long each behavior cycle is. The robot uses a certain amount of energy to move in one behavior cycle, which also depends on this modulator value.

b) **Externality** indicates how fast it moves through the path.

c) **Precision** indicates how far its sensory range to obstacles is and how often it updates the sensory information.

d) **Focus** indicates how often it deviates from the route. If it concentrates on its task, it moves to the goal directly along the route (the dashed line in Fig.4). If not, it deviates from the route. It also indicates how far its sensory range to light resources and the goal is.

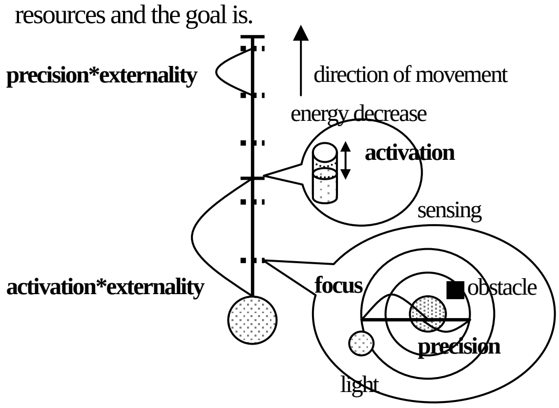

Fig. 3 Modulations of the robot behavior.

3 Evolutionary Simulations

3.1 Environmental setting

We conducted evolutionary simulations based on our definition of emotions so as to verify the evolutionary adaptivity. In the simulations, a robot moved "emotionally" from the start point to the goal point in the environments with various physical conditions [1](Fig. 4) including a hazard area (Zone A) where the robot suffers serious damage every second, a narrow path (Zone B) where it is difficult for the overly cautious robot to move through, a poorly-lighted area (Zone C) where the visual range of the robot is limited, and a light-rich area (Zone D) where the robot can fill in its energy if it finds a light source.

[1] Plain area without any particular physical conditions is also in the environment.

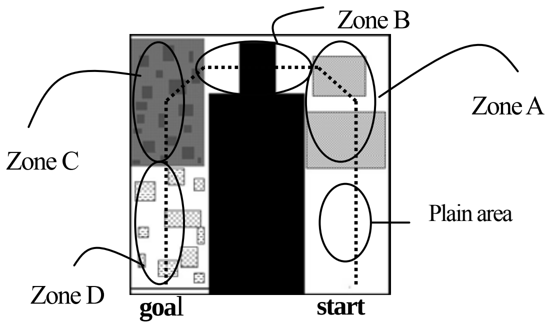

Fig. 4 An environment with various physical conditions.

3.2 Experiments with a single type of zones

Each individual contained 4 modulator values directly in its genome, and was evolved in an environment with one type of conditions by a genetic algorithm. The fitness function was defined as the level of the energy when the robot completed the task. Fig. 5-9 shows the result of the experiments. It is shown that particular modulation patterns representing the typical emotions emerged corresponding to the given environments. For example, the individuals with the anger-like modulation pattern were adaptive in the environment with a hazard area. Also, it is shown that expression of sadness and excitement in action was adaptive in the environment with poorly-lit and light-rich area respectively. Environments with a narrow path evolved the individuals expressing somewhat angry behavior.

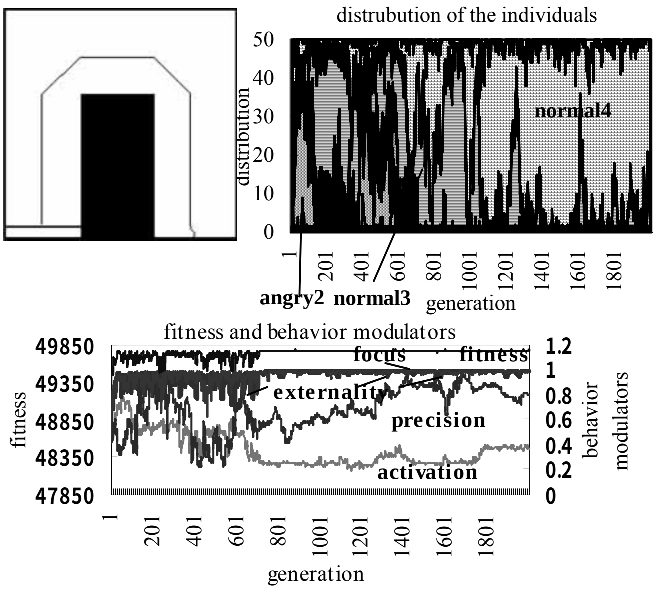

Fig. 5 The results of the simulation in the environment without any particular physical conditions: a sketch of the robot trajectories in 2000 generation (upper left), the distribution of the individuals[1] (upper right), and the average fitness and the behavior modulators of 50 individuals (lower).

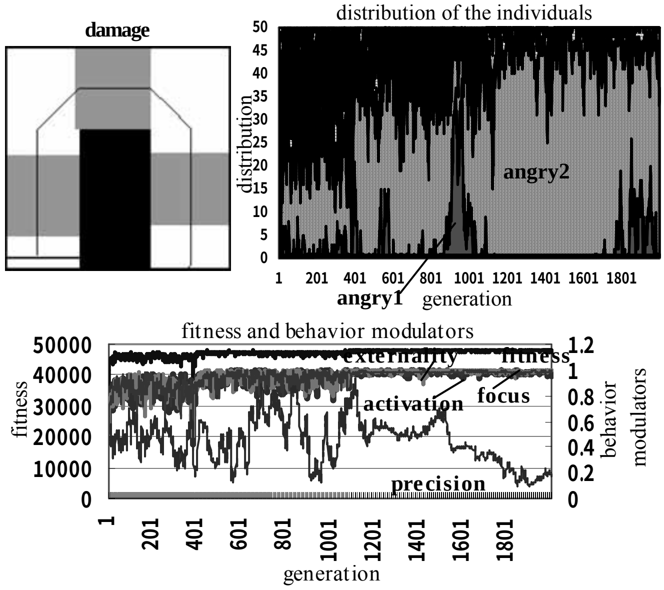

Fig. 6 The results of the simulation in a hazard area.

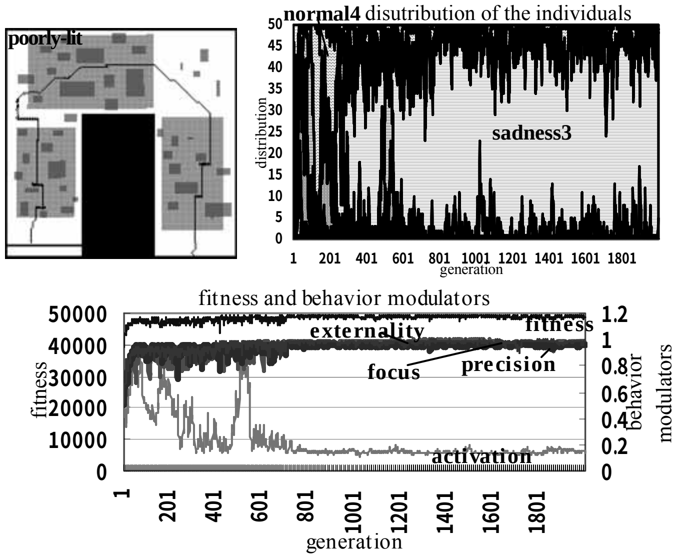

Fig. 7 The results of the simulation in a poorly-lit area.

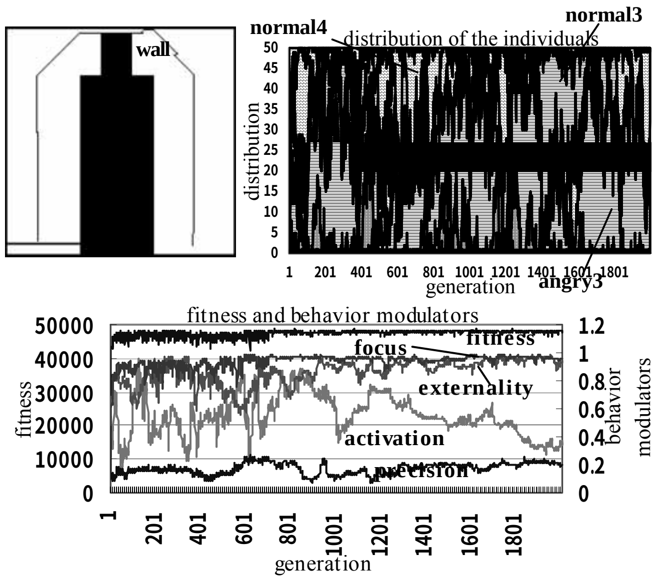

Fig. 8 The results of the simulation in the environments with a narrow path.

[1] Hamming distance between four modulators of individuals and modulation patterns of six emotions (Tab. 1) are used to classify the emotion of individuals. The smaller the suffix number is, the closer to the basic six emotions.

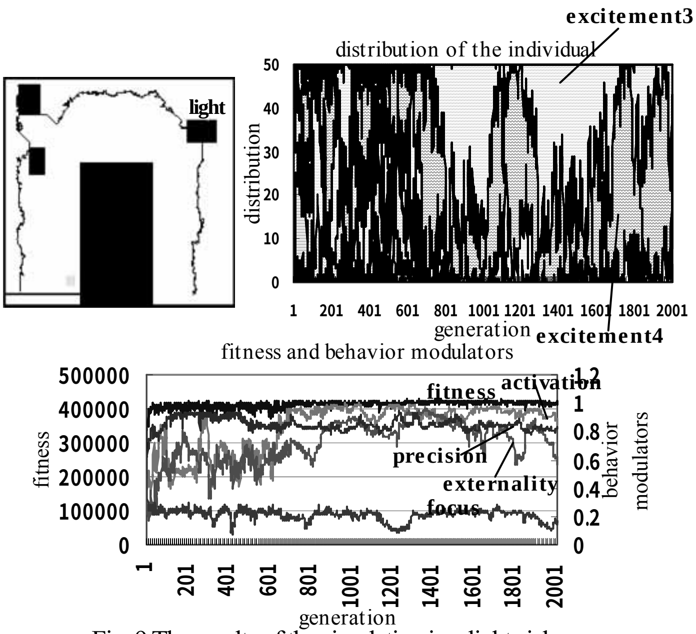

Fig. 9 The results of the simulation in a light-rich area.

3.3 Experiments with mixed types of zones

In the next experiment, the robot has a simple three-layer neural network (three input neuron, five hidden neurons and four output neurons), in which input was the explicitly expressed type of conditions of the area and the output was the modulator values. Each individual contained the synaptic weights, and evolved to move in the environment shown in Fig. 4 effectively by changing their emotions corresponding to the type of the area they were in. We also conducted another experiment using the same environment but evolving directly four modulator values as shown in 3.2 to evaluate and compare the results.

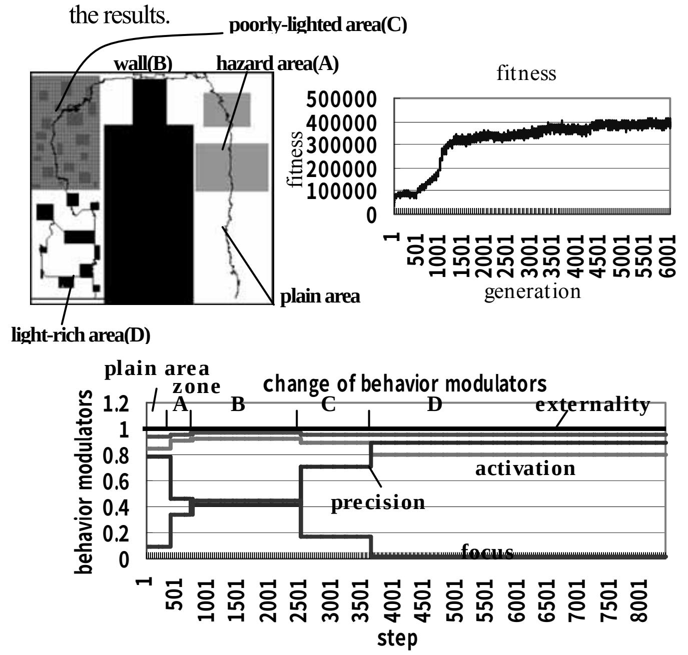

Fig. 10 The results of simulation in the environment with mixed types of physical conditions: a sketch of the robot trajectories in generation 6000 (upper left), the average fitness of 50 individuals (upper right), the change of the behavior modulators corresponding their location in generation 6000 (lower).

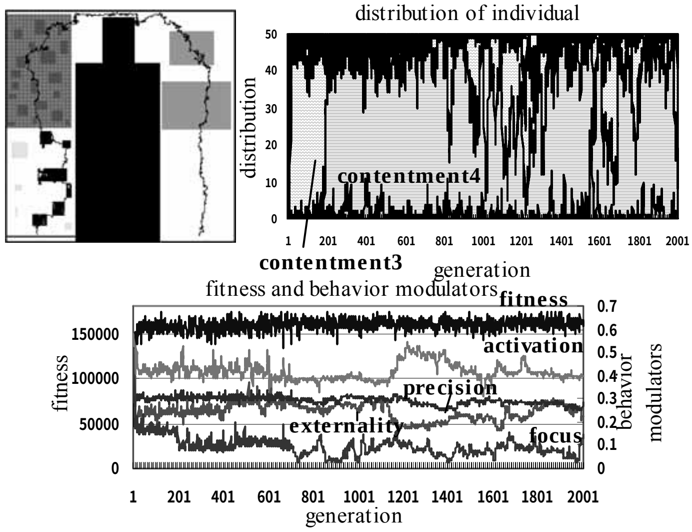

Fig.11 The results of simulation in the environment with mixed types of zones in the same setting as in 3.2.

The results of both experiments are shown in Fig. 10 and Fig. 11 respectively. We see from Fig. 10 that the robot was evolved to adjust its behavior modulators properly corresponding to the type of the area where it moved. The fitness of the robot with the evolved neural network in the last generation was $4.46*10^4$ and the fitness of the robot with evolved fixed modulator values in the last generation was $1.74*10^4$, which clearly shows the effectiveness of the robot behavior with dynamically changing its emotion corresponding to the environmental change.

4 Conclusion

We have conducted evolutionary simulations based on the definition of emotions in robots and have shown that particular modulation patterns representing the typical emotions emerged corresponding to the particular physical conditions. It has also been shown that the robot with a simple neural network moved effectively by changing their emotions corresponding to the environmental change. These results show that possession of emotion is adaptive for robots, which is parallel with a selectionist view that emotion in humans is the product of adaptive evolution. We are now conducting more practical evolutionary simulations in which robots change their emotions according to their actual sensor values and their internal states.

References

[1] Tomoko Kato and Takaya Arita, "A Robotic Approach to Emotion from a Selectionist Perspective", *Proceedings of the 8th International Symposium on Artificial Life and Robotics*, pp. 601-604, 2004.

[2] D. Doerner, H. Schaub, T. Staeudel and S. Strohschneider, "Ein system zur handlungs- regulation oder die interaktion von emotion, kognition und motivation", *Sprache & Kognition*, Vol. 4, pp. 217–232, 1988.

[3] D. Doerner and K. Hille, "Artificial souls: Motivated emotional robots", *Proceedings of the International Conference on Systems, Man and Cybernetics*, pp. 3828-3832, 1995.

[4] K. Hille, "Synthesizing Emotional Behavior in a Simple Animated Character", *Artificial Life*, Vol. 7, No. 3, pp. 303-313, 2001.

The Tenth International Symposium on Artificial Life and Robotics 2005(AROB 10th '05),
B-con Plaza, Beppu, Oita, Japan, February 4-6, 2005

Models of individuals for constructive approach to dynamic view of language and society

T. Hashimoto
hash@jaist.ac.jp

T. Sato
stakashi@jaist.ac.jp

A. Masumi
a-masumi@jaist.ac.jp

School of Knowledge Science
Japan Advanced Institute of Science and Technology (JAIST)
1-1, Tatsunokuchi, Ishikawa, Japan, 923-1292

Abstract

In order to understand dynamic nature of our world and ourselves, we propose three models of individuals that can be used in multi-agent systems for dynamic linguistic or social simulations. They are developing word-web, simple recurrent network with self-influential connection (SRN-SIC), and coupled NZ maps. We briefly summarize the architecture of these models and show some dynamic behavior in multi-agent simulations composed by these models[1].

Keywords: Developing Word-Web, Simple Recurrent Network with Self-Influential Connection (SRN-SIC), Coupled NZ Maps, Constructive Approach, Dynamic View of Language, Dynamic View of Society

1 Introduction

One of the main aims in complex systems studies including Artificial Life is to understand dynamics of our world dynamically, namely, not eliminating the essential dynamics. The theory of nonlinear dynamical systems and chaos is a useful tool for the aim. The constructive approach also has power to produce deep understanding of dynamical nature of the world[1]. This approach is a methodology to understand an objective system by constructing it and operating the system constructed. Artificial Life is originally constructive studies of biological systems. The constructive approach has expanded its applicable domains to cognitive, linguistic, and social systems. In these domains, the important step for understanding such systems constructively is to make a good model abstracting individuals engaged in cognitive/linguistic/social activities, since such systems usually consists of one or many individuals and dynamics of the systems are often induced by activities of individuals.

The dynamic view of language is to understand language as an activity of meaning creation by language users at the situation of using it such as communication. This is on the tradition of the viewpoint of language as processes insisted by Tokieda[2] and the individualistic subjectivism view of language addressed by Bakhtin[3].

The dynamic view of society conceptualizes society and social structures as dynamically changing. Blumer[4] argues that humans are subjective entities actively interacting with objects and that societies consisting of such humans are dynamically and transitionally changing. Heyek asserted the spontaneous order of society, in which individuals actively gather and develop knowledge and social structures spontaneously emerges as results of subjective actions of such individuals[5].

While such thinkings have been developed so long, the constructive approach can contribute to work out further such dynamic concepts. In order to perform the development, we need appropriate models dynamic individuals, which can be used in constructive studies. In this paper, we introduce three models of individuals developed for studying linguistic and social systems using nonlinear dynamical systems, based on the dynamic viewpoint of language and society. Analyzing features of the models and results of simulations using the models, we advocate the advantage of the models and of taking the dynamic viewpoint for understanding the cognitive, linguistic, and social systems.

2 Developing Word-Web

The first model to be introduced is the Developing Word-Web model[6], which is suited for the study

[1]Due to the space limitation, the description of the models and the results are concise. Please refer cited papers for details.

of dynamics and evolution of language[7]. It consists of a word-web, relationships among words, as individual's linguistic knowledge. The web develops through conversational interaction with other individuals. Namely, the web, implemented as a matrix, is updated by uttering and accepting a sentence. The update algorithm is a modification of a word relation calculation method proposed in corpus linguistics in order to update incrementally for using in conversation, not in corpus.

Simulating conversations between some individuals using the Developing Word-Web model, we have found that they come to acquire prototypical categorical structures, which are thought of as the important structure of categories in natural languages[8]. Figure 1 depicts a change of the relationship among words at some point in a simulated conversation. Two corresponding words, before and after accepting a sentence containing a word used in a new usage, are connected by arrows. Words form clusters as shown by circles. Since words in a cluster move in a coherence way, the whole structure does not change drastically. A word indicated by a dotted circle moves in completely different way from other words in a cluster. This word is used in a new usage. Thus, the structure can adapt to a new usage.

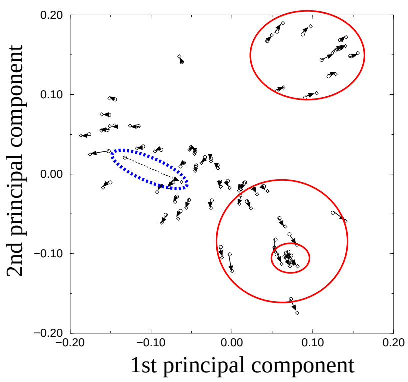

Figure 1: The dynamics of cluster structure. This is a scatter diagram of a word relationship matrix dealt with the principal coordinate analysis. The horizontal and vertical axes are the first and the second principal coordinates, respectively

This result indicates that the model shows the coexistence of stability and adaptability of a category system. Further, we have shown that the simulated language system realizes the coexistence of commonality and individuality. These features are intrinsic for mutual understanding in linguistic communication and creative development of natural language systems.

3 Simple Recurrent Network with Self-Influential Connection (SRN-SIC)

The second model is Simple Recurrent Network with Self-Influential Connection (SRN-SIC)[9], which is a modification of Elman network[10] by adding an additional recurrent connection between output and input layers (Fig. 2). The system's own past output affects its behavior through the additional connection. This is a model of an individual having internal dynamics that is indispensable to humans as cognitive systems.

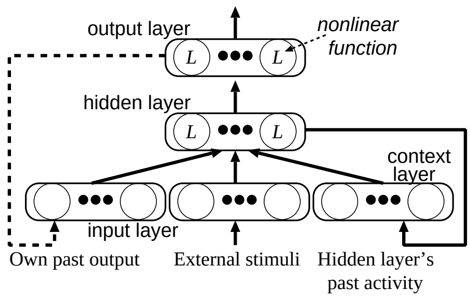

Figure 2: The basic architecture of SRN-SIC. It is a Elman-type neural network with an additional recurrent connection (dashed line) between the output and the input layers. The circles are neurons and arrows are connections.

We are engaged in a simulation of a social system consisting of individuals implemented by SRN-SIC playing the Minority Game (MG)[11] which is a many players' game in which players selecting a minority choice from two alternative choices win. The individuals play the MG continuously with given past minority side, and intermittently change their behavioral rule through learning the past time series of the minority side. Thus, this simulation is equipped with a interaction loop between micro (individuals) and macro (society) levels.

By analyzing the time series of the minority side, we observed itinerant change of dynamical state of the time series (Fig. 3). The dynamical states of the game change frequently among fixed points and various periodic cycles via aperiodic motions. It is a similar dynamics to chaotic itinerancy, a spontaneous transition among attractors[12].

This itinerant dynamics at the macro level is interpreted as a continual change of social structures, since the fact that the system with many individuals is in a low dimensional dynamical state means the system has some sort of order, that is, structurized.

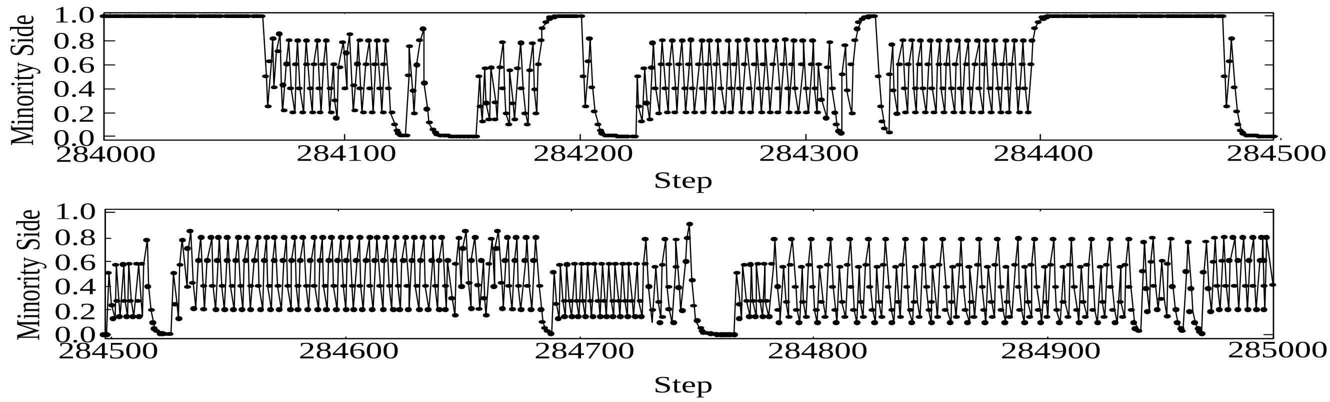

Figure 3: An example of itinerant dynamics at the macro level between learning. The horizontal and the vertical axes are the time steps and the minority sides converted to real numbers, respectively.

4 Coupled NZ Maps

The third model is a coupled chaotic maps, called NZ map[13]. The map changes its function shape and dynamical state by changing a parameter (Fig. 4). The coupled system change autonomously the parameter of each map. This dynamic change of functions induce dynamic behavior of the coupled system. It is known that the system shows chaotic itinerancy. This model of an individual also reflects the dynamic perspective of cognitive system[14, 15].

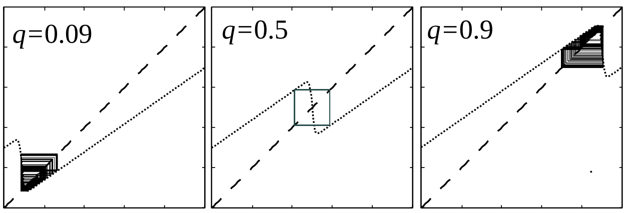

Figure 4: The change of the shape of maps and dynamics of a NZ map for different values of a parameter. Each box shows a unit interval, the horizontal and vertical axes are the value of a variable at time t and $t+1$, respectively. The dotted and the solid lines shows the shape and the dynamics of the map, respectively.

This model is used for modeling symbol formation[16]. In this model, symbols are represented with attractors and manipulation rules of symbols by transition among attractors. We can embed some orthogonal patterns into the system. We have confirmed that this system shows a transition among the patterns according to input sequences(5). This means that the model may show two important feature of symbols, representing something and manipulated in accordance with some rules. Although an order in the transition among the attractors, representing rule of symbol manipulation, is not found, the model has a potential to represent a process of symbol formation.

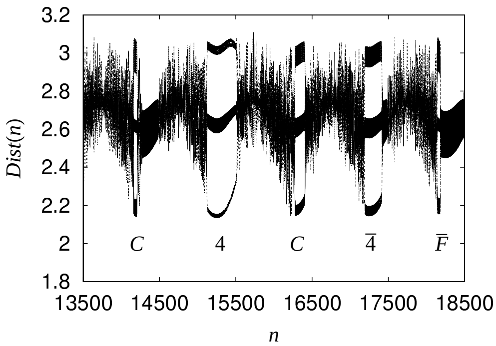

Figure 5: Transition among embedded attractors. The horizontal axis is time step. The vertical axis is a distance measure from embedded patters. A sinusoidal input sequence is given. When the orbits stay at a pattern, it is labeled. The labels $C, F, 4$ are embedded patterns and $\bar{C}, \bar{F}, \bar{4}$ are their reversed patterns.

5 Conclusion

We have introduced three models of dynamic individuals. Each model and multi-agent system consisting of the models show dynamic behavior such as: category formation and its change by Developing Word-Web model, dynamics of social structure by SRN-SIC, and transition among embedded patterns induced by external inputs by the coupled NZ maps. We insist that these models can be used for progressing the dynamic view of language and society.

The importance of dynamic nature of humans as cognitive systems are recently recognized[14, 15]. Several mathematical and computational models have been proposed. This paper summarize our effort, especially for understanding the dynamics of linguistic and social systems.

Fukaya and Tanaka studies sense-making process, which shares the dynamic view of language, through observations of conversations and other communicational activities[17]. Although Developing Word-Web model is not enough for a complete model of the sense-making process, the constructive study using the model can develop the dynamic view of language[6]. Actually, we are studying the evolution of language[7], especially the evolution of lexical (categorical) structure, using this model.

Shiozawa advocated that the micro-micro loop is a key notion to understand the dynamics of social structure [18]. However, no effective actual simulation models has been proposed to implement both the loop and individuals acting in such dynamic loop. We can construct a dynamic social simulation using SRN-SIC and show that the micro-macro loop actually plays an important role to form and maintain the dynamics of social structures[19].

Acknowledgements

This research is supported by the following grants: Canon Foundation Europe Fellowship; a Grant-in-Aid for Scientific Research (No.12780269 and No.15700183) from the Ministry of Education, Culture, Sports, Science and Technology of Japan and by the Japan Society for the Promotion of Science; and JAIST research grant (grant for in-house research projects).

References

[1] K. Kaneko and I. Tsuda, "Constructive complexity and artificial reality: an introduction, *Physica D*, **75**, 1–10, 1994.

[2] M. Tokieda, *Kokugo-gaku Genron (The Principles of Japanese Linguistics)*(in Japanese), Iwanami Shoten, 1941.

[3] V. N. Vološinov, *Marxism and Philosophy of Language*, Harvard University Press, 1986.

[4] H. G. Blumer, *Symbolic Interactionism: Perspective and Method*, Prentice-Hall, 1969.

[5] J. Gray, *Hayek on Liberty*, Basil Blackwell, 1984.

[6] T. Hashimoto, " The constructive approach to the dynamical view of language", A. Cangelosi and D. Parisi (Eds.), *Simulating the Evolution of Language*, Springer, pp.307–324, 2002.

[7] T. Hashimoto, "What is problem of language evolution? – from constructive perspective" (in Japanese), *The Proceedings of 18th Annual Meeting of Japanese Society of Artificial Intelligence*, 2004.

[8] J. R. Taylor, *Linguistic Categorization – Prototypes in Linguistic Theory*, Oxford University Press, 1995.

[9] T. Sato and T. Hashimoto, "Dynamic social simulation with multi-agents having internal dynamics", *New Frontiers in Artificial Intelligence*, Springer, 2005 (in prinitng).

[10] J. L. Elman, "Finding structure in time", *Cognitive Science*, **14**(2), 179–211, 1990.

[11] D. Challet and Y. C. Zhang, "Emergence of cooperation and organization in an evolutionary game", *Physica A*, **246**, 407–418, 1997.

[12] K. Kaneko and I. Tsuda, "Chaotic itinerancy", *Chaos*, **13**(3), 926–936, 2003.

[13] H. Nozawa, "A neural network model as a globally coupled map and applicatoins based on chaos", *Chaos* **2** (3), 377–386, 1992.

[14] T. van Gelder, "The dynamical hypothesis in cognitive science", *Behavioral and Brain Sciences* **21**, 615–665, 1998.

[15] I. Tsuda, "Toward an interpretation of dynamic neural activity in terms of chaotic dynamical systems", *Behavioral and Brain Sciences*, **24**(5), 793–847, 2001.

[16] T. Hashimoto and A. Masumi, "Learning and transition of symbols in chaotic dynamical system: toward dynamical model of symbolic individual", *The Proceedings of 2nd. International Symposium on Emergence and Evolution of Linguistic Communication*, 2005 (forth coming).

[17] M. Fukaya and S. Tanaka, *Kotoba no ⟨Imiduke-ron⟩ (A Theory of ⟨Sence-Making⟩ of Language)* (in Japanese), Kinokuniya Shoten, 1996.

[18] Y. Shiozawa, *Fukuzatsusa no Kiketsu (Consequences of Complexity)* (in Japanese), NTT Shuppan, 1997.

[19] T. Sato and T. Hashimoto, "Dynamic social simulation with multi-agents having internal dynamics", submitted to *Artificial Life.*

The Tenth International Symposium on Artificial Life and Robotics 2005(AROB 10th '05),
B-con Plaza, Beppu, Oita, Japan, February 4-6, 2005

Grasping the Distributed Entirety

Peter Sapaty [1] Masanori Sugisaka [2] Nikolay Mirenkov [1] Minetada Osano [1] Robert Finkelstein [3]

[1] University of Aizu
Aizu-Wakamatsu, Fukushima-ken 965-8580 Japan
+ 81-242-37-2604, + 81-242-37-2553 (fax)
{ sapaty, nikmir, osano}@u-aizu.ac.jp

[2] Oita University
700 Oaza Dannoharu, 870-1192 Japan
+ 81-97-554-7831, + 81-97-554-7841 (fax)
msugi@cc.oita-u.ac.jp

[3] Robotic Technology Inc.
11424 Palatine Drive, Potomac, Maryland 20854
+ 1-301-983-4194, + 1-301-983-3921 (fax)
RobertFinkelstein@compuserve.com

Abstract. A flexible WAVE-WP ideology and technology, aimed at creation of new and penetration into other distributed systems of different natures and at different levels, are described. Supported by a high-level spatial programming language, the technology allows us to grasp large distributed systems as a whole, study and manage their behavior, and direct evolution. Programming examples combining swarm behavior of an unmanned group with a hierarchical command and control are presented, providing integrity, flexibility, and openness within the same solution. Other application areas of the paradigm are discussed too.

Keywords: parallel distributed processing, spatial navigation, WAVE-WP language, cooperative robotics, swarm behavior, distributed command and control, open systems, over-operability.

1 Introduction

To understand the mental state of a handicapped person, of what the life and soul really mean, problems of economy and ecology, or how to win market or battlefield, we must consider the system as a whole – not just as a collection of parts. The situation complicates dramatically if the systems are dynamic and open, spread over territories, comprise unsafe or changing components, and cannot be observed in their entirety from a single point.

Usually the whole can be comprehended and decisions made only by a single human brain -- that is why we still have queens, kings, presidents, prime-ministers and commanders-in-chief. However, due to physical limitations, the brain cannot perceive the entire system in detail, and uses simplifications. Hierarchical systems are common too, where decisions on different levels are made by single brains on restricted information, with averaging and abstracting on higher levels. This is usually inherited by automatic systems using computers and computer networks mimicking human hierarchies. The hierarchical systems with predetermined partitioning onto levels often become static and clumsy, and may not operate efficiently in changeable environments.

In this paper, as an alternative to existing manned or unmanned control systems, we are describing flexible WAVE-WP (or World Processing) ideology and technology aimed at creating new or penetrating other systems and their organizations. Supported by a high-level spatial programming language, WAVE-WP allows us to grasp large systems as a whole, study their behavior and direct evolution in the way required. On the implementation layer, the technology widely uses self-spreading mobile cooperative program code dynamically covering and matching distributed systems. This often allows us to get solutions orders of magnitude more compact than by other approaches. The internal system organization, including partitioning into components and specific command and control, can be a function of the environment and the mission scenario in WAVE-WP; it may change at runtime while preserving the overall system operability and goal orientation.

Practical applications (with code examples) will be presented in relation to collective behavior of a robotic group, which integrates a swarm-based movement with hierarchical command and control.

The proposed approach allows us to grasp and manage the integrity and wholeness of large dynamic systems in highly parallel and fully distributed mode, often contrary to the human experience, also to the systems modeling human behavior, with a real potential to outperform them.

2 The WAVE-WP Spatial Automaton

The WAVE-WP automaton [1,2,3] effectively inherits the integrity of traditional sequential programming over localized memory, but for working now with the real distributed world, while allowing its parallel navigation in an active pattern flow and matching mode, as a single spatial process. The automaton may start from any point of the distributed world to be controlled, dynamically covering its parts or the whole, and mounting of a variety of parallel and distributed knowledge and control infrastructures. Implanting distributed "soul" into the system organization, the automaton increases system's integrity, capability of pursuing local and global goals, assessing distributed situations, making autonomous decisions, and recovering from indiscriminate damages. Many spatially cooperating or competing parallel WAVE-WP automata may evolve on the same system body serving, say, as deliberative, reactive, and/or reflective spatial processes.

One of the distinguishing features of WAVE-WP is the representation of distributed worlds it operates in. *Physical world* (or PW) is continuous and infinite in WAVE-WP. Existing at any its point, and possibly performing a job, is considered as residing in a *node* having physical coordinates. Such a node, reflecting only occupancy at the point, vanishes with the termination of all occupancies in it. *Virtual world* (or VW) is discrete and interlinked in WAVE-WP, being represented similar to WAVE [4] by a distributed Knowledge Network (KN). Its persistent nodes may contain established concepts or facts, and (also persistent) links (oriented and non-oriented, connecting the nodes) may reflect different relations between the nodes.

The same model can also operate with the *united (or PVW) world*, in which any element may have features of the both worlds. A variety of effective access mechanisms to nodes, links and their groups, say, by physical coordinates, electronic addresses, by names, via traversing links, etc. (classified as *tunnel* and *surface* navigation) abound in the model, using both selective and broadcasting access modes.

Solutions of any problems in this formalized world in WAVE-WP are represented as its coordinated parallel *navigation* (or *exploration*, *invasion*, *grasping*, *coverage*, *flooding*, *conquest*, etc.) by some higher-level forces, or *waves* [2,4] These bring local operations, control and transitional data directly into the needed points of the world. The obtained results, together with the same or other operations may invade the other world parts, and so on.

During the world navigation, which may be loose and free or strictly (both hierarchically and horizontally) controlled, waves can modify the very world they evolve in and move through, as well as create it from scratch (including any distributed structures and topologies). Waves may also settle persistent cooperative processes in world's different points, subsequently influencing its further development and evolution in the way required.

3 WAVE-WP Language

The system language expressing full details of this new control automaton has been developed. Having recursive space-navigating and space-penetrating nature, it can operate with both information and physical matter. The language can also be used as a traditional one, so no integration with (and/or interfaces to) other programming models and systems may be needed for solving complex distributed knowledge processing and control problems.

Very compact syntax of the language, as shown in Fig.1, see also [1,2], makes it particularly suitable for direct interpretation in distributed environments, being supported by effective program code mobility in computer networks.

wave	→	{ *advance* ; }
advance	→	{ *move* , }
move	→	*constant* | *variable* | { *move act* } | [*rule*] (*wave*)
constant	→	*information* | *physical-matter*
variable	→	*nodal* | *frontal* | *environmental*
act	→	*flow-act* | *fusion-act*
rule	→	*forward-rule* | *echo-rule*

Fig.1. Syntax of WAVE-WP language.

In this description, braces set up zero or more repetitions of a construct with a delimiter at its right; square brackets identify an optional construct; semicolon allows for sequential, while comma for parallel invocation of program parts; and parentheses are used for structuring of WAVE-WP programs (or *waves*). Successive program parts, or *advances*, develop from all nodes of the set of nodes reached (SNR) by the previous advance, whereas parallel or independent parts, *moves*, constituting the advances, develop from the same nodes, while splitting processes and adding their own SNRs to the resultant SNR of the advance.

Elementary *acts* represent data processing, hops in both physical and virtual spaces, and local control. *Rules* establish non-local constraints and contexts over space-evolving waves like, for example, the ability to create networks, also allowing WAVE-WP to be used as a conventional language. *Variables*, called *spatial* (as being dynamically scattered in space), can be of the three types: *nodal*, associated with virtual or physical nodes and shared by different waves; *frontal*, propagating with waves as their sole property; and *environmental*, accessing elements of internal and external environments navigated by waves.

This recursive navigational structure of the language allows us to express highly parallel and fully decentralized, albeit strongly controlled and coordinated, operations in distributed worlds in a most compact way – in the form of integral space processing and transformation formulae. These resemble data processing expressions of traditional programming languages, but can now *operate in and process the whole distributed world*.

4 Implementation Basics

On the implementation layer, the automaton widely uses high-level mobile cooperative program code self-spreading and replicating in networks, and can be easily implemented on any existing software or hardware platform. As the automaton can describe direct movement and processing in physical world, its implementation may need to involve multiple mobile hardware, with or without human participation. A network of (hardware or software) communicating WAVE-WP language interpreters (or WIs), which can be mobile if installed in manned or unmanned vehicles, should be embedded into the distributed world to be controlled, in most sensitive points, see Fig. 2.

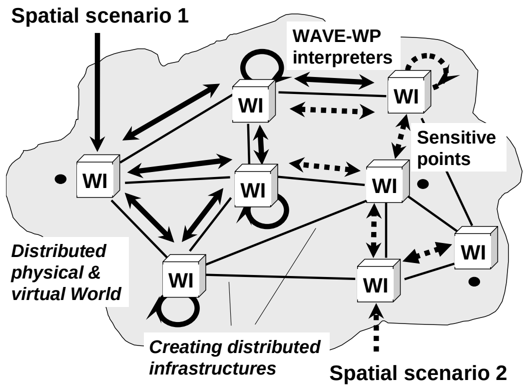

Fig.2. A network of WAVE-WP interpreters.

During the spatial execution of system scenarios in WAVE-WP, individual interpreters can make local information and physical matter processing, as well as physical movement in space. They can also partition, modify and replicate program code, sending it to other interpreters (along with local transitional data), dynamically forming *track-based distributed interpretation infrastructures*.

The automaton can exploit other systems as computational and control resources too, with or without preliminary consent, i.e. in a (remotely controlled) virus-like mode. For example, many existing network attacks (especially DDoS) may be considered as a possible malicious, simplified and degenerated implementation of the automaton. WAVE-WP can also effectively integrate with other advanced systems managing distributed resources, like, for example, J-UCAS [5], within their orientation on rescue and crisis relief missions.

5 Programming Example: Integration of Swarm Behavior with Distributed Command and Control

Effective integration of swarm behavior [6] with strict command and control for robotic teams may help fulfill complex objectives and survive in dynamic environments.

Different forms of group behavior can coexist within WAVE-WP model of parallel and distributed processing and control. Written in a higher-level spatial language, with considerable code reduction, the combined system scenarios can start from any component, covering at runtime the whole system that may be dynamic and open.

A distributed organization has been programmed which, for example, makes all units of a scout platoon move in a swarm, but at the same time regularly redefining the topologically central unit and creating a fresh, most efficient, neighborhood-based hierarchical infrastructure covering all units. It fuses targets seen by the units, distributing them back to all units for an individual selection and impact.

We will consider here only some very simplified examples of the WAVE-WP code expressing different distributed operations of the platoon, along with their unity.

5.1 Swarm Movement

The initial, casual, distribution of mobile units in space may be as shown in Fig. 3. The simple program below activates all units in the group (say, unmanned scout platoon), making them move in a swarm.

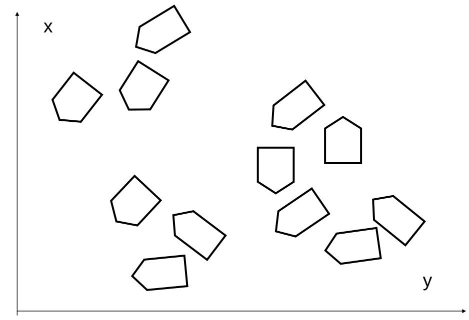

Fig. 3. Distributed group of mobile units: initial order.

Each unit randomly chooses next step within a given global direction, if the planned new position is not too close to other units, otherwise the next step is being redefined unless a suitable move is found. The program (let us call it ***swarm-move***) may start from any node, making all units fully autonomous and independent, and communicating only locally with other units:

```
Flimits = (dx0_dy-2, dx8_dy5);
Frange = r5; direct # all;
repeat(
  [Fshift = Flimits ? random;
   (direct # Fshift;
    direct ## Frange)== nil;
   WHERE += Fshift
  ];
)
```

A possible snapshot of the group during the work of this distributed program is shown in Fig. 4.

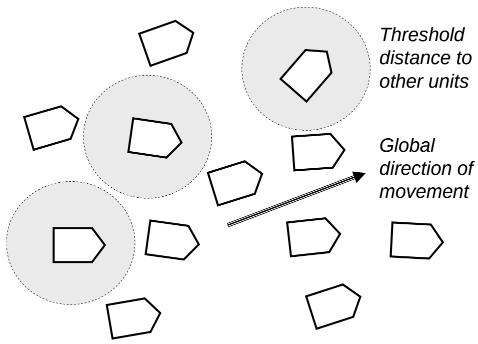

Fig. 4. Moving in a swarm with a threshold distance between units.

5.2 Finding Topologically Central Unit

Let us consider now the finding of a topologically central unit of the group for a certain moment of time (as the units may be constantly moving and changing positions to each other). Starting from *any* unit, this can be done by the following program (calling it ***find-center***):

```
Faver = average(direct # all; WHERE);
Ncenter =
  min(
   direct # all;
   (Faver, WHERE) ? distance _ ADDRESS
  ) : 2
```

5.3 Creating a Hierarchical Infrastructure

Let us create a hierarchical infrastructure starting from the central unit found and covering all other units. It can be most efficient if based on a physical neighborhood principle, with the next layer nodes lying from a current node, say, within a certain physical range. This can be accomplished by the following program (calling it ***infra-build***):

```
Frange = r20;
repeat(
 direct ## Frange;
 grasp(
  (all #) == nil; [create(-infra # BACK)]
 )
)
```

An example of such an infrastructure built over a swarm of Fig. 4 is shown in Fig. 5.

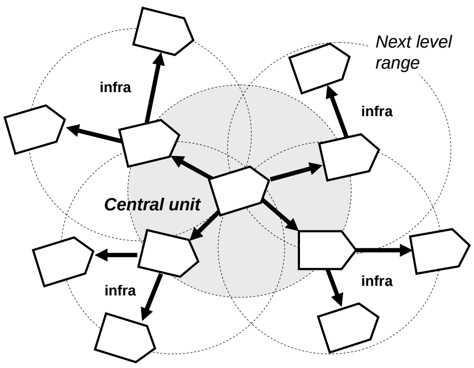

Fig. 5. Creating a neighborhood-based infrastructure from the most central unit.

Such an infrastructure can be effectively used for different purposes within the distributed command and control, with a possible one discussed below.

5.4 Hierarchical Fusion and Distribution of Targets

Starting from the same root node, the created hierarchical infrastructure can be repeatedly used for collecting targets discovered by the sensors of all units (ascending the hierarchy in parallel), with subsequent distribution of the collected list of targets back to all the units (descending the hierarchy, in parallel too, with the target list replicated in nodes). The units may be allowed to choose suitable targets individually, impacting them by the available means. All this can be achieved by the following spatially-recursive program (named ***collect-distribute***):

```
F1={(+infra#; ^F1), ?detect};
F2={(+infra#; ^F2), Fseen?selectImpact};
repeat([Fseen=(^F1); Fseen!=nil; ^F2])
```

The work of this program is explained in Fig. 6.

5.5 The Combined Scenario

All these programs can be effectively combined within a single scenario, with the center constantly migrating when units move in the swarm, and a new hierarchical infrastructure being rebuilt each time and frequently used for parallel and distributed vision and impacting targets.

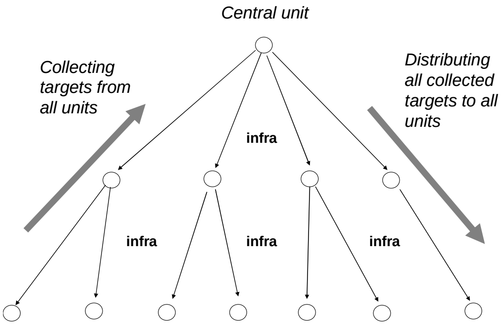

Fig. 6. Hierarchical fusion and distribution of targets.

To achieve this, we will also need removing of the previous infrastructure each time before creating of a new one from, possibly, a new central unit, which can be easily done by the following program (symbolically called ***infra-remove***):

```
direct # all; all #; LINK = nil
```

The united program, combining all the previous programs within a single distributed scenario, which can originally be injected from any mobile unit, will be as follows.

```
swarm-move,
repeat(
  find-center; direct # Ncenter;
  [infra-remove]; [infra-build];
  orparallel(
    collect-distribute,
    TIME += 300
  )
)
```

The named constituent programs, discussed before, can participate in it directly by their full texts, or by calls to them if represented as procedures. The program allows the regularly updated infrastructure to be used for fusing-distributing targets for some period of time (here 300 sec.), after which it finds the topologically central unit and new infrastructure from it again, after removing the previous infrastructure, and so on. All units continue moving in a swarm (with the details given before) independently of the infrastructure updating, targets collecting, distributing, and impacting processes.

As can be seen from the programming examples above, WAVE-WP is a completely different language from conventional terms, allowing us to express complex operations and control directly in distributed dynamic spaces, with programs often orders of magnitude more compact than in other known languages.

6 Other WAVE-WP Applications

The technology has numerous practical applications in other areas too, summarized in [1-4]. Some exemplary projects are as follows.

- *Distributed knowledge representation and processing.* Dynamically creating arbitrary knowledge networks in distributed spaces, which can be modified at runtime, WAVE-WP can implement any knowledge processing and control systems in parallel and fully distributed way. A program package had been developed for basic problems of the graph and network theory, where each graph node could reside on a separate computer.
- *Operating in physical world under the guidance of virtual world.* Operating in the unity of physical and virtual worlds, the WAVE-WP model can effectively investigate physical worlds and create their reflection in the form of distributed virtual worlds. The latter can guide further movement and search in the distributed PW, and so on.
- *Intelligent network management.* Integrating traditional network management tools and systems, and dynamically extracting higher-level knowledge from raw data via them, WAVE-WP establishes a higher, intelligent layer allowing us to analyze varying network topologies, regulate network load and redirect traffic in case of line failures or congestions. It also can be used for essentially new, universal and intelligent network protocols.
- *Advanced crisis reaction forces.* Smaller, dynamic armies, with dramatically increased mobility and lethality, represent nowadays the main direction in the development of advanced crisis reaction forces, which may effectively use multiple unmanned units. The WAVE-WP technology can quickly assemble a highly operational battle force from dissimilar (possibly casual) units, setting intelligent command and control infrastructures over them.
- *Distributed road and air traffic management.* Distributed computer networks working in WAVE-WP, covering the space to be controlled, can be efficiently used for both road and air traffic management. The model provides simultaneous tracking of multiple objects in PW by mobile intelligence spreading in VW, via computer networks.
- *Autonomous distributed cognitive systems.* While cognitive systems include reactive and deliberative processes, they also incorporate mechanisms for self-reflection and adaptive self-modification. The WAVE-WP paradigm allows for the description of interacting deliberative, reactive, and reflective processes on a semantic level, representing the whole mission rather than individual robots. This provides new, important degrees of freedom for autonomous robotic teams.
- *Distributed interactive simulation.* The technology allows for highly efficient, scalable distributed simulation of complex dynamic systems, like battlefields, in open computer networks. Due to full distribution of the simulated space and entities operating in it, there is no need to broadcast changes in terrain or positions of entities to other computers, as usual. Each entity operates in its own part of the simulated world, communicating locally with other entities. Entities can move freely through the simulated space (and between computers) if needed.
- *Intelligent global defense and security infrastructures.* WAVE-WP can also be used in a much broader scale, especially for the creation of intelligent international infrastructures widely using automated and fully automatic control and advanced robotics. The global system may effectively solve problems of distributed air defense, where multiple hostile objects penetrating the air space can be simultaneously discovered, chased, analyzed, and destroyed using computerized radar networks as a collective brain.

7 Conclusions

The WAVE-WP technology allows for a more rational and universal integration, management and simulation of large complex systems. This is being achieved by establishing a higher level of their vision and coordination, symbolically called "over-operability" [2] versus (and in supplement) to the traditional "interoperability".

Distributed system creation and coordination scenarios in WAVE-WP are often orders of magnitude simpler and more compact than usual, due to high level and spatial nature of the model and language.

This helps us to effectively grasp and manage large, dynamic and open systems and solutions in them as a whole, often avoiding tedious partitioning into pieces (agents) and setting their communication and synchronization.

These and other routines are effectively shifted to the automatic implementation by dynamic networks of WAVE-WP interpreters. Traditional software or hardware agents may have sense within this approach only when required, during the spatial development of parallel system scenarios.

A detailed description of the WAVE-WP model and its extended applications can soon be available from [7].

References

[1] P. Sapaty, N. Mirenkov, M. Sugisaka, and M. Osano, "Distributed Artificial Life Using World Processing Technology", Proc. of the Fifth Int. Conference on Human and Computer (HC-2004), September 1-3, 2004, The University of Aizu, Japan, 2004.

[2] P. S. Sapaty, "Over-Operability in Distributed Simulation and Control", The MSIAC's M&S Journal Online, Winter 2002 Issue, Volume 4, No. 2, Alexandria, VA, http://www.msiac.dmso.mil/journal/WI03/sap42_1.html.

[3] P. Sapaty, M. Sugisaka, "WAVE-WP (World Processing) Technology", Proc. 1st International Conference on Informatics in Control, Automation and Robotics, 25-28 August 2004, Setubal, Portugal.

[4] P. S. Sapaty, "Mobile Processing in Distributed and Open Environments", John Wiley & Sons, ISBN: 0471195723, New York, February 1999, 436 p.

[5] "Joint Unmanned Combat Air Systems (J-UCAS)", www.darpa.mil.

[6] R. Finkelstein, "Swarm Intelligence: Application to the 4/DRCS and the Scout Platoon Mission", White Paper, Robotic Technology Inc., USA, 2004.

[7] P. S. Sapaty, "Ruling Distributed Dynamic Worlds", John Wiley & Sons, ISBN: 0471655759, New York, June 2005, 256p., www.wiley.com.

The Tenth International Symposium on Artificial Life and Robotics 2005(AROB 10th '05),
B-con Plaza, Beppu, Oita, Japan, February 4-6, 2005

Motion control of biped robot bending the knee

Koji Umezaki　Masanori Sugisaka

Dept. of Electrical and Electronic Engineering, Oita University.
700 Dannoharu Oita 870-1192 Japan.
E-mail:msugi@cc.oita-u.ac.jp

Abstract

In this research, it experiment about the stable walk by leveling by a static walk. The robot manufactured this is the biped robot without the portion of the upper half of the body, such as an arm, of only a lower half of the body.

Then, walk operation using center of gravity movement with a crotch and an ankle was created, and angle change of the servomotor in this mechanism on either side was compared. The large step and walk was able to be obtained by carried out moveable of the knee this time.

A future problem is to raise the biped robot's stability from now on, and to enable it to perform various operation.

1. Introduction

In these years, the humanoid robot which can harmonize with a life of human attracts attention many biped robots are studied developed. Those many think entertainment nature as important. In future it live together and cooperates with human in activity of human's ever day, and it is thought that the demand of a robot with the practicality which can perform work and support increases.

In this research, in order to perform a walk on step or slope, it amide at performing walk motion which separated the leg from the floor certainly.

The walk preformed this is static walk. With static walk, it progresses in front little by little, maintaining "static balance" in every moment. Therefore, in static walk even if it stops walk operation on the way it is possible to maintain balance and to continue stopping at a state as it is. On the other hand, dynamic walk carries out maintaining "dynamic balance" on the assumption that it moves. If dynamic walk is stopped during walk operation for movement which will be the requisite, balance will be broken down and it will fall.

2. Structure of biped robot

2. 1 Specific of biped robot

Size and degree of freedom of biped robot are shown in a Table1.

Table1　Specific and degree of freedom

size	height449[mm]×width 200[mm] ×length 120[mm]
degree of freedom	hip joint 3×2 knee joint 1×2 ankle joint 2×2　(Total 12)

2. 2 Structure and system of biped robot

The biped robot manufactured for the first time at this laboratory had attached the upper half of the body. However, load was applied and damaged to the servomotor of knee joints for weight. Then, biped robot which removed fixation of knee joint was manufactured last year. However, in order to mitigate the burden of a knee joint, the upper half of the body is removed.

The biped robot manufactured this time is shown in Fig.1.

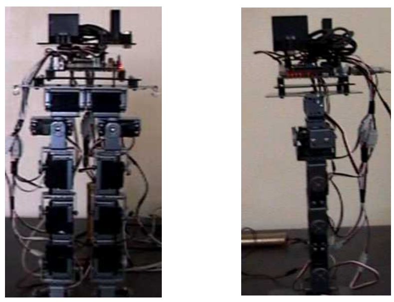

Fig.1　Photograph of developed robot

The Tenth International Symposium on Artificial Life and Robotics 2005(AROB 10th '05),
B-con Plaza, Beppu, Oita, Japan, February 4-6, 2005

3. Experiment of walking cycle

3. 1 The experiment method

The motion which a robot is made to perform was created using the manufactured biped robot. In creation to each servomotor was determined by trial and error. The flow of motion creation is shown in Fig.2.

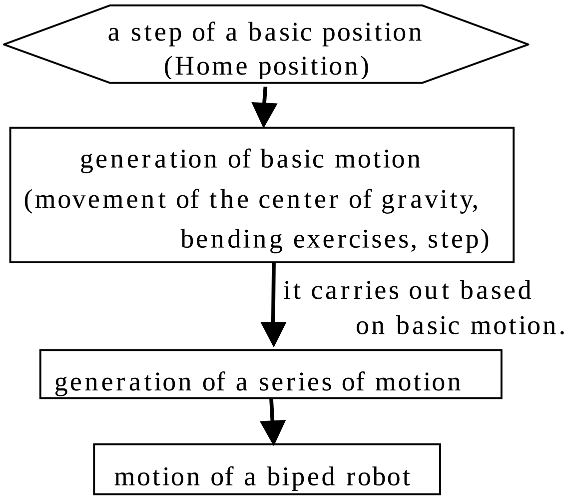

Fig.2 The creation of the motion

3. 2 Walk operation of biped robot

The rate of double stance phase and single stance phase in a biped robot's walking cycle is shown in Table2. Angle change of the instruction value of the servomotor of each joint is shown in Fig.3.

Double stance phase is a period which stands both legs, arriving at the ground and switches a leg. Moreover, single stance phase is a period which stands by one leg and carries idling leg in front from back.

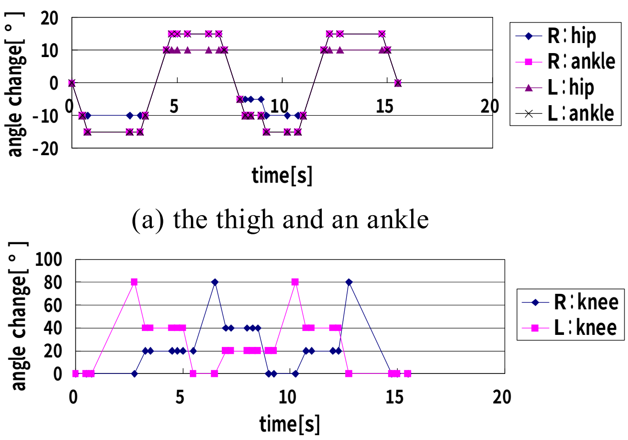

(a) the thigh and an ankle

(b) a knee

Fig.3 Servomotors value of each joints

Table2 Robot walking cycle

double stance phase	37%
single stance phase	63%

Fig.3 shown that the knee joint on either side is performing symmetrical change. However, at a hip joint and ankle joint on either side, the instruction value is not change symmetrical. This is because it will have fallen if the center of gravity is moved to right-and-left symmetry. The following thing can be considered as this reason. It is that the interval of a leg on either side becomes narrow for a robot's weight , when performing walk operation.

Moreover, in walk operation, it turns out that the knee joint is performing operation to bend and operation to lengthen by a unit of two times.

3. 3 Walking analysis of human

The rate of double static phase and single static phase in human walking cycle is shown in Table.3.

Table3 Human walking cycle

double stance phase	20%
single stance phase	80%

Human walking cycle, the hip joint is operation to bend and operation to lengthen by a unit of one times. Moreover, the knee joint and the ankle joint are performed by a unit of two times.

3. 4 Comparison of a robot and human being in a walking cycle

From Table2 and Table3, biped robot walking cycle is understood the rate of double stance phase is long as compared with human thing. This is because walk operation of biped robot is static walk. Usually, by comparison of dynamic walk which human is performing this thing for time to movement of the center of gravity as a reason. Dynamic walk is taken out with the leg near at hand simultaneously with movement of the center of gravity. However, static walk is performing separately operation issued before movement and the leg of the center of gravity.

4. Up rise of step

4. 1 Relation between a step and the sole

In order for me to make it go up a step, biped robot's sole and position of a step were considered. The model and size of a sole of biped robot are shown in Fig.4 and Table4.

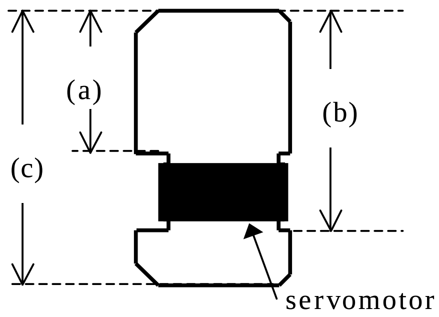

Fig.4 The model of sole

Table4 The size of sole

part	size [mm]
(a)	65
(b)	100
(c)	125

The following thing was considered from this. However, it is the case where both legs are placed just before a step. When a pace less than 100[mm], it become like Fig.5.

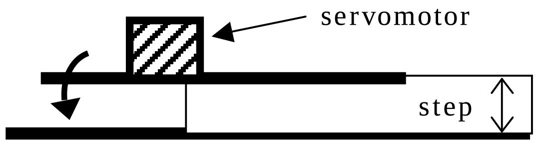

Fig.5 A pace less than 100[mm]

I thought that there may be no center of gravity on step, and it might fall back for this. Moreover, when a pace is larger than 100[mm], it is become like Fig6. I thought that there may be center of gravity on step and it could be a step.

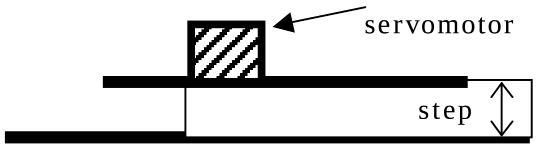

Fig.6 A pace larger than 100[mm]

4. 2 Motion which go up to step.

Biped robot shows the angle change of each servo motor in operation which reaches a step in Fig8. It is the hip joint and the ankle joint on either side which are shown in Fig8. Moreover, link mechanics of biped robot is shown in Fig.9.

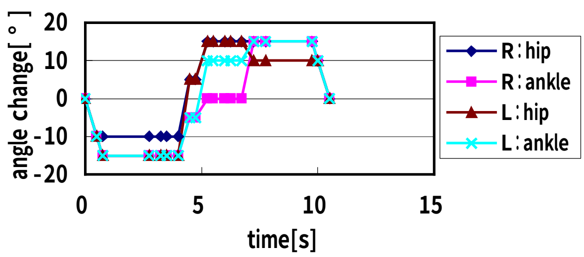

Fig.8 Servomotors value of each joints (a step)

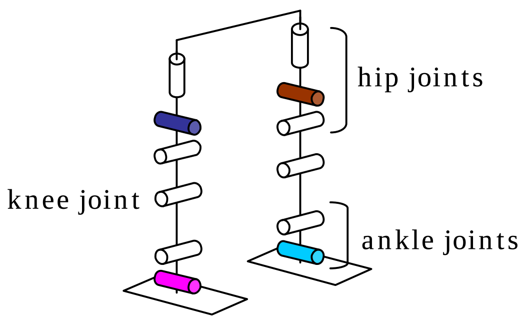

Fig.9 Link mechanics of biped robot

There servo motors are mainly used for movement of the center of gravity on either side. Fig shows moving the center of gravity finely, when moving the center of gravity to the leg before being on a step. This is because movement of the center of gravity on either side and center of gravity of order are moved separately. From this, it seldom needs to maintain balance by movement of the center of gravity of order by the case of the flat ground at the time of movement of the center of gravity on either side. However, in the case of a step, I thought that it was required to maintain balance at movement of the center of gravity of order.

5. Conclusion

Walking motion which separated biped robot's leg from the floor completely was able to be made to perform this time. It become possible to make a step reach by this, and operation was generated. However, many condition are required in order to operate.

6. Challenges for the future

The environment which can be operated for the influence of friction with the sole and a floor is limited. Moreover motion is generated by trial and error this time. Therefore, the position of the center of gravity cannot be grasped. In order to act, the center of gravity is important. From now on, it is necessary to consider move transition of the position of the center of gravity. As for the rest, stable operation is aimed at by using technology, such as a sensor and image processing.

Reference

[1] Nikkei mechanical・Nikkei design joint compilation "Robolution" Nikkei BP Co. p.40～41 2001

[2] Ryuichi Nakamura, Hiroshi Saito "Basic Kinematics" Isiyaku publication Co. Ltd p.334～342 2002

The Tenth International Symposium on Artificial Life and Robotics 2005(AROB 10th '05),
B-con Plaza, Beppu, Oita, Japan, February 4-6, 2005

Acquisition of common symbols with development of cooperative behaviors

Yoshimitsu Hashizume, Jun Nishii
Faculty of Science
Yamaguchi University
1677-1 Yoshida, Yamaguchi
zenko@bcl.sci.yamaguchi-u.ac.jp

Abstract

How and why did human being acquire the ability of verbal communication? To consider the problem concerned with the origin of a verbal communication, we should consider why verbal communication brings a profit for the survival of an individual. In this study we examine the condition under which common words to express objects emerge without mutual mimicry of words among agents who pursue their own profit. Various reward conditions for a food and an enemy are prepared and the conditions under which a common word for an object and a cooperative behavior emerge are investigated. The results suggest that the emergence of a common word would be possible without mutual mimicry under some conditions, however, the profit of the existence of common words should not be taken as a matter of course.

keywords

Language evolution, Cooperative and non-cooperative behaviors, Communication

1 Introduction

How and why did human being acquire the ability of verbal communication? Some simulation studies have been done to consider this problem. In most of these studies a word (or a symbol) to express an object is assumed to be acquired among agents by a mutual mimicry of words for an object through common experiences, which implies that a learning mechanism of common words is prepared a priori in these studies[1][2][3]. To consider the problem concerned with the origin of a verbal communication, we should consider the problem why verbal communication brings a profit for the survival of an individual. In this study we examine the condition under which common words to express objects emerge without mutual mimicry of words among agents who pursue their own profit.

2 Simulation method

2.1 Virtual field

A simulation experiment was performed in a two dimensional torus composed of 10×10 cells. In the virtual field foods and enemies, objects giving positive and negative rewards for agents, respectively, are put on each cell with the probability of 1/10 and 1/20, respectively, as an initial condition, and added to empty cells with the probability of 1/50 and 1/100, respectively, for every simulation step. If an agent stays at a cell with an enemy for three consecutive steps, the enemy will disappear. If an agent stays at a cell with a food five steps, the food will disappear.

2.2 Agents

An agent has a transformation matrix which determines an input-output relation, and communication is carried out with agents which are in the eight neighboring cells. The moving range for every step of an agent is its nine neighboring cells including the current position. The direction of a movement in the next step and a word to speak to neighbors are determined according to the output vector given by a multiplication of an input vector and the transformation matrix. Each element of a matrix and an input vector takes 0 or 1. When the element of an output vector takes a non-binary value it is replaced by the remainder of the value divided by 2. An input vector consists of two sub-vectors. One shows the word transmitted from neighbors, a 4-bit binary (b in Fig.1), and the other shows the information on the current position (a in Fig.1) : the existence of a food (01), an enemy (10), and nothing (00). When an agent receives more than one word at the same time, the agent chooses one at random. An output vector consists of two sub-vectors. One shows a word emitted (d in Fig.1) and the other shows the action taken at the next step (c in Fig.1) : moving to the cell where the word is emitted (01), moving to a cell where no word is emitted (10), staying at the current cell (11), and moving to neigh-

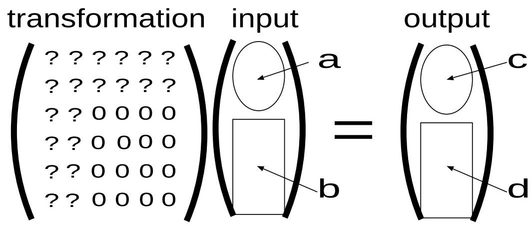

Figure 1: The determination method of an action and a word to speak. The direction of a movement in the next step and a word to speak to neighbors are determined according to the output vector given by a multiplication of an input vector and the transformation matrix. Sub-vector a shows the information on the current position, b is the word transmitted from neighbors, c is the action taken at the next step, and d is the word emitted.

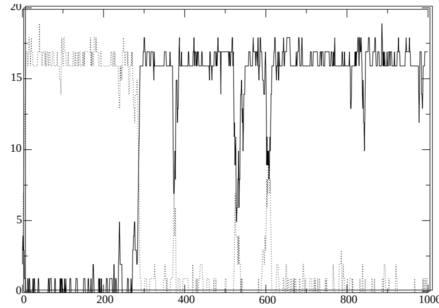

Figure 2: The example of transition of words expressing a food. The solid line shows the number of agents which emitted '1010' to express a food. The dashed line shows the number of agents which emitted '1110' to express a food. A horizontal axis is the number of times of learning, and a vertical axis is the number of agents. The reward condition is $x = 1$ and $y = 0$.

bors or current cell at random (00). The elements of the transformation matrix are improved by a Genetic Algorithm according to the total reward obtained for every fixed period, 1000 simulation steps, and one simulation involves 1000 times of learning. The number of agents on the field was set as 20.

2.3 Reward conditions

If an agent is in a cell with an enemy, it obtains a reward of -10. If more than one agents meet an enemy at the same time, agents can beat the enemy and obtain a reward of y ($0 \leqq y \leqq 50$). If an agent is in a cell with a food, it obtains a reward of n^x ($-5 \leqq x \leqq 5$) depending on the number of the agent n in the same cell. The conditions of the reward which an agent obtains, x and y, were changed for each simulation.

3 Results and discussions

The simulation was performed 10 times and the average ratio of agents who take each action for each object over each simulation was obtained for each combination of x and y. The 10 averaged ratios for each condition are averaged again and its variance is obtained in order to know the tendency of the choice of an action independent of random process of each simulation. Fig.4, 5, 6 and 7 show the average and variance of the rate of agents who take each action, going to the cell where a word expressing an enemy is emitted, not going to the cell where a word expressing an enemy is emitted, going to the cell where a word expressing a food is emitted and not going to the cell where a word expressing a food is emitted, respectively. We define here 'a word expressing a food' as 'a word emitted by an agent when he goes to a cell with a food'.

The result was divided into three types : type 1 is a case that most of the agents approach the cell where a word expressing a food is emitted ($x > 0$), type 2 is a case that most of the agents approach the cell where a word expressing an enemy is emitted ($x < 0$ and $y > 40$), and type 3 is a case that most agents do not approach the cell where a word expressing a food or an enemy are emitted ($x < 0$ and $y < 30$).

3.1 Type 1

For the reward conditions $x > 0$ most of the agents tend to go to the cell where words expressing a food is emitted (Fig.6 (a)). Low variance of the action indicates that the action is stably observed (Fig.6 (b)). Such action would bring benefit for agents because reward for a food increases by sharing it in these reward conditions. On the other hand, high variance of the action of approaching the cell where a word expressing an enemy is emitted indicates that the action is not stably observed (Fig.4 (b) and Fig.5 (b)). In these reward conditions a word expressing a food was stabilized and the word turned into a common word for most of the agents over a long time (Fig.2). On the other hand, the common word expressing an enemy also emerged but changed in a shorter span than the common word expressing a food.

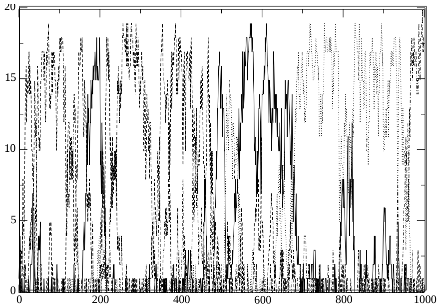

Figure 3: The example of transition of words expressing an enemy. The horizontal axis shows the number of times of learning, and the vertical axis shows the number of agents. The reward condition is x = -5 and y = 50.

3.2 Type 2

For the reward conditions $x < 0$ and $y > 40$, most of the agents do not go to the cell where words expressing a food is emitted (Fig.6 (a)), and on average about the half of the agents avoid the cell (Fig.7 (a)). The reason is that it would be more advantageous to look for new foods rather than to go to the cell with a food in these conditions, because the reward for a food for an agent becomes smaller by sharing it. On the other hand, most of the agents tend to go to the cell where the words expressing an enemy is emitted (Fig.4 (a)), because large reward is expected by gathering at a cell with an enemy. Low variance of the action of approaching an enemy indicates that the action is stably observed (Fig.4 (b)). Common words expressing a food and an enemy emerged but the common words changed in a shorter span than the common word expressing a food in type 1 (Fig.3).

3.3 Type 3

For the reward conditions, $x < 0$ and $y < 30$, sharing a food brings smaller reward and expected reward by going to the cell with an enemy would be also small. In these conditions, most agents do not go to the cells where words expressing a food and an enemy are emitted (Fig.4 (a) and Fig.6 (a)), and on average about the half of the agents avoid such cells (Fig.5 (a) and Fig.7 (a)). However, the rate of the agents which take the action to avoid the cells is not higher than the rate of those which take the action to approach the cells where words expressing a food and an enemy in type 1 or type 2. This result suggests that cooperative behaviors to obtain rewards tend to be emerged but those to avoid negative reward are hardly emerged. In these conditions common words expressing a food and an enemy changed in a very short span, and were scarcely stabilized.

4 General discussion

Simulation results indicate that the word which points out an object becomes stable and a cooperative relation emerges when agents can obtain more profit by cooperation from the object, and when there is no merit for cooperation, neither stabilization of a word nor a cooperative relation is emerged. When an agent pursues only its profits, the action to tell the existence of a negative object to others would not be advantageous because such behavior might decrease the relative predominance of the speaker. These results also suggest that the emergence of the cooperative and the non-cooperative relations between individuals have a close relation to the balance of reward and damage, and stabilization of a word.

In real world we tell the existence of non-profitable objects, such as an enemy, each other to avoid such objects. On what conditions do such cooperative relations emerge? The merit for the survival of various levels, such as not only the merit for an individual but also for blood relatives and a species, might have to be taken into considerations. The relation between the preservation of a species and language stability might be strong, because there is little word shared over species.

References

[1] Cangelosi A, Parisi D, *Simulating the evolution of language*, Springer Verlag, London, 2002.

[2] Arita T, Unno K, Kawaguchi K, "A model for evolution of communication in a population of artificial organisms," *The journal of Information processing society of Japan (in Japanese)*,Vol. 36, pp. 859-867, 1995.

[3] Hashimoto T, "Constructive modeling of symbol formation based on the dynamic view of language," *Proc. of the symposium of the 16th distributed-autonomous-system (in Japanese)*, pp. 125-130, 2004

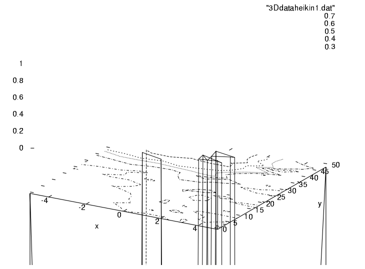

(a)

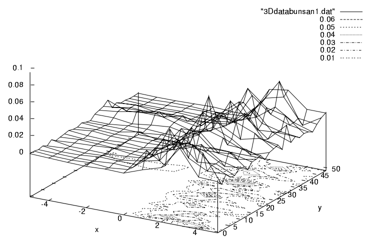

(b)

Figure 4: The rate of agents which go to the cell where a word expressing an enemy was emitted for each reward condition x and y. (a) shows the average of the rate during 10 times of the simulation, and (b) shows its variance.

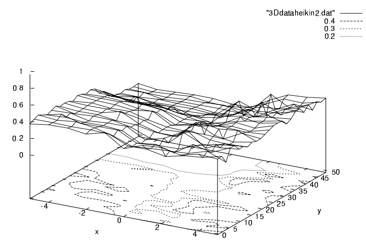

(a)

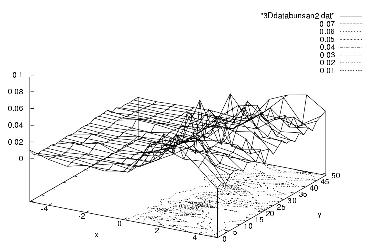

(b)

Figure 5: The rate of agents which do not go to the cell where a word expressing an enemy was emitted for each reward condition x and y. (a) shows the average of the rate during 10 times of the simulation, and (b) shows its variance.

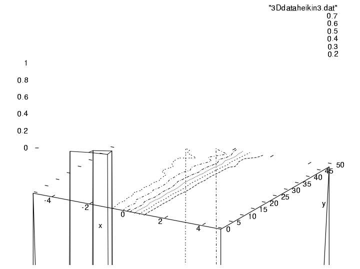

(a)

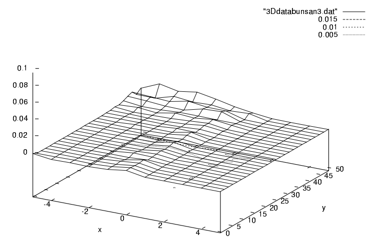

(b)

Figure 6: The rate of agents which go to the cell where a word expressing a food was emitted for each reward condition x and y. (a) shows the average of the rate during 10 times of the simulation, and (b) shows its variance.

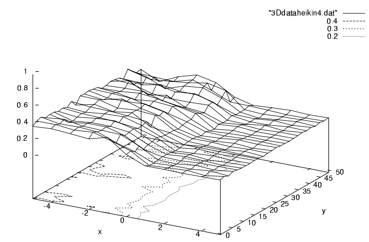

(a)

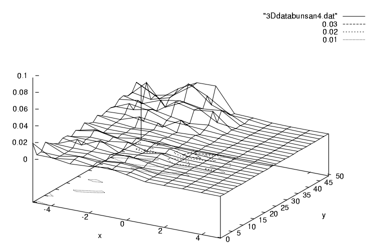

(b)

Figure 7: The rate of agents which do not go to the cell where a word expressing a food was emitted for each reward condition x and y. (a) shows the average of the rate during 10 times of the simulation, and (b) shows its variance.

The Tenth International Symposium on Artificial Life and Robotics 2005(AROB 10th '05),
B-con Plaza, Beppu, Oita, Japan, February 4-6, 2005

A hierarchical learning model for basic locomotor patterns

Tomoko Hioki† ††, Jun Nishii†
† Faculty of Science, Yamaguchi University, 1677–1 Yoshida, 753–8512 Yamaguchi, Japan
†† Department of Electronic Information, Yamaguchi Junior College, 1346–2 Daido, Hofu, 747–1232 Yamaguchi, Japan
{hioki,nishii}@bcl.sci.yamaguchi-u.ac.jp

Abstract

Most animal locomotor patterns are produced by two control systems: a higher center such as the cerebellum and the CPG (Central Pattern Generator) which is located in the spinal cord of vertebrates. We take notice of the following two questions. How are firing patterns of the CPG well coordinated? How do two motor commands from the CPG and a higher center work without confliction in order to realize a target motion? In order to answer these questions, we propose a motor learning model that a higher center learns an appropriate motor command which works as a supervisory signal for the CPG and an appropriate firing pattern of the CPG is learned by the signal. We applied this model to the learning control of a one-dimensional hopping robot. As a result, higher center and the CPG learned proper motor commands for the target motion.

Key words Central pattern generator, Learning, Motor control, Hierarchical architecture

1 Introduction

Most animal locomotor patterns, such as walking and swimming, present cyclic movements, which are produced by properly patterned firing of neurons of the CPG (Central Pattern Generator) in the central nervous system. The CPG receives feedback signals from a musculoskeletal system, however it is capable of generating motor commands even in an immobilized animal [1].

Although a firing pattern of the CPG is genetically determined at some level, learning and coordination of an adequate firing pattern would be necessary to respond to the change of body parameters due to growth and injury. However it has not been known how firing patterns of the CPG are learned. In the learning of the CPG a kind of teacher signals from a higher center to the CPG would be necessary because the CPG is situated at the lower part of a nervous system.

An experimental result with decerebrate cat indicates that smooth movements require not only the control by the CPG but also by a higher center [2]. Yanagihara et al. (1994) reported that climbing fiber responses in cerebellar vermal Purkinje cells in decerebrate cats increased during perturbed locomotion [3]. This result shows that the responses of climbing fibers represent error signals in control of movements. Therefore a higher center would be monitoring the sequence of normal gait controlled by the CPG and generating motor commands to recover from the perturbation. However it is not clear how do two motor commands from the CPG and a higher center work without confliction? To avoid this confliction, a higher center must monitor the activity of the CPG and sends a signal to control the CPG. Projections, from the brainstem of a lamprey to the CPG is observed and a stimuli to such region in the brainstem makes the lamprey take a certain postures, or swims front or back, or turns around [4]. This experimental result indicates that the neural activity of the brainstem exerts a strong influence over the activity of the CPG, and suggests that the brainstem controls the neural activity of the CPG. It has been also reported that the neural activity of the brainstem is largely affected by the firing of the CPG [5], which suggests that the brainstem is monitoring the activity of the CPG.

On the basis of these neurophysiological knowledge, we propose a hierarchical learning model of the CPG and a higher center, which solves the problems of the confliction of multiple control signals and the learning of the CPG.

2 A hierarchical learning model

Figure 1 shows a schematic representation of a hierarchical motor learning model that a higher center learns an appropriate motor command which works as a supervisory signal for the CPG to learn an appropriate firing pattern (Fig. 1). In this model, a higher center sends control signals to the CPG according to the states of the musculoskeletal system and the CPG.

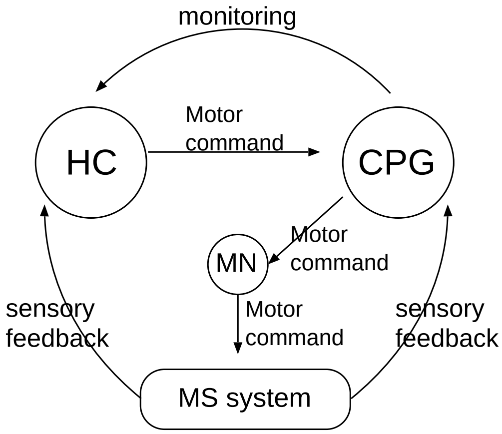

Figure 1: Schematic representation of the proposed motor control model by a higher center and the CPG. A control signal generated by a higher center is sent to a motor neuron through the CPG. HC is a higher center, MN is a motor neuron, and MS system is the musculoskeletal system.

The control signal works as a reset signal for the CPG to cause an immediate firing which induces the firing of the motor neuron and as a suspend signal to delay the firing of the CPG, and are tuned so as to realize a target action. By sending a motor command from a higher center to motor neurons through the CPG, the state of the CPG can be controlled, by which confliction of two motor commands would be avoided.

3 Simulation method

By applying the proposed model to the learning control of a one-dimensional hopping robot, we examined the learning performance of the proposed model. The one-dimensional hopping robot consists of a trunk and a leg with a spring component and a damping component (Fig. 2 [6]). When the motor neuron receives a control signal, a force is generated between the trunk and the toe. If the force is applied to the robot in an appropriate timing in a hopping cycle, the robot can keep hopping with target height. In this simulation, the CPG is assumed to be a phase oscillator.

3.1 A learning model of its higher center

Q-learning [7] was applied to the learning of the control signals of a higher center, and the lowest height of the trunk, x_0 [m], and the phase of the CPG, θ,

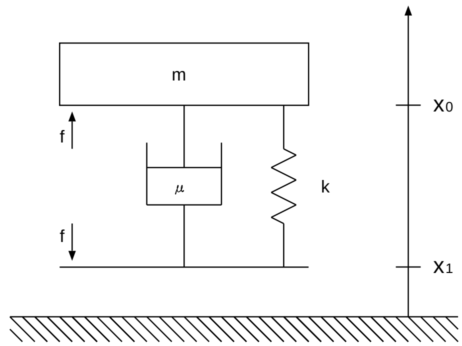

Figure 2: One-dimensional hopping robot [6]. m is the mass of the robot, x_0 and x_1 are positions of the toe and the trunk, respectively, k and μ are an elastic coefficient and a damping coefficient of the leg, respectively, and f is the force applied between the trunk and the toe when a motor neuron receives a control signal.

are used as the states for Q-learning. When the robot reaches the lowest position, an action which the higher center takes is chosen from (1) sending an excitatory signal to the CPG δ seconds later ($\delta = 0.001 \times a$ [s], $a = 0 \ldots 57$), (2) sending an inhibitory signal to the CPG at the moment, and (3) sending no signal to the CPG during a hopping cycle. Reward function is set as $10e^{-\frac{(\hat{x}_0 - x_0)^2}{0.2^2}}$. When a higher center sends a control signal to the CPG, negative reward (-5) is added to the total reward, by which it is expected that the learning of a control signal from a higher center proceeds so as that a higher center sends no signal to the CPG when the CPG sends a correct signal to the motor neuron.

3.2 A model of the CPG and a learning rule

In this simulation the phase dynamics of the CPG is assumed to take the following form:

$$\dot{\theta} = \omega + \sum_i W_i P(\theta - \varphi_i) Q(t) + P(\theta) Q_{HC}(t),$$

where θ is the phase of the oscillator, ω is the intrinsic frequency of the CPG, $P(\theta)$ is the function which shows the effect of input signals to the oscillator and is assumed to be $P(\theta) = -\sin 2\pi\theta$, φ_i indicates the phase delay of the effect, $Q(t)$ is a sensory feedback signal to the oscillators, W_i is its weight of the connection, and $Q_{HC}(t)$ is a signal from a higher center.

We use $Q(t) = \frac{v}{<|v|>}$ as the sensory feedback signal, where <> means the time average (see Appendix A).

We define the signal of a higher center as $Q_{HC}(t)$=20 for action (1) in section 3.1, $Q_{HC}(t)$=-1.0 for 0.01 [s] for condition (2), and otherwise $Q_{HC}(t)$=0. The CPG sends a pulse signal to a motor neuron when the phase of the CPG becomes $\theta = 0$, which results in the force generation f =0.4 [N] for 0.15 [s] between the trunk and the toe.

We apply the learning rule proposed by Nishii(1998) [8] to the learning of the intrinsic frequency ω of the CPG and the weights W_i. The learning rule takes the form as follows:

$$\dot{\omega} = \epsilon_\omega \left\{ \sum_i W_i \langle P(\theta - \varphi_i) Q(t) \rangle + \langle P(\theta) Q_{HC}(t) \rangle \right\},$$
$$\dot{W}_i = \epsilon \langle P(\theta - \varphi_i) Q(t) \rangle \cdot \langle P(\theta) Q_{HC}(t) \rangle,$$

where ϵ and ϵ_ω are parameters determining the learning rate.

By this learning rules, the timing of the output signals of the CPG becomes in phase with the control signal from a higher center and the effect of the control signal on the phase dynamics becomes zero. Thus it is expected that only the CPG can generate an appropriate signal after learning even if the signal from a higher center is blocked.

Because continuous hopping of the robot is necessary for the learning of an appropriate control signal, we set the initial parameters of the CPG so as to enable the continuable hopping. Parameters in this simulation are shown in Appendix A.

3.3 Results

Figure 3 shows the time profile of the time averaged height of the trunk of the robot ($\bar{x}_0$) during learning. It is shown that an appropriate control signal is acquired for each target height $\hat{x}_0$ =1.1, 1.3, 1.5 [m]. Figure 4 shows the time profile of the time averaged height of robot's trunk when only the CPG sends motor control signals after learning. The robot continues hopping at desired heights, which indicates that the parameters of the CPG are tuned properly.

4 Conclusion

In our study, we proposed a hierarchical motor learning model composed of a higher center and the CPG. In this model a higher center learns an appropriate motor command, and sends it to the CPG as a supervisory signal. The CPG coordinates its natunal frequency and weights of connections with sensory feedback for an appropriate firing pattern on the basis of the signal. This model solves the problem of confliction of two motor commands, and enables the CPG to learn an appropriate control signal. In living bodies multiple control systems as the proposed model would make animal locomotor patterns robust.

By applying the proposed model to the learning control of one-dimensional hopping robot, desired hopping was successfully acquired. Although we applied the model to a simple model with single degree of freedom in this article, we expect that the model could be applied to a complicated movement such as walking and swimming.

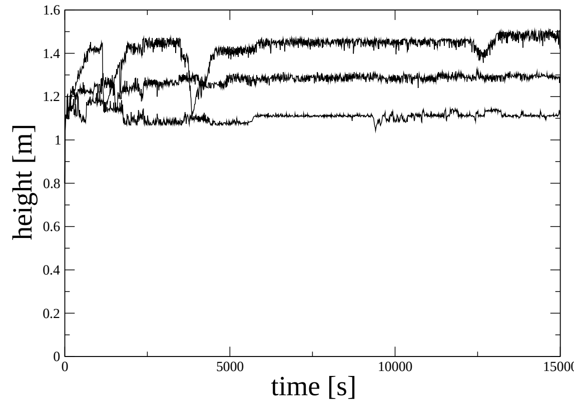

Figure 3: The time profile of the time averaged height of the trunk of the robot ($\bar{x}_0$) during learning. The target heights are set as $\hat{x}_0$=1.1, 1.3, 1.5 [m].

A The parameters of the CPG during learning

The parameters of the CPG are given as follows.
$\omega = 1.0$, $W_1 = 0.2$, $W_2 = -0.4$, $\varphi_1 = 0$, $\varphi_2 = 0.8$, $\epsilon = 0.5$, $\epsilon_\omega = 0.5$.

Time average is used first-order lag low-pass filter, and time constant is 5 [s].

References

[1] S. Grillner, J. T. Buchanan, P. Wallen, and L. Brodin, *Neural Control of Rhythmic Movement in Vertebrate*, Wiley-Interscience Publication, 1988.

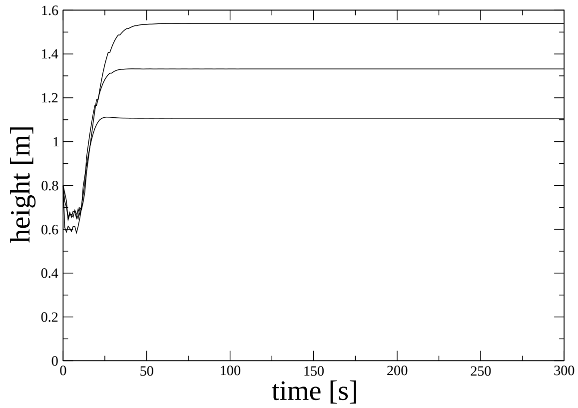

Figure 4: The time profile of the time averaged height of the trunk of the robot ($\bar{x}_0$) after learning.

[2] G. M. Shepherd, *Neurobiology*, Oxford University Press, 1994.

[3] D. Yanagihara, M. Udo, "Climbing fiber responses in cerebellar vermal Purkinje cells during perturbed locomotion in decerebrate cats", *Neuroscience Research*, Vol.19, pp.245-248, 1994.

[4] C. M. Rovainen, "Physiological and anatomical studies on large neurons of central nervous system of the sea lamprey (*Petromyzon marinus*). I. Muller and Mauthner cells", *Journal of Neurophysiology*, Vol.30, pp.1000-1023, 1967.

[5] S. Grillner, P. Wallen and L. Brodin, "Neuronal network generating locomotor behavior in lamprey: circuitry, transmitters, membrane, properties and simulation", *Annual Review of Neuroscience*, Vol.14, pp.169-199, 1991.

[6] J. Nishii , "An adaptive control model of a locomotion by the central pattern generator" *Natural to Artificial Neural Computation, Lecture Notes in Computer Science*, Vol. 930, pp. 151–157, Springer, Berlin Heidelberg, 1995.

[7] R. S. Sutton, A. G. Barto, *Reinforcement Learning: An Introduction*, MIT Press, 1998.

[8] J. Nishii, "A learning model for oscillatory networks", *Neural Networks*, Vol.11, pp.249-257 1998.

Artificial Life-Based Search Technique on the Solution of Singular Configurations Concerning Screw Parameters in Helicoidal Robots

Ignacio Juárez Campos

Nachito Robotics Group
Privada de Antimonio 56, Col. Industrial 58130
Morelia, Michoacán, México
+52 443 3172656
ijcunam@att.net.mx

Facultad de Ingeniería Mecánica, UMSNH
Ciudad Universitaria, Edif. W, Santiago Tapia S/N,
Col. Felicitas del Río 58120
Morelia, Michoacán, México
+52 443 3167207

ABSTRACT

The screw-based robot manipulators belonging to the *SBMF6* and *SBMF7* present closed-form equations describing joint variables as functions of end-effector coordinates; the mentioned closed-form equations depends on the so called screw parameters that, in some conditions, can not be determined because present singularities. It means that the inverse kinematics solved by this technique is not robust enough. The paper presents an auxiliary technique that will be helpful in finding the corresponding inverse kinematics. The mentioned technique is an artificial life-based search method that will be used only for those cases in which singularities are present and closed-form equations fail.

Key words: Artificial Life, Artificial Intelligence, Genetic Algorithms, Robotics, Inverse kinematics

1. INTRODUCTION

The *SBMF6* and *SBMF7* are sets containing manipulators having a particular mechanical architecture capable of transporting 3-dimensional work pieces by means of the helical or screw-based motions. This singular way of transferring work pieces from one pose (position and orientation) to another one is based on the well-known Chasles' Theorem and the Rodrigues' Formula [1], [2], [3], [4], [5], [6]. The *SBMF6* possesses the PPSP, RRSP, SPRP and RPSP arrangements, while the *SBMF7* contains the PPSPP, RRSPP, SPRPP and RPSPP manipulators; all these manipulators are named as *Helicoidal Manipulators*. The elements contained by the set *SBMF6* have 6 degrees of freedom, while elements belonging to the *SBMF7* posses 7 degrees of freedom. In all cases, *Helicoidal Manipulators* were designed according to the screw transformation that says that a piece described by three non-collinear points P, Q and R is brought from an initial to a final one by means of a screw displacement [1], [2], [3], [4], [5], [6]. In order to transfer a work piece from the initial pose to the final one, it is necessary to find the corresponding joint displacements; it is the duty of the inverse kinematics which is expressed by a set of closed-form equations depending on the screw parameters found by Rodrigues in 1840 [6]. These parameters can not be found for some initial and final positions and orientations of the work piece. This is a singular configuration dealing with the screw motion. In this case, it is necessary the aid of and auxiliary method to find the corresponding screw parameters. In this case, a search technique, based on the way species find the solution to the survival problem, was selected.

2. GOAL

To present an auxiliary technique employed to find the screw parameters when traditional or closed-form solutions fail. The mentioned screw parameters are necessary because the corresponding inverse kinematics is expressed in terms of them. This adjacent technique is an artificial life-based search method (ALBSM) because it uses the mechanisms employed by living species to be successful [5].

3. GENERAL SCREW DISPLACEMENT

Suppose that two poses of an object at time $t = 0$ and at time $t = t_f$ are given and it is necessary to find the screw motion that interpolate them, then the description of computing pose interpolating screw parameters can be done as follows: it is a known fact that three non-collinear points $\mathbf{P_1}$, $\mathbf{Q_1}$ and $\mathbf{R_1}$, belonging to a work piece, are brought to positions $\mathbf{P_2}$, $\mathbf{Q_2}$ and $\mathbf{R_2}$ by a screw displacement (ϕ, d) about an axis with direction $\hat{e}$ passing through a point defined by $\bar{s}_0$ [1], [2], [3], [4], [5], [6]. They are called "screw parameters". (1), (2), and (3) present the mentioned functions and are known as the Rodrigues' formulae [6].

$$\bar{p}_2 - \bar{p}_1 = (\tan(\phi/2))\hat{e} \otimes (\bar{p}_2 + \bar{p}_1 - 2\bar{s}_0) + d\hat{e} \quad (1)$$

$$\bar{q}_2 - \bar{q}_1 = (\tan(\phi/2))\hat{e} \otimes (\bar{q}_2 + \bar{q}_1 - 2\bar{s}_0) + d\hat{e} \quad (2)$$

$$\bar{r}_2 - \bar{r}_1 = (\tan(\phi/2))\hat{e} \otimes (\bar{r}_2 + \bar{r}_1 - 2\bar{s}_0) + d\hat{e} \quad (3)$$

Where $\bar{p}_i$, $\bar{q}_i$, $\bar{r}_i$ are the position vectors describing $\mathbf{P_i}$, $\mathbf{Q_i}$ and $\mathbf{R_i}$ when i=1, 2. Symbol $\otimes$ represents the cross product.

It is possible to find the corresponding four screw parameters in terms of the three mentioned points by using (4), (5) and (6).

$$\tan\left(\frac{\phi}{2}\right)\hat{e} = = \frac{\{[(\bar{r}_2-\bar{q}_2)-(\bar{r}_1-\bar{q}_1)]\otimes[(\bar{p}_2-\bar{q}_2)-(\bar{p}_1-\bar{q}_1)]\}}{\{[(\bar{r}_2-\bar{q}_2)-(\bar{r}_1-\bar{q}_1)]^T[(\bar{p}_2-\bar{q}_2)+(\bar{p}_1-\bar{q}_1)]\}} \quad (4)$$

$$\bar{s}_0 = \tfrac{1}{2}\begin{bmatrix} \bar{p}_1+\bar{p}_2+(\hat{e}\otimes(\bar{p}_2-\bar{p}_1)/\tan(\phi/2))- \\ -(\hat{e}^T(\bar{p}_2+\bar{p}_1))\hat{e} \end{bmatrix} \quad (5)$$

Where $\hat{e}^T\bar{s}_0 = 0$

$$d = \hat{e}^T(\bar{p}_2-\bar{p}_1) \quad (6)$$

4. ANALYSIS OF MATHEMATICAL SINGULARITIES

Consider (7) which is the denominator of (4). It is not possible to find the screw axis and the rotation angle when (7) becomes null. As a result, the other two screw parameters, (5) and (6), can not be found because they depend on the screw axis and the rotation angle.

$$den = [(\bar{r}_2-\bar{q}_2)-(\bar{r}_1-\bar{q}_1)]^T[(\bar{p}_2-\bar{q}_2)+(\bar{p}_1-\bar{q}_1)] \quad (7)$$

The mentioned denominator becomes zero when position vectors $[(\bar{r}_2-\bar{q}_2)-(\bar{r}_1-\bar{q}_1)]$ and $[(\bar{p}_2-\bar{q}_2)+(\bar{p}_1-\bar{q}_1)]$ rest perpendicular. In some cases it is desirable for the pick and place operation to have particular initial and final position and orientations, but they could make (4) singular, so then, inverse kinematic equations, depending on screw parameters, can not be found. This is the main reason to use a method whose robustness ignores limitations dealing with this singularity [5].

5. THE ARTIFICIAL LIFE-BASED SEARCH METHOD (ALBSM)

5.1 GENOTYPE

The member *n*, belonging to the species of sets of screw parameters and representing a particular solution, must contain the most basic information, responsible for the determination and transmission of hereditary characteristics corresponding to the four screw parameters (8).

$$solution(n) = \langle\langle\hat{e}_g\rangle\langle\phi_g\rangle\langle\bar{s}_0\rangle\langle d_{\hat{e}}\rangle\rangle \quad (8)$$

Where $\langle\hat{e}_g\rangle$ represents the screw axis which contains three elements due to the fact that it is a Cartesian vector (9).

$$\langle\hat{e}_g\rangle = \langle\langle a_1\rangle\langle a_2\rangle\langle a_3\rangle\rangle \quad (9)$$

So then, (10) must be used to obtain the screw axis.

$$\hat{e}_g = \frac{1}{\sqrt{\sum_{i=1}^{3} a_i^2}}(a_1 \quad a_2 \quad a_3)^T \quad (10)$$

The second part of (8), $\langle\phi_g\rangle$, representing the rotation angle, is constituted by one genetic structure, (11).

$$\langle\phi_g\rangle = \langle b_1\rangle \quad (11)$$

The third part of (8), $\langle\bar{s}_0\rangle$, contains four genetic structures, (12).

$$\langle\bar{s}_0\rangle = \langle\langle c_1\rangle\langle c_2\rangle\langle c_3\rangle\langle c_4\rangle\rangle \quad (12)$$

These four elements help to find the position vector describing the point where the screw axis passes, (13).

$$\bar{s}_0 = \left(\frac{1}{\sqrt{\sum_{i=1}^{3} c_i^2}}\begin{pmatrix} c_1 \\ c_2 \\ c_3 \end{pmatrix}\right) c_4 \quad (13)$$

The last part of (8), $\langle d_{\hat{e}}\rangle$, is a scalar parameter related to the linear displacement along the screw axis, (14).

$$d_{\hat{e}} = d_1 \quad (14)$$

So then, equation (8) can be expressed by (15).

$$solution(n) = \langle\langle a_1\rangle\langle a_2\rangle\langle a_3\rangle\langle b_1\rangle\langle c_1\rangle\langle c_2\rangle\langle c_3\rangle\langle c_4\rangle\langle d_1\rangle\rangle \quad (15)$$

5.2 LENGTH OF BASIC GENETIC STRINGS

The length of the genetic vectors or strings depends on the length of the domain of the search space and the required precision [5]. The chromosomes corresponding to $\langle a_i\rangle$; $i = 1,2,3$, $\langle b_1\rangle$, $\langle c_i\rangle$; $i = 1,2,3$, $\langle c_4\rangle$ y $\langle d_1\rangle$ by means of binary strings are given by (16)-(20), taking in account that $b_{*,*} = 0, 1$.

$$\langle a_i\rangle = \langle b_{K1-1,ai}\ldots b_{2,ai}b_{1,ai}b_{0,ai}\rangle \quad (16)$$

$$\langle b_1 \rangle = \langle b_{K2-1,b1} \ldots b_{2,b1} b_{1,b1} b_{0,b1} \rangle \quad (17)$$

$$\langle c_i \rangle = \langle b_{K3-1,ci} \ldots b_{2,ci} b_{1,ci} b_{0,ci} \rangle \quad (18)$$

$$\langle c_4 \rangle = \langle b_{K4-1,c4} \ldots b_{2,c4} b_{1,c4} b_{0,c4} \rangle \quad (19)$$

$$\langle d_1 \rangle = \langle b_{K5-1,d1} \ldots b_{2,d1} b_{1,d1} b_{0,d1} \rangle \quad (20)$$

The problem consists in finding K1, K2, K3, K4 and K5 in (16)-(20) satisfying the search space and the precision requirements [5].

5.3 PHENOTYPES

The mapping from binary strings into real numbers can be done by (21)-(25).

$$a_j = -1 + \left(\sum_{i=0}^{K1-1} b_{i,aj} 2^i\right)\left(\frac{2}{2^{K1}-1}\right); \quad j = 1,2,3 \quad (21)$$

$$b_1 = \left(\sum_{i=0}^{K2-1} b_{i,b1} 2^i\right)\left(\frac{2\pi}{2^{K2}-1}\right) \quad (22)$$

$$c_j = -1 + \left(\sum_{i=0}^{K3-1} b_{i,cj} 2^i\right)\left(\frac{2}{2^{K3}-1}\right); \quad j = 1,2,3 \quad (23)$$

$$c_4 = \left(\sum_{i=0}^{K4-1} b_{i,c4} 2^i\right)\left(\frac{c_{MAX}}{2^{K4}-1}\right) \quad (24)$$

$$d_1 = \left(\sum_{i=0}^{K5-1} b_{i,d1} 2^i\right)\left(\frac{d_{MAX}}{2^{K5}-1}\right) \quad (25)$$

Where c_{MAX} and d_{MAX} are the upper limits of the search spaces.

5.4 EVALUATION FUNCTION

The evaluation function takes in account the final pose acquired by the work piece. If the object is close to the required final pose, then the corresponding solution is evaluated with a high score, otherwise, it will have a poor effectiveness. Each solution, generated by the ALBSM, provides a final pose described by $\mathbf{P_2(n)}$, $\mathbf{Q_2(n)}$, $\mathbf{R_2(n)}$. The comparison between the required final pose ($\mathbf{P_2}$, $\mathbf{Q_2}$, $\mathbf{R_2}$) and ($\mathbf{P_2(n)}$, $\mathbf{Q_2(n)}$, $\mathbf{R_2(n)}$) will permit evaluate solution *n*. It is important to take in account that whatever points ***S*** and ***S(n)*** are represented by sets of three coordinates:

$$S([w_1,s],[w_2,s],[w_3,s]) \quad (26)$$

And,

$$S(n)([w_1,s](n),[w_2,s](n),[w_3,s](n)) \quad (27)$$

With this in mind, it is possible to define the scalar $g_{S,wi}$ as follows,

- If $\|[w_i,s](n)\| \geq \|[w_i,s]\|$ then $g_{S,wi} = \dfrac{[w_i,s]}{[w_i,s](n)}$.
- If $\|[w_i,s](n)\| < \|[w_i,s]\|$ then $g_{S,wi} = \dfrac{[w_i,s](n)}{[w_i,s]}$.

Then, the proximity of the work piece corresponding to solution *n* is expressed by $sum(n) \in [-9, 9]$, (28).

$$sum(n) = \sum_{S=P,Q,R}\left(\sum_{i=1,2,3} g_{S,wi}\right) \quad (28)$$

The final evaluation function, $eval(n) \in [0, 1]$, is defined by (29).

$$eval(n) = \frac{9 + sum(n)}{18} \quad (29)$$

Obviously, the exact solution corresponds to $eval(n) = 1$, belonging to the member *n*, Fig 1.

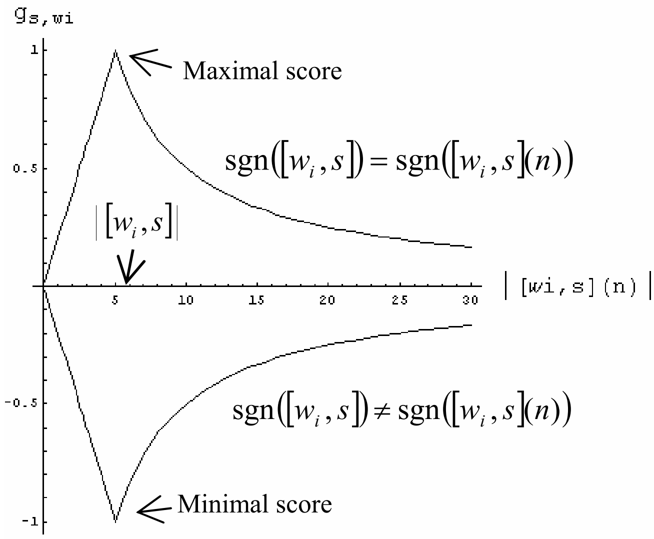

Fig. 1 Evaluation function for the coordinate $[w_i,s](n)$ belonging to the member *n*

5.5 THE ALBSM FLOWCHART

Fig. 2 presents the flowchart representing the different stages followed by the ALBSM.

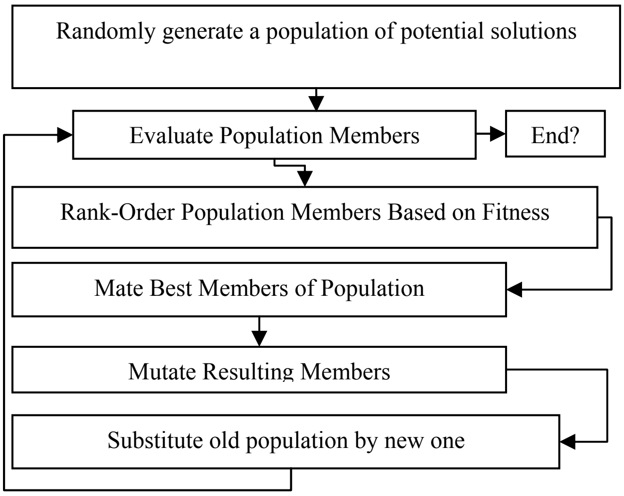

Fig. 2 Flowchart representing the different stages of the ALBSM

6. EXPERIMENTATION

It is necessary to transfer a work piece from the initial and final positions described in table 1.

Object	coordinates
$\mathbf{P_1}$	(2, 2, 0)
$\mathbf{Q_1}$	(3, 2, 0)
$\mathbf{R_1}$	(2, 3, 0)
$\mathbf{P_2}$	(2, 2, 0)
$\mathbf{Q_2}$	(1, 2, 0)
$\mathbf{R_2}$	(2, 1, 0)

Table 1. Initial and final poses

For the mentioned initial and final poses presented in table 1, (4) becomes singular. The screw parameters, shown in table 2, were found with the aid of the ALBSM.

Screw Parameters	
$\hat{e}$	$(0 \quad 0 \quad 0.995)^T$
ϕ	179.898º
$\bar{s}_0$	$(1.997 \quad 2.001 \quad 0.003)^T$
d	0

Table 2. Screw parameters resulting from the ALBSM

The exact values of the screw parameters are shown in table 3. The comparison of both tables, It is concluded that the ALBSM provides a suitable result.

Screw Parameters	
$\hat{e}$	$(0 \quad 0 \quad 1)^T$
ϕ	180º
$\bar{s}_0$	$(2 \quad 2 \quad 0)^T$
d	0

Table 3. The exact screw parameters

7. CONCLUSIONS

The ALBSM has demonstrated its effectiveness in finding the solution of singular configurations. However, this method should be only used for those cases in which it is not possible to find the screw parameters by other means. It is necessary to take in account that the ALBSM is an iterative one; therefore, it spends more time to find the solution in comparison to the closed-form equations. The main advantage resides in its robustness because this method does not use the equations that could become singular. All the manipulators, belonging to the *SBMF6* and *SBMF7*, have their own inverse kinematics, but these equations depends on the screw parameters, so then, the ALBSM can be applied to all the screw-based manipulators.

8. REFERENCES

[1] Ignacio Juárez Campos, Beatriz Juárez Campos, Oracio García Lara. (2004) *The Inverse Kinematics of the SPRP Screw-Based Manipulator*. Proc. of the 10th IASTED International Conference on Robotics and Applications, RA 2004, August 23-25, Honolulu, Hawaii, USA, pp. 34-40.

[2] Ignacio Juárez Campos et al. (2004) *The Inverse Kinematics of the PPSP Helicoidal Robot Manipulator*. Proc. of the 10th IASTED International Conference on Robotics and Applications, RA 2004, August 23-25, Honolulu, Hawaii, USA, pp. 22-27.

[3] Ignacio Juárez Campos, Oracio García Lara, Beatriz Juárez Campos. (2004). *The Inverse Kinematics of the RPSP Screw-Based Robot Manipulator*. Proc. of the 4th Int. Conf. on Advanced Mechatronics, ICAM'04. October 3-5, Asahikawa, Hokkaido, Japan.

[4] Ignacio Juárez Campos, Oracio García Lara, Beatriz Juárez Campos. (2004). *Trajectory Planning for the PPSP Helicoidal Robot Manipulator*. Proc. of the 4th International Symposium on Robotics and Automation ISRA 2004. August 25-27, 2004. Querétaro, Qro, México, pp. 287-294.

[5] Ignacio Juárez Campos, Beatriz Juárez Campos. (2004). Síntesis Evolutiva de un Mecanismo de Tornillo, *Proc. 9th SOMIM Conf. on Mechanical Engineering*, Veracruz, Ver, Mexico. pp 35-40.

[6] O. Bottema, B. Roth (1979) *Theoretical Kinematics* (North Holland Publishing Company, Amsterdan, New York, Oxford.

The Tenth International Symposium on Artificial Life and Robotics 2005(AROB 10th '05),
B-con Plaza, Beppu, Oita, Japan, February 4-6, 2005

Human-following Robot Using the Particle Filter in ISpace with Distributed Vision Sensors

Tae-Seok Jin, Kazuyuki Morioka, and Hideki Hashimoto

Institute of Industrial Science, the University of Tokyo
4-6-1 Komaba, Meguro-ku, Tokyo 153-8505, Japan

Abstract

We present a method for representing, tracking and human following by fusing distributed multiple vision systems in intelligent space, with application to pedestrian tracking in a crowd. In this context, particle filters provide a robust tracking framework under ambiguity conditions. The particle filter technique is used in this work, but in order to reduce its computational complexity and increase its robustness, we propose to track the moving objects by generating hypotheses not in the image plan but on the top-view reconstruction of the scene. Comparative results on real video sequences show the advantage of our method for multi-object tracking. Simulations are carried out to evaluate the proposed performance. Also, the method is applied to the intelligent environment and its performance is verified by the experiments.

Keywords: Multi-vision sensors, Tracking, Intelligence Space, Mobile robot, Particle filter

1. Introduction

Video object tracking in dense visual clutter, although being notably challenging, has many practical applications in scene analysis for automated surveillance, such as the detection of suspicious moving objects (pedestrians or vehicles), or the monitoring of an industrial production [1][2][3][4]. The quality of an object tracking system is very much dependent on its ability to handle ambiguous conditions, such as occlusion of an object by another one. To cope with such ambiguities, multi-hypotheses techniques have been developed [5]. In the standard techniques using multi-hypotheses for the state estimation and tracking, the Kalman filter is used under the premise that the noise distributions are Gaussian and the system dynamics are linear [6]. However, when tracking human movements, non-linear and non-stationary assumptions make it suboptimal to use. In this context particle filter algorithms are attractive because they are both simple and very general. The particle filter algorithms track objects by generating multiple hypotheses and by ranking them according to their likelihood. They suppose that the correct hypothesis is retained [7][8]. Many tracking filters have been proposed using this approach, defining the states as being each static posture or position of the objects and modeling a motion sequence by the composition of these states with some transitional probabilities [9][10]. Those state-of-the-art techniques perform efficiently to trace the movement of one or two moving objects but the operational efficiency decreases dramatically when tracking the movement of many moving objects because systems implementing multiple hypotheses and multiple targets suffer from a combinatorial explosion, rendering those approaches computationally very expensive for real-time object tracking.

Our intelligent environment is achieved by distributing small intelligent devices which don't affect the present living environment greatly. Color CCD cameras, which include processing and networking part, are adopted as small intelligent devices of our intelligent environment. We call this environment "Intelligent Space (ISpace)" [3]. Intelligent Space is constructed as shown in Fig.1. In this paper, how to represent feature vectors of multiple objects using particle filter is described. Then, the technique to achieve the tracking by using color information is described.

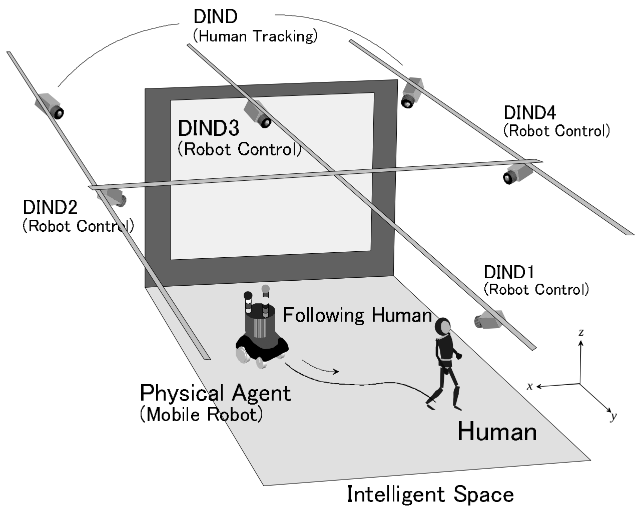

Fig. 1. Intelligent environment by distributed Cameras.

2. Vision Systems in Intelligence Space

2.1 Basic Scheme

Fig.2 shows the system configuration of distributed cameras in Intelligent Space. Since many autonomous cameras are distributed, this system is autonomous distributed system and has robustness and flexibility. Tracking and position estimation of objects is characterized as the basic function of each camera. Each camera must perform the basic function independently at least because over cooperation in basic level between cameras loses the robustness of autonomous distributed system. On the other hand, cooperation between many cameras is needed for accurate position estimation, control of the human following robot[4], guiding robots beyond the monitoring area of one camera[5], and so on. These are advanced functions of this system. This distributed camera system of Intelligent Space is separated into two parts as shown in Fig.2. This paper will focus on the tracking of multiple objects in the basic function.

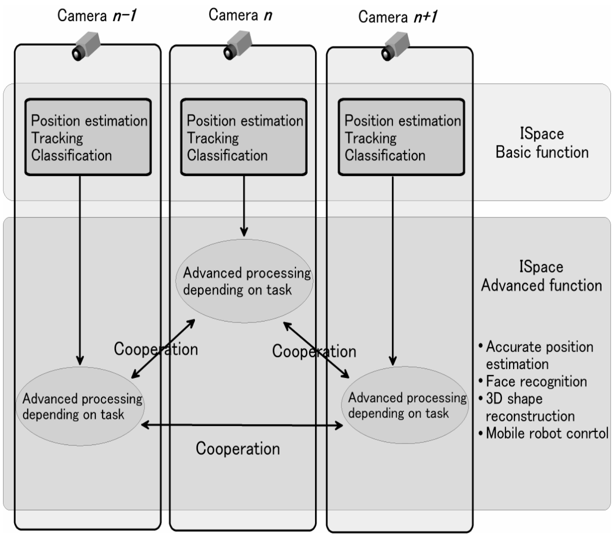

Fig. 2. Configuration of distributed camera system.

2.2 Previous Research for Moving Object Tracking

Various tracking methods of moving objects using a vision system have been investigated. These can be separated in two major compartments. One is the method of matching and clustering of feature points extracted from an input image. For example, optical flows are extracted in a image, and tracking is achieved by clustering of them[11]. The other is the method that the knowledge on objects is given to the system as an object model in advance and the model and an input image are compared. For example, the 3D ellipse model is used for human tracking in [12]. The former has the merit that various feature points can be extracted according to image processing, because the whole of the captured image can be always observed. However, matching of feature points between successive frames become difficult and computational cost increases, according to number of the feature points in the complicated scene and by the effect of noise. The other hand, in the latter method, only comparison between the model and input image is required. Tracking of moving objects is achieved by comparing the real image with the model. Computational cost is lower than the former. However, tracking systems have to prepare the models of the objects in advance. For example, human tracking for surveillance system needs human models[8] and vehicle tracking for ITS needs vehicle models[9]. Tracking cannot be achieved without object models. It is impossible to build a model of every object which exists in our daily life.

3. Processing Flow

3.1 Extraction of Objects

Our system uses many low-cost cameras to improve recognition performance. Position and viewing field of all cameras are fixed. Each camera is connected to a normal computer with a video capture board. It is necessary to extract only the moving objects robustly in order to simplify the matching process. Background subtraction is simple and efficient to recognize the moving objects in fixed camera image. Following process based on background subtraction is performed to extract the object region.

Fig.3 shows the example of results of this object extraction process mentioned above. Fig. 3(a) is the raw image captured by the CCD camera. Extracted objects, which are human and robot, are shown in Fig. 3(b), 3(c). It is clear that this can extract the multiple objects simultaneously. When the image of the size of 320X240 pixels is captured and Pentium III 866 MHz PC is used, this process is performed at the speed of 28 to 30 frames per second. In this process, a lot of processing time is not required. Matching process of the objects between successive frames is based on the information acquired from these extracted objects.

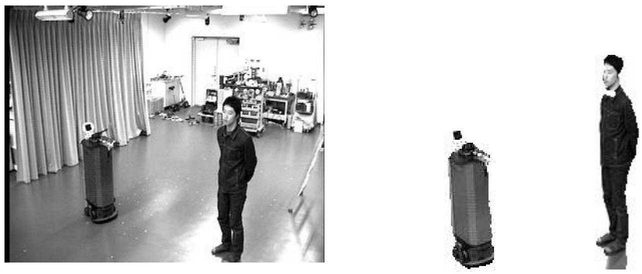

(a) (b) (c)

Fig. 3. Captured image and extracted objects.

3.2 Target regions encoded in a state vector Using Particle filter

Particle filtering provides a robust tracking framework, as it models uncertainty. Particle filters are very flexible in that they not require any assumptions about the probability distributions of data. In order to track moving objects (e.g. pedestrians) in video sequences, a classical particle filter continuously looks throughout the 2*D*-image space to determine which image regions belong to which moving objects (target regions). For that a moving region can be encoded in a state vector.

In the tracking problem the object identity must be maintained throughout the video sequences. The image features used therefore can involve low-level or high-level approaches (such as the colored-based image features, a subspace image decomposition or appearance models) to build a state vector.

A target region over the 2*D*-image space can be represented for instance as follows:

$$r = \{l, s, m, \gamma\} \quad (1)$$

where l is the location of the region, s is the region size, m is its motion and γ is its direction. In the standard formulation of the particle filter algorithm, the location l, of the hypothesis, is fixed in the prediction stage using only the previous approximation of the state density. Moreover, the importance of using an adaptive-target model to tackle the problems such as the occlusions and large-scale changes has been largely recognized. For example, the update of the target model can be implemented by the equation

$$\bar{r}_t = (1-\lambda)\bar{r}_{t-1} + \lambda E[r_t] \tag{2}$$

where λ weights the contribution of the mean state to the target region. So, we update the target model model during slowly changing image observations.

4. Tracking moving objects

4.1 State-space over the top-view plan

In a practical particle filter implementation, the prediction density is obtained by applying a dynamic model to the output of the previous time-step. This is appropriate when the hypothesis set approximation of the state density is accurate. But the random nature of the motion model induces some non-zero probability everywhere in state-space that the object is present at that point. The tracking error can be reduced by increasing the number of hypotheses (particles) with considerable influence on the computational complexity of the algorithm. However in the case of tracking pedestrians we propose to use the top-view information to refine the predictions and reduce the state-space, which permits an efficient discrete representation. In this top-view plan the displacements become Euclidean distances. The prediction can be defined according to the physical limitations of the pedestrians and their kinematics. In this paper we use a simpler dynamic model, where the actions of the pedestrians are modeled by incorporating internal (or personal) factors only. The displacements $M^t_{topview}$ follows the expression

$$M^t_{topview} = A(\gamma_{topview})M^{t-1}_{topview} + N \tag{3}$$

where $A(.)$ is the rotation matrix, $\gamma_{topview}$ is the rotation angle defined over top-view plan and follows a Gaussian function $g(\gamma_{topview};\sigma_\gamma)$, and N is a stochastic component. This model proposes an anisotropic propagation of M : the highest probability is obtained by preserving the same direction. The evolution of a sample set is calculated by propagating each sample according to the dynamic model. So, that procedure generates the hypotheses.

4.2 Estimation of region size

The size of the search region represents a critical point. In our case, we use the *a-priori* information about the target object (the pedestrian) to solve this tedious problem. We assume an averaged height of people equal to 160 cm, ignoring the error introduced by this approximation. That means, we can estimate the region size s of the hypothetical bounding box containing the region of interest $r = \{l, s, m, \gamma\}$ by projecting the hypothetical positions from top-view plan in Fig. 4. A camera calibration step is necessary to verify the hypotheses by projecting the bounding boxes. So this automatic scale selection is an useful tool to distinguish regions. In this way for each visual tracker we can perform a realistic partitioning (bounding boxes) with consequent reduction in the computational cost. The distortion model of the camera's lenses has not been incorporated in this article. Under this approach, the processing time is dependent on the region size.

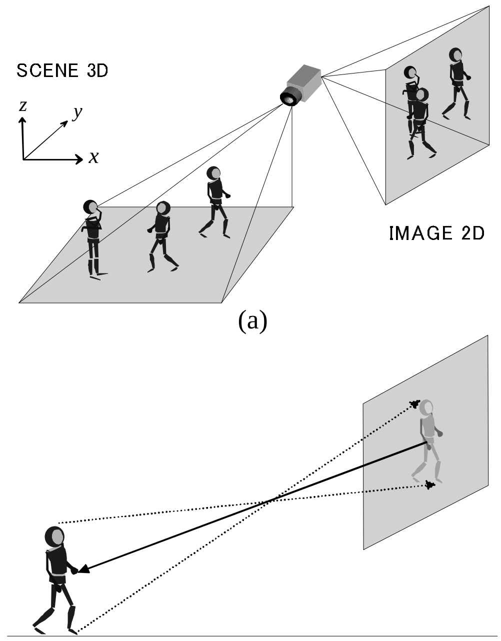

(a)

(b)

Fig. 4. (1) the approximation of Top-View plan by image plan with a monocular camera, (2) size estimation

4.3 Tracking experiments

Some experiments are performed to verify this tracking method. Fig.5 shows the experimental environment and objects that should be tracked by this method. Three objects, which are human, a mobile robot and a chair, exist in this environment. In this experiment, the system does not have object models for these objects in advance. A mobile robot and a chair are static at the beginning and human is walking between them afterward. Since only one camera is used for this experiment, occlusion between human and the other objects is supposed to happen as shown Fig. 5(a). Fig. 5(b) shows the clustering result of the feature vectors obtained in a given time, when three objects exist in the space as shown in Fig. 5(c).

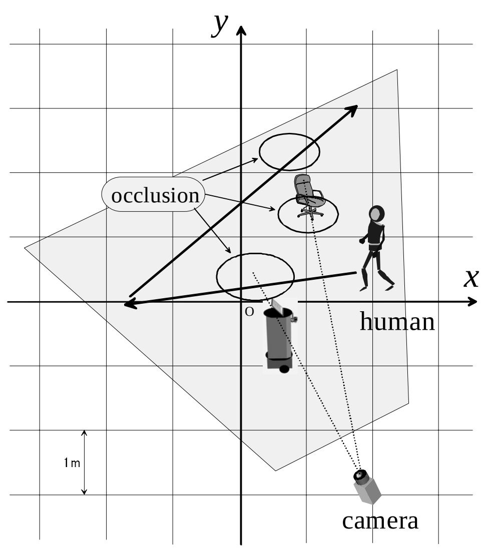

(a)

(b)

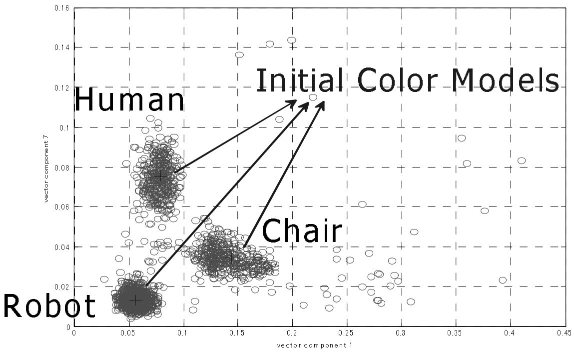

(c)

Fig. 5. Experiment: moving area and models.

Fig. 6 shows the captured image by a camera in this experiment. Experimental result of multiple objects tracking is shown in Fig. 7. X axis and Y axis represent X and Y pixel coordinate of captured image respectively. Central pixels of each object are plotted. Although occlusion between human and other objects was observed during tracking of walking human, matching and tracking of each object achieved without fail. In this case, this system doesn't have the complex object models, however tracking of multiple objects was performed in low processing time.

Fig. 6. Multi-Objects detection and tracking in ISpace.

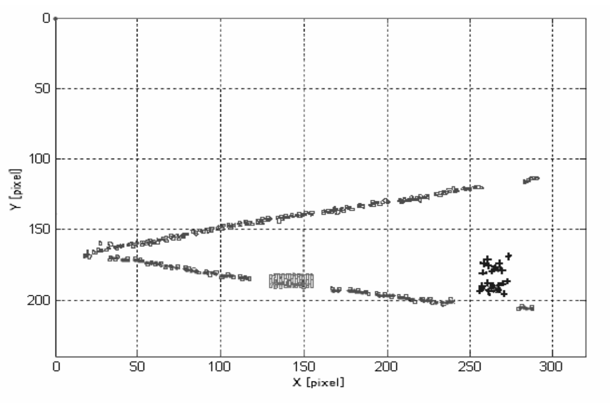

Fig. 7 Experiment results: Multi Objects tracking.

5. Conclusion

In this paper, the basic function of the vision system in Intelligent Space was described. The vision sys tem of Intelligent Space needs real time processing, tracking of multiple objects, extension to cooperative multiple cameras network and overcoming partial occlusion. To realize them, it is required that model based method and feature based method are combined efficiently. Then, new tracking strategy was proposed based on extracting the objects by background subtraction and creating color appearance model dynamically with particle filter. This strategy achieved real-time and robust tracking of multiple objects. Especially, correct matching had been kept after the occlusion among objects happened in the experimental results.

As a future work, representation method of objects that are close to achromatic color will have to be investigated. Next, recognition of the wide area using the distributed cameras should be performed. It will need that different cameras share information about clusters and the feature space. Then, sharing method of the information that each camera acquires will be investigated.

References

[1] A. W. Senior, "Tracking with Probabilistic Appearance Models," in *Proc ECCV workshop on Performance Evaluation of Tracking and Surveillance Systems*, pp 48-55, June 2002.

[2] M. Bierlaire, G. Antonini and M.Weber, "Behavioural Dynamics for Pedestrians," *in K. Axhausen (Ed.), Moving through nets: the physical and social dimensions of travel*, pp. 1-18, Elsevier. 2003.

[3] Joo-Ho Lee, Hideki Hashimoto, "Intelligent Space -concept and contents", Advanced Robotics, Vol.16, No.3, pp.265-280, 2002.

[4] Kazuyuki Morioka, Joo-Ho Lee, Hideki Hashimoto, "Human Centered Robotics in Intelligent Space", IEEE International Conference on Robotics and Automation(ICRA'02), Washington D.C., USA, May 2002.

[5] K. Choo, and D.J. Fleet, "People tracking using hybrid Monte Carlo filtering," In *Proc. Int. Conf. Computer Vision*, vol. II, pp. 321-328, Vancouver, Canada, 2001.

[6] B. Anderson, and J. Moore, *Optimal Filtering*, Prentice-Hall, Englewood Cliffs, 1979.

[7] A. Doucet, N. de Freitas, and N. Gordon, *Sequential Monte-Carlo Methods in Practice*, Springer Verlag, April 2001.

[8] G. Kitagawa, "Monte Carlo Filter and Smoother for Non-Gaussian Nonlinear State Space Models," Journal of Computational and Graphical Statistics, Vol. 5(1), pp. 1-25, 1996.

[9] K. Nummiaro, E. Koller-Meier, L.J. Van Gool, "Object Tracking with an Adaptive Color-Based Particle Filter," *DAGM-Symposium Pattern Recognition*, pp. 353-360, 2002.

[10] J. Vermaak, A. Doucet and P. Perez, "Maintaining Multi-Modality through Mixture Tracking," *International Conference on Computer Vision*, ICCV2003, Nice, France 2003.

[11]Peter Norlund and Jan-Olof Eklundh, "Towards a Seeing Agent", Proceedings of First International Workshop on Cooperative Distributed Vision, pp.93-120, 1997.

[12]Nakazawa Atsushi, Kato Hirokazu, Hiura Shinsaku, Inokuchi Seiji, "Tracking Multiple People using Distributed Vision Systems", Proceedings of the 2002 IEEE International Conference on Robotics & Automation, pp.2974-2981, Washington D.C, May 2002.

The Tenth International Symposium on Artificial Life and Robotics 2005(AROB 10th '05),
B-con Plaza, Beppu, Oita, Japan, February 4-6, 2005

On Vector Autoregressive Model for Action of Human Arm's

Kenji TOMIZAWA
Department of Computer and Systems Engineering
Tokyo Denki Univ.
Ishizaka,Hatoyama,Hiki, Saitama,350-0394
tomisan@hanalab.k.dendai.ac.jp

Kunihiko OURA
Department of Electrical and Electronics Engineering
Kokushikan Univ
4-28-1,Setagaya,Setagaya-ku, Tokyo,154-8515
kuni@kokushikan.ac.jp

Izumi HANAZAKI
Department of Computer and Systems Engineering
Tokyo Denki Univ.
IshizakaHatoyama,Hiki, Saitama,350-0394
hana@k.dendai.ac.jp

Keywords:Vector autoregressive model,AIC, Rate of contribution

Abstract

Human arm's pose is determined by the angles of the shoulder and the elbow. In this paper, we will estimate the relation between the angles of the arm in action using a vector autoregressive model.

1 Introduction

Recently, analysis of human pose and action becomes important in the fields, such as medical treatment, welfare and robotics. The authors proposed the fuzzy models to describe the human-like arm's pose. There wear two types of fuzzy models which depended on the domain's where the hand moved.

In this paper, we propose a vector autoregressive model to estimate the action of the arm.

2 The model of an arm's pose

2.1 Description of the arm's pose

By using the D-H method, we can build the virtual posture model to human's upper limbs. We set coordinates to the body, shown in Figure 1. The arm's pose can be described by the angles of the joints. Considering the constraints of the joints, human-like arm's model is estimated.

a_1 shows the breadth of its shoulders. a_2 shows the length from the shoulder to an elbow. a_3 shows the length from the elbow to the wrist. d_1 shows the length of the body.

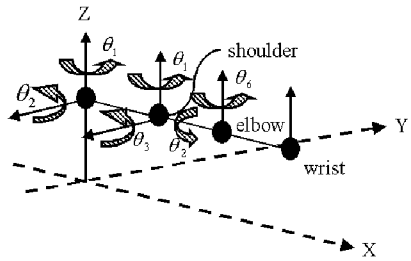

Figure 1: Coordinates of D-Hmethod length between the neck and the shoulder

2.2 Relation between a hand position and each joint angle

Hand position is denoted by (X, Y, Z). Each joint angle is denoted $\theta_i (i = 1 \cdots 6)$. The relation between the hand position and each joint angle is shown below.

$$X = a_3(C_{12}C_{34}C_5 - S_{12}S_5) + a_2C_{12}C_3 + a_1C_1 \quad (1)$$

$$Y = a_3(C_{12}C_{34}C_5 + C_{12}S_5) + a_2S_{12}C_3 + a_1S_1 \quad (2)$$

$$Z = a_3S_{34}C_5 + a_2S_3 + d_1 \quad (3)$$

where

$$C_i = \cos\theta_i, S_i = \sin\theta_i,$$
$$C_{ij} = \cos\theta_i + \theta_j, C_{ij} = \sin\theta_i + \theta_j$$

Angle γ and δ are set such that Figure 2 shows.

The coordinates of the hand, the elbow, and the shoulder are (x_h, y_h, z_h), (x_e, y_e, z_e), (x_s, y_s, z_s), respectively.

The distances A, B, C, and D shows in Figure 2 is as follows.

$$A = \sqrt{(x_e - x_h)^2 + (y_e - y_h)^2} \quad (4)$$

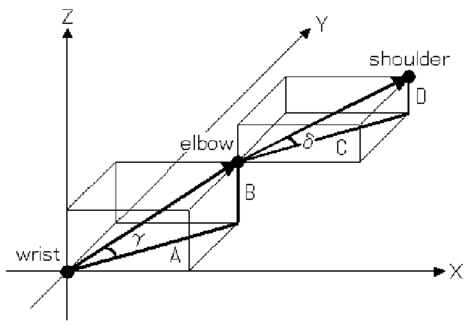

Figure 2: The angles of hand, elbow, and shoulder

$$B = | z_e - z_h | \tag{5}$$

$$C = \sqrt{(x_s - x_e)^2 + (y_s - y_e)^2} \tag{6}$$

$$D = | z_s - z_e | \tag{7}$$

From (4) and (5),we get

$$\tan\gamma = \frac{z_e - z_h}{\sqrt{(x_e - x_h)^2 + (y_e - y_h)^2}} \tag{8}$$

$$\gamma = \tan^{-1}\frac{z_e - z_h}{\sqrt{(x_e - x_h)^2 + (y_e - y_h)^2}} \tag{9}$$

From (6) and (7),we get

$$\tan\delta = \frac{z_s - z_e}{\sqrt{(x_s - x_e)^2 + (y_s - y_e)^2}} \tag{10}$$

$$\delta = \tan^{-1}\frac{z_s - z_e}{\sqrt{(x_s - x_e)^2 + (y_s - y_e)^2}} \tag{11}$$

3 Vector autoregressive model

$X(n) = (x_1(n), \cdots, x_k(n))$ denote the time series. $U(n)$ is white noise sequence. Vector autoregressive model is as follews. It is shown in (12).

(1)The autoregressive model

$$X(n) = \sum_{m=1}^{M} A(m)X(n-m) + U(n) \tag{12}$$

$$A(m) = \begin{bmatrix} A_{11}(m) & \cdots & A_{1k}(m) \\ \vdots & \ddots & \vdots \\ A_{k1}(m) & \cdots & A_{kk}(m) \end{bmatrix} \tag{13}$$

(2)Autoregressive coefficient

The Mth coefficient is decided by (14).

$$c_i(m) = A_{ii} \qquad m = 1, \cdots, M \tag{14}$$

Cofficients $A(m)$ is estimated by Levinson-Durbin Algorithm.

(3)Impulse response function

The impulse response function from $x_j(n)$ to $x_i(n)$ is calculated by (15) and (16).

$$a_{ij}(m) = A_{ij}(m) + \sum_{k=1}^{m-1} c_i(k)a_{ij}(m-k) \tag{15}$$

$$a_{ij}(m) = \sum_{k=1}^{M} c_i(k)a_{ij}(m-k) \tag{16}$$

Variable $x_i(n)$ is obtained by (17).

$$x_i(n) = \sum_{j=1}^{k}\sum_{m=1}^{M} a_{ij}(m)x_j(n-m) + u_i(n) \tag{17}$$

The frequency response function from $x_j(n)$ to $x_i(n)$ is calculated by (18).

$$a_{ij}(f) = \sum_{m=1}^{M} a_{ij}(m)e^{-2\pi imf} \tag{18}$$

The power spectrum of noise($u_i(n)$) is set to (19). σ^2 is variance of $u_i(n)$.

$$P_{ui}(f) = \frac{\sigma^2}{| 1 - \sum_{m=1}^{M} c_i(m)e^{-2\pi imf} |^2} \tag{19}$$

$$A(f) = \begin{bmatrix} 1 & -a_{12}(f) & \cdots & -a_{1k}(f) \\ -a_{21}(f) & 1 & \cdots & \cdots \\ \vdots & \vdots & \ddots & \vdots \\ -a_{k1}(f) & \cdots & \cdots & 1 \end{bmatrix} \tag{20}$$

The power spectrum of $x_i(n)$ can be decomposed into (21) and K ingredients. (22) is the noise portion of $x_i(n)$. (23) can calculate the rate of noise contribution.

$$P_{ii}(f) = \sum_{j=1}^{k} | b_{ii}(f) |^2 \, P_{uj}(f) \tag{21}$$

$$q_{ij}(f) = | b_{ij}(f) |^2 \, P_{uj}(f) \tag{22}$$

$$r_{ij}(f) = \frac{q_{ij}(f)}{P_{ii}(f)} \tag{23}$$

The Tenth International Symposium on Artificial Life and Robotics 2005(AROB 10th '05),
B-con Plaza, Beppu, Oita, Japan, February 4-6, 2005

4 Experiment

4.1 Measurement conditions

Experiments are performed as follows.

1. A subject is sat down in the chair.
2. The subject moves his hand on a desk.
3. The height of a desk is same as the height of his navel.
4. Positions of his right shoulder, his right elbow, his right-hand head, his navel, and his throat are mesured by motion capture.
5. Sampling interval of observation is 0.0084[ms].
6. Repetition operation is measured in the domain where the subject moves his hand easily.
7. Same action is repeated 50 times.

It is shown in Figure 3.

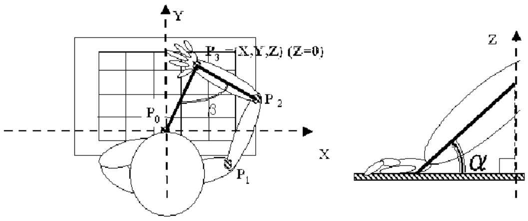

Figure 3: The situation of the experiment

4.2 The measured waveform

The measured waveform is shown in Figure 4, 5, and 6. The number of data is 2000. The angle γ and δ are calculated from these date and are shown in Figure 7, 8.

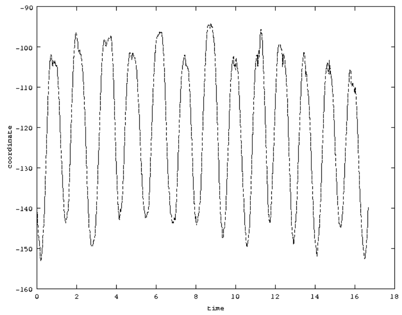

Figure 4: Coordinates x of the wrist

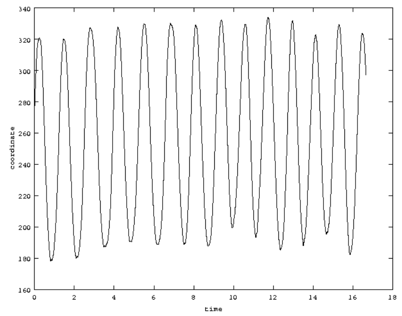

Figure 5: Coordinates y of the wrist

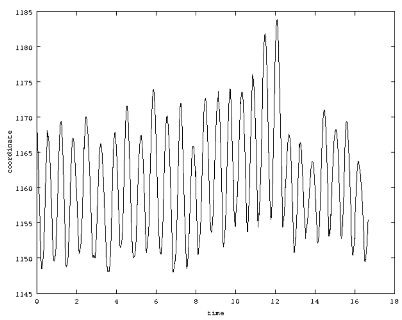

Figure 6: Coordinates z of the wrist

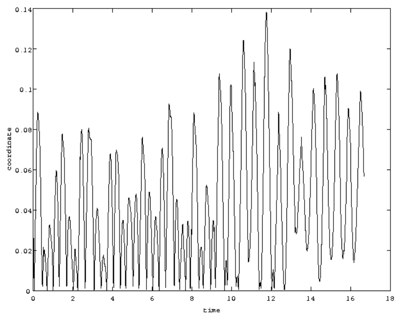

Figure 7: Angles γ

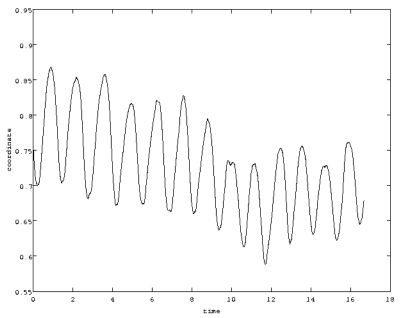

Figure 8: Angles δ

4.3 Application of vector autoregressive model

The relation between angle γ and δ is estimated by vector autoregressive model. The order of the model is determined by AIC.

It was decided that we would be the 10th order. The rate of contribution is calculated from (7) and (8). A result is shown in Figure 9.

The motion of the wrist and the motion of an elbow are interlocking. If frequency becomes high, the tendency for which a motion of an elbow depends on a motion of a wrist will become strong.

5 Conclusion

We estimated the pose of the upper limbs in action by using vector autoregressive model. Estimated model described the relation between the angles of the wrist and the elbow. And gave the contribution rate to show the dependence between the movement of the wrist and the elbow. In this experiment, the action was performed only in the domain where the subject move his arm easily.

In the future, we will determine the model of the

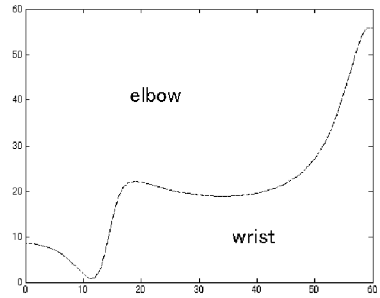

Figure 9: The rate of contribution

action out of this domain.

References

[1] Peter J.Brockwell, Richard A.Davis, "Introduction To Time Series and Forecasting 2nd edition", *Center for Academic Publications*, 2004.

[2] Lennart Ljung, "System Identification Theory for the User Second Edition," *PRENTICE HALL*, 1999.

The Tenth International Symposium on Artificial Life and Robotics 2005(AROB 10th '05),
B-con Plaza, Beppu, Oita, Japan, February 4-6, 2005

Outwit game – a dynamical systems game for market dynamics

M. Konno
m-konno@jaist.ac.jp

T. Hashimoto
hash@jaist.ac.jp

School of Knowledge Science
Japan Advanced Institute of Science and Technology (JAIST)
1-1, Tatsunokuchi, Ishikawa, Japan, 923-1292

Abstract

A dynamical systems game model of market, called Outwit Game, is proposed. In the game, individual behavior in a market is abstracted as orienting majority and orienting minority. We suppose that individuals' profit changes with a course of these two actions. Through computer simulations, we show that an index representing both micro and macro dynamics show a power law distribution.

Keywords: Outwit Game, Dynamical Systems Game, Market Dynamics, Micro-Macro Loop, Power Law Distribution

1 Introduction

In this paper, we propose a game model, called Outwit Game (OG), for capturing dynamics of market by considering individuals behavior in a market. In neo-classical economics, the assumptions of the perfect competitive market and the perfect rationality make the market model static. However, any market, in reality, dynamically changes. Therefore, in order to understand the real market, we need a model that includes dynamics of market and individual behavior.

The real market is composed of interactions among individuals in a game theoretic situation. Namely, others' action affects decision making and consequences of actions by an individual and vice versa. In addition to the interactions among individuals, there exist interactions between individuals' actions, that is, micro dynamics, and change of a market, that is, macro dynamics. This circular interacting causation is called "micro-macro loop" by Shiozawa[1]. We think that the essence of market dynamics consists of endogenous change induced by individuals' actions, interaction among individuals, and the micro-macro loop.

Constructing a game theoretic model of a market, we put importance on the following points:

- The perfect competition should not be assumed for a model of markets.
- The perfect rationality should not be assumed for a model of individuals.
- The model should include dynamic and strategic interaction among individuals.

In order to focus on the dynamical change of market, we adopt a framework of dynamical systems game[2]. It is an extension of the game theory for describing changes of game environment such as payoff matrix, options by players.

2 Individuals' Actions in Market

At first, we consider the properties of individual behavior in a market. Keynes[3] likens a market to a beauty contest, in which the prize goes to a parson who is voted at most and the voters for the winner earn. In this beauty contest, people try to vote for a parson who is thought of as the most beautiful by most of the people, not for a parson they themselves think as the most beautiful. In financial market, people try to invest a company that many investors invest. This is an action pursuing a trend and orienting a majority.

Investors do not always follow trends. They invest in a company that is not in a trend at present and may be in future, invest to a new business, or sell stocks they have before the upward trend ceases. Namely, people try to make a trend by themselves. This action is not to do the same action as others and favors minority.

In the market, people change over these two actions, orienting majority and orienting minority and gain or loss. Switching two actions may be a trigger of change of trends. The market change is often induced by the trend changes. Although the people favor majority or minority intentionally, the consequence of an action is determined by the market. This is an uncertainty of market.

3 Outwit Game

Based on the above discussion, we introduce a game abstracting the real market. In the game, individuals' actions have features of orienting majority and minority, that changes with the state of market. This type of game is named as Outwit Game (OG).

We define two versions of the OG, Simple Outwit Game (SOG) and Monetary Outwit Game (MOG). The MOG is relatively complex version than the SOG. In the MOG, so as to approach to the dynamics of real market, two forms of profit, capital gain and realized gain, are considered. These two games share the essential part. We analyze the SOG at first and report in this paper. The MOG is not treated in this paper.

3.1 Definition of Simple Outwit Game

The procedure of the SOG is the followings:

1. Each player selects one of two alternative moves at each time step t.
2. The majority and minority sides are decided from all players' moves.
3. Each player is grouped into the majority or the minority according to his/her move and given the payoff $p(t)$ defined by Table 1.

Table 1: The payoff matrix of Simple Outwit Game

move	payoff
Majority	$p(t) = \dfrac{N^{\mathrm{M}}(t) - N^{\mathrm{M}}(t-1)}{N}$
Minority	$p(t) = 0$

In Table 1, $N^{\mathrm{M}}(t)$ and $N^{\mathrm{M}}(t-1)$ are the number of majority players at the present (t) and the previous step $(t-1)$, respectively, and N is the number of all players. Note that $N^{\mathrm{M}}(t)$ and $N^{\mathrm{M}}(t-1)$ change with time, the players have the possibility both to gain and to loss when they keep in the majority side. If they are in the minority side, they are always risk-free.

3.2 Players' Action

In a game theoretic model, players pursue their own profit. In SOG, the player must predict the number of majority and decide the move at the next step according to the prediction in order to pursue his/her profit. Namely, they decide their move as

$$l(t+1) = \begin{cases} \text{Majority} & (\tilde{N}^{\mathrm{M}}(t+1) > N^{\mathrm{M}}(t)) \\ \text{Minority} & (\text{otherwise}) \end{cases} , \quad (1)$$

where $l(t+1)$ is the side of majority or minority and $\tilde{N}^{\mathrm{M}}(t+1)$ is the predicted number of majority at the next step. Note that the players cannot certainly be a majority/minority when they want to be so. They must predict which move is the majority/minority as well. Accordingly, SOG has double uncertainty in the prediction of the number of majority and its move.

4 Players' Model for Simulation of SOG

We analyze the characteristics of SOG using computer simulations. In the simulation, we use a model of players with prediction and learning. Because of the space limit, we briefly explain the players' model.

Each player has two kind of prediction functions for the number and the move of majority from the present information. At first a player predict the number of majority in the next step,

$$\tilde{N}^{\mathrm{M}}(t+1) = P^{\mathrm{N}}(N^{\mathrm{M}}(t), m^{\mathrm{M}}(t), m(t)) \ . \quad (2)$$

This expression represents that a player produce a predicted number of majority $\tilde{N}^{\mathrm{M}}$ at the next step $t+1$, based on the number of majority, $N^{\mathrm{M}}(t)$, the move of the majority side, $m^{\mathrm{M}}(t)$, and the move of the player itself, $m(t)$, at the present step t.

Further, using the same information at the present and the output from the prediction function, P^{N}, the player try to predict the move of the majority $\tilde{m}^{\mathrm{M}}(t+1)$ at the next step using the other prediction function P^{m},

$$\tilde{m}^{\mathrm{M}}(t+1) = P^{\mathrm{m}}(N^{\mathrm{M}}(t), m^{\mathrm{M}}(t), m_i(t), \tilde{N}^{\mathrm{M}}(t+1)) \ . \quad (3)$$

Every time step, the players adjust the prediction function according to success and unsuccess of the predictions.

5 Simulation Results

We analyze the dynamic behavior and statistical properties of the game. The total number of players is 51, two moves are -1 and 1.

5.1 Dynamics of Game

To see the dynamics of SOG, we observe the transition of the players' payoffs. The most of players can gain the payoffs averagely. Three examples of the transitions of accumulated payoffs,

$$S_i(t) = \sum_{t'=0}^{t} p_i(t') \ , \qquad (4)$$

are depicted in Fig. 1, where $p_i(t)$ is the payoff of the i-th agent at the time step t. We find three types of the transition: rapid increasing in a long range, slow increasing, and decreasing.

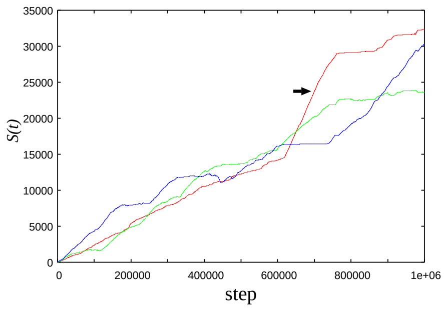

Figure 1: The transition of the accumulated payoff $S_i(t)$ of tree typical players. The x axis is time step, the y axis is the accumulated payoff. The arrow indicates a player depicted in Fig. 2.

The increasing of the accumulated payoff means that the players are able to predict the transition of the majority and it's move to some extent. We observe more closely the dynamics of the game in order to know how they obtain the payoff (Fig. 2). Figure 2(a) depicts the accumulated payoff of a player whose accumulated payoff grows rapidly in the period from 630000 to 730000 steps in Fig. 1 (indicated by an arrow). The player gains some payoff every three steps. The time series of the player's moves is period three (-1, -1, 1) as shown in Fig. 2(b). Figure 2(c) is the time series of the majority's move. This shows period three dynamics (-1, 1, -1). Namely, the player's belonging group changes as (majority, minority, minority). Finally, we draw the change of the number of minority from last step, that is, $N^{\mathrm{M}}(t) - N^{\mathrm{M}}(t-1)$, in Fig. 2(d). This value also shows period three dynamics as (positive, negative, negative). Accordingly, the player belongs to the majority when he/she can gain and to the minority when he/she may loss. In other words, he/she can appropriately outwit.

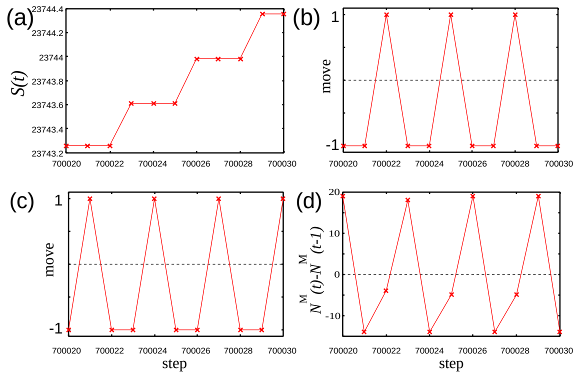

Figure 2: Transitions of (a) the accumulated payoff, $S(t)$ of a player, (b) the moves of the player, (c) the majority's move, and (d) the number of change of majority per one step, $N^{\mathrm{M}}(t) - N^{\mathrm{M}}(t-1)$, at the period of time step (the x axis) between 700020 and 700030.

5.2 Power Law Distribution of Players' and Market Dynamics

We observe some statistical characteristics of SOG. Figure 3(a) shows a distribution of the length that the players continue to take the same move. The straight line is a fitting taken at the range longer than 30. This observation value obeys a power law distribution in the range of longer length, while in the range of shorter length the value is much larger than the extrapolation of the power law fitting in the longer range. This means that the players mostly change their move shortly, but some players often do not change their moves very long periods.

Figure 3(b) is a distribution of the length that the majority continues to take the same move, namely a version of global value or market dynamics of Fig. 3(a). This value also obeys a power law.

6 Discussion

6.1 Power Law Distribution in Market

We found the power law distributions in the length of consecutive time steps that individuals take the same move and that the majority is in the same move. The former can be thought of as a characteristic of individual action, that is, a micro dynamics, and the latter as that of market, that is, a macro dynamics. If we interpret the latter index as the length of trends, this result means that infinitely long trends can occur in a market. Namely, there is possibilities of large

The Tenth International Symposium on Artificial Life and Robotics 2005(AROB 10th '05),
B-con Plaza, Beppu, Oita, Japan, February 4-6, 2005

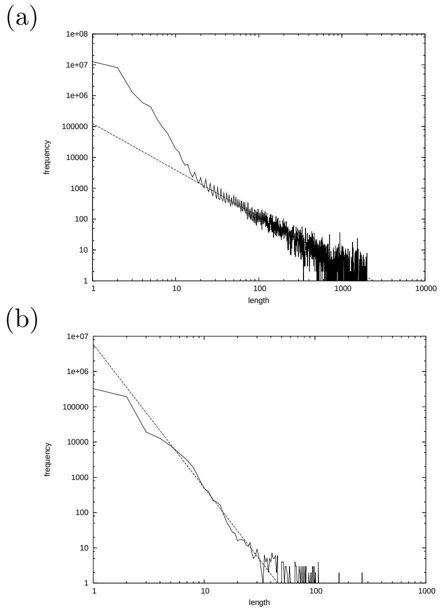

Figure 3: The distribution of the consecutive length of the same move taken by (a) the players and (b) the majority side. The x and y axes are the length and the frequency, respectively. The straight lines are fitting by pow functions at ranges that length is (a) longer than 30, and (b) 1 to 100.

stock bubbles, long term inflations and deflations in financial markets.

Power laws have been found in several indices in real financial markets. We have not, however, made correspondence between such power laws and the power law distribution in our game model. The reason why such power law is observed in our game model is also an open problem.

6.2 Comparison with Minority Game

A game that can be considered as a model of market is the Minority Game (MG)[4]. The Outwit Game (OG) is thought of as a modification of MG. The differences between the OG and the MG are the followings:

1) In the OG, two kind of actions, orienting majority and minority are taken into consideration, while the MG takes only the action orienting minority.

2) The OG has a payoff matrix that changes with time (explicitly includes a time variable t), while the payoff matrix of MG is fixed[1].

[1] As a simple modification of the MG, the number of majority can be given to the minority. Although the relative value of the payoff changes with time in this modification, the essential payoff structure that the minority is always win does not change.

3) In the OG, to win the game, players should select the majority/minority appropriately responding to changes of game situations, while in the MG to be the minority is always to win.

6.3 SOG as Tragedy of a Common

The SOG has a characteristic of tragedy of a common. If a player in the SOG change from the majority to the minority in order to avoid a loss, the other players in the majority suffer a loss. For example, when n players are in the majority, suppose a player changes to the minority. Since the number of the majority decreases to $n-1$, the players remaining in the majority lose their payoff. But the player changed to the minority eludes a loss. Namely, an action pursuing individual's own profit conflicts with profit of the whole.

7 Conclusion

We propose a new dynamical systems game theoretic model of financial market. This game is named the Outwit Game. The simplest version of the game, the Simple Outwit Game, is analyzed using computer simulations. We show that indices corresponding to a micro and macro dynamics obey the power law. Thus, it can be said that the Outwit Game reflect some nature of market dynamics. The analysis of the Outwit Game should be progressed for showing the utility of this game model for understanding market dynamics.

Acknowledgements

The authors are grateful to Makoto Nishibe and Susumu Egashira for their fruitful suggestions.

References

[1] Y. Shiozawa, "On micro-macro loop" (in Japanese), *Keizai Ronsou (Kyoto University)*, **164**(5), 1–73, 1999.

[2] E. Akiyama, K. Kaneko, "Dynamical systems game theory and dynamics of game", *Physica D*, **147**, 221–258, 2000.

[3] J. M. Keynes, *The General Theory of Employment, Interest, and Money*, Macmillan Cambridge University Press, 1936

[4] D. Challet and Y. C. Zhang, "Emergence of cooperation and organization in an evolutionary game", *Physica A*, *246*, 407–418, 1997.

The Tenth International Symposium on Artificial Life and Robotics 2005(AROB 10th '05),
B-con Plaza, Beppu, Oita, Japan, February 4-6, 2005

Artificial Ecosystem on the Resource Conservative Tierra Structure

Shuichi Matsuzaki*, Hideaki Suzuki**, Minetada Osano*

*Graduate School of Computer Science and Engineering, Aizu University
Aizu-Wakamatsu City, Fukushima 965-8580 Japan

**ATR Network Informatics Laboratories
2-2-2 Hikaridai Seika-cho, Soraku-gun, Kyoto 619-0288 Japan

Abstract

In this paper, we present an Artificial Life system with a remodeling of Tierra. This system provides a rule for a system environment, which is induced by the natural resource property: "matter resources" will be conserved and recycled through biochemical reactions. Because of that point, fundamental components (as matter) of digital creatures being conserved (never being added/deleted) are introduced into this system. Consequently, the system forces the creatures to recycle their program ingredients in order to self-replicate. We have developed two distinct ancestor programs called "Plants" and "Animals," which they can recycle resources by executing photosynthesis/preying. Our experimental results demonstrate that particular interactions, which are similar to a *food web*, appeared as a result of the recycling actions, and such interactions stabilized the population equilibrium among groups of Plants and Animals. In addition, co-adaptive evolutionary behaviors caused by predator-prey interactions are also observed.

Keywords: Tierra, self-replication, resource conservative system

1. Introduction

The Cambrian explosion, an example of Adaptive radiation with the sudden appearance of many animal body plans, produced most types of higher taxonomic categories of actual animals [1]. It is assumed that the rich environmental resources of "space" and "matter" mainly caused this outstanding evolutionary event.

Tierra is an artificial life (Alife) system designed to realize such biological behaviors in computer architectures [2,3]. A Tierran digital creature that consists of a self-replicating program and a CPU create its replicant (copy of itself), and also evolve it through mutations. For example, one class of mutants called "parasites" appears in Tierra experiments, and these parasites will self-replicate by partly depending on other programs. In addition, Network Tierra, a following study of Tierra, modeled digital creatures that are organized by several distinct programs, and showed that the programs can differentiate into more specialized units [3,4]. Having shown such evolutionary behaviors in artificial systems, a kind of extraordinary evolution of the natural ecosystem can be reproduced by the Alife systems, while another type of evolutionary phenomenon in which it will continuously affect creatures with far tinier changes is hardly shown in such systems.

In principle, natural creatures belong to a particular trophic level, and their evolutions are affected by mutual interactions (such as predator-prey interactions) in order to stabilize an entire food web (the resource-recycling system). In terms of this, an aspect of the preservation of space/matter resources, which is a type of abiotic rule, causes creature interaction. In contrast to such a system, resources become freely available (with looser limits) within the above-mentioned systems that Tierra shows. From these points, we consider that a strong restriction of the resources may produce one kind of evolutionary behavior, while a weak one causes another kind.

In this paper, we present an Alife system with a remodeling of the Tierran structure. The remodeling focuses on the appearance of a spontaneous interaction of digital creatures and the global systems resulting from the interaction. A theory proposed by Suzuki *et al*. [5] formed the underlying concept of this study: the theory of "Symbol Resource Conservation". This theory suggests that the component symbols (or symbol ingredients) in which matter is equivalent be conserved in each elementary reaction. A set of Tierran instruction words, represented by bits, composes a self-replicating program. Those bits are regarded as a fundamental matter of the system. The instruction words, however, can be copied/overwritten by elementary reactions (computations). Hence, the Tierra Operating System (OS; namely, a higher-level manager) prohibits overwriting on "active instruction words" (components of active programs). Nevertheless, the total number of active instruction words explodes in the RAM unless a *reaper* perpetually eliminates creatures. If no elimination occurs, the system will not be able to function due to memory overflow. Without conserving matter, systems with a conserved (limited) space will experience this problem in principle. Consequently, we have assumed that the instruction words of Tierra should be given more rational characteristics as matter. Our model introduces an environmental rule whereby each instruction word is conserved, and because of this rule, creatures recycle the words to self-replicate. We show here two types of creature designed with distinct manners of recycling the words.

In the next section, we introduce the digital creatures and some important rules of the system. Following that, we show several of our experimental results, and then provide concluding remarks.

2. The Model

2.1. Self-Replicating Programs

Our model characterizes a "word" with the following two aspects: on the one hand it is represented by six bits (each order corresponds to a type); on the other hand, each of its appropriate sets represents a self-replicating program. The system produced by this model conserves every bit as the ingredient of the words. All–possible combinations of six-bit sets are classified into two categories: *instruction words* and *no-instruction words* (the CPU will decode instruction words into particular computations, but will not decode no-instruction words). These words are necessary for digital creatures to use/reuse in their self-replication, and such actions are included within a copy procedure of our ancestor programs (thus, this part of the Tierra program has been almost fully renewed). We have developed the following two types of ancestor program with distinct copy procedures.

(1) Plant Ancestor

In principle, creatures in this model can replicate one instruction word within one replicating cycle (thus, self-replication will be accomplished by finishing all the cycles).

An ancestor program called a "Plant" synthesizes no-instruction words during each replication cycle, and then produces instruction words. Figure 1 shows an actual example of a replication cycle, and each of its actions (1-7) is described as follows:

1. Identify an instruction word that a creature will replicate during this cycle.
2. Obtain an arbitrary no-instruction word (Element A) by searching entire memory space.
3. Obtain another arbitrary no-instruction word (Element B) by searching entire memory space.
4. Produce an instruction word (Product. It is equivalent to what is identified in **1**) by using and arranging 12 bits within Elements A and B.
5. Produce an arbitrary instruction word (By-product) by using and arranging six bits that are not used in **4**.
6. Move the Product to an address allocated for a replicant.
7. Move the By-product to the address where Element B was.

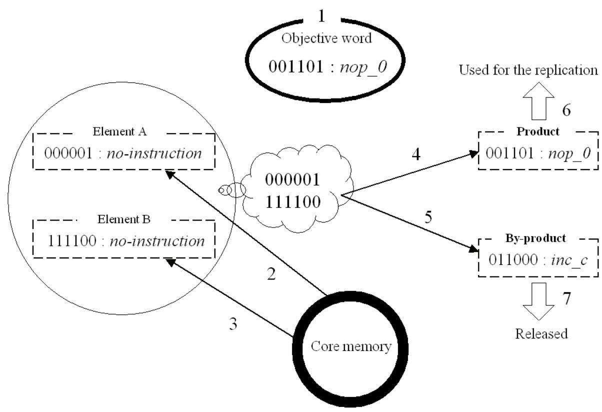

Figure 1. An example of the replication cycle for Plants.

In brief, in order to replicate each word, ingredients of two no-instruction words (obtained in **2** and **3**) will be recycled to ingredients of two instruction words (**4** and **5**). Since this action will increase the number of instruction words in a system, Plants are considered as a producer of instruction words in a system.

(2) Animal ancestor

In each replicating cycle, Animals first identify an instruction word that they will replicate during this cycle (the same manner as Plant's), after which they will begin searching this instruction word by checking each address outward in both directions (within the range of 350). Then, Animals will obtain the instruction word and finish the cycle if they can satisfy the following conditions in parallel:

(a) If the creature finds the instruction word;
(b) If its "CPU state" equals *True*.

The condition of (a) will be satisfied when the search reveals a corresponding instruction word. In the next condition, the CPU state represents a kind of Boolean register (*True*/*False*) equipped in the CPU, and the state existing at the every beginning of replication cycles is fixed to *False*. It can only be changed with "template matching," which will be executed in parallel with the search. The search template, which has been installed on the Animal programs, will look for a corresponding template matching itself (such a manner is similar to that of Tierra). On matching the search template with another template, the CPU state will switch to another state: *True* →*False* or *False*→*True*.

To take the case of Animal ancestor, a matching of its search template with its own "membrane template" (templates which exist at beginning and end of each program) will occur, and the Animal changes its CPU state (*False*→*True*). Having changed its CPU state to *True*, the Animal satisfies the condition of (b), and it will obtain a word to replicate when it satisfies the condition of (a) after this. However, by matching its search template with another membrane template afterward, it will change its CPU state again (*True*→*False*), and it will not obtain words.

Animals can obtain not only non-active instruction words (not a component of programs), but also active instruction words, enabling them to take component instruction words away from the other self-replication programs. Since such behavior of Animals can eliminate other creatures, it is regarded as predation in our model.

2.2 System environments

(1) Death

A function of OS for eliminating a creature removes a CPU from the system and changes the state of component words into the non-active one. This function will eliminate a creature in which at least one of the following conditions is fulfilled:

- By losing an instruction word necessary to self-replicate, the OS will eliminate the creature. Predations and some mutations (wrong cases) can remove/modify instruction words, and they might make a self-replicating program an invalid one.
- By failing to execute any of its own instruction words within 3,000 steps, the OS will eliminate it. An *instruction pointer* might jump incorrectly to other programs by errors/mutations, but will rarely return to its own program.
- By failing to replicate an instruction word in 100 cycles, the OS will eliminate this creature at 10%.

(2) Resource Management

The OS sets the following rules relating to an existence of words.

- If the number of active instruction words amounts to 80% of the total, the OS will prohibit creatures from obtaining any more words. Without this rule, creatures use most of the words for their own self-replication, giving rise to result that none of them will be able to obtain enough further words to self-replicate.
- If a non-active instruction word has not been used by any creatures during those first 100 steps, the OS will change it into an arbitrary no-instruction word. As we have already seen, since Plants will synthesize instruction words from no-instruction words, the number of instruction words will unilaterally increase. In this respect, this rule will make up a balance of the two word types. In comparison with the natural world, this rule is regarded as a kind of dissimilation: the process of gradually changing materials of dead bodies into other materials by chemical reactions.

3. Experiments

3.1. Basic Experiment

Here we present experimental results of a system in which Plant and Animal ancestors are initially inoculated. First, Fig. 1 shows variables for populations of Animals and Plants.

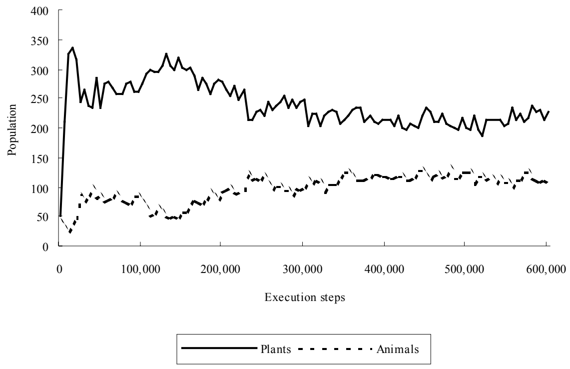

Figure 2. Populations of Animals and Plants.

In the early steps the system explodes its population of Plants and brings the population almost to its maximum possible size. The system then starts increasing its population of Animals, decreasing the Plant population inversely. Although the population equilibrium between them fluctuates during the several-hundred-thousand steps of the experiment, it does gradually stabilize after a while. With respect to these results, we have considered the following:

1. The words are randomly given initially (the total number is fixed). Plants can obtain sufficient no-instruction words, and they increase. On the other hand, Animals can rarely gather enough instruction words for self-replication because there are few available instruction words around them.
2. By increasing the population of Plants, an increase in the total number of instruction words will follow, after which the Animal population will start to increase. However, having decreased the number of no-instruction words, further replications of Plants becomes increasingly difficult.
3. A decrease in the total production of instruction words will follow a decrease in the Plant population (and an increase in the Animal population). Through the function of the OS (see 2.2(2)), the number of instruction words will also decrease after that. Thus, further replications of Animals become ever more difficult. However, having boosted the number of no-instruction words, the population of Plants will start to increase again. As a result of these interactions, the population equilibrium between Animals and Plants will stabilize.

Next, we describe another experimental result that illustrates predator-prey interactions. In the system, the interaction by which predators attempt to gain the instruction words of prey is regarded as a predation. Before every predation occurs, the predator checks that its search template can match a membrane template of the prey. If these templates match, the prey will be protected from the predator. Therefore, It is considered that a diversity of matching patterns of the membrane template is a measure of a creature's ability to protect itself against enemies (by making a template longer, the membrane template will come to match more types of short templates representing the search templates in most cases). For this reason, we use the Matched Template Number (MTN) as the measure that indicates a prey's ability to protect its entire program against predation. The MTN of each creature represents the total number of template matchings in which its membrane templates match templates of "all possible four-letter words" (the search template basically contains four-letter words). Figure 3 shows variables of the MTN (maximum: 32) of each group.

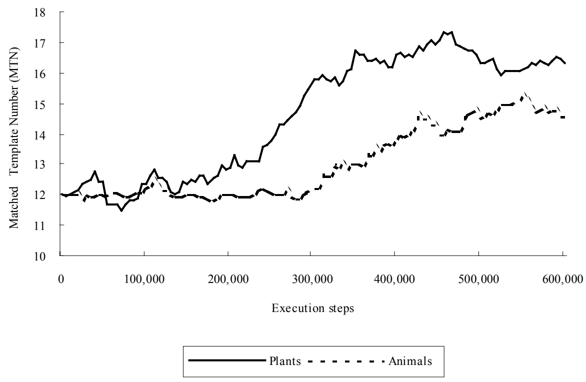

Figure 3. Matched Template Number.

The MTN of each group keeps increasing almost through the experiment. In addition, the MTN of Plants is higher than that of Animals in most cases. An increasing MTN actually indicates a lengthening of templates, and places the heavier load on self-replication; however, it has been observed perpetually in the experiment, that is to say, this result shows mutations in creatures for adapting to predations by other Animals.

As we have seen above, the experimental results in Figs. 2 and 3 indicate that this system produces two varieties of creature interaction that influence creature behaviors. We finally summarize the consideration given in the experiment.

- In this resource-conservative system, a particular relationship between Animals and Plants in which each group indirectly cooperates with each other has appeared through their reactions of the resource-recycling process.
- In local reactions, competition among individual creatures has been observed, causing creatures to mutate in order to adapt to each other.

3.2. Experiment with a Simple Replicator

It is considered as one of the advantages of resou-rce-conservative systems that they may limit an explo-sion of trivial replicators with a simple structure. These systems will preserve the digital creatures from being expelled by such trivial replicators. From this point, we have planned an experiment in which simple replicators are deliberately inoculated. We have conducted the experiments not only in our model, but also in Tierra, to compare the results. We prepared a simple replicating program with 20 instruction words that were all composed by Tierran instruction words. Therefore, this program can perform within both of those models.

Figure 4 shows the results of the experiments where the simple replicator is added in 3,000 steps.

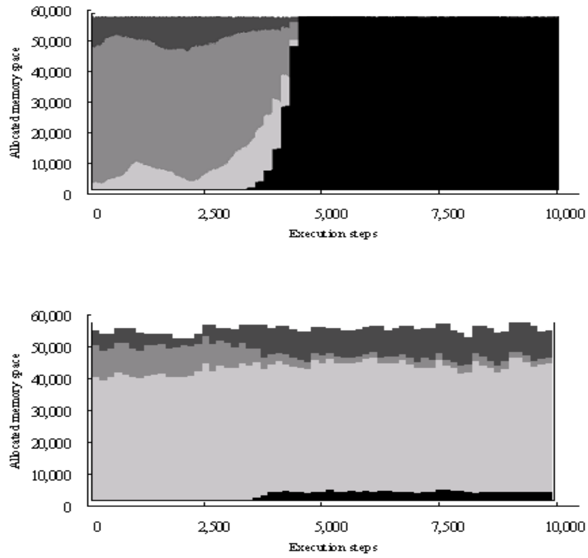

Figure 4. Results of an experiment with a simple replicator. Both of these graphs, Tierra (upper) and our model (lower), show the balance of power among creature groups. The Tierra experiment evaluates the balance between simple replicators (black) and normal creatures (other colors). The experiment conducted with our model evaluates the balance among three groups: simple replicators (black), Plants (light gray), and Animals (gray/dark gray).

In the Tierra experiment, the group of simple replicators drastically expands, reducing groups of normal creatures. Then, it occupies an entire space, and the others disappear. In our model, the group of simple replicators expands slightly at the beginning, but it hardly changes at all afterward.

Since the simple replicators are actually capable of self-replicating almost six times faster than the ancestor creatures, the Tierra result is considered natural at this point. In contrast, the results from our model will contradict that, with the following principles:

- Reducing the number of Plants will make the obtaining of instruction words difficult.
- Only a few kinds of word are necessary for a simple program to self-replicate, and they will be consumed within a short period. Then, only these words will become insufficient, and this will restrain the simple program from self-replication.
- A simple program has few templates, and seldom avoids predation (by Animals).

These results demonstrate the robustness of our mechanism of our system compared with that of Tierra against the simple replicating program, and owing to it this system keeps such replicators under control. In general, any creature that cannot be placed in a cycling rule of this system will be weak, even if it can self-replicate faster than the others.

4. Conclusion

We have proposed an artificial system that had been designed based on the Tierra structure. The system ruled that any program component regarded as matter is conserved. We also introduced two self-replicating programs (Animals and Plants) in which processes to recycle the components are preprogrammed. We then, demonstrated the evolutionary performances of such digital creatures. First, particular creature interactions caused by the recycling processes were observed that stabilized the population equilibrium existing among creature groups. Next, we showed predator-prey relationships through local inter-creature competition. As a result of such competition, creatures mutated their programs in order to adapt to each other. Finally, the robustness of this system against a trivial replicator was proved by a comparison with Tierra.

Acknowledgements

The second author's research work was supported in part by the National Institute of Information and Communications Technology and Doshisha University's Research Promotion Funds.

References

[1] Sole R, V. Salazar-Ciudad I., & Garcia-Fernandez J. Landscapes, (2000). *Gene Networks and Pattern Formation: on the Cambrian Explosion*. Adv. Complex Systems 2, 313-337.

[2] Ray T, S. (1994). *An Evolutionary Approach to Synthetic Biology: Zen and the Art of Creating Life*, Artificial Life Vol.1, 179--209.

[3] Ray, T. S. (2001). *Overview of Tierra at ATR.* Technical Information, No.15, Technologies for Software Evolutionary Systems. ATR-HIP. Kyoto, Japan.

[4] Ray, T. S., & Hart, J. (1998). *Evolution of differentiated multi-threaded digital organisms*. In: Adami, C., Belew, R.K., Kitano, H., and Taylor, C.E. (eds.): Artificial Life VI: Proceedings of the Sixth International Conference on Artificial Life, MIT Press, Cambridge, MA 295--304

[5] Suzuki H., Ono N., & Yuta K. (2003). *Several Necessary Conditions for the Evolution of Complex Forms of Life in an Artificial Environment*, Artificial Life Vol.9, No.2, 537-558

The Tenth International Symposium on Artificial Life and Robotics 2005(AROB 10th '05),
B-con Plaza, Beppu, Oita, Japan, February 4-6, 2005

Rule ecology dynamics for studying dynamical and interactional nature of social institutions

T. Hashimoto
hash@jaist.ac.jp

School of Knowledge Science,
Japan Advanced Institute of
Science and Technology (JAIST)
1-1, Tatsunokuchi,
Ishikawa, Japan, 923-1292

M. Nishibe
nishibe@hucc.hokudai.ac.jp

Graduate School of Economics
and Business Administration,
Hokkaido University
Kita 9 Nishi 7, Kita-ku,
Sapporo, Japan, 060-0809

Abstract

In this paper, we address a new concept to view a social system as consisting of diversified institutions interacting with each other and dynamically changing through actions of individuals in a society. A mathematical framework for the concept is formalized. The framework, called Rule Ecology Dynamics (RED), is an extension of multi game dynamics, in which players play plural games simultaneously, by introducing time dependent weights for the plural games and a "meta-rule". The meta-rule is a rule to determine the change of rules. We show simulation results of two kind of meta-rules , average payoff type and inverse standard deviation type. We discuss that this framework is a realization of rule dynamics and it has certain relevance to describe real phenomena of institutional dynamics.

Keywords: Rule Ecology Dynamics, Formation and Change of Institutions, Replicator Equation, Multi-Game Dynamics, Evolutionary Game Theory, Rule Dynamics

1 Introduction

Social institutions are rules for individuals' behavior and cognition broadly accepted and used in a society. In our society, there exist various institutions/rules ubiquitously. Seiyama[1] describes such situation as "We are living with institutions, such as family, commuter passes, trains, universities, telephones, postal services, E-mails, meetings, lectures, laws, norms, conventions and so on. There is no one that is not institutional. We engage in our daily life postulating such institutions. They are omnipresent. It is very difficult to pick out non-institutional aspect, even only one, from our daily life." As we can easily imagine, each institution has different importance or influence for individuals' behavior.

Aoki and Okuno-Fujiwara[2] discusses that diversity of institutions exists in different social systems. But, as quoted above, there are great diversity of institutions in a society. Aoki and Okuno-Fujiwara[2] point out the important feature of institutions, that is an institutional complementarity. When an institution provides a reason to exist another institution, these two institutions are refereed to as in the relationship of institutional complementarity. Since only one of such institutions cannot change independently, Aoki and Okuno-Fujiwara insist that they are stable. However, social institutions often changes and many institutions interact with each other. Accordingly, a change of an institution induces changes of other institutions. The chain of change may go on to all institutions.

This chain of change through interaction among institutions is like an ecological system of biological species. In this paper, we conceptualize such dynamic and interactional nature of institutions as an ecology of rules. Here we use a term 'rule' as a more abstract version of institutions. We propose a new framework to formalize the ecology of rules and its dynamics as an extension of evolutionary game theory. This framework is named "Rule Ecology Dynamics (RED)[1]". This framework can integrate two game theoretical treatment of institutions, one treats institutions as game rules, and the other as equilibria of games[3].

[1]The previous version of the framework was called "Meta-Evolutionary Game Dynamics" since it is an extension of game dynamics (replicator dynamics) introducing a meta-rule[3].

2 Rule Ecology Dynamics

In our framework, rules and individual behaviors are modeled by games and strategies of players in the games, respectively. We start the formalization of the RED from the replicator equation that governs the dynamics of population of each strategy[4]:

$$\dot{x}_i = x_i(u_i - \bar{u}) \qquad (i = 1 \cdots N) \ , \tag{1}$$

where x_i is a population share of the i-th strategy and satisfies $\sum_{i=1}^{N} x_i = 1$, u_i is a payoff of the i-th strategy, $\bar{u} = \sum_{i=1}^{N} x_i u_i$ is the average of the payoffs, and N is the number of strategies.

To represent various compositional rules, multiple games that all players play are brought in, as proposed in Multi Game Dynamics[5]:

$$\begin{aligned} \dot{x}_{i_1 \cdots i_M} &= x_{i_1 \cdots i_M} \sum_{g=1}^{M} (u^g_{i_1 \cdots i_M} - \bar{u}^g) \qquad (2) \\ & \qquad (g = 1 \cdots M) \ , \end{aligned}$$

where $x_{i_1 \cdots i_M}$ is a population share of a strategy $(i_1, i_2, \cdots, i_M)$, which means that a player plays the strategy i_1 at the game 1, the strategy i_2 at the game 2 and so on, satisfying $\sum_{i_1=1}^{r^1} \sum_{i_2=1}^{r^2} \cdots \sum_{i_M=1}^{r^M} x_{i_1 \cdots i_M} = 1$, where r^g is the number of options at the game g, $u^g_{i_1 \cdots i_M}$ is a payoff of the strategy $(i_1, i_2, \cdots, i_M)$ at the game g, $\bar{u}^g$ is the average payoff at the game g, and M is the number of games.

We introduce a weight for each game to treat the degree of influence or importance of each rule. The weight of each game change with time through individual behavior. The change of the game weights is governed by a meta-rule. A meta-rule is a more basic and stabler rule than focal rules. It is for determine which rules are relatively desirable or relatively strong in influence for individual behavior. Introducing a meta-rule is a representation of the hierarchical structure of interaction and stability of rules. Thus, the meta-rule corresponds to the constitution or social values and norms, which are relatively not easy to change. In our framework, it is modeled as an evaluation function of games. The RED is defined by the following three equations:

$$\begin{aligned} \dot{x}_{i_1 \cdots i_M} &= x_{i_1 \cdots i_M} \sum_{g=1}^{M} w^g (u^g_{i_1 \cdots i_M} - \bar{u}^g) \ , && (3) \\ \tau \dot{w}^g &= w^g (\lambda^g - \bar{\lambda}) \ , && (4) \\ \lambda^g &= \lambda^g(\boldsymbol{x}, \boldsymbol{u}^g) \ , && (5) \end{aligned}$$

where w^g is the weight of the g-th game, satisfying $\sum_{g=1}^{M} w^g = 1$, λ^g is an evaluation of the g-th game, and $\bar{\lambda} = \sum_{g=1}^{M} w^g \lambda^g$ is the weighted average of the evaluations of games, τ is a time coefficient for the changing velocity of the games relative to that of the strategy populations, $\boldsymbol{x} = (\{x_{i_1 \cdots i_M}\})$ $(i_g = 1 \cdots r^g)$ is the strategy profile that is a vector of population share of each strategy, and $\boldsymbol{u}^g(\boldsymbol{x}) = (\{u^g_{i_1 \cdots i_M}(\boldsymbol{x})\})$ is the combined payoff or the payoff profile that is a vector of the payoff of each strategy.

The equation (5) is a meta-rule to give evaluation of each game. The variables of the evaluation function is the strategy profile $\boldsymbol{x}$ and the combined payoff $\boldsymbol{u}^g(\boldsymbol{x})$. This setting makes an interaction loop among individual behavior, the rules and the meta-rule closed. Namely, the change of rules depends on the consequences of the behavior under the rules.

3 Simulation Result

We show simulation results of the system for tow settings of the meta-rule. The meta-rule should be considered appropriately for the objective system to be modeled.

The first example is the average type meta-rule

$$\lambda^g_{\mathrm{A}}(\boldsymbol{x}, \boldsymbol{u}) = \sum_{i_1, \cdots, i_M} x_{i_1 \cdots i_M} u^g_{i_1 \cdots i_M} \ . \tag{6}$$

This is a model of a market economics and each rule is thought of as describing a market. We suppose in the market economics that the more profit a market or a rule gives for individuals/organizations, the more important the market/rule is, as in stock markets.

The simulation result is depicted in Fig. 1[2]. In this case, a phenomenon like globalization is observed. Namely, the system is monopolized by a strategy and then games in which the monopoly strategy wins develop their weights.

The second example of the meta-rule is to describe the egalitarianism that is the doctrine of the equality of mankind and the desirability of political, economic and social equality. This meta-rule is formalized as the inverse of standard deviation of agents' payoffs:

$$\lambda^g_{\mathrm{IV}}(\boldsymbol{x}, \boldsymbol{u}) = \sum_{i_1, \cdots, i_M} \left\{ x_{i_1 \cdots i_M} \left(u^g_{i_1 \cdots i_M} - \bar{u}^g \right)^2 \right\}^{-1} \ . \tag{7}$$

[2] In the following simulations, we simplify the RED (Eq.(3)-(5)) as follows: The number of options of all games are the same, $r^g = N$ $(g = 1 \sim M)$ and each strategy is limited to take the same one at the all games and thus the strategy share is indicated as $x_{i_1 \cdots i_M} \equiv x_i$.

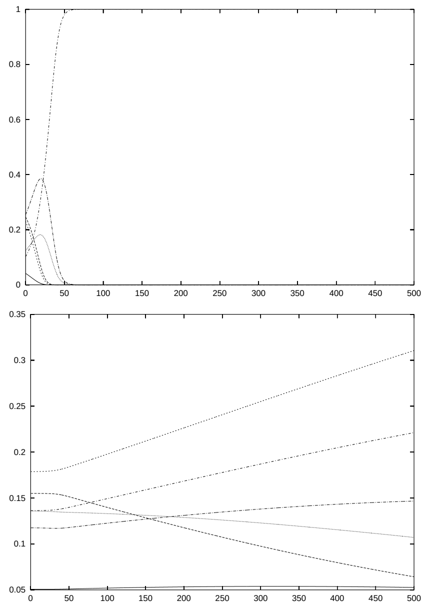

Figure 1: An example of dynamics of RED with the average type meta-rule (Eq.(6)). The y axes are the strategy distribution for the top graph and the weights of games for the bottom, respectively. The x axis is time steps. The system size is $N = 6, M = 7$.

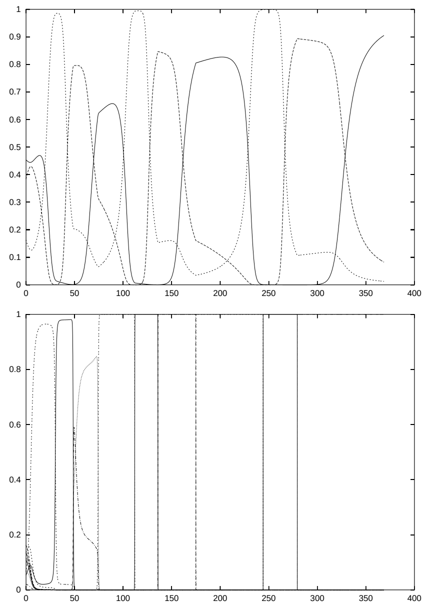

Figure 2: An example of dynamics of RED with the the inverse standard deviation type type meta-rule (Eq.(7)). The y axes are the strategy distribution for the top graph and the weights of games for the bottom, respectively. The x axis is time steps. The system size is $N = 3, M = 10$.

The dynamics of the strategy share and the games' weights are shown in Fig. 2. This case gives revolutionary changes of predominant rules. Namely, no one game and no one strategy can dominate the system stably and temporarily prevalent games and strategies change continually. It is a rather paradoxical situation that egalitarianism induces destabilization of established rules and revolutions.

4 Discussion – RED as Framework for Rule Dynamics

When we try to understand some object, it is often described by a set of states and a system of static functions. The functions are rules to govern the change of states. In other words, the rules are operators and the states are operands. Describing with static functions implies that the decomposability between rules and states is presupposed. The decomposability may occasionally not be able to be presupposed. This undecomposability between rules and states, or between operators and operands is one of the main features of complex systems[6]. In complex systems, rules are often not static but dynamically changing. The typical phenomena are found in evolution, development, learning, adaptation and emergence. We call such dynamic phenomena rule dynamics.

The social rule is also an example having undecomposability between operators and operands. Social structures such as institutions and norms are formed, maintained and changed with time. The remarkable dynamic nature in such systems are self-modification. Individuals behave under some institutions and change the institutions.

Some efforts to study and to describe rule dynamics have been launched [7, 8, 9, 10]. The RED proposed here is also a framework to describe the rule dynamics, especially observed in social systems. Actually, RED (Eqs.(3)-(5)) can be written in a matrix form as

$$\dot{\boldsymbol{x}} = \left(G_{\mathrm{T}}(t)\boldsymbol{x} - \boldsymbol{x} \cdot G_{\mathrm{T}}(t)\boldsymbol{x}\right)\boldsymbol{x} \ , \qquad (8)$$

where $G_{\mathrm{T}} = \sum_{g=1}^{M} w^g A^g$ is a total game that is the weighted some of all games and A^g $(g = 1, \cdots, M)$ is the payoff matrix of the g-th component game. It is clearly seen that RED is a replicator equation with time dependent interaction matrix $G_{\mathrm{T}}(t)$.

The RED can be resolved into a multi-population replicator system[11] of the individual strategies and the rules:

$$\dot{x}_{i_1\cdots i_M} = [(A\boldsymbol{w})_{i_1\cdots i_M} - \boldsymbol{x}\cdot A\boldsymbol{w}]\,\dot{x}_{i_1\cdots i_M}\ , \quad (9)$$

$$\tau\dot{w}_g = \left[\lambda^g - \bar{\lambda}\right] w^g \quad (10)$$

where the element of a matrix A is $(A)_{i_1\cdots i_M g} = u^g_{i_1\cdots i_M}$. This representation clearly show that RED is interactions between the individual strategies and the rules.

5 Conclusion

We have proposed a new model for studying the dynamics of social institutions. The model called Rule Ecology Dynamics (RED). The key concept of RED is that rules in a society is diverge and ubiquitous, interact with each other and change through behavior of individuals acting under the rules. The ecological interaction of rules is described by a modification of the replicator equation. The notable point is to incorporate not only the interactions among individuals but also those of rules. In RED, an interaction loop between individual behavior and rules is realized by introducing a meta-rule. Accordingly, RED is a mathematical model of the micro-macro loop proposed by Shiozawa[12] to understand economic dynamics.

The formation and the change of social institutions is a representative of rule dynamics phenomena, which is a key feature of complex systems. We show that our model is a framework to describe rule dynamics. We also show that RED describes the interaction (game) between individual behavior and rules.

By setting two kind of meta-rules, the average type and the inverse standard deviation type, we show the simulation results that show actually the dynamics of rules and support certain effectiveness of RED to study the dynamics of institutions.

We need to promote the relevance of the RED for describing the real phenomena of rule dynamics. We can suggest a concrete example of the rule dynamics to be described by RED. It is changes of monetary credit systems in Argentina where a local currency, GRT, has been used. Since the crash of national currency, Peso, caused by the governmental default in 2002, the credit of the national and the local currencies, mechanisms to establish and support the currencies, relationship between them, users' impression about them have changed. All of these factors constitute institutions and interact with each other ecologically. This phenomena may be able to be modeled with RED. Through such effort, the framework of RED come to be a tool of designing institutions from the viewpoint of evolutionary economics.

Acknowledgements

This research is partly supported by Canon Foundation Europe; and a Grant-in-Aid for Scientific Research (No.15700183) from the Ministry of Education, Culture, Sports, Science and Technology of Japan and by the Japan Society for the Promotion of Science.

References

[1] K. Seiyama, *Seidoron no kouzu (The plot of institution theory)* (in Japanese), Soubunsha, 1995.

[2] M. Aoki, M. Okuno-Fujiwara (Eds.), *Comparative Institutional Analysis: A New Approach to Economic Systems* (in Japanese), University of Tokyo Press, 1996.

[3] T. Hashimoto, Y. Kumagai, "Meta-evolutionary game dynamics for mathematical modelling of rules dynamics", *Advances in Artificial Life*, W. Bnzhaf, *et al.* (Eds.), Springer, pp. 107-117, 2003.

[4] P. Taylor, L. Jonker, "Evolutionary stable strategies and game dynamics", *Mathematical Biosciences*, **40**, 145–156, 1978.

[5] K. Hashimoto, "Multi-game dynamics" (in Japanese), *Suri-Kagaku*, **495**, 75-83, 2004.

[6] T. Hashimoto, "Complex systems", *Knowledge Science* (in Japanese), K. Sugiyama *et al.* (Eds.), Kinokuniya Shoten, pp.126–131, 2002.

[7] N. Kataoka and K. Kaneko, "Functional dynamics I: articulation process", *Physica D*, **138**, 225-250, 2000.

[8] N. Kataoka and K. Kaneko, "Functional dynamics II: syntactic structure", *Physica D*, **149**, 174-196, 2001.

[9] G. Masumoto, T. Ikegami, "Lambda game system – an approach to a meta game–", *Advances in Artificial Life*, J. Kelemen, P. Sosik (Eds.), Springer, pp.695-699, 2001.

[10] J. Namikawa, T. Hashimoto, "Dynamics and computation in functional shifts", *Nonlinearity*, **17**, 1317-1336, 2004.

[11] J. W. Weibull, *Evolutionary Game Theory*, MIT Press, 1995.

[12] Y. Shiozawa, *Fukuzatsusa no kiketsu (Consequences of Complexity)* (in Japanese), NTT Shuppan, 1997.

The Tenth International Symposium on Artificial Life and Robotics 2005(AROB 10th '05),
B-con Plaza, Beppu, Oita, Japan, February 4-6, 2005

Interactive musical editing system for supporting human error and offering personal preferences for an automatic piano

- Preference database for crescendo and decrescendo -

Eiji Hayashi

Department of Mechanical Information Science and Technology
Kyushu Institute of Technology
680-4, Iizuka City, Fukuoka, Japan, 820-8502
haya@mse.kyutech.ac.jp

Yasuya Takamatsu

Graduate School of Computer Science and System Engineering
Kyushu Institute of Technology
680-4, Iizuka City, Fukuoka, Japan, 820-8502
yasuya@mmcs.mse.kyutech.ac.jp

Abstract

We have developed an automatic piano that can accurately control the motion of both the keys and the pedal, based on performance information data that a user has elaborated for the piece of music. However, this system cannot perform a new piece of music by sight, as in a simulation of a human's expressive performance, because the user must first elaborate his or her desired interpretation of a new piece of music. Therefore, we have developed a program that can memorize and use knowledge databases and the user's preferences concerning an interpretation of a piece of music.

In this paper, we describe the interactive music editing system, the pianist's analysis of preferences regarding crescendos and decrescendos, and the resulting preference database that was developed.

Key words: automatic piano, knowledge database, music interface, user's preference, computer music

1. Introduction

In recent years, with the progress of electronic technology, electronic musical instruments are developing rapidly. However, when comparing the performance of a pianist and the performance of a player piano in the present situation, the timbre and interpretation by the electronic instrument are not a good representation of the live performer. When working with an electronic piano, the user must arrange the respective tones at a given tempo, dynamic, and so on. In the case of piano music, there can be over a thousand notes in even a simple score, which means a very large amount of time is needed for editing the input.

We are attempting to develop a performance information editing support system to edit music more efficiently[1]~[9]. The system has the function to change performance information automatically and the function to provide the user music knowledge and so on (see Figure 1). We structured the database to store knowledge about the musical grammar, the score, and the user's preferences[10]. Moreover, we have developed an automatic editing system based on musical rules.

In this research, we analyzed the data of some performances to investigate pianists' performance preferences. The main object of the analysis was data about crescendos and decrescendos. We considered the parameters that would express preferences. Also, we structure of the database which stored preferences to have taken out and developed the automatic editing system[11].

In this paper, the preference database and a developed interactive editing system are described.

Figure 1. View of the automatic piano

2. Format of Performance Information

The performance information to be edited is shown in table 1 and table 2.

The automatic piano that we have developed uses a music data type structure that is similar to MIDI. We defined performance information, dividing it into two categories, the notes and the pedals.

There are six note information parameters: the key (note), velo(velocity), gate, step, bar, and timing involved in producing a tone. The velocity is dynamics, given by the value of 1～127. The gate is the duration of the note in milliseconds. The step is the interval of time until the next note, and it also exhibits tempo. The bar is the vertical line placed on the staff to divide the music into measures.

There are four pedal information parameters: the key (indicating the kind of pedal, "Damper" or "Shifting"), velo (the pedaling quantity), time (the duration of applying the pedal), and bar.

Table 1. The parameters of note information

Parameter	Key	Velo	Gate	Step	Time	Bar
Unit	-	-	m sec	m sec	m sec	-
Reference	21〜108	1〜127	-	-	-	-

Table 2. The parameters of pedal information

Parameter	Key	Velo	Time	Bar
Unit	-	-	m sec	
Reference	Damper or Shift	0〜127	-	-

3. Editing Process with Databases

3.1 System Architecture

The structure of the system is shown in Figure 2. The user edits music via the user's interface on the computer display, which is shown in Figure 3. Also, the user can access a database that has musical grammar, the user's preferences, and so on. As a result, editorial work is reduces and efficient editing becomes possible.

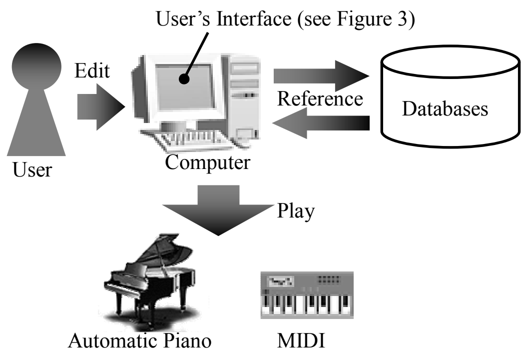

Figure 2. Structure of the editing system

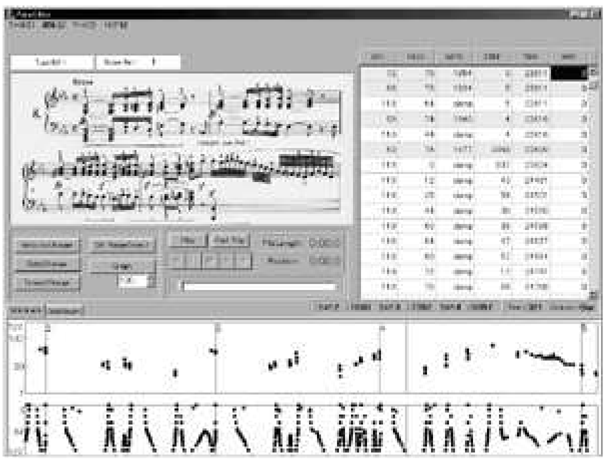

Figure 3. User's interface on the computer display

3.2 Editing Support Process

The procedure of the editing by the system is shown in Figure 4.

Temporary music data (TMD) is the data of a piece of music without expression. For example, the TMD of a part of the first movement of Beethoven's Sonata No. 8, which is shown in Figure 5, is shown in Figure 6. Because expression has not been added, the necessary editing of the TMD is extensive.

Therefore, the TMD is translated into original music data (OMD; This data may or may not be automatically translated using databases at the beginning of editing, and after that, the user can start to edit it. The data structure is similar to that of the TMD.) by the automatic translation of the system and is provided for the user (see Figure 7). The automatic translation program uses a Score Database, Musical Rules Database, and Preference Database (the details of the databases are described later). The user adds editing to the OMD and makes slight adjustments. When editing, the system watches over the data the user enters and music knowledge is provided. Concurrently, a phrase in the music is discovered. When the phrase with the same pattern exists in the music, it is automatically translated. After editing, the system extracts the expressions and the preferences which are peculiar to the user from the OMD. These expressions are stored in the Preference Database, which is then used when editing other music, which results in improved editorial efficiency.

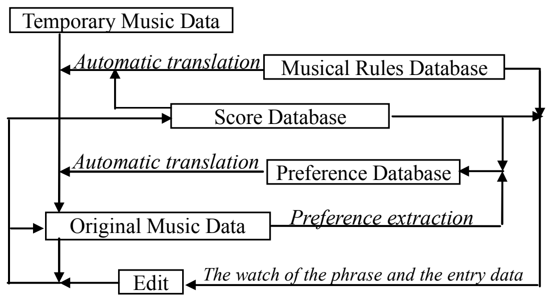

Figure 4. The editing procedure

Figure 5. Bars 1~2 of Sonata No. 8

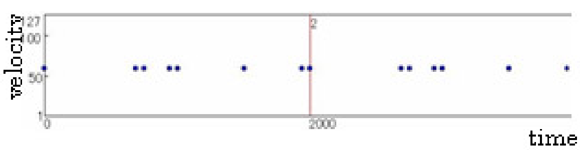

Figure 6. Temporary music data

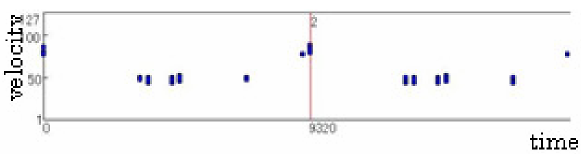

Figure 7. Original music data

3.3 Details of the Databases

3.3.1 Score Database

This database has symbols including notes and time signature rests and so on in standard musical notation. Symbols were pulled together in order of bar, and also in a bar symbol was arranged in time series.

This database is composed of three tables, the "Element table" (showing the position of the note and the composition of the chord), the "Symbol table" (showing the position of the music symbol) and the "Same table" (showing the position of the repetition of the phrase). Recently, we added "field of the note value" and "field of the pitch of melody" to the "Element table". The overview of the Score Database is shown in Table 3.

3.3.2 Musical Rules Database

This database has the architecture of the musical grammar necessary to interpret symbols in musical notation. This database is composed of five tables containing "Dynamics marks", "Articulation marks", "Symbol of the Changing Dynamics or the Changing Tempo (Symbol that affects the speed of a note or the increase or decrease of the volume.)", "Time signature" and "Tempo marks".

Dividing a music symbol according to every usage allows efficient information processing by the system. The overview of the Musical Rules Database is shown in Table 4.

3.3.3 Preference Database

This database contains the expressions of the user's characteristic performance. The expressions show the relationship between tempo and dynamic. The basic data structures used in this database are shown in Table 5.

The "Edit" selection in the user's interface of Figure 3 gives the user access to the parameters for expression. A user can edit his or her parameters, and the respective databases will automatically change at least one of their parameters.

The main theme of this paper is the development of that part of the Preference Database dealing with "Crescendo and Decrescendo". We analyzed the performance data of the pianist to make it, to pick up the featuring and expressed parameter. Those analysis results are described in the following section.

3.4 Analysis of Crescendo and Decrescendo

We analyzed the pianist's performance data in terms of crescendos and decrescendos to clarify the editorial tendency of the performance information. The graphs of the analysis results are shown in Figure 8-1 to 8-4. The horizontal axis of each graph is time (in milliseconds), and the vertical axis is velocity (1 to 127).

These graphs are a result of using the music of Beethoven's "Moonlight" piano sonata. The straight line is the regression line of the notes with a crescendo or a decrescendo. Figure 8-1 is the result of drawing a regression line except for the note of the melody from the performance data. Figure 8-2 is the result including the note of the melody. The graph may appear confusing at first, but inspection will reveal that the graph in Figure 8-2 expresses a crescendo better than that in Figure 8-1.

The considering which was compared by presenting a sound to this actually in MIDI is included. Figures 8-3 and 8-4 can be more easily understood. The straight line with 3 colors in the graph is the notes played with the right hand, the notes played with the left hand, and the notes of the melody. Therefore, when we considered the right hand, the left hand, and the notes of melody and drew the regression line, we were able to show a linear crescendo (or decrescendo). Figure 8-4 shows that a crescendo (or decrescendo) is strongly influenced by the expression mark, the dynamics mark, and so on. In the range of our analysis, this rule applied to any case.

Based on these results, we developed a Preference Database that includes crescendos and decrescendos. An overview of the Preference Database is shown in Table 6.

Table 3. Structure of the Score Database

Table	Summary
Element	The position of the note, the role of the note and so on.
Symbol	The range where the position, the symbol of the symbol show an effect
Same	The position of the phrase with the same pattern

Table 4. Structure of the Musical Rules Database

Table	Summary	Example
Dynamics mark	This specifies the dynamics of the note.	*ff*, *mp*
Articulation mark	This changes the length and the strength of one note.	*staccato*, *fermata*
Changing mark	This changes the strength and the speed of the note in the specific range gradually.	rit., cresc.
Time signature	Defining both the number of beats in a measure and the type of note that fills one beat.	$\frac{3}{4}$
Tempo mark	This specifies the tempo of the music.	Allegro.

Table 5. Structure of the Preference Database

Table	Summary
Phrase vector	The vector* of all notes of the phrase.
Symbol vector	The vector* of the note which had a symbol.
Gate rate	The ratio of Gate to Step.(Gate/Step)

*The ingredient of the vector is Velo and Step.

Table 6. Preference Database for crescendo and decrescendo

Record	Summary
ChangeNum	Kind of Symbol; Cresvendo or Decrescendo
DyNum	Kind of the dynamics mark which is before and behind
PsNum	Kind of the articulation mark which is before and behind
Unit	Cresc and Decresc are connecting or no.
NoteValue	First note value of the Cresc or Decresc.
Slope	Slope of the regression line
Intercept	Intercept of the regression line

4. Example of the Automatic Translating

4.1 Case by Musical Knowledge

The TMD of the first movement of Beethoven's Moonlight Sonata, which is shown in Figure 9, is shown in Figure 10.

Figure 11 is the OMD, which is derived from the TMD, changed automatically using the Musical Rules Database and Score Database. When observing Figures 10 and 11, OMD was changed from the TMD that Velocity was constant into the data which the expression which is certain degree of was added to.

4.2 Case by User's Preference

A result of applying the developed Preference Database for crescendo and decrescendo to the OMD (Figure 11) is shown in Figure 12, which can be seen to differ from Figure 11. With sufficient editing by such an automatic translation, the performance can eventually approach the performance of the user's preference. Eventually, the editorial efficiency, too, will improve.

5. Conclusion

We developed a Preference Database specific to a user. Specifically, it stored the preferences regarding crescendos and decrescendos. Also, we developed a interactive musical editing system that translates performance information automatically using the developed Preference Database. Then we input information about the music to the Score Database. The added information included the note value and note of melody. As a result of this improvement, the system became able to extract the user's preference regarding every melody or note value.

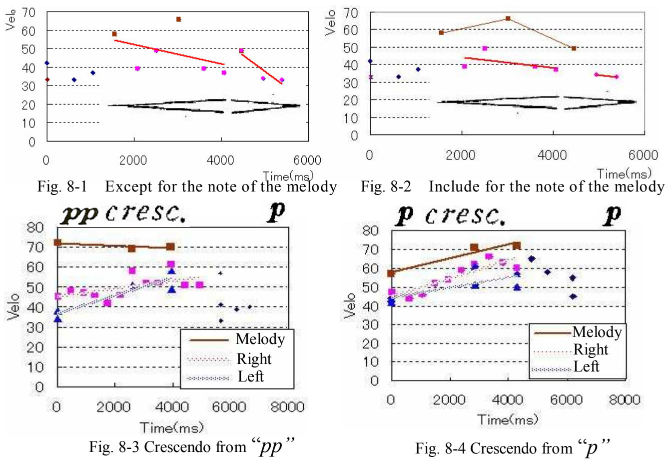

Fig. 8-1 Except for the note of the melody
Fig. 8-2 Include for the note of the melody
Fig. 8-3 Crescendo from "pp"
Fig. 8-4 Crescendo from "p"

Figure 8. The results of analysis

Figure 9 Bars 16～18 of Moonlight Sonata

Figure 10. TMD

Figure 11. OMD

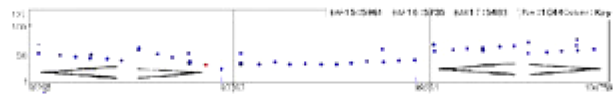

Figure 12. Result of applying the user's preferences

References

[1] Hayashi, E. et al, "Behavior of piano-action in a grand piano.I", Journal of acoustical Society of America, Vol.105, pp.3534-3544, 1999.

[2] Hayashi, E. et al, "Development of a Piano Player", Proc. of the 1993 International Computer Music Conference, pp.426-427, 1993.

[3] Hayashi, E. et al, "Development of Moving Coil Actuator for an Automatic Piano", International Journal of Japan Society for Precision Engineering, Vol.28 No.2, pp164-169, 1994.

[4] Hayashi, E. et al, "Development of piano player 1st. Analysis of behavior of piano-action until string-striking of hummer", Journal of the Japan Society of Mechanical Engineers, vol.60 No.579, pp.325-331, 1994. (*in Japanese*)

[5] Hayashi, E. et al, "Development of piano player 2nd. Study on repetition of same key based on Analysis of behavior of piano-action", Journal of the Japan Society of Mechanical Engineers, Vol.61 No.578, pp.339-345, 1995. (*in Japanese*)

[6] Hayashi, E. et al, "Behavior of piano-action in a Grand Piano for an Automatic Piano", Proc. of 1st Pioneering International Symposium on Motion and Vibration Control in Mechatronics, pp.80-85, 1999.

[7] Asami, K and Hayashi, E. et al, "Intelligent Edit of Support for an Automatic Piano", Proc. of the 3rd International Conference on Advanced Mechatronics, pp.342-347, 1998.

[8] Asami, K and Hayashi, E. et al, "An intelligent supporting system for editing music based on grouping analysis in automatic piano", IEEE Proceedings of RO-MAN'98, 672-7, 1998.

[9] Hayashi, E et al, "Interactive musical editing system for supporting human errors and offering personal preferences for an automatic piano", Proc. of the 7th International Symposium on Artificial Life and Robotics, Vol.2, pp 513-516, 2002.

[10] Takamatsu, Y., Hayashi, E., et al, "Study on the Performance Information Edit Support System for an Automatic Piano", Technical Report of Information Processing Society of Japan, MUS-52, pp.111-118, 2003. (*in Japanese*)

[11] Arimatsu, M., Takamatsu, Y. and Hayashi, E., "Development of Performance Information Edit Support System for an Automatic Piano", The bachelor's degree paper of Kyushu Institute of Technology, 2004. (*in Japanese*)

The Tenth International Symposium on Artificial Life and Robotics 2005(AROB 10th '05),
B-con Plaza, Beppu, Oita, Japan, February 4-6, 2005

The role of population structure in language evolution

Yoosook Lee* Travis C. Collier Edward P. Stabler Charles E. Taylor
Dept. of EEB Dept. of EEB Dept. of Linguistics Dept. of EEB
University of California, Los Angeles
Los Angeles, CA 90095

Abstract

The question of language evolution is of interest to linguistics, biology and recently, engineering communicating networks. Previous work on these problems has focused mostly on a fully-connected population. We are extending this study to structured populations, which are generally more realistic and offer rich opportunities for linguistic diversification. Our work focuses on the convergence properties of a spatially structured population of learners acquiring a language from one another. We investigate several metrics, including mean language coherence and the critical learning fidelity threshold.

1 Introduction

The question of linguistic divergence is of interest to linguistics[1, 2, 3, 4, 5], biology[6, 7],and engineering communicating networks[8, 9, 10, 11]. For linguists the question is: "What causes languages to change[12, 13, 14], and why do humans have so many different languages?[15, 16, 17]". From an engineering point of view, how to achieve convergence to a single language in a distributed adaptive system[18, 19] is an important issue, as in adversarial conditions, where we would like to maintain high coherency among "friendlies" with minimal understanding from the adversary.

More generally, the dynamics of language evolution provides insight into convergence to a common understanding where distributed learning is a goal. At a theoretical level, these issues are fundamentally similar. The evolution of language takes on special importance for robotics and artificial life because it provides a superb platform for studying the emergence of united behavior from distributed, separate agents.

Previous work on these problems has focused mostly on a fully-connected population where all individuals have an equal probability of learning from each other and the fitness contribution of language is evaluated using the frequency among the entire population[20, 21]. We are extending this study to structured populations, which are generally more realistic and offer rich opportunities for diversification. Our work focuses on the convergence properties of a population of learners acquiring a language from one another under different connectivity connectivity conditions, called *topologies*. This approach is motivated in part by studies indicating that whom a person learns language from can heavily influence one's language [22, 23, 24, 25].

Breaking the symmetry that a fully-connected population provided makes finding an analytical solutions much more difficult, though perhaps not impossible. Therefore, we are using simulations to explore the convergence properties of variety of distinct topologies. We compare the topologies on several metrics, including mean language coherence and critical error-threshold. Our results show that topology has a large effect on overall convergence and can create stable multi-language solutions.

The multi-language solutions are a third distinct phase of local convergence between no-convergence ("Tower of Babel") on the one hand, where all languages are represented in roughly equal frequencies, and global convergence ("Lingua Franca"), where a single language and its close variants predominate. In a multi-language solution, the average individual belongs to a neighborhood predominated by a single language, but no single language dominates across the entire population.

In our paper these simulations are described and discussed. Among our conclusions is that local convergence has important implications for developing systems such as sensor networks where adaptive communication between agents in a heterogeneous environment is desirable.

*yoosook@ucla.edu

The Tenth International Symposium on Artificial Life and Robotics 2005(AROB 10th '05),
B-con Plaza, Beppu, Oita, Japan, February 4-6, 2005

2 Methods

Our system is constructed with each individual possessing a parameterized grammar, in the principles and parameters tradition, which can be encoded as a sequence of symbols. However, for the baseline tests we report here, each grammar consists of a single symbol and all grammars have the same expressive power and equal distance from each other. This is a necessary simplification to make our results comparable to the analytic results from Komarova *et. al.*[20].

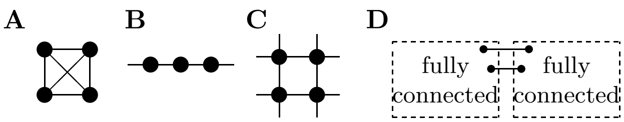

Figure 1: Topologies: (**A**) Fully-connected, denoted FC. The number of connection for each individual n_c is $N-1$. (**B**) Linear, $n_c = 2$. (**C**) A von Neumann lattice with $r = 1$, denoted VN, $n_c = 4$. (**D**) Bridge, which has multiple fully-connected subpopulations and a fixed number of connections between subpopulations.

Each individual exists within a topology defining a set of neighboring individuals. We explore four different topologies: fully-connected (FC), linear, von Neumann lattice (VN), and bridge, illustrated in Figure 1.

The fitness of an individual has two parts: the base fitness, denoted as f_0, and a *linguistic merit* proportional to the probability that the individual could successfully communicate with its neighbors. In the simplified system, linguistic merit is proportional to the number of neighbors which share the same grammar. In the fully-connected topology, each individual of a given grammar will have the same fitness, but this does not hold for other topologies.

Specifically, the fitness of individual i, f_i, is f_0 plus the sum over each neighbor j of the similarity between i's grammar and j's grammar.

$$f_i = f_0 + \frac{1}{2}\sum_{j=1}^{n_c}(a_{ij} + a_{ji}) \tag{1}$$

Each time step, an individual is chosen proportional to its fitness to reproduce. Reproduction can be thought of as the chosen individual producing an offspring which inherits the parent's grammar and replaces one of the parent's neighbors. The offspring learns the parent's grammar with a certain *learning fidelity*, q. This learning fidelity is properly a function of the specifics of the learning method the child uses and the complexity of the grammar, but in the simplified system the learning fidelity is reducible to a transition probability function between grammar G_i and grammar G_j equal to q for $i = j$, and $(1-q)/(n-1)$ for $i \neq j$.

The algorithm of our program is as follows:

```
for each individual i in a population P
    set a random language L_i of i
end for
for each individual i ∈ P
    compute fitness f_i of i
end for
do until number of updates is met
    select an individual k ∈ P
    select a random neighbor j of individual k
    replace the neighbor j with an offspring of individual k
        the offspring becomes an individual j
        if the offspring is mutant( mutation rate = μ)
            get a random language for L_j
        else
            Lj = L_k
        end if
        update fitness of the individual j
end do
```

One important metric is the *dominant* grammar frequency. We measure this directly each time step by counting the abundance of each grammar. Which grammar is the dominant one may change each time it is measured; in other words, the dominant grammar is whichever grammar happens to be at the highest frequency at the time.

The linguistic coherence, denoted as ϕ, is measured using the following equation:

$$\phi = \frac{1}{N}\sum_{i=1}^{N}\frac{1}{2}\sum_{j=1}^{n_c}(a_{ij} + a_{ji}) \tag{2}$$

Various different "levels" of coherence exist as defined by the set of individuals in n_c the second summation occurs over. *Local coherence*, ϕ_0, only sums over the neighbors of each individual and is proportional to mean fitness (equal if $f_0 = 0$). ϕ_1 is the coherence measured over the set of neighbor's neighbors, and generally, ϕ_i is measured using the set of (neighbor's)^i neighbors. *Global coherence*, ϕ_∞, corresponds to summation is over the entire population. In the fully-connected topology, all of these convergence levels reduce to the same value.

For the experiments, we used a population size N of 500, except for the von Neumann lattice which was a 22×22 torus giving a population size of 484. The similarity of between languages a was set at .5, the base fitness f_0 was 0, and the number of different possible grammars n was 10. All relevant parameters are summarized in Table 1.

Parameter	FC	Linear	VN	Bridge
	Topologies			
a			0.5	
f_0			0	
n (# grammars)			10	
N (pop size)	500	500	484	500
# subpops				2
subpopsize				250
# connections				10
# time steps	10^5	10^6	5×10^5	10^5

Table 1: Parameters. Note that 10 connections of bridge topology are randomly selected from each subpopulation.

The experiments, or runs, are done for a set number of time steps that varies with topology. The goal is to make each run long enough that the system will very probably reach an equilibrium. A set of 5 replica runs, varying only the random number generator seed, were done at each q value between 0.65 and 1 at 0.01 intervals.

3 Analytic Model

For the fully-connected topology given a uniform similarity a between n different grammars, and the learning fidelity of q, three equilibrium solutions for grammar frequency were derived by Komarova *et. al.*[20]:

$$X_0 = 1/n \tag{3}$$

$$X_\pm = \frac{(a-1)(1+(n-2)q) \mp \sqrt{D}}{2(a-1)(n-1)} \tag{4}$$

where

$$D = 4[1 + a(n-2) + f_0(n-1)](1-q)(n-1)(a-1) + (1-a)^2[1+(n-2)q]^2$$

Below a specific learning fidelity q_1, D is negative and there is no real solution for $X_\pm$. Therefore, for $q < q_1$, only the symmetric solution X_0 exists and no grammar dominates. Solving for q when $D = 0$ determines the critical leaning fidelity threshold q_1, which corresponds to the *error threshold* in molecular evolution.

$$q_1 = \frac{4 - 2f_0(n-1)^2 - 3n - a(2n^2 - 7n + 6)}{(1-a)(n-2)^2} + \frac{2(n-1)^{\frac{3}{2}}\sqrt{1 + f_0[1 + a(n-2) + f_0(n-1)]}}{(1-a)(n-2)^2} \tag{5}$$

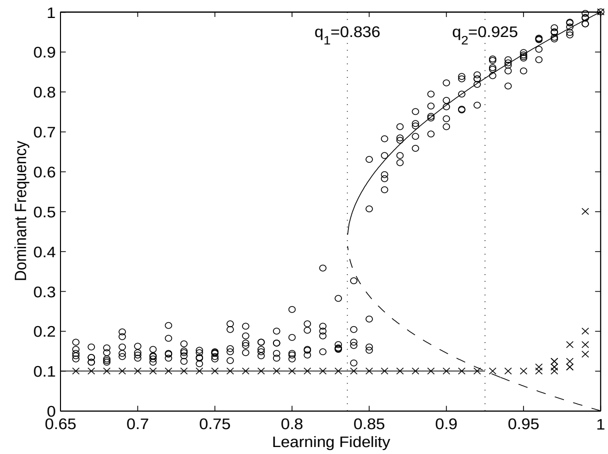

Figure 2: The dominant(○) and average(×) grammar frequency at the last time step of a set of fully-connected runs, overlaid with symmetric (horizontal line) and asymmetric (curved line) analytic solutions for $a = 0.5$, $n = 10$, $f_0 = 0$.

When $q_1 < q < q_2$ for a specific q_2, both the symmetric $X_\pm$ and asymmetric X_0 solutions exist and are stable. For $q > q_2$ however, only the asymmetric solution where one grammar dominates the population is stable. This q_2 value is the point where $X_0 = X_-$, giving:

$$q_2 = \frac{n^2(f_0 + a) + (n+1)(1-a)}{n^2(f_0 + a) + 2n(1-a)} \tag{6}$$

Komarova *et. al.* provide much more detail and proofs[20]. We plot these solutions and compare them to experimental results in Figure 2.

4 Results

The empirical results for the fully-connected topology well match the expectation from the analytic results arrived at by Komarova *et. al.*[20], as shown in Figure 2. In the region where only the symmetric solution is stable ($q < q_1$), the average grammar frequency is $1/n$. The dominant grammar frequency appears high because it is the upper end of a distribution of grammar frequencies which has a non-zero variance due to the finite population size.

In the bi-stability region ($q_1 < q < q_2$), a discrepancy between the analytic and empirical results presumably derives from a lack of runs settling at the symmetric solution. With a finite population, the basin of attraction of the symmetric solution in this region is very weak. Choosing which individual reproduces each

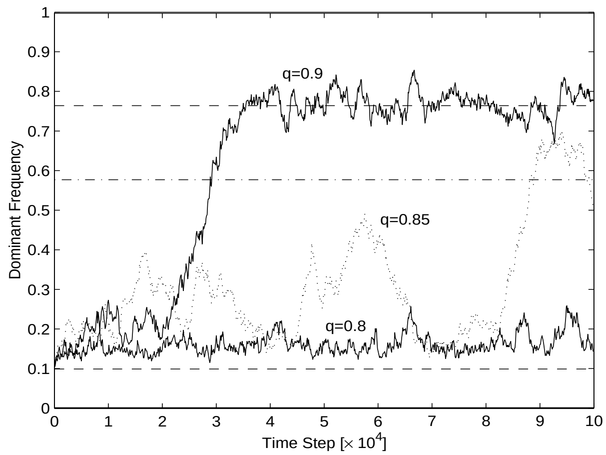

Figure 3: Time-series of fully-connected single runs. The dash line(--) is X_+ for $q = 0.9$, the upper dot-dash line(·-) is X_+ for $q = 0.85$, the lower dot-dash line is X_0. When $q = 0.8$, only the X_0 is stable.

time step is stochastic. This combined with stochastic learning errors appear to be sufficient perturbation to make the symmetric solution unstable empirically in this region.

The time series of single runs with three different learning fidelities in the fully-connected topology are shown in Figure 3. These learning fidelities correspond to the three different regions of stable solutions. The run in the region where symmetric and asymmetric solutions are possible shows the very weak attraction of the symmetric solution. Even starting with every individual in the population being initialized to the same grammar, a dominant frequency of 1, runs at this learning fidelity settle into a similar pattern (data not shown).

For topologies other than fully-connected, convergence provides a more clear picture of system dynamics than dominant frequency. Global coherence ϕ_∞ correlates very closely with dominant frequency, but local coherence ϕ_0 corresponds directly to the linguistic contribution to fitness and is directly operated on by the evolutionary process.

Figure 4 shows the coherence values by taking the average values at the end-points of the 5 replica runs at each q value. The learning fidelity threshold, or error-threshold, for the emergence of a dominant grammar is where indicated by the inflection point in the coherence curve. The emergence of a dominant universal grammar among the entire population is reflected in the global coherence curve.

The bridge topology with 2 subpopulations of size 250 and 10 random connections between subpopula-

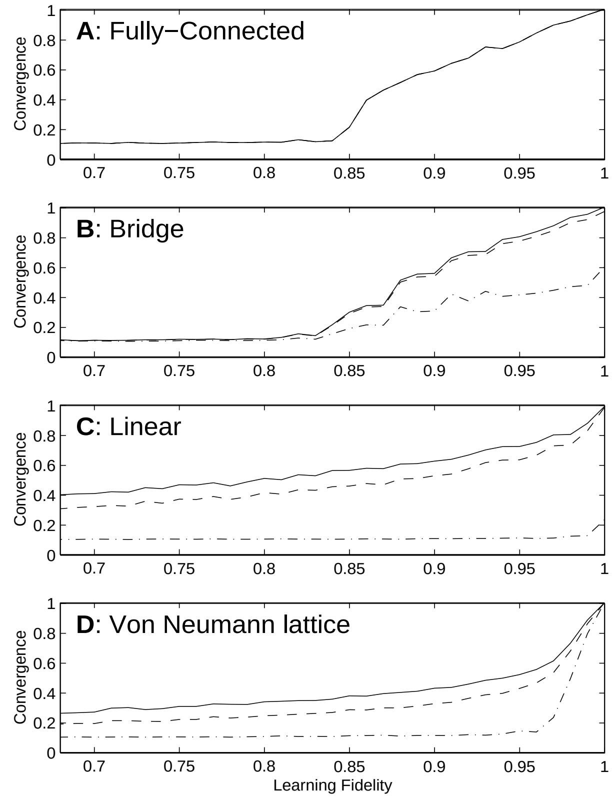

Figure 4: Linguistic coherence. The solid line(–) for ϕ_0, the dash line(--) for ϕ_1, and the dot-dashed line(·-) for global coherence ϕ_∞.

tions (Figure 4 B) is indistinguishable from two isolated fully connected populations. It demonstrates a very similar learning fidelity threshold, $q_1 \approx 0.84$, as the fully-connected run shown in panel A. However, global convergence is never achieved reliably in excess to the probability that both subpopulations individually converge to the same grammar by chance. The up-tick in the ϕ_∞ line at $q = 0$ is not statistically significant due to this effect. Additionally, ϕ_1 is extremely close to ϕ_0 while ϕ_∞ only rises to approximately 0.5, indicating that there is a large degree of separation between many individuals.

For the linear topology shown in Figure 4 C, ϕ_0 and ϕ_1 slowly rise over the entire range shown, and the trend extends all the way from $q \approx 0.2$ where learning error makes each offspring essentially random (data not shown). Since ϕ_1 trends upward along with ϕ_0, we can conclude that extended "patches" of individuals with the same grammar form. Near $q \approx 0.99$, ϕ_1 begins to approach ϕ_0, and ϕ_∞ shows a slight uptick. However, even with perfect learning fidelity, ϕ_∞ is only slightly different from the symmetric solution

$1/n$. There appears to be no possible global convergence learning fidelity threshold for this topology.

In contrast to the linear topology, the toroidal von Neumann lattice topology (VN) shows a clear learning fidelity threshold for all three coherence metrics at $q \approx 0.96$. Below this threshold, the VN topology behaves similarly to the linear topology with an expected decrease in ϕ_0 and ϕ_1 due to the doubling of neighbors.

5 Discussion

Empirical results using agent-based simulations closely match the analytic results produced by Komarova, Nowak, and others for the fully-connected topology. However, a relatively small population size combined with stochastic scheduling and learning errors lead to sufficient perturbations that empirical results show less stability than the pure math would suggest.

The instability of the fully-connected model at learning fidelities just above the critical threshold q_1 tempts the conclusion that human languages exist in this "edge of chaos" region. Humans exist in complex social connectivity networks, which are probably closer to the bridge topology. The instability of human language is more probably related to changing connectivity and topology than a specific learning fidelity.

Topologies other than fully-connected can behave quite differently. The bridge topology for the parameters we have tested quickly and stably converges to two independent grammars, one for each subpopulation, above a critical learning fidelity. A linear topology fails to converge to a single dominant grammar, but does converge to many "patches" that increase in size as q increases. Both of these cases correspond to stable multi-language solutions which do not exist in the fully-connected topology.

Additionally, the bridge topology has parameters that quite likely change its dynamics. At a higher number of connections between subpopulation and/or a higher number of smaller subpopulations, there is probably a global coherence threshold.

The lack of apparent learning fidelity threshold for the linear topology and similarity to the behavior of the VC topology below its threshold suggests that there is a critical connectivity value that a regular lattice must exceed before global convergence is possible. This result, while only hinted at here, would fit very well with percolation theory. Percolation theory may also provide insight into what parameterized random graph topologies a learning threshold exists for.

The fully-connected topology provides the scenario with the lowest critical learning fidelity, but it also requires the most intensive communication. A topology with much more limited connectivity such as a lattice or clustered graph may still globally converge with much more limited communication. For many engineering situations such as adaptive sensor networks, this is an important consideration.

Language in this study is sufficiently abstract that these results apply to many situations where agents adapt by learning from one another and convergence is desirable. In an adaptive sensor network setting, it may be beneficial for sensor nodes to adapt their communicative coding and recognition/detection systems based on the specific topology of deployment and the actual inputs to the network. An evolutionary strategy where nodes adopt successful schemes from their neighbors with a fitness bonus for agreement is a general option with great promise. Such a system maps directly onto the linguistic systems we present.

6 Summary

We demonstrated the role of topology is critical in determining the degree of linguistic coherence and the learning fidelity threshold through empirical studies informed by the theoretical results for an idealized population. The reality of complex population structure makes evident the importance of topology in studying the dynamics of language acquisition and language evolution. Further investigation on various topologies with different parameter settings may provide a more in depth understanding of language evolution and diversification.

Acknowledgements

This work was supported by the UCLA Center for Embedded Network Sensors, the Defense Advance Research Projects Agency (DARPA), administered by the Army Research Office under Emergent Surveillance Plexus MURI Award No. DAAD19-01-1-0504, and DARPA MURI award administered by the US Airforce No. F49620-01-1-0361. Any opinions, findings, and conclusions or recommendations expressed in this publication are those of the authors and do not necessarily reflect the views of the sponsoring agencies.

References

[1] S. Kirby. Fitness and the selective adaptation of language. In J. R. Hurford, M. Studdert-Kennedy, and C. Knight, editors, *Approaches to the Evolution of Language: Social and Cognitive Bases*, Cambridge, 1998. Cambridge University Press.

[2] K. Smith. Natural selection and cultural selection in the evolution of communication. *Adaptive Behavior*, 10(1):25–44, 2002.

[3] G. Jäger. Evolutionary game theory and linguistic typology: a case study. In *Proceedings of the 14th Amsterdam Colloquium*. ILLC, 2003.

[4] M. A. Nowak, D. C. Krakauer, and A. Dress. An error limit for the evolution of language. *Proc. Roy. Soc. Lond. B.*, pages 2131–2136, 1999.

[5] N. Grassly, A. von Haesler, and D. C. Krakauer. Error, population structure and the origin of diverse sign systems. *J. theor. Biol.*, 206:369–378, 2000.

[6] S. Nowicki, W. A. Searcy, M. Hughes, and J. Podos. The evolution of birdsong: male and female response to song innovation in swamp sparrows. *Animal Behaviour*, 62:1189–1195, 2001.

[7] W. J. Sutherland. Parallel extinction risk and global distribution of languages and species. *Nature*, 423:276–279, 2003.

[8] T. C. Collier and C. E. Taylor. Self-organization in sensor networks. *Journal of Parallel and Distributed Computing*, 64(7), 2004.

[9] D. Livingstone and C. Fyfe. Modelling the evolution of linguistic diversity. In J. N. D. Floreano and F. Mondada, editors, *ECAL99*, pages 704–708, Berlin, 1999. Springer-Verlag.

[10] L. Steels and F. Kaplan. Stochasticity as a source of innovation in language games. In C. Adami, R. Belew, H. Kitano, and C. Taylor, editors, *Proceedings of Artificial Life VI*, pages 368–376, Cambridge, MA, June 1998. The MIT Press.

[11] T. Arita and C. E. Taylor. A simple model for the evolution of communication. In L. Fogel, P. J. Angeline, and T. Bäck, editors, *The Fifth Annual Conference On Evolutionary Programming*, pages 405–410. MIT Press, 1996.

[12] A. Fox. *Linguistic Reconstruction*. Oxford University Press, Oxford, UK, 1995.

[13] H. H. Hock and B. D. Joseph. *Language History, Language Change, and Language Relationship: An Introduction to Historical and Comparative Linguistics*. Mouton de Gruyter, Berlin, 1996.

[14] A. M. S. McMahon. *Understanding Language Change*. Cambridge University Press, Cambridge, UK, 1 edition, 1994.

[15] M. Ruehlen. *The Origin of Language*. John Wiley & Sons Inc., New York, 1994.

[16] L. L. Cavalli-Sforza, P. Menozzi, and A. Piazza. *The History and Geography of Human Genes*. Princeton University Press, 1994.

[17] L. L. Cavalli-Sforza. gene, peoples and languages. *Proc. Natl. Acad. Sci. USA*, 94:7719–7724, 1997.

[18] L. Steels. Language games for autonomous robots. *IEEE Intelligent systems*, pages 17–22, October 2001.

[19] H. Yanco and L. A. Stein. An adaptive communication protocol for cooperating mobile robots. In J.-A. Meyer, H. Roitblat, and S. Wilson, editors, *From Animals to Animats 2: Proceedings of the Second International Conference on the Simulation of Adaptive Behavior*, pages 478–485. The MIT Press/Bradford Books, 1993.

[20] N. L. Komarova, P. Niyogi, and M. A. Nowak. Evolutionary dynamics of grammar acquisition. *Journal of Theoretical Biology*, 209(1):43–59, 2001.

[21] M. A. Nowak, N. L. Komarova, and P. Niyogi. Evolution of universal grammar. *Science*, 291:114–118, 2001.

[22] S. Pinker. *The Language Instinct*. HarperPerennial, New York, NY, 1995.

[23] A. Senghas and M. Coppola. Children creating language: How nicaraguan sign language acquired a spatial grammar. *Psychological Science*, 12:323–328, 2001.

[24] J. Kegl, A. Senghas, and M. Coppola. Creation through contact: Sign language emergence and sign language change in nicaragua. In M. DeGraff, editor, *Language Creation and Language Change:Creolization, Diachrony, and Development*, pages 179–237. MIT Press, Cambridge, MA, 1999.

[25] L. Steels. Social language learning. In M. Tokoro and L. Steels, editors, *The Future of Learning*, pages 133–162, Amsterdam, 2003. IOS Press.

The Tenth International Symposium on Artificial Life and Robotics 2005(AROB 10th '05),
B-con Plaza, Beppu, Oita, Japan, February 4-6, 2005

Truth Table Language for Generating Self-replicating Systems

Hajime Harada and Yukihiko Toquenaga
Integrative Environmental Sciences
University of Tsukuba
Ibaraki 305-8572, Japan
E-mail: hajime@pe.ies.life.tsukuba.ac.jp

Abstract

In Artificial Life studies, a self-replicating system is considered to have mostly perfect copying capacity. However this feature is sensitive external to perturbation. We proposed a simple self-replication system with self-irreplicable individuals. The system consists of truth table relations for generating individual notations. The system incorporating 1-D spatial configuration showed cyclic behavior. Within the cycle, the system acquired replication redundancy, or offspring was of the same species irrespective of which neighboring individual was chosen as a mate. Another feature of this system was its robustness; when one or more individuals were altered by noise effect, the system absorbed the perturbation. Creating a Truth Table Language (TTL) and a self-replicating system is for the purpose of orienting to a platform for bioinformatic research. Dealing with TTL systems as study subjects, we may further propose new techniques for analyzing TTL systems, which can be used as feedback into bioinformatics.

keywords: Artificial Life, truth table, redundancy, cyclic behavior, bioinformatics.

1 Introduction

Most self-replicating systems coined in Artificial Life studies start from one or several ancestral species or individuals that are capable of perfectly copying themselves. In the field of Artificial Life, many experiments, such as artificial chemistry[1, 2], Tierra[3], Avida[4], random access language[5], machine and tape dynamics[6], and binary string system[7, 8], have been performed in order to study self-reproduction systems.

However, these studies focused on perfect replication in self-reproduction. In such systems, perturbation by mutation and other evolutionary operations, which work against the self-copying process, generate lucky variants in species which later prevail within the system. Thus, making perfectly self-replicating ancestral species becomes the key to constructing artificial self-replicating systems. Additionally redundant and robust language should be used for self-replication in order to protect against genetic perturbation so as to prevent the core of the self-replication processes from generating variant species which are not capable of self-replication.

What happens when not all ancestral species are self-replicating, but some of them reproduce in hypercycles? Hypercycle[9] is recognized as the common theory of replication cycles, in which each member catalyzes the replication of the next in the cycle, and may be dynamic in the sense that members of each hypercycle change both temporally and spatially. The coexistence of multiple dynamic hypercycles as an integrated whole can realize a self-replication system. Such a system may be robust and hence resistant to external perturbation, similar to immune systems realized in biological systems. However, several studies have argued that hypercycles seem to be adversely affected by noise or perturbations, causing errors in replication, and that they are unstable in regards to persistence at higher phases[10, 11].

In this article, we propose the Truth Table Language (TTL) for generating a self-replication system that starts with many self-irreplicapable species and a pair of self-replicating species. It has a simple structure, but shows some interesting behavior against external noise.

2 Model

For self- or other-replication, we used bit-matching rules applying 16 possible rules in the truth table (Fig. 1). The system consists of individuals, each of which is coded by a specified length of a binary bit-string (Fig. 2A). For example, in the case of a 6-bit length, there were 64 types of individuals in the system. Pairs were then formed among the individuals for producing offspring. Each individual was able to select one individual to pair with, so that the direction went from one individual to another. Individuals in a pair were defined as "Self" and "Mate" to clarify the direction of producing offspring; the Self individual produced offspring with the Mate individual.

(A)

Self	Mate	Combination of bit-pattern
(1 ,	1)	case 1
(1 ,	0)	case 2
(0 ,	1)	case 3
(0 ,	0)	case 4

(B)

Decimal number	Logic function name	Inputs (Self, Mate) (1, 1) case1	(1, 0) case2	(0, 1) case3	(0, 0) case4
0	ALL0	0	0	0	0
1	NOR	0	0	0	1
2		0	0	1	0
3		0	0	1	1
4		0	1	0	0
5		0	1	0	1
6	XOR	0	1	1	0
7	NAND	0	1	1	1
8	AND	1	0	0	0
9	XNOR	1	0	0	1
10		1	0	1	0
11		1	0	1	1
12		1	1	0	0
13		1	1	0	1
14	OR	1	1	1	0
15	ALL1	1	1	1	1

Figure 1: Truth Table. (A):2-bit input.(B):16 possible combinations

The bit pattern of an offspring was determined by locus-wise bit-matching between the two aligned bit-strings of the parents (Fig. 2B), and each individual had a head and tail position in the bit pattern. The length of individuals in the system was the same, so that the alignment of two individuals' bit patterns was simply a matter of aligning each individual's head or tail position. After alignment, each locus had a position in one of four possible patterns (00, 01, 10, or 11) (Fig. 1A).

At this point, we considered the bit pattern as input for producing a 1-bit pattern of the offspring's locus. When an offspring's 1-bit pattern is determined using a pair's 2-bit pattern on one locus, there are 16 patterns possible (there are 2 single-bit patterns, and there are four 2-bit patterns for one locus. Thus the combination is $2^4 = 16$). These input and output patterns are just as a 2-state and 2-input truth table (Fig. 1B).

The bit-pattern at a locus (00, 01, 10, or 11) was then decoded with one of the 16 possible truth table functions for 2-bit patterns. To make the truth table, we needed to extract four bits, which were used for deciding the new 1-bit pattern (Fig. 2B). The pattern consisted of four bits, surrounding the target locus, used to determine which truth table was applied for

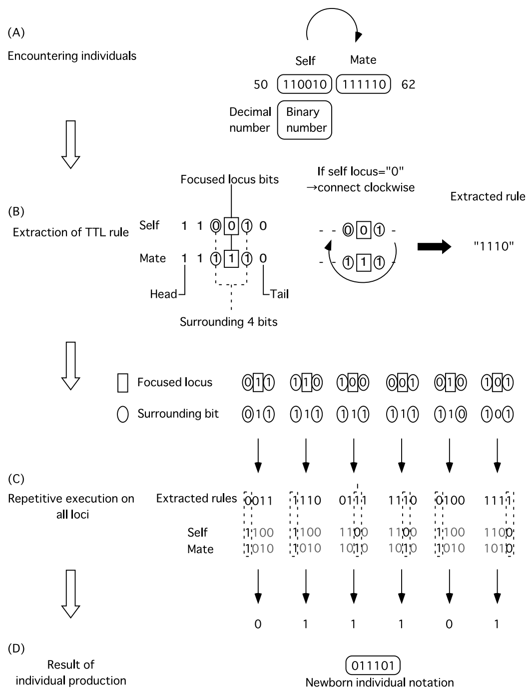

Figure 2: Individual production schema

locus-wise translation. At the locus point, Self's locus bit was the focus for deciding the linking order for extracting four bits. When the focal locus bit was "0", the four bits neighboring the locus were linked in a clockwise sequence, which started from the Self's lower bit, through the Mate's lower and upper bits, and finished at the Self's upper bit. When the Mate's bit was "1", four bits were linked in a counterclockwise sequence. This method, which linked four bits to one sequence, is not biased, and can extract all sorts of 16 rules on the truth table. An extra step was applied only to the loci in the head and tail positions. In these positions, the bit sequence of an individual was defined as a circular structure, so that the bits of head and tail loci were defined as adjacent bits for the execution of the above extraction methods. When the head locus was focal, the tail locus was considered adjacent, and vice versa. Thus, the production of a new individual was completely deterministic and depended solely on the bit-patterns of the two parent individuals.

3 TTL Systems

In this system, exactly one offspring was generated at each reproduction event. The parent individual was then replaced by the newborn offspring, and hence, the total number of individuals was kept constant. As each individual had a fixed length, the number of pairings between Self and Mate individuals was finite. For example, the number of pairings (sorts) between 6-bit individuals was $4,096(2^6 \times 2^6)$, because of the existence of a one-way production direction for Self individuals. As can be seen by the absence of a grayscale line running diagonally from the top left to the bottom right of the diagrams in Figure 3, perfectly replicating individuals did not, for the most part, exist within the system. Only the pairs of each 00...0s and 11...1s individuals were able to produce offspring identical to the Self and Mate individuals' bit strings. A few pairs were able to reproduce an individual identical to Self, though these were not perfect copies in the sense that Mate's bit string was not identical to the offspring's, and vice versa.

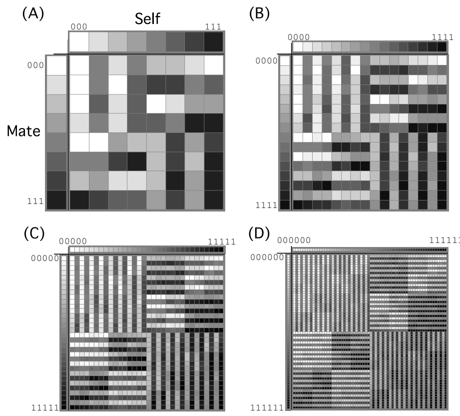

Figure 3: The matrixes of individual combinations: Individuals ordered as binary digits are suggested as grayscale. (00...0): white, (11...1): black. Each matrix shows the individual length: (A)3, (B)4, (C)5, and(D)6.

If there was no spatial structure (Fig. 4A), a small number of bit-patterns (species) were able to persist. After a transient phase, the system dynamics converged into cyclic behavior; each location in the loop was occupied by a specific series of individual species. The word "convergence" does not mean a stable state in which an individual is producing an identical individual with same bit-string, but rather that the group, which consists of specific individuals, is sequentially producing individuals of each other, in which case the dynamics of production by the group are closed. Thus, we incorporated a 1-D spatial constraint; individuals were arranged in a loop and a reproducing individual interacted with one of its one-step neighbors (Fig. 4B).

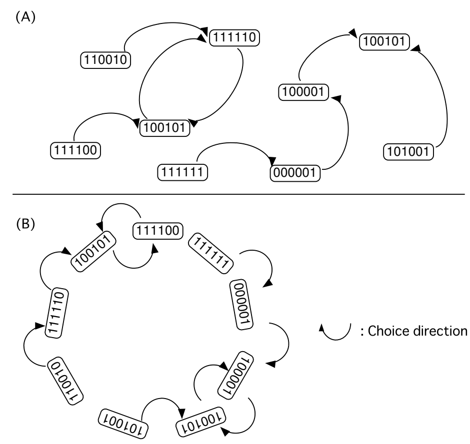

Figure 4: Spatial settings. (A): non-spatial. (B): 1-D spatial restriction

4 Results

The results obtained by incorporating 1-D spatial restrictions are as follows. The composition of individuals in the loop at the state of convergence was not estimated from these initial compositions. Nevertheless the production process by the parents is predictable. Although the initial configuration strongly influenced the system, the diversity of emerging individuals was maintained.

The cyclic behavior of individual production was revealed either when all individuals in the loop had the same bit-string, or when a Self individual was able to reproduce an individual with a bit-string matching that of the Mate, irregardless of whether or not it matched the Self's bit-string. Within the cycle, the same species was reproduced as an offspring irrespective of which neighboring individual was chosen as Mate (Fig. 5).

Another feature of the system with 1-D restrictions is its robustness. When one or more individuals were replaced by randomly selected individuals of a different species, the system absorbed the perturbation. Individual replacement is the same as noise injection directly onto a bit-string (Fig. 6). In Figure 6, after the first replacement occurred, the inserted individual reproduced a bit-string different from that of the previous series. Replacement did not seem to have a wide range of effects in the loop domain. The loop structure has absorbing capabilities. This behavior influences the phenomenon of early convergent generations. Thus, the loop of individuals achieved a stable cyclic transition with redundant reproduction, and proved to be robust in regards to external perturbation.

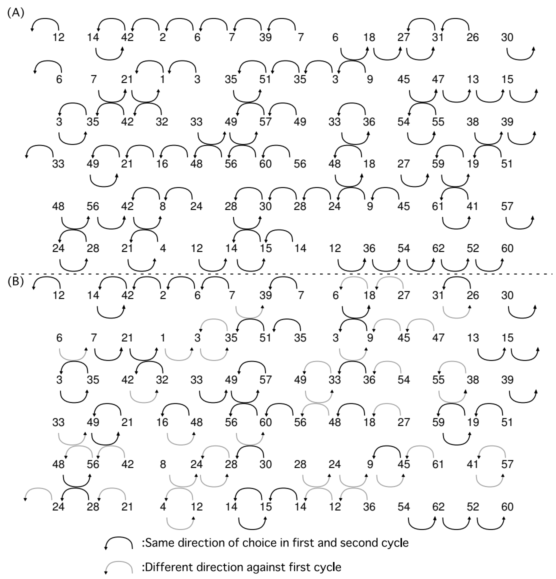

Figure 5: The result of selection behavior. (A): First cycle. (B): Second cycle. Despite random individual selection, each cycle has the same individual production.

5 Discussion

The proposed TTL system with 1-D spatial structure showed robustness in regards to external perturbation and redundant reproduction as a whole. However, it was not our intent that these phenomena emerge during the process of individual production. The structure of each individual as well as the TTL system applied to individual production are simple, and are not intended to intrinsically replicate perfectly.

We may be able to extract one generation from the results of the 1-D restriction system, and consider it as a coded biological string, such as a DNA string, by transposing the string into a DNA sequence and analyzing it with bioinformatic tools. If meaningful results are produced, we must ask ourselves how they should be interpreted. These bioinformatic tools merely suggest the homology between the strings and the character data coded by the base (A, T, G, and C). They show neither the informational relation between the function of the TTL system nor the biological meanings between an artificial string and a biological string. If these bioinformatic tools suggest the homology of some genes, they may find some "biased" patterns affected through production within a TTL system (Fig. 7).

Individuals on 1-D restricted space

Generations	Loop structure									
149	13	9	0	36	45	37	52	38	54	51
150	38	36	0	18	54	50	26	19	27	57
151	19	18	0	9	27	25	13	41	45	60
152	41	9	0	36	45	44	38	52	54	30
153	52	36	0	18	54	22	19	26	27	15
154	26	18	0	9	27	11	41	13	45	39
155	13	9	0	36	45	37	52	38	54	51
156	38	36	0	18	54	50	26	19	27	57
157	19	18	0	9	27	25	13	41	45	60
158	41	9	0	36	45	44	38	52	54	30
159	52	36	0	18	54	22	19	26	27	15
160	26	18	0	9	27	11	41	13	45	39
161	13	9	<31>	36	45	37	52	38	54	51
162	38	36	(45)	(43)	54	50	26	19	27	57
163	19	18	[54]	(57)	(23)	25	13	41	45	60
164	41	9	[27]	(58)	(45)	44	38	52	54	30
165	52	36	[45]	(61)	(53)	22	19	26	27	15
166	26	18	[54]	[62]	[58]	11	41	13	45	39
167	13	9	[27]	[31]	(45)	(21)	52	38	54	51
168	38	36	[45]	[47]	(46)	(10)	(58)	19	27	57
169	19	18	[54]	[55]	[23]	(21)	(61)	(9)	45	60
170	41	9	27	[59]	[43]	[42]	[62]	52	54	30
171	52	36	45	[61]	[53]	[21]	[31]	26	27	15
172	26	18	54	[62]	[58]	[42]	[47]	13	45	39
173	13	9	27	31	[29]	[21]	[55]	38	54	51
174	38	36	45	47	[46]	[42]	[59]	19	27	57
175	19	18	54	55	23	[21]	[61]	41	45	60
176	41	9	27	59	43	42	62	52	54	30
177	52	36	45	61	53	21	31	26	27	15
178	26	18	54	62	58	42	47	13	45	39
179	13	9	27	31	29	21	55	38	54	51
180	38	36	45	47	46	42	59	19	27	57
181	19	18	54	55	23	21	61	41	45	60
182	41	9	27	59	43	42	62	52	54	30

< >: Modified individual by external noise(or replaced indiviual)
( ): Affected newborn individuals by the neighborhood replacement
[ ]: Newborn individuals cyclic behavior produced by noise-affected individuals

Figure 6: Noise effect on 1-D spatial restriction.

What is the sequence pattern? How does the pattern emerge? The bioinformatic tools are considered to "··· look for patterns and make predictions without a complete understanding of where biological data comes from and what it means[12](p.4)." However the supreme goal of genome sciences should be to solve the algorithms that realize homologous or similar sequence patterns in the comparisons between extracted DNA data.

6 Future Direction

The TTL system is limited in fixed individual length for individual production, and so requires system improvements. Creating the TTL and a self-replicating system is not our final goal. In this paper, we proposed the present self-replicating system as a platform for bioinformatic research.

- Generally, one can only infer the evolutionary events from real biological data. However, the present system includes true trees and lineages for specific evolutionary events, and all histories

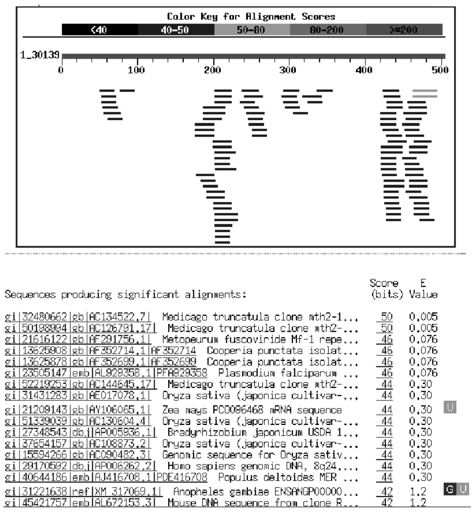

Figure 7: An example of BLASTN results with TTL system output (extended neighborhood selection: length 1→2). http://www.ncbi.nlm.nih.gov/BLAST/

for the "life". Such a system may prove to be advantageous in analysing evolutionary events in more detail.

- There are biases in the usage of truth tables similar to the codon bias in DNA data. These biases suggest that the TTL system does not merely output data at random. Thus, it is the meaningful experiments that we try to analyze these outputs, which have been generated randomly by initial settings.

Dealing with TTL systems as study subjects, we can evaluate the conventional techniques for analyzing molecular data. We may further propose new techniques for analyzing TTL systems, which can be used as feedback for bioinformatics.

References

[1] Fontana W. (1992). Algorithmic chemistry. In Langton CG, Taylor C, Farmar JD, Rasmussen S, editors, *Artificial Life II*, pages 159–209. Addison-Wesley, Redwood City, CA.

[2] Dittrich P, Ziegler J, Banzhaf W. (2001). Artificial chemistries — a review. *Artificial Life*, 7(3):225–275.

[3] Ray TS. (1992). An approach to the synthesis of life. In Langton CG, Taylor C, Farmar JD, Rasmussen S, editors, *Artificial Life II*, pages 371–408. Addison-Wesley, Redwood City, CA.

[4] Adami C. (1998). *Introduction to Artificial Life.* TELOS, Springer–Verlag, New York.

[5] Rasmussen S, Knudsen C, Feldberg R. (1992). Dynamics of programmable matter. In Langton CG, Taylor C, Farmar JD, Rasmussen S, editors, *Artificial Life II*, pages 211–254. Addison-Wesley, Redwood City, CA.

[6] Ikegami T , Hashimoto T. (1995). Active mutation in self-reproducing networks of machines and tapes. *Artificial Life*, 2(3):305–318.

[7] Banzhaf W. (1993). Self-replication sequence of binary numbers. foundation I and II: General and strings of length n=4. *Biological Cybernetics*, 69:269–281.

[8] Dittrich P, Banzhaf W. (1998). Self-evolution in a constructive binary string system. *Artificial Life*, 4:203–220.

[9] Eigen M, Schuster P. (1977). The hypercycle. a principle of natural self-organization. part a: Emergence of the hypercycle. *Naturwissenschaften*, 64:541–565.

[10] Barbieri M. (2003). *The Organic Codes : An Introduction to Semantic Biology.* Cambridge.

[11] Szathmáry E, Smith JM. (1997). From replicators to reproducers : the first major transitions leading to life. *Journal of Theoretical Biology*, 187:555–571.

[12] Gibas C, Jambeck P. (2001). *Developing Bioinformatics Computer Skills.* O'REILLY.

The Tenth International Symposium on Artificial Life and Robotics 2005(AROB 10th '05),
B-con Plaza, Beppu, Oita, Japan, February 4-6, 2005

Effectiveness of Emerged Pheromone Communication in an Ant Foraging Model

Yoshiyuki Nakamichi
Graduate School of Human Informatics
Nagoya University
Furo-cho, Chikusa-ku, Nagoya 464-8601, Japan
nakamiti@create.human.nagoya-u.ac.jp

Takaya Arita
Graduate School of Information Science
Nagoya University
Furo-cho, Chikusa-ku, Nagoya 464-8601, Japan
arita@nagoya-u.jp

Abstract

The collective behavior of social insects has been a puzzling problem for scientists for a long time. In particular, it is well known that ants solve difficult problems, for instance selecting the shortest pathway by communicating with each other via pheromone. How is it possible for such simple creatures to coordinate their behaviors and to solve problems as a whole? This paper focuses on the emergence of the pheromone communication system based on an ant foraging model in which neural networks of ant agents evolve according to the result of foraging. The computer experiments show that the ant agents using emerged communication with one type of pheromone are more adaptive than the ant agents not using pheromone communication or the ant agents using human-designed communication with 2 types of pheromone. This paper also discusses the reason for this superiority of the evolved pheromone communication.

Key words: ant colony, pheromone communication, swarm intelligence, artificial life.

1 Introduction

Complex and adaptive behavior of population emerges in social insects like ants and bees, though individuals seem to follow a relatively simple set of rules. The last decade has seen an explosion of research in fields variously referred to as swarm intelligence or collective intelligence. Especially in ants, pheromone communication is the key to understanding their swarm intelligence. The fundamental question regarding pheromone communication is: How have the pheromone communication systems emerged? This topic is not only a biological one, but, at the same time, a cross-disciplinary one [1, 2, 3, 4].

As a first step towards the origin of pheromone communication, we focus on the adaptive property of pheromone communication in population of agents, depending on the kind of pheromone communication. There can be two computational approaches to this issue, one is to define, a priori, both the meaning of pheromone and the rules of behavior for agents, and the other is to let them establish communication autonomously through learning or evolution. The latter is effective especially when the specific knowledge for solving the problems is limited or unknown. However, it is quite difficult to establish communication without a priori knowledge because pheromone communication doesn't function at all until the following two rules autonomously emerge in accordance with each other: "In what kind of situation should the agents secrete some kind of pheromone?" and "How should they act when they detect some kind of pheromone?".

To pursue this issue, some models have been proposed, including the pioneering model by Collins and Jefferson in which the mechanism for the evolution of pheromone communication was implemented [5] and a simple model by Kawamura and Ohuchi in which pheromone communication emerged in the environment where two colonies of artificial ants competed for food resources [6]. Based on these studies, we developed an ant foraging model, in which there can be several kinds of pheromone [7]. This paper reports our current state of the research based on the computer experiments using a simple model for evolution of pheromone communication, in which neural networks of ant agents evolve based on the result of foraging.

2 The ant foraging model

This section offers the brief summary of our ant foraging model which was proposed in our previous paper [7]. The model is based on multi-agent modeling and is inspired by foraging ants in nature. Foraging ant agents move around the $X \times Y$ grid environment in which there are food resources, pheromone and a nest. Each colony consists of N_a ant agents and their objective is to look for and carry to their nest as many food resources as possible.

Ant agents could secrete several types of pheromone in the same environment. The type of pheromone is identified by the subscript v ($v = 1, 2, \cdots$). They have no effect on each other. Each ant agent can drop pheromone on the ground by dropping action. Dropped pheromone gradually evaporates and diffuses in the air. Ant agents can detect diffusing pheromone only. Dropped pheromone and diffusing pheromone at position (x, y) are represented by $T_v(x, y)$ and $P_v(x, y)$ respectively. Then the diffusion process is defined by the partial differential equation as follows.

$$T_v^*(x,y) = (1-\gamma_{eva})T_v(x,y) + \sum_{k=1}^{N_a} \Delta T_v^k(x,y) \quad (1)$$

$$\Delta T_v^k(x,y) = \begin{cases} Q_p & \text{if } k\text{-th ant agent on the grid } (x,y) \text{ put the pheromone } v \\ 0 & \text{otherwise} \end{cases} \quad (2)$$

$$P_v^*(x,y) = P_v(x,y) + \gamma_{dif}(P_v(x-1,y) + P_v(x,y+1) + P_v(x,y-1) + P_v(x+1,y) - 5P_v(x,y)) + \gamma_{eva}T_v(x,y) \quad (3)$$

where the parameters γ_{eva} and γ_{dif} are the evaporation rate and diffusion rate of pheromone per a time respectively. Also, the letter "*" in superscript means that this represents intensity of pheromone at time $t+1$, and Q_p is the intensity of pheromone dropped by an ant agent.

All ant agents in each colony are homogenous, and have the same mechanism for action decision. Each agent performs actions in the following order. 1) The ant agent senses whether a food resource exists on the grid, senses whether the grid is a part of nest, and recognizes whether it is carrying a food resource. 2) The ant agent might drop a certain type of pheromone depending on the output of the neural network. Each ant agent can use V types of pheromone. In case $V=2$, ant agents can use pheromone $v=1$ and pheromone $v=2$ in the experiment. 3) When there is a food resource, if the ant agent carries no food, it picks it up, and if the ant agent has a food resource and is on the nest, the ant agent drops it. 4) If the ant agent did not perform the previous action, it selects and perform one action from 5 options according to the output of the neural network: "wait (do nothing)", "move forward", "turn backward", "turn left", "turn right". If the ant agent selects an action that is impossible to do, it waits instead.

All ant agents have the same simple two-layer neural network with $3+4V$ sensory input and $5+2V$ output neurons. Action selection is stochastically decided according to the probability from output value of a neural network.

The output value I_i $(i = 1, \cdots, 3+4V)$ of i-th sensory input neuron of an ant agent is defined as follows.

$$I_1 = \begin{cases} 1 & \text{if food is present} \\ 0 & \text{otherwise} \end{cases} \quad (4)$$

$$I_2 = \begin{cases} 1 & \text{if the ant agent is on the nest} \\ 0 & \text{otherwise} \end{cases} \quad (5)$$

$$I_3 = \begin{cases} 1 & \text{if the ant agent has food} \\ 0 & \text{otherwise} \end{cases} \quad (6)$$

$$I_{4+4(v-1)\sim 7+4(v-1)} = \begin{cases} 1 \text{ if the } P_v^s \text{ is satisfied} \\ 0 \text{ otherwise} \end{cases} \quad (7)$$

Here, the position of an ant agent is assumed to (x,y), and its neighbor position is $(x',y') \in \{(x-1,y),(x+1,y),(x,y-1),(x,y+1)\}$. $P_v^s(x',y')$ is the probability to fire input neuron of pheromone sensory input neurons. This stochastic firing function is used when obtaining the discrete values of $I_{4+4(v-1)\sim 7+4(v-1)}$, which depends on the gradient of density of pheromone and is defined as follows.

$$P_v^s(x',y') = \frac{1}{1+\exp\left(-\frac{P_v(x',y') - P_v^{\#}(x,y)}{T}\right)} \quad (8)$$

where the function $P_v^{\#}$ indicates the average intensity among neighbor grids.

The output value O_j $(j = 1, \cdots, 5+2V)$ of j-th output neuron is calculated by using following regular equations.

$$O_j = f\left(\sum_{i=1}^{3+4V} w_{ij} I_i - \theta_j\right) \quad (9)$$

$$f(x) = 1/\left(1+\exp(-x)\right) \quad (10)$$

where w_{ij} and θ_j are the weight and the threshold of the neural network. The values of 5 outputs $(O_{1\sim 5})$ correspond to "wait", "move forward", "turn backward", "turn left" and "turn right" actions respectively and the value of $2V$ outputs $(O_{6+2(v-1)}$ and $O_{6+2(v-1)+1})$ correspond to "dropping pheromone v" and "doing nothing about pheromone v" actions.

The genetic algorithm (GA) is adopted to evolve the neural networks of ant agents. A set of weights and thresholds describing a neural network is directly encoded to each genotype. The population size is N and all genotypes are initialized to random values of $[-0.5, 0.5]$. A fitness function is defined to be 1 plus the number of food resources that have been stored in the nest. New generation with N individuals is generated by the roulette wheel selection and mutation. The mutation operator is defined as adding a random real number of $[-0.5, 0.5]$ to the value in each locus with the mutation probability P_m. These processes are repeated until the final generation $g_{\max}$.

3 Computer experiments

The parameters of ant foraging and GA were set as $(X, Y, N_a, t_{\max}, Q_p, \gamma_{eva}, \gamma_{dif}, T) = (50, 50, 40, 1000, 1, 0.1, 0.1, 0.002)$ and $(N, g_{\max}, P_m) = (20, 2000, 0.05)$. The size of the nest was 5×5 and it was located in the center of the environment. 72 food resources were put on a randomly selected 3×3 area at the time $t=0$. Each grid in the area had 8 food resources. Under these conditions, several trials were conducted for each V $(V = 0, 1, 2)$.

Fig. 1 shows the moving average of food resources stored in the nest. It increased sharply to the range between 7 and 10 by 3000 generations in all graphs, and from then on, transitions differed depending on the parameter V. In the case of $V=0$, most trials showed that each moving average remained at around 7. In the case of $V \geq 1$, transitions were classified into two typical classes, and thus, it would be supposed that there are at least two evolutionary pathways. One was the case that moving average remained between 7 and 10, which is similar to the case of $V=0$. The cases 1a and 2a correspond to this class. The other was the case that moving average increased beyond 10. The cases 1b and 2b correspond to the class. The moving average had a tendency of swinging between 15 and 25 in 1b and it gradually increased beyond 7 in 2b. We see that the case 1b outperformed the other cases.

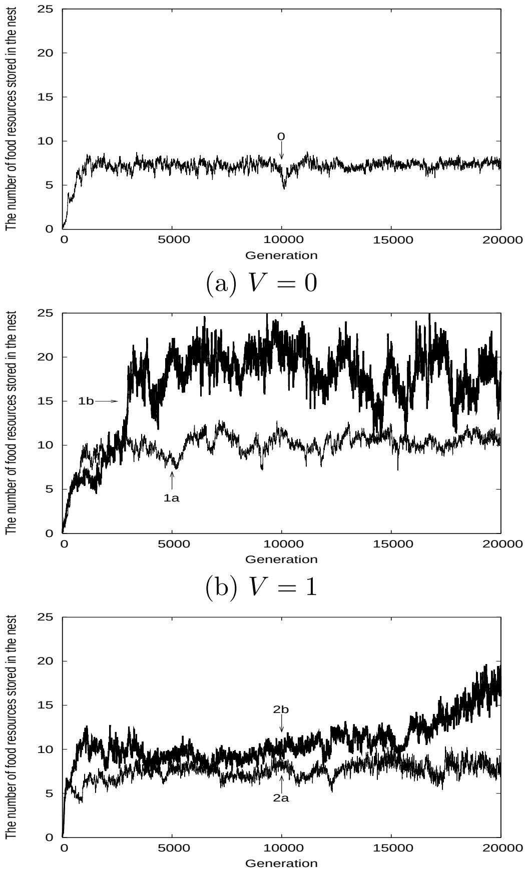

(a) $V = 0$

(b) $V = 1$

(c) $V = 2$

Figure 1: Moving average of the number of stored food resources.

It was found from the analysis of neural network that the ant agents in case 1b behaves as follows. Overall, the ant agents move forward with probability of about 90% and it turns right with probability of about 10%. However, the ant agents turns right with probability of about 40% only in cases in which they exist on the falling gradient of pheromone. Therefore, we can assume that the pheromone moderately indicates the presence of both food and a nest. The ant agents without food hardly secrete pheromone. The ant agents with food secrete pheromone with the probability of 40% and they on the nest secrete pheromone by the probability of 20% even if they aren't carrying food. Therefore, the pheromone moderately indicates the presence of both food and a nest.

We conducted additional experiments on the ant agents with human-designed pheromone communication (Fig. 2) in order to evaluate the effectiveness of emerged pheromone communication. The ant agents used two types of pheromone (food pheromone and nest pheromone) and were expected to do shuttling behavior between the nest and the food locations efficiently by using them. In the experiments, human-designed ant agents and the evolved ant agents (in the 20000th generation in all cases shown in Fig. 1) performed the foraging task 1000 times each. It is clearly shown from Table 1 that evolved

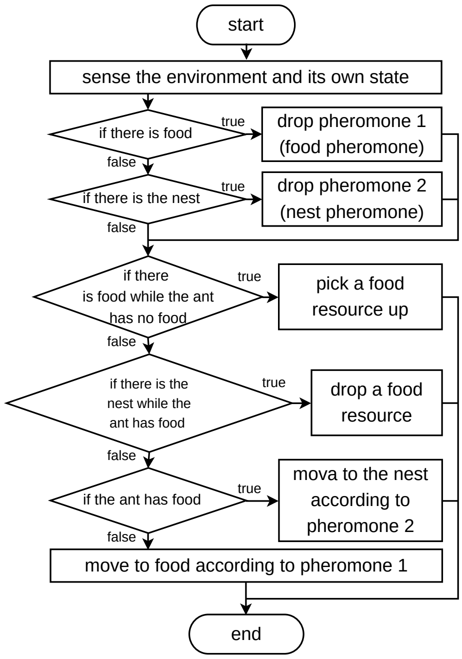

Figure 2: Behavior of human-designed ant agents.

Table 1: Average number of stored food resources.

Ant agent	Average
0 ($V = 0$)	8.8
1a ($V = 1$)	18.9
1b ($V = 1$)	28.0
2a ($V = 2$)	14.4
2b ($V = 2$)	24.7
human-designed	12.4

pheromone communication outperformed the human designed pheromone communication, in other words, some clever pheromone communication beyond human design emerged through evolution.

4 Superiority of emerged pheromone communication

The results of the first experiments are summarized as follows. The ant agents using pheromone ($V \geq 1$) could be clearly more adaptive than the ant agents without pheromone ($V = 0$). In other words, emergent pheromone communication could be adaptive. However, the results also show that it is not necessarily true that the more the number of available pheromone type increases, the more the ant agents could be adaptive. This might be because of the difficulty in establishing the meaning of pheromone or communication protocol based on multiple types of pheromone. We believe that more sophisticated and powerful mechanisms of learning or evolution could make pheromone communication work better.

The results of the second experiments show that emerged pheromone communication outperformed

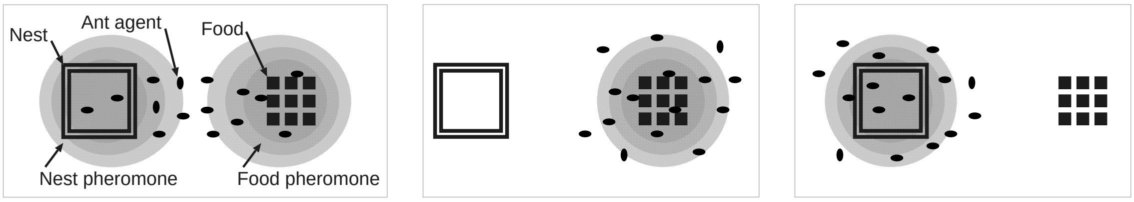

(a) The ideal state (b) An ill-balanced state (c) An ill-balanced state

Figure 3: The ideal and the ill-balanced states in the case of 2 types of pheromone.

human-designed pheromone communication. Why did emerged pheromone communication outperform human-designed one? To answer why emerged pheromone communication performed better, we observed the behavior of ant swarms and the spatial distribution of pheromone across the environment.

In the case of human-designed ant agents, it seems an ideal state that equal amount of two types of pheromone exist in the environment (Fig. 3 (a)). However, we found that ill-balanced states (Fig. 3 (b) and (c)) frequently happened, which mean inefficient concentration of the ant agents around the food or the nest. This unexpected result shows the difficulty in controlling the behavior of ant agents by using pheromone communication, which was caused by its emergent property.

In contrast, ant agents hardly crowded the food or the nest in case 1b. The results shown in previous section suggests that the ant agents in case 1b behaved as follows. Ant agents secrete one type of pheromone with high probability both when they are in the nest and when they have food. So, in this case, the pheromone moderately indicates the presence of both food and the nest in the emerged pheromone communication. Ant agents have evolved to have a tendency to move to the places with more intensive pheromone. Therefore, ant agents move around the peripheries of both food and the nest. These ant agents don't behave optimally, because it has no way of distinguishing food and nest by using only one type of pheromone. However, it is a significant fact that we hardly observe the ill-balanced states which appeared frequently in the case of human-designed ant agents.

Above discussion is summarized as follows. While the uniquely existing type of pheromone acquired a moderate meaning of the presence of both food and the nest through evolution, the diversity of pheromone distribution and the diversity of the ant agents' collective behavior got to be maintained at proper levels, which realized the robust foraging behavior of ant agents.

5 Conclusion

This paper describes the ant foraging model for the evolution of pheromone communication and discusses the result of the computer experiments. The computer experiments show that the ant agents using emerged communication with one type of pheromone are more adaptive than the ant agents not using pheromone communication or the ant agents using human-designed communication with 2 types of pheromone. The reason for the superiority of the evolved pheromone communication is the diversity of pheromone distribution and the diversity of the ant agents' collective behavior got to be maintained at proper levels, which realized the robust foraging behavior of ant agents.

Acknowledgments

This work was supported by a Grant-in-Aid for the 21st Century COE "Frontiers of Computational Science".

References

[1] T. Arita, *Artificial Life: A Constructive Approach to the Origin/Evolution of Life, Society, and Language*. IGAKU-SHUPPAN, revised 2nd ed., 2002.

[2] M. Dorigo, *Optimization, Learning and Natural Algorithms*. PhD thesis, Politecnico di Milano, 1992.

[3] E. Bonabeau, M. Dorigo, and G. Theraulaz, "Inspiration for optimization from social insect behaviour," *Nature*, vol. 406, pp. 39–42, July 2000.

[4] D. Payton, M. Daily, R. Estkowski, M. Howard, and C. Lee, "Pheromone robotics," *Autonomous Robots*, vol. 11, no. 3, pp. 319–324, 2001.

[5] R. J. Collins and D. R. Jefferson, "Antfarm: Towards simulated evolution," in *Artificial Life II* (C. G. Langton, C. Taylor, J. D. Farmer, and S. Rasmussen, eds.), pp. 579–601, 1992.

[6] H. Kawamura and A. Ohuchi, "Evolutionary emergence of collective intelligence with artificial pheromone communication," in *Proceedings of IECON-2000*, pp. 2831–2836, 2000.

[7] Y. Nakamichi and T. Arita, "An evolutionary simulation of the origin of pheromone communication," in *Proceedings of the 5th International Conference on Simulated Evolution and Learning*, pp. 1–6 (STP–1–93), 2004.

The Tenth International Symposium on Artificial Life and Robotics 2005(AROB 10th '05),
B-con Plaza, Beppu, Oita, Japan, February 4-6, 2005

Foraging Behavior of Ant-Like Robots with Virtual Pheromone

Ken Sugawara[1] and Toshiya Kazama[2]
[1] Department of Liberal Arts, Tohoku Gakuin University, Sendai, JAPAN
[2]Graduate School of Information Systems, Univ. of Electro-Communications, Tokyo, JAPAN

Abstract

In multi-robot system, communication is indispensable for effective cooperative working. To apply chemical method to the communications of multi-robot system is challenging topic, but it is not easy to treat real chemical materials for the robots because of some technical difficulties. In this paper, we show virtual pheromone system in which chemical signals are simulated with the graphics projected on the floor, and in which the robots decide their action depending on the color information of the graphics. We examined the performance of this system through the foraging task, which is one of the most popular tasks for multi-robot system.

1 Introduction

Recently, research in the area of multi-robot systems has been very active, and many researchers are currently studying the behavior of these types of systems[1, 2]. One of the most important aspects in a multi-robot system is the ability of robots working cooperatively. Working together, they complete tasks that a single robot cannot.

For effective working, mutual communication between units is indispensable. Many researchers have introduced the direct communication, and in most cases, physical media such as light, sound, radio wave are used for the communication. Those media are also employed in biological system: for example, fireflies make use of light as a mating signal, and crickets use the sound as the signal. However, as we know, not only physical signals but also chemical signals are used for the communication. It is well-known that some insects use the chemical signals, which are generally called pheromone. They show very interesting behaviors depending on the properties of pheromones. One of the most popular pheromone-controlled behaviors is foraging of ants. Here, pheromone released by organism enables individuals to communicate with each other.

Pheromones are available not only for direct communication but also for indirect communication. In insect world, pheromones are used for various purposes: alarm, aggregation, sex attractant, recruitment, defense, trail-making, and so on.

2 Properties of Pheromone

Important characteristics of pheromones as a chemical signal are described as follows:

•Marking

Most pheromones do not disappear immediately and remain in the field for some time. It means agents can share an information based on the pheromones even in the absence of signal source agent. Foraging ants, for example, move from the food source to their nest laying "recruit pheromone" while food remains at the source, and they can find out the food efficiently thanks to this property.

•Diffusion

Most pheromones are volatile and spread over a large area. This characteristic is used for long range communication, for generating chemical gradient field, and so on.

•Evaporation

Pheromone disappears by evaporation because of its volatility. This characteristic leads to the erase of needless/useless information. In case of ant societies, less food remains at the food source, less pheromone the ants lay. As a result, they can avoid useless energy consumption for foraging.

•Diversity

There is a lot of materials which are used as pheromones, and moreover, some of them are used in combination. In ant societies, for example, each individual can distinguish its colony's mates and ones of other colonies based on the difference of mixture rate of some pheromones.

3 Virtual Dynamic Environment for Autonomous Robots (V-DEAR)

As described above, communication by chemical material such as pheromone has some interesting characteristics that physical communication system does not have, but few researches treat real chemical materials as a communication media for physical robot system[3]. We can consider following reasons. At this stage, it is not easy to treat chemical material comparing with the physical medium, and it is also not easy to get proper chemical sensors. Moreover, chemical materials, especially gas, are invisible and it is quite difficult to observe how they spread and affect robots' behaviors.

Here we propose "Virtual Dynamic Environment for Autonomous Robots (V-DEAR)" for real robot experiment. In this system, pheromones are replaced with graphics projected on the ground. Robots decide their actions following the color information of the projected CG. As virtual pheromones are represented as CG, we can avoid the problems described above. In addition, we can easily control the rate of diffusion, evaporation, diversity, etc. of the virtual chemical materials.

Fig. 1 shows the schematic and photo of this system. This is composed of LC projector to project the CG and the CCD camera to trace the position of the robots in the field. The robot moving on the field has sensors on the top to detect the color and brightness of the field, and determine its actions autonomously based on the condition of the CG on the floor.

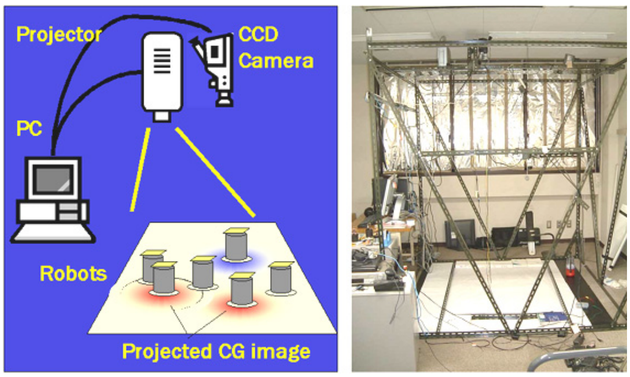

Figure 1: Virtual Dynamic Environment for Autonomous Robots (V-DEAR). Schematic (left) and photo (right).

Combining the position information of the robots acquired from CCD camera and the projected CG by projector, we can realize the dynamic interaction between the environment and the robots.

In this paper, we will show you the performance of this system through the foraging task by the interacting robots. This is one of the most popular tasks in the study of multi-robot system, but almost all of them treat physical communication methods[4, 5, 6, 7, 8].

4 Experiment

4.1 Robot for Experiment

•Robot

Each robot has the five fundamental behaviors as follows: "searching," "attracted," "recruiting," "homing," and "avoidance" (Fig. 2). When a robot in searching state finds food, it stays there for a short time and picks up some of the food. After that, it moves to home leaving a pheromone. When arriving at home, it lays the food there and goes searching food again. The robot which detects the pheromone follows the trail, if it has no food.

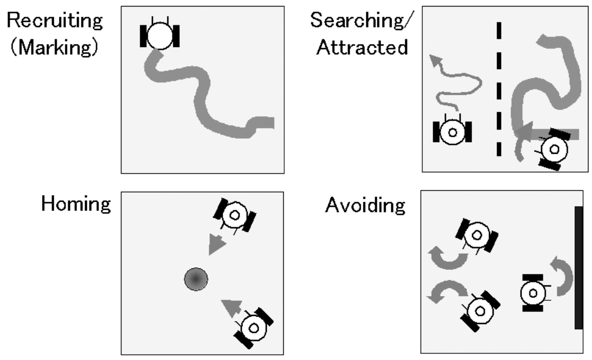

Figure 2: Fundamental robot behaviors. "Recruiting","searching," "attracted","homing," and "avoidance."

The robot used in this experiment is shown in Fig. 3. It has touch sensors extended to 8-directions to detect collision, a pair of infrared sensors to return to home, three color-sensors to detect field condition, bottom sensors to detect "Home", and 1 LED to indicate its state.

•Pheromone

Dynamics of pheromone is described as

$$\dot{\rho} = \delta + D\nabla^2\rho - k\rho, \tag{1}$$

where ρ is the concentration of pheromone, δ is injection concentration, D is a diffusion coefficient, and

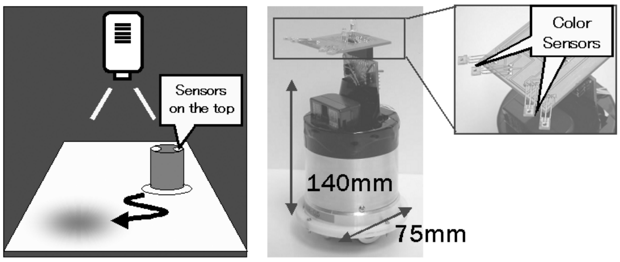

Figure 3: Robots detect the field condition by sensors on the top.

k is the rate of evaporation.

Fig. 4 shows the basic behavior of the foraging robots. On discovering a food, the robot turns on a LED on the top and moves towards the nest. The V-DEAR system detects the LED and projects a CG pheromone trail during the LED is turned on. When the robot arrives at the nest, it turns off the LED and changes into the searching state. If it finds the pheromone trail, it follows the trail.

Here you can see the trail pheromone, or a band of light is projected following the homing route of the robot (a), and a robot traces a band (b) in Fig. 4.

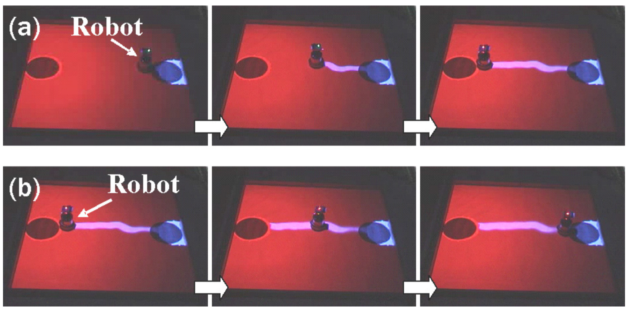

Figure 4: Basic behavior of the foraging robot. (a) On discovering food, the robot lays chemical trail while returning to nest. (b) The robot detecting the pheromone follows the trail.

4.2 Field for Experiment

•Field
The field for this experiment was an 90 × 90 cm black surface with the wall at the boundary. A nest is represented with a yellow circle on the ground and IR-LED array is placed there.

•Food distribution
We can consider various types of food distribution. In this experiment, we chose homogeneous and localized distributions.

In homogeneous distribution, 24 food points are projected on the field. When a robot in searching state detects the color of food point, the robot turns on the LED on the top and changes its state to homing state. When the V-DEAR system detects the LED, it erases the corresponding food point and starts to draw the virtual pheromone following the robot's homing route.

In localized field, the behavior of robots is same as the case of homogeneous distributed field, but the quantity of food is assumed to be infinite, i.e. the food point is not erased.

4.3 Results

Fig. 5 is the snapshot and the trajectories of the foraging by a robot in the homogeneously food-distributed field, where Fig. 5(a) and (b) are the case of ($D = 0.05, k = 0.1$) and ($D = 0, k = 0$), respectively. In case that the evaporation rate of the pheromone is high, the pheromone hardly remains. On the other hand, when the evaporation rate and the diffusion coefficient are too low, the pheromone remains clearly in the field. Here the trajectory shows that the robots are trapped by their own pheromone and tend to do useless searching.

Fig. 6 is the snapshot of the foraging by two robots in the locally distributed field, where fig. 6(a) and (b) are the case of ($D = 0.15, k = 0.01$) and ($D = 0.15, k = 0.002$),respectively. In case that the evaporation rate of the pheromone is high, the pheromone hardly remains. However, the evaporation rate is low, a stable trail is formed between the food point and their nest. In this case, the robots can search and carry the foods by tracing the laid pheromone effectively, which can be observed from the trajectory.

Fig. 7 shows the relation between the evaporation rate and the number of collected foods. Fig. 7(a) is the result of homogeneously food-distributed field, and (b) is the result of locally food-distributed field. The parameter in these graphs is the number of robots (1∼3).

These graphs clearly show that less pheromone is left in the field, more foods are collected in homogeneous field, and that the performance becomes better when a pheromone trail is formed continuously in localized field.

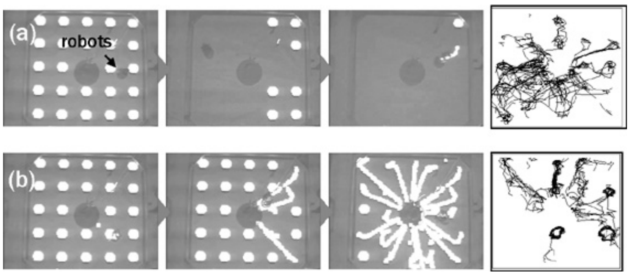

Figure 5: Snapshot of experiment in homogeneously distributed field. (a)$D = 0.05, k = 0.1$, (b)$D = 0, k = 0$.

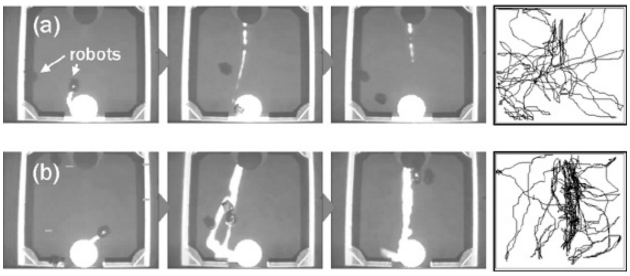

Figure 6: Snapshot of experiment in locally distributed field. (a) $D = 0.15, k = 0.01$ (b) $D = 0.15, k = 0.002$.

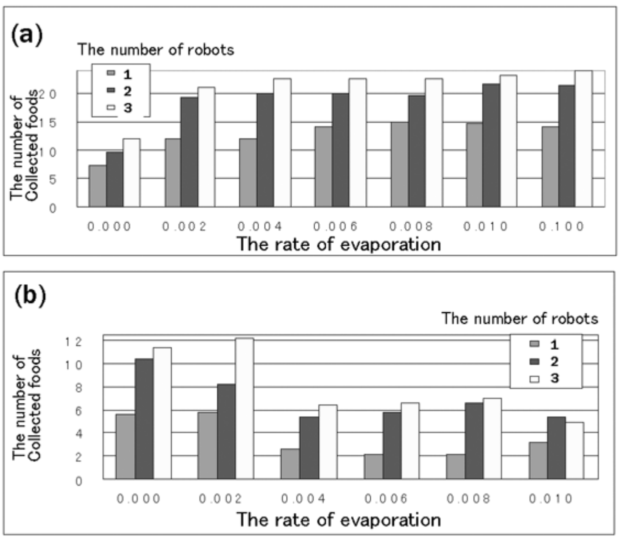

Figure 7: Relation between the evaporation rate and the number of collected foods. Parameter is the number of the robot. (a) Homogeneous field. (b) Localized field.

5 Conclusion

In this paper, we treat indirect communication by chemical signal between the robots, and investigate a foraging behavior by multi-robot system. Here we proposed a Virtual Dynamic Environment for Autonomous Robots (V-DEAR), where we can simulate chemical system such as pheromone, and discussed the foraging by the experiment.

This work was partially supported by a Japanese Grand-in-Aid for Encouragement of Young Scientists from the Ministry of Education, Science and Culture (No.15760291).

References

[1] Y.U.Cao, A.S.Fukunaga and A.B.Kahng, "Cooperative Mobile Robotics:Antecedents and Directions," *Autonomous Robots*, 4, (1997) pp.7-27.

[2] L.E.Parker, "Current Research in Multi-Robot Systems", Journal of Artificial Life and Robotics, vol. 7 (to appear).

[3] A.T. Hayes, A. Martinoli, and R.M. Goodman, "Distributed Odor Source Localization", *IEEE Sensors*, Vol. 2, No. 3 (2002) pp.260-271.

[4] L. Steels, "Cooperation between distributed agents through self-organization," *Proc. of the First European Workshop on Modeling Autonomous Agents in a Multi-Agent World*, (1990) pp. 175-195.

[5] A. Drogoul and J. Ferber, "From Tom Thumb to the Dockers: Some Experiments with Foraging Robots," *Proc. Simulation of Adaptive Behavior*, (1993) pp.451-459.

[6] T. Balch and R.C. Arkin, "Communication in Reactive Multiagent Robotic Systems," *Autonomous Robots*, 1, (1994), pp. 27-52.

[7] R. Beckers, O.E. Holland and J.L. Deneubourg, "From Local Actions To Global Tasks: Stigmergy and Collective Robotics," *Artificial Life IV*, MIT Press, (1994) pp. 181-189.

[8] M.J.B. Krieger, J.B. Billeter, "The call of duty: Self-organized task allocation in a population of up to twelve mobile robots", *Robotics and Autonomous Systems*, Vol.30 (2000) pp.65-84.

The Tenth International Symposium on Artificial Life and Robotics 2005(AROB 10th '05),
B-con Plaza, Beppu, Oita, Japan, February 4-6, 2005

Information-theoretic approach to embodied category learning

Gabriel Gómez[1], Max Lungarella[2] and Danesh Tarapore[3]
[1] *Artificial Intelligence Laboratory, University of Zurich, Switzerland*
[2] *Dept. of Mechano-Informatics, the University of Tokyo*
[3] *Autonomous Systems Lab., EPFL, Lausanne, Switzerland*
gomez@ifi.unizh.ch, maxl@isi.imi.i.u-tokyo.ac.jp, danesh.tarapore@epfl.ch

Abstract

We address the issue of how statistical and information-theoric measures can be employed to quantify the categorization process of a simulated robotic agent interacting with its local environment. We show how correlation, entropy, and mutual information can help identify distinct informational structure which can be used for object classification. Further, by means of the isometric feature mapping algorithm, we analyze the weights of a neural network designed to find clusters based on these distinct information theoretic characteristics of the object's shape, size and color. We conclude that an understanding of the information-theoretic implications of categorization could help design robots with improved categorization and better exploration strategies.

1 introduction

In our daily lives, we are exposed to a barrage of multimodal sensory stimulation (e.g., visual, tactile, proprioceptive). Perceptual categorization can be conceptualized as the ability to identify regularities in this continuously changing stream of sensory information, and to treat similar, but not necessarily identical objects and events, as being somehow equivalent. Recently, evidence has been accumulating showing that perceptual categorization is not a mere mapping from a set of sensory nodes to a set of category nodes – as previously assumed – but is instead the result of a process of sensorimotor coordinated interaction between an embodied agent and its local environment. Such interaction has been hypothesized to be one of the major information theoretic implications of embodiment, because it allows an agent to actively generate constraints in its sensory input ([1, 2, 3, 4]). Such constraints, in turn, simplify the problem of learning categories by inducing spatio-temporal correlations, and by reducing drastically – in an information theoretic sense – the number of degrees of freedom (dimensionality) of the sensory space.

This paper aims at quantitatively underpinning this hypothesis (see also [1, 2, 5, 6, 7, 8]). We present the analysis of data collected by a simulated robotic agent by means of correlation, mutual information, geometric separability index, and isometric feature maps. We conclude that an information-theoretic approach to the study of categorization leads to a better (quantitative) understanding of how embodied interaction simplifies category learning despite the high dimensionality of the sensorimotor data sets. This approach may also shed light on the characteristics of the objects being categorized, and reduce the time required by the agent to learn.

2 Experimental Setup

We simulated a two-wheeled robot moving in a closed environment cluttered with randomly distributed, colored objects. Objects in the environment were red cubes and cylinders.

The robot was equipped with 11 proximity sensors (d_{0-10}) and a pan-controlled image sensor or camera unit (see Fig. 1b). The proximity sensors had a position-dependent range (see caption of Fig. 1). The output of each sensor was affected by additive white noise, and was partitioned into a space having 32 discrete states, leading to sensory signals with a 5 bit resolution. To reduce the dimensionality of the input data, we divided the camera image into 24 vertical rectangular slices (i_{0-23}). We computed the amount of "effective" red color in each slice as R=r-(b+g)/2.

For the control of the robot we opted for the Extended Braitenberg Architecture [3] (see Fig. 2). To pick up the regularities induced by the sensorimotor coordination we used a Kohonen feature map [9].

Before being projected onto the Kohonen map, the 28-dimensional input vector consisting of the ac-

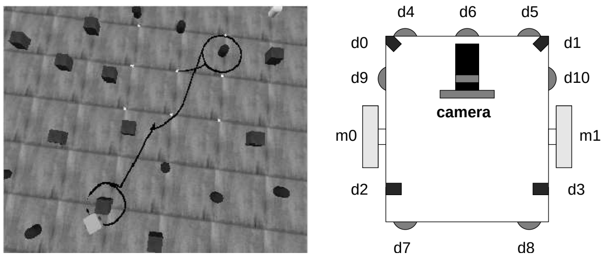

(a) (b)

Figure 1: (a) Bird's eye view of the robot and its ecological niche. The trace represents a typical path of the robot during an experiment. (b) Schematic representation of the agent. The distance sensors have a range that depends on their position. If rl is the length of the robot, then the range of d_0, d_1, d_9, and d_{10} is $1.8\,rl$, the one of d_2 and d_3 is $1.2\,rl$, and the one of d_4, d_5, d_6, d_7, and d_8 is $0.6\,rl$.

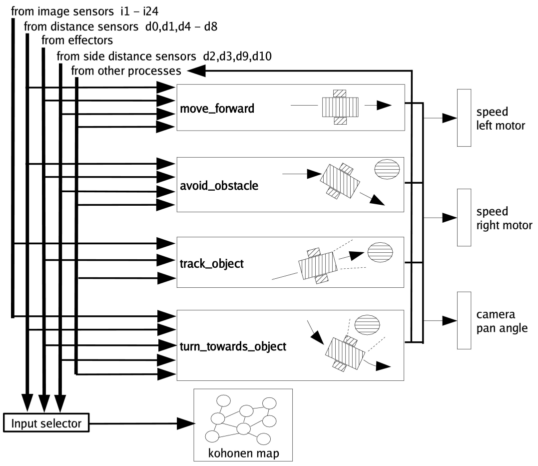

Figure 2: Block diagram of the control architecture.

tivations of 24 red channels, the activations of two out of four proximity sensors located on the same side of the robot (that is, either the pair d_2,d_9, or the pair d_3,d_{10}), as well as the left and right motor activation values (m_l,m_r), was preprocessed by the "input selector" (see Fig. 2). If the agent circled an object counter-clockwise – i.e., the object was on its left – the input vector of the Kohonen map was $[i_0, i_1, \ldots, i_{23}, d_2, d_9, m_l, m_r]^T$. However, if the agent circled an object clockwise – i.e., the object was on its right – the input vector was $[i_{23}, i_{22}, \ldots, i_0, d_3, d_{10}, m_r, m_l]^T$. That is, the vector ($i_0$,...,$i_{23}$) was fed to the Kohonen map in reverse order (i_{23} was the first element, followed by d_3 and d_{10}, and the right and left motor activation). The reason for this re-ordering operation was to avoid having the Kohonen map discriminate between objects, based on the direction of circling.

The 28-dimensional output vector of the input selector was normalized to unit length, and each of its elements was projected onto each of the neurons of the Kohonen map (that is, the input layer was fully connected to the map layer). The Kohonen map consisted of 576 neurons, arranged in the form of two-dimensional lattice with N_r=24 rows and N_c=24 columns. The network's 24x24x28=16128 initial synaptic weights were chosen from a random set. The dependence of the learning-rate parameter η on discrete time n was chosen to be $\eta(n) = \eta_0\, e^{-n/\tau_1}$, where η_0=1.0 was the initial value of the learning parameter, and $\tau_1 = 2.2^{\log N_r N_c}$. That is, the learning rate decreased exponentially over time. Another feature of the Kohonen map was that the size of the neighborhood of each neuron shrank over time. The dependence on discrete time n was $\sigma(n) = \sigma_0\, e^{-n/\tau_2}$, where σ_0=9.0 and $\tau_2 = 2.0^{\log N_r N_c}$.

3 Behavioral specification

At the outset of each experimental run the behavioral mode of the robot was set to "exploring." In this mode the robot roams through the environment at a constant speed while avoiding obstacles. Upon detection of a salient red object, the robot approaches it under guidance of the visual system ("tracking" mode). As soon as the object is close, the robot starts circling around it keeping it in the center of its visual field by adjusting the camera's pan-angle ("circling" mode). Concurrently, a habituation signal starts increasing. While the robot circles the object, the values of the input signal (24 image sensors,a pair of side distance sensors, and two motor activations) – after being appropriately re-organized by the input selector – are projected onto the Kohonen feature map; the synaptic weights of the network are updated, and the learning-rate parameter decreased. The robot keeps circling around the object for a while and then resumes the exploration of its environment. The trace of a typical experimental run is shown in Fig. 1a. The entire experiment comprised 78 such experimental runs, each run consisting of approximately 6000 data samples. All samples were stored into a time series file for subsequent analysis.

The categorization error as the percentage of misclassified objects per unit of time is shown in Fig. 3. Clearly, the network learned to discriminate between

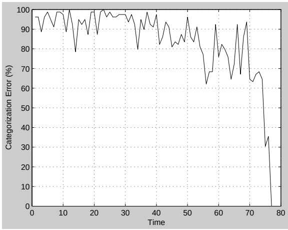

(a)

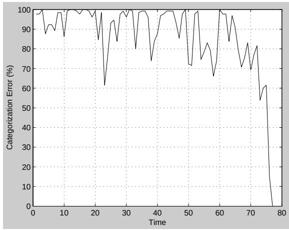

(b)

Figure 3: Categorization error (vertical axis) versus time (horizontal axis). (a) cubes; (b) cylinders.

cubes and cylinders: The classification error after timestep 77 dropped to almost zero.

4 Methods

In this section, we describe the statistical and information theoretical measures employed in this paper. The correlation $Corr(X,Y)$ quantifies the amount of linear dependency between two random variables X and Y (e.g., two sensory channels), and is given by $\sum_{x\in X}\sum_{y\in Y} p(x,y)\,(x-m_X)(y-m_Y))/\sigma_X\,\sigma_Y$, where $p(x,y)$ is the second order (or joint) probability density function, m_X and m_Y are the mean, and σ_X and σ_Y are the standard deviation of x and y computed over X and Y. The entropy of a random variable X is a measure of its uncertainty, and is defined as $H(X) = -\sum_{x\in X} p(x)\,log\,p(x)$, where $p(x)$ is the first order probability density function associated with X (in a sense entropy provides a measure for the sharpness of $p(x)$). Similarly, the joint entropy between variables X and Y is defined as $H(X,Y) = -\sum_{x\in X}\sum_{y\in Y} p(x,y)\,log\,p(x,y)$. For entropy as well as mutual information, we assumed the binary logarithm. Using the joint entropy $H(X,Y)$, we can define the mutual information between X and Y as $MI(X,Y) = H(X) + H(Y) - H(X,Y)$.

To get a better grasp on the regularities in the sensory space, we computed also the Geometric Separability Index (GSI) introduced in [10]. Geometric separability is a generalization of linear separability, and quantifies how close regions in the sensory space belonging to the same object are to each other. The GSI is computed by checking for every sensory pattern whether the nearest pattern (in terms of the Euclidean distance) is part of the same class. It is calculated as follows:

$$\sum_{i=1}^{n} \frac{(f[x_i] + f[x_i{}^*] + 1)\,mod\,2}{N},$$

where $f[x_i] = 0$, if x_i belongs to one class, and $f[x_i] = 1$, if x_i belongs to the other class (f is also called the category function); x_i is the i-th sensory pattern (N-dimensional vector), and $x_i{}^*$ is the nearest neighbor of x_i. If the nearest pattern in sensory space always belong to the same class of the currently perceived object the GSI is 1. High values of the GSI thus indicate that the sensory patterns belonging to the two categories are quite separated in the input space and easy to discriminate, while value close to 0.5 indicate that the sensory patterns corresponding to the two categories completely overlap.

In addition to these three measures, we also used the isometric feature mapping, or Isomap, algorithm described in [11]. Isomap solves the problem of dimensionality reduction by using local metric information to learn the underlying global geometry of a data set. It discovers – given only the unordered high-dimensional input – the low-dimensional representations of the data. Although the classical techniques for dimensionality reduction such as Principal Component Analysis (PCA) and Multi Dimensional Scaling (MDS) are simple to implement and efficiently computable, many data sets contain non linear structures that are invisible to PCA and MDS. Isomap combines the major algorithmic features of PCA and MDS with the flexibility to discover nonlinearity in the input data.

5 Data Analysis and Results

Correlation

While the robot circled the object, we observed negative correlation between the left and right motors. The circling behavior also induced negative correlation between pairs of proximity sensors located on the same side of the robot, that is, between (d_2,d_9), (d_0,d_2) and (d_2,d_4) when the robot circled the object in the counter-clockwise direction. (see Fig. 4).

There is a high discrepancy in the (d_0,d_2) sensor correlation between cubes (-0.3083) and cylinders (0.7109). In the case of cylinders, due to their smooth surface, the sensors d_2 as well as d_0 will always be in contact with the object. Due to the corners of the cubes, as well as the length of its edge, this positive correlation will not be evident.

Correlation	Cubes	Cylinders
(d_2,d_9)	-0.4995	-0.3189
(d_0,d_2)	-0.3083	0.7109
(d_2,d_4)	-0.4476	0.0540

Table 1:

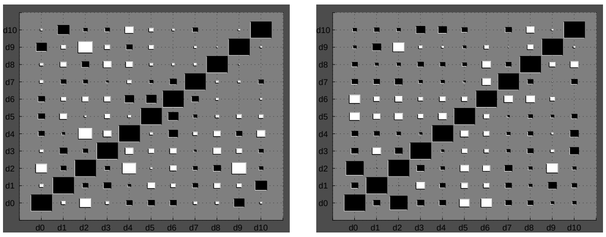

(a) (b)

Figure 4: Distance sensor correlation matrix obtained from the pair-wise correlation between pairs of distance sensors (indexes d_0 to d_10) for (a) cubes and (b) cylinders . The behavioral state is "circling". The higher the correlation the larger the size of the square.

While the robot was circling around a cube, strong correlations between the output of all the 24 red channels (i_1 to i_{24}) could be observed. The average correlation amounted to 0.5628 (see Fig. 5a). For cylindrical objects, the average correlation between the same red channels (i_1 to i_{24}) was 0.1321.

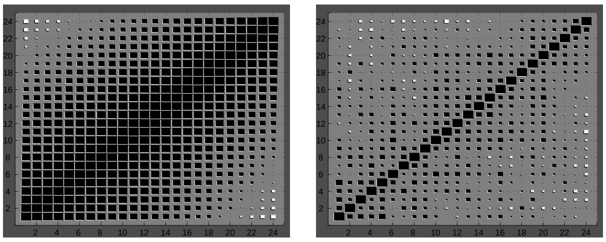

(a) (b)

Figure 5: Image sensor correlation matrix obtained from the pair-wise correlation between pairs of image sensors (indexes 1 to 24) for (a) cubes and (b) cylinders. The behavioral state is "circling". The higher the correlation the larger the size of the square.

Entropy and mutual information

The pair-wise mutual information between the 24 image sensors, and the 11 proximity sensors is shown in Fig. 6 and Fig. 7. The diagonals of the plots represent the entropy of the sensory stimulation.

While the robot circled the object, we observed high mutual information between pairs of proximity sensors located on the same side of the robot, that is, between (d_2,d_9), (d_0,d_2) and (d_2,d_4) when the robot circled the object in the counter-clockwise direction.

Mutual Information	Cubes (bits)	Cylinders (bits)
(d_0,d_0)	0.0464	0.1752
(d_2,d_2)	3.0225	3.0439
(d_9,d_9)	1.0292	0.9103
(d_0,d_2)	0.0252	0.1475
(d_2,d_4)	0.1956	0.0506
(d_2,d_9)	0.1919	0.0858

Table 2:

There is a high discrepancy in the sensor d_0 entropy between cubes (0.0464) and cylinders (0.1752). This discrepancy is also observed in (d_0,d_2) mutual information between cubes (0.0252) and cylinders (0.1474).In the case of cylinders, due to their smooth round surface, the sensor d_0 will always be in contact with the object. However the sharp corners of the cube prevent this contact from occurring as frequently. We also observe a high discrepancy in (d_2,d_4) mutual information between cubes (0.1956) and cylinders (0.0506).

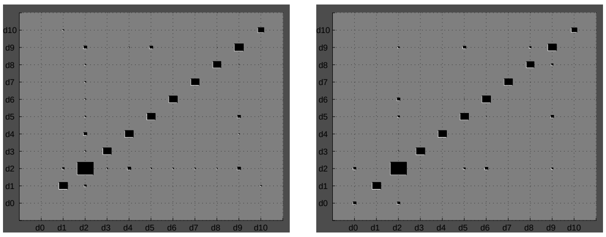

(a) (b)

Figure 6: Distance sensor mutual information matrix obtained from mutual information between pairs of distance sensors (d_0 to d_{10}), in one particular experimental run. The behavioral state is "circling" (a) cubes and (b) cylinders. The higher the mutual information the larger the size of the square.

While the robot was circling around a cube, high mutual information between the output of all the 24 red channels (i_1 to i_{24}) could be observed. The average mutual information amounted to 0.8166 bits (see Fig. 7a). For cylindrical objects, the average mutual information between the same red channels (i_1 to i_{24}) was 0.2676 bits.

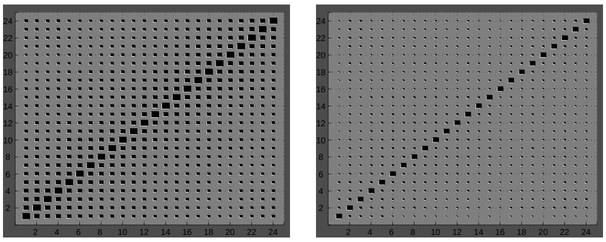

(a) (b)

Figure 7: Image sensor mutual information matrix obtained from the pair-wise mutual information between pairs of image sensors (indexes 1 to 24), in one particular experimental run. The behavioral state is "circling" (a) cubes and (b) cylinders. The higher the mutual information the larger the size of the square.

Geometric Separability Index (GSI)

The GSI identifies the regularities founded by the Kohonen map in the sensory space, allowing us to predict the Kohonen map's learning performance. A GSI of 0.9989 when the robot has learnt to classify the cubes and cylinders. Sensory motor interactions indicates the presence of clusters in the data, which the Kohonen map has extracted. Indeed, the "circling" behavioral mode by inducing constraints in the input space, made cubes and cylinders discernible because data points belonging to one object were close to each other in the data space (correlation). The data points belonging to different objects are far apart.

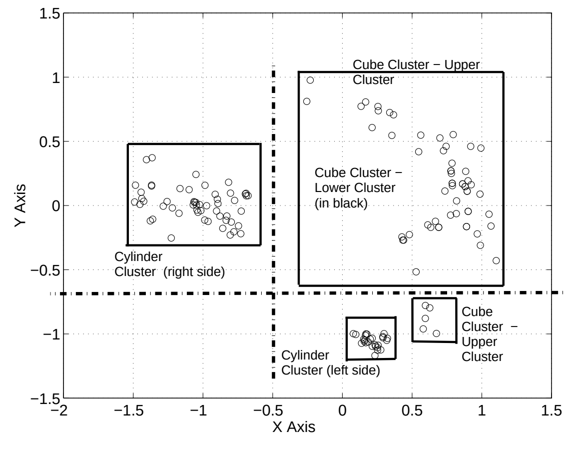

Figure 8: Dimensionality reduction of the 28-dimensional sensory input vector. Applied to N=576 vectors with K=7, Isomap learned a two-dimensional embedding of the data's informational structure.

Isometric feature mapping

To get a grasp on the high-dimensional space spanned by the sensory data, we used the Isomap algorithm. By applying Isomap to the 28-dimensional input space, we were able to compress it to a two-dimensional space. In Fig. 8, the clusters have been enclosed in boxes. The X axis shows positive correlation with a linear combination of the following factors: a) the difference between distance sensors d_2-d_9 or d_3-d_{10}: cubes are clustered by higher values of this difference and cylinders by the lower values; b) the difference of right and left motor m_R-m_L: the cubes are clustered according to higher values of this difference compared to the cylinders; and c) the sum of the image sensor values focused on the object being circled: cubes display a larger number of image sensor activations than cylinders.The total correlation considering all these factors was 0.931.

Activation of the sensor d_2 orients the robot toward objects (attraction); activation in d_9, on the other hand, makes the robot turn away from objects (repulsion). For cubes, due to their flat surfaces and sharp corners, attraction prevails on repulsion. This results in cubes being associated with larger values of the differences d_2-d_9, and d_3-d_{10}. In the case of cylinders, however, attraction prevails on repulsion, causing the cylinders to be associated with low values of the difference d_2-d_9 or d_3-d_{10}. Due to the sudden turns the robot has to make when circling cubes, the differencem_R-m_L is higher for cubes than for cylinders. When circling cubes, the robot is closer to it than for cylinders. The reason behind this is that in the case of cylinders, the robot starts circling the object, when one of its distance sensors d_4 or d_5 detects the object ahead. However, in the case of cubes, the distance sensors d_4 or d_5 do not detect the cube. Rather, it is detected by the center distance sensor d_6 which has a much shorter range. This causes the robot to be much closer to the encircled object in the case of cubes (larger number of image sensor activations) than in the case of cylinders (smaller number of image sensor activations).

6 Further discussion and conclusion

Does sensorimotor coordinated activity induce discernible regularities or structure in the sensorimotor space? As shown by the statistical and information-theoretic analyses of the recorded sensory and motor data, appropriate coordinated motor activity leads to a characteristic "fingerprint" of the sensorimotor interaction – that is, spatio-temporal patterns in the sensorimotor space reproducible across multiple experimental runs (for a similar result see also [7]). Such patterns can be identified, and exploited to simplify subsequent discrimination tasks.

It is important to note that the categorization for the robot is based on a 28-dimensional vector of sensorimotor values, where each of the sensors take 32 values (each sensor has a 5 bit resolution). Indeed, this results in a very large space of potential sensorimotor configurations (28^{32}). The circling behavior of the robot, allows the agent to generate constraints in its sensory input that lead to a drastic dimensionality reduction of the sensory space. This greatly reduces the search space of the robot. In other words, the circular behavior, akin to the object rotation behavior found in human infants [12], or exploration strategies observed in adults exploring objects with their hands [13], induces spatio-temporal correlations among the sensory patterns. These correlations are a further indication of the fact that the sensorimotor coupling leads to a reduction of the degrees of freedom in the input space [2].

The high values of correlation that we have observed in the "circling" behavioral state allow us to infer that while in this state, the agent generates redundancy in the sensory signals, which can picked up by the agent itself. In turn, such redundancy is a prerequisite for learning, and provides a basis for some sort of "self-cognition." That is, the agent can acquire a notion of its own emergent behavior.

We further note that while it is possible, at least in simple cases, to characterize exploration strategies by means of information theoretic and statistical measures, the proposed measures are by no means equivalent, but complement each other. For instance, in contrast to linear correlation, mutual information takes into account also nonlinear dependencies between various stochastic variables. The geometric separability index, on the other side, discerns sensory input based on how linearly separable it is, that is, based on where it falls respect to a hyperplane. Isomap, finally, tries to isolate nonlinear degrees of freedom in the data set. It would be of interest to understand if the agent could perform such "analyses" on its own. By characterizing its interactions with the environment, it would form the basis on which to build its own individual experiences, its memory. In future work, we also plan to study more complex agent-object interactions, and to experiment with more sophisticated robots.

Acknowledgements

Gabriel Gómez would like to thank the EU-Project ADAPT (IST-2001-37173) for funding. Max Lungarella would like to thank the University of Tokyo for funding and Yasuo Kuniyoshi for support and encouragement.

References

[1] R. Pfeifer and C. Scheier. Sensory-motor coordination: The metaphor and beyond. *Robotics and Autonomous Systems*, 20:157–178, 1997.

[2] C. Scheier, R. Pfeifer, and Y. Kuniyoshi. Embedded neural networks: Exploiting constraints. *Neural Networks*, 11:1551–1569., 1998.

[3] R. Pfeifer and C. Scheier. *Understanding Intelligence.* MIT Press, 1999.

[4] M. Lungarella, T. Pegors, D. Bulwinkle, and O. Sporns. Methods for quantifying the informational structure of sensory and motor data. *Neuroinformatics (submitted)*, 2004.

[5] M. Lungarella and R. Pfeifer. Robots as cognitive tools: information-theoretic analysis of sensory-motor data. In *Proc. of 2nd Int. IEEE/RSJ Conf. on Humanoid Robotics*, pages 245–252, 2001.

[6] O. Sporns. Generating structure in sensory data through coordinated motor activity. In *Proc. of Joint Conf. on Neural Network*, page 2796, 2003.

[7] D. Tarapore, M. Lungarella, and G. Gómez. Quantifying patterns of agent-environment interaction. *Robotics and Autonomous Systems (accepted for publication)*, 2005.

[8] R. Te Boekhorst, M. Lungarella, and R. Pfeifer. Dimensionality reduction through sensory-motor coordination. In *Proc. of the Joint Int. Conf. ICANN/ICONIP*, pages 496–503, 2003.

[9] T. Kohonen. *Self-organization and associative memory.* Springer, Berlin, 1988.

[10] C. Thornton. Separability is a learners best friend. In *Proc. 4th Neural Computation and Psychology Workshop: Connectionist representations*, pages 40–47, 1997.

[11] J. Tenenbaum, V. de Silva, and J. Langford. A global geometric framework for nonlinear dimensionality reduction. *Science*, 290:2319–2323, 2000.

[12] H. A. Ruff. Infants' manipulative exploration of objects: effects of age and object characteristics. *Developmental Psychology*, 20:9–20, 1984.

[13] S. J. Lederman and R. L. Klatzky. Haptic exploration and object representation. In M. Goodale, editor, *Vision and Action: The Control of Grasping*, pages 98–109. New Jersey: Ablex, 1990.

The Tenth International Symposium on Artificial Life and Robotics 2005(AROB 10th '05),
B-con Plaza, Beppu, Oita, Japan, February 4-6, 2005

On the Diversity of HIV using Cellular Automata Approach

Hiroshi UEDA[1] Yukio IWAYA[1] Toru ABE[2] Tetsuo KINOSHITA[2]

[1] Research Institute of Electrical Communication, Tohoku University
2-1-1 Katahira, Aoba-ku, Sendai, 980-8577 Japan
{uep, iwaya}@fir.riec.tohoku.ac.jp

[2] Information Synergy Center, Tohoku University
2-1-1 Katahira, Aoba-ku, Sendai, 980-8577 Japan
beto@isc.tohoku.ac.jp, kino@riec.tohoku.ac.jp

Abstract

Diversity of HIV (Human Immunodeficiency Virus) in vivo has been reported. In this study, we propose a CA (Cellular Automata) model about interaction between the immune system and HIV, and examine the effect of this diversity. Originality of our CA model is that it has not only four states (HIV, Virgin, Dead, Infect) but diversity of HIV and T-Cells. Growing maximum value of the diversity, we performed computer simulation with the CA model. The results demonstrated that growth of the diversity have an effect on cell population and simulations steps. Additionally, we observed CA state corresponds to infection, incubation period and development of AIDS. In on our CA model, it is demonstrate that the diversity of HIV is the major factor which HIV can escape the immune response.

Keywords: Cellular automata, HIV, Immune system

1 introduction

From the late in the 1980s, many active researches about infection of HIV (Human Immunodeficiency Virus) and development of AIDS (Acquired Immunodeficiency Syndrome) are current in progress. Medical works have been reported diversity of HIV which is due to its high mutation rate and variability in HIV-specific T cell epitope sequences [1, 2, 3], but its functionality to develop HIV infection against the immune response is not clear in vivo. Nowak and May have proposed a mathematical model considered with diversity of HIV strains[4]. According the model, there exists *antigenic diversity threshold* of HIV.

On the other hand, many scientists and engineers have proposed CA (cellular automata) model to investigate physical, chemical, life, traffic and economical processes. Advantage of CA model is that can simplify complicated interaction into local interaction.

Since it is considered to that the immune system responses based on local interaction between immune cells and antigens [5], many CA models about HIV infection has been proposed [6, 7, 8, 9, 10, 11, 12].

But until now, no work has focused on diversity of HIV with CA model. In this study, we proposed CA model considering diversity of HIV and investigated its behavior.

2 Model

We consider two-dimensional CA, the cells of which being arranged in a square lattice. Each cell has four states (*HIV, Virgin, Dead, Infect*) and *Type i* ($i = 0, 1, 2, \cdots, T_{max} - 1$) as follows:

HIV[i]: A state being HIV type *i* which is from outside the body, other lymphocyte or host cell. Although there exists only one HIV strain (*HIV[0]*) at the beginning of infection, it mutates into strain *HIV[1], HIV[2],* $\cdots$*, or* $HIV[T_{max} - 1]$ in each proliferate process.

Virgin[i]: Uninfected healthy host cell which can only response and eliminate against $Infect[i]$.

Dead: Nothing exists. After moving $HIV[i]$ or $Infect[i]$ was eliminated.

Infect[i]: A state corresponds to host cell ($Virgin[\ ]$) infected by $HIV[i]$.

$HIV[\ ]$, $Virgin[\ ]$ and $Infect[\ ]$ imply any type of HIV, host cell and infected cell respectively. T_{max} stands for antigenic diversity of HIV and the immune system in the CA model. In fact, this is the originality of our model.

Parameters of the model are maximum value of the diversity of HIV, T_{max} and small initial infection fracture $pHIV$. The initial CA configuration is composed of $Virgin[\ ]$ with $pHIV$ of $HIV[0]$. Type i and the placement chosen randomly.

In one time step the entire lattice is updated in a synchronized parallel way, according to the rules described below. The updated state of a cell is dependent on the states of its *Moore* neighbors in a square lattice.

We determine this process will continue until all the $HIV[\ ]$ and $Infect[\ ]$ or $Virgin[\ ]$ is eliminated.

Rule 1 *Moving of HIV:* If $HIV[\ ]$ has at least one $Virgin[\ ]$ or *Dead* neighbor, it becomes *Dead* with probability (the number sum of $Virgin[\ ]$ and *Dead*)/8. This rule represents that HIV moves to the cite nothing exists or infects to another virgin host cell.

Rule 2 *Being infected of virgin host cell with HIV:* If $Virgin[\ ]$ has at least one $HIV[i]$, it becomes $Infect[i]$ with probability (the number of $HIV[i]$)/8. This rule represents that virgin host cell is infected with HIV.

Rule 3 *Mutation and emergence of HIV:* **(a)** If *Dead* has at least one $Infect[\ ]$, it becomes $HIV[\ ]$ since HIV mutates before emergence, with probability (the number of $Infect[\ ]$)/8 . This rule represents that HIV emerges from infected host cell. **(b)** If *Dead* has at least one $HIV[i]$, it becomes $HIV[i]$ with probability (the number of $HIV[i]$)/8. This rule represents that moving of HIV from another cite.

Rule 4 *Update of infected cell:* **(a)** If $Infect[\ ]$ has at least one $Virgin[i]$, it becomes $Virgin[i]$ with probability (the number of $Virgin[i]$)/8. This rule represents that infected cell is eliminated by type i activated virgin host cell. **(b)** Otherwise it becomes $HIV[i]$ since HIV eliminate infected cell.

We performed computer simulations of the model, using periodic boundary condition, on a 100   100 lattice, $pHIV = 0.05$ with T_{max} from 1 to 35. For each T_{max}, we performed 1000 times trial runs.

3 Results and Discussion

Fig. 1 and 2 show the relation between average number of cells and *antigenic diversity* of HIV, T_{max}. $HIV[\ ]$,$Empty$ increased with T_{max}. In addition, decrease of $Virgin[\ ]$ was also observed. Mutation of HIV in vivo has

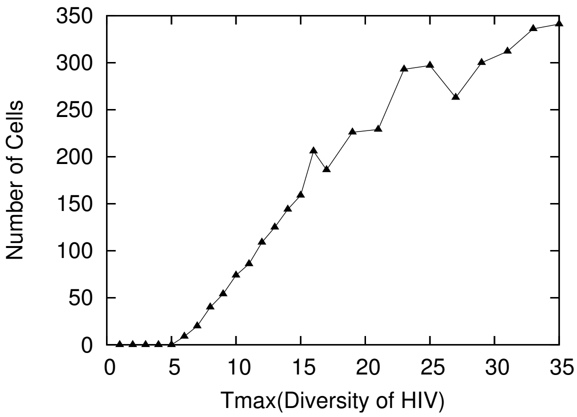

Figure 1: Average number of $HIV[\ ]$ cells versus T_{max}.

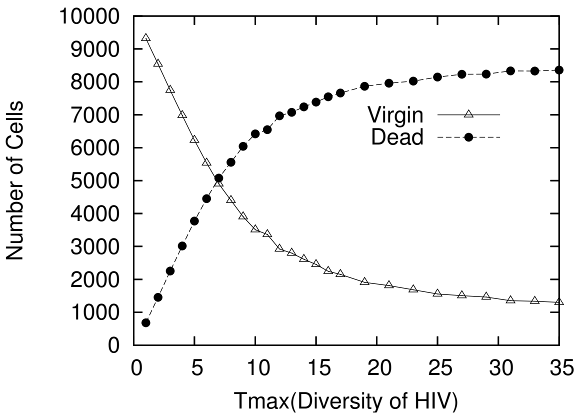

Figure 2: Average number of $Virgin[\ ]$ and $Empty$ cells versus T_{max}.

been reported. From these results, it seem to suggest that *antigenic diversity* of HIV has great effect on the model.

Fig. 3 shows the relation between average simulation steps and T_{max}. The simulation steps increased with T_{max}. Long time incubation period of HIV has been known. This result corresponds to HIV infect phenomenon in vivo.

Main points are described below:

First, since the decrease of $Virgin[\ ]$ depend on HIV infection in the model, the situation that immune system cannot response was assumed to be due to increase of *antigenic diversity* of HIV (Fig. 1, 2). In detail, if no responsible immune cells exist on its *Moore* neighbors, HIV can escape the immune response in the CA model.

Second, Fig. 3 points out that long time steps were needed to stop simulation in the situation high *antigenic diversity* of HIV.

Fig. 1-3 indicate only average value of 1000 times runs.

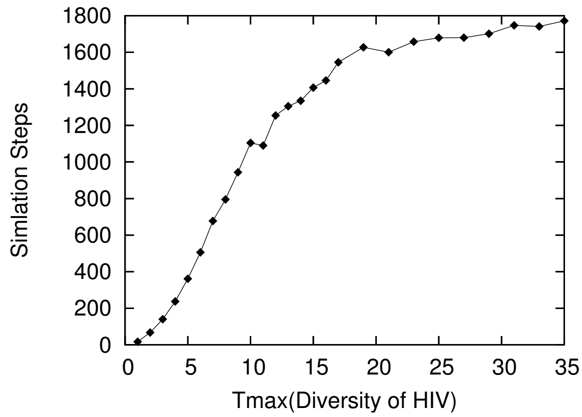

Figure 3: Average simulation steps versus T_{max}.

Since the CA model is not deterministic, the simulation result of one trial run (namely whether HIV is control or not) is not depend on parameters. Fig. 4-6 show the time-evolution of CA state. In early stage (Fig. 4), a volume of $Infect[\ ]$ was observed. This state seem to correspond to initial infection. In contrast, only a few $Infect[\ ]$ cells was observed in fig. 5. This state seem to correspond to incubation period in which being controlled of $HIV[\ ]$. Moreover, since CA is filled with *Dead* in fig. 6, this state seem to correspond to *break down* of the immune system, that is AIDS.

4 Conclusion

In this study, we modeled the interaction between HIV and the immune system with CA approach to examine the effect of antigenic diversity of HIV. We make a point that CA approach which is based on local interaction is very useful to investigate the interaction between HIV and the immune system.

Our CA model contrasts with deterministic model because simulation result of each trial runs is different at same parameters. Since all the HIV carrier don’t have an onset of AIDS; variety of time in incubation period has reported, this property of CA model is correspond with phenomenon in vivo.

Originality of out CA model is that takes into consideration of antigenic diversity of HIV. We have taken *antigenic diversity* of HIV as parameter. Simulation results suggest that increase of *antigenic diversity* of HIV has great impact on the immune system.

By taking account for *antigenic diversity* in CA model, we make a point that HIV which has diversity can escape from local immune response and proliferate.

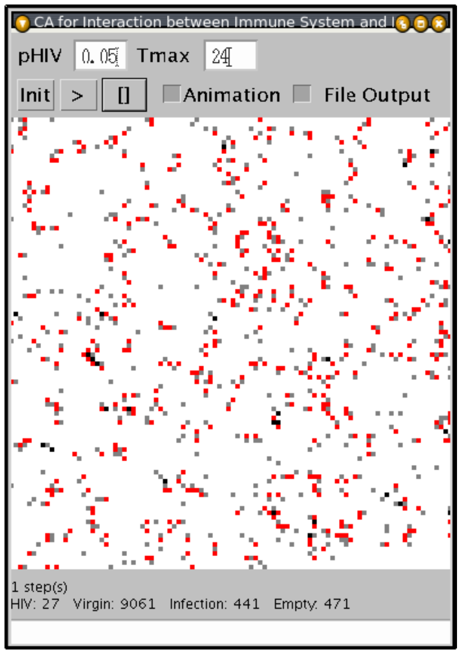

Figure 4: Snapshot of CA state at step 1. Red: $Infect[\ ]$, Black: HIV, White: $Virgin[\ ]$, Gray: $Dead$. Parameters are: $T_{max} = 24, pHIV = 0.05$

These results depend on that interaction between HIV and the immune system is sum of local interactions. We are currently performing studies to determine CA model to compute Moore neighbor. Therefore, it is interesting to change condition of neighbor.

Further studies to analyze development of *antigenic diversity* of HIV and pattern which is formulated by CA are required.

In summary, the present work shows that the the CA model taking account for *antigenic diversity* of HIV can examine interaction between HIV and the immune system successfully.

Acknowledgments

A part of this research was supported by Research Grant of Kiban (B): No.6300011 from Ministry of Education, Science and Culture, Japan.

References

[1] A. S. De Groot *et al.*, “Engineering immunogenic consensus T helper epitopes for a cross-clade HIV vaccine,” *Methods*, vol. 34, no. 4, pp. 476–487, 2004.

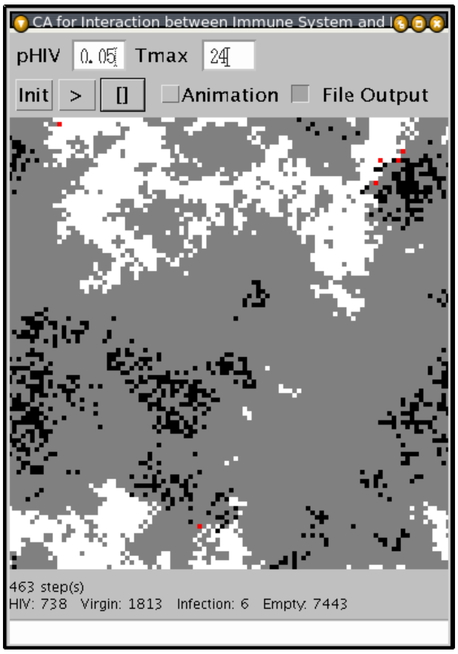

Figure 5: Snapshot of CA state at step 463. Parameters are same to Fig. 4

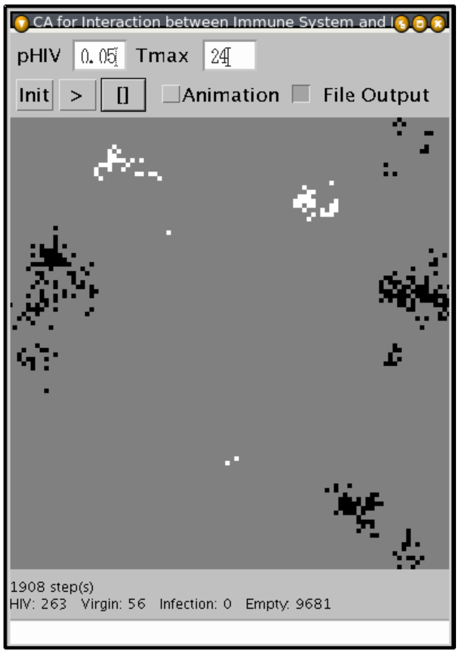

Figure 6: Snapshot of CA state at step 1908. Parameters are same to Fig. 4

[2] D. Turner *et al.*, "Variability in the PR and RT genes of HIV-1 isolated from recently infected subjects," *Antiviral Chemistry & Chemotherapy*, vol. 15, pp. 255–259, September 2004.

[3] P. J. R. Goulder *et al.*, "Evolution and transmission of stable CTL escape mutations in HIV infection," *Nature*, vol. 412, pp. 334–338, July 2001.

[4] M. A. Nowak *et al.*, "Antigenic diversity thresholds and the development of AIDS," *Science*, vol. 254, pp. 963–969, Novemver 1991.

[5] N. K. Jerne, "The immune system," *Scientific American*, vol. 229, no. 1, pp. 52–60, 1973.

[6] R. B. Pandey and D. Stauffer, "Immune response via interacting three dimensional network of cellular automata," *Le Journal de Physique*, vol. 50, pp. 1–10, January 1989.

[7] R. B. Pandey, "Cellular automata approach to interacting cellular network models for the dynamics of cell population in an early HIV infection," *Physica A*, vol. 179, no. 3, pp. 442–470, 1991.

[8] R. M. Z. dos Santos and S. Coutinho, "Dynamics of HIV infection: A cellular automata approach," *Physical Review Letters*, vol. 87, no. 16, pp. 168102–1–168102–4, 2001.

[9] F. Kougias and J. Schulte, "Simulating the immune response to the HIV–1 virus with cellular automata," *Journal of Statistical Physics*, vol. 60, no. 1/2, pp. 263–273, 1990.

[10] P. Sloot, F. Chen, and C. Boucher, "Cellular automata model of drug therapy for HIV infection," in *ACRI* (S. Bandini, B. Chopard, and M. Tomassini, eds.), vol. 2493 of *Lecture Notes in Computer Science*, pp. 282–293, Springer, 2002.

[11] R. B. Pandey and D. Stauffer, "Metastability with probabilistic cellular automata in an HIV infection," *Journal of Statistical Physics*, vol. 61, no. 1/2, pp. 235–240, 1990.

[12] T. Tomé and J. R. D. de Felício, "Probabilistic cellular automaton describing a biological immune system," *Physical Review E*, vol. 53, no. 4, pp. 3976–3981, 1995.

The Tenth International Symposium on Artificial Life and Robotics 2005(AROB 10th '05),
B-con Plaza, Beppu, Oita, Japan, February 4-6, 2005

Construction and strategy of a soccer team by the agent using immune concept

Nagahisa Kogawa †

Masanao Obayashi ‡

Kunikazu Kobayashi ‡

Takashi Kuremoto ‡

†Graduate School of Science and Engineering
Yamaguchi University
2-16-1 Tokiwadai Ube , Yamaguchi
755-8611 Japan

‡Faculty of Engineering
Yamaguchi University
2-16-1 Tokiwadai Ube , Yamaguchi
755-8611 Japan

Abstract

In recent years, the immune system of a living body attracts attention as a new biological information processing based paradigm. In this paper, the concept of the immune system is adapted to the soccer problem which is the standard one of multi-agent system. And new soccer agent is proposed. In the proposed method, appropriate antibodies (agent's actions) corresponding to various antigens (game's environment) are produced and learned. It is verified that agents select optimal and cooperative actions in a dynamic environment using The RoboCup Soccer Simulator.

1 Introduction

Multi-agent system attracts attention as the important research technique of complex system. The reason is it becomes the key to analyzing complex system. Which appears unexpected aspect as the whole system as a result of interaction between agents who become composite element.

Many soccer agents on The RoboCup soccer simulator have been proposed. On construction of effective agent group, performance of the whole system can be clearly evaluated based on an explicit criterion, such as the number of goals. However it is difficult to determine when and how and in what situation agent takes action for team from evaluation point of view and also from selection point of view. It is expected that various knowledge acquired in construction of effective agent group is applicable to general multi-agent system [1]. Murata et al. proposed a method of dynamically arranging soccer agent using genetic Algorithms [2]. Irie et al. presented the way that action value function of various local goal was designed [3]. Kumada et al. showed a soccer agent with ability to predict other agents [4].

The biological information processing mechanism is roughly divided into four parts; a brain nerve system, a genetic system, an internal secretion system, and an immune system. From the engineering point of view, the brain nerve system is modeled as neural networks, the genetic system is also modeled as genetic algorithms and they have been used in many fields. On the other hand, although both the internal secretion system and the immune system have an advanced information processing mechanism, there are few examples applied in engineering.

The immune system came to be especially known well with the latest development of medicine and physiological research. It has an important function how to retain self in dynamic environments except for the simple function eliminating the invaded thing from the external world. An advanced immune processing mechanism is realized. Because each cell takes communication mutually in biological field.

In this paper, we focus on the immune system described above. Immune system of a living body is large-scale system equipped with complicated defense function. This system has function of memory and learning using interaction between cells, such as stimulus and suppression. And this system has the robustness by diversity and the adaptation capability by variation and selection in the immune system. Ishiguro et al. proposed a method of arbitrating between mobile robots using immune network [5].

In the present research, we focus on features of immune system; adaptation capability by variation and selection and robustness by diversity. Concept of immune system is applied to soccer problem. Then soccer agent group using immune concept is proposed. It is verified that appropriate strategies are acquired through simulation using The RoboCup soccer simulator.

2 Immune type system

Immune type system has features that processing information of immunity. It has the similar adaptation and learning capability to artificial neural network which consists of unit corresponding to immune cell. Unique feature of immune type system is summarized in the following [6].

2.1 Dynamic network

B cells in a living body are seen as a network through antibody. There is hypothesis that B cells build Idiotypic network through antibody. The Idiotypic network has three features; mutual recognition, existence of internal image and relation among immune memory. The network is recognized as a dynamic system of suppression and stimulus between cells. And equilibrium point may move or may add or may delete as a nonlinear dynamic system.

The network of structure of immune system can be flexibly changed as compared with neural network. Namely immune system is a distributed cooperative system with mutual reference.

2.2 Adaptation system by variation and selection

Immune system has mechanism which prepares various antibodies to a strange antigen. However it is impossible to prepare antibody which fit strictly to any antigens in advance. Then in process of immune response, mechanism which adaptively enhances affinity between the antigen and an antibody is prepared by variation of a part of gene corresponding antibodies.

2.3 Robust system by versatility

Coping with unexpected situations, the policy mainly taken by traditional engineering prepares reserves. That is based on redundancy and this realized robustness and fault tolerance. However Antibodies can be almost freely copy. And the reproduced antibodies are slightly different each other. Therefore strategy corresponding to strange element is possible by the above versatility.

3 Proposed system

It is proposed that concept of immune system is applied to soccer problem. First, environmental information which each agent obtains is defined as antigen. Next, soccer team is regarded as one living body. Then action against antigen is determined using a group of antibodies which the team holds. Each agent chooses antibody corresponding to the obtained antigen and determines action.

The proposed system has mechanism which prepares various antibodies to a strange antigen. In soccer problem, it is difficult to set up suitable action to environment in advance. Hence the group of antibodies is changed to select suitable action to environmental information through learning.

3.1 Problem setting

In the present paper, soccer problem is treated. A team is constituted of ten players except for a goalkeeper. Strategy that acquired by the proposed system is analyzed through many games.

3.2 Definition of antibody

Antibody consists of three parts as shown in Figure 1; field position (FP), attribute and action part. Moreover environmental part of antibody is the same structure as antigen which is environmental information.

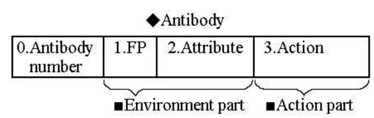

Figure 1: Structure of antibody

3.2.1 Field position (FP)

The size of soccer field is ($64 + \alpha$) $\times$ ($105 + \alpha$), where is α is a margin. Soccer field is divided into a total of 40 areas of height 5 and width 8. The definition of FP is shown in Figure 2.

3.2.2 Attribute

Attribute expresses environment around each agent. It consists of position of a ball and an own team's agents and opponents and is used for classification of agent's environment. Perceptive area is shown in Figure 3.

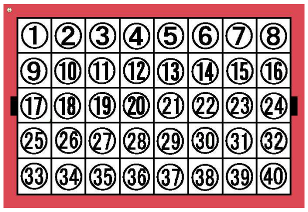

Figure 2: Definition of field position

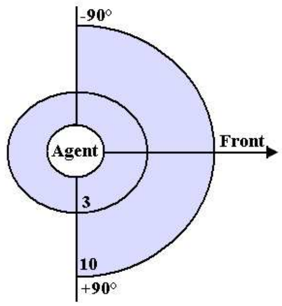

Figure 3: Perceptive area of agent

3.2.3 Action

Action part consists of basic action, an action parameter, and selective value, and basic action is four kinds, kick, path, dribble, and movement. The action parameter is used to decide direction or to choose an own team's agent to pass a ball. Selective value is value which determines probability that antibody will be chosen. The basic action presents a series of actions. For example in case of kick a series of action means agent approaching a ball until it is kicked.

3.2.4 Selection of antibody

In the proposed system, each agent chooses four antibodies which have different basic actions corresponding to antigen from group of antibodies after each agent obtains antigen. Next, antibodies are reproduced in the proportion of there selective values. At this time, small variation is given to action parameter of the original antibody to reproduce difference with antibody. In this way, adaptation capability by variation and selection is given. One antibody is chosen from group of antibodies and action is determined.

3.3 Learning method

As the learning method of the proposed system, the two methods are used when the team gets a goal and agents choose basic actions and practice them.

The learning method when basic action is chosen and practiced is performed if agent's action is successful. Action parameter of selected antibody is approached to that of the reproduced antibody. And this selective value is increased. For example in case of kick judgment of action is decided by whether ball is kicked or not.

In present research, it is noted that a FP is highly important from strategic point of view. So the learning when the team gets a goal is performed by Profit Sharing for every FP.

Furthermore when one antibody is learned, it is rational to perform for antibodies similar to the antibodies. Then learning is performed for FP around FP of selected antibody for the sake of learning convergence.

The equations for learning are described as

$$p_n = p_o + \frac{p_c - p_o}{1.0 + \sqrt{v_o}} \tag{1}$$

$$v_n = v_o + r_b \tag{2}$$

$$v_n = v_o + r_p(t) \qquad (t = 0, \ldots, T-1) \tag{3}$$

where p_o is a action parameter, p_c is an action parameter of reproduced antibody, v_o is a selective value, r_b is a reward for basic actions, $r_p(t)$ is a reward for Profit Sharing, T is the length of history of PS every FP. and v_n, p_n is renewed value.

4 Computer simulation

Each team is constituted using the proposed system. All the soccer games are played on The RoboCup soccer simulator. In one experiment, 50 games of usual The RoboCup soccer are conducted.

For basic action the reward of learning is set to the following values. The reward for kick, dribble, pass and movement is set to 0.1, 0.2, 0.3, and 0.01, respectively. When the team gets a goal, the maximum reward of learning by PS is set to 1.0.

Figure 4 shows the probability to select basic action in case of existence of a ball, two or more friends and opponents in the perceptive area for FP23. As shown in Figure 4, the optimal selection near the goal for kick is realized. Figure 5 illustrates the probability to select basic action in case of existence of a ball, no friend and opponent in the perceptive area for FP24. As shown in Figure 5, the wrong selection near the goal for movement is appeared.

The number of selected antibodies is shown in Table 1. In this table normal means the number of selected antibodies not including 8 neighbors (8 adjacent FPs) for learning. Then the second row is the number of selected antibodies including 8 neighbors for learning of basic action and third row is furthermore considering PS. After learning the agents in the adjacent FPs tend to select the similar actions to the agent in a FP. In addition there is no remarkable difference in the results whether including 8 neighbors or not.

Selective value of antibodies seldom chosen during games did not be enhanced. Moreover the phenomena that agents are gathering to a ball are seen. This is regarded as one of the reason that capability to search for state is reduced.

The experiment shows optimal actions are partially selected. A cooperative action was not able to be produced as a team. Therefore, improvement is required.

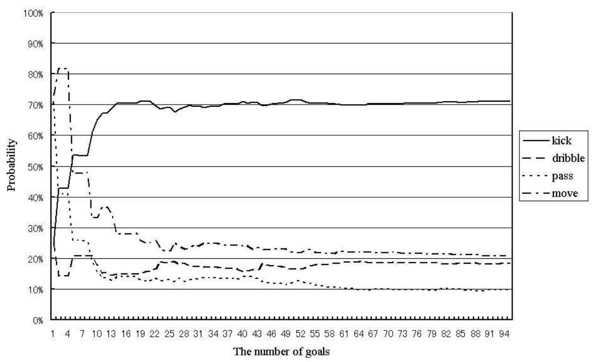

Figure 4: Transition of probability to select basic action when a ball exists and two friends and opponents exists in FP23

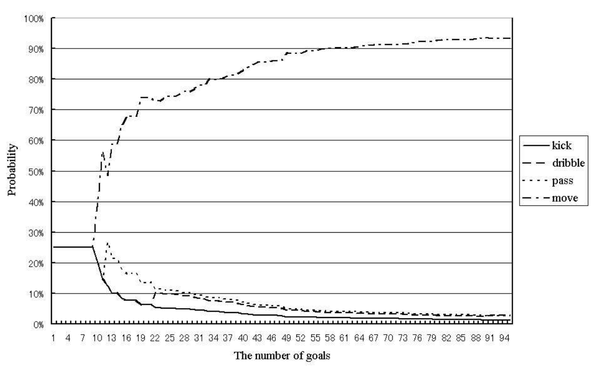

Figure 5: Transition of probability to select basic action when a ball exists and no friend and opponents in FP24

Table 1: The numbers of selected antibodies

Probability to select	more than 80 %	more than 70 %	more than 60 %
normal	3	25	92
including 8 neighbors (only for basic action)	1	20	82
including 8 neighbors (for basic action and PS)	0	0	2

5 Conclusion

In the present research, soccer team by agent using immune concept was proposed. Computer simulation was conducted on The RoboCup soccer simulator, and it is verified that appropriate strategy acquired.

Future problem is to improve learning ability incorporating stimulus and suppression.

References

[1] A. Ohuchi, M. Yamamoto, H. Kawamura, *Theory and Application of Multi-agent Systems -Computing Paradigm from Complex Systems Engineering-*, Corona Publishing, 2002 (in Japanese)

[2] T. Murata, K. Suzuki, A. Ohuchi, "Dynamic Position Arrangements of Soccer agents with Genetic Algorithms", *Journal of the Japanese Society for Artificial Intelligence*, Vol. 14 No.3, pp. 446-454, 1999 (in Japanese)

[3] T. Irie, N. Inui, Y. Kotani, "Design of an Action Value Function of various Local Goal in RoboCup Soccer", *Research of Information Processing Society of Japan Game Informatics*, Vol.4 No.8, pp. 47-54, 2000 (in Japanese)

[4] Y. Kumada, K. Ueda, "Acquisition of Cooperative Tactics by Soccer Agents with Ability of Prediction and Learning", *Journal of the Japanese Society for Artificial Intelligence*, Vol.16 No.1, pp. 120-127, 2001 (in Japanese)

[5] A. Ishiguro, T. Kondo, Y. Watanabe, Y. Shirai, Y. Uchikawa, "An Evolutionary Construction of Immune Network-Based Behavior Arbitration Mechanism Mobile Robot", *IEEJ Transactions on Electronics, Information and Systems*, Vol.117-C No.7, pp.865-873, 1997 (in Japanese)

[6] Y. Ishida etc., *Immunity-Based Systems and Its Applications -Intelligent Systems by Artificial Immune Systems -*, Corona Publishing, 1998 (in Japanese)

[7] A. Ohuchi etc., *Paradigm of Calculation from life complex system*, Morikita Publisher, 2003 (in Japanese)

The Tenth International Symposium on Artificial Life and Robotics 2005(AROB 10th '05),
B-con Plaza, Beppu, Oita, Japan, February 4-6, 2005

An Investigation into State-Change Complexities in Synchronization Algorithms for Cellular Automata

Kouhei Matsumoto
Univ. of Osaka Electro-Communication
Neyagawa-shi, Hatsu-cho 18-8
Osaka, 572-8530, Japan

Hiroshi Umeo
Univ. of Osaka Electro-Communication
Neyagawa-shi, Hatsu-cho 18-8
Osaka, 572-8530, Japan

Abstract

This paper presents a comparative study of state-change complexity in optimum- and linear-time synchronization algorithms for a large-scale of cellular automata on one- and two-dimensional arrays. We implement most of the synchronization protocols developed so far and investigate their state-change complexities on a computer.

1 Introduction

In recent years cellular automata (CA) have been establishing increasing interests in the study of modeling real phenomena occurring in biology, chemistry, ecology, economy, geology, mechanical engineering, medicine, physics, sociology, public traffic, etc. Cellular automata are considered to be a nice model of complex systems in which an infinite one-dimensional array of finite state machines (cells) updates itself in synchronous manner according to a uniform local rule.

The synchronization in cellular automata has been known as firing squad synchronization problem since its development, in which it was originally proposed by J. Myhill to synchronize all parts of self-reproducing cellular automata [9]. The firing squad synchronization problem has been studied extensively for more than 40 years [1-18].

The complexity of synchronization algorithms has received much attention, and those synchronization algorithms have been studied from viewpoints of time complexity, number of internal states of the automata, and number of transition rules. Vollmar [15, 16] introduced a concept of state-change complexity as a measure of energy consumption in the cellular spaces and showed that any optimum-time synchronization algorithms operating on one-dimensional array need $\Omega(n \log n)$ state-changes for synchronizing n-cells.

In this paper, we give a comparative study of state-change complexity in the synchronization algorithms developed so far. The synchronization algorithms being compared in this paper are seven optimum- and linear-time algorithms developed by Balzer [1], Fischer [2], Gerken [3], Mazoyer [8], Minsky [9], Waksman [17] and Yunés [18] . The state-change complexity in several synchronization algorithms on two-dimensional arrays are also studied in the last section.

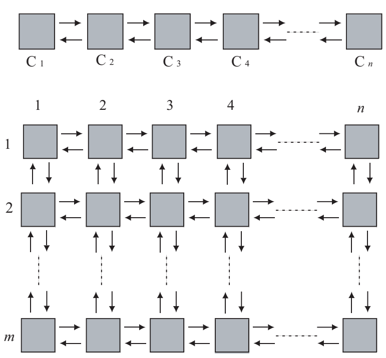

Figure 1: Cellular automata.

2 Firing squad synchronization problem on one-dimensional cellular automaton

In this section we give informal definitions of cellular automata, firing squad synchronization problem and a measure of state-change complexity for synchronization algorithms on one-dimensional cellular automata.

2.1 One-dimensional cellular automaton

Figure 1 (above) shows a finite one-dimensional cellular array consisting of n cells, denoted by C_i, where $1 \le i \le n$. Each cell is an identical (except the border cells) finite-state automaton. The array operates in lock-step mode in such away that the next state of each cell (except border cells) is determined by both its own present state and the present states of its left and right neighbors. All cells, except the left end cell, are initially in a *quiescent* state at time $t = 0$. The quiescent state has a property that the next state of a quiescent cell with quiescent neighbors is the quiescent state again.

2.2 Firing Squad Synchronization Problem

The firing squad synchronization problem is formalized in terms of the model of cellular automata. All cells (*soldiers*), except the left end cell, are initially in the *quiescent* state at time $t = 0$. At time $t = 0$ the left end cell (*general*) is in the *fire-when-ready* state, which is an initiation signal to the array. The firing squad synchronization problem is stated as follows. Given an array of n *identical* cellular automata, including a *general* on the left end which is activated at time $t = 0$, we want to give the description (*state set* and *next-state function*) of the automata so that, *at some future time*, all of the cells will *simultaneously* and, *for the first time*, enter a special *firing* state. The set of states and the next-state function must be independent of n. Without loss of generality, we assume that $n \geq 2$. The tricky part of the problem is that the same kind of soldier having a fixed number of states must be synchronized, regardless of the length n of the array.

2.3 State-change complexity in one-dimensional synchronization algorithms

Vollmar [15, 16] introduced a state-change complexity in order to measure the efficiency of cellular algorithms and showed that $\Omega(n \log n)$ state changes are required for the synchronization of n cells in $(2n-2)$ steps.

[Theorem 1][16] $\Omega(n \log n)$ state-change is necessary for synchronizing n cells in $(2n-2)$ steps.

3 State-change complexity in one-dimensional synchronization algorithms

3.1 Optimum-time synchronization algorithms

Waksman [17] presented a 16-state optimum-time synchronization algorithm. Afterward, Balzer [1] and Gerken [3] developed an eight-state algorithm and a seven-state synchronization algorithm: Gerken I, respectively, thus decreasing the number of states required for the synchronization. In 1987, Mazoyer [8] developed a six-state synchronization algorithm which, at present, is the algorithm having the fewest states. The state change complexity for those algorithms is investigated on a computer, and the next theorem is established.

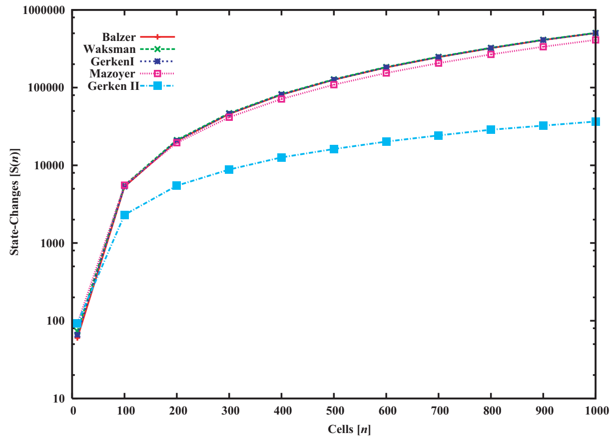

Figure 2: State-changes in optimum-time synchronization algorithms.

[Theorem 2] Each optimum-time synchronization algorithm developed by Balzer [1], Gerken [3], Mazoyer [8] and Waksman [17] has an $O(n^2)$ state-change complexity, respectively.

Figure 2 shows a comparison between state-changes of the optimum-time synchronization algorithms. Gerken [3] has shown that his 155-state algorithm has $\Theta(n \log n)$ state-change complexity.

3.2 Linear-time synchronization algorithms

The firing squad synchronization problem was first solved by J. McCarthy and M. Minsky [9] who presented a $3n$-step algorithm. Fischer [2] gave a 15-state implementation for the $3n$-step synchronization scheme. Both of the algorithms were based on the divide-and-conquer scheme that were realized with 1/1- and 1/3-speed signals interacting each other. These signals look like threads in the time-space diagram and the $3n$-step synchronization algorithm based on the scheme is said to be *thread-like* algorithm. Yunés [18] presented a seven-state implementation based on the thread-like algorithm. In his construction, the width of the threads is larger than the pre-

The Tenth International Symposium on Artificial Life and Robotics 2005(AROB 10th '05),
B-con Plaza, Beppu, Oita, Japan, February 4-6, 2005

vious design. We can get the state change complexity for the $3n$-step thread-like synchronization algorithms with finite-width threads.

[Theorem 3] Any $3n$-step finite-width thread-like synchronization algorithm has an $\mathrm{O}(n \log n)$ state-change complexity.

[Theorem 4] Each linear-time $3n$-step synchronization algorithm developed by Fischer [2], Minsky and MacCarthy [9], and Yunés [18] has an $\Omega(n \log n)$ state-change complexity, respectively.

Figure 3 shows a comparison between state-changes of the $3n$-step synchronization algorithms with finite-width threads.

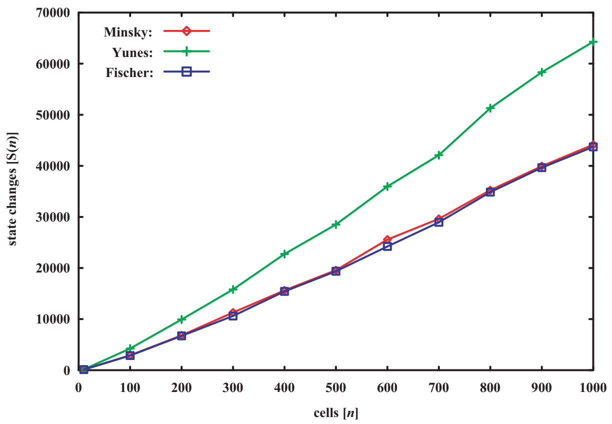

Figure 3: State-changes in $3n$-step synchronization algorithms.

4 State-change complexity in two-dimensional synchronization algorithms

Figure 1 (below) shows a finite two-dimensional (2-D) cellular array consisting of $m \times n$ cells. Each cell is an identical (except the border cells) finite-state automaton. The array operates in lock-step mode in such a way that the next state of each cell (except border cells) is determined by both its own present state and the present states of its north, south, east and west neighbors. All cells (*soldiers*), except the north-west corner cell (*general*), are initially in the quiescent state at time $t = 0$ with the property that the next state of a quiescent cell with quiescent neighbors is the quiescent state again. At time $t = 0$, the north-west corner cell $\mathrm{C}_{1,1}$ is in the *fire-when-ready* state, which is the initiation signal for synchronizing the array. The firing squad synchronization problem is to determine a description (state set and next-state function) for cells that ensures all cells enter the *fire* state at exactly the same time and for the first time. The set of states must be independent of m and n. Maeda and Umeo [5] developed a simple and efficient mapping scheme that enables us to embed any one-dimensional firing squad synchronization algorithm onto two-dimensional arrays without introducing additional states. We see that any configuration on a 1-D CA consisting of $m + n - 1$ cells can be mapped onto 2-D $m \times n$ arrays. Therefore, when the embedded 1-D CA fires $m+n-1$ cells in $T(m+n-1)$ steps, the corresponding 2-D CA fires the $m \times n$ array in $T(m+n-1)$ steps. We can design state-efficient synchronization algorithms based on the mapping. Those algorithms are stated as follows:

[Theorem 5][5,14] There exists a 6-state firing squad synchronization algorithm that can synchronize any $m \times n$ rectangular array in $2(m + n) - 4$ steps.

[Theorem 6][4,5,14] There exists a 13-state firing squad synchronization algorithm that can synchronize any $m \times n$ rectangular array in optimum $m + n + \max(m, n) - 3$ steps.

In Fig. 4 (left), we show snapshots of the 13-state optimum-time generalized firing squad synchronization algorithm. Shaded squares in Fig. 4 (right) mean cells that change their states in the computation. Figure 5 shows a comparison of the state-change complexity of the algorithm in the case where the initial general is located on C_1,$\mathrm{C}_{n/4}$ and $\mathrm{C}_{n/2}$. Figure 6 illustrates the state-change complexities between those two linear- and optimum-time algorithms for rectangular arrays.

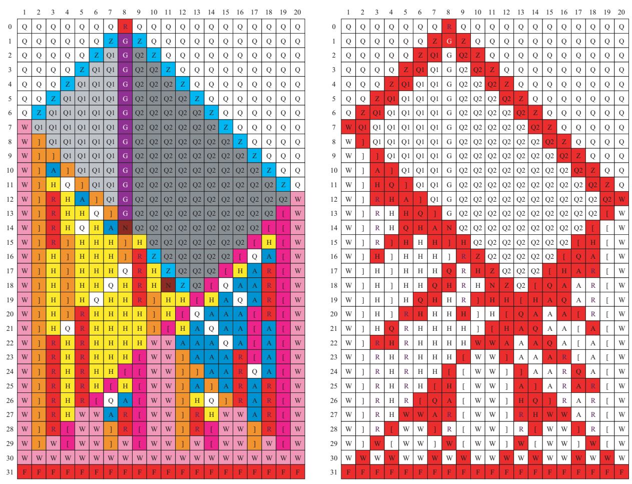

Figure 4: Snapshots of the generalized 13-states synchronization algorithm.

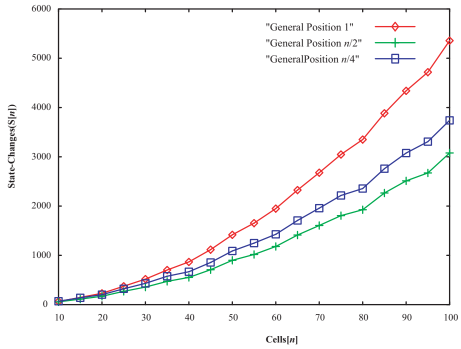

Figure 5: Comparison of state-changes in the generalized 13-states synchronization algorithm.

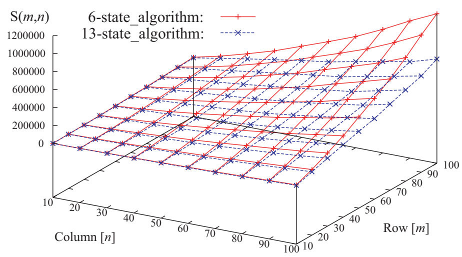

Figure 6: State-changes in the two-dimensional synchronization algorithms.

5 Conclusions

We have implemented most of the synchronization algorithms developed so far and investigated their state-change complexities on a computer. A comparative study of the state-change complexity in optimum- and linear-time synchronization algorithms on one- and two-dimensional cellular arrays has been presented.

References

[1] R. Balzer: An 8-state minimal time solution to the firing squad synchronization problem. *Information and Control*, vol. 10 (1967), pp. 22-42.

[2] P. C. Fischer: Generation of primes by a one-dimensional real-time iterative array. *J. of ACM*, vol. 12, No. 3 (1965), pp. 388-394.

[3] Hans-D., Gerken: Über Synchronisations-Probleme bei Zellularautomaten. Diplomarbeit (1987), Institut fur Theoretische Informatik, Technische Universitat Braunschweig, pp. 50.

[4] M. Hisaoka, M. Maeda and H. Umeo: An implementation of two-dimensional optimum-time firing squad synchronization algorithms. *Proc. of Annual Conference IEICE*, D-1-9(in Japanese), (2004).

[5] M. Maeda and H. Umeo: A design of two-dimensional firing squad synchronization algorithms and its implementation. *Proc. of Cellular Automata 2001*, pp.102-107(in Japanese), (2001).

[6] K. Matsumoto, T. Sogabe and H. Umeo: State-change complexity for firing squad synchronization algorithms on one-dimensional cellular automata. *Proc. of IEEJ*, 3-099, pp.143-144(in Japanese), (2004).

[7] K. Matsumoto and Hiroshi Umeo: A State-Change Complexity in Synchronization Algorithms for Cellular Automata. *SICE Annual Conference 2004 in Sapporo (SICE2004)*, P-57, (2004).

[8] J. Mazoyer: A six-state minimal time solution to the firing squad synchronization problem. *Theoretical Computer Science*, vol. 50 (1987), pp. 183-238.

[9] M. Minsky: *Computation: Finite and infinite machines.* Prentice Hall, (1967), pp. 28-29.

[10] E. F. Moore: The firing squad synchronization problem. in *Sequential Machines, Selected Papers* (E. F. Moore, ed.), Addison-Wesley, Reading MA.,(1964), pp. 213-214.

[11] P. Sanders, R. Vollmar and T. Worsch: Cellular automata: Energy consumption and physical feasibility. *Fundamenta Informaticae*, 52(2002) 233-248.

[12] H. Umeo, T. Sogabe and Y. Nomura: Correction, optimization and verification of transition rule set for Waksman's firing squad synchronization algorithm. *Proc. of the Fourth Intern. Conference on Cellular Automata for Research and Industry*, Springer, pp. 152-160(2000).

[13] H. Umeo, M. Hisaoka and T. Sogabe: A comparative study ofoptimum-time synchronization algorithms for one-dimensional cellular automata -A survey-. *Proc. of the 6th International Conference on Cellular Automata for Research and Industry*, LNCS 3305, Springer-Verlag, pp.50-60(2004).

[14] H. Umeo, M. Maeda and N. Fujiwara: An efficient mapping scheme for embedding any one-dimensional firing squad synchronization algorithm onto two-dimensional arrays. *Proc. of the 5th International Conference on Cellular Automata for Research and Industry*, LNCS 2493, Springer-Verlag, pp.69-81(2002).

[15] R. Vollmar: On Cellular Automata with a Finite Number of State Change. *Computing, Supplementum*, vol. 3(1981), pp. 181-191.

[16] R. Vollmar: Some Remarks about the "Efficiency" of Polyautomata. *International Journal of Theoretical Physics*, vol. 21, No. 12(1982), pp. 1007-1015.

[17] A. Waksman: An optimum solution to the firing squad synchronization problem. *Information and Control*, vol. 9 (1966), pp. 66-78.

[18] J. B. Yunés: Seven-state solution to the firing squad synchronization problem. *Theoretical Computer Science*, 127 (1994), pp.313-332.

The Tenth International Symposium on Artificial Life and Robotics 2005(AROB 10th '05),
B-con Plaza, Beppu, Oita, Japan, February 4-6, 2005

A State-Efficient Implementation of Synchronization Algorithms for Two-Dimensional Cellular Automata -Extended Abstract-

Masato Teraoka†, Masaya Hisaoka†, Masashi Maeda† and Hiroshi Umeo†

†Univ. of Osaka Electro-Communication
Neyagawa-shi, Hatsu-cho 18-8
Osaka, 572-8530 Japan

1 Introduction

The synchronization in cellular automata has been known as firing squad synchronization problem since its development, in which it was originally proposed by J. Myhill to synchronize all parts of self-reproducing cellular automata [5]. The firing squad synchronization problem has been studied extensively for more than 40 years [1-10]. The present authors are involved in research on firing squad synchronization algorithms on two-dimensional (2-D) cellular arrays.

In this paper, we first propose a new linear-time generalized synchronization algorithm that can synchronize any $m \times n$ rectangular array in $m + n + \max(r + s, m + n - r - s + 2) - 4$ steps with the general at an arbitrary initial position (r, s) of the array. The algorithm is based on a state-efficient mapping scheme for embedding a restricted class of generalized one-dimensional optimum-time synchronization algorithms onto 2-D rectangular arrays. The embedding can be implemented with providing two additional states. We show that the linear-time 14-state solution developed yields an optimum-time synchronization algorithm in the case where the general is located at the north-east corner. Due to the space available, we omit proofs of the theorems.

2 Firing Squad Synchronization Problem on Two-Dimensional Cellular Automata

Figure 1 shows a finite two-dimensional (2-D) cellular array consisting of $m \times n$ cells. Each cell is an identical (except the border cells) finite-state automaton. The array operates in lock-step mode in such a way that the next state of each cell (except border cells) is determined by both its own present state and the present states of its north, south, east and west neighbors. All cells (*soldiers*), except one *general* cell, are initially in the quiescent state at time $t = 0$ with the property that the next state of a quiescent cell with quiescent neighbors is the quiescent state again. At time $t = 0$, any one cell on the array is in the *fire-when-ready* state, which is the initiation signal for synchronizing the array. The firing squad synchronization problem is to determine a description (state set and next-state function) for cells that ensures all cells enter the *fire* state at exactly the same time and for the first time. The set of states must be independent of m and n. We call the synchronization problem *normal*, when the initial position of the general is restricted to north-west corner of the array. We consider a *generalized* firing squad synchronization problem, in which the general can be initially located at any position on the array. As for the normal synchronization problem, several algorithms have been proposed, including Beyer [1], Grasselli [2], Kobayashi [3], Shinahr [7], Szwerinski [8] and Umeo, Maeda and Fujiwara [9]. Umeo, Maeda and Fujiwara [9] presented a 6-state two-dimensional synchronization algorithm that fires

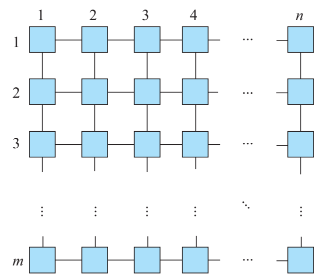

Figure 1: A two-dimensional cellular automaton.

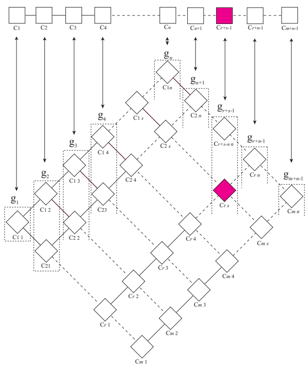

Figure 2: Correspondence between 1-D and 2-D cellular arrays.

any $m \times n$ arrays in $2(m+n)-4$ steps. The algorithm is slightly slower than the optimum ones, but the number of internal states is considerably smaller. Beyer [1] and Shinahr [7] presented an optimum-time synchronization scheme in order to synchronize any $m \times n$ arrays in $m + n + max(m,n) - 3$ steps. To date, the smallest number of cell states for which an optimum-time synchronization algorithm has been developed is 28 for rectangular array, achieved by Shinahr [7]. On the other hand, Szwerinski [8] proposed an optimum-time generalized 2-D firing algorithm with 25,600 internal states.

3 Linear- and Optimum-Time Firing Squad Synchronization Algorithms

Now we consider a generalized firing squad synchronization problem, in which the general can be initially located at any position on the array. Before presenting the algorithm, we propose a simple mapping scheme for embedding one-dimensional generalized synchronization algorithms onto two-dimensional arrays.

Consider a correspondence between 1-D array of length $m+n-1$ and 2-D array of size $m \times n$, shown in Fig. 2. Each black square corresponds to initial *general* cell on the array. The 2-D array of size $m \times n$ is divided into $m+n-1$ groups g_k, $1 \le k \le m+n-1$, that is defined as follows:

$$g_k = \{C_{i,j} | (i-1)+(j-1) = k-1\}, \text{ i.e.,}$$

$g_1 = \{C_{1,1}\}$,
$g_2 = \{C_{1,2}, C_{2,1}\}$,
$g_3 = \{C_{1,3}, C_{2,2}, C_{3,1}\}$,
.
.
.
,
$g_{m+n-1} = \{C_{m,n}\}$.

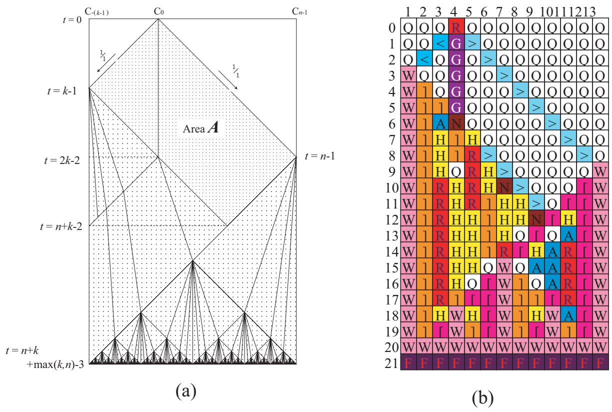

Figure 3: Time-space diagram for optimum-time generalized firing squad synchronization algorithm and snapshots for a 12-state implementation of the generalized firing squad synchronization algorithm with the property $\mathcal{Q}$ on 13 cells with a general on C_4.

The objective of our correspondence is to embed configurations of 1-D generalized synchronization algorithms onto 2-D arrays.

Property $\mathcal{Q}$: We say that a generalized firing algorithm has a *property* $\mathcal{Q}$, where any cell, except the general cell C_k, keeps a quiescent state *in the area* A of the time-space diagram shown in Fig. 3(a).

For any 2-D array M of size $m \times n$ with the general at $C_{r,s}$, where $1 \le r \le m$, $1 \le s \le n$, there exists a corresponding 1-D cellular array N of length $m+n-1$ with the general at C_{r+s-1} such that the configuration of N can be mapped on M, and M fires if and only if N fires. The transition table for N consists of four parts, one is a transformation rule set (Type (I)) that is for the inner cells of 2-D array and the other two sets (Type (II) and Type (III)) are for the state transition of cells $C_{1,1}$ and $C_{m,n}$. The fourth part is a new set of transition rules (omitted) for the transmission of *general* state in the diagonal direction. Let $\delta_1(a,b,c) = d$ be any transition rule of M, where $a, b, c, d \in \{Q - \{w\}\}$. Then, N has seven Type (I) transition rules, as shown in Fig. 4. The first rule (1) in Type (I) is used by an inner cell that does not include border cells amongst its four neighbors. Rules

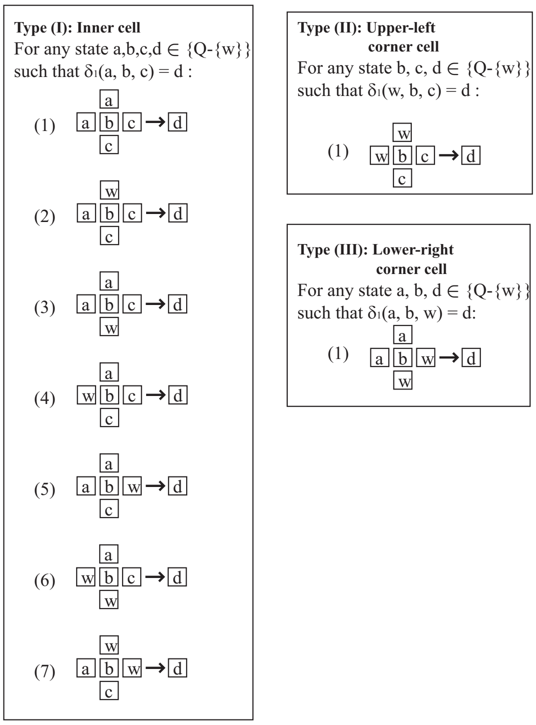

Figure 4: Construction of transition rules for 2-D linear-time firing squad synchronization algorithm.

(2)-(5) are used by an inner cell that has a border cell as its upper, lower, left, right, lower left, or upper right neighbor, respectively. Here the terms *upper*, *right* etc. on the rectangular array are interpreted in a usual way, shown in Fig. 2, although the array is rotated by 45° in the counterclockwise direction. Rules (6)-(7) in Type (I) are used by an inner cell that has border cells in its left-lower and right-upper neighbors, respectively.

Let S_i^t, $S_{i,j}^t$ and $S_{g_i}^t$ denote the state of C_i, $C_{i,j}$ at step t and the set of states of the cells in g_i at step t, respectively. Then, we can establish the following lemma.

[Lemma 1] The following two statements hold:

1. For any integer i and t such that $1 \le i \le m+n-r-s+1$, $r+s+i-3 \le t \le T(m+n-1, r+s-1)$, $\| S_{g_i}^t \| = 1$ and $S_{g_i}^t = S_i^t$. That is, all cells in g_i at step t are in the same state and it is equal to S_i^t, where the state in $S_{g_i}^t$ is simply denoted by $S_{g_i}^t$.

2. For any integer i and t such that $m+n-r-s+2 \le i \le m+n-1$, $2m+2n-r-s-i-1 \le t \le T(m+n-1, r+s-1)$, $\| S_{g_i}^t \| = 1$ and $S_{g_i}^t = S_i^t$.

[Theorem 2] Let M be any s-state generalized synchronization algorithm with the property $\mathcal{Q}$ operating in $T(k, \ell)$ steps on one-dimensional ℓ cells with a general on the k-th cell from the left end. Then, based on M, we can construct a two-dimensional $(s+2)$-state cellular automaton N that can synchronize any $m \times n$ rectangular array in $T(m, m+n-1)$ steps. The one-dimensional generalized firing squad synchronization algorithm with the *property* $\mathcal{Q}$ can be easily embedded onto two-dimensional arrays with a small overhead. Fig. 3(b) shows snapshots of our 12-state optimum-time generalized firing squad synchronization algorithm with the *property* $\mathcal{Q}$.

[Theorem 3] There exists a 12-state one-dimensional cellular automaton with the property $\mathcal{Q}$ that can synchronize ℓ cells with a general on the k-th cell from the left end in optimum $\ell - 2 + \max(k, \ell - k + 1)$ steps.

Based on the 12-state generalized 1-D algorithm given above, we obtain the following 2-D generalized synchronization algorithm that synchronizes any 2-D array of size $m \times n$ in $m+n-3+\max(r+s-1, m+n-r-s+1) = m+n+\max(r+s, m+n-r-s+2)-4$ steps.

[Theorem 4] There exists a 14-state 2-D CA that can synchronize any $m \times n$ rectangular array in optimum $m+n+\max(r+s, m+n-r-s+2)-4$ steps with the general at an arbitrary initial position (r, s).

Two additional states are required in our construction (details omitted). Szwerinski [8] also proposed an optimum-time generalized 2-D firing algorithm with 25,600 internal states that fires any $m \times n$ array in $m+n+\max(m, n)-\min(r, m-r+1)-\min(s, n-s+1)-1$ steps, where (r, s) is the general's initial position. Our 2-D generalized synchronization algorithm is $\max(r+s, m+n-r-s+2)-\max(m, n)+\min(r, m-r+1)+\min(s, n-s+1)-3$ steps larger than the optimum algorithm proposed by Szwerinski [8]. However, the number of internal states required to yield the firing condition is the smallest known at present. Snapshots of our 14-state generalized synchronization algorithm running on a rectangular array of size 7×9 with the general at $C_{4,5}$ are shown in Fig. 5.

Our linear-time synchronization algorithm is interesting in that it includes an optimum-step synchronization algorithm as a special case where the general is located at the north-east corner. By letting $r = 1$, $s = n$, we get $m+n+\max(r+s, m+n-r-s+2)-4 = m+n+\max(n+1, m+1)-4 = m+n+\max(m, n)-3$. Thus the algorithm is a time-optimum one. We have:

[Theorem 5] There exists a 14-state 2-D CA that can synchronize any $m \times n$ rectangular array in $m + n + \max(m, n) - 3$ steps.

4 Conclusions

We have proposed a state-efficient mapping scheme for embedding a restricted class of generalized one-dimensional synchronization algorithms onto 2-D rectangular arrays, then based on the scheme, a new linear-time generalized synchronization algorithm with fourteen states has been presented that can synchronize any $m \times n$ rectangular array in $m + n + \max(r + s, m + n - r - s + 2) - 4$ steps with the general at an arbitrary initial position (r, s) of the array. It is shown that the linear-time 14-state solution developed yields an optimum-time synchronization algorithm in the case where the general is located at the north-east corner.

References

[1] W. T. Beyer: Recognition of topological invariants by iterative arrays. Ph.D. Thesis, MIT, (1969), pp. 144.

[2] A. Grasselli: Synchronization of cellular arrays: The firing squad problem in two dimensions. *Information and Control*, vol. 28(1975), pp. 113-124.

[3] K. Kobayashi: The firing squad synchronization problem for two-dimensional arrays. *Information and Control*, vol. 34(1977), pp. 177-197.

[4] M. Minsky: *Computation: Finite and infinite machines.* Prentice Hall, (1967), pp. 28-29.

[5] E. F. Moore: The firing squad synchronization problem. in *Sequential Machines, Selected Papers* (E. F. Moore ed.), Addison-Wesley, Reading MA., (1964), pp. 213-214.

[6] H. B. Nguyen and V. C. Hamacher: Pattern synchronization in two-dimensional cellular space. *Information and Control*, vol. 26(1974), pp. 12-23.

[7] I. Shinahr: Two- and three-dimensional firing squad synchronization problems. *Information and Control*, vol. 24(1974), pp. 163-180.

[8] H. Szwerinski: Time-optimum solution of the firing-squad-synchronization-problem for n-dimensional rectangles with the general at an arbitrary position. *Theoretical Computer Science*, vol. 19(1982), pp. 305-320.

[9] H. Umeo, M. Maeda and N. Fujiwara: An efficient mapping scheme for embedding any one-dimensional firing squad synchronization algorithm onto two-dimensional arrays. *Proc. of the 5th International Conference on Cellular Automata for Research and Industry*, LNCS 2493, Springer-Verlag, pp.69-81(2002).

[10] H. Umeo, M. Hisaoka, K. Michisaka, K. Nishioka and M. Maeda: Some generalized synchronization algorithms and their implementations for a large scale cellular automata. *Proc. of the Third International Conference on Unconventional Models of Computation, UMC 2002*, LNCS 2509, Springer-Verlag, pp.276-286(2002).

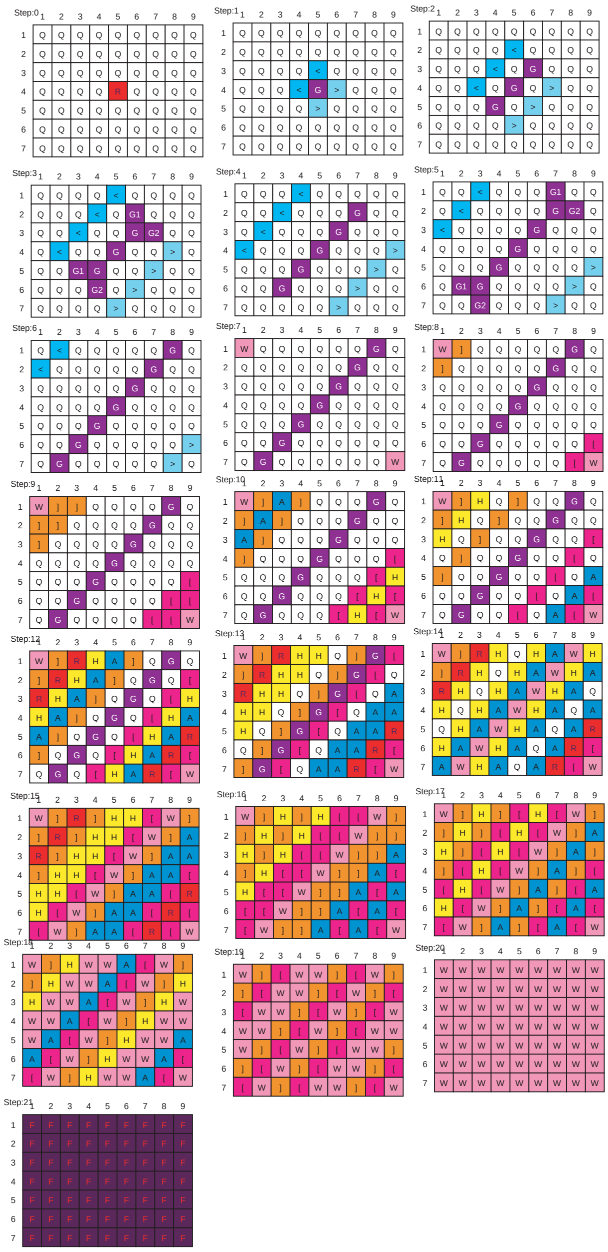

Figure 5: Snapshots of the 14-state linear-time generalized firing squad synchronization algorithm on rectangular arrays.

The Tenth International Symposium on Artificial Life and Robotics 2005(AROB 10th '05),
B-con Plaza, Beppu, Oita, Japan, February 4-6, 2005

A Study of the Basic Concept of Information in a Complex System

Yasuo Kinouchi
Department of Information Systems
Takashi Komiyama
Department of media and cultural studies
Tokyo University of Information Sciences
kinouchi@rsch.tuis.ac.jp
komiyama@rsch.tuis.ac.jp
1200-2 Yatoh-cho, Wakaba-ku, Chiba, 265-8501 Japan

Abstract

Neither the basic concept of information nor its fundamental properties have yet been clarified. A basic concept of information and its fundamental properties are given from the original viewpoint that information is both a kind of method of natural recognition and a kind of conceptual structure. The information properties that contribute to constructing actual complicated systems are also clarified.

Key words: basic concept of information, conceptual structure, and complex system

1. Introduction

In our modern society, which is a very complicated system, information fulfils an important role, along with energy and materials. In the world of living things, from humans to bacteria, complicated mechanisms operate based on information. Pure information systems, such as computer systems and the Internet, are the most complicated systems that human beings have ever produced. There are now many complex systems based on information. However, Wiener, Shannon, Noguchi, Bateson and Yoshida showed their concepts of information, they are different from each other. The basic concept of information and its fundamental properties have not yet been clarified. [1]-[6]

In this paper, we first clarify the basic concept of information and its fundamental properties. We then show that the fundamental properties of information greatly contribute to constructing actual complicated information systems, such as computer systems and network systems.

We work from the original viewpoint that information is a kind of method of natural recognition. From this viewpoint, as well as from modeling of a physical phenomenon as a conceptual structure composed of components and clearly defined relations, an information-based phenomenon can also be modeled as a kind of conceptual structure. This structure has the following features, differing from the model of a physical phenomenon:
(1) The components and the relations between components in the structure must be expressed in forms that do not depend on their physical properties. (2) Each component one-sidedly determines the effects of other components according to their relationships. (3) Each component has inputs, inner states, and outputs.

The property that information can be copied by using a small amount of energy is based on the model being expressed as a conceptual structure and having feature (1). Feature (2) represents the property of receiving information with sensitivity or susceptibility. The inputs and outputs in feature (3) correspond to transmitting information between components, while the inner states represent the memory or recording functions of information. In addition, the information quantity proposed by Shannon can be defined as a measure of the variety of stimuli from other components at the input interfaces of a component. By using this model, the properties of information can be clearly explained, and the main previous information concepts proposed by Wiener, Yoshida, and Noguchi can be systematically integrated.

Moreover, because information can be described as a structure, and a structure generally has the properties of facilitating easy generation of new components by combining multiple components and of enabling resolution of one component into multiple components, information systems combining computers and networks can be made extremely complicated. In addition, these properties are drastically accelerated through the digitization of information in computers and networks.

2. Previous views of information

2.1 Wiener and Shannon's concepts of information

In the middle of the twentieth century, Wiener advocated using the name "cybernetics" for the entire field of control and communication theory, whether in machines or in animals. Information thus fulfils a very important role in cybernetics, and Wiener wrote that "Information is a name for the content of what is exchanged with the outer world as we adjust to it, and make our adjustment felt upon it. The process of receiving and of using information is the process of our adjusting to the contingencies of the outer environment, and of our living effectively within that environment." [1][2] Though feeding is an important exchange activity with the external world of animal, this is clearly not included. Hence, information does not include exchanges of energy or materials.

At the same period, Shannon established the basis of communication theory, in which communication functions by utilizing an information source, a transmitter, a channel, a receiver, and a destination. He discussed only the "quantity" of information without mentioning its "meaning," and he advocated that that quantity of information is measured by a decrease in entropy. [3] Since an information source and a transmitter are assumed with regard to information transmission in Shannon's model, his concept of information has a narrower meaning than Wiener's.

2.2 Noguchi's concept of information

In 1974, Noguchi, a Japanese economist, gave the widest definition of an information concept, which was based on the capability of copying. He wrote that "The basic concept of information is the capability to copy it by using a very small amount of energy while leaving the original information in the same condition afterward. Although the copying capability is an important property of information, more precisely, something that can be copied is called information itself." [4]

The capability of copying as the definition of information can be intuitively understood from the routine work of copying paper documents with copy machines. However, information is not the only thing with the property of having the capability to be copied. For example, consider an iron bridge over which cars pass. It is possible for a similar purpose to be achieved by building an iron bridge of equal composition or structure in another place. In addition, it is possible for cars to pass over a wooden bridge, instead of an iron bridge. In general, the equivalent purpose can be achieved by any similar "structure" of stone, iron, or wood, which can be considered a kind of copying. However, a bridge with a similar structure cannot be copied by using only a very small amount energy, and thus, Noguchi thought that a copied bridge was not information. From a different viewpoint, consider the world of micromachining. The copied machines in this case also are not information, even though various structures can be copied with a very small amount of energy. Therefore, the capability of copying by using a very small amount of energy in Noguchi's definition should be reexamined in terms of structure. In addition, we must consider the fact that where Wiener regarded as system receiving information as important, Noguchi regarded the copied content as important.

2.3 Bateson and Yoshida's concepts of information

Bateson showed a view of information based on "difference" in his book, Steps to an Ecology of Mind, as follows: "The technical term 'information' may be succinctly defined as *any difference which makes a difference in some later event*. This definition is fundamental for all analysis of cybernetics systems and organization. … What is a difference? A difference is a very peculiar and obscure concept. A difference is an abstract matter. …What we mean by information– the elementary unit of information –is a *difference which makes a difference*, and it is able to make a difference because the neural pathway along which it travels and is continually transformed are provided with energy." [5]

Bateson defined information by referring to the information transfer in a neuron as "the difference which makes the difference," as shown above. On the key concept of "difference," however, he said only that it is abstract. It has not yet been clearly defined. Consider a system receiving multiple external stimuli. In this case, there are two viewpoints on determining whether these stimuli differ or resemble each other. One viewpoint is to mutually compare the multiple stimuli. The other viewpoint is to compare the effects that each stimulus has on the system. Whether the stimuli mutually differ or resemble each other depends on the properties selected for the comparison, which are limitless in their diversity. We think that the difference necessary for defining information must be based on the differences in the effects of the stimuli on the system. These differences are not abstract and can be treated very concretely. Bateson's concept of information must be reexamined from this viewpoint. In addition, Bateson's indication that neural pathways are provided with energy means a kind of physical condition for copying or transmitting information by using very little energy.

In addition to Bateson, the Japanese philosopher, Yoshida, has advocated the basic concept of information based on "difference". Moreover, he used the word "informational phenomena" in his argument. [6] Usually we express and model natural phenomena related to chemistry or physiology by using the terms chemical phenomena or physiological phenomena. It is very interesting that natural phenomena related to information can be similarly expressed and modeled in terms of "informational phenomena."

2.4 Watanabe's view

The Japanese physicist, Watanabe, who is investigating a mathematical model of information propagation, claims that the "sensitivity" of the receiver is very important, because the effect of information is greatly different as received by each person, even if it is the same information. [7] As described above, both Wiener and Bateson mentioned the importance of the component receiving information, but Watanabe clearly and intuitively conceptualized the importance by using the word "sensitivity."

3. Informational phenomenon and informational structure

In this section, we give our view of information in the widest sense.

3.1 Information and informational phenomenon as a method of natural recognition

We clarify information in the widest sense as a phenomenon reduced to a physical phenomenon. However, information cannot be clarified, even if we microscopically observe the mutual relationships between materials. It cannot be expected that information or functions of information are recognizable from the relationships between material particles under gravity. As shown in Figure 1, there are chemical phenomena in which materials react in chemical relations, and physiological phenomena overlaying the chemical phenomena. In addition to these phenomena, we recognize a phenomenon related to information as an “informational phenomenon,”as shown by the dashed ellipse. We thus recognize information as a kind of method of natural recognition, so that chemistry and physiology may also be methods of natural recognition. As an example of recognizing a complicated system, there are macroscopic observation or a method of coarse graining. Though it differs from these methods, a physical phenomenon of some kind plainly be grasped by recognizing its nature as an information phenomenon of information. Also, the basic concept of information can be clarified by modeling this informational phenomenon.

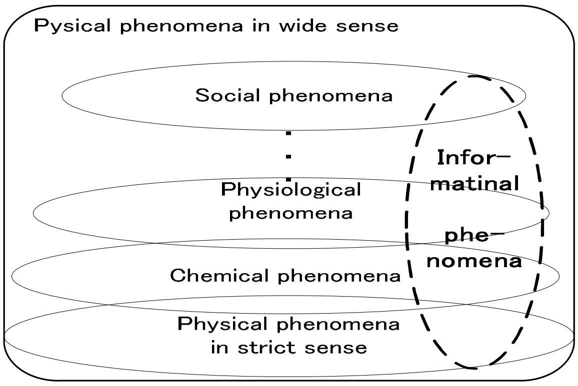

Fig.1 The positioning of informational phenomena

3.2 Modeling informational phenomena

The technical terms used here are defined as follows in order to discuss the idea of an informational phenomenon. We define the term “system” as “a sets of components or elements standing in interrelation,” according to the definition of Bertalanffy in his book, General system theory. [8] A “system” is classified into two categories: a real system, and a conceptual system. The real system is entities that really exists, such as a solar system, a machine, a dog, a cell, or an atom. On the other hand, the conceptual system does not really exist but is a symbolic construct, such as mathematics, physical laws, or the plan of a bridge. We classify the conceptual system expressing a model of nature as shown in Fig. 2.

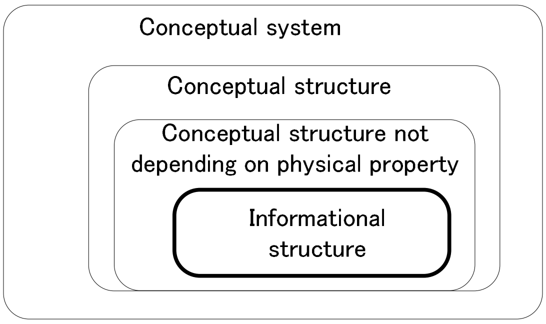

Fig.2 The positioning of informational structure

(1) Conceptual structure: A subset of a conceptual system, in which the relationships among components must be defined clearly. (An example is a model using physical laws.)
(2) Conceptual structure not depending on physical properties: A subset of a conceptual structure, in which the relationships among components must be expressed in forms that do not depend on physical properties. (A physical property means a property of a physical phenomenon in the widest sense, including chemical and physiological property, and so on. An example is a model using mathematical expressions.)
(3) Informational structure: A subset of a conceptual structure not depending on physical properties. An informational structure represents or models informational phenomenon and has the following properties:
a. Each component one-sidedly determines the effects of other components according to their relationships. (This property represents the sensitivity of a receiver.)
b. Each component has inputs, inner states, and outputs. Each component determines its outputs and inner states as functions of inputs and previous inner states.

In an informational structure, transmission, memory, and processing of information are carried out as follows. The relationship between components that send out or receive changes corresponds to “transmission.” In some cases, these changes occur as physical stimuli originating from light, sound, or electric current. In other cases, they occur as a result of transferring material, such as DNA or document. The setting or retaining of the inner states of a component corresponds to “memory,” and the conversion from input states to output states in the component corresponds to “processing.”

The digital computer is an example of an informational structure modeling an informational phenomenon. Each logical circuit in a digital computer certainly works according to a very complex physical phenomenon based on the motion of electrons, where these actions are described by chains of ON or OFF values, whose effects are one-sidedly determined by adjoining circuits and as a whole are not dependent on physical properties.

3.3 Reexamination of the previous information concepts based on the informational structure

Recognizing information as a kind of process according to the view of Wiener and Bateson corresponds to recognizing the relations in an informational structure whose components are an animal, a neuron, and an environment. Components receiving various stimuli in a real system distinguish whether it is “information” by using the “difference” advocated by Bateson and Yoshida. In an informational structure, the “difference” is converted to a quantity that does not depend on physical properties. Under conditions that functions of the component receiving information are not changed in the informational structure, we can replace input stimuli or entities to the component by different ones in the corresponding real system. This capability of replacement corresponds to the capability of copying as the basic concept of information, as advocated by Noguchi, because a copy is a kind of replacement that maintains the same effects on the component receiving information.

The information quantity of Shannon shows whether a component receiving information recognizes the outside of the component to a certain degree of fineness. The input of information with a quantity of n bits enables the component to recognize the outside as a space composed of 2^n pieces.

4. Contributions of information properties to constructing complex systems

As shown above, an informational structure has the following three properties.

a. An informational structure is not dependent on physical properties.

b. The actions of an informational structure function in uni-directionally.

c. A real system represented by an informational structure can be simply replaced with different materials, or components while still maintaining all functions. Then information can be copied easily.

In addition, the next important property should also be applied.

d. Development is easy in an informational structure, and the result of the development is easily implemented as a real system.

Here, "development" means the generation of a new component from multiple components and the resolution of a component into multiple components. Generally, development is easy for the conceptual structure, as the mathematics is developable. The informational structure also has the property that the result of development becomes easy to implement as a real system, based on the properties of easy replacement and copying, and the lack of dependence on physical properties. Since these four properties work comprehensively, the construction of a complex system becomes very easy by applying them. By digitizing the informational structure, this tendency can be further accelerated. Representative examples include today's computer systems and communication network systems.

5. Conclusion

The basic concept of information and its fundamental properties have been clarified from the original viewpoint that information is both a kind of method of natural recognition and a kind of conceptual structure, called an “informational structure.” Relations, actions, and states in this informational structure model “information” itself and its functions. This model can account for previous information concepts, such as those of Wiener, Shannon, Bateson, and Noguchi. The properties of information showed here greatly contribute to constructing complex systems.

Acknowledgments

We thank Prof. Shuji Hashimoto of Waseda University and Mr. Shoji Inabayashi of Pacific Technos Corp. for useful suggestion. This work was supported by Frontier Project of the MESC.

References

[1] N.Wiener(1948), Cybernetics: or control and Communication in the Animal and the Machine, MIT Press

[2] N.Wiener(1954), The Human Use of Human Beings - Cybernetics and Society, Da Capo Press

[3] C.E.Shanonn(1948), Mathematical theory of communication, The Bell system technical journal Vol.27, pp379-423,623-656, (1948)

[4] Yukio Noguchi(1974), Economical theory of information (in Japanese), Toyo keizai sinpohsya

[5] G.Bateson (1972), Steps to an ecology of mind, The University of Chicago Press

[6] TamitoYoshida (1990), Informational science of self-organization(in Japanese), Shinyohsya

[7] Tadashi Watanabe and Takeo Ebisu(2003), A Mathematical Model for Information Propagation(in Japanese), Journal of Tokyo University of information sciences, Vol. 6 No.2, pp27-38

[8] L.V. Bertalanffy(1968), General System Theory –Foundations, Development, Applications, George Braziller

The Tenth International Symposium on Artificial Life and Robotics 2005(AROB 10th '05),
B-con Plaza, Beppu, Oita, Japan, February 4-6, 2005

Quantitative analysis of self-organizing multiagent interaction with entropy and mutual information

Koji Nishikawa Hidenori Kawamura Masahito Yamamoto Azuma Ohuchi

Graduate School of Information Science and Technology, Hokkaido University
Nishi 9, Kita 14, Kita-ku, Sapporo, Hokkaido, 060-0814, Japan
{koji, kawamura, masahito, ohuchi}@complex.eng.hokudai.ac.jp

Abstract

In the research of a multiagent system, the indicators such as a task achievement ratio and a payoff have been used for analyzing a system. These indicators are important for the point that agents need to accomplish a task. However they are inadequate to make clear the entity of phenomena that occur in complex system, because they are specialized in the target system and the analysis is also specialized. In these respects the approaches that analyze a system quantitatively are begun to investigate in recent years. In our research, we propose the approach that analyzes a multiagent system quantitatively by focusing on the dynamics of a system and interaction among multiagents. We use two indicators, i.e., entropy and mutual information, for analyzing a system. Entropy estimates the behavior of an agent and mutual information estimates interactions between two agents. For verifying these propositions, we conduct verification experiment in the simple slime mold model. The result shows a relationship between agents' behavioral patterns and two indicators, therefore our approach using entropy and mutual information is available for analyzing a multiagent system.

Keywords. Multiagent system, Quantitative analysis, entropy, mutual information, interaction

1 Introduction

The researchers who construct multiagent systems must deal with the complex behavior of self-organization. Self-organization in multiagent systems emerges from agents' behavior, which is independently autonomous but corporately structured by interactions among agents and the environment. Researchers want to reveal these interactions because the coherence of the agents' local behavior and the system's overall behavior is required in designing systems.

Historically, researchers analyze system's overall behavior with the indicators such as a task achievement ratio and a payoff. These indicators are important for the point that agents need to accomplish a task. However they are inadequate to make clear the entity of complex systems and it is difficult to say why and how the task is achieved or how we get higher score. Since they are specialized in the target system and the analysis is also specialized. Therefore analyses that quantify the entity of systems universally are required. In these respects, there are researches that comprehend the dynamics of systems and agents with the concept of entropy [1], [2], [3], [4]. In these researches they consider about the behavioral diversity and the constraint with variance of entropy, and attempt to quantify the system.

In this paper, we propose the approach that analyzes a multiagent system quantitatively by focusing on the dynamics of a system and the interaction among multiagents as the entity of systems. In particular, we quantify the system's overall behavior and the intensity of interactions among agents and analyze systems.

2 Analysis of multiagent interaction

The interactions among multiagent in self-organization systems are considered to be interchange of information about the state of agent. The discussion of the relationship between these information and entropy is done historically [5]. In particular, decrease of entropy is great issue, and it is said that

- gain of information causes decrease of entropy and emerge constraint and
- gain of information constantly keeps up these constraint.

Therefore it is considered that information and entropy are important to capture the entity of multiagent interaction.

The concept of entropy is defined three contexts, i.e., thermodynamics, statistical mechanics and information theory; particularly information theory definition is called information entropy or Shannon's entropy [6]. Though informational definition does not inherit two other definitions, there are common entities because of the sameness of these formulas. With using information entropy, analysis of multiagent systems are studied in thermo dynamics perspective [1] and nonequilibrium thermodynamics perspective [2]. Therefore we use informational theoretical approach to quantify the entity of multiagent system.

Our analysis method uses two indicators entropy and mutual information, where mutual information is the indicator of the value of information. In our approach we can analyze

1. agent's behavior, e.g., stability, constraint or complexity with entropy and
2. the intensity of interactions between two agents with mutual information.

When one computes these indicators, what to observe as states is the great issue. Then consider about an agent, it is the autonomous individual that takes input from environment through its sensors and outputs through these input and decision-making process. At this time, agent's decision-making is followed its internal state, which can be variously designed. For capturing the essential states of agent that is not specialized in systems, agent's internal state depends systems and is not just as well. Whereat we use agent's input and output as the state of agent.

3 Experimental setup

We experiment with these concepts using a simple model of self-organization, slime mold model. In this section we describe the experiment in the slime mold model and how one measures entropy and mutual information.

3.1 Slime mold model

The group behavior of slime mold cells is the famous focus for models of self-organization [7]. Normally they move around as individual amoebas throughout their substrate, performing a simple random walk. But when the environmental situation worsens, they suddenly change their behavior and aggregate to a single multi-cellular body. During this aggregation process, they emit a chemical signal called cAMP to guide the collective movements. As they move, they follow the cAMP gradient in the environment.

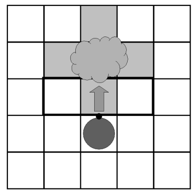

Figure 1: The environment of slime mold model

The whole process is a self-organization. Though all amoebas act with local information around them and without any other guidance such as coordinating the aggregation, they aggregate.

In the slime mold model, amoeba agents are placed on the grid world as Figure 1. An agent and environment model are described as follows.

Agent model

An agent acts as described below at each step.

1. Put cAMP on the current grid.
2. Sense the density of cAMP on the forward 3 grids in 8 neighbors.
3. Move to the grid that has the most cAMP.

Environment model

In the environment, cAMP is defined on the grid as parameters $T(x,y)$ and $P(x,y)$. $T(x,y)$ denotes the amount of cAMP on the grid (x,y), and $P(x,y)$ denotes the density of cAMP over the grid (x,y). An agent can sense the density of cAMP over the grid.

As time passes, cAMP evaporates and diffuses. By evaporation and diffusion, $T(x,y)$ and $P(x,y)$ changes into $T^*(x,y)$ and $P^*(x,y)$ at each step

$$T^*(x,y) = (1-\gamma_{eva})T(x,y) + \Delta T \tag{1}$$

$$\Delta T = \{ \begin{array}{cc} Q & \text{if an agent exists on grid } (x,y) \\ 0 & \text{otherwise} \end{array} \tag{2}$$

$$\begin{aligned} P^*(x,y) = P(x,y) + \gamma_{dif}\{P(x-1,y) + \\ P(x+1,y) + P(x,y-1) + P(x,y+1) \\ -5P(x,y)\} + \gamma_{eva}T(x,y) \end{aligned} \tag{3}$$

where Q denotes the amount of cAMP put by an agent in 1 step, and γ_{eva} and γ_{dif} denotes the evaporation rate and the diffusion rate of cAMP, which defines the property of cAMP.

3.2 The parameter of slime mold model

In the slime mold model, the cAMP's property that is defined by evaporation and diffusion rate affects the pattern of agents' self-organizational process. We compare these various patterns and the distribution of entropy and mutual information in our experiment, and verify our proposition.

The environment is 50×50 grid world, and contained 50 agents. We change cAMP's property to vary information's property among agents in respect of time length and accuracy, and the value of evaporation and diffusion rate is set to 4 different values, i.e.,

a. $\gamma_{eva} = 0.1$, $\gamma_{dif} = 0.1$

b. $\gamma_{eva} = 0.1$, $\gamma_{dif} = 0.3$

c. $\gamma_{eva} = 0.5$, $\gamma_{dif} = 0.1$

d. $\gamma_{eva} = 0.5$, $\gamma_{dif} = 0.3$.

We experiment with these setups at 1000 steps.

3.3 Measuring entropy and mutual information

Computing entropy and mutual information requires that we measure

1. the set of an agent X's states $x \in \{x_1, \cdots, x_n\}$ (i.e. input and output) and
2. the probability $p(x)$ of being those states,

where the agent's input is the discrete density of cAMP that exist on agent's forward 3 grids, and output is the agent's moving direction toward its facing direction.

Measuring those states is observation of the agent at each step. To measure the probability, we take Monte Carlo approach. By counting those states in whole step of 1 experiment, we estimate the probability.

With using these variables, entoropy of an agent X and mutual information among an agent X and Y is defined in following equations,

$$H(X) = -\sum_x p(x) \log p(x) \tag{4}$$

$$I(X:Y) = \sum_x \sum_y p(x,y) \log \frac{p(x,y)}{p(x)p(y)} \tag{5}$$

Table 1: The distribution of agents' entropy and mutual information in the slime mold model (in 100 trials)

	$\bar{I}$	$V(I)$	$\bar{H}$	$V(H)$	r_{Id}
a.	0.21	5.2×10^{-3}	0.53	1.5×10^{-2}	-0.31
b.	0.048	3.1×10^{-4}	0.34	4.5×10^{-3}	-0.41
c.	0.23	4.9×10^{-3}	0.54	1.1×10^{-2}	-0.34
d.	0.056	6.8×10^{-5}	0.39	3.3×10^{-4}	-0.11

4 Experimental results

Table 1 shows entropy and mutual information in each setup, a $\sim$ d, where $\bar{I}$ and $V(I)$ denote the average and variance of mutual information for randomly selected 100 pairs of agents. $\bar{H}$ and $V(H)$ denote the average and variance of entropy for all agents. r_{Id} denotes correlation coefficient between mutual information and Euclidean distance of pairs of agents. The results show that the average of mutual information is larger in the setting a and c than b and d, and it is considered that agents interact more intensive in the setting a and c. The average of agents' entropy is smaller in the setting b and d, and the states of agents will be stable.

On the other hand, we look the states of agents in visible by Figure 2 $\sim$ 5. In the setting a and c, many agents form clusters by self-organization. On the contrary many agents act independently in the setting b and d. These behavioral patterns are same as we see the difference of mutual information in each setup on the point of the intensity of interactions. Moreover, the value of r_{Id} shows tendency that the closer two agents are, the intensive they interact.

In addition, we look the process of forming cluster to look the stable of the system. In the setting a and c, because of the intensity of interactions, the agents form various cluster one after another in 1 experiment. While in the setting b and d, when the agents form a cluster, they seldom go out from this cluster and keep it up because the cAMP dropped by the agent out of them is weak and not enough to draw them in. These behavioral patterns are also same as the analysis by entropy, i.e., the states of agents are more stable in the setting b and d than a and c.

5 Summary

In this paper, we proposed the quantitative analysis of multiagent interaction with entropy and mutual

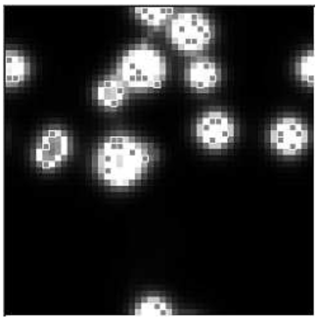

Figure 2: The look of the system at 1000 step in the setting a. The agents form some clusters.

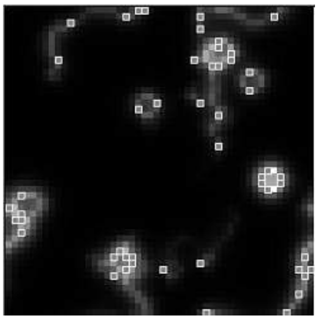

Figure 3: The look of the system at 1000 step in the setting b. The agents form small clusters, and some agents act independently.

Figure 4: The look of the system at 1000 step in the setting c. The agents form big cluster.

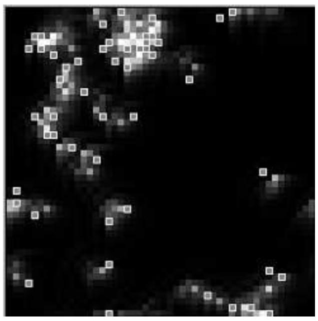

Figure 5: The look of the system at 1000 step in the setting d. Many agents act independently.

information. We conducted verification experiment in the slime mold model to quantify the interactions in self-organizational process. The results show the relationship between agents' behavioral patterns and our analysis, and validity of our proposal method.

References

[1] H.Van Dyke Parunak, Sven Brueckner, "Entropy and Self-Organization in Multi-Agent Systems", Proceedings of the Fifth International Conference on Autonomous Agents, pp.124-130, 2001

[2] Stephen Guerin, Daniel Kunkle, "Emergence of Constraint in Self-Organizing Systems", Journal of Nonlinear Dynamics in Psychology and Life Sciences, Vol. 8, No. 2, 2004

[3] Mikhail Prokopenko, Peter Wang, "Evaluating Team Performance at the Edge of Chaos", In Proceedings of the 7th RoboCup-2003 Symposium, 2003

[4] Tucker Balch, "Hierarchic Social Entropy: An Information Theoretic Measure of Robot Team Diversity", Autonomous Robots, Vol. 8, No. 3, 2000

[5] Christoph Adami, "Introduction to Artificial Life", Springer-Verlag, New York, 1998

[6] Claude E. Shannon, Warren Weaver, "The Mathematical Theory of Communication", University of Illinois Press, 1949

[7] Mitchel Resnick, "Turtles, Termites, and Traffic Jams: Explorations in Massively Parallel Microworlds", MIT Press, 1997

The Tenth International Symposium on Artificial Life and Robotics 2005(AROB 10th '05),
B-con Plaza, Beppu, Oita, Japan, February 4-6, 2005

Transforming Information to Knowledge and Intelligence*

Yi. X. ZHONG
University of Posts & Telecommunications
Beijing 100876, P.R.CHINA
e-mail: yxzhong@ieee.org

Abstract: Intelligence is regarded as the most precious wealth among all kinds of capabilities. It would be of great interest and significance if the formation mechanism of intelligence could be understood. It is our discovery that intelligence is activated from knowledge and the latter in turn is refined from information and the transformations of information to knowledge and further to intelligence and that is the secrets of intelligence formation. These discoveries will be reported in the article as what could be followed for building intelligent machine. As an interesting by-product, the three existing approaches to AI research have also been unified in the article.

Key Words: Information, Knowledge, Intelligence, Transformation from Information to Knowledge and to Intelligence

1, Introduction

As the most attractive, powerful, and unique attributes to human beings, intelligence has been received more and more attentions from scientific circles. It would be a great scientific breakthrough in history if human intelligence, or even part of it, can steadily be transferred to machines.

What is the essence of intelligence we should understand in the context? What is the technically feasible mechanism for intelligence formation? Would it be really possible for humans to make machines intelligent? How to make machines intelligent, if possible? And what if intelligent humans can eventually utilize and manage the intelligent machines?

Based on the observations and results accumulated during his research, the author of the article would like to give some of the answers toward the questions above. Due to the space limitation we have for the article, the answers will be concise and brief.

2, Model of Human Intelligence Process

To begin with, a model of intelligence process performed by humans is necessarily given as a basis of the discussions that will be carried on in the article. In Fig.1 below shows a model of human intelligence process in the boxes of which are human organs (the sensors, nerve system, brain and actuators) while outside the boxes are the functions the organs perform (information acquisition, information transferring, information cognition & decision

----

* The work is supported in part by National Project 863-2001AA114210-13

making, and strategy execution) and alongside

The model tells how human beings solve the problems they face in the real world and how the intelligent strategies and accordingly the intelligent actions are produced from knowledge and information.

3, The Transformations

The mechanisms embedded in the process of intelligence formation consist of a number of transformations that will be explained in the following sub-sections. Due to the limitation of the space we have for the paper, only the nucleus, the transformations of information to knowledge and then to intelligence are dealt with in the paper.

3-1 The Transformation: from Information to Knowledge

The first step is to deal with the transformation from information to knowledge and here the information is the so-called epistemological information as is shown in Fig.1. The related concepts can be given below.

$$K \Leftarrow \bigcap\{I_E\} \qquad (1)$$

where the symbol ∩ in (1) stands for induction operator; $\{I_E\}$ the sample set of the epistemological information; and K the knowledge produced by $\{I_E\}$. In some cases, there may need some iterations between induction and deduction and the deduction itself can be expressed as

$$K_{new} \Leftarrow \Re\{K_{old}, C\} \qquad (2)$$

where C stands for the constraint for deduction. Fig.3 shows the general process of transformation from epistemological information to knowledge.

Definition 1 Epistemological Information *of an object is a description, given by the subject (observer or user), concerning the object's states and the manner including their forms, meanings and utilities and are respectively termed as the* *Syntactical Information, Semantic Information* *and* *Pragmatic Information,* see [1].

Definition 2 Knowledge: *Knowledge concerning a category of objects is the description, made by subjects, on various aspects of the states at which the objects may stay and the law with which the states may vary. The first aspect is the form of the states and law and that is termed the formal knowledge, the second aspect is the meaning of the states and law that is termed the content knowledge and the third aspect is the value of the states and law with respect to the subject that is termed the value knowledge. All the latter three aspects constitute a trinity of knowledge* [2].

The definitions 1 and 2 indicate that the transformation from epistemological information to knowledge can be implemented through inductive algorithms:

More specifically, the formal knowledge can be refined from syntactic information, content knowledge can be refined by semantic information, and utility knowledge can be refined by pragmatic information through induction/deduction as indicated below:

$$K_F \Leftarrow \bigcap\{I_{sy}\} \qquad (3)$$

$$K_V \Leftarrow \bigcap\{I_{pr}\} \qquad (4)$$

$$K_C \Leftarrow \bigcap\{\Re(I_y, I_{pr}, C)\} \qquad (5)$$

where the symbols K_F , K_V and K_C respectively stand for formal, content and value knowledge while I_{sy} and I_{pr} for syntactic and pragmatic information. The general algorithms related to （3）,（4）and（5）can be referred to [2].

Knowledge, in accordance with its maturity in the process of growth, can roughly be further classified into three categories: the experiential knowledge, the regular knowledge and the knowledge in common sense.

Definition 4 Empirical Knowledge: *The knowledge produced by induction yet without verification is named the empirical knowledge. It may also be called the potential knowledge, or pre-knowledge, sometimes.*

Definition 5 Regular Knowledge: *The regular knowledge can be defined as matured knowledge. It is the normal stage of knowledge growth.*

Definition 6 Knowledge in Common Sense: *There exist two sub-categories: axiom and reflection with or without conditions. Learning and reasoning process are not needed in the category. Knowledge can also be called the popular knowledge.*

3-2 Transformation: from Knowledge to Intelligence

The task for decision-making in Fig.1 is to create an intelligent strategy, based on the knowledge and information, as the guidelines for problem solving intelligently. The strategy is the embodiment of the related intelligence.

Definition 7 Strategy: *A Strategy for problem solving is sort of procedure, produced based on the related knowledge and information, along which the given problem could be satisfactorily solved, meeting the constraints and reaching the goal. It is the embodiment of intelligence and is therefore also called intelligent strategy.*

The transformation from knowledge and information to strategy can be expressed as

$$I_S : (P, E, G; K) \mapsto S \tag{6}$$

where I_S denotes the strategy, P the problem to be solved, E the constraints given by environment, G the goal of problem solving, K the knowledge related to the problem solving and S the space of strategies. Theoretically speaking, for any reasonably given P, E, G and K, there must exist a group of strategies such that the problem can be solved satisfactorily and among the strategies there will be at least an optimal one guaranteeing the optimal solution.

The specific form of the transformation will be dependent on the properties of the problem faced and the knowledge possessed. For empirical knowledge, the form of the transformation can obviously be implemented via learning/training and testing. In fact, this is the mechanism of neural network's learning [3].

As for the regular knowledge, the transformation can be implemented via a series of logic inferences. More specifically, for the given problem, constraints, goal and the related knowledge, it is possible to form a tentative strategy for the selection of rules for applying to the problem and producing a new state of the problem. Diagnosing the new state by comparing it with the goal and making analysis based on the related knowledge, the tentative strategy can thus be improved or maintained. A new rule can then be selected to apply to the new state and new progress may be made. This process will be continued until the goal is reached, the constraints are met. In the meantime, the strategy is also formed.

Evidently, this is the mechanism of strategy formation in the so-called Expert System [4].

In the case of common-sense knowledge, the mechanism of intelligent strategy formation can be implemented by directly linking the input pattern and the strategies. As long as the input pattern is recognized the strategy for control can immediately be determined based on the common-sense knowledge direct related to the problem without any inferences needed. This is the typical feature of strategy formation sensor-motor category [5].

Summary: *As it is indicated in Fig.1, there are four categories of functional units in the entire information process (also intelligence process). The units of information acquisition and execution are two kinds of interface between intelligent system and the external world: the former acquires the ontological information from the external world while the latter exert strategic information to the external world. On the other hand, the units of information cognition and decision-making are the two kinds of inner core of the intelligent system: the former create knowledge from information and the latter produce strategy from the knowledge. Only by the synergetic collaboration among all the four functions could make intelligence practical.*

4. Unified Theory of Intelligence: A By-Product

It is interesting to note that in a long history of Artificial Intelligence development there have been three strong approaches to the research in literature, the structuralism also called as connectionism, the functionalism also termed as symbolism, and the behaviorism or senor-motor approach, that seem distinctive to each other.

As is seen in last section, however, all the three approaches have well been unified into one same mechanism of intelligence formation, that is, the transformations from information to knowledge and further to intelligence. In views of the mechanism of intelligence formation, there is a unified theory of intelligence, realizing the unification among the three approaches. This is shown in Fig.2.

It is clearly enough to see from Fig.2 that the real difference among the three traditional approaches lies only on the categories of knowledge in use while the core mechanisms of cognition and decision-making are always necessary.

As stated in section 3-2 and shown in Fig.2, if the knowledge to be used must be refined from information directly and instantly (this is the first category of knowledge, or experiential knowledge), the implementation of cognition and decision-making will have to employ the training and testing procedure by using, for example, the artificial neural networks approach. This is so-called Structuralism because Artificial Neural Networks are designed by following the Biological Neural Networks in principle.

If the knowledge to be used can be obtained from somewhere and not necessary to be refined from information (this is the second category of knowledge, or regular knowledge), the cognition is simply be performed by the system designers while the decision-making can be implemented via logic inference. This is the approach emphasizing on the functions of the system without considering the structure.

When the knowledge to be used is the third category, the common sense knowledge about the relationships between the input patterns and output actions, there is of course no need for else knowledge. This is behaviorism approach.

After all, the three approaches in Artificial Intelligence research are by no means in contradiction. They, Artificial Neural Networks Approach, Expert Systems Approach, and Senor-Motor Approach, are well complementary to each other and no one can take the other's place.

This, the author believes, is an important conclusion resulted from the studies in the core transformations in intelligence creation.

References

[1] Y. X. Zhong, *Principles of Information Science*, BUPT Press, 2002 (The Third Edition)
[2] Y. X. Zhong, *A Framework of Knowledge Theory*, China Engineering Science, Vol.2, No.9, p.50-64, 2000
[3] J. M. Zurada, *Introduction to Artificial Neural Systems*, West Publisher, New York, 1992
[4] N. J. Nilsson, *Principles of Artificial Intelligence*, Springer-Verlag, Berlin, 1982
[5] R. A. Brooks, *Intelligence without Representation*, Artificial Intelligence, 4, 139-159, 1991

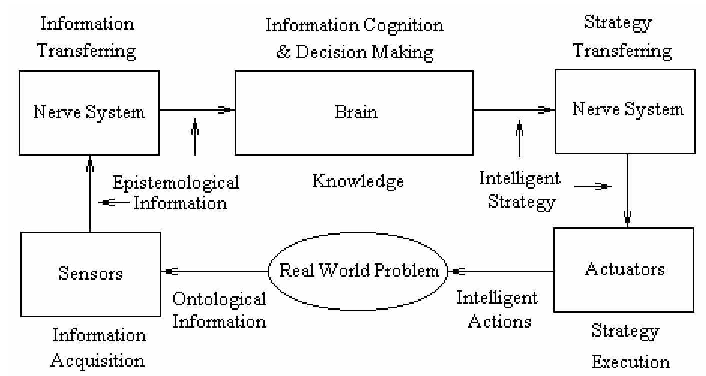

Fig.1 Model of Human Intelligence Process

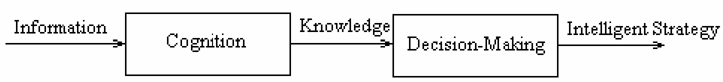

Epistemological Information	Training	Empirical Knowledge	Neural Network	Structuralism
Epistemological Information	Manually Creation	Regular Knowledge	Expert System	Functionalism
Epistemological Information	Machine Sensing	Common-Sense Knowledge	Sensorimotor	Behaviorism

Fig.2 Intelligence Theory Unification

The Tenth International Symposium on Artificial Life and Robotics 2005(AROB 10th '05),
B-con Plaza, Beppu, Oita, Japan, February 4-6, 2005

Establishment of sound-corresponce laws of word-initial consonants between Finnish/Uralic and Malayo-Polynesian/Proto-Austronesian languages: Towards making comparative analysis of word-initial consonant frequencies

[1] Koji Ohnishi, [2]Shigeki Akiyama, [3]Yusuke Murayama, and [4]Masaki Goda

[1,3] Dept .of Biology and [2]Dept of Mathematics, Faculty of Sciences,
and [4]Faculty of Engeneering, Niigata University, Niigata, 950-2181, Japan.
[1]E-mail: ohnishi@sc.niigata-u.ac.jp

Abstract

In order to make comparative analysis of word-initial sound (or consonant) frequencies among different languages or language families, it is most important for us to find basic knowledge concerning consonant-correspondence laws among related languages. However, we have very few knowledge about such laws useful for comparing distantly related language families. In this paper, Finnish-Austronesian sound-correspondence laws were analyzed by using comparative dictionaries, and Finnish (Uralic)-Austronesian sound correspondence laws were established for most of word-initial Finnish (and proto-Uralic) consonants, as shown in Tables 1 and 2. This establishment provides us with a very important tool not only for evolutionary Uralic language studies, but also for comparative analyses of word-initial sounds (or consonants) among distantly related Eurasian languages.

Word-initial consonant frequencies in Finnish suggested an interesting phenomenon, which however needs more evidence based on detailed comparative and statistical analyses.

1. Introduction

Comparative linguistics has had shown that sound-correspondence laws are most important for comparative and evolutionary analyses of languages. Whether Zipf's law can be found or not in the distribution of word-initial consonants is an interesting problem of theoretical linguistics. In order to begin comparative analyses of word –initial sound-(or consonant-)frequencies between Uralic (URA) and Austronesian (AN) language families, we attempted to elucidate sound-correspondence laws between these two language families. This approach is based on the findings of Austronesiian origins of various Eurasiatic and Pacific-rim languages (Ohnishi, 1999).

2. Establishment of word-initial sound-correspondence laws between URA and AN

For finding sound-correspondences in cognate words ("evolutionarily related words"= "homo-logous words") between URA and AN, cognates were extensively searched by using "Uralisches Etymologisches Woeterbuch", "Austronesian Comparative Dictionary" and others. which are listed in the "References" portion of Table 1.

Extensive comparative search for cognates between Finnish (Finn.) (and other Uralic languages such as Hungarian (Hung.), etc.) and Austronesian languages has revealed that many basic Urklic words have their own cognates in Austronesian, especially in Malayo-Polynesian (MP) subfamily consisting of Western MP (W.MP), Central MP (C.MP) and Oceanic (OC). Based on these cognate relations listed in Table 1, sound-correspondence-laws between Finn.(, URA and prpto-URA) and AN (mostly MP) for word-initial consonants were analysed and elucidated, as summarized in Table 2. Very beautiful sound-correspondence laws have now been established for nearly all Finnish word-initial consonants, which means that Uralic language family have evolved from a branch of MP subfamily of the AN language family.

3. Analyses of word-initial consonant frequencies

In the next step of our research, sound-frequencies in word-initial positions were analyzed in representative URA and AN languages. By letting x_N denote the number of pages of the words(in A. Wuolle "Finnish–English and Emglish-Finnish Dictionary", Helsinki, 1978) for the N-th most frequent consonant in word-initial position, the relationship between N and x_N was found as shown in Fig. 1, suggesting a simple relation, $\ln x_N = a - k N$, i.e., $x_N = A e^{-kN}$, where a, A, k are constants (> 0). Further analyses are needed for confirming this phenomenon.

4. References: See references in Table 1.

N = {1, 2, 3, 4, 5, 6, 7, 8, 9, 10, 11, 12, 13, 14, 15, 16, 17, 18, 19, 20}

= {k, #, s, t, p, v, h, l, m, r, n, j, o, i, y, u, b, d, f, g}

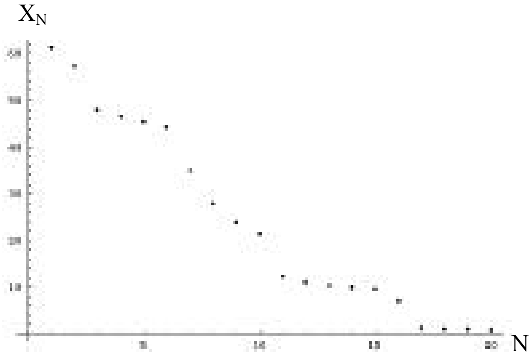

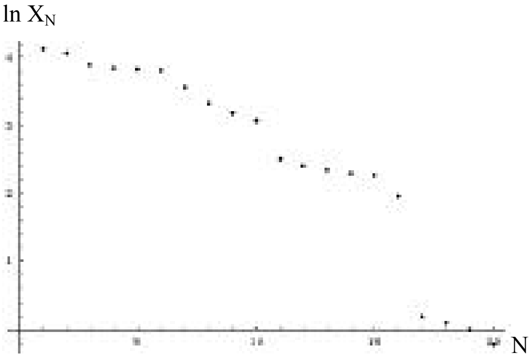

Fig.1. Relationship between N and x_N, where x_N, denotes the No. of pages (proportional to the No. of words) in Finnish–English Dictionary for the N-th most frequent word-initial consonants. "#"(in N={})= None.

x_N = {61.1, 57.2, 48., 46.3, 45.3, 44.2, 34.8, 27.7, 23.7, 21.3, 12.2, 11., 10.3, 9.9, 9.6, 7., 1.2, 1.1, 1., 0.8}

Table 1. Sound-correspondence laws of Finnish/Uralic word-initial consonants to Austronesian consonants. List of Uralic-Austronesian cognate words.

Abbreviations:
General: *xxxx = reconstructed form, "A < B", "B > A" = A has/had been derived from B, B has/had converted to B, "A < > B" = A is phylogenetically related to B. ; pXX = proto-XX (e.g., pURA, pAN, pEsk), dial.= dialect , Wr.= Written, Mod.= Modern, Mid.= Middle
Language nanes:
URA=Uralic: (1) FU=Finno-Ugric (Finn.= Finnish, Est.= Estonean, Lapp.= Lappish (N = Norwayish-Lappish dial.), Zyr.= Zyrian, Hung.= Hungarian), FV= Finno-Volgaic, FP= Finno-Permian. (2) SAM= Samoyedic.
AN= Austronesian : (1) FORM.= Formossan.
(2) MP = Malayo-Polynesian: W.MP= Western MP { Taga. = Tagalog, Kal.L.= Kalinga Limos, Sar.Blaan= Sarangani Blaan, Bang.Sama= Bangingi Sama, Goron. = Gorontaro, SND= Sundic (Minang.= Minangkabau, IndoN= Indonesian, Java.= Javanese, Bali.= Balinese) ; SLW= Sulawesi }, C.MP = Central MP (Mangg.= Manggarai), SHWNG = South Halmahera-West New Guinean, OC. = Oceanic [ADMI:= Admiralties, W.OC.= Western Oceanic, C.E.OC= Central-Eastern OC {NwCAL= New Caledonian, C.Pac.= Central Pacific (E.Fiji./W.Fiji. = Eastern/Western Fijian, MelN= Melanesian, PolyN= Polynesian)}].
Other languages: Esk= Eskimo, Esk-AL.= Eskimo-Aleut, ALT= Altaic, Trkc= Turkic, MONGc= Mongolic (Wr.Mong.= Written Mongolian), TNG= Tungus, JR= Japanese-Ryukyuan (Ml.Jpn.= Mailland Japanese, RYU= Ryukyuan), KOR= Korean, IE= Indo-European, MxZq= Mixe-Zoquean, STb= Sino-Tibetan, TbB= Tiberto-Burman
References: Most materials are obtained from; CAD*= Comparative Austronesian Dictionary (Tryon,1995), UEW*= Ualisches Etymologisches Wörterbuch (Rédei, 1988), CED*= Comparative Eskimo Dictionary, YH* = Nihongo no Tanzyou ("The Birth of the Japanese Language") (Yasumoto and Honda, 1978), MelL*= The Melanesian Languages (Codrington, R., Oxford, 1885), EML*= "Evolution of Mongoloid Languages" (Ohnishi, 1999)
Reconstructions: Redi* (from UEW*), Zorq*(from CAD*), Coh* (Cohen, E.M.K., "Fundermentals of Austronesian Roots and Etymology", ANU, Camberra, 1999), K.O.* (by Koji Ohnishi). ||| See EML* for other abbreviations not shown above.

1. [Finn.] m- |||| $ 1.1. [Finn.][Hung.] m- < [pURA] *m- < [pAN] *m- ; (W.MP) m- /[pEsk] *m- ||| # DAUGHTER-IN-LAW: [pURA] *minä || FU: [Finn.] miniä /[Hung.] mëny || SAM: [Yurak] ḿeje ||| W.MP: (SLW)[Uma] minia /[Wolio] mania
EARTH: [Finn.] maa "earth, land, country" ||| OC: (PolynN) [Tongan] maamani, maama "world" (< *maa-ma < *maa-maa < *maa)
to GO: [pURA] *mene- "to go" || FU: [Finn.] mene- /[Est.] min- /[Zyr] mun- /[Ostyak] mĕn- /[Hung.] mĕn- "to go" || SAM: [Kamas] mən- "to go" ||| W.MP: [Bugis] menreʔ "to go up" (< *men-reʔ < *men- "to go" + *-reʔ)) || OC: (W.OC)[Kilivila] -mʷena "to go up" (< * -mʷen-a), [Yabem] -mèŋ /[Kaulong] me "to come" ||| Esk-AL: [pEsk] *mənət- "to leave someone out during distribution", [Altiiq Alaskan Yupiq] məŋtə- "to go strait to destination without stopping"
to WASH: [pURA] *muśke- (mośke-) "to wash" || FU: [Finn.] ? /[Est.] mõske- /[Hung.] mos "to wash" || SAM: [jenisey samojedisch] musua- /[Selkup] muselǯa- "to wash" (UEW*, p.289) ||| W.MP: [pPHIL] *hiDamʔus /[Aklanon] hilaʔmus "to wash face" (< *hiDa-mʔus)

2. [Finn.] p- |||| $ 2.1. [Finn.] p- /[Hung.] f- < [pURA] *p- < (W.MP) p- < [pMP] *p- < [pAN] *p- ||| # to BLOW: URA: [pURA] *puwз- (*puɣз-) /[Mordvin] puva- /[Hung.] fúj "to blow" (<*puwa < *pua) || SAM: ||| OC: (W.OC)[Mekeo] e-pua /[Roviana] ivua /[Maringe] ifu "to blow" (< *i-pua ~ *e-pua) ||| [Ainu] pui-se "to blow as out of the mouth, to spray"
to DIG: [Finn.] päivä < *paiwa < *pai-a ~ *βai-a) ||| OC: (W.OC) [Motu] βai-a "to hollow out"(< *pai-a)
||| North Halmahera: [Sahu] paiti "to dig" (< *pai-ti).
HEAD: [pURA] *päŋe ~ *päŋ(e)a "head" (*päŋe, UEW*, p.365) || FU: [Finnish] pää /[Est.] pea "head" (< *pea < *peŋa, [Mordvin] pe, pä "end", [Hung.] fey, fő (accisative form: fejet) (< *peŋe-) ||| OC: (W.OC) [Manam] peŋa-na, paŋa-na "head" ; [Tolai] pepe "hair", pepe-ŋa-ulu "hair of head"
"HASELHUHN": [pURA] *piŋe (päŋe) "Haselhuhn" (< [pURA] *päŋe < *pəjŋə < *pəŋŋə < *päŋnə < *pəŋinə "hen") || FU: [Finn.] pyy /[Moldovin] povo "Haselhuhn", [Est.] püü "Feldhuhn", [Hung.] fogoly "Red- or Feldhuhn" || SAM: [Selkup] pēke, pēkä "Haselhuhn" (UEW*, p.383) ||| W.MP: (SND) [Bali.] pəŋinə "hen" (< *pəŋ-ninə < *pəŋ- "bird" + ninə "female" ; Cf. [Sasak] manuk ninə "hen = female chicken", manuk "bird".) ||| Gilyak: (Amur dial.) pəjŋa "bird"

bőr "skin, shell" (most plausibly, < *pőr, under the influence of *r*: UEW*, p.374) ; Probably related to; [Vogul] pār "Lappen", šašpār "bark" (UEW*) || SAM: [Koibal] pere "bark" ||| OC: (C.-E.OC, NwCAL) [Aji'e] pʌřʌ "shell" ||| ALT: (MONGc) [Wr.Mong.] arasu / [Mod.Mong] aris "skin" (< *ara-su < *para-su "bark ?" < *para- "skin ~ shell" + *-su "?")

3. [Finn.] v- |||| $ 3.1. [Finn.] v- /[Hung.] ø- /[Kamas] b- < [pFU] *v- (~ *w-) /[pSAM] *b- < [pURA] *b- (~ *β- ~ *v-) < [pMP][pAN] *b- |||| # ALL: [pURA] *ba(n)ćз "all" (Cf. *we(n)ćз , UEW*, p.568) || [pFU] *wećз / [Finn.] veśe, veśi, väśij /[Zyrian] vać "all", [Ostyak] wotśa "zusammen", ot'aśa "ganz" ; [Hung.] ősszе "together, all" || SAM: [Twg] bansa "all", [Kamas] bɯššа "ganz" (UEW*, p.547) ||| C.MP: [Roti] basa "all" || OC: (C.-E.OC)[Paamese] vasī "all" (< *basī), ?[Xaracuu] wani "all".
BELLY: FU: [pFU] *waća ~ *watta (or, *vaća ~ *vatta) (Cf. *waća, UEW*, p.547) "belly" (< [pURA] *watta /*vatta ~ *batta) ; [Finn.] vatsa, (dial.) watta "belly, stomach, inside", [Est.] vats (Gen. vatsa) "belly" ; [Vogul] vaś "stomach" ||| ?FORM: [Paiwan] vəçəkad-an "middle, center" (< *baCa- ~ *batta- ?) || W.MP: (SND)[Javanese] wətəŋ /[Balinese] basaŋ //(SLW)[Konjo] battaŋ "stomach" (< *battaŋ) || SHWNG: [Irarutu] ɸəta "stomach" ||| JR: [pJR] *batta /[RYU] (Yaeyaman) batta, bata, (Northern RYU) bata, wata "belly", [Old Ml.Jpn.][Ml.Jpn.] wata "bowels, cotton" ||| IE: [Shinhalese] bada "belly"
FIVE: [pURA] *bii-sí ~ *biju- (K.O.*) (< *bili- ~ *bili-su(g) "hand" < *bili-) "five" || FU: [pFU] *wiisí (< *biisig "hand") (Cf. [pFU] *witte (UEW*) < *wit-te < *wiis-t ~ *viis-t)) : [Finn.] viisí /[Est.] viis / [Lapp.] (Lule dial.) viht(t)a /(Notozero dial.) vīht, viht /[Mordvin] vet'e (< *viis-te) /[Chremis] (Uržum dial.) wić, wizə̑t /[Votyak] vit /[Ostyak] wet "five" ; [Hung.] öt "five" || SAM: [Enets] bjəʔn /[Kamas] bjəʔn /[Koibal] bet, bi /[Motor] bi (< [pSAM] *biet ~ *biit) "five" (UEW*, p.577) ||| ALT: (Turkic) [Uighur] biyeši /[Turkish] beş "five" (< *biy-eši < *bili- "hand") ||| ([Finn.] vii-sí < *vili-sí < *vili- "five, arm" < *bili) OC: (Santa cruz)[Nifole] vili //(Banks Islands)[Santa Matia(Lacon dial.)] tivilem /[Vanua Lava] 'evelem /[Melikolo] tavalim /[Santa Maria] tevelim //(New Hebrides)[Aurora] tavalima "five" (< *tava-lima < *tava "?" + *lima "hand") (Data from MelL*) || W.MP: [Tagalog] bīsig "arm" (< *biisig < *biisugi < *bili-sigi < *bili- "hand" + *siku(h) (= [pPHIL] *sikuh "elbow". Cf. (OC) [Leper's Island] bisugi "finger" < *bii- + *sugi ~ *sigi < > [Wolio] sigi "elbow".) || OC: [Kaulong] βili-n "hand" || OC: [Raga] bihu- "finger", [Saddleland] (Volow dial.) bihigi /[Leper's Island] bisugi /[Aurora] bisui "finger" (MelL*, p.43) (< *biisugi "finger" < *bili-sugi) ; (MelN languages from MelL*, pp.235-236.) (Santa cruz)[Nifole] vili //(Banks Lslands)[Santa Matia(Lacon dial.)] tivilem /[Vanua Lava] 'evelem /[Melikolo] tavalim /[Santa Maria] tevelim //(New Hebrides)[Aurora] tavalima "five" (< *tava-lima < *tava "?" + *lima "hand")
WATER: [pURA] *vu (< *bu) || FU: [Votyak] vu "water", [Finn.] vuotta- "to pour" ; [Hung.] önt "to pour" (probably, < *vu-ont) || SAM: [pSAM] *bu /[Kamas] bɯ /[Motor][koibalisch] bu "water" ||| W.MP: [Da'a] buvu (< *bubu < *bu) /[Gorontaro] butu "spring, well", [Uma] βuβu "well" ; (?)[Bang. Sama] bohe "water" || OC: [Yabem] bu "water" ; [E. & W. Fijian] βure "spring, well", (?)[Roviana] bukaha "spring bubbling out of ground" (< *bu-kaha ?)
$ 3.2. [Finn.][Hung.] v- < [pURA] *w- < [pAN] *w- |||| # WATER: [pURA] wit "water" < *weit < *wehit < *wahi- ?) || FU: [Finnish] vesi (Gene. *veden*) /[Mordvin] ved', väd' /[Zyr.] va /[Hung.] víz (< *wesi < *wehi- < *wahiR "water") || SAM: [Yurak] wit "water" ||| AN: [pMP] *wáhiR "fresh water" || W.MP: [Kagayanen] waig /[Bugis] wae (< *wai) /[Old Balinese] air < *aiR) /[Madurese] aiŋ "water" (< *waiR < *wahiR) || C.MP: [Mangg.][Ngada] vae "water", [Buru] wae "water, river" (< *wai) || OC: [Raga] wai /[E.&W. Fijian] wai /[Tongan, Samoan] vai "water", [Paamese] oai (< *uai < *wai < *wahiR) ; [Lewo] wī /[Nemi] we /[Mekeo] vei, ui "water"(< *wei < *wai) ||| JR: [Ml.JPN] wi, wi-zu-mi /[Ryukyuan] (Tokunoshima dial.) ʔiʒuN (< *ʔi-ʒu-mi) "well, spring" < [pJR] *wi /[pMl.Jpn.] *wi /[pRyu.] *ʔi "well, spring" < *wī < *wei < *wai < [pAN] *wáhiR "water")
SMALL/LITTLE/FEW: [Finn.] vähä /[Est.] vähe ||| OC: [Cemuhi] wáhin
SMALL: [Mordovin] viška "small" ||| OC: [Roviana] visvisa "little (quantity)" (< *vis-visa < *visa)

4. [Finn.] t- |||| $4.1. [Finn.][Hung.] t- < [pURA] *t- < [pAN] *t- ||| # to COME: [pURA] *tule- /[Finn.][Est.] tule- "to come" ||| W.MP: (SLW) [Uma] tu-mai "to come" ||| Note: Cf. [Finn.] tulla "to come" (< *tu-lla < *tu- "come" + *-lla "to go, to walk") ||| W.MP: [Batak Toba] laɔ /[Bugis] lao /[Sasal] lalo "to go" || C.MP:

Table 1. (Continued.)

[Ngada] laʔa "to go, to walk" || OC: [Manam] alale /[Mbula] -la /[W.Fijian] lā "to go"
FEATHER: [pURA] tulka "feather, wing" (< *tul-ka < *tolu "bird" (< "egg") + *-ka) ; [Lapp.] dol'ge /[Mordvin] tolga /[Hung.] toll (dialogs; tollu, tolu, tolyu, etc.) : [Finn.] sulka "feather" (< *tulka) ||| C.MP: [Dobel] toru "fowl", [Roti] manu-tolo "egg" || W.MP: [Murut] taluʔ /[IndoN] təlur /[Sasak] təlo /[Da'a] tolu /[Uma] ^{n}tolu /[Wolio] o^{n}tolu "egg" ||| JR: [Ml.Jpn.] tori "bird"
FIRE: [pURA] *tule /[Finn.] tuli /[Hung.] tüz /[Samoyed] tū "fire" ||| W.MP: [Goron.] tulu "fire" ; [Palawan, Molbog, Batak Toba] tutuŋ /[Wolio] tunu "to burn (v.t.)" || OC: [Mbula][Yaben] -tuŋ "to light, to ignite" || FORM: [Atayal] ma-čuɬiŋ "to burn (v.i.)", ši-čuɬiŋ "to burn (v.t.)"
to KILL /to STRIKE: [pURA] *tappa- "mit dem füβen stampfen, schlagen, klopfen"|| FU:[Finn.] tap-pa- "to kill", [Zyr.] tap-tap kar "einigemal klopfen,, schlagen" (kar- "to do, to make") || SAM: [Yurak] tapar- "mit dem Fuss treten, stoβen" ||| W.MP: [Isnag] tappit "to strike, to beat" (< *tap-) ||| IE: [Old French] taper "to tap"

<u>5. [Finn.] n-</u> ||| $ 5.1. [Finn.] n- < [pURA] *n- < [pAN] *n- |||| # FOUR: [Finn.] neljä /[Est.] neli ||| OC: (W.OC)[Kaulong] nal, mnal (< m-nal)
to SEE: [Finn.] nähdä "to see" ||| ?W.MP: [Da'a] naᵑgita "to see"
SUN: [Hung.] nap ||| OC: [Kwaio] napʷ "fire"
WOMAN/WIFE: [pFU] *naje "woman, wife, fire" (< *naŋe "fire, sun" < > [Buang] naŋʷaɣ "fire") ; [Finn.] nainen /[Est.] naine "woman" ; [Ostyak] (Vach dial.) näj "lady, fire, sun", näj-öɣi "fire" (öɣi "Tochter, Mädchen") ||| OC: [Buang] nəŋʷaɣ "fire" (< *naŋ-waɣi < *naŋ- "fire ~ sun" + *uagi "wife ?". || W.MP: [Buang] nəŋʷaɣ "fire" (< *naŋ-waɣi < *naŋ- "sun ~ fire" + *waɣi "wife ?", where *waɣi < *uaɣi < > (SHWNG)[Irarutu] a uagə "wife" (< *uagi ?), and where *naŋ- "sun ~ fire" is related to (OC)[N.Tanna] naŋam /[Kwaio] napʷ "fire" and (URA)[Hung.] nap "sun".) ||| STb: [pTbB] *nəy "sun, day" (< *naŋ- "sun ~ fire")

$ 5.2. [Finn.] n /[Zyr.][Mordvin][Yurak] ń- /[Kamas] n- < [pURA] *ń- < [pMP] *ŋ- |||| # to LICK: [pURA] *ńole //(FU)[Finn.] nuole- /[Hung.] nyal- //(SAM) [Selkup] ńu- /[Kamas] nɯ- "to lick" (< *ŋole) ||| OC: [Port Sandwitch] ŋole "to lick"
NAME: [pURA] *nime (or, *nime ~ *nəme ?) "name" || FU: [Finn.][Est.] nimi /[Ostyak] nem [Votyak] ńim, ńem /[Hung.] név || SAM: [Yurak] ńim /[Kamas] nim, nəm "name" ||| OC: [Cemuhi] nî /[Xaracuu] nĩ /[Ajie] nē "name" ; [Yabem] ŋae "name" (< *ŋaa < *ŋara-n < *ŋaɬan < [pAN?] (Zorq*)] *ŋájan /[pAN] *ŋáZan (K.O.) "name") || C.MP: [Buru] ŋaa-n /[Sika] nara-n /[Ngada] ŋaza "name" || W.MP: [Yami] ŋaẓan /[Molbg] ŋadan /[Aklanon] ŋaɬan "name" ||| Turkic: [Chuvash] yat /[Uighur] at /[Turkish] ad "name" (< *ŋad) ||| JR: [Ml.Jpn.] na "name" (< *ŋa)

$ 5.3. [Finn.] n- /[Hung.] m(y)- < [pFU] *ń- ((OC) ŋ- ?) ||| # ARROW: [pFU] *ńōle (UEW*) ~ ńuole /[Finn.] nuoli /[Hung.] myil "arrow" (< *ŋōle ~ *ŋuole < *ŋu- "arrow" + *(o)le "bow") ||| OC: [Mekeo] ŋuŋu "arrow" || C.MP: [Ngada] leʔe "bow" (< *lele ? < *le "bow")

<u>6. [Finn.] l-</u> |||| $ 6.1. [Finn.][Hung.] l- < [pURA] *l- < (MP) *l- ||| # BIRD: [pFU] *lintu /[Finn.] lintu /[Estonean] lind "bird" (< *lindu(ŋ) "cook") ||| W.MP: [Sar. Blaan] lunduŋ "cook, rooster" (< *linduŋ)
BONE: [Finn.] luu ||| C.MP: [Sika] luri-ŋ
to FLY: [Finn.] lentää "to fly" (< lentä- < *leŋ-te- < *leŋ- "to jump" + *-te(ŋ) "to fly, to jump") //// (1) *leŋ- "to jump" ||| W.MP: [Sasak] leŋkak-aŋ "to jump" (< *leŋ-kak-) || OC: [Samoan] lele /[Tahitian] rere (< *le-le < *le-) "to fly" //// (2) *-te(ŋ) "to fly, to jump" ||| OC: [Cemuhi] tȅ "to fly", [Kaulong] teŋ "to jump" || W.MP: [Uma] ᵑkali-tene "to jump" (< *-te-ne) # to SEE: [Hung.] lát- "to see" (< *liat) ||| W.MP: [Bali.] ŋ-liat "to look, to look at"
SOUL: [pURA] *lewlз "soul, air, breath" || FU: [Lapp.] (N) lewˈlu "vapour-bath" (< *lewˈleu "vapour" < *laulau "soul"), [Finn.] lõyly "Badehitze;vapour"; [Votyak] lul "breath, air, soul, ghost, mind, heart, life" ; [Hung.] lélĕk "soul, ghost, mind (Gemüt), heart, peraon" || SAM: [Yurak] lũl, jũl (probably, < *lũl) "smoke" ||| OC: (W.OC) <u>[Mekeo]</u> lau-lau "spirit, soul, image, idea, reflction, shadow, aura", (North-Western Mekeo) laulau "ghost", (Eastern Mekeo) laupa "presence, aura" ; [Motu] lauma (< *lau-ma) "soul, spirit" | (C.-E.OC, Polynesian) [Tongan] laumālie "soul, spirit"

$ 6.2. <u>[Finn.] -ll-</u> < *lVl- < *d_2Vl- (V = vowel) **||||** # INSIDE: [Finn.] -llä, -lle "inside" ||| AN: [pAN] *d_2á+lem + i- "inside" || W.MP: [Kal.L.] dālom / [Murut] da dalom /[IndoN][Minang.] di dalam /[Madurese][Sasak] daləm /[Bugis] ri-laliŋ /[Konjo] i-lalaŋ /[Uma] rala "inside, in" || C.MP: [Buru] lale-n "inside, in" || [Mbula] lela /[Yabem] lelom /[Mot] lalo-nai /[Lau] ilalo /[Rotuman] laloŋa "inside, in"

<u>7. [Finn.] r-</u> ||| $ 7.1. [Finn.] r- < [MP] *r- ~ *R- |||| # to FLY: [Finn.] räppä (Gen. räpän) "knappernder Schlag", räpyttä- "to flatter" ; (?)[Hung.] rĕpít- "(auf)-fliegen lassen, rĕpül "to fly" ||| W.MP: (SLW)<u>[Konjo]</u> ʔa-ribbaʔ "to fly" (< *-ribbak < [pMP] *Rebbek "to fly" < *Reb-baek)
?# FOX: [pFU] *repä /[Finn.] repo /[Est.] rebane /[Lapp.](N) riebân "fox" ||| ?W.MP: [IndoN] rubah "fox"

$ 7.2. [FU] r- < (MP) r- < [pAN] (Zorc*) *d_2-. [pMP](Dem*) *d- |||| # WARM/HEAT: [proto-Ugric] *reŋз (*rekз) "warm, heat" (< *räŋi < [MP] *raŋi "hot, to heat" ; [Ostyak] (O.) răw "heat", [Vogul] räj "warm, heat" ||| [pAN] (Zorc*) *d_2a(ŋ)-d_2aŋ "to heat, to warm oneself by fire", [pMP](Dem*) da(n)daŋ "to heat" || W.MP: [Wolio] ma-rani "hot" (< *rani < *rani ~ *raŋi) || OC: [Raga] raraŋi "to roast" (< *ra-raŋi "to roast" < [pMP(K.O.)] *raŋi ~ *laŋi ? "to heat; hot")

$ 7.3. [pFU] *r- < [pMP] *z- (Zorc*), *d'- (Dem*) |||| # [pFU] *rakka "near" ; [Finn.] rakas (Gen. rakkaan) "lieb, innig, befreundet, geliebt" ; [Lapp.] (N) rakkes, rakˈkas "dear, actionate, loving", (L) rāhkēs "verliebt" (< *rāh-kēs < *raN-kas < *zaNi "near" + *-kasu "near") ; [Hung.] rokon "near" ||| AN: [pAN] *zaNí "near" ([pMP](Dem*) *ɗahit "nähen") || W.MP: (PHIL) [Isnag] adanni /[Kal.L.] adani /[Kaga] dani "near" (< [pAN] *zaNí "near" (< *zanni ?) ; (SND) [IndoN] dəkat][Minang.] dakeʔ /[Sundanese] dɨkɨt "near" (< *daŋ-kat < *zaN-kat) ; (SLW) [Wolio] ma-kasu (< *kasu) "near" || C.MP: [Buru] b-raŋi-n "near" (< *-raŋi- < *zaNí), [Dobel] ren "near" || SHWNG: [Sawai] rakɛn (< *dake-n) || OC: [Maringe] ɽeña "near" (< *deNa < *zaN-a)

<u>8. [Finn.] s-</u> ||| $ 8.1. [Finn.][Zyr.] s- /[Chremis] š- /[Hung.] ø- /[Kamas] t- < [pURA] *s- < (W.MP) *s- < [pAN] *s- |||| # BLOOD VESSEL: [pURA] *sẹne (šöne) /[Finn.] suoni / [Churemis] šũn /[Zyr.] sẹn "blood vessel, sinew", [Hung.] ín "sinew" ||| OC: [Mbula] siŋi- "blood" ||| TNG: [Wr.Manchu.] seŋgi "blood" ||| IE: [Old English] sinewe (oblique form of *seonu, sinu*) "sinew"
BLOOD VESSEL: [pFU] *särз (< *serз) "blood vessel, vein, root", (FU)[Chremis] šär, wũr-šer /[Votyak] ver-ser /[Hung.] ér "blood vessel, vein" (< [pFU] *ver-ser ~ *wũr-ser <blood" + *ser "rope") ||| OC: [E.Fijian] sere-ka /[W.Fijian] here-kia "to unite" (< *sere-kia < *sere- "(probably,) rope")
Note: Cf. Unrelated to; [Ponnapean] salī "to tie, to bind", [Ponn.] sal /[E.Fiji.] dali /[W.Fijian] tali /[Java.] tali /[Paiwan] ¢aļis "rope" (< [pAN] *CaliS "rope")
CHACOAL: [Twig] simi "Kohl" ||| W.MP: [Konjo] sumiʔ "charcoal" ||| [Jpn.] sumi "charcoal"
FECES: [pURA] *sitta (< *sikta) "feces, excrement", (FU) [Finn.](dial.) sitta /[Est.] sitt "feces (Dreck)", [Lapp.] sikta, siksta "feces of anilals (Losung)" | (SAM)[Selkup](Ket-dial.) tytti "Kot" ||| OC: [Tongan] siko /[Mele-Fila] jiko "to deficate"
to ROW: [pURA] *suɣe- (< *su-ɣe) //(FU)[Finn.] souta- /[Chremis] šua- /[Vogul] yow- //(Samoyedic)[Selkup] tua- /[Kamas] tu- "to row" ||| OC: [Rotuman][Mele-Fila] sua /[Raga] hua "to row"
SISTER(of father or mother) /AUNT: [pFU] *säće "sister (of father or mother)" (< *ʔasasi); [Lapp] siessa "father's sister, parental aunt", [Zyr.] soć "sister" ; [Ostyak] śaśə "yonger sister of mother" ||| OC: [Rotuman] sɔsiŋa "yonger sister" || C.MP: [Dobel] ʔasasi "aunt" ||| IE: [Eng.] sis-ter /[Old Norse] systir "sister"
?# SKIN / BARK: [pFU] *śuka "skin, bark" ||| Tungus: [Wr.Tungus-Manchu.] sukû "skin" ||| AN: [Takia] sukulo-n "skin"

$ 8.2. [Finn.] s- < [pFP] *s- < *S- |||| # FLESH: [pFP] *siwз-lˈз "flesh" (*siwз- < [pFP] *siwə- < *siə < *Siə ~ *Ssiə) < [pAN?] *Sisi "meat, flesh" ~ *Si- "meat ?". cf. [pAN] *Si-káʔen "fish" < *Si- "meat "?" + *káʔen "to eat") ; [Mordvin] sivel', śivel' / [Chremis] šəl, šə̃l, śil' "flesh" ||| W.MP: [Aceh] siə "meat" ; [Yami] aşişi /[Bang.Sama] [Da'a] isi "flesh", [Konjo] assi "meat" || C.MP: [Ngada] isi /[Roti] isi-k /[Buru] isi-n "flesh" ||| JR: [Ml.Jpn.] sisi "wild bore, deer, lion" (< *Sisi "meat") ||| STb: [pTbB] *sya-n (< *Sia)"animal, flesh, meat", [Old Chinese] śióg "animal" (Matsisoff*, p.162, p.177)

$ 8.3. [Finn.] s- < [pAN] *C- |||| #SMOKE: [Finn.] savu (< *Cavu < *Cavu) ||| [Paiwan] ¢avulʸ "smoke"

$ 8.4. [Finn.] s- (< [pFU] *ś-)

$ 8.4a. [Finn.] s- /[Hung.] sz- < [pURA] *ś- < *d_2- |||| # to PUSH: [pFU] *śurwa- /[Finn.] survaa- /[Chremis] šure- "to push", [Hung.] szúr- "stechen" ||| FORM: [Paiwan] z-əm-uruŋ "to push" (< *$d_2$uruŋ) || W.MP: [IndoN] mən-doroŋ "to push" || C.MP: [Mangg.] dūr "to push" || OC: [Tawala] dudu /[Roviana] dudua

Table 1. (Continued.)

"to push" || Note: Cf. W.MP: [pW.MP] *suruŋ "to push foward", [Madurese] suruŋ /[Sasak] soroŋ "to push"

??$ 8.4b. [Finn.] sy- < [pFU] *śi- < (MP) *ti-

EYE: [pURA] *śilmä /[Finn.] silmä /[Hung.] szëm /[Koibal] sima "eye" (< *śil-mä < *sil-mä ~ *til-mä < *sil- ~ *til- "to see ~ to look at" + *-mä "eye") ||| OC: [Samoan] sila-sila "to see" (polite), [Mele Fila] sirea /[Tongan] sio "to see", [Samoan] tolo-tilo "to look at" || Note: *-mä "eye" cognates with; OC: [Lau][Kwaio] mā /[Marshallese] mæc (< [pAN] *maCa) "eye", or [Paamese] me-tok /[[Ajie] pie-mɛ "eye"

SPIT(TLE): [pFU] *śilʲke, *śülʲke /[Finn.] sylki, sylke- /[Est.] sülg "spit, spittle", (< *śilkü < *tiliku "spit") ||| W.MP: (SLW)[Uma] n-tiliku "spit"

$ 8.5. [Finn.] su- < [pURA] *ću- < (MP) ču- |||| # FLEA: [pFU] *ćoŋča ||| W.MP: [Bugis] čuŋŋo ||| ?STb: (pTbB] *dyuŋ

HILL: [pURA] *ćukkз "hill, Spitz", [Lappish] (Nothern dial.) čokʲkâ-kk- "summit, mountain top", [Finn.] (?) sukki "spitzfindig, listig", [Zyr.] čuk "bugor (б у г о р)" ||| W.MP: [Sundanese] ñuŋ-čuŋ (< čuŋ-čuŋ) /[Madurese] kuñ-čuʔ "pointed", [Bali.] mə-muñ-čuk "having a pointed extremity", [Sar.Blaan] tukəʔ "tip"

NARROW: [pFU] *ćuppa /[Finn.] (?) suppa "narrow" (< *čup-pa) , [Zyr.] śopi̮d "eng, dicht" (< * ||| W.MP: [Kalinga Limos] sūpit /[Batak Toba] sↄppit /[Bali.]čupit /[Java.] səmpit "narrow", ([Konjo] seppaŋ "narrow")

<u>9. [Finn.] h- (< [pFU] *č-)</u> |||| $ 9.1. [Finn.] h- / [Votyak] (Kazan dial.) ž- /[Ostyak] č- < [pFU] *č- < (W.MP) t-, č- /(FORM)[Paiwan] *ḑ- < [pAN] *dʒ- ||| # BACK: [pFU] *čänčä "back (Rücken)" , [Finn.] häntä /[Est.] händ "tail", [Ostyak] čĕṇč "back (Rücken)" ||| W.MP: [Java.] čəŋəl /[Isnag] taŋŋad /[IndoN] təŋ-kuk "nape", [Madurese] təŋŋa "back" || C.MP: [Mangg.] təŋu "nape" || FORM: [Paiwan] ḑəŋəḽan "nape"

to CHOKE (ersticken), to be DROWNED: [pFU] *čäkkз- "to choke, to be drowned" (< "narrow") , [Votyak] (Kazan dial.) žə̂kal- "to choke, to be drowned", žə̂kə̂t "narrow, thick", [Zyr.](Sysola dial.) ʒagal- "erhängt", [Ostyak] čäkən- "to choke" ||| W.MP: [Bugis] ma-čikke "narrow" || OC: [Ponapean] ţiki-ţik "small", ā-ţikiţik "slender"

WARM/ DUMP: [pFU] *čenke "dump, warm" (< *čen- < *dəŋ- < *(a-)ḑaŋ- < *ḑaŋə < *ḑaraŋə "hot ?"), [Finn.] henki "breath", [Votyak] žog "very warm, drückend heiss", [Ostyak] čeŋk "warm, heat" ||| OC: [E.&W. Fijian] ðeŋu "breath", [Yabem] (ŋ-)aⁿdaŋ "hot", ?[Woleaian] yaŋi "air" (< *daŋi ?) [|| FORM: [Rukai] n-ḑaraŋə-ḑaŋə "hot"

$ 9.2. [Finn.] ? /[Zyr.][Votyak] š- /[pFU] *č- < *š- < *sy- ||| # SOUR: [pFU] *čemз- "sour" (< *šem < *asyem < *asiem < *asilem < *ha-silam < [pAN] *qa-silam "sour".) ; [Votyak] šę̈m, šə̂m "sour", [Zyr.] šu̇m "acid (noun)" ; [Ostyak] č im "gären" ||| [pAN(Zorc*)] *qal+sem (< [pAN(K.O.)] *qa-silam) /[pHN] *la + sem "sour" || W.MP: (PHIL)[Taga.] asim /[Akl.] aslum /[Kal.L.] sīlom "acid, sour" (< *a-silom < *ma-silam ?) ; (SND) [Sundanese] hasɨm /[IndoN] asam /[Bali.] masəm (< *hasiam < *qa-silam "sour") || Note: Possibly cognates with; ALT: [Mod.Mong.] čuu "sour" ||| JR: [Ml.Jpn.] su- "acid, sour" (< *(a)sum < *(qa)sillam ?).

<u>10. [Finn.] k-</u> ||| $ 10.1. [Finn.] k- / [Hung.] h- < [pURA] *k- < [pMP] *k- || [pESK] *q- ||| # BACK: [pURA] *kutt3 "back, behind" ; [Ostyak] (Jugan dial.) kutəʌ (juw kutəʌ-nə "im Schutz des Baums"); [Vogul] (Pelymka dial.) kūtəɣ "im Schatten, im Schutz" : [Hung.] hát "back, behind" (UEW*, p.225) ||| W.MP: [Minang.] kuduᵊʔ / [Aceh] kudoʔ "nape of neck" || C.MP: [Ngada] koti "nape of neck" || OC: [Nengone] wakod "nape of neck" (< *wa-kod), haḓi "north" (probably, < *kaḓi "behind") || Note: Further cognates with; [pAN] *likúd "back" (< *li-kúd) || (W.MP)[Yami] likoḓ "back", [Isnag] likud /[Aceh] likot "behind", [Taga.] likod /[Akl.][Paqlawan] likud "back, behind" ; (?)[Kal.L.] lāgud "north" (< "behind, backwards") || OC: [Marshallese] lik "behind".

EAR: [Finnish] korva (< *koru-a ~ *kor-va) ||| FORM: [Tsou] koru

FISH: [Finn.] kala /[Hung.] hal ||| ESK-AL: [pESK] iqałuɣ /[GRI] iqaluk "fish (esp. salmon)" (< *ikałuɣ) ||| W.MP: [Kal.L.][Minang.][IndoN] ikan || C.MP: [Ngada][Buru] ika || OC: [Tongan] ika /[Manam][Lau] iʔa ||| JR: [Jpn.] ika "squid" |||[Gilyak] kalim "whale" ||| [Mongolian][Manchurian] kalimu "whale".

to HEAR: [Hung.] hall "to hear" (< *kall), [Nenets] ha (= xa) "ear" ||| W.MP: [Bang.Sama] kale /[Bugis] eŋ-kaliŋa "to listen" || OC: [Dami] karĩ "to listen"

Note: Cf. [Finn.] kuule- /[Mari] kola- "to hear".

SKIN: [Finn.] kuori /[Est.] koor "skin", [pURA] *kora (UEW*), *koora (K.O.*) (< *kuora) "skin" ||| OC: [Kiribati] kuora "to peel"

$ 10.2. [Finn.] k- /[Hung.] h- < [pFU][pURA] *k- < [pAN] *q (FORM: [Atayal][Pai.] ķ- (= q-), [Tsou] ø- | W.MP: [Sundanese] h-, [Kal.L.] g-, [Yami][Taga.][IndoN] ø- | OC: [Tolai][Kilivila][Mbula] [Motu][Nemi] k-, [Tawara][Nengone] g- , [Tongan] ʔ, [Takia] ø-) || [pEsk] *q- ||| # ASHES: [Finn.] ? /[Hung.] hamu (< *kamu < *qaβu ?) ||| [pAN] qabúH || FORM: [Atayal] ķaβu-ɬiʔ /[Paiwan] ķavu /[Tsou] fū || W.MP: [Kal.L.] gabu /[Akl.] abuh /[Taga.] abo /[Molbog, Sar.Blaan, Minang., IndoN, Bali.] abu /[Java.] awu "ashes" || OC: (W.OC) [Tolai] kəbu /[Tawala] gahuwei /[Motu] kahu

Note: Etymology in UEW*, p.194, is probably wrong.

APEX /WOODPECKER: [Finn.] kärki (Gen. kärjen) "point, apex, tip, end; woodpecker", kärjekäs "pointed" (< *kärj-ekäs < *kärj- < *qali-) ; [pFV] *kärke /[Est.] kärg (Gen. käru) /[Chremis] keryе "woodpecker" (< [pURA] *kär(i)ɣe) ||| Esk-AL: [pEsk] *qalliʀ or qaðliʀ topmost or outermost thing"; [SPI] qalliq /[GRI] qaɬɬiq "topmost one, scab" ||| FORM: [Paiwan] ķaḽiw "top"

BELLY: [pFU] *kač3 ""Etwas gebogenes" (< "belly" < "liver") (< *qacy < *qaCey "liver") ||| [Hung.] has "belly" ||| [pAN] *qaCéy "liver" || FORM: [Paiwan] ķaȼay "liver" || W.MP: [Sundanese] hati /[Yami, Taga., Aklanon, Kaga., Bang.Sama] atay /[Aceh, Sasak, Konjo, Da'a] ate /[Malagasi M., Minang., Bali.] ati "liver" || C.MP: [Mangg.] ati /[Ngada] ate /[Roti] ate-k "liver" || OC: [Tolai] kati- /[Kilivila] kate- /[Takia] ate-n /[Mbula] kete- /[Nemi] kec /[Nengone] guat /[Tongan] ʔate "liver" ; [Aceh] boh ate "kidney"

Note: Cf. Might cognate with; [Votyak] (dialects) gač, gaš "auf dem Ruecken liegen" ||| OC: [Nengone] guat "liver"

(?)# to BITE: [Hung.] harap- "to bite" (< *hara-p- < *gara- ~ *qara-) ||| W.MP: [Batak Toba] harat "to bite" (< *qarat) || C.MP: [Dobel] ʔa-ʔara "to bite" ||| OC: [Manam] ʔarati "to bite" ||| Note: Cf. Possibly related to; OC: [Adzera] gara- /[Tolai] kərət /[Roviana] ɣarata "to bite".

TASS /HAND: [pFW] käppä /[Est.] käpp (Gen. käppa) "tass, hand", [Mordvin] kepe, käpä "barfuss" ||| FORM: [Atayal] ķaβaʔ "hand, arm" || OC: [Lau] ʔaba "hand, arm", [Rotuman] ʔu-hapa "hand" (< *-hapa < *qappa)

$ 10.3. [Finn.] k- /[Hung.] k- < [pFU] *k- < (OC) *g- ||| # HAND: [Finnish] käsi /[Hung.] kés "hand" (< *gesu "wrist" < *lima-gesu "wrist = hand-neck") ||| OC: [<u>Yabem</u>] lima-gesu "wrist" (lema "hand" + gesu "neck")

ROUND: URA: (FU) [pFU] *kerä (< *geri- ~ *gere- < *gele-) //[Finn.] kiereä /[Hung.] kerek "round", [pFU] *kere "circle, ring" ||| AN (C.MP)[Manggarai] gelep //(OC)[Kwaio] gari (< *gəri) "circle"

STONE: [pFU] *kiwe (< *give < *gibe ~ *kibe) /[Finn.] kivi (genetive: kiven) /[Vogul] (dialects) küv, käv /[Hung.] kő "stone" ||| W.MP: [Sar.Blaan] kbɨ "cliff, presipice" || OC: [Ajie] gʷẽ̃wɛ "mountain, hill" (< *givɛ < *kibɛ ?) ||| JR: [Ml.Jpn.](Shikoku dial.) kibu- "steep (of rocky mountain)"

<u>11. [Finn.] h- (< *h-)</u> ||| $11.1. (?) [Finn.] h- < [pURA] *h- (K.O.) < (MP) *h- ||| # TOOTH: [Finn.] hammas "tooth" ||| OC: [Roviana] hamhamu "to chew"

AIR: URA: [Finn.] höyry "air" (< *höy-ry < *höŋ(i)-rŋ(i) ? < *hāŋi-lŋi < *hāŋi-ləŋi ? < *hāŋi- "air" + *-laŋi "sky, wind") ||| W.MP: [pMP] *háŋin "air" : [Tagalog][Aklanon] hāŋin /[Isnag] [Kagayasnen] āŋin /[Kagayanen] [Murut] [Balinese] aŋin /[Konjo] aŋiŋ "air, wind" , [Aceh] aŋɛn /[Minangkabau, Sundanese, Javanese, Balinese, Sasak] aŋin /[Bugis] aŋŋiŋ "wind" || C.MP: [Sika] ani-n /[Roti] anin "wind" ||| ALT: [Wr.Mong.] aGar / [Mod. Mong.] а г а а р "air" (< *aŋar < *aŋal < *aŋ-alʸ ? < *aŋ- (< *hāŋi- "air") + *alʸ, where *alʸ < *aly < *aləŋ < *ləŋi "sky, wind" ?) ||| ?[Quechua] wayra "air" (< *hāyra < *hāŋ(i)-ra ?)

<u>12. [Finn.] j-</u> ||| $ 12.1. [Finn.] j- < *j- < *ǰ- (< *D-) ||| (OC) j- (= y-) ?, (W.MP) [Sundic, Slawesh] ǰ-, (C.MP) ǰ- ||| # to DANCE: [pFU] *jekk3 "to dance" (< *jegg3 < *jegt < *jeget < *ǰoget "to dance") ; [Votyal] ekt- /[Zyrian] jǒkti "to dance", [Ostyak] jek̥ , jok "dance" ||| W.MP: [Sasak] ǰoget /[Konjo] aʔ-ǰoge "to dance" || ?OC: [Kaulong] yik "to dance" (< *yek ? < *yege < *ǰoge)

RIVER: [Finn.] joki "river" ||| C.MP: [Mangg.] ǰōk "gulf, bay" || OC: [Mbula] yok /[Takia] you "river, stream" ; [Ajie][Xaracuu] ɟↄ "to flow"

Note: W.MP: [Yami] ayo "river, stream"

ROOT/ NEWLY: [pFW] jure "root" (UEW*, p.639) ; [Finn.] juuri "root, foot, origin, ground; just, newly, freshly" (probably, < [pURA] *juu-ri < *ǰulu- "new" < > [Minang.] ǰoloŋ "new"), [Est.] juur "root" ||| W.MP: [<u>Minang.</u>] ǰoloŋ "new" (< *ǰoloŋ ~ ǰuluŋ < [pMP] *Doloŋ ~ *Duluŋ) ||| [pIE] *i̯uwn̥-ti "youth" (< *juuŋ- <

Table 1. (Continued.)

*ǰuuŋ < *ǰuluŋ "new" < > [Minang.] ǰoloŋ) ||| JR: [Ml.Jpn.] yuri "lily" (< *juu-ri "root (of lily)" < *ǰulu- "new")

SWAMP: [pURA] *jäŋkä "swamp" ||| W.MP: [Konjo] ǰanna ~ ǰenna "inland, fresh water"
Note: Might cognate with; (W.MP)[Bali.] danu /[Minang.][Aklanon] danaw "lake"
Note: Cf. (C.MP)[Dobel] yek^{w}al "swamp".

$ 12.2. [Finn.][Hung.] j- < [pAN] *Z- ||| # to WALK /FOOT: [Hung.] jär "to walk" (< *ǰala < *Zalan), [Finn.] jalka /[Est.] jalg "foot" (< *jal-g), jalan "on foot" (< *jal(a)- "to walk" < *Zalan "road") ||| [pAN] *Zalan "road" || W.MP: [Batak Toba] mar-dalan /[Bali.] mə-ǰalan /[Madurese] ǰ^{h}alan /[Minang.] ba-ǰalan /[IndoN] bər-ǰalan "to walk" ; [Chamorro] chalan / [Kal.L.] dālan /[Molbog][Murut][Java.] dalan /[Minng.] ǰalan /[Da'a] ǰala /[Wolio] ɗala "road" || C.MP: [Ngada] zala /[Sika] lala-ŋ /[Mangg.] salaŋ / [Dobel] sala "path" || OC: [Nyindrou] san /[Takia] dal /[Mbula] zāla /[Motu] dala /[Lau][Kwaio] tala /[Raga] hala /[Woleaian] yařa /[Tongan] hal "road, path" ||| [Ainu] ra "passage" (Bachelor, 1938)

<u>13. [Finn.] y-</u> || $ 13.1. [Finn.] y- /[Hung.] ē̈- ~ é- < *i- ~ *yi- ||| # to DRINK: URA: [pURA] *ir3- (ür3-) || FU: [Mordvin] iŕed'e- (< *(y)ir-) || SAM: [Taiga] örsu- ||| OC: [Marshallese] irāk /[Woleaian] üřümī (< *ir- ?) || W.MP: [Gorontaro] moŋilu (= yilumo + moN-)

NIGHT: [pFU] eje (üje) "night" (< [pFU] *idjâ (K.O.) < *idjiaŋ < > [Adzera] i<u>dz</u>iaŋ "night") ; [Finn.] yö /[Est.] öö "night", [Lapp] (dialects) iggjâ, idja, ijj, éjj "night" (ijj < *üjja < [proto-Lapp.] *üdjâ ~ *idja "night" < i<u>dz</u>ia-ŋ "night"), [Hung.] éj, éjjel "night" ||| OC: [Adzera] i<u>dz</u>iaŋ "night" ||| JR: [Old Ml.Jpn.] yö /[Mod. Ml.Jpn.] yo "night"

MALE PERSON, SON: [pFU] *irkä (ürkä) "male person (Mann), son" (< *yir-kä ~ *yer-kä), [Finn.] yrkä "Junggesel, Freier", yrkö "male person (Mann)" ; [Chremis] erɣə "son" ; [Hung.] -ĕr, -ér "parson (Mensch), male person (Mann)" ||| C.MP: [Dobel] yil "man (male)" || OC: [Lewo] yerim^{w}ene /[North Tanna] [Kwaio] ierman "man (male)" (< *yeri- ~*ieri- "man (male)")

ONE: [pFP][pFU ?] *ikte (ükte) "one" (< *ik-te ~ *yik-te < (OC) *ik- "little" + *-te "?"), [Finn.] yksi /[Est.] üks /[Chremis] (dialects) ik', ikte, iktət "one" ||| OC: [Tolai] ik "little (of amorphous stuff)"

<u>14. [Hung.] ø-</u> || $ 14. 1. [Finn.] ? /[Hung.] øu- < *yu- < *diu- < [pAN] *diRu- ||| # to BATHE: [Hung.] usz-kal "to bathe", usz-as "bathing (n.)" (< *usz- < *yus- < *ǰus < *dus < *dius < *diʔus < *diRus "to bathe") ||| Turkic: [Turkish] yüz-me "to bathe" ||| JR: [Ml.Jpn.] yu "bath, hot spring, hot water" ||| AN: [pHN] *diRus (Zorq) /[pMP] *DiRus, *zîus "to bathe" || W.MP: [Isnag] mag-digut /[Malagasy Merina] man-ḑru /[Murut] diuʔ /[Java] adus (< *a-dus) /[Bali.] mañ-ǰus (-ǰus < *dus < *dius) /[Da'a] nan-ⁿdiu "to bathe" || OC: [Motu] digu /[Lau] sisiu (< *siu < *diu) "to bathe" ||| [Ainu] sus "to bathe" (< *dus)

Table 2. Word-initial sound-correspondence laws of consonants between Finnish/Uralic and Austronesian

1. [Finn.] m- ||| $1.1. [Finn.][Hung.] m- < [pURA] *m- < [pAN] *m-. (W.MP) m- /[pEsk] *m-
2. [Finn.] p- ||| $2.1. [Finn.] p- / [Hung.] f- < [pURA] *p- < (W.MP) p- < [pMP] *p- < [pAN] *p-
3. [Finn.] v-
  $3.1. [Finn.] v- /[Hung.] ø- /[Kamas] b- < [pFU] *v- (~ *w-) /[pSAM] *b- < [pURA] *b- (or *v-) < [pAN] *b-
  $3.2. [Finn.][Hung.] v- < [pAN] *w-
4. [Finn.] t- < [pURA] *t- < [pAN] *t-
5. [Finn.] n-
  $5.1. [Finn.] [Hung.] n- < [pURA] *n- < [pAN] *n-
  $5.2. [Finn.] n /[Zyr.][Mordvin][Yurak] ń- /[Kamas] n- < [pURA] *ń- < [pMP] *ŋ-
  $5.3. [Finn.] n- /[Hung.] m(y)- < [pFU] *ń- ((OC) ŋ- ?)
6. [Finn.] l-
  $ 6.1. [Finn.][Hung.] 1- < [pURA] *1- < (MP) *1-
  $ 6.2. [Finn.] -ll- < *-lVl- < *-d_2Vl- (V = vowel)
7.[Finn.] r-
  $ 7.1. [Finn.] r- < [MP] *r- ~ *R-
  $ 7.2. [FU] r- < (MP) r- < [pAN] (Zorc*) *d_2-. [pMP](Dem*) *d-
  $ 7.3. [pFU] *r- < [pMP] *z- (Zorc*), *d'- (Dem*)
8. [Finn.] s-
  $ 8.1. [Finn.][Zyr.] s- /[Chremis] š- /[Hung.] ø- /[Kamas] t- < [pURA] *s- < (W.MP) *s- < [pAN] *s-
  $ 8.2. [Finn.] s- < [pFP] *s- < [pAN] *S-
  $ 8.3. [Finn.] s- < [pAN] *C-
  $ 8.4. [Finn.] s- (< [pFU] *ś-)
    $ 8.4a. [Finn.] s- /[Hung.] sz- < [pURA] *ś- < *d_2-
    ??$ 8.4b. [Finn.] sy- < [pFU] *śi- < (MP) *ti-
  $ 8.5. [Finn.] su- < [pURA] *ću- < (MP) ču-
9. [Finn.] h- (< [pFU] *č-)
  $ 9.1. [Finn.] h- / [Votyak] (Kazan dial.) ž- /[Ostyak] č- < [pFU] *č- < (W.MP) t-, č- /(FORM)[Paiwan] *ḑ- < [pAN] *d_3-
  $ 9.2. [Finn.] ? /[Zyr.][Votyak] š- /[pFU] *č- < *š- < *sy-
10. [Finn.] k-
  $ 10.1. [Finn.] k- / [Hung.] h- < [pURA] *k- < [pMP] *k- || [pESK] *q-
  $ 10.2. [Finn.] k- /[Hung.] h- < [pFU][pURA] *k- < [pAN] *q (FORM: [Atayal][Pai.] ķ- (= q-), [Tsou] ø- | W.MP: [Sundanese] h-, [Kal.L.] g-, [Yami][Taga.][IndoN] ø- | OC: [Tolai][Kilivila][Mbula] [Motu][Nemi] k-, [Tawara][Nengone] g- , [Tongan] ʔ, [Takia] ø-) || [pEsk] *q-
  $ 10.3. [Finn.] k- /[Hung.] k- < [pFU] *k- < (OC) *g-
11. [Finn.] h- ||| $11.1. (?) [Finn.] h- < [pURA] *h- (K.O.) < (MP) *h-
12. [Finn.] j-
  $ 12.1. [Finn.] j- < *j- < *ǰ- (< *D-)
  $ 12.2. [Finn.][Hung.] j- < [pAN] *Z-
13. [Finn.] y- || $13.1. [Finn.] y- /[Hung.] ē̈- ~ é- < *i- ~ *yi-
14. [Hung.] ø- || $14. 1. [Finn.] ? /[Hung.] øu- < *yu- < *diu- < [pAN] *diRu-

The Tenth International Symposium on Artificial Life and Robotics 2005(AROB 10th '05),
B-con Plaza, Beppu, Oita, Japan, February 4-6, 2005

Effect of action selection on the emergence of one-way communication using Q-learning

Masanobu Nakanishi, Katsunari Shibata
Dept. of Electrical and Electronic Engineering, Oita University
700 Dannoharu Oita 870-1192 Japan

Abstract

In this paper, the effect of action selection in the learning of one-way communication between two agents using Q-learning is examined. The ratio of successful learning becomes larger when the receiver agent's action selection is greedy and the transmitter agent's action selection is not completely greedy but with a small random factor. From the analysis of the learning process, it is known that inappropriate mapping from states to signals in the transmitter agent sometimes breaks the mapping from signals to action severely in the receiver agents. Accordingly, the transmitter agent needs to find an appropriate mapping through exploration, while the receiver agent decides its action after the mappings is fixed in the transmitter. Accordingly, no exploration is necessary in the receiver agent.

1. Introduction

Communication plays a very important role in the supplement of insufficient observation, collision avoidance and cooperative action in multi-robot and multi-agent systems. In order to learn a purposive communication autonomously, evolutionary method[1] or reinforcement learning[2][3] has been used. Autonomous acquisition of one-way communication to supply the receiver's insufficient observation has been examined[1][2]. However, it was not examined what kind of information should be transmitted, and whether the optimal communication can be acquired in any cases. Then, we also focused on the learning of one-way communication that supplies the receiver's insufficient observation. For simple analysis, the number of agents is limited to two, those are a transmitter agent and a receiver agent. We have examined the reason why state confusion occurred in some simulations[4]. In this paper, the effect of action selection in the learning of one way communication between two agents using Q-learning that the authors discovered through the simulations is examined.

2. Learning of one-way communication

2-1 Task description

In this paper, the learning of one-way communication that supplies the receiver's insufficient observation is focused on. The simulation environment was decided referring to [1][2]. Fig.1 shows the image of one-way communication learning. Two agents called "male" and

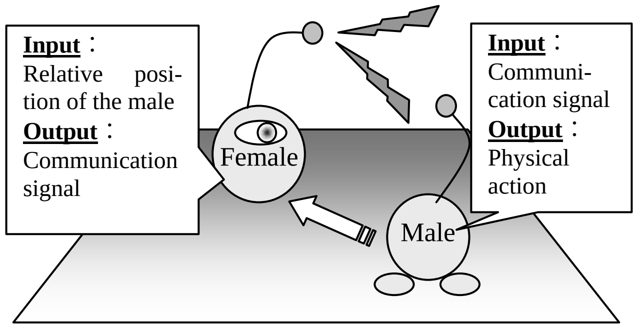

Fig.1 Learning of one-way communication

"female" are assumed in a discrete environment. The male can move, but does not have sight. On the other hand, the female can't move, but can transmit some signals to the male. The female's input is the relative position of the male, and its output is a communication signal. The male's input is the communication signal and its output is a physical action. If the male touches the female, a reward is given to the both agents. The meaning of the communication signal is not given to either agent at all beforehand. Therefore, a transmitter agent has to learn what communication signal should be transmitted and a receiver agent have to learn to generate appropriate actions from the signal. If some common language can be built up between the male and the female, the contact can be repeated efficiently.

2-2 Learning method for the both agents

For the learning of the both agents, Q-learning is used. In Q-learning, state-action pairs are evaluated, and the action value is called Q-value. An agent chooses an action with the probability calculated from the Q-values. It is usually applied on a discrete action space.

The algorithm of Q learning is as follows.

(1) The agent observes a state.
(2) The agent selects and executes an action.
(3) The agent observes the state after the transition.
(4) A reward r_{t+1} is received from the environment.
(5) Q-value is modified as

$$Q(s_t, a_t) \leftarrow (1-\alpha)Q(s_t, a_t) + \alpha\left[r_{t+1} + \gamma \max_a Q(s_{t+1}, a)\right] \tag{1}$$

where α is a learning rate $(0 < \alpha \le 1)$
γ is a discount factor $(0 \le \gamma < 1)$

(6) t -> $t+1$, and the flow returns to the step(2).

For the female, the state s is the male's relative position, and the action a is the communication signal. For the male, the state s is the communication signal, and the action a results in a state transition. α is 0.1, and γ is 0.9 here.

2-3 Action selection

2-3-1 Boltzman selection

When the state is x, the probability of the action a is calculated as,

$$p(a \mid x) = \frac{\exp(Q(x,a)/T)}{\sum_{i \in A} \exp(Q(x,i)/T)} \qquad (2)$$

where A is a set of actions, and T is a temperature coefficient. An action is selected almost randomly when T is large. As opposite to it, when T is close to 0, a little difference of Q-value has a great influence on the action selection, in other words, the action selection is almost greedy. In the following simulations, the initial value of T is 1.0, and it is gradually decreased exponentially to 0.005. In the rest of trials, it was fixed at 0.005. The reason is that when it becomes smaller than 0.005, the computation on our computer becomes impossible.

2-3-2 Greedy selection

In greedy selection, there is no probabilistic factor and the action with the maximum Q-value is always selected.

2-4 Flow of the learning

The agents act in accordance with the following cycle.

(1) The female detects the male's state.
(2) The female's Q-value at t-1 is modified.
(3) The female transmits a signal to the male.
(4) The male receives the female's signal.
(5) The male's Q-value at t-1 is modified.
(6) The male makes an action.
(7) If the both agents touch each other, the trial finishes, and they get a reward. In that case, they learn their Q-values at t according to Eq.(1) with $\max Q(s_{t+1}, a) = 0$ and the flow returns to (1). If the trial finished, t=0, otherwise t->$t+1$.

When t=0, the step(2)or(5) is not executed.

3. Simulation

A simulation environment is shown in Fig.1. In this environment, the number of states, signals and actions are decided to be the same to match the condition of the both agents. All the initial Q-values are 1.0 here. When all the initial Q-values are set to be high, which is called Optimistic initial value, the effect of exploration can be realized even in greedy selection[5].

In this simulation, the number of the trials until the temperature coefficient reaches the minimum is varied for each agent in the case of Boltzmann selection, and successful learning ratio was observed.

When the temperature coefficient T reaches the minimum value at the N-th trial, the temperature at the k-th trial is calculated as

$$\begin{aligned} T(k) &= 0.005^{\frac{k}{N}} \quad if\,(k < N) \\ &= 0.005 \quad otherwise \end{aligned} \qquad (3)$$

N is varied from 200 to 1000 with the interval of 200 in each agent. The total number of trials is 1000. Furthermore, the greedy selection is also employed. The average successful ratio over 1000 simulation runs for each combination of exploration ways of two agents is shown in Table 1.

From this figure, it is known that the successful ratio is high when the male's action selection is greedy, and the female's one is Boltzmann selection with the temperature decreased fast. On the other hands, the successful ratio is low when the female's action selection is greedy.

Next, in order to examine the effect of the small exploration factor remaining due to the lower bound of the temperature, greedy selection was employed when the temperature reaches the minimum value 0.005. In the previous simulation, the action which does not have the maximum Q-value sometimes selected because of the probabilistic selection after the temperature coefficient reaches the minimum. On the other hand, in this simulation, the action that has the maximum Q-value is always selected after the temperature coefficient reaches the minimum.

The results are shown in Table 2. The successful ratio is higher than in Table 1 when the male's action selection is greedy, and the female's selection is Boltzmann selection. However, when the female's action selection is greedy, and the male's action selection is Boltzmann selection, the successful ratio is lower than in Table 1. The reason why the successful ratio is high when the male temperature coefficient is decreased faster than the female can be thought that the male's action selection becomes greedy in the early stage of the total trials.

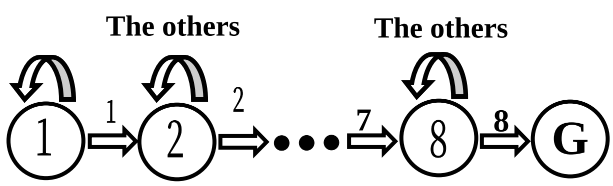

Fig.2 Simulation environment

Table 1: Success ratio according to the number of trials when the temperature reached 0.005

		The male's number of trials until T=0.005					
		greedy	200	400	600	800	1000
The female's number of trials until T=1000	Greedy	87.1	44.7	38.7	30.2	19.8	9.8
	200	100.0	82.0	77.0	61.1	32.2	7.6
	400	99.9	80.1	78.8	61.0	36.0	9.9
	600	99.1	64.8	62.4	57.4	34.9	9.0
	800	81.9	41.0	36.4	32.1	21.8	7.6
	1000	62.8	6.1	6.9	5.6	2.7	0.4

Table 2: Success ratio according to the number of trials when the action was changed to greedy selection after the temperature reached 0.005.

		The male's number of trials until T=0.005					
		greedy	200	400	600	800	1000
The female's number of trials until T=1000	greedy	87.1	84.0	67.2	40.5	20.3	9.8
	200	90.5	86.9	75.9	47.9	22.4	10.4
	400	90.5	90.9	83.4	65.2	28.7	11.9
	600	90.4	87.9	85.9	77.8	53.0	14.4
	800	83.8	84.4	85.8	79.3	54.5	18.6
	1000	62.8	61.5	56.8	36.7	6.8	0.4

Then, in order to investigate the reason of the difference of successful ratio depends on the action selection of the both agents, the change of Q-values in the learning process is observed. The change of Q-values when the female's action selection is greedy from the beginning is shown in Fig.3. The change when Boltzmann selection was employed and the temperature coefficient was fixed at 0.005 from the beginning is shown in Fig.4. Fig.(a) shows the change of female's Q-values when the male is in the state 8 that is located 1 step before the goal, and Fig.(b) shows the change of male's Q-values for the action 8 that takes the agent from the state 8 to the goal, but is not rational for the other states.

From Fig.3,4, it is known that only one Q-value is higher after learning progressed in some degree, and the signal with the highest Q-value in the female corresponds to the signals with the highest Q-value in the male. It is also known that the signal with the maximum Q-value was switched several times. Finally the female decides to select a signal in the state 8, and the male decides to select the proper action from the signal. The both corresponding Q-values converged to 1.0. In Fig.3, the male's maximum Q-value became large in the early stage of learning, but it decreased drastically. On the other hand, in Fig.4, the male's Q-learning is slightly oscillating around a comparatively small value. It can be said that, in greedy selection, reconstruction of the signal-action pair occurs often and drastically, but in the Boltzmann selection, the learning is more stable.

Then, the reason why the difference of successful ratio and the change of Q-value due to the female's exploration factor in action selection is examined. An example to show the influence of one agent's learning to the other agent's learning is shown in Fig.5. The failure of the female's learning means that the female selects the same signal in two or more states. For example, when the female transmitted the signal 1 in the both state 1 and 8, the male continues to select the action 8 as long as the signal 1 is received and the action for the signal 1 is not switched by the greedy selection of the both agents. Accordingly, signal-action mapping is broken not only in the state 1 but in the state 8, and learning has to be done again from scratch.

On the other hand, in the case of the failure of the male's learning, the male selects the same action for the different signals even though the female assigned signals appropriately. For example, although the female transmits the signal 1 at the state 1 and transmits the signal 2 at the state 8, the male selects the action 8 in either case of the signal 1 or the signal 2. Then, for the male, Q-value of the action 8 on the signal 1 decreases, and for the female, Q-value of the signal 1 on the state 1 also decreases. However, in this case, it gives no influence on the Q-values at the state 8. So, insufficient learning of the female breaks the generation of the right action also in other states in the male, while insufficient learning of the male breaks the signal only at the state in the female. That is supposed to be the reason why the successful ratio becomes larger when the male's action selection is greedy, and the female's action selection is not completely greedy, but with a small random factor.

Finally, in order to investigate how the learning progressed in the both agents, the number of steps since which the action with the maximum Q-value was not switched was observed. The result shows that the action with the maximum Q-value began to be fixed from the state that is close to the goal, and then, the range where the action was fixed spreads to the far states from the goal gradually. Furthermore, the time when the female fixed its signal is slightly earlier than the number of steps when the male fixed its action. That must be also because the female's insufficient learning sometimes breaks the male's proper mapping from the signal space to the action space.

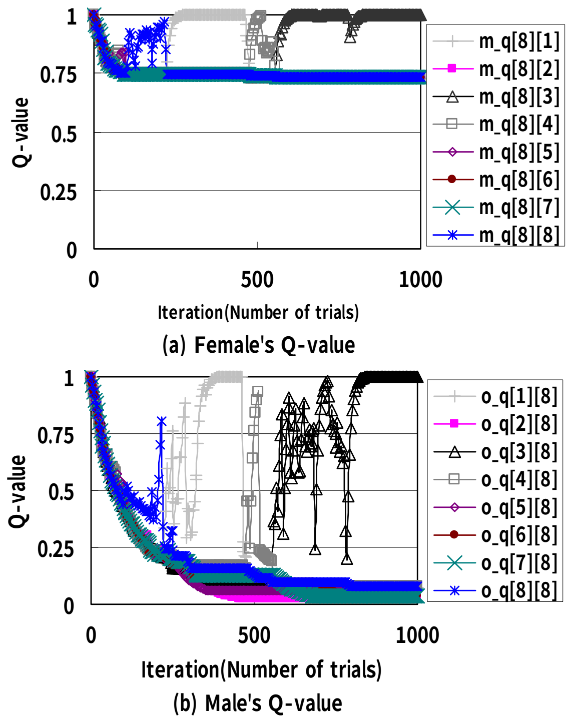

Fig.3 Change of the Q-values when the female's action selection in greedy selection

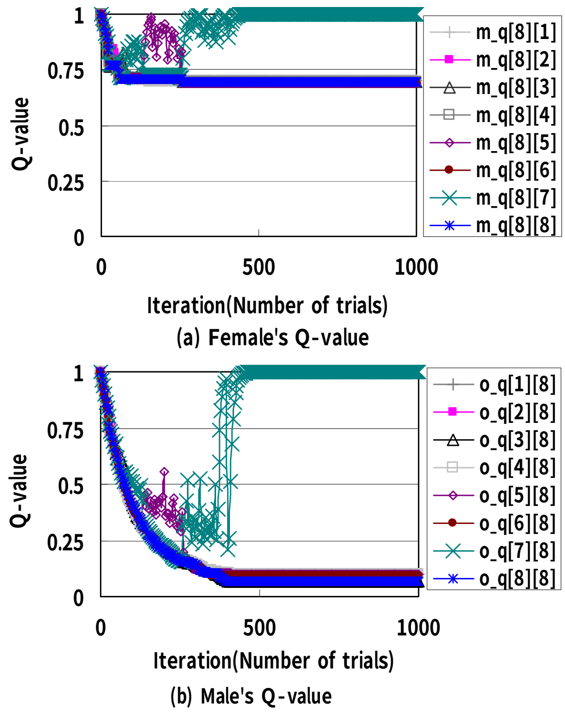

Fig.4 Change of the Q-values when the female's action selection is Boltzmann selection

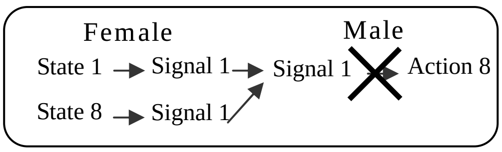

(a) When the mapping in the female is not appropriate

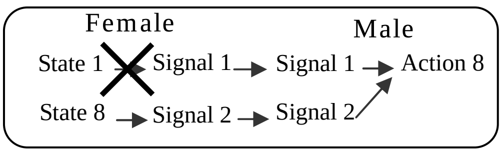

(b) When the mapping in the male is not appropriate

Fig.5 The influence of one agent's learning to the other's learning

4. Conclusion

In this paper, the effect of action selection in the learning of one-way communication between two agents using Q-learning was examined. The successful ratio became higher when the receiver agent's action selection is greedy, and the transmitter agent's is not completely greedy but has a small random factor.

By observing the change of Q-values and the number of the steps when the both agents determine their actions, it is found that insufficient learning in the female may break learning fatally.

Acknowledgement

This research was partially supported by the Japan Society for the Promotion of Science, Grants-in-Aid for Scientific Reearch, # 14350227 and # 15300064.

Reference

[1] G.M. Werner & M. G. Dyer : Evolution of Communication in Artificial Organizing System, Proc.of Artificial life II, 1-47(1991)

[2] N.Ono, T. Ohira, and A. T. Rahmani: Emergent Organization of Interspecies Communication in Q-Learning Artificial Organism,*Advances in Artificial Life*, pp. 396-405 (1995)

[3] K. Shibata and K. Ito: Learning of Communication for Negotiation to Avoid Some Conflicts of Interests-Learning of Dynamic Communication Using a Recurrent Neural Network- Trans. of SICE Vol.35, No.11, 1346-1354 (1999) (in Japanese)

[4] Masanobu Nakanishi, Masanori Sugisaka & Katsunari Shibata: Occurrence of State Confusion in the Learning of Communication Using Q-leaning,Proc. of The 9th AROB (Int'l Sympo. on Artificial Life and Robotics), Vol. 2, pp. 663-666, (2004)

[5] R.S. Sutton and A.G.Barto,: Reinforcement Learning, The MIT Press,1998

DESIGN OF A ROBUST ADAPTIVE CONTROLLER FOR A CLASS OF UNCERTAIN NONLINER SYSTEMS WITH TIME-DELAY INPUT

Thi-Minh-Huong NGUYEN, Thi-Nga DINH
Center for Automation Technology – CAT
thiminhhuong_nguyen@yahoo.com

Thi-Ngoc NGUYEN, Van-Truong TRAN
Center for Automation Technology – CAT,
Hanoi, Vietnam

Abstract

This paper presents a systematic analysis and a simple design of a robust adaptive control law for a class of nonlinear systems with modeling errors and a time-delay input. The theory for designing a robust adaptive control law based on input-output feedback linearization of nonlinear systems with uncertainties and a time-delay in the manipulated input by the approach of parameterized state feedback control is presented. The main advantage of this method is that the parameterized state feedback control law can effectively suppress the effect of the most parts of nonlinearities, including system uncertainties and time-delay input in the pp-coupling perturbation form and the relative order of nonlinear systems is not limited.

Keywords: nonlinear, robust control, adaptive control, time-delay

1 Introduction

Recent developments in the theory of differential geometry provide useful methods for a class of nonlinear systems. The central concept of this approach is to algebraically transform the nonlinear system dynamics into an equivalent linear system, such that the conventional linear control techniques can also be applied [1, 2]. Generally, the feedback linearization techniques require the accurate mathematical model for the plant to achieve exact linearization of the close loop system. However, for many real processes, there exist inevitable uncertainties in their constructed structure models. Therefore, design of a robust controller for a nonlinear system is important subject.

In this paper, we present a systematic analysis and a simple design of an adaptive control law for a class of nonlinear systems with modeling errors and a time-delay input. The so-called matching conditions [3] for controlled nonlinear systems and the Smith predictor are not necessary. System uncertainty is considered as the non-vanishing case in the desired operating condition. Using the parameterized coordinate transformation, the original nonlinear system can be transformed to a class singular perturbation problem having distinct fast and slow dynamics. An adjustable parameter can be detuned to satisfy the desired control specification. When the lumped nonlinearity, including uncertainty and time-delay input, is constrained to a closed bounded set and satisfy the local Lepschitz condition [4], its effect on the output trajectory can be effectively suppressed using the proposed technique. More precisely, to treat the tracking problem, an ultimate bound of tracking error is investigated under the specific reference model.

2 Preliminaries and problem formulation

Consider the uncertain single input single output (SISO) nonlinear system with time-delay input:

$$\dot{x}(t)=f(x(t))+Df(x(t))+[g(x(t))+Dg(x(t))]u(t-d) \quad (1)$$
$$y(t)=h(x(t))$$

, where $x \in R^n$ is the state variable, $u \in R$ is the manipulated input, $d>0$ is the time delay in the manipulated input, $y \in R$ is the output .f(•), g(•), Df(•) and Dg(•) are smooth vector fields on R^n, and h(•) is a smooth function. The nominal system is then defined as follows:

$$\dot{x}(t)=f(x(t))+g(x(t))u(t) \quad (2)$$
$$y(t)=h(x(t))$$

, i.e. assume that Df(•) = 0, Dg(•) = 0, and d=0 in (1).

There has been a great deal of research in recent years over the development of a complete theory for explicitly linearizing the input-output map of the nominal system (2) using state feedback. Here we introduce some notations from differential geometry, namely the Lie derivative, which is frequently used in this paper. For more general treatment in this area, readers are advised to look in [1], [5]. Given a scalar function h(x(t)) and a vector field f(x(t)) on R^n, one can define a new scalar function $L_f h(x(t))$, called the Lie derivative of h(x(t)) with respect to f(x,t):

$$L_f h(x(t))=\frac{\partial h(x(t))}{\partial x(t)} f(x(t)) \quad (3)$$

Thus, the Lie derivative $L_f h(x(t))$ is the directional derivative of h(x(t)) along the direction of the vector f(x(t)). Higher order Lie derivative can be defined recursively as:

$$L_f^0 h(x(t))=h(x(t)) \quad (4)$$

$$L^k_f(x(t))=\sum_{j=1}^{n}\frac{\partial}{\partial x(t)}[L^{k-1}_f h(x(t))]f_j(x(t)),\ k = 1, 2, 3, \ldots \quad (5)$$

if g(x)is another smooth vector field on R^n, then one can define the Lie derivative of h(x(t)) with respect to two different vector fields:

$$L_g L_f^k h(x(t))= \sum_{j=1}^{n}\frac{\partial}{\partial x(t)}[L^k_f h(x(t))]g_j(x(t)),$$
$$k=1, 2, 3, \ldots \quad (6)$$

Furthermore, the minimum eigenvalue of a hermitian is denoted as $\lambda_{min}(\bullet)$ and $\lambda_{max}(\bullet)$, where as the transpose of the vector or of a matrix is written as $(\bullet)^T$ and $\|\bullet\|$ denotes the Euclidean norm.

An important property of a nonlinear system is its relative degree. For a linear system defined in transfer function form, the relative degree is usually defined as the order of the denominator minus the order of a numerator. Amore general definition is used for nonlinear systems:

Definition 1: The system (eqn.2) is said to have a constant relative degree r [6], if there exists a positive integer $1<=r<=\infty$,such that

$L_gL_f^kh(x(t))=0, k< r-1$ (7)

$LgLfr-1h(x(t))!=0$ for all $x\in R^n$ and $t\in [0,\infty)$ (8)

Throughout this paper, we assume that the nominal system (2) possesses a relative degree r. Based on the assumption, it has been shown that [1] there exits a neighborhood U of the operating point x_s such that the mapping:

p: U-> R^n (9)

defined as

$p_i(x(t))=E_i(t)=L_f^{i-1}h(x(t)), i=1,2,3,...,r$ (10)

$p_k(x(t))=N_k(t), \quad k=r+1,r+2,...,n$ (11)

, and satisfying:

$L_gp_k(x(t))=0, k=r+1,r+2,...,n$ (12)

, is a diffeomorphism onto image. To obtain a linear input-output relation of (2), start with the external dynamics:

$$E'_1(t)=\frac{\P p_1}{\P x}\frac{dx}{dt}=\frac{\P h}{\P x}\frac{dx}{dt}=L_fh(x(t))=p_2(x(t))=E_2(t) \quad (13)$$

…

$$E'_{r+1}(t)=\frac{\P p_{r-1}}{\P x}\frac{dx}{dt}=\frac{\P L_f^{r-1}}{\P x}\frac{dx}{dt}=L_f^{r-1}h(x(t))$$

$$=p_2(x(t))=E_r(t) \quad (14)$$

$$E'(t)=\frac{\P p_r}{\P x}\frac{dx}{dt}=\frac{\P L_f^{r-2}}{\P x}\frac{dx}{dt}$$

$$=L_f^rh(x(t)) + L_gL_f^{r-1}h(x(t))u(t) \quad (15)$$

Set

$$a(E(t)), N(t)=L_gL_f^{r-1}h(x(t))u(t)\,|_{x=p}^{-1}\,(E(t),N(t)) \quad (16)$$

$$b(E(t), N(t))=L_gL_f^{r}\,h(x(t))u(t)\,|_{x=p}^{-1}\,(E(t),N(t)) \quad (17)$$

(15) can be written as:

$E'_r(t) = b(E(t),N(t))+a(E(t),N(t))u$ (18)

Next, under eqn.12 the integral dynamics is considered as:

$$N'_k(t) = \frac{\P p_k}{\P x}(f(x(t))+g(x(t))u(t) = L_fp_k(x(t))+$$

$$L_gp_k(x(t))u(t) = L_fp_k(x(t)), k=r+1,r+2,r+3, \ldots \quad (19)$$

Thus, in short, the state space description of the system in the new co-ordinates as follows:

$E'_i(t)=E_{i+1}(t), i=1,2,3, \ldots$ (20)

$E'_r=b(E(t),E(t))+a(E(t),N(t))u(t)$ (21)

$N'(t)=q(E(t),N(t))$ (22)

$y(t)=E_1(t)$ (23)

, where $q_i(E(t),N(t)) = L_fp_k(x(t))\,|_{x=p}^{-1}\,(E(t),N(t))$, k = r+1,r+2, …, n

Generally, (20), (21) are called the external dynamics of the system, and (22) is called the internal dynamics of the system. The proper choice of a linearizing control law is now apparent from (21). As b(E(t),N(t)) is bounded away from zero, its inverse is well defined. Thus the following linearising feedback law can be derived from (16), (17) and (21):

$$u(t)=f(t),v(t)) = (L_gL_f^{r-1}h(x(t))^{-1}(-L_f^rh(x(t))+v(t))$$

$$=a^{-1}(E(t),N(t))[-b(E(t),N(t))+v(t)] \quad (24)$$

, where v(t) is a new external control to be designed for the purpose of tracking signals. Note that the control law of (24) makes the state vector N(t) completely unobservable at the output. Since we are interested in achieving stable state tracking, it is required that N(t) remain bounded for the bounded E(t). However, we observe that E(t) can be thought as an external input vector with respect to the dynamics of N(t). Since E(t) is expected to track arbitrary time functions, it is clear that the boundedness of N(t) is entirely depend on the vector field q(E(t),N(t)). It can be easily verified that the equation:

$E'(t)=q(0,N(t))$ (25)

, is referred to as the zero dynamics [1]. The system in which the zero dynamics is asymptotically stable referred to as the minimum phase system. Stable tracking requires a stronger stability criterion for the dynamics

$E'(t)=q(E(t),N(t))$ (26)

be bounded input bounded state (BIBS) stable. In addition to the relative degree assumption, a further property of the zero dynamics required. This is illustrated in the following assumptions:

Assumption 1: The zero dynamics of eqn.25 is exponentially stable. Moreover, the function q(E(t),N(t)) is Lepchitz uniformally in N(t).

Remarks:

(i)Since the zero dynamics is exponentially stable by assumption therefore by a converse theorem of Lyapunov [7], there exists a Lyapunov Vo(N(t))which satisfies the following properties:

$K1°N(t)°^2<= Vo(N(t))<=K2°N(t)°^2$ (27)

$$\frac{\P Vo(N(t))}{\P N(t)}q(0,N(t)) <=-K3°N(t)°^2 \quad (28)$$

$$\left\|\frac{\P vo(N(t))}{\P N(t)}\right\|<=K4°N(t)° \quad (29)$$

,, where K1, K2, K3 and K4 are some appropriate positive constants.

(ii) Due to the fact that q(E(t),N(t)) is Lepschitz in E(t) there exists a positive constant L such that

$°q(E(t),N(t))- q(0,N(t))°<=L°E(t)°, N(t)\in R^{n-r}$ (30)

, and Lis called a Lepschitz constant of q(E(t),N(t)) [1].

Now, we are ready to design the tracking controller for the system (1) to minimize the trajectory error and to stabilize the close loop control system in the presence of system uncertainties and time-delay input.

3 Results of research

In this part, the robust control objective is to design a parameterized feedback linearizing control law such that the desired output trajectory of the close loop system is achieved and the effects of system uncertainty attenuated while maintaining the boundedness of all signals inside the control loops. For simplicity, all uncertain components can be lumped and the uncertain nonlinear system can be reduced to

$\dot{x}(t)=f(x(t))+g(x(t))u(t-d)+\Sigma(x(t),u(t-d))$

$y(t)=h(x(t))$ (31)

, where $\Sigma(x(t),u(t-d))=Df(x(t))+Dg(x(t))u(t-d)$.

Applying the nominal change of co-ordinates of equations (10)-(12) and the nonlinear state feedback of (24) to the system (1) yields

$$\dot{E}_1(t)=E_2+\frac{\partial h(x(t))}{\partial x(t)}(\Sigma(x(t),u(t-d))) \quad (32)$$

…

$$\dot{E}_{r-1}(t)=E_r(t)+\frac{\partial L_f^{r-2}h(x(t))}{\partial x(t)}\Sigma(x(t),u(t-d)) \quad (33)$$

$$\dot{E}_r(t)=v(t)+\frac{\partial L_f^{r-1}}{\partial x(t)}\Sigma(x(t),u(t-d))+g(x(t)(u(t-d)-u(t)) \quad (34)$$

$$\dot{N}_1(t)=q_1(E(t),N(t))+\frac{\partial p_n}{\partial x(t)}\Sigma(x(t),u(t-d)) \quad (35)$$

$$\dot{N}_{n-r}(t)=q_{n-r}(E(t),N(t))+\frac{\partial p_{r+1}}{\partial x(t)}\Sigma(x(t),u(t-d)) \quad (36)$$

Taking advantage of the identities in the nominal transformations and by some derivations, it can be easily verified the equations (32)-(36) can be transformed into:

$\dot{E}(t)=AE(t)+Bv(t)+DA(x(t),u(t), u(t-d))$ (37)

$\dot{N}(t)=q(E(t),N(t))+D\Phi(x(t),u(t-d))$ (38)

$y(t)=CE(t)$ (39)

, where $E=[E_1,E_2,\ldots, E_n]^T$, $N=[N_1,N_2,\ldots, N_{n-r}]^T$,

$$DA=[DA_1, DA_2, \ldots, DA_r]^T=\begin{bmatrix}\frac{\partial h(x(t))}{\partial k(t)}\Sigma(x(t),u(t-d)) \\ \ldots \\ \frac{\partial L_f^{r-2}h(x(t))}{\partial x(t)}\Sigma(x(t),u(t-d)) \\ \frac{\partial L_f^{r-1}h(x(t))}{\partial x(t)}\Sigma(x(t),u(t-d)+g(x(t))u(t-d)-u(t)\end{bmatrix}$$

$$, DA\in R^{r\times 1}, D\Phi=\begin{bmatrix}\frac{\partial p_{r+1}}{\partial x(t)}(\Sigma(x(t),u(t-d))) \\ \ldots \\ \frac{\partial p_n}{\partial x(t)}(\Sigma(x(t),u(t-d)))\end{bmatrix}\in R^{(n-r)\times 1}$$

$$A=\begin{bmatrix}010.0 \\ 001.0 \\ \ldots.. \\ 000.1 \\ 00000\end{bmatrix}\in R^{r\times r},$$

$B=[0\ \ 0\ \ldots\ 0]^T\in R^{r\times 1}$, $C=[0\ \ 0\ \ldots\ 0]^T\in R^{1\times r}$

Consider that the output y(t) will track the output $y_d(t)$ of the reference model. The desired model reference is

$\dot{z}(t)=A_0z(t)+B_0y_{sp}(t)$ (40)

where z(t) is the state variable, A_0,B_0,C_0 are matrices and vectors with appropriate dimensions. $Y_{sp}(t)$is the external input, and $y_y(t)$is the desired output trajectory. The following assumptions are needed to achieve the desired output trajectory:

Assumption 2:

The desired trajectory output and its first r derivatives are all uniformly bounded, and satisfy:

$\|(y_d(t)\ y_d^{(1)}(t)\ \ldots.\ y_d^{(r)}(t))\|<=B_d$ (41)

, where B_d is the some positive constant.

Remark:

(iii) The fact that the model reference must be of relative order of r, to avoid the use of differentiators in the controller. Furthermore, if the desired trajectory and its derivatives are uniformly bounded, one can make the output tracking error, $y(t)-y_d(t)$, as minimum as possible and the whole system states locally stable. This is further verified in the subsequent theorem:

Define: $e_i(t)=E_i(t)-y_d^{(i-1)}(t)$, $i=1,2,\ldots,r$ (42)

Then equations (24) and (37)-(39) become:

$\dot{e}(t) = Ae(t)+B(v(t)-y_d^r(t)) + DA(x(t),u(t),u(t-d))$ (43)

$\dot{N}(t) = q(E(t),N(t)) + D\Phi(x(t),u(t-d))$ (44)

$e_1(t)=Ce(t)$ (45)

Define the tracking error with parameterization

$e_i^*(t)=pp^{i-1}e_i(t)$, $i=1,2,\ldots,r$ (46)

, for a positive constant pp<=1. Then we obtain the following equations:

$pp\dot{e}^*(t)=Ae^*(t) + pp^rB(v-y_d^{(r)}+ppDA^*(x(t),u(t),u(t-d)$ (47)

$\dot{N}(t)=q(E(t),N(t)) + D\Phi(x(t),u(t-d))$ (48)

$e_1(t)=Ce^*(t)$ (49)

, where $DA^*=[DA_1\quad ppDA_2\ \ldots\ pp^{r-1}A_r]^T$

Now, we propose the control law v(t) of the following form:

$$v(t)=\Phi_0(e^*(t),y_d^{(r)}(t))=y_d^{(r)}(t)-pp^{-r}\sum_{i=1}^{r}a_ie^*_i(t)$$
$$=y_d^{(r)}(t)+\Gamma(a,pp)e(t) \quad (50)$$

, where $\Gamma(a,pp) = [-pp^{-r}a_1,\ldots, -pp^{-1}a_r]$

Note that $a_1,a_2,\ldots,a_r$ are chosen such that

$s^r + a_rs^{r-1} + \ldots +a_1$ (51)

is a Hurwitz polynomial and s is the Laplace operator. By some derivations we obtain a standard singularly perturbed system of the form:

$pp\dot{e}^*(t)=A_ce^*(t)+ppDA^*(x(t),u(t),u(t-d))$ (52)

$\dot{N}(t)=q(E(t),N(t))+D\Psi(x(t),u(t-d))$ (53)

, where $A_c=\begin{bmatrix}0 & 1 & 0 & 0 & 0 \\ 0 & 0 & 1 & 0 & 0 \\ . & . & . & . & . \\ 0 & 0 & 0 & 0 & 1 \\ -a_1 & -a_2 & . & . & -a_r\end{bmatrix}$ is companion matrix.

Moreover, we define P as a symmetric positive define matrix satisfying the Lyapunov equation:

$A_c^TP + Pa_c = -I$ (55)

, where I is an identity matrix.

Intuitively, to reduce the effects of the nonlinearity including state and input perturbations to the tracking error e(t) while maintaining the boundedness of N(t), we can choose a large gain in the control law v(t) eqn.50. However, the input error between the delay in put u(t-d) and the desired control law u(t) will be large due to inappropriate high gain feedback control. Therefore how to choose a suitable tuning parameter pp in the present control law, which guarantees the overall system stability and good performance, is the main key issue of in this paper.

Owing to state feedback control the resulting closed loop system of (52) and (53) may include state delay and input delay. Hence, the bound information of the delayed state x(t-d) and current state x(t) is a priori. This is addressed in the following assumption.

Assumption 3:

Consider that $W(e^*(t))=ppe^*(t)^Tpe^*(t)$ is a positive define function, where $e^*(t)$ is the parameterized variable as shown in eqn.46, and P satisfies eqn.55. If there exists

$$W(e^*(t-d))<=\varepsilon^2 c^{*o}e^*(t)^o \qquad (56)$$

where c^* is the ratio between maximum and minimum eigenvalues of matrix P.

Remarks:

(iv) This assumption is based on the stability theorem of Razumikhin [7]. Under the continuous inversion of parameterized co-ordinate transformation (equations (10), (11), (42), (46)), i.e.:

$$x_I(t) = p_k^{-1}(E_i(t),N_j(t)) = p_k^{-1}(e_i(t)+y_d^{i-1}(t),N_j(t))$$
$$= p_k^{-1}(pp^{1-i}e_i^*(t)+ y_d^{(i-1)}(t)N_j(t)),\ \ i=1, 2, \ldots$$

The result of (56) represents that if the current state x(t) is bounded, the delayed state x(t-d)is uniformly bonded. This assumption had been used in the literature for state-delayed systems [8].

From the assumptions above, the error can be expressed further as follows:

$$^3u(t-d)-u(t)^3= {}^3\Phi(x(t-d),v(t-d) - \Phi(x(t),u(t)))$$
$$^3={}^3-a^{-1}(E(t-d),N(t-d))$$
$$b(E(t-d),N(t-d))+y_d^{®}(t-d)a^{-1}(E(t-d), N(t-d)) –$$
$$y_d^{®}(t)a^{-1}(E(t),N(t))+\Gamma(a,pp)$$
$$a^{-1}(E(t-d),N(t-d))e(t-d)-a^{-1}(E(t),N(t))e(t))^3 \qquad (57)$$

After taking derivation of Lepschitz Jacobian near the origin, one can show that:

$$^3u(t-d)-u(t)\ {}^3<=pp^{-r}(c_1{}^oE(t-d)-E(t)\ {}^o+ c_2{}^oN(t-d)-N(t)\ {}^o+$$
$$c_3<=k^*/pp^r \qquad (58)$$

, where c_1,c_2,c_3 and $k^*$are positive constants.

Based on the ongoing analysis, a simple design procedure for better output tracking in the presence of plant uncertainties and time delay is proposed. The basic principle is to design the parameterized state feedback control law for getting a good system response and to tune the parameter pp for achieving robust stability and performance specification.

The control structure is shown in Figure 1, and the design procedure consists of five steps:

Step 1: Select the controlled output and calculate the co-ordinate transformation based on the nominal system as shown in equations (10)-(12).

Step 2: Transform the nonlinear system into an equivalent linear system as shown in equations (20)-(23).

Step 4: Calculate the desired reference model based on the specific specification as shown in equation (40).

Step 5: Adjust the tuning parameter pp to satisfy the performance specification.

4 Conclusions

The theory for designing a robust adaptive control law based on input-output feedback linearization of nonlinear systems with uncertainties and a time-delay in the manipulated input by the approach of parameterized state feedback control has been presented. The main advantage of this method is that the parameterized state feedback control law can effectively suppress the effect of the most part of nonlinearities, including system uncertainties and time-delay input in the pp-coupling perturbation form and the relative order of nonlinear systems is not limited.

References

[1] Kravaris, A., et al (1987), Nonlinear state feedback synthesis by global input/output linearization, *AIchJ*.

[2] Sastry, S., et al, Adaptive control of linearizable systems, *IEEE Trans.,* AC 34, 1123-1131.

[3] Narebdra, K.S, et al (1986), robust adaptive control in the presence of bounded disturbances. *IEEE Trans. On Aut. Control* AC, 306-315.

[4] Bethtash S. (1990), Robust output tracking for nonlinear systems*, Int.J.Control*,1381-1407.

[5] Campion, G. and g. Bastin (1990) Indirect adaptive state feedback control of linearly paramiterized nonlinear systems.*Int.J of adaptive control and Signal processing,* 4,345-358.

[6] Peterson, B. B., et al (1982), Bounded error adaptive control. *Trans. On IEEE Aut. Control,* AC-27.

[7] Reed,J.,S, et al ,(1984)Instability analysis and robust control of robotic manipulator, *IEEEJ.of robot and Automation,* 15.

[8] Lioa, T., et al (1990) Adaptive robust tracking of nonlinear systems and with an application to a robotic manipulator. System and control Letters, 15, 339-348.

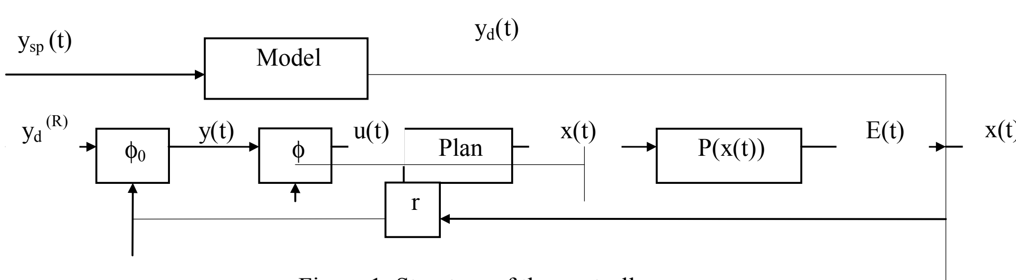

Figure 1: Structure of the controller

The Tenth International Symposium on Artificial Life and Robotics 2005(AROB 10th '05),
B-con Plaza, Beppu, Oita, Japan, February 4-6, 2005

Optimization of Camera Positions for Taking All Indoor Sceneries by GA

Yusuke TOMINARI
Faculty of Engineering
University of Miyazaki
1-1,Gakuen Kibanadai-Nishi,
Miyazaki, 889-2192,Japan

Takumi NAKAGAWA
Faculty of Engineering
University of Miyazaki
1-1,Gakuen Kibanadai-Nishi,
Miyazaki, 889-2192, Japan

Kunihito YAMAMORI
Faculty of Engineering
University of Miyazaki
1-1, Gakuen Kibanadai-Nishi,
Miyazaki, 889-2192, Japan

Ikuo YOSHIHARA
Faculty of Engineering
University of Miyazaki
1-1, Gakuen Kibanadai-Nishi,
Miyazaki, 889-2192, Japan

Haruo TAKEDA
Office of Strategic Planning
Systems Development Laboratory
Hitachi, Ltd
Kawasaki, Japan

Abstract

CG images consisting of all indoor sceneries are usually used in movies, virtual reality applications, etc. This paper addresses a GA-base method to find the optimal camara positions to synthesize a complete indoor image from multiple photographs. For this objective, we use a efficiency crossover operation. Our method is evaluted by computer simluations that find the camera positions which can take all walls in the building. The experimental results show that our method can take all walls in the building by the small number of cameras.

Keyword: Genetic Algorithm, CG, Composition of a seamless image

1 Introduction

Recently, Computer Graphics (CG) are used in many fields such as movies, games and so on. Many CG engineers have developed sophisticated techniques to produce photo-realistic CG images. In particular, movies use many CG images to synthesize scenes which are hard to film. This field reruires an easy way to get a complete in image a building. Some CG engineers synthesize the complete indoor image from multiple photographs.

If has two problems to synthesize a complete indoor image from multiple photographs; how to determine the minimum number of cameras to take all indoor scenery, and how to determine the optimal camera positions and view angles. In addition a photograph needs to have appropriate overlap areas between the neighboring photographs to make a seamles image as shown in Figure.1.

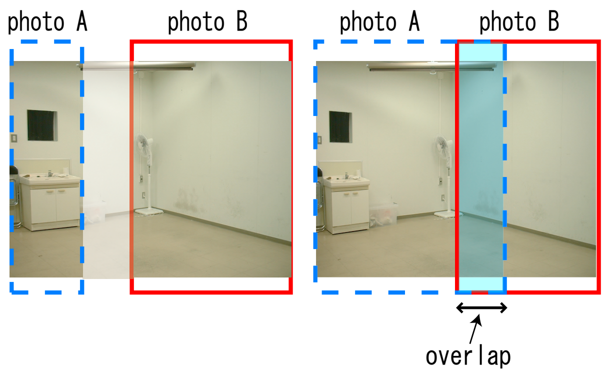

Figure 1: Overlap to compose a seamless image

2 Definition of the problem

The final goal is to compose a seamless image from the minimum number of photographs with suitable overlaps, and the seamless image takes all indoor scene in the building. For this objective we derive the optimal camera positions by GA under the following assumptions and constraints.

2.1 Assumptions

To simplify the problem, we suppose the following four assumptions.

- There is no furniture in the room.
- Building is described as two dimensional floor map.
- Cameras are allowed to put on the descrete position. The interval of positions is given by user.
- The view angle of camera is 48 degree, that is as the same as that of standard lens of 35mm camera. And the focus range is given by user.

2.2 Constrains

To compose a seamless image from multiple photographs, the image has to satisfy the following two constraints.

- The seamless image has to take a complete view in the view building. In other words, the seamless image has to take all walls in the rooms.
- Each photographs has to have suitable overlap areas between neighboring photographs as shown in Figure.1. Since the wall taken by more than two cameras is redundant, it is not used as the overlap.

2.3 Optimal camera position

We define the optimal camera position that satisfies the constraints under the assumptions by the minimum number of cameras. However the minimum number of cameras is not generally decided by the probabilistic search such as GA. Therefore we decide the smallest number of cameras through computer simulations. Concretely, if N cameras put on the appropriate positions can satisfy the constraints, and if $N-1$ cameras can not satisfy them, N is the minimum number of cameras. This N is decided through all computer simulations.

3 Genetic Algorithms

3.1 Genetic Coding

A camera has three parameters; the horizontal position, the vertical position and the angle from the horizontal axis. These three parameters are arranged as an individual. X_i and Y_i denotes the horizontal and vertical coordinates of the camera i, respectively. X_i and Y_i have descrete values as described in the assumption. θ_i denotes the angle of from the horizontal axis. The range of θ_i is ± 180 degree by one degree step.

3.2 Genetic operations

3.2.1 Parents Selection and Crossover

The numbers of cameras in an individual are affected by the crossover operation. To reduce the number of cameras effectively, it is desired that a camera take more area of the walls. For this reason, the selection of parents is operated as follows;

1. "Parent-A" is chosen in order of the fitness value defined by Equation (1) in Section 3.2.2.
2. A temporary individual A' is made from the "Parent-A" . The individual A' is almost the same as the "Parent-A", but some cameras taking a wall that has the smallest area are removed. The wall taking by the removed cameras is called as the "WorstWall-A".
3. "Parent-B" that takes the largest area of the "WorstWall-A" is chosen from the population. Camera is called as the "BestCamera-B".
4. A temporary individual B' is made from the "Parent-B". The individual B' only includes the "BestCamera-B".

The "BestCamera-B"are inserted into Individual A' in one by one as shown in Figure.2 . Finally, new offspring is created.

3.2.2 Fitness Function

The fitness function is defined by Equation (1) where j is ID of walls. N is the number of walls in floor map.

$$f_g = \Sigma_j (P_j + Q_j), \tag{1}$$

$$P_j = \frac{l_{ja} + l_{jb} - \lambda}{L_j} \times 100(\%), \tag{2}$$

$$Q_j = \begin{cases} 100 & P_j\textit{=100(\%)} \quad \textit{and} \\ & \lambda > (1-\alpha)M \\ 0 & \textit{other} \end{cases}, \tag{3}$$

In Equation (2), l_a and l_b denote the length on the wall j taken by the camera A and the camera B, respectively. λ denotes the length of the wall j taken by both of the camera A and the camera B (overlap). L_j is the length of the wall j. These parameters are also illustrated in the Figure 3 . When the wall j is completely taken by the camera A and the camera B, P_j becomes 100.

Q_j becomes 100 if the wall j is completely taken, and the photographs include desirable overlap to compose a complete image. The parameter α $(0 \leq \alpha \leq 1)$ and M are given by user.

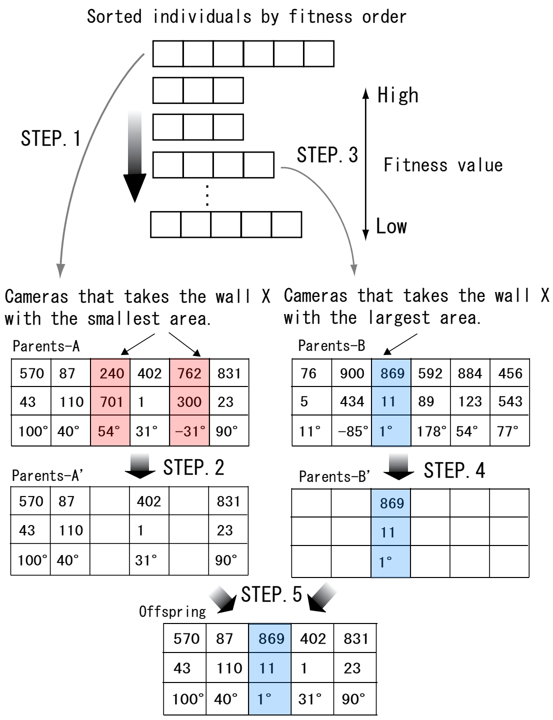

Figure 2: Crossover

Thus the maximum of fitness value for each wall is 200 when all the walls are taken, and it has appropriate overlaps between photographs.

3.2.3 Mutation

In GA, the contents of an individual are randomly changed by the mutation. It means that the direction and the position of the camera are changed by the mutation in this application. However, this mutation causes low fitness value at the last stage of evolutional process. Therefore we use the following two operations as the mutation.

If a camera takes only one wall, this camera is deleted from the individual to reduce the number of cameras. If a photograph taken by camera A is completely included the other photograph, the camera A is deleted from the individual.

3.2.4 Local search

Since GA is a kind of the probabilistic search, it dose not guarantee to find the optimum solution. To improve the quality of solution, local search operation is employed. The local search is operated as follows;

1. Change of the camera direction

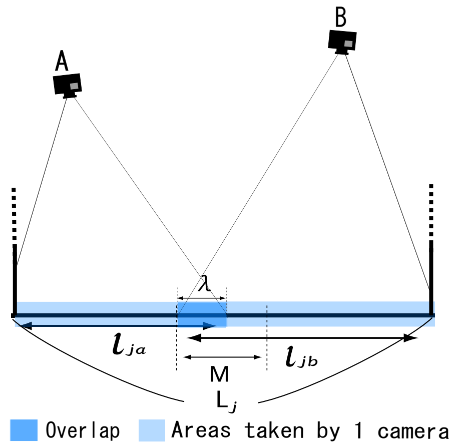

Figure 3: Parameters to calculate fitness

   (a) The angle of all cameras are changed from 0 to 360 degree at random. The angle with the highest fitness value is set to the new angle for each camera.

   (b) After above operation, the individual that have more than 90% of the elite's fitness values are selected. The angle of these cameras is changed within ±10 degree by one degree step, then the angle with the highest fitness value is selected.

2. Change of the camera position

   At first, the camera is provisionally moved to the eight neighbors of the current position. Then the camera is moved to the position with the highest fitness value.

4 Experiments and Discussions

4.1 Experimental conditions

For the experiments, we prepare a floor map based on the actual building in University of Miyazaki.

4.2 The parameter of GA

Parameters of GA for the experiments are described in below. These parameters are derived from the preliminary computer simulations.

- Maximum number of generations: 100
- Number of individuals: 100

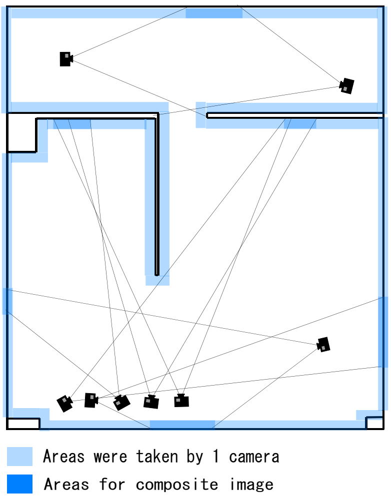

Figure 4: An example of camera layout at 100-th generation

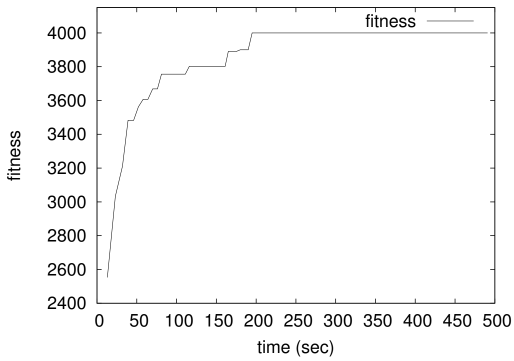

Figure 5: Change of fitness

- Number of offspring generated by Crossover: 100
- Initial number of cameras: 12
- Camera position interval: 0.5 (m)
- Walls in the floor map: 20
- Number of simulations: 30
- Desirable overlap length M: 0.03 (m)
- α :0.3

4.3 Experiments Results

In the 0-th generation, some walls are taken by more than two cameras, and some walls are not taken by any cameras. Figure.4 shows the camera position of an elite individual after 100 generations. As shown in Figure.4, all cameras take more than two walls with suitable overlap. In addition the number of cameras was decreased into 8. In this case, the fitness of the individual was arrived at the maximum value 4000. As a result, it is showed that our method could take multiple photographs including desirable overlap to synthesize a seamless indoor image of the building. Figure.5 shows changes of fitness value. As shown in Figure.5, the fitness reached the maximum value after 200 (sec) execution.

5 Conclusion

Recent progress of image processing technology leads many applications in real world. In particular composition of a seamless image from the multiple photographs taken from many viewpoints attracts attention in the movie fields. We propose a method to composition a seamless image by the minimum number of photographs. For this objective, we employed the genetic algorithm to find an appropriate layout of the cameras. To reduce the computation time we allowed the cameras to place on the discrete positions, and employ a powerful local search method to find the better camera layout. Simulations results showed that our method could derive the suitable camera layout that makes be possible to compose of a seamless image.

Future works remain as the experiments in the floor map containing some funiture, and we try to apply our method to 3-D buildings.

References

[1] H.Kitano,*Genetic Algorithm*, Sangyou tosho, 1993.

[2] M.Tanaka and M.Sakawa, *Genetic Algorithm*, Assakura shoten, 1999.

[3] H.Takeda, M.Yamasaki, T.Moriya, T.Minakawa, F.Beniyama and T.Koike,*A video-based virtual reality system*, ACM VRST'99 (ACM Symposium on Virtual Reality Software and Technology), pp.19-25, 1999.

[4] J.H. Holland, *Adaptation in Natural and Artificial Systems*, University of Michigan Press, 1975.

[5] D.E. Goldbreg, *GeneticAlgorithm in Search, Optimization and Machine Learning*, Addison Wesley, 1983.

The Tenth International Symposium on Artificial Life and Robotics 2005(AROB 10th '05),
B-con Plaza, Beppu, Oita, Japan, February 4-6, 2005

Real-Time Structure Preserving Image Noise Reduction For Computer Vision On Embedded Platforms*

Walter Nistico, Uwe Schwiegelshohn, Matthias Hebbel, Ingo Dahm
Department of Electrical Engineering
Computer Engineering Institute
University of Dortmund
Otto-Hahn-Str. 4, D-44221, Dortmund, Germany
name.surname@udo.edu

Abstract

A camera is often the main sensor of autonomous robots. As those embedded platforms offer minor computing power only, it is a challenge to provide a fast and robust image processing. This paper describes a new real-time structure preserving noise reduction operator based on the so-called SUSAN filtering approach. We use a correlation function to determine which part of a pixel's neighborhood has to be included in the smoothing process. Thus, the smoothing process takes place only inside homogeneous regions of the image, without blurring edges and bi-dimensional features which are needed for object recognition.

1 Introduction

With the recent development of autonomous mobile applications, embedded platforms have become a viable and convenient option for robotics (e.g. Sony ERS-7).However, embedded robotic platforms are severely limited in terms of processing resources, due to the space and power constraints which are a consequence of autonomous operation. Furthermore, low power consumption cameras can exhibit significant amounts of noise in the images they capture [1]. Linear noise reduction convolution operators, such as Gaussian smoothing filters, are relatively inexpensive in terms of computing power. Yet, they significantly alter crucial features for computer vision such as edges and corners. Non-linear operators which selectively determine what part of the convolution kernel to include in the smoothing process, exhibit satisfactory performance in terms of image structure preservation while effectively reducing noise [2]. On the other hand, as we will show, the computational cost of such filters makes them not suitable for real-time applications on embedded platforms.

*This work was supported by the Deutsche Forschungsgemeinschaft DFG under program of emphasis SPP 1125

2 Noise Reduction Filtering

Conventionally, noise reduction is done by cutting the high frequency components of an image. Thus, all relevant information of the high frequency part of the spectrum of the image is lost. This is why non-linear operators try to preserve image structures by selectively determine which part of a pixel's neighborhood has to be included in the smoothing process.

2.1 SUSAN Noise Filtering

The SUSAN noise reduction filter achieves this by applying a correlation function to calculate the similarity of the brightness of a pixel to be filtered with a neighborhood defined by a fixed convolution mask [2]:

$$c(p, p_0) = e^{-\left(\frac{I(p)-I(p_0)}{t}\right)^2} \tag{1}$$

In Equation 1 $c(p, p_0)$ represents the Gaussian correlation function, where the so-called nucleus $p_0 = (x_0, y_0)$ is the pixel which is going to be filtered, $p = (x, y)$ is a pixel which belongs to the convolution mask around the nucleus, and t is the brightness threshold which controls the width of the Gaussian. In the spatial domain, the SUSAN filter also makes use of a Gaussian weighing. Accordingly, the overall equation of the filter is given by Equation 2:

$$I'(p_0) = \frac{\sum\limits_{p \neq p_0} I(p) \cdot e^{-\frac{r^2}{2\sigma^2} - \left(\frac{I(p)-I(p_0)}{t}\right)^2}}{\sum\limits_{p \neq p_0} e^{-\frac{r^2}{2\sigma^2} - \left(\frac{I(p)-I(p_0)}{t}\right)^2}} \tag{2}$$

Here, $I(x, y)$ is the brightness of a pixel before filtering, $I'(x, y)$ is the filtered brightness , and σ determines the spatial Gaussian weighing.In case the denominator of such a function for a given pixel is zero, it means that its whole neighborhood is uncorrelated with it, and hence it's treated as pulse noise. This is dealt with by using as an estimate for the pixel brightness the *median* of its 8 closest neighbors [3].

2.2 Going Real-Time

An efficient implementation of such a filter is to precalculate the non-linear correlation function for a chosen t in a look-up-table L. Using the Sony ERS-7 as a reference implementation, the total size of such a table is 2044 byte. In the following, this will be referred to as

$$L_{corr.}[\Delta I] := exp \quad -\left(\frac{\Delta I(x,y)}{t}\right)^2\Bigg) \tag{3}$$

Further, it has to be specified the spatial scale of the smoothing σ, which can be also precalculated and stored in the convolution mask of neighbors:

$$L_{mask}[\Delta x][\Delta y] := exp\left(-\frac{(\Delta x)^2 + (\Delta y)^2}{2\sigma^2}\right) \tag{4}$$

Now for each pixel in the mask of neighbors, applying Equation 2 can be done at the cost of 2 look-ups, a division and several multiplications and additions(depending on the mask size).

If the denominator of Equation 2 equals zero, the eight closest neighbor's brightnesses have to be put in an array which has to be sorted, and the 2 median values averaged. Due to efficiency reasons, we recommend the use of the insertion sort algorithm [4].

In all other cases, the division is the most complex and expensive operation in terms of execution time, followed by the multiplication [5, 6].

In order to avoid one source of multiplications involved in the original algorithm, we chose to replace the correlation function with a $rect_{2\tau}(p, p_0)$: having a sharper cutoff, the optimal threshold τ is somehow more dependent from the amount of noise present in the images ([2]), however having a binary co-domain for the function means that we can represent it with integer values, and use the smallest data type offered by the processors for that purpose, which is the byte, reducing the size of the look up table to $\frac{1}{4}$ of the original, for a total of 511 byte. This can be further reduced, in case of processors with very limited cache amounts, by introducing a quantization $n : 1$ (with $n = 2^i$, works well for $i = 1, 2$) in the domain of the function, which has the only negative effects of an increase of granularity of the threshold value (which can then assume only values $mod_n(t) = 0$) and require an additional shift operation of ΔI by i positions. The multiplication can be avoided, by using $c(p, p_0) = -rect_{2\tau}(p, p_0) \in \{0, -1\}$ whose domain is represented in signed byte format respectively as 00000000 and 11111111, hence the correlation weighing can be performed with a simple bitwise logical operation $AND\,\langle I(p), c(p, p_0)\rangle$. The remaining multiplications can be avoided by approximating the original Gaussian spatial weighing with a special mask that is illustrated by Figure 2. Then, no spatial weighing multiplications are required, because the neighbors whose weight is 0 in the mask are simply not included in the numerator and denominator sums n and d. As a result, let $M = \{(1, 1); (1, -1); (-1, 1); (-1, -1)\}$ represent the neighbors considered by the algorithm, the equation of the new filter is:

$$I'(p_0) = \frac{\sum\limits_{p \in M} I(p) \cdot rect_{2\tau}\left(I(p) - I(p_0)\right)}{\sum\limits_{p \in M} rect_{2\tau}\left(I(p) - I(p_0)\right)} \tag{5}$$

In order to speed-up the division operation, we first have to note that the denominator d of such a function can assume only 5 possible values: $d \in \{0, 1, 2, 3, 4\}$, which represents how many neighbors are "similar" to the nucleus for a given pixels. The statistical incidence of each case is dependent on the threshold τ of the correlation function: obviously, for $\tau = 0 \overset{\forall(x,y)}{\Rightarrow} d(x, y) = 0$, while for $\tau = 255 \overset{\forall(x,y)}{\Rightarrow} d(x, y) = 4$. Using a sample of 100 images captured from the on-board camera of our robot (Aibo ERS7) from real-world situations, we have measured that for values of $\tau \geq 6$ case $d(x, y) = 4$ totally dominates with more than 80% of occurrences (which become $> 91\%$ for $d(x, y) = 10$): following the criterium of making the common case fast, we have replaced the division with a series of nested conditional branches, such that in the most common case only one conditional branch is performed, followed by the second most common with 2, and so on.

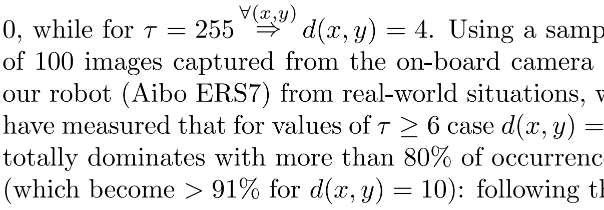

The following case differentiation shows, what operations should performed according to the denominator value d in order to achieve optimized processing speed:

- d=4: replace division by a shift-right instruction by two positions: $I'(x,y) = n(x,y) >> 2$
- d=3: approximation: add nucleus to numerator and divide by four $I'(x,y) = (n(x,y) + I(x,y)) >> 2$
- d=2: replace devision by a shift-right instruction by one bit $I'(x,y) = n(x,y) >> 1$
- d=1: nothing to divide
- d=0: perform median filtering: just discard the maximum and minimum, then average the remaining.

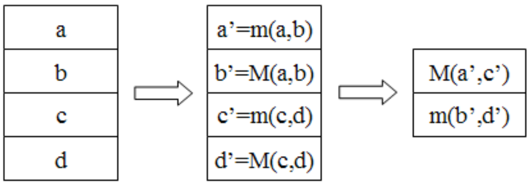

Figure 1: Calculating the median. $\{a,b,c,d\}$ is the set of neighbours, $m(x,y)$ stands for the minimum and $M(x,y)$ for the maximum of elements x and y, the 2 final values have to be averaged.

3 Performance Analysis

To better evaluate the performance of our new approach, we have separated our tests into two categories: structure preservation in noisy images, and run-time measurements. The latter is particularly important for our application domain, since the filter is meant to be used on a robot with limited computational resources in a dynamic and competitive environment, where it has to quickly react to the changing situations. As a reference, we have compared our filter, that here will be referred to as "SUSAN RealTime", with the following operators:

- the original SUSAN, presented with the smallest mask suggested by its authors (3×3), in order to minimize its running time;
- the Gaussian, with mask size also 3×3, in the most popular and computationally efficient variant, as shown in Figure 2.

0	1	0
1	0	1
0	1	0

1	2	1
2	4	2
1	2	1

Figure 2: Masks of neighbors, integer approximation of the original gaussians. Left: SUSAN RealTime mask. Right: Gaussian with $\sigma^2 \approx 0.64$.

3.1 Running Time

We measured the running time of each filter over 100 images captured by the camera of the robots: on the robot Sony Aibo ERS7 the camera has a resolution of 208×160 pixel, 24 bit per pixel. In all cases, the filters were running in normal conditions of operations, thus in parallel with other system threads. While the SUSAN RealTime execution time is dependent on the brightness threshold used, we have empirically derived the optimal for the noise present in the images ($\tau = 14$), and we have verified that its speed is only $\approx 1\%$ slower than the best case which is ($\tau = 255$).

ERS7 576MHz, 208×160 pixel image			
Filter	*Average(ms)*	*Min*	*Max*
SUSAN RT $\tau = 14$	9.904	9.8	10
SUSAN $\tau = 12$	50.796	50.65	50.95
Gaussian $\sigma^2 \approx 0.64$	5.864	5.75	6

As can be seen, the SUSAN RT is ≈ 5 times faster than the original algorithm, and in tests where the latter used the same mask, our approach was still ≈ 3 times faster. Compared to the gaussian, it's ≈ 1.7 times slower, which is a very good result for a non-linear filter. A more detailed comparison can be found in [7].

3.2 Noise Reduction

To evaluate the noise reduction and structure preservation capabilities, we have followed a similar approach as in the original SUSAN article ([2]), but with a notable exception: the results will be measured after a single application of each filter, this because in our domain the total execution time is critical, making unfeasible a repeated iteration until the error variance reaches 0. For each filter which requires to determine a threshold, we have used in all tests the value which provided the overall best score: using different thresholds in different tests would yield higher scores, but this doesn't reflect the real usage, since several kinds of noise are present simultaneuosly inside real images, and the amount of edges and bi-dimensional structures is varying continuously depending on the objects present in the scene.

Edge Preservation, 10% of Noise, final gradient			
Filter	*Gaussian*	*Pulse*	*Uniform*
SUSAN RT $\tau = 24$	55.51	53.45	54.44
SUSAN $\tau = 19$	55.09	51.56	54.35
Gaussian $\sigma^2 \approx 0.64$	34.72	33.54	34.03

Table 1: The reference image is a perfect step edge of 300 pixel length, with gradient of ($\Delta = 55$). Higher numbers mean a better score.

Corner Preservation, 10% of Noise, final σ			
Filter	*Gaussian*	*Pulse*	*Uniform*
SUSAN RT $\tau = 24$	4.39	6.07	4.68
SUSAN $\tau = 19$	3.77	10.93	4.33
Gaussian $\sigma^2 \approx 0.64$	4.60	10.77	4.78

Table 2: The reference image is 102×102, with a uniform brightness of 112, which contains 100 squares of size 5×5 and brightness 135, so the feature strength is ($\Delta = 25$). Lower numbers mean a better score.

For all the experiments we have made, it must be noted that the SUSAN RealTime is performing better than the original in presence of pulse noise: this is a consequence of having a smaller mask, so that the chances of finding two similar noise spikes inside it are lower, and because of the sharper correlation function. The gaussian filter performed badly, reducing the strength of edges and corners; the original SUSAN overall provided the best filtering, however the new SUSAN RealTime scored very close to it, and proved to be very well balanced in all test conditions.

4 Results

We have used the SUSAN RealTime filter in the image processor of our RoboCup team *Microsoft Hellhounds* (which is part of the GermanTeam that won RoboCup 2004 in Lisbon) to take part at several RoboCup competitions: GermanOpen 2004, AustralianOpen 2004, AmericanOpen 2004, and JapanOpen 2004. The average running time of the whole image processor, on the Sony ERS7 robot, was 17ms for a frame processing rate of 28.5 fps, which was more than adequate to track fast moving objects. The performance of the suggested approach is analyzed both in terms of noise filtering and structure preservation as well as in terms of running time on different CPU architectures. We proved that this filter combines the benefits of non linear structure preserving operators with processing times comparable to linear ones. We presented a practical application for the RoboCup Four-Legged Soccer League. Furthermore, we showed that the limits of this approach (the lack of scalability in terms of noise filtering due to the spatial constraints and the rippling behavior in the high frequency range) cannot be overcome with traditional approaches as well within the typical processing constraints of real-time applications on embedded platforms. Compared to existing algorithms, the suggested approach provides an excellent ratio between image quality and runtime behavior. As a final conclusion, this efficient algorithm for image processing helps to save processing power which can be used for less time-critical applications like AI or task scheduling.

References

[1] J. Bunting, S. Chalup, M. Freeston et.al., "Return of the NUbots! The 2003 NUbots Team Report," Tech. Rep. N.N., Newcastle Robotics Laboratory, The University of Newcastle, Australia, 2003.

[2] S. M. Smith and J. M. Brady, "SUSAN - A New Approach to Low Level Image Processing," *Int. Journal Computer Vision*, vol. 23, no. 1, pp. 45–78, 1997.

[3] M. Singh and P. K. Bora, "Two-Dimensional Linear Prediction Based Median Filtering," 2002.

[4] R. Sedgewick, *Algorithms*, ch. 9, pp. 120–125. Addison-Wesley, 2nd ed., 1984.

[5] D. A. Patterson and J. L. Hennessy, *Computer Organization & Design. The Hardware/Software Interface*, ch. 4. Morgan Kaufmann, 1994.

[6] J. L. Hennessy and D. A. Patterson, *Computer Architecture - A Quantitative Approach*, ch. 3, 5, Appendix H. Morgan Kaufmann, 3rd ed., 2003.

[7] W. Nistico, U. Schwiegelshohn, M. Hebbel, and I. Dahm, "SUSAN RealTime - Structure Preserving Noise Reduction For Computer Vision," Tech. Rep. 1004, University of Dortmund, 2004.

The Tenth International Symposium on Artificial Life and Robotics 2005(AROB 10th '05),
B-con Plaza, Beppu, Oita, Japan, February 4-6, 2005

Model-less Visual Servoing Using Modified Simplex Optimization

K. Miura, K. Hashimoto, H. Inooka
Graduate School of Information Sciences
Tohoku University
Aramaki aza aoba01,
Aoba-ku, Sendai, 980-8579, Japan

J. A. Gangloff, M. F. de Mathelin
LSIIT UMR CNRS 7005
Louis Pasteur Strasbourg University
Bd. S. Blant,
67412 Illkirch Cedex, France.

Abstract

In this paper, we present a robot positioning task with respect to a static target by visual servoing. The vision system is uncalibrated and the kinematic model of the robot may be totally unknown. The displacements of the robot in joint level are generated in real time in order to minimize an objective function. The objective function includes the quadratic error between the current and the desired target images. A *simplex* method is used to minimize the objective function, and a Newton-like method is also used near the convergence. We successfully validate this method with simulations under the graphic library OpenGL.

1 introduction

Most of the previous works on visual servoing assume that the kinematic model of the robot and the camera intrinsic parameters are known. Most of these methods could work with weak calibration, but they would fail if the robot and the vision system were fully unknown.

Uncalibrated and model-less visual servoing has been addressed by Hosoda *et al.* [1], and Jägersand [2]. They use an on-line estimation of the Jacobian between the joint velocities of the robot and the feature velocities in the image plane. Their approach assumes the on-line identification of a large number of parameters. In the presence of noise, this type of approach may lead to a badly estimated Jacobian matrix if the motions of the robot do not guarantee identifiability of the parameters.

In previous research, we proposed a novel approach for uncalibrated and model-less visual servoing using a modified *simplex* iterative search method is proposed. We successfully demonstrated the algorithm with a industrial manipulator[4]. However, it usually requires a lot of iteration to complete the positioning task accurately.

In this paper, a Newton-like optimization algorithm is adopted for quicker convergence. The simulations are carried out in the case where the kinematic model of the robot is unknown, assuming that the joint limits are known. The intrinsic parameters of the camera are also unknown. The improvement of the convergence speed is discussed with the simulation results.

2 Simplex method and its modification for visual servoing

2.1 Conventional simplex method by Nelder and Mead

Simplex method is an unconstrained optimization technique. Note that it is different from the linear programming technique method also called "simplex". This method was originally proposed by Spendley, Hext, and Himsworth [7] and was developed later by Nelder and Mead [5].

This section deals with the methods for solving the minimization problem:

$$\text{Find } \boldsymbol{X} = \{x_1, x_2, \ldots, x_n\} \text{ which minimize } F(\boldsymbol{X}) \quad (1)$$

The geometric figure whose vertices are defined by a set of $n+1$ points in an n-dimensional space is called a simplex. For example, in two dimensions, the simplex is a triangle, and in three dimensions, it is a tetrahedron.

The basic idea in the simplex method is to compare the value of the objective function at the $n+1$ vertices of a simplex and move the simplex gradually toward the optimum point during the iterative process, known as reflection, contraction, and expansion.

If $\boldsymbol{X}_h$ is the vertex corresponding to the highest value of the objective function among the vertices of a simplex, we can expect the point $\boldsymbol{X}_r$ obtained by reflecting the point $\boldsymbol{X}_h$ in the opposite face to have a smaller value. Mathematically, the reflected point $\boldsymbol{X}_r$ is given by;

$$\boldsymbol{X}_r = \alpha(\boldsymbol{X}_o - \boldsymbol{X}_h) + \boldsymbol{X}_o \quad (2)$$

where $\boldsymbol{X}_o$ is the centroid of all the points $\boldsymbol{X}_i$ except $i = h$, and α is the reflection coefficient ($\alpha > 0$).

In the case $f(\boldsymbol{X}_r)$ gives the smallest cost between all the vertices, one can generally expect to see the function value decrease further by expanding $\boldsymbol{X}_r$ to $\boldsymbol{X}_e$;

$$\boldsymbol{X}_e = \gamma(\boldsymbol{X}_r - \boldsymbol{X}_o) + \boldsymbol{X}_o \quad (3)$$

where γ is called the expansion coefficient ($\gamma > 1$).

If the reflection process gives a worst value, $\boldsymbol{X}_r$ is contracted to $\boldsymbol{X}_c$;

$$\boldsymbol{X}_c = \beta(\boldsymbol{X}_h - \boldsymbol{X}_o) + \boldsymbol{X}_o \quad (4)$$

where β is called the contraction coefficient ($0 \leq \beta \leq 1$).

If the contracted point still has worst value, the contraction process will be a failure, and in this case we apply a reduction process, *i.e.* all $\boldsymbol{X}_i$ are replaced by;

$$\mathrm{new}\boldsymbol{X}_i = \frac{1}{2}(\boldsymbol{X}_i + \boldsymbol{X}_l) \quad i = 1, 2, \ldots, n+1 \quad (5)$$

with $\boldsymbol{X}_l$, the vertex where the objective function is minimum. Then, we restart the reflection process.

The method is assumed to reach convergence whenever some stopping criteria have been met, e.g.:

$$\sqrt{\sum_{i=1}^{n+1} \frac{\{F(\boldsymbol{X}_i) - \bar{F}\}^2}{n+1}} \leq \varepsilon_1, \ \textit{with} \ \bar{F} = \sum_{i=1}^{n+1} \frac{F(\boldsymbol{X}_i)}{n+1} \quad (6)$$

$$\text{or} \quad F(\boldsymbol{X}_l) \leq \varepsilon_2 \quad (7)$$

2.2 Modified simplex method for real-time visual servoing

We slightly modify the Nelder and Mead simplex method for the particular case of visual servoing with a robot. The main idea is to use a simplex like optimization algorithm to move the robot from an initial position to a goal position, so that the robot is performing the optimization. Since the vision system acquires images continuously and assuming that joint angles are also measured, the cost function can be computed along the trajectory of the robot while it is moving from a vertex to its reflection point. Therefore, the optimum could be selected along that vertex. In real-time, in other words, this is equivalent to modifying the Nelder and Mead simplex method by adding a line search procedure during the reflection, expansion, or reduction process. With this technique, the contraction process is omitted and faster convergence is expected.

3 Newton-like optimization method

Assuming that m features are detected in the image, let define $f(\boldsymbol{X})$ as the m-dimensional vector of the feature errors, where $\boldsymbol{X}$ is the vector of size n defining the position of the robot (e.g., $\boldsymbol{X}$ are the joint angles). Hence, the feature error vector $f(\boldsymbol{X}) = 0$ if $\boldsymbol{X} = \boldsymbol{X}^*$, the desired position of the robot. Therefore, the positioning task using visual servoing is achieved by minimizing the following objective function:

$$F(\boldsymbol{X}) = \frac{1}{2} f(\boldsymbol{X})^\top f(\boldsymbol{X}) \quad (8)$$

$$\text{with} \quad f(\boldsymbol{X}) = \begin{pmatrix} f_1(\boldsymbol{X}) \\ \vdots \\ f_m(\boldsymbol{X}) \end{pmatrix} \quad (9)$$

Indeed, the feature error value $f(\boldsymbol{X}^*) = 0$ minimizes $F(\boldsymbol{X})$.

A Newton-like algorithm is given by:

$$\boldsymbol{X}_{k+1} = \boldsymbol{X}_k - \alpha_k (J_k J_k^\top)^{-1} J_k f(\boldsymbol{X}_k) \quad (10)$$

where, $0 < \alpha_k$ is the step size in the descent direction, and $J(\boldsymbol{X})$ is the $n \times m$ Jacobian matrix of the feature errors:

$$J_{ij}(\boldsymbol{X}) = \frac{\partial f_j(\boldsymbol{X})}{\partial x_i} \quad (11)$$

and $J_k = J(\boldsymbol{X}_k)$.

If the Jacobian matrix is unknown, it must be estimated on-line. Piepmeier *et al.* [6] presented a moving target tracking task based on the quasi-Newton optimization method. The Jacobian of the objective function is estimated on-line with a Broyden's update formula (equivalent to a LMS algorithm). This approach is adaptive, but cannot guarantee the stability of the visual servoing scheme in presence of large errors in the image or if the motions of the robot do not guarantee identifiability of the parameters.

It should be pointed out that the Newton optimization algorithm has local properties of convergence, i.e., it will converge toward the nearest local minimum of $F(\boldsymbol{X})$

The Tenth International Symposium on Artificial Life and Robotics 2005(AROB 10th '05),
B-con Plaza, Beppu, Oita, Japan, February 4-6, 2005

4 Simulation

4.1 Experimental procedure

The model of robot manipulator is a 6DOF industrial manipulator, and the target object is a cylindrical white cup in Fig. 1. The task consists in bringing the end-effector fitted with a camera (eye-in-hand configuration) at the vertical of the object. To compare several optimization runs, we use the same starting positions.

Three procedures are compared with respect to the number of iterations and the accuracy of the convergence:

Scheme1: A positioning task is carried out only with the simplex optimization.

Scheme2: During simplex iterative search, on-line Jacobian estimation using a Broyden's update formula is carried out using the information at the simplex vertices. Once the simplex optimization arrives near the minimum, the process switches to the Newton-like optimization with Eq. 10.

Scheme3: The process switches to the Newton-like optimization without on-line Jacobian estimation during the simplex optimization phase. The Jacobian matrix is estimated with small movement around the current position.

Furthermore, to accelerate the convergence, a hybrid scheme combining an optimization algorithm with an image-based partial visual servoing loop is proposed. The idea is to bring the target object to the center of the image, during the optimization process. Thus the target will not be lost during the iterative search, which is a well known problem in visual servoing (cf. E. Malis [3]). The manipulator has six joints, and the image-based centering scheme is assigned to two joints near the end-effector. Three joints are controlled by the simplex and Newton-like optimization, and a joint is fixed.

4.2 Objective function

The objective functions are usually selected as sum of square of feature errors. A possible objective function could have the following features:

- The distance between the end-effector and the object is given by its size in the image.
- The angle between the object axis (cylinder axis) and the optical axis of the camera is given by the form factor of its image (form factor = 1 when this angle is zero). This angle can be decomposed in two elementary angles (*e.g.* roll and pitch).

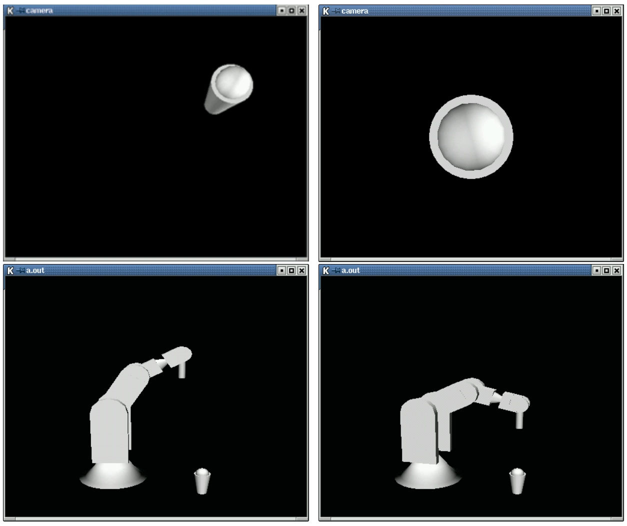

(a)start position (b)final position

Figure 1: Start and goal position of the robot and their images taken at the end-effector

We also use the sum-of-square-difference (SSD) of each pixel intensity between the current and the reference image of the object as an error. Note that SSD does not need feature extraction.

For this task, we propose the following objective/cost function:

$$F(\boldsymbol{X}) = \frac{1}{2} f(\boldsymbol{X})^\top f(\boldsymbol{X}) \tag{12}$$

where,

$$\begin{aligned} f_1(\boldsymbol{X}) &= W_1 \left(\frac{s}{S} - 1 \right) \\ f_2(\boldsymbol{X}) &= W_2 \left(\frac{l_{long}}{l_{short}} - 1 \right) \\ f_3(\boldsymbol{X}) &= W_3 \sum_{i,j} \left(P_{cur}(i,j) - P_{ref}(i,j) \right)^2 \end{aligned}$$

where s and S are the actual and the desirable size of the object in the image, l_{long} is the longest distance from the center of the object to its contour, and l_{short} is the shortest one. Therefore $\frac{l_{long}}{l_{short}}$ is the form factor of the object image. P_{cur} and P_{ref} are pixel intensities of the current and the reference image, respectively. Finally, W_1, W_2, and W_3 are the respective weights of feature errors in the cost function.

5 Results and Discussion

Simulations were carried out comparing several schemes. All schemes were executed with modified simplex optimization until rough convergence. Termination tolerance in Eq.6 and Eq.7 were decided experimentally.

Scheme1 converged, but it took more iteration near the minimum. The modified simplex roughly converged with 16 iterations, and the process took 27 iterations near the minimum. The vertices of the simplex often fell into a small local minimum, and the simplex restarted the process again.

Scheme 2 did not converged. The estimated Jacobian was not close enough to the true Jacobian. Though this type of estimation method guarantees the accuracy in a small area, the estimation used the image data at the vertices of the simplex in a large area. A solution is to have a large forgetting factor λ, however, it may lead to a badly estimated Jacobian matrix in the presence of noise.

Scheme 3 converges quicker than simplex near the minimum with 36 total iterations. The trajectory was also very simple, as shown in Fig. 2. However, this scheme was not always robust when the objective function had large noise at the initial position of the Newton-like optimization process.

All these experiments make it clear that the optimization with only the simplex method takes many iterations near the minimum. Newton-like method with on-line Jacobian estimation converged faster, since the Newton optimization algorithm has better local properties of convergence. However, it has a risk of a badly estimated Jacobian matrix in the presence of noise.

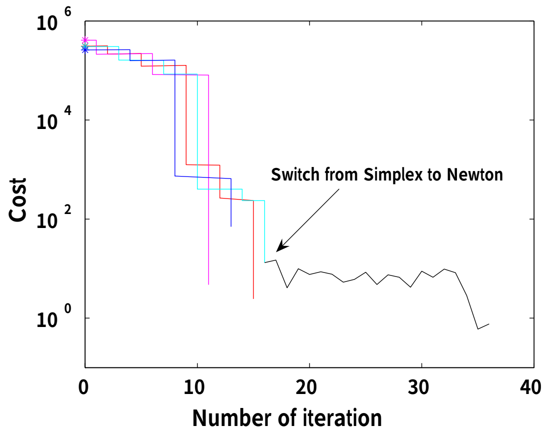

Figure 2: Trajectory of the optimization process

6 Conclusion

In this paper, we used the modified simplex optimization techniques for a positioning task by visual servoing. This method does not need a model of the robot and does not require the estimation of Jacobian matrices. Thus, a robot never goes in the wrong direction due to the bad estimation. Moreover, the objective function does not need to be differentiable.

Since the simplex method took more iterations near the minimum, the Newton-like method with on-line Jacobian matrix estimation was also executed in order to have quicker convergence. We successfully demonstrated the proposed scheme with simulations.

Improvements are needed for stable convergence. Jacobian matrix estimation was not always correct because of the large motions of the robot between the vertices of the simplex that do not guarantee sufficient excitation for the identification of the parameters.

For the future works, it is important to find the objective function without noise, which may cause a badly estimated Jacobian matrix.

References

[1] K. Hosoda, and M. Asada, Versatile Visual Servoing without Knowledge of True Jacobian, Proc. of the IEEE/RSJ Int. Conf. on Intelligent Robots and Systems, Munchen, September 1994.

[2] M. Jägersand, O. Fuentes, and R. Nelson, Experimental Evaluation of Uncalibrated Visual Servoing for Precision Manipulation, Proc. of the 1997 IEEE Int. Conf. on Robotics and Automation, New Mexico, April 1997.

[3] E. Malis, F. Chaumette, and S. Boudet, *2 1/2 D Visual Servoing*, IEEE Transactions on Robotics and Automation, Vol. 15, No. 2, pp. 238–250, 1999.

[4] K. Miura, J. A. Gangloff, and M. F. de Mathelin, *Robust and Uncalibrated Visual Servoing without Jacobian using a Simplex Method*, Proceedings of the 2002 IEEE/RSJ International Conference on Intelligent Robots and Systems, Lausanne, September 2002.

[5] J. A. Nelder, and R. Mead, *A simplex method for function minimization*, Computer Journal, Vol. 7, No. 4, pp. 308–313, 1965.

[6] J. A. Piepmeier, G. V. MacMurray, and H. Lipkin, Uncalibrated Dynamic Visual Servoing, IEEE Transactions on Robotics and Automation, Vol. 20, No. 1, pp.143–147, 2004.

[7] W. Spendley, G. R. Hext, and F. R. Himsworth, *Sequential application of simplex designs in optimization and evolutionary operation*, Technometrics, Vol. 4, pp. 441–461, 1962.

The Tenth International Symposium on Artificial Life and Robotics 2005(AROB 10th '05),
B-con Plaza, Beppu, Oita, Japan, February 4-6, 2005

Impulsive noise reduction using M-transform and wavelet with applications to AFM signals

Hiroshi Harada, Kumamoto University, hiroshi@mech.kumamoto-u.ac.jp, Japan
Su-Kyun Jeon, Kumamoto University, jsk4544@hotmail.com, Japan
Hiroshi Kashiwagi, Kumamoto University, kashiwa@gpo.kumamoto-u.ac.jp, Japan

Abstract

The authors propose here a new method for reducing both impulsive noise and white noise by use of M-transform and wavelet shrinkage. M-transform is a new signal transformation proposed by the authors, and any periodic time signal can be considered as the output of a filter whose input is an M-sequence. By using the properties of M-tarnsform, it is shown that both impulsive noise and white noise can be eliminated by use of first M-transform and then wavelet shrinkage. This method is applied to the signal obtained in Atomic Force Microscope(AFM) signal which usually contains many impulsive noise and withe noise. The result of experiments show that this method can be widely applied to practical situations for reducing both impulsive and white noise.

1 Introduction

In this paper, the authors propose a new method for impulsive noise reduction by using M-transform and wavelet shrinkage. Various filters such as Wavelet shrinkage have been proposed for the removal of white noise included in a signal[1]. However, these methods are based on assumption that the removed noise is a Gaussian white noise. Therefore, when a white noise and an impulsive noise are included in the observed signal, the impulsive noise can not be removed.

The authors have recently proposed a new signal processing technique called M-transform[2]. By using M-transform, both impulsive noise and a white Gaussian noise are converted into a small-amplitude random signal. By combining M-transform and Wavelet shrinkage, a new method is proposed here to remove both impulsive noise and white noise simultaneously in Atomic Force Microscope(AFM) signal. From the results of computer simulation, the proposed method is shown to be very efficient to remove both impulsive noise and white noise in AFM signal.

2 M-transform

M-transform is a new signal processing technique proposed by the authors[2]. This transform is based on the pseudo-orthogonal property of a pseudo-random M-sequence. Just like in case of Fourier transform where any time signal can be expressed as a sum of sinusoidal signals by use of Fourier transform, any periodic time function can be considered to be a weighted sum of M-sequences.

Let $\{a_i\}$ ($a_i = 1$ *or* 0) be an n-th order M-sequence. Then, we provide a new sequence $\{m_i\}$ as is defined in Eq.(1).

$$m_i = 1 - 2a_i \ (0 \le i \le N-1) \tag{1}$$

Here, $N = 2^n - 1$ is a period of the M-sequence.

A matrix M_i of $N \times N$ degree is defined by the next equation.

$$M_i = \begin{bmatrix} m_i, m_{i-1}, \cdots, m_{i-N+1} \\ m_{i+1}, m_i, \cdots, m_{i-N+2} \\ . \\ . \\ m_{i+N-1} \cdots\cdots, m_i \end{bmatrix} \tag{2}$$

Let X_i be an arbitrary periodic discrete time signal represented as

$$\begin{aligned} X_i &= (x(i), x(i+1), \cdots, x(i+N-1))^T \quad (3) \\ x(i) &\triangleq x(i\Delta t) \end{aligned}$$

where Δt is a sampling period. Then, M-transform A of the signal X_i is uniquely determined as

$$X_i = M_i A \tag{4}$$
$$A = (M_i^T M_i)^{-1} M_i^T X_i \tag{5}$$

The definition of M-transform is shown in Fig.1.

Any periodic time signal X_i can be considered as the output of a filter whose input is an M-sequence.

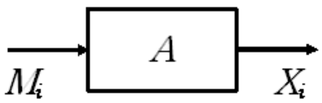

Figure 1: M-transform

Impulsive noise is converted into small-amplitude random signals through M-transform. Let P be a periodic time signal, in which a single impulse is included.

$$P(i) = (0, 0, \cdots, p_l, 0, \cdots, 0)^T \tag{6}$$

Here, l means a position of the impulse and p_l is the amplitude of the impulse. Substituting Eq.(6) into Eq.(5), M-transform A_p of the signal P is given as

$$A_p = (\alpha_p(0), \alpha_p(1), \cdots, \alpha_p(N-1)) \tag{7}$$

$$\alpha_p(i) = \frac{1}{N+1}(m_{i+l} - 1)p_l \tag{8}$$

Since the amplitude p_l is a constant, it is clear that the impulsive noise is converted into a small amplitude M-sequence. M-transform of a time signal is equivalent to calculating the cross-correlation between the time signal and M-sequence. Since white noise does not correlate with an M-sequence, M-transform of a white signal also becomes a random signal having small amplitude. Thus, these two different kinds of noise become the small-amplitude random signal through M-transform.

3 Wavelet Shrinkage

In the method called wavelet shrinkage, the noise included in the signal is removed according to the following procedures[1]. Let $u(i)$ be a discrete time original signal and $e(i)$ be a Gaussian white noise. Then, the observed signal $x(i)$ is given by the next equation.

$$x(i) = u(i) + e(i) \quad (i = 0, 1, \cdots, L-1) \tag{9}$$

Here, L is a length of the signal. Computing a level J_L orthogonal wavelet transform of the observed signal $x(i)$, the wavelet coefficient $W_x^{(j)}(k)$ is given by the next expression.

$$\begin{aligned} &W_x^{(j)}(k) = W_u^{(j)}(k) + W_e^{(j)}(k) \\ &(j = 1, \cdots, J_L; k = 0, 1, \cdots, L_j - 1) \end{aligned} \tag{10}$$

Here, L_j is a length of the wavelet coefficient at level j. Since wavelet transform is a linear transformation, the wavelet coefficients $W_e^{(j)}(k)$ of the white noise become also white noise. On the other hand, when the original signal $u(i)$ does not contain high-frequency component, the coefficients $W_u^{(j)}(k)$ become 0. Thus, the white noise can be removed by removing the coefficient $W_x^{(j)}(k)$ below a threshold level λ. For the thresholding, Donoho[1] used the following equation.

$$W_x^{'(j)}(k) = \begin{cases} sgn(w_x^{(j)}(k)(|w_x^{(j)}(k)| - \lambda) \cdots \\ \qquad \cdots (if\ |w_x^{(j)}(k)| > \lambda) \\ 0 \cdots\cdots\cdots (if\ |w_x^{(j)}(k)| \le \lambda) \end{cases} \tag{11}$$

Here, $sgn(x)$ is a function satisfying,

$$sgn(x) = \begin{cases} 1\ (x > 0) \\ -1\ (x < 0) \end{cases} \tag{12}$$

This method is called soft-thresholding. If the standard deviation σ of the Gaussian noise is already known, the threshold level λ can be determined by

$$\lambda = \sigma\sqrt{2\ log\ L} \tag{13}$$

Noise reduction is completed by reconstructing the signal by using the coefficient $W_x^{'(j)}(k)$ processed by Eq.(11).

4 Impulsive noise reduction method

The noise reduction method for both impulsive noise and white noise in AFM signal by using M-transform and wavelet shrinkage is as follows[4].

Let $x(i)$ be a time signal which includes both impulsive noise $p(i)$ and white noise $e(i)$.

$$x(i) = u(i) + e(i) + p(i) \tag{14}$$

$$X_n = (x(0), x(1), \cdots, x(N-1))^T \tag{15}$$

Then, M-transform A of the noisy signal X_n is calculated by Eq.(5).

$$A = A_u + A_e + A_p \tag{16}$$

Here, A_u, A_e and A_p are the M-transform of the original signal, white noise and impulsive noise, respectively. As mentioned above, both impulsive noise

$p(i)$ and white noise $e(i)$ are converted into small-amplitude random signals through M-transform. So, if we apply the wavelet shrinkage method to the M-transform $\alpha(i)$ intead of the time signal $x(i)$, it is possible to remove both impulsive noise and white noise.

The method for noise reduction proposed in this paper is as follows. First, M-transform A of the AFM signal $x(i)$ is calculated. Then, the wavelet shrinkage method is applied to the M-transform A. After the wavelet shrinkage, the filtered signal is transformed into time domain through the inverse M-transform and the noise reduction procedure is completed.

Fig.2 shows the procedure of the proposed noise reduction method.

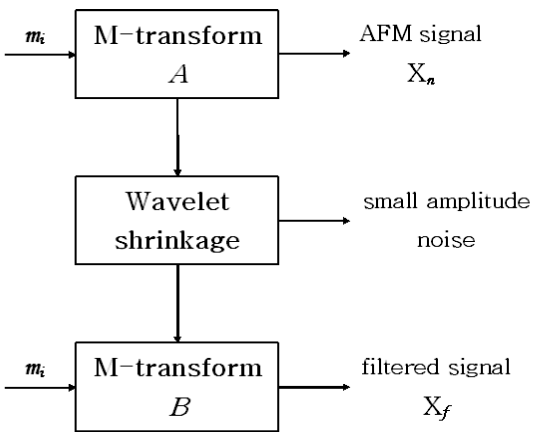

Figure 2: Procedure of the proposed noise reduction method

5 Application of the proposed method to atomic force microscope signal

Atomic force microscope(AFM) can measure the surface profile very precisely by using the atomic force operating between a probe and the sample surface. A schematic configuration of AFM is shown in Fig. 3. AFM mainly consists of three parts, a cantilever, a displacement sensor and scanning element. The cantilever converts the atomic force that is received by a probe into displacement. The displacement sensor detects the deflection of the cantilever. The scanning element is used to move the sample in high accuracy in three-dimensional space. AFM has the following features.

1. AFM possesses the spatial resolution at an atomic level.

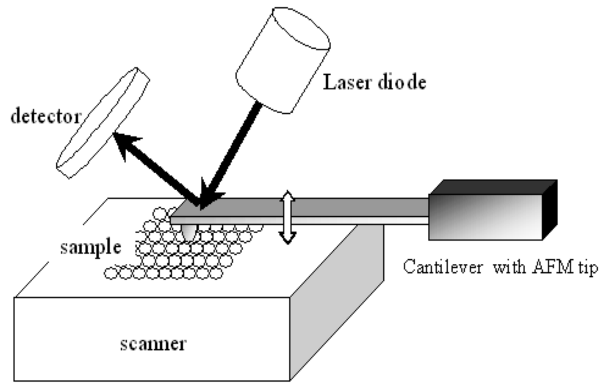

Figure 3: Structure of AFM

2. AFM does not need a special operating environment, and be able to measure the surface profile in atmosphere, in liquid, and in the vacuum.

3. Unlike the scanning electron microscope, AFM can measure surfaces of the conductive material, ceramics, the polymeric material, and the biological material.

4. AFM can measure various kinds of force such as van der Waals force, repulsive force and adhesive force.

In order to shorten the measuring time, it is necessary to increase the scanning speed of a probe that traces the surface of the test piece. However, when the scanning speed becomes faster, impulsive noise is likely to occur, and it becomes impossible to measure the precise surface profile. Those impulsive noises cannot be removed by using ordinary low-pass filter or a nonlinear median filter.

The AFM used in this paper is SPI3700 manufactured by SEIKO Instruments Inc., Japan, and the measuring range of the AFM is from $1\mu m \times 1\mu m$ to $150\mu m \times 150\mu m$. The maximum resolution of displacement is 0.2nm in th x-y place and 0.01nm in z axis direction.

An example AFM signal which includes impulsive noise is shown in Fig. 4. Here, the sample used for the measurement was a silicon plate which was polished like a mirror finished surface. In this sample, the scanning speed is 1Hz and the measure range is $25.57\mu m \times 25.57\mu m$. In Fig. 4, 127×127 pixels of a measured image of 256×256 pixels are displayed. From this figure it is clear that a lot of impulse noises are included in the AFM signal, and it is not possible to measure accurate surface profile of the sample.

The proposed noise reduction method is applied to the AFM signal. Since the size of the image shown in Fig. 4 is 127×127, the degree of M-sequence is chosen to be 7 and the characteristic polynomial f(x) is

$$f(x) = x^7 + x^4 + x^3 + x^2 + 1 \tag{17}$$

The level j of the Wavelet transform is j=3.

The result of the noise reduction is shown in Fig. 5. Although, there remain some impulsive noises, most the impulsive noises were removed from the original AFM signal.

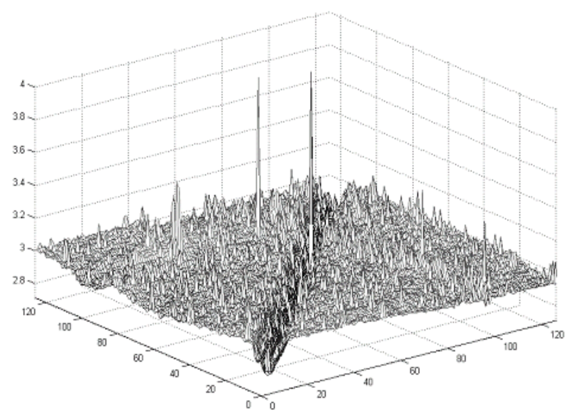

Figure 4: AFM signal which includes both impulsive noise and white Gaussian noise

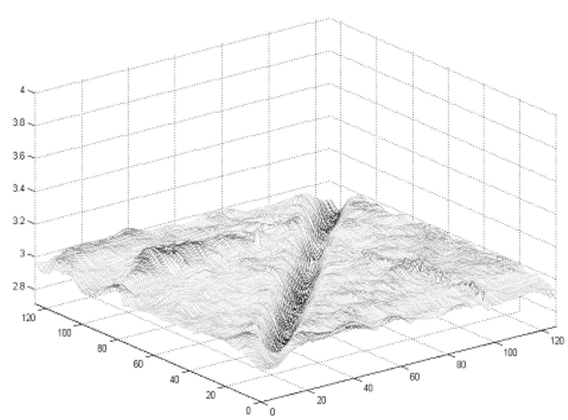

Figure 5: AFM signal after impulsive noise and white noise reduction by using M-transform and wavelet shrinkage

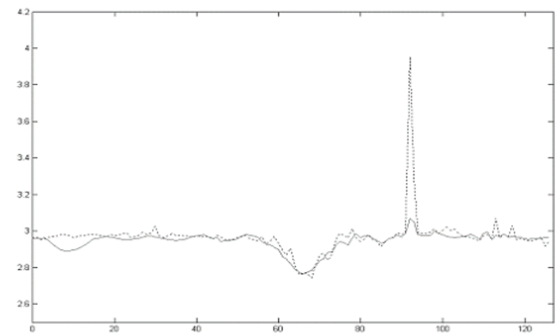

Figure 6: Original signal and noise reduced signal

An example of a column of AFM signal containing original signal and noise reduced signal is shown in Fig. 6. The dotted line is the original signal, and the solid line is noise reduced signal by using M-transform and wavelet shrinkage. From this figure, we see the proposed method is very effective for impulsive noise reduction.

6 Conclusion

In this paper, the authors propose a new method for impulsive noise reduction by using M-transform and wavelet shrinkage. From the results of computer simulation, it is shown that the proposed method is very efficient to remove both impulsive noise and white noise in AFM signals.

References

[1] Donoho, D.L., "De-noising by soft-thresholding",*IEEE Trans. Information Theory*, Vol.41 (1995), No.3, pp.613-627.

[2] Kashiwagi, H., M.Liu, H.Harada and T.Yamaguchi, "M-transform and its application to System Identification",*Trans. of SICE*, Vol.E-1(2002), No.1, pp.289-294.

[3] Harada, H., H.Kashiwagi, T.Andoh and K.Kaba, "Impulsive noise reduction by use of M-transform",*Trans. of SICE*, Vol.39(2003), No.7, pp.688-690.(in Japanese)

[4] Harada, H., H.Kashiwagi, K.Kaba and T.Yamaguchi, "Impulse noise reduction by using M-transform and wavelet shrinkage", *Proc. ICSS held in Wroclaw, Poland*,(2004), pp.313-319.

The Tenth International Symposium on Artificial Life and Robotics 2005(AROB 10th '05),
B-con Plaza, Beppu, Oita, Japan, February 4-6, 2005

DNA Computing Approach to Evolutional Reasoning Algorithm by Using Restriction Enzyme

Yusei Tsuboi, Zuwairie Ibrahim, and Osamu Ono

Institute of Applied DNA Computing
Graduate School of Science & Technology
Meiji University
1-1-1 Higashimita, Tama-ku, Kawasaki-shi, Kanagawa, 214-8671 JAPAN
e-mail: tsuboi@isc.meiji.ac.jp

Abstract

In this paper, we describe how to encode SMC and propose a new reasoning algorithm as experimental protocol of DNA computing techniques, which are enhanced by a concept derived from ADCA. When the SMC is encoded into DNA sequences, the enzyme recognition site involves in each encoded ssDNA representing nodes and edges. The reasoning algorithm shows an object is reasoned out. The ssDNAs are mixed and anneal to complementary sequences under defined conditions in a test tube. In order to retrieve a correct dsDNA which means an object reasoned, a following cycle is repeated. First, the restriction enzyme such as EcoR I cuts a specific part of dsDNAs, reading enzyme recognition sites of the sequence. Second, the cut products are annealed. Finally, the generated products are analyzed by gel electrophoresis. Even if once annealing process runs, the cutting process enables to evolutionarily reuse the same DNA molecules for computation. This repetition stops, when correct strands remain at the analysis process. If the strands do not remain in spite of several repetitions of the cycle, we can say "No". As an output, DNA chips will display the name of the object reasoned.

Keywords: DNA computing, Semantic Network, Algorithm, AI application

1 Introduction

In 1994, L. Adleman's [1] ground-braking work demonstrated the way to use DNA molecules for computational purposes. This experience also contributed into a better understanding where to go with DNA machines, namely, to try to develop memory machines that are machines with very large memory that implements rather simple search operations.

In 2004, a semantic model was proposed and described theoretically for DNA-based memories by Tsuboi, *et al* [2]. This model, referred to as 'semantic model based on molecular computing' (SMC) has the structure of a graph formed by the set of all attribute-value pairs contained in the set of represented objects, plus a tag node for each object. The objects representing double-stranded DNAs (dsDNAs) will be formed via parallel self-assembly, from encoded single-stranded DNAs (ssDNAs) representing the attribute attribute-value pairs (nodes), as directed by splinting ssDNAs representing relations (edges) in the network. The computational complexity of the implementation is estimated via simple simulation, which indicates the advantage of the approach over a simple sequential model. According to this report, if such reasonable computation is realized in *vitro*, a huge number of DNA molecules will be needed in advance as the size of the graph increases. Thus, we have to generates massive initial pools in the first implementation step and then filter the candidate solutions which satisfy the given conditions. To successfully decrease the initial pools, there are a few different initial pool generation methods, parallel overlap assembly (POA) introduced by Stemmer [3], the mix and sprit method introduced by Faulhammer *et al*. [4], with their own advantages and disadvantages. In addition to these methods, the adaptive DNA computing algorithm (ADCA) with a feedback structure was introduced by Yamamoto*, et al*. [5] in 2004. We strongly support the ADCA because this algorithm requires only simple and reliable operations: annealing, cutting by a restriction enzyme, polymerase chain reaction (PCR) and gel electrophoresis. The ADCA is applied to a shortest path problem for a mobile robot. The simulation results indicated to extremely reduce the number of DNA molecules needed as compared with a simple Adleman's model.

In this paper, we propose an evolutional reasoning algorithm which uses the SMC and the ADCA. We will review the ADCA in section 2 and the SMC in section3. Section 4 explains the evolutional reasoning algorithm by using a restriction enzyme, as experimental protocols. Section 5 presents the discussion and conclusion.

2 Encoding Scheme

Many works on DNA computing have employed the encoding scheme presented by Adleman. In Adelman's experiment, each of edges and nodes within the small

Hamiltonian path graph presented by him is represented by ssDNAs of 20 nucleotides respectively. These codes were constructed at random; the length 20 is enough in order to ensure that the codes are "sufficiently different". The edge *u*→*v* from node *u* to node *v* is described to be Watson-Crick complementary to the node sequences derived from the 3' 10- mer of the node *u* and from the 5' 10-mer of the node *v*. For instance, the codes of the node 1, 2 and the edge 1→2 specified below

node1: 5'TATCGGATCGGTATATCCGA3'
node2: 5'GCTATTCGAGCTTAAAGCTA3'
edge1→2: 3'CATATAGGCTCGATAAGCTC5'

As for an encoding scheme of ADAC, let us suppose that we have code α, β and complementary code $\overline{\alpha}$, $\overline{\beta}$ which are parts of recognition site of a restriction enzyme EcoR I. α and β are respectively assigned 'AATTC' and 'G'. That is to say, $\overline{\alpha}$ and $\overline{\beta}$ are respectively assigned 'TTAAG' and 'C'. A dsDNA involving codes α, β, $\overline{\alpha}$, $\overline{\beta}$ is cut at the set part by EcoR I as shown in Figure 1.

α and β code are embedded between the sequences derived from the 3' 10- mer of the node *u* and from the 5' 10-mer of the node *v*. $\overline{\alpha}$ and $\overline{\beta}$ are attached to the 5'end of the edge *u*→*v*. In this way, the codes of the node 1, 2 and the edge 1→2 are modified below,

node1: 5'TATCGGATCG | α β | GTATATCCGA3'
node2: 5'GCTATTCGAG | α β | CTTAAAGCTA3'
edge1→2: 3'CATATAGGCTCGATAAGCTC| $\overline{\alpha}$ $\overline{\beta}$ |5'

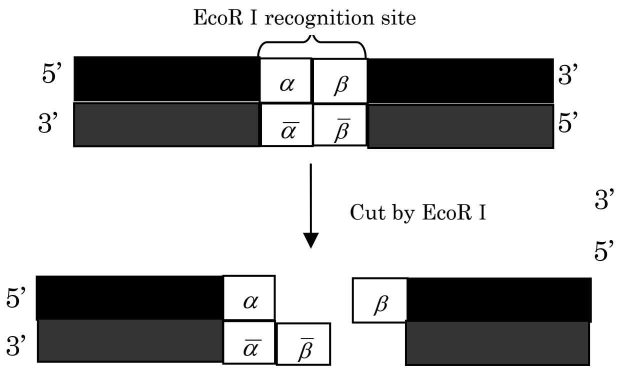

Figure 1 A dsDNA is cut by enzyme EcoR I

3 Semantic Model Based on Molecular Computing (SMC)

Figure 2 describes an SMC formed by the union of a set of some objects. It is made of three relations: object, O; attribute, A; and attribute-value, V. This list representation is denoted as follows:

$$\{<O, A_i, V_{ji}> \mid i=1, 2,\ldots, m; j=1, 2,\ldots, n\}$$

A tag as a name of an object is set to an initial node in the graph. Both the attribute and attribute-value are also set to another node following by the tag node. The nodes denote either a name of the object or both the attribute and the attribute-values. In short, one path from an initial node to a terminal node means one object named on the tag. The model represents an object, as reasoned out by the combinations between the nodes connected by the edges. An SMC contains all attributes common to every object as well as each attribute-value. Attribute layers consist of attribute-values, lined up. If an object has no value of a certain attribute, the attribute value is assigned '*no value*'.

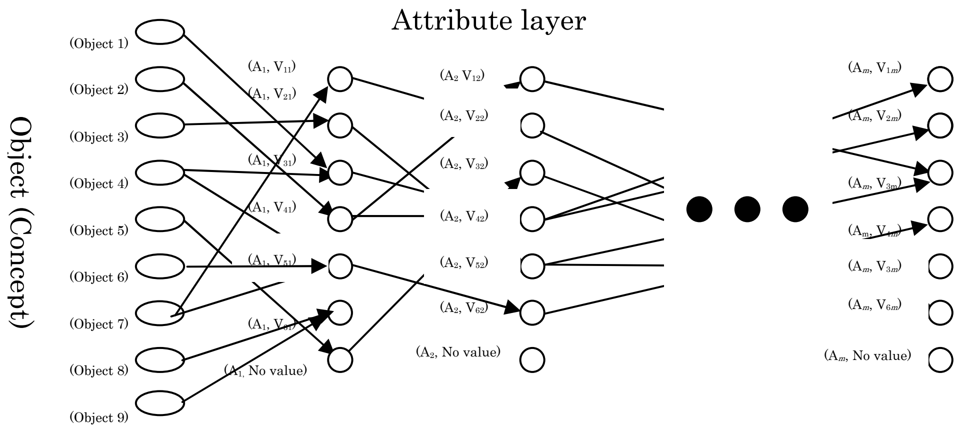

Figure 2 A semantic model based on molecular computing (SMC), which collectively models a set of objects, given a total number of attribute layers, *m*.

4 Methodology

In this section, we propose a reasoning algorithm by using a restriction enzyme, which are enhanced by a concept derived from the ADCA.

4.1 DNA Representation of SMC

Each of the nodes and edges within an SMC may be represented by a DNA library. In the DNA library, a row shows attributes and a column shows attribute-values. DNA sequence is designed by these relations so that it might not be overlapping with the other sequences at random. Firstly, with Adleman's encoding scheme, except for initial and terminal edge, each nodes and edges is assigned ssDNA oligonucleotide of length 20. As for tag nodes, the sequences are also assigned by random 20 bases. The initial and terminal edges are respectively represented by the size which suits the end of the DNA pieces exactly. Here, an important thing is that every sequence is designed according to these relations to prevent mishybiridization via other unmatching sequences. Next, we innovate the concept of ADAC encoding scheme in the Adleman's encoding scheme. The code α, β $\overline{\alpha}$ and $\overline{\beta}$ of the enzyme recognition site of EcoR I involves in each encoded ssDNA representing nodes and edges, except for the initial node, the terminal node and the terminal edge. Figure 3 shows DNA representation of one of the object within the SMC.

4.2 Algorithm

The reasoning algorithm shows an object is reasoned out by DNA computing techniques. Semantic information of some reference objects is stored in a semantic memory as knowledge bases. The algorithm reveals that which reference object several input objects are classified into with DNA molecules all at once. Figure 4 explains overall procedures of DNA operations required for solutions.

A set of DNA representing reference objects and an input object fragments, formed by the combinations of oligonucleotides, are synthesized as follows:

- Reference object

The ssDNA of each edge and tag node in the network is synthesized as a set of *knowledge based molecules.*

- Input object

Attribute-values are extracted from an input object according to determined attribute A_i. Using the attributes and the attribute-values, an ssDNA is synthesized as a set of *input molecules* with the sequence defined by the DNA library.

The ssDNAs are mixed and anneal to complementary sequences under defined conditions in a test tube. In order to retrieve a correct dsDNA which means an object reasoned, the generated products are analyzed from DNA length by gel electrophoresis. If they remain, say "Yes": the object is reasoned out, otherwise, we should consider about two cases. The one is "No": the object is not reasoned out. The other is that the number of DNA molecules prepared in advance is too few to form the correct dsDNAs. To distinguish the two cases, a following cycle is repeated. First, the EcoR I cuts the all the analyzed products, reading the enzyme recognition site of the sequences. Second, the cut products are annealed again. Figure 5 illustrates ligation & hybridization process after the cutting. Finally, the generated products are analyzed as well. Even if once annealing process runs, the cutting process enables to evolutionarily reuse the same DNA molecules for computation. This repetition stops, when correct strands remain at the analysis process. If the strands do not remain in spite of several repetitions of the cycle, we can say "No".

4.3 Output

DNA Chips, output in readable format is accomplished by attaching the cloned, coding sequences to an array. Thus, each spot would represent an object. Readout occurs directly form sensing fluorescent tags attached to a tag sequence of the correct strands, as probes.

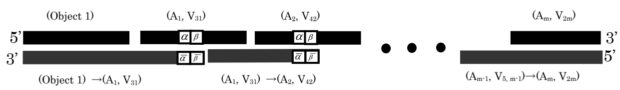

Figure 3 DNA representation of one of the objects

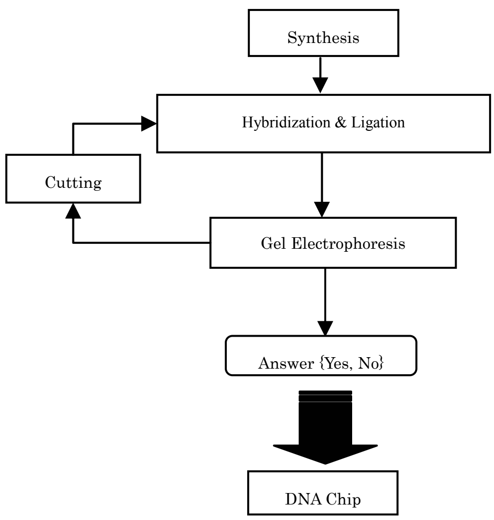

Figure 4 Overall procedures of DNA Operations

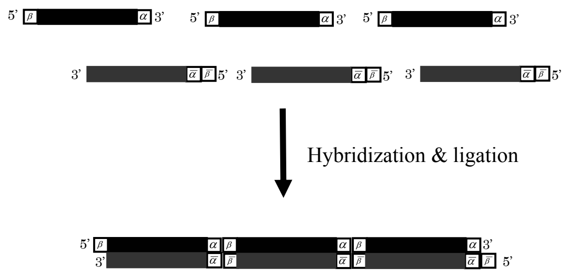

Figure 5 Hybridization & ligation process after cutting

5 Discussion & Conclusion

We have been discussed an evolutional reasoning algorithm by using DNA computing techniques. This paper provides a necessary DNA computing-chemical process including experimental operations. An adopted protocol is very simple. Standard genetic engineering techniques such as annealing, ligation, cutting and gel electrophoresis are required. Several experiments have been conducted to assess the performance of DNA-based databases realized by biochemical reactions. Within the SMC, attributes and attribute-values are represented by random (0-20) oligonucleotides {A, T, C, G}. There are two issues to consider length and sequences design of DNA. The one is that if a set of knowledge increases, oligonucleotides, length 20 are not fully assigned to each of nodes and edges in the network. Such length limits to represent a lot of objects. This issue would be resolved simply by assigning longer oligonucleotides length. The other is that in practical sequences design, we have to consider an effective way to select proper sequence to avoid mismatched, error hybridization will have to be devised. Word design strategies for DNA-based computation have been investigated so far. Substantial progress has been reported on this issue [6]-[10]. We expect that this issue will be satisfactorily resolved in the near future. Thus, these issues are very crucial to obtain a correct answer. In the light of these issues, we will have to design best sequences with adequate length, when a laboratory experiment is done.

The SMC is one of the models for applying DNA computing techniques to the research field of artificial intelligence. Its application has many incredible advantages, whereas the reasonable performance demands a huge number of molecules. The proposed algorithm will enable to minimize useless molecules synthesized. In addition, it repeats cutting, annealing and analysis processes to reach the solution only, which interests us in terms of an intelligent mechanism based on DNA computing. It is expected that the proposed algorithm would extend many AI applications, knowledge bases, pattern matching, etc. As a future work, to achieve reliable performance, some parameters of reactions-temperatures, concentrations of oligonucletides, times of reactions, etc. will be experimentally tested.

Reference

[1] L. Adleman, "Molecular computation of solutions to combinatorial problems", *Science* 266, pp.583-585, 1994.

[2] Y. Tsuboi, Z. Ibrahim, and O. Ono, "Semantic model for artificial Intelligence based on molecular computing", Proc. of *The 8th International Conference on Knowledge-Based Intelligent Information and Engineering Systems*, Lecture Notes in Artificial Intelligence (LNAI), Vol. 3213, pp. 32-39, 2004.

[3] W. Stemmer, "DNA shuffling by random fragmentation and reassembly: in vitro recombination for molecular evolution, Proc. of Natl. Acad. Sci., pp.10747-10751, 1994.

[4] D. Faulhammer, A. R. Cukras, R. J. Lipton, and Laura F. Landwever, "Molecular computation: RNA solutions to chess problems, Proc. of *Natl. Acad. Sci.*, pp1385-1389, 2000.

[5] O. Ono, Y. Tsuboi, T. Yamamoto, Z. Ibrahim, and S. Watanabe, "Computation algorithm based on adaptive DNA molecules by using polymerase chain reaction", Pcoc. of *20th Fuzzy System Symposium* pp. 83-86, 2004 (in Japanese).

[6] R. Daton, M. Garzon, R. C. Murphy, J. A. Rose, D. R. Franceschetti, and S. E. Stevens Jr, "Reliability and efficiency of a DNA-based computation", *Phys. Review Letters* 80, pp.417-420, 1998.

[7] R. Deaton, C. R. Murphy, M. Garzon, D. R. Franceschetti, and S. E. Stevens Jr.,"Good encodings for DNA-based solutions to combinatorial problems", Proc. of *DNA Based Computers DIMACS Series in Discrete Mathematics and Theoretical Computer Science*, Vol.44, pp.247-258, 1999.

[8] J. A. Rose, R. Deaton, D. Franceschetti, M. Garzon, and S. E. Stevens Jr., "A statistical mechanical treatment of error in the annealing biostep of DNA computation", Proc. of *Genetic and Evolutionary Computation Conference*, pp.1829-1834, 1999.

[9] J. SantaLucia, H. Allawi, and P. Seneviratne, "Improved nearest-neighbor parameters for predicting DNA duplex stability", *Biochemistry,* Vol.35, No.11, pp.355-356, 1996.

[10] R.Penchovsky, and J. Ackermann, "DNA library design for molecular computation", *Journal of Computational Biology*, Vol.10, No.2, pp.215-229, 2003.

The Tenth International Symposium on Artificial Life and Robotics 2005(AROB 10th '05),
B-con Plaza, Beppu, Oita, Japan, February 4-6, 2005

A Model for Coevolution

K. Makino
Dept. of Mech. and Ctrl. Eng
Tokyo Institute of Technology
makino@mylab.ctrl.titech.ac.jp

K. Nakano
School of Bionics
Tokyo University of Technology
nakano@cc.teu.ac.jp

keywords : coevolution, differentiation of species, genotypic gene, phenotypic gene

Abstract

In the natural world, many kinds of animals and plants have been evolving mutually influenced. This study aims to investigate how the differentiation of species occurs through coevolution. We have constructed a model by computer simulation, which is compared to coevolution of bees and flowers. By the use of the model, the process of breading have been examined. The influence on correspondence between genotypic genes and phenotypic genes has been examined as well.

1 Introduction

For the evolution of creatures, mutual interaction is important. This is called coevolution. Competitive relation between gnus and lions, and cooperative relation between bees and flowers are good examples of coevolution. The aim of this research is to construct a model for coevolution and to investigate the mechanisms of differentiation of species through coevolution[1].

We start with introducing an example of coevolution, that is, the relation between hammer orchids and wasps. A hammer orchid has a sort of lure, which resembles a female wasp in its shape and pheromone (Fig. 1-a). A male wasp catches the dummy by mistake (Fig. 1-b). It tries to fly with the dummy and touches the pollen, because the flower is connected to the stem with a hinge (Fig. 1-c). It transfers pollen from flower to flower (Fig. 1-d). This is the example we focus on to construct a model for coevolution.

Every creature has genes (genotype) as biological information. Different genes do not necessarily describe different observable characteristics (phenotype). We introduce genotype and phenotype to our model. For simplicity of the argument, it is assumed that there are only two kinds of creatures in the world, one is "FLOWER" and the other is "BEE". First, our model

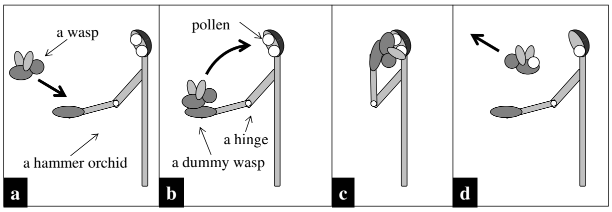

Figure 1: A hammer orchid and a wasp.

of bees and flowers is introduced. The characteristics of creatures are decided by the phenotype that is described by the genotype. In this model, a bee flies to a flower whose color is its favorite. If the shape of the bee fits to that of the flower, the bee can get pollen. It can also get nectar (that is, energy), if the nectar of the flower is its favorite one. After bees' gathering the nectar and transferring the pollen, the bees and the flowers bear their children. Probability of mating of a flower increases according to the number of times it received pollen. The number of mating of a bee is decided by the amount of the energy that it gathered. This is how we model the cooperative relation between bees and flowers. Secondly, we discuss the differentiation of species through coevolution and show that such differentiation occurs in our model. In addition, it is confirmed that differentiation of species is influenced by the relation between genotype and phenotype and by the condition of mating.

2 Model of Bees and Flowers

In this section, the detail of our model is described. The model consists of bees and flowers. Hereafter we denote BEE's and FLOWER's for those in the model. Since an accurate model is not necessary for our purpose, there is neither a queen bee nor the difference between a male and a female. BEE's and FLOWER's have genes. The genes have genotypic and phenotypic expression. The detail is described in section 2.1.

In section 2.2, the behavior of BEE's and FLOWER's are explained. There are two phases. One is pollinating phase, where BEE's fly to FLOWER's to get nectar and transfer pollen. The other is breeding phase, where BEE's and FLOWER's bear children. A sequence of a pollinating phase and a breeding phase is called a cycle.

2.1 Phenotype and Genotype

BEE's and FLOWER's have genotypic genes. The same observable characteristic does not necessarily correspond to the same genotypic gene. Sometimes, a few genotypic genes express the same characteristic. This characteristic expression is called phenotype. A BEE has three genotypic genes each of which is composed of 4 bits. Totally they are represented by 12 bits $x_1x_2x_3x_4|x_5x_6x_7x_8|x_9x_{10}x_{11}x_{12}$, and corresponding phenotypic genes are $X_1X_2X_3$. In the same manner, genotypic genes of a FLOWER are represented by $y_1y_2y_3y_4|y_5y_6y_7y_8|y_9y_{10}y_{11}y_{12}$, and phenotypic genes are $Y_1Y_2Y_3$. Y_1, Y_2, and Y_3 describe a color, shape, and nectar, respectively, where each of them takes a value out of A, B, and C. X_1, X_2, and X_3 are the BEE's favorite color, fitting shape, and favorite nectar, respectively. Each of them also takes a value out of A, B, and C. DNA and a characteristic in a real creature correspond to genotype and phenotype, respectively. In our model, we define the correspondence between genotype and phenotype, and investigate how coevolution happens through interactions. One example of such correspondence is shown in Fig. 2 as relation rule 1, and another in Fig. 3 as relation rule 2. Though in the model, both coding of genes and the relation rule are quite different between bees and flowers, the same coding and the same rule are applied to BEE's and FLOWER's. The essence of coevolution still exists in the model. In Fig. 2, each of the genotypic genes is assigned to a phenotypic gene at random. In Fig. 3, similar genotypic genes are assigned to the same phenotypic gene, that is, genes with zero and single 1's are assigned to phenotype A, with two 1 to B, and with three and four 1's to C. The lines indicate the relation between two genotypic genes where 1 bit is inverted.

Table 1 shows an example of relation between genotypic and phenotypic genes adopting relation rule 1 in Fig. 2. There are a BEE with ABA and a FLOWER with ABB. The BEE likes the color of the FLOWER and fits to it in the shape, and can take the pollen and the nectar, but the nectar is not nutrient for the BEE.

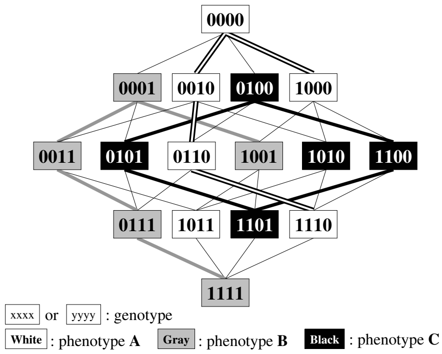

Figure 2: Relation between genotype and phenotype (relation rule 1).

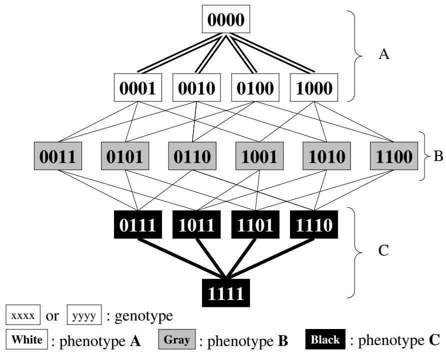

Figure 3: Another relation rule (relation rule 2).

It is assumed that creatures with the same phenotypic genes constitute one species.

2.2 Pollinating and Breeding Phase

The details of the behavior of BEE's and FLOWER's in pollinating phase and breeding phase are described as follows.

Pollinating phase The pollinating phase consists of 3 steps. Every BEE acts as step 1 $\sim$ 3.

Step 1 A BEE flies to a few FLOWER's (five FLOWER's for example) that have its favorite color and spends some energy. If the energy becomes zero, the BEE dies. The BEE finishes flying to any FLOWER, if there is no FLOWER with its favorite color.

Step 2 If the shape of the FLOWER fits to that of the BEE, it gives the FLOWER pollen which it has taken from another FLOWER and takes new pollen from the FLOWER. The BEE does nei-

	genotypic genes	phenotypic genes
BEE	0000 0001 0110	ABA
FLOWER	1000 1001 0001	ABB

Table 1: An example of genes of a BEE and a FLOWER in the case of relation rule 1.

ther give nor take pollen if it dose not fit to the FLOWER in the shape.

Step 3 Presume that BEE's can recognize whether the nectar is nutrient for it or not. If the nectar is nutrient, the BEE gathers the nectar (some energy), and the FLOWER looses a part of the nectar. Therefore, a BEE can not gather the nectar from the FLOWER which lost all the nectar. The nectar is recovered at the end of the cycle.

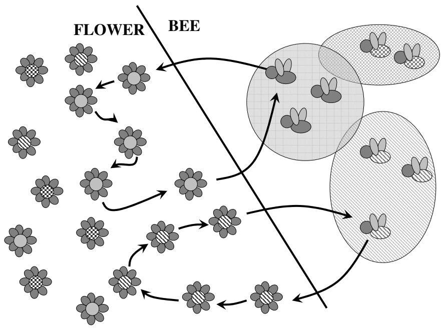

Figure 4: BEE's fly to FLOWER's.

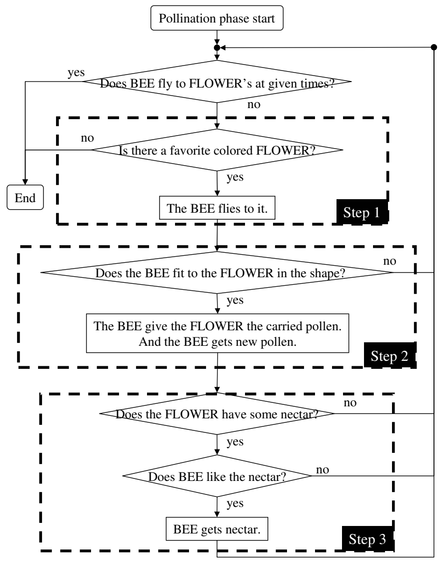

Figure 5: Flowchart of pollinating phase.

Figure 4 illustrates that BEE's fly to five FLOWER's with their favorite color one by one. And a flowchart of this phase is shown in Fig. 5.

The BEE in the breeding phase : A BEE can bear children in proportion to its energy. Whether two BEE's are able to mate or not, is not decided by phenotype but by genotype. First, two BEE's are chosen at random. Secondly, a similarity of their genotypic genes is examined. Finally, the BEE's bear a child through mating, if their genotypic genes are similar. Mutation can happen at this point. The similarity is evaluated by the Hamming distance between their genotypic genes. The maximum of the difference, where mating is possible, is defined as **MPD** (Maximum Permitted Difference). In other word, two BEE's can bear a new BEE, when different bits between their genotypic genes are less than MPD. This parameter is important in the following simulations. Mating is performed in every gene but not in every bit. In addition, the BEE's give certain energy to the child.

The FLOWER in the breeding phase : A FLOWER and the transferred pollen bear a new FLOWER as the BEE's. Maximum number of FLOWER's is limited. That is, randomly chosen FLOWER's bear new FLOWER's until the maximum number is reached.

In addition, BEE's and FLOWER's are given a lifetime. They die of the lifetime, after breeding phase.

3 Differentiation of Species though Coevolution

After the process described in the previous section, BEE's and FLOWER's with new genes appear. The creatures with the same phenotypic genes constitute a sub-species. Most of the sub-species can not survive because the population is small, but a few of them survive where the population increases to make new species. Fig. 6 shows an example of the differentiation of species through the coevolution. In initial condition, there are only two species, BEE's with AAA and FLOWER's with AAA. It is assumed that a new sub-species of FLOWER's with BAA appeared after some cycles. The sub-species survives by chance. If BEE's with BAA appear and increase after some cycles from the appearance of FLOWER's with BAA, BEE's with BAA and FLOWER's with BAA mutually cooperate with and survive. Also, the BEE's with BAB and the FLOWER's with BAB survive.

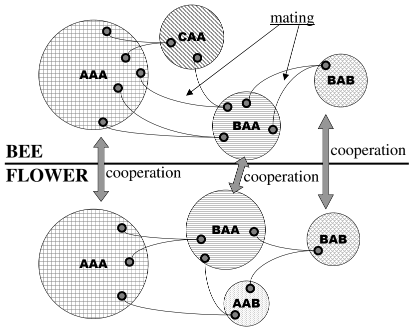

Figure 6: Differentiation of species though coevolution.

4 Simulation

The basic parameters are chosen as in Tab. 2. At the initial point, there are 10 BEE's and 10 FLOWER's. Their genotypic genes are 0000 0000 0000. Every BEE flies to 5 FLOWER's. First, a basic simulation is shown in section 4.1. As the result, it has been confirmed that differentiation of species occurs. Secondly, the influence of MPD on differentiation of species is analyzed in section 4.2. Finally, in section 4.3, another relation table is adopted.

item	value
Initial energy of a BEE	5 [point]
Initial energy of a FLOWER	10 [point]
Energy that is necessary to fly to a FLOWER	1 [point]
Energy that a BEE gets from a FLOWER	2 [point]
Energy that a FLOWER gives to a BEE	2 [point]
Energy that two BEE's give to a new BEE	5 [point]
Lifetime	5 [cycle]

Table 2: Definition of basic parameters.

4.1 Basic Simulation

This simulation is performed with a relation rule in Fig. 2 and MPD = 4 [bit]. The results are shown in Fig. 7-a, b. These figures show time evolution of the population BEE's and FLOWER's of every species at every cycle. There are many species at the same time. It means that differentiation of species has occurred.

In addition, two interesting phenomena are observed. One is that two new species of BEE's with BAA and CAA, that have different favorite color from the original one (AAA), have appeared. The BEE's with AAA can not gather enough nectar to mate, because the maximum number of FLOWER's and the amount of the nectar that a FLOWER generates are limited. If FLOWER's that has different color appear, the BEE's that like the color can gather more nectar than the BEE's of other species. Then, the new BEE's and the new FLOWER's increase. For this reason, increase and decrease of species are repeated. On the other hand, FLOWER's that have the same color and shape as the original one but have different nectar appear. The FLOWER's can survive, because they attract the BEE's and receive pollen. However, even if the FLOWER's increase, many BEE's that fly to them can not gather the nectar, because it is not their favorite one. The BEE's decrease, because the energy is not enough to bear children. It is considered that the model is stable at the condition that the number of the FLOWER is small.

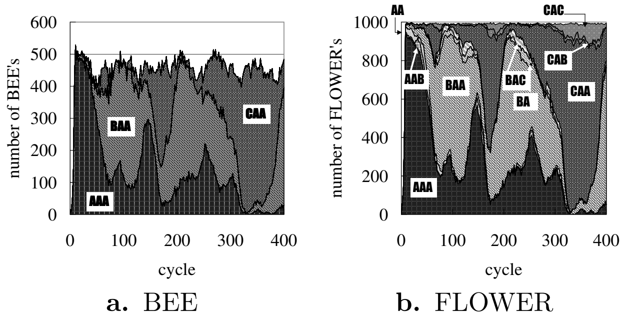

Figure 7: Time evolution of the population of every species at every cycle with relation rule 1 and MPD = 4.

4.2 Influence on the MPD

First, the simulation has been performed in the case of MPD = 0. The results are illustrated in Fig. 8. It is confirmed that differentiation of species does not occur.

Next, the simulations under the condition of MPD = 2 and MPD = 3 have been tried to investigate how MPD influences the differentiation Fig. 9 and Fig. 10 show that different species is easier to occur, as MPD increases.

4.3 Influence of Relation between Genotype and Phenotype

Figure 11 shows the result when relation rule 2 in Fig. 3 is adopted. In this case, differentiation of species does not occur. The reason is considered as

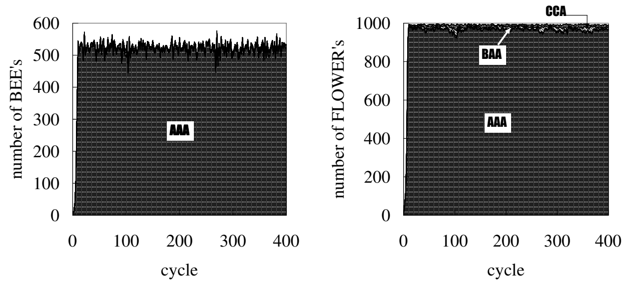

a. BEE **b.** FLOWER

Figure 8: Time evolution of the population of every species at every cycle with relation rule 1 and MPD = 0, that is, their genotypic genes must be exactly the same in order to mate.

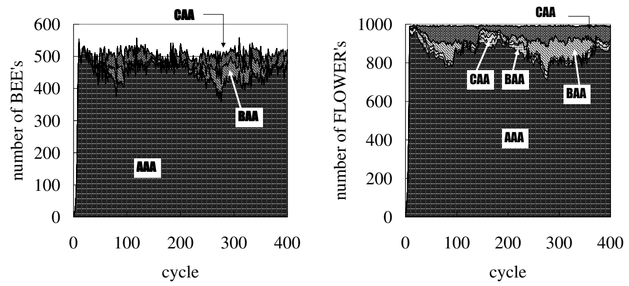

a. BEE **b.** FLOWER

Figure 9: Time evolution of the population of every species at every cycle with relation rule 1 and MPD = 2.

follows: when the genotypic genes have a close relation with phenotypic genes, two creatures belonging to different species can not mate with each other. Therefore the sub-species that appears from original one can not survive for a long time.

5 Conclusion

We constructed a model for coevolution of bees and flowers. Using the model, we confirmed that the differentiation of species occurs through coevolution. Influence of various parameters to the process of evolution is investigated. The differentiation of species is influenced by the relation between genotype and phenotype. It easily occurs when relation rule 1 (randomly constructed) is adopted. Next, it is easier to occur, as MPD (Maximum Permitted Difference) is larger. It has been found that lifetime of creatures, number of FLOWER's which a BEE flies to, getting and consuming energy, and maximum number of FLOWER's do not make much influence on the differentiation of

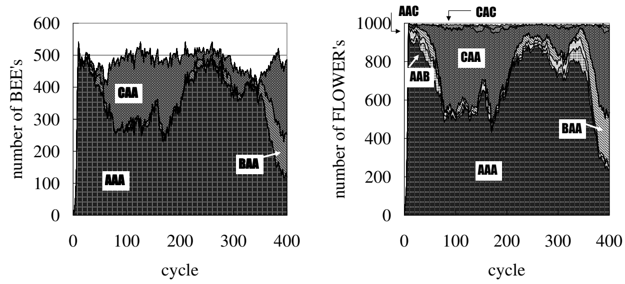

a. BEE **b.** FLOWER

Figure 10: Time evolution of the population of every species at every cycle with relation table 1 and MPD = 3

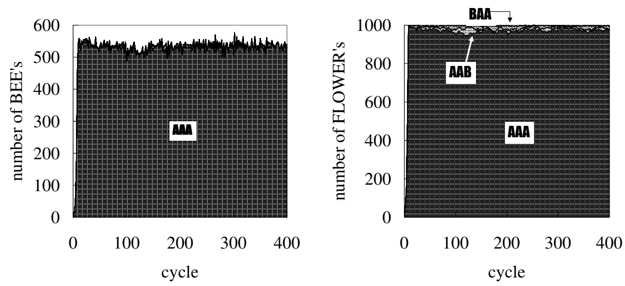

a. BEE **b.** FLOWER

Figure 11: Time evolution of the population of every species at every cycle with relation rule 2 and MPD = 4.

species.

To investigate the behavior of more complicated bio-systems composed of many kinds of animals and plants is one of our future works.

Reference

[1] K. Makino and K. Nakano, "The 66th National Convention of IPSJ," *Information Processing Society of Japan* ,Vol. 2, pp. 15-16, 2004.

The Tenth International Symposium on Artificial Life and Robotics 2005(AROB 10th '05),
B-con Plaza, Beppu, Oita, Japan, February 4-6, 2005

Simultaneous State and Parameter Estimation of Nonlinear Models by Evolution Strategies Based Particle Filters*

Katsuji Uosaki Toshiharu Hatanaka
Department of Information and Physical Sciences
Graduate School of Information Science and Technology, Osaka University
Suita, Osaka 565-0871, Japan

Abstract

Recently, particle filters have attracted attentions for nonlinear state estimation. In this approaches, a posterior probability distribution of the state variable is evaluated based on observations in simulation using so-called importance sampling. We proposed a new filter, Evolution Strategies based particle (ESP) filter to circumvent degeneracy phenomena in the importance weights, which deteriorates the filter performance, and apply it to simultaneous state and parameter estimation of nonlinear state space models. Results of numerical simulation studies illustrate the applicability of this approach.

Keywords. Nonlinear filtering, particle filters, Bayesian approach, evolution strategies, importance sampling, selection.

1 Introduction

The problem of state estimation of dynamic systems using a sequence of their noisy observations has been an active research area in control system sciences for many years. We focus here on Bayesian estimation approaches, that is, inference on the unknown state can be performed according to the posteriori probability density function (pdf), which is obtained by combining a prior pdf for the unknown state with a likelihood function relating to the observations. When observations come sequentially in time, recursive state estimation is often interested, where the evolving posterior pdf is evaluated recursively in time. However, in many realistic problems, state space models include nonlinear and non-Gaussian elements that preclude a closed form of expression for the posteriori pdf, and hence many approximations have been proposed such as the extended Kalman filter (EKF) and Gaussian sum filter [6]. Recent progress of computing ability allowed to the rebirth of Monte Carlo integration and its application of Bayesian filtering, or Monte Carlo filters. A class of Monte Carlo filters, known as "particle filters" [4, 2] is discussed here. In this approach, the integrals in Bayes' rule is approximated by a weighted sum based on the discrete grids with associated weights sequentially chosen by the importance sampling. A common problem in the particle filter is the degeneracy phenomenon, where almost all importance weights tend to zero after some iteration and a large computational effort is wasted to updating the particles with negligible weights. In order to resolve this difficulty, several modifications have been proposed such as resampling particle filter (SIR) [5] that introduces a resampling steps. Applying the concept of Evolution Strategies [7], we also developed the Evolution Strategies based prticle (ESP) flter [8]. In this paper, the ESP filter is applied to simultaneous state and parameter estimation of nonlinear state space models. Numerical simulation studies have been conducted to exemplify the applicability of this approach.

*This work is partially supported by the Grant-in-Aid for Scientific Research from the Japan Society for the Promotion of Science (C)(2)14550447.

2 Particle Filters

Consider the following nonlinear state space model.

$$x_{k+1} = f(x_k, v_k) \tag{1}$$
$$y_k = g(x_k, w_k) \tag{2}$$

where x_k and y_k are the state variable and observation, respectively, f and g are known possibly nonlinear functions, v_k and w_k are independently identically distributed (i.i.d.) system noise and observation noise sequences, respectively. We assume v_k and w_k are mutually independent. The main objective here is to find the best estimate of the state variable x_k in some sense based on the all available data of observations $y_{1:k} = \{y_1, y_2, \dots, y_k\}$. We can solve the problem by calculating the posteriori pdf of the state variable x_k of time instant k based on all the available data of observation sequence $y_{1:k}$.

The posteriori pdf $p(x_k|y_{1:k})$ of x_k based on the observation sequence $y_{1:k}$ satisfies the following recursion:

$$p(x_k|y_{1:k-1}) = \int p(x_k|x_{k-1})p(x_{k-1}|y_{1:k-1})dx_{k-1} \tag{3}$$

$$p(x_k|y_{1:k}) = \frac{p(y_k|x_k)p(x_k|y_{1:k-1})}{p(y_k|y_{1:k-1})} \tag{4}$$

with a prior pdf $p(x_0|y_0) \equiv p(x_0)$ of the initial state variable x_0. Here normalizing constant

$$p(y_k|y_{1:k-1}) = \int p(y_k|x_k)p(x_k|y_{1:k-1})dx_k$$

depends on the likelihood $p(y_k|x_k)$, which is determined by the observation equation (2).

Since a closed form solution of recursions (3) and (4) is not admitted except in very restrictive cases including linear Gaussian state space models, where the Kalman filter [1] can be applied, some approximations should be introduced such as the extended Kalman filter (EKF)[6] and particle filters [4, 2]. Since EKF uses a linearization technique based on a first order Taylor expansions of the nonlinear system and observation equations about the current estimate and approximates the posteriori pdf to be Gaussian, it can never describe the true non-Gaussian density well. Particle filters approximate the true posteriori pdf $p(x_k|y_{1:k})$ by a large set of $n \gg 1$ particles $\{x_k^{(i)},\ (i = 1,\ldots,n)\}$, where each particle has an assigned relative weight, $\{w_k^{(i)},(i = 1,\ldots,n)\}$, $w_k^{(i)} > 0$, $\sum_{i=1}^n w_k^{(i)} = 1$ as follows:

$$p(x_k|y_{1:k}) \approx \sum_{i=1}^{n} w_k^{(i)}\delta(x_k - x_k^{(i)}) \tag{5}$$

where $\delta(\cdot)$ is Dirac's delta function ($\delta(x) = 1$ for $x = 0$ and $\delta(x) = 0$ otherwise).

Here, the particles are generated and associated weights are chosen using the principle of "importance sampling". If the samples $x_k^{(i)}$ in (5) were drawn from an importance density $q(x_k^{(i)}|y_{1:k})$, then the associated normalized weights are defined by

$$w_k^{(i)} \propto \frac{p(x_k^{(i)}|y_{1:k})}{q(x_k^{(i)}|y_{1:k})}. \tag{6}$$

When the importance density $q(x_k|y_{1:k-1})$ is chosen to factorize such that

$$q(x_k|y_{1:k}) = q(x_k|x_{k-1}, y_{1:k})q(x_{k-1}|y_{1:k-1}), \tag{7}$$

we can obtain samples $x_k^{(i)}$ by augmenting each of the existing samples $x_{k-1}^{(i)}$ sampled from the importance density $q(x_{k-1}|y_{1:k-1})$ with the new state sampled from $q(x_k|x_{k-1}^{(i)}, y_{1:k})$.

Noting that the posteriori pdf can be rewritten using Bayes' rule as

$$\begin{aligned} p(x_k|y_{1:k}) &= \frac{p(y_k|x_k, y_{1:k-1})p(x_k|y_{1:k-1})}{p(y_k|y_{1:k-1})} \\ &\propto p(y_k|x_k)p(x_k|x_{k-1})p(x_{k-1}|y_{1:k-1}) \end{aligned} \tag{8}$$

and inserting (7) and (8) into (6), the weights are recursively updated as

$$w_k^{(i)} \propto w_{k-1}^{(i)} \frac{p(y_k|x_k^{(i)})p(x_k^{(i)}|x_{k-1}^{(i)})}{q(x_k^{(i)}|x_{k-1}^{(i)}, y_{1:k})}. \tag{9}$$

The particle filter with these steps is called "Sequential Importance Sampling Particle Filter" (SIS).

It is known that the SIS filter suffers from the degeneracy phenomenon, where all but one of the normalized importance weights are very close to zero after a few iterations. By this degeneracy, a large computational effort is wasted to updating trajectories whose contribution to the final estimate is almost zero. In order to prevent this phenomenon, several modifications have been introduced. Among them, resampling process, which eliminates trajectories whose normalized importance weights are small, is a common approach. It involves generating new grid points $x_k^{*(i)}$ $(i = 1,\ldots,n)$ by resampling from the grid approximation (5) randomly with probability

$$\Pr(x_k^{*(i)} = x_k^{(j)}) = w_k^{(j)} \tag{10}$$

and the weights are reset to $w_k^{*(i)} = 1/n$, when

$$\hat{N}_{eff} = \frac{1}{\sum_{i=1}^n (w_k^{(i)})^2} \tag{11}$$

with the associated normalized weight $w_k^{(i)}$ is less than a predefined threshold $N_{thres} < 1$. Particle filter with this resampling process is called "Sampling Importance Resampling Particle Filter" (SIR).

3 Evolution Strategies Based Particle Filter

Evolution Strategies (ES) is one of the Evolutionary Computation approaches, computational models simulating natural evolutionary processes to design and implement computer-based problem solving systems (see the extensive surveys, for examples[3]. It has been applied to continuous function optimization in real-valued n-dimensional space via selection and perturbation processes called mutation. Mutation process is realized by the additive process.

$$\begin{aligned} \sigma'_j &= \sigma_j \exp(\tau' N(0,1) + \tau N_j(0,1)) \\ x'_j &= x_j + \sigma'_j N_j(0,1) \end{aligned} \tag{12}$$

where $N(0,1)$ and $N_j(0,1)$ denote a realization of normal random variable and normal random variables sampled anew for counter j with zero mean and unit variance, respectively, and σ_j denotes the mean step size. The factors τ and τ' are chosen dependent on the population size. The μ individuals of higher fitness are chosen deterministically out of the union of μ parents and λ offspring ($(\mu + \lambda)$-selection) or λ offspring only ((μ, λ)-selection) to form the parents of the next generation in order to evolve towards better search region. It can be seen that SIR and ES have similarities; both the importance sampling process in SIR filter and mutation process in ES give perturbation to the parent individuals $x_{k-1}^{(i)}$ with extrapolation by $f(x_{k-1}^{(i)})$, and both resampling process in SIR filter and selection process in ES select offspring among the perturbed individuals. However, there is a difference between them, i.e., resampling in SIR is carried out randomly and the weights are reset as $1/n$, while the selection in ES is deterministic and the fitness function is never reset. Hence, by replacing the resampling process in SIR by the selection process in ES, we can derive a new particle filter as follows.

Based on the particles $\{x_{k-1}^{(i)},\ (i=1,\ldots,n)\}$ sampled from the importance density $q(x_{k-1}|\, y_{1:k-1})$, we generates ℓ samples $\{x_k^{(i,j)},\ (j=1,\ldots,\ell)\}$ according to the importance density function $q(x_k|\, x_{k-1}^{(i)}, y_{1:k})$. Corresponding weights $w_k^{(i,j)}$ are evaluated by

$$w_k^{(i,j)} \propto w_{k-1}^{(i)} \frac{p(y_k|\, x_k^{(i,j)})p(x_{k-1}^{(i,j)}|\, x_{k-1}^{(i)})}{q(x_k^{(i,j)}|\, x_{k-1}^{(i)}, y_{1:k})} \tag{13}$$

From the set of $n\ell$ particles and weights $\{x_k^{(i,j)}, w_k^{(i,j)}, (i=1,\ldots,n,\ j=1,\ldots,\ell)\}$, we choose n sets with the larger weights, and set as $x_k^{(i)}, w_k^{(i)} (i=1,\ldots,n)$. This process corresponds to $(n, n\ell)$-selection in ES. Hence, we call this particle filter using $(n, n\ell)$-selection in ES as Evolution Strategies based particle filter Comma (ESP(,)). When we add the particles $x_k^{(i,0)} = f(x_{k-1}^{(i)}),\ (i=1,\ldots,n)$ in addition to $n\ell$ $x_k^{(i,j)},\ (i=1,\ldots,n,\ j=1,\ldots,\ell)$ sampled from the importance density function $q(x_k|x_{k-1}^{(i)}, y_{1:k})$ as above and evaluate the weights $\{w_k^{(i,j)}, (i=1,\ldots,n, j=0,\ldots,\ell)\}$ by (13), and then choose n sets of $(x_k^{(i)}, w_k^{(i,j)})$ with larger weights from the ordered set of $n(\ell+1)$ particles $\{x_k^{(i,j)}, w_k^{(i,j)},\ (i=1,\ldots,n,\ j=0,\ldots,\ell)\}$, we can obtain another ESP filter. Since this ESP filter uses the selection corresponding to $(n+n\ell)$-selection in ES, we can call this filter as Evolution Strategies based particle filter Plus (ESP(+)).

4 Simultaneous State and Parameter Estimation by Evolution Strategies Based Particle Filter

The proposed ESP filter is applied here to simultaneous state and parameter estimation of nonlinear systems. Consider the nonlinear state space model (1) with unknown parameter θ and (2), where a posteriori pdf $p(x_k, \theta|y_{1:k})$ should be approximated to estimate state and parameter simultaneously, Application of Bayes' rule (4) provides

$$\begin{aligned} p(x_{k+1}, \theta|y_{1:k+1}) \quad &\propto \quad p(y_{k+1}|x_{k+1}, \theta)p(x_{k+1}|\theta, y_{1:k+1}) \\ &\quad\quad \times p(\theta|y_{1:k+1}) \end{aligned}$$

Since the form of the theoretical pdf $p(\theta|y_{1:k})$ is not known for unknown parameter case, we replace θ by θ_k at time k, and simply include θ_k in an augmented state vector $\boldsymbol{x}_k = (x_k, \theta_k)^T$, where θ_k evolves as

$$\theta_{k+1} = \theta_k + \eta_k \tag{14}$$

and η_k is a normal random disturbance with zero-mean and very small variance. Then approximation of the true posteriori pdf is given by

$$p(\boldsymbol{x}_k|y_{1:k}) \approx \sum_{i=1}^{n} w_k^{(i)} \delta(\boldsymbol{x}_k - \boldsymbol{x}_k^{(i)}) \tag{15}$$

If particles $\boldsymbol{x}_k^{(i)}$ in (15) were drawn from an importance density

$$\begin{aligned} q(\boldsymbol{x}_k^{(i)}|\boldsymbol{x}_{k-1}^{(i)}, y_{1:k}) \quad &= \quad q_x(x_k^{(i)}|x_{k-1}^{(i)}, \theta_{k-1}^{(i)}, y_{1:k}) \\ &\quad\quad \times q_\theta(\theta_k^{(i)}|x_{k-1}^{(i)}, \theta_{k-1}^{(i)}, y_{1:k}) \end{aligned} \tag{16}$$

with importance densities for x_k and θ_k, $q_x(x_k^{(i)}|x_{k-1}^{(i)}, \theta_{k-1}^{(i)}, y_{1:k})$ and $q_\theta(\theta_k^{(i)}|x_{k-1}^{(i)}, \theta_{k-1}^{(i)}, y_{1:k})$, and the associated normalized weights are evaluated by

$$\begin{aligned} w_k^{(i)} \quad &\propto \quad w_{k-1}^{(i)} \frac{p(y_k|x_k^{(i)}, \theta_k^{(i)})}{q_x(x_k^{(i)}, \theta_k^{(i)}|x_{k-1}^{(i)}, \theta_{k-1}^{(i)}, y_{1:k})} \\ &\quad\quad \times \frac{p(x_k^{(i)}, \theta_k^{(i)}|x_{k-1}^{(i)}, \theta_{k-1}^{(i)})}{q_\theta(\theta_k^{(i)}|x_{k-1}^{(i)}, \theta_{k-1}^{(i)}, y_{1:k})}. \end{aligned} \tag{17}$$

Then, the SIS, SIR and ESP filters are defined as above.

4.1 Numerical Examples

Numerical simulation are carried out to exemplify the applicability of the proposed ESP filter. First, we consider the following nonlinear state space model

$$\begin{aligned} x_k &= \frac{x_{k-1}}{2} + \frac{\theta x_{k-1}}{1+x_{k-1}^2} + 8\cos(1.2k) + v_k \\ &= f(x_{k-1}, \theta) + v_k \end{aligned} \tag{18}$$

$$y_k = \frac{x_k^2}{20} + w_k \tag{19}$$

where v_k and w_k are i.i.d. zero-mean normal random variables with variance 10 and 1, respectively, and value of the parameter θ is known to be 25. The normal distribution with mean $f(x_{k-1}^{(i)})$ and variance 10 is chosen as the importance density $q(x_k|x_{k-1}^{(i)}, y_{1:k})$. Sample paths of the estimates by the proposed ESP(,) ($n=100, \ell=4$) and EKF as well for comparison are given in Fig.1. Proposed ESP filter works well in nonlinear state estimation, while the estimate by EKF cannot follow the true state.

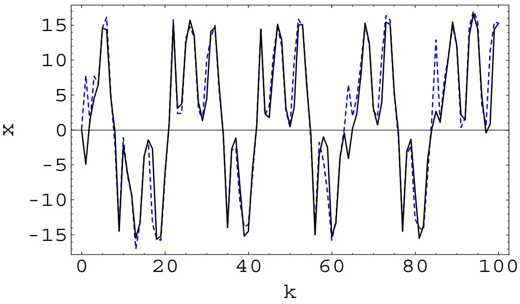

(a) Estimate by ESP(,)

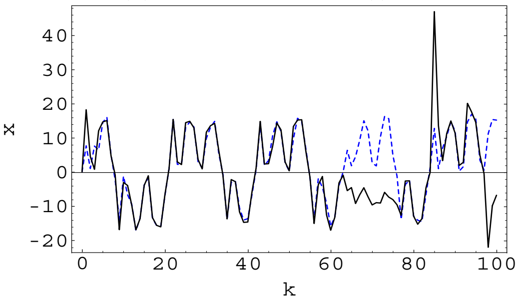

(b) Estimate by EKF

Figure 1: Sample paths of state estimates (dashed line: estimate, solid line: true state)

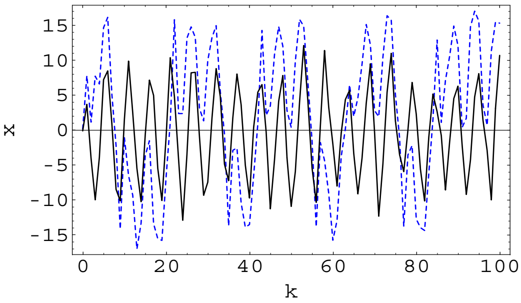

(a) A sample path of the state estimate

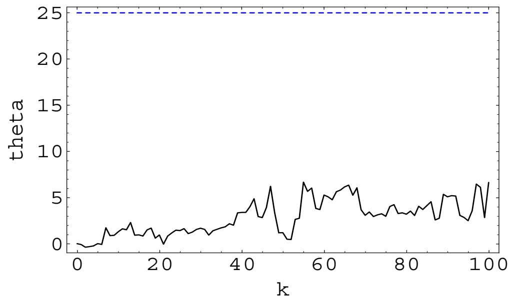

(b) A sample path of the parameter estimate

Figure 2: Simulation results in simultaneous state and parameter estimation by ESP(,)

Next, we consider the unknown parameter case where the true value of $\theta = 25$ in (18) is not known. Here, only the results by ESP(,) with the importance densities $q_x(x_k^{(i)} \,|x_{k-1}^{(i)}, \theta_{k-1}^{(i)}, y_{1:k}) \sim \mathcal{N}(f(x_{k-1}^{(i)}, \theta_{k-1}^{(i)}, 10)$ and $q_\theta(\theta_k^{(i)}|x_{k-1}^{(i)}, \theta_{k-1}^{(i)}, y_{1:k}) \sim \mathcal{N}(\theta_{k-1}^{(i)}, 0.01)$ are shown in Fig.2 since the EKF does not work as before. Though the estimate approach to the true ones, the convergence speed is slow and the filter leaves much for improvement. For examples, better choice of design parameters n, N_{eff} and ℓ and choice of evolution operations should be pursued since the estimation performance, of course, depends on the choice of them.

5 Conclusions

The novel particle filter, which is developed by recognizing the similarity and the difference between the importance sampling and resampling processes in the SIR filter and mutation and selection processes in ES and substituting (μ, λ)-selection in ES into resampling process in SIR, is applied to simultaneous state and parameter estimation of nonlinear state space models. It works stably and provides small mean square errors compared to EKF filter. Application of other evolution operations such as crossover and modification of mutation will have the potential to create much higher performance particle filters.

References

[1] B. D. O. Anderson and J. B. Moore: *Optimal Filtering*, Prentice-Hall, 1979.

[2] S. Arulampalam, S. Maskell, N. Gordon and T. Clapp: A tutorial on particle filters for on-line non-linear/non-Gaussian Bayesian tracking, *IEEE Trans. on Signal Processing*, SP-50, No.2, pp.174–188, 2002.

[3] T. Bäck, *Evolutionary Algorithms in Theory and Practice: Evolution Strategies, Evolutionary Programming, Genetic Algorithms.* Oxford University Press, 1996.

[4] A. Doucet, N. de Freitas and N. Gordon (Eds.): *Sequential Monte Carlo Methods in Practice*, Springer-Verlag, 2001.

[5] N. Gordon, D. Salmond and A. Smith: A novel approach to nonlinear/non-Gaussian Bayesian state estimation, *IEE Proc. on Rader and Signal Processing*, 140, pp.107-113, 1993.

[6] A. H. Jazwinski: *Stochastic Process and Filtering Theory*, Academic Press, 1970.

[7] H.-P. Schwefel: *Evolution and Optimum Seeking*, J. Wiley, 1995.

[8] K. Uosaki, Y. Kimura and T. Hatanaka: State estimation of nonlinear stochastic systems by evolution strategies based particle filter. *Proc. 9th Int. Symposium on Artificial Life and Robotics*, pp.406–409, 2004.

The Tenth International Symposium on Artificial Life and Robotics 2005(AROB 10th '05),
B-con Plaza, Beppu, Oita, Japan, February 4-6, 2005

Evaluating a solution of Tour Planning Problem based on the partially exhaustive exploration Monte Carlo Method

Masaki Onodera* Hidenori Kawamura* Azuma Ohuchi*

*Graduate School of Information Science and Technology, Hokkaido University
Kita 14, Nishi 9, Kita-ku, Sapporo, Hokkaido, 060-0814, Japan
{onodera, kawamura, ohuchi}@complex.eng.hokudai.ac.jp

Abstract

Researches on a planning, which includes the uncertainty that a result to a single solution cannot be determined uniquely, have been done. In such problems, a solution needs to be evaluated based on the uncertainty. In this paper, as the evaluation function based on such uncertainty, expected value estimated using the Monte Carlo Method is suggested. Moreover, the partially exhaustive exploration Monte Carlo Method is proposed to improve the accuracy of the estimation. As an example of the problem, the Tour Planning Problem is suggested and the proposed method is applied to this problem. From experimental results, it has been confirmed that the accuracy is improved by the proposed method. The proposed method can estimate the expected value as accurately as the standard Monte Carlo Method using the fewer samples. There is a probability of improving the effectiveness of searching because more solutions can be evaluated.

Keywords: Monte Carlo Method, uncertainty, Tour Planning Problem

1 Introduction

Researches on a planning, such as the automatic decision-making by the software or the combinatorial optimization problem containing probabilistic parameter, have been done [1][3][4]. These problems include the uncertainty that a result cannot be determined uniquely. In short, in such problems, a single solution may produce different results. Therefore, a solution needs to be evaluated based on the uncertainty. In the case where all possible results and each probability are known, the simplest evaluation function includes the expected value. However, if the number of possible results is large, it is difficult to calculate the expected value actually because of the time constraints.

In this paper, we suggest the expected value estimated using the Monte Carlo Method (MCM) [2] as the evaluation function based on the uncertainty and propose the partially exhaustive exploration Monte Carlo Method to improve the accuracy of the estimation using a few samples. Furthermore, we suggest the Tour Planning Problem as an example including such uncertainty. We apply the proposed method to this problem.

The remainder of the paper is organized as follows: In section 2, the Tour Planning Problem is formulated. In section 3, the partially exhaustive exploration Monte Carlo Method is proposed. In section 4, we apply the proposed method to the Tour Planning Problem and discuss the effectiveness. Finally, concluding remarks are given in Section 5.

2 Tour Planning Problem

2.1 Overview

The purpose is to plan a tour, which maximizes the total score within the time limit, when there are multiple tourist facilities. In traditional model, it is assumed that the each time cost involved with transferring between the facilities or staying at each facility is constant. We introduce the probability distributions as each time cost. It cannot be defined that whether a tour exceeds the time limit or not because each time cost is not defined uniquely.

We compared two evaluation functions about a tour in the preliminary experiment. One is the expected score. The other is the score, which is got when it is assumed that each cost is the average of given probability distribution. From experimental results, it is confirmed that using the expected value can search for a tour, which rarely exceeds the time limit and gets high score averagely. Therefore, we formulate the Tour Planning Problem as the combinatorial optimization problem aiming at maximizing the expected score.

2.2 Formulation

A set of node, which corresponds to a tourist facility, is denoted by V, and a set of time is denoted by T.

$$V = \{v_1, \cdots, v_n\}, \quad (1)$$
$$T = \{t_r | t_r = t_1 + (r-1) \cdot \delta t, r = 1, 2, \cdots\}, \quad (2)$$

where δt is unit time. The v_i has the opening time o_i and closing time e_i $(o_i, e_i \in T)$. A set of time cost involved with moving from v_i to v_j and staying at v_i is denoted by W_{ij} and W_i $(v_i, v_j \in V)$, respectively.

$$W_i = \{w_{ik} | w_{i,k+1} = w_{ik} + \delta t, k = 1, \cdots, m_i\}. \quad (3)$$

$$W_{ij} = \{w_{ijk} | w_{i,j,k+1} = w_{ijk} + \delta t, k = 1, \cdots, m_{ij}\}. \quad (4)$$

The v_i has the probability distribution denoted by $p_i(w_{ik})(\sum_k p_i(w_{ik})=1,\ p_i(w_{ik})\geq 0)$, which indicates the probability of staying at v_i for w_{ik}. Moreover, the probability distribution denoted by $p_{ij}(w_{ijk})(\sum_k p_{ij}(w_{ijk})=1,\ p_{ij}(w_{ijk})\geq 0)$, which indicates the probability of taking w_{ijk} to move from v_i to v_j, is defined. Given starting point v_s, goal v_g, departure time D_s and time limit D_g, the objective of Tour Planning Problem is to maximize

$$\sum_{b \in B} (S(A,b) \cdot p(b)) = E\left[S(A,b)\right]. \quad (5)$$

$$A = (a_{ui})_{u=1,\cdots,n, i=1,\cdots,n} \ (a_{ui} \in \{0,1\}). \quad (6)$$

$$S(A,b) = \begin{cases} \sum_{u=2}^{L-1} s_{a(u)}(t_u) : t_L \leq D_g \\ 0 \qquad\qquad\qquad : t_L > D_g \end{cases}. \quad (7)$$

$$s_i(t) = \begin{cases} s_i : o_i \leq t \leq e_i \\ 0 : otherwise \end{cases}. \quad (8)$$

$$B = W_{a(1)} \times \cdots \times W_{a(L)} \times W_{a(1),a(2)} \times \cdots \times W_{a(L-1),a(L)}. \quad (9)$$

$$b = (c_{a(1)}, \cdots, c_{a(L)}, c_{a(1),a(2)}, \cdots, c_{a(L-1),a(L)}). \quad (10)$$

$$p(b) = \prod_{u=1}^{L} p_{a(u)}(c_{a(u)}) \times \prod_{u=1}^{L-1} p_{a(u),a(u+1)}(c_{a(u),a(u+1)}). \quad (11)$$

$$t_\xi = D_s + \sum_{u=2}^{\xi-1} c_{a(u)} + \sum_{u=1}^{\xi-1} c_{a(u),a(u+1)}. \quad (12)$$

$$L = \sum_{u=1}^{n} \sum_{i=1}^{n} a_{ui}. \quad (13)$$

$$a(u) = \sum_{i=1}^{n} (a_{ui} \cdot i). \quad (14)$$

subject to

$$a_{1,s} = a_{L,g} = 1. \quad (15)$$

$$\sum_{u=1}^{n} a_{ui} \leq 1. \quad (16)$$

$$\sum_{i=1}^{n} a_{u+1,i} \leq \sum_{i=1}^{n} a_{ui}. \quad (17)$$

Equation (5) represents the expected score. The matrix (6) represents a tour. If $a_{ui} = 1$, the u-th node that a client visits is v_i. Equation (7) represents the total score. In this model, the score for the case of exceeding the time limit is set to zero because we assume the time limit as the departure time of the airplane or the train that a client will take. Therefore, if to exceed the time limit is allowed somewhat, it is possible that not zero but the function of a certain penalty is used as such score. Equation (8) is a score of v_i in the time t. Equation (9) represents a direct product consisted of combination of time cost. As (10) shown, b $(\in B)$ represents the combination of arbitrary costs. Where c_i and c_{ij} are arbitrary time costs determined according to $p_i(w_{ik})$ and $p_{ij}(w_{ijk})$. The value of (11) is occurrence probability of b. In short, $p(b)$ is a probability that arbitrary c_i and c_{ij} are selected at the same instant. Equation (12) represents the time that a client arrives at ξ-th node. The value of (13) is the total number of node that a client visits. The value of (14) represents the number of u-th node that a client visit. Equations (15)-(17) are the constrained conditions.

3 Proposed method

3.1 Estimation of expected score

Because it is difficult to search for the optimum solution, we search the approximate solution by the heuristic search. However, if the expected score is calculated actually, it takes time granted that heuristic search is used. Therefore, we propose the expected score estimated by the MCM as the evaluation function. Some combinations of c_i and c_{ij}, which is b, is selected randomly according to $p_i(w_{ik})$ and $p_{ij}(w_{ijk})$ as samples. Then, the MCM estimates the expected score. The number of samples is denoted by M. The M has to be set a low value because of the time constraints. Therefore, we propose the partially exhaustive exploration Monte Carlo Method to improve the accuracy of the estimation using a few samples.

3.2 Partially exhaustive exploration Monte Carlo Method

This method uses the feature that the b with the high occurrence probability can be enumerated without exploring all combinations of time costs. As above, the $p(b)$ is calculated as a product of $p_i(c_i)$ and $p_{ij}(c_{ij})$. Therefore, a certain threshold is set when the $p(b)$ is calculated. If a product is below the threshold in the course of calculation of $p(b)$, the rest of all the calculation about the combination is omitted. By this tree pruning, the cost for enumeration can be reduced.

The procedure to estimate the expected score about an A is as follows. First, a certain threshold is determined and the set B is divided into two sets. One is the set of b, which has the higher $p(b)$ than the threshold. The other is the set of other b. The former is denoted by $B^{(1)}$ and the latter is denoted by $B^{(2)}$. The number of samples used for estimation about $B^{(1)}$ is M_1 and about $B^{(2)}$ is M_2. M is the sum of M_1 and M_2. Secondly, all b contained in $B^{(1)}$ are explored exhaustively. Therefore, M_1 equals $|B^{(1)}|$. The E_1, which is answer of exhaustive exploration about $B^{(1)}$, is calculated.

$$E_1 = \sum_{b \in B^{(1)}} (S(A, b) \times p(b)) \; . \qquad (18)$$

Thirdly, the MCM estimates the expected score about $B^{(2)}$. The M_2 samples are generated randomly according to $p_i(c_i)$ and $p_{ij}(c_{ij})$. They are denoted by ξ_q. However, the $p(\xi_q)$ may be higher than the threshold. Such sample cannot be used. Therefore, the number of the samples, which can actually be used, may be less than M_2. The number of samples, which can be used, is denoted by M_2^{true}. The E_2, which is expected score estimated about $B^{(2)}$, is calculated.

$$E_2 = \frac{1}{M_2^{true}} \sum_{q=1}^{M_2^{true}} S(A, \xi_q). \quad (M_2^{true} \leq M_2) \qquad (19)$$

Finally, the expected score E is calculated.

$$E = E_1 + \sum_{b \in B^{(2)}} p(b) \cdot E_2 \; . \qquad (20)$$

In the preliminary experiment, it is confirmed that the larger there is deviation between the occurrence probabilities, the more this method is effective. When there is not deviation so much, the effect cannot be expected. However, because it is difficult to define that the Tour Planning Problem is contained in which, it is necessary to investigate.

4 Experiment

4.1 Experimental setup

We design the model based on fourteen tourist facilities in Sapporo city, Japan. The $p_{ij}(w_{ijk})$ is determined as follows. First, standard time cost involved with moving from v_i to v_j, which is denoted by μ_{ij}, is calculated using the store-bought map software. Secondly, $_{ij}$ is calculated as μ_{ij} divided by K. This K is parameter to set the variation of the time cost. Finally, $p_{ij}(w_{ijk})$ is determined by dividing a normal distribution $N(\mu_{ij}, \; _{ij})$ according to δt as Figure 1. The $p_i(w_{ik})$ is determined in the same way as $p_{ij}(w_{ijk})$. The standard time cost μ_i is determined referring to some guidebooks. Each o_i and e_i is the actual value. In this experiments, $\delta_t = 5$, and $K = 15$ are used.

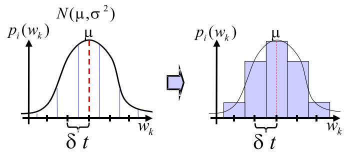

Figure 1: The calculation of the occurrence probability

Table 1: The three kinds of setups about client

	v_s	v_g	D_s	D_g
Client 1	13	0	840	1380
Client 2	0	0	480	1080
Client 3	0	13	540	1260

4.2 Comparison with the standard MCM

To compare the accuracy of estimation, the expected score is estimated about one thousand solutions each ten thousand times by each MCM. Then, to evaluate the accuracy, a error rate to a true expected score is calculated. Three kinds of client are prepared as shown in Table 1. In the setting of client 1, some nodes will be closed depend on the time. In the setting of client 2, some nodes do not stay open at first. In the setting of client 3, more time can be used than other settings. Furthermore, two kinds of settings about M, M=200 and M=500 are used. In this paper, we used the M as an indicator of the calculation cost. Because it is thought that the computation time depends on the feature of the problem or efficiency of programs, we fixed not the computation time but M.

4.3 Results of the first experiment

Figure 2 - 7 show the average error rate. The "1.0" in figures represents the standard MCM. About clients 1 and 2, the proposed method could estimate the expected score more accurately than the standard MCM. In the case of M=500 of client 1, accuracy was improved about one to two percent. In view of the fact that the Standard MCM can estimate the expected score comparatively accurately, it is thought that the accuracy was improved considerably. In other words, the proposed method can estimate the expected score as accurately as the standard MCM using the fewer samples. Furthermore, the accuracy differs depending on the balance between the threshold and the number of samples M. Therefore, the threshold is very important. About client 3, there is not so much of a difference between the proposed method and the Standard MCM. Because client 3 can visit more nodes, the combination of time cost increases. Each $p(b)$ becomes low and almost all $p(b)$ becomes lower than a threshold. As a result, the proposed method is not so different from the standard MCM. Next, client 1 that the accuracy is most improved is considered selectively.

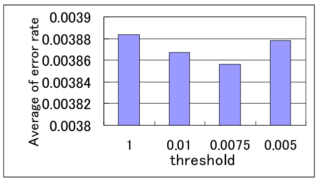

Figure 2: The average error rate about client 1 (M=200)

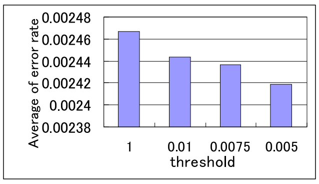

Figure 3: The average error rate about client 1 (M=500)

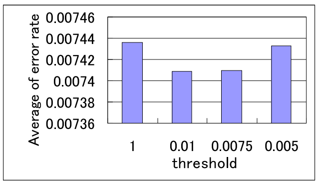

Figure 4: The average error rate about client 2 (M=200)

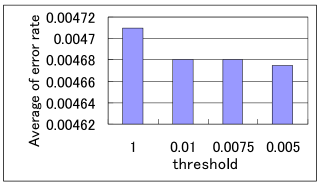

Figure 5: The average error rate about client 2 (M=500)

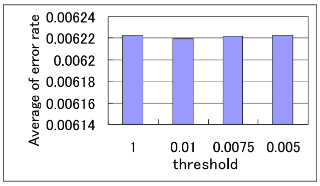

Figure 6: The average error rate about client 3 (M=200)

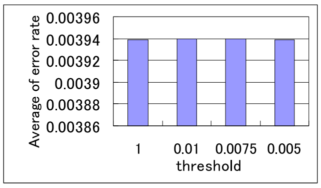

Figure 7: The average error rate about client 3 (M=500)

4.4 Comparison of effectiveness of searching

To discuss the effectiveness of searching by each method, we search for a tour 500 times actually about the setting of client 1 and compare the tours, which are selected finally. We use the simulated annealing (SA) because of the ease of implementation. The parameters are determined in the preliminary experiments. A tour is expressed as permutation of the visited node number.

4.5 Results of the second experiments

Figure 8 shows the average of true expected scores of 500 tours selected by 500 trials of SA. There is not so much of a difference between the two methods. It is thought that a tour, which finally is selected, is much the same because the expected score is estimated comparatively accurately whichever method. However, as stated in section 4.3, the proposed method can estimate the expected score as accurately as the standard MCM using the fewer samples. As a result, more solutions can be evaluated. Therefore, there is a probability of improving the effectiveness of searching by the proposed method. Figure 9 shows the average of probability that a selected tour exceed the time limit.

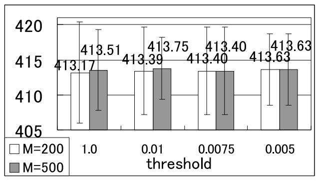

Figure 8: The average of true expected scores of 500 tours

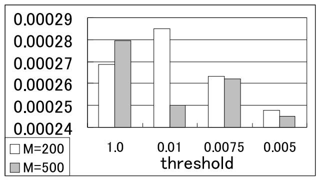

Figure 9: The average of probabilities of breach to time limit

The selected tours rarely exceed the time limit. The computation time of the proposed method is similar to that of the standard MCM within four seconds.

5 Conclusion

In this paper, we suggest the expected value estimated using the MCM as the evaluation function based on the uncertainty. Moreover, the partially exhaustive exploration Monte Carlo Method is proposed to improve the accuracy of the estimation. Furthermore, the Tour Planning Problem is suggested as an example of the problem including the uncertainty. From results of experiments, it has been confirmed that the accuracy is improved by the proposed method. In other words, the proposed method can estimate the expected value as accurately as the standard MCM using the fewer samples. There is a probability of improving the effectiveness of searching because more solutions can be evaluated. Moreover, a reasonable tour, which rarely exceeds the time limit and gets high score averagely, can be searched by using the expected score as the evaluation function. As the future works, we have to design the means to adjust a threshold automatically. Moreover, we have to discuss a case that it is difficult to estimate an expected value.

Acknowledgment

Our special thanks are due to Mr. Koichi Kurumatani, National Institute of Advanced Industrial Science and Technology for considerable cooperation and valuable advice.

References

[1] E.L.Lawler, et al. *The TRAVELING SALESMAN PROBLEM*, October, 1986.

[2] Arnaud Doucet, et al. *Sequential Monte Carlo Methods in Practice*, Springer-Verlag, January 2001.

[3] M. Wellman, et al. *Designing the Market Game for a Trading Agent Competition*, IEEE INTERNET COMPUTING, March/April (2001. 8) :p43–51

[4] Michael P. Wellman, et al. *Path Planning under Time-Dependent Uncertainty**, the Eleventh Conference on Uncertainty in Artificial Intelligence, August, 1995.

The Tenth International Symposium on Artificial Life and Robotics 2005(AROB 10th '05),
B-con Plaza, Beppu, Oita, Japan, February 4-6, 2005

A Comprehensive Evaluation of the Methods for Evolving a Cooperative Team

Yasuyuki Suzuki Takaya Arita
Graduate School of Information Science
Nagoya University
yasu@create.human.nagoya-u.ac.jp arita@nagoya-u.ac.jp

Abstract

This paper focuses on the techniques of evolutionary computation for generating players performing tasks cooperatively. However, in using evolutionary computation for generating players performing tasks cooperatively, one faces fundamental and difficult decisions including the one regarding the so-called "credit assignment problem". We believe that there are some correlations among design decisions and therefore a comprehensive evaluation for them is essential. We first list three fundamental decisions and possible options in each decision in designing methods for evolving a cooperative team. We find that there are 18 typical combinations available to execute. Then we describe the ultimately simplified soccer game played on one-dimensional field as a testbed for comprehensive evaluation for these 18 candidate methods. The results are analyzed in this paper.

1 Introduction

Some problems can be efficiently solved only by teams consisting of cooperative autonomous players. Many researchers have developed methods that don't require human designers to define specific behaviors of players for each problem. The work reported here focuses on the techniques of evolutionary computation, which has been regarded as one of the most promising approaches to solve such complex problems. However, in using evolutionary computation for generating players performing tasks cooperatively, one faces fundamental and difficult decisions including the one regarding the so-called "credit assignment problem" [1]. For example, if we can only evaluate the global performance of each team, how do we divide up the team's performance among the participating players? We believe that there are some correlations among design decisions and therefore a comprehensive evaluation for them is essential, although not a few researchers have proposed evolutionary methods for evolving teams performing specific tasks.

The rest of the paper is organized as follows. In Section 2, we list three fundamental decisions and possible options in each decision in designing methods for evolving a cooperative team. We find that there are 18 typical combinations available to execute. Then, in Section 3, we describe the ultimately simplified soccer game played on one-dimensional field as a testbed for comprehensive evaluation for these 18 candidate methods. Section 4 reports on the results of the comprehensive evaluation of these methods, and Section 5 summarizes the paper.

2 Methods for Evolving a Team

Three fundamental decisions are necessary when one designs an evolutionary computation method for generating players performing tasks cooperatively, and there may be not a few combinations of the options in these decisions.

The first decision is: How many evolving populations are there? The answer is derived by considering whether or not the population structure depends on the number of the teams in the game or the number of the player roles in the game (Figure 2). Suppose that the game is played by 2 teams consisting of 3 players. We can assume an evolutionary computation with 2 populations corresponding 2 teams, with 3 populations corresponding 3 players, or with 6 populations corresponding to 2 teams and 3 players. So, the typical options for the number of the populations are 1, R, T and $T \cdot R$ (T: Number of teams in the game, R: Number of the player roles in the team).

The second decision is: What does each individual (genome) represent? Typical options are a player and a team. In case of that each genome represents a player, there can be two further options: all players in the team share one genome ("homogeneous players") and all players are represented by different genomes ("heterogeneous players"). Also in case that each genome represents a team, there can be two further options: whether or not the roles of the players represented in each genome are fixed. In case that the roles of the player is fixed, for example, if a part of a genome represents a defender in the game, this part always represents a defender.

The third decision is: How is the fitness function evaluated? One option is that fitness is evaluated for a team as a whole. In this case, if each genome represents a player, each player in a team is supposed to have the same fitness. The other option is that the fitness is evaluated for each player directly or indirectly. Direct evaluation of players in a cooperative team is sometimes a very difficult task, as in general altruistic behavior is important or essential in the establishment and maintenance of cooperation in population. Some methods for indirect evaluation has been proposed [2]. We adopt a method as this option in which the fitness of a player is defined as the decrease in the fitness of the team when the player is replaced by a predefined "primitive player" which has a minimum set of behavior rules.

Therefore, there could be 18 combinations available to execute for evolving players performing tasks cooperatively as shown in Table 1.

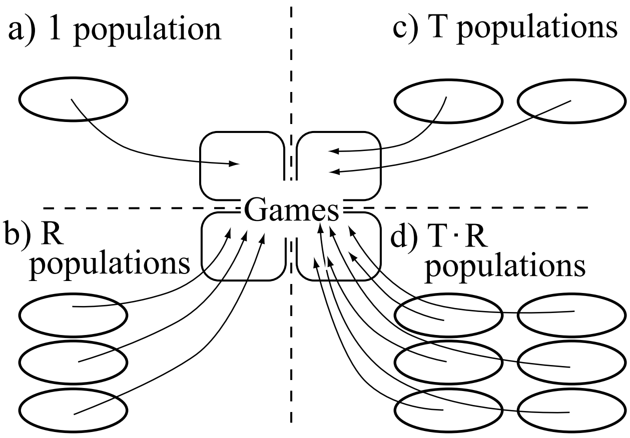

Figure 1: 4 options for the population structure. a) The population represents all player roles in all teams. b) Each population represents one player role in all teams. c) Each population represents all player roles in each team. d) Each population represents one player role in each team.

3 Ultimately-Simplified Soccer Game

The ultimately-simplified soccer game is defined as a testbed for comprehensive evaluation for these 18 candidate methods. It is a 2 vs. 2 player game played on one-dimensional cellular field as shown in Figure 2 (field[1-20]). Players are homogeneous except their starting positions (Left team: player1 (field[8]), player2 (field[5]), Right team: player1 (field[13]), player2 (field[16])), and each player makes a run, dribbles a ball, makes a shot on goal or put a ball up to the player of his/her team. One of the action is decided to take based on the relative locaton of all players and the ball (72 patterns). Action is taken in turn alternatively between 2 teams. Each step in the game is composed of 4 actions by all players.

Multiple players can't be in a cell. The ball is always in a cell where a player resides. Moving action of a player with a ball means dribbling. Players move to either of the neigboring cells, but when a player moves to the cell with a player, it skips the neigboring player (it cannot skip more than one player). In this case, if both are in opposite teams and one of them has a ball, the ball moves to the other player with a certain probability (P_{steal}). If there is an opponent player between the passer and the receiver, the ball-passing becomes failure with a certain probability (P_{cut}), and in this case the ball moves to the cell where the oppenent player resides. The success rate for shooting is anti-proportional to the length between the player's position and the goal irrespective of the presence of the oppsite players. In case of scoring a goal, the game restarts with initial player-location. In case of the failure, the game restarts after the ball moves to the opposite player nearer to the goal post.

We expect two types of altruistic behavior which could lead to the emergence of cooperation in the game. One is putting a ball up to the other player in his/her team instead of dribbling the ball or getting a shot at the goal. The other type is making a run in the opposite direction but not toward the goal. The former type of altruistic behavior is analyzed in 4.3.

4 Evaluation

4.1 Expression of the Players

Each player selects next action deterministically based on the positional relationship of players and the ball. In the recognition of each player, opponent players are not distinguished. So, to be precise, genetic information of each player decides the next action of the player based on one of 48 patterns, in which each pattern is associated to one of the four actions: running/dribbling to the right, running/dribbling to the left, feeding (passing) the ball to the player of his/her

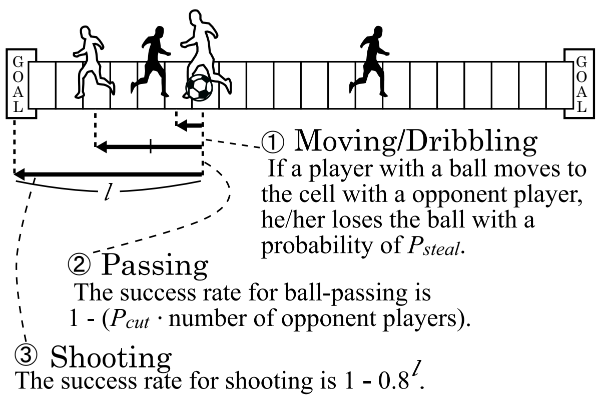

Figure 2: The ultimately simplified soccer game.

Table 1: Classification of the methods for evolving a team.

Population structure depends on T?	Population structure depends on R?	Number of populations	Each genome represents		Unit of fitness evaluation is		Code name
No	No	1	a player	heterogeneous players	a player	by direct evaluation	1-PHe-PD
						by indirect evaluation	1-PHe-PI
					a team (same fitness in a team)		1-PHe-T
				homogeneous players	a team (same fitness in a team)		1-PHo-T
			a team	fixed player-roles	a team		1-TFi-T
				unfixed player-roles	a team		1-TUn-T
	Yes	R	a player	heterogeneous players	a player	by direct evaluation	R-PHe-PD
						by indirect evaluation	R-PHe-PI
					a team (same fitness in a team)		R-PHe-T
Yes	No	T	a player	heterogeneous players	a player	by direct evaluation	T-PHe-PD
						by indirect evaluation	T-PHe-PI
					a team (same fitness in a team)		T-PHe-T
				homogeneous players	a team (same fitness in a team)		T-PHo-T
			a team	fixed player-roles	a team		T-TFi-T
				unfixed player-roles	a team		T-TUn-T
	Yes	$T \cdot R$	a player	heterogeneous players	a player	by direct evaluation	TR-PHe-PD
						by indirect evaluation	TR-PHe-PI
					a team (same fitness in a team)		TR-PHe-T

(T: Number of teams in a game, R: Number of player roles in a team)

team, making a shot on goal. Therefore each player is represented by 96 bits genetic information.

4.2 Evaluation Setting

The evaluation is conducted through two steps: an evolution step and an evaluation step. In the evolution step, populations are evolved for 2000 generations using 18 methods independently. Each population has 40 individuals in all methods. The round-robin tournament of the ultimately-simplified game of 200 steps is held to evaluate the fitness in each generation. The parameters P_{steal} and P_{cut} are set to 0.8 and 0.4 respectively in both steps. In case of <team-evaluated> option, fitness is calculated as the goals the team acquired minus the goals the opponent team acquired. In case of <direct-player-evaluated> option, fitness is calculated as the goals the player acquired minus the opponent team's goals divided by 2. Then tournament selection (selecting repeatedly the individuals with higher fitness as a parent by comparing randomly picked 2 individuals), crossover with a 60% probability and one-point mutation with a 3% probability are adopted as genetic operators. In case of <indirect-player-evaluated> option, we use a primitive player designed a priori as follows. In case of the player keeps a ball, if he (or she) is behind the other player he passes the ball to the other player, otherwise he makes a shoot. In case of the player doesn't keep a ball, if he is behind the other player, he moves back, otherwise he moves toward the goal. In the evaluation

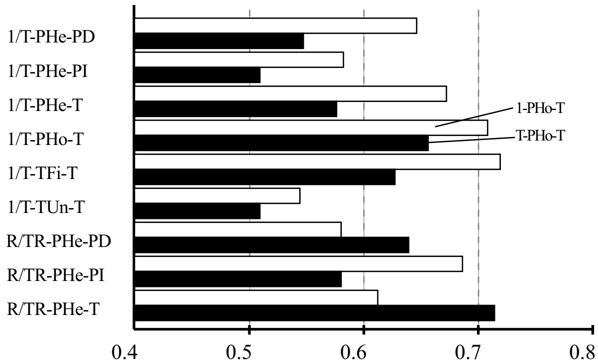

Figure 3: The average winning ratio of the best 10 teams evolved by each of 18 methods.

step, the best team is selected in each of the last 50 generations in the evolution step, and selected 50 18 teams conduct the other round-robin tournament of the game of 1000 steps.

4.3 Evaluation Results

Figure 3 shows the winning ratio of the teams evolved by 18 methods, each of which is the average of winning ratio of the best 10 teams from 50 teams in the all-play-all tournament described above. Table 2 (the left-hand in the results) also shows it. Each pair of bars shows the results of the strategies with same options in genome representation and fitness evaluation except the population structure option (Upper white bars: <$1/R$-population> options, Lower black bars: <$T/T \cdot R$-populations> options).

It is shown that the top 3 methods in this evaluation are <1-population, team-represented with fixed player-roles, team-evaluated>, <$T \cdot R$-population, heterogeneous-player-represented, team-evaluated>, and <1-population, homogeneous-player-represented, team-evaluated>. Their winning ratios are 74.6%, 74.1% and 73.5% respectively. An additional evaluation using the team consisting of 2 primitive players showed that its winning ratio was 16.0%. This ratio could be a measure for the performance of the methods.

Regarding to population structure, <$1/R$-populations> options performed better than <$T/T \cdot R$-populations> options in general. This might be because of the ill-balanced evolution, over-specialization or "round and round going". Adoption of an asymmetric game as a testbed would make this tendency weaker. Regarding to genome representation, <homogeneous-player-represented> option performed well in general. Also, <team-represented with fixed player-roles> option performed well, though <team-represented with unfixed player-roles> option performed badly. Regarding to fitness evaluation, <team-evaluated> option performed well in general as the fact that 5 methods among top 6 methods adopt this option has shown. The performance of <indirect-player-valuated> option depended largely on the other options.

We have observed interesting separation of roles among 2 players in the teams with high winning ratio. For example, in some teams the forward player tended to play near the goal and the backward player tended to move in order to intercept the ball, and in some teams both players seemed to use man-to-man defense.

Next we examined the relationship between altruistic behavior which could lead to cooperative behavior and the winning ratio. Here we focus on the following behavior pattern. A player with a ball makes a pass for the other player, who receives the ball without being intercepted and then successfully shoots a goal immediately or after dribbling. We termed this series of actions as "assisted goal". Table 2 shows the assist ratio, which is the ratio of assisted goals among all goals, and winning ratio of the teams evolved by 18 methods. We see from this table that good performing teams have a tendency to also have a high assist ratio. In contrast, it is not necessarily the case that teams with a high assist ratio have a tendency to have a high winning ratio. This means that above-defined assisting behavior is a necessary requirement for the teams to perform well.

It is a remarkable fact that <indirect-player-evaluated> option made the assist ratio much higher compared with the winning ratio. As this option, we adopted a method in which the fitness of a player is the decrease in the fitness of team when the player is replaced by the primitive player. This method should generate the strong interaction between 2 players because it tends to make large decrease when the player is replaced. Therefore the teams generated by the indirect evaluation method have a higher assist ratio despite having the relatively low winning ratio.

Table 2: Average winning ratio and assist ratio.

Code name	Results			
	Winning ratio	Rank	Assist ratio	Rank
1-PHe-PD	0.673	7	0.146	15
1-PHe-PI	0.609	11	0.289	10
1-PHe-T	0.699	5	0.310	9
1-PHo-T	0.735	3	0.390	5
1-TFi-T	0.746	1	0.342	7
1-TUn-T	0.571	16	0.336	8
R-PHe-PD	0.607	12	0.109	16
R-PHe-PI	0.713	4	0.503	1
R-PHe-T	0.639	10	0.402	3
T-PHe-PD	0.574	15	0.080	17
T-PHe-PI	0.536	17	0.391	4
T-PHe-T	0.603	14	0.242	12
T-PHo-T	0.683	6	0.226	13
T-TFi-T	0.654	9	0.260	11
T-TUn-T	0.536	18	0.214	14
TR-PHe-PD	0.666	8	0.077	18
TR-PHe-PI	0.607	13	0.388	6
TR-PHe-T	0.741	2	0.416	2

5 Conclusion

This paper has focused on the methods for evolving a cooperative team by conducting a comprehensive evaluation for 18 methods. We have found that some methods performed well and at the same time that there are complex correlations among design decisions. Also, further analysis has shown that cooperative behavior can be evolved and can be a necessary requirement for the teams to perform well in even such a simple game. Future work includes more detailed analysis of cooperative behavior and extension of the ultimately-simplified soccer game.

References

[1] Thomas Haynes, Sandip Sen, Dale Schoenefeld and Roger Wainwright, "Evolving a Team", *Working Notes for the AAAI Symposium on Genetic Programming*, pp. 23-30, 1995.

[2] Thomas Miconi, "A Collective Genetic Algorithm", *Proceedings of the Genetic and Evolutionary Computation Conference (GECCO 2001)*, pp. 876-883, 2001.

The Tenth International Symposium on Artificial Life and Robotics 2005(AROB 10th '05),
B-con Plaza, Beppu, Oita, Japan, February 4-6, 2005

A Fast Algorithm in Finding Communities of Book Network

Shijun Wang, Changshui Zhang
State Key Laboratory of Intelligent Technology and Systems, Department of Automation,
Tsinghua University, Beijing 100084, China
wsj02@mails.tsinghua.edu.cn, zcs@mail.tsinghua.edu.cn

Abstract

In this paper, we present a new fast algorithm named NDBC in finding communities within large network systems. The algorithm is developed based on DBSCAN and makes use of the structural information of complex networks. We test NDBC on the book network which is constructed by the readers' borrowing behaviors. The experimental result shows that it can quickly find communities of a big network which contains thousands upon thousands vertices.

Keywords: complex network, community, book network

1. Introduction

Many systems in the real world can be abstracted as complex networks. The examples of complex network include the Internet, science collaboration network, neural networks, metabolic networks, food web, etc. [1]. Recent research on complex networks has revealed a number of distinctive statistical properties that most networks seem to share [1] [2] [3], such as power law distribution of degree, high clustering coefficient and short average path length.

"It is widely assumed that most social networks show "community structure", i.e., groups of vertices that have a high density of edges within them, with a lower density of edges between groups." [4] How to discover communities in large network systems within a short time is an interesting problem.

A recent influential algorithm that has been used is based on the idea of betweenness, proposed by Girvan and Newman [5] [6]. The betweenness of an edge is defined as the number of shortest paths that traverse it. Their method iteratively removes edges which lie between two clusters and has highest betweenness from the network. In this method, the time involved to discover the community structure of the graph scales as $O(n^3)$, with n the number of vertices in the network.

In the computer science literature, there are a number of fast heuristics, such as "FM-Mincut". Flake et al. [7] use a maximum flow/minimal cut algorithm to define the edges and vertices that act as boundary between communities.

Wu et al. [8] present a method which is based on notions of voltage drops across networks that are both intuitive and easy to solve. However, their algorithm has to specify the number of communities beforehand.

Zhong Su et al. [9] present a recursive density-based clustering algorithm for web document clustering based on DBSCAN [10]. In order to cut off the bridge between two clusters, their algorithm varies *Eps* and *MinPts* whenever necessary.

In this paper we present a new method named NDBC that can discover communities within networks of arbitrary size in a very short time. The key idea of our method is that we combine the clustering algorithm DBSCAN with the structural information of complex networks in finding communities. We apply our method to finding communities of book network. The result shows that NDBC is very efficient because we just need scan the vertices of the data set once. Moreover, it does not require a predetermined cluster number to operate. Our method achieves the same goal as Zhong Su [9] but need only one constant predefined in the algorithm.

The outline of this paper is as follows. In Sec. 2 we introduce the book network. In Sec. 3 we show the key idea of DBSCAN and its drawback in finding communities. In Sec. 4 our algorithm NDBC is described. The dataset and experimental results are listed in Sec. 5. In Sec. 6 we give our conclusions.

2. Book Network

In the book network, the vertices are the books, and two vertices have a common edge if the corresponding books have been borrowed together by the same person. That means if two books occur in someone's book borrowing records, then the two books are associated. If these two books are borrowed together by more than one person, then the weight of link between them are accumulated. So the book network is a weighted and undirected network.

If two books are borrowed together by N persons separately, we define the distance between those two books is $1/N$. Set D as the book set. The *Eps*-

neighborhood of a book p is defined as $N_{Eps}(p) = \{q \in D \mid dist(p, q) \le 1/MinTime\}$ where $Eps = 1/MinTime$. *MinTime* is the least times that two books are borrowed together.

A clustering CL of book set D with respect to *Eps*, *MinPts* is a set of density-connected [10] sets with respect to *Eps*, *MinPts* in D. For any points in a space, where a point corresponds to a book, the more books that co-occur with it in some reader's borrowing records, the higher its density is.

3. DBSCAN

The clustering algorithm DBSCAN [10] based on sample density is designed to discover clusters of arbitrary shape as well as to distinguish noise.

"The key idea of a density-based cluster is that for each point of a cluster it's *Eps*-neighborhood for some given $Eps > 0$ has to contain at least a *MinPts* minimum number of points, i.e. the "density" in the *Eps*-neighborhood of points has to exceed some threshold." [11]

In order to find communities of book network, we first tried DBSCAN to the book network. The result shows that DBSCAN often leads to a single, giant cluster which is not desirable. The reason why all these books are connected together lies in the inherent nature of DBSCAN. As pointed above, DBSCAN is based on sample density. For many popular books and reference books of various categories, the probability that they are borrowed together is very high. For example, book A is a science fiction and book B is a reference book of physics. If A and B are borrowed together many times, then the weight between them is high. So A and B serve as a bridge between science fictions and references of physics and these two clusters are connected together. This is illustrated in Fig. 1.

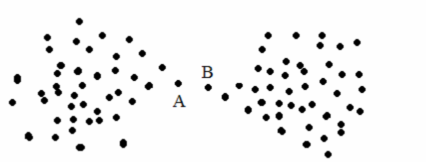

Figure 1. Bridge between two communities

4. NDBC: Neighbor Density Based Clustering algorithm

To solve this problem, we propose a clustering algorithm called NDBC that attempts to overcome the drawback of DBSCAN in finding communities by utilizing the high clustering of complex network.

4.1. Clustering Coefficient

The DBSCAN algorithm just considers the distances of samples from each other, but in a complex network, there is also structural information between vertices besides distance information. The edges between vertices form the topology of a network.

In order to describe the connections in the environment closest to a vertex, we often use the so-called clustering coefficient [1]. "For the network with undirected edges, the number of all possible connections of the nearest neighbors of a vertex μ ($z_1^{(\mu)}$ nearest neighbors) equals $z_1^{(\mu)}(z_1^{(\mu)}-1)/2$. Let only $y^{(\mu)}$ of them be present. The clustering coefficient of this vertex, $C^{(\mu)} \equiv y^{(\mu)} / \left[z_1^{\mu}(z_1^{\mu}-1)/2 \right]$, is the fraction of existing connections between nearest neighbors of the vertex." [2] The clustering coefficient C of the network is the average of $C^{(\mu)}$ over all vertices of a network. The clustering coefficient is the probability that two nearest neighbors of a vertex are nearest neighbors also of one another.

In simple terms the clustering coefficient of a book in the book network tells us the likelihood a book's neighbors are borrowed together.

4.2. NDBC

Most complex networks exhibit a large degree of clustering [1] [2] [4]. In a network with high clustering coefficient, though two communities may be connected by a bridge, the vertices on the bridge belonging to different communities have few common neighbors. Based on the phenomena observed above, we can cut off the bridge between these two communities by neighborhood check. From the statistics of clustering coefficient of book network, illustrated in Fig. 4, we can see that the clustering coefficient of book network is very high compared with random network. This means the neighbors of a book are often connected. So based on the high clustering coefficients of most complex networks, we extend DBSCAN by considering the superposition degree of neighbors between a seed vertex and it's subsequent seed vertex in the expansion progress of a cluster.

If vertex A as a seed belongs to community C1 and vertex B as A's neighbor belongs to community C2, suppose that there are enough neighbors of A at given *Eps*, then at the expansion of this cluster from seed A, vertex B's relationship with A's neighbor is checked. If B is connected with most of A's neighbors, then B is assigned the same label with A; otherwise, B is treated as a noise. A constant called *superposition* is defined as a threshold in order to check the superposition degree of these two vertices' neighbors. Because most of A's neighbors belong to C1 and most of B's neighbors belong to C2, the number of common neighbors of A and B is small. By means of checking two vertices' neighbor superposition degree, the bridge between two different communities is truncated.

The algorithm is listed below:

```
Algorithm NDBC(DB, MinTime, MinBook)
For each  v∈DB   do
  If v is not yet assigned to a cluster then
     Expand(v, MinTime, MinBook);
     Assign them to a new cluster or noise;
```

```
Expand(v, MinTime, MinBook)
Find v's neighbors NSet with weight greater  than
MinTime;
Find vertices whose neighbors have few
superposition with v's neighbors, and delete them
from NSet;
If the size of NSet is greater than MinBook
  Expand the cluster from vertices of Nset;
```

Figure 2. Neighbor Density Based Clustering algorithm

4.3. Analytical Evaluation

The runtime of NDBC is $O(n*$ *runtime of a neighborhood query*$)$: n objects are visited and exactly one neighborhood query is performed for each of them [11]. Thus, the overall runtime depends on the performance of the neighborhood query. Fortunately, all the interesting neighborhood predicates are based on adjacency matrix – like distance predicates – which can be efficiently supported by sparse matrix when the network contains many vertices. So the runtime of NDBC is very short.

5. Experiment

5.1. Data Set

```
b1010768x;03-04-08 15:35;p10583956
b10107939;03-04-08 10:18;p10824522
b10126235;03-04-08 09:28;p10809545
b10255977;03-04-08 14:05;p10633716
```

Figure 3. Book borrowing records

We first analyze the data set under consideration. Our experiments draw on data collected from Library of Tsinghua University, China. Fig. 3 is an example of Tsinghua University Library's book borrowing records. The first column is ID of book and the third is ID of reader. It consists of book borrowing records from 15:35:00 March 4, 2003 through 11:21:00 November 12, 2003. In this period there are 573,862 book borrowing records in which 142,081 books appear.

The average clustering coefficient for the book network is 0.6188 with 170 isolated vertices. The distribution of clustering coefficients for the book network is shown in Fig. 4.

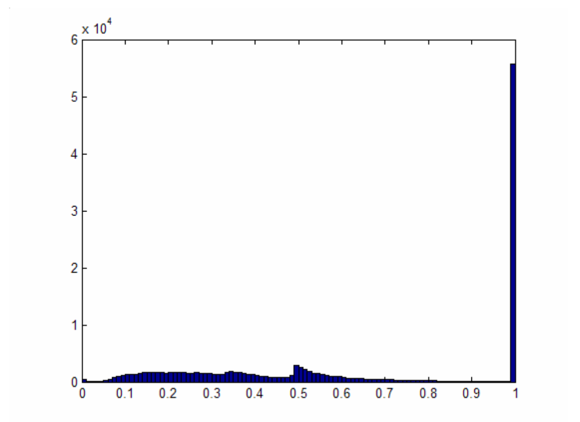

Figure 4. Distribution of Clustering Coefficients

5.2. Experimental Results

To find the communities which DBSCAN can't, we applied our community-finding method to the same book network from Library of Tsinghua University.

In Table 1 we show several communities found by NDBC. By examining the names of books belonging to the same cluster, we can see that the clusters found by NDBC are more reasonable than that found by DBSCAN since similar books are indeed grouped together.

Table 1: Some clutering results using NDBC.

Cluster ID	Book Name
77	Basic algebra Sheaves on manifolds Algebraic geometry Lectures on algebraic topology Geometric integration theory …
71	A physicist's guide to Mathematics Classical mechanics Quantum mechanics Computational fluid dynamics The universe in a nutshell Modern physics …
122	Thinking in C+ + C+ + Primer The design and evolution of C+ + The Annotated STL Sources (Using SGI STL) …
…	…

In Fig. 5 we illustrate 3 clusters of the result from the application of our algorithm to the book network. It shows community structures clearly.

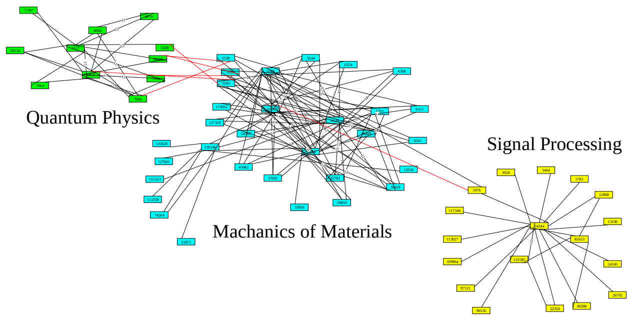

Figure 5. 3 Clusters of Book Network

Table 2 and Figure 6 show the clustering result and efficiency comparison between the two clustering algorithms (Runtime of Table 2 does not include the time reading data from disk). We see that using NDBC, we obtain more clusters for the book network and generate clusters with more even distribution than DBSCAN. In the result of DBSCAN, we can see from Fig. 6 that a cluster contains books far more than that of other clusters. The runtimes of these two algorithms are approximate.

Table 2. Comparison of NDBC and DBSCAN

	NDBC	DBSCAN
Number of Books	142081	142081
Runtime (Sec)	4	3
Eps/*MinPts*	0.125/10	0.125/10
Number of Clusters	142	69

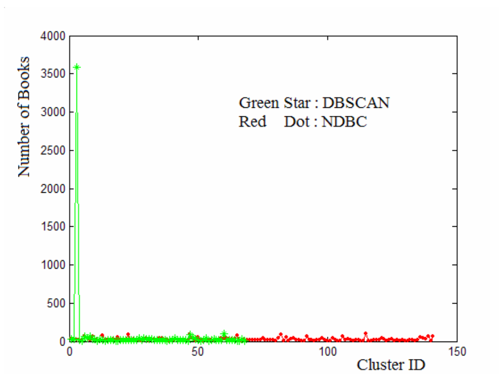

Figure 6: Number of Books in every Cluster

Our algorithm seems to find two types of communities: pure community and complex community. The pure community just contains books belonging to the same subject; the complex community often contains books belonging to several subjects. From the result of clustering, we find that the books relating to computer programming often appear in the same cluster with some books of other subjects. The phenomenon reveals that many students studying in different subjects are interested in programming. It shows that the Computer Science is closely related with other subjects.

6. Conclusions

In this paper we present a new method that allows the quick discovery of communities within a big network. The traditional clustering method DBSCAN fails in the discovery of communities of complex networks. In order to overwhelm the shortcoming of DBSCAN, we introduce structural information of complex networks in finding communities. By utilizing the high clustering coefficients of complex networks, our method succeeds in cutting of the bridge between two communities. Moreover, we do not have to specify the number of communities we wish to divide the network into.

We test the algorithm by applying it to book network. The experimental result shows its validity.

A possible defect of our method is that in order to divide the popular books coming from different categories, we select a high *MinTime*. Unfortunately, the books which are rarely borrowed together with popular books within the same category are treated as noise. In some sense, we just find the cores of the book network communities.

In spite of possible shortcoming we believe that the algorithm we have presented is valid and fast when trying to quickly find communities within large complex networks.

References

[1] R. Albert and A. Barabasi, Statistical mechanics of complex networks, *Reviews of Modern physics*, 2002, pp. 74.47.
[2] S.N. Dorogovtsev and J.F.F. Mendes, Evolution of networks, *Adv. Phys.*, 2002, pp. 51, 1079-1187.
[3] Steven H. Strogatz, Exploring complex networks, *Nature* 410, March 2001.
[4] M. E. J. Newman, The structure and function of complex networks, *SIAM Review*, 2003, pp. 45, 167-256.
[5] M. Girvan and M. E. J. Newman, Community structure in social and biological networks, *Proc. Natl. Acad. Sci.* USA 99, 2002, pp. 8271-8276.
[6] M. E. J. Newman and M. Girvan, Finding and evaluating community structure in network, *Phys. Rev. E*, 2003.
[7] Gary Flake, Steve Lawrence, and C. Lee Giles, Efficient identification of web communities, *In Sixth ACM SIGKDD*, Boston, MA, August 20-23 2000, pp. 150-160.
[8] Fang Wu and Bernardo A. Huberman, Finding communities in linear time: a physics approach, *cond-mat/0310600*, 2003.
[9] Zhong Su, Qiang Yang, Hongjiang Zhang, Xiaowei Xu and Yuhen hu, Correlation-based document clustering using web logs, *34th Annual Hawaii International Conference on System Sciences*, 2001, pp. 5022.
[10] M. Ester, H.P Kriegal, J. Sander, and X. Xu, A density-Based algorithm for discovering clusters in large spatial databases with noise, *KDD 96*, 1996.
[11] M. Ester, H.P Kriegal, J. Sander, and X. Xu. Density-Based Clustering in Spatial Databases: The Algorithm GDBSCAN and its Applications, *Data Mining and Knowledge Discovery* , Kluwer Academic Publishers, Norwell, MA, June 1998, pp. 169-194.

The Tenth International Symposium on Artificial Life and Robotics 2005(AROB 10th '05),
B-con Plaza, Beppu, Oita, Japan, February 4-6, 2005

Autonomous evolutionary machine vision systems.

Jeffrey Johnson and Valerie Rose
Department of Design and Innovation
The Open University
Milton Keynes, MK7 6AA, England
j.h.johnson@open.ac.uk and vrose@ukonline.co.uk

Abstract

We propose a radical new approach to machine vision based on biological principles in the context of a multilevel architecture of representation and reconstruction.

1. Introduction

Machine vision is a notorious bottleneck in robotics and automated systems. We seek a method of creating very flexible machine vision systems that can evolve in particular environments to recognise anything that an operator has indicated as being 'interesting' in that environment. For example, Figure 1 shows an object that a house-tidying robot might encounter during its everyday duties.

Figure 1.Contouring an object

Our intention is that non-programmers can train our vision systems by 'pointing' at an object in a scene, *e.g.* drawing a contour round it, with the system to evolving the ability to recognise such objects automatically. Our approach is based on new combinatorial structures supporting an *architecture* that allows vision systems to generalise and adapt to recognise new classes of objects. This architecture is based on new combinatorial mathematics in the science of complex systems [1].

There are many approaches to machine vision, including algorithmic knowledge-based programming, neural systems that learn from examples, and combinations of both. Many practical systems are based on algorithms or procedures making opportunistic use of special features of particular objects and scenes. Although this may give acceptable performance for a given application, there is usually a poor ability to *generalise* to other similar scenes, and no ability to generalise to different environments. A system designed to inspect industrial parts is unlikely to be incorporated in a mobile planetary robot.

It is common for human programmers to *design* vision systems so that data are optimised for the particular problem and classification technique being used. The generality is that machine vision systems are hand-crafted to give the best results for a particular application, but are brittle and perform poorly outside their narrow specification, and lack any ability to adapt.

We seek machine vision systems that can:

- use point-and-learn training
- work for cluttered scenes
- adapt to changes in objects and scenes
- adapt to any scene or environment

To achieve this we propose a multilevel architecture in which machine vision systems

- evolve appropriate retinal configurations
- evolve connectivities to represent spatial relationships
- abstract their own higher level constructs
- levels are integrated by new relational mathematics

The key feature of the architecture is the ability of the system to abstract its own constructs from data in a multilevel algebraic representation. This allows the system to learn objects that may change through time, and to adapt to learn radically new objects and scenes without the need to change the underlying program. These requirements are very demanding and beyond any existing machine vision systems.

2. The Fundamental Structures

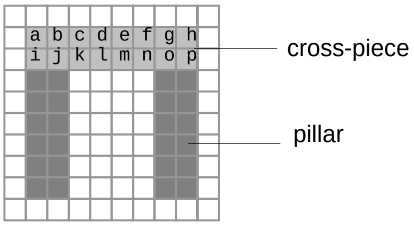

Figure 2. An image of an arch.

The fundamental idea behind our architecture is that of *n-ary relations*. To illustrate this consider the image of an arch in Figure 1. As we view it, we see two *pillars* supporting a *crosspiece*. The crosspiece, for example, is made up of the pixels marked a, b, c, d, e, f, g, h, i, j, k, l, m, n, o, and p. These sixteen pixels are *assembled* by a 16-ary relation, R_{RB}, into a rectangular block.

The *construct* 'rectangular block' defines a set of objects which will be written RB = {x | x is a rectangular block} .In order to be operational, this requires a *pattern recogniser*, P_{RB}, which is able to say of any candidate for membership, x, that x is a rectangular block, $P_{RB}(x)$ = True, or that x is not a rectangular block, $P_{RB}(x)$ = False.

Generally pattern recognisers need to refer to a set of features of the object. In this case there are sixteen features, $\{x_1, x_2, \ldots, x_{16}\}$, the pixels used to make up the block. Each of these x_i needs to be of the right type, so the overall pattern recogniser requires a set of sub-pattern recognisers, $P_{RB,i}$, with the requirement that $P_{RB,i}(x_i)$ = True.

Now it can be seen that the pattern recognition involves two types of decision:

(i) for each x_i, it is necessary that x_i is of the right type, here a dark pixel. $P_{RB,i}(x_i)$ = True.
(ii) given that all the x_i are pixels, it is necessary to established that they are assembled properly so that the relational structure holds with $P_{RB}(x_1, x_2, \ldots, x_{16})$ = True.

Clearly (i) comes before (ii). There is no point applying expensive pattern recognition procedures to objects which are of the wrong type to form the pattern. However, there is danger of an infinitive regress: To test R_{RB} it is necessary to test $R_{RB,i}$ for each x_i. But to test $R_{RB,i}$ it is necessary to reduce x_i to its parts, and test them. And so on. Where can it all end? In robotics and machine vision the answer to this question is easy. Top-down reductionism ends when the pattern recognisers are *grounded* in sensor data. In other words the sensors 'ground' everything the machine can know about its environment (Figure 3).

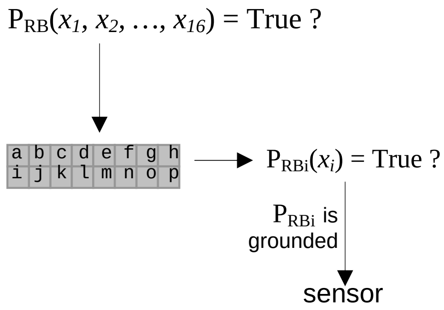

Figure 3. Reductionist grounding prevents infinite regress in pattern recognition

When $P_{RB}(x_1, x_2, \ldots, x_{16})$ = True for a particular set of features, {*a, b, c, …*}, we give the resulting object a name, here **C**, and write σ(**C**)= ⟨ a, b, c, d, e, f, g, h, i, j, k, l, m, n, o, p; R_{RB}⟩. σ(**C**) is called a *simplex* and the elements ⟨a⟩, ⟨b⟩, ⟨c⟩, etc are called its *vertices*. The parts or features of an object can be said to lie at a lower level in its representation than the object itself. If the parts are drawn within an Euler circle (ellipse), the name of the object can be drawn as the apex of a *hierarchical cone*, as illustrated in Figure 4.

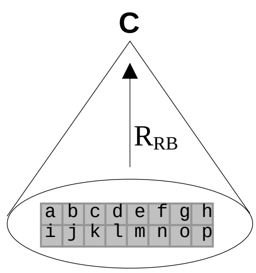

Figure 4. A hierarchical cone.

The relation R_{RB} and all its reductionist sub-relations will be called a *construct*. Clearly, in order for a construct to be operational, it must be grounded. Generally constructs are *named*, and they define sets of named objects. E.g., we can use the name 'rectangular blocks', and write rectangular blocks = { x | x is a rectangular block } , which is an intensional definition. Alternatively we can write Rectangular Blocks = { RB_1, RB_2, …, RB_n} ,

where each of RB_i is the name of a particular rectangular block.
Figure 5 shows the two stages of assembly of the arch; which is defined as structured set of blocks. The blocks are defined as structured sets of pixels; and the pixels are grounded in reality through the camera sensor.

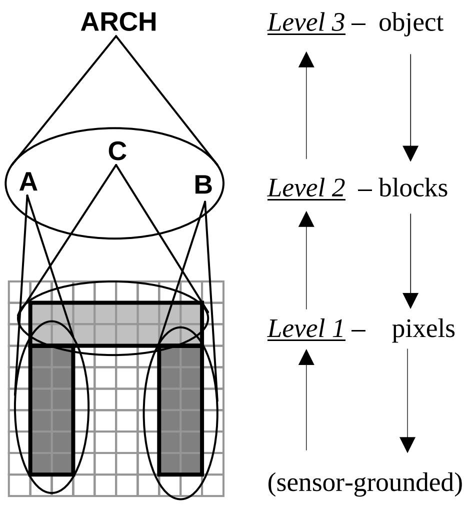

Figure 5. Multilevel construct aggregation

The pillars named as A and B in the image are also structured sets of pixels, as shown in Figure 5. The intermediate constructs A, B and C can be assembled by a 3-ary relation, R_{arch} to form the construct called an ARCH. Thus we have σ(ARCH) = ⟨ A, B, C; R_{arch} ⟩. In this way we build primitive structures from *atomic constructs* (pixels), we build *intermediate constructs* from these at a higher level in the multilevel representation, and so on, until we recognise objects within scenes at the highest level. At every level we use named constructs to reference the objects abstracted.

This example illustrates a major problem in machine vision. The notions of 'pillars' and 'crosspieces' are social constructs inside programmers' heads. Vision systems are highly dependent on programmers' ways of construing the visual universe. It is well known that this can be very different between different people [2], and there is no guarantee that a given programmer will choose the most appropriate constructs. Much better to have the vision system abstract these constructs for itself.

3. Low level pixel configurations

In the proposed multilevel architecture, let the pixels define a base level, *Level 1*. (Lower level sub-pixel constructs are possible, (e.g. Johnson and Picton, 1985), but not discussed here. At this level of representation are the usual greyscale histograms.
The next level of representation must be characterised by sets of pixels structured by relations – nothing else is possible! So, *Level 2* in the representation will consist of sets of pixels under *n*-ary relations. To illustrate this, consider the pixel configurations shown in Figure 6. To establish them at the lowest level in the representation, these will be called *retinal constructs*.

In Figure 6(a) there is a central sensor, such as light-sensitive rod, responding to relative darkness, surrounded by six other sensors, numbered 0, 1, 2, 3, 4 and 5. There are $2^6 = 64$ configurations of light-.dark for these six *satellite* sensors. The configurations have been designed to have a topology corresponding more closely to packed cells than the usual Cartesian grid. Also they are designed using the 'next but one' *neighbours* according to Simon's three pixel principle [3][4].

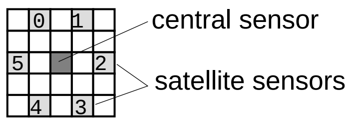

(a) hexagonal array of pixel sensors

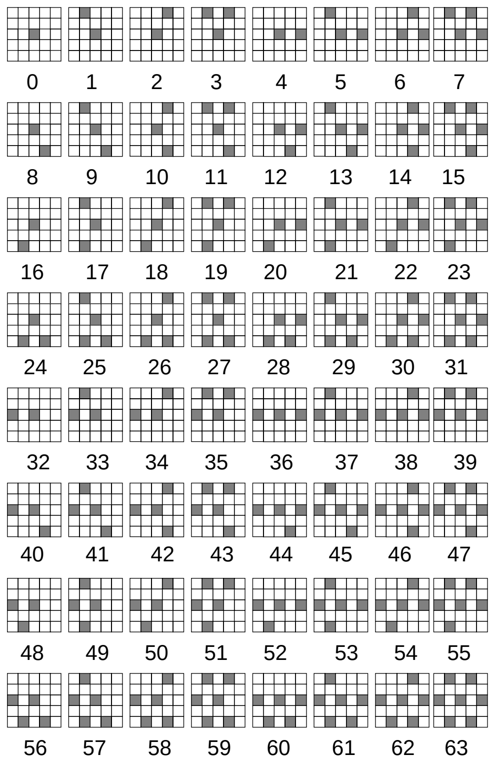

(b) the 64 retinal configurations

Figure 6. Hexagonal pixel constructs

These configurations are examples of *masks* or *filters* which are widely used in machine vision. As such they have been *designed* by the programmer (me!) and have the problem of subjective selectivity. Although I find these configurations attractive for a number of reasons, how can I be sure that they are the most appropriate for any particular objects in any particular environment?

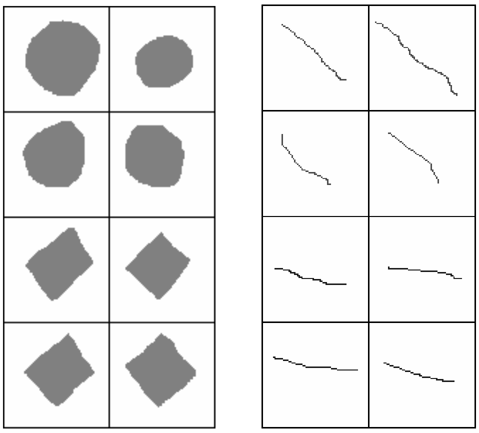

(a) circle and diamonds (b) line segments

Figure 7. Examples object classes

The sixty four retinal configurations in Figure 6 were used to analyse eighty hand-drawn shapes, forty 'circles' and forty 'diamonds', similar to those shown in Figure 7. Each dark pixel in the shapes was analysed by inspecting its surrounding pixels and assigning to it one of the sixty four retinal configurations. As a first level of analysis, the numbers of each configuration were counted, giving a 64-element vector for each configuration. The vectors of the configurations with non-zero frequencies are given in Table 1.

4. Single Level Neural Classification

Inspection of Table 1suggests that the frequency vectors alone are sufficient for classification of the simple circle and diamond shapes, and indeed they are. For example, configurations 14 and 31 have much higher frequency for the circles than the diamonds, reflecting their natural response to vertical left and right edges respectively. Similarly, configurations 7, 30, 51 and 57 favour the diamond shape by responding well to oblique edges.

In principle, a conventional multilayer perceptron neural network will classify such data well, assuming convergence. Note that in Table 1, twenty nine of the sixty four possible configurations respond to the eighty shapes, leaving thirty five retinal configurations that do not respond to these shapes. Training the network with all sixty four configurations as inputs increases the computation and the possibility of non-convergence.

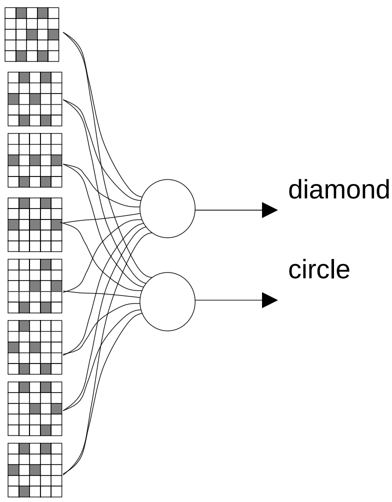

Figure 5. A single level vector neural classifier

Table 2 gives the configuration counts for the line segments shown in Figure 4(b). The response of these objects to the retinal configurations is completely different to that for the shapes. These response vectors can also be used for robust classification between the steep and shallow line segments. It is encouraging that a single layer neural classifier can discriminate these line segments, since it is believed that animal vision uses such primitives.

diamond

3	**4**	**6**	**7**	**12**	**14**	**15**	**24**	**28**	**30**	**31**	**32**	**33**	**35**	**39**	**46**	**47**	**48**	**49**	**51**	**53**	**55**	**56**	**57**	**59**	**60**	**61**	**62**	**63**
2	1	1	22	1	1	21	2	25	24	0	1	2	21	0	1	21	1	2	25	1	21	18	24	2	0	17	24	978
2	1	1	25	1	2	21	1	14	26	1	0	1	18	1	1	24	1	2	18	0	17	25	27	0	2	23	12	885
1	0	1	27	2	4	23	0	27	17	3	0	0	25	2	0	25	2	2	28	0	22	28	19	0	4	26	25	1256
2	0	0	30	1	3	17	2	26	29	0	0	0	22	5	0	28	1	3	28	0	20	21	31	0	3	20	25	1292

circle

3	**4**	**6**	**7**	**12**	**14**	**15**	**24**	**28**	**30**	**31**	**32**	**33**	**35**	**39**	**46**	**47**	**48**	**49**	**51**	**53**	**55**	**56**	**57**	**59**	**60**	**61**	**62**	**63**
0	0	2	14	0	8	20	0	25	19	6	0	1	11	31	0	12	0	22	17	0	8	10	14	19	21	6	21	1322
0	0	0	18	2	18	10	0	6	18	16	0	0	8	33	0	14	2	16	18	0	4	17	13	14	32	15	4	1253
0	0	2	13	1	11	37	0	10	12	10	0	0	12	28	0	11	1	14	16	0	8	27	15	11	23	24	7	1375
0	0	1	18	1	14	10	2	14	18	12	0	1	8	23	0	15	1	22	14	0	5	10	12	20	19	9	13	1083

Table 1. Frequencies of retinal configurations in the shapes of Figure 4.

However, these classifier soon break down when the number of objects to be classified gets large, as is required for recognising a comprehensive set of line segments.

steep lines

0	1	4	5	8	9	32	36	40
9	0	13	2	0	0	13	21	2
3	0	11	1	1	0	12	27	0
8	1	17	1	0	0	16	15	2
7	0	11	0	0	0	11	28	0

shallow lines

0	1	4	5	8	9	32	36	40
21	7	5	1	7	4	5	1	1
32	4	0	0	4	5	0	0	0
30	10	1	1	10	18	1	0	1
28	11	1	3	13	10	3	0	1

Table 2. Line segments frequencies (Fig 4)

The approach to pattern recognition illustrated here map the object to a vector of numbers counting the frequency of 'interesting' features of the objects, interprets the vector as a point in multidimensional space, and classifies the points according to some notion of 'similarity'. In terms of our objects it begs two questions:

1. where do the 'interesting' features come from?
2. is a single level of processing adequate to discriminate objects in complex scenes?

In answer to first question, in our illustrative application, the 'interesting' features were designed in by the programmer. Delegating the selection of 'interesting' features to a programmer inevitably means that the system will be limited in its ability to recognise objects, and unable to adapt to recognise objects that are very different from the design specification.

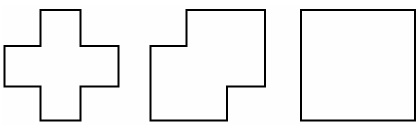

Figure 9. Shapes with equivalent vertical and horizontal lengths

It is easy to show that this kind of single level of classification is inadequate in general for object recognition in vision. For example, the objects in Figure 9 all have the same length of vertical and horizontal edges. Conceivably the corners would have different retinal configurations, but the numbers would be small, and robust discrimination between the objects by a single vector of retinal configurations is unlikely.

The answer to the second question must be that a single level of classification is not adequate. If it were, objects and scenes could be presented to a network as an input vector, to deliver recognition of classified objects. Even if this were possible in theory, it would be impractical because combinatorial explosion mean that the necessary input vectors would have astronomic numbers of elements.

5. Interpreting the data as constructs

In the previous section it has been seen how some retinal configurations can be associated with constructs such as 'oblique', 'vertical', 'left and 'right' edges. These are human constructs that can be imposed on the data. The machine, of course, does not share these constructs explicitly in its representation. Thus there is a co-relation between our concept of a 'round edge' and, say, the pixel configuration 49, , taking a relatively high value for circular objects.

Put like this is becomes possible to understand why conventional approaches to machine vision have failed so comprehensively. As programmers we seek appropriate descriptors or constructs to represents objects to be recognised. We look at an object, and abstract properties such as 'roundness' and 'straightness', that our language conveniently has terms to describe. We then seek machine-based abstractions that match these linguistic constructs.

But as animals we constantly recognise objects for which there is no explicit name. For example, most readers will recognise the shape  as being one of those in Figure 9, even though this shape has no explicit common name. Since I want to talk about it I will give the name of 'double-square shape'. Then I can say things like 'the double square shape is between the cross and the square in Figure 9, and even begin to reason about double-square shapes. However, if such a shape were to be recognised within a machine, it can simply be named implicitly by the data structures, possibly, its position in memory.

Freeing ourselves from serendipity abstractions in a particular programmer's head, and designing machines to form their own constructs is here seen as the way forward. To some extent this is what multilayer neural networks do, and some researchers assert that each neuron is processing a construct. However, that approach is relatively blunt, since the constructs are always implicit.

5. Multi-Level Pattern Recognition

Figure 10 shows one of the diamond shapes of Figure 7 with its numbered retinal pixel responses letter-coded as follows: A (7), B (14), C (15), D(24), E (25), F (30), G (35), H(47), I (49), J (51), K (53), L (55), M(56), N (57), O (61), P (62), dot (63), and X (all others). Note that on the bottom edge the sequence ACH ( ) recurs along the bottom left edge. This can be written as a simplex, ⟨ A, C, H; $R_{\text{horizontal}}$ ⟩, in the terms of Section 2. This can be considered to be a configuration of retinal configurations, and exists at a higher level of aggregation.

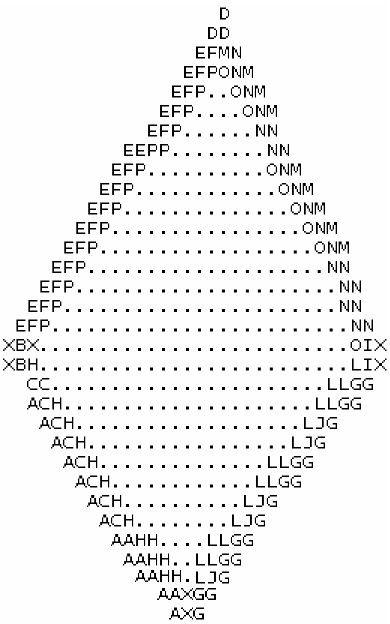

Figure 10. ⟨ A, C, H; $R_{\text{horizontal}}$ ⟩ as an emergent construct

The ACH configuration emerges from the diamond shape, Let it be denoted σ_{ABC}. Then pairs of such configurations can form the structure ⟨ $\sigma_{ACH,i}$, $\sigma_{ACH,j}$; $R_{\text{above\_left}}$ ⟩, at yet another level of aggregation. Let this structure be denoted by the symbol $\sigma_{ACH,}$. Then these too can be aggregated to form a structure that eventually aggregate into structures involving all seven of the ACH sequences. From a human perspective this could be called a *straight edge*. From a machine perspective this is a learned or evolved structure, physically embedded in the machine that has emerged because there is advantage in it doing so.

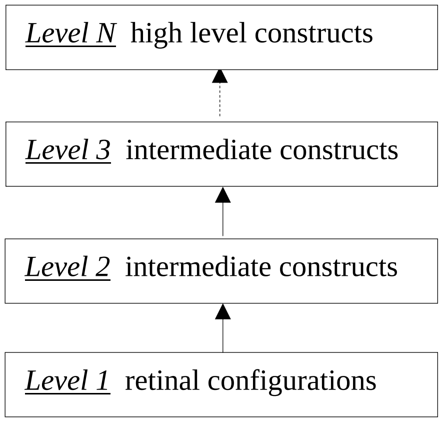

(a) Iterated assembly up the representation

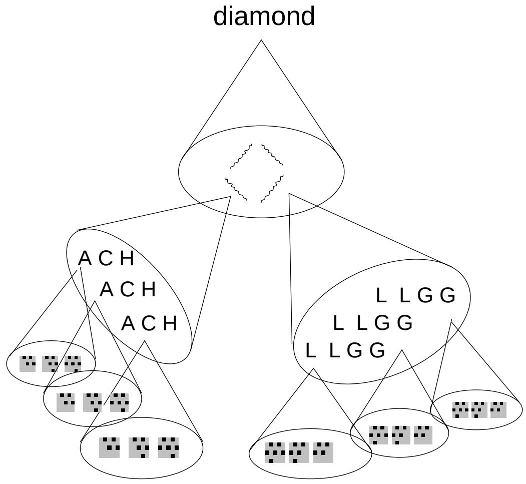

(b) iterated assembly through cones

Figure 11. Multi-level aggregation

6. Spatial Relationships

The configurations in machine vision inherently involve spatial relationships. Conventional approaches to machine vision often take a highly geometric approach to spatial relationships, based on the Cartesian geometry of the pixel grid. It is interesting to consider whether Cartesian geometry is a product of the human mind, or part of the fundamentals of its workings.

From our perspective it is much easier, in principle, to represent multilevel spatial structure through multilevel tessellations and connections between levels. In other words, we propose to proceed on the basis of spatial relationships being hard-wired into the substrate of the vision system. This idea is illustrated in Figure 12, where four objects have been recognised, and the spatial relationship between them is established (and computed) by located connections between the site of response and higher level processing that recognises the object.

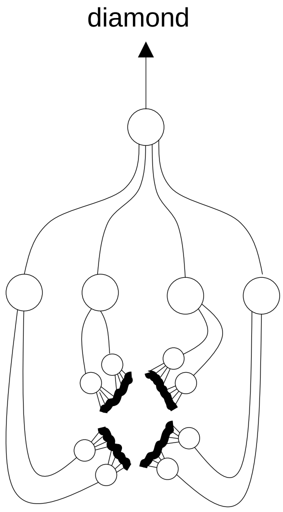

Figure12. Hard-wired spatial relationships

7. Segmentation

One of the most difficult tasks in machine vision is to segment a complex scene into 'relevant' parts. Generally one seeks areas that contain discrete objects, such as the coffee mug shown in Figure 10. In Figure 10(a) we show a training object identified by a user. This low-skilled method of teaching the system is the only kind of input the trainer gives. Following this, the system has to find discrete objects in the image to be recognised as of the same type as the training items.

Figure 10(b) illustrates the many problems involved in segmenting images. The mug has no well defined contour, since neither it nor the background are homogeneous in greyscale. In some places the mug merges into the dark background, while in other places it is a relatively light grey due to the reflected light.

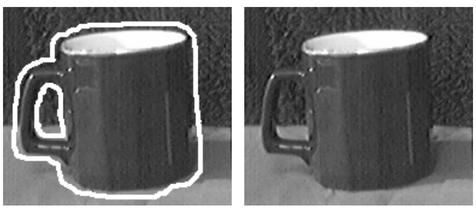

(a) user defined object (b) how to segment?

Figure 10. The segmentation problem

The white ellipse is a strong signal to humans that this is a cylindrical object, but the machine knows nothing of this *a priori*. In many places the mug has highlights, making it visually very variable. In the first instance we do not assume that that our system will have top-down context knowledge such as 'if the scene contains an ellipse, then it contains a cylinder'.

Although the examples in this paper have been pre-segmented binary images, the methods developed here are highly applicable to greyscale and coloured images. The relational method can be very powerful when, for example, the satellite pixels are compared to the centre and classified as light/darker. This approach can lead to areas with varying greyscales but homogeneous greyscale gradient. This approach has been successfully applied in scientific measurement systems. The details are beyond the scope of this paper, but further details can be found in [3][4].

8. The architecture

The research described in this paper, in the context of our objectives leads us to the following principles:

Principle 1. Low retinal configurations will aggregate to form higher level constructs

Principle 2. The constructs will depend on spatial relations

Principle 3. The retinal configurations should not be constrained by design, but should be allowed to emerge from the images and scenes in its environment

Principle 4. The spatial relations in the system should be implicit in its topology so that Cartesian geometry need not be used

Principle 5. Higher level spatial configurations should not be constrained by design, but should be allowed to emerge from the images and scenes in its environment

Principles 1 and 2 are the fundamental theoretical underpinning of our approach. They are supported by algebraic mathematics that can be implemented as data structures in real computers.

Principle 3 is based on the need for the system to adapt to new things. Any system with pre-designed primitives is constrained by what the designer puts in. This *spans* the space of possibilities. Any object not in that space cannot be recognised. This is one reason why conventional machine vision collapses outside its design domain.

If the low level configurations are not to be designed in, where can they come from? We have experimented with forming low level constructs by random configurations of pixels. We have found that generating random masks gives some discrimination between the circular and diamond shapes discussed earlier. However, there remain many open questions, including the optimum diameter for a retinal configuration.

A similar argument suggests there can be no fixed multilevel architecture, and this too must incorporate random processes. Thus the 'relevant' configurations of configurations, and the resulting 'construct' have to be discovered by the machine.

Thus there are two parts to our architecture. The simplest involves the machine learning particular objects and scenes within a given hardware topology. In other words, in the simplest case the machine is fixed, and recognition takes place by values and parameters changing within that structure.

The more demanding part of the architecture involves evolutionary principles to generate and select 'appropriate' retinal primitives, and to generate and select appropriate topologies to support relational structure throughout the multilayer aggregation. This lies at the heart of our research programme to achieve autonomous evolutionary machine vision systems.

9. Discussion and conclusions

In this paper we have illustrated some of the basic ideas of our research programme, and reported briefly some preliminary experiments on evolving retinal configurations. Those experiments combined with the experiments reported on designed retinal configurations suggest that this part of the research will be relatively straight forward. In other words, the research on the evolution of retinal configurations has already begun and we are beginning to understand this part of the challenge relatively well.

By far the greatest challenge is in implementing the multilayer architecture to support the hierarchical assembly of information towards object and scene recognition. One major unresolved challenge in this is to design spatial structure into the system in a way that overcomes combinatorial explosion. The human brain has some ten billion neurons with five to ten thousand connections per neuron. This apparently huge amount of processing power and information distribution ability appears more modest when compared to the numbers of ways that retinal configurations can be defined and connected in a multilevel architecture. Furthermore, we expect to implement our architecture on standard computers with orders of magnitude less memory and orders of magnitude less computational ability than biological vision systems.

Currently our idea is that spatial structure is determined by the initial connections to the retinal configurations, where the image is grounded, and subsequent connections are through the multilayer system. There is a major challenge in establishing a theoretical architecture that can be implemented in practice, followed by the major practical challenge of inducing the system to self-organise as it adapts to new visual environments.

We are aware of the difficulty of the research we propose. We are optimistic that success is possible because the combinatorial mathematics underlying our research contains some of the essential structures necessary to achieve our objectives.

References

[1] Johnson, J.H., 'Some structures and notation of Q-analysis', *Environment and Planning B*, **8**, 73-86, 1981.

[2] Gregory, R. L., *Eye and brain: the psychology of seeing*, Oxford University Press, 1998.

[3] Johnson, J.H., Picton, P.D., *Mechatronics: Concepts of Artificial Intelligence*, Butterworths (London), 1985

[4] Johnson, J.H., Simon, J-C, 'Fundamental Structures for the Design of Machine Vision Systems', *Mathematical Geology*, Vol. **33,** No.3, 2001.

[5] Marr, D., *Vision*, W Freeman and Company, (New York), 1982.

[6] Rose, V., Results of experiments in shape-recognition through random selection of sets of pairs of pixels within 75x75 pixel binary images of various simple shapes. Mimeo Open University, 2004.

The Tenth International Symposium on Artificial Life and Robotics 2005(AROB 10th '05),
B-con Plaza, Beppu, Oita, Japan, February 4-6, 2005

Real-time adaptive maintenance for performance improvement on daily-use computer

Shinichi Hirose
Graduate School of Information Science and Technology,
Hokkaido University
Kita 14, Nishi 9, Kita-ku, Sapporo, Hokkaido,
060-0814, Japan
E-mail: s.hirose@complex.eng.hokudai.ac.jp

Shinichiro Yoshii
Graduate School of Information Science and Technology,
Hokkaido University
Kita 14, Nishi 9, Kita-ku, Sapporo, Hokkaido,
060-0814, Japan
E-mail: yoshii@complex.eng.hokudai.ac.jp

Abstract

When it continues using a personal computer, it has often come to operate slowly rather than the time of having purchased it. In this paper, the authors argue about the easy tuning method of personal computers. The general users without much deep special knowledge will be able to use it easily. By using the simple genetic algorithm, we search for the optimized set of the parameters of the operating system. the effect is verified in an experiment. The authors propose the adaptive method for the improvement in performance for personal computers.

1. Introduction

It has been long time since the personal computers turned to be daily commodities. As being used for a long time, the personal computer comes to lose its quickness. For example, it comes to take a long time to boot up. So the personal computer users have often come to feel inconvenience for use. The most of general users do not have deep knowledge as much as IT professionals. Therefore, general users cannot help making a uniform improvement in performance by installing the packaged software for tuning, or returning their personal computers to the initial state by installing the operating system again. However, since various factors for the prolongation of the booting up time and the other inconvenient phenomena can be considered, these methods do not necessarily become better solution.

Several system integration companies have proposed the self-control function in the information systems called Autonomic Computing in enterprise field [1]. But it is expected that the maintenance method of personal computers as daily commodities is more adaptive than the packaged software for tuning and simpler than Autonomic Computing. The authors focused on tuning parameters of the operating system as the maintenance method of personal computers.

2. Genetic algorithm

Genetic algorithms bases on the research of J. H. Holland [2] in University of Michigan in the 1960s. He made the model in engineering paying attention to the genetical mechanism in a nature. The algorithms based on such a view have been studied as various and concrete techniques. The most fundamental kind of genetic algorithm in them is called simple genetic algorithm [3]. Hereinafter, we explain the simple genetic algorithm .

A certain individual is formed based on the genetic code described in its chromosome. The chromosome is constituted as a gene arrangement with which two or more genes were located in a line, and it is decoded when an individual is born. The character of the individual decoded and generated is called phenotype. On the other hand, the pattern of the gene of the origin of it is called genotype. In genetic algorithms, it is usually assumed that the individual has only one chromosome. The gene information will be recorded by the following arrangement S in the individual with n genes.

$$S = \langle s_1, s_2, \cdots, s_n \rangle, \qquad s_i \in \{0,1\}$$

The position of each gene on a chromosome is called locus, and the gene in the position specifies a certain characteristic character. For example, s_2 is recording the information on the color of the eye of an individual etc. The candidate of the gene that can be taken on a locus is called allele. As mentioned above, an individual will be born to environment by decoding and expressing a genetic code from a chromosome. And a set of an individual is called population. The individual with the high degree of adaptation to the environment survives by high probability. The evaluation value is called fitness.

Generally the genetic algorithm is advanced by the following procedures. When solving an optimization problem, it is necessary to express a problem to optimize with a gene and to set up end conditions.

(1) initialization : Building the individuals by generating their chromosomes randomly
(2) evaluation : Calculating the fitness for each individual according to the evaluation function
(3) selection : Selecting the individuals by their fitness
(4) crossover : Generating the chromosomes of the new individuals by crossover two parents' chromosomes
(5) mutation : Generating the chromosomes of the new individuals by the probability of mutation
(6) reproduction : Replacing with all or some of new generations
(7) repetition of (2) to (6) until fulfilling end conditions

3. Experiment

Generally, that users feel some inconvenience to computer systems becomes the opportunity that tunes them up. In many cases, after the tuning target is set up, a method required in order to attain the target is examined. The tuning is performed according to the plan. The phenomenon which user feels inconvenient is various. There may be two or more tuning methods for the same phenomenon.

3.1 Tuning method

In order to improve the prolonged startup time of the personal computer, we search for the optimized set of parameters of the operating system by the simple genetic algorithm. In this experiment, Microsoft Windows XP, which is the most popular operating system among general users, was taken up. The parameters of operating system of Microsoft Windows, which are called registry, can be set with the numerical values other than 0 or 1, or character strings, or binary data, etc. The authors selected the 14 target parameters, which can be set with 0 or 1, taking account of their roles with expertise acquired through professional practice of system engineering. We coded to genotypes the set of parameters chosen in this way. Instead of using the defined evaluation function, we used the starting time actually obtained by measurement in the set of parameters as each individual's evaluation. In order to measure the starting time of a personal computer, we referred the document [4] that provided guidelines for system manufacturers to improve boot and the tool introduced there.

We summarized some main genetic operators and parameters of the simple genetic algorithm for our experiment in Table 1.

	GA operators	GA parameters
(1)	initialization	N (population of individuals) = 30
(2)	selection (elitist preserving selection)	G (generation gap) = 0.8
(3)	crossover (uniform crossover)	p_c (probability of crossover) = 0.8
(4)	mutation	m_c (probability of mutation) = 0.01

Table 1. The genetic operators for the experiment

3.2 Experiment System

Figure 1 shows the experiment environment. We experimented on the virtual operating system that was realized by this emulation software.

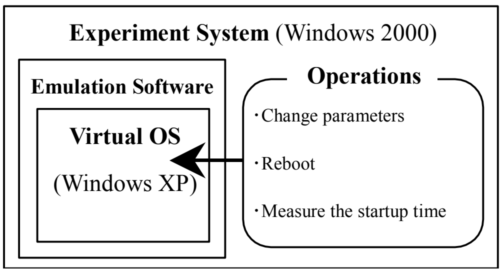

Figure 1. The experiment environment

This emulation software had the function that rollbacks the operation to the virtual operating system, and we used this one when acquiring an individual's evaluation. Because the internal environment of the operating system is changed by the repeating configuration of the registries, it is impossible to acquire the exact starting time of the personal computer.

3.3 Results

We repeat the reboot of the virtual operating system supposing the situation that the personal computer was used daily. In the case A and B, after rebooting the virtual operating systems 100 times and 300 times respectively, we measured the start time without tuning parameters. Similarly, in the case A' and B', after rebooting the virtual operating systems 100 times and 300 times respectively, we measured the start time with tuning parameters. Table 2 shows the results. When a case A and A' were compared, 9.58% of improvement was found, and when a test case B and B' were compared, 16.52% of improvement was found.

	Boot Times	Startup time [s]	effect
Case A	100	50.64	—
Case A'	100	45.79	△ 9.58 %
Case B	300	68.81	—
Case B'	300	57.44	△ 16.52 %

Table 2. The experiment of the results

4. Conclusion

We consider that a certain amount of improvement was found.

In an experiment of this paper, it is hardly taking into consideration that the state of the hardware and software comes to change with using the personal computer. The remaining issues will be to build the model that realizes the method of tuning up the value of the parameters with taking into account the change state of hardware environment, and to check it in the experiment.

References

[1] IBM Corporation, Autonomic Computing, http://www-3.ibm.com/ autonomic/index.shtml, 2004.
[2] J. H. Holland, Adaptation in Natural and Artificial Systems, MIT Press 1992.
[3] M. Sakawa and M. Tanaka, Genetic Algorithm, Asakura-Syoten, 1995.
[4] Microsoft Corporation, Fast System Startup for PCs Running Windows XP, http://www.microsoft.com/whdc/ system/sysperf/fastboot/fastboot-winxp.mspx, 2002.

Swarm Search for Fast Face Detection with Neural Networks

Xinjian Fan, Masanori Sugisaka
Department of Electrical and Electronic Engineering, Oita University, Japan
Email: {msugi, fxinjian}@cc.oita-u.ac.jp

Abstract: This paper presents the application of particle swarm optimization (PSO) to improve the search speed of neural network based face detection problems. The method is based on the idea that the task of finding a well-matched subwindow (face) can be formulated as an integer nonlinear optimization problem (INLP). To find a face, we only need to find a local maximum filter response which value is above a given threshold. The proposed method has been tested and examined with a set of 42 images to demonstrate its effectiveness. The results confirm the potential of the proposed approach and show its superiority over the classical technique.

1. Introduction

Face detection is a very important task that serves as the first step of a large area of applications: automated face recognition, secure access control, advanced human-computer interfaces, etc. Its accuracy and efficiency have a direct impact on the usability of the whole system.

Face detection has been a well researched problem and there are many approaches on it [1]. Up to now one kind of the most successful methods is known as neural network-based methods [2-7]. In these methods, a face model (filter) is first learned from a large number of examples (face images and non-face images). And then a sliding window is used to scan all possible subwindows across multiple-scale images.

However, these methods are generally computationally expensive because: (a) the search window is a high-dimensional vector that has to be classified in a very non-linear space; (b) there are hundreds of thousands of windows to search. Although many efforts have been done to reduce the runtime of neural network based methods, most of them focused on reducing the computational complexity of classifiers [4],[5]. Only a few attentions were given to improving the search efficiency. In Ref. [6], the search window moves every q pixels (q=3~5) instead of every pixel. Thus the number of searched windows is only about $1/q^2$ of the exhaustive search, but with the disadvantage of lowering the system's performance. Many methods use skin color information to limit the search area [6],[7]. But color information is not always able to be used and it is very difficult to build a skin color model robust to illumination changes.

In this paper, to reduce computational cost while retaining high detection accuracy, we propose a new method to speed up neural network (NN) based face detection systems. The method is based on the idea that the face search (FS) problem can be formulated into an integer nonlinear optimization problem (INLP). To find a face, we only need to find a local maximum filter response which is above a threshold. The integer variables are parameters that represent a subwindow in the image. The objective function is based on the output of the face filter.

PSO is a novel evolutionary computation (EC) technique [8], which has been improved and applied to various problems. Although the original algorithm was basically developed for continuous optimization problem, it can be expanded to handle discrete variables easily. Furthermore, PSO has only a few parameters that make it easy-adjusted to get better performance. Therefore, PSO is expected to be suitable for FS formulated as an INLP.

Based on a NN-based face filter, this paper presents a PSO for the FS problem formulated as an INLP. The feasibility of the proposed method is demonstrated and compared with the exhaustive search method on a set of 42 test images with promising results. In this paper, we assume that there is only one face contained in the test image. The extension of the method to detect multiple faces will be done in our future work.

2. Neural network based face filter

The purpose of the face filter is to classify a window of size 20×20 pixels extracted from an image, as a face or as a non-face.

We use a retinally connected neural network [3] to serve as the face filter. The network takes a 20×20 pixel window as input. Each hidden unit receives inputs only from part of the input layer (called a receptive field). There are 3 kinds of receptive fields: four 10×10 pixel regions, sixteen 5×5 pixel regions, and six 20×5 pixel overlapping horizontal stripes. Each of these receptive fields has full connection to two hidden neurons. It has a single output. The output is a real value from -1.0 to 1.0, giving the likelihood as to what extent the input window looks like a face.

3. Formulation of FS as an INLP

Figure 1 shows a 3D plot of the neural network output with the image on the left as input. The highest peak represents the face location. It can be seen that the face filter is very selective: it responds strongly within a several pixel radius of the face while its output on the background is low. Moreover, around the face, the output of the neural filter is a monotonous and growing function. The properties lead to the following heuristic:

The face search (FS) problem can be formulated as an integer nonlinear optimization problem (INLP). To find a face, we only need to find a local maximum filter response which value is above a threshold. Let **T** represent an input image, **SW** represent a subwindow and *dv* be its detection value (the corresponding output of the neural network). With these notations the FS problem can be stated as:

$$\arg\max_{\mathrm{SW}} dv(\mathbf{SW}) \qquad \forall \mathbf{SW} \in \mathbf{T} \tag{1}$$

If $dv(\mathbf{SW})$ is higher than a given threshold, the corresponding portion of **SW** is declared as a face.

4. Particle swarm optimization

Particle swarm optimization (PSO) is a novel evolutionary computation method, modeled after the social behavior of flocks of birds [8]. PSO is a population based search process where individuals, referred to as particles, are grouped into a swarm. Each particle in the swarm represents a candidate solution to the optimization problem at hand. The performance of particles is measured using a predefined fitness function which encapsulates the characteristics of the optimization problem.

Each particle i maintains the following information: $\mathbf{X}_i$, the *current position* of the particle; $\mathbf{V}_i$, the *current velocity* of the particle; $pbest_i$, the personal best position discovered by the particle so far, and also the best position found by the entire swarm so far, denoted by *gbest*. All particles start with randomly initialized velocities and positions. At iteration step t, the current velocity and position (searching point in the solution space) are updated by:

$$\mathbf{V}_i(t+1) = \omega \mathbf{V}_i(t) + c_1 r_1(t)(pbest_i - \mathbf{X}_i(t)) + c_2 r_2(t)(gbest - \mathbf{X}_i(t)) \tag{2}$$

$$\mathbf{X}_i(t+1) = \mathbf{X}_i(t) + \mathbf{V}_i(t+1) \tag{3}$$

where w is the inertia weight, c_1 and c_2 are the acceleration constants, $r_1(t)$ and $r_2(t) \sim$ U(0, 1). The velocity of a particle will be set to a predetermined maximum velocity ($\mathbf{V}_{\max}$) if it exceeds $\mathbf{V}_{\max}$.

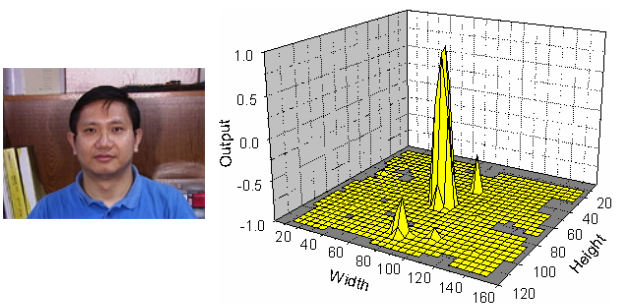

Fig. 1 *left*: an input image; *right*: 3D view of the neural network output, obtained by superposing the outputs of subwindows at all scales.

The features of the algorithm can be summarized as follows:

(a) PSO searches the solution space using a group of searching points like genetic algorithm (GA) and the searching points gradually get close to the optimal point using their *pbests* and the *gbest*.

(b) As explained in Ref. [9], the first term of the right side of Equ. (2) is corresponding to the exploration of the search space. The second and third terms of that are corresponding to the exploitation of the best solutions found so far. Namely, the method has a flexible and well-balanced mechanism to utilize exploration and exploitation in the search procedure.

(c) The original PSO was originally developed for nonlinear optimization problems with continuous variables. However, the method can be expanded to discrete problems easily [10].

(d) Because the update process of PSO is based on simple equations, the algorithm is easy to implement and computing economically. In addition, only a few input parameters need to be adjusted in PSO which makes it easy-adjusted to get better performance.

Due to the above features, PSO is expected to be suitable for the FS problem formulated as an INLP.

5. Face search using PSO

The main steps of the proposed method are shown in Figure 2. In the following, we will describe the approach in detail.

5.1 Encoding and rescaling

In our problem, each particle represents a subwindow in the input image. We use its center (C_x, C_y) and length S to encode a subwindow. To evaluate subwindows of different sizes using the neural network, we should rescale them to the size of 20×20 (the input size of the neural network). However, if this computation is done on every size of subwindows, it will be very time-consuming. To avoid it, we first build an image pyramid†:

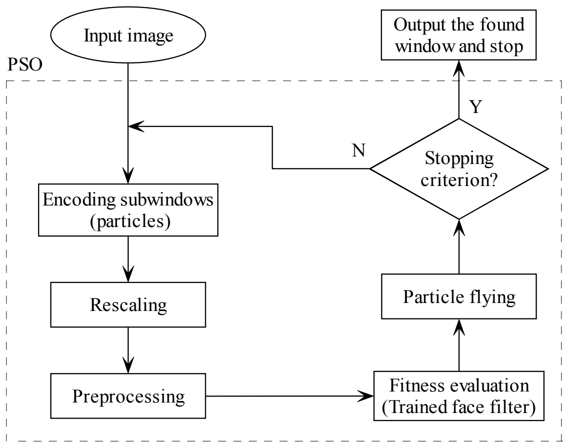

Fig. 2 Main steps of the proposed method

$$W \times H,\ \frac{W}{q} \times \frac{H}{q},\ \cdots,\ \frac{W}{q^k} \times \frac{H}{q^k},\ \cdots,\ \frac{W}{q^L} \times \frac{H}{q^L} \qquad (4)$$

where W and H are the width and height of the input image respectively, and q is the scale factor. The top level (level L) should have a size more than 20×20:

$$\frac{\min(W,\ H)}{q^L} \geq 20 \text{ , gives}$$

$$L = \left\lfloor \frac{\ln(\min(W,\ H)) - \ln 20}{\ln q} \right\rfloor \qquad (5)$$

Then we let S to be chosen among the following geometric sequence†:

$$20,\ 20q,\ \cdots,\ 20q^k\ \cdots,\ 20q^L \qquad (6)$$

For a subwindow $\mathbf{SW} = (C_x, C_y, \lfloor 20q^k \rfloor)^T$, we find its mapped 20×20 window $\mathbf{SW}' = (C_x', C_y', 20)^T$ in level k of the pyramid by:

$$C_x' = \left\lfloor \frac{C_x}{q^k} \right\rfloor,\ C_y' = \left\lfloor \frac{C_y}{q^k} \right\rfloor \qquad (7)$$

So each particle $\mathbf{X}$ is constructed as $\mathbf{X} = (C_x, C_y, k)^T$. C_x, C_y and k are defined in [10, W-10], [10, H-10] and [0, L] respectively.

5.2 Preprocessing

Before a 20×20 window is passed to the trained neural network, it is preprocessed with lighting correction (by subtracting a best fit linear function) and histogram equalization as in Ref. [2],[3]. The former reduces the effect of different lighting conditions and the latter improves contrast across the window.

5.3 Fitness evaluation

To evaluate each particle (subwindow), we directly use its detection value (the corresponding output of the neural filter): the larger its detection value (dv), the more the subwindow resembles a face. The fitness function $f(\mathbf{SW})$ is given as

$$f(\mathbf{SW}) = dv(\mathbf{SW}) \quad \mathbf{SW} \in \mathbf{T} \qquad (8)$$

where $\mathbf{T}$ is the input image and $\mathbf{SW}$ is a subwindow, $dv(\mathbf{SW}) \in [-1,\ 1]$.

The corresponding subwindow of a particle may go beyond the image's boundary even if all its variables lie in the search boundary. To guarantee feasibility of solutions, a random repair method (RRM) is investigated in this paper. If a particle is checked to be infeasible, it will be forced to "fly" to a new position, which is randomly generated but feasible. The method works as follows:

If $\mathbf{SW} \notin \mathbf{T}$, then

Step 1: Randomly generate a new position $\mathbf{SW}'$.

Step 2: If $\mathbf{SW}' \in \mathbf{T}$, replace $\mathbf{SW}$ with $\mathbf{SW}'$; otherwise, go to step 1.

† Each term in Equ. (4) and (6) is transformed from a real value to an integer value by using the floor function.

The proposed RRM has proven more efficient for our problem than the traditional penalty approach [11].

5.4 Particle flying

Based on their fitness, particles in the swarm are guided by Equ. (2) and (3) to fly to possible face regions in the image. New (C_x, C_y, k) generated by Equ. (2) and (3) are real values. When corresponding to a subwindow in the input image, they are transformed into integers by using the floor function. During flying, if a variable extends the defined search boundary, it will be set to the closest limit, i.e.

$$x_j = \begin{cases} x_{j\min} & \text{if } x_j < x_{j\min} \\ x_{j\max} & \text{if } x_j > x_{j\max} \end{cases} \qquad (9)$$

where x_{jmin} and x_{jmax} are respectively the lower and upper search limit of variable x_j, $x_j \in \mathbf{X}$.

5.5 Stop criterion

The algorithm is stopped when 1) a "face" is found – the detection value of the best particle is above the given threshold or 2) the maximum iteration number is reached.

6. Experiments

A number of experiments were performed to evaluate the proposed method. The experiments were performed on 42 images with complex backgrounds. Some of the images were chosen from CMU Test Set [12] and other Internet resources; the others were taken by us in an indoor environment using a CCD camera. Each image contains only one face and all the faces can be detected by the neural filter. All the images have the same size of 320×240 and the face size ranges from 34×34 to 178×178. The threshold of the neural network output was set to 0.1.

According to pre-simulation, the parameters of PSO were set as:

c_1, c_2: 0.2,

w: 1.2,

$\mathbf{V}_{\max}$: 0.2×($\mathbf{X}_{\max}$-$\mathbf{X}_{\min}$),

Swarm size P: 60,

Maximum iteration number *MaxIt* is set to 70. But one restart is allowed, i.e., if the algorithm fails to find a face within *MaxIt* it will be re-initialized and perform a new search.

For each image in the test set, we ran our algorithm 100 times. The total detection results are listed in Table 1. Some examples are shown in Figure 3. The time consuming was reported on an AMD Athlon 750 MHz PC with Windows 2000 as its OS.

As shown in Table 1, the proposed search method yielded a high success rate (93.6%) on average (the best is 100% and the worst is 72%). Moreover, about 39% of the failures are because PSO fell into a false detection, the other failures are due to non-convergence. A further reduction of false detections can be achieved by arbitrating among multiple networks [3]. From the

Table 1: Experimental results

Success	False	Non-convergence	ANSEs	APT (ms)
93.6%	2.52%	3.88%	1965	250

False: false detection rate; ANSEs: Average Number of Subwindow Evaluations; APT: Average Processing Time.

Fig. 3 Examples from the test set

examples shown in Figure 3, we can see that the proposed method maintains robustness in images which contain faces under a very wide range of conditions including scale, pose, position, complex backgrounds, illumination conditions, etc.

Table 2 gives the comparison of the proposed search method (called *swarm search*) with the exhaustive search method. It's clear that the time consuming and the number of subwindow evaluations of the proposed method are much less than those of the exhaustive search. Although with a little loss of detection rate (due to non-convergence), a great speedup has been achieved by using the swarm search compared to using the exhaustive search.

The method proposed by Viola and Jones [13] is about 2.7 times faster than ours even performing an exhaustive search. The reason is that they use a computationally extremely efficient face filter, which is made of a boosted cascade of classifiers built with the AdaBoost algorithm. However, it is possible to combine our swarm search method with their face filter to make a more powerful face detection system.

7. Conclusion

This paper presents a new search method for NN-based face detection. The proposed method formulates the problem of face search into an integer nonlinear optimization problem (INLP) and expands the basic PSO to solve it. The feasibility of the proposed method is demonstrated on a set of 42 images with promising results. With fine-adjusted parameters, PSO only requires less than 2000 evaluations of subwindows for finding the face in an image. The result is much more effective and superior over the classical exhaustive search method. Many object detection problems can be formulated as an INLP and the results indicate the possibility of PSO as a practical tool for various INLPs of object detection.

However, we have found that the method doesn't work well on some images, especially when the face size is very small. How to improve the robustness is the future work.

Table 2: Swarm search vs. exhaustive search

	Swarm search	Exhaustive search*	Ratio
ANSEs	1965	193737/2	1 : 49
APT (ms)	250	20169/2	1 : 40

* Because we only consider the single-face detection problem in this paper, for fair comparison, we suppose that it takes only half of an exhaustive search to find a face.

References

[1] M.H. Yang, D. Kriegman and N. Ahuja, "Detecting faces in images: a survey", IEEE Trans. Pattern Anal. & Mach. Intell., vol.24, no.1, pp.34-58, 2002.
[2] K.K. Sung and T. Poggio, "Example-based learning for view-based human face detection", IEEE Trans. Pattern Anal. & Mach. Intell., vol.20, pp.39-50, 1998.
[3] H.A. Rowley, "Neural Network-Based Face Detection", Thesis submitted for the degree of Doctor of Philosophy, School of Computer Science, Carnegie Mellon University, 1999.
[4] L. Huang, A. Shimizu, Y. Hagihara and H. Kobatake, "Face detection from cluttered images using a polynomial neural network", Proc. Conf. on Image Processing, pp.669-672, Thessaloniki, Greece, 2001.
[5] B. Fasel, "Fast multi-scale face detection", Technical Report COM-98-04, IDIAP, 1998.
[6] R. Feraud, O. J. Bernier, J. Viallet, and M. Collobert, "A fast and accurate face detector based on neural networks", IEEE Trans. Pattern Anal. & Mach. Intell., vol.23, no.1, pp.42-53, Jan. 2001.
[7] S. Karungaru, M. Fukumi and N. Akamatsu, "Human face detection in visual scenes using neural networks", IEEJ Trans., vol.122-C, no.6, pp.995-1000, 2002.
[8] J. Kennedy and R. Eberhart, "Particle swarm optimization", Proc. IEEE Int'l Conf. on Neural Networks, vol.4, pp.1942-1948, Perth, Australia, 1995.
[9] Y. Shi and R. Eberhart, "A modified particle swarm optimizer", Proc. IEEE Int'l Conf. Evolutionary Computation, pp.69-73, Anchorage, 1998.
[10] H. Yoshida, Y. Fukuyama, K. Kawata, S. Takayama, and Y. Nakanishi, "A particle swarm optimization for reactive power and voltage control considering voltage security assessment", IEEE Trans. Power Systems, vol.15, no.4, pp.1232-1239, 2001.
[11] Z. Michalewicz, "A survey of constraint handling techniques in evolutionary computation methods", Proc. 4th Annual Conf. on Evolutionary Programming, MIT Press, Cambridge, MA, pp.135-155, 1995.
[12] CMU Test Set: http://vasc.ri.cmu.edu/idb/images/face/frontal_images/images.tar
[13] P. Viola and M. Jones, "Robust real-time object detection", Proc. 2nd Int'l Workshop on Statistical and Computational Theories of Vision, Vancouver, Canada, 2001.

Development of the Fuzzy Control for a GPS-located Airship

Masanori Sugisaka [1], Fengzhi Dai [2], Yutaka Fujihara [2], Takumi Kamioka[3]

[1] Oita University, Oita, Japan. msugi@cc.oita-u.ac.jp
[2] Matsue National College of Technology, Japan. daifz (fujihara)@matsue-ct.jp
[3] Nara Institute of Science and Technology, Nara, Japan

Abstract

The purpose of the work is to develop the fuzzy control for the experimental GPS-located airship, which has the overall length of 5.8m and the maximum diameter is 2.2m. The basic technology including the hardware and the program to control the airship navigating along the shortest flight path to the target point is developed. Fuzzy control is used because the kinematics and dynamics features of an airship are non-linear and it is difficult to describe the motion equations. At last, to compare the efficiency, PD control is also applied. The result of comparison shows the validity of the fuzzy control.

Keywords：Autonomous airship, GPS, Side thruster, Fuzzy control

1. Introduction

For many situations, autonomous green flight systems are needed and important. They have been developed for uses such as mine detecting, crop dusting and military surveillance. Aerosonde [1], which is developed by Aerosonde Robotic Aircraft Pty Ltd., PREDETOR [2] by Inc. of General Atomics Aeronautical Systems, and RQ-4A Global Hawk [3] by Northrop Grumman Corporation are examples of these kinds of flight systems. Also the development of helicopter system was reported by Sugeno et al [4, 5] and an airship by Ouchi et al [6]. Suzuki et al have studied the control of the airship by reinforcement learning [7, 8].

In this study, the experimental airship is proposed, which can remain stationary in the sky and since it uses helium gas, it has low fuel consumption. In the paper, the basic technology including the hardware and the control method by which the airship navigates along the shortest path to the target point is discussed.

2. Structure of the system

Figure 1 shows the structure of the airship. The balloon is elliptical and has an overall length of 5.8m, a maximum diameter of 2.2m and a volume of 17.5m^3. Helium gas is used for buoyancy. The gondola at the bottom contains a notebook computer, controllers, motors, batteries, a geomagnetic sensor and ballast. For navigation, GPS (Global Positioning System) is mounted and an antenna for receiving GPS signals is fixed to the head of the balloon.

The power sources consist of a side thruster and two main fan ducts. The side thruster is used to rotate the airship around the vertical axis (yawing rotation shown in Figure 2). Two main fan ducts are used to control the airship going up, down, forward and backward.

In Figure 2, the *ox* axis is coincident with the axis of symmetry of the envelope and the *oxz* plane

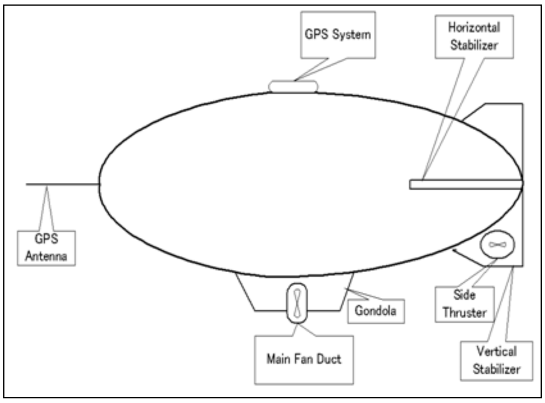

Figure 1 Structure of airship

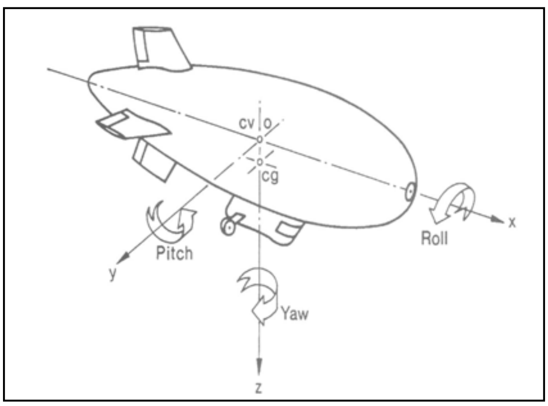

Figure 2 kinematics of airship

coincides with the longitudinal plane of symmetry of the airship. Since the volume of the gondola is negligible compared with that of the envelope, it is reasonable to assume that the *cv* (center of volume) lies on the axis of symmetry of the envelope.

The airship is able to move in translation and rotation in three dimensional spaces. Rotation around the x axis is called rolling, around the y axis is pitching and around the z axis is yawing. In this study the rotation of the airship is mainly yawing.

3. Control method

3.1 General algorithm

The flow chart of the automatic control algorithm is shown in Figure 3. When it starts, the airship flies up first. Next, the notebook computer receives data from each sensor. Subsequently, the position of the airship compares with the target point. When it reaches the target, the program terminates and the airship hovers. Otherwise the computer calculates the direction and distance to the target point shown in Figure 4. Values of control parameters are outputted to each motor. Eventually by repeating these processes, the airship arrives to the target point.

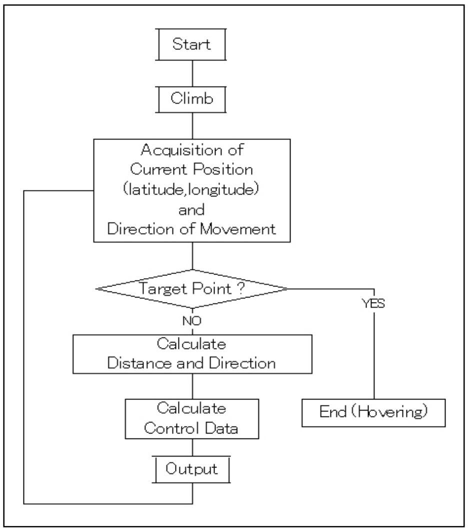

Figure 3 Flow chart

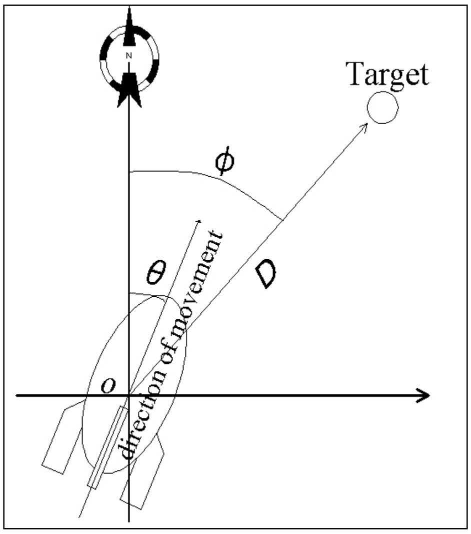

Figure 4 Coordinate of the airship to target

3.2 Control of side thruster

3.2.1 PD control

The side thruster is first controlled by PD adjustment as comparison. The thrust S_t is determined by the angular difference $\theta_d = \phi - \theta$ shown in Figure 4, the angular velocity ω (= $d\theta_d/dt$) and the angular acceleration α (= $d^2\theta_d/dt^2$). Thus the thrust of the side thruster is expressed as follows:

$$S_t = K_\theta(0-\theta_d) + K_\omega(0-\omega) + K_\alpha(0-\alpha) \quad (1)$$

where K_θ, K_ω and K_α are constants and the target point is set to (0, 0, 0). However, it is difficult to determine these parameters because the airship is slow to respond and the characteristic of the airship is non-linear. Therefore, these constants are adjusted and determined by repeating the experiment.

3.2.2 Fuzzy control

As the other control method for the side thruster, fuzzy control is applied. Figure 5 shows the membership functions being used [9]. Inputs are the angular difference θ_d and the angular velocity ω. The membership functions have triangular forms and seven vertices. Each set is labeled NL, NM, NS, ZR, PS, PM and PL, meaning negative large, negative medium, negative small, zero, positive small, positive medium and positive large for each symbol.

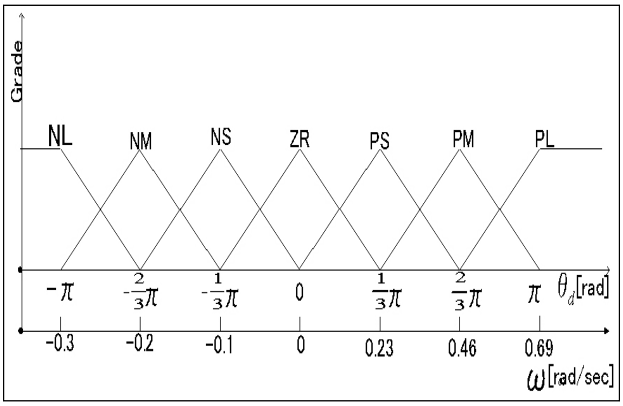

Figure 5 Membership functions

The fuzzy rules are as follows

If θ_d is A_{11} and ω is A_{12}, then S_t is B_1
If θ_d is A_{21} and ω is A_{22}, then S_t is B_2

Where A_{ij} and B_i are labels of each fuzzy set. The fuzzy output set B_i is discrete. These rules are expressed as the rule table shown in Table 1.

Table 1 Rule table for S_t

ω \ θ_d	NL	NM	NS	ZR	PS	PM	PL
NL	0	0.5	1	1	1	1	1
NM	0	0.4	0.7	0.3	1	1	1
NS	-0.7	0.3	0.5	0.1	0.3	1	1
ZR	-1	-0.5	-0.3	0	0.1	0.4	1
PS	-1	-1	-0.6	-0.4	-0.6	-0.4	0.6
PM	-1	-1	-1	-0.5	-0.8	-0.5	0
PL	-1	-1	-1	-1	-1	-0.6	0

4. Experiment

4.1 Procedure of experiment

The purpose of the experiment is to confirm that the airship navigates to the target point and to compare the two control methods for controlling the side thruster. Since the power of the motors is not very large, it is desirable that the experiment is conducted indoors, where there is little effect to disturb the flight. The space for experiment needs an area of over 1000m^2 and a height over 20m due to the size of the airship. And since GPS signals cannot be received in a reinforced concrete building, the experiment is done in wooden building Izumo dome.

4.2 Result and Discussion

The result is shown in Figure 6. It gives two trajectories of the flight path, plotting longitude along the ordinate and latitude along the abscissa. By PD control, the airship flew changing the direction right and left before arriving at the target point. The main cause is that gains of K_θ, K_ω, K_α in equation (1) were not able to be adjusted properly. The adjustment is very difficult without analyzing the dynamic characteristics of the airship. By fuzzy control, the airship could autonomously navigate by the almost shortest flight path. The flight time is 1 minute and 27 seconds by PD control, and 20 seconds by fuzzy control.

The results of this experiment show that the fuzzy control method is more effective than the PD control method from viewpoint of tuning parameters, and the PD control method is not suitable for the autonomous airship system in the present situation.

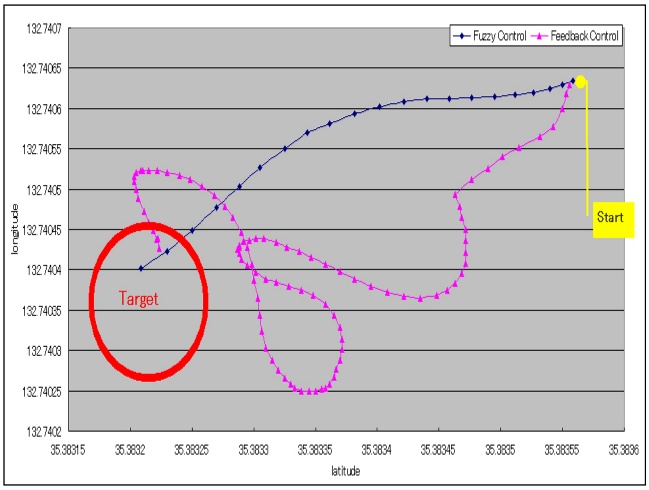

Figure 6 Results of flight controlled by Fuzzy and PD

5. Conclusions

In this paper, we proposed the control system and the algorithm for the airship to navigate autonomously to the target point. To control the side thruster, the PD and fuzzy control are applied as comparison. As the result, it is clear that the fuzzy control is better for the airship to finish the task of flying to the target point.

Further work of image processing and recognition by the CCD camera and the technology of the telecommunication are being considered. Telecommunication needs to communicate mutually the data between the computer mounted on the airship and the computer at the base station. The monitoring program using wireless LAN is developed in the project. It enables us to monitor the condition of the airship from a remote location. In the near future, we will develop integrated monitoring and operating software.

Reference

[1] Web site of Aerosonde Robotic Aircraft Pty Ltd: http://www.aerosonde.com
[2] Web site of General Atomics Aeronautical systems, Inc: http://www.uav.com/home/index.html
[3] Web site of Northrop Grumman Corporation: http://www.is.northropgrumman.com/products/usaf_products/global_hawk/global_hawk.html
[4] S. Nakamura, K. Kataoka and M. Sugeno (2000), “A study on autonomous landing of an unmanned helicopter using active vision and GPS”. Journal of the Robotics Society of Japan, Vol.18, No.2, pp252-260, 2000.
[5] S. Nakamura, A. Sato, H. Shibata and M. Sugeno (2000), “A study on autonomous searching and tracking by an unmanned helicopter based on GPS and image information”. Journal of the Robotics Society of Japan, Vol.18, No.6, pp862-870, 2000.
[6] Web site of Tomakomai. C. T: http://www.tomakomai-ct.ac.jp/mech/thermal/sotuken2001/airplane_cont.files/frame.htm
[7] K. Suzuki, Y.Akisato and A Ohuchi (1999), “Micro airship control based on reinforcement learning”. Proceedings of 99th robotics and mechatronics conference on JSME, No.99-9, 1999.
[8] K. Motoyama, M. Yamamoto, K. Suzuki, A. Ohuchi (1999), “Evolutionary state space configuration for RL applied to airship control”. Proceedings of the 9th intelligent system symposium on JSME, No.99-18, 1999.
[9] Yutaka Fujihara, Takumi Kamioka, et al (2004), “Development of the autonomous airship by fuzzy control”. Proceedings of the Seventh International Conference on Industrial Management (ICIM’2004), Okayama, Japan, Nov. 15-17, 2004, pp. 183-190.

The Tenth International Symposium on Artificial Life and Robotics 2005(AROB 10th '05),
B-con Plaza, Beppu, Oita, Japan, February 4-6, 2005

Fuzzy Information Retrieval Based on Weighted Power-Mean Averaging Operators

Won-Sin Hong*, Shyi-Ming Chen*, and Shi-Jay Chen**

*Department of Computer Science and Information Engineering, National Taiwan University of Science and Technology, Taipei, Taiwan, R. O. C.

**Department of Information Management, Ching-Yun University, Jung-Li, Taiwan R. O. C.

Abstract

In recent years, some researchers used averaging operators (i.e., Infinite-One operators, Waller-Kraft operators, P-Norm operators and GMA operators) to deal with AND and OR operations of users' queries for fuzzy information retrieval, but they still have some drawbacks, e.g., sometimes query results do not coincide with the intuition of the human being. In this paper, we present new averaging operators, called weighted power-mean averaging (WPMA) operators, based on the weighted power-mean for dealing with fuzzy information retrieval to overcome the drawbacks of the existing methods. The proposed WPMA operators are more flexible and more intelligent than the existing averaging operators to deal with users' fuzzy queries for fuzzy information retrieval.

1 Introduction

In [1], [2], [3], [4] and [5], the T-operators (i.e., T-norms and T-cornorms) are used to deal with fuzzy information retrieval. Although T-operators support the ranking facility, they still have some drawbacks, e.g., sometimes query results do not coincide with the intuition of the human being. In [6], Lee et al. pointed out that three averaging operators (i.e. Waller-Kraft operators [7], P-Norm operators [8] and Infinite-One operators [9]) have been proposed to achieve high retrieval effectiveness for fuzzy information retrieval, where these three averaging operators can avoid the drawbacks of T-operators. However, in [10], Chen et al. pointed out that these three averaging operators still have some drawbacks, i.e., it is subjective and hard to determine appropriate values for the parameters of these averaging operators, respectively. Thus, in [10], Chen et al. presented new averaging operators based on the geometric mean, called the geometric-mean averaging (GMA) operators, to overcome the drawbacks of the Waller-Kraft operators, the P-Norm operators and the Infinite-One operators. However, the GMA operators still have some drawbacks, i.e., in some specific situations, the retrieval results do not coincide with the intuition of the human being. Thus, it is necessary to develop new averaging operators to overcome the drawbacks of the existing averaging operators for dealing with fuzzy information retrieval.

In this paper, we present new averaging operators, called weighted power-mean averaging (WPMA) operators, based on the concept of the weighted power-mean [8] to deal with fuzzy information retrieval. We also prove that the proposed WPMA operators are "positively compensatory" operators. In [3] and [6], Kim et al. pointed out that operators which have the "positively compensatory" property could provide high retrieval effectiveness. The proposed WPMA operators are more flexible and more intelligent than the average operators presented in [7], [9], [10] and [11] for dealing with fuzzy information retrieval.

2 Preliminaries

In [8], the definition of the weighted power means is defined as follows:

Definition 2.1: Assume that $\underline{a}$ and $\underline{w}$ are two positive n-tuples and $r \in R$, then the *rth* power mean $M_n^{[r]}(\underline{a},\ \underline{w})$ of $\underline{a}$ with weight $\underline{w}$ is define as follows:

$$M_n^{[r]}(\underline{a},\ \underline{w}) = \left(\frac{1}{W_n} \sum_{i=1}^{n} a_i^{\ r} w_i \right)^{\frac{1}{r}}, \tag{1}$$

where $W_n = w_1 + w_2 + \cdots + w_n$.

Since $M_n^{[1]} = A_n$ and $M_n^{[-1]} = H_n$, in [8], Bullen et al. defined $M_n^{[0]} = G_n$ and proved that the definition of the weighted power mean is reasonable. Thus, the weighted power means form a natural extension of elementary means. Furthermore, when $r \to \infty$, $M_n^{[r]}(\underline{a},\ \underline{w}) = \max \underline{a}$; when $r \to -\infty$, $M_n^{[r]}(\underline{a},\ \underline{w}) = \min \underline{a}$.

In [3], Kim et al. pointed out that an information retrieval system based on the conventional fuzzy set model is defined by a quadruple < T, Q, D, F> , where

(1) T is a set of index terms, T= $\{t_1, t_2, \cdots, t_m\}$, where these index terms are used for representing queries and documents.
(2) Q is a set of queries, where query $q \in$ Q is a Boolean expression composed of index terms t_j, $1 \le j \le$ m, and the logical operators "AND", "OR"

and "NOT".

(3) D is a set of documents, $D=\{d_1, d_2, \cdots, d_n\}$, where each document $d_i \in D$ is represented by $((t_1, e_{i1}), (t_2, e_{i2}), \cdots, (t_m, e_{im}))$, e_{ij} denotes the degree of strength of term t_j in document d_i, $e_{ij} \in [0,1]$, $1 \le i \le$ n, and $1 \le j \le$ m.

(4) F is an evaluation function,

$$F\text{: D} \times \text{Q} \to [0, 1], \tag{2}$$

which assigns a real value in the closed interval $[0,1]$ to each pair (d, q). It is a similarity measure between document d and query q.

From [12], we can see that the weight e_{ij} of term t_j in document d_i is determined either subjectively by domain experts or objectively by some algorithmic procedures, where $1 \le i \le$ n and $1 \le j \le$ m. One way for determining the degree of strength e_{ij} of term t_j in document d_i objectively is to consider the frequency of occurrence of index term t_j in document d_i.

3 Fuzzy Information Retrieval Based on the Weighted Power-Mean Averaging Operators

In this section, we present new averaging operators, called the Weighted Power-Mean Averaging (WPMA) operators, for fuzzy information retrieval, shown as follows:

$$F(d_i,\ \text{q}_{\text{AND}}) = F(d_i,\ \text{t}_1 \text{ AND t}_2 \text{ AND } \cdots \text{AND t}_\text{m}) = \left[\frac{1}{m^2}\sum_{k=1}^{m}(2m-2k+1)\, {e^*_{ik}}^{r}\right]^{\frac{1}{r}}, \tag{3}$$

$$F(d_i,\ \text{q}_{\text{OR}}) = F(d_i,\ \text{t}_1 \text{ OR t}_2 \text{ OR } \cdots \text{OR t}_\text{m}) = 1-\left[\frac{1}{m^2}\sum_{k=1}^{m}(2k-1)(1-e^*_{ik})^{r}\right]^{\frac{1}{r}}, \tag{4}$$

where $r \in \{0.0001, 0.5\}$, e_{ij} denotes the degree of strength of term t_j in document d_i, e^*_{ik} denotes the kth smallest value of e_{ij}; the weight of the term in document d_i which is associated with the kth smallest value of e_{ij} in the AND query q_{AND} is $2m-2k+1$; the weight of the term in document d_i which is associated with the kth smallest value of e_{ij} in the OR query q_{OR} is $2k-1$, $1 \le i \le n$, $1 \le j \le m$, $1 \le k \le m$, $F(d_i,\ q_{\text{AND}}) \in [0,1]$ and $F(d_i,\ q_{\text{OR}}) \in [0,1]$.

In the following, we use two cases to discuss how the proposed WPMA operators are controlled by a parameter r. Assume that there are four documents d_1, d_2, d_3 and d_4, and assume that there are two queries q_1 and q_2, shown as follows:

$d_1 = \{(t_1, 0), (t_2, 0)\}$,
$d_2 = \{(t_1, 0), (t_2, 1)\}$,
$d_3 = \{(t_1, 1), (t_2, 0)\}$,
$d_4 = \{(t_1, 1), (t_2, 1)\}$,
$q_1 = t_1$ AND t_2,
$q_2 = t_1$ OR t_2.

Case 1: If the parameter $r = 0.0001$, then the degree of satisfaction $F(d_3,\ q_1)$ of the document d_3 with respect to the query q_1 and the degree of satisfaction $F(d_2,\ q_2)$ of the document d_2 with respect to the query q_2 can be evaluated, shown as follows:

$$F(d_3,\ q_1) = \left[\frac{1}{4}\left(3\times 0^{0.0001} + 1\times 1^{0.0001}\right)\right]^{10000} = 0,$$

$$F(d_2,\ q_2) = 1-\left[\frac{1}{4}\left(1\times(1-0)^{0.0001} + 3\times(1-1)^{0.0001}\right)\right]^{10000} = 1.$$

In the same way, we can calculate the values of $F(d_1,\ q_1)$, $F(d_2,\ q_1)$, $F(d_4,\ q_1)$, $F(d_1,\ q_2)$, $F(d_3,\ q_2)$ and $F(d_4,\ q_2)$, respectively, as shown in Table 1. From Table 1, we can see that when $r = 0.0001$, the proposed WPMA operators become the traditional Boolean operators. The operator graph [10] of the proposed WPMA operators is shown in Fig. 3.

Table 1. Query Result of the Proposed WPMA Operators (when r = 0.0001)

Documents	Terms		Queries	
	t_1	t_2	$q_1 = t_1$ AND t_2	$q_2 = t_1$ OR t_2
d_1	0	0	0	0
d_2	0	1	0	1
d_3	1	0	0	1
d_4	1	1	1	1

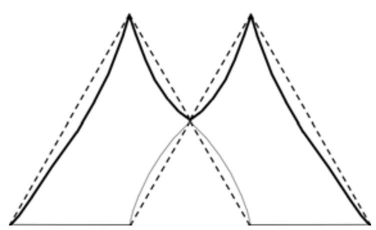

Fig. 3. The operator graphs of the proposed WPMA operators (when $r = 0.0001$).

Case 2: If the parameter $r = 0.5$, then the degree of satisfaction $F(d_3,\ q_1)$ of the document d_3 with respect to the query q_1 and the degree of satisfaction $F(d_2,\ q_2)$ of the document d_2 with respect to the query q_2 can be evaluated, shown as follows:

$$F(d_3,\ q_1) = \left[\frac{1}{4}\left(3\times 0^{0.5} + 1\times 1^{0.5}\right)\right]^2 = 0.063,$$

$$F(d_2,\ q_2) = 1 - \left[\frac{1}{4}\left(1\times(1-0)^{0.5} + 3\times(1-1)^{0.5}\right)\right]^2 = 0.938.$$

In the same way, we can calculate the values of $F(d_1,\ q_1)$, $F(d_2,\ q_1)$, $F(d_4,\ q_1)$, $F(d_1,\ q_2)$, $F(d_3,\ q_2)$ and $F(d_4,\ q_2)$, respectively, as shown in Table 2. From Table 2, we can see that when $r = 0.5$, the proposed WPMA operators are compatible with the extended Boolean operators [11]. The operator graph of the proposed WPMA operators is shown in Fig. 4.

Table 2. Query result of the Proposed WPMA Operators (when $r = 0.5$)

Documents	Terms		Queries	
	t_1	t_2	$q_1 = t_1$ AND t_2	$q_2 = t_1$ OR t_2
d_1	0	0	0	0
d_2	0	1	0.063	0.938
d_3	1	0	0.063	0.938
d_4	1	1	1	1

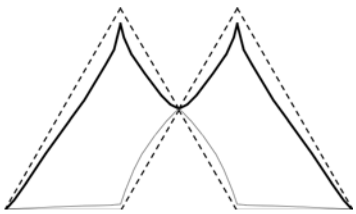

Fig. 4. The operator graph of the proposed WPMA operators ($r = 0.5$).

In [6], Lee pointed out that an operator which has the "*positively compensatory*" property could provide higher retrieval effectiveness. The "*positively compensatory*" operators are functions of the form $p:[0,1]\times[0,1]\to[0,1]$. They must satisfy the following two properties:

(1) $p(x,x) = x$; i.e., p is an idempotent function.

(2) $Min(x,y) < p(x,y) < Max(x,y)$, where $x \neq y$.

In the following, we assume that $0 \le x \le 1$, $0 \le y \le 1$, and prove that the proposed WPMA operators satisfy the following two properties.

Property 3.1: $F(d,\ t_1\ \text{AND}\ t_2)$ and $F(d,\ t_1\ \text{OR}\ t_2)$ are idempotent, where document $d = \{(t_1,\ x),\ (t_2,\ x)\}$, t_1 and t_2 are terms, and $0 \le x \le 1$.

Proof: Based on formula (3), we can see that

$$F(d,\ t_1\ \text{AND}\ t_2) = \left[\frac{1}{4}(3\times x^r + 1\times x^r)\right]^{\frac{1}{r}} = \left[x^r\right]^{\frac{1}{r}} = x.$$

Based on formula (4), we can see that

$$\begin{aligned} F(d,\ t_1\ \text{OR}\ t_2) &= 1 - \left[\frac{1}{4}(1\times(1-x)^r + 3\times(1-x)^r)\right]^{\frac{1}{r}} \\ &= 1 - \left[(1-x)^r\right]^{\frac{1}{r}} \\ &= 1-(1-x) \\ &= x. \end{aligned}$$

Thus, the proposed WPMA operators are idempotent.

Q.E.D.

Property 3.2: Assume that there is a document $d = \{(t_1,\ x),\ (t_2,\ y)\}$, where t_1 and t_2 are terms, and $0 \le x \le 1$ and $0 \le y \le 1$. Then, $Min(x,y) < F(d,\ t_1\ \text{AND}\ t_2) < F(d,\ t_1\ \text{OR}\ t_2) < Max(x,y)$, where $x \neq y$.

Proof:

(i) If $x > y$, then we can see that $Min(x,y) = y$ and $Max(x,y) = x$. Furthermore, based on formula (3), we can see that

$$F(d,\ t_1\ \text{AND}\ t_2) = \left[\frac{1}{4}(3\times y^r + 1\times x^r)\right]^{\frac{1}{r}}$$

$$\Rightarrow \left[\frac{1}{4}(3\times y^r + 1\times y^r)\right]^{\frac{1}{r}} < \left[\frac{1}{4}(3\times y^r + 1\times x^r)\right]^{\frac{1}{r}} < \left[\frac{1}{4}(3\times x^r + 1\times x^r)\right]^{\frac{1}{r}}$$

$$\Rightarrow F(d,\ t_2\ \text{AND}\ t_2) < F(d,\ t_1\ \text{AND}\ t_2) < F(d,\ t_1\ \text{AND}\ t_1)$$ (by formula (3))

$$\Rightarrow y < F(d,\ t_1\ \text{AND}\ t_2) < x$$ (by Property 3.1)

$$\Rightarrow Min(x,y) < F(d,\ t_1\ \text{AND}\ t_2) < Max(x,y).$$

Based on formula on (4), we can see that

$$F(d,\ t_1\ \text{OR}\ t_2) = 1 - \left[\frac{1}{4}(1\times(1-y)^r + 3\times(1-x)^r)\right]^{\frac{1}{r}}$$

$$\Rightarrow 1 - \left[\frac{1}{4}(1\times(1-y)^r + 3\times(1-y)^r)\right]^{\frac{1}{r}} < 1 - \left[\frac{1}{4}(1\times(1-y)^r + 3\times(1-x)^r)\right]^{\frac{1}{r}} < 1 - \left[\frac{1}{4}(1\times(1-x)^r + 3\times(1-x)^r)\right]^{\frac{1}{r}}$$

$$\Rightarrow F(d,\ t_2\ \text{OR}\ t_2) < F(d,\ t_1\ \text{OR}\ t_2) < F(d,\ t_1\ \text{OR}\ t_1),$$ (by formula (4))

$$\Rightarrow y < F(d,\ t_1\ \text{OR}\ t_2) < x,$$ (by Property 3.1)

$$\Rightarrow Min(x,y) < F(d,\ t_1\ \text{OR}\ t_2) < Max(x,y).$$

Then, we prove "$F(d,\ t_1\ \text{AND}\ t_2) < F(d,\ t_1\ \text{OR}\ t_2)$" based on formulas (3) and (4), shown as follows:

$$F(d,\ t_1\ \text{AND}\ t_2) = \left(\frac{y^r + y^r + y^r + x^r}{4}\right)^{\frac{1}{r}} <$$

$$\left(\frac{y+y+y+x}{4}\right) < \left(\frac{y+x+x+x}{4}\right) =$$
$$1-\left(\frac{(1-y)+(1-x)+(1-x)+(1-x)}{4}\right) <$$
$$1-\left(\frac{(1-y)^r+(1-x)^r+(1-x)^r+(1-x)^r}{4}\right)^{\frac{1}{r}}$$
$$= F(d,\ t_1 \text{ OR } t_2).$$

From the above discussions, we can see that $Min(x, y)$ $< F(d,\ t_1 \text{ AND } t_2) < F(d,\ t_1 \text{ OR } t_2) < Max(x, y)$.

(ii) In the same way, if $x < y$, we can get

$F(d,\ t_1 \text{ AND } t_1) < F(d,\ t_1 \text{ AND } t_2) < F(d,\ t_2 \text{ AND } t_2)$, (by formula (3))

$x < F(d,\ t_1 \text{ AND } t_2) < y$, (by Property 3.1)

$F(d,\ t_1 \text{ OR } t_1) < F(d,\ t_1 \text{ OR } t_2) < F(d,\ t_2 \text{ OR } t_2)$, (by formula (4))

$x < F(d,\ t_1 \text{ OR } t_2) < y$, (by Property 3.1)

and $F(d,\ t_1 \text{ AND } t_2) < F(d,\ t_1 \text{ OR } t_2)$. (by formulas (3) and (4))

Thus, $Min(x, y) < F(d,\ t_1 \text{ AND } t_2) < F(d,\ t_1 \text{ OR } t_2) <$ $Max(x, y)$, where $x \neq y$. Q.E.D.

According to the above properties, we can see that the proposed WPMA operators have the "*positively compensatory*" property. Moreover, they have neither the "single operand dependent" property nor the "negatively compensatory" property. Therefore, they can overcome the drawback of the T-operators.

4 Conclusions

In this paper, we have presented the weighted power-mean averaging (WPMA) operators for fuzzy information retrieval. The proposed WPMA operators are more flexible and more intelligent than the averaging operators presented in [7], [9], [10] and [11] to deal with users' fuzzy queries for fuzzy information retrieval due to the fact that the proposed WPMA operators have the following advantages:

(1) The proposed WPMA operators can overcome the drawbacks of the existing averaging operators for fuzzy information retrieval.
(2) The retrieval results of the proposed WPMA operators are much closer to the intuition of the human being than the existing averaging operators.
(3) We can easily determine appropriate values for the parameters of the proposed WPMA averaging operators. If we use the proposed WPMA operators to deal with traditional Boolean query processing for fuzzy information retrieval, then we can set the parameter $r = 0.0001$; if we use the proposed WPMA operators to deal with extended Boolean query processing for fuzzy information retrieval, then we can set the parameter $r = 0.5$.

Acknowledgements

This work was supported in part by the National Science Council, Republic of China, under Grant NSC 93-2213-E-011-018.

References

[1] D. A. Buell, "A problem in information retrieval with fuzzy set," *Journal of the American Society for Information Science*, Vol. 36, pp. 398-401, 1985.

[2] D. H. Kraft and D. A. Buell, "Fuzzy set and generalized Boolean retrieval systems," *International Journal of Man-Machine Studies*, Vol. 19, pp. 45-56, 1983.

[3] M. H. Kim, J. H. Lee, and J. Lee, "Analysis of fuzzy operators for high quality information retrieval," *Information Processing Letters*, Vol. 46, pp. 251-256, 1993.

[4] D. Lucaralla and R. Morara, "FIRST: Fuzzy information retrieval system," *Journal of Information Science*, Vol. 17, pp. 81-91, 1991.

[5] S. Miyamoto, *Fuzzy Sets in Information Retrieval and Cluster Analysis*, Kluwer, Dordrecht, 1990.

[6] J. H. Lee, "Properties of extended Boolean model in information retrieval," *Proceedings of the Seventeenth Annual ACM Conference on Research and Development in Information Retrieval*, Dublin, pp. 182-190, 1994.

[7] W. G. Waller and D. H. Kraft, "A mathematical model of a weighted Boolean retrieval system," *Information Processing and Management*, Vol. 15, pp. 235-245, 1979.

[8] P. S. Bullen, D. S. Mitrinovic, and P. M. Vasic, *Means and Their Inequalities*, D. Reidel Publishing Company, Dordrecht, 1988.

[9] M E. Smith, *Aspects of the P-Norm Model of Information Retrieval: Syntactic Query Generation, Efficiency and Theoretical Properties*, Ph.D. Dissertation, Cornell University, New York, 1990.

[10] S. J. Chen and S. M. Chen, "A new method for fuzzy information retrieval based on geometric-mean averaging operators," *Proceedings of the 2002 International Computer Symposium: Workshop on Artificial Intelligence*, Hualien, Taiwan, Republic of China, 2002.

[11] G. Salton, E. A. Fox, and H. Wu, "Extended Boolean information retrieval," *Communications of the ACM*, Vol. 26, pp. 1022-1036, 1983.

[12] G. J. Klir and B.Yuan, *Fuzzy Sets and Fuzzy Logic: Theory and Applications*, Prentice Hall, New Jersey, 1995.

The Tenth International Symposium on Artificial Life and Robotics 2005(AROB 10th '05),
B-con Plaza, Beppu, Oita, Japan, February 4-6, 2005

Temperature Prediction Based on Genetic Simulated Annealing Techniques and High-Order Fuzzy Time Series

Li-Wei Lee*, Li-Hui Wang**, and Shyi-Ming Chen*

*Department of Computer Science and Information Engineering, National Taiwan University of Science and Technology, Taipei, Taiwan, R. O. C.
**Department of Finance, Chihlee Institute of Technology, Panchiao, Taipei, Taiwan, R. O. C.

Abstract

In this paper, we present a new approach for temperature prediction based on genetic simulated annealing techniques and high-order fuzzy time series, where the simulated annealing techniques are used to deal with the mutation operations of genetic algorithms. The proposed method uses genetic simulated annealing techniques to adjust the length of each interval in the universe of discourse to increase the forecasting accuracy rate. It can get a higher forecasting accuracy rate than the existing methods.

1 Introduction

It is obvious that people are always interested in oncoming events, where an event may be affected by many factors. If we can consider these many factors for dealing with forecasting problems, then we can get a higher forecasting accuracy rate. In recent years, some methods have been presented for dealing with forecasting problems [1]-[15].

In this paper, we present a new method for temperature prediction based on genetic simulated annealing techniques and high-order fuzzy time series, where the simulated annealing techniques [16] are used to deal with mutation operations of genetic algorithms. The proposed method uses genetic simulated annealing techniques to adjust the length of each interval in the universe of discourse for increasing the forecasting accuracy rate. It can get a higher forecasting accuracy rate than the existing methods.

2 Fuzzy Time Series

In [10]-[12], Song and Chissom presented the concepts of fuzzy time series based on the fuzzy set theory [17]. In the following, we briefly review the definitions of fuzzy time series from [3], [11] and [13].

Definition 2.1: Let $Y(t)$ ($t = \cdots, 0, 1, 2, \cdots$) be the universe of discourse and be a subset of R. Assume that $f_i(t)$ ($i = 1, 2, \cdots$) is defined in the universe of discourse $Y(t)$, and assume that $F(t)$ is a collection of $f_i(t)$ ($i = 1, 2, \cdots$), then $F(t)$ is called a fuzzy time series of $Y(t)$ ($t = \cdots, 0, 1, 2, \cdots$).

Definition 2.2: Let $F(t)$ be a fuzzy time series. If $F(t)$ is caused by $F(t-1)$, $F(t-2)$, $\cdots$, and $F(t-n)$, then the nth-order fuzzy logical relationship is represented by

$$F(t-n), \cdots, F(t-2), F(t-1) \rightarrow F(t), \tag{1}$$

where $F(t-n)$, $\cdots$, $F(t-2)$, $F(t-1)$ and $F(t)$ are fuzzy sets, "$F(t-n)$, $\cdots$, $F(t-2)$, $F(t-1)$" is called the current state of the nth-order fuzzy logical relationship, and $F(t)$ is called the next state of the nth-order fuzzy logical relationship.

3 Basic Concepts of Simulated Annealing Algorithms and Genetic Algorithms

In [16], Kirkpatrick et al. proposed the simulated annealing algorithm. A simulated annealing algorithm takes into account not only downhill move, but also permits uphill moves with an assigned probability depending on the "state temperature". The basic concept of a simulated annealing algorithm is derived by observing the change of energy in a process in which materials solidify from the liquid state to the solid state. When the system's temperature decreases gradually in the annealing schedule, if the energy of the material in a new state is lower than the energy of the material in the current state, then the system will replace the current state by the new state. Otherwise, whether the new state can be accepted or not depends on the probability p shown as follows:

$$p = e^{\frac{-\Delta E}{kT}}, \tag{2}$$

where p denotes the probability that the system accepts the new state, T denotes the current system temperature, k denotes the Boltzmann's constant, and ΔE denotes the difference between the energy of the new state and the energy of the current state.

The concept of genetic algorithms was proposed by Holland [18], where a population consists of chromosomes and a chromosome consists of genes. The number of chromosomes in a population is called the "population size". The reproduction operation, crossover operation and mutation operation of genetic algorithms can refer to [18], [19] and [20].

4 A New Method for Temperature Prediction Based on Genetic Simulated Annealing Techniques and High-Order Fuzzy Time Series

In this section, we present a new method for temperature prediction based on genetic simulated annealing techniques and high-order fuzzy time series.

The method is essentially a modification of the method presented in [7]. Table 1 shows the historical data of the daily average temperature from June 1996 to September 1996 in Taipei, Taiwan [21]. Table 2 shows the historical data of the daily cloud density from June 1996 to September 1996 in Taipei, Taiwan [21]. In [2], the daily average temperature is called the "Main-Factor" of the fuzzy time series and the daily cloud density is called the "Second-Factor" of the fuzzy time series. First, based on Table 1, Table 2 and [7], we define the universe of discourse of the daily average temperature U = [23, 32] and define the universe of discourse of the daily cloud density V = [0, 100].

Table 1. Historical Data of the Daily Average Temperature from June 1996 to September 1996 in Taipei, Taiwan (Unit: °C) [21]

Day \ Month	June	July	August	September
1	26.1	29.9	27.1	27.5
2	27.6	28.4	28.9	26.8
3	29.0	29.2	28.9	26.4
4	30.5	29.4	29.3	27.5
5	30.0	29.9	28.8	26.6
6	29.5	29.6	28.7	28.2
7	29.7	30.1	29.0	29.2
8	29.4	29.3	28.2	29.0
9	28.8	28.1	27.0	30.3
10	29.4	28.9	28.3	29.9
11	29.3	28.4	28.9	29.9
12	28.5	29.6	28.1	30.5
13	28.7	27.8	29.9	30.2
14	27.5	29.1	27.6	30.3
15	29.5	27.7	26.8	29.5
16	28.8	28.1	27.6	28.3
17	29.0	28.7	27.9	28.6
18	30.3	29.9	29.0	28.1
19	30.2	30.8	29.2	28.4
20	30.9	31.6	29.8	28.3
21	30.8	31.4	29.6	26.4
22	28.7	31.3	29.3	25.7
23	27.8	31.3	28.0	25.0
24	27.4	31.3	28.3	27.0
25	27.7	28.9	28.6	25.8
26	27.1	28.0	28.7	26.4
27	28.4	28.6	29.0	25.6
28	27.8	28.0	27.7	24.2
29	29.0	29.3	26.2	23.3
30	30.2	27.9	26.0	23.5
31		26.9	27.7	

Table 2. Historical Data of the Daily Cloud Density from June 1996 to September 1996 in Taipei, Taiwan (Unit: %) [21]

Day \ Month	June	July	August	September
1	36	15	100	29
2	23	31	78	53
3	23	26	68	66
4	10	34	44	50
5	13	24	56	53
6	30	28	89	63
7	45	50	71	36
8	35	34	28	76
9	26	15	70	55
10	21	8	44	31
11	43	36	48	31
12	40	13	76	25
13	30	26	50	14
14	29	44	84	45
15	30	25	69	38
16	46	24	78	24
17	55	26	39	19
18	19	25	20	39
19	15	21	24	14
20	56	35	25	3
21	60	29	19	38
22	96	48	46	70
23	63	53	41	71
24	28	44	34	70
25	14	100	29	40
26	25	100	31	30
27	29	91	41	34
28	55	84	14	59
29	29	38	28	83
30	19	46	33	38
31		95	26	

The proposed method is now presented as follows:

Step 1: Partition the universe of discourse $U = [U_{min}, U_{max}]$ into n intervals $u_1, u_2, \cdots, u_n$, where $u_1 = [U_{min}, x_1]$, $u_2 = [x_1, x_2], \cdots, u_n = [x_{n-1}, U_{max}]$, U_{min} denotes the minimum value in the universe of discourse U, U_{max} denotes the maximum value in the universe of discourse U, and $x_1 \le x_2 \le \cdots \le x_{n-1}$. Partition the universe of discourse $V = [V_{min}, V_{max}]$ into m intervals $v_1, v_2, \cdots, v_m$, where $v_1 = [y_1, V_{max}]$, $v_2 = [y_2, y_1], \cdots, v_m = [V_{min}, y_{m-1}]$, V_{min} denotes the minimum value in the universe of discourse V, V_{max} denotes the maximum value in the universe of discourse V, and $y_1 \ge y_2 \ge \cdots \ge y_{m-1}$. Define each chromosome consisting of n-1 "X genes" and m-1 "Y genes", where the contents of each chromosome are represented by an array $<x_1, x_2, \cdots, x_{n-1}, y_1, y_2, \cdots, y_{m-1}>$, $x_1 \le x_2 \le \cdots \le x_{n-1}$, and $y_1 \ge y_2 \ge \cdots \ge y_{m-1}$. In this paper, we assume that a population consists of 30 chromosomes and assume that the system randomly generates 30 chromosomes as the initial population.

Step 2: Define linguistic terms of the main-factor represented by fuzzy sets $A_1, A_2, \cdots, A_n$, shown as follows:

$$A_1 = 1/u_1 + 0.5/u_2 + 0/u_3 + 0/u_4 + 0/u_5 + \cdots + 0/u_{n-2} + 0/u_{n-1} + 0/u_n,$$
$$A_2 = 0.5/u_1 + 1/u_2 + 0.5/u_3 + 0/u_4 + 0/u_5 + \cdots + 0/u_{n-2} + 0/u_{n-1} + 0/u_n,$$
$$A_3 = 0/u_1 + 0.5/u_2 + 1/u_3 + 0.5/u_4 + 0/u_5 + \cdots + 0/u_{n-2} + 0/u_{n-1} + 0/u_n,$$
$$\vdots$$
$$A_n = 0/u_1 + 0/u_2 + 0/u_3 + 0/u_4 + 0/u_5 + \cdots + 0/u_{n-2} + 0.5/u_{n-1} + 1/u_n.$$

Define linguistic terms of the second-factor represented by fuzzy sets $B_1, B_2, \cdots, B_m$, shown as follows:

$$B_1 = 1/v_1 + 0.5/v_2 + 0/v_3 + \cdots + 0/v_{m-2} + 0/v_{m-1} + 0/v_m,$$
$$B_2 = 0.5/v_1 + 1/v_2 + 0.5/v_3 + \cdots + 0/v_{m-2} + 0/v_{m-1} + 0/v_m,$$
$$B_3 = 0/v_1 + 0.5/v_2 + 1/v_3 + \cdots + 0/v_{m-2} + 0/v_{m-1} + 0/v_m,$$
$$\vdots$$
$$B_m = 0/v_1 + 0/v_2 + 0/v_3 + \cdots + 0/v_{m-2} + 0.5/v_{m-1} + 1/v_m.$$

Based on [22], fuzzify the historical data of the main-factor and the second-factor, respectively, based on each chromosome of the population. For example, if the value of the main-factor of day i belongs to interval u_j, and fuzzy set A_j whose maximum membership value occurs at interval u_j, then the value of the main-factor of day i is fuzzified into A_j, where $1 \le j \le n$; if the value of the second-factor of day i belongs to interval v_s, and fuzzy set B_s whose maximum membership value occurs at v_s, then the value of the second-factor of day i is fuzzified into B_s, where $1 \le s \le m$.

Step 3: Construct two-factors kth-order fuzzy time series relationship groups, where $k \ge 2$.

Step 4: Forecast the values based on the principles presented in [7].

Step 5: Perform the reproduction operations based on the roulette wheel selection method [19]. In this paper, the average forecasting error rate (AFER) is used as the fitness value of each chromosome in the genetic algorithm for temperature prediction, where.

$$\text{AFER} = \frac{\sum_{i=1}^{n} \left| (\text{Forecasted Value of Day } i - \text{Actual Value of Day } i)/\text{Actual Value of Day } i \right|}{n} \times 100\%. \quad (3)$$

The smaller the fitness value (Note: The fitness value is the average forecasting error rate) of a chromosome, the higher the chance of the chromosome to be chosen for put into the mating pool. In this paper, the system chooses chromosomes from the current population into the mating pool according to their reciprocal fitness values. For example, let f_i denote the fitness value of the ith chromosome and let r_i be the reciprocal f_i, i.e., $r_i = 1/f_i$. The selected probability p_i of the ith chromosome is denoted by $p_i = r_i \Big/ \sum_j r_j$. The larger the selected probability of a chromosome, the higher the chance of the chromosome to be chosen for put into the mating pool. Repeatedly perform the reproduction operations, until the number of chromosomes in the mating pool is the same as the number of chromosomes in the current population. Then, let the mating pool become the current population.

Step 6: Randomly select two chromosomes from the population to perform the crossover operations, until all chromosomes in the population have been selected. If the system randomly generates a real value between zero and one that is smaller than or equal to the crossover rate, then the system randomly selects a crossover point of a X gene and a crossover point of a Y gene from the two selected chromosomes of the current population to exchange genes after the crossover point. Otherwise, the selected chromosomes will not perform the crossover operation. In this paper, the crossover rate is set to 0.8. When performing the crossover operation, the system randomly selects one crossover point of X genes and one crossover point of Y genes, where the crossover point of X genes is an integer between 1 and n-1, n is the number of X genes, the crossover point of Y genes is an integer between 1 and m-1, and m is the number of Y genes. Furthermore, if the derived values of the chromosomes are not sorted by the values of genes in an ascending sequence, the system will sort the values of genes in the chromosomes in an ascending sequence.

Step 7: Use the simulated annealing mutation (SAM) algorithm shown in Fig. 1 to perform the mutation operations. For each chromosome in the population, the system generates a real value between zero and one to determine whether the system performs the simulated annealing mutation or not. If the real value generated by the system for a chromosome is smaller than or equal to the mutation rate (Note: In this paper, the mutation rate is 0.05), then the system applies the simulated annealing mutation algorithm to perform the mutation operation on this chromosome. Otherwise, the system will not perform the mutation operation on this chromosome. In Fig. 1, $T_{initial}$ denotes the initial temperature; T denotes the current system temperature; T_{frozen} denotes the frozen temperature; C and C' denote the current chromosome C and the newly generated chromosome C', respectively; we use the average forecasting rate (AFER) shown in formula (3) as the fitness value of each chromosome in the genetic algorithm for temperature prediction; Δf denotes the difference between the fitness value fitness(C') of the newly generated chromosome C' and the fitness value fitness(C) of the current chromosome C; α denotes the annealing constant. First, the system randomly chooses the ith X gene and the jth Y gene from current chromosome C, and then replaces the value x_i of the ith X gene and the value y_j of the jth Y gene of current chromosome C by the random numbers x_i^* and y_j^*, generated by system, respectively, to form the new generated chromosome C'. Then, the system calculates the fitness value of chromosome C and chromosome C', respectively, and then calculates their difference Δf. If Δf is smaller than or equal to zero, then the newly generated chromosome C' is always allowed to replace the current chromosome C. Otherwise, the system is allowed to accept the newly generated chromosome C' depending on the probability $e^{(-\Delta f/T)}$. In this situation, if the random number generated by the system is smaller than the probability $e^{(-\Delta f/T)}$, then the newly generated chromosome C' replaces the current chromosome C. Repeatedly perform the above process, until the current system temperature T is smaller than the frozen temperature T_{frozen}. In this case, the simulated annealing mutation process finishes.

```
Procedure SAM (T_initial, T_frozen, α)
begin
    T ← T_initial;
    while (T > T_frozen) do
        Randomly choose the ith X gene and jth Y gene
        of chromosome C, where 1 ≤ i ≤ n, 1 ≤ j ≤ m, n
        is the number of X genes of chromosome C,
        and m is the number of Y gene from
        chromosome C, and replace the value x_i of the
        ith X gene and the value y_j of the jth Y gene of
        chromosome C by the random numbers x_i* and
        y_j* generated by the system, respectively, to
        derive newly generated chromosome C'(i.e., C'
        ← < x_1, x_2, ⋯, x_i*, ⋯, x_n, y_1, y_2, ⋯, y_j*, ⋯,
        y_m>);
        Let Δf ← fitness(C') – fitness(C);
        r ← random number between 0 and 1 generated
        by the system;
        if   Δf ≤ 0 or r < e^(-Δf / T) then C ← C';
        T ← T × α;
    end;
    return C
end.
```

Fig. 1. Simulated annealing mutation algorithm.

Step 8: Based on formula (3), calculate the average forecasting error rate (AFER) of each chromosome in the population. If the system has evolved a predefined number of generations, then the chromosome that has the smallest average forecasting error rate is the optimal solution to be used to deal with the forecasting problem; **Stop**. Otherwise, go to Step 5.

We have implemented the proposed method using Visual Basic version 6.0 on a Pentium 4 PC. We use the average forecasting rate (AFER) shown in formula (3) as the fitness value of each chromosome in the genetic algorithm for temperature prediction. We use different annealing constants in the simulated annealing mutation algorithm to forecast the daily average temperature from June 1996 to September 1996 in Taipei, Taiwan, where we partition the universe of discourse U of the main-factor (i.e., the daily average temperature) into 9 intervals and partition the universe of discourse V of the second-factor (i.e., the daily cloud density) into 7 intervals. In other words, each chromosome in a population consists of 8 X genes and 6 Y genes. A comparison of average forecasting error rates of the proposed method with the existing methods is shown in Table 3, where the average forecasting error rates are calculated by executing the proposed method three times, and the number of generations, the population size, the crossover rate, the mutation rate, the initial temperature and the frozen temperature are 1000, 30, 0.8, 0.05, 100 and 0.0001, respectively. From Table 3, we can see that the proposed method gets smaller forecasting error rates than the methods presented in [2] and [7]. That is, the proposed method gets higher forecasting accuracy rates than the methods presented in [2] and [7] for dealing with temperature prediction.

Table 3. A Comparison of the Average Forecasting Error Rates of the Proposed Method with the Existing Methods

		Month	Window Basis							
Chen's Method [2]			w = 2	w = 3	w = 4	w = 5	W = 6	w = 7	w = 8	
		June	2.88%	3.16%	3.24%	3.33%	3.39%	3.53%	3.67%	
		July	3.04%	3.76%	4.08%	4.17%	4.35%	4.38%	4.56%	
		August	2.75%	2.77%	3.30%	3.40%	3.18%	3.15%	3.19%	
		September	3.29%	3.10%	3.19%	3.22%	3.39%	3.38%	3.29%	
Lee et al's Method [7]		Month	Order							
			First Order	Second Order	Third Order	Fourth Order	Fifth Order	Sixth Order	Seventh Order	Eighth Order
		June	1.44%	0.47%	0.50%	0.49%	0.49%	0.50%	0.49%	0.46%
		July	1.33%	0.46%	0.50%	1.50%	0.50%	0.49%	0.50%	0.50%
		August	1.16%	0.48%	0.48%	0.49%	0.50%	0.49%	0.50%	0.49%
		September	1.28%	0.98%	1.02%	1.12%	1.02%	0.74%	0.86%	0.50%
The Proposed Method	Annealing Constant α	Month	Order							
			First Order	Second Order	Third Order	Fourth Order	Fifth Order	Sixth Order	Seventh Order	Eighth Order
	0.25	June	0.79%	0.44%	0.42%	0.42%	0.42%	0.44%	0.40%	0.40%
		July	0.66%	0.45%	0.42%	0.41%	0.41%	0.40%	0.41%	0.40%
		August	0.64%	0.43%	0.47%	0.40%	0.41%	0.38%	0.40%	0.45%
		September	0.69%	0.58%	0.59%	0.57%	0.56%	0.57%	0.58%	0.47%
	0.5	June	0.84%	0.50%	0.45%	0.42%	0.38%	0.43%	0.39%	0.46%
		July	0.66%	0.50%	0.47%	0.44%	0.40%	0.38%	0.44%	0.42%
		August	0.69%	0.40%	0.38%	0.37%	0.37%	0.39%	0.42%	0.45%
		September	0.66%	0.62%	0.59%	0.59%	0.56%	0.54%	0.56%	0.53%
	0.9	June	0.79%	0.46%	0.42%	0.44%	0.42%	0.41%	0.46%	0.39%
		July	0.62%	0.46%	0.45%	0.44%	0.44%	0.41%	0.40%	0.40%
		August	0.66%	0.40%	0.40%	0.40%	0.36%	0.41%	0.39%	0.44%
		September	0.62%	0.59%	0.61%	0.57%	0.54%	0.59%	0.57%	0.50%

5 Conclusions

In this paper, we have presented a new method for temperature prediction based on genetic simulated annealing techniques and high-order fuzzy time series, where the simulated annealing techniques are used to deal with the mutation operations of the genetic algorithms. The proposed method uses genetic simulated annealing techniques to adjust the length of each interval in the universe of discourse for temperature prediction to increase the forecasting accuracy rate. From Table 3, we can see that the proposed method gets smaller average forecasting error rates than the methods presented in [2] and [7]. That is, the proposed method gets higher forecasting accuracy rates than the methods presented in [2] and [7].

Acknowledgements

This work was supported in part by the National Science Council, Republic of China, under Grant NSC 93-2213-E-011-018.

References

[1] S. M. Chen, "Forecasting enrollments based on fuzzy time series," *Fuzzy Sets and Systems*, Vol. 81, pp. 311-319, 1996.

[2] S. M. Chen and J. R. Hwang, "Temperature prediction using fuzzy time series," *IEEE Transactions on Systems, Man, and Cybernetics-Part B: Cybernetics*, Vol. 30, pp. 263-275, 2000.

[3] S. M. Chen, "Forecasting enrollments based on high-order fuzzy time series," *Cybernetics and Systems: An International Journal*, Vol. 33, pp. 1-16, 2002.

[4] J. R. Hwang, S. M. Chen, and C. H. Lee, "Handling forecasting problems using fuzzy time series," *Fuzzy Sets and Systems*, Vol. 100, pp. 217-228, 1998.

[5] K. Huarng, "Effective lengths of intervals to improve forecasting in fuzzy time series," *Fuzzy Sets and Systems*, Vol. 123, pp. 387-394, 2001.

[6] K. Huarng, "Heuristic models of fuzzy time series for forecasting," *Fuzzy Sets and Systems*, Vol. 123, pp. 369-386, 2001.

[7] L. W. Lee and S. M. Chen, "Temperature prediction using genetic algorithms and fuzzy time series," *Proceedings of the 2004 International Conference on Information Management*, Miaoli, Taiwan, Republic of China, pp. 299-306, 2004.

[8] L. W. Lee, L. H. Wang, S. M. Chen, and Y. H. Leu, "A new method for handling forecasting problems based on two-factors high-order fuzzy time series," *Proceedings of the 2004 Ninth Conference on Artificial Intelligence and Applications*, Taipei, Taiwan, Republic of China, 2004.

[9] Q. Song and B. S. Chissom, "Some properties of defuzzification neural networks," *Fuzzy Sets and Systems*, Vol. 61, pp. 93-89, 1994.

[10] Q. Song and B. S. Chissom, "Fuzzy time series and its models," *Fuzzy Sets and Systems*, Vol. 54, pp. 269-277, 1993.

[11] Q. Song and B. S. Chissom, "Forecasting enrollments with fuzzy time series – Part I," *Fuzzy Sets and Systems*, Vol. 54, pp. 1-9, 1993.

[12] Q. Song and B. S. Chissom, "Forecasting enrollments with fuzzy time series – Part II," *Fuzzy Sets and Systems*, Vol. 62, pp. 1-8, 1994.

[13] Q. Song and R. P. Leland, "Adaptive learning defuzzification techniques and applications," *Fuzzy Sets and Systems*, Vol. 81, pp. 321-329, 1996.

[14] Q. Song, "A note on fuzzy time series model selection with sample autocorrelation functions," *Cybernetics and Systems: An International Journal*, Vol. 34, pp. 93-107, 2003.

[15] J. Sullivan and W. H. Woodall, "A comparison of fuzzy forecasting and Markov modeling," *Fuzzy Sets and Systems*, Vol. 64, pp. 279-293, 1994.

[16] S. Kirkpatrick, C. D. Gelatt, Jr., and M. P. Vecchi, "Optimization by simulated annealing", *Science*, Vol. 220, pp. 671-680, 1983.

[17] L. A. Zadeh, "Fuzzy sets", *Information and Control*, Vol. 8, pp. 338-353, 1965.

[18] J. H. Holland, *Adaptation in Natural and Artificial Systems,* MIT Press, Cambridge, MA, 1975.

[19] M. Gen and R. Cheng, *Genetic Algorithms and Engineering Design,* John Wiley & Sons, New York, 1997.

[20] D. E. Goldberg, *Genetic Algorithm in Search, Optimization, and Machine Learning,* Addison-Wesley, MA, 1989.

[21] Central Weather Bureau, *The Historical Data of the Daily Average Temperature and Daily Cloud Density* (from January 1995 to September 1996), Taipei, Taiwan, R. O. C., 1996.

[22] L. X. Wang and J. M. Mendel, "Generating fuzzy rules by learning from examples," *IEEE Transactions on Systems, Man, and Cybernetics*, Vol. 22, pp. 1414-1427, 1992.

The Tenth International Symposium on Artificial Life and Robotics 2005(AROB 10th '05),
B-con Plaza, Beppu, Oita, Japan, February 4-6, 2005

Design of a Fuzzy Expert System for Electric Vehicle Speed Control

Masanori SUGISAKA & MBAÏTIGA Zacharie
Oita University, Department of Electrical & Electronic Engineering ,msugi@cc.oita-u.ac.jp ,
zack145@oita-cc.cc.oita-u.ac.jp

Abstract

Fuzzy logic systems have demonstrated through numerous application areas, to be an effective procedure for hardware control problems. The basic concept of fuzzy controller is to formulate the control protocol of a human operator in a way that is tractable for microcomputer-based controller. The present paper describes the fuzzy expert system applied to control the speed of the autonomous electric vehicle (EV). The parameters of the speed to be followed by the vehicle during the driving operation at each moment are defined by a set of fuzzy rules and have two inputs and one output. The following two points are the main points of this control. The accelerator pedal position that governs the vehicle speed and the speed categories to be used. The experimental result obtained proves the merit of the control method as the controller accomplishes a satisfactory speed control of three categories.

Key Words: Electric vehicle, fuzzy expert system

1. Introduction

As an alternative to conventional control technique, fuzzy control is gaining increased interests, both in the academic world as well as in the industrial field. For those systems whose accurate mathematical models are not available or are difficult to formulate, fuzzy control can often provide a good solution by incorporating linguistic information from human expert and which is considered as an efficiency tool for hardware control. Due to its efficiency, many researchers have used it in the domain of robot speed control and vehicles speed control in the open literature [1, 2, 3]. In the proposed method of [4], the fuzzy approximator and sliding mode control scheme are considered. The fuzzy logic theory is applied to design the sliding mode controller then a simple adaptive law is used to approximate the unknown function f that defines the motor parameters via fuzzy logic system. However, its only drawback is that the controller does not provide a continuous performance of the motor, due to the considerable number of overshoot. In [5] the paper presents the speed and position control of a permanent magnet (PM) motor, with a sinusoidal flux distribution using fuzzy Logic. Two approaches were proposed and compared with each other; one was based on the voltage model of the motor and other was based on the current model. This control was very successfully in the open loop control of fuzzy control system. But unfortunately the starting procedure from standstill was very difficult under the proposed method, due to the use of both voltage and current for estimation of the rotor position by sensor drive. Therefore no information was available before starting. The other reason is that some incremental control inputs to the motor have been not determined from the fuzzy logic subset. Normally, to well control the speed of any system with a complex hardware such as for example, robot, EV as in our case etc., the choice of the parameters for decision making is the most important part. In this paper, we develop a fuzzy expert control system algorithm for electric vehicle speed, which allows the EV to adapt to three speed levels, based on the knowledge acquired from fuzzy rules base. This method provides, in addition to the well-known efficiency of the fuzzy system in control a continuous running performance of the vehicle.

2. Drive system of the electric vehicle

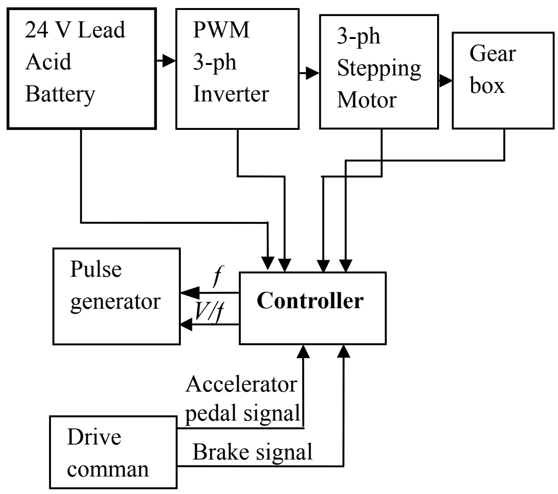

Fig.1 Block diagram of the drive system

The stepper motor use in the electric vehicle is a variable speed; multi-task three phase permanent magnet with 16 stator teeth per stack.. Its maximum output is 5.2 KW at 72V, 50 Hz. The rated slip is only 2 percent to minimize the motor copper loss and to behave stiffer characteristic. The rated iron loss is only 15 W; the reduction of iron is an important factor because of the high frequency harmonics induction by the PWM. The motor frame is made of aluminum alloy to minimize the weight and the frame size is 130. The drive system of the electric vehicle is shown in fig.1.The PWM inverter converts the battery pack dc voltage into a variable voltage, variable frequency ac in-sinusoidal voltage for supply of the three-phase stepping motor. The motor then drives the wheels through a variable ratio gearbox assembly. The power path is reversed in the case of regeneration i.e., the motor becomes an induction generator and the inverter rectifies the ac power into dc and recharges the battery. In the battery system, a range prediction device (RPD) has been connected to the battery. The device provides a real-time estimation of the remaining battery capability as well as residual range of the EV by means of compensated ampere-hour measurement method. The device takes care of the recharging case; it renews the value of remaining ampere-hours by adding the value of recharged ampere-hours, which are obtained by integrating the recharging current. The device also was proven to be essential for providing reliable information to the EV about the state of the charge of battery and the EV residual. The drive command, gear box, etc., are slaved under the controller. The controller gathers the information of voltage, current, brake signal, accelerator pedal position, motor speed and other signals; then the controller gives a proper control to the motor according to the designed control strategy.

3. Fuzzy Expert System Control

A fuzzy expert system as you know or you may read somewhere is a collection of membership functions and rules that uses to reason about data. Unlike conventional control methods, whose strongly relies on the accuracy of the analytic control model, which are mainly symbolic reasoning engines, fuzzy expert systems are oriented toward numerical processing. Like other control mechanisms, fuzzy control is also a feedback control system as presented in Fig. 2

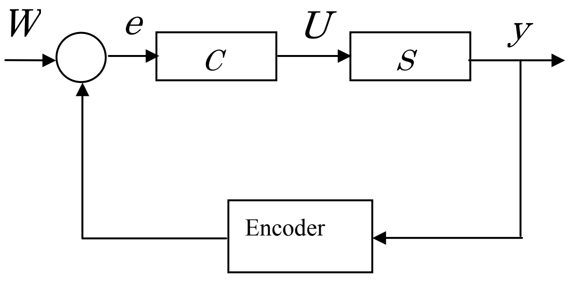

Fig.2 A feedback control system

The object to be controlled is called the *system*, denoted as *S*, which is the vehicle speed in our case. The controller denoted as *C*, is to generate a desired response of the output *y,* i.e., keeping the output *y* close to the reference point *W* (keeping *e* small). The output *U* of the controller *C*, is the control action in our application. In essence, the fuzzy control relies on a set of IF…..THEN inference rules which have the general form:

If x is A and B is y then z is C

Where, x is the input variable, and y is the output variable. The values A, B, C are expressed linguistically rather than numerical forms. Example of linguistics values is *very low, low, high, very high.* Using the concept of fuzzy set proposed by L.A Zadeh in 1965, these linguistics values can be translated into numerical values to perform calculations.

4. Control strategy using fuzzy expert system

In this section, our fuzzy expert system is described in detail. We first present the construction of its knowledge base, before describing the three main steps. The membership functions of the input variables, the membership functions of the output variables, and the creation of the rule base have been done

5. Construction of Knowledge Base

As mentioned before, the knowledge base rule in a fuzzy expert system consists of a data base and a rule base. The data base includes the membership functions of inputs and output, and the rule base contains the inference rules. Our fuzzy control system has two inputs and one output. The input variables are the speed level and the accelerator pedal position (current pedal position- desired pedal position) and throughout the rest of this paper we will note it AccPP. The accelerator pedal as for any road vehicle governs the motor speed and its position reflect the vehicle speed. The output variable is a vehicle speed that depends on the accelerator pedal position and we have used some error tolerance modulator to adjust the error speed. The input variable here is used to describe the level of the desired AccPP rate and to evaluate the perceived vehicle speed result, while the output variable is used to determine the required vehicle action. Next we need to create one set of membership functions for each input and output variable. The membership functions defined on the input variables are applied to their actual values, to determine the degree of truth for each rule premise. If a rule's premise has a nonzero degree of truth, then the rule is said to fire. Then we compute the truth value for the premise of each rule and applied to the conclusion part of each rule. This result is one fuzzy subset to be assigned to the output variable of the rule.

6. Membership functions of input variables

To define the membership function of the AccPP, we divided the range of the AccPP into five linguistic sets, Negative-Big (NB), Negative Small (NS), Zero (ZO), Positive Small (PS), and Positive Big (PB), and the membership functions are shown in figure 3. In the figure, the horizontal axis indicates the desired accelerator pedal position to be used, which is the difference between the the cuurent and expected position. The vertical axis denotes the membership value of a given AccPP. This value is used to indicate the degree to which a difference belongs to a linguistic set. For example, from the figure we can see that the degree of AccPP of 0.8 to PS is 0.6, and the degree of AccPP of 0.8 to ZO is 0.4. In this example a precise AccPP value is mapped to two linguistic sets. The objective of this research is to control the electric vehicle using on-board computer of which its operation will be done via mouse, therefore the choice of the speed to be used during each task is very important. So the speed level is divided into threecategories, "High (H)", "Medium (M)", and "Low (L)", and the membership functions are shown in figure 4. The value of 500 is the value of acceleration and deceleration time when accelerate or decelerate the motor and is set in millisecond.

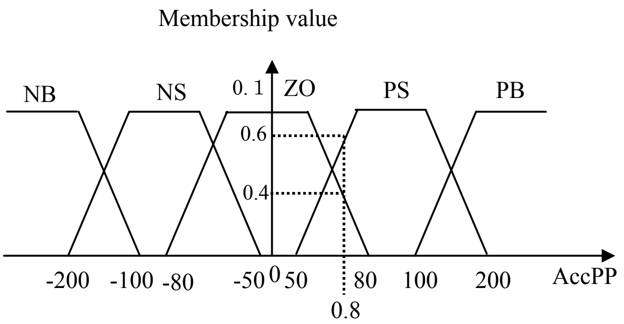

Fig.3 Membership function for input: Accelerator pedal position

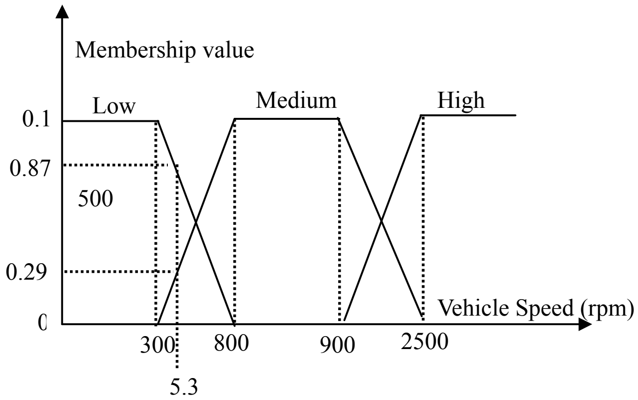

Fig.4 Membership function for input: Speed level

7. Membership functions of output variables

To define the membership function of the output variable, the value of the vehicle speed is categorized into fifteen linguistic sets, which are: LNB, LNS, LZO, LPS, LPB, MNB, MNS, MZO, MPS, MPB, HNB, HNS, HZO, HPS and HPB. We have used fifteen output linguistic sets because there are three levels of vehicle speed, L, M, H, and five levels of accelerator pedal position as follows, NB, NS, ZO, PS, PB. That results in fifteen different combination and we have used a singleton membership function to represent each of the linguistic set, as it is easy to perform defuzzification. Figure 5 shows five output singleton membership functions.

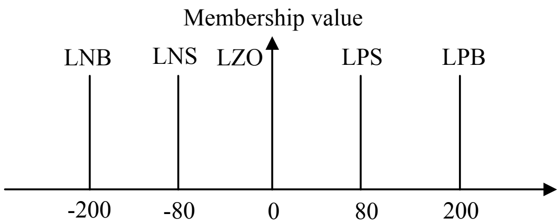

Fig.5 output singleton membership functions

To determine the singleton values for the linguistic sets, we need to perform the profiling runs. The singleton is an impulse function, and is defined by simply assigning a single numeric value to each sub-domain of the output. For example the "crisp "output of our control must be in the range between 0 and 2500 rpm and that allow us to define the speed as follows: Low speed = 300 rpm, medium speed = 900 rpm and high speed =1500 rpm. These values of the output singleton sets are used to get the exact desired speed in the linguistic sets for the three speed categories (Fig. 7, 8,9). If the values of the output singleton are not used it will be very difficult for the operator to know the speed to be selected for the vehicle navigation. Table 1 shows the parameters of the control. Column 1 shows that the speed level is categorized into three levels (H, M, L).. To obtain the singleton values for the output linguistic sets HNS, MNS, and LNS,we averaged the error tolerance modulation values for each of the three speed level categories (High, Medium, and Low). Other singleton values can be obtained in the same way.

8. Creation of rule base

In this step, we construct the fuzzy reasoning rules that governs the relations between the input and output variables. As our present system has two inputs and one output, the form of each rule is: " IF speed level is A and the accelerator pedal position is B, then the vehicle speed is C", where A is chosen from "L", "M", "H", B is chosen from "NB", "NS", "ZO", "PS", "PB" and C is a singleton output. A sample rule can be written as follows: If the speed level is L, and the accelerator pedal position is PB, then the vehicle speed is LPB. The following is the overall of the control base.

Table 1 Fuzzy reasoning rule base

	NB	NS	ZO	PS	PB
H	HNB	HNS	HZO	HPS	HPB
M	MNB	MNS	MZO	MPS	MPB
L	LNB	LNS	LZO	LPS	LPB

9. Experimental Results

The proposed algorithm was carried out using a three phase stepping motor MFA05KEV connected to an oriental rotary encoder E6C2-CWZ62 for recording data during the test operation whose specifications is given in Table 3. The output of the encoder is directly input into IN04, IN05 and IN06 of the CPU unit for using these three points as built-in high-speed counter.

Table 2 Motor parameter specifications

Rate output	0.59 kw (1H)
Max. Output	5.2 kw (3min)
Max. Revolution	6000 rpm

Power supply	72 DC V
Rate torque	98 kgf
Torque constant	0.532 kg fcm

The single-phase response speed is 5 KHz, and the two-phase response speed is 2.5 KHz. The counter value is within a range between 65,535 in incremental mode, which uses only phase A and 32,767 in decrement mode. The electrical ratings of the encoder are as follows: current consumption 80ms, maximum response frequency 100 KHz, insulation increases 100M Ω min and output phases A, B and Z (reversible). We tested the effectiveness of our fuzzy expert control system under two different scenarios. Firstly the brake signal that determines the desire braking torque is sent to the controller allowing the operator to manipulate the gear i.e., changing it from Neutral position to Drive or Reverse. The brake control part is not reported in this paper but it will be reported in the coming month. We have mentioned here in order to well explain how the algorithm has been tested. Secondly the accelerator pedal signal that determines the required vehicle speed is sent to the motor driver through the controller to drive the vehicle. The controller is required to control the motor speed very accurately to achieve and maintain speed from 0 to 2500 rpm.

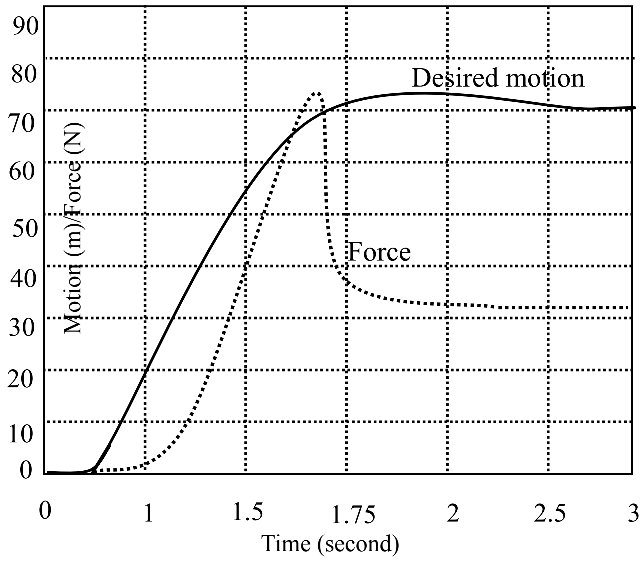

Fig.6 Motion and force trajectories

But during the test of our algorithm, we have limited the high speed to 1500 rpm in order to well control the vehicle. In the Fig.6 that shows the motion trajectory and force trajectory, the desire motion obtained consists of three segments. From the initial position of 0 m to approximately 75 m the vehicle moves progressively to the goal position in 3 minutes. The first segment from 0 m to about 67 m is the approaching phase having the fastest motion. In this phase the fuzzy reasoning created a rule base that selected the AccPP for medium speed in order to avoid producing a large impact force, which might results in loss of control. During this phase, the desired interaction force is increased from 0 to a value of 75 N at 1.65 second and decreased from 75 N to a value of 33 N at 2.3 s. The decrease of the force indicates that the vehicle is approaching to its target position, so the fuzzy reasoning again create the rule base that start to decrease the speed to a low speed before falling to zero. During the acceleration, the equilibrium position is maintained between 12.5 and 15.5 steps ahead of rotor position, and during the deceleration the equilibrium position is also maintained between 12.5 and 15.5 steps behind of rotor position, and the angle between the stator and rotor flux was kept close to 90°. The test practice has been done on the road in front of the department of electrical and electronic engineering till the venture business laboratory (VBL) that is built at the end of this road. The distance between the two buildings is approximately 150 m.

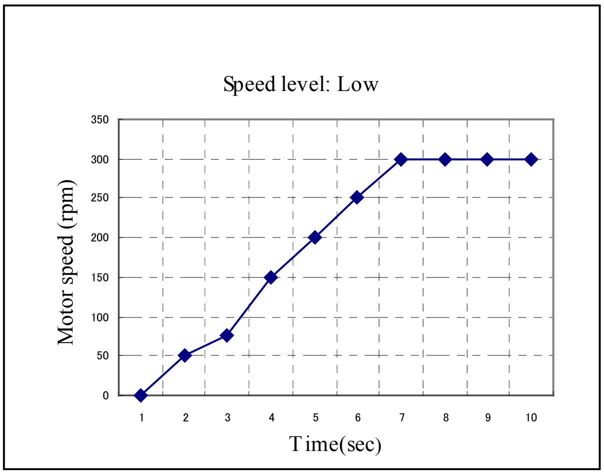

Fig.7 Low speed

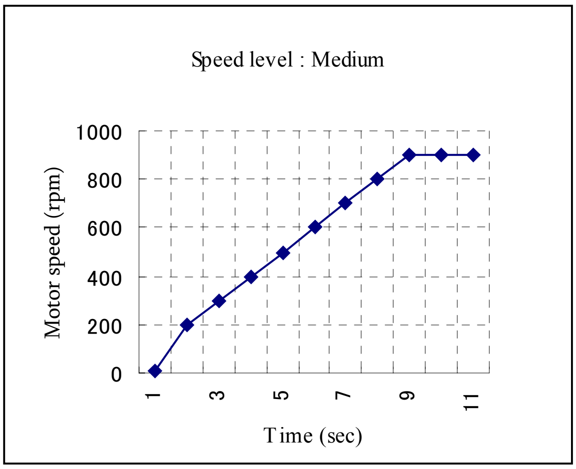

Fig.8 Medium speed

Fig.7, Fig.8 and Fig.9 show the three speed levels variation under the fuzzy expert controller and that agree with the membership function for input (speed level) shown in Fig.4 during the software design. Fig.7 and Fig.8 are the low and medium speed of which the motor increase gradually then stabilize at the corresponding limited speed level at 7 and 9 second respectively. At this stage, the vehicle keep moving smoothly without changing the speed rate till we released the acceleration pedal in order to bring the vehicle to a complete stop. When we released the acceleration pedal, the fuzzy controller through the inference rules sends a signal to the pedal. This signal is passed particularly through a sensor, which release the force applied previously to the accelerator pedal. Hence pedal release.

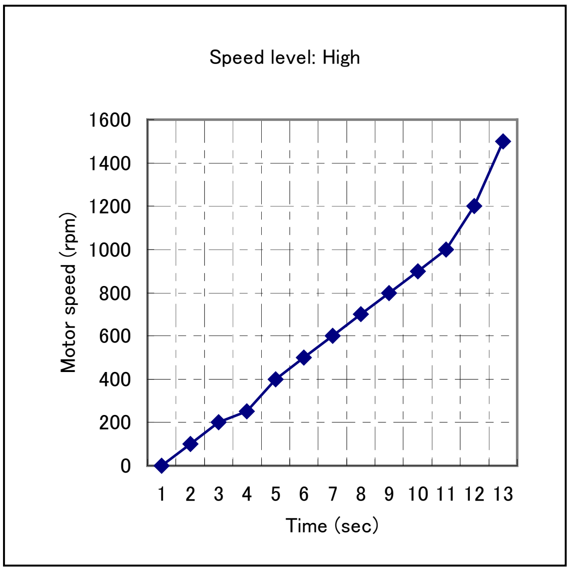

Fig.9 High speed level

In Fig.9, when the acceleration pedal signal is sent to the motor driver by the controller, again the motor starts and very quickly reaches 1000 rpm and gains its maximum peak speed of approximately 1500 rpm at around 13 Seconds, which is followed by the increase of the interaction force. The advantage of our technique is that, during the running test, if the hardware has some technical problems the controller notified the operator about the problem and stop the motor 2 second after the notification.

7. Conclusion

We have presented the EV motor speed control using fuzzy expert controller. Our algorithm allows the operator to control the vehicle without the need to have extensive knowledge about the data. It provides a continuous running performance of the vehicle, and can automatically select the desired speed level, when the speed is about to reach a certain level that can produce a large impact force, and that might results in loss of control. Since we have started to test the running perfornace of the vehice under the fuzzy expert, so far there was no overshoot and noise. In this paper the construction of the knowledge base of the fuzzy expert controlller and the following three main steps, fuzzyfication, fuzzy reasoning and defuzzification have been described.

References

1) C.C. Lee, "fuzzy logic in control system: fuzzy logic controller-part I, II." IEEE Transaction on system, Man, and cybernics. SMC-20 No.2, pp. 404-435, 1990
2) Xinyue Li and Han-Wein Shen, " Adaptive volume rendering using fuzzy logic," The Ohio state university Columbus, Department of science and information science magazine, vol. 45, pp. 56-59, 2004
3) Ch, S. Kim, W. H. Seo,, S. H. Han, S. Ch. Fan, S. H. Lee,"Fuzzy logic control of a robot manipulator based on visual servoing," Proceedings of the ISIM 2000, Oct, 4-7, kyongnam, Korea, pp 390-395.
4) Byung. Yoo, Sacheul, Jeoung, Woochl. Han, "Adaptive slinding mode control using fuzzy logic system", Proceedings of the ISIM- 2000, Oct, 4-7, kyongnam, Korea, pp. 26-29
5) C. C Chan, " speed and position control strategy for electric vehicles," IEEE Transaction on industrial electronics vol. IE-34, No.4, pp.447-456, 1987

A Harness Line Color Recognition Method Based on Fuzzy Similarity Measure

Youn Tae Kim, Hyeon Bae, Young In Kim, Sungshin Kim

School of Electrical and Computer Engineering, Pusan National University, Busan, Korea

Pusan National University 30 Changjeon-dong, Keumjeong-ku, Busan 609-735, Korea
E-mail: dream0561@pusan.ac.kr, baehyeon@pusan.ac.kr, kyi98@pusan.ac.kr, sskim@pusan.ac.kr

Abstract

Conventional methods for color separation in computer-based machine vision has weak performance because of the environmental dependency like light source, camera sensitivity, etc. In this paper, we propose an improved color separation method using RGB, HLS, color coordination space and fuzzy similarity measure. RGB that consists of red, green, blue is light's three primary colors. HLS that includes hue, light, saturation is human's color recognition elements. A fuzzy similarity measure is employed for evaluating the similarity among fuzzy colors with six features in RGB and HLS. Color recognition system for the harness line is designed and implemented as a testbed to evaluate the physical performance. The proposed color separation algorithm is tested with different kind of harness lines.

Keywords: color recognition, fuzzy entropy, fuzzy measure

1. Introduction

By the development of high efficiency computer recently, image processing algorithm and improvement of image devices helped test systems to improve the performance. What is called, it is given a name field that is artificial vision. Artificial vision is not concept of conventional contact-based sensor but concept of information-based sensor that comes from videotex in short or long distance using camera. The status of target is recognized through suitable digital image processing algorithm or numerical solution.

Many parts of several functions in the artificial vision are implemented and used for industrial equipments. But, the part of color recognition has still many problems to be solved. One of the underlying problems is the subject measurements that come from several values according to strength, direction, and color temperature of light and quality of the material of product. We normally try to recognize and represent an object as one color but the object consists of many color elements which is called natural color.

If a red color electric line in harness line is captured from camera, we recognize the line as a red color but the information of the pixels includes variable colors such as brown, black, etc. Because of these problems, the conventional color recognition methods in natural color image has many restricts. Many intelligent methods have been developed to overcome these problems. Several intelligent approaches for color recognition are:

- Fuzzy colors
- Neural networks
- Fuzzy similarity measure

But, intelligence methods generally require too many arithmetic operations to handle complicated algorithm.

In this paper, we propose a simple algorithm for natural color recognition with low computational burden. First, the HLS color coordination system that converted from RGB information is introduced. The HLS color coordinate system is similar to the human's color recognition system. Second, fuzzy memberships based upon the RGB and HLS information is represented. Third, fuzzy similarity measure of each color are computed and compared for the color recognition. Finally, the proposed algorithm is applied to the harness line color recognition system and the performance is discussed.

2. RGB and HLS Color Coordination

2.1 RGB

RGB coordinate of reflex gives us information about three dimensional spaces that consist of red (R), green color (G) and blue color (B). Three dimensional spaces are represented as a color cube. Here, the origin of the cube displays and means pure black. Color density is increased as the value in the each axis of coordinates is receded from origin. Image device that follows NTSC rules basically shows the RGB information. Image processing based on RGB information has an advantage in time aspect because the pretreatment process is not necessary. For these reasons, RGB color coordinate system is more popular than other color coordinate systems in image processing until present.

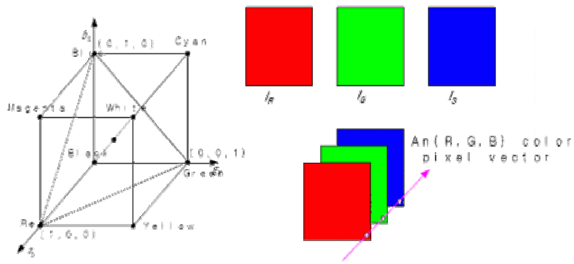

Fig. 1 RGB color cube.

2.2 HLS

The coordination of human's color recognition for an object is based upon the HLS color coordination (hue, light and saturation) [2]. Alternative method to express color information consists of hue, saturation and light. The hue marks color frequency that is represented as chromaticity graph as shown in Fig. 2. The saturation mixing with white and density expresses luminance of object or realized brightness. Structure of this coordinate is cone style. Distance is density from cone top and position of archetype. Cross section of cone is hue and distance from origin to outside is saturation. The hue is put according to order of spectrum (on right from observer red and left blue, green). HLS is color space that marks brightness to specified frequency fastest.

Proved that more correct recognition is possible than RGB in color recognition by H. Palus, D. Bereska. For these reason, HLS information through HLS conversion of RGB is utilized by means of color awareness along with RGB information.

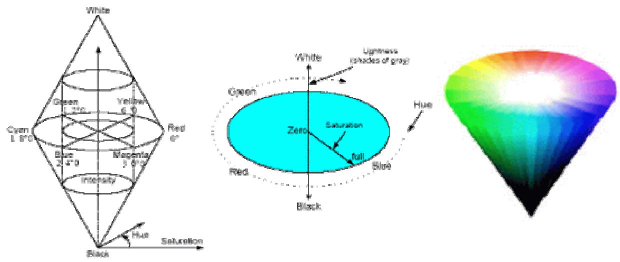

Fig 2 HLS Graph.

2.3 HLS Conversion Using RGB Information

HLS can be easily converted from RGB information by the following arithmetic expressions.

$$r=\frac{R}{255},\ g=\frac{G}{255},\ B=\frac{B}{255} \qquad (1)$$
$$I_{\max}=\max(r,g,b),\ I_{\min}=\min(r,g,b)$$

$$H=\begin{cases} 60*\left(\frac{g-b}{I_{\max}-I_{\min}}\right) & if\ \ r=I_{\max} \\ 60*\left(2+\frac{g-b}{I_{\max}-I_{\min}}\right) & if\ \ g=I_{\max} \\ 60*\left(4+\frac{g-b}{I_{\max}-I_{\min}}\right) & if\ \ b=I_{\max} \\ 0 & if\ \ I_{\max}=I_{\min} \end{cases} \qquad (2)$$
$$H=H+360 \quad if\ \ H<0$$

$$L=\frac{I_{\max}-I_{\min}}{2} \qquad if\ \ H<0 \qquad (3)$$
$$L^{'}=1-\frac{|L-0.5|}{0.5}$$

$$S=\begin{cases} 0 & if\ \ I_{\max}=I_{\min} \\ \frac{I_{\max}-I_{\min}}{I_{\max}+I_{\min}}*L^{'} & if\ \ L<0.5 \\ \frac{I_{\max}-I_{\min}}{2-(I_{\max}+I_{\min})}*L^{'} & otherwise \end{cases} \qquad (4)$$

3. Fuzzy Similarity Measure

In this section, we introduce some preliminary results of fuzzy measures. Measure of fuzziness is an interesting topic in the fields of pattern recognition or decision theory. Measure of crisp set can be determined by classical mathematical study, whereas the concepts of fuzzy measures and fuzzy integrals had been proposed by Sugeno[8]. Recently, Liu suggested three axiomatic definitions of fuzzy entropy, distance measure and similarity measure as Definitions [9]. Among these definitions, we used fuzzy similarity's concept for color recognition.

Definition 1 [9] A real function $s: F^2 \rightarrow R^+$ is called a similarity measure on $F(X)$ if d satisfied the following properties:

(S1) $s(A,B)=s(B,A),\ \ \forall A,B\in F(X)$

(S2) $s(A,A^c)=0\ \ \forall A\in F(X)$

(S3) $s(D,D)=\max_{A,B\in F} s(A,B),\ \ \forall D\in P(X),$
$\forall A,B\in F(X)$

(S4) $\forall A,B,C\in F(X), if\ A\subset B\subset C, then\, s(A,B)$
$\leq s(A,C)\, and\ s(B,C)<s(A,C)$.

Above definitions are the axiomatic, Liu also pointed out that there is an one-to-one relation between all distance measure and all similarity measures, $d+s=1$.

We used a mathematical expression in equation (5) as a similarity measure that satisfies definition 1.

$$s(M_1,M_2)=\frac{\sum_{i=1}^{n}\min(\mu_{M_1}(i),\mu_{M_2}(i))}{\sum_{i=1}^{n}\max(\mu_{M_1}(i),\mu_{M_2}(i))} \qquad (5)$$

4. Experimental Results

4.1 Color Recognition Using Fuzzy Similarity Measure

We verify, in this section, the proposed color recognition algorithm and demonstrate experiment result that uses fuzzy similarity measure. First we make color fuzzy membership functions for RGB and HLS. 100 samples are acquired from color information for each color in image to make color distribution. We make distribution of acquired RGB and HLS information that converted from RGB information.

The prepared data use to generate membership information through the following calculation:

$$\mu_M(i) = \frac{n}{N} \qquad i = 0,1,\cdots 255 \quad ,if\ R,G,B,L,S \quad (6)$$

Where μ_M are membership values, n is number of member data and N is the number of whole data. But a hue is different from the other data, discontinuous data. Because of this reason we don't make hue membership information.

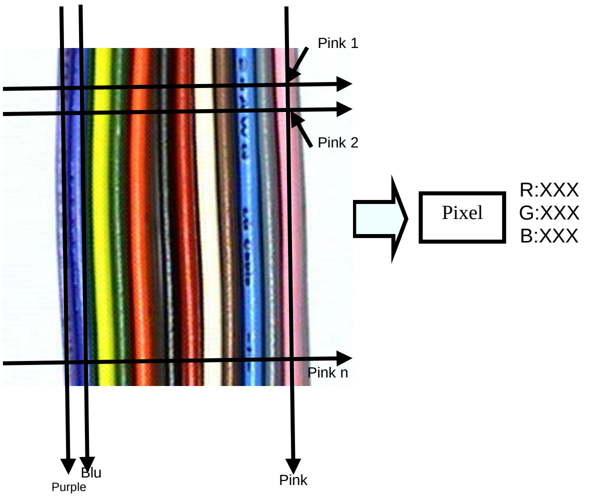

Fig 3 Gathering color information.

In this research, our sample of color information acquired from harness image of twelve different colored lines. The following among line of other colors, red line's color information will R, G, B, L and S distributions of each line.

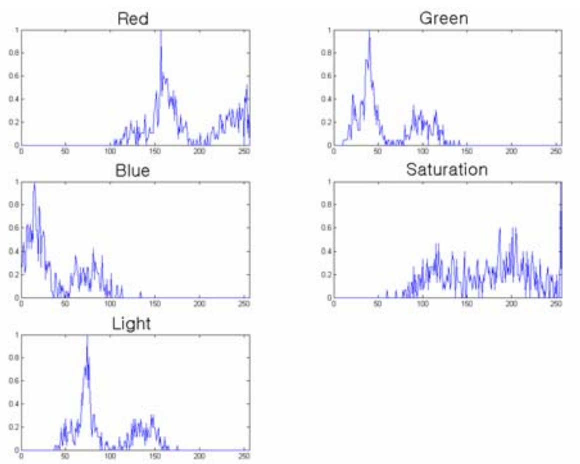

Fig. 4.2 Distribution graph of R, G, B, L, S (red line).

Figure 4.2 is non-convex form. It doesn't treat to fuzzy set. Also, connect out-line of this distribution chart apply concept to compensate information that was lost by digitizing and then changed in form of fuzzy membership.

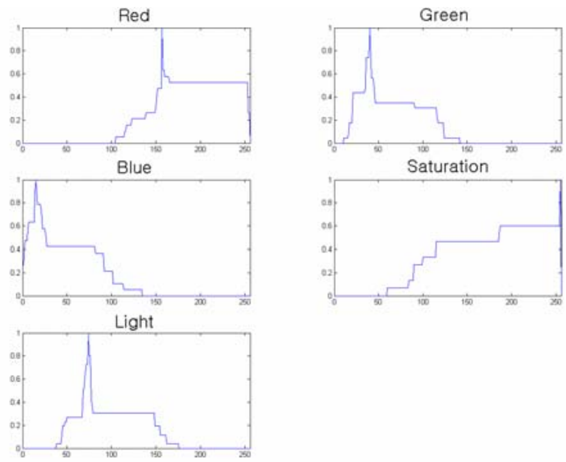

Fig. 4.3 Fuzzification of color distribution (red line).

Color of Harness line that used by this research has pink, blue, white, black, violet, blue, green, yellow, orange, red, brown and gray of 12 colors.

After data of a set that consist of 12 colors makes membership by prior method, compare template fuzzy membership to unknown fuzzy membership in each color.

In table 1, you can see distribution special quality of each color Hue values. Various Hue values appear in achromatic color, but chromatic color has only one hue value. It can gain advantage that may not do comparison calculation between unnecessary each membership except achromatic color using this nature.

Table 1 Color distribution by hue value

Hue value	Colors
0 value (Red like)	BROUN, RED, ORANGE, PINK
120 value (Green like)	GREEN
240 value (Blue like)	BLUE, SKY-BLUE
Uniformly distributed	BLACK, YELLOW, PURPLE, GRAY, WHITE

After consider this Hue condition, we can recognize the color using fuzzy similarity measure method and we have displayed red and gray color recognition result of algorithm.

Table 2 Results of color recognition (red line)

Input data	Red line, Hue values are all 0.				
Comparison (Red like)	**R.**	**G.**	**B.**	**S.**	**L.**
Brown	0.2084	0	0.0219	0.0329	0.0635
Red	0.2344	0.4468	0.4624	0.5773	0.3813
Orange	0.0044	0.0152	0.2181	0.5549	0.0223
Pink	0.0630	0	0	0	0.0016
Max value	0.2344	0.4468	0.4624	0.5773	0.3813
Result	Red	Red	Red	Red	Red

Table 3 Results of color recognition (blue line)

Input data	Blue line, Hue values are all 240.				
Comparison (Blue like)	**R.**	**G.**	**B.**	**S.**	**L.**
Blue	0.4461	0.2980	0.6661	0.5961	0.4786
Sky Blue	0.4439	0.1788	0.0975	0.3427	0.1972
Max value	0.4461	0.2980	0.6661	0.5961	0.4786
Result	Blue	Blue	Blue	Blue	Blue

Table 4 Results of color recognition (gray line)

Input data	Gray line, Hue values are uniformly distribute				
Comparison (Red like)	**R.**	**G.**	**B.**	**S.**	**L.**
Black	0.0082	0.0055	0.0081	0.0092	0.1188
Yellow	0.0361	0.0105	0	0.3073	0
Gray	0.2609	0.2921	0.3252	0.5952	0.3063
Purple	0.1338	0.0995	0.6525	0.3144	0.0855
White	0.0038	0.0056	0.2633	0.0460	0.3243
Max value	0.2609	0.2921	0.6525	0.5952	0.3243
Result	Gray	Gray	Purple	Gray	Gray

4.2 Color Recognition Using Fuzzy Similarity

We manufacture the harness line color recognition system on the basis of algorithm that introduced in session 4.1 and verified performance. Fig 4.2 shows this system and tested harness. System of Fig 4.2 can recognize harness's line color and distinguishes whether order of line is right.

Fig 4.2 Test system and picture of harness.

We confirmed the recognition rate of actuality Harness's line color using this system. Harness that used in experiment has 12 colors (order of black, brown, red, ash color, blue, green color, blue color, yellow, orange, pink, violet and white). Result of an experiment appeared to Table 5. An experiment has 10th trial and show the 100% recognition rate.

5. Conclusion

Color recognition which use color information of a pixel or mean value of neighbor pixels that is method that is accomplishing main current in existent research had limit. In this paper, we did so that can analyze color distribution of objects that describe person's index process to a these alternative method and color recognition is more exactly.

Table 5 Results of harness's line order recognition

Tested harness's line order: BK BR RD GY SB GR BL YL OR PK PP WH												
No.	Test Result (Order of Harness's line color)											
1	BK	BR	RD	GY	SB	GR	BL	YL	OR	PK	PP	WH
2	BK	BR	RD	GY	SB	GR	BL	YL	OR	PK	PP	WH
3	BK	BR	RD	GY	SB	GR	BL	YL	OR	PK	PP	WH
4	BK	BR	RD	GY	SB	GR	BL	YL	OR	PK	PP	WH
5	BK	BR	RD	GY	SB	GR	BL	YL	OR	PK	PP	WH
6	BK	BR	RD	GY	SB	GR	BL	YL	OR	PK	PP	WH
7	BK	BR	RD	GY	SB	GR	BL	YL	OR	PK	PP	WH
8	BK	BR	RD	GY	SB	GR	BL	YL	OR	PK	PP	WH
9	BK	BR	RD	GY	SB	GR	BL	YL	OR	PK	PP	WH
10	BK	BR	RD	GY	SB	GR	BL	YL	OR	PK	PP	WH

References

[1] Rafael C. Gonzalez and Richard E. Woods, "*Digital Image Processing*," Prentice Hall, 2002.

[2] Been-Chian Chien and Ming-Cheng Cheng, "*A Color Image Segmentation Approach Based on Fuzzy Similarity Measure*," IEEE, 2002.

[3] Cox, E. *The Fuzzy Systems Handbook*, Academic Press Professional, pp.21-105, 1994.

[4] Klir, G. J. and Folger, T. A., *Fuzzy Sets, Uncertainty, and Information*, Pretice-Hall, Englewood Cliffs, 1988.

[5] Takagi, H. and Hayashi, I., "*NN-Driven Fuzzy Reasoning*," International Journal of Approximate Reasoning, Vol. 5, pp.191-212, 1991.

[6] S. Wesolkowski, R. D. Dony, and M. E. Jernigan, "*Global color image segmentation strategies: Euclidean distance vs. vector angle*," Nueral Networks for Signal Processing 4. Proceedings of the 1999 IEEE Signal Processing Society Workshop, pp 419-428, 1999.

[7] D. Yining, B. S Manjunath, and H. Shin, "*Color image segmentation*," Computer Vision and Pattern Recognition, IEEE Computer Society Conference, Volume 2, 1999.

[8] Z. Wang and G. T. Klir, *Fuzzy measure theory*, New York : Plenum Press, 1992.

[9] B. Kosko, *Neural Networks and Fuzzy Systems*, Prentice-Hall, Englewood Cliffs, NJ, 1992.

An Electric Power Steering Control by Fuzzy logic in HILS system

Mun Ki Lee, Sung Ki Ha
Department of Interdisciplinary Program in Mechatronics
Pusan National University
Busan, 609-735, KOREA

Ju Yong Choi
Department of Mechanical and Intelligent Systems Engineering
Pusan National University,
Busan, 609-735, KOREA

Man Hyung Lee
School of Mechanical Engineering,
Pusan National University,
Busan, 609-735, KOREA

Abstract

This paper discusses a DC motor equipped electric power steering (EPS) system and demonstrates its advantages over a typical hydraulic power steering (HPS) system. The tire-road interaction torque at the steering tires is calculated using the 2 d.o.f. bicycle model, which is verified with the J-turn test of a real vehicle. By using hardware-in-the-loop simulation(HILS), the control responses of the vehicle are obtained. In previous EPS systems, the assisting torque for the measured driving torque is developed as a boost curve similar to that of the HPS system. To improve steering stiffness and returnability of the steering system, assisting torque map is determined by fuzzy logic.

1 Introduction

Recently the automotive industry has focused on improving vehicle performance, safety and convenience for drivers. Steering assist systems play an important role in each area. The conventional HPS system, which is made up of an engine-driven hydraulic pump and a hydraulic actuator, decreases engine efficiency but requires complex hydraulic components. To cope with the deficiencies of HPS, an EPS system has been vigorously researched. Since the EPS system uses an engine-independent motor without complex hydraulic units, the weight and volume of steering systems can be reduced. Thus, EPS systems achieve better fuel and space economy and maintains the feel of the steering even during quick changes in driving conditions through software. Moreover no harm is done the environment because no hydraulic fluid is used [1].

To improve steering stiffness and returnability of the steering system, steering feel should be set up. Adams, F. J. [2] researched the feel of power steering and Norman, K. D. [3] introduced on center handling performance. Gary P. Bertollini and Robert M. Hogan [4] drew up a preference curve as a function of vehicle speed based on the effort needed for steering by various drivers using VTI driving simulators. Rakan C. C. and Le Yi Wang [5] used boost curves of assist torque for a given vehicle speed. Based on these objective indices, Camuffo, et al [6] tuned an EPS to have the steering feel of an HPS. Generally EPS systems are controlled by comparing the measured steering torque with the reference steering torque. Using a steer-by-wire EPS, Tong Jin Park, et al [7] utilized the steering wheel motor to alter the steering feel according to vehicle speed and controlled the front wheel motor by PID Control to minimize the error between steering angle and wheel angle. With steering wheel angle and torque sensors attached to a steering column, Anthony W. Burton [1] calculated assistance torque by summing the high gain related to steering torque and the low gain related to steering position. To improve returnability, M. Kurishige, et al [8] developed a control strategy based on an estimation of alignment torque generated by tires and road surfaces without sensors. Since steering torque assistance and returnability are not active at the same time, Kim and Song [9] separated the two control algorithms where the reference steering torque was determined by the torque map based on vehicle speed and steering wheel position.

In this paper, the 2 d.o.f. bicycle model will be used to calculate the tire road interaction torque. Although the steering of a vehicle affects its rolling motion, a description of the rolling system is beyond the scope of this dissertation since an EPS does not control the active driving angle but the assisting torque. In previous EPS systems [5], assisting torque for the measured driving torque was making a chart as a boost curve like the HPS of Adams's research [2]. In the research of Kim and Song [9], the reference steering torque depended on vehicle speed and steering wheel angle by encoder. The evaluated assisting torque map by fuzzy logic will be simulated in HILS system [10]. The fuzzy logic is useful for nonlinear system and decision making for controllers.

The organization of the paper is as follows: Chapter 2 describes a vehicle system and a hydraulic servo system and verifies the mathematical models for the vehicle system. Chapter 3 presents HILS system for EPS. In chapter 4, the assisting torque map is proposed by fuzzy logic. The control results in HILS are discussed in chapter 5. Finally, the main conclusions are given in chapter 6.

2 Tire-road Interaction Torque

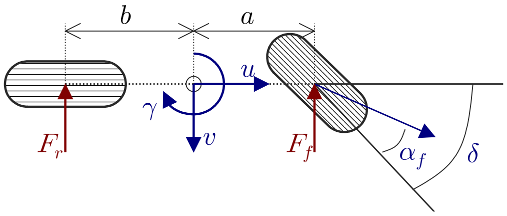

Fig. 1. Coordinate of the single-track model

To find the tire-road interaction torque, τ_t, the kingpin torque [11] is obtained as

$$\tau_k = \tau_V + \tau_L + \tau_A \quad , \tag{1}$$

where τ_V and τ_L are the vertical torque and the lateral torque, respectively. And the third term, τ_A, is aligning torque. Because of the kingpin offset angle, d, and a lateral inclination angle, λ, the vertical force, F_z, on the tire produces the vertical torque, τ_V. When the kingpin offset angle and the lateral inclination angle are small, the vertical torque generated by the vertical force can be approximated by

$$\tau_V = -F_z\, d \sin\lambda \cdot \sin\delta, \tag{2}$$

where δ is the steering angle. Since the lateral force, F_y, acting at the tire center produces a torque through the longitudinal offset resulting from the caster angle, the lateral torque generated by the lateral force is given by

$$\tau_L = F_y\, r_t \tan\nu, \tag{3}$$

where r_t is a tire radius and ν is a caster angle. The lateral force, F_y, is developed by a tire at a point behind the tire center. So the aligning torque is written as

$$\tau_A = p_t F_y \cos\sqrt{\lambda^2 + \nu^2}\ , \tag{4}$$

where p_t is the pneumatic trail distance. Considering the length from kingpin to rack-bar, the rack-bar force is written by

$$F_r = \frac{\tau_k}{\{l_0 \cos(\theta_0 - \delta) + l_0 \cos(\theta_0 + \delta)\}} \quad , \tag{5}$$

where l_0 is the length of the tie-rod and θ_0 is the tie-rod angle.
The ground reactions on the tire are described by

$$\tau_t = F_r \cdot r_p, \tag{6}$$

where r_p is the radius of the pinion. Additionally the friction torque, τ_f, is defined as follows:

$$\tau_f = C_{fric} \cdot \mathrm{sign}(\dot\theta)\,. \tag{7}$$

where C_{fric} is the friction gain. Although the steering system has more complex frictions, these are ignored here. The classical single-track model [12] is obtained by lumping the two front wheels into one wheel in the centerline of the vehicle, the same is done with the two rear wheels as shown in figure 1. For the lateral direction and the yaw axis, the vehicle kinetics at the center of gravity (C.G.) are describes as

$$m\, a_y = 2(F_f + F_r)\,, \qquad I_{zz}\dot\gamma = 2a(F_f - F_r)\,, \tag{8}$$

where a_y and γ are the lateral acceleration and the yaw rate, m and I_{zz} are the vehicle total mass and the yaw moment of inertia, F_f and F_r are the lateral forces at the front and the rear tire, and a is the distance from the vehicle C.G. to front axle. Since tires can be modeled as linear within $|a_y| \le$ 0.3 g, the lateral forces at the front and the rear tires are obtained as

$$F_f = C_f \cdot \alpha_f, \quad F_r = C_r \cdot \alpha_r, \tag{9}$$

where C_f and C_r are the front and the rear cornering stiffnesses. Usually to verify the steering performance, a J-turn test is fulfilled. For the verification, the steering wheel angle, θ, is stepped up to 34° within 0.2 sec when the longitudinal velocity, u, is 22 m/s. Figure 2 shows the J-turn results for the single-track model and the actual vehicle. The lateral acceleration, a_y, and the yaw rate, γ, settled to around 3.4 ㎨ and 8.3 deg/s. The integrals of time muliplied by the absolute magnitude of the error (ITAE) for the lateral acceleration and the yaw rate are 0.29 ㎨ and 0.42 deg/s, where the nonlinearity of the tire may be the main factor for the errors. As a result, the single-track model has characteristics almost similar to the actual vehicle's. A hydraulic servo system is used for realization of the lateral force in HILS system. In this paper, there are several assumption. A velocity difference between going and returning is regarded as disturbance, servo valve is symmetric, supplied-pressure and falling-pressure at the valve orifice are constant, returned-pressure is zero, and there is no loss of friction at the pipe.

3 HILS System for an Electric Power Steering

For the design, implementation and testing of control systems, some actuators are real, and the process and the sensors are simulated. The reason is that actuators and the control hardware very often form one integrated subsystem, also actuators are difficult to model precisely and to simulate in real time. By using this HILS, the effects of faults and failures of actual sensors and computers on the overall system can be tested in spite of extreme and dangerous operating conditions. The expenditure of developing cost and time can be cut down since experiments are reproducible and frequently repeatable [13]. Especially, HILS systems are useful for the active or semi-active vehicles. By using HILS, the control responses of the vehicle for the various conditions of speed, steering angles, and disturbances are obtained precisely, safely, cheaply, and rapidly. The tire-road force related to the vehicle dynamics is calculated by software and is exerted on rack-bar by hydraulic actuator, where steering torque is measured by torque sensor attached on the steering column. Steering system organized by steering wheel, steering column, and rack-bar is embodied in hardware. In figure 2, ECU makes the EPS motor generate a proper torque which is dependent on vehicle speed, u, and measured driving torque, τ_s. A hydraulic actuator controlled by a servo-valve realizes lateral force, which is calculated steering wheel angle by potentiometer and vehicle speed by dial. By Visual

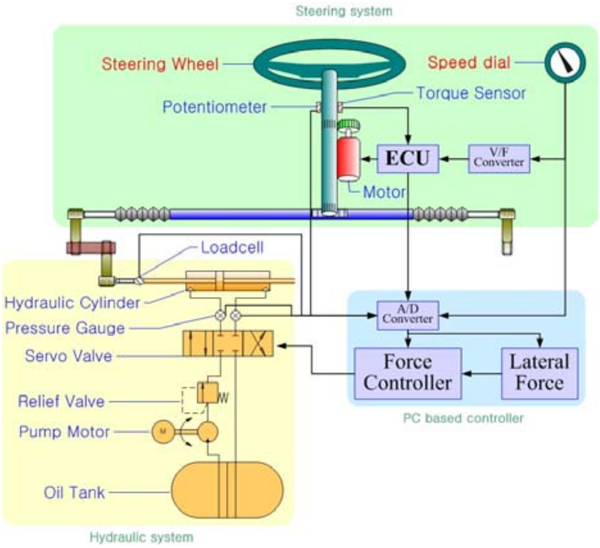

Fig. 2. Constitution of HILS system

C++ under MS window 98, the 2 d.o.f. vehicle dynamics yields lateral force, yaw rate, and lateral acceleration. To control the hydraulic actuator precisely, LMI based H_∞ controller is used and the force is measured by loadcell. And also the output of sensors are displayed by indicators and an emergency button is setup for the malfunction. The EPS (C-EPS of KOYO SEIKO Co.) mounted on a column axis provides an assist force to a column shaft via a worm gear. The optimal value of a current required for a motor is calculated by ECU (Electronic Control Unit), based on a electric signal from a torque sensor and a signal from a vehicle speed sensor. The torque sensor sends the signal depending on a torsional angle of a torsion bar mounted in the inner part of a column axis, which is proportional to a steering force. This EPS system adopts a brushless DC motor which has a lot of advantages versus a brushed motor. By non-contact electronic switching of brushless motor, the life cycle is lengthened, and the absence of brushed and commutator enables the motor to be downsized and reduces the noise of it. In addition, lower inertia of the brushless motor gives good steering feel because there is no permanent magnets as the rotor [16]. Commonly, it is not necessary to measure a steering wheel angle, since an EPS system is related with a steering torque. However, lateral force in the HILS system is determined by the vehicle speed and the steering wheel angle, which is measured by a potentiometer(Model 534, Vishey Co.). The resolution of measured angle is doubled by 2:1 gear between the potentiometer and the steering column. Vehicle speed has influence on the lateral force at tire and the EPS system. By dial-gauge equipped potentiometer, vehicle speed is set up in the HILS system. The realized speed as analog voltage is adopted by DAQ and used for the calculation of the lateral force. However, ECU (Electronic Control Unit) in vehicles recognizes the speed by accumulating the pulse of speed. So the speed as voltage type should be converted to the pulse type.

The output range of frequency is tuned by 104 μF condenser, where the maximum frequence is 200 Hz for the maximum speed of vehicle, $u_{\max}$ =83 m/s. The servo-valve is a proportional valve, direct operated, which provides both directional and non-compensated flow control according to the electronic reference signals. This operates in association with electronic drivers, which supplies the proportional valves with correct current signal to align valve regulation to the reference signal supplied to the electronic driver. This valve has a 4-way spool, sliding into a 5-chambers and directly operated by solenoids. In order to make the accurate lateral force, axile force on rack bar should be measured and controlled. Sensors and actuators in the HILS system need the sources of electricity. Because they are operated by DC, transformer with bridge circuit converts AC into DC. To stabilize the supplied voltage, linear voltage regulators and condensers are used, where the suppling states are checked by LED. The sensor signals are acquired by PIC-MIO-16X-4 of National Instrument Co.

4 Steering Feel and Assisting Torque Map

Vehicle dynamics and steering systems behave strongly nonlinear which causes difficulties in developing a classical controller system. Fuzzy logic however facilitates such system designs and improves tuning abilities [10]. A Fuzzy logic controller is used to give a desired assisting torque. The longitudinal speed of a vehicle, u, and the measured torque, τ_m, are applied to a Fuzzy controller. The membership functions are composed of the triangular and the trapezoidal functions. Table 1 shows the rule base for the Fuzzy controller. By the Mamdani's fuzzy implication and the max-min composition, the control surface is made up as shown in figure 3.

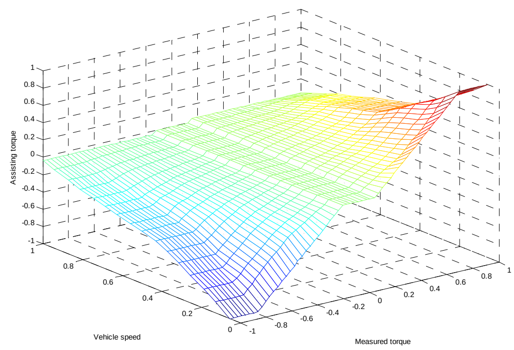

Fig. 3. Normalized control surface

Table 1. Fuzzy rule-base for EPS controller

u \ τ_m	NB	NM	NS	ZE	PS	PM	PB
ZERO	NX	NB	NM	ZE	PM	PB	PX
LOW	NB	NM	NS	ZE	PS	PM	PB
MID	NM	NS	NS	ZE	PS	PS	PM
HIGH	NS	NS	NS	ZE	PS	PS	PS

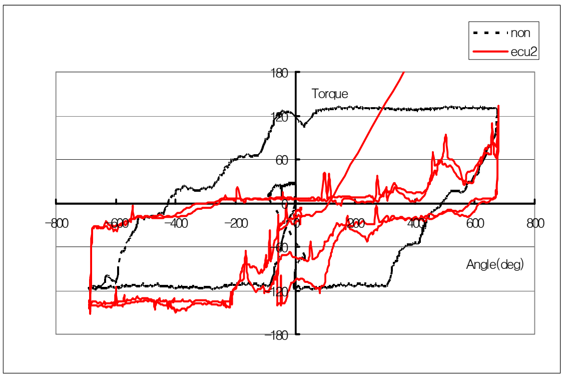

Fig. 4. Plot of steering angle vs. steering torque (u = 0 m/s)

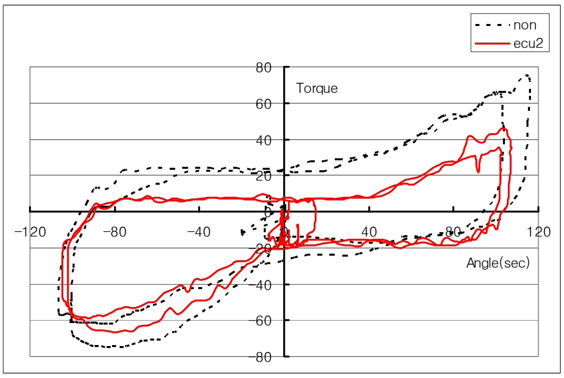

Fig. 5. Plot of steering angle vs. steering torque (u = 11.1 m/s)

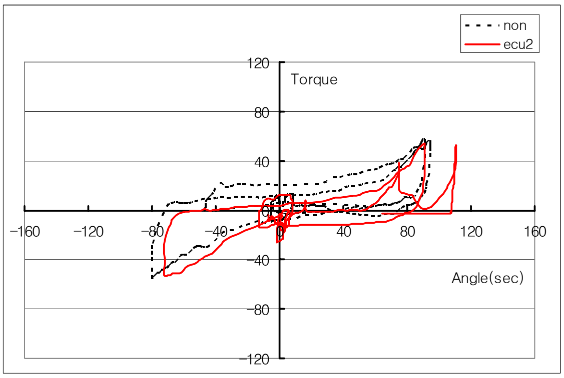

Fig. 6. Plot of steering angle vs. steering torque (u = 16.6 m/s)

5 Experimental Results

Figures 4-6 show the plots of steering wheel angles versus steering torques. When a vehicle is stopped as shown in figure 1, the EPS system helps a driver to park. As the speed of vehicle is increased, the assisting torque by the EPS system is decreased.

6 Conclusions

In this paper, the vehicle model utilized 2 d.o.f. bicycle model and was verified by the J-turn test of a real vehicle. We introduced a cubic curve as a torque map. To improve steering stiffness and returnability of the steering system, assisting torque map was drawn by fuzzy logic. This proposed torque map waw simulated in HILS system with a real steering system. By using this map, the EPS system was improved sufficiently.

Acknowledgements

This research was financially supported by Korea Science and Engineering Foundation(KOSEF) through the Engineering Research Center for Net Shape and Die Manufacturing(ERC/NSDM) at Pusan National University and by Pusan National University Research Grant.

References

[1] Anthony W. Burton, "Innovation Drivers for Eletric Power-Assisted Steering," *IEEE Control Systems Magazine*, pp. 30-39, 2003.

[2] Adams F. J., 1983, "Power Steering Road Feel," *SAE Paper* 830998, 1983.

[3] Norman K. D, "Objective evaluation of On-center Handling Performance," *SAE Paper* 840069, 1984.

[4] Gary P. Bertollini, Robert M. Hogan, "Applying Driving Simulation to Quantify Steering Effort Preference as a Function of Vehicle Speed," *SAE Paper* 1999-01-0394,1999.

[5] R. C. Chabaan, L. Y. Wang, "Control of Electrical Power Assist Systems : H∞ design, torque estimation and structural stability," *JSAE Review* 22, pp. 435-444, 2001.

[6] I. Camuffo, G. Caviasso, L. Pascali, M. Pesce, E. Alviano, "Simulation Tools and Evaluation Criteria for Steering Wheel Feel Improvement of an Electric Power Steering System," *SAE Paper* 2002-01-1593, 2002.

[7] Tong Jin Park, et al, "The Design of a Controller for the Steer-by-Wire System Using the Hardware-In-the-Loop-Simulation System," *SAE Paper* 2002-01-1596, 2002.

[8] M. Kurishige, et al, "A New EPS Control Strategy to Improve Steering Wheel Returnability," *SAE Paper* 2000-01-0815, 2000.

[9] J. H. Kim, J. B. Song, "Control Logic for an Electric Power Steering System Using Assist Motor," *Mechatronics* 12, pp. 447-459, 2002.

[10] F. Tahami, R. Kazemi, and S. Farhanghi, "A Novel Driver Assist Stability System for All-Wheel-Drive Electric Vehicles," *IEEE Transactions on vehicular technology*, Vol. 52, No. 3, pp. 683-692, 2003.

[11] Thomas D. Gillespie, *Fundamentals of Vehicle Dynamics*, SAE Inc., pp. 284-291, 1992.

[12] J. Y. Choi, et al, "Lateral Control of Autonomous Vehicle by Yaw Rate Feedback," *KSME International Journal*, Vol. 16, No. 3, pp. 338-343, 2002.

[13] R. Isermann, J. Schaffnit, and S. Sinsel, "Hardware-in-the-loop simulation for the design and testing of engine-control systems," Control Engineering Practice 7, pp. 643-653, 1999.

The Tenth International Symposium on Artificial Life and Robotics 2005(AROB 10th '05),
B-con Plaza, Beppu, Oita, Japan, February 4-6, 2005

The Analysis for the Movement Characteristics of the Flying Object with Genetic Algorithms

Ryuji Goto
Graduate School of IT Professional Course,
Hosei University:1914-7, Kosuzume-cho,Totsuka-ku,Yokohama-shi 244-0004, Japan
E-mail: rgoto@paw.hi-ho.ne.jp

Yuji Sato
Faculty of Computer and Information Science,
Hosei University:3-7-2, Kajino-cho, Koganei-shi
Tokyo 184-8584, Japan
E-mail: yuji@k.hosei.ac.jp

Abstract

Issues such as multiobjective optimization, time-series prediction, the analysis from noisy observation data, and the solution of implicit functions are all crucial in the consideration of real world problems, and research into the applicability of evolutionary computer techniques to these problems has already begun [1–9,13]. However, there are only a few examples of studies where evolutionary computer techniques have been applied to problems that involve all of these issues at the same time. One such examples are previous studies in which we reported on the effectiveness of genetic algorithms (GA) as a tool for tracking objects as they move towards a destination while making evasive maneuvers in order to avoid pursuit or attack. In another study, we reported on the effectiveness of GA as a tool for tracking objects in the earth orbit. All our previous reports are based on the active observed data. In this paper, we verify the applicability of GA to the problem of analyzing the movement characteristics of flying objects based on only passive observed data. **Key words:** Tracking, Analysis based on observed passive data, Analysis from noisy data.

1 Introduction

In previous reports, we considered the two dimensional movement of an object whose evasive motion was assumed to consist of constant-velocity straight-line, simple sinusoidal and sawtooth motion [10, 11]. In another previous report, we considered the three dimensional path elements of the moving objects in a earth orbit whose motion consists of circles, ellipses [12]. These previous analysis are based on active observed data gathered by radar, laser or active sonar. In this paper, we report the three dimensional movements analysis for the flying object like a fighter in the air, from passive observed data without the active observed data. The passive observed data means that they can be gathered by the observation equipment in its surveillance mode without radiation of electric-magnetic wave(EMW), only by observation of the EMW radiated by the flying object. The passive observed data consist of the bearing and elevation angles from observer. Active observed data means that they can be gathered by the observation equipment in its radiation mode of the EMW. Active observed data contain distance component.

The movement characteristics to be analyzed based on the passive observed data must contain the distance components. If the flying object is enemy aircraft for the observer, the observer should not radiate the EMW for concealing the existence of observer itself, because the enemy aircraft may starts counter attack operation to the observer. Therefore, the analysis for the movement characteristics of the flying object based on the passive observed data has the tactical meanings. The movement characteristics are the present distance, the velocity and the three dimensional proceeding course of the flying object. The other hand, to analyze the movement characteristics of the flying object rightly from only the passive observed data, it is necessary that the removal observer changes the velocity or course of itself at least one times during the analysis, because there are infinite solutions in case of no changing of the velocity and course of observer. This can be took the place by the plural foxed position observers arranged different places. Even though, the movement of the flying object has constant velocity and course in short period, this analysis has the problems such as described in the beginning of abstract.

2 Tracking of a Flying Object in the Air

2.1 Earth Surface coordinates and Movement Characteristics of the Flying Object

The relationship between the earth surface coordinates *xyz* and the movement characteristics is illustrated in Figure 1. This shows a flying object is proceeding to the destination. Its velocity and course are assumed as constant in the period of analysis. The velocity is V. East-West(x) components of velocity V is Vx. North-South(y) components is Vy. Radius direction of the earth component(y) is Vz. Proceeding horizontal course measured clockwise from the north direction (y) of the flying object is Cmh, vertical course measured upward from surface is Cvm. Initial position of the observer is $Xo(t0)$,$Yo(t0)$,$Zo(t0)$. This point is the origin of the earth surface coordinates. Exact values of them are 0, 0, 0. The position of the observer at time tn is $Xo(tn)$, $Yo(tn)$, $Zo(tn)$. Initial position of the flying object is $Xm(t0)$, $Ym(t0)$, $Zm(t0)$ and position of time tn is $Xm(tn)$, $Ym(tn)$, $Zm(tn)$. The observer observes the bearings and elevations of flying object intermittently as removing on the ground. This removal observer must change its velocity or course at least one times during the analysis because there are infinite solutions in case of no changing. This can be took

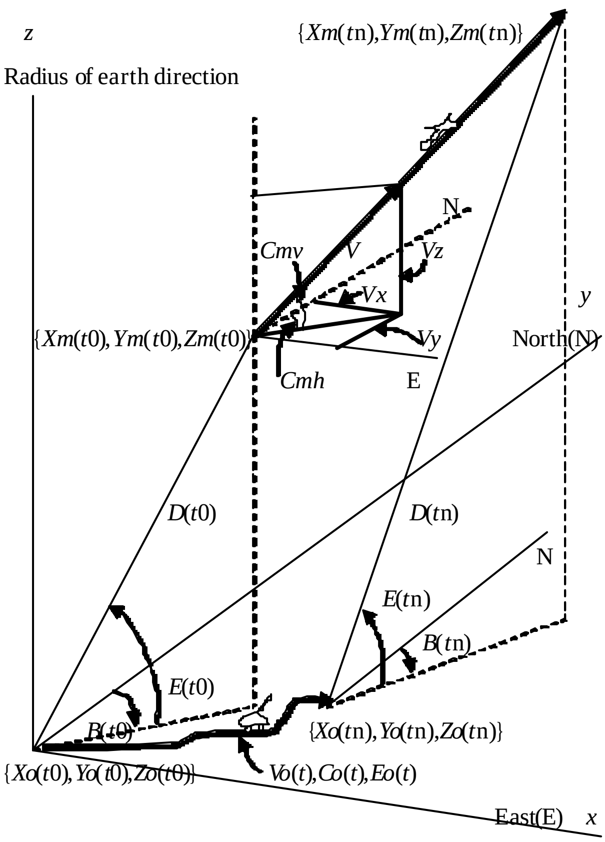

Xo(*tn*):observer X position of time *tn*
Yo(*tn*):observer Y position of time *tn*
Zo(*tn*):observer Z position of time *tn*
Xm(*tn*):mover X position of time *tn*
Xm(*tn*):mover Y position of time *tn*
Xm(*tn*):mover Z position of time *tn*
B(*tn*):bearing of time *tn*
E(*tn*):elevation of time *tn*
D(*tn*):distance of time *tn*
V:velocity of mover
Vx:East(*x*) component of *V*
Vy:North(*y*) component of *V*
Vz:Radius of earth(*z*) component of *V*
Cmh:mover horizontal course
Cmv:mover vertical course
Vo(*t*): observer velocity of time *t*
Co(*t*): observer horizontal course of time *t*
Eo(*t*): observer vertical course of time *t*

Figure 1: The movement of the flying object and the observer at time from *t*0 to *tn* in the coordinates *xyz*.

the place by the plural fixed position observers arranged different places. Initial bearing is $B(t0)$ and bearing at time tn is $B(tn)$. Initial elevation is $E(t0)$ and elevation at time tn is $E(tn)$. Intial distance from observer to the flying object is $D(t0)$ and distance at time tn is $D(tn)$.

2.2 Formulation of Analysis for the Movement Characteristics of the flying object

In the following, we show the relationship between the inferred values of the movement characteristics—initial distance $D(t0)$, East-West components of velocity Vx. North-South components of velocity Vy. Radius direction of the earth component velocity Vz —and flying object's bearing $B(tn)$ and elevation $E(tn)$ at time tn.

Position of the observer at time tn is expressed by equation (1).

$$\left.\begin{aligned} Xo(tn) &= \int_{t0}^{tn} Vo(t)\cos Eo(t)\cos Co(t)dt \\ Yo(tn) &= \int_{t0}^{tn} Vo(t)\cos Eo(t)\sin Co(t)dt \\ Zo(tn) &= \int_{t0}^{tn} Vo(t)\sin Eo(t)dt \end{aligned}\right\} \text{......(1)}$$

Position of the flying object at time $t0$ is expressed by equation (2) as the function of initial distance $D(t0)$.

$$\left.\begin{aligned} Xm(t0) &= D(t0)\cos E(t0)\sin B(t0) \\ Ym(t0) &= D(t0)\cos E(t0)\cos B(t0) \\ Zm(t0) &= D(t0)\sin E(t0) \end{aligned}\right\} \text{............(2)}$$

Position of the flying object at time tn is expressed by equation (3) as the function of x,y,z component of flying object's velocity.

$$\left.\begin{aligned} Xm(tn) &= Xm(t0) + Vx*(tn-t0) \\ Ym(tn) &= Ym(t0) + Vy*(tn-t0) \\ Zm(tn) &= Zm(t0) + Vz*(tn-t0) \end{aligned}\right\} \text{...............(3)}$$

Distance x,y,z components of the flying object from the observer at time tn is expressed by equation (4).

$$\left.\begin{aligned} Dx(tn) &= Xm(tn) - Xo(tn) \\ Dy(tn) &= Ym(tn) - Yo(tn) \\ Dz(tn) &= Zm(tn) - Zo(tn) \end{aligned}\right\} \text{.....................(4)}$$

Distance at time tn is expressed by equation (5).

$$D(tn) = \sqrt{(Xm(tn)-Xo(tn))^2 + (Ym(tn)-Yo(tn))^2 + (Zm(tn)-Zo(tn))^2} \text{......................(5)}$$

Bearing at time tn is expressed by equation (6).

$$B(tn) = \tan^{-1}\frac{Xm(tn)-Xo(tn)}{Ym(tn)-Yo(tn)} \quad \text{..........................(6)}$$

Elevation at time tn is expressed by equation (7).

$$E(tn) = \tan^{-1}\frac{Zm(tn)-Zo(tn)}{\sqrt{(Xm(tn)-Xo(tn))^2+(Ym(tn)-Yo(tn))^2}} \quad \text{....(7)}$$

Velocity of the flying object is expressed by equation (8).

$$V = \sqrt{Vx^2+Vy^2+Vz^2} \quad \text{..................(8)}$$

Horizontal course of the flying object is expressed by equation (9).

$$Cmh = \tan^{-1}\frac{Vx}{Vy} \quad \text{............................(9)}$$

Vertical course of the flying object is expressed by equation (10).

$$Cmv = \tan^{-1}\frac{Vz}{\sqrt{Vx^2+Vy^2}} \quad \text{.....................(10)}$$

Accordingly, the problem addressed in this paper — i.e., that of analyzing the three dimensional movement of a flying object — can be formulated as an inverse problem involving complex implicit functions where it is necessary to find the four characteristics—initial distance $D(t0)$, velocity x component Vx, y component Vy, z component Vz—of a flying object by working backwards from noisy time-series observations of its bearing and elevation obtained from the observer. The present distance $D(tn)$, velocity V, horizontal course Cmh, vertical course Cmv of the flying object are calculated from $D(t0)$, Vx, Vy, Vz by equation (5), (8), (9), (10).

3 Method to Apply Genetic Algorithms

3.1 The Movement Characteristics Determined by Genetic Algorithms

Four movement characteristics — initial distance $D(t0)$, flying object velocity x component Vx, y component Vy, z component Vz — constitute a complex implicit function, so we will try to use genetic algorithms to determine their values. Initial distance $D(t0)$ can be biased by offset value because observer can detect the existence of the flying object before it approach to certain minimum area of distance to the observer. If bias value is $Dbias$, GA operation value for initial distance Dga is $D(t0)$-$Dbias$.

3.2 Chromosome Coding Method

We defined chromosomes respectively corresponding to the characteristics──initial distance Dag and flying object velocity x component Vx, y component Vy, z component Vz. And we expressed a single individual as a set of these characteristics as sub chromosomes. But the sub-chromosome of the initial distance Dga and the velocity Vx,Vy,Vz consist of different length bits according to range of its value and necessary resolution. The initial distance Dga consists of integer 18 bits, velocity of Vx,Vy,Vz consists of integer 17 bits.

The physical range over which each sub chromosome are expressed are set considering the possible range of distance and velocity of flying object, analysis period of time and the observation precision of passive observations. Assumed range of initial distance is 50,000m~200,000m, assumed range of velocity is ±500m/sec and assumed bearing and elevation error is less than 0.1degree. Analysis period of time to get effective accuracy should be less than 100sec.

The minimum units of these sub chromosome are set as follows by considering above conditions: initial distance $D(t0)$ is 1m, flying object velocity component Vx, Vy, Vz is 1/100m/sec. In exact physical calculation of this simulation, initial distance $D(t0)$ is biased by constant value $Dbias$=50,000m (Dga= $D(t0)$-$Dbias$).

3.3 Fitness Function

We determine the angles error between the observed angles(bearing and elevation) data of the moving object and the angles data inferred by GA, and we defined the fitness of an individual based on the reciprocal of the square root of the sum of these errors. The fitness function is shown in Equation (11).

$$f = k(n+1)/\{\sum_{i=0}^{i=n}\sqrt{dB(ti)^2+dE(ti)^2}\} \quad \text{..................(11)}$$

Where

$$dB(ti) = esB(ti) - oB(ti), \quad dE(ti) = esE(ti) - oE(ti)$$

Here, $esBti$, $esEti$ are the bearings and elevations estimated by GA at time ti, $oBti$ and $oEti$ are the bearings and elevations observed at time ti, $n+1$ is the number of observations, and k is a suitable constant. For example, case of k=1, it is set so that f=1.0 when the average angle difference is 1.0 degree.

3.4 Genetic Operation

The method for selecting the group of individuals carried forward to the next generation from the current generation is shown in Figure 2. All individual (the total number of chromosomes)P sent from the previous generation is evaluated by calculation of fitness and sorted in descending order. Fixed proportion E from the highest fitness individual is retained as elite, and the number of discarded individuals are supplemented by roulette selection to preserve the original population P. M (=P-E) is the number of discarded individuals. Making up of the deficit for M is done as follows. One pair of individual is chosen as parent by roulette selection from all individual P of the current generation. The sub chromosomes Dga, Vx, Vy, Vz of this one pair of individual is then subjected to single point crossover between each of the same kind of sub chromosomes independently (i.e. crossover between Dga and Dga, Vx and Vx, Vy and Vy, Vz and Vz,of both individual) to produce one pair of child individual.

After crossover operation, all sub chromosome of produced one pair child individual is subjected to spontaneous mutation independently. Through the crossover and spontaneous mutation processes, one pair of new individual is produced and carried forward to the

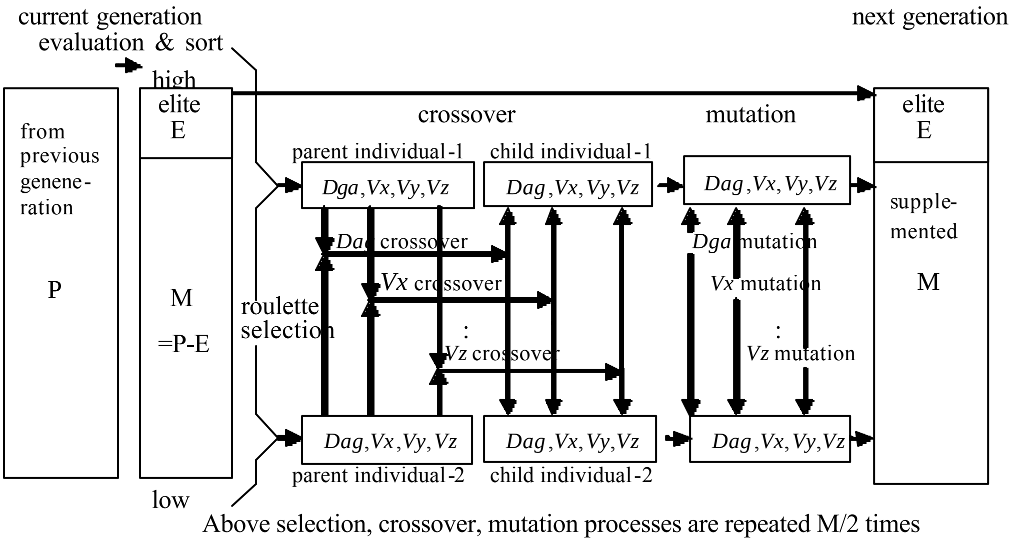

Figure 2: Flowchart of genetic operation. 1 pair of chromosome is selected by roulette selection, and crossover and spontaneous mutation are done for each sub-chromosome respectively.

next generation. Above processes are repeated until the making up of the deficit for M is completed (M/2 times). In preliminary trials we found two phenomena.

The first of those phenomena is that the solution starts to converge around the 20th generation, so for subsequent generations we reduced the spontaneous mutation rate for all sub chromosomes. We did those to avoid destroying the sub chromosome that had already approached convergence. In the exact simulation, the spontaneous mutation rate is changed from the 20th generation onwards as described in Section 4.2 Simulation Data. The results of the reducing the spontaneous mutation rate is described in Section 4.3 Results of Simulation.

The second phenomenon is as follows. From the 10th generation onwards, new two type individuals (chromosome) are effective for the earlier convergence. One of them is calculated as much 2% uniform random numbers of the sub chromosomes contained in the fittest individual of the current generation. The other is calculated as much 2% uniform random numbers of the sub chromosomes contained in the roulette selected individuals from the current generation. The number of these new two type individual are 10% for total number of individual. The results of the supplement the modified sub chromosomes is described in Section 4.3 Results of Simulation.

4 Evaluation Tests

4.1 Evaluation Method

We made a software system shown in Figure 3 for the evaluation of this research. This system consists of three modules of software, Observed data Generator, Estimated value Generator and Estimated value Evaluator. They do cooperative works for evaluation.

Observed data Generator

Based on the theoretical movement characteristics of a flying object provided by the operator, the observed data generator calculates the theoretical values of the object's, bearing (Bti) and elevation (Eti) at time ti for 1-second intervals from the time $t0$ at which the observation starts. It then adds normal random number errors $ebti$ and $eeti$ to the calculated theoretical values to simulate the errors produced by an observation system, such as electric magnetic wave beam fluctuations, instrumentation errors, and conversion errors, to produce the observed bearing ($oBti$) and observed elevation ($oEti$).

As the observation time ti is increased, the observed data generated for experimental use are stored along with the observation time ti in the database for observed data. This observation data gathering cycle is continued until simulation ends.

Estimate value Generator

The Estimated value Generator generates the estimated bearing ($esBti$) and estimated elevation ($esEti$) based on estimated sub chromosomes in the chromosomes. The initial values of the sub chromosomes are set randomly to values in the defined ranges by using uniform random numbers. and uses genetic algorithms to renovate the estimated values of sub chromosomes. The values of $esBti$ and $esEti$ ($t0 \le ti \le tn$) are calculated by Equations (6), (7) based on the renovated values of sub chromosomes. These renovated $esBti$ and $esEti$ are sent to the Estimated value Evaluator.

Next, we will describe how the GA is used to renovate the estimated values of the sub chromosome. In the Estimated value Generator, the values of $esBti$ and $esEti$ corresponding to each individual are sent to the Estimated value Evaluator.

Next, based on the received fitness values, the method described in section 3.4 is used to select the fittest individuals and perform crossovers and spontaneous mutations, thereby updating the generation i.e., renovating the estimated values of the sub chromosomes.

Here, the renovating of the estimated values of the sub chromosomes using a genetic algorithm is started at the point when a certain set of observed data is stored into the

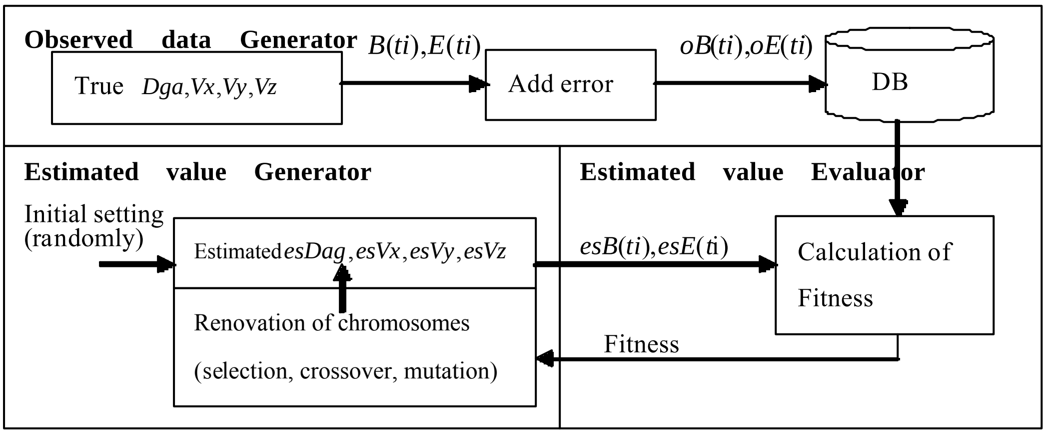

Figure3: The flowchart of GA evaluation system. The GA evaluation system consists of Observed data Generator, Estimated value Generator and Estimated value Evaluator.

database for observed data. Spontaneous mutation rate are changed at around convergence generation of the analysis in order to broaden the search space before convergence and to avoid destroying the solution after convergence.

Estimated value Evaluator

For every observation time, the Estimated value Evaluator calculates the fitness of each individual according to Equation (11) based on the values of the observed bearing (*oBti*) and elevation (*oEti*) input from the database for observed data and the estimated bearing (*esBti*) and estimated elevation (*esEti*) input from the Estimated value Generator. These calculated fitness values are sent to the Estimated value Generator, where they are used for genetic manipulation. The above processes of generating observed values, generating estimated values and performing evaluation are repeated until a stopping criterion is met. The stopping criterion was taken to be the fulfillment of either of two conditions: that an individual appears whose fitness exceeds a preset standard fitness, or that the number of generations of genetic manipulation becomes greater than a certain value.

4.2 Simulation Data

In this simulation, the parameters of genetic operation were set as follows:
(1)maximum genetic manipulation generation:50 (2) observed data set prior to GA start: 60 (3) number of total individuals: 6000 (4)number of elite:60 (5)crossover ratio: 0.8 (6)spontaneous mutation rate: 0.00001 before the 20th generations, and 0.000005 from the 20th generation onwards.

The physical parameters are as follows:
(1) Initial distance : 150000m (2) Initial bearing : 5.0deg
(3) Initial elevation : 5.0deg (4) Velocity of flying object : 340m/s (5): Horizontal-course of flying object:110.0deg
(6) Vertical-course of flying object : 5.0deg (7)observing: by two observers arranged 5km apart. (8) observation error (maximum) : 0.004 deg, 0.020deg, 0.100deg

4.3 Results of Simulation

Figure 4 shows how the best fitness for three kinds of error of the observation vary with the number of generations in cases where the movement of the flying object is assumed to be linear movement. To obtain a maximum fitness value of 1.0, the fitness *fg* on the vertical axis in this figures is the normalized value obtained from the relationship $fg = 1 - 1/f$, where f is the fitness defined in Equation (11). The observations are made at 1-second intervals by the observer having an bearing and elevation observation errors. At the time of

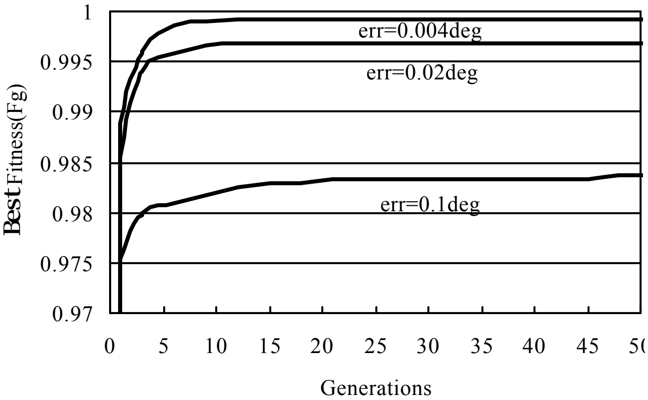

Figure4: The maximum and average fitness for generations.

Table1: The accuracy of analyzed initial distance $D(t0)$, velocity component *Vx, Vy, Vz*, velocity *V*, horizontal course *Cmh* and vertical course *Cmv*.

sub-chromo	$D(t0)$(m)	Vx(m/s)	Vy(m/s)	Vz(m/s)
theory	150000	333.6	-58.8	29.6
err=0.004o	37	0.1	0.1	0.1
err=0.020o	155	0.6	1.2	0.2
err=0.100o	522	0.8	4.0	0.3

out put	V(m/s)	Cmh(deg)	Cmv(deg)
theory	340.0	100.0	5.0
err=0.004o	0.1	0.0	0.0
err=0.020o	0.5	0.2	0.1
err=0.100o	0.6	0.7	0.2

the 60th observation (i.e., 60 seconds after the observations are started), the first generation of GA starts. Figure 4 shows the best fitness (Fg) of three kinds of observation error grow up sharply and they converge around at 7~15th generation. The fitness of the observation error 0.004deg grows up at the earliest generation. The fitness of observation error 0.1deg grows up last. Table 1 shows the accuracy of the analyzed movement characteristics (sub chromosomes) for the three kinds observation error at the 50th generation. The accuracy of the observation error 0.004deg is the best and the accuracy of observation error 0.1deg is the worst among three kinds of error. Reducing the spontaneous mutation described in Section 3.4 Genetic Operation is effective for the early convergence by several %. New two type chromosomes described in Section 3.4 effects to make the convergence generation earlier by more than 10%. These data are average values of 20 trials.

4.4 Discussion

From the above experimental results, it can be judged that by applying GA to the analysis for the movement characteristics of a flying object whose four characteristics are all unknown, it is possible to analyze these values only from time-series values of the observed bearing and elevation of the flying object obtained from observation equipment. Since the analysis results are all based on observation data, it can be judged that the necessary time for the completion of analysis is effected by the errors contained in observed bearing and elevation. The smaller the errors contained in observed data are, the faster and the more accurately the analysis completes. However, even though, the errors contained in the bearing and elevation extend to around 0.1 degrees, the accuracies of the results and the completion time of the analysis are still in effective range.

To shorten the analysis time, we must do furthermore investigation for the effect of the parameters of GA. These parameters are number of stored data prior to analysis start, number of chromosome, number of elite, crossover rate and mutation rate. Also, we must deepen the quantitative analysis of the effectiveness of reducing spontaneous mutation and new two type chromosome described in Section 4.3 Results of simulation.

5 Conclusion

As a problem including various issues such as multiobjective optimization, time-series prediction, the analysis from noisy observation data, and the solution of implicit functions, we have investigated the applicability of genetic algorithms to the analysis of the three dimensional and dynamic linear movement of a flying object in the air based on the passive observed data. In the future ,we aim to demonstrate that genetic algorithms are suitable for solving three dimensional and non linear movement analysis problems for objects moving in the air and seawater by expanding this technique in a practical amount of time and practical level of precision. Also, we aim to demonstrate that genetic algorithms are suitable for the more wide and complex analysis for the facts in the noisy data.

References

[1] Oakley, H.: Two Scientific Applications of Genetic Programming: Stack Filters and Non-Linear Equation Fitting to Chaotic Data. in K.E. Kinnear, Jr (ed.), Advances in Genetic Programming, pp. 369-389, The MIT Press (1994).

[2] Reynolds, C.W.: Evolution of Obstacle Avoidance Behavior: Using Noise to Promote Robust Solutions. In K.E. Kinnear, Jr (ed.), Advances in Genetic Programming, pp. 221-241, The MIT Press (1994).

[3] Sato, Y., and Nagaya, S.: Evolutionary Algorithms that Generate Recurrent Neural Networks for Learning Chaos Dynamics. Proc. The 3rd. IEEE Intl. Conf. on Evolutionary Computation, pp. 144-149 (1996).

[4] Tamaki, H., Kita, H., and Kobayashi, S.: Multi-Objective Optimization by Genetic Algorithms: A Review. Proc. The 3rd. IEEE Intl. Conf. on Evolutionary Computation, pp. 517-522 (1996).

[5] Beyer, H-G., and Arnold, D.V.: Fitness Noise and Localization Errors of the Optimum in General Quadratic Fitness Models. Proc. The 1999 Genetic and Evolutionary Computation Conference, pp. 817-824 (1999).

[6] Parmee, I.C., and Watson, A. H.: Preliminary Airframe Design Using Co-Evolutionary Multiobjective Genetic Algorithms. Proc. The 1999 Genetic and Evolutionary Computation Conference, pp. 1657-1665 (1999).

[7] Blumel, A.L., Hughes, E.J., and White, B.A.: Fuzzy Autopilot Design Using A Multiobjective Evolutionary Algorithm. Proc. The 2000 Congress on Evolutionary Computation, pp. 54-61 (2000).

[8] Yoshihara, I., Aoyama, T., and Yasunaga, M.: GP-Based Modeling Method for Time Series Prediction with Parameter Optimization and Node Alternation. Proc. The 2000 Congress on Evolutionary Computation, pp. 1475-1481 (2000).

[9] Tominaga, D., Koga, N., and Okamoto, M.: Efficient Numerical Optimization Algorithm Based on Genetic Algorithm for Inverse Problem. Proc. The 2000 Genetic and Evolutionary Computation Conference, pp. 251-258 (2000).

[10] Goto R., and Sato Y.: Motion Analysis of Moving Objects with Genetic Algorithms. Proc. The 2001 Genetic and Evolutionary Computation Conference, pp.1276-1283 (2001).

[11] Goto R., and Sato Y.: Applicability of Genetic Algorithms to Motion Analysis of a Moving Object. Proc. The 2002 Congress on Evolutionary Computation, pp. 765-770 (2002).

[12] Goto R., and Sato Y.: Analysis for the Path of an Object in Earth Orbit with Genetic algorithms. Proc. The 2004 Artificial Life and Robotics, pp. 253-258 (2004).

[13] Goto R., and Sato Y.: The Analysis for the Characteristics of Time Series Signals with Genetic Algorithms. Proc. The 2004 International Conference on Computing, Communications and Control Technologies, Volume I, pp. 267-272 (2004).

The Tenth International Symposium on Artificial Life and Robotics 2005(AROB 10th '05),
B-con Plaza, Beppu, Oita, Japan, February 4-6, 2005

Proposal of Serially and Dynamically Separating Genetic Algorithm and Its Application to Optimization of Robot Control Systems

Koichi NAKAYAMA[1),2)] Hirokazu MATSUI[3)] Katsunori SHIMOHARA[2)] Osamu KATAI[1)]
1) Graduate School of Informatics, Kyoto Univ.
2) ATR Network Informatics Lab. 3) Faculty of Engeenering, Mie Univ.
Address 2-2-2 Hikari-Dai, Keihanna Science City, Kyoto 619-0288, Japan
voice: [+81](0774)95-1098; e·mail: knakayama@atr.jp

Abstract

In this paper, we propose a Serially and Dynamically Separating Genetic Algorithm (sDS-GA), and apply it to optimize an agent-oriented control system for an intelligent robot. The conventional DS-GA is inapplicable as a learning algorithm for a single hardware unit such as an intelligent robot. By the extension of a dynamically separating mechanism, the proposed sDS-GA becomes applicable as an optimization algorithm for a single hardware unit. We conducted experiments with sDS-GA that optimize the parameters of a control system for an intelligent robot called MieC. The sDS-GA obtained not short-term but long-term optimality. We also found that sDS-GA is efficient for the optimization of an actual intelligent robot under an unknown and dynamic environment.

1 Introduction

There have been many studies of control systems for robots[1, 2]. In particular, many intelligent robots operate by agent-oriented programming. However, in agent-oriented programming, it is difficult to design the entire agent optimally beforehand. In this paper, we focus on a Dynamically Separating Genetic Algorithm (DS-GA)[3, 4] as an optimization algorithm for agents in an intelligent robot that is controlled by agent-oriented programming.

An intelligent robot must be designed taking the following into account. It has to do various processing at the same time, such as target determination, image processing, data transferring, and arm and wheel control. The priority of the processing changes in response to the influences of external factors and internal factors, such as interaction with humans, and the residual quantity of the battery. The optimal parameters for processing are dynamically changed by these factors. As such, an adaptation algorithm is required.

In the environment of an actual robot, there is a time lag between the decision of the agent's action and the action of the robot. Whether or not the action is appropriate is determined after a certain time's passing. In order to optimize the control system of an actual robot, because of the above environment, an algorithm that can obtain not short-term but long-term optimality is required.

DS-GA has the ability to increase system-level optimality by the autonomous learning of agents based on local information by using the dynamic separation of the agent's interaction. In other words, system-level information emerges from collective agent-level information by "Swarm-Sensing," which is a characteristic of DS-GA. We expect that extended DS-GA will have the ability to increase long-term optimality by the autonomous learning of agents based on short-term information.

The conventional DS-GA uses the dynamically separating mechanism of its agents. However, in the case where an agent controls a single hardware unit such as an intelligent robot, the DS-GA is inapplicable as a learning algorithm for a robot. In order to optimize a single hardware unit that is designed by an agent-oriented control system such as an intelligent robot, we extend DS-GA to form a Serially and Dynamically Separating Genetic Algorithm (sDS-GA) that includes the time-separating mechanism of the agents.

In DS-GA, many agents act simultaneously, and the interactions of many agents are restricted in a colony. In sDS-GA, a control-agent is chosen serially and the influence of the agent's action is decreased with time. In order to reduce an interaction with an agent that belongs to other colonies, the agents who belong to the same colony are chosen continuously.

In order to verify the validity of the proposed sDS-GA, we applied the sDS-GA to an object tracing task for a Movable Intelligent Evolutional Computer (MieC) as an actual robot.

The Tenth International Symposium on Artificial Life and Robotics 2005(AROB 10th '05),
B-con Plaza, Beppu, Oita, Japan, February 4-6, 2005

2 Serially and Dynamically Separating Genetic Algorithm (sDS-GA)

In this section, we propose the Serially and Dynamically Separating Genetic Algorithm (sDS-GA) as an applicable DS-GA for an actual robot. The conventional DS-GA uses dynamic separation as follows. Agents that are separated into colonies act simultaneously. The interactions of agents are restricted in a colony, and an agent cannot contact any agent that belongs to another colony. The colonies change dynamically according to the number of agents they contain. When the number of agents in a colony increases, the colony is divided into two halves. A colony is extinguished when the number of agents it contains becomes 0.

We propose sDS-GA for use as a control system for an actual robot. The basic idea of sDS-GA is as follows. In sDS-GA, control-agents are separated into colonies. Agents in a colony control a robot in a period serially. In a certain period, control-agents who belong to a certain colony are chosen randomly, and they control the robot serially. In the next period, control-agents who belong to the next colony are chosen randomly, and they control the robot serially.

As a result, the interval of control by an agent that belongs to the same colony is much shorter than the interval of control by an agent that belongs to other colonies. In other words, the influence by a certain agent's action is strong for the agent that belongs to the same colony, and weak for the agent that belongs to other colonies. Serial separation is realized by such a mechanism. We show the main routine of the algorithm using sDS-GA in **Fig. 1**.

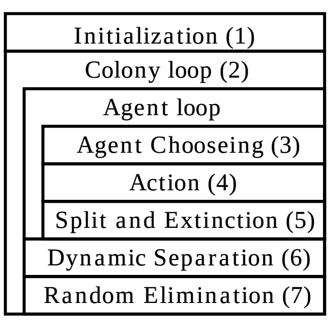

Figure 1: Main routine of the sDS-GA shown by NS chart.

Specifically, in the experiments described in this paper, the evolution of a population is based on the split or extinction of agents according to their private performance, e.g., accumulated profit. Consequently, an agent's autonomy is not spoiled and agents can still learn by means of evolution. The learning algorithm used by the DS-GA is as follows.

(1) Initialization: $N_A(t)$ agents at $t = 0$ are created and separated into colonies. The number of agents in a colony is $N_{Lim}/2$. The evaluation value of an agent a, $E_A(a,t)$, is initially set to $E_A(a,0)$ and its action determination gene, $Gene_{Act}(a)$, is initially randomly chosen.

(2) Colony Loop: Every colony takes charge of the control in order.

(3) Agent Choosing: An agent is chosen from the colony for robot control randomly.

(4) Action (Robot control of agent): The agent acts for robot control. Details are shown in section 3. The agent changes its own evaluation value based on the result of the action.

(5) Split and Extinction of Agents: An agent is split into two agents when the evaluation value by an agent becomes more than twice the initial value ($E_A(a,0)$). The two agents inherit half of the original agent's evaluation value. An action gene is mutated according to the mutation probability P_{mut}. An agent is extinguished from the colony when its evaluation value becomes less than or equal to zero.

(6) Dynamic Separation of Colonies: When the number of agents in a colony exceeds the limit N_{Lim}, the agents are separated into two half-colonies. The difference in the number of agents between the two colonies is either 1 or 0.

(7) Random Elimination: When the total number of agents that can exist in the robot control system becomes greater than the initial number of agents (N_{Lim}), a colony is eliminated at random.

In the experiments, the number of initial agents was set to $N_A(0) = 100$, the number of maximum agents in a colony was set to $N_{Lim} = 20$, the mutation probability $P_{mut} = 0.1$, and the initial accumulated profit $E_A(a,0) = 100$ for all agents.

3 Experiment

Each agent has an evaluation value for its own task achievement, and has no information about the other task achievements. We think that the total of their evaluation values is maximized, so that the system becomes optimal. But, it is not always maximized as an entire system, even if each agent acts in order to maximize its task achievement, i.e., the system may have a dilemma on a task achievement such as the following. An agent may be unable to use computer resources to do a task, if another is doing a task by using computer resources. An agent may be unable to maximize a task achievement in a longer term, if it maximizes a task achievement in a shorter term.

In this section, we verify experimentally that sDS-GA is efficient for actual intelligent robots. Here, we use an auto guided tracked vehicle with a camera, called (MieC) as an actual intelligent robot.

Concretely, applying sDS-GA, the control parameters of MieC are optimized when MieC traces a ball that moves on the same plane.

3.1 Movable Intelligent Evolutional Computer (MieC)

Here, we use the Movable Intelligent Evolutional Computer (MieC) shown in **Fig. 2**as an actual intelligent robot. MieC has two motors as movable actuators, two encoders for the motors as internal sensors, and a camera as an external sensor.

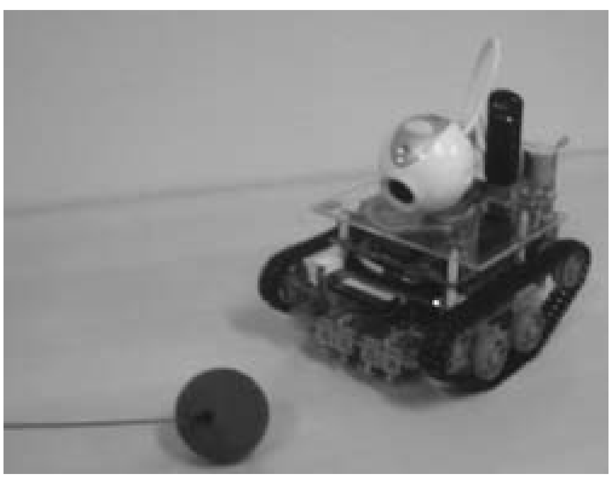

Figure 2: Movable Intelligent Evolutional Computer (MieC)

3.2 Tracing Control

The flow of target tracing control is shown in **Fig. 3**. This control flow is one of the simplest in this case. (1) The current position of the target is solved by processing an image from the camera. (2) The position command of MieC is determined by the error between the target position and the current position. (3) The target rotation angles of the left and the right tracks are calculated from the position command, considering the inverse kinematic of MieC. (4) The voltage commands to motors are determined by the errors between the target positions and the value current positions, respectively. (5) The motors are rotated by the voltage commands, respectively. (6) Return to (1).

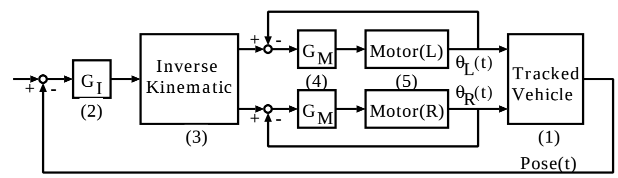

Figure 3: The block diagram for the target tracing of the traced vehicle

In steps (2) and (4), the commands are determined by the errors and the gains G_I and G_M. Here we treat the gains G_I and G_M as proportionality constants, although the gains have to be determined, considering the weight and the inertia moment of MieC and the characteristics of the motors, etc. The execution cycle (1)∼(3) and the execution cycle (4)∼(5) depend on the execution speeds of image-processing and motor-control, respectively. These execution cycles are considered to determine the gains G_I,G_M. Here, these parameters G_I,G_M are optimized applying sDS-GA.

3.3 sDS-GA Coding

We give each agent gene G_I or G_M. G_I takes one of 10 quantized values 0.0, 0.1, 0.2, $\cdots$, 0.9. G_M takes one of 10 quantized values 0.0, 0.3, 0.6, $\cdots$, 2.7. The agents with gene G_I and gene G_M can call the cycle(1) ∼(3) and the cycle(4)∼(5), respectively. However, the agent cannot call a cycle before the same cycle is completed. Each agent is evaluated by how much and how fast MieC can trace the target during the time in its duty.

3.4 Experiments and Discussion

We gained the following results. The histories of the population ratios of G_I(0.0, 0.1, 0.2, $\cdots$, 0.9) and G_M(0.0, 0.3, 0.6, $\cdots$, 2.7) are shown in **Fig. 4**, respectively. The horizontal axes express the number of times the colony loop was performed. The vertical axes express the ratios of G_I and G_M with each of 10 quantized values, respectively.

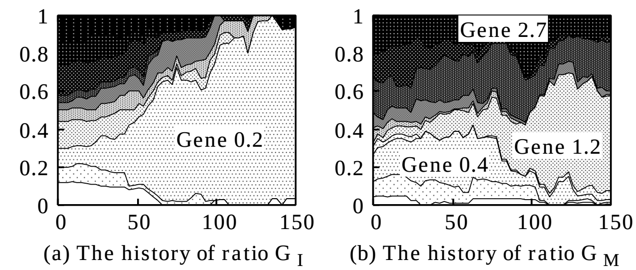

Figure 4: The history of the population ratio

G_I converged on the optimal value 0.2. G_M did not converge, but the average of G_M in each colony converged near the optimal value 1.8. It is believed that the action time of each agent is so short in this case that an agent's action affects not itself but other agents in the same colony, evenly. In other words, agents in the same colony evenly affect each other. As the results, the average in each colony converged, but the agents did not converge. Therefore, a single agent with G_M cannot aquire the optimal value, but aquires the optimal value as the average. On the other hand, a single agent with G_I aquired the optimal value. It is believed that the average was equal to the value of the agent, since only a few agents with G_I are in the same colony.

From the above discussion, it is believed that both G_I and G_M are optimized by applying sDS-GA. The sDS-GA is efficient for the optimization of a control system for MieC as an actual intelligent robot under an unknown environment.

4 Conclusion

In this paper, we proposed the Serially and Dynamically Separating Genetic Algorithm (sDS-GA) as an optimization algorithm for an actual intelligent robot control system.

In order to verify the validity of sDS-GA for the optimization of intelligent robot control, we applied sDS-GA to a target tracing task for a Movable Intelligent Evolutional Computer (MieC) as an actual intelligent robot.

Experimental results show that even if there is a time lag between the decision of the agent's action and the action of the robot, and even if the agent learns based on short-term information, sDS-GA can obtain not short-term but long-term optimal parameters of the control system. These characteristics of sDS-GA are similar to the characteristics of the conventional DS-GA, which obtains system-level optimality by agents' learning based on local information by the use of "Swarm-Sensing". These results suggest that sDS-GA is efficient for the optimization of an actual robot control system under an unknown environment.

Acknowledgements

This research was conducted as part of 'Research on Human Communication' with funding from the National Institute of Information and Communications Technology.

References

[1] A. Mori, F. Naya, N. Osato, T. Kawaoka, "Multiagent-Based Distributed Manipulator Control," *Proceedings of the 1996 IEEE/SICE/RSJ International Conference on Multisensor Fusion and Integration for Intelligent Systems*, pp. 289-296, 1996.

[2] J.D. Morrow, "Sensorimotor Primitives for Programming Robotic Assembly Skills," *Ph.D. Thesis, Robotics Institute, Carnegie Mellon University*, 1997.

[3] K. Nakayama, H. Matsui, Y. Nomura, "Dynamically Separating GA (DS-GA)," *IPSJ Transactions on Mathematical Modeling and Its Applications (In Japanese)* , Vol. 43, No. SIG 10 (TOM 7), pp. 95-109, 2002.

[4] K. Nakayama, K. Shimohara, O. Katai, "Dynamically Separating GA: A New Method of Achieving the System-level Optimality in MAS," *The journal of three dimensional images*, Vol.16, No.4, pp. 177-183, 2002.

The Tenth International Symposium on Artificial Life and Robotics 2005(AROB 10th '05),
B-con Plaza, Beppu, Oita, Japan, February 4-6, 2005

Proposal of Genetic Operations Reducing the Evaluator Workload to the Voice Quality Conversion Using Interactive GA

Takenori Nishizono Satoshi Noami Yuji Sato
Graduate School of Computer and Information Sciences, Hosei University
3-7-2 Kajino-cho, Koganei-shi, Tokyo, Japan
i04t0014@k.hosei.ac.jp

Abstract

We have already proposed the voice quality conversion system using interactive evolution. Users can convert our voice to various voice qualities because it does not require a codebook. However the practical application of the system requires reducing the evaluator workload. This paper proposes two kinds of genetic operations, that is, "individual complement" and "adjustment after genetic operations" that aim to reduce the evaluator workload by improving the efficiency of tournament selection. The experimental result using the expediential function shows the proposed operations have effect of reduction of the workload.

Keywords: Interactive Evolution; Evolutionary Computation; Voice Quality Conversion;

1. Introduction

The growth of communication technology increases variety of the online communication methods. In these days, as typified by online meeting services, we can communicate by our real voice on line. The development of voice processing technology is important for the growth of application area of these.

The usual voice modification system realizes a specified voice quality by modifying another specified voice according to a codebook. It requires getting the voice data of conversion object and creating the codebook corresponding to the conversion. Therefore, it is only used to improve synthetic voice quality and to convert between the specified speakers. On the other hand, we have already proposed the voice modification system using interactive evolution [1]. Users can convert a voice selected freely to various voice qualities with it because it does not require the codebook. However a system using interactive evolution requires reducing the evaluator workload to put into practical use [2].

We applied tournament selection for evaluator workload reduction to the system. For further improvement, this paper proposes two kinds of genetic manipulation that aims to improve the efficiency of tournament selection, and reports the evaluation result.

2. Voice modification system using interactive GA

Fig. 1 shows the voice modification system using interactive evolution. The system is trisected by a voice conversion part which converts input voice with conversion coefficients, a learning part which search the conversion coefficients with genetic algorithms (GA), and a GUI part. This section explains the system with the focus on the voice conversion part and the learning part.

The voice conversion part treats three prosodic elements – voice frequency, voice amplitude, and speech tempo – as control information. It creates new voice quality by compressing or expanding the above elements according to conversion coefficients that are real number. This paper describes the conversion coefficient of frequency as PIT, of amplitude as POW, and of speech tempo as TMP. The learning part searches PIT, POW, and TMP which realize the target voice quality.

The learning part repeats the search process explained below until the system detects the target. This section explains it by assuming the population size is 2N if it does not apply the operation proposed in this paper. The individuals in population consist of three kinds of chromosome. The each chromosome keeps PIT, POW, and TMP as bit string. First the process performs tournament selection that a user chooses one candidate among three. The selection is repeated N times. Therefore, it has N individuals after finishing the selection. Then it creates new N individuals by performing one-point crossover and mutation to the selected N individuals. At last it creates the population in net generation by adding the N individuals before and

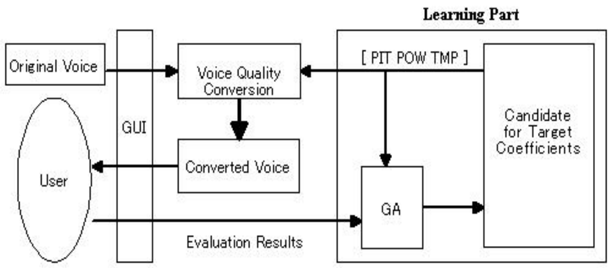

Fig. 1: The system configuration outline of voice quality conversion system.

after performing the crossover and mutation.

The selection presents individual in population at least one time, and forbids selecting a candidate twice. Although the selection reduces the evaluator workload required in one generation, it may increase the generation number until convergence. For further reduction, the next section proposes two kinds of genetic manipulation to reduce the search time.

3. Proposal of genetic operations reducing the evaluator workload

This section proposes two kinds of genetic operations in order to reduce the evaluator workload. First the section 3.1 proposes "individual complement" for reduction of evaluation times required in one generation. The section 3.2 proposes "adjustment after genetic operations" for diversity maintenance of population. At the last of this section, we show the search process which applying the proposed operation.

3.1. Individual complement

The reduction of evaluator workload is realized by curtailment of evaluation times in one generation. However it has adverse effect to search ability because it cut down the population size. The operation "individual complement" realizes the curtailment by complementing the reduction of individuals with individuals created based on the individuals selected in same generation. In addition, this operation aims at improvement of search ability by complementing with individuals created based on bit information of the selected individuals. This operation creates the individuals a reduction number of evaluation times, and uses these to complement.

This section below explains how to create the individual to complement the individual reduction. The individual consists of PIT, POW, and TMP chromosomes that are created by a process explained below. This section explains the process if it creates a PIT chromosome. A similar process creates the others. First the process takes PIT chromosome form the individuals selected in same generation, and creates a group of PIT chromosome. Next it investigates the maximum and the minimum of real-valued PIT kept in the group. Then it calculates an absolute value of difference between the maximum and the minimum of PIT. If the absolute value is over a threshold which is set beforehand, it creates the PIT chromosome by using the upper creation method in Fig. 2. It choices one chromosome from the group, and makes it the PIT chromosome of individual for complement. If the absolute value is under the threshold, it uses the lower method in Fig. 2. It investigates the percentage of bit value in each digit of PIT chromosome in the group of PIT, and creates a probability table of bit value as shown in Fig. 2. Then it creates bit string according to the table, and makes the created bit string the PIT chromosome of the individual for complement.

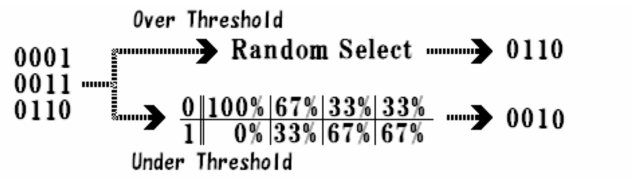

Fig. 2: The creation method of chromosome based on chromosome group

3.2. Adjustment after genetic operations

Next this section proposes the operation "adjustment after genetic operations" in order to maintain diversity of population. The "individual complement" proposed in previous section promotes early detection of the target individual. However it may make the population drop into premature convergence because it reduces diversity. The operation proposed in this section maintains diversity, and tries to improve the effect of the individual complement.

This operation is illustrated by Fig. 3. First it investigates whether the population has two same individuals. If the population has, it performs mutation to chromosome in the one individual with fixed probability. This mutation makes a chromosome mutate within about between -0.256 and 0.256 from the original value if the chromosome has 3 decimal places. In Fig. 3, the lower individual in the squared two individuals in mutated. The convergence speed is easy to become blunt by the target individual. Therefore, this mutation does not take very big mutation amount.

The purpose of this operation is near to the purpose of heterogeneous recombination in CHC (cross generational elitist selection, heterogeneous recombination, and cataclysmic mutation) [3]. However this operation differs from the heterogeneous recombination because this operation maintains the

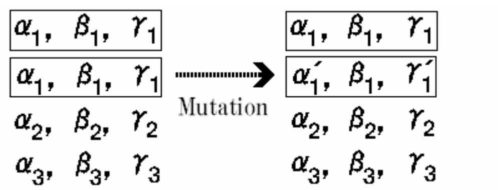

Fig. 3: The image of adjustment after genetic operations

number of individuals. This operation increases diversity with keeping the number of individuals, and maintains the number of candidate's kinds. According to the above, this operation aims at the early detection of target individual.

At last, we explains the search process if the system applies the proposed operations. We assume that the population size is 2N to contrast with the search process explained in section 2. First the process performs tournament selection with threefold choice. The selection is performed 2N/3 times in one generation. The number of evaluation times is decided by the lowest times required to bring up all individuals with the threefold choice evaluation. As the result of this selection, 2N/3 individuals are selected. Next it increases the number of the individuals to N by performing the "individual complement". After that, it creates new N individuals by performing one-point crossover and mutation to the N individuals. It creates 2N individuals by adding the N individuals before and after performing crossover and mutation. Finally, it performs the "adjustment after genetic operations" to the 2N individuals, and makes the individuals the population in next generation. By performing the proposed operations as described above, the operations aims at improvement of efficiency of tournament selection.

4. Evaluation experiment

4.1. Evaluation method

Since the voice modification system adopts interactive GA, repeating the experiment of this system tasks the evaluator. Therefore, as a matter of convenience, this paper experiments with an evaluation function described below.

The evaluation function calculates a point of each candidate, and choices a candidate which has the lowest point. The point of a candidate is decided by a total of three values. These are absolute value of difference between each conversion coefficient of the target and the candidate. The experimental system searches the target with it, and records the generation number when the system detects the target.

This experiment was performed with the parameters below. The population size was 30. Therefore, it performs the selection 10 times in one generation if the system applies the "individual complement", and performs 15 times if it does not apply. PIT and TMP have 3 decimal places, and POW has 2. The bit length of PIT or TMP chromosome is 13, and that of POW is 11. The crossover rate is 1.0. The mutation rate was 0.3. The threshold used in the individual complement was set 0.0025 to PIT or TMP, and set 0.025 to POW. The mutation rate in the adjustment after genetic operations was set 0.4. A coefficient value of the initial individuals was created randomly within the range from 0.4 to 2.5 if it is PIT, within the range from 0.4 to 2.5 if it is POW, and within the range from 0.5 to 2.5 if it is TMP.

4.2. Experimental results

This section reports the evaluation results. We performed experiment to the 4 kinds of the system; the system that does not apply the proposed operations, that applies one of the proposed operations, and that applies both proposed operations. Each experiment is performed 5000 times, and graph-ized the result. The target conversion coefficients of these experiments were set 1.5 to PIT, set 4.0 to POW and set 0.8 to TMP.

First we show the result applying the individual complement by Fig. 4. The horizontal axis of the graph shows the generation number when the system detected the target. The vertical axis shows the number of times which the system could detect on the generation number of the horizontal axis. The result shows the operation decreased the average number of generation required until detection from 50.5426 to 43.314, the shortest number form 19 to 16, and the maximum number from 128 to 110. On the other hand, the application of adjustment after genetic operations decreased the shortest number of generation required until the target detection from 19 to 14, and the maximum number from 128 to 98. However, it had little effect to the average number.

Next, this section shows the result when the system applied both proposed operations. Fig. 5 shows the experimental result. This experiment took the best result in this paper. The average number of generations was 38.3840, the shortest number was 12, and the maximum number was 84. In addition, as shown in Fig. 6, we compare this result with the result in the case the system applied half of the proposed operations. Although the adjustment after genetic operations had little effect to the average number in the previous result, it had effect when it is applied with the individual complement. By applying it to the system that applies the individual complement, it decreased the average number of generations from 43.3140 to 38.3840, the shortest number from 110 to 84, and the maximum number from 16 to 14.

4.3. Discussion

Fig. 4 shows the individual complement is effective to improve the efficiency of tournament selection. It decreases evaluation times required in one generation by 2/3 in addition to the reduction effect of the generation number. The adjustment after genetic operations did not have effect to the average number of generations required until target detection. However, Fig. 7 shows it reduces the average number when applied system applied the individual complement. We consider that this result shows the adjustment after genetic operations complements diversity which is decreased by the individual complement.

The section below estimates how much the evaluation times were reduced by the proposed operations according to the experimental results. If the system did not apply the proposed operations, it performed evaluation 15 times in one generation and required 50.5426 generations until target detection on an average. Therefore, it gave users 758.139 times evaluation on an average. On the other hand, if the system applied, it evaluated 10 times and required 38.3840 generations. Therefore, it required 383.84 times evaluation on an average. Altogether, the proposed operations decreased the evaluation times by about 49%. It means that the proposed operations are effective to the efficiency improvement of tournament selection.

5. Conclusion

This paper proposed the "individual complement" and the "adjustment after genetic operations" to reduce the evaluator workload in the voice modification system using interactive GA which applied tournament selection. As a result of the experiment using a function which evaluates voices replaced by users, the proposed operations reduced the evaluation times required until target detection about 49%. In future, the system requires further improvement of a system side and interface side to the system easy to use.

References

[1] Sato Y.:"Voice Conversion Using Interactive Evolution of Prosodic Control", Proc. Of the 2002 Genetic and Evolutionary Computation Conference (GECCO-2002), Morgan Kaufmann Publishers, pp.1204-1211 (2002).

[2] H. Takagi: Interactive Evolutionary Computation: Fusion of the Capabilities of EC Optimization and Human Evaluation. In: "Tutorial Book of the 2001 Congress on Evolutionnary Compuation", IEEE Press, 2001.

[3] D.E. Goldberg, "Genetic Algorithms in Search, Optimization, and Machine Learning", Addison-Wesley, 1989.

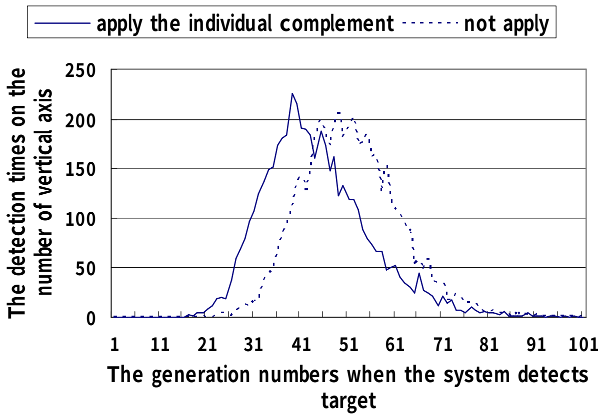

Fig. 4: The result applying the individual complement

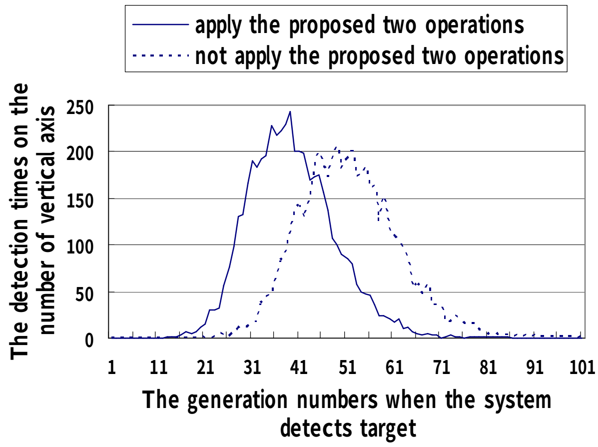

Fig. 5: The result applying the proposed operations

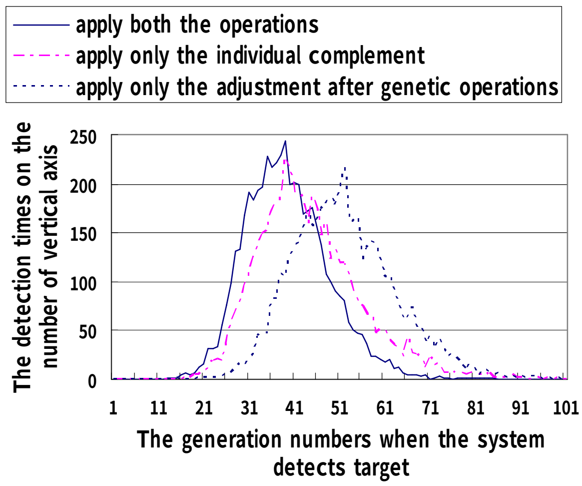

Fig. 6: The comparison between the result applying the proposed operations and the result applying the one-half of operations

The Tenth International Symposium on Artificial Life and Robotics 2005(AROB 10th '05),
B-con Plaza, Beppu, Oita, Japan, February 4-6, 2005

Fitness Modification in Genetic Algorithms for Function Optimization Problems

Takanori Yoshida, Tomoharu Nakashima, and Hisao Ishibuchi
College of Engineering, Osaka Prefecture University
Gakuen-cho 1-1, Sakai, Osaka 599-8531, Japan
{dayoshi, nakashi, hisaoi}@ie.osakafu-u.ac.jp

Abstract

In this paper, we propose a fitness modification method to improve the performance of genetic algorithms. In the proposed method, the distance from each individual to the best one in the current population is used to modify its fitness value. First we examine the behavior of a genetic algorithm for various function optimization problems from the viewpoint of diversity of the population. Next we demonstrate that the performance of the genetic algorithm is improved by the proposed method for those problems that are difficult for the genetic algorithm to efficiently find optimal solutions. Finally, we examine the performance of our fitness modification method on a dynamically changing function optimization problem.

1 Introduction

The balance between exploration and exploitation is undoubtedly a key issue in the research of genetic algorithms. In genetic algorithms, this issue can be discussed in terms of the diversity and the selection pressure. That is, the diversity in the population corresponds to the exploration ability and the selection pressure corresponds to the exploitation ability of genetic algorithms. It is, however, difficult to find the best balance between the diversity and the selection pressure. For example, if one tries to keep a large diversity in the population, the search speed may slow down. On the other hand, if the selection pressure is high, the population is likely to converge to a local optimal solution. This issue has been discussed in various literature (for example, see [1]).

In this paper, we examine the effect of fitness modification on the performance of genetic algorithms from the viewpoint of diversity of the population. The aim of our fitness modification is to have high search ability with a large diversity in an entire population. We also examine the performance of the fitness modification method in a dynamic function optimization problem where the shape of the objective function changes over generation.

2 Performance of GAs

This section examines the performance of genetic algorithms on some function optimization problems. The performance is measured from the viewpoint of diversity as well as the search ability.

2.1 Function Optimization Problems

In the computer simulations in this paper, we use the following functions for function optimization. All of them are to be minimized.

$$\mathrm{F1}: f_1(x_i|1 \le i \le n) = \sum_{i=1}^{n} x_i^2, \quad x_i \in [-5.12, 5.11], \tag{1}$$

$$\mathrm{F2}: f_2(x_i|1 \le i \le n) = 10 \times n + \left[\sum_{i=1}^{n} x_i^2 - 10\cos(2\pi x_i)\right], \quad x_i \in [-5.12, 5.11], \tag{2}$$

$$\mathrm{F3}: f_3(x_i|1 \le i \le n) = \sum_{i=1}^{n-1}\left[100\left(x_{i+1} - x_i^2\right)^2 + \left(1 - x_i\right)^2\right], \quad x_i \in [-2.048, 2.047], \tag{3}$$

$$\mathrm{F4}: f_4(x_i|1 \le i \le n) = \sum_{i=1}^{n-1}\left(100\left((i+1)y_{i+1} - (iy_i^2)\right)^2 + \left(1 - iy_i\right)^2\right), \quad y_i = x_i/i, \quad x_i \in [-2.048, 2.047]. \tag{4}$$

Function F1 is the first function of the DeJong's test suite, Function F2 is the Rastrigin function, Function F3 is the Rosenbrock function and Function F4 is the ill-scaled Rosenbrock function. The optimization problems of the above functions are static (that is, they do not change their shapes during the execution of optimization algorithms).

2.2 Entropy

In this paper, we use entropy as a measure of the diversity of the population [2]. The entropy measure of a population P is calculated as follows:

$$E(P) = -\sum_{l}^{L}\{p_l \log p_l + (1 - p_l)\log(1 - p_l)\}, \qquad (5)$$

where p_l is the proportion of the value 1 in the l-th bit in the population P, and L is the length of a bit string (i.e., an individual). We examine the entropy measure of the following subpopulations: $20 \times m$ neighboring individuals for best one in genotype space, where $m = 1, 2, 3, \cdots$. Figure 1 shows the subpopulations of which we examine the entropy. A low entropy measure means that a large number of individuals are the same bit string.

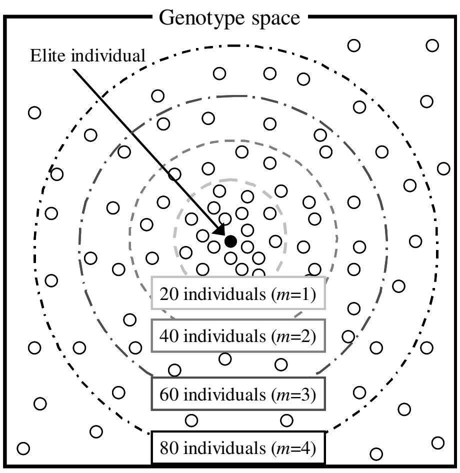

Figure 1: Examined subpopulations (m=1,2,3,4)

2.3 Experiments

We applied a genetic algorithm to each function optimization problem ten times. During the execution of the algorithm, we monitored the diversity of the subpopulation as well as the function values of elite individuals. Parameter specifications of the genetic algorithm in our experiments are shown in Table 1.

Table 2 shows the average function value of the obtained solutions over ten runs and the number of successful runs (R) where the optimal solution was found. We can see that the genetic algorithm could not find the optimal solution of F3 nor F4. In Figure 2 and Figure 3, we show the entropy measure of 20 neighboring individuals for the best individual and the entropy measure of the entire population, respectively. From these figures, we can see that during the execution for F3 and F4 the genetic algorithm keeps higher diversity maintained in 20 neighboring individuals and in the entire population than for F1 and F2. This is why the genetic algorithm could not find the optimal solution of F3 nor F4. We also show in Figure 4 the distribution of individuals in the final generation for F3. From this figure, we can see that the population does not converge around the optimal solution.

Table 1: Parameter settings

Population size	400
Crossover probability	1.0
Mutation probability	0.05
Stopping criterion (no. of generations)	500

Table 2: Simulation results for each problem

	Function value	R
F1	0.0	10
F2	0.0	10
F3	0.000219	0
F4	0.000155	0

3 Fitness Modification

In this section, we propose a fitness modification method and demonstrate that the performance of the genetic algorithm is improved by our fitness modification method.

3.1 Fitness Modification Method

In our fitness modification method, the best individual with the lowest function value in the population is selected from the current population. The selected

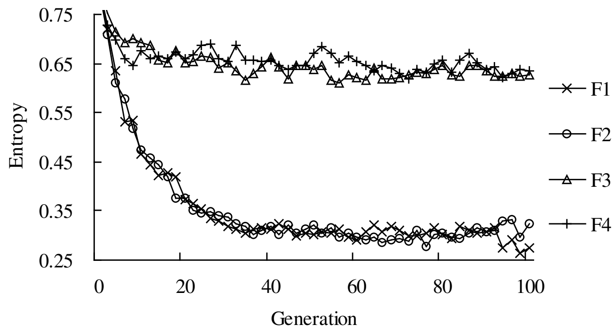

Figure 2: Entropy measure of 20 neighboring individuals for the best individual

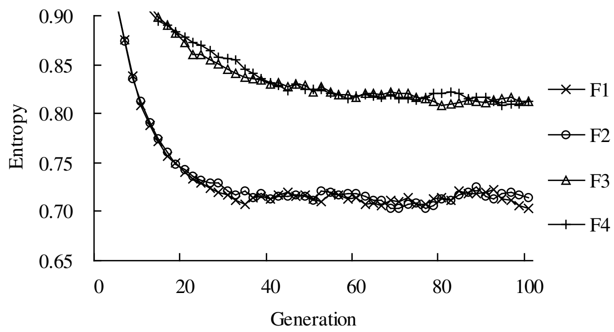

Figure 3: Entropy measure of the entire population

individual is called a reference individual. The fitness value is calculated for each individual in the population for a function minimization problem as follows:

$$fitness_i = F_i \times \left\{ \left(\frac{10 d_i}{D} \right)^2 + 1 \right\}, \tag{6}$$

where F_i is the function value of the i-th individual, d_i is the phenotype distance from the i-th individual to the reference individual, and D is the length of the diagonal line in the phenotype search space.

The proposed fitness modification method in (6) means that the fitness value is increased if d_i is large (i.e., if the i-th individual is far from the reference individual.). On the other hands, if d_i is not large, the fitness value of an individual is almost the same as its objective function value.

3.2 Experiments

In this section, we use F3 and F4 in computer simulations. We applied the genetic algorithm with our fitness modification method to each function optimization problems ten times.

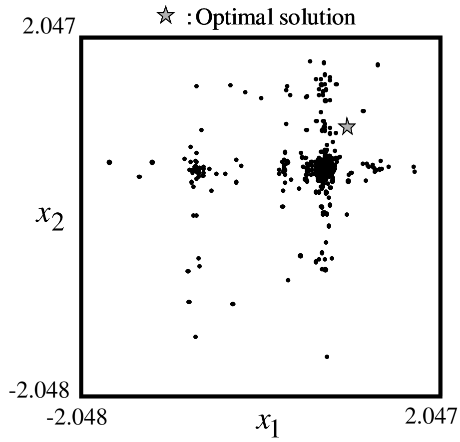

Figure 4: Distribution of individuals in the final generation for F3

Table 3 shows the average function value of obtained solutions over ten runs and the number of runs where the optimal solution was found. In this table, the genetic algorithm (GA) with our fitness modification method is denoted as GA+. From this table, we can see that the performance of genetic algorithms was improved by our fitness modification method. Figure 5 shows the entropy of various subpopulations in the final generation. From this figure, we can see that the entropy was decreased by our fitness modification method.

Table 3: Simulation results for F3 and F4

		Function value	R
F3	GA	0.000219	0
	GA+	0.0	10
F4	GA	0.000155	0
	GA+	0.0	10

4 Adaptability for Dynamic Environment

Dynamic environments form a difficult class of optimization problems for evolutionary algorithms. Branke [3] suggests that his memory-based genetic algorithm is able to efficiently adapt to changing environments. In this section, we examine the performance of our fitness modification method for a dynamically changing function.

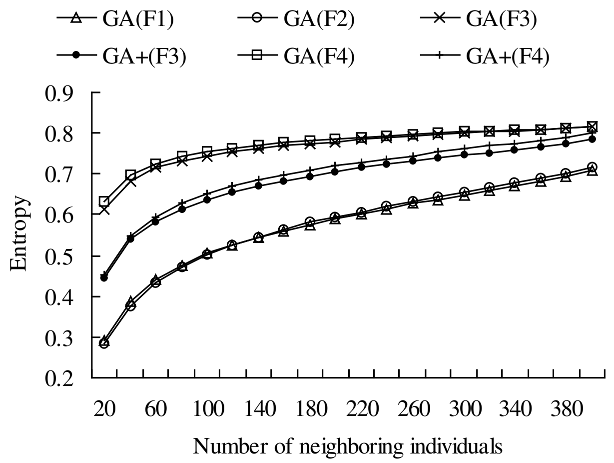

Figure 5: Entropy measure of subpopulations in the final generation

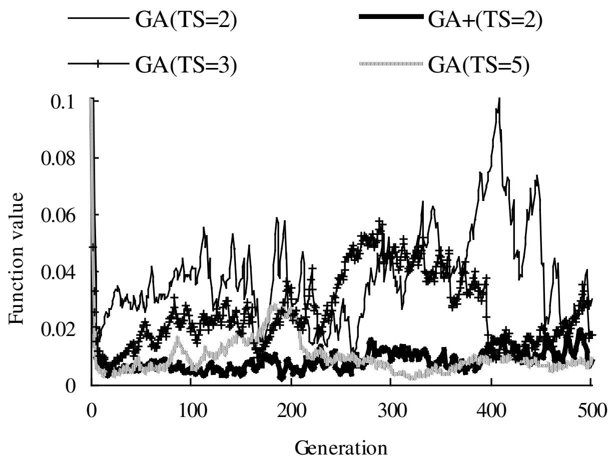

Figure 6: Best function value for F5

4.1 Function Optimization Problems

In this section, We examine the performance of our method on the following function:

$$\begin{aligned} \text{F5}: & f_5(x_i|1 \leq i \leq n) \\ &= \sum_{i=1}^{n-1} \left[100\big(y_{i+1} - y_i^2\big)^2 + \big(1 - y_i\big)^2 \right], \\ & y_i = x_i - (\frac{t}{500} - 1), \quad x_i \in [-2.048, 2.047] \end{aligned} \tag{7}$$

where t is the index of the generation, which serves as a time index during the execution of genetic algorithms. The characteristic feature of the above function is that the optimal point gradually moves over generations while the optimal function value is always the same (i.e., 0.0).

4.2 Experiments

We examine the performance of the genetic algorithm and the genetic algorithm with our fitness modification method on the dynamically changing function optimization problem in (7). The genetic algorithms were executed ten times in the same manner as in the previous section. In the genetic algorithm, we examined three specifications of the tournament size (TS): TS=2, 3, 5. Figure 6 shows the best function value for F5 at each generation of each algorithm. From Figure 6, we can see that the modified version of the genetic algorithm (GA+) is more adaptable to the changing environment than the original version without the fitness modification method.

5 Summary

In this paper, first we examined the behavior of the genetic algorithm for several function optimization problems from the viewpoint of the diversity of the population. Next, we examined the effect of our fitness modification method for difficult problems where the genetic algorithm can not efficiently find their optimal solutions. In our computer simulations, we showed that the performance of the genetic algorithm was improved by our fitness modification method. Finally, we examined the performance of our fitness modification method on a dynamically changing function optimization problem. It was shown that the fitness modification method improved the adaptability of the genetic algorithm.

References

[1] D. Whitley, "The GENITOR Algorithm and Selection Pressure: Why Rank-Based Allocation of Reproductive Trials is Best", *Proc. of the third International Conference on Genetic Algorithms*, pp. 116–121, 1989.

[2] E. K. Burke, S. Gustafson, G. Kendall, "Diversity in Genetic Programming: An Analysis of Measures and Correlation with Fitness", *IEEE Trans. on Evolutionary Computation*, Vol. 8, No. 1, pp. 47-62, 2004.

[3] J. Branke, "Memory Enhanced Evolutionary Algorithms for Changing Optimization Problems", *Proc. of Congress on Evolutionary Computation*, pp. 1875-1882, 1999.

The Tenth International Symposium on Artificial Life and Robotics 2005(AROB 10th '05),
B-con Plaza, Beppu, Oita, Japan, February 4-6, 2005

Data Mining using Genetic Network Programming

Takeshi FUKUDA* Kaoru SHIMADA* Kotaro HIRASAWA* Takayuki FURUZUKI*
*Graduate School of Information, Production and Systems, Waseda University
2-7 Hibikino, Wakamatsu-ku, Kitakyushu-shi, Fukuoka 808-0135, Japan
e-mail: kurt2@moegi.waseda.jp

Abstract

Recently, Data Management System (DMS) is used in various fields, and the importance of data mining extracting important rules from a large-scale database has been recognized widely. Although the conventional data mining using statistical techniques has been developed, a novel algorithm of data mining using Genetic Network Programming (GNP)is proposed in this paper. The proposed system using GNP with directed graph structures can extract automatically the correlation rules showing the importance of data. GNP has been proposed and studied as a new method of evolutionary computations. GNP is constructed by the network structure whose gene consists of the directed graph, so it is possible to search solutions effectively by the implicit memory function of the network structure. Until now, the applicability and availability of GNP to the real-world applications have not been studied, whereas it has been applied to virtual-world examples such as Tile-world and its effectiveness has been proved through the comparison with GP. We describe a method to extract correlation rules automatically using support and confidence, and experimental results are described to show the effectiveness of the proposal method.

Keywords: Data Mining, Correlation Rule, Genetic Network Programming, Evolutional Algorithm.

1 Introduction

Information is spreading in the information-oriented society almost every day. In this circumstance, Data Management System (DMS) has been attracted recently. People interested in DMS have not only managed the data but tried to extract knowledge from the data, and this has become important theme in these days. In this sense, data mining capable of extracting hidden knowledge from an enormous database has been noticed recently. Database techniques using statistical techniques such as decision tree, correlation rule, and cluster analysis have been proposed in order to carry out data mining efficiently.[1][5]

Finding the correlation rules[1][5], that is, discovering the relevance or pattern existing in the set of items of the records, is one of the methods which can be easily understood.

But, the cost of extracting the correlation rules using the traditional statistical techniques is fairly high.

In this paper, we propose a novel data mining technique using Genetic Network Programming (GNP)[2] whose gene has directed graph structures in order to overcome the disadvantages of the conventional methods.

A complex mathematical algorithm could not solve the problems caused by the large size of database but an evolutional algorithm could do it because GNP has such features as *1)* reusing the nodes and *2)* having the directed graph structure. In other words, GNP can extract correlation rules efficiently using the directed graph structure and keeping the size of the individuals fixed due to the reused nodes.

The fitness of GNP having a number of correlation rules is calculated and GNP is evolved by the calculated fitness.

Data mining and GNP are briefly discussed in section 2 and 3, respectively. The basic structure of the proposed method is described in section 4, followed by simulation results in section 5, and the conclusions in section 6.

2 Data Mining (Market Basket Analysis)

In this section, the market basket analysis is reviewed briefly, which is used in the simulation of this paper as the benchmarking problem.

When we deal with the shopping cart filled with goods in a supermarket, we can talk about the market basket analysis.[1][5] The shopping cart tells what a customer buys. Each customer buys a quality of different items because the characteristics of customers are different from each other. Therefore, we can get a lot of information through them.

We can analyze the purchase lists of buyers in the market basket analysis to understand the general trend of the purchase of customers. The market basket analysis can give us the insight about the information on buying goods and can suggest us the new design of the shopping site because it shows us what combination of the goods is sold well. Furthermore it can show us where better sites for special goods are.

Merits of the market basket analysis are the availability and clearness of the results expressed by correlation rules. The correlation rules have intuitional properties because they express what kinds of relations the goods on the shelves have each other. Namely, the merits of finding the correlation rules by the conventional methods are:

1. It is easy to understand the correlation results clearly.
2. It is powerful to analyze the complicated data.
3. It is suitable to the data with variable size.
4. It is simpler than other algorithms for analyzing the data.

However they have several shortcomings:

1. The cost of calculating correlation rules increases exponentially with the size of problems.
2. It is difficult to deal with rare items.

We will show that the proposal method can overcome the above shortcomings by analyzing the market basket analysis using GNP in this paper.

3 Genetic Network Programming

In this section, Genetic Network Programming (GNP) is explained in detail. Basically, GNP is an extension of GP in terms of gene structures. The original idea is based on the more general representation ability of graphs than that of trees.[2]

3.1 Basic structure of GNP

The basic structure of GNP is shown in Fig.1. As shown in Fig.1, the directed graph structure is used to represent individuals. GNP is composed of plural

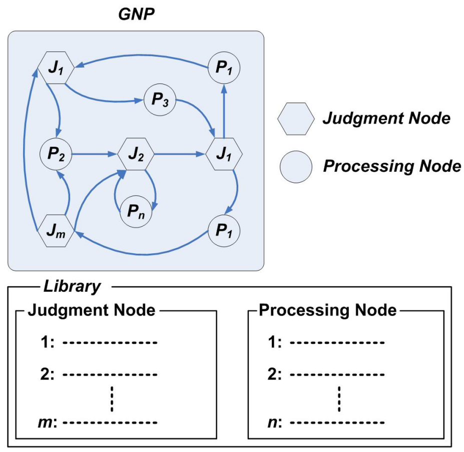

Figure 1: The basic structure fo GNP individual

nodes which are roughly classified into two kinds of nodes: `JUDGEMENT NODE` and `PROCESSING NODE`.

`JUDGEMENT NODE`s correspond nearly to elementary functions of GP and `PROCESSING NODE`s correspond almost to terminal symbols of GP. `JUDGEMENT NODE`s are the set of $J_1, J_2, \cdots, J_m$, which work as some kinds of judging functions. On the other hand, `PROCESSING NODE`s are denoted by the set of $P_1, P_2, \cdots, P_n$, which work as some kinds of action/processing functions. The practical roles of these nodes are predefined and stored in the library by supervisors.[3]

GP's elementary functions and terminal symbols are repeatedly used in a tree structure. In the same way, there are some $J_{1s}, J_{2s}, P_{1s}, P_{2s}$ and so on in GNP as shown in Fig.1. These `JUDGEMENT NODE`s and `PROCESSING NODE`s are the essential elements of GNP. The number of these nodes may be determined as a result of evolution like GP. Actually, GNP can use this strategy, in other words, GNP can adopt evolving the genotypes with variable number of nodes, but in this paper GNP evolves only the networks with the predefined number of nodes. It would be better to say that GNP here evolves the genotypes with fixed number of nodes. We set the number of each node in GNP equal to each other, e.g., $J_1 \times 3, J_2 \times 3, \cdots, P_1 \times 3, P_2 \times 3, \cdots$, and so on.

Additional specific nodes, start node S, is involved in GNP. Start node indicates the start point of GNP, which corresponds to GP's root node.

Once GNP is booted up, the execution starts from the start node, then the next node to be executed is determined according to the connection from the current activated node. If the activated node is `JUDGEMENT`

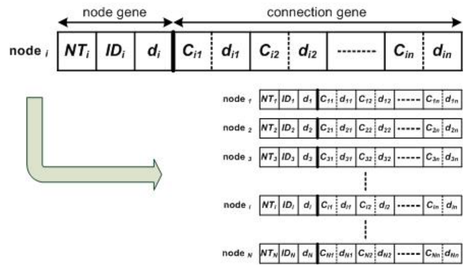

Figure 2: The genotype expression of GNP node

NODE, the next node is determined by the judgement at the activated JUDGEMENT NODE. When PROCESSING NODE is executed, the next node is uniquely determined by the single connection from PROCESSING NODEs.

The genotype expression of GNP node[4] is shown in Fig.2. This describes the gene of node i, then the set of these genes represents the genotype of GNP individuals. All variables in these genes are described by integer. NT_i describes the node type, $NT_i = 0$ when the node i is JUDGEMENT NODE, $NT_i = 1$ when the node i is PROCESSING NODE. ID_i is an identification number, e.g., $NT_i = 0$ and $ID_i = 1$ mean node i is J_1. $C_{i1}, C_{i2}, \cdots$, denote the nodes which are connected from node i firstly, secondly, $\cdots$, and so on depending on the arguments of node i. The total number of connection genes depends on the arity of the node's function. d_i and d_{ij} are the delay time. They are the time required to execute the processing of node i and delay time from node i to node C_{ij}, respectively. GNP can become materialized more realistically by setting these delays.

3.2 Genetic operator of GNP

The following genetic operators[4] shown in Fig.3 and 4 are used in GNP. Mutation operator affects one individual. All the connections of each node are changed randomly by mutation rate of P_m (shadowed in Fig.3). Crossover operator affects two parent individuals All the connections of the uniformly selected corresponding nodes in two parents are swapped each other by crossover rate of P_c between the two parents (shadowed in Fig.4). GNP evolves the fixed number of nodes, as I mentioned before, crossover is applied to the corresponding nodes selected uniformly in two parent genotypes as shown in Fig.4.[2][3][4]

Note that these genetic operators will not change any node functions, they only change the connection among the nodes. Therefore GNP doesn't evolve the functions of the nodes, but evolves the connections between nodes.

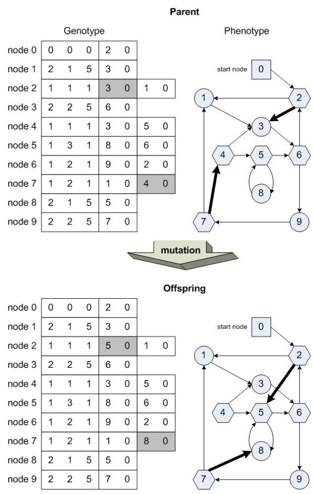

Figure 3: Mutation of GNP

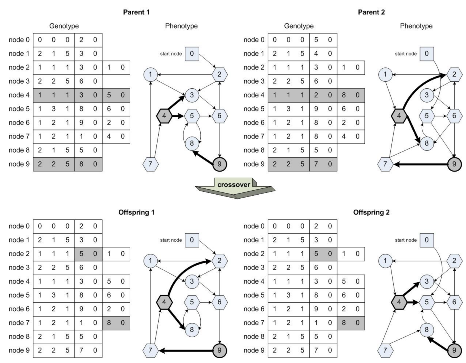

Figure 4: Crossover in GNP

4 Data Mining Structure using GNP

In this section, the proposed method for extracting correlation rules is described. First, we describe the fundamental concept dealing with the application of GNP to data mining.

1. Set the structural condition of GNP to extract correlation rules effectively.
2. Express a correlation rule by transition from the group of judgment nodes to the group of processing nodes in GNP.

3. Determine if the extracted rules are good enough or not using the support and the confidence.

4.1 Expression of Correlation Rules with GNP

Here, how to express the correlation rules using GNP is stated. The correlation rule shows the following relation between attributes in database,

$$if\ X\ then\ Y\ (X \subset I,\ Y \subset I,\ I : item\ set) \quad (1)$$

JUDGEMENT NODE corresponds to each element of set X, while PROCESSING NODE deal with each element of set Y, when a correlation rule is expressed by GNP. We define a correlation rule as the transition from the starting node S to the PROCESSING NODE following a JUDGEMENT NODE J. For example, a correlation rule of $if\ A, B\ then\ C, D$ is expressed by the node connection like Fig.5.

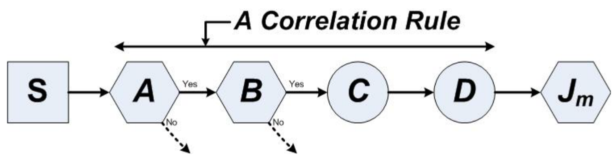

Figure 5: The expression of the correlation rule using nodes in GNP

4.2 Support and Confidence

When the correlation rule is expressed by $(X \Rightarrow Y)$, where X is called antecedent and Y is called consequent, we define *Support* as the ratio of the records satisfying both X and Y, and $Confidence$ as the ratio of records satisfying Y among the records containing X.[1][5] The following *Support* and $Confidence$ are used as the index to evaluate the importance of the correlation rule.

$$\begin{aligned} Support(X \Rightarrow Y) \\ Confidence(X \Rightarrow Y) \end{aligned} \quad (2)$$

For example, *Support* of $(X(A, C) \Rightarrow Y(D))$ is 0.25, and the $Confidence$ is 0.5 in Table.1. In the case of $(X(B, C) \Rightarrow Y(E))$, *Support* is 0.5 and $Confidence$ of it is 1.0.

Comparing with the conventional data mining method (apriori algorithm[1]) that extracts all the rules having more than minimum *Support* and $Confidence$ values in database, GNP has a feature that it can extract correlation rules having high fitness considering the structural condition of GNP.

Table 1: Database example

Database					
TID	ITEM				
	A	B	C	D	E
1	1	0	1	1	0
2	0	1	1	0	1
3	1	1	1	0	1
4	0	1	0	0	1

4.3 Fitness

Individuals of GNP are evolved by an evolutionary algorithm using *Support* and $Confidence$ as the index of fitness. The fitness of the proposed algorithm uses the following:

$$Fitness = \frac{1}{|L|} \left(\sum_{l \in L} Support(l) \times Confidence(l) \right) \quad (3)$$

L	:	set of the number of rules in GNP
Support(l)	:	Support of rule l in GNP
Confidence(l)	:	Confidence of rule l in GNP

4.4 Extracting correlation rules by GNP

We set up several constraints to extract the correlation rules effectively in designing GNP. First, GNP reuses the nodes. If the node already used is reused at JUDGEMENT NODEs, a loop is created among JUDGEMENT NODEs. To overcome the loop problem, we set up several JUDGEMENT NODEs in GNP which express the same item.

In addition, we set several starting nodes connecting to JUDGEMENT NODEs, which means that all the rules are created by searching all the tuples in the database from the starting nodes.

The method to generate correlation rules using GNP is as follows:

1. Generate if part of the rule by searching the tuples in the database.

2. Generate then part of the rule by transfering the PROCESSING NODEs in GNP.

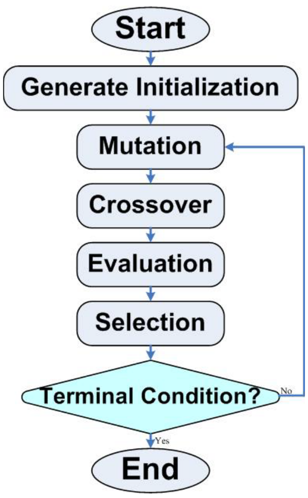

Figure 6: The flow chart of the proposed algorithm

We use a general evolutionary algorithm and select the better individuals for the next generation.

The flow chart of the proposed algorithm is as follow (See Fig.6).

1. Initialize GNP randomly.
2. Apply genetic operations to GNP.
3. Generate correlation rules using GNP.
4. Evaluate the generated rules by $Support$ and $Confidence$ of the rules.
5. Calculate the fitness of each individual.
6. Select the better individuals to the next generation.
7. Move to 2, until a terminal condition meets.

5 Simulation

The effectiveness of the proposed algorithm is studied by extracting the correlation rules from the database having 10 attributes.

5.1 Simulation Parameters

200 individuals of GNP are used considering that many rules should be extracted in a short running time. The mutation probability and the crossover probability were set at 0.01 and 0.1 respectively[2][3][4]. We also used the elite strategy to move the elite individual to the next generation.[2]

5.2 Simulation Results

Database is made up of 10 attributes (from A to J) and 100 records. Each attribute is a binary code. Assuming the market basket analysis as an benchmarking problem, 0 denotes that the customer doesn't buy the item and 1 indicates that he buys the item. Moreover, the database used in the simulation is made artificially. For example, we set five artificial rules in the database like the records from 1 to 6 are the ones for extract-

Table 2: $Support$ and $Confidence$ of the given 5 kinds of rules

	Correlation Rule	Support	Confidence
1	$A \Rightarrow J$	0.050000	0.500000
2	$B \Rightarrow E$	0.060000	0.461538
3	$C \Rightarrow D$	0.070000	0.636364
4	$F \Rightarrow G$	0.060000	0.666667
5	$H \Rightarrow I$	0.060000	0.428571

Table 3: The results wiht evolutionary algorithm

	Correlation Rule	Support	Confidence
1	$A \Rightarrow J$	0.050000	0.500000
2	$B \Rightarrow E$	0.060000	0.461538
3	$C \Rightarrow D$	0.070000	0.636364
4	$F \Rightarrow G$	0.060000	0.666667
5	$H \Rightarrow I$	0.060000	0.428571
6	$A \Rightarrow C$	0.010000	0.100000
7	$BE \Rightarrow D$	0.010000	0.166667
8	$B \Rightarrow H$	0.010000	0.076923
9	$E \Rightarrow D$	0.030000	0.214286
10	$C \Rightarrow J$	0.020000	0.181818
11	$I \Rightarrow H$	0.060000	0.400000
12	$D \Rightarrow E$	0.030000	0.250000
13	$J \Rightarrow A$	0.050000	0.416667
14	$DJ \Rightarrow C$	0.010000	1.000000
15	$I \Rightarrow G$	0.030000	0.200000
16	$C \Rightarrow G$	0.020000	0.181818
17	$DF \Rightarrow E$	0.010000	1.000000
18	$J \Rightarrow C$	0.020000	0.166667
19	$G \Rightarrow F$	0.060000	0.375000
20	$B \Rightarrow G$	0.000000	0.000000
21	$I \Rightarrow A$	0.010000	0.066667
22	$D \Rightarrow C$	0.070000	0.583333
23	$E \Rightarrow B$	0.060000	0.428571

Table 4: Comparing the elite individual at each generation

Generation	The total number of extracted rules	Fitness
300	89	0.076441
500	92	0.078151
1000	89	0.080956

ing ($A \Rightarrow J$), the records ($7 \sim 12$) are for ($B \Rightarrow E$), the records ($13 \sim 18$) are for ($C \Rightarrow D$), the records ($19 \sim 24$) are for ($F \Rightarrow G$), and the records ($25 \sim 30$) are for ($H \Rightarrow I$). The records from 31 to 100 are made randomly.

Table.2 shows *Support* and *Confidence* of the given 5 kinds of rules and Table.3 shows the results with the proposed algorithm. Comparing Table.2 and Table.3, we can see that the rules from 1 to 5 in Table.2 and.3 are the same. The results from 6 to 23 in Table.3 denote the rules extracted from the records (31 to 100). These results show that it is possible to extract rules using the proposed algorithm.

Table.4 shows the total number of rules and the fitness from the elite individual at each generation. According to Table.4, we can see the elite individual extracted 92 rules at 500th generation, which are more than the ones of 1000th generation. However, we also see the fitness at 1000th generation is higher than 500th generation. We can see the elite individual at 1000th generation extracted better rules than the one at 500th generation according to the proposed algorithm because the fitness of 1000th generation is higher than that of 500th generation, although the elite individual at 500th generation extracted more rules than that at 1000th generation.

The simulation results show that *Support* and *Confidence* of the extracted rules increase as generation goes on. This indicates that the proposed algorithm is useful to extract rules and can extract many effective rules through generations.

Fig.7 denotes the fitness of the elite individual, the average fitness values over all individuals, and the worst fitness at each generation. We extracted the rules of Table.3 from the elite individual.

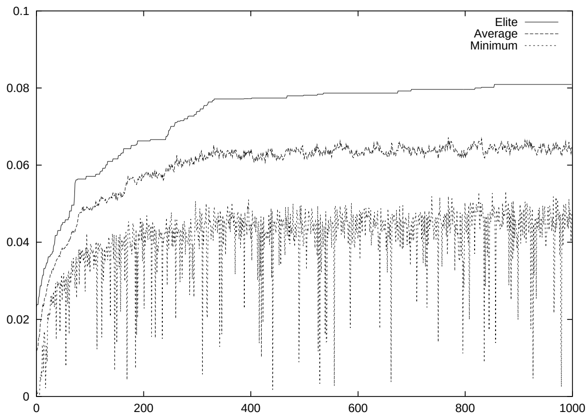

Figure 7: Simulation result

6 Conclusions

We proposed the data mining technique using GNP in this paper. And we studied the effectiveness of the proposed method in terms of extracting rules. Concretely, the fitness of each individual is calculated using *Support* and *Confidence* of the database, the better individuals having the higher fitness are selected, and finally the effective rules from the elite individual are extracted.

We have studied the effectiveness of the data mining using the proposed algorithm so far. The comparison of the proposed method with other methods is going underway.

References

[1] T. Fukuda, Y. Morimoto, and T. Tokuyama, "Data Mining - in japanese -", *Kyoritsu Press*, 2002.

[2] K. Hironobu, K. Hirasawa, J. Hu, J. Murata, M. Kosaka, "Network Structure Oriented Evolutionary Model : Genetic Network Programming", *Trans. of the Society of Instrument and Control Engineers, Vol.38, No.5, pp.485-494*, 2002.

[3] K. Hirasawa, M. Okubo, J. Hu, J. Murata, Y. Matsuya, "Co-evolution of Hetero Multiagent Systems using Genetic Network Programming", *IEEJ Trans. EIS, Vol.123, No.3, pp.554-551*, 2003.

[4] K. Hironobu, K. Hirasawa, J. Hu, J. Murata, "Variable Size Genetic Network Programming", *IEEJ Trans. EIS, Vol.123, No.1, pp.57-66*, 2003.

[5] David J. Hand, Heikki Mannila, Padhraic Smyth "Principles of Data Mining", *MIT Press*, 2001.

The Tenth International Symposium on Artificial Life and Robotics 2005(AROB 10th '05),
B-con Plaza, Beppu, Oita, Japan, February 4-6, 2005

Performance Comparison between Fuzzy Rules and Interval Rules in Rule-Based Classification Systems

Satoshi Namba, Yusuke Nojima, and Hisao Ishibuchi
Department of Industrial Engineering
Osaka Prefecture University
Gakuen-cho 1-1, Sakai, Osaka 599-8531, Japan
{snamba, nojima, hisaoi}@ie.osakafu-u.ac.jp

Abstract

In this paper, we compare the performance of fuzzy rule-based classification systems with that of interval rule-based classification systems on real-world data sets. We generate multiple rule-based classification systems using an evolutionary multiobjective optimization (EMO) algorithm. In our EMO approach, the classification accuracy of rule sets is maximized, while their complexity is minimized. A number of non-dominated rule sets with different accuracy and different complexity are obtained by its single run. Through computational experiments on some data sets, we compare the generalization ability of fuzzy rule-based systems with that of interval rule-based systems using the ten-fold cross-validation technique. Furthermore, we perform the same computational experiments with fuzzified interval rule-based classification systems. From experimental results, we clearly demonstrate characteristics of each classification system: fuzzy rule-based classification systems have high generalization ability on test data, interval classification systems can achieve high accuracy on training data, and fuzzified interval classification systems have these advantages of two other classification systems.

1 Introduction

Fuzzy rule-based systems have been applied to various problems such as control, function approximation and pattern classification. The tradeoff between the accuracy and the complexity of fuzzy rule-based systems was often discussed in recent studies [1, 2]. When we design fuzzy rule-based classification systems, it should be noted that the maximization of the accuracy on training data often leads to the overfitting, which degrades the actual performance of fuzzy rule-based classification systems on test data.

Fuzzy rule-based systems are interpretable for human users. In our former study on fuzzy rule extraction [2], antecedent fuzzy sets in fuzzy rule-based classification systems are homogeneously triangular. Homogeneous fuzzy discretization works well because there are significant overlaps between adjacent fuzzy sets. Decision boundaries are adjustable over those overlapping regions using the certainty grade of each fuzzy rule. On the other hand, antecedent intervals in interval rule-based classification systems are generated from given numerical data using an entropy measure in some approaches to the design of decision trees [3]. We combine some advantages of fuzzy rule-based systems and interval ones into fuzzified interval rule-based classification systems. That is, the antecedent fuzzy sets in fuzzified interval rule-based classification systems are derived from intervals in the interval rule-based systems by fuzzification.

In this paper, we compare the performance of fuzzy rule-based classification systems with that of interval rule-based classification systems. All the rule-based classification systems are constructed by using our EMO approach [2]. Furthermore, we perform the same computational experiments with fuzzified interval rule-based classification systems. Experimental results show that interval rule-based classification systems can obtain high accuracy on training data, while high generalization ability on test data can be obtained by fuzzy rule-based classification systems. It is also shown that the generalization ability of the interval rule-based classification systems can be improved by their fuzzification.

2 Rule-Based Classification Systems

We use the following type of rules for an n-dimensional pattern classification problem:

$$\text{Rule } R_q : \text{If } x_1 \text{ is } A_{q1} \text{ and } \dots \text{ and } x_n \text{ is } A_{qn} \text{ then Class } C_q \text{ with } CF_q, \quad (1)$$

where $\mathbf{x} = (x_1, ..., x_n)$ is an n-dimensional pattern vector, $\mathbf{A}_q = (A_{q1}, ..., A_{qn})$ is an antecedent part (i.e., fuzzy sets in fuzzy rule-based systems, and intervals in interval ones), C_q is a consequent class, and CF_q is a rule weight (i.e., certainty grade). First we explain how the consequent class C_q of the classification rule R_q in (1) is specified from numerical data. Let us assume that we have m labeled patterns $\mathbf{x}_p = (x_{p1},...,x_{pn})$, $p = 1,2,...,m$ from M classes. We define the compatibility grade $\mu_{\mathbf{A}_q}$ of each training pattern $\mathbf{x}_p$ with the antecedent part $\mathbf{A}_q$ of the rule R_q using the product operator as

$$\mu_{\mathbf{A}_q}(\mathbf{x}_p) = \mu_{A_{q1}}(x_{p1}) \cdot \mu_{A_{q2}}(x_{p2}) \cdot \ldots \cdot \mu_{A_{qn}}(x_{pn}), \quad (2)$$

where $\mu_{A_{qi}}(\cdot)$ is the membership function of an antecedent set A_{qi}. We first calculate the confidence of the classification rule "$\mathbf{A}_q \Rightarrow$ Class h" in the field of data mining:

$$c(\mathbf{A}_q \Rightarrow \text{Class } h) = \sum_{\mathbf{x}_p \in \text{Class } h} \mu_{\mathbf{A}_q}(\mathbf{x}_p) \Big/ \sum_{p=1}^{m} \mu_{\mathbf{A}_q}(\mathbf{x}_p). \quad (3)$$

The consequent class C_q of the rule R_q is specified by identifying the class with the maximum confidence as

$$c(\mathbf{A}_q \Rightarrow \text{Class } C_q) = \max_{h=1,2,...,M} \{c(\mathbf{A}_q \Rightarrow \text{Class } h)\}. \quad (4)$$

Using the confidence measure, we specify the rule weight CF_q as

$$CF_q = c(\mathbf{A}_q \Rightarrow \text{Class } C_q) - \sum_{\substack{h=1 \\ h \neq C_q}}^{M} c(\mathbf{A}_q \Rightarrow \text{Class } h). \quad (5)$$

If the rule weight CF_q is negative, we do not generate the rule "$\mathbf{A}_q \Rightarrow$ Class h".

Let S be a set of classification rules. A new pattern $\mathbf{x}_p$ is classified by a single winner rule R_w, which is chosen from the rule set S as

$$\mu_{\mathbf{A}_w}(\mathbf{x}_p) \cdot CF_w = \max\{\mu_{\mathbf{A}_q}(\mathbf{x}_p) \cdot CF_q \mid R_q \in S\}. \quad (6)$$

The winner rule R_w has the maximum product of the compatibility grade and the rule weight in S.

2.1 Fuzzy Rules

All attribute values are normalized into real numbers in the unit interval [0, 1]. As antecedent fuzzy sets, we use *"don't care"* and 14 homogeneous triangular fuzzy sets in Fig. 1 (see [2]).

2.2 Interval Rules

The whole domain interval is divided into K intervals. To specify $(K-1)$ cutting points for each attribute, we use an optimal splitting method [3] based on the class entropy measure:

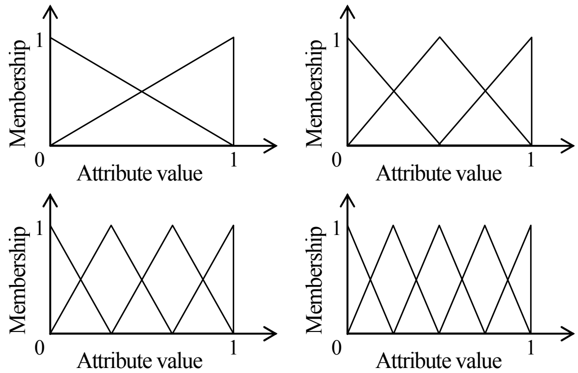

Figure 1: Four fuzzy partitions used in our computer simulations.

$$H(A_1, ..., A_K) = -\sum_{j=1}^{K} \frac{|D_j|}{|D|} \sum_{h=1}^{M} \left(\frac{|D_{jh}|}{|D_j|} \cdot \log_2 \frac{|D_{jh}|}{|D_j|} \right), \quad (7)$$

where $(A_1, ..., A_K)$ are K intervals generated by the discretization of an attribute, D_j is the set of training patterns in the interval A_j, and D_{jh} is the set of training patterns from Class h in D_j. We can efficiently find the optimal $(K-1)$ cutting points that minimize the class entropy measure in (7). In computational experiments, we use five partitions with K intervals where $K = 1,2,3,4,5$ as in Fig. 2 (see [4]).

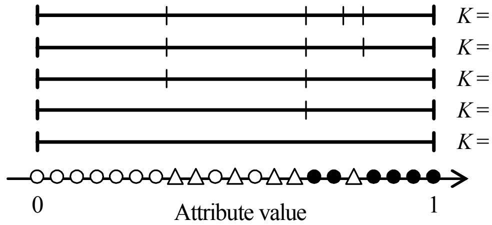

Figure 2: Five partitions with different granularities.

2.3 Fuzzified Interval Rules

We also examine the performance of fuzzy rule-based systems of the antecedent fuzzy sets in Fig. 3. The antecedent fuzzy sets of those rules are generated by fuzzifying intervals in Subsection 2.2. For more details on our fuzzification, see [5].

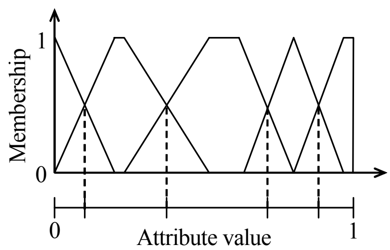

Figure 3: Fuzzy sets derived from intervals.

3 Heuristic Rule Extraction and Genetic Rule Selection

As in our former studies on the design of fuzzy rule-based classifiers [2], we handle knowledge extraction as the following three-objective rule selection problem:

$$\text{Maximize } f_1(S) \text{ and minimize } f_2(S) \text{ and } f_3(S), \quad (8)$$

where S is a subset of candidate rules, $f_1(S)$ is the number of correctly classified training patterns by S, $f_2(S)$ is the number of fuzzy rules in S, and $f_3(S)$ is the total rule length in S. The number of antecedent conditions of each fuzzy rule is referred to as the rule length in this paper. To solve (8), we apply a two-step method (i.e., heuristic rule extraction and genetic rule selection).

First, in heuristic rule extraction, a pre-specified number of candidate rules with the largest values of the following criterion are found for each class.

$$f_{\text{SLAVE}}(R_q) = s(\mathbf{A}_q \Rightarrow \text{Class } C_q) - \sum_{\substack{h=1 \\ h \neq C_q}}^{M} s(\mathbf{A}_q \Rightarrow \text{Class } h), \quad (9)$$

where $f_{\text{SLAVE}}(\cdot)$ is a modified version of a rule evaluation criterion in an iterative genetic learning algorithm called SLAVE [6], and $s(\cdot)$ is the support defined as follows:

$$s(\mathbf{A}_q \Rightarrow \text{Class } h) = \frac{1}{m} \sum_{\mathbf{x}_p \in \text{Class } h} \mu_{\mathbf{A}_q}(\mathbf{x}_p). \quad (10)$$

For designing rule-based systems with high comprehensibility, only short rules are examined as candidate rules. This restriction on the rule length is consistent with the third objective (i.e., to minimize the total rule length) of our three-objective formulation in (8).

Second, in genetic rule selection, let us assume that N rules have been extracted as candidate rules using the SLAVE criterion (i.e., N/M rules for each class). A subset S of the N candidate rules is represented by a binary string of the length N as

$$S = s_1 s_2 \cdots s_N, \quad (11)$$

where $s_j = 1$ and $s_j = 0$ mean that the j-th candidate rule is included in S and excluded from S, respectively. Since rule sets are represented by binary strings, almost all multiobjective genetic algorithms are applicable. In this paper, we use the NSGA-II [7] because its search ability is high and its implementation is relatively easy. We incorporate two problem-specific heuristic tricks into the NSGA-II. One is biased mutation where a larger probability is assigned to the mutation from 1 to 0 than that from 0 to 1. This is for efficiently decreasing the number of rules. The other is the removal of unnecessary rules. Since we use the single winner-based method for classifying each pattern, some rules in S may be chosen as winner rules for no patterns. We can remove those rules without degrading the first objective with respect to the classification accuracy. At the same time, the second and third objectives with respect to the complexity are improved by removing unnecessary rules. Thus, we remove all rules that are not selected as winner rules for any training patterns from the rule set S. The removal of unnecessary rules is performed after the first objective is calculated for each rule set and before the second and third objectives are calculated.

4 Computational Experiments

4.1 Settings of computational experiments

We use six data sets in Table 1. These data sets are available from the UC Irvine machine learning repository. We do not use incomplete patterns with missing values in our computational experiments. All attributes are handled as continuous attributes in this paper.

We evaluate the performance of our EMO approach by ten independent executions (with different data partitions) of the whole ten-fold cross-validation (10CV) procedure (i.e., 10×10CV) in [3]. We extract 300 candidate rules for each class in the heuristic greedy manner using the SLAVE criterion (i.e., 300M candidate rules in total where M is the number of classes).

The NSGA-II [7] is applied to the extracted 300M candidate rules to find non-dominated rule sets with respect to the three objectives. Each of the obtained rule sets is evaluated by test data. We use the following parameter values in the NSGA-II:

Population size: 200 strings,
Crossover probability: 0.8 (uniform crossover),
Biased mutation probabilities:
$p_{\text{m}}(0 \to 1) = 1/300M$ and $p_{\text{m}}(1 \to 0) = 0.1$,
Stopping condition: 5000 generations.

During ten executions of the whole 10CV procedure, the NSGA-II is employed 100 times. We examine the average error rates only for combinations of the number of rules and the average rule length obtained from more than 30 (out of 100) runs. We also calculate the average error rates on training data and test data using the majority vote where all the obtained rule sets in each run except for too small ones are used for the classification of each pattern. Due to their poor performance, we do not use small rule sets with less rules than the number of classes.

Table 1: Data sets used in our computational experiments.

Data set	Attributes	Patterns	Classes
Breast W	9	683*	2
Diabetes	8	768	2
Glass	9	214	6
Heart C	13	297*	5
Sonar	60	208	2
Wine	13	178	3

* Incomplete patterns with missing values are not included.

4.2 Experimental Results

We show the result on the Cleveland heart disease data set (i.e., Heart C in Table 1) in Fig. 4. A number of non-dominated rule sets with different accuracy and different complexity were obtained for each classification system. In the comparison between fuzzy rules and interval rules, we can see that interval rule-based classification systems can obtain high accuracy on training data, while high generalization ability on test data can be obtained by fuzzy rule-based classification systems from this figure. We can also see that fuzzified interval rule-based classification systems are comparable to interval rule-based classification systems on training data, while their generalization ability outperforms two other classification systems.

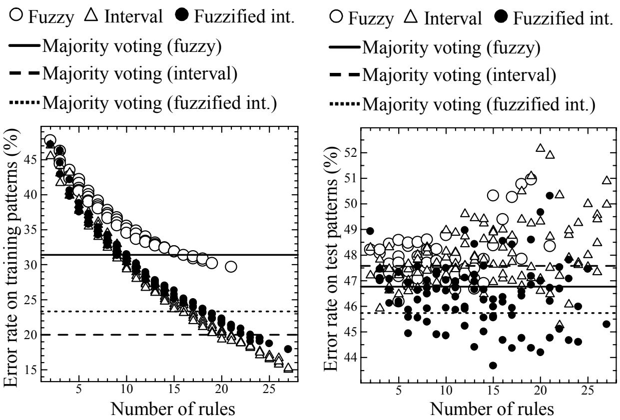

(a) Error rates on training patterns. (b) Error rates on test patterns.

Figure 4: Error rates for the Cleveland heart disease data set.

Table 2: Error rates on test data by majority voting. The best result for each data set is shown by boldface.

Data set	Fuzzy	Interval	Fuzzified int.
Breast W	3.75	4.06	**3.31**
Diabetes	25.73	25.27	**24.29**
Glass	39.31	**30.60**	32.67
Heart C	46.77	47.58	**45.74**
Sonar	**22.16**	25.58	23.59
Wine	**4.15**	5.00	4.78

Table 2 shows error rates on test data by majority voting for each data set. The results show that the generalization ability of the interval rule-based classification systems can be improved by their fuzzification for almost all data sets.

5 Summary

We generated multiple rule-based classification systems using an EMO algorithm with respect to the classification accuracy and the complexity, and compared the performance of fuzzy rule-based classification systems with that of interval rule-based classification systems on some benchmark data sets. Experimental results showed that interval rule-based classification systems can obtain high accuracy on training data, while high generalization ability on test data can be obtained by fuzzy rule-based classification systems. It was also shown that the generalization ability of the interval rule-based classification systems can be improved by their fuzzification.

References

[1] H. Roubos and M. Setnes, "Compact and transparent fuzzy models and classifiers through iterative complexity reduction," *IEEE Trans. on Fuzzy Systems*, vol. 9, no. 4, pp. 516-524, August 2001.

[2] H. Ishibuchi and T. Yamamoto, "Evolutionary multiobjective optimization for generating an ensemble of fuzzy rule-based classifiers," *Lecture Notes in Computer Science 2723: Genetic and Evolutionary Computation Conference - GECCO 2003*, pp. 1077-1088, Springer, Berlin, July 2003.

[3] T. Elomaa and J. Rousu, "General and efficient multisplitting of numerical attributes," *Machine Learning*, vol. 36, no. 3, pp. 201-244, September 1999.

[4] H. Ishibuchi and S. Namba, "Evolutionary multiobjective knowledge extraction for high-dimensional pattern classification problems," *Lecture Notes in Computer Science 3242: Parallel Problem Solving from Nature - PPSN VIII*, pp. 1123-1132, Springer, Berlin, October 2004.

[5] H. Ishibuchi and T. Yamamoto, "Performance evaluation of fuzzy partitions with different fuzzification grades," *Proc. of IEEE International Conference on Fuzzy Systems*, pp. 1198-1203, Hawaii, USA, May 2002.

[6] A. Gonzalez and R. Perez, "SLAVE: A genetic learning system based on an iterative approach," *IEEE Trans. on Fuzzy Systems*, vol. 7, no. 2, pp. 176-191, April 1999.

[7] K. Deb, A. Pratap, S. Agarwal, and T. Meyarivan, "A fast and elitist multiobjective genetic algorithm: NSGA-II," *IEEE Trans. on Evolutionary Computation*, vol. 6, no. 2, pp. 182-197, April 2002.

The Tenth International Symposium on Artificial Life and Robotics 2005(AROB 10th '05),
B-con Plaza, Beppu, Oita, Japan, February 4-6, 2005

Design of an Augmented Automatic Choosing Control with the Weighted Automatic Choosing Functions Using Hamiltonian and Genetic Algorithm

Toshinori Nawata
Department of Information and Computer Sciences,
Kumamoto National College of Technology,
Kumamoto, Japan. 861-1102

Hitoshi Takata
Department of Electrical and Electronics Engineering,
Faculty of Engineering, Kagoshima University,
Kagoshima, Japan. 890-0065

Abstract

In this paper we consider a nonlinear feedback control called augmented automatic choosing control (AACC) for nonlinear systems with constrained inputs. It is designed by making use of the LQ controls and the weighted automatic choosing functions. Constant terms which arise from sectionwise linearization of a given nonlinear system are treated as coefficients of a stable zero dynamics. Parameters included in the control are suboptimally selected by minimizing the Hamiltonian with the aid of the genetic algorithm.

1 Introduction

A genetic algorithm (GA)[1] is one of evolutionary computing algorithms to carry out some designing problems in engineering. It has been used to solve such complicated tasks as nonlinear global optimization problems. The purpose of this paper is to present a nonlinear feedback control called AACC (Augmented automatic choosing control), which is designed by making good use of the GA.

Generally, it is easy to design the optimal control laws for linear systems, but it is not so for nonlinear systems, though they have been studied for many years[2]~[7]. One of most popular and practical nonlinear control laws is synthesized by applying a linearization method by Taylor expansion and the linear optimal control method to a given nonlinear system. This is only effective in a small region around the steady state point or in almost linear systems[2]~[4].

To overcome these weakness, the AACC is proposed for nonlinear systems with constrained inputs and its design procedure is as follows. Assume that a system is given by a nonlinear differential equation. Choose a separative variable, which makes up nonlinearity of the given system. The domain of the variable is divided into some subdomains. On each subdomain, the system equation is linearized by Taylor expansion around a suitable point so that a constant term is included in it. This constant term is treated as a coefficient of a stable zero dynamics. The given nonlinear system approximately makes up a set of augmented linear systems, to which the optimal linear control theory is applied to get the linear quadratic (LQ) controls. These LQ controls are smoothly united by using the weighted automatic choosing functions of sigmoid type to synthesize a single nonlinear feedback controller.

This controller is of a structure-specified type which has some parameters, such as the number of division of the domain, regions of the subdomains, points of Taylor expansion, weights and gradients of the automatic choosing functions, and coefficients of the zero dynamics. These parameters must be selected optimally to be just the controller's fit. Since they lead to a nonlinear optimization problem, we are able to solve it by using the GA suboptimally and successfully. The suboptimal values of these parameters are obtained by minimizing the Hamiltonian in this paper.

This approach is applied to a field excitation control problem of power system to demonstrate the splendidness of the AACC. Simulation results show that the new controller using the GA can improve performance remarkably well.

2 Augmented Automatic Choosing Control

Assume that a nonlinear system is given by

$$\dot{x} = f(x) + g(x)u, \quad x \in \mathbf{D} \tag{1}$$

subject to

$$u_{j,min} \leq u[j] \leq u_{j,max} \quad (j = 1, \cdots, r) \tag{2}$$

where $\cdot = d/dt$, $x = [x[1], \cdots, x[n]]^T$ is an n-dimensional state vector, $u = [u[1], \cdots, u[r]]^T$ is an r-dimensional control input vector, $f(x) : \mathbf{D} \rightarrow R^n$ is a nonlinear vector-valued function with $f(0) = 0$ and is continuously differentiable, $g(x) : \mathbf{D} \rightarrow R^{n \times r}$ is a driving matrix with $g(0) \neq 0$ and is continuously differentiable, $u_{j,min}$: the minimum value of $u[j]$, $u_{j,max}$: the maximum value of $u[j]$, $\mathbf{D} \subset R^n$ is a domain , and T denotes transpose.
Considering the nonlinearity of the system (1), introduce a vector-valued function $C : \mathbf{D} \rightarrow R^L$ which

defines the separative variables $\{C_j(x)\}$, where $C = [C_1 \cdots C_j \cdots C_L]^T$ is continuously differentiable. Let D be a domain of C^{-1}. For example, if $x[2]$ is the element which has the highest nonlinearity of (1), then

$$C(x) = x[2] \in D \subset R \quad (L = 1)$$

(see Section 4). The domain D is divided into some subdomains: $D = \cup_{i=0}^{M} D_i$, where $D_M = D - \cup_{i=0}^{M-1} D_i$ and $C^{-1}(D_0) \ni 0$. $D_i (0 \le i \le M)$ endowed with a lexicographic order is the Cartesian product $D_i = \Pi_{j=1}^{L}[a_{ij}, b_{ij}]$, where $a_{ij} < b_{ij}$.
Introduce a stable zero dynamics :

$$\dot{x}[n+1] = -\sigma_i x[n+1] \tag{3}$$

$$(x[n+1](0) \simeq 1, \quad 0 < \sigma_i < 1),$$

where the value of σ_i shall be selected so that $\sigma_i = -\dot{x}[n+1]/x[n+1] \le -\dot{x}[k]/x[k]$ holds for all $k (k = 1, \cdots, n)$. This tries to keep $x[n+1] \simeq 1$ for a good while when the system (1) is not on $C^{-1}(D_0)$.
Combine (1) with (3) to form an augmented system

$$\dot{\mathbf{X}} = \bar{f}(\mathbf{X}) + \bar{g}(\mathbf{X})u \tag{4}$$

where

$$\mathbf{X} = \begin{bmatrix} x \\ x[n+1] \end{bmatrix} \quad \in \mathbf{D} \times R$$

$$\bar{f}(\mathbf{X}) = \begin{bmatrix} f(x) \\ -\sigma_i x[n+1] \end{bmatrix}, \bar{g}(\mathbf{X}) = \begin{bmatrix} g(x) \\ 0 \end{bmatrix}.$$

Let a cost function be

$$J = \frac{1}{2}\int_0^{\infty} \left(\mathbf{X}^T\mathbf{Q}\mathbf{X} + u^T\mathbf{R}u\right) dt \tag{5}$$

where

$$\mathbf{Q} \quad = \quad \begin{bmatrix} Q & 0 \\ 0 & q \end{bmatrix}, \quad R \ni q > 0,$$

$Q = Q^T > 0$ and $\mathbf{R} = \mathbf{R}^T > 0$ which denote positive symmetrix matrices. Values of $\mathbf{Q}$ and $\mathbf{R}$ are properly determined based on engineering experience.
On each D_i, the nonlinear system is linearized by the Taylor expansion truncated at the first order about a point $\hat{X}_i \in C^{-1}(D_i)$ and $\hat{X}_0 = 0$:

$$\begin{aligned} f(x) + g(x)u &\simeq A_i x + w_i + B_i u \\ &\simeq A_i x + w_i x[n+1] + B_i u \end{aligned} \tag{6}$$

where

$$\begin{aligned} A_i &= \partial f(x)/\partial x^T|_{x=\hat{X}_i}, \; B_i = g(\hat{X}_i), \\ w_0 &= 0, \; w_i = f(\hat{X}_i) - A_i\hat{X}_i. \end{aligned}$$

That is, an approximation of (4) is

$$\dot{\mathbf{X}} = \bar{A}_i\mathbf{X} + \bar{B}_i u \quad \text{ on } \; C^{-1}(D_i) \times R \tag{7}$$

where

$$\bar{A}_i \quad = \quad \begin{bmatrix} A_i & w_i \\ 0 & -\sigma_i \end{bmatrix}, \bar{B}_i = \begin{bmatrix} B_i \\ 0 \end{bmatrix}.$$

An application of the linear optimal control theory[3] to (5) and (7) yields

$$u_i(\mathbf{X}) = -\mathbf{R}^{-1}\bar{B}_i^T\mathbf{P}_i\mathbf{X} \tag{8}$$

where the $(n+1) \times (n+1)$ matrix $\mathbf{P}_i$ satisfies the Riccati equation :

$$\mathbf{P}_i\bar{A}_i + \bar{A}_i^T\mathbf{P}_i + \mathbf{Q} - \mathbf{P}_i\bar{B}_i\mathbf{R}^{-1}\bar{B}_i^T\mathbf{P}_i = 0. \tag{9}$$

Introduce an automatic choosing function of sigmoid type with weight d_i:

$$\begin{aligned} I_i(x) \quad = \quad d_i \prod_{j=1}^{L} \Bigg\{ 1 &- \frac{1}{1 + \exp\left(2N\left(C_j(x) - a_{ij}\right)\right)} \\ &- \frac{1}{1 + \exp\left(-2N\left(C_j(x) - b_{ij}\right)\right)} \Bigg\} \end{aligned} \tag{10}$$

where d_i and N are positive real values, $-\infty \le a_{ij}$ and $b_{ij} \le \infty$. $I_i(x)$ is analytic and almost unity on $C^{-1}(D_i)$, otherwise almost zero(see Figure 1).

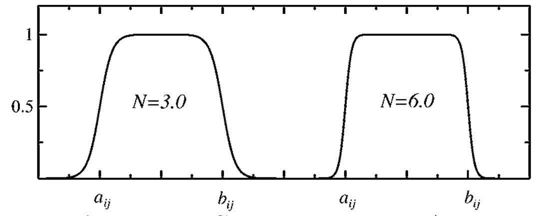

Figure 1: Automatic Choosing Function(N=3.0, 6.0) when $d_i = 1.0$

Uniting $\{u_i(\mathbf{X})\}$ of (8) with $\{I_i(x)\}$ of (10) yields

$$\begin{aligned} \hat{u}(\mathbf{X}) \quad &= \quad [\hat{u}(\mathbf{X})[1], \cdots, \hat{u}(\mathbf{X})[j], \cdots, \hat{u}(\mathbf{X})[r]]^T \\ &= \quad \sum_{i=0}^{M} u_i(\mathbf{X})I_i(x). \end{aligned}$$

We finally have an augmented automatic choosing control which is satisfied with the constraint condition (2) by

$$u(\mathbf{X}) = [u(\mathbf{X})[1], \cdots, u(\mathbf{X})[j], \cdots, u(\mathbf{X})[r]]^T \tag{11}$$

where

$$u(\mathbf{X})[j] = \begin{cases} u_{j,max} & \text{if} \quad \hat{u}(\mathbf{X})[j] \ge u_{j,max} \\ u_{j,min} & \text{if} \quad \hat{u}(\mathbf{X})[j] \le u_{j,min} \\ \hat{u}(\mathbf{X})[j] & \text{otherwise} \end{cases}$$

$$(1 \le j \le r).$$

3 Parameter Selection by GA

The Hamiltonian for Eqs.(4) and (5) is given by

$$H(\mathbf{X},u,\lambda) = \frac{1}{2}\left(\mathbf{X}^T\mathbf{Q}\mathbf{X}+u^T\mathbf{R}u\right) + \lambda^T\left(\bar{f}(\mathbf{X})+\bar{g}(\mathbf{X})u\right). \quad (12)$$

Assume that the adjoint vector $\lambda(\mathbf{X}) \in R^{n+1}$ is defined by

$$\lambda(\mathbf{X}) = [\lambda^I(\mathbf{X})^T, \lambda^{II}(\mathbf{X})^T]^T \quad (13)$$

where $\lambda^I(\mathbf{X}) = [\lambda[1],\cdots,\lambda[r]]^T = -(G^T(x))^{-1}\mathbf{R}u(\mathbf{X})$, $\lambda^{II}(\mathbf{X}) = [\lambda[r+1],\cdots,\lambda[n+1]]^T = [\mathbf{0},E]\hat{\lambda}$,

$$\hat{\lambda} = \sum_{i=0}^{M}\{(\bar{B}_i-\bar{g}(\mathbf{X}))\bar{g}(\mathbf{X})^\dagger+E\}^T\mathbf{P}_i\mathbf{X}I_i(x) \quad \in R^{n+1},$$

$\bar{g}(\mathbf{X})^\dagger\bar{g}(\mathbf{X}) = E$, E is an appropriate-dimentional unit matrix, and † denotes pseudo inverse.
The necessary condition of the optimality is $\partial H/\partial u = 0$ or $u = -\mathbf{R}^{-1}\bar{g}(\mathbf{X})^T\lambda = -\mathbf{R}^{-1}G^T(x)\lambda^I(\mathbf{X})$, which is satisfied with Eq.(11) from Eq.(13). By it, Eq.(12) becomes

$$H(\mathbf{X},u,\lambda) = \frac{1}{2}\mathbf{X}^T\mathbf{Q}\mathbf{X} - \frac{1}{2}u^T\mathbf{R}u + \bar{f}^T(\mathbf{X})\lambda. \quad (14)$$

Thus we can define a performance

$$PI = \int_{\mathbf{D}}|H(\mathbf{X},u,\lambda)|/\mathbf{X}^T\mathbf{X}d\mathbf{X}. \quad (15)$$

A set of parameters included in the control (11):

$$\bar{\Omega} = \left\{M,N,d_i,a_{ij},b_{ij},\hat{X}_i\right\}$$

is suboptimally selected by minimizing PI with the aid of GA[1] as follows.

<ALGORITHM>
step1:A-priori: Set values $\bar{\Omega}_{apriori}$ appropriately.
step2:Parameter: Choose a subset $\Omega \subset \bar{\Omega}$ to be improved and rewrite it by $\Omega = \{M,N,d_i\cdots\} = \{\alpha_k : k=1,\cdot\cdot,K\}$.
step3:Coding: Represent each α_k with a binary bit string of $\widetilde{L}$ bits and then arrange them into one string of $\widetilde{L}K$ bits.
step4:Initialization: Randomly generate an initial population of $\widetilde{q}$ strings $\{\Omega_p : p=1,\cdot\cdot,\widetilde{q}\}$.
step5:Decoding: Decode each element α_k of Ω_p by $\alpha_k = (\alpha_{k,max}-\alpha_{k,min})\,A_k/\left(2^{\widetilde{L}}-1\right)+\alpha_{k,min}$ where $\alpha_{k,max}$:maximum, $\alpha_{k,min}$:minimum, and A_k:decimal value of α_k.
step6:Control: Design $u = u(\mathbf{X})_p \quad (p=1,\cdots,q)$ for Ω_p by using Eq.(11).
step7:Adjoint: Make $\lambda = \lambda(\mathbf{X})_p \quad (p=1,\cdots,q)$ for Ω_p by using Eq.(13).
step8:Fitness value calculation: Calculate

$$PI_p = \int_{\mathbf{D}}\left|\frac{1}{2}\mathbf{X}^T\mathbf{Q}\mathbf{X} - \frac{1}{2}u(\mathbf{X})_p^TRu(\mathbf{X})_p + \bar{f}^T(\mathbf{X})\lambda(\mathbf{X})_p\right|/\mathbf{X}^T\mathbf{X}d\mathbf{X} \quad (16)$$

by Eq.(15), or fitness $F_p = -PI_p$.
Integration of (16) is approximated by a finite sum.
step9:Reproduction: Reproduce each of individual strings with the probability of $F_p/\sum_{j=1}^{\widetilde{q}}F_j$.
step10:Crossover: Pick up two strings and exchange them at a crossing position by a crossover probability P_c.
step11:Mutation: Alter a bit of string (0 or 1) by a mutation probability P_m.
step12:Repetition: Repeat step5∼step11 until prespecified G-th generation. If unsatisfied, go to step2.

As a result, we have a suboptimal control $u(\mathbf{X})$ for the string with the best performance over all the past generations.

4 Numerical Example

Consider a field excitation control problem of power system which is described[6][7] by

$$\widetilde{M}\frac{d^2\delta}{dt^2} + \widetilde{D}(\delta)\frac{d\delta}{dt} + P_e(\delta) = P_{in}$$
$$P_e(\delta) = E_I^2Y_{11}\cos\theta_{11} + E_I\widetilde{V}Y_{12}\cos(\theta_{12}-\delta)$$
$$E_I + T'_{d0}\frac{dE'_q}{dt} = E_{fd}$$
$$E_I = E'_q + (X_d - X'_d)I_d(\delta)$$
$$I_d(\delta) = -E_IY_{11}\sin\theta_{11} - \widetilde{V}Y_{12}\sin(\theta_{12}-\delta)$$
$$\widetilde{D}(\delta) = \widetilde{V}^2\left\{\frac{T''_{d0}(X'_d-X''_d)}{(X'_d+X_e)^2}\sin^2\delta + \frac{T''_{q0}(X_q-X''_q)}{(X_q+X_e)^2}\cos^2\delta\right\},$$

where δ: phase angle, $\dot{\delta}$: rotor speed, $\widetilde{M}$: inertia coefficient, $\widetilde{D}(\delta)$: damping coefficient, P_{in}: mechanical input power, $P_e(\delta)$: generator output power, $\widetilde{V}$: reference bus voltage, E_I: open circuit voltage, and E_{fd}: field excitation voltage. Put x=$[x[1],x[2],x[3]]^T$=$[E_I-\hat{E}_I, \delta-\hat{\delta}_0, \dot{\delta}]^T$ and $u = E_{fd}-\hat{E}_{fd}$, so that

$$\begin{bmatrix}\dot{x}[1]\\ \dot{x}[2]\\ \dot{x}[3]\end{bmatrix} = \begin{bmatrix}f_1(x)\\ f_2(x)\\ f_3(x)\end{bmatrix} + \begin{bmatrix}g_1(x)\\ 0\\ 0\end{bmatrix}u \quad (17)$$

where

Table 1: Performances $\widetilde{J}$

Method	$x^T(0)$				
	[0, 0.4, 0]	[0, 0.6, 0]	[0, 1.2, 0]	[0, 1.35, 0]	[0, 1.39, 0]
LOC	0.954	×	×	×	×
AACC(d_i:fix)	1.121	2.065	3.155	2.769	×
AACC(d_i:GA)	1.364	2.478	2.723	2.165	2.496

× : very large value

$$\begin{aligned}
f_1(x) &= -\frac{1}{kT'_{d0}}\left(x[1]+\hat{E}_I\right) \\
&\quad +\frac{(X_d-X'_d)\widetilde{V}Y_{12}}{k}x[3]\cos\left(\theta_{12}-x[2]-\hat{\delta}_0\right) \\
f_2(x) &= x[3] \\
f_3(x) &= -\frac{\widetilde{V}Y_{12}}{\widetilde{M}}\left(x[1]+\hat{E}_I\right)\cos\left(\theta_{12}-x[2]-\hat{\delta}_0\right) \\
&\quad -\frac{Y_{11}\cos\theta_{11}}{\widetilde{M}}\left(x[1]+\hat{E}_I\right)^2-\frac{\widetilde{D}(x)}{\widetilde{M}}x[3]+\frac{P_{in}}{\widetilde{M}} \\
\widetilde{D}(x) &= \widetilde{V}^2\left\{\frac{T''_{d0}(X'_d-X''_d)}{(X'_d+X_e)^2}\sin^2\left(x[2]+\hat{\delta}_0\right)\right. \\
&\quad \left.+\frac{T''_{q0}(X_q-X''_q)}{(X_q+X_e)^2}\cos^2\left(x[2]+\hat{\delta}_0\right)\right\} \\
g_1(x) &= \frac{1}{kT'_{d0}}, \quad k=1+\left(X_d-X'_d\right)Y_{11}\sin\theta_{11}.
\end{aligned}$$

Assume that the constrained input is subject to

$$u_{min}+\hat{E}_{fd}\le E_{fd}\le u_{max}+\hat{E}_{fd}.$$

Parameters are $\widetilde{M}=0.016095[pu]$, $T'_{d0}=5.09907[sec]$, $\widetilde{V}=1.0[pu]$, $P_{in}=1.2[pu]$, $X_d=0.875[pu]$, $X'_d=0.422[pu]$, $Y_{11}=1.04276[pu]$, $Y_{12}=1.03084[pu]$, $\theta_{11}=-1.56495[pu]$, $\theta_{12}=1.56189[pu]$, $X_e=1.15[pu]$, $X''_d=0.238[pu]$, $X_q=0.6[pu]$, $X''_q=0.3[pu]$, $T''_{d0}=0.0299[pu]$, $T''_{q0}=0.02616[pu]$.

Steady state values are $\hat{E}_I=1.52243[pu]$, $\hat{\delta}_0=48.57°$, $\hat{\dot{\delta}}_0=0.0[deg/sec]$, $\hat{E}_{fd}=1.52243[pu]$. Set $\mathbf{X}=[x^T,x[4]]^T=[x[1],x[2],x[3],x[4]]^T$, $n=3$, $\hat{X}_0=\hat{\delta}_0=48.57°$, $C(x)$=$x[2]$, $L=1$, $\mathbf{Q}$=diag(1,1,1,1), $\mathbf{R}$=1, $d_0=1$ and $x[4](0)=1$. Experiments are carried out for the new control(AACC) and the ordinary linear optimal control(LOC)[2][3].

1) AACC(d_i:GA):
The parameters are suboptimally selected along the algorithm of section 3. $u_{max}=-u_{min}=0.5$. Ω={$M,N,d_i,a_{ij},b_{ij},\hat{X}_i$}. $\widetilde{G}$=100, $\widetilde{q}$=100, $\widetilde{L}$=8, P_c=0.8, P_m=0.03, $\mathbf{D}$=[-1,1]×[-1,1.5]×[-5,5]×[0,1.5]. It results that $M=1$, $N=8.34$, $d_1=0.20$, $a=49.0°$, $\hat{X}_1=75°$.

2) AACC(d_i:fix):
The parameters are suboptimally selected by using a similar way of the **AACC**(d_i:GA) when the weight is fixed at $d_i=1(i=1,\cdots,M)$. Ω={$M,N,a_{ij},b_{ij},\hat{X}_i$}. It results that $M=1$, $N=6.65$, $a=74.9°$, $\hat{X}_1=75°$.

Table1 shows performances by the AACC and the LOC. The cost function of Table1 is $\widetilde{J}=\frac{1}{2}\int_0^{20}\left(\mathbf{X}^T\mathbf{Q}\mathbf{X}+u^T\mathbf{R}u\right)dt$. These results indicate that the AACC is better than the LOC.

5 Conclusions

We have studied an augmented automatic choosing control using the weighted automatic choosing functions for nonlinear systems with constrained inputs. This approach have been applied to a field excitation control problem of power system. Simulation results have shown that this controller using the GA can improve performance remarkably well.

References

[1] D. E. Goldberg, "Genetic Algorithms in Search, Optimization, and Machine Learnings", *Addison-Wesley Pub. Co. Inc.*, 1989.

[2] Y. N. Yu, K. Vongsuriya and L. N. Wedman, "Application of an Optimal Control Theory to a Power System", *IEEE Trans. Power Apparatus and Systems*, 89-1, pp.55–62, 1970.

[3] A. P. Sage and C. C. White III, "Optimum Systems Control (2nd edition)", *Prentice-Hall, Inc.*, 1977.

[4] M. Vidyasagar, "Nonlinear Systems Analysis", *Prentice-Hall, Inc.*, 1978.

[5] A.Isidori, "Nonlinear Control Systems : An Introduction (2nd edition)", *Springer-Verlag*, 1989.

[6] Y.Takagi and T.Shigemasa, "An Application of State-Space Linearization to a Power System Stabilizer", *Proc. 29th CDC*, TA8-1, pp.1553–1558, 1990.

[7] H.Takata, "An Automatic Choosing Control for Nonlinear Systems", *Proc. 35th CDC*, FA10-5, pp.3453–3458, 1996.

The Tenth International Symposium on Artificial Life and Robotics 2005(AROB 10th '05),
B-con Plaza, Beppu, Oita, Japan, February 4-6, 2005

Evolution and Niche Construction in NKES Fitness Landscape

Reiji Suzuki and Takaya Arita

Graduate School of Information Science, Nagoya University
Furo-cho, Chikusa-ku, Nagoya 464-8601, Japan
{reiji, arita}@nagoya-u.jp

Abstract

Niche construction is known as the process whereby organisms, through their metabolism, their activities, and their choices, modify their own and / or each other's niches. Our purpose is to clarify the interactions between evolution and niche construction by focusing on non-linear interactions between genetic and environmental factors shared by interacting species. We have constructed a new fitness landscape model termed NKES model by introducing the environmental factors and their interactions with the genetic factors into Kauffman's NKCS model. Then, we conducted the evolutionary experiments based on the hill-climbing and the niche-constructing processes of species on this landscape. Experimental results have shown that the average fitness among species strongly depends on the ruggedness of the fitness landscape (K) and the degree of the effect of niche construction on the fitness of genes (E). Especially, we observed two different roles of niche construction which brought about the high average fitness. One of the roles prevents the species from getting stuck in the local optimums when K is large and E is small. The other role yields the completely stable state which maintains the high average fitness when K is small and E is large.

Keywords: NKES fitness landscape, niche construction, ecological inheritance, epistasis, artificial life.

1 Introduction

Organisms can modify their own and / or each other's niches (sources of selection) through their metabolism, their activities, and their choices. This process is calld "niche construction", and there are many evidences that it has strong effects on the evolution of organisms in various taxonomic groups although it had been neglected for a long time in evolutionary biology [1]. A typical example of niche-constructing organism is earthworms that change the structure and chemistry of soils through their burrowing behaviors. These changes are accumulated over generations, and then bring about different environmental conditions which expose successive population to different selection pressure. This effect is also called "ecological inheritance" which makes the generation inherit both genes and a legacy of modified selection pressures from ancestral organisms.

The effects of niche construction on evolution have been mainly investigated in population genetics. For instance, Laland et al. constructed two-locus models, in which one locus affects the niche-constructing behavior which produces the resources in the environments and the fitness of the other locus is affected by the amount of accumulated resources [2]. They have shown that niche construction and ecological inheritance yield unexpected results such as the maintenance of polymorphisms, evolutionary momentum and so on. However, previous studies were based on simplified cases as described above despite the fact that real biological systems are more complex in the sense that existing species have mutually affected their courses of evolutions by niche-constructing their shared environment, although only a few individual-based models which focused on the perturbational effects of niche constructions were investigated recently [3].

Our purpose is to clarify the complex relationships between evolution and niche construction by focusing on non-linear interactions between genetic and environmental factors shared by interacting species. For this purpose, we have constructed a new fitness landscape model termed NKES model by introducing the environmental factors and their interactions with the genetic factors into Kauffman's NKCS model [4]. Then, we conducted the evolutionary experiments based on the hill-climbing and the niche-constructing processes of species on this landscape, in which each species can increase its own fitness by changing not only its genetic factors but also the environmental factors. Based on experiments using various settings of the ruggedness of fitness landscape and the strength of the effect of niche construction on the fitness of genetic factors, we clarify how niche-constructing behaviors can facilitate the adaptive evolution of interacting species via the shared environment.

2 Model

2.1 NKES fitness landscape

We constructed NKES model by introducing environmental factors and their interactions with the genetic factors into Kauffman's NKCS model. There are S species who share the same environment of which properties are described as N-length binary values e_i (i=0, $\cdots$, N-1). We define e_i as environmental factors which represent abstract conditions of the shared environment such as the chemistry of soil, the temperature, the humidity, the existence of burrow or nest and so on. Each species s_i (i=0, $\cdots$, S-1) has N genetic factors which are represented as binary values $g_{i,j}$ (j=0, $\cdots$, N-1).

The fitness of each genetic factor $g_{i,j}$ has epistatic interactions not only with other K genetic factors $g_{i,j+k mod N}$ (k=1, $\cdots$, K) in its own species but also has non-linear interactions with E environmental factors e_i (i=0, $\cdots$, E-1). The fitness contribution of each genetic factor caused by interactions among genetic and environmental factors is defined in similar manner to the NKCS model. For each $g_{i,j}$, we prepare a lookup table which defines its fitness corresponding to all possible (2^{K+E+1}) combinations of interacting genetic and environmental factors. The value of each fitness in the lookup table is randomly set within the range of $[0.0, 1.0]$. Thus, the parameter K represents the ruggedness of the fitness landscape of each species and E represents the strength of the effect of niche construction on the fitness of genetic factors in this model. Figure 1 shows an example image of this model when N=5, K=1, E=2 and S=3. Each table represents the value of genetic or environmental factors, and thin arrows that issue from these values represent the existence of non-linear interactions with values of other genetic or environmental factors.

2.2 Evolution and niche construction

In each generation, each species independently chooses the process which yields the best increase in its own fitness from "evolution", "niche construction" or "doing nothing" by using the following procedures: First, we calculate the fitness of the species when randomly selected one genetic factor is flipped. At the same time, we also calculate its fitness when randomly selected one environmental factor is flipped. The former value corresponds to the expected result caused by the evolutionary process and the latter corresponds to that by the niche-constructing process. Then, the species adopts the process which brings about the best fitness by comparing these two fitness and its current fitness. If the current fitness is the best, it does nothing in this generation. After all species have chosen the processes, they actually conduct the adopted processes at the same time. Note that if some species decide to flip the same environmental factor, it is flipped only once in each generation.

The outlined arrows in Figure 1 represent examples of evolutionary process and niche-constructing process. If one species flips the environmental factor by niche construction, this can change the fitness contributions of the other species' genetic factors, and then can bring about different evolutionary or niche-constructing dynamics of the other species. There are indirect interactions among species via niche constructions instead of the direct interactions among them like NKCS model.

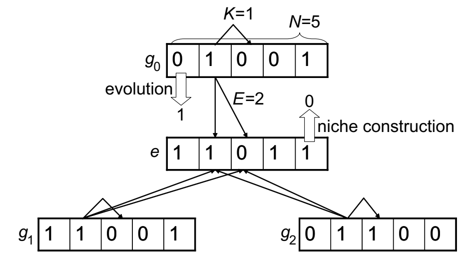

Figure 1: An example of NKES model when N=5, K=1, E=2 and S=3.

3 Experimental results

3.1 General analyses

We have conducted experiments using various settings of K and E (N=80 and S=3) for 100000 generations. The initial values of genetic and environmental factors were randomly decided. Firstly, we focus on the effects of K and E on the average fitness among all species. This index does not only represents how the species could evolve on the current environment but also shows how the environment was modified and become better for all species through niche constructions.

Figure 2 shows the average fitness among all species during the last 1000 generations in various cases of K and E. The x and y axes correspond to the conditions of K and E, and the z axis represents the average fitness on corresponding conditions. Each value is the averages over 20 trials. The first thing we notice is that the average fitness is large (exceeds 0.75) when either K or E is relatively small. In particular, there are two different conditions which brought about the peaks of the average fitness: the cases when K=4 and E=1 (0.78), and when K=1 and E=4 (0.77). Figure 3 also shows the proportion of trials in which the population completely converged to the stable state (the condition that the fitness of any species can not be improved by neither evolution nor niche construction). There is a peak of the proportion of convergence (0.95) in the latter condition, while it is 0.0 in the former condition. It implies that different dynamics of evolution and niche construction brought about the high average fitness under both conditions.

3.2 Evolutionary dynamics when K=4 and E=1

Here, we investigate the two conditions which brought about the high fitness respectively in detail. First, we focus on the case when K=4 and E=1. In this case, it should be noticed that the average fitness

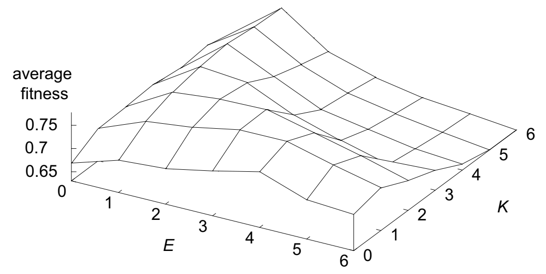

Figure 2: The average fitness in various cases of K and E.

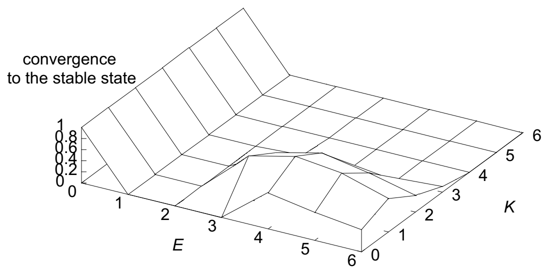

Figure 3: The proportion of the convergence to stable state in various cases of K and E.

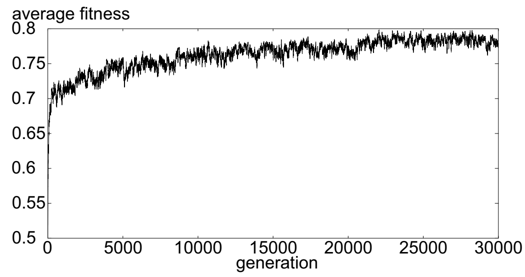

Figure 4: The transition of the average fitness when K=4 and E=1.

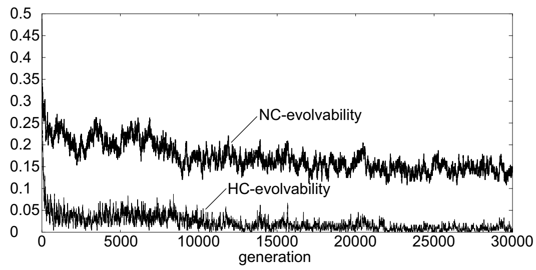

Figure 5: The transitions of the HC-evolvability (thin line) and NC-evolvability (thick line) when K=4 and E=1.

was higher than the corresponding condition without niche construction (K=4 and E=0). When E=0, the evolution of each species rapidly gets stuck in the local optimum because each species is able to climb the fitness landscape to increase its fitness only by changing its genetic factors (not shown). Actually, Figure 3 shows that the population always converged to the stable state in all cases of E=0.

However, when E=1, each species can change its fitness landscape by the niche-constructing process. Figure 4 shows a sample transition of the average fitness among species during the first 30000 generations. Note that the transition of the fitness of each species was approximately similar to that of the average fitness, although it tended to fluctuate around the average fitness. We can see that the species gradually and smoothly increased their fitness and fluctuated around 0.78, but they never converged to the stable state.

In this model, the niche construction does not only simply increase the fitness of performer of the niche construction, but also can decrease the other species' fitness by changing their fitness landscapes. The difference in the average fitness between with and without niche construction is mainly caused by the latter effect of niche construction. Figure 5 shows the transition of the evolvability provided by hill climbing (HC-evolvability) and the evolvability provided by niche construction (NC-evolvability) in the same experiment as Figure 4. The HC-evolvability (or NC-evolvability) represents the average proportion of genetic (or environmental) factors for each species which can increase its own fitness by flipping them. These indices measure how often each species can apply the evolutionary or niche-constructing process in order to increase its fitness. Figure 5 shows that the NC-evolvability kept a relatively large value, while the HC-evolvability approached to almost 0.0 after the drastic decrease in both indices until a few hundreds generation. This means that the species were almost getting to local optimums, but the continuous niche constructions through generations prevented them from getting stuck in the local optimums by slightly changing their landscapes and enabled them to obtain higher fitness regardless of their high ruggedness. Thus, the niche construction worked as a moderate perturbation on the other species' hill-climbing processes in this case.

3.3 Evolutionary dynamics when K=1 and E=4

The other condition which yielded the high average fitness is the case of K=1 and E=4. The important difference compared with the previous condition is that the population converged to the stable state in almost all trials as shown in Figure 3. Figure 6 and 7 show the sample transitions of indices respectively. We observe the average fitness completely converged to 0.78 around 22000th generation after its temporal increase and sub-

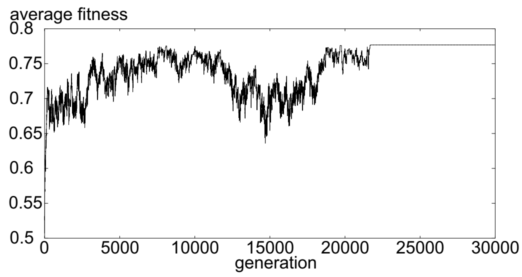

Figure 6: The transition of the average fitness when K=1 and E=4.

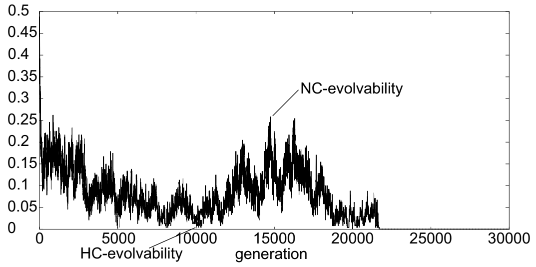

Figure 7: The transitions of the HC-evolvability (thin line) and NC-evolvability (thick line) when K=1 and E=4.

sequent decrease from the initial population. Such a temporal decrease is interesting because all species are always trying to increase their own fitness in our model. Also, the transitions of two indices in Figure 7 were quite similar and the HC-evolvability was just slightly smaller than the NC-evolvability.

These phenomena are supposed to occur due to the reason as follows: As shown in Figure 3, the high average fitness was caused by the convergence to the stable state in this case. It means that the HC-evolvability and NC-evolvability became 0.0 at the same time as shown in Figure 7. When K=1, the NC-evolvability tends to approach to the smaller value as E increases (not shown). It is because that the strong effects of niche construction on the fitness of genetic factors make the species difficult to improve its fitness by niche construction likewise the species more easily gets stuck in the local optimum on the standard NK fitness landscape as K increases. Simultaneously, the increase in E also brings about the large fluctuation around the relatively large value in NC-evolvability (not shown). It is because that as E becomes large, the change in the environmental factor by niche construction of one species more drastically changes the other species' fitness landscapes and draws them back into the bottom of their landscapes. Thus, NC-evolvability frequently approaches to 0.0 when these effects are well-balanced. Also, when E is large, the transition of HC-evolvability tends to be synchronized with the NC-evolvability as shown in Figure 7, and the fluctuation in HC and NC-evolvability becomes larger as K increases (not shown). Thus, the convergent state occurs the most frequently only when K is small and E is large. In addition, the temporal decrease in the average fitness in this case is supposed to be caused by the strong perturbational effects of niche construction as described above.

4 Conclusion

We have discussed the universal nature of interactions between evolution and niche construction by using the NKES fitness landscape model. We found that the average fitness among species strongly depends on the ruggedness of fitness landscape (K) and the strength of the effect of niche construction on the genetic factors (E). It should be emphasized that the two qualitatively different roles of niche construction brought about the high average fitness in different conditions. When K is large and E is small, the niche construction by one species works as moderate perturbation on the other species' hill-climbing processes on the highly rugged landscapes, which prevents them from getting stuck in the local optimums. On the other hand, when K is small and E is large, the strong effect of niche constructions on the fitness of genetic factors yields the convergence to the completely stable state which maintain the high average fitness. Future work includes investigations into the effects of the other parameters on the roles of niche construction and the introduction of learning into the model.

Acknowledgements

This work was supported in part by a Grant-in-Aid for the 21st Century COE "Frontiers of Computational Science".

References

[1] F. J. Odling-Smee, K. N. Laland and M. W. Feldman, *Niche Construction -The Neglected Process in Evolution-*, Princeton University Press, 2003.

[2] K. N. Laland, F. J. Odling-Smee and M. W. Feldman, "Evolutionary Consequences of Niche Construction: A Theoretical Investigation Using Two-locus Theory", *Journal of Evolutionary Biology*, 9: 293–316, 1996.

[3] T. Taylor, "Niche Construction and the Evolution of Complexity", *Proceedings of Artificial Life IX*, pp. 375–380, 2004.

[4] S. Kauffman, *The Origins of Order: Self-Organization and Selection in Evolution*, Oxford University Press, 1993.

The Tenth International Symposium on Artificial Life and Robotics 2005(AROB 10th '05),
B-con Plaza, Beppu, Oita, Japan, February 4-6, 2005

Solving Constrained Motion Problems Using the GI Method[1]

Y. Y. Fan
Department of Civil and Environmental Engineering
University of California
Davis, CA 95616, United States
Email address: yyfan@ucdavis.edu

Abstract Derivation of equations of motion is the central part of analytical dynamics, which is important in the design of machines and prosthetic devices and in the motion control of spacecraft, robotic devices, and human bodies. This paper summarizes some recent developments of a new method for deriving equations of motion that was originally invented by Kalaba and Udwadia. Through simple examples, we demonstrate the simplicity of this method, its easy numerical implementation in modern computing environment, and its advantage of handling modification of constraints.

Key Words Analytical dynamics, nonideal nonholonomic constraints, generalized inverses of matrices, equation of motion

Introduction

Multibody dynamic mechanical systems occur in many classical and modern fields in science and engineering, such as in the design of vehicles, machines, and prosthetic devices, in the motion control of spacecrafts, robots and human bodies, and in the dynamic machinery control that can be integrated into active structural control against earthquake risk. For example, studies of human motion often begin with a simplified mechanical system of point masses and rigid bodies with constraints on motion. Flexible building structures (for protection against earthquakes) can be represented by a lumped system of point masses and springs. All efforts in modeling, simulating and controlling such dynamic systems start with the derivation of equations of motion, which is the central part of analytical dynamics.

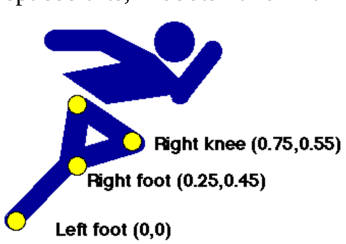

As the classical field of analytical dynamics still serves as the theoretical foundation for many problems in modern science and technology, the complexity and large scale of most challenging and exciting new problems usually demand interdisciplinary collaboration and the aid of modern computers. The advanced mathematical concepts in classical Lagrangian mechanics are often difficult to understand outside of classical mechanics. In addition, most classical methods were developed before the computer era. Their formulation and derivation do not allow us to make the best use of the modern computing environment. Lastly, much of the classical analysis is based on the principle of virtual work, an assumption that Lagrange made to avoid thermodynamics concerns. Thus, constraints that involve forces that *do* work, such as friction, have been ruled out of classical methods. This limitation makes modeling difficult in situations where friction is not insignificant. For instance, in studies of the motion of sports-injured and the elderly, friction is often the driving force that causes great pain and limits the motion and cannot therefore be neglected. Therefore, new methods, together with extension and generalization of classical methods, are required for theoretical and practical reasons.

Recent development [1,2] on equations of motion for constrained mechanical systems opens possibilities for addressing the above mentioned limitations of classical methods. This new method exploits the advantages of the modern computing environment. It begins the analysis directly from the constraints of motion imposed on the systems, and arrives at an explicit set of equations of motion by using the chain rule of differentiation and the concept of generalized inverses (GI) of matrices. No generalized coordinate systems or any physical assumptions are required in the derivation. This new method handles *nonholonomic*[2] constraints with the same ease as holonomic constraints. More importantly, it takes into account the *nonideal*[3] constraints in a systematic and convenient manner. For brevity, the new method for deriving equations of motion will henceforth be referred to as the "GI method".

Recent Development of the GI Method

The original GI method [1] is equivalent to the classical methods such as Lagrange equation, Gibbs-Appel Equation, Hamilton Equation, and Gauss's

[1] This special presentation is dedicated to Prof. Robert Kalaba (September 1926 - September 2004) by his last student Dr. Yueyue Fan. The work is based on their most recent collaboration on analytical dynamics.

[2] Nonholonomic constraints depend on time, displacement, and velocity, and are nonintegrable.
[3] Nonideal constraints involve forces that *do* work on the system in a virtual displacement.

principle of least constraint. However, the GI method has the advantages of providing an *explicit* equation of motion, easily handling nonholonomic constraints, and requiring no extra effort in treating dependent but consistent constraint equations. Later, the GI formula was further extended to systems including *non-ideal* constraints [3]. Further studies on its relation to other classical principles and its potential contribution to theory toward general dynamic and underdetermined systems are still ongoing [4].

Suppose that a mechanical system that contains p point masses is subjected to m holonomic or nonholonomic equality constraints of the form

$$f_i(x, \dot{x}, t) = 0, \; i = 1, 2, \ldots, m, \tag{0}$$

where x is the displacement vector of the system of dimension $3p = n$. We also introduce the mass matrix M, which is of dimension $3p$ by $3p$, is a diagonal matrix, is positive definite, and has the masses $m_1, m_2, \ldots, m_p$ down the main diagonal in groups of three, with zeros elsewhere. As usual, $\dot{x}$ is the time derivative of x. Use of the chain rule of differentiation leads to a set of m equations that are *linear* in $\ddot{x}$, of the form

$$A\ddot{x} = b, \tag{1}$$

where A is an m by $n = 3p$ matrix function of x, $\dot{x}$, and t, and b is an m by 1 column vector that may depend upon x, $\dot{x}$, and t. Given the initial conditions on x and $\dot{x}$, Eq. (1) is equivalent to Eq. (0).

If only ideal constraint forces are considered, it has been shown that the actual system acceleration vector is given by the explicit formula

$$\ddot{x} = a + M^{-1/2}(AM^{-1/2})^{+}(b - Aa), \tag{2}$$

where $(AM^{-1/2})^{+}$ denotes the usual pseudoinverse of the matrix $AM^{-1/2}$. Vector a is the free motion acceleration if there were no constraint. Refer to reference [1] for the details.

Later, the GI formula was further extended to systems including *non-ideal* constraints [3]. The general equation of motion is

$$M\ddot{x} = F^N + F^L + F^C, \tag{3}$$

where

$$F^N = Ma, \tag{4}$$

$$F^L = M^{1/2}(AM^{-1/2})^{+}(b - Aa), \tag{5}$$

$$F^C = M^{1/2}[I - (AM^{-1/2})^{+}AM^{-1/2}]M^{-1/2}c, \tag{6}$$

and a is the free motion acceleration vector, and c is an arbitrary vector, both being of dimension 3n by 1. The notation recalls the names of Newton, Lagrange, and Coulomb. It has been shown in reference [3] that F^N is the newtonian impressed force vector, that F^L is a constraint force that does no work on the system in a virtual displacement v, and that F^C is a constraint force that *does* work on the system in a virtual displacement v. The type of force represented by F^C is called non-ideal constraint force, which includes sliding friction.

Eq. (3) is the most general possible equation of motion that is compatible with the constraint condition $A\ddot{x} = b$, assuming, of course, that the matrix M is nonsingular. Only two essential mathematical ideas are essential in the derivation of Eq. (3): the chain rule of differentiation and generalized inverses of matrices. Modern computing environments, such as Matlab, have built-in commands for calculating the generalized inverse of a matrix, so it makes the approach highly suitable for numerical studies. On the physical side the notions of mass, distance and time occur. There is no mention of kinetic energy, potential energy, moments, etc.. In the applications to specific systems, of course, the customary centripetal and Coriolis forces, moments, and so on do appear. These notions emerge naturally from the terms in the right side of Eq. (3), but no prior exposure to them is needed.

In classical analytical mechanics, it is assumed that the constraint force does no work in a virtual displacement. This means that the fundamental assumption of classical analytical mechanics is that $F^C = 0$, so that the equations of motion, Eq (3) reduce to Eq. (2). More generally, though, as in situations in which sliding friction is significant, we shall have $F^C \neq 0$, in which case the more general equation of motion, Eq. (3), will apply.

A Simple Example

A simple example is used to illustrate how the GI formula works. Consider a double pendulum system subjected to ideal constraints. The rectangular coordinates (x_1 y_1), (x_2 y_2) are as shown in Figure 1. The two constraints on the system are

$$x_1^2 + y_1^2 = l_1^2, \tag{7}$$

and

$$(x_2 - x_1)^2 + (y_2 - y_1)^2 = l_2^2. \tag{8}$$

Eqs. (7) and (8) on two differentiations give

$$A\ddot{x} = b, \tag{9}$$

where

$$A = \begin{bmatrix} x_1 & y_1 & 0 & 0 \\ x_1 - x_2 & y_1 - y_2 & x_2 - x_1 & y_2 - y_1 \end{bmatrix}, \tag{10}$$

and

$$b = \begin{bmatrix} -(\dot{x}_1^2 + \dot{y}_1^2) \\ -[(\dot{x}_2 - \dot{x}_1)^2 + (\dot{y}_2 - \dot{y}_1)^2] \end{bmatrix}. \tag{11}$$

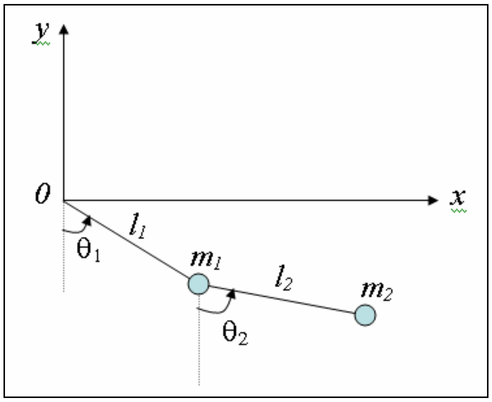

Figure 1: A Double Pendulum

Under ideal constraints, Eq. (2) is the equation of motion for this double pendulum system, with A and b defined by Eqs. (10) and (11). The mass matrix in this two-dimensional problem is

$$M = \begin{bmatrix} m_1 & 0 & 0 & 0 \\ 0 & m_1 & 0 & 0 \\ 0 & 0 & m_2 & 0 \\ 0 & 0 & 0 & m_2 \end{bmatrix}.$$

Let the initial position be $x_1 = l_1$, $y_1 = 0$, $x_2 = l_1 + l_2$, and $y_2 = 0$. Let the initial velocity of both particles be zero. The position and the velocity of the two particles at any time t can be obtained by integrating Eq. (2) with the given initial conditions.

Next, we will show how this double pendulum problem would have been solved in the classical Lagrangian mechanics. Lagrange considered mechanical systems as being characterized by potential energy, kinetic energy and the constraint function, with an emphasis on the use of generalized coordinates to describe the current configuration.

Let us use the two generalized coordinates θ_1 and θ_2 as shown in Figure 1. The virtual work done by the force of gravity is $m_1 g \delta y_1 + m_2 g \delta y_2$. But

$$y_1 = L_1 \cos\theta_1, \tag{12}$$

so that

$$\delta y_1 = L_1 \sin\theta_1 \delta\theta_1, \tag{13}$$

and

$$y_2 = L_1 \cos\theta_1 + L_2 \cos\theta_2, \tag{14}$$

so that

$$\delta y_2 = -(L_1 \sin\theta_1 \delta\theta_1 + L_2 \sin\theta_2 \delta\theta_2). \tag{15}$$

Using these expressions in the expression for virtual work, we get

$$\begin{aligned} Q_1\delta\theta_1 + Q_2\delta\theta_2 &= -[m_1 g L_1 \sin\theta_1 \delta\theta_1 \\ &+ m_2 g(L_1 \sin\theta_1\delta\theta_1 + L_2 \sin\theta_2\delta\theta_2)] \\ &= -(m_1 + m_2) g L_1 \sin\theta_1 \delta\theta_1 - m_2 g L_2 \sin\theta_2 \delta\theta_2 . \end{aligned} \tag{16}$$

Therefore, the generalized forces are

$$Q_1 = -(m_1 + m_2) g L_1 \sin\theta_1 \delta\theta_1, \tag{17}$$

and

$$Q_2 = -m_2 g L_2 \sin\theta_2 \delta\theta_2 . \tag{18}$$

The kinetic energy can be written as

$$T = \frac{1}{2}(m_1 + m_2) L_1^2 \dot{\theta}_1^2 + m_2 L_1 L_2 \dot{\theta}_1 \dot{\theta}_2 \cos(\theta_1 - \theta_2) + \frac{1}{2} m_2 L_2^2 \dot{\theta}_2^2 . \tag{19}$$

The first Lagrange equation

$$\frac{d}{dt}\left(\frac{\partial T}{\partial \dot{\theta}_1}\right) - \frac{\partial T}{\partial \theta_1} = Q_1 \tag{20}$$

yields

$$\frac{d}{dt}[(m_1 + m_2) L_1^2 \dot{\theta}_1 + m_2 L_1 L_2 \dot{\theta}_2 \cos(\theta_1 - \theta_2)] + m_2 L_1 L_2 \dot{\theta}_1 \dot{\theta}_2 \sin(\theta_1 - \theta_2) = -(m_1 + m_2) g L_1 \sin\theta_1, \tag{21}$$

and the second equation

$$\frac{d}{dt}\left(\frac{\partial T}{\partial \dot{\theta}_2}\right) - \frac{\partial T}{\partial \theta_2} = Q_2 \tag{22}$$

becomes

$$\frac{d}{dt}[m_2 L_2^2 \dot{\theta}_2 + m_2 L_1 L_2 \dot{\theta}_1 \cos(\theta_1 - \theta_2)] - m_2 L_1 L_2 \dot{\theta}_1 \dot{\theta}_2 \sin(\theta_1 - \theta_2) = -m_2 g L_2 \sin\theta_2 . \tag{23}$$

Differentiating the left hand members of Eqs. (21, 23) with respect to time, we obtain the equations of motion of the system,

$$\begin{bmatrix} (m_1 + m_2) L_1^2 & m_2 L_1 L_2 \cos(\theta_1 - \theta_2) \\ m_2 L_1 L_2 \cos(\theta_1 - \theta_2) & m_2 L_2^2 \end{bmatrix} \begin{pmatrix} \ddot{\theta}_1 \\ \ddot{\theta}_2 \end{pmatrix} = \begin{pmatrix} -m_2 L_1 L_2 \dot{\theta}_2^2 \sin(\theta_1 - \theta_2) - (m_1 + m_2) g L_1 \sin\theta_1 \\ m_2 L_1 L_2 \dot{\theta}_1^2 \sin(\theta_1 - \theta_2) - m_2 g L_2 \sin\theta_2 \end{pmatrix} \tag{24}$$

By integrating Eq. (24) with the initial conditions $\theta_1(t_0) = 0$ and $\theta_2(t_0) = 0$, we obtain the results of the position of the two particles in the generalized coordinate system. These results, after being converted to the rectangular coordinate system, are compatible with the results from the GI formula.

In an ideal situation, the GI formula and the classical methods are equivalent. However, the derivation of the equations of motion using the classical method is quite complicated even for this simple example.

Handling Modification of Constraints

Most engineering design of mechanical systems involves modification of constraints on the base model. Handling such modification using the classical Lagrange mechanics requires change of the generalized coordinate system, and thus requires change of the generalized forces and the kinetic energy. Each time a constraint is modified, we will have to solve a completely new problem starting from the beginning. However, modification of constraints can be easily handled by the GI formula. Changing constraints of the system only changes matrix A and vector b in the equation of motion, Eq. (4). The rest of the procedure and the data required all remain the same. We will demonstrate this easy implementation using two examples below.

First, let us remove the first constraint in the double pendulum problem. Because only the second constraint is imposed on the system, as given in Eq. (8), only the second row of matrix A and vector b remains. Thus, we have

$$A = \begin{bmatrix} x_1 - x_2 & y_1 - y_2 & x_2 - x_1 & y_2 - y_1 \end{bmatrix}, \tag{25a}$$

and

$$b = -[(\dot{x}_2 - \dot{x}_1)^2 + (\dot{y}_2 - \dot{y}_1)^2]. \tag{25b}$$

Given initial position and velocity of the two particles, the problem can be solved by integrating the equation of motion with the new A and b.

Next, let us add an extra constraint to the original double pendulum problem

$$y_2 = -d \tag{26}$$

to keep the second particle moving along a horizontal line. Differentiate both sides of Eq. (26) twice, we have

$$\ddot{y}_2 = 0, \tag{27}$$

which adds a third row to the original constraints $A\ddot{x} = b$. The new A and b become

$$A = \begin{bmatrix} x_1 & y_1 & 0 & 0 \\ x_1 - x_2 & y_1 - y_2 & x_2 - x_1 & y_2 - y_1 \\ 0 & 0 & 0 & 1 \end{bmatrix}, \tag{28a}$$

and

$$b = \begin{bmatrix} -(\dot{x}_1^2 + \dot{y}_1^2) \\ -[(\dot{x}_2 - \dot{x}_1)^2 + (\dot{y}_2 - \dot{y}_1)^2] \\ 0 \end{bmatrix}. \tag{28b}$$

These are the only changes needed for solving the modified problem. The rest of the procedure remains the same. However, this one-degree-of-freedom problem cannot be easily handled if we were to use the classical methods. To express the kinetic energy and potential energy of the system in terms of single variable can be quite messy.

Conclusions and Discussion

In this paper, we have shown that the GI formula is suitable for the modern computing environment, and has potential to facilitate the analysis and control of large and complex mechanical systems. The only inputs required are the equations of the constraints and the initial conditions on the system. The rest of the procedure, such as differentiating the given functions, computing the generalized inverses of matrices, and integrating systems of differential equations, can be automated for execution by a computer. In order to fully utilize the advantage of the GI formula, a necessary step for future research is to automate the entire analysis of constrained mechanical systems. Full development of the new theory will require long-term cross-disciplinary collaboration from many scholars in mechanics, computational mathematics, and system optimization and control. We hope this paper will serve as an introduction of this GI method to the community of biomechanics and robotics design and will inspire further interest in applying and extending this new method.

References

1. Udwadia FE and Kalaba RE (1992), A New Perspective on Constrained Motion, Proceedings of the Royal Society of London, Series A, v. 439, pp. 407-410.
2. Udwadia FE and Kalaba RE (1996), Analytical Dynamics, Cambridge University Press, New York.
3. Kalaba RE and Udwadia FE (2001), Analytical Dynamics with Constraint Forces that Do Work in Virtual Displacements, Applied Mathematics and Computation, v. 121, pp. 211-217.
4. Fan YY, Kalaba RE, Natsuyama HH, and Udwadia FE, Reflections on the Gauss's Principle of Least Constraint, to appear in Journal of Optimization Theory and Applications.

The Tenth International Symposium on Artificial Life and Robotics 2005(AROB 10th '05),
B-con Plaza, Beppu, Oita, Japan, February 4-6, 2005

Moving Robot Path Search including Obstacles by GA using Quadrant Idea

Hidehiko Yamamoto* and Etsuo Marui

Faculty of Engineering,
Gifu University
1-1, Yanagido, Gifu-shi, 501-1193, Japan
* yam-h@cc.gifu-u.ac.jp

Abstract

This paper describes the problem to search the robot path. We solve this problem by using GA system. To operate GA system for searching the path, Quadrant Usage to Improve Zone (QUIZ), to reduce the search space by using a quadrant idea is proposed. QUIZ also includes new method, Split Coordinates and Avoid Method (SCAM), to avoid obstacles in the maze by splitting zones surrounding the obstacles and to find the path. The Quiz including SCAM is applied to some path search examples. As a result, it is ascertained that QUIZ is useful.

Key words: Path search, GA, Obstacles, Initial individuals

1. Introduction

This research describes the problem to search the robot path. The search is done in the space including obstacles and the robot visits some places in the space. The path search research has been done [1]. Our research finds the path by using Genetic Algorithm (GA). We have developed the path search by using GA [2][3]. This paper proposes the new idea to use the quadrant of an x-y axis to decrease the search space in creating initial individuals of GA. By using the idea, we develop the system to search the path and apply it to some examples.

2. Environments

The problem of the paper is to search the moving robot path in the space including obstacles. As shown in Fig.1, the environments of the research have the maze including many square obstacles. We will search the path that a moving robot moves via some points and solve it by using GA system.

The research for the path problem solved by using GA system has been done. The conventional research environments are simple and it did not include complicated obstacles.

3. QUIZ and SCAM

To operate GA system for searching the path, the paper proposes the new method, Quadrant Usage to Improve Zone (QUIZ), to reduce the search space by using a quadrant idea. QUIZ also includes new method, Split Coordinates and Avoid Method (SCAM), to avoid obstacles in the maze by splitting zones surrounding the obstacles and to find the path. The path search including QUIZ considers a moving path as finding the path by arranging the x-y coordinates in the moving space where a moving robot moves and indicating the coordinate points.

Fig. 2 shows the outline of GA system including QUIZ. Though the conventional GA system carry out to generate initial individuals, calculate fitness for each individual generated and to give crossover and mutation, our GA system starts QUIZ before generating initial individuals. The fitness used in our GA system is adopted as the distance between the robot current point and the next point. The smaller the distance is, the better the fitness is.

The characteristics of QUIZ are to reduce the search space in order to create the excellent individuals beforehand and to create initial individuals corresponding to the ones that will not collide with obstacles or will not become lethal individuals by SCAM system.

3-1. QUIZ

Quiz is the method to limit the search space by excluding useless points beforehand in order that a moving robot does not visit these points. The strategy of QUIZ is to consider the 4 quadrants (1st quadrant, 2nd quadrant, 3rd quadrant and 4th quadrant) that divides the robot moving space with the orthogonal axis (x-y axis) whose origin of the coordinates is the robot current point and consider the search space as one of the 4 quadrants. Because of the strategy, the search space can be reduced to a quarter.

The algorithm of QUIZ is as follows.

Step1: Consider the start point and the end point as $A_i(x_i,y_i)$ and $A_z(x_z,y_z)$ for each.
Step2: Calculate the value k of the equation (1) and, by using the value, C_1 of the equation (2) and C_2 of the equation (3) are acquired. The next rules are carried out and the quadrant that A_x exists is found.

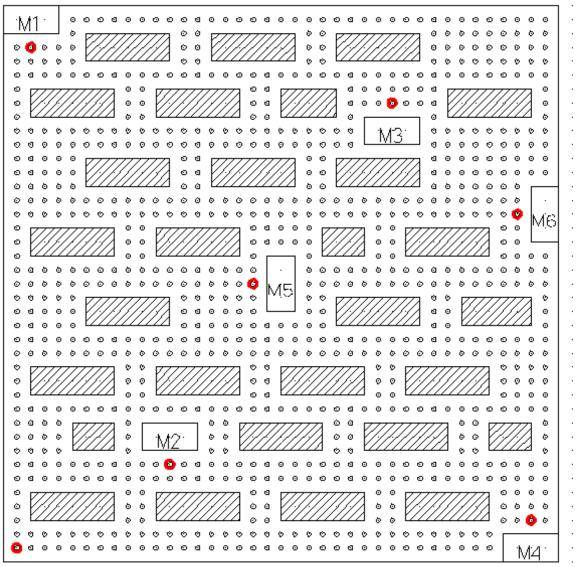

Fig. 1 Search space including obstacles

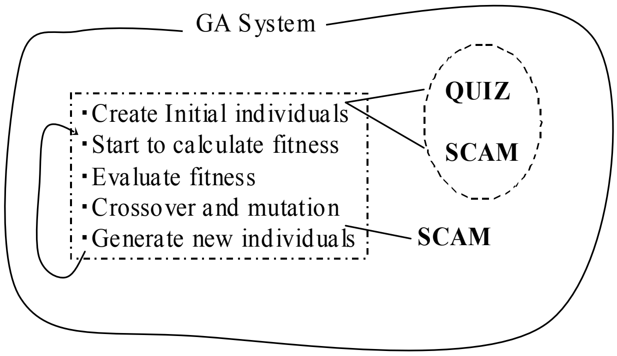

Fig. 2 Outline of GA system

$$k = \sqrt{(x_z - x_i)^2 - (y_z - y_i)^2} \cdot \cdot \cdot \quad (1)$$

$$c_1 = \frac{y_z - y_i}{k} \cdot \cdot \cdot (2)$$

$$c_2 = \frac{x_z - x_i}{k} \cdot \cdot \cdot (3)$$

if: $c_1 \geq 0, c_2 \geq 0$, then: A_z exits in the 1st quadrant
if: $c_1 \geq 0, c_2 < 0$, then: A_z exits in the 2nd quadrant
if: $c_1 < 0, c_2 < 0$, then: A_z exits in the 3rd quadrant
if: $c_1 < 0, c_2 \geq 0$, then: A_z exits in the 4th quadrant

Step 3: Express all points set in the quadrant where A_z exists as Set(A_q), from among the set, select one element and express it as A_n.
Step 4: Carry out SCAM system (judgments to avoid obstacles) between the point A_i and the point A_n. If there is an obstacle, return to Step 3 and if not, consider A_n as the next A_i and go to Step 5.
Step 5: Search a new A_n from among the Set(A_q) and if $A_n = A_z$, go to Step 6, if not, return to Step 4.
Step 6: Consider Ai and the A_n value sequence acquired in Step 3~5 as an initial individual and finish the algorithm. □

In this way, in the process of Step 2, QUIZ searches the quadrant where the current point and the end point exist. In other words, QUIZ calculates the values of $\sin\alpha$ and $\cos\alpha$ in Fig. 3 and searches the quadrant depending on the positive and negative numbers of the values. Because of this, whenever each gene of an initial individual is decided, QUIZ searches the quadrant corresponding to the search space and can reduce the search space as shown in Fig. 4.

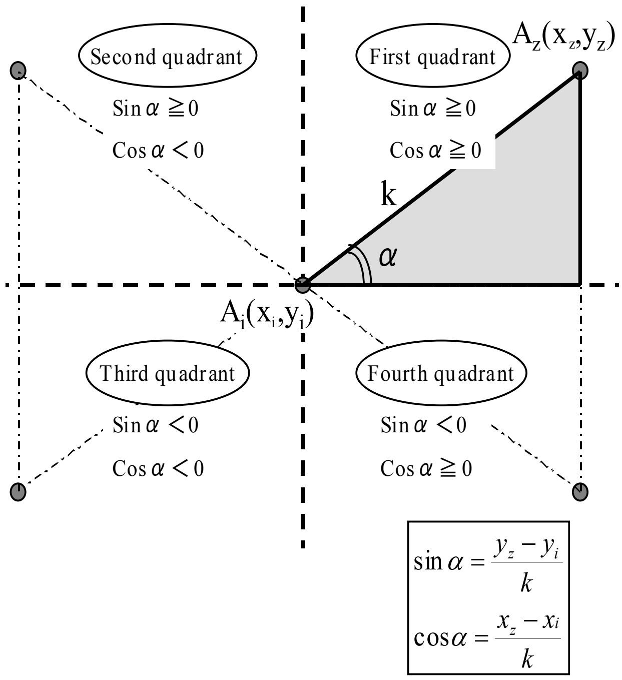

Fig. 3 Quadrant of QUIZ

3-2. SCAM

SCAM is the system to judge whether there is an obstacle between two points a moving robot visits or not. The obstacles of the paper are square. When the straight line that links the current point and the corners of an obstacle is found as shown in Fig. 5, SCAM judges the existence of an obstacle whether the next point is included in the shaded portion or not. In other words, if the next point exists in the shaded portion, it is judged that there is an obstacle between the two points.

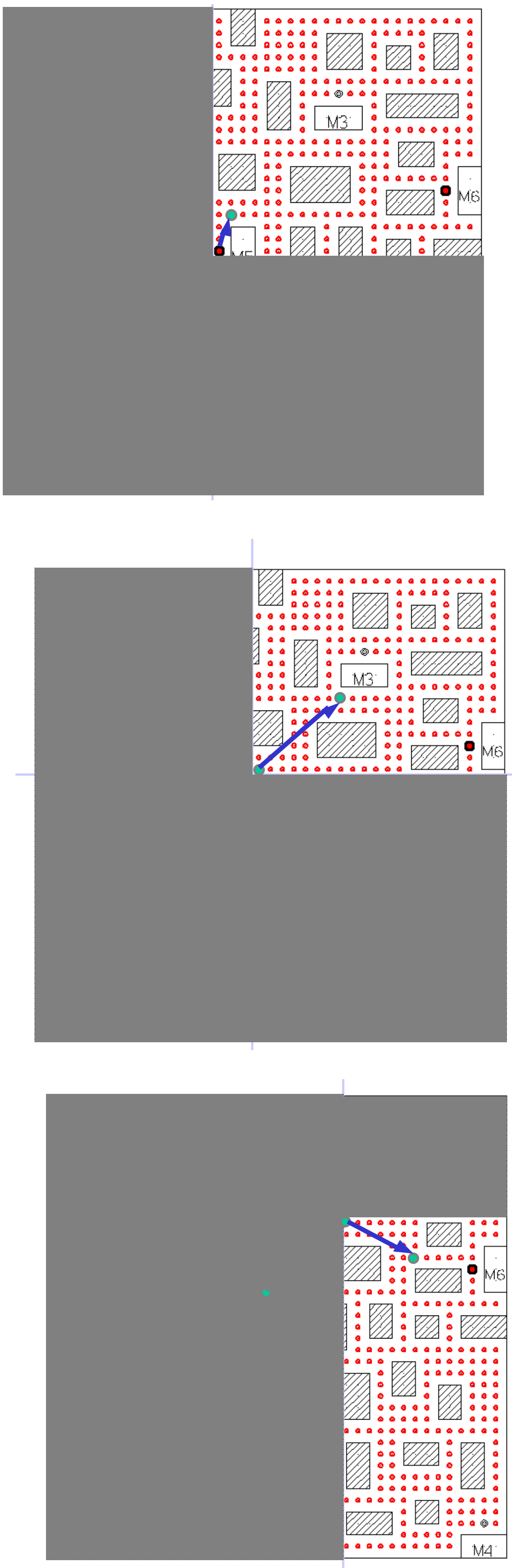

Fig. 4 Example to deduce search space

4. Application Examples

The developed QUIZ including SCAM was applied to some examples. The examples are that moving robots visit some machine (M1~M6) and finally get the end point in the space including obstacles. Fig. 6 and Fig. 7 are the search results.

The examples' moving robots start M1, visit M2, M3, M4, M5 and M6 in turn and finally return M1. In the figures, red marks indicate the bays of each machine and moving robots visit there. Fig. 8 shows the change curves for the maximum fitness of the result used QUIZ and the one not used QUIZ. The curve of Quiz converged earlier and it acquired higher fitness. Judging from the results, it is ascertained that the research to use QUIZ and SCAM is useful.

5. CONCLUSIONS

The research described the path search problem that a moving robot gets the final destination via some points in the space including obstacles by using GA system. Specifically, the idea of the quadrant in the x-y coordinate space was adopted in order to find better individuals in generating initial individuals in GA system. The idea can limit the solution space and converge early to find the solution. The idea is called as QUIZ and in the process of QUIZ, SCAM system not to generate lethal genes corresponding to the path that collides with an obstacle was adopted.

After applying the developed system to some path search examples, it is ascertained that the developed system can get better paths and earlier converge.

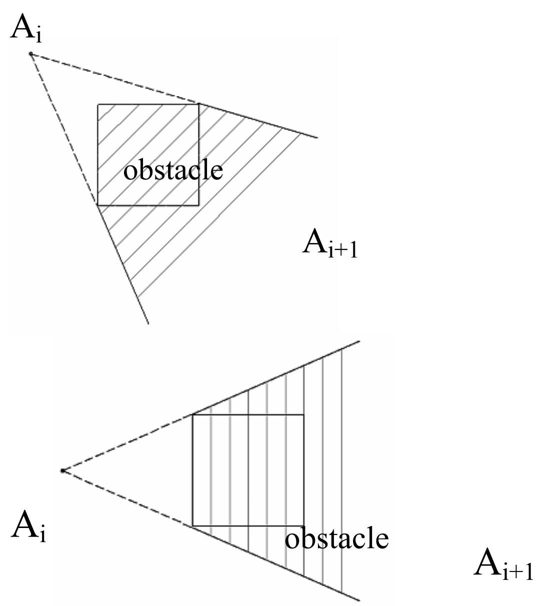

Fig. 5 Obstacles and moving points

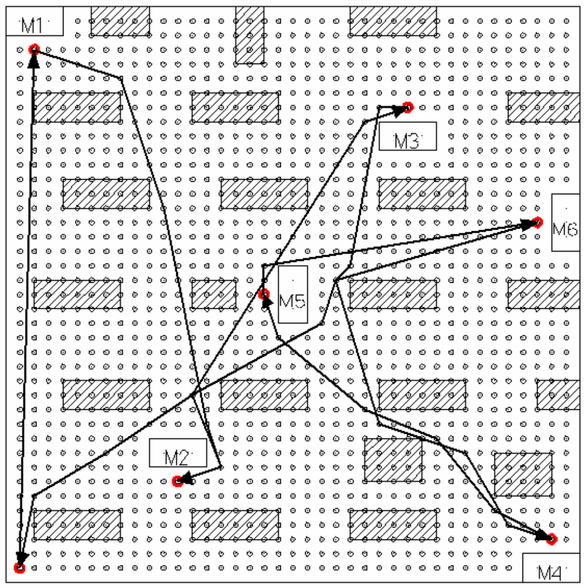

Fig. 6 Acquired path result 1

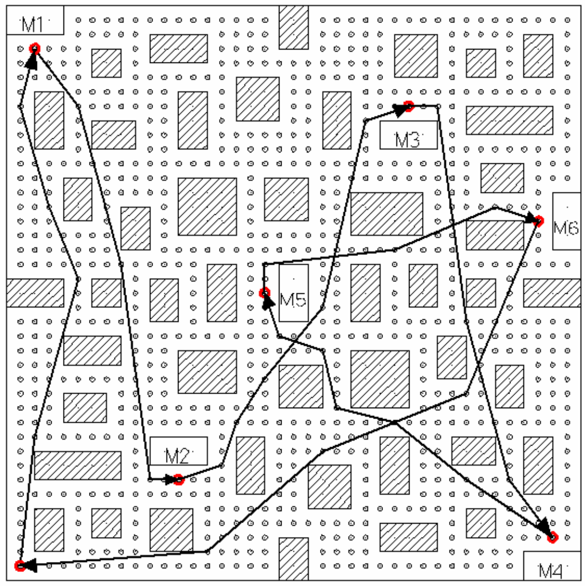

Fig. 7 Acquired path result 2

References

[1] Barraquand, J and Latombe, JC, A Montecaro Algorithm for Path Planning with Many Degrees of Freedom, IEEE International Conference on Robotics and Automation, pp.1712-1717, 1990.

[2] Yamamoto, H. Robot Path Search Including Obstacles by GA, Proc. of the 4th International Symposium on Artificial Life and Robotics, Vol.1, pp.270-273, 1999.

[3] Yamamoto, H. Robot Path Planning for Visiting FA Working Points by Obstacle Avoiding Using GA, Proc. of the 6th International Symposium on Artificial Life and Robotics, Vol.2, pp.524-527, 2001.

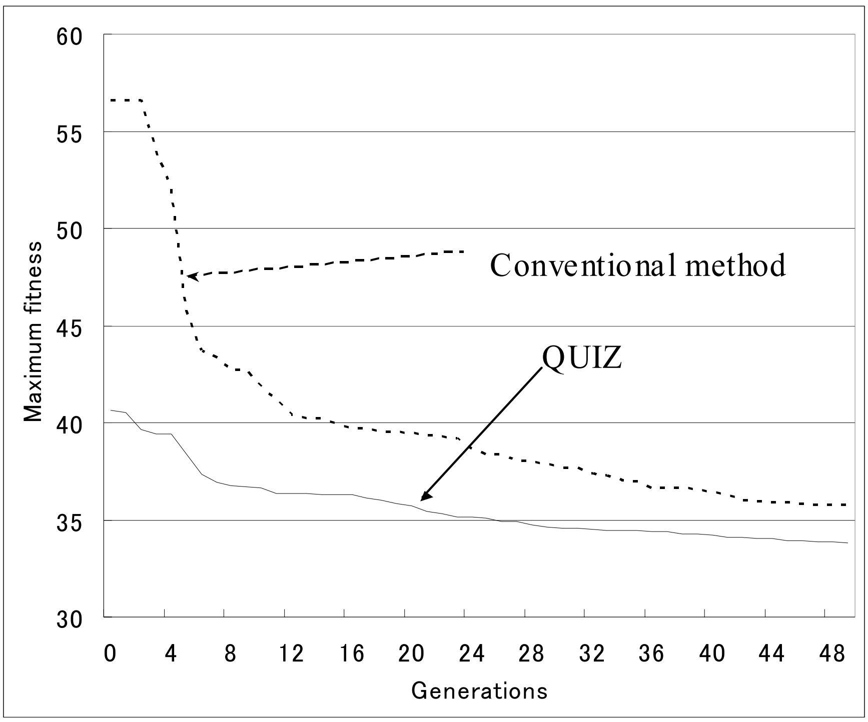

Fig. 8 Maximum fitness curves

The Tenth International Symposium on Artificial Life and Robotics 2005(AROB 10th '05),
B-con Plaza, Beppu, Oita, Japan, February 4-6, 2005

Design of Novel Adaptive Routing by Mimicking Enzymic Feedback Control Mechanism in the Cell

Takashi Kawauchi*, Masahiro Okamoto**
Dept. of Bioinformatics,
Graduate School of Systems Life Sciences,
Kyushu University,
Fukuoka, 812-8581 Japan
*** kawauchi@brs.kyushu-u.ac.jp**
**** okahon@brs.kyushu-u.ac.jp**

Miwako Hirakawa***
Dept. of Digital Media,
Fac. of International Communications,
Fukuoka International University,
Dazaifu, Fukuoka, 818-0193 Japan
***** miwako@fukuoka-int-u.ac.jp**

ABSTRACT

The routing algorithm of SPF (Shortest Path First) [1] is widely distributed in large scale network such as internet. Since this routing algorithm is designed in order to improve throughput of each packet which is sequentially generated at the nodes, it is not suitable for averaging load balance in the network. The enzymic feedback in the cell is the typical and basic control mechanism which can realize homeostasis of the value of every reactant in the metabolic pathway. The purpose of this study is to design an adaptive routing in which the packets generated at the nodes can be sent to the final destinations with avoiding the partial and time-variant traffics in the network, and the load balance in the network can be averaged. We have proposed here a new adaptive routing algorithm by introducing an enzymatic feedback control mechanism in the cell.

Keywords: Adaptive routing, Biomimetics, Enzymatic feedback, Homeostasis and Fault-tolerant network topology

1. INTRODUCTION AND BACKGROUND

The metabolic pathway in the cell is so-called "a stream of water" and is composed of a lot of enzymic reaction steps in which reactant (substrate) is converted to the product by unique "enzyme" (catalyzed protein), and the produced product is converted to the product by enzyme at the subsequent reaction step and so on. Enzymes are proteins which catalyze the turnover of substrates without being consumed themselves and without changing the equilibrium of the biochemical reaction. In metabolic pathways, the product of a late (or the last) step frequently acts as an inhibitor of the first committed step in this pathway ("negative feedback control"). This way, the end product of a pathway controls its own synthesis and prevents useless accumulation of intermediates. Enzymic feedback control can be considered to be a bandwidth control; rate velocity of consumption of substrate can be represented by the function of substrate (A) and feedback inhibitor (B). There are so many function mechanisms of feedback control in the cell, however, for example, when the B is assumed to control the rate velocity of A with a manner of competitive inhibition [2] (one of the feedback functions), the rate velocity of A (d[A]/dt, t represents time) can be mathematically written as follows:

$$\mathrm{d[A]/dt} = -\frac{V\max[A]}{Km(1+[B]/Ki)+[A]} \qquad (1)$$

where *Vmax* represents maximum velocity (reaction rate) of enzyme activity, *Km* is the value of substrate giving 0.5*Vmax*, *Ki* is the feedback coefficient. Anyway, d[A]/dt is the function of the substrate A and the feedback inhibitor B. In the case of accumulation of B, the absolute value of the term in the right-side of eq.(1) become to be small. Since the B is the end product of the pathway, we can easily considered that the accumulation of B corresponds to be "traffic" of the pathway; the absolute value of the term in the right-side of eq.(1) represents new metric of "traffic" from the view point of network routing. Thus, in this study, we define the following metric of routing by mimicking enzymic feedback control in the cell:

$$k = p / V\max \quad (2)$$

$$p = \frac{V\max[a]}{Km(1+[b]/Ki)+[a]} \quad (3)$$

where [a] represents the reserved sending packet size (Byte) to the nearest node, [b] is the total accumulated packet size (Byte) at the nearest node, *Vmax* is maximum sending rate (Mbps), and *Km* and *Ki* are the arbitrary coefficients. The value of k in eq.(2) decreases with the increase in "traffic". Furthermore, we define the following weighted multi-objective *f*:

$$f = (1-\alpha)k + \alpha(1/h) \qquad 0<\alpha<1 \quad (4)$$

where α represents arbitrary coefficient; if α=1, the network routing will be performed according to the SPF (Shortest Path First) algorithm.

At the branching of node-pathways, the value of *f* at each branching pathway is calculated and it determines the node to be sent with having the larger value of *f*. This is the outline of the proposed dynamic adaptive routing algorithm where most of the packets will be sent to the final destination with escaping from the traffic nodes; the QOS (quality of service) of the proposed algorithm is expected to be "averaging the load within the network".

2. CASE STUDY AND VALIDATION

The following node-network was used in order to evaluate our algorithm, where the numeral (0 to 5) represents the node-number, and the bold line is the connection pathway between nodes:

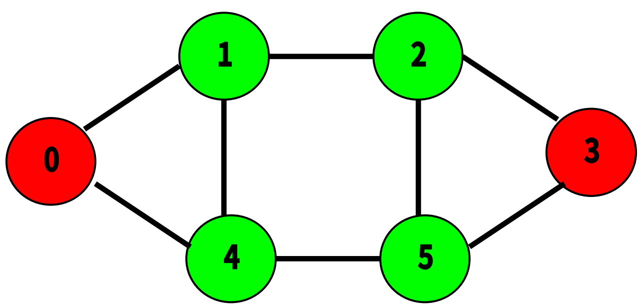

Fig. 1 6 nodes-network

Supposing the three kinds of sequential packets to be sent randomly in the network (total number of packets is 300); one is the packets generated at the starting node 0 and sent to the destination node 3, second is those generated at the starting node 0 and sent to the destination node 2, and the last one is those generated at the starting node 0 and sent to the destination node 5. Each packet has 3072B size and is generated at every 150 μsec. The maximum sending rate between binding nodes is fixed at 100Mbps. The control packet (64B) is sending to the nearest node at every 5000 μsec. This control packet involves the information of the value of [b] (total accumulated packet size) in eq.(3). The time between the generating and arriving at the final destination (passage) of every packet and transient sending route of every packet were examined. The default route was supposed to be 0 → 1 → 2 → 3 for the packets sending to the node 3 and to be 0 →1→ 2 for the packets sending to the node 2 and to be 0 → 4 → 5 for the packets sending to the node 5 ; the route 0 → 1 → 2 is overlapped which will lead to the traffic of the packets at this route.

For comparison, the passage profile with packets to be sent was examined in the case of SPF algorithm; every packet is sent to the final destination according to the default route. The results can be summarized as follows: As shown in Fig. 2, the passage increases with the packet ID that means the traffic is occurred at the route between the nodes 0 and 2.

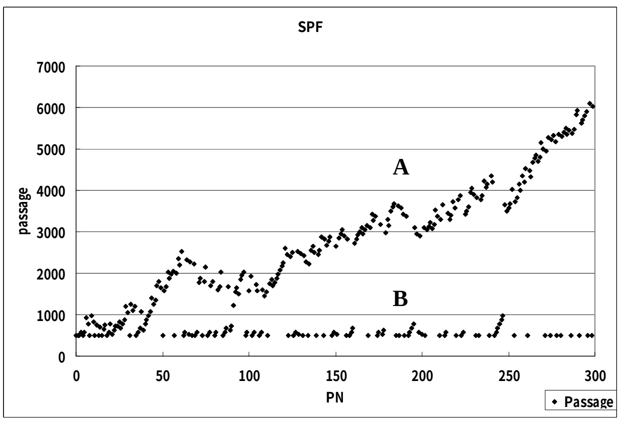

Fig. 2 Passage profile with packet by using SPF algorithm. The abscissa and the ordinate represent data packet ID and passage (μsec), respectively. A, packet sending to the nodes 2 and 3; B, packet sending to the node 5.

Fixed the value of α in eq.(4) at 0.5, the passage profile with packets to be sent was examined by introducing our proposed algorithm. The results are shown in Fig. 3. Also the passage profiles for the packets sending to the node 3 and for those sending to the node 2 and for those sending to the node 5 are shown in Figs. 4, 5 and 6, respectively. The average, minimum and maximum passage of Figs. 2 and 3 are summarized in Tables 1 and 2, respectively. Those of Figs. 4, 5 and 6 are also summarized in Tables 3, 4 and 5, respectively.

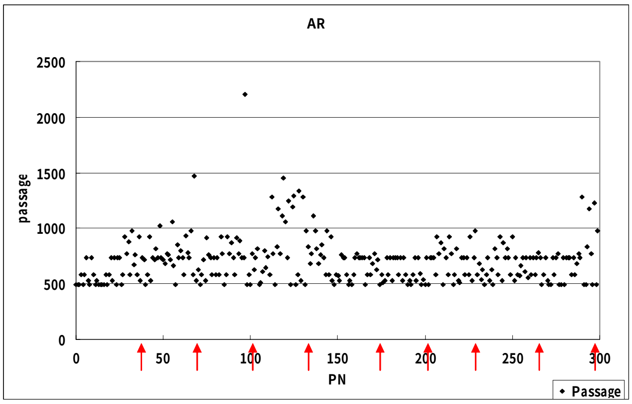

Fig. 3 Passage profile with packet by using the proposed routing algorithm. The abscissa and the ordinate represent data packet ID and passage (μsec), respectively. The arrow shows the time-point when the control packet was sent to the nearest node.

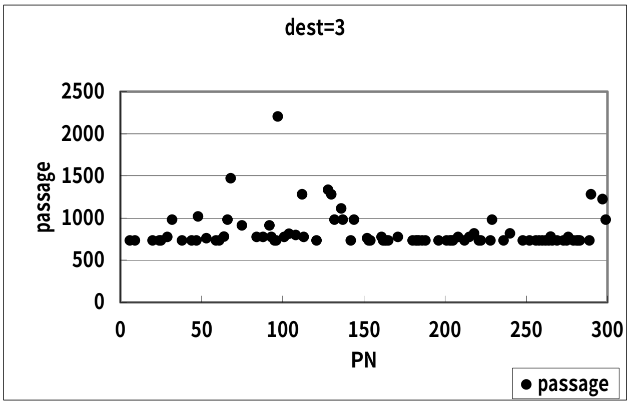

Fig. 4 Passage profile with packet sending to the node 3 by using the proposed routing algorithm. The abscissa and the ordinate represent data packet ID and passage (μsec), respectively.

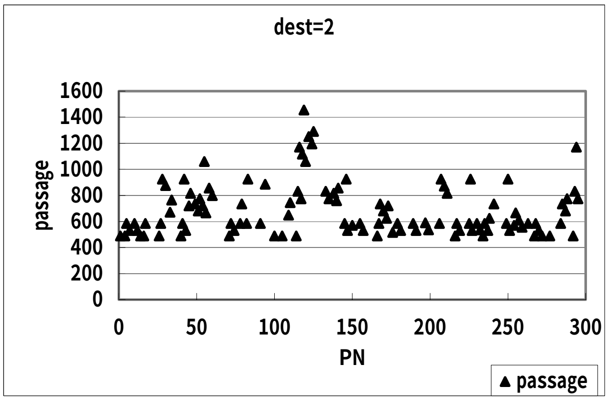

Fig. 5 Passage profile with packet sending to the node 2 by using the proposed routing algorithm. The abscissa and the ordinate represent data packet ID and passage (μsec), respectively.

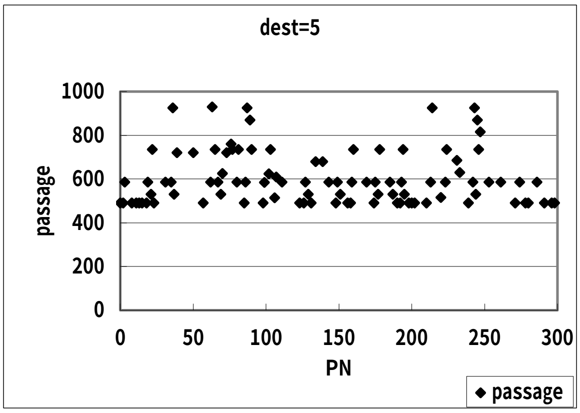

Fig. 6 Passage profile with packet sending to the node 5 by using the proposed routing algorithm. The abscissa and the ordinate represent data packet ID and passage (μsec), respectively.

Table 1 Summary of passage profile shown in Fig. 2.

Total number of data packets	300
Average of passage (μsec)	2129
Standard deviation of passage	1592
Minimum passage (μsec)	490
Maximum passage (μsec)	6090

Table 2 Summary of passage profile shown in Fig. 3.

Total number of data packets	300
Average of passage (μsec)	702
Standard deviation of passage	206
Minimum passage (μsec)	490
Maximum passage (μsec)	2205

Table 3 Summary of passage profile shown in Fig. 4.

Total number of data packets	89
Average of passage (μsec)	831
Standard deviation of passage	217
Minimum passage (μsec)	735
Maximum passage (μsec)	2205

Table 4 Summary of passage profile shown in Fig. 5.

Total number of data packets	114
Average of passage (μsec)	688
Standard deviation of passage	201
Minimum passage (μsec)	490
Maximum passage (μsec)	1455

Table 5 Summary of passage profile shown in Fig. 6.

Total number of data packets	98
Average of passage (μsec)	601
Standard deviation of passage	123
Minimum passage (μsec)	490
Maximum passage (μsec)	930

As shown in Figs. 2 and 3, and Tables 1 to 5, most of the passages of data packets were averaged, which means that our proposed algorithm is effective for dynamic adaptive routing. According to Figs. 2 and 3, part of the transient passage profiles of packets and route sending to the final destination by using SPF algorithm and by using the proposed algorithm are summarized in Tables 6 and 7, respectively.

In Table 7, the shadowed columns represent the packets which were sent by using the non-default routes (default routes are 0→1→2→3 for the packets sending to the node 3, 0→1→2 for those sending to the node 2, and 0→4→5 for those sending to the node 5). In Table 7, most of the packets sending to the node 2 or 5 were sent by using the default route, however, focused on the packets between 242 and 247 their routes are flexible such as 0→4→5, 0→1→4→5 and 0→1→2→5 with escaping from the traffic nodes. The routes for the packets sending to the node 3 are most flexible; the route 0→4→5→3 is another short-cut route and the routes 0→1→4→1→2→3 and 0→1→4→5→3 are alternative ones with escaping from the traffic nodes. Since the maximum sending rate between all binding nodes is fixed at 100Mbps and the each data packet size is 3072B, the minimum required time sending to the nearest node is 245μsec (minimum required time sending from the node to the node 3 is 245 x 3 = 735μsec). The passages for PID=290, 297 and 299 are 1280, 1225 and 980μsec, respectively, which were near to 245 multiplied by the number of hops; 1280 is approximately equal to 245 x 5, and 1225 and 980 are quite equal to 245 x 5, 245 x 4, respectively. These results show the proposed algorithm can find alternative non-traffic routes with considering the smaller number of hops to the destination.

Even if each packet arrives at the final destination with escaping from the traffic nodes, it is key issue that all packets, which constitute one data-file, arrive at the final destination in the order of sending from the starting node. For example, when the packet 3 arrives at the final destination prior to the packets 1 and 2, sorting process can not be performed until both of these packets arrive. In the case where this waiting time is larger than a given threshold value, routing system should request to the sending node for re-sending of packets. In the 6-node network shown in Fig. 1, we examined the waiting time at the final destinations (node 2, 3 and 5). The simulation conditions are as follows: (1)three kinds of sequential packets to be sent randomly from node 0. (2)total number of packets is 300, and the number of packets to the nodes 2, 3 and 5 is 100, respectively. (3)each packet has 3072B size and is generated at every 125 μsec. Figure 7 shows the histogram of waiting time at the node 3 when the weighting coefficient α in eq. (4) is fixed at 0.5. The ordinate represents the relative frequency at each class. The abscissa shows class of histogram, for example, 1000 and 2000 means 0-1000μsec and 1001-2000μsec, respectively. Figure 7 shows the average of 10 trails. Next we change in α value according to the following algorithm and examined waiting time with the same conditions above:

$$
\begin{aligned}
& if\,(sHop > Cnt) \\
& \alpha = 0.5 \\
& if\,(sHop \le Cnt < 2sHop) \\
& \alpha = 0.5 + \frac{0.2}{sHop} \times (Cnt - sHop) \qquad (5) \\
& if\,(Cnt > 2sHop) \\
& \alpha = 0.7
\end{aligned}
$$

where, *sHop* and *Cnt* represent the number of the shortest hops from stating node to the final destination node, and the accumulated number of nodes for the packet to pass through, respectively.

Table 6 Transient passage profiles of packets by using SPF algorithm.

Packet ID	generate	arrive	passage	route
240	36150	40500	4350	0>1>2>3
241	36300	40500	4200	0>1>2
242	36450	36940	490	0>4>5
243	36600	37185	585	0>4>5
244	36750	37430	680	0>4>5
245	36900	37675	775	0>4>5
246	37050	37920	870	0>4>5
247	37200	38165	965	0>4>5
248	37350	40990	3640	0>1>2>3
249	37500	40990	3490	0>1>2
250	37650	41235	3585	0>1>2
251	37800	41480	3680	0>1>2
252	37950	41970	4020	0>1>2>3
275	41400	46625	5225	0>1>2>3
276	41550	46870	5320	0>1>2>3
277	41700	46870	5170	0>1>2
278	41850	42340	490	0>4>5
279	42000	47360	5360	0>1>2>3
280	42150	42640	490	0>4>5
281	42300	47605	5305	0>1>2>3
282	42450	47850	5400	0>1>2>3
283	42600	48095	5495	0>1>2>3
284	42750	48095	5345	0>1>2
285	42900	48340	5440	0>1>2
286	43050	43540	490	0>4>5
287	43200	48585	5385	0>1>2
288	43350	48830	5480	0>1>2
289	43500	49320	5820	0>1>2>3
290	43650	49565	5915	0>1>2>3
291	43800	44290	490	0>4>5
292	43950	49565	5615	0>1>2
293	44100	49810	5710	0>1>2
294	44250	50055	5805	0>1>2
295	44400	50300	5900	0>1>2
296	44550	45040	490	0>4>5
297	44700	50790	6090	0>1>2>3
298	44850	45340	490	0>4>5
299	45000	51035	6035	0>1>2>3

Table 7 Transient passage profiles of packets and the route sent to the final destination by using the proposed algorithm

Packet ID	generate	arrive	passage	route
240	36151	36966	815	0>1>2>3
241	36301	37036	735	0>4>1>2
242	36451	37036	585	0>4>5
243	36601	37526	925	0>1>4>5
244	36751	37281	530	0>4>5
245	36901	37771	870	0>4>5
246	37051	37786	735	0>1>2>5
247	37201	38016	815	0>4>5
248	37351	38086	735	0>1>2>3
249	37501	38086	585	0>1>2
250	37651	38576	925	0>4>1>2
251	37801	38331	530	0>1>2
252	37951	38686	735	0>4>5>3
275	41401	42136	735	0>1>2>3
276	41551	42326	775	0>4>5>3
277	41701	42191	490	0>1>2
278	41851	42341	490	0>4>5
279	42001	42736	735	0>1>2>3
280	42151	42641	490	0>4>5
281	42301	43036	735	0>1>2>3
282	42451	43186	735	0>4>5>3
283	42601	43336	735	0>1>2>3
284	42751	43336	585	0>1>2
285	42901	43636	735	0>4>1>2
286	43051	43636	585	0>4>5
287	43201	43881	680	0>1>2
288	43351	44126	775	0>1>2
289	43501	44236	735	0>4>5>3
290	43651	44931	1280	0>1>4>1>2>3
291	43801	44291	490	0>4>5
292	43951	44441	490	0>1>2
293	44101	44931	830	0>1>2
294	44251	45421	1170	0>4>1>2
295	44401	45176	775	0>1>2
296	44551	45041	490	0>4>5
297	44701	45926	1225	0>1>4>1>2>3
298	44851	45341	490	0>4>5
299	45001	45981	980	0>1>4>5>3

For example, in the case of packets generating at the node 0 and sending to the node 3, *sHop* is 3 and when *Cnt* is over 3, α value increases linearly to 0.7 with the *Cnt*; α value is 0.7 at *Cnt* = 2*sHop* (6 in this case) and fixed at 0.7 when *Cnt* is over 2*sHop*. Figure 8 shows the histogram of waiting time where α value is variable according the above schedule.

Compared Fig. 8 with Fig. 7, changing in α value is efficient method for reducing the waiting time; in Fig. 7, the sum-up of relative frequency at the classes over 4000 is 16.1%, whereas in Fig. 8, the corresponding frequency is 0%.

3. DISCUSSION

The OSPF (Open Shortest Pass First) [3] is the routing protocol by using various cost parameters as metrics; the

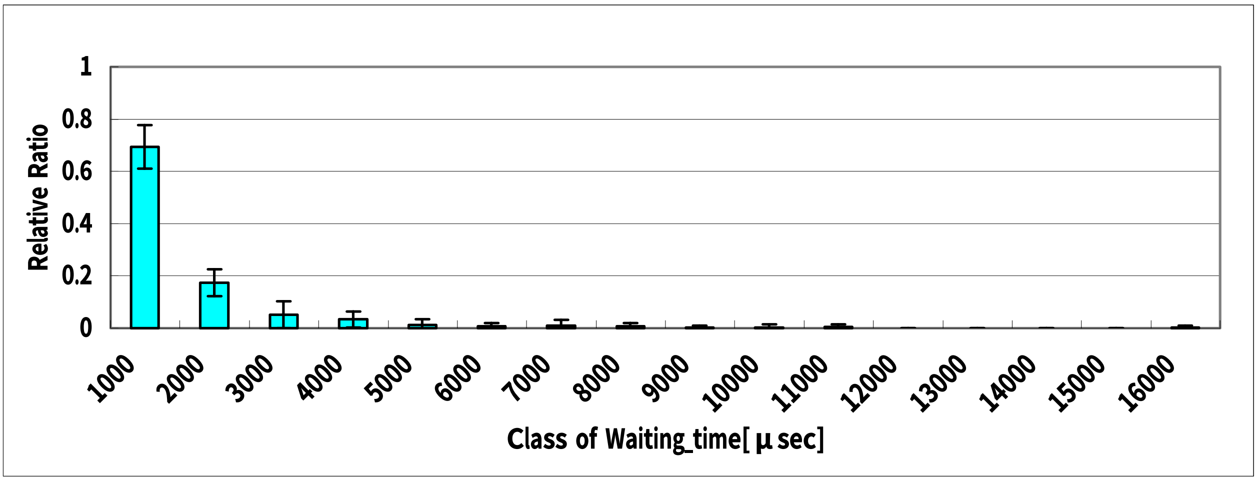

Fig. 7 Histogram of Waiting_time at the node 3 under fixing the α value in eq.(4) at 0.5.

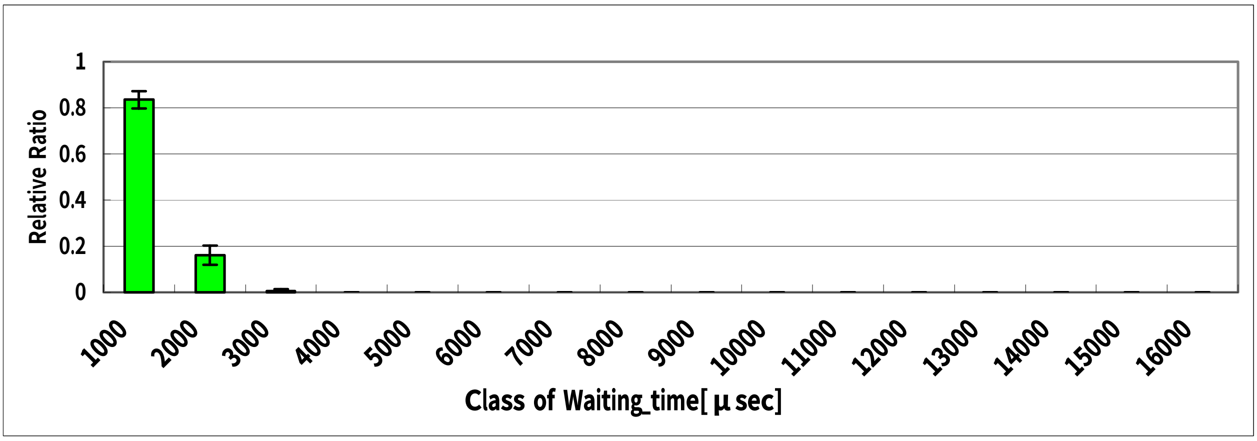

Fig. 8 Histogram of Waiting_time at the node 3 under the condition where theα value changes with schedule (5).

followings are considered to be cost parameter: reliability, delay, bandwidth, load, maximum transfer unit, communication cost. In this study, we proposed here eqs. (2), (3) and (4) by mimicking the mechanism of enzymatic feedback function in the cell. As shown in eq. (3), the p is the integrated parameter considering both the current traffic status between the self-node and the nearest bonding node (the [a] in eq. (3) numerically reflects this information) and the most recent traffic status between the nearest bonding node and the subsequent nodes (the [b] in eq. (3) numerically reflects this information). The Km represents the [a] value giving the half speed of maximum sending rate (*Vmax*); the smaller *Km* value gives the steeper decrease of p-value. The *Ki* determines steepness of the *p*-value *vs.* [a]-value; the smaller *Ki* value represents the stronger feedback control. In metabolic pathways in the cell we can observe various kinds of feedback function mechanisms except for eq. (1) or (2) [2]. These functions including eq. (3) have high possibility to be acceptable as new metrics in OSPF.

REFERENCES

[1]Dikjstra,E.W.: A note on two problem in connection with graphs, Numerische Mathematik, 1, pp269-271(1959)

[2]Okamoto, M., Takeda, Y., Aso, Y., Hayashi, K.: Steady-state approximation of enzyme activation and inhibition, Biotechnol. and Bioengineer., 25, pp1453-1463 (1983)

[3]Thomas M. Thomas II: OSPF Network Design Solutions 2nd. ed., Cisco Press (2003)

The Tenth International Symposium on Artificial Life and Robotics 2005(AROB 10th '05),
B-con Plaza, Beppu, Oita, Japan, February 4-6, 2005

Agent based plant allocation and transfer routing of products in case of emergency

Al-Sehaim Sulaiman, Graduate School, Okayama University
Masami Konishi, Faculty of Engineering, Okayama University
Kazuo Nose, Faculty of Engineering, Osaka Sangyo University

Abstract

In this paper, two problems, plant allocation problem and that of transfer routing from plants to customers, are considered simultaneously. Especially, adaptation scheme for emergency cases are checked. To solve these problems, decentralized agent based optimization procedures are used. In our study, oil production and products transfer in Saudi Arabia are treated. Through numerical experiments, practicability of the proposed method is verified.

Keywords: decentralized agents, optimization, oil production, ant system, allocation problem, conveyance planning

1. Introduction

In recent years, the system optimization technologies are studied briskly and applied widely to production and distribution problems. These advancements are supported both by the progress of computer technologies and that of the optimization technologies for large scale system.[1] This research deals with an optimization problem for oil production planning and its transfer control in case of emergency. When an emergency occurs, it becomes necessary to determine once again the appropriate allocation of plants and transfer routes from plants to customers. To the purposes, a decentralized agent method for optimizing both the allocation of plural oil plants and the transfer route of oil products in a wide area are studied. Optimization of oil production and products distribution system are taken up as the aimed problem of real scale. In order to optimize the arrangement of oil production plants, delivery routes of a product are taken into consideration simultaneously.

2. Problem Description

To treat the problem, 48 nodes representing consumer places are arranged in Saudi Arabia and 3 production plants are set up on the corresponding nodes. The delivery route of a product shall be constituted by the adjoining node sequence. The tracks made with a uniform velocity are belonged to each plant.

[Emergency cases]

In this research, there are two kinds of emergency cases. One is plant damage or building a new plant to cover consumer's demands for plants in work. The other is the interruption of transfer to some reason such as the destruction of a proper transfer rout to consumer cities.

3. Mathematical description

In our treatment, the time required for movement between nodes is made one unit period and all tracks are assumed to have a uniform velocity. The mathematical models for track operations are described in the following. Decision variables are [0,1] variables representing moving from one node to the adjacent node whose attributes are track number, corresponding to nodes, time and plant number. In the following, these definitions will be described mathematically together with restrictive conditions and objective functions for optimization.

3.1 Notation for variables

Variables, parameters and functions used in our paper are summarized as follows.

C : city number $(C=1,\cdots,48)$, $S_C(t)$: Volume of inventories , $D_C(t)$: amount of demands , $R_C(t)$: amount of consumption , p : Plant number, Ω_p :Plants Quantity of production, X_α :search track (main agent) of plant arrangement , X_β : transportation track of an oil product (sub agent), a_β : freight per track, b_β : loading of a track (if b = 1), $l_{p\bullet c}$: distance form plant to city , $f_\alpha(l_{i\bullet j})$: arrangement cost of a plant, $f_\beta(l_{i\bullet j})$: transfer cost between a city and a plant , I_α :evaluation function for optimum plants arrangement, I_β : evaluation function for optimization of sub agent's transportation (conveyance route length), ΔW_α : amount of pheromone of a main agent, ΔW_β : amount of pheromone of a sub agent, ρ_α : evaporating ratio of pheromone of a main agent, ρ_β : evaporating ratio of a sub agent, Q : penalty cost reflecting the number of consumption nodes which is not delivered,

3.2 Restrictive Conditions

Conditions for continuation are as follows.

$$\sum_{j\notin N_i} x_{i,j,t}^{k,m} = 0 , \quad \sum_{j\in N_i} x_{i,j,t}^{k,m} = 1 \qquad (1)$$

Where *Ni* denotes a set of adjacent nodes of node

$\#i$. As shown here, decision variable is x that express the movement of a track between adjacent nodes in unit time. Variable $x^{k,m}_{\beta,i,j,t}$ takes 1 when a track $\#k$ belonging to the plant $\#m$ moves from node $\#i$ to node $\#j$ at time period t.

Condition for shipment from a plant is as follows.

$$H_m = g(\Omega_m - a \sum_{k,j \in N_{n(m)}} x^{k,m,1}_{\beta_{n(m)},j,t}) \qquad (2)$$

Where, Ω_m, $N(m)$ and a are the quantity of production of a plant$\#m$, a set of nodes corresponding to plant$\#m$ and the capacity of a truck.

Condition for inventory volume at consumer place is given by

$$S_C^{Min} < S_C < S_C^{Max} \qquad (3)$$

Where, S_C^{Min}, S_C^{Max} and $R_{C,t}$ are minimum volume of stock, maximum volume of stock and current stock at a consumer node.

3.3 Objective functions for plants arrangement

Delivery cost is used for the objective function in plants arrangement problem. Namely, the objective function I_α is defined by equation (4).

$$I_\alpha = \sum_{i,j,m,t} f_{\alpha,i,j} x^{k,m}_{\alpha,i,j,t} + \gamma_1 Q \rightarrow Min \qquad (4)$$

In equation (4), penalty cost Q depending on the number of consumption nodes which is not delivered is added to the transfer cost.

3.4 Objective function for transfer routing

Objective function for transfer routing is defined by

$$W = H^e + H^o + \gamma_2 H^\upsilon + \mu H_m \qquad (5)$$

Where, H^e, H^o, H^υ and H_m show the transfer costs of approaching, returning, penalty value for inventory volume at consumers and penalty for excessive loading of a truck. Except H_m, these are defined as follows.

$$H^e = \sum_{i,j,k,m,t,b=1} f^e_\beta(l_{i,j}) x^{k,m,b}_{\beta_{i,j,t}} \qquad (6)$$

$$H^o = \sum_{i,j,m,t,b=0} f^o_\beta(l_{i,j}) x^{k,m,b}_{\beta_{i,j,t}} \qquad (7)$$

$$H^\upsilon = f(\Delta S) \quad , \quad \Delta S = f \sum_i (S_{Ci} - S_i^{Min}) \qquad (8)$$

Where, f^e and f^o show the cost per unit distance for movement in approach and return respectively. $f(y)$ is a nonlinear function whose value takes positive large one if the sign of y becomes negative.

As for the parameters in equation (6), $f^b_{\beta,i,j}$ is the delivery cost between nodes i,j. Where, b denotes parameter showing approach or return route of a track. The value of b is one when a track is on an approach route and is zero for return.

4. Algorithm for optimization

In our method the decentralized agent method is adopted for the optimization. [2]-[4] As shown in Figure 1, agents corresponding to plant accompanied by tracks autonomously search their locations and distribution area including transfer routes.

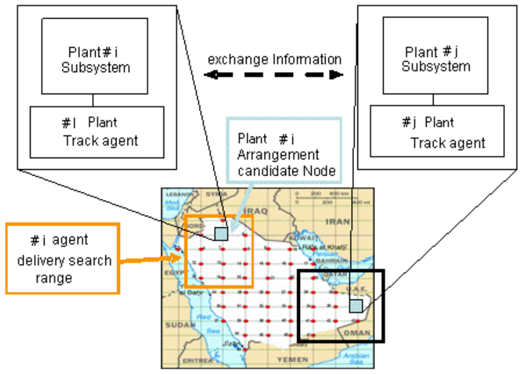

Fig.1 planning plant location and transfer routes by decentralized agents

4.1 Search algorithm for optimal plant allocation

Step1. input number of plants.

Step2. generate the node of a plant location. The Plant node number is not allowed to overlap the node number of other plants.

Step3. search delivery route for a track randomly. These serve as a primary solution candidate.

Step4. sprinkle pheromone ΔW_α on delivery nodes employing the following relation.

$$Ph_k^\alpha = \Delta W_\alpha \qquad (9)$$

Ph_k^α : amount of accumulated pheromone.

Step5. calculate evaluation of primary solution.

Step6. search again the delivery course of a track randomly, This serves as a secondary solution candidate.

Step7. compare pheromone information for primary and secondary solution

$$Ph_k^{\alpha,2} \geq \sum_{k' \neq k} Ph_{k'}^{\alpha,1} \qquad (10)$$

If the amount of pheromone for a secondary solution is larger, then go to Step 9, else go to Step8.

Step8. calculate probability of adoption of a secondary solution candidate, $R_a(k)$

$$R_\alpha(k) = \max\left[\exp\left[\frac{r_\alpha(k)}{T_{R_\alpha}}\right], R_o\right] \quad (11)_1$$

$$r_\alpha(k) = Ph_k^{\alpha,2} - \sum_{k' \neq k} Ph_{k'}^{\alpha,1} \quad (11)_2$$

If it becomes $r_\alpha(k) < 0$, return to Step6. with probability $R_\alpha(k)$. Otherwise, go to Step9.

Step9. pheromone is sprinkled on nodes of a secondary solution.

Step10. compare cost of the primary solution and that of the secondary. If the secondary solution is better than the primary solution, go to Step12. If not good, go to step 11.

Step11. calculate probability of adoption of the secondary solution even if its cost is not good.

$$P_\alpha(k) = \exp\left[\frac{I_\alpha^1(k) - I_\alpha^2(k)}{T_P}\right] \quad (12)$$

When not improved, go to step 12 with probability $P_\alpha(k)$. Otherwise, return to step 6.

Step12. Secondary solution is exchange with primary solution.

Step13. Convergence condition is investigated to finish the iterations. When convergence is not attained, returns to Step6.

4.2 Algorithm for transfer routing

In transfer routing after plant allocation Algorithm is over plan node number and plant transfer area nodes, or in emergency case the arc cant be used are passing to transfer routing Algorithm.

Step1. Input plants node number, delivery node numbers.

Step2. Create the track primary solution in random, and calculate Evaluation.

Step3. Sprinkle pheromone ΔW_β on delivery nodes.

$$Ph_k^\beta = \Delta W_\beta \quad (13)$$

Ph_k^β the amount of accumulation pheromones.

Step4. Create the track Secondary solution, calculate Evaluation.

Step5. Compare pheromone information for primary and secondary solution

$$Ph_k^{\beta,2} \geq \sum_{k' \neq k} Ph_{k'}^{\beta,1} \quad (14)$$

If the amount of pheromones of a secondary solution is large then go to Step 7, else go to Step6.

Step6. Probability it calculates.

$$R_\beta(k) = \max\left[\exp\left[\frac{r_\beta(k)}{T_{R_\beta}}\right], R_o\right] \quad (15)_1$$

$$r_\beta(k) = Ph_k^{\beta,2} - \sum_{k' \neq k} Ph_{k''}^{\beta,1} \quad (15)_2$$

$r_\beta(k) < 0$ If it becomes, it will return Step6. By probability $R_\beta(k)$. Otherwise, it progresses to Step9.

Step7. a pheromone is sprinkled on a secondary solution node.

Step8. Compare the Cost of a primary solution and Secondary solution. If Secondary solution Cost is better than the primary solution, it will progress to Step6. If bad, it will progress to next.

Step9.

$$P_\beta(k) = \exp\left[\frac{I_\beta^1(k) - I_\beta^2(k)}{T_P}\right] \quad (16)$$

When not improved, it returns to Step6 by probability $P_\beta(k)$ Otherwise, it progresses to Step10.

Step10. replace a Secondary solution and primary solution .

Step11. Convergence situation of a solution is investigated. When convergence is not enough, it returns to Step6. It will end, if it is converging.

5. Experimental conditions

Numerical experiment was conducted in order to verify the effect of the algorithm stated above. The problem of plants arrangements and distribution from plants to consumers was solved simultaneously. In the experiment, the number of plants was set as 3. The production data of oil plants are given together with data of customers in Table 1.

Table 1. Plants production and customers number

Plant	producing	No of track	customers
1	11	1	48 nodes 76 arcs
2	21	1	
3	16	1	

Parameters for decentralized agents stated above are given as shown in Table 2.

Table 2. Constant in algorithm

ρ	ΔW	T_P	T_R
0.3	4.0	12.0	18.0

6 Experimental results

Using the algorithm and conditions described in the preceding sections, numerical experiments were carried out.

6.1 Plant allocation design

Plants allocation search is made by decentralized agent algorithm explained in the above sections. The transition of evaluation function, cost, is shown in Figure 2. In the figure, three examples of calculated customer cities by plant #1 is shown with excess of iterations. According to the change in cost, numbers of customers converge to its final solution. The delivery zone from each plant in the target area which is the converged solution is shown in Fig. 3.

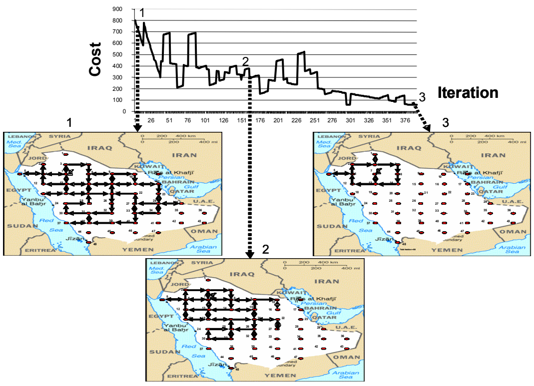

Fig.2 Transition of Cost during search procedure

The result of the plant arrangement node and cost which used and searched for this algorithm is shown in Table 3. In Table 3, calculated numbers of customers for 3 plants are shown together with their costs. As shown in the table, calculated number of customers (nodes) of a plant coincides with production rate of the corresponding plant. Costs in the table mean summation of arcs on each transfer route.

Table 3 Numerical experiment result (cost and the optimal solution)

	Production of plant	optimal solution	
		Node	Cost
Plant 1	11	11	14
Plant 2	21	21	26
Plant 3	16	16	18

Thus, the solution corresponding to the plant capability and the demand in a consumer place is obtained.

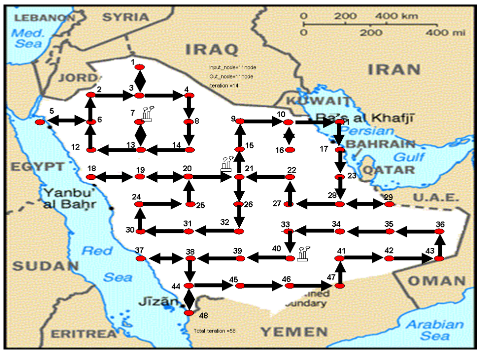

Fig.3 Simulation result

To check the validity of the proposed algorithm, pheromone consumption on the selected transfer route is checked. Fig.4 shows the accumulated amount of pheromone corresponding to plant #1 at nodes #7 and #19. As is shown in figure 3, node #7 is served by plant #1 and node #19 is not served.

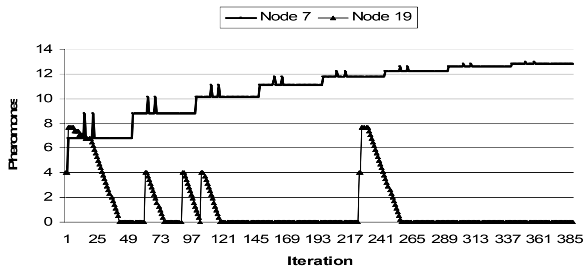

Fig.4 Change of pheromone accumulation (Plant #1)

As shown in figure 4, accumulated amount of pheromone increased with iteration. Contrary to this, that of #19 decreased with iterations.

5.2 Results for emergency cases

As for emergency, case of route destruction is considered. As shown in Figure 5, arc between node #8 and #14 is destructed. As the results, the other transfer route except this arc should be determined. Using the proposed method, surrogate transfer route was determined as such shown in Figure 6.

As shown in figure 6, new arc is created between nodes #7 and #8. Addition to this, transfer direction is changed to fulfill the minimization of transfer distance. As the result, total traveling distance of the surrogate route is the same before the destruction of transfer route.

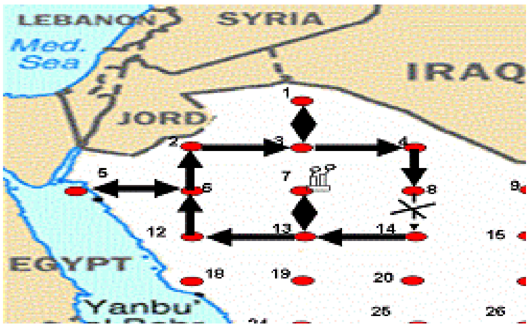

Fig.5 Emergency case of route destruction

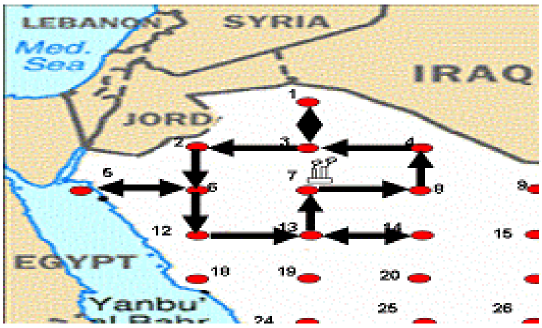

Fig.6 Finding of surrogate transfer route

Next, as the second case of emergency, #1 plant is forced to shut down due to emergency. In this case, two plants must cover the whole consumers in the area. Figure 7 shows the result of two plants case. As shown in figure 7, two plants #2 and #3 could successfully cover the whole consumer cities.

Fig. 7 Solution for #1 plant shutdown

6. Conclusion

This research examined the subject about the arrangement of oil production plants, where to locate and to what consumer places the oil products are to be delivered, and how to employ the distribution routes. In the proposed method, a delivery tracks was set up as a distributed agents, and it tried for these agents to search for an appropriate solution autonomously.

Using the developed program for planning, the arrangement of three plants and the delivery problem to 48 cities were set up supposing cities in Saudi Arabia, and the solution was calculated. Consequently, the very suitable solution could be found and the validity of the proposed method has been checked. The proposed method is expected to extend for more advanced problems about optimization of both production base planning and logistics in a wide area.

Based on the result, further research will be made to solve the problem of seven plants of a real scale, and 48 cities under the various conditions.

Acknowledgments

The authors gratefully represent acknowledgments for the financial support by the Japan society for the promotion of science

References

[1] Osaki, Akagi, Fujiwara, and Kikuchi: production system technique, Kyotitsu syuppan (Tokyo) pp.162-184

[2] Al-Sehaim Sulaiman, Masami Konishi, Kazuo Nose, Ryuji Otani: Scheduling Method by Decentralized Agents for Soft Drinks Production Line the Japan society for production management, Vol.10, No2 (2003), PP35-43

[3] Al-Sehaim Sulaiman, Masami Konishi, Kazuo Nose: Simulation Model for Production and Logistics of Petroleum, Preprint of the Japan society for production management, (Sept. 2003), PP 245-248

[4] Al-Sehaim Sulaiman, Masami Konishi, Kazuo Nose: Optimization of Production Control and Logistics for Oil Products- Decentralized Optimization of Conveyance Planning for Oil Products , Preprint of the Japan society for production management, (March 2004), PP107-110

The Tenth International Symposium on Artificial Life and Robotics 2005(AROB 10th '05),
B-con Plaza, Beppu, Oita, Japan, February 4-6, 2005

Decision Method of Reference Input Time Interval and Sampling Time Interval that Considered Contour Control Performance in Software Servo System

S. Sato*, M. Nakamura* and S. Goto*, N. Egashira** and N. Kyura †

* Department of Advanced Systems Control Engineering, Saga University, Saga 840-8502, Japan

** Kurume National College of Technology, Fukuoka, 830-8555, Japan

† Department of Electrical and Computer Engineering, Kinki University, Fukuoka 820-8555, Japan

E-mail : sato@cntl.ee.saga-u.ac.jp

Abstract

In a software servo system, reference input time interval and sampling time interval are two important control parameters. In this paper, these two control parameters are adjusted to achieve high performance of contour control for circle drawing. The performance is analyzed through mathematical models concerning two critical control performance criteria, namely decrease in radius and surface roughness. Further, validity of the analytical equations is confirmed through experiments in an actual software servo system.

Keywords: contour control, linear interpolation, sampling time interval, reference input time interval, decrease in radius, surface roughness, average radius, padé approximation, software servo system

1 Introduction

From 1980's, mechatronics servo system has been changed from hardware servo system to software servo system. The change causes some problems in the contour control especially the following 2 points.

1. Input command became changed from the pulse allocation method of the hardware circuit to linear interpolation by the microcomputer computation. Therefore, small fluctuation appears in input command.

2. The reference input time interval and the sampling time interval of the control system become remarkably shorten by high performance of the microprocessor in recent years. Therefore, an input command wave changes largely according to the ratio of the reference input time interval and sampling time interval.

The control performance, i.e., the decrease in radius and surface roughness in circular have not been investigated. The above control performance is analyzed mathematically in this paper. The appropriateness is also shown by a real machine experiment.

2 Mathmatical Model of Software Servo System

Software servo system is modelled by the first order system including dead time, where the essence of the sampling control is considered[1]. The block diagram of software servo is shown in Fig. 1.

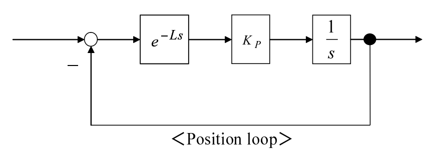

Figure 1: Block diagram of software servo system.

In Fig. 1, $K_p(\mathrm{s}^{-1})$ shows the position loop gain and $L(\mathrm{s})$ shows the dead time. The total dead time is expressed by computation time delay and the delay of 0th order hold as $L = 1.5\Delta t_p$[1].

where $\Delta t_p(\mathrm{s})$ is the sampling time interval of the servo system.

3 Relationships among Reference Input Time Interval, Sampling Time Interval and Shape Error

3.1 Relationship between time intervals and decrease in radius

3.1.1 Average radius

In case of the circular tracking approximated by the linear interpolation, command locus becomes the polygon shape. Namely the circle becomes a polygon. Therefore the radius of an actual circle drawn by the software servo system must be considered. Then, the radius of the circle approximated by the polygon is investigated. An example of the linear interpolation is shown in Fig. 2. From the reference input time interval T(s) and the input angular frequency ω_i(rad/s) of circle drawing, division several N of the circle is calculated by eq.(1).

$$N = 2\pi / (\omega_i T) \tag{1}$$

Next, area $S(\mathrm{m}^2)$ of a triangle inside the polygon is calculated by eq.(2).

$$S = r^2 \cos(\theta/2)\sin(\theta/2) \tag{2}$$

where θ is set as $360/N$. Therefore all the area $S'(\mathrm{m}^2)$ of the polygon can be calculated by NS. By using the ratio between the area of the real circle and all the area of the polygon, the equivalent circular radius of the approximated polygon is obtained by eq.(3).

$$\bar{r} = r\sqrt{(1/\omega_i T)\sin\omega_i T} \tag{3}$$

Here, this radius $\bar{r}$(m) is defined as "average radius". From eq.(3), the radius of the circle which is approximated the polygon linear interpolation, is smaller than the radius of the real circle. The radius is fluctuated for the approximated polygon.

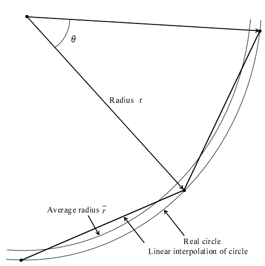

Figure 2: Concept of average radius.

3.1.2 Derivation of decrease in radius

The circular drawing by the interpolated straight line is considered for the control system of Fig. 1. In the circular drawing in radius r(m) and tangential speed v(m/s), the response of the servo system is the syntheses of 2 axis (X, Y axis) motion. The decrease in radius is obtained by the gain corresponding to the circular drawing speed in continuous system. The same idea is used for sampling control system.

The transfer function of the software servo system in Fig. 1 is given in eq.(4).

$$G(s) = \frac{K_p e^{-Ls}}{s + K_p e^{-Ls}} \tag{4}$$

It is not easy to be treated just as the eq.(4) because of the nonlinear term e^{-Ls} of the dead time. Therefore, e^{-Ls} is transformed into the (1,1) order padê approximation[2]. From the Padê approximation, the software servo system eq.(4) is approximated by eq.(5).

$$G(s) = \frac{K_p 2/L - s}{s^2 + (2/L - K_p)s + 2K_p/L} \tag{5}$$

From eq.(5), the gain $|G(j\omega_i)|$ of the frequency response function is eq.(6).

$$|G(j\omega_i)| = \sqrt{\frac{\omega_i^2 + (2K_p/L)^2}{(2K_p/L - \omega_i^2)^2 + ((2/L - K_p)\omega_i)^2}} \tag{6}$$

From the gain of eq.(6) and the average radius $\bar{r}$, the decrease in radius by delay of the servo system is obtained. Actual radius is reduced in the average radius from the radius of a real circle with that approximated the polygon. Therefore decrease in radius Δr of the circle by the interpolated straight line is derived by eq.(7).

$$\Delta r = \quad r - \bar{r}|G(j\omega_i)| \tag{7}$$

From eq.(7), decrease in radius depends on the position loop gain K_p, reference input time interval T, sampling time interval Δt_p and input angular velocity ω_i.

3.2 Relationship between time intervals and the surface roughness

3.2.1 Consideration of input in linear interpolation

When input command is interpolated by the straight line in the case of circular drawing, the circle becomes a polygon approximation, and command causes by some fluctuation. Furthermore the reference input time interval is divided by the sampling time interval of the servo system. Shape of the input wave differs from the difference of the ratio of the sampling time interval and the reference input time interval, as shown in Fig. 3. Here, the ratio of the reference input time interval and the sampling time interval is set as $q(= T/\Delta t_p)$. Generally q equals to or greater than 1.

From Fig. 3, one piece of command of small fluctuation becomes the stairs shape with the sampling

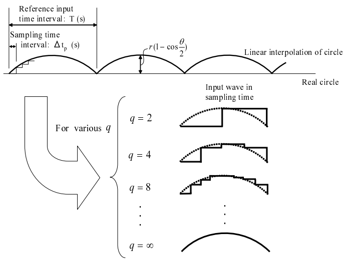

Figure 3: Concept of input wave by difference of q(=reference input time interval T/sampling time interval Δt_p).

time interval with the difference of q. DFT (Discrete Fourier Transform) is used for analyzing the wave of the stairs form. By using DFT, the main frequency component is obtained and the surface roughness is derived. DFT is expressed by eq.(8).

$$F(n) = \sum_{k=0}^{N-1} f(k) e^{-j\frac{2n\pi k}{N}} \tag{8}$$

Here $f(k)$ is the function of DFT derivation. Table 1 shows the DFT results for the input wave for various q from the eq.(8).

Table 1: DFT results of input wave for various q(q = (reference input time interval T/sampling time interval Δt_p), k = ordinary).

q \ k	1 st	2 nd	3 rd	4 th	5 th
2	1.270	0	0.419	0	0.247
3	1.01	0.454	0	0.271	0
4	0.943	0.313	0.250	0	0
5	0.898	0.269	0.169	0.177	0
10	0.860	0.223	0	0	0
20	0.850	0.213	0	0	0
50	0.846	0.209	0	0	0

Table 1 shows the normalized amplitude between the real circle and string for each order of the frequency component where $r(1-\cos(\theta/2))$=1. From Table 1, in the case that q is small, the higher order frequency components needs to be considered to represent the input wave. Zeros in Table 1 means the amplitude is small compared with 1 order and is able to be neglected.

3.2.2 Derivation of surface roughness

From the consideration of the previous paragraph, the input wave of the interpolated straight line is made by the base frequency as N times of input angular velocity ω_i. The input wave of higher hamonics is expressed with the basic wave. In the case that q is big, the basic wave and the 2nd order harmonics wave components must be considered. However, in the case that q is small (q=5 or less), the higher harmonics wave components to the 2∼5th order must be considered. The conceptual figure of the derivation of surface roughness, is shown in Fig. 4.

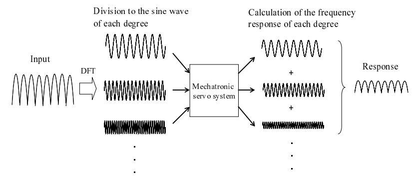

Figure 4: Consideration of surface roughness.

As shown in Fig. 4, the surface roughness is derived from principle of superposition. Surface roughness is calculated by the summation of gain for each frequency. However, the above study is considering only the gain. Therefore, the value corresponds to the maximum value of the quantity.

Gain $|G(j\omega_i N)|$ of the division number N of the circle is obtained by eq.(9).

$$|G(j\omega_i N)| = \sqrt{\frac{(\omega_i N)^2 + (2K_p/L)^2}{\left(2K_p/L - (\omega_i N)^2\right)^2 + ((2/L - K_p)\,\omega_i N)^2}} \tag{9}$$

When q changes, the higher harmonics order number of the input wave must be considered as shown in Table 1. Therefore, surface roughness changes $\omega_i N$ of the eq.(9) with 1,2... times and obtains the gain. Therefore, the surface roughness Δm in particular q is obtained the eq.(10).

$$\Delta m = r \sum_{k=1}^{5} \left(1 - \cos\left(\omega_i T/2\right)\right) l_{q,k} |G\left(jk\left(\omega_i N\right)\right)| \tag{10}$$

Here, $l_{q,k}$ is the coefficient in Table 1. Also, q shows the vertical axis and k is the horizontal axis of the Table 1. Also from the eq.(10), surface roughness changes by K_p, T, Δt_p and input angular velocity ω_i.

4 Inspection by Experiment

4.1 Setting of experimental device constitution and experimental conditions

Surface roughness is confirmed by a real machine experiment. The experiment system is the numerical control unit consisted of SPX-8000 (techno Co., Ltd. Mfg.). As shown in Fig. 5 the experiment system is composed of ball screw systems of 2 axes (X-axis, Y axis) that used 2 units of AC servo motor and the servo controller and also the motion controller board (SPX-8000). The motion controller board gives command to the servo controller and PC (personal computer).

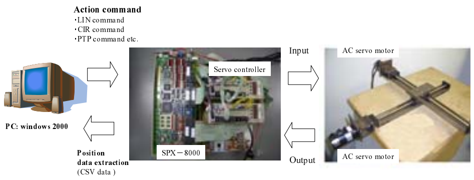

Figure 5: Schematics of experimental.

The experimental conditions are as follows. The condition of big fluctuation is choosed to check the influence (polygon approximation) by linear interpolation.

1. ω_i=1rad/s, r=50mm, Δt_p=2ms, T=260ms, q=130, N=24
2. ω_i=1rad/s, r=50mm, Δt_p=2ms, T=130ms, q=65, N=48

Furthermore, the position loop gains of the servo controllers of 2 axis are adjusted with K_p=40s^{-1}. Also AC servo motor and servo controller for the experiment is 100W (Yasukawa Electric Mfg).

4.2 Experimental results of decrease in radius and surface roughness

The size of decrease in radius and surface roughness are confirmed by a actual machine experiment. The experimental results are shown in Fig. 6. Here the left side of Fig. 6 is the input wave in the experiment. The wave on the right side of Fig. 6 is the error between the reduced synthesis locus of the position detection device of 2 motors from the real circle. In Fig. 6(a), the division number N of the circle is 24, the output wave is smooth and the same as an input wave. However, in Fig. 6(b) the division number N is 48 is distorted. This causes the low resolution of the position detection device of 2048pulse/rev.

The experimental results and the analyzed results of the decrease in radius and surface roughness are shown in Table 2. In the case of the division number of the circle 24, as for decrease in radius and surface roughness one of the analysis solution is bigger than the experimental results. This is caused that eq.(10) of surface roughness are not considered the phase. Also the size of decrease in radius and surface roughness almost become the same, in the case of division several N of the circle 48. As for this the influence of the phase is almost disappearing, because the size of the input of originally is small with that the reference input time interval becomes short. Appropriateness of decrease in radius and surface roughness is confirmed from the results of Table 2.

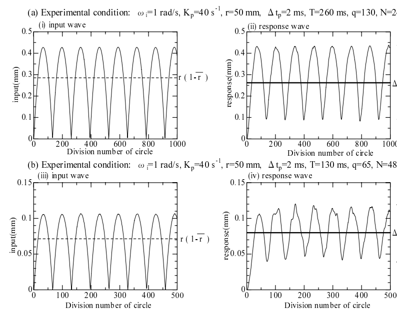

Figure 6: Experimental results.

Table 2: Comparison between analytical solutions and experimental results.

	Condition (a)		Condition (b)	
	Analysis	Experiment	Analysis	Experiment
Decrease in radius Δr (μm)	297	262	83	80
Surface roughness Δm (μm)	383	343	73	70

5 Conclusion

The analysis equations of the decrease in radius and surface roughness were derived, that becomes the control performance guideline of the circular drawing that was represented to the contour control. Appropriateness was confirmed by the experimental results.

References

[1] M. Nakamura, H. Kouda, N. Kyura, "Determination of Required Sampling Rate for Sampling Control of Continuous Contour Control by Servo System," *SICE*, vol.28, No.5, pp.649-651 (1992).

[2] JOHN G. TRUXAL, *Automation Feedback Control System Synthesis*, McGraw-Hill book Company, Inc., pp.548-550 (1955)

The Tenth International Symposium on Artificial Life and Robotics 2005(AROB 10th '05),
B-con Plaza, Beppu, Oita, Japan, February 4-6, 2005

AN AUTOMATIC DECOUPLING CONTROL SYSTEM FOR SHIP HARBOR MANEUVERS AND ITS ROBUSTNESS EVALUATION

Minh - Duc LE,
Vietnam Shipbuilding Industry Corporation (VINASHIN),
Hanoi, Vietnam
le_minh_duc@yahoo.com

Anh – Tuan DANG,
Shipbuilding Industrial Software Joint Stock Company
(SHIPSOFT JSC.)
Hanoi, Vietnam

Abstract

Presented and discussed in this paper are mathematical model used for expressing ship motions, application of Decoupling Control Methodology to construct the automatic control system and corresponding designing issues. Computer simulation results for a Very Large Crude Carriage (VLCC) in a typical harbor maneuver are given to verify the designing of the control method. Excellent effects of the automatic control system are showed by very good simulation results of ship motions during several 180 deg. turning maneuvers under various strong wind conditions. Robustness of the control system against parameters' uncertainty, strong environment disturbances such as strong wind and currents is also studies and presented in this paper.

Keywords: Nonlinear control, Decoupling control, Ship dynamic, Robustness

1 Introduction

Controlling ship motions in harbor areas is always one of the most sophisticated actions carried out by human operators. When a ship moving at a low speed approaches or leaves a berth, the ship is often in the most complicated and dangerous operation. Therefore, to keep ships' safety, it is a very important task to construct an automatic control system for ships' harbor maneuvers.

To develop such an automatic control system for large ships, several problems must be solved. Among them the most difficult is the how to lead the ships follow a desired trajectory precisely. Then a suitable mathematical model of ship maneuvering motions in harbors and a proper control method are necessary. Since ship dynamics in harbor maneuvers are fundamentally non-linear in nature, a multi-term mathematical model of ship motions should be adopted to describe a wide range of ship maneuvering motions in harbors. The model used here was based on a well-known and widely applied one, known as the MMG model that expresses surge, sway and yaw motions of ship by open-water characteristics of hull(s), propeller(s), rudder(s) individually and interaction terms among them [1]. The model was originally presented by K. Kose et al. [2] and has further been developed by Le and Kose [3], [4] recently. All the parameters (in the model) for a Very Large Crude Carriage (VLCC) have also been estimated with high accuracy, and used in this study for simulation purpose.

Besides, to automatically control such a non-linear system, a robust control methodology must be employed. Over the last three decades, the problems of achieving decoupling, or non-interaction, in MIMO control systems has been widely studied and Decoupling Control Method (DCM) has been motivated by the needs of a wide range of applications. Because of highly coupled nature of ship dynamics, high performance requirements, and possibility to divide ships' maneuvering motions in harbors into elemental motions for practical purposes [5], the DCM can be seen as the best solution for this study.

Recently several studies concerning automatic control systems for ships' harbor maneuvers have been carried out [6] - [10], however, in most of those studies, bow and stern thrusters were used as the means to provide controlling forces and moment. But in practical handling of ships, control of large ships in harbor areas, especially in berthing and de-berthing maneuvers, usually involves the use of tugboats. This study applies the DCM to construct an automatic control system for large ships in harbor maneuvers through the use of tugboats. Excellent effectiveness of the automatic control system is illustrated by simulation results of the VLCC in a typical pattern of approaching and berthing maneuvers. Moreover, not only the accuracy of the position tracking is emphasized, but the robustness of the control system is also considered carefully.

2 The mathematical model and a typical pattern of approaching and berthing for large ships

The non-linear, multi-term mathematical model

The MMG model [1] shown in formula (1) (non-dimensional form) consists of the open-water characteristics of hull(s), propeller(s) and rudder(s) individually and interaction terms among them:

$$\begin{aligned} m^*(\dot{u}^* - v^*r^* - x_G^* r^{*2}) &= X_H^* + X_P^* + X_R^* + X_E^* \\ m^*(\dot{v}^* + u^*r^* + x_G^*\dot{r}^*) &= Y_H^* + Y_P^* + Y_R^* + Y_E^* \\ I_{zz}^*\dot{r}^* + m^*x_G^*(\dot{v}^* + u^*r^*) &= N_H^* + N_P^* + N_R^* + N_E^* \end{aligned} \tag{1}$$

Here, u^*, v^*, r^* are the ship's surge, sway and yaw velocities, respectively and $\dot{u}^*, \dot{v}^*, \dot{r}^*$ are their corresponding derivatives with respect to time; m^*, I_{zz}^* are ship mass and moment of inertia; x_G^* is distance from mid-ship to the ship's center of gravity; X, Y, N terms with subscripts H, P, R, E respectively are forces in longitudinal and lateral directions and moment induced by ship hull(s), propeller(s), rudder(s) and external effects, respectively. With the aim of controlling large ships in harbors, only the forces and moment produced by hull(s) and tugboats are considered in this study.

The forces and moment induced by ship hull(s) in low speed motions are described by a multi-terms mathematical model [2], its form is given in formula (2).

$$\begin{aligned} X_H^* &= -m_x^*\dot{u}^* + X_{uu}^* u^{*2} + X_{vv}^* v^{*2} + (X_{vr}^* + m_y^*) v^* r^* + \\ &\quad X_{|v|vr}^* |v^*| v^* r^* / U^* + X_{vvu}^* v^{*2} u^* / U^* + X_{|v|u}^* |v^*| u^* \\ Y_H^* &= -m_y^*\dot{v}^* + Y_v^* v^* + Y_{|v|v}^* |v^*| v^* + Y_r^* r^* + \\ &\quad (Y_{ur}^* - m_x^*) u^* r^* + Y_{rrr}^* r^{*3} + Y_{vvru}^* v^{*2} r^* u^* / U^{*2} \\ N_H^* &= -J_{zz}^*\dot{r}^* + (Y_v^* v^* + Y_{|v|v}^* |v^*| v^*)(L_2^* + L_3^* b) + \\ &\quad N_r^* r^* + N_{uur}^* u^{*2} r^* + N_{rrr}^* r^{*3} + N_{vvru}^* v^{*2} r^* u^* / U^{*2} + \\ &\quad N_{|v|vr}^* |v^*| v^* r^* + N_{uvr}^* u^* v^* r^* \end{aligned} \tag{2}$$

, here: $U^* = \sqrt{u^{*2} + v^{*2}}$ and $\tan b = -(v^*/u^*)$, m_x^*, m_y^*, J_{zz}^* are added mass and moment of inertia in the forward, transverse, and yaw directions, respectively.

Figure 2 shows the coordinate systems used in this study. All the terms in the above mathematical model are expressed in the ship-fixed coordinate system XYZ with the origin at the center of symmetry of the hull, and the Earth-fixed coordinate system is $X_0Y_0Z_0$.

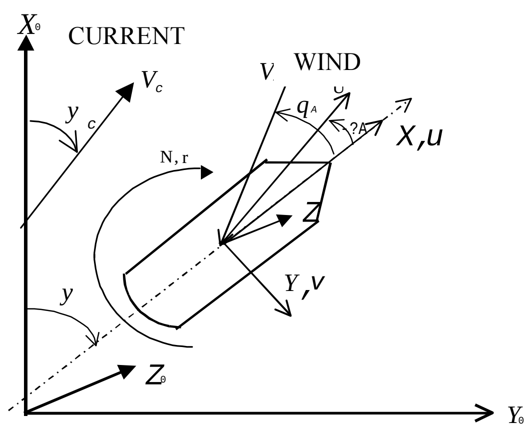

Figure 1. The coordinate system

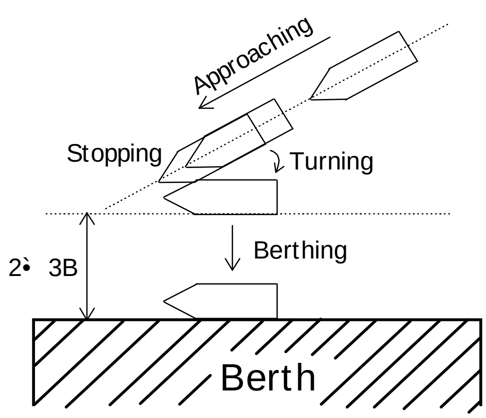

Figure 2. A typical pattern of approaching and berthing for large ships.

Typical patterns for harbor maneuvers of large ships

A typical pattern of harbor maneuvers for a large tanker [5] is shown in Fig. 2. The ship firstly enters the approaching maneuver, stops at some point located in front of a berth (this position is called as a "false goal"). There is enough safety distance between the false goal and the real berth (about 2-3 B, where B is the ship breadth molded [5]). The ship then turns around the false goal, her heading is adjusted parallel to the real berth, her longitudinal position is also adjusted to the just in front of the berth. Lastly, the ship enters the berthing maneuver by shifting laterally to the berth.

3 Application of the decoupling control methodology

Decoupling control methodology applied to the non-linear model of ship in harbor maneuvers

System of equations (1) and (2) can be rewritten in the following form of non-linear equation system:

$$M\dot{n} + N(n,h) = T \tag{3}$$

$$\dot{h} = J(h)n \tag{4}$$

, where $h = [x\ y\ y]^T$ and $n = [u\ v\ r]^T$ are the vectors that express ship position (and Euler angle) and velocity in the horizontal plane (surge, sway, yaw), respectively. Both h and n are usually assumed to be measured. M , N , T are matrices expressing influence of inertia, damping part, and control forces and moment as well as environment effects, respectively; J is transformation matrix that expresses the relationship between the $X_0Y_0Z_0$ and XYZ coordinate systems (see Fig. 1).

$$J = \begin{bmatrix} \cos y & -\sin y & 0 \\ \sin y & \cos y & 0 \\ 0 & 0 & 1 \end{bmatrix} \tag{5}$$

Equation (3) suggests a non-linear solution q_n (in the body-fixed reference frame) that satisfies:

$$T = Mq_n + N(n,h) \tag{6}$$

Taking differentiation of both sides of the equation (4) with respect to time yields:

$$\ddot{h} = J(h)\dot{n} + \dot{J}(h)n \quad \text{or} \quad \dot{n} = J^{-1}(h)[\ddot{h} - \dot{J}(h)n] \tag{7}$$

Denoting:

$$M_h = J^{-T}(h)MJ^{-1}(h) \text{ and } a_h = \dot{J}(h)n + J(h)a_n \tag{8}$$

, and using equations (3) and (6) with notation (8), the following result is derived:

$$M_h[\ddot{h} - a_h] = 0 \tag{9}$$

This equation suggests that $\ddot{h} - a_h$ should have the form of a 2nd order differential expression:

$$\ddot{h} - a_h = \ddot{\tilde{h}} + K_d\dot{\tilde{h}} + K_p\tilde{h} \tag{10}$$

, where $\tilde{h} = h - h_d$ and h_d denotes the desired vector of state variables, K_d and K_p are two positive definite matrices. In order to keep the error dynamics of the control system stable, the real part of solutions of the characteristic equation $S^2 + K_d S + K_p = 0$ for (10) should be negative.

The commanded acceleration should be chosen as:

$$a_h = \ddot{h} - (\ddot{\tilde{h}} + K_d \dot{\tilde{h}} + K_p \tilde{h}) = \ddot{h}_d - K_d \dot{\tilde{h}} - K_p \tilde{h} \quad (11)$$

4 Compute simulation results and robustness of the control system

Simulation results of a typical harbor maneuver

Applying the above described method, a position and attitude tracking controller was designed for the VLCC [4], [11]. To illustrate the application, let examine ship motions in a simple harbor trajectory similar to the typical pattern of approaching and berthing maneuvers described Fig. 2, with position and heading (x, y, Psy) of marked points in the ship trajectory given as:

- Starting position: (1000m, 900m, -145deg.),
- False goal: (0m, 150m, -180deg.),
- Real berth: (0m, 0m, -180deg.).

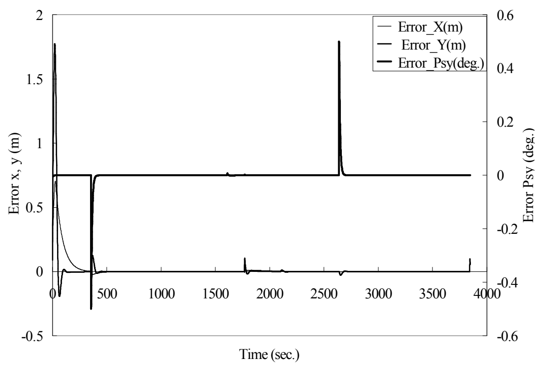

Figure 3. Tracking errors of the controller during a typical pattern of approaching and berthing

Figure 3 shows tracking errors (deviations from the designed trajectory) of the controller. Except for some small periods when the ship entered new manoeuvres, the tracking errors are considerably small and the final errors were limited to the allowable values for harbour manoeuvres (of the order of decimetre level).

Robustness of the control system again parameters' uncertainty

Since in de-berthing process ships often have to turn 180deg. in a very limited space, it is important to study the turning ability of the ship in this manoeuvre. Denoting the largest distance from initial mid-ship position to any point in the ship during ship manoeuvring by $R_{\max}$, the minimum required diameter (non-dimensional) of the basin's space for that manoeuvre is given by:

$$D_{\min} = 2R_{\max} / L \quad (12)$$

, where L is the ship length. The smaller the value of D_{min} is achieved, the better the controller is.

Suppose that M and N respectively are the true values of added mass and moment, and damping coefficients in the formula (3) while M_e and N_e are the corresponding estimated values of M and N.

Defining the relative values:

$$m = M_e / M \text{ and } n = N_e / N \quad (13)$$

, then the relations between the values of m, n and the corresponding values of D_{min} show the influence of the coefficients' mismatch on the performance of the automatic control system.

Simulation results of these relations are shown in Fig. 4, for 5 values of m and n: 0.25, 0.5, 1.0, 2.0, and 4.0. $m = 1.0$ means that there is no coefficients' mismatch on added mass and moment. Similar thing does for damping coefficients. For the cases of added mass and moment coefficients' mismatch, it is clear that the coefficients' mismatch has almost no influence on the control results. For damping coefficients' case, although the value $D_{min} = 1.07$ when $n = 4.0$ is little bit larger compared to other values of D_{min} (about 1.01), the influence of coefficients mismatch is not significant. In other words, the controller can well compensate influence of the uncertainty of model's coefficients.

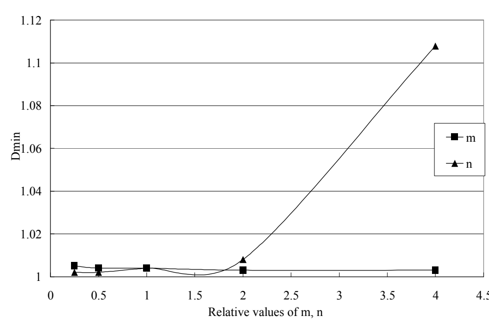

Figure 4. Influence of the coefficients' mismatch on the control results during 180 deg. turning

Robustness of the automatic control system again environmental disturbances

To study the ability of the controller in dealing with influence of environmental disturbances, several simulations of the VLCC's motions in the 180 deg. turning maneuver under various wind conditions were carried out. Simulations were carried out with the wind direction varied each 30deg. in the range from –180deg. to 180deg., while wind velocities varied with 5 values of m and n: 0.25, 0.5, 1.0, 2.0, and 4.0. Fig. 5 gives overall results of influences of the 15 m/s wind and coefficients' mismatch on the 180 deg. turning. In the case of added mass and moment coefficients' mismatch, although the value of D_{min} varies with the change of the wind direction, value of D_{min} is only a little different from the corresponding value where no mismatch has occurred ($m = 1$ and $n = 1$). In the case of damping coefficients' mismatch, results are quite different. If $N_e \leq N$ (or $n \leq 1$), value of D_{min} is as small as the in the situation of no mismatch, no environmental disturbances. But if $N_e > N$ (or $n > 1$), values of D_{min} are a bit larger than the corresponding value of D_{min} when there is no mismatch occurred. However, even in this case values of D_{min} are smaller than 1.2 and that shows excellent effect of the controller on cancelling the influence of the wind since the value 1.3 is considered as desired value for advanced controllers.

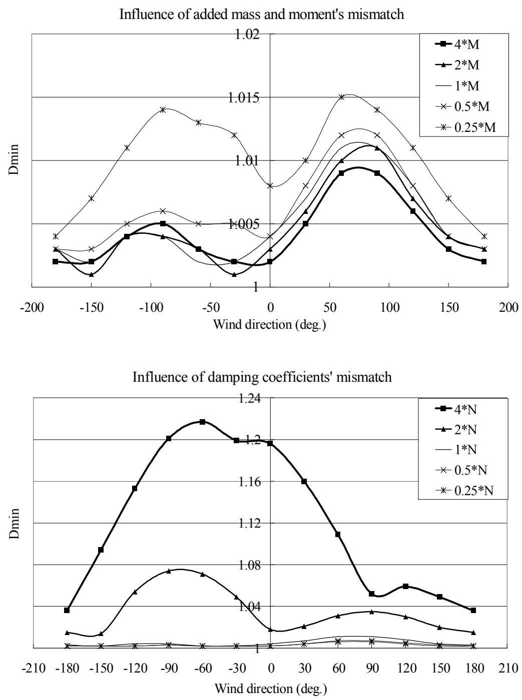

Figure 5. Influences of coefficients' mismatch and 15m/s strong wind on the control results during the 180 deg. turning manoeuvre.

5 Conclusions and future works

The Decoupling Control Methodology has been applied to design an automatic control system using a non-linear model of ship harbor maneuvers. The control method helps to reduce the complicity of the ship control system. Excellent simulation results of a typical pattern of approaching and berthing maneuvers using the control system show that the automatic control system can very well deal with the non-linear dynamics of ship motions in harbor maneuvers. The Decoupling Controller also produces extremely robustness in canceling influences of the parameter uncertainty and the environmental disturbances such as strong wind.

Some future works can be pointed out as follows: more effective methods to deal with the influence of strong current and shallow water conditions in harbour are necessary. Another possible future work is to study the use of tugboats in practice, including an optimal method for allocation of required control forces and moment to the tugboats.

Acknowledgements

The deepest gratitude is expressed to Prof. Kuniji Kose of Hiroshima University for his guidance in this study. Sincere acknowledgements is extended to members of "Low Speed Model" team (Lab. of Ship Maneuvering and Motion Control, Hiroshima Univ.) for their cooperation in carrying out the experiments, which resulted in the ship mathematical model used in this study. Hearty thanks are expressed to Mrs. Houmyou Saitou and Mr. Shodo Seta of Houryuji (Hiroshima, Japan), for their encouragement and financial support during the time this study was carried out.

References

[1] Kose K., et al (1989), "Practicalization of ship Manoeuvring Mathematical Model at Low Speed" (in Japanese), Transactions of Japan Society of Naval Architects, Vol. 721, pp. 403-411.

[2] Le M. D., and Kose K. (2000), "Estimation of Ship Hydrodynamic Coefficients at Low Speed Range and Application to Control Ships", The Journal of Japan Institute of Navigation, Vol. 103, pp. 33-39.

[3] Le M. D., and Nguyen D. H. (2000), "Estimation of ship hydrodynamic coefficients in harbour manoeuvres and its applications", Preprints of IFAC Workshop, Control Applications of Optimization, CAO2000, pp. 227-232, Saint Petersburg.

[4] Kose K., (1987) "Study on A Computer Aided Manoeuvring System in Harbors", Proceedings of the 8th Ship Control Systems Symposium, Vol. 2, pp. 1-13, The Hague.

[5] Iwamoto S. (1999), "An Automatic Control System Design of Berthing Manoeuvring with Decoupling Control" (in Japanese), The Journal of Japan Institute of Navigation, Vol. 101, pp. 75-82.

[6] Ogawara Y., and Iwamoto, S. (1998), "Studies on the Control System Design of Ship Manoeuvring Motion with Decoupling Control", Proceedings of IFAC Conference, Control Applications on Marine Systems, CAMS'98, pp. 147-153, Fukuoka.

[7] Berge S. P., et al (1998), "Non-linear Control of Ships Minimizing the Position Tracking Errors", Proceedings of IFAC Conference, Control Applications on Marine Systems, CAMS'98, pp. 141-146, Fukuoka.

[8] Ohtsu K., et al (1991), "A Fully Automatic Berthing Test Using the Training Ship Shioji Maru", The Journal of Navigation, Vol. 41, pp. 213-223.

[9] Fossen T., Guidance and Control of Ocean Vehicles, Great Britain, John Wiley & Sons, 1994, Chapter 4, pp. 93-165.

[10] Kose K. (1982), "On a New Mathematical Model of Manoeuvring Motions of A Ship and Its Applications", International Shipbuilding Progress, Vol. 336, pp. 201-219.

The Tenth International Symposium on Artificial Life and Robotics 2005(AROB 10th '05),
B-con Plaza, Beppu, Oita, Japan, February 4-6, 2005

CPU Resource Double Auction System with an Anonymous Protocol

Takashi Matsumoto Hidenori Kawamura Azuma Ohuchi

Graduate School of Information Science and Technology, Hokkaido University
Nishi 9, Kita 14, Kita-ku, Sapporo, Hokkaido, 060-0814, Japan
{matumo, kawamura, ohuchi}@complex.eng.hokudai.ac.jp

Abstract

CPU resource of a computer has a case of using all the power and a slight amount of the power, according to time and circumstances. A company wants to buy CPU resource when large-scale processing or processing of emergency is performed, and wants to sell CPU resource when it uses a slight amount of the power. The way of marketing an electronic auction is performed actively. In a general way of auction, it has problem that the auctioneer finds out identity of bids. In case an auction is performed among companies, it can not make use of the auction with a sense of security unless such problem is solved. Since, if a company bids, a trend of the company leaks out as a company secret from the bid price whether it goes through or not. Moreover, if a company finds out that the trading partner is rival company, there is possibility of adverse effect to the auction. In this paper, we describe a set of protocols of CPU resource electronic double auction system among companies for protect identity of bid from other companies and the auctioneer by using Secret Sharing Scheme, public key encryption, and particular method for sending data.

keywords:resource, auction, Secret Sharing Scheme

1 Introduction

CPU resource of a computer has a case of using all the power and a slight amount of the power, according to time and circumstances. Thus research on utilization of idle CPU resource is increasing in recent years, suchlike grid computing [1].

As a general trend, company has large-scale CPU resource and there are often two distinguishing situations. One is a case of using all the power when large-scale processing or processing of emergency is performed, in this instance the company wants to buy CPU resource from other companies at a low price to speed up processing. The other is a case of using a slight amount of the power, in this instance the company wants to sell idle CPU resource for profit.

In the way of marketing, an auction is the best mechanism for price setting since a product of the auction can be sold at a price determined by interactions in the auction. Moreover, the Internet is the most suitable for carrying out a real time auction since participants can bid anytime regardless of a particular place. Therefore, at present an electronic auction spread. However, an auction has problem of leaking of personal information from bid history or a corrupt auctioneer.

Especially in case trading among companies, it is necessary to conceal identity of a bid for protecting an intellectual property. Since a company must not know worth of CPU resource needlessly. Moreover, it is necessary to conceal trading partner too. Since if it turns out that a trading partner is a rival company, there is possibility of adverse effect to the auction. On the other hand, buying and selling prices are published to all participants since trading are made easy to do.

Kikuchi et al. [2], propose anonymous protocols based on a multiparty secret computation protocol [3]. This auction protocol is based on that identity of seller is known by the auctioneer, and bid price distribution is concealed to the auctioneer and all participants. In double auction, both seller's identity and buyer's identity should be concealed, and bid price distribution is published to all participants. Therefore, this protocol is not able to use double auction system.

In this paper, we describe a set of protocols of CPU resource electronic double auction system among companies for performing protected identity of bid. An identity means the thing of what can be specified a participant, such as IP address, account which was assigned by the auctioneer and so on, in paper.

In our system, there are four features.
First, the system conceals an identity of bid from the auctioneer and all participants of the auction. Second, the system publishes selling and buying price distribution to all participants. Third, the system makes known an identity of participant whose trading was decided to only the auctioneer. Fourth, the system conceals trading partner from a participant whose trading was decided.

For realizing these terms, the following things are required.
· A bid data, which is sent when a participant bid,

has the feature that the bid-price is found out and the identity can not be found out. Moreover when trading goes, only the auctioneer finds out the identity.

· It is necessary to change a method of sending bid data, since by using a usual auction method an identity of the bidder founds out from IP address.

· It is necessary to work out the way of processing using the bought CPU resource.

These tasks are realized by using Secret Sharing Scheme (SSS), public key encryption, and particular method for sending data. At the following section, we describe details of the auction-protocol.

2 Proposed Protocol

2.1 Auction Style

We consider an electronic double auction formed by the auctioneer and participants registered by the auctioneer.

A participant can bid a selling and buying price and cancel a previous bid any time one likes. A participant sends these orders to the auctioneer as a bid. The auctioneer publishes selling and buying price distribution obtained from these bids to all participants, and selects pair of bid to trade.

In case a trading goes through, only the auctioneer can know identity of the pair of bids, and a participant can know his bid were decided except identity of his trading partner.

In order to conceal a trading partner, the following procedure is done. A participant which bought CPU resource from other participant hands over a process to the auctioneer, and a seller participant receive the process from the auctioneer and return the result to the buyer participant through the auctioneer.

In this auction, volume of CPU resource is defined as B_i which is possible number of processing which was decided beforehand in a unit of time. B_i is assigned interger value.

2.2 Bid data

A selling or buying bid data is sent to the auctioneer. If the bid data includes identity of the bidder, the auctioneer finds out it. Therefore, it is necessary to divide the bid data into a price-data, denoted by p-$data_i$, including selling or buying price from an identity-data, denoted by i-$data_i$ including account, denoted by ac_i, which was assigned by the auctioneer. A p-$data_i$ is sent to the auctioneer ($i \in N$:N is a set of participants). The auctioneer selects trading partners from p-$data_i$. But an i-$data_i$ can not afford to be sent to the auctioneer, since auctioneer finds out identity of bid. Therefore, an i-$data_i$ is kept by participant.

If a bidder own self i-$data_i$, there is fear, such as a participant who is not bidding the selected bid insists on his bid, and a participant who bided the selected bid erase the i-$data_i$ for misbehave. Therefore, an i-$data_i$ is kept by all participants. But in this way, they can see i-$data_i$ of other participant. Though a bidder encrypts a i-$data_i$ with a public key of the auctioneer, a participant can see i-$data_i$ of others by at most one participant cooperates with the auctioneer. Therefore, a bidder encodes the ac_i into multiple distributed codes by SSS.

2.3 (k, n) threshold SSS

(k, n)threshold SSS make the number of n distributed data, denoted by $w_j (1 \leq j \leq n)$, from secret-data [4]. It has a feature that if the number of k or more of w_j are collected the secret-data can restore, but in case less than the number of k it can not restore even partial information of the secret-data.

A bidder makes the number of n i-$data_i$s, denoted by W_{ij}, including one of w_{ij} which is distributed from ac_i, and one of them own himself and remainder sends to other participants.

Figure 1A shows destination of p-$data_i$ and W_{ij}.

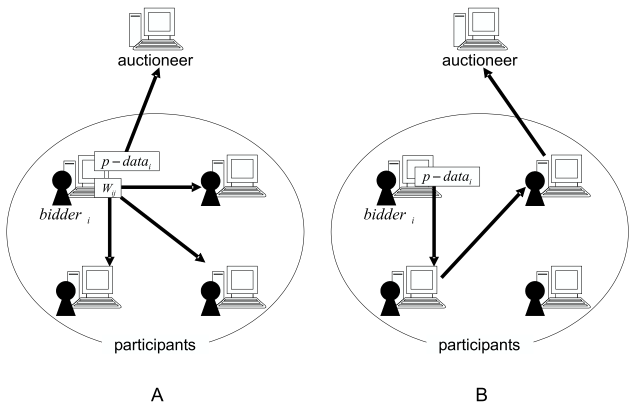

Figure 1: A:Destination of p-$data_i$ and W_{ij}. B:Method for sending data

It is impossible that restore variable ac_i of other participant unless the number of k or more participants cooperate and misbehave by using this method.

Figure 2 shows image of this method.

This algorithm is shown below. A bidder obtains the j-th distributed data (w_{ij}), by evaluating a $k-1$ polynomials of the form

$$f(x) = a + r_1 x + r_2 x + ... + r_{k-1} x^{k-1} \ (mod\, p)$$

at $x = j$:

$$w_{ij} = f(j)$$

where p is a large prime number greater than any of the coefficients and is made available to all participants

sign	type	explanation
ac_i	integer value of optional digit	identity of a participant which was assigned by the auctioneer
B_i	integer value	possible number of processing which was decided beforehand
$price_i$	integer value	selling or buying bid price
$M1_i$	string	result from SHA algorithm of a bid time and ac_i
$M2_i$	string	result from SHA algorithm of $M1_i$
$p\text{-}data_i$	$\{M1_i,\, B_i,\, price_i\}$	be sent to the auctioneer
w_{ij}	integer value of	destributed data of ac_i by using SSS
W_{ij}	$\{M2_i,\, w_{ij}\}$	be sent to other participants

Table 1: Contents of data

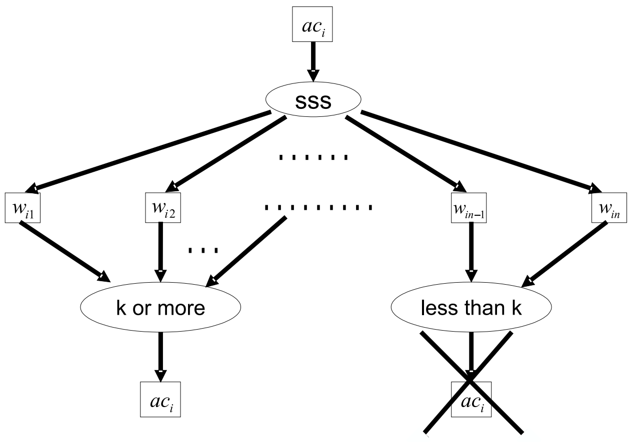

Figure 2: image of using SSS

and the auctioneer, and the coefficient a is account of the bidder while other coefficients $r_1, r_2, ..., r_{k-1}$ are all randomly chosen. W_{ij} includes one of these w_{ij}.

When a trading goes through and the auctioneer collects the number of k or more of W_{ij}s, it can reconstruct the original polynomial by solving a set of linear equations over a finite field $GF(p)$. Assume that the auctioneer collects the number of k w_{ij}s, which is $w_{i1}, w_{i2}, \cdots, w_{ik}$, from the number of k W_{ij}s. The original polynomial $f(x)$ can be restored by Lagrange interpolation.

$$f(x) = \sum_{i=1}^{k} (w_i \cdot \prod_{j=1, j\neq i}^{k} \frac{x-j}{i-j})\ (mod\, p)$$

The variable ac_i can be restored by calculating $f(0)$.

2.4 Marks

When the auctioneer collects W_{ij}, a mark which associates a p-$data_i$ with W_{ij} is necessary. The auctioneer selects trading partners from p-$data_i$ and when pair of bids are selected, and collect the W_{ij} based on this mark.

On the other hand a participant cancels a bid, a mark which associates a cancel order with bid is necessary too.

If these marks are equal, a participant can cancel a bid of other participant since participant has a mark of others W_{ij}. Therefore, these two makes have to different things. Moreover, it is necessary to be connected with two marks.

These two marks must not overlap with it of other participants. Since, if same marks exist in database of the auctioneer, the marks can not be recognized. Therefore, these two marks are assigned a value of one-way function.

This algorithm is shown below. First, a bidder calculates the value, denoted by $M1_i$, from SHA algorithm, which is one-way function, of a present time and his account. Next, bidder calculates the value, denoted by $M2_i$, from SHA algorithm of the $M1_i$. $M1_i$ and $M2_i$ are assigned by string. $M1_i$ is attached to p-$data_i$ and $M2_i$ is attached to W_{ij}. In case cancel a bid, it is necessary to $M1_i$. A participant can not cancel bid of other participant by using this method, since it is very difficult to calculate $M2_i$ from $M1_i$. When a trading goes through, the auctioneer collects W_{ij} based on a value $(M2_i)$ from SHA algorithm of the $M1_i$ which is attached p-$data_i$.

Table 1 shows compilation of these data.

2.5 Method for sending data

When a participant sends p-$data_i$ to the auctioneer, the data is sent to the auctioneer not directly but through several participants selected at random. Since, if the data is sent to the auctioneer directly like Figure 1A, the auctioneer finds out the identity of the sender.

If a number of roam participants is decided, the original sender is found out from the number. Therefore, the number is decided from probable. Moreover time limit of roam participants is set, since it has possibility that the p-$data_i$ is hard to be sent to the auctioneer.

The algorithm is shown below. First, a bidder chooses integer number, denoted by NUM_i, from 1 to 10, and set a limit time. Next, a bidder sends $p\text{-}data_i$ to a participant selected at random. Participants who receive the $p\text{-}data_i$ check the limit time and NUM_i. In case run past the limit time or NUM_i equal to 0, the participant sends the $p\text{-}data_i$ to the auctioneer; the other case, the participant subtracts 1 or adds 1 from NUM_i, leaves it, or is set to 0 by restrictive probability, and sends the price-data to other participant selected at random. This operation is repeated until the $p\text{-}data_i$ is sent to the auctioneer.

But using this method, a participant can see $p\text{-}data_i$ of others. Therefore, bidder encrypts a $p\text{-}data_i$ with a public key of the auctioneer.

Figure 1B shows an example of $p\text{-}data_i$'s path.

In case of sending W_{ij}, it is in the same way that sending $p\text{-}data_i$, since it has same problem. Therefore, W_{ij} includes a destination of sending. Moreover, a bidder encrypts a W_{ij} with a public key of a participant of destination of sending, since a participant who receives k or more of W_{ij} can restore the account.

3 Procedure

3.1 Selling or Buying Bid

When a participant bids selling or buying bid, the same procedure is performed. Here is a procedure of the algorithm.

Step 1: A participant makes $M1_i$ and $M2_i$, to use method of described at preceding section.

Step 2: A participant makes $p\text{-}data_i$ include $M1_i$, B_i, and $price_i$.

Step 3: A participant encrypts the $p\text{-}data_i$ with a public key of the auctioneer, and attach NUM_i and time limit.

Step 4: A participant sends the encrypted data to the auctioneer, to use method of described at preceding section.

Step 5: A participant make w_{ij} from ac_i, to use method of described at preceding section.

Step 6: A participant makes W_{ij} include $M2_i$ and one of w_{ij}.

Step 7: A participant encrypts W_{ij} with a public key of a participant of destination of sending, and attach NUM_i and time limit.

Step 8: A participant sends the encrypted data to a participant of destination, to use method of described at preceding section.

3.2 Cancel a previous Bid

When a participant bids cancel bid, the procedure is equal to Step 1 to Step 4 of selling or buying bid. In case a participant cancels bid, he uses $M1_i$ and $M2_i$ which restored at bid the selling or buying bid and the value of B_i and $price_i$ is set to 0.

3.3 Auctioneer

Role of the auctioneer in auction is publishes price distribution which be sent as a $p\text{-}data_i$, selects trading partners, collects pair of W_{ij} and restores a variable ac_i of participant whom dealings determined, and relays process between participants. Here is a procedure of collect pair of W_{ij} and restore a variable ac_i.

Step 1: The auctioneer selects trading partners from $p\text{-}data_i$, and calculates $M2_i$ from SHA algorithm of $M1_i$ of the $p\text{-}data_i$.

Step 2: The auctioneer collects W_{ij} of the $M2_i$ from all participants, and order them to delete the W_{ij}.

Step 3: The auctioneer restores a variable ac_i from the W_{ij}, to use method of described at preceding section.

4 Conclusion

We presented protocol of CPU resource electronic double auction system among companies. Using this proposed protocol, identity of bid will not become clear to the auctioneer and all participants unless k, that is threshold, or more participants cooperate and misbehave. Moreover, only selling and buying price distribution is published to all participants and the auctioneer.

If the auctioneer collects W_{ij} unjustly, a bidder notices this misbehave since the bidder owns one of his W_{ij}. Therefore, the auctioneer who has the authority to collect W_{ij} can not misbehave either.

It should be noted that in a general protocol of electronic double auction, auctioneer can find out identity of all bids. A construction of a system using the proposed protocol will be studied in future work.

References

[1] William E. Johnston et al."Grids as Production Computing Environments :The Engineering Aspects of NASA's Information Power Grid", *Proceedings of 8th IEEE Symposium on High Performance Distributed Computing*, IEEE Press, 1999.

[2] H. Kikuchi et al. "Multi-round Anonymous Auction Protocols", *Proceedings of the First IEEE Workshop on Dependable and Real-Time E-Commerce Systems*, June, pp. 62-69, 1998.

[3] D. Chaum et al."Multi-party unconditionally secure protocols", *Proceedings of ACM STOC '88*, pp. 11-19, 1988.

[4] A. Shamir. "How to share a secret", *Communication of the ACM*, Vol. 22, No.11, pp. 612-613, 1979.

The Tenth International Symposium on Artificial Life and Robotics 2005(AROB 10th '05),
B-con Plaza, Beppu, Oita, Japan, February 4-6, 2005

Issues and Application on Robot Control Using Internet

Masanori Sugisaka[1] Desa Hazry[2,]
[1]Department of Electrical and Electronic Engineering
[2] Graduate School of Engineering, Department of Electrical and Electronics Engineering
The University of Oita, 700 Oaza Dannoharu, Oita, 970-1192, Japan
Tel: + 81-97-554-7831, Fax: + 81-97-554-7841,
e-mail: msugi@cc.oita-u.ac.jp hazry@cc.oita-u.ac.jp

Abstract:
Robot control using internet basically uses the internet as command transmission medium and obtain feedback signals. This paper introduces the fundamentals of such robot control relationships. Four variations of robot control relationship have been identified and they are one to one, one to many, many to one and many to many. Samples for each of the relationship are given. The development of internet are further considered in the various applications areas. The applications made by various projects are referred. Some research issues and problems brought up by the projects are also reflected. The issues directed are time delay, communication, dynamic environment and dispersing the whole robot system on the internet.

Keywords: Internet robot, robot control

1 Introduction
Robot control using internet basically uses the internet as command transmission medium and obtain feedback signals. Our laboratory is developing a technique to remote control a group of autonomous mobile robots (Tarou) by mobile phone or via the internet [1]. The remote control equipment used in Tarou is transmitter/receiver RDIS/LT-08 which has 8 input ports, 8 output ports, 2 analog input ports and RS232 port.

2 Robot Control Architecture
Internet operated robot generally uses hardware which includes the robot, the robot server workstation, web server workstation and other user computers [2]. The user access the worldwide web and give commands. The web server receives these commands and transmits them to the robot server. The robot server decides the robot motion and behavior. The tasks are transmitted to the robot which is supposed to carry out the commands. The relationship of the user and the control system can be classified into four control architectures which are; one to one, one to many, many to one and many to many.

2.1 One to one
An interesting internet controlled pet robot with arithmetical inclination has been developed within this architecture [3]. The robot is programmed to recognize the image signals of the arithmetic operation using the binary method. If the equation is right it will nod and if the equation is wrong it will shake its head

2.2 One to many
The ARMAGRA Project [4] also depicts the same robot control architecture. It involves a few robots with an assistance system for disable persons. Both robot projects illustrated uses a decentralize system which enables each part of hardware to be develop individually. The flexibility of decentralize system is also economical as the web server workstation can be shared through LAN or a WAN. Our robot TAROU allows one remote user to control a group of autonomous robots. The operator sends commands using interface in HTML to the internet host onto the internet system. The command is received by RDIS/LT which is attached to Tarous body. Upon execution of command, reports are generated by Tarous and sent to the operator.

2.3 Many to one
A system that allows multiple users to control and industrial arm robot has been developed [2]. Each users monitors different sensors and submits control inputs based on different control information. The inputs are combined to a single control signal for the robot. However, time delay and transmission latency remain as two prominent areas of concerns.

2.4 Many to many
Marin *et all* [5] has described an experiment on multirobot internet based architecture. In the experiment, they tested on several telerobotic configurations that enable access from multi-users. They highlighted that having many robots connected to the servers manager would cause a bottleneck and proposed a configuration for the synchronization of the robots operation and

specification for reliable multirobot tasks.

3 Application

The literature reviews have revealed many aspect of internet robot. Many of it has focused on the technical aspect of the robot system development. This part of the paper discusses the research of internet robot which has been developed within an application area. The recent developments in the research and development for internet based robot have been focused on eight areas of application. The areas identified are; industrial robot, medical robot, entertainment robot, autonomous robot, service robot, hazardous environment robot, educational robot and other types of robot.

3.1 Industrial Robot

Industrial robots are used in various areas in manufacturing and production environment. The robot are used to assemble parts, paint, weld and do other tasks. An internet based robotic assembly planning system namely the WebROBOT has been developed using a modular architecture [6]. User can model desired assembly sequence using a variety of parts in the assembly area. The objects are classified onto two categories which are the stationary objects and the movable objects. Users plan an assembly sequence using the movable objects onto the stationary objects. A common assembly done by the robot involves placing five cylindrical parts into an array of holes of a block in polar fashion. This way the user can specify the assembly operation while the robot converts the orders into detailed robot path by computing robot joint positions using inverse kinematics. The ability to automatically generate the robot path enable the WebROBOT to carry out robot programming at the task level compared to the commonly used strategies which is at joint level or teach-in type robot programming.

An added feature of industrial robot has been developed using the Virtual Reality Modeling Language VRML model [7]. The VRML model is developed using various software components and it has the capability to control and monitor the robot via the internet. The system is designed as such it allows users to control the robot without the need to know the details of the programming language used. In factory environment, it allows the operators or managers to visualize the robot system in the factory online at remote locations.

3.2 Medical Robot

The main advantage of medical robots in ultrasound examinations is it alleviates the problems of human physical conditions among the sonographers [8]. This robot assisted system for medical diagnostic ultrasound helps to reduce the problem of having to perform awkward body positions in doing the test. The system comprises of a master hand controller, a slave manipulator and a computer control system. It enables the operator to remotely position the ultrasound transducer onto the targeted patients body parts. The teleoperated quality enable the operator to position the ultrasound at ease with additional assistance of machinery force and image controllers enable the robot to be remotely position and used in telemedicine.

Another medical robot system is developed by the Kanagawa Institute of Technology in the area of Face Robot [9]. The robot system is within a personal computer (PC). The purpose of the robot is to remind the patients when and which medication is to be taken using facial expression, a voice communication system and a display on the PC.

3.3 Entertainment Robot

Entertainment robots are developed as a variation of amusement means. However its potentials can be extended for other arising needs. The interesting internet controlled pet robot with arithmetical inclination has been explained earlier is a good extension of entertainment robot. Apart from the basic movements of walking, seating and standing up it can also do fundamental mathematics calculations. The pet robot can determine the equation of addition, subtraction; multiplication and division are correct or otherwise. If the equation right the pet robot will nod and if it is wrong, the pet robot will shake its head. Another entertainment robot is being developed by the LunaCorp Inc. and Carnegie Mellon University [10]. They aimed to operate a pair of teleoperated robotic vehicles on the surface of the moon with a television network as customer.

3.4 Service Robot

The service robot can provide many services in home or office. Sawasaki *et all* [11] describe the application of Humaniod robots to building and home management service. The system enables users to remote control humanoid robot in home environment. Another service robot WorkPartner has been developed to perform tasks like garden work, transferring of light weight obstacles and environment mapping. The centaur like service robot is a hybrid, lightweight outdoor robot [12]. Its hybrid system combines both legged and wheeled locomotion, providing good terrain negotiation and large velocity range.

3.5 Autonomous Robot

Unlike the conventional conveyance robot system which uses the line trace system, the autonomous robot can make judgment and equipped with dynamic sensors. Ohchi *et all* [13] described its robot which can follow the infrared rays emitted by a transmitter on a guide and move to the destination. An interesting autonomous robot with book browsing system has been developed [14]. The development has been made with consideration on the application and usability in book browsing environment. The aspects of movement towards the bookshelf, extraction and return of book and book perusal have been developed.

3.6 Hazardous Environment Robot

Environment such as managing spent nuclear fuels is obviously hazardous due to its high radioactivity nature. Cragg and Hu [15] proposed an integrated architecture which combines the strengths of available distributed computing, autonomous multiple robot and internet robot architectures for the use in nuclear decommissioning environment. Korea Atomic Energy Research Institute (KAERI) has developed a 3D graphic simulator to monitor the operation of multiple devices operated in such hostile environment [16]. Most of the devices are operated within a hot cell involving various sensors. They have successfully transmit the operational information from the actual system to the graphic workstation in realtime and visualization of the operating devices was simulated successfully in the virtual workcell.

3.7 Educational Robot

Safaric [17] has made an application of internet robot for education and training in using expensive equipment. The trainees uses offline virtual environment for task planning which then, exported to remote physical hardware through the internet for robot execution. This method has increases the training possibility and it is low cost. The downtime of the critical equipment is minimized while the gaining of valuable experience is minimized.

3.8 Other Internet Based Robotic

A space robot experiment ROTEX has been carried out [18]. One of its control modes operated from the ground using predictive computer graphics.

4 Research Issues

Most recent researches highlighted the issues concerning the robot work environment, communication delay and the tools needed for robot performance.

4.1 Usage in Dynamic Environment

Using such robot in dynamic environment is a concern due to a few reasons. One of the concern is on the information gap about the robot remote workplace. Virtual Reality (VR) is one of the common counter measure [16]. 3D graphic simulator is usually used as the human interface for robot in remote place operation. It is also used to visualize the work place environment in offline simulation to preview the robot movements in virtual workcell before operating the real robot. The KAERI project uses real time monitoring by gathering the task based operation data from the sensor to the graphic workstation which is then used to simulate the operation of the real device [16]. They proposed dedicated communication protocols and dividing the simulation programs into a number of small modules to execute each event massage from the control computer.

4.2 Communication, Time Delay and Other Unresolved Issues

The underlying problems of communication and time delay are rooted in the data transmission of the robot and the operator. The whole system also can be upset due to irregular time delay. Accumulation of these problems then leads to time varying system which requires various control methods. Kikuchi *et all* [19] proposed a system which consist of three subsystems; a bilateral teleoperation subsystem, a visual information subsystem and an environment predictive display subsystem. The first subsystem is stabilized using the virtual time delay method and the second subsystem transfers the visual information. Finally the third subsystem predicts the behavior of the environment for the operator. Other theories proposed on maintaining the system stability and synchronization of operator and robot terminal. This would involve predictive methodology including traditional predictive control, internal model control and Kalman filtering [20]. Other issues involve having the whole robot system being disperse on the internet. The sensor, the operator and controller are located in different nodes and coordinated via internet connection [21]. A perfect example would be a homeland security robot which have sensors at various locations, operator and the robot at remote places, all connected through the internet for full execution.

Conclusion

The direction of research for robot control using internet is patterned on having the operator and the robot in remote areas. The capitalization on true quality of the internet should be reap for closer correlation.

References

[1] M. Sugisaka and M. R. M Johari, "Remote Control of Autonomous Robot via Internet," *ICCAS 2004*, Bangkok Thailand, August 2004, pp.25-27

[2] Ren C. L, Kuo L. S, Shen H. S and Kuo H. T, "Networked Intelligent Robots Through the Internet: Issues and Opportunities," *Proc. of the IEEE*, Vol. 91, No.3, March 2003, pp.371-382

[3] Ren C. L, Kuo L. S, and S. H. Phang, "Multisensor Based Control of Pet Robot Through the Internet," *The 27th Annual Conference of IEEE Industrial Electronics Society (IECON'01)*, 2001, pp.416-421

[4] G. Pradel and O. Comfaits, "A Framework for a Web-based Supervisory Control of Mobile Robots," IEEE Int. Workshop on Robot and Human Interactive Communication, 2001, pp.249-255

[5] R. Marin, P. J. Sanz, P. Nebot and R. Esteller, "Multirobot Internet-Based Architecture for Telemanipulation: Experimental Validation," *Systems, Man and Cybernetics IEEE Int. Conf.*, Vol. 4, Oct. 5-8, 2003, pp.3565-3570

[6] V. B. Sunil and S. S. Pande, "WebROBOT: Internet based robotics assembly planning system," *Science Direct Computers in Industry 54*, 2004, pp.191-207

[7] H. Vermeulen, T. I. Niekerk, J. Huang, D. Hattingh, "VRML to Monitor and Control an Industries Robot via the Internet," *AFRICON, IEEE Int. Conf.*, Vol.1, Sept. 28-Oct. 1, 1999, pp.561-564

[8] P. Abolmnesumi, S. E. Salcudean, W. H Zhu, M. R Sirouspour and S. P. DiMaio, "Image-Guided of a robot for Medical Ultrasound," *IEEE Transactions on Robotics and Automation*, Vol. 18, No.1, Feb. 2002, pp.11-23

[9] Y. Takahashi, H. Goto and T. Saito, "Health Care System using Face Robot and Tele-operation via Internet," *7th Int. Conf. on Control, Automation, Robotics And Vision (ICARCV'02)*, Dec 2002, Singapore, pp.1025-1030

[10] K. Taylor and B. Dalton, "Internet Robots: A New Robotics Niche," *IEEE Robotics and Automation Magazine*, March 2000, pp.27-34

[11] N. Sawasaki, T. Nakajima, A. Shiraishi, S. Nakamura, K. Wakabushi and Y. Sugawara, "Application of Humanoid Robots to Building and Home Management Services," *Proc. IEEE Int. Conf. Robotics and Automation*, Taipei Taiwan, Vol. 3, Sept.14-19, 2003, pp.2992-2997

[12] S. J. Ylonen and A. J. Halme, "WorkPartner-Centaur like Service Robot," *Proc. IEEE/RSJ Int. Conf. Intelligent Robots and Systems*, Lausanne Switzerland, Vol. 1, Sept.30-Oct.5, 2002, pp.727-732

[13] M. Ohchi, T. Furukawa, M. Takayama and S. Yanagi, "Development of Autonomously Mobile Robot with Control System Connected by TCP/IP Network," *The 27th Ann. Conf. IEEE Industrial Electronics Society (IECON'01)*, 2001, pp.311-316

[14] T. Tomizawa, A. Ohya, S. Yuta, "Book Browsing System using an Autonomous Mobile Robot Teleoperated via the Internet," *Proc. of the 2002 IEEE/RSJ Inl. Conf. Intelligent Robots and Systems*, Lausanne Switzerland, Oct. 2000, pp.1284-1289

[15] L. Cragg and H. Hu, "Application of Mobile Agents to Robust Teleoperation of Internet Robots in Nuclear Decommissioning," *Int. Conf. IEEE Industrial Technology (ICIT 2003)*, Maribor Slovenia, Vol.2, Dec.10-12, pp.1214-1219

[16] S. H. Hong, J. W. Jeon, J. S. Yoon, "A Robot Graphic Simulator for Tele-operation," *Proc. of the IEEE Industrial Electronic (ISIE 2001)*, Pusan Korea, Vol. 1, June 12-16, pp.195-200

[17] R. Safaric, M. Debevc, R. M. Parkin and S. Uran, "Telerobotics Experiments via Internet," *IEEE Trans. Industrial Electronics*, Vol. 48, No.2, April 2001, pp.424-431

[18] G. Hirzinger, B. Brunner, J. Dietrich and J. Heindl, "Sensor-based space robotics-ROTEX and its telerobotics features," *IEEE Trans. Industrial Electronics*, Vol. 9, Oct. 1993, pp.649-663

[19] J. Kikuchi, K. Takeo, and K. Kosuge, "Teleoperation System via Computer Network for Dynamic Environment," *Proc. IEEE Int. Conf. Robotics and Automation*, Leuven Belgium, May 1998, pp.3534-3539

[20] X. Huo and J. Su, "New Approaches to Internet Based Intelligent Robotic System," *Proc. IEEE Int. Conf. Robotics and Automation*, New Orleans LA, April 2004, pp.3363-3368

[21] X. Huo and J. Su, "A Distributed Architecture for Internet Robot," *Proc. IEEE Int. Conf. Robotics and Automation*, New Orleans LA, April 2004, pp.3357-3362

Hard / soft switching particle filters for efficient real-time visual tracking

Takashi Bando[1,4] Tomohiro Shibata[1,2,4] Kenji Doya[2,3,4,1] Shin Ishii[1,4]

[1] Nara Institute of Science and Technology
[2] ATR Computational Neuroscience Laboratories
[3] Initial Research Project, Okinawa Institute of Science and Technology
[4] CREST, Japan Science and Technology Agency
takash-b@is.naist.jp

Abstract

Particle filtering is an approach to Bayesian estimation of intractable posterior distributions from time series signals with non-Gaussian noises. Several particle filters employing different sampling methods have been proposed for approximating Bayesian computation with finite particles. Our previous work first studied the difference between two filters, Condensation and Auxiliary Particle Filter. They can be considered compensatory in terms of accuracy and robustness under severe circumstances having unknown occluders and/or distracters. We then proposed a new particle filtering scheme, called switching scheme, which allows robust and accurate visual tracking under severe circumstances. This scheme utilizes the two complementary sampling algorithms above by switching them based on the confidence of filtered state of the visual target. This article presents an alternative switching method called soft switching while we call the previously proposed method hard switching. The soft switching method softly changes the population ratio of each sampling method for assigning particles. We examine their properties in terms of accuracy and robustness via real visual tracking experiments as well as computer simulations.

keywords – particle filter, sampling, real time, visual tracking, switching

1 Introduction

Particle filtering is an approach to Bayesian estimation of intractable posterior distributions from time series signals with non-Gaussian noise. This approach has been attracting attention in various research areas, including real-time visual processing which deals with images contaminated by non-Gaussian noises due to not only signal noises but also the existence of obstacles and/or distracters. Several particle filters have been proposed for approximating Bayesian computation with finite particles. The performances of such algorithms have not, however, been fully evaluated under circumstances specific to real-time vision systems, i.e., there are unknown occluders and distracters. It is important for real-time visual tracking systems to realize high accuracy and robustness, coping with these difficulties.

Our previous work studied the difference between two filters, Condensation [1] and Auxiliary Particle Filter [2] (APF). Condensation employs the Sampling Importance Resampling (SIR) method, and can run on a cheap standard PC. Condensation, however, has a problem called an outlier problem, i.e., large difference between prior and true distribution causes crude approximation of the posterior distribution. Unfortunately the outlier problem often occurs in a real-time visual tracking task due to unknown occlusions, distracters and target dynamics. APF was proposed to solve the outlier problem using the information of current observation. These two filters can be considered compensatory in terms of accuracy and robustness under the circumstances specific to real-time vision systems. To exploit their advantages, we proposed a new filtering scheme that switches these filters according to a simple criterion [3].

This article presents an alternative switching method called soft switching while we call the previously proposed method hard switching. The soft switching method softly changes the population ratio of each sampling method for assigning particles. We, then, examine their properties of accuracy and robustness via computer simulations that model realistic circumstances include occlusion and distracters. Next, the effectiveness of our methods are demonstrated by real visual tracking experiments. In our tasks, the tracking target is a red ball, and the ball moves sinusoidally behind a board as an occluder. Because there are in addition many objects similar to the tracking target in the background as distracters, they are realistic visual tracking tasks.

2 Particle Filters

Particle filters are based upon point-mass representation of probability densities. A continuous state vector of a target object at time step t is denoted by $\mathbf{x}_t \in \mathcal{R}^{N_x}$, and a measurement vector is $\mathbf{z}_t \in \mathcal{R}^{N_z}$. Using a sample set $\{(\mathbf{x}_t^{(n)}, \pi_t^{(n)}), n = 1, ..., N\}$ at time step t, the posterior density is approximated as

$$p(\mathbf{x}_t|\mathbf{z}_t) = k_t p(\mathbf{z}_t|\mathbf{x}_t)p(\mathbf{x}_t|\mathbf{z}_{t-1}), \qquad (1)$$

where k_t is the normalization term. Then, prediction density $p(\mathbf{x}_t|\mathbf{z}_{t-1})$ as prior is approximated as

$$p(\mathbf{x}_t|\mathbf{z}_{t-1}) \approx \sum_n \pi_{t-1}^{(n)} p(\mathbf{x}_t|\mathbf{x}_{t-1}^{(n)}). \qquad (2)$$

The weights $\pi_t^{(n)}$ are determined by $\pi_t^{(n)} = p(\mathbf{z}_t|\mathbf{x}_t^{(n)})$.

If we can prepare sufficient large number of particles, Eq.2 becomes accurate. However, we cannot prepare such a large number of particles for real-time processing.

In Condensation, $p(\mathbf{x}_t|\mathbf{x}_{t-1})$ used as the proposal density is independent of observation $\mathbf{z}_t$ at each time step t, and the state space is explored regardless of $\mathbf{z}_t$. This property suffers from the outlier problem [2], i.e., model-implausible observations may occur when there are unexpected occluders, distracters, and changes in the target motion.

Auxiliary Particle Filter [2] proposed by Pitt and Shepherd employs elegant resampling method that solves the outlier problem. In their approach, likelihoods are calculated as weights at any likely point that characterizes $p(\mathbf{x}_t|\mathbf{x}_{t-1}^{(n)})$, e.g., mean or mode. Then, by resampling with the weights that include information of current observation $p(\mathbf{z}_t|\mathbf{x}_t)$, the estimation around the likely points tends to be more accurate in APF than in Condensation. The diversity of particles, however, is lower in APF than in Condensation. For particle filters, we need to prepare an observation model, or likelihood function, of the target to be tracked. In this article, we employ the same observation model as that in [3].

3 Hard / Soft Switching Particle Filters

As described in the last section, Condensation emphasizes prediction of target transition (prior) more than APF, while APF emphasizes observation more than Condensation for estimating current target state. Emphasis on observation makes tracking accurate, while emphasis on prior would make tracking robust especially under the severe circumstances having unknown occluders and distracters. To exploit their advantages, we previously presented switching sampling scheme based on the confidence of filtered state of the visual target [3]. Our proposed method fully switched the two sampling algorithms according to a simple criterion, the variance of current estimated target states as confidence in the estimation. We call it hard switching method. The variance of the current estimated target states is defined as

$$V_{\text{est}}(t) = (\sigma_{\text{est},1}^2, ..., \sigma_{\text{est},N_x}^2)^T \qquad (3)$$

$$= \frac{\sum_n \pi_t^{(n)}(\hat{\mathbf{x}}_t - \mathbf{x}_t^{(n)})(\hat{\mathbf{x}}_t - \mathbf{x}_t^{(n)})^T}{N-1}, \qquad (4)$$

where, $\hat{\mathbf{x}}_t = \sum_n \pi_t^{(n)} \mathbf{x}_t^{(n)}$. Then, using threshold vector γ, the hard switching method is described as

if $\sigma_{\text{est},i} > \gamma_i$ $(\exists i)$, then use APF,
otherwise, use Condensation.

The vector γ is a thresholding parameter that discriminates successful tracking from unsuccessful tracking based on the confidence of the current estimated target states. We set γ at the variance of estimated target states during successful tracking. For example, in our experiments described later, γ was set as follows. We assume that the ball size on the image plane is invariant and $x_i (i = 1, 2)$ are independent of each other for simplicity. Under such assumption, the covariance components of the current estimated target state are expected to be 0, and all we have to do is to compare the threshold vector $\gamma_i (i = 1, 2)$ to the standard deviation of the current estimated target state $\sqrt{V_{\text{est}}(t)}$. If we cannot assume the component-wise independence of state vector, we need to extend the variance $V_{\text{est}}(t)$ to the variance-covariance matrix. In our experiments we employ the target ball radius as threshold γ because we found the standard deviation of the current estimated target states during successful tracking were almost equal to the ball radius.

In this article, we propose an alternative switching method called soft switching. Although the soft switching method is the same as the hard switching method except that it controls the population ratio of each sampling method for assigning particles, based on confidence level of estimation. The number of particles sampled by each sampling method, N_{cond} and N_{apf}, are determined as

$$N_{\text{cond}} = N - N_{\text{apf}},\ N_{\text{apf}} = \max_i N_{\text{apf},i},$$

$$\begin{cases} N_{\text{apf},i} = 0 & (\sigma_{\text{est},i} < \gamma_{\min,i}) \\ N_{\text{apf},i} = \frac{N(\sigma_{\text{est},i} - \gamma_{\min,i})}{\gamma_{\max,i} - \gamma_{\min,i}} & (\gamma_{\min,i} \le \sigma_{\text{est},i} \le \gamma_{\max,i}) \\ N_{\text{apf},i} = N & (\sigma_{\text{est},i} > \gamma_{\max,i}) \end{cases},$$

meaning that the more confident of tracking the tracker has, the larger number of particles are sampled by Condensation, while the less confident of tracking it has, the larger number of the particles are sampled by APF.

The threshold vectors in the soft switching method are also determined using the target ball radius. We set $\gamma_{\min}$ at smaller than the ball radius, and $\gamma_{\max}$ at larger than the ball radius. We will examine the performance of the soft switching method with various combinations of $\gamma_{\min}$ and $\gamma_{\max}$ in the next section.

4 Simulation Results

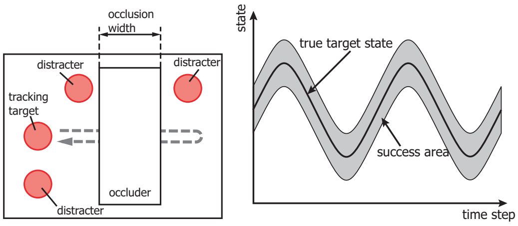

Figure 1: The setting of the computer simulations (left) and the success area defined encompassing the true target state (right).

To investigate the performance under realistic circumstances, we prepared simulated image sequences in which occlusion width, distracter size and positions varied (cf. Figure 1 (left)). The radius of the target was 5 pixels, and the target moved sinusoidally with amplitude 200 pixels and frequency 1 Hz. The occlusion width varied from 5 to 100 pixels with step size 5 pixels. For each image sequence, three distracters were randomly chosen from six candidate positions, and their radius were varied from 1 to 20 pixels. The length of each image sequence was set to 60 frames.

First, the hard switching method ($\gamma = 5$) and the soft switching method ($\gamma_{\min} = 4, \gamma_{\max} = 20$) were tested for the simulation image sequences. We examined robustness of the two methods in terms of the tracking success rate, where "success" means the number of failure frames in which estimated target state deviated from the success area (cf. Figure 1 (right)) was smaller than 15 frames. Their accuracies were also examined based on the mean tracking error in successful trials.

To examine difference in the success rate, we used the χ^2 test. Figure 2 (left) shows results of the χ^2 test ($p < 0.01$), indicating the hard switching method is more robust against unknown occluder and distracters except for too severe conditions, i.e., large occlusion and distracters, or very simple conditions, i.e., small occlusion and distracters.

To examine difference in the tracking error, we applied the Wilcoxon test because the tracking errors and the number of successful trials were too small for the t-test under the severe condition with low success rate. Figure 2 (right) shows results of the Wilcoxon test ($p < 0.05$), indicating the hard switching method

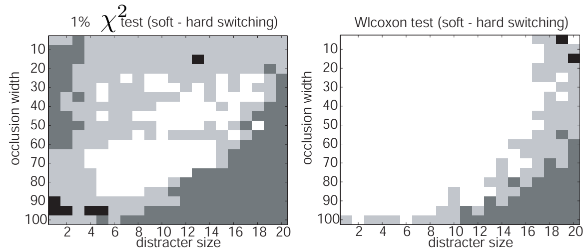

Figure 2: Result of the χ^2 test (left) and the Wilcoxon test (right). White, black, gray, dark gray colors mean that the hard switching method was better significantly, the soft switching method was better significantly, there was no significant difference between their performances, and neither the χ^2 test nor the Wilcoxon test was not applied because of the too small number of successful trials, respectively.

maintain its accuracy of tracking under the broad conditions better than the soft switching method.

In order to use switching methods, switching threshold γ must be set beforehand. Although we found that the target ball radius was enough in our experiments, the switching methods depends on this parameter, which is more salient for the hard switching method. An inappropriate parameter causes failure tracking because the tracker misses timing of switching and then the balance of divergence and convergence of particles is broken. As for the soft switching method, setting $\gamma_{\min}$ at smaller than the ball radius, and $\gamma_{\max}$ at larger than the ball radius adding a margin to the timing of switching leads to robust tracking. The soft switching method becomes equivalent to the hard switching method in terms of the number of particles sampled by each sampling method if $\gamma_{\min} = \gamma_{\max}$. When sufficient resource cannot be allocated as in real-time visual tracking, the hard switching method is more efficient than the soft switching method if the precise switching threshold can be predetermined.

5 Real Experiments

In this section, we compare the performance of the hard and soft switching methods with Condensation, APF and Unscented Particle Filter (UPF) [4]. Similar to APF, UPF proposed by Merwe et al. emphasizes the information of current observation. Its proposal distribution is estimated by Unscented Kalman Filter for maintaining accurate estimation of target states. Because we cannot calculate $\mathbf{x}_t$ from $\mathbf{z}_t$, we use weighted mean by redness at each pixel as an observation in UPF. We evaluate the effectiveness by comparing the number of lost-target frames and mean error in successful trials.

5.1 Experimental Setup

The task was to track a red ball moved sinusoidally either by hand or by a robot manipulator. Real video images were taken by a digital video camera and processed by a Pentium 4 (2 GHz) Linux PC. These images were downloaded to the PC by Video for Linux at a resolution of 640 × 480 pixels, then reduced to 320 × 240. We also need to determine the number of particles. From simulation results using artificial images, we set the number of particles to 800 to maintain the accuracy and real-time quality. Our system processed one frame in about 8 msec.

5.2 Tracking with an Occluder and distracters

To statistically compare the performance of different particle filters under usual circumstances for vision systems, we prepared an environment in which we placed a board as an occluder between a red ball and a camera, cf. Figure 3. There were also some distracters, i.e., red objects around the trajectory and the board.

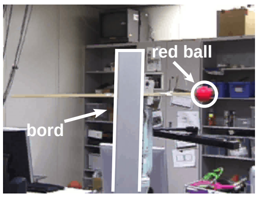

Figure 3: A sample image in the our task.

Figure 4 (left) shows histograms of "lost" frames (length of video sequence is 423 frames for 14 sec). "Lost" means that the estimated target state deviated from the success area defined around the true target state (cf. Figure 1 (right)). Figure 4 (right) shows the mean absolute position error of each tracker in successful trials. A successful trial means that the number of lost frames was less than 100.

These figures show that our switching scheme outperforms the other filters including UPF. Because APF takes particular note of the current observation, it sometimes failed in tracking the target due to distracters, especially as it crossed behind the board. Condensation was more robust for crossing the board, but subsequent convergence to the target was very slow and not promising. The UPF was more robust and accurate than those two filters, but its accuracy was much worse than that of the switching methods. Because the current target state cannot be observed directly from the image (only the redness at each pixel is observed), we choose the weighted mean of pixels using their redness as the observed state in UPF. In spite of inaccurate observation, UPF worked well. In a severe circumstance with occlusion and distracters, however, UPF was not able to keep accurate tracking.

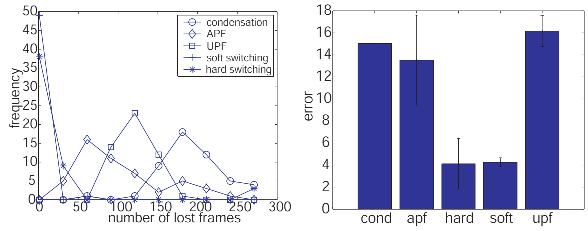

Figure 4: Lost frames (left) and mean absolute position errors (right).

6 Summary

We have examined new particle filtering methods, hard and soft switching particle filters, devised for duality with real-time vision systems. These filters employ two particle filters, Condensation and Auxiliary Particle Filter (APF), which incorporate different resampling algorithms. To exploit their advantages, our proposed filters switch them dynamically according to a simple criterion: the confidence level of the current estimated target state. The two methods, hard switching and soft switching, were examined in their properties in terms of accuracy and robustness via computer simulations that model realistic circumstances include occlusion and distracters. The simulation results showed that the soft switching method is more tolerant to the switching threshold, although the hard switching method is more efficient if precise switching threshold is pre-determined, especially when sufficient resource cannot be allocated as in real-time visual tracking. We also demonstrated that the switching methods outperform other well-known particle filters through real visual tracking experiments.

Automatic determination of the threshold parameter can be regarded as learning of a hyper-parameter, which will be our future work.

References

[1] M. Isard and A. Blake, "CONDENSATION-conditional density propagation for visual tracking," *IJCV*,Vol. 29, pp. 5-28, 1998.

[2] M. k. Pitt and N. Shephard, "Filtering via Simulation: Auxiliary Particle Filter," *J. of American Statistical Association*, Vol. 99, pp. 590-599, 1999.

[3] T. Bando, T. Shibata, K. Doya, and S. Ishii, "Switching Particle Filters for Efficient Real-time Visual Tracking," *ICPR*, Vol. 2, pp.720-723, 2004.

[4] R. v d Merwe, A. Doucet, N. de Freitas, E, Wan, "The Unscented Particle Filter," *NIPS 13*, 2001.

The Tenth International Symposium on Artificial Life and Robotics 2005(AROB 10th '05),
B-con Plaza, Beppu, Oita, Japan, February 4-6, 2005

Robotics and the Q-analysis of Behaviour

Pejman Iravani — p.iravani@open.ac.uk — Computing Department
Jeffrey Johnson — j.h.johnson@open.ac.uk — Design and Innovation
Lucia Rapanotti — l.rapanotti@open.ac.uk — Computing Department
*
The Open University, Milton Keynes, MK7 6AA, UK

Abstract

A new method is presented for the analysis of complex multi-agent robotic behaviours, based on observing behaviour and abstracting models on which to base control. This involves (i) building an appropriate representation of the scene using the 'best' features, (ii) classifying each scene by its features, and (iii) learning the correlation between scene classes and the actions performed in each. A novel aspect is the use of *Q-analysis* to investigate relational structure between many possible observable features, and configurations in the scene. Q-analysis helps in the selection of appropriate features and is the basis of our combinatorial classification. The methods and algorithms presented are experimentally validated using data from the RoboCup simulation league. We conclude that Q-analysis could be a powerful new approach in robot control.

1 Introduction

We refer to *behaviour analysis* as the task of constructing a model of the behaviour exhibited by an agent or multiagent system (MAS) using observations. In this paper the agents are autonomous robots working together as a team to play soccer.

Behaviour analysis starts by observing *scenes* as the interaction between agents and their environment. Scenes have sub-scenes, here called *configurations*. In the first step, the configurations are described by a set of *observed features*, for example, 'opponent to left', 'ball moving fast', 'team-mate to right', 'close to goal', or any other 'relevant' characteristic. In the second step, the configurations are classified, based on combinations of their features. Finally, the configuration classes are correlated to the observed *actions* performed by the agents. This is then used as the basis of control for the agents, effectively giving a *learned behaviour* [1, 2]. In order to analyse behaviours in this manner, the following issues need to be addressed:

1. Which features "best" describe a scene?
2. How can the features be used to classify scenes?
3. How can relationships be learned between configuration classes and the agent control actions?

The first issue, known as *feature extraction* in pattern recognition, relates to which features should and should not be part of the representation. In general, adding irrelevant features "obscures" the effects of relevant features. Thus it is desirable to find a method to include only 'relevant' features in the representation. The second issue is a general problem in classification, which relates to finding an appropriate criteria of 'similarity' between instances. The third issue is related to machine learning, in finding a method for learning from classified observed behaviours.

This paper develops a framework for behaviour analysis based on the *Methodology of Q-analysis* [3, 4]. As explained in the next section, Q-analysis is a multidimensional generalisation of network theory, able to model general *n-ary* relations between features and configurations. Through its notion of 'q-connection' it provides a graded method of classification according to shared features.

This is in marked contrast to methods of classification that map objects into multidimensional data spaces, and cluster them into components based on similarity metrics. The essential difference is that Q-analysis is very sensitive to the selection of features, and this can be exploited to detect and remove features that add little or no information.

Before starting the discussion, we establish some basic notation. A *scene* is an instantaneous observation of the system including the robots and environment. Scenes have sub-scenes associated with subsets of players that we will call *configurations*. In this paper we are concerned with selecting *features* to describe those configurations, and classifying the configurations for control purposes.

2 The Methodology of Q-analysis

2.1 Classifying Multidimensional Data

Of the large literature on classification, we can abstract two complementary approaches. To illustrate this, consider a set of objects to be classified, $A = \{a_1, a_2, ..., a_m\}$, and a set of *classificatory features*, $B = \{b_1, b_2, ..., b_n\}$. An *observation* of an object a_i consists of making two decisions for each b_j:

1. is object a_i related to feature b_j?
2. what is the strength of that relationship, weighted as a number?

Behind the first of these questions is a subtlety often lost by unquestioning use of standard classificatory techniques. Whether or not an object is related to a feature is a binary yes/no decision. For example, consider whether or not a battery-powered robot has a power source. If the battery is removed it does not (relationship). Suppose the robot has a battery fitted, but the battery is flat. Then it does have a power source (relationship), currently capable of delivering zero power (number).

This distinction makes a big difference in the application of classification techniques. When 'non-present' characteristics are included in the classification with weight zero, this impacts on the classification. In particular, it established 'similarity' between objects weakly related to a feature, and objects that are logically unrelated to that feature. In the case that the feature represents a dimension with little or no information, this creates spurious similarities.

This is one of the reasons why it is not possible to solve all problems using fully connected neural networks as classifiers. Neural networks such as the multilayer perceptron effectively map an m-dimensional input space to an n-dimensional output space. The distinction being made above corresponds to there being no connection between input x_i and neuron y_j (not related), and there being a connection for which all the input values are zero, or the weight, w_ij, being held at zero. In fact this last possibility cannot be guaranteed within the standard multilayer perceptron architecture, and the only way to achieve the required effect is to cut the link between x_i and y_j.

The practical implications of this are profound. The idea that one can throw any combination of 'data' at a network, or any other classifier, founders on combinatorial complexity. In principle the network will filter out the 'irrelevant' data by assigning low weights to their connections. In practice a network with a million inputs will never converge.

Thus, the classification of multidimensional data addressed by many clustering techniques often begs the essential question: *what are the relevant dimensions for the particular application?*

As we will show, Q-analysis is an approach that stays very close to the data. At times its sensitivity to the dimensions used can be frustrating, as can the effects of objects that dominate the structure. But often, this just reflects the nature of the system under investigation.

2.2 Similarity

In classification, *geometric* models are often used to evaluate the similarity between instances. Geometric models represent instances as points in a multidimensional coordinate space and define similarity between instances as the Euclidean distance separating them. This means that the information stored in a set of dimensions is subsumed into a distance value, and thus, it is critically important that this distance reflects accurately the relevant information in the data [5]. Figure 1 illustrates an example of geometric similarity; on the left, three robots (R1,R2,R3) are positioned with respect to a goal, on the right, two different coordinate spaces are used to represent each situation. Following the top coordinate space, robots R1 and R3 are in more similar situations than R2. On the bottom coordinate space, the angle feature (α) has been scaled differently (e.g. changed representation units), as an effect R1 and R2 are now more similar. This exemplifies the importance of finding a distance value that accurately represents similarity among instances.

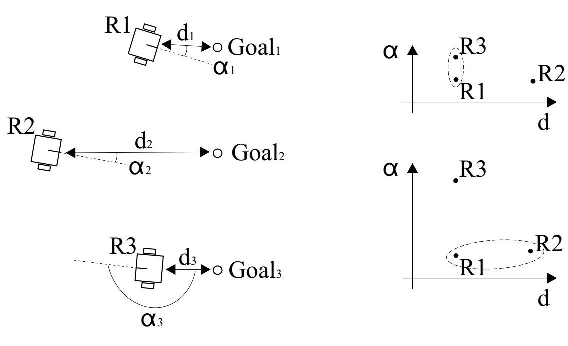

Figure 1: Mobile robots in different situations with respect to a goal and their similarity based on Euclidean distance.

2.3 Representing relations by simplices

Given the limitations of geometric models based on geometric similarity metrics, the Methodology of Q-analysis offers new insights to the concept of similarity. This analysis is especially suited for discovering *relational structure* in multidimensional data. In Q-analysis, similarity is no longer defined as a distance, but is based on structural ideas of connectivity between particular instances.

Q-analysis provides a *set-theoretic* approach to the study of relationships. In general a relation R between a set of elements, $\{x_0, x_1, ..., x_p\}$, can be considered to determine a new object called a *simplex*, denoted $\langle x_0, x_1, ..., x_p; R\ \rangle$.

Simplices can be represented by *polyhedra* in multidimensional spaces. Let the individual x_i be called *vertices*, denoted as $\langle x_i \rangle$. Then a simplex with one vertex is a point, a simplex with two vertices is a line, a simplex with three vertices is triangle, a simplex with four vertices is a tetrahedron, a simplex with five vertices is a 5-hedron, and so on. This is illustrated in Figure 2, where (a) and (b) are tetrahedra, (c) is a triangle, and (d) is line. As can be seen, a simplex with $p+1$ vertices is a p-dimensional object. Thus we refer to a simplex with $p+1$ vertices as a *p-simplex*.

We illustrate this using an example from robotics. Let $\{x_0, x_1, ..., x_p\}$ be a set of features describing a sub-scene, or configuration, in a robot soccer game. Let a configuration be denoted by c_j, so that each x_i is R-related to c_j. Then we can write the simplex associated with c_j as $\sigma(c_j) = \langle x_0, x_1, ..., x_p; R\ \rangle$.

To illustrate this consider a matrix M representing five configurations, $\{c_1, c_2, c_3, c_4, c_5\}$, related to subsets of six binary features $\{x_1, x_2, ..., x_6\}$:

$$\mathbf{M} = \begin{array}{c|cccccc} & x_1 & x_2 & x_3 & x_4 & x_5 & x_6 \\ \hline c_1 & 1 & 1 & 0 & 1 & 1 & 0 \\ c_2 & 0 & 1 & 1 & 1 & 0 & 1 \\ c_3 & 0 & 1 & 0 & 1 & 0 & 1 \\ c_4 & 0 & 0 & 0 & 0 & 1 & 1 \\ c_5 & 1 & 1 & 0 & 1 & 1 & 0 \end{array}$$

Table 1: a configuration-feature incidence matrix.

Each row, i, of matrix, M, can be represented by a *simplex*, $\sigma(c_i)$. Thus $\sigma(c_1)$ and $\sigma(c_5)$ are the 3-simplex or tetrahedron $\langle x_1, x_2, x_4, x_5 \rangle$ (Figure 2(a)). $\sigma(c_2)$ is also a 3-simplex, $\langle x_2, x_3, x_4, x_6 \rangle$, (Figure 2(b)). $\sigma(c_3)$ is a 2-simplex or triangle, $\langle x_2, x_4, x_6 \rangle$, (Figure 2(c)), and $\sigma(c_4)$ is a 1-simplex or line, $\langle x_5, x_6 \rangle$ (Figure 2(d)).

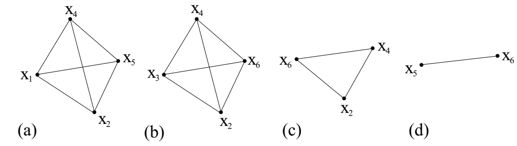

Figure 2: Some examples of different simplices.

An important idea in Q-analysis is that high dimensional simplices can be decomposed into their lower order simplices called their *faces*. For example, the simplex representing, $\sigma(c_1)$, (Figure 2a) can be decomposed into the following face simplices of dimension q:

q	#	simplices
3	1	$\sigma(c_1) = \langle x_1, x_2, x_4, x_5 \rangle$
2	4	$\langle x_1, x_2, x_4 \rangle \langle x_1, x_2, x_5 \rangle \langle x_1, x_4, x_5 \rangle \langle x_2, x_4, x_5 \rangle$
1	6	$\langle x_1, x_2 \rangle \langle x_1, x_4 \rangle \langle x_1, x_5 \rangle \langle x_2, x_4 \rangle \langle x_2, x_5 \rangle \langle x_4, x_5 \rangle$

2.4 q-nearness and structural similarity

Let the intersection of two simplices be defined to be their shared face. For example, $\sigma(c_1) \cap \sigma(c_2) = \langle x_1, x_2, x_4, x_5 \rangle \cap \langle x_2, x_3, x_4, x_6 \rangle = \langle x_2, x_4 \rangle$ (Figure 3).

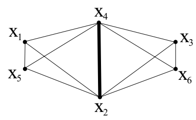

Figure 3: Q-connectivity of two simplices.

More generally, two simplices σ and σ' are said to be *q-connected* if there is a chain of pairwise p-near simplices between them, $p \geq q$.

When the relation is represented by a binary matrix, M the q-nearness can be calculated as, $MM^T - \mathbf{1}$, where, M^T, is the transpose of M and $\mathbf{1}$ is a matrix with all elements equal to 1.

	c_1	c_2	c_3	c_4	c_5
c_1	3	1	1	0	3
c_2	1	3	2	0	1
c_3	1	2	2	0	1
c_4	0	0	0	1	0
c_5	3	1	1	0	3

Table 2: A shared face matrix.

For example, the symmetric matrix above represents the q-nearness of the simplices in M given in the previous section. The diagonal of this matrix represents the dimension of each simplex, this value is also known as *q-top*.

This *shared face matrix* represents the direct connectivity of the simplices based on their shared vertices. Every p-simplex is p-near to itself. In this case, c_1 is 3-near to c_5 because they are related to the same set of vertices, and are *identical* with respect to this vertex set. On the other hand, c_1 and c_2 are both 3-simplices (tetrahedra), but they are only 1-near because they share only a 1-dimensional face.

The *conjugate matrix*, calculated using $M^T M - \mathbf{1}$, gives the number of configurations shared by pairs of features. It represents the connectivity between features, and we call it the *feature shared face* matrix.

3 Q-analysis in Behaviour Analysis

This section investigates the suitability of the Q-analysis framework for behaviour analysis, defined in the Introduction.

The underlying hypothesis is that classes of 'similar' configurations can form more abstract *concepts*. These can be associated with particular control actions that have been experienced previously by the robot as successful. Thus the classification is the means of *generalising* from particular experiences.

The study is conducted by analysing the example of robot football *passing behaviour*. The data for this come from observing 'passing configuration' from the Log-Files of the RoboCup 2003 Competition, and constructing a model of a passing behaviour. As seen earlier, to construct such model the following issues need to be addressed: (i) selecting 'relevant' feature, (ii) using these 'relevant' features to best classify 'similar' configurations, (iii) using these classes as the basis for learning behaviour.

3.1 Representing Configurations

The number of possible features that could be used to describe a configurations, or position, in a robot soccer game is enormous. Also, there is no obvious *a priori* 'best-set' of features. We constructed our set of features as follows.

Figure 4a illustrates a 'passing scene', simplified to 5 players per team rather than the 11 used in this experiment. Player, p, is the one holding the ball, while the players a_i are on the same team as p, and players b_j are the opposition team.

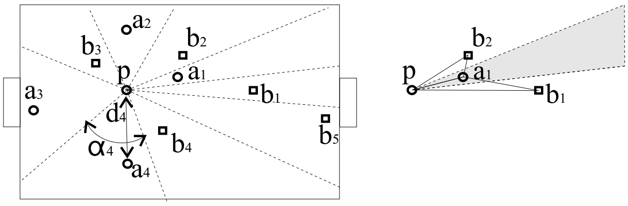

Figure 4: a) Passing scene. b) Player configuration

For a configuration, many features could be abstracted. For example, let player p have possession of the ball. Then each other player has an associated triangular area of 'controlled space' defined by p and the positions of other neighbouring players (Figure 4(a)). Then each triangle has an angle, α_i, and a distance, d_i between the player and p.

Both, α_i and d_i are continuous variables that are segmented into four intervals, 'very-small', 'small', 'big', and 'very-big', denoted as vs, s, b, vb. Two relations indicating whether or not the right and left neighbouring players are of the passer's team are also represented. We also use the feature of whether or not an opponent player is closer to the ball than a teammate. Many other features could be incorporated, but we arbitrarily select these 11 binary variables:

4 distances: d_{vs}, d_s, d_b, d_{vb}
4 angles: $\alpha_{vs}, \alpha_s, \alpha_b, \alpha_{vb}$
2 neigbours: $R_{neigh\_own\_team}, L_{neig\_own\_team}$
1 opponent closer: opp_{closer}

Thus, each configuration (Figure 4(b)) can be described by simplex with vertices subsets of these eleven features. As will be explained, these vertices themselves were the result of a selection process according to relevance.

3.2 Feature Selection using Q-analysis

Given an arbitrary set of features, which ones are the most 'relevant'? The usual approach to this question has been to *leave it to the designers intuition* to decide which are the most important features, whether new ones need to be added or if any need to be discarded. In this context, a method to evaluate features as 'relevant' or otherwise, could be helpful to human robot designers, and in the longer term, could lead into automating the feature selection process. Here we present a method of feature selection based on Q-analysis.

Let X be a configuration represented by n binary features, $X_i = \{x_1, x_2, ..., x_n\}$. For illustration it will be assumed that each configuration is classified by experience into 'passing configuration' and 'non-passing configuration'. Thus the configurations will be denoted $c_{j,passing}$ and $c_{k,non-passing}$. Some features add no discriminative information for a classification, while others give complete information.

For the simplest cases, we will define a feature to be 'distracting' when observing it adds little information in its context. For example, a feature related to *all* configurations adds no information, and a feature related to *no* configurations adds no information. The first case would apply when a thermometer always recorded $x_{temperature}$ above a safety threshold in all cases, associated with the action "sound alarm", while second case would apply when a thermometer always recorded $x_{temperature}$ as below the safety threshold associated with action "do nothing".

A feature x_i is a *perfect classifier* if all configurations of one class are are related to that feature, and no configuration from other classes is related to that feature. This last occurs when, for example, $x_{temperature}$ below a safety threshold is related to a class "do nothing", or otherwise "sound alarm".

In this paper we are concerned with discovering features that are neither distracting or perfect classifiers, but become relevant in combination with other features. In order words seek features that form the vertices of classifying simplices. These simplices can be considered to be 'concepts' at a higher level or representation [1, 2, 6].

In the next section we will illustrate a number of heuristics for selecting 'relevant' features for the case of passing and non-passing configurations. These heuristics amount to seeking feature simplices that are faces of many configuration simplices. In other words, we seek *combinations* of feature vertices that give the most powerful discrimination, and we seek features vertices that belong to many such combinations.

3.3 Q-analysis of a Games

To investigate the use of Q-analysis as a classification method, we took the Final game of RoboCup 2003 and studied the passing behaviour observed in it. Let, S, be the set of successful passing configurations (passer and receiver players belong to the same team) observed in that game.

For every pass that is made, the pitch can be divided into 21 triangular configurations, one for each of the 21 players not possessing the ball. Of these we focus on the areas of the 10 team-mates of the passing player.

Each of the ten 'team-mate' areas can be described by the eleven features defined above. Some of these are mutually exclusive, and the maximum dimension of the simplices representing the triangular configurations is $q = 4$. The pass can only be made to one of these areas, so the remaining nine become 'non-passes'.

We now apply Q-analysis on this data to study whether any structural difference emerges between the pass and non-pass simplices, both enabling us to isolate powerful classificatory simplices, and thereby relatively the powerful features that make up their vertices.

3.3.1 The Shared Face Connectivity Matrices

	x_1	x_2	x_3	x_4	x_5	x_6	x_7	x_8	x_9	x_10	x_11
x_1	12	0	0	0	7	1	4	0	5	2	11
x_2	0	45	0	0	13	9	13	10	10	18	30
x_3	0	0	44	0	11	10	16	7	20	15	33
x_4	0	0	0	17	8	4	2	3	8	4	10
x_5	7	13	11	8	39	0	0	0	12	16	35
x_6	1	9	10	4	0	24	0	0	8	8	19
x_7	4	13	16	2	0	0	35	0	21	14	23
x_8	0	10	7	3	0	0	0	20	2	1	7
x_9	5	10	20	8	12	8	21	2	43	11	34
x_10	2	18	15	4	16	8	14	1	11	39	33
x_11	11	30	33	10	35	19	23	7	34	33	84

(a)

	x_1	x_2	x_3	x_4	x_5	x_6	x_7	x_8	x_9	x_10	x_11
x_1	33	0	0	0	10	13	6	4	17	7	24
x_2	0	108	0	0	29	38	29	12	46	54	76
x_3	0	0	187	0	68	58	41	20	82	73	116
x_4	0	0	0	734	465	211	48	10	300	315	344
x_5	10	29	68	465	572	0	0	0	243	233	314
x_6	13	38	58	211	0	320	0	0	136	150	172
x_7	6	29	41	48	0	0	124	0	57	54	60
x_8	4	12	20	10	0	0	0	46	9	12	14
x_9	17	46	82	300	243	136	57	9	445	164	308
x_10	7	54	73	315	233	150	54	12	164	449	307
x_11	24	76	116	344	314	172	60	14	308	307	560

(b)

Figure 5: a) Pass shared face matrix, M. (b) Non-pass shared face matrix, $\tilde{M}$

Let M be the incidence matrix of the relation between the set of triangular configurations associated with passing. Let $\tilde{M}$ be the incidence matrix of the relation between the set of triangular configurations not associated with passing. Then we form the two shared face matrices $M^T M$ and $\tilde{M}^T \tilde{M}$, for the passing and non-passing configurations. Figure 5 illustrates these matrices.

The diagonal entries of the two shared face matrix give the number of passes or non-passes related to the diagonal feature. For example, out of 118 passes, x_1 is related to 12 of them while x_{11} is related to 84 of them. There are many more non-passes (1062) than passes, and x_1 is related to 33 of them while x_{11} is related to 560 of them.

Already it is clear that the vertices are responding differently to pass and non-pass configurations. For example, a comparison of the diagonals of the matrices using the 'normalised ratio' formula $(M^T M_{ii}/((\tilde{M}^T \tilde{M}_{ii})/9)$ gives the following:

x_1	x_2	x_3	x_4	x_5	x_6	x_7	x_8	x_9	x_{10}	x_{11}
0.3	0.2	0.5	4.8	1.6	1.5	0.4	0.2	1.1	1.3	0.7

This means, for example, that x_1 is related to relatively less non-pass positions than it is pass positions $(1 : 0.3)$, as is x_{11} ($1 : 0.7$). However, x_4 has a relative large ratio of ($1 : 4.8$)in favour of non-pass positions. This is easy to explain, since x_4 means "large distance to team mate". In fact x_4 approaches being a perfect classifier, as far as non-passes are concerned.

The further the ratios are from unity in the table above, the more discriminating are the features, x_i. As we have noted, some numbers are less that unity (better response to pass configurations) and some are above unity (better response to non-pass configurations). In combination these features may exploit these differences to give robust classification.

For example, recall that there are 118 passes and 1062 non-passes in the data. $\langle x_7 \rangle$ is related to 35 passes (30%), $\langle x_9 \rangle$ is related to 43 passes (36%), while $\langle x_7, x_9 \rangle$ is related to 21 passes (18%). In contrast, $\langle x_7 \rangle$ is related to 124 non-passes (11%), $\langle x_9 \rangle$ is related to 445 passes (42%), while $\langle x_7, x_9 \rangle$ is related to 57 passes (5%). Thus the q-nearness analysis suggests that x_7 and x_9, in combination, have more subtle discriminating power. In other words we should classify by simplices rather than vertices.

3.3.2 Star-Hub Analysis

Given any set of simplices, $\sigma_1, \sigma_2, ..., \sigma_n$, their *hub*, is the largest face of them all. Thus hub$(\sigma_1, \sigma_2, ..., \sigma_n)=$ $\cap_{i=1}^{n} \sigma_i$. In the light of the comment at the last section, we should be seeking those simplices that have a relatively large hub for the 'passing' class, and a relatively small hub for the 'non-passing' class. For our set of eleven features its is possible to examine all of its 128 possible combinations $(4 \times 4 \times 2 \times 2 = 128)$. Table 4 shows a summary of this star-hub analysis.

hub simplex	# pass	%	# non-passes	%
$\langle x_4, x_5, x_9, x_{10}, x_{11} \rangle$	1	1%	57	5%
$\langle x_4, x_6, x_9, x_{10}, x_{11} \rangle$	0	0%	35	3%
...	...	...	...	...
$\langle x_3, x_7, x_9, x_{10}, x_{11} \rangle$	4	3%	7	1%
$\langle x_3, x_8, x_9, x_{10}, x_{11} \rangle$	1	1%	1	0%
...	...	...	...	...
$\langle x_3, x_9, x_{10}, x_{11} \rangle$	7	6%	36	3%
$\langle x_3, x_7, x_9, x_{11} \rangle$	8	7%	13	1%
...	...	...	...	...
$\langle x_4, x_5, x_{10}, x_{11} \rangle$	2	2%	120	11%
$\langle x_5, x_9, x_{10}, x_{11} \rangle$	2	2%	74	7%
...	...	...	...	...
$\langle x_4, x_5, x_{11} \rangle$	6	5%	232	22%
$\langle x_4, x_6, x_9 \rangle$	2	2%	86	8%
$\langle x_5, x_{10}, x_{11} \rangle$	14	12%	157	15%
...	...	...	...	...
$\langle x_7, x_9, x_{11} \rangle$	15	13%	42	4%
$\langle x_3, x_7, x_9 \rangle$	12	10%	16	1%
$\langle x_2, x_5, x_{11} \rangle$	12	10%	23	2%
...	...	...	...	...
$\langle x_9, x_{11}, \rangle$	34	29%	308	29%
$\langle x_4, x_{11} \rangle$	10	8%	344	32%
$\langle x_4, x_5 \rangle$	8	7%	465	44%
...	...	...	...	...
$\langle x_2, x_{11}, \rangle$	30	25%	76	7%
$\langle x_7, x_{11} \rangle$	23	19%	60	6%
$\langle x_7, x_9 \rangle$	21	18%	57	5%
...	...	...	...	...
$\langle x_4 \rangle$	17	14%	734	69%
$\langle x_5 \rangle$	39	33%	572	54%
$\langle x_{11} \rangle$	84	71%	560	53%
...	...	...	...	...
$\langle x_2 \rangle$	45	38%	108	10%
$\langle x_3 \rangle$	44	57%	187	18%
$\langle x_8 \rangle$	20	17%	46	4%

Table 3: A selection of hubs and their frequencies.

Any discussion of Table 3 must be qualified by the observation that the frequencies are small, especially for passes. Nonetheless, distinct patterns emerge. For example, even at the relatively high dimension of $q = 4$, the $\langle x_4, x_5, x_9, x_{10}, x_{11} \rangle$ is associated with 5% of non-passes and almost no passes. At $q = 3$ there is a marked difference for $\langle x_4, x_5, x_{10}, x_{11} \rangle$ between 2% passes and 11% non-passes. At $q = 2$, for example, $\langle x_3, x_7, x_9 \rangle$ accounts for 10% of the passes and just 1% of the non-passes. At $q = 2$ $\langle x_2, x_{11} \rangle$ accounts for 25% of the passes and 7% of the non-passes. At $q = 0$ it can be seen that the vertices alone have considerable discriminating power. For example $\langle x_4 \rangle$ is a strong precursor for a non-pass (14% passes to 69% non-passes, while $\langle x_2 \rangle$ is a strong precursor for a pass (38% passes to 10% non-passes).

4 Discussion

In this paper we have identified passing configurations in robot soccer. When a player makes a pass, they have a choice of ten other members of their team to pass to. Each team member has a structure, relative to the player possessing the ball, determined as combinations of the eleven features (simplices) to characterise the game. In simple systems any one such feature or simplex would be sufficient to classify the configurations as 'pass' or 'non-pass'. In more complicated cases it is not so clear cut. We have shown that particular vertices and simplices may have strong predispositions toward one class or another.

The 'better' the vertices, the stronger will be the discriminating power. It is suggested that 'weak' vertices can be identified by belonging to few 'powerful' simplices, while 'strong' vertices can be identified by belonging to many simplices with strong discrimination between classes. Elsewhere we develop this idea towards a methodology providing heuristics for the inclusion and exclusion of features in the classification of objects determined by relational data [8].

4.1 The dynamic context

In the current context, the classification of the position is intended to underlie the decision as to which team member to pass to. In practice this is only part of the story, since the passing decision may also depend on the current (static) system state being part of a (dynamic) trajectory of states [7]. However, in this context a player may decide that the demands of the trajectory to pass the ball to particular player should be over-ridden by the strong possibility that this could lead to loss of possession given the structural position. In this circumstance the player may abort the previous plan and initiate a new trajectory.

4.2 Learning from observed populations

The examples given here have come from a single game, the 2003 RoboCup Simulation League Final, which 118 pass configurations and 1062 non-pass configurations. As the tables show the frequencies of some configurations are relatively small - probably too small for any reliable generalisation on which to base learning. Although they are outside the scope of this paper, the research prompts the following questions:

Question 1: for any given simplex used to discriminate two classes such as pass/non-pass, what is the minimum number of observations required to make the discrimination 'significant?

Question 2: can the observed frequencies for one game be added to those of another game in a meaningful way for this kind of analysis?

Question 3: can the observed frequencies of one team be added to those of another team in a meaningful way for this kind of analysis?

Question 4: what is the impact of adding features on generalisation - does combinatorial explosion reduce the frequencies to statistically insignificant levels?

These issues are studied by Iravani [8]. There he reports that the patterns observed here persist for the same team in different games, and between different teams. This suggests that data from many games can be combined to give much larger sample sizes as a more robust basis for machine learning.

Iravani also addresses the issue of machines learning over time, and even changing their tactics based on experience. For example, a particular configuration may give a good outcome initially, but then given a bad outcome when another team invokes a new strategy. In such circumstances the frequencies associated with the particular simplex(es) will 'drift' from pass to non-pass, or *vice-versa*, and the robot's behaviour will change as it learns and adapts.

References

[1] P. Iravani, 'Behaviour-based architecture for abstract control and learning', *Proc. TAROS*, 2004

[2] P. Iravani, Johnson, J.H., Rapanotti, L., 'Applications of concept grounding techniques to reduce the dimensionality in sensorory-motor space', STAIRS, 2004

[3] Atkin, R.H., *Multidimensional Man*, Penguin (Harmondsworth), 1981.

[4] Johnson, J.H., 'Some structures and notation of Q-analysis', *Environment and Planning B*, **8**, 73-86, 1981.

[5] Gordon, A. D., *Classification*, Chapman & Hall, 1999.

[6] Johnson, J., H., 'Stars, Maximal Rectangles, and Lattice: a new persepctive on Q-analysis', *International Journal of Man-Machine Studies*, **24**, 293-299, 1986.

[7] Johnson, J. H., 'Visual communication in swarms of intelligent robot agents', *Artifical Life and Robotics*, **5**, 1-9, 2001.

[8] P. Iravani, 'An architecture for multilevel learning and robotic control base on concept generation', Ph.D. Thesis, The Open University, 2004.

The Tenth International Symposium on Artificial Life and Robotics 2005(AROB 10th '05),
B-con Plaza, Beppu, Oita, Japan, February 4-6, 2005

Cooperative Behavior Acquisition for Multiple Autonomous Mobile Robots

Koji Nakano*

Masanao Obayashi**

Kunikazu Kobayashi**

Takashi Kuremoto**

* Graduate School of Science and Engineering
Yamaguchi University
2-16-1 Tokiwadai Ube, Yamaguchi 755-8611 Japan

** Faculty of Engineering
Yamaguchi University
2-16-1 Tokiwadai Ube, Yamaguchi 755-8611 Japan

Abstract

This paper proposes a method for multiple autonomous mobile robots to acquire cooperative behaviors through a garbage-collection problem. In the proposed method, robots select the most available target garbage for cooperative behaviors by visual information in unknown environments, and move to the target avoiding obstacles. The learning system in the robot uses Profit sharing (PS), which is one of the reinforcement learning, and the feature of this method is using two kinds of PS-tables. The one is to learn cooperative behaviors using information of other robot's positions, the other is to learn how to control movements. This paper demonstrates effectiveness of the proposed method through simulation and real experiments.

1. Introduction

Recently, many researches on solving problems cooperatively with plural agents have been studied enthusiastically. Specially, a research field that agents get cooperative behavior through reinforcement learning in a dynamic environment has gotten a lot of attention.

Reinforcement learning is a method that agents will acquire the optimum behavior by trial and error by being given rewards in an environment as a compensation for its behaviors. Most of studies on reinforcement learning have been done for a single agent learning in a static environment. Q-learning which is a typical learning method is proved that it converges to an optimum solution for Markov Decision Process (MDP). However, in a multiagent environment, as plural agents' behavior may effect state transition, the environment is considered as non Markov Decision Process (non-MDP), and we must face critical problems whether it is possible to solve.

In such situation, Arai et al.[1] evaluated both Q-learning and PS for the pursuit problem which is one of the multiagent tasks, and suggested that PS is suited to a multiagent environment more than Q-learning.

In this paper, we propose a learning method for a multiagent environment based on PS. And the feature of this method is using two kinds of PS-tables. The one is to learn cooperative behaviors using information of other agent's position and present state, the other is to learn how to control own basic behavior like movements.

We apply the proposed method to garbage collection problem which is one of the multiagent tasks, and demonstrate effectiveness of the proposed method through computer simulation and real experiment.

2. Reinforcement Learning

Reinforcement learning is to learn what to do (how to map situations to actions) so as to maximize a numerical reward signal [2].

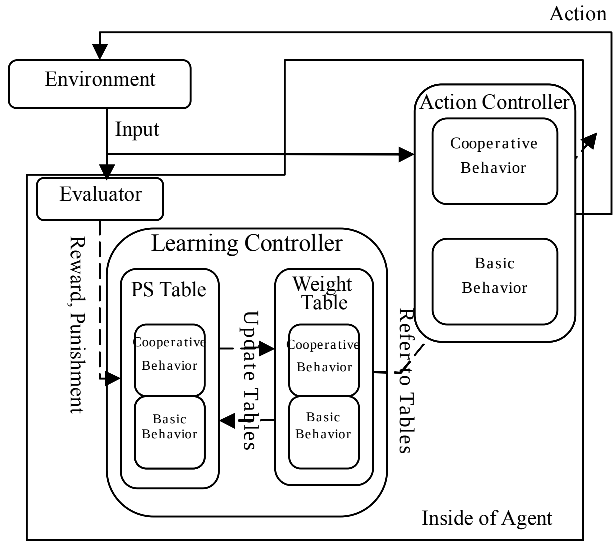

Figure 1. System architecture.

Profit sharing (PS) is one of the learning methods. PS defines a pair of state s and action a as a rule. Rules are stored in PS table each step, and when a learner achieves a goal PS reinforces weight w(s,a) based on PS table. W(s,a) is updated with equation (1).

$$w(s_t, a_t) \leftarrow w(s_t, a_t) + f(t, r) \qquad (1)$$

w(s,a) : weight of rule (s,a)
f : reinforcement function
t : time , r : reward

3. Proposed System

3.1 System architecture

Figure 1 shows proposed system architecture. The system is composed of three parts; action controller, learning controller and evaluator. The feature of the system is to divide behavior of agent into cooperative and basic behavior to learn separately. The learning of cooperative behavior is using information of the other agent's position and present state. The learning of basic behavior is to learn how to control own basic behavior like movements. In a general learning method, when an agent acquires a reward it can hardly estimates own action whether it can cooperate or not. To solve this problem, the proposed system divides the learning into two kinds of behavior, and each behavior is evaluated using different criteria.

3.2 Action controller

The agent controls its action based on w(s,a). It selects an action using following Boltzmann distribution which is one of the probability action selections (equation (2)).

$$p(a \mid s) = \frac{e^{w(s,a)/T}}{\sum_{a_i \in A} e^{w(s,a_i)/T}} \qquad (2)$$

p(a|s) : probability of a on s
T : temperature parameter
A : set of all actions

3.3 Learning controller

The agent learns using PS (as shown in Section 2.1). The parameter w(s,a) is updated by equation (3) and the reinforcement function uses geometric decreasing function.

$$w(s_t, a_t) \leftarrow w(s_t, a_t) + r \cdot \gamma^t \qquad (3)$$

γ : rate of attenuation

3.4 Evaluator

The behavior of the agent is evaluated using next state s'. The evaluation of behavior is similarly established by two criteria.

4. Experiment

We apply the proposed method to garbage collection problem which is one of the multiagent tasks. There are plural agents, garbage and one trash can in the environment, and agents collect garbage and take it to the trash can. Agents learn cooperative behavior and basic behavior by themselves.

4.1 Computer Simulation

Figure 2 illustrates the simulation environment which field size is 21x21 and there are 10 garbage, 2 agents and a trash can on the field. One trial is defined as until all garbage are collected, and 100 trials are considered as 1 episode. We calculate the

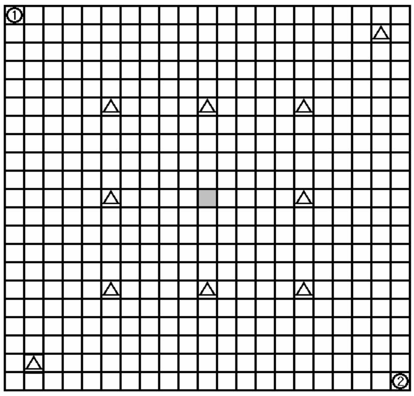

①,② : agent
△ : garbage
■ : trash can

Figure 2. Initial positions of agents, garbage, and trash can.

Table 1. The average number of steps to the goal one agent can observe the other or not.

	agent can observe	agent cannot observe
conventional method	118.7	111.1
proposed method	113.3	123.8

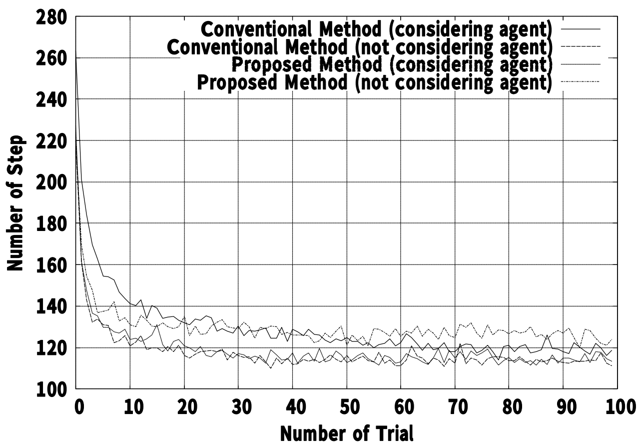

Figure 3. Change of the number of steps.

number of average steps after repeating 100 episodes. At this time, w(s,a) are initialized for each episodes. To verify the effectiveness of the proposed method, we compare the proposed method with the conventional method which also learns using a PStable.

Figure 3 and Table 1 show the result of the

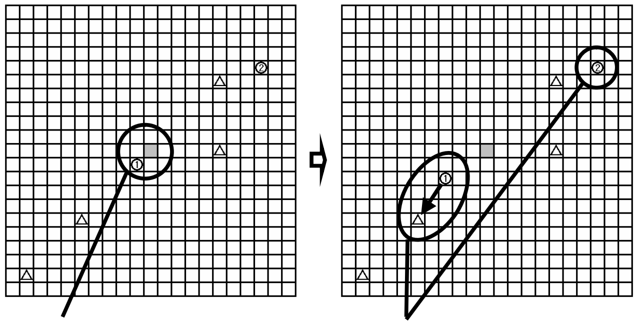

(a)Agent 1 arrives at the trash can.

(b)Agent 1 goes to garbage opposite to agent 2

△ : garbage
①、② : agent
■ : trash can

Figure 4. Cooperative behavior acquired by the experiment with observing the other agent.

experiment. In the case that one agent can observe the other, the agent using the proposed method learns faster than the agent using conventional method. However, when the agent is compared with the agent which is using the conventional method and do not observe the other agent, the performance of the proposed agent is similar to that of the conventional agent.

Figure 4 illustrates a cooperative behavior observed in the experiment in which agent observes the other one. After agent 1 took garbage to the trash can (Figure 4 (a)), it do not select the garbage near agent 2 as the object, but another one opposite to agent 2 (Figure 4 (b)). Such behavior often occurred after learning with observing the other agents.

4.2 Real Experiment

Figure 5 illustrates the field of the experiment which field size is 1x1(m) large and has 5 garbage, 2 robots and a trash can. We try following three kinds of the experiments.

Exp 1: Using weights which are learned in the computer simulations repeating for 10 trials in Figure 5(a)

Exp 2: Using weights which are learned in the real experiments repeating for 10 trials in Figure 5(a)

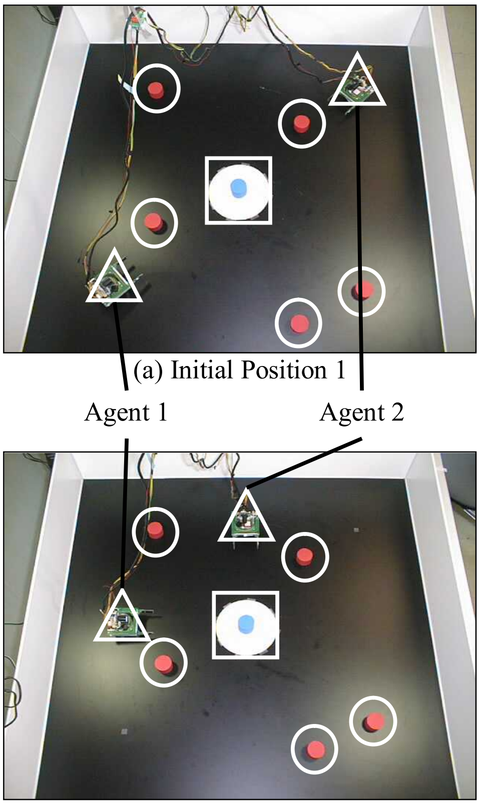

(a) Initial Position 1

(b) Initial Position 2

△ : robot
○ : garbage
□ : trash can

Figure 5. Initial positions of robots, garbage, and trash can.

Table 2. The number of average steps to garbage collection in the experiment 1-3.

	Number of average steps
Exp 1	201.9
Exp 2	178.2
Exp 3	161.1

Exp 3: Using weights which are the same as Exp 2 repeating for 10 trials in Figure 5(b)

Table 2 illustrates the result of the experiment. Table 2 illustrates that the number of average steps of Exp 2 is decreased compared with Exp 1. Thus the weights learned in computer simulation are available for the real environment, and furthermore, the proposed method can learn flexibly in real environment. On the other hand, the number of average steps in Exp 3 is not increased compared with Exp 2. Thus the weights learned in real environment are applicable to different environments, and this shows that the proposed system is robust.

5. Conclusion

In this paper, we proposed the method which separates the learning of the cooperative behavior and the learning of the basic behavior for a multiagent environment. We demonstrated availability of the method through computer simulation and real experiment, and confirmed that the agents learned quickly and behaved cooperatively.

However, there are two problems in the proposed method. The first is that most of cooperative behaviors are emerged by agents acting basic behaviors each other, so it is difficult to separate the learning of the cooperative behavior and the learning of the basic behavior in other multiagent tasks. Therefore, to apply the proposed method to many multiagent tasks, it should be generalized more. The second is that separating two ways of learning may restrict emergences of cooperative behavior. The cooperative behavior should be emerged fundamentally. Therefore we should establish the framework of the learning of the cooperative behavior not restricting emergences of the cooperative behavior.

References

[1] S. Arai, K. Miyazaki, S. Kobayashi: Methodology in Multi-Agent Reinforcement Learning -Approaches by Q-Learning and Profit Sharing-, Artificial intelligence, Vo.13, No.4, pp.609-618, 1998 (in Japanese)

[2] Richard S. Sutton, Andrew G. Barto: Reinforcement Learning An Introduction, MIT Press, 1998

Multi-agent Learning Mechanism Based on Diversity of Rules : from the Viewpoint of LCS *

Hiroyasu Inoue*† Yutaka Leon Suematsu*† Keiki Takadama†‡
Katsunori Shimohara*† Osamu Katai*

* Kyoto University Graduate School of Informatics, Yoshida Honmachi, Sakyo-ku, Kyoto 606-8501 Japan
† ATR Network Informatics Laboratories 2-2 Hikaridai, Keihanna Science City, Kyoto 619-0288 Japan
‡ Tokyo Institute of Technology 4259 Nagatsuta-cho, Midori-ku, Kanagawa 226-8502 Japan
E-mail: hir_inoue@atr.jp

Abstract

Multi-agent learning requires effective means because of its vast learning space. One means is that agents share their knowledge. However, thoughtless knowlege sharing can disturb its learning process. In this paper, we investigate the relatioship between the effect of knowledge sharing and information on other agents' positions.

We proposed a novel rule-sharing mechnism employing LCS. Through experiments using simplified soccer, we demonstrated that if agents can find other agents, sharing rules is effective; if not, then sharing rules is ineffective.

Keywords: multi-agent, learning, rule sharing, learning classifier system

1 Introduction

Arai [1] and others have shown that multi-agent learning includes many difficulties. Those problems include the simultaneous learning problem, the reward-assignment problem, and so on. Another problem is that even if a single agent has a small learning space, the whole learning space is enormous because of the number of possible combinations. Thus, a more effective method is required for multi-agent learning. One means of this is that agents share their knowledge.

Generally, it seems that two conditions should be fulfilled to achieve knowledge sharing. The first is that representation of knowledge is sharable, while the second condition is that imported knowledge from other agents can be interpreted. One approach that fulfills these conditions is that agents have the same mechanical functions so as to interprete knowledge from each other, and to employ a rule-based system for importing and exporting their knowledge. Though such agents can share knowledge, thoughtless knowlege sharing can disturb the learning process, since knowledge sharing homogenizes agents' knowledge. Inoue [2] showed that the effect of knowledge diversity has a relationship with position information on other agents. This paper focuses on this problem.

In this paper, we investigate the relationship between the effect of knowledge sharing and information on other agents' positions.

This paper is organized as follows. Section 2 starts with a description of the rule-sharing mechanism. Section 3 explains the experimental settings, and Section 4 provides the results. Section 5 we discuss the results, and conclude in Section 6.

2 Rule-Sharing Mechanism

There are various possible mechanisms for sharing rules. For the purpose of this paper, we should consider a general mechanism. An inevitable aspect of the general mechanism is sharing priorities of rules. In accordance with this, in this section we propose a novel mechanism based on the Learning Classifier System (LCS: proposed by Holland [4]).

LCS is a general learning system in which a set of condition-action rules called classifiers compete to control a target system, gaining reward from the environment. We employ ZCS (Zeroth level Classifier System) proposed by Wilson [5], which has no message list, and propose the Rule-Sharing Learning Classifier System (RS-LCS), extending ZCS to share rules between agents.

RS-LCS has the following differences to ZCS: (1) RS-LCS does not use GA because the effectiveness of GA is ambiguous and still under discussion. Also, RS-LCS does not use #. # is used to condition parts of rules and matches any condition. # does not work

*This research was conducted as part of 'Research on Human Communication' with funding from the National Institute of Information and Communications Technology.

effectively without GA. (2) The covering process in RS-LCS creates rules so that all kinds of actions can be chosen. (3) RS-LCS does not use the roullette selection process. Twenty percent of all actions are random, while the rest are chosen from the rule that matches conditions and has the highest priority. (4) RS-LCS does not use a bucket brigade process; instead it uses a profit-sharing process proposed by Grefenstette [6] because the profit-sharing process fits multi-agent learning. We employ Miyazaki's profit-sharing process [7], and its decreasing ratio is 0.9.

LCS, including ZCS, is basically a mechanism for single agents. Hence, RS-LCS should include an extension for rule sharing. This paper has the assumption that agents simultaneously acquire a reward from the environment. Based on this, agents share their rules every ten reward events. In the rule-sharing process, all of the agents' rules are merged, an if any of those rules have the same condition parts and action parts, their strengths are averaged. The merged rules are then returned to each agent.

3 Experimental Setting

3.1 Simplified Soccer

We employ simplified soccer as an example. The following is a discription.

Figure 1 shows the landscape of simplified soccer. (The meaning of dotted lines is described in the following section.) The field has 8×30 squares, and there are two teams, a left team and a right team, and a ball. Each team has three agents. The vertical line on the right side is the left team's goal, and vice versa.

At every step, all agents move simultaneously, to the left, right, above, or below squares. Agents can also stay in the same squares, and the agents and the ball can freely move into the same square. If at least one agent moves into the same square as the ball, the ball is moved (kicked). If more than two agents move into the same square, one agent is selected randomly, and the ball is moved. If the left team's agent moves the ball, the ball moves 12 squares to the right, and also moves vertically and horizontally by less than two squares. This is also applied to the right team, but the direction of movement is left. If the ball goes over the left goal, the left team gets a goal, and vice versa. If the ball goes over the horizontal lines, it goes back to within the range of the horizontal lines.

At the beginning of experiments, or after a goal, positions of the agents and the ball are reset. The ball is set randomly from a choice four squares in the center of the field. The left agents are set to the left half of the field randomly, and the right agents are also set in the same way.

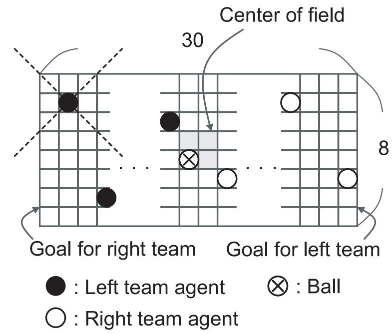

Figure 1: Simplified Soccer

Each right agent has a greedy mechanism, which always makes an agent chase the ball. Through all experiments, the right agents' mechanism is the greedy mechanism. On the other hand, left agents have RS-LCS implemented. By fixing the right agents, performance comparisons with the left agents are possible.

The greedy mechanism does not need any additional description. To use RS-LCS, however, sensor description is necessary, which is provided in the following section.

3.2 Left Agent Sensor

In Section 2, the substance of the sensor was not mentioned. In fact, the sensor includes six bits in total.

The first four bits are assigned to information on positions of other agents in the left team [1]. The dotted lines in Fig. 1 are two imaginary lines for an agent. Based on those two lines, the field is divided into four areas. The squares on the border are included in the right area, or left area, and the square in which the agent sits is included in the right area. If at least one other of the left agents is found in an area, the bit for that area is set to 1, if not, it is set to 0.

Next, three bits are assigned to directions of the ball. If the ball is in the right area, 000 is set. (The distance is not considered.) In the same way, left, above, below are set to 001, 010, 011, respectively. The remaining areas, upper-right, upper-left, lower-right, and lower-left, are set to 100, 101, 110 ,111.

The last one bit is assigned to the distance of the ball. The horizontal difference of position between the agent and the ball is calculated and its absolute value is taken. If the sum of the horizontal value and the

[1] Position information of right team's agents can be included. But because of large learning space experiments are difficult to conduct. Hence this information is omitted here.

vertical one is larger than 10, the bit is set to 0. If not, it is set to 1.

3.3 Reward Assignment

As we mentioned in Section 1, the reward-assignment problem for multi-agent is still being discussed. Hence we describe a specific method of reward assignment for the simplified soccer problem, because the validity of reward assignment cannot be discussed.

To assign a reward, an episode of moving the ball is recorded. This episode records a left agent moving the ball every step. If no left agent moves the ball, that is also recorded. When the left team scores a goal, left agents obtain a reward. The last agent that moved the ball gets a 1.0 reward. After that the episode is traced back, and at every one step the reward is multiplied by 0.9. If a record of an agent is found, the reward is given at that step. However if the agent has already received a reward, the reward is not given. After tracing back the episode, the agents which did not receive a reward get a 0.0 reward, and the episode is cleared.

If the right team scores a goal, all left agents get 0.0 reward. The episode is then cleared.

3.4 Experimental Combinations

The purpose of this paper is to verify whether or not sharing rules is always effective. Therefore we conduct the following experiments. (1) Left agents cannot find other teammates, and cannot share their rules. (2) Left agents cannot find other teammates, and can share their rules. (3) Left agents can find other teammates, and cannot share their rules. (4) Left agents can find other teammates, and can share their rules.

4 Results

Figure 2 shows the two experimental results. The vertical axis represents the number of goals every 2,000 steps, and the horizontal axis representss the steps. Both results are the average of ten trials. In both experiments, agents cannot find other teammates. In one experiment, agents can not share their rules, whereas in the other, they can. At the start, the number of no share agents' goals is smaller than that of share agents' goals. At the end, however, no share agents overtake share agents.

Figure 3 shows the two other experimental results. The axes of Figure 3 are identical to those in Fig. 2. In both experiments, agents could find other teammates. At the start, the number of share agents' goals is larger

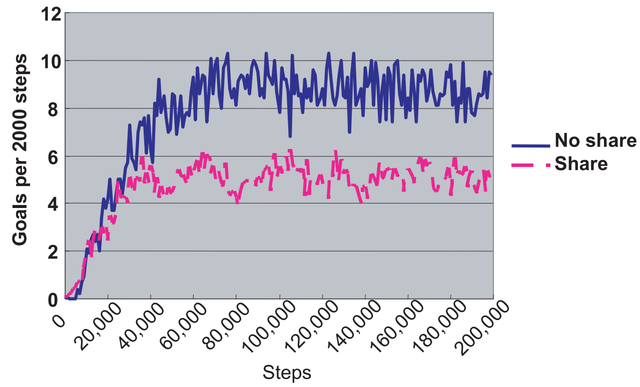

Figure 2: Result (Agents cannot find other teammates)

than that of no share agents' goals, but the number of finite goals is similar between two agents.

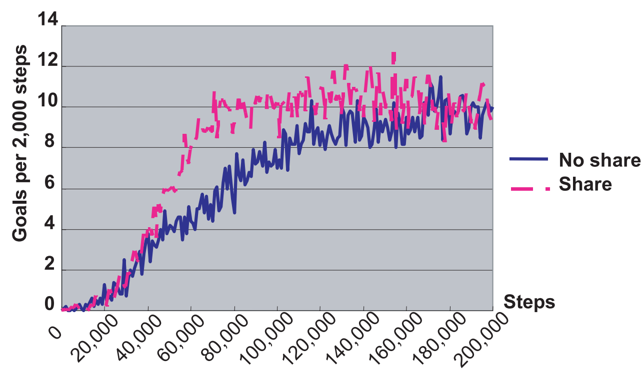

Figure 3: Result (Agents can find other teammates)

5 Discussion

5.1 Construction on Results

If left agents take the same greedy strategies as right agents, the performance should be identical between them. The performance, however, is not identical: the left agents are superior to the right agents. (Because of space restrictions, the right agents' results can not be included.) This is because each left agent performs different roles, which enables them to pass the ball to each other so as to outwit right agents. The important point is the method of performing those roles. The difference between Fig. 2 and 3 can be analyzed in light of this point.

In these experiments, role assignments are similar to positioning. That is, left agents try to take their appropriate posiions. If left agents cannot find other teammates (Fig. 2), each agent has to take a specific position; otherwise they may conflict in their positions. This specialty can only be realized by the difference of rules. Hence, if agents share their rules, that specialization collapses, and the performance deteriorates.

If left agents can find other teammates (Fig. 3), none of the agents have to take a specific position because they can arrange their positions dynamically. Thus even if agents share their rules, the performance does not deteriorate.

Sharing rules makes agents homogeneous, and vice versa. As we mentioned in Section 1, there are concerns with the results. This is because heterogeneity between agents is necessary when agents cannot find other agents, as Inoue [2] demonstrated.

From the above discussions, we could show the relationship between the effect of sharing rules and information of other agents' positions. Especially, if agents can find other agents, rule sharing is effective. If not, rule sharing is not effective.

5.2 Open Problems

This research has only just started. Therefore, many open problems still remain, as the described bellow.

5.2.1 Constraints of Problems

In this paper, agents do not communicate with each other. It should be investigated as to whether the finding of this paper is still valid, if agents do communicate with each other.

Rule-sharing has a cost, which is not discussed in this paper. Not only the ability to find other agents, but also the cost should be taken into account.

5.2.2 Rule-Sharing Mechanism

A rule-sharing mechanism has many parameters. For example, the number of rules for sharing, the timing of rule sharing, and so on. The sensitivities of these parameters need to be investigated.

This paper's rule-sharing mechanism has all agents merge their rules. However, there are various kinds of merger. For example, specific two agents always merge their rules.

Another important open problem is the contradiction of rules between agents. There are some solutions to this problem proposed by Inoue [8], but these are not insufficient.

Although this paper's rule-sharing mechanism has agents merge their rules, agents do not necessarily merge their knowledge. One such mechanism has been proposed by Inoue [9]. In that mechanism, agents retain other agents' rules as different rule sets and exploit them according to the situation the agent faces.

6 Conclusion

Multi-agent learning requires effective means because of its vast learning space. One means is that agents share their knowledge. We proposed a novel rule-sharing mechnism employing LCS. Through experiments using simplified soccer, we demonstrated the relationship between the effect of sharing rules and information of other agents' positions. In particular, if agents can find other agents, sharing rules is effective. If not, it is not effective.

References

[1] Arai S (2001), Multiagent reinforcement learning frameworks: Steps toward practical use (in Japanese). *Journal of Artificial Intelligence* 16(4):476-481

[2] Inoue H, Takadama K, Shimohara K, et al. (2003), Exploring Conditions of Heterogeneous Knowledge for Effective Multi-agent Systems (in Japanese). *The Second Joint Agent Workshops and Symposium*, 208-215

[3] Takadama K, Hajiri K, Nomura T, et al. (1998), Organizational Learning Model for Adaptive Collective Behaviors in Multiple Robots. *Advanced Robotics (The International Journal of the Robotics Society of Japan)*, 12(3):243-269

[4] Holland H (1985), Properties of the Bucket Brigade Algorithm. *The 1st International Conference on Genetic Algorithms* 1-7

[5] Wilson S (1994), ZCS: A Zeroth Level Classifier System. *Evolutionaly Computation* 2(1):1-18

[6] Grefenstette J.J. (1988), Credit assignment in rule discovery systems based on genetic algorithms. *Machine Learning*, 3:225-245

[7] Miyazaki K, Arai S, Kobayashi S (1999), A theory of profit sharing in multi-agent reinforcement learning (in Japanese). *Journal of Artificial Intelliegence*, 14(6):1156-1164

[8] Inoue H, Takadama K, Shimohara K, et al. (2002), Learning Classifier System Enabling Adaptation to Mixed Known Environments (in Japanese). *The Journal of Three Dimensional Images*, 208-213

[9] Inoue H, Takadama K, Shimohara K, et al. (2000), Agent Architecture Based on Self-Reflection Learning Classifier System. *The 5th International Symposium on Artificial Life and Robotics*, 454-457

The Tenth International Symposium on Artificial Life and Robotics 2005(AROB 10th '05),
B-con Plaza, Beppu, Oita, Japan, February 4-6, 2005

Gradual emergence of communication in a multi-agent environment

Shinjiro Tensho*, Satoshi Maekawa†, Junichiro Yoshimoto*,‡, Tomohiro Shibata* and Shin Ishii*
*Nara Institute of Science and Technology, 8916-5 Takayama, Ikoma, Nara, 630-0192 JAPAN
†National Institute of Information and Communications Technology, 3-5 Hikaridai Seika, Soraku, Kyoto, 619-0289 JAPAN
‡Initial Research Project, Okinawa Institute of Science and Technology, 12-22 Suzaki, Gushikawa, Okinawa, 904-2234 JAPAN
E-mail: shinji-t@is.naist.jp

Abstract

Communication is one of the most important keys for agents in a multi-agent environment to find global or semi-optimum policies. It has been attracting not only biologists but also engineers to make communication emerged in compliance with a given problem. Such emergence, however, is very difficult to realize from the computational viewpoint because it requires both sender and receiver agents to acquire the corresponding functions for communication individually but concurrently; such an emergent system tends to be evolutionally unstable. This article presents a new mechanism for emergent communication in a competitive multi-agent system. The key point of our mechanism is to introduce an environmental event (or factor) that agents have to learn to cope with. The acquired function for the environmental factor, then, drives the emergence of communication. Simulation results show that our approach allows gradual emergence of communication, which makes the agents to acquire higher fitness as compared with the case without communication.

keywords: communication, competitive environment, gradual emergence, reinforcement learning, evolution

1 Introduction

In recent years, studies of communication in multi-agent systems have been popular because they are important especially when dealing with large-scale problems that are intractable by single-agent approaches; potential targets are rescue robot systems and Robocup soccer systems for example.

In the engineering field, primitive functions of communication, such as protocol and encoding/decoding schemes, are often manually designed and built into agents. This approach may be effective in a completely specified and stationary domain, but would not be able to cope with partially known and/or non-stationary problems. An adaptive mechanism to emerge communication has possibility to avoid this defect.

In this article, we define that "communication" between agent A and agent B is to maximize acquired reward or to minimize suffered risk when agent A takes an action a_a then agent B takes an action a_b in response to the agent A's action. We call action a_a and a_b "communicative action" for agent A and agent B, respectively.

It is generally difficult to emerge communication concurrently in a multi-agent environment because a communicative action often costs. In addition, it is not guaranteed that the optimality of communication between two agents is generalized in a multi-agent environment, in which various interactions among agents affect each other and make the problem ill-conditioned [1].

This article presents a new mechanism to acquire communication emergently in a multi-agent competitive environment. The key point is to introduce time-invariant danger as an environmental event (or factor) that agents have to learn to cope with. The acquired function for the environmental factor, then, drives the emergence of communication making agents to acquire higher fitness than in the case without communication.

2 Setup

2.1 Agent's model

Figure 1 shows the agent's model used in this article. Each agent can observe four types of information at an arbitrary time step: 1) whether a big sound exists in the environment, 2) whether the agent faces another agent, 3) whether the agent is faced with resources, and 4) whether the agent occupies any resources in his hand. These sensory inputs are denoted by binary variables $s_i \in \{0,1\}$, where $s_i = 0$ ($s_i = 1$) indicates that

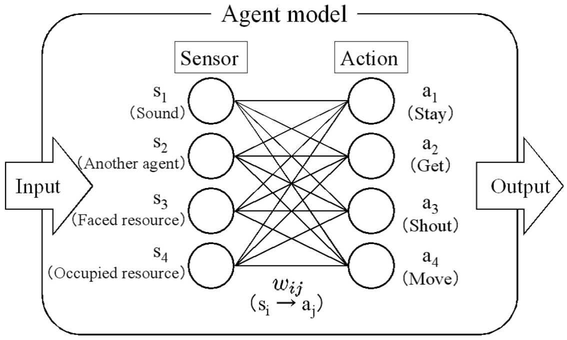

Figure 1: Agent model

the i-th information is true (false). For example, $s_1 = 1$ if the agent hears a big sound, and $s_4 = 0$ if the agent does not occupy any resource. After obtaining sensory inputs $S \equiv (s_1, \ldots, s_4)$, the agent takes one of four actions: 1) "*Stay*", 2) "*Get*", 3) "*Shout*" and 4) "*Move*". Here, "*Stay*" and "*Get*" are to keep the current situation and to pick up resources in front of it, respectively. "*Shout*" and "*Move*" are to raise a loud cry and to run away from the situation, respectively. Let a_i be the i-th action, e.g., a_1 indicates "*Stay*". Which action the agent takes for given sensory inputs is stochastic and the probability of a_i, π_j, is given by

$$\pi_j = \frac{e^{u_j}}{\sum_k e^{u_k}} \tag{1}$$

$$u_j = \sum_{i=1}^{4} w_{ij} s_i, \tag{2}$$

where $w_{ij} (i, j = 1, \ldots, 4)$ are connection weights that specify agent's behaviors.

Getting a resource increases agent's fitness to the environment. If an agent successfully obtains resources whose amount is denoted by r_t at time step t, the fitness f is increased by

$$f := f + r_t. \tag{3}$$

The aim of each agent is to maximize the fitness in its lifetime.

The colony of agents has two types of adaptation mechanism with different time scale [2]. One is the individual learning of connection weights based on the actor-critic method [3], and another is evolution. The learning process at time step t is as follows:

1. **Calculating TD-error** δ

$$\delta := r_t + \gamma V(S_t) - V(S_{t-1}) \tag{4}$$

where S_t denotes a sensory input at time step t and $V(S)$ is a value function for state S. $\gamma \in (0, 1)$ is a discount rate.

2. **Updating the value function** $V(S)$

$$V(S_{t-1}) := V(S_{t-1}) + \alpha\delta \tag{5}$$

where $\alpha \in (0, 1)$ is the learning rate.

3. **Updating connection weight** w_{ij}

$$w_{ij} := w_{ij} + \beta\delta s_i \tag{6}$$

where $\beta \in (0, 1)$ is a step size parameter.

After agents live fixed time steps, they move to the next generation. At the beginning of the new generation, N agents with the highest fitness at the end of the previous generation are duplicated whereas N agents with the lowest fitness are deleted. Accordingly, the population size in generations are fixed. To keep the diversity in agents, the non-deleted agents at the T-th generation are initialized as follows:

1. **Initializing fitness** f

$$f := 0 \tag{7}$$

2. **Initializing value function** $V(S)$

$$V(S) := 0, \quad \text{for all } S. \tag{8}$$

3. **Inheritance of the initial connection weight** w_{ij}

$$w^0_{ij}(T) = w^0_{ij}(T-1) + \epsilon, \tag{9}$$

where $w^0_{ij}(T)$ denotes the initial connection weight at the T-th generation. ϵ is a Gaussian noise.

4. **Initializing the initial connection**

$$w_{ij} = w^0_{ij}(T) \tag{10}$$

This genetic procedure called "Darwinism" [4] is the other type of adaptation, for the agents' colony, in our model.

2.2 Environment

We consider a multi-agent environment where all agents have an identical model explained in the previous subsection. Resources are distributed in the environment. If an agent takes a "*Stay*" action, nothing occurs and the fitness does not change. If an agent takes a "*Move*" action, the agent discards R_i resources in his hand and runs away to another situation. This results in decreasing the fitness by R_i. If an agent takes a "*Shout*" action, the fitness decreases by c_v because the action is assumed to require resources of c_v. If an agent takes "*Get*" when facing free resources, the agent gets them and the fitness increases by R. If an agent takes "*Get*" when facing another agent that holds resources, a fight between these agents occurs and the former agent steals R resources from the latter agent. Since the fight costs d resources, the fitness of the former agent (the latter agent) increases by $R-d$ $(-R-d)$. The immediate reward r_t at time step t corresponds to the increase or decrease in the fitness. If an agent takes "*Get*" when facing another agent that does not hold resources, a fight between these agents occurs but nobody wins. Since the fight costs d resources, the fitness of each agent just decreases by $-d$.

The objective of each agent is to maximize the fitness in its lifetime. If we assume that agents are able to know every information of the environment, it is easy to achieve their objective. Since our agent's sensors are not able to distinguish whether resources are free or occupied by another agent, however, an agent without any additional information may suffer from getting into fights by trying to acquire resources in front of it. Communication is one possible way to produce such additional information and hence to increase fitness by avoiding fights.

2.3 Mechanism

In our mechanism, the existence of dangers is the key to emerge communication, although the avoidance of the dangers are not directly related to communication. The dangers are distributed in the environment, and accompanied by a loud sound. Each agent probabilistically encounters a danger.

If an agent encounters a danger and does not avoid it, the agent suffers from big damage more than the reward through a fight between agents. Unless an agent acts "*Move*" when being faced with a danger, it receives a negative reward of $-d_d$ and the fitness decreases by $-d_d$. In this way, the sense of a danger naturally drives agents to associate it with running away as a policy. Note that an agent cannot recognize a danger directly, but a loud sound is an indirect signal associated with a danger. Thus, it is expected that all agents acquire the same policy for the case when they meet a danger.

Based on the above mechanism, in a competitive environment, if an agent is able to express the sense of a danger against other agents, it can avoid fighting and keep the current resources without any risk. Therefore, an action "*Shout*" emitted to another agent holding resources encourages the agent to take "*Move*", which is a communicative action.

Note that it is not natural or easy for the agents to acquire such a peaceful policy since expressing the sense of a danger is accompanied by paying a cost. For example, in a competitive situation, if an opponent agent has not acquired a policy to avoid a danger, a fight may occur even when the agent produces a loud sound like the big sound representing a danger. At this time, the opponent agent cannot distinguish resources occupied by the agent from those existing freely in the environment, which will not make the opponent agent to take a "*Move*" action. A risk of the agent is increased in this situation, therefore, the policy "*Shout*" is difficult to be acquired.

3 Simulation Results

We conducted simulation studies. Our setup includes a few symbols each of which has no meaning before learning. Table 1 presents parameters and their values used in simulations.

Table 1: Parameters

Number of agents	100
Transition probability $P_i(i = 1...4)$ with the danger (none, danger, agent, resource) without the danger (none, danger, agent, resource)	 (0.55,0.05,0.2,0.2) (0.6,0,0.2,0.2)
Time step per generation, t_{max}	100
Generation step, T_{max}	500
Sensor dimensionality, S_t	4
Action simensionality, A_t	4
Cost for making a sound, c_v	0.1
Damage by a danger, d_d	20
Damage by a fight, d	5
Resource in environment, R	5
Occupied resource, R_i	consumption 1 per a time step
Learning rate, α	0.9
Discounted rate, γ	0.9
Step size parameter, β	0.5
Number of breeding(dying) per generation	5
Gaussian noise, ϵ	N(0, 0.01)

Figure 2 shows the time course of fitness summed over all agents in each generation. Figure 3 shows histograms of actions selected at states during learning in an environment in which dangers exist, while Figure 4 shows histograms of actions selected at states during learning without dangers. As shown in Figure 3, communication emerged so that useless fighting that makes each agent's fitness to decrease were avoided. Hence, the sum of acquired fitness in each generation was larger in the environment with dangers than in that without dangers. Without dangers, we observed that the agents either ran away from their opponent or fought with it depending on their states including the past experiences.

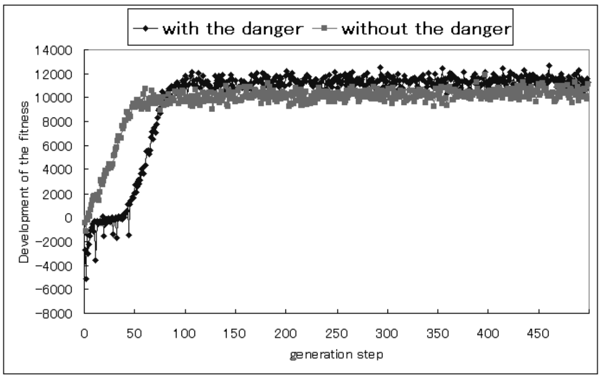

Figure 2: Development of the fitness

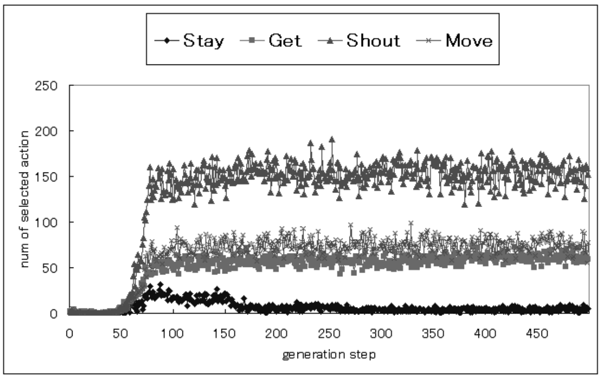

Figure 3: Development of actions by agents in an environment with dangers

4 Conclusion

We have demonstrated that the existence of dangers in the environment encourages the agents to develop communication appropriate for acquiring higher fitness by avoiding useless fights.

In a scientific view, it is believed that every organism have evolved the way "to use what can be used" in the history of living. All the symbols might be meaningless originally, but gradual assignment of meanings profitable for adapting to the environment makes the agents to utilize them; this would be the emergence of communication. The result shown in this article can be regarded as an example of such emergence process of communication.

In the future, we will try to examine the essence of communication such to increase communicative symbols of agents.

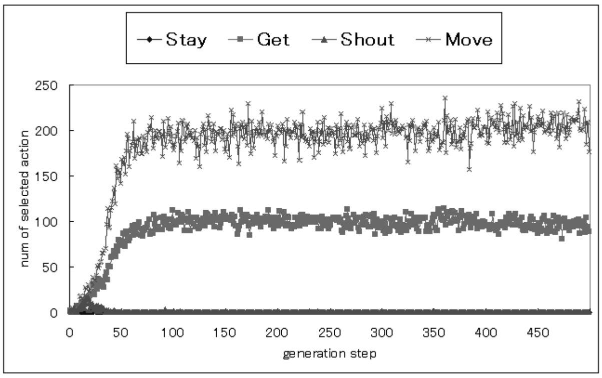

Figure 4: Development of actions by agents in an environment without dangers

References

[1] B.MacLennan: Synthetic Ethology -An Approach to the Study of Communication-, Artificial Life II, pp.631-658, 1991

[2] D.Ackley and M.Littman: Interaction Between Learning and Evolution, Artificial Life II, pp.487-509, 1991

[3] R.S.Sutton and A.G.Barto: "Reinforcement Learning : An Introduction", MIT Press, Cambridge, MA, 1998

[4] T.Sasaki and M.Tokoro: Adaptation of Evolutionary Agents towards the Dynamic Environment, Computer Software, Vol.14, No.4, pp.33-46, 1997

The Tenth International Symposium on Artificial Life and Robotics 2005(AROB 10th '05),
B-con Plaza, Beppu, Oita, Japan, February 4-6, 2005

Nanoparticles as biosensors components - a brief review

Tomasz Kubik† Masanori Sugisaka*

† Institute of Cybernetics Engineering, Wrocław University of Technology,
Janiszewskiego 11/17, Wrocław 50-372, Poland
E-mail: tkubik@ict.pwr.wroc.pl
* Department of Electrical and Electronic Engineering, Oita University,
700 Dannoharu, Oita 870-1124, Japan
E-mail: msugi@cc.oita-u.ac.jp

Keywords: nanoparticles, biosensors.

Abstract

Biosensors are chemical sensors, in which recognition processes rely on biochemical mechanisms utilization. There are several kinds of nanoparticles that can be used as biosensors components. Most of them work as probes recognizing and differentiating an analyte of interest for diagnostic and screening purposes.

The probes are used to bind and signal the presence of a target in a sample by their color, mass, or other physical properties. This paper provides a brief description of the following nanoprobes: quantum dots, nanobarcodes, metallic nanobeads, silica nanoparticles, magnetic beads, carbon nanotubes, and nanopores.

1 Introduction

The most common definition of nanotechnology is that of manipulation, observation and measurement at a scale of less than 100 nanometers (one nanometer is one millionth of a millimetre). In biology and chemistry nanoscale operations are involved in the synthesis of inorganic, organic and hybrid nanomaterials for use in nanodevices, the development of novel nanoanalytical techniques, and the manipulation of biological molecules such as DNA and the evolution of molecular machines. This review is focused on the potential of nanotechnology in the developing and constructing artificial nanodevices, such as biosensors.

Biosensors consist of a biological element (responsible for sampling), and a physical element (transmitting sampling results for further processing) [1, 2]. The biological element of a biosensor contains a biosensitive layer, which can either contain bioreceptors or be made of bioreceptors covalently attached to the physical element. The type of biological element defines biological specificity conferring mechanism used. The physical element translate information from the biological element into a chemical or physical output signal with a defined sensitivity.

There are several kinds of nanoparticles that can be used as biosensors components. Most of them work as probes recognizing and differentiating an analyte of interest for diagnostic and screening purposes. In such applications biological molecular species are attached to the nanoparticles through a proprietary modification procedure. The probes are used then to bind and signal the presence of a target in a sample by their color, mass, or other physical properties. The other biosensors employ nanoparticles in a different way. They work as sieves through which charged molecules are transported in an electrical field.

In the next section a short description of nanoparticles used in biosensors as nanoprobes and nanosieves is provided.

2 Nanoparticles as parts of biosensors

Most of nanoparticles used in biosensors work as probes translating information from the biological element into measurable signal. Nanoparticles made of solid-state materials currently available (see Figure 1) are presented in the foregoing paragraphs.

Nanocrystals, quantum dots – these particles are inorganic crystals of cadmium selenide, 200–10000 atoms wide, coated with zinc sulphide. They emit fluorescent light when irradiated with low-energy light. The size of the dots (< 10 nm) determines the frequency of light emitted. The dots usually have a polymer coating with multivalent bio-conjugate attached, or are embedded into microbeads. Collection of dots of different size embedded to a given microbead emits distinct spectrum of colors - spectral bar code specific for this bead. Detection technique with the use of 10

intensity levels and 6 colors could theoretically provide 106 distinct codes. Quantum dots, for example CdSe-ZnS nanocrystals, do no emit in the near infrared, so they cannot be used for analysis in blood [3].
Area of use: multicolor optical coding for biological assays [4]; labelling of the breast cancer marker HeR2 on the surface of fixed and live cancer cells; stain actin and microtubule fibbers in the cytoplasm; detection of nuclear antigens in side nucleus [5]; immunohistochemical analysis of paraffin-embedded tissue sections [6]; *in vivo targeting* [7].

Nanobarcodes are cylindrical nanoparticles with specific patterns of submicron stripes of noble metal ions, produced by alternating electrochemical reduction of the appropriate metals. They are between 12 nm and 15 μm in width and 1-50 μm in length. The striping patterns make them distinctive under light, or fluorescent microscopy, or mass spectrometry. Nanobarcodes are easy to make in a nearly unlimited number of uniquely identified flavors [8, 9].
Area of use: coding in multiplexed assays for proteomics, population diagnostics and in point-of-care hand-held devices; proteins detection by either mass spectrometry or fluorescence measure.

Metallic nanobeads are made of noble metals with diameters between 15 to 60 nm [10, 11]. They can be detected by the transmissive and reflective light measure, plasmon resonance, quartz crystal microbalance, and differential pulse voltametry.
Area of use: cancer diagnosis [11]; DNA detection assay [10]; DNA diagnostics [12].

Silica nanoparticles are synthesized using standard water-in-oil microemulsion method (60nm in diameter.) They are silanised, and coated by oligonucleotide before use (DNA immobilization.) They are observable by fluorescence measurements methods [13].
Area of use: efficient nucleic acid hybridisation; detection of nanomolar range target DNA probes; ultra-small nano-biosensors for trace analysis [13].

Ferrofluid magnetic nanoparticles are particles (25–100 nm in radius) consisting of a magnetic core surrounded by a polymeric layer (biological substrate) coated with affinity molecules, such as antibodies. Macro magnetic beads are bigger in size. They might be coated with streptavidin to bind to biotin with a single-stranded DNA probes specific for a bioagent or sample DNA attached. They are detectable trough amperometry or resistance measure. They can be also manipulated in a magnetic field [14].

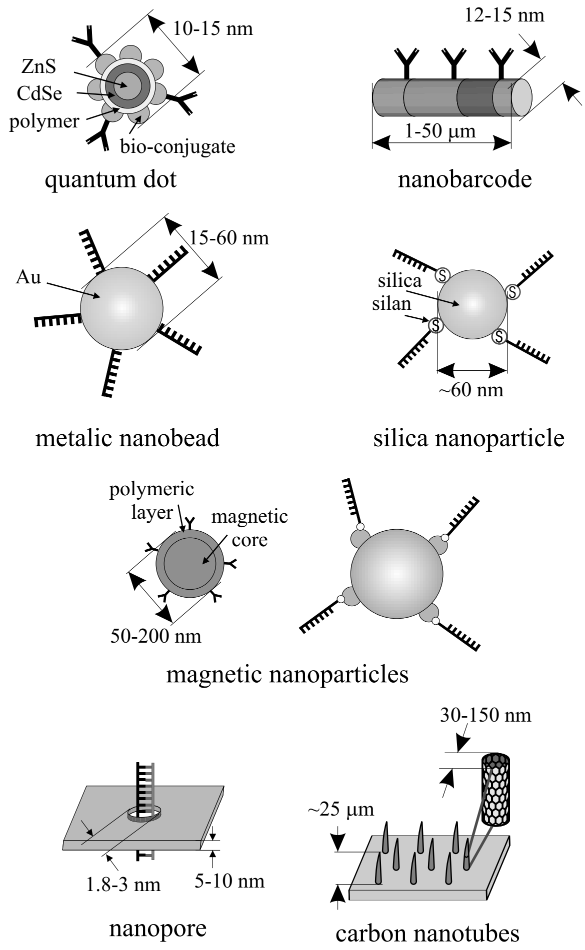

Figure 1: Schemes of different nanoparticles used for diagnostic and screening purposes.

Area of use: imaging specific molecular targets using nanoparticles as magnetic resonance contrast agents [15]; very sensitive cells or other tissue samples capture and/or separation.

Carbon nanotubes are carbon cylinders rising in the process of folding graphitic layers. The cylinders have remarkable strength and unique electrical properties making them insulting, semiconducting or conducting depending on their structure. They may be composed of a single shell single-walled nanotubes (SWNTs), or of several shells multi-walled nanotubes (MWNTs) [16, 17]. They are produced by microwave plasma enhanced chemical vapor deposition. Carbon nanotubes may be grown on a wide variety of substrates (including quartz and glass slides, platinum substrates) in the presence of catalyst (like nickel.)

Average length of these nanoparticles is of 25 mm order. Mean diameter may vary from 30 nm up to 150 nm. But with the use of super-lattice nanowire pattern transfer individual semiconductor nanowires can be created that are as little as 8 nm in diameter with the same distance between each wire [18]. In most cases electrical properties of carbon nanotubes are utilized for measurement purposes. When used in biosensing, carbon nanotubes have specific biomolecules attached. Area of use: promotion of electron transfer reactions when used to fabricate electrodes for the oxidation of biomolecules including dopamine, protein and b-nicotinamide adenine dinucleotide [19, 20]; extracellular analysis[21]; *in vivo* diagnostics.

Optical fibres are made from optical fibres pulled down to tips having distal end sizes of approximately 3060 nm. Fabrication procedure involves pulling from a larger silica optical fibre using a special fibre-pulling device what yields fibre with submicron diameters. One end of such fibre is polished from 600-mm silica/silica to a 0.3 mm finish. The other end is pulled then to a submicron length using a fibre puller. Thus the distal end of the fibre reaches 60 nm size. To prevent light leakage of the excitation light on the tapered side of the fibre, the side wall of the tapered end can be coated with a thin layer of silver, aluminium or gold (100-300 nm) leaving the distal end of the fibre free. These nanoparticles are not subject to electromagnetic interferences from static electricity, strong magnetic fields, or surface potentials. Fibreoptic nanoprobes can be covalently bound either with bioreceptors, such as antibodies, or with other, synthetic receptors, such as cyclodextrins [22, 23].
Area of use: in situ measurements of benzopyrene tetrol in single cells with the antibody-based nanoprobe [24, 1]; specific detection of target DNA at zeptomole levels, in the presence of non-cDNA [25]; analysis of mRNA isoforms in human cancer cell lines in conjunction with a new enzymatic detection method termed RNA-based annealing, selection and ligation (RASL) [26].

Nanopores are molecular-scale pores fabricated from variety solid-state materials (like silicon nitride) by ion-beam sculpting technique [27, 28]. The technique uses low-energy ion beams to slowly shape the surface of a material, while a feedback loop enables single-nanometre control over the pore dimension. Nanopores can be fabricated in two ways: they can be created from a cavity in the membrane under conditions where the sputtering erosion process dominates, or can be made by filling in larger pores under conditions where the lateral mass transport process dominates. The depth of nanopore fabricated in a membrane 510 nm thick is smaller than the molecule persistence length (50 nm for dsDNA), and a pore diameter 3-nm is slightly larger than the cross-sectional size of the molecule (∼2 nm.) In another attempt nanopores are created as an array of cylindrical gold nanotubes with as small as 1.6 nm inner diameter [29]. Area of use: manipulation and electronically registering of single DNA molecules in aqueous solution [30]; discrimination and characteristic of unlabelled DNA molecules at low copy number [31].

3 Conclusion

This paper highlighted few examples of nanoparticles with their applications. Nowadays technology provides tools which allow researchers to produce several kinds of nanoparticles. Over the next couple of years it is widely anticipated that nanotechnology will continue to evolve and expand in many areas of life and science, and the achievements of nanotechnology will be applied in medical sciences, including diagnostics, drug delivery systems and patient treatment.

References

[1] T. Vo-Dinh, B. Cullum, and D. Stokes: Nanosensors and biochips: frontiers in biomolecular diagnostics. *Sensors and Actuators, B: Chemical Sensors and Materials*, 74(1-3):2–11, (2001).

[2] S. Mohanty: Biosensors: A Survey Report. Technical report, Dept. of Comp. Sc. and Eng. University of South Florida Tampa, FL 33620, USA, (2001).

[3] S. Rosenthal: Bar-coding biomolecules with fluorescent nanocrystals. *Nature Biotechnology*, 19:621–622, (2001).

[4] M. Han, X. Gao, J. Su, et al.: Quantum-dot-tagged microbeads for multiplexed optical coding of biomolecules. *Nature Biotechnology*, 19:631–635, (2001).

[5] X. Wu, H. Liu, J. Liu, et al.: Immunofluorescent labeling of cancer marker HeR2 and other cellular targets with semiconductor quantum dots. *Nature Biotechnology*, 21:41–46, (2003).

[6] A. Sukhanova, L. Venteo, J. Devy, et al.: Highly stable fluorescent nanocrystals as a novel class of

labels for immunohistochemical analysis of paraffin-embedded tissue sections. *Lab. Invest.*, 82:1259–1261, (2002).

[7] M. E. Akerman, W. C. Chan, P. Laakkkonen, S. N. Bhatia, and E. Ruoslahti: Nanocrystal targeting in vivo. *Applied Biological Sciences*, 99(20):12617–12621, (2002).

[8] S. Nicewarner-Pena, R. Freeman, B. Reiss, et al.: Submicrometer metallic barcodes. *Science*, 294:137–141, (2001).

[9] H. Zhou, S. Roy, H. Schulman, and M. Natan: Solution and chip arrays in protein profiling. *Trends in Biotechnology*, 19(10):S34–S39, (2001).

[10] H. Cai, N. Zhu, Y. Jiang, P. He, and Y. Fang: CuAu alloy nanoparticle as oligonucleotides labels for electrochemical stripping detection of DNA hybridization. *Biosensors and Bioelectronics*, 18(11):1311 – 1319, (2003).

[11] H. Zhao, L. Lin, J. Li, et al.: DNA Biosensor with High Sensitivity Amplified by Gold Nanoparticles.. *Journal of Nanoparticle Research*, 3(4):321–323, (2001).

[12] A. Csaki, R. Moller, and W. Fritzsche: Gold nanoparticles as novel label for DNA diagnostics.. *Expert Review in Molecular Diagnostics*, 2(2):187–93, (2002).

[13] L. Hilliard, X. Zhao, and W. Tan: Immobilization of oligonucleotides onto silica nanoparticles for DNA hybridization studies. *Analytica Chimica Acta*, 470(1):51–56, (2002).

[14] C. Aston: Biological Warfare Canaries. *Cover Story : IEEE Spectrum*, (2001).

[15] D. Emerich and C. Thanos: Nanotechnology and medicine. *Expert Opin. Biol. Ther.*, 3(4):655–63, (2003).

[16] S. Iijima: Helical Microtubules of Graphitic Carbon. *Nature*, 354:56–58, (1991).

[17] S. Iijima and T. Ichihashi: *Nature*, 363:603, (1993).

[18] C. Zandonella: Cell nanotechnology: The tiny toolkit.. *Nature*, 423(6935):10–2, (2003).

[19] J. Davis, M. Green, H. Hill, et al.: The immobilization of proteins in carbon nanotubes. *Inorg. Chim. Acta*, 272:261, (1998).

[20] M. Musameh, J. Wang, A. Merkoci, and Y. Liu: Low-potential stable NADH detection at carbon-nanotube-modified glassy carbon electrodes. *Electrochem. Commun.*, 4(10):743–746, (2002).

[21] S. Wang, Q. Zhang, R. Wang, et al.: Multi-walled carbon nanotubes for the immobilization of enzyme in glucose biosensors. *Electrochemistry Communications*, 5(9):800–803, (2003).

[22] W. Vercoutere and M. Akeson: Biosensors for DNA sequence detection. *Current Opinion in Chemical Biology*, 6(6):816–822, (2002).

[23] J. Lu and Z. Rosenzweig: Nanoscale fluorescent sensors for intracellular analysis. *Fresenius' Journal of Analytical Chemistry*, 366(6-7):0569 – 0575, (2000).

[24] T. Vo-Dinh, G. Griffin, J. Alarie, et al.: Development of Nanosensors and Bioprobes.. *Journal of Nanoparticle Research*, 2(1):17–27, (2000).

[25] J. Epstein, M. Lee, and D. Walt: High-density fiber-optic genosensor microsphere array capable of zeptomole detection limits.. *Anal. Chem.*, 74:1836–1840, (2002).

[26] J. Yeakley, J.-B. Fan, D. Doucet, et al.: Profiling alternative splicing on fiber-optic arrays. *Nature Biotechnology*, 20:353–358, (2002).

[27] A. Storm, J. Chen, X. Ling, et al.: Fabrication of solid-state nanopores with single-nanometre precision. *Nature Materials*, 2:537–540, (2003).

[28] R. Austin: Nanopores: The art of sucking spaghetti. *Nature Materials*, 2:567–568, (2003).

[29] M. Nishizawa, V. Menon, and C. Martin: Metal nanotubule membranes with electrochemically switchable ion-transporter selectivity. *Science*, 268:700–702, (1995).

[30] O. Saleh and L. Sohn: An artificial nanopore for molecular sensing. *Nano Lett.*, 3:37–38, (2003).

[31] A. Meller, L. Nivon, E. Brandin, et al.: Rapid nanopore dicrimination between single polynucleotide molecules. *PNAS*, 97(3):1079–1084, (2000).

The Tenth International Symposium on Artificial Life and Robotics 2005(AROB 10th '05),
B-con Plaza, Beppu, Oita, Japan, February 4-6, 2005

P systems with dynamic channels transporting membrane vesicles

Rudolf FREUND Marion OSWALD
Faculty of Informatics
Vienna University of Technology
Vienna, Austria
rudi@emcc.at marion@emcc.at

Abstract

Based on the biological model of cell-to-cell communication proposed by A. Rustom et al. in [5] we consider cells able to dynamically form connections (channels) between them according to specific constraints possibly relying on some attribute assigned to the membranes of the cells as well as of their contents. From a theoretical point of view, such P systems with dynamic channels transporting membrane vesicles are computationally complete even when using only some of the characteristic features of the general model. Also the efficiency of modelling specific processes in various application areas depends on the specific features of the chosen model of P systems with dynamic channels transporting membrane vesicles.

1 Introduction

Membrane systems were introduced in 1998 by Gh. Păun in [2] as a parallel distributed model of computation abstracted from cell functioning. In a membrane structure (that can be represented as a tree in P systems or as an arbitrary graph in the more general case of tissue P systems), multisets of objects can evolve according to given evolution rules. Many variants of membrane systems (P systems) have been considered so far, see [3] for a comprehensive overview and [4] for the actual status of research.

Like in the biological model of cell-to-cell communication proposed by A. Rustom et al. in [5], in this paper we consider cells (like in tissue P systems) able to dynamically form connections (channels or *nanotubes* in the sense of [5]) between them according to specific constraints possibly relying on some attributes assigned to the membranes of the cells as well as of their contents. In contrast to the P systems considered so far, through these nanotubes (channels) of P systems with dynamic channels transporting membrane vesicles, multisets of elementary objects are transported in a membrane vesicle, which is the most important new feature of the model introduced in this paper. Attributes assigned to the cell membranes, for example, can be their electrical charges (polarizations) as this was formally already considered in P systems with active membranes. Moreover, the transport of a membrane vesicle through a nanotube between two cells may depend on the contents of the membrane vesicle itself as well as on the objects contained in the two cells connected by this nanotube and on the specific attributes assigned to the cell membranes and the membrane of the vesicle to be transported through the nanotube.

As it is often observed in the P systems area, processes may happen in parallel according to a universal clock; yet although in nature many processes are carried out in parallel, they are not synchronized. Therefore, to model these biological systems as described by A. Rustom et al., we consider P systems with dynamic channels transporting membrane vesicles also working in the asynchronous mode (an arbitrary number of rules that do not interfere with each other can be carried out in parallel in one derivation step) or in the sequential mode (exactly one rule is carried out in one derivation step); for an overview on P systems working in the asynchronous or in the sequential mode see [1]. On the other hand, processes in computers as for simulating mobile software agents can be simulated by P systems with dynamic channels transporting membrane vesicles working in the maximally parallel mode (which means that as many processes as possible are carried out in parallel).

In the second section, we now will introduce the general model of P systems with dynamic channels transporting membrane vesicles. From a theoretical point of view, P systems with dynamic channels transporting membrane vesicles are computationally complete, i.e., in the sense of Turing we can simulate the actions of Turing machines; depending on the working mode (sequential, asynchronous or maximally parallel), different variants of rules and corresponding membrane attributes are needed to obtain this computational universality (we will prove universality for one specific variant working in the sequential mode in the third section). Also the efficiency of modelling specific processes in various application areas depends on the specific features of the chosen model of P systems with dynamic channels transporting membrane vesicles as we will discuss in the fourth section.

2 The General Model

In this section we describe the general model of P systems we are going to investigate in this paper. Intuitively, we consider cells enclosed by a membrane which allows for communication with the environment as well as for dynamically forming connections (channels or *nanotubes* in the sense of A. Rustom et al. in [5]) between cells that transport (multisets of) objects enclosed in a membrane (*vesicle*).

A *P system with dynamic channels transporting membrane vesicles* (in the following we shall use the notion *P system* only) Π is a construct

$$(O, O_T, O_\infty, C, Q, F, I, R)$$

where

- O is the set of *objects*;
- $O_T \subseteq O$ is the set of *terminal* objects;
- $O_\infty \subseteq O$ is the set of objects occurring infinitely often in the environment of the cells;
- $C \subseteq O$ is the set of *catalysts*; a catalyst is never changed or moved by a rule;
- Q is the set of *states* for the channels between cells;
- F is the set of *attributes* assigned to a cell or a vesicle;
- I specifies the initial contents of the environment (only those objects not occurring in an infinite number of copies, which were already specified by O_∞) as well as the cells and the vesicles and their initial contents the system starts with (observe that we assume no channels to exist at the beginning);
- R is a set of *rules*.

The set of rules R itself consists of several sets of different types of rules:

- $R_{e,c}$ is a set of evolution rules for objects in a cell;
- $R_{e,v}$ is a set of evolution rules for objects in a vesicle;
- $R_{c,e}$ is a set of communication rules for exchanging (multisets of) objects between a cell and the environment;
- $R_{c,v}$ is a set of communication rules for exchanging (multisets of) objects between a vesicle in a cell and the surrounding cell;
- $R_{c,c,i}$ is a set of rules initializing a channel (nanotube) between two cells (or a cell and the environment);
- $R_{c,c,t}$ is a set of rules transporting a vesicle through a channel (nanotube) between two cells (or a cell and the environment);
- $R_{c,c,d}$ is a set of rules deleting a channel (nanotube) between two cells (or a cell and the environment; a vesicle sent out from a cell into the environment gets the status of a cell).

In some restricted variants, the sets $R_{c,c,l}$, $l \in \{i, t, d\}$, may be combined in only one set $R_{c,c}$ of rules which establish a channel between two cells for moving a vesicle from one cell to another one (or between a cell and the environment for expelling a vesicle into the environment) and immediately after having moved this vesicle deletes the channel again.

- R_d is a set of rules eliminating a vesicle in a cell (in a biological sense, this deletion of a vesicle reflects a kind of phagocytosis);
- R_g is a set of rules generating a new vesicle in a cell.
- R_δ is a set of rules eliminating the membrane of a vesicle and expelling its contents into the surrounding cell;
- R_μ is a set of rules generating a new vesicle containing the whole contents of a cell.

All the rules described above may depend on the features currently assigned to the involved cell(s) and/or the involved vesicle and possibly also change these features. In static variants of the general model, we omit the sets of rules R_d, R_g, R_δ, and R_μ and do not allow vesicles to be expelled into the environment.

Moreover we should like to point out that all the sets in the general model described above need not be finite, e.g., the set of objects may be the set of strings over a given alphabet, and the set of attributes may be infinite, too. If the sets of rules are infinite, we assume that given an instance of the P system, we are able to effectively list the rules applicable to this instance and to decide whether a set of rules chosen so far is maximal or not.

The P system Π may work in different derivation modes: In the maximally parallel mode, for each derivation step we choose such a subset of the rules in R that cannot be extended any more; in the asynchronous mode, an arbitrary number of rules is applied in parallel; in the sequential mode, exactly one rule is applied.

3 Theoretical Results

The general model of *P systems with dynamic channels transporting membrane vesicles* introduced in the previous section is very powerful from a theoretical point of view, i.e., not all possible features are needed to obtain computational completeness. Moreover, we may use these P systems for different tasks, e.g., as generating devices or as accepting devices (*P automata*), but also for modelling different processes carried out by other devices, yet needing only specific features of the general model for obtaining efficient simulation results. We here restrict ourselves to a model which works in the sequential mode and only uses communication rules (*antiport rules*) as well as, of course, rules for transporting vesicles from one cell to another one, and we show how in this restricted model we can simulate graph-controlled grammars (which are devices well known to be computationally complete (e.g., see [6]).

Now let us consider a finite set of elementary objects constituting O and a subset O_T to be the set of terminal objects. A *graph-controlled grammar* G_C then is a construct

$$(O, O_T, w, R, L_{in}, L_{fin})$$

where w is the initial multiset over O, R is a finite set of rules r of the form $(l(r) : p(l(r)), \sigma(l(r)), \varphi(l(r)))$, with $l(r) \in Lab(G_C)$, $Lab(G_C)$ being a set of labels associated (in a one-to-one manner) with the rules r in R, $p(l(r))$ is a rewriting rule of the form $a(r) \to u(r)$ with $a(r) \in O$ and $u(r)$ being a multiset over O, $\sigma(l(r)) \subseteq Lab(G_C)$ is the *success field* of the rule r, and $\varphi(l(r)) \subseteq Lab(G_C)$ is the *failure field* of the rule r; $L_{in} \subseteq Lab(G_C)$ is the set of initial labels, and $L_{fin} \subseteq Lab(G_C)$ is the set of final labels. For $r = (l(r) : p(l(r)), \sigma(l(r)), \varphi(l(r)))$ and v, u being two multisets over O we say that (u, k) is directly derivable from $(v, l(r))$ if and only if

- **either** $p(l(r))$ is applicable to v, v is the result of the application of $p(l(r))$ to u, and $k \in \sigma(l(r))$,
- **or** $p(l(r))$ is not applicable to v, $u = v$, and $k \in \varphi(l(r))$.

The language generated by G_C is the set of all multisets u such that (u, k) can be derived in an arbitrary number of steps from (w, l) for some $k \in L_{fin}$ and $l \in L_{in}$.

We now define a restricted variant of the general model of P systems with dynamic channels transporting membrane vesicles that allows for the simulation of graph-controlled grammars: Let

$$(O, O_T, w, R, L_{in}, L_{fin})$$

be a graph-controlled grammar (without loss of generality, we may assume L_{in} and even L_{fin} to contain only one label and, moreover, $l(r) \notin \sigma(l(r))$ for all r). Then we construct the P system with dynamic channels transporting membrane vesicles Π working in the sequential mode

$$(O, O_T, O_\infty, C, Q, F, I, R_\Pi)$$

as follows:

We do not use catalysts, and we do not need states for the channels to be created dynamically; therefore, we omit C and Q, as well as O_∞, because we assume all objects from O to be available in the environment in an unbounded number, hence, Π is specified as a quintuple (O, O_T, F, I, R_Π) only.

As set of attributes F we take $Lab(G_C) \cup \{-, 0, +\}$, where we assume $Lab(G_C) \cap \{-, 0, +\} = \emptyset$. The initial configuration consists of $card(Lab(G_C))$ cells having the labels from $Lab(G_C)$ as attributes; moreover, the cell with attribute $l(r)$ contains the multiset $u(r)$, and finally, the initial cell (having the initial label from L_{in} as attribute) also contains a vesicle with attribute 0 and the contents w (i.e., the initial multiset from G_C). The rules in R_Π simulate the rules in R as follows:

- $(l(r), 0, a(r)/u(r), +) \in R_{c,v}$: In the cell with attribute $l(r)$, $a(r)$ in a vesicle (with attribute 0 which by the application of this rule is changed to $+$) contained in this cell is replaced by $u(r)$ which is taken from the cell and regained by

- $(l(r), a(r)/u(r)) \in R_{c,e}$; in that way, one application of the rule r is simulated.
- $(l(r), 0, \neg a(r), \lambda/\lambda, -) \in R_{c,v}$: Provided that the symbol $a(r)$ is not present in a vesicle contained in the cell with attribute $l(r)$, the attribute of the vesicle is changed from 0 to $-$ (without communicating symbols between the vesicle and the cell, which is indicated by the notion λ/λ, where λ denotes the empty word).
- $R_{c,c}$ consists of all rules of the form $(i, k, j, 0)$ such that
  - $k = +$ and $j \in \sigma(i)$ or
  - $k = -$ and $j \in \varphi(i)$.

  The application of $(i, k, j, 0)$ means establishing a channel between the cells with attributes i and j for transporting a vesicle with attribute k from cell i to cell j thereby changing the attribute of the vesicle from k to 0.

As results of a computation in Π we take the contents of any vesicle which appears in the final cell (i.e., the cell carrying the attribute from L_{fin}) and contains only terminal symbols. In that way Π generates the same set of terminal multisets as G_C.

As is well-known (see the results cited in [1]), P systems with antiport rules are computationally complete in only one membrane when working in the maximally parallel mode, whereas in the sequential mode universality cannot be reached even with an arbitrary number of membranes. The proof sketched above takes advantage of the inherently new feature of P systems with dynamic channels transporting membrane vesicles allowing for transporting the complete multiset of symbols in a vesicle from one cell to another one.

4 Variants for Applications

The biologically motivated model of P systems with dynamic channels transporting membrane vesicles introduced in this paper can be used for modelling various mechanisms in different application areas. Again the main feature we have to take advantage of is the possibility to establish connections between cells and to transport whole multisets of objects from one cell to another one in a single step.

As the model of P systems with dynamic channels transporting membrane vesicles incorporates several other features well motivated from biology, it can be used for modelling various aspects of artificial life. The cells themselves are organisms that may interact in an unguided manner via the environment or else, in a direct way, by establishing channels for exchanging complete sub-organisms (vesicles). By using suitable evolution rules, the organisms may develop also based on the development (evolution) of their components mostly represented by the vesicles contained in them, which usually happens in a parallel but unsynchronized way (and which corresponds with the asynchronous working mode of the P systems).

On the other hand, the vesicles can also be seen as packages of information transported from one computer (cell) to another one or as autonomous agents performing their tasks on different servers. In that case, these agents work in parallel, either in an unsynchronized way (which corresponds with the asynchronous mode of the P system) or even in a synchronized way (which corresponds with the maximally parallel mode of the P system); using sufficiently powerful operations (evolution rules) in the vesicles, we are able to describe the processes taking place in distributed systems.

Acknowledgements

The work of Marion Oswald was supported by FWF-project T225-N04.

References

[1] R. Freund, Asynchronous P systems, Proceedings WMC5 (2004), 12-28

[2] Gh. Păun, Computing with membranes. Journal of Computer and System Sciences 61 (1), 108-143

[3] Gh. Păun, Membrane computing - an introduction, Springer-Verlag, Berlin, 2002

[4] The P systems webpage: http://psystems.disco.unimib.it

[5] A. Rustom, R. Saffrich, I. Markovic, P. Walther, HH. Gerdes, Nanotubular highways for intercellular organelle transport, Science 303 (2004), 1007-1010

[6] A. Salomaa, G. Rozenberg (eds.), Handbook of Formal Languages, Springer-Verlag, Berlin, 1997

The Tenth International Symposium on Artificial Life and Robotics 2005(AROB 10th '05),
B-con Plaza, Beppu, Oita, Japan, February 4-6, 2005

Design of Soccer-ball-shape DNA Molecules and Preliminary Experiments in Vitro

Yutaka Kita* Atsushi Kameda** Masahito Yamamoto*,** Azuma Ohuchi*,**

*Graduate School of Information Science and Technology, Hokkaido University
Nishi 9, Kita 14, Kita-ku, Sapporo, Hokkaido, 060-0814, Japan
ki-yu, masahito, ohuchi@complex.eng.hokudai.ac.jp

**CREST, Japan Science and Technology Agency (JST)
Honmachi 4-1-8, Kawaguchi 332-0012, Japan
kameda@complex.eng.hokudai.ac.jp

Abstract

DNA molecules are functional materials to apply to nanotechnology. DNA polyhedra are one of DNA nanostructures and are expected to be implemented to nanomachines and other fields. There are many technical difficulties to construct DNA polyhedra. We employ some techniques developed in DNA computing research to construct DNA polyhedra. In this paper, we design Soccer-ball-shape (truncated icosahedron) DNA Molecules by means of gradual self-assembly using circular single-stranded DNA molecules (ssDNA). Then we report some preliminary experimental results toward the construction of the whole soccer-ball-shape structure.

key words: DNA nanotechnology, DNA polyhedra, constructive method

1 Introduction

1.1 DNA nanotechnology

DNA nanotechnology is a research field that aims at a construction of nanostructures, nanodevices, and nanomachines using DNA molecules [1]. DNA molecules have some advantages as follows. DNA molecules are stable materials. DNA molecules have ability to associate with and to recognize other DNA molecules by means of Watson-Crick complementarity. Watson-Crick complementarity is that four nucleotides A (adenine), T (thymine), C (cytosine), and G (guanine) form two complementary base pairs (A, T), (G, C). Therefore the states of DNA molecules can be controlled by using the hybridization of ssDNA. Moreover, by using properly designed DNA sequences, we can control a self-assembly of DNA molecules in order to construct a target structure.

1.2 DNA nanosturctures

DNA tiles and DNA polyhedra belong to DNA nanostructures. DNA tiles are formed structures that some double-stranded DNA molecules (dsDNA) crossover their ssDNA at some point. DNA tiles are utilized as a two-dimensional periodic structure and a scaffold for the production of a nanowire [2]. DNA polyhedra are three-dimensional structures. Since DNA polyhedra have a characteristic that can trap some materials within them, DNA polyhedra are expected to be applied to a drug delivery and crystal structure analysis etc. However, a construction of DNA polyhedra have many technical difficulties in itself, DNA polyhedra have not reached to be utilized actually yet. Hence we employ some techniques developed in DNA computing research to construct DNA polyhedra. In DNA computing, reactions of DNA molecules must be controlled with more remarkable accuracy than traditional molecular biology. Therefore we can use experimental methods and protocols researched in DNA computing to perform a self-assembly of DNA molecules. Moreover, we can use the sophisticated sequence design methods developed in DNA computing to construct a certain structure of DNA molecules because a lot of constraints used in DNA nanotechnology are common to that of DNA computing.

In this paper, we design Soccer-ball-shape DNA Molecules by means of gradual self-assembly using circular ssDNA as the basic structures. Soccer-ball-shape DNA Molecules have 90 edges, 60 vertexes, and 32 faces. Each edge of Soccer-ball-shape DNA Molecules consists of 22-mer oligonucleotides. The diameter of Soccer-ball-shape DNA Molecules is approximately 40 nm. The more faces DNA polyhedra have, the more difficult the material trapped in them escape outside. Therefore our proposed Soccer-ball-shape DNA Molecules are more effective in terms of feature as the cages that trap some materials than typical DNA polyhedra such as DNA cube [3] and DNA octahedron [4].

2 Design of Soccer-ball-shape DNA Molecules

2.1 Structure design

To construct DNA polyhedra, several constructive methods are proposed as follows.

The first method is self-assembly of one DNA three-arm junction that same DNA three-arm junctions are formed from three ssDNA by hybridization reactions and self-assemble into DNA cages [5]. This constructive method is simple and required sequence number is only three. However, to construct desired structures are unfavorable. The second method is stepwise self-assembly that substructures are formed from multiple ssDNA and gradually self-assembly into desired structures. This method can construct desired structures confirming construction of substructures gradually. However, this method requires more sequence than the first method. DNA cube [3] is constructed this method. The third method is self-assembly utilizing DNA foldings that one long ssDNA folds into polyhedra by several short ssDNA help. The advantage of this method is that long ssDNA can amplify by the polymerase chain reaction. However, one long ssDNA sequence must be designed in one DNA polyhedra. DNA octahedron [4] is constructed this method.

In view of constructing Soccer-ball-shape DNA molecules, the products may contain many undesirable polyhedra in the first method. Designing long ssDNA folding into soccer-ball-shape is difficult in the third method because truncated icosahedron has more faces than octahedron. Therefore we design Soccer-ball-shape DNA Molecules based on the second method. When required sequence set is designed in accordance with the edge length, the number of required sequence is 90 in total edge number of Soccer-ball-shape DNA Molecules. However, there is a trade-off between the size of sequence set and the constraint of sequence. Therefore we propose reutilization of edge sequence subset that utilized at previous reaction and is expected not to affect next. Thus we succeed in reducing required number of designed sequences to 14.

The construction step is shown in Fig. 1. Firstly we synthesize circular ssDNA corresponding to the pentagon of Soccer-ball-shape DNA Molecules. Sequences of circular ssDNA are designed that all edge have either same sequence or unique. Secondly we construct the intermediate unit that is made from circular ssDNA concatenated and intertwined by multiple arm molecules. Arm molecules are 44-mer ssDNA molecules that associate with circular ssDNA and formed hexagons. In consideration of the reaction efficiency, we design and utilize two types of the arm molecules: the type 1 arm molecules are concatenated by circular ssDNA help; the type 2 by hybridization of sticky-end is formed by two arm molecules. The intermediate unit consists of six pentagons and five hexagons. Finally Soccer-ball-shape DNA Molecules is completed concatenating two intermediate units by the arm molecules. The details of Soccer-ball-shape DNA Molecules in Fig. 2. Each edge of Soccer-ball-shape DNA Molecules forms dsDNA (20 base pairs). Bulged T_2 loops are placed at each of the junctions to give flexibility at vertexes of Soccer-ball-shape DNA Molecules [6].

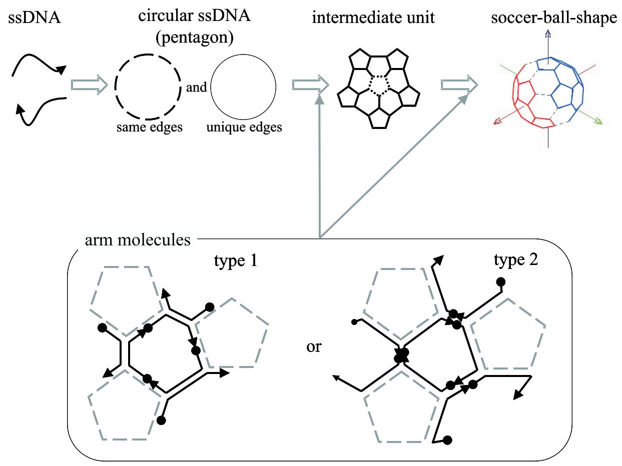

Figure 1: Construction step of Soccer-ball-shape DNA Molecules.

2.2 Sequence design

In using DNA molecule, experimental accuracy and efficiency depend on DNA sequences as well as experimental methods. To construct DNA polyhedra, DNA sequences must avoid mis-hybridization and folding undesirable secondly structures. With the reduction of sequence number by structure design, we can design DNA sequences satisfy strict constraints and decrease the undesirable reactions.

The sequence design process is proceeded as follows. Firstly we make a sequence set that consists

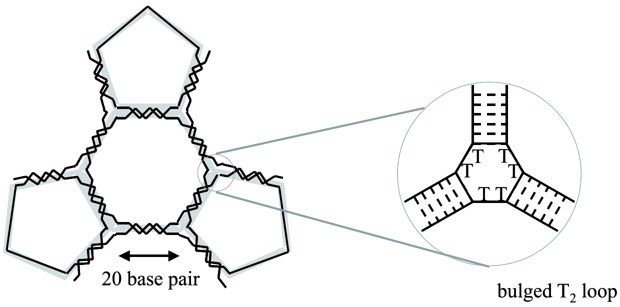

Figure 2: The ditails of structure.

of sequence satisfy constraints such as Energetic constraints, Hamming Distance, and Consecutive Match by Two-Step search algorithm [7]. Secondly we use Mfold [8] as a sieve to eliminate undesirable sequences that are expected to fold secondly structure from sequence set.

3 Gradual self-assembly by chemical experiments

We practically performed experiments in vitro. 5' end of ssDNA are phosphorylated for ligation reactions that concatenate ssDNA. We generally perform ligation reactions at 16°C for over 1 hour. We use constant denaturing polyacrylamide gel electrophoresis (CDPAGE) to detect the desired structures.

3.1 Synthesis of circular ssDNA

The synthesis of circular ssDNA is shown in Fig. 3. First, we mix 56-mer, 54-mer, and complementary ssDNA (non phosphorylated) to form circular structure by hybridization reactions at room temperature. Next, we concatenate ssDNA by ligation reactions. Next, we confirmed these products circularly concatenated or not by restriction enzyme digestion reactions with ExonucleaseIII. Finally, we purify circular ssDNA with the column purification.

3.2 Construction of intermediate unit

The construction of two intermediate units with the type 1 arm molecules is shown in Fig. 4. First, we mix circular ssDNA (c1) and the arm molecules. All edge of c1 are same sequence. The conditions of hybridization reactions are: room temperature, heated at +5.0°C/s, 94°C for 10 s (denaturation), cooled at

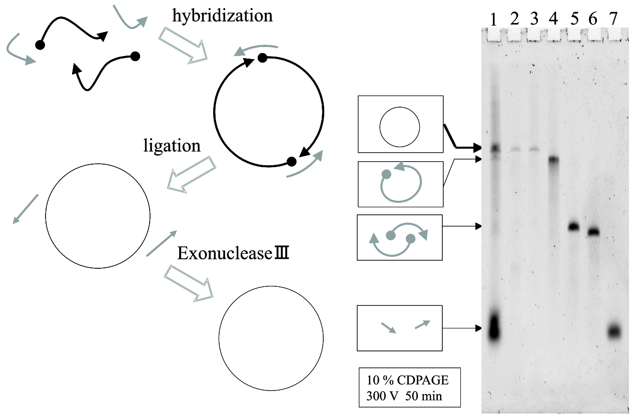

Figure 3: Result of synthesizeing circular ssDNA. Lane 1:after ligation; lane 2:after digestion; lane 3:after purification; lane 4, 5, 6:110 mer, 56-mer, and 54-mer ssDNA; lane 7:complementary ssDNA. Since a new band excepts the material ssDNA are appeared in lane 1 and remain lane2, we obtain circular ssDNA.

−0.01°C/s, 4°C for over 1 hour (annealing). Next, we mix the mixture and other circular ssDNA (c2 or c3). All edge of c2 and c3 are unique sequence. Next, we mix the arm molecules that concatenate between c2 or c3 at 4°C and perform ligation reactions.

The construction with the type 2 is shown in Fig. 5. First, we mix each circular ssDNA and corresponding the arm molecules that associate with circular ssDNA and form sticky-ends. We use equal condition of hybridization reactions in type 1 arm molecules. We label after hybridization products as $c1\_h$, $c2\_h$, and $c3\_h$ that c1, c2, and c3 circular ssDNA hybridize with the corresponding five arm molucules. Next, we mix $c1\_h$ with $c2\_h$ and $c3\_h$ at 4°C and perform ligation reactions.

4 Conclusion

We proposed design of Soccer-ball-shape DNA Molecules and significantly reduced required number of designed sequences by our methods. Reutilization of DNA sequences will be indispensable for meeting more complex needs in DNA nanotechnology. Moreover, we reported some experimental results of the synthesis of circular ssDNA and the construction of the intermediate units toward the construction of the whole soccer-ball-shape structure. We confirmed construction of the ring structure that several circular ssDNA

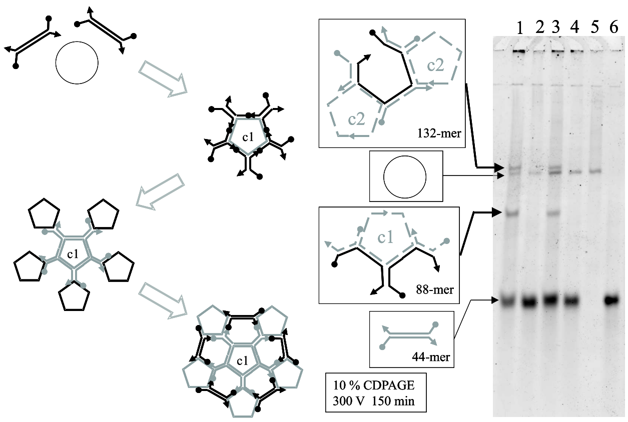

Figure 4: Construction of the intermediate units with the type 1 arm molocule. Lane 1, 2:after and before ligation with c2; lane 3, 4:after and before ligation with c3; lane 5, 6:circular ssDNA and the arm molecules. Compare with after and before ligation reactions, new bands appeared in lane 1, 3 are partial products;lower bands are 88-mer and upper are 132-mer ssDNA that two and three arm molucules are concatenated

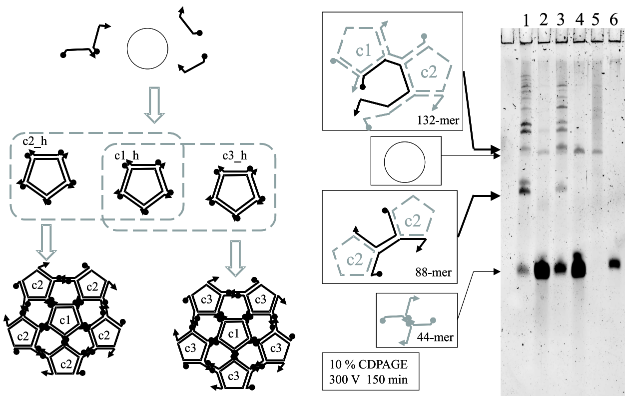

Figure 5: Construction of the intermediate units with the type 2. Lane 1,2:after and before ligation with $c1\_h$ and $c2\_h$; lane 3, 4:after and before ligation with $c1\_h$ and $c3\_h$; lane 5, 6:circular ssDNA and the arm molecules. New bands of 88-mer and 132-mer ssDNA are apppeared in lane 1, 3 as well as with the type 1. Moreover, new bands are appeared upper 132-mer ssDNA. Since density of circular ssDNA bands in lane 1, 3 are thinner than that of in lane 2, 4, circular ssDNA and arm molecules form the ring structures that several circular ssDNA are intertwined. However, we cannot detect the construction of the intermediate unit yet.

intertwined. Since our detection method of CDPAGE is unfavorable to detect complex structure, we must additionally use other detection methods such as a scanning probe microscope using in nanothecnology field.

As the future work, we will improve experimental protocols and methods to construct Soccer-ball-shape DNA Molecules.

References

[1] N. C. Seeman, "DNA in a material world", *nature*, Vol. 421, pp. 427-431, 2003.

[2] H. Yan, S. H. Park, G. Finkelstein, J. H. Reif and T. H. LaBean, "DNA-Templated Self-Assembly of Protein Arrays and Highly Conductive Nanowires", *science*, Vol. 301, pp. 1882-1884, 2003.

[3] J. Chen and N. C. Seeman, "The synthesis from DNA of a molecule with the connectivity of a cube", *nature*, Vol. 350, pp. 631-633, 1991.

[4] W. M. Shih, J. D. Quispe and G. F. Joyce, "A 1.7-kilobase single-stranded DNA that folds into a nanoscale octahedron", *nature*, Vol. 427, pp. 618-621, 2004.

[5] K. Matsuura, T. Yamashita, Y. Igami and N. Kimizuka, "'Nucleo-nanogages': designed ternary oigodeozyribonucleotides spontaneously form nanosized DNA cages", *Chem Comm* pp. 376-377, 2003.

[6] P. Sa-Ardyen, N. Jonoska, and N. C. Seeman, "Self-assembling DNA Graphs", *Eighth International Meeting on DNA-Based Computers (DNA8), in Lecture Notes in Computer Science*, pp. 1-9, 2003.

[7] S. Kashiwamura, A. Kameda, M. Yamamoto, A. Ohuchi, "Two-Step Search for DNA Sequence Design", *IEICE (The Institute of Electronics, Information and Communication Engineers) TRANSACTION. FUNDAMENTALS*, Vol. E87-A, No.6, pp. 1446-1453, 2004.

[8] M. Zuker, "Mfold web server for nucleic acid folding and hybridization prediction" , *Nucleic Acids Res*, Vol. 31, pp. 1-10, 2003.

The Tenth International Symposium on Artificial Life and Robotics 2005(AROB 10th '05),
B-con Plaza, Beppu, Oita, Japan, February 4-6, 2005

Amoebic ability to arrive at signal sources in an obstacle-rich space

Shin I. Nishimura
Graduate School of Engineering
Nagoya University
Nagoya 464-8061, Japan
shin@sasai.human.nagoya-u.ac.jp

Sasai Masaki
Graduate School of Information Science
Nagoya University
Nagoya 464-8061, Japan
sasai@info.human.nagoya-u.ac.jp

Abstract

Amoebic cells are able to trace signal molecules and arrive at sources of those molecules. An interesting problem is on how amoebic cells can avoid obstacles and find the correct way to reach the signal source. To answer this problem, we develop a discrete model of amoeba. We put a wall in the model space with a hole through which the amoeba can migrate. The wall also has a dummy hole or "permeable membrane" through which the signal permeates but the amoeba can not pass. If we place the cell near by the permeable membrane, the cell initially tries to pass it but finally finds the true hole and succeeds in passing it.

1 Introduction

Amoebic cells are widely seen in many eukaryotic species. Cellular slime mold at the unicellular period, for example, moves and searches foods with the amoebic locomotion [1]. Human neutrophils which attack the external microbes are also well-known examples of amoebic cells [2].

One of important features of amoebae is "chemotaxis". Immune cells migrate from vessels to the inflamed tissue in order to destroy the external microbes. Cells in the inflamed tissue are known to produce signal molecules (usually called "chemokine"). Immune cells detect the gradient of the signal and move along the gradient to get to the tissue.

The mechanism that amoebae can detect the very small difference in signal density between their head and tail, which is often as small as the signal fluctuation, has been a challenge to researches, and many secrete mechanisms of chemotaxis have been brought to light through intensive studies [3, 4, 5, 6, 7].

However, many problems remain elusive. One of interesting problems is the mechanism that amoebic cells can migrate among tissue cells which are constructed as if a maze in animal bodies. There suppose to be dead-ends, narrow holes, and other unexpected difficulties. In order for amoebic cells such as immune cells to arrive at appropriate tissues, they need to avoid these difficulties. The aim of this paper is to elucidate amoebic abilities of migration in an obstacle-rich space.

2 Model

Our model has discrete two-dimensional grids on which some concentrations of molecules are defined. A cell is defined on the grids as a domain. We adopt hexagonal grids for convenience. A grid is either external or in the cellular domain. When the grid is in the cellular domain, three real numbers are defined on the grid, which indicate densities of activator, inhibitor and actin filaments. We give four rules in order to move the cell: Kinetics, Diffusion, Cellular domain extension and Keeping the cell. The following paragraphs explain those rules.

(1) **Kinetics**: Both activator and inhibitor are produced by the stimulation of the external signal[8]. The activator enhances polymerization of actins, whereas the inhibitor suppresses the polymerization. First, this rule selects a grid in the cellular domain randomly. If densities of activator, inhibitor and actin filaments at the selected grid j are expressed as A_j, I_j and F_j, respectively, those variables are changed obeying the following equations:

$$A'_j = A_j + \quad S_j \quad k \quad A_j \tag{1}$$

$$I'_j = I_j + \quad S_j \quad k \quad I_j \tag{2}$$

$$F'_j = F_j + \begin{cases} k_f F_j & (\frac{A}{I} > h) \\ k_f F_j & (\text{otherwise}) \end{cases}, \tag{3}$$

where , , , k , k , k_f, and h are constants. S_j indicates the concentration of chemoattractants or the strength of the external signal at the jth grid. Grids at the border of the cellular domain are regarded as

The Tenth International Symposium on Artificial Life and Robotics 2005(AROB 10th '05),
B-con Plaza, Beppu, Oita, Japan, February 4-6, 2005

the cellular membrane. We call the grid in the cellular domain the membrane if at least one of its six nearest grids is external. S_j is set to zero if the jth grid is in the cellular domain but not in the membrane. The functional form of S_j represents the chemical gradient. A schematic picture of the kinetics is depicted in Figure 1

(2) **Difiusion**: Only the inhibitor diffuses into the whole cytoplasm[8]. This rule selects a grid from the whole cellular domain. At the selected jth grid and its nearest cellular lth grid, I_j and I_l obey the following equations:

$$I'_j \;=\; I_j \quad DI_j \qquad (4)$$

$$I'_l \;=\; I_l + \frac{DI_j}{n}, \qquad (5)$$

where D is the diffusion constant. n is the number of the nearest cellular grids. D should be smaller than 1 by definition.

(3) **Cellular domain extension**: The rule randomly selects a grid from the membrane. When F_j at the selected jth grid in the membrane exceeds the threshold F_{th}, an external grid in the six nearest grids of the jth grid is turned into a cellular grid. When there are two or more than two external grids around the jth grid, a grid is randomly selected. If this grid is referred to as l, $F_l = F_j/2$ and other variables are set to zero. F'_j equals to $F_j/2$ by definition, where the prime indicates the value at the next time step.

(4) **Keeping the cell**: We also give a rule to prevent cell from breaking into pieces. The cellular volume is kept and the cellular surface length is constrained to be as small as possible. This rule randomly selects a grid from the membrane. Then the rule decides either to remove the grid or to add a new cellular grid around the grid. This rule checks the cellular "tension" by calculating energy of tension as:

$$E = (V \quad V_0)^2 + cL^2, \qquad (6)$$

where V and L are the cellular volume and length of the membrane and V_0 and c are constants. When E' denotes the energy after either removing or adding a cellular grid, we define the probability P as follows:

$$P = \exp\left(\quad \frac{E' \quad E}{kT} \right), \qquad (7)$$

where kT is a constant. We generate a random number between 0 and 1 and then compare the number with P. If the number is smaller than P, we "undo" the event of removing/adding. From the definitions of P and E, the volume of the cell tends to be V_0 and the length of the membrane becomes as small as possible. Note that if removing is chosen, the values of A, I and F in the removed grid are added into the nearest cellular grid.

We also give the "master" rule that randomly selects one of the above rules. Each rule has the probability of selection. The probabilities of selection for rules from (1) to (4) are written as P_1, P_2, P_3 and P_4. $P_1 + P_2 + P_3 + P_4$ should equal to 1. When the master rule selects one of the four rules, the selected rule is executed. We iterate this process several millions times.

External signal is defined in external grids. The signal diffuses over external grids but not into cellular grids. When S_k is the signal density in the external grid k, S_k is updated to S'_k by the following equation:

$$S'_k = S_k \quad D_s S_k + D_s \sum_l S_l/n_l, \qquad (8)$$

where l indicates the lth nearest external grid, n_l is the number of nearest external grids around the lth grid, and D_s is constant. Although this equation looks similar to Equations 4 and 5, it should be noted that signal densities are synchronously updated at all external grids. After the master rule randomly selects the rules n_c times, it executes Equation 8 once, and this cycle is repeated. The reason why we adopt the synchronous updating rule for external signal densities is that the external signal diffuses much more rapidly than intracellular molecules. External signal does not diffuse into cellular grids. We define rectangle boundary grids in which the external signal sinks: The signal flows into the boundary grids but not from the grids. When a signal source is defined at the kth grid, S_k is kept constant instead of Equation 8 as $S_k = S_0$ at the source grid.

We calibrate parameters in the model by examining how our cell moves in a simple linear gradient. The initial diameter of the cell is set to be 30 grids. The cell goes up the linear gradient as observed experimentally [9] when the following set of parameters are chosen: $= 1.0$, $= 0.1$, $k \; = 0.9$, $k \; = 0.02$, k_f, $D = 0.45$, $h = 1.0$ $P_1 = 0.0419$, $P_2 = 0.03$, $P_3 = 0.03$, $P_4 = 0.898$, $V_0 = 900$, $c = 10^5$, $kT = 100$, $D_s = 0.3$, $S_0 = 0.5$ and $n_c = 10$.

Although we have not yet exhaustively tried different parameter sets, we expect that the cell behaviors are robust against the parameter change. We use 95 95 grids in which both external and cellular grids are defined. Simulation is designed to terminate before the cell reaches the boundary of the grid space.

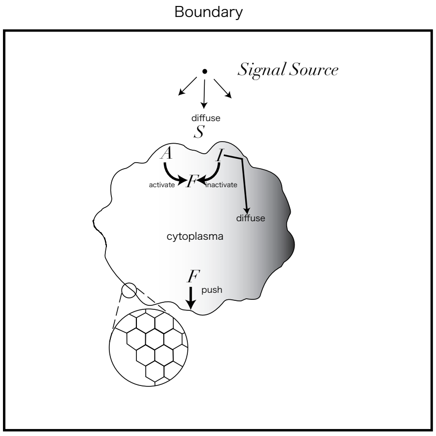

Figure 1: A schematic picture of a cell in the space with boundary through which signal drops out of the space. Both activator A and inhibitor $I$are produced by the stimulation S of the external signal. The activator enhances polymerization of actins F, whereas the inhibitor suppresses the polymerization. Only the inhibitor diffuses into the whole cytoplasm. External signal diffuses from signal sources.

3 Results

First we put a source near by the cell. When the cell touches the source, the source is eliminated from the grid space. This operation naively represents "phagocytosis" . Does the cell arrive at the source as reaching "food"? Figure 2 shows that the cell succeeds in reaching the food.

If there are multiple foods, how does the cell behave? Interestingly, the cell moves to one of foods and "eats" it. It then goes to the next one and eats all the foods in the end. (Figure 3).

Figure 4 shows that there is a wall with a hole and a "permeable membrane" through which the signal can permeate but the cell cannot pass. When the cell starts near by the permeable membrane, the cell stays at the membrane for a while then moves to the true hole and reaches the source.

4 Discussion

In actual animal bodies amoebic cells seem to select suitable paths by avoiding obstacles or local maxima of signal density. Results in the last section showed that the model amoebic cell can also choose a suitable path as natural amoebic cells do: When multiple foods are placed in the space, the simulated cell did

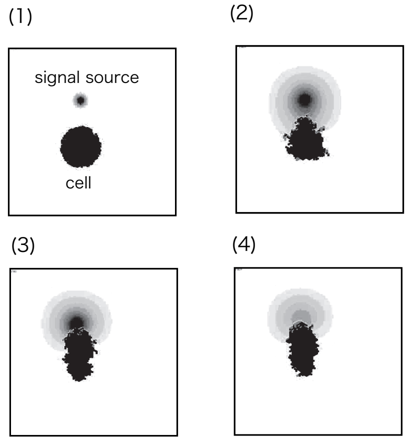

Figure 2: Snapshots of a cell moving to a signal source as if to eat a "food". A large, dark gray area is the cell. The signal density is indicated with gray scale. A sinal source is a small dark gray area. Around the source, contour lines of signal density are shown. In Subfigure (4), a dark small area has vanished because the source has been touched by the cell and removed.

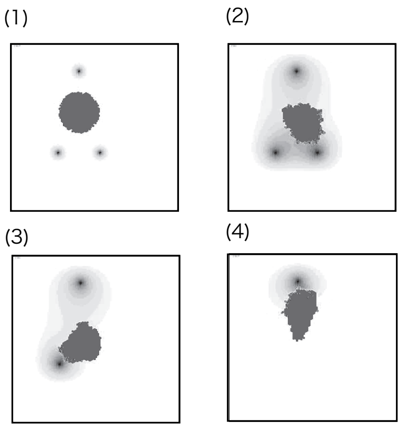

Figure 3: Snapshots of a cell "eating" three foods. The cell moves to the right bottom, then to the left bottom, and finally to the top.

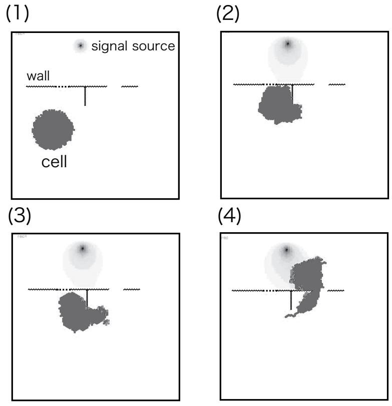

Figure 4: Snapshots of a cell moving in the space separated by a wall. The wall has a membrane indicated by a dashed line at the left part, through which the signal permeates. The wall also has a hole at the right part. A vertical part of the wall is a stand in cell's way.

not freeze but chooses one food to another to gain as much food as possible. When the obstacle is placed between the food and the cell, the cell can find out the proper way to get round the obstacle to reach the food. Simplicity of our model leads to the idea that such seemingly complex motion is based on the essentially simple mechanism. Although the real biological process is supported by enormous numbers of different types of proteins, the key mechanism underlying the behavior might be the nonlinear and history-dependent response of cell to the external stimuli as demonstrated in the model.

Our next task is to quantify the efficiency of amoebic strategy by using our model. Such works will be done in future publications.

References

[1] J. Ishikawa, J. Okano, K. Ohki, A. Amagai, Y. Maeda, and H. Miyata. Phagocytosis of Dictyostelium discoideum studied by the particle-tracking method. *Experimental Cell Research*, 288(2):286–276, 2003.

[2] I. Roitt, J. Brostoff, and D. Male. *Immunology.* Mosby International Ltd., 1998.

[3] F. I. Comer and C. A. Parent. PI 3-Kinases and PTEN: How Opposites Chemoattract. *Cell*, 109:541–544, 2002.

[4] T. D. Pollard. The cytoskeletion, Cellular Motility and the Reductionist Agenda. *Nature*, 422:741–745, 2003.

[5] T. D. Pollard and G. G. Borisy. Cellular Motility Driven by Assembly and Disassembly of Actin Filaments. *Cell*, 112:453–465, 2003.

[6] M. Iijima, Y. E. Huang, and P. Devreotes. Temporal and Spatial Regulation of Chemotaxis. *Dev. Cell*, 3:469–478, 2002.

[7] A. B. Verkhovsky, T. M. Svitkina, and G. G. Borisy. Self-polarization and Directional Motility of Cytoplasm. *Curr. Biol.*, 9:11–20, 1999.

[8] A. Levchenko and P. A. Iglesias. Models of Eukaryotic Gradient Sensing: Application to Chemotaxis of Ameobae and Neutrophils. *Biophys. J.*, 82:50–63, 2002.

[9] S. I. Nishimura and M. Sasai. Inertia of amoebic cell locomotion as an emergent collective property of the cellular dynamics. *Phys. Rev. E.* in press.

The Tenth International Symposium on Artificial Life and Robotics 2005(AROB 10th '05),
B-con Plaza, Beppu, Oita, Japan, February 4-6, 2005

A Controller Design Method for an Articulated Vehicle Employing Self-Oraganizing Relationship(SOR) Network

Takanori Koga, Keiichi Horio, Takeshi Yamakawa
Graduate School of Life Science and Systems Engineering
Kyushu Institute of Technology
2-4 Hibikino, Wakamatsu-ku, Kitakyushu-shi, Fukuoka, 808-0196, Japan

Abstract

In this paper, we design a trailer-truck back-up controller by using the Self-Organizing Relationship (SOR) network with fuzzy inference based evaluation. The proposed method facilitates embedding designers' know-how and observation-based knowledge to controller design. Furthermore, the controller designed by using proposed method is robust against physical parameter variation.

1 Introduction

Trailer-truck back-up control is very difficult even for expert drivers as well as non-experts, because the mechanism of the trailer-truck includes nonlinearities and instabilities. Besides, the control has to be achieved while avoiding an uncontrollable state called jackknifed-state. Therefore, trailer-truck back-up control is well-known benchmark in the field of nonlinear control. Generally, the controllers are designed by using nonlinear control theories[1] or soft-computing techniques[2][3]. In the former method, mathematical model of the trailer-truck and advanced mathematical knowledge are required. In the latter one, typical methods are based on neural networks and rule-based fuzzy controls. However, correct I/O relationship (*i.e.* supervisor) of the controller is required for learning of neural networks. A detailed knowledge of the I/O relationship has to be given by experts to design rule-based fuzzy controllers. In addition, fine adjustment of the fuzzy if-then rules is required. It means that, to design the trailer-truck back-up controller using traditional methods are difficult for non-expert designers.

In this paper, we design the trailer-truck back-up controller employing the Self-Organizing Relationship (SOR) network[4]. The SOR network is effective when the desired I/O relationship of the controller is not available but can be evaluated. The desired I/O relationship is extracted by learning of the SOR network using I/O vectors and their evaluations. The evaluation of the I/O vectors should be given quantitatively when the SOR network is applied to control problems. However, it is difficult to represent an evaluation function for the I/O vectors of SOR network in complicated applications such as trailer-truck back-up control. In order to calculate the evaluation values for the I/O vectors without mathematical evaluation functions, we propose a new method in which a fuzzy inference is used. In proposed method, designers' know-how and observation-based knowledge can be embedded to the evaluation of the controllers I/O relationship. Therefore, the knowledge-based controller can be designed easily by using the SOR network with fuzzy inference based evaluation.

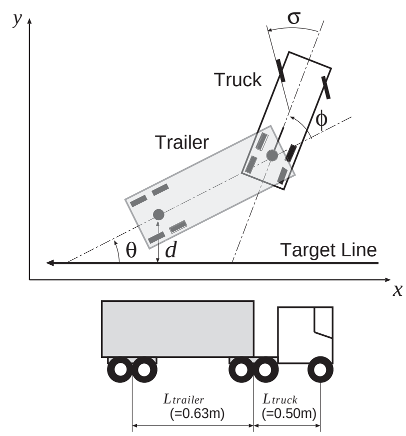

Figure 1: *Model of the semi-trailer.*

2 Trailer-Truck Back-Up Control

The model of the semi-trailer type trailer-truck used in this paper is shown in Fig.1. The control objective is to make the trailer-truck follow a straight target line only backward movement at constant velocity from various initial states. In other words, a 3-input-1-output regulator should be designed. The inputs are the connection angle between trailer and truck ϕ, the angle of the trailer θ and the distance between the

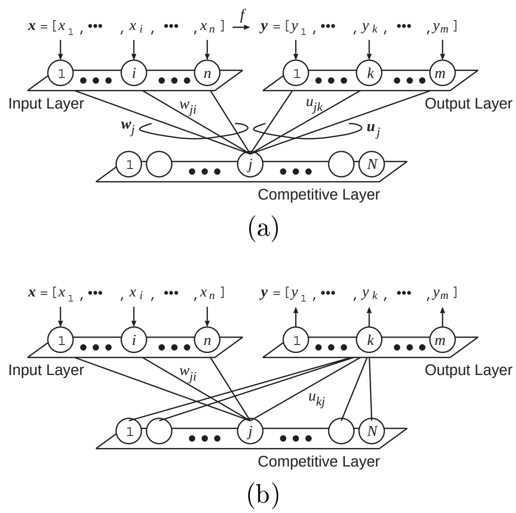

Figure 2: *The structure of SOR network. (a)Learning mode, (b)Execution mode.*

trailer-truck and the target line d, and, the output is the front wheel angle of truck σ.

3 Controller Design

3.1 The SOR Network

The SOR network[4] consists of the input layer, the output layer and the competitive layer, in which n, m, and N units are respectively included as shown in Fig.2. The j-th unit in the competitive layer is connected to the units in the input and the output layers with weight vectors respectively. The network can be established by learning in order to approximate the desired I/O relationship of the object system. The SOR network has two modes, learning mode and execution mode. In learning mode (Fig.2(a)), the random I/O vectors are applied as learning vectors, to the input and the output layers together with the evaluation for the I/O vector pair. The evaluation may be assigned by the network designer, given by the intuition of the user or obtained by examining the system under test. The value of evaluation is positive and negative in accordance with judgment of the designer, preference of the user or score of examination. The positive causes the self-organization of attraction to the learning vector and the negative one does that of repulsion from the learning vector. The weight vectors are arranged in area where desired I/O vector pairs exist by learning. After the learning the SOR network is ready to use as the I/O relationship generator in execution mode (Fig.2(b)). The output of the network represents the

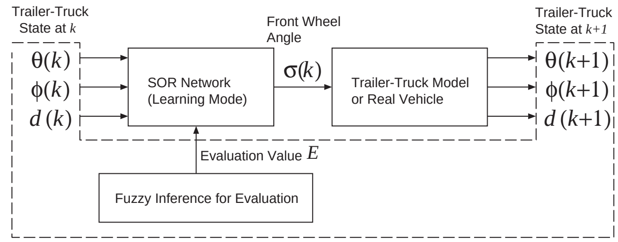

Figure 3: *Data acquisition and evaluation process.*

weighted average of output vectors by the similarity measure between the reference vector and the actual input vector.

3.2 Data Acquisition and Evaluation

In computer simulation, it is assumed that the kinematics model of the trailer-truck is given. Fig.3 shows procedure of learning vectors acquisition. At first, the state of the trailer-truck at k $(\phi(k), \theta(k), d(k))$ is randomly given. Then, front wheel angle $(\sigma(k))$ is randomly given as an operation at state k. These values are elements of the learning vectors. As a result of operation, the state at $k+1$ is calculated using kinematics model. The designer should evaluate the I/O relationship of the controller with fuzzy inference by observing the state at k and $k+1$. The antecedent variables of the fuzzy inference are the state of the trailer-truck $(\phi(k), \theta(k), d(k))$ at k, and the consequent variable is the decreace of the error between state k and $k+1$. The decreace of the error is normalized and its range is from -1 to 1. These fuzzy if-then rules are constructed based on four fundamental control strategies given by designers' commonsense.

(Strategy 1) If the connection angle ϕ is large, it should be decreased to avoid jackknifed-state.

(Strategy 2) If the trailer-truck is directed away from the target line, the direction should be corrected to meke the trailer-truck approach the target line.

(Strategy 3) If the trailer-truck move in a direction opposite to the target direction, the direction should be corrected to meke the trailer-truck move in the target direction.

(Strategy 4) If the control strategies 1-3 are satisfied, the trailer-truck should be controlled to follow the target line while regulating both the distance d and the angle θ.

Particularly, the strategy 1 is most important, because the trailer-truck should be controlled while avoiding falling into uncontrollable state. These strategies are represented by fuzzy if-then rules and fuzzy membership functions shown in Fig.4(a)(b).

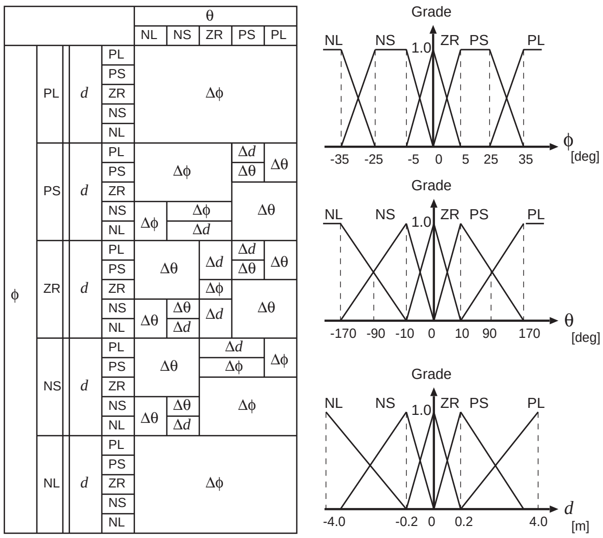

(a) (b)

Figure 4: *Fuzzy if-then rules for evaluation. (a)Rule table. (b)Membership functions. The consequent variables $\Delta\phi$, $\Delta\theta$, Δd represents normalized decrease of error between state k and $k+1$.*

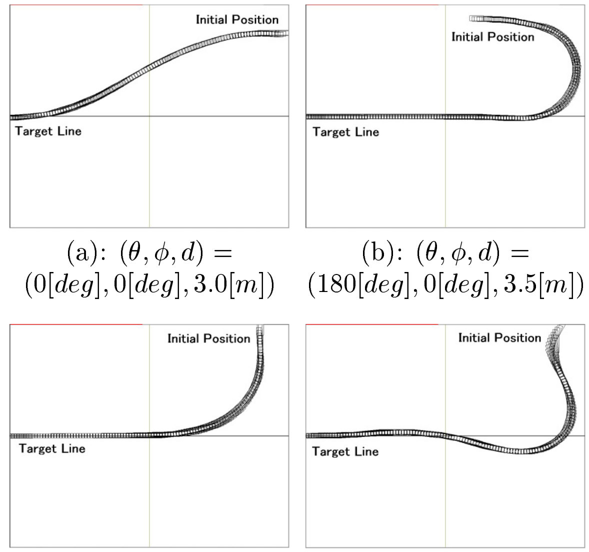

(a): $(\theta, \phi, d) = (0[deg], 0[deg], 3.0[m])$
(b): $(\theta, \phi, d) = (180[deg], 0[deg], 3.5[m])$
(c): $(\theta, \phi, d) = (90[deg], 0[deg], 3.0[m])$
(d): $(\theta, \phi, d) = (90[deg], -30[deg], 3.0[m])$

Figure 5: *Simulation results from various initial states.*

3.3 Learning of SOR network

As the learning vectors, 50000 vectors are acquired and evaluated by the proposed method. For details of learning process, refer to references [4][5].

4 Simulation Results

Simulation results are shown in Fig.5. In each figure, the lengths of the work space are 10.0m and 8.0m for the x and y axes, respectively. The trailer-truck is controlled to satisfy the control objective from the various initial states while avoiding jackknifed-state. Fig.6 shows that the time series of the I/O variables of controller in case of Fig.5(c). It should noted that the trailer-truck-specific operation "countersteering" is achieved at the beginning of the control, though details of the operation were not supervised in evaluation process.

Generally, the difficulty of the trailer-truck back-up control mainly relies on variation of the length ratio between trailer and truck. To verify the robustness of the controller against length ratio variation, some trailer-trucks with different length ratio are controlled by the controller which is designed for the trailer-truck with length ratio $L_{trailer}/L_{truck} = 1.26$. The values of length ratio are, 0.75, 1.0, 1.26, 1.50, 1.75, 2.0. Fig.7 shows trajectories in phase space. The controller is stable for the range from 1.26 to 2.0 though the overshoot becomes large as the ratio increases. On the other hand, the controller is unstable for the ratio 0.75, and the trailer-truck fell into jackknifed-state. In case that the ratio is 1.0, the controller is narrow stable. This is because the back-up control becomes difficult as the trailer length becomes short. In case that the ratio takes off significantly, the controller should be re-designed.

5 Practical Experimental Results

In the experimental system, the coordinates of three markers attached to trailer-truck are detected by CCD cameras and motion capture system. In the PC, the angles ϕ, θ and the distance d are calculated and the front wheel angle σ (*i.e.* the output of the SOR network) is calculated. The weight vectors of the SOR network used in the experiment are the same to those used in the computer simulation. Fig.8 shows the experimental result. Each picture was taken every five seconds. The black line in the figures is the target line. The initial values of the distance and angles are $\phi = 0$[degree], $\theta = 135$[degree], and $d = 2.5$[m] as shown in Fig.8 (a). The angle of the trailer becomes smaller and the trailer-truck follows the target line finally. In cases of other initial values, it is confirmed that the trailer-truck can follow the target line.

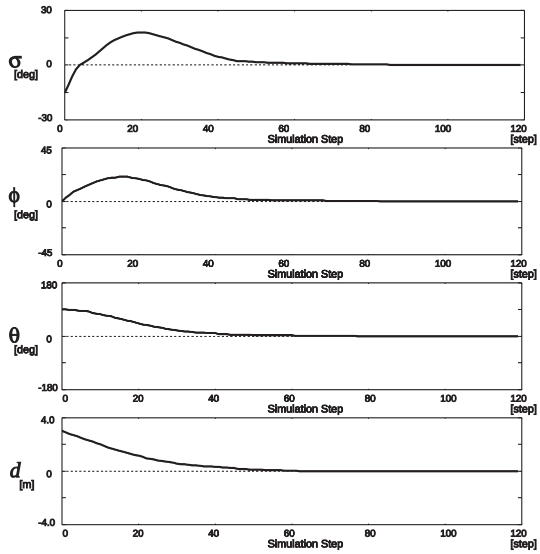

Figure 6: *Time series of I/O variables of controller.*

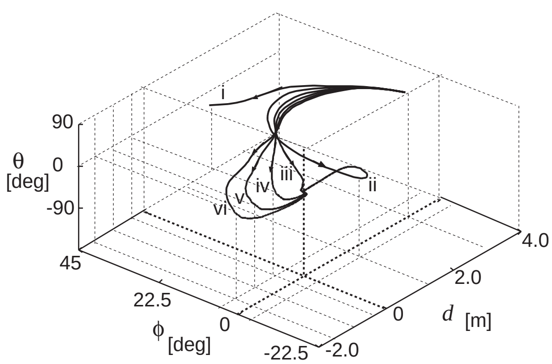

Figure 7: *Trajectories in phase space. Initial state:* $(\phi, \theta, d) = (0[deg], 90[deg], 3.0[m])$. *The length ratio=* $i : 0.75$, $ii : 1.0$, $iii : 1.26$, $iv : 1.50$, $v : 1.75$, $vi : 2.00$.

6 Conclusion

In this paper, we proposed a controller design method for trailer-truck back-up control by using SOR network with fuzzy inference based evaluation. The back-up controls both in computer simulations and practical experiments are successfully achieved by using the proposed method. The controller design is achieved with only common sense (special knowledge of experts is not needed) which is used for evaluating I/O relationship. Furthermore, the controller designed by the proposed method is robust against physical parameter variation of the trailer-truck.

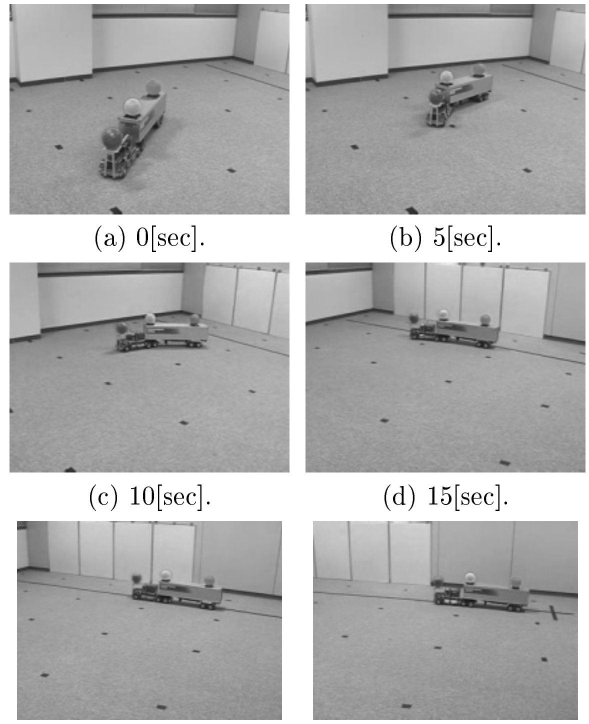

(a) 0[sec]. (b) 5[sec].

(c) 10[sec]. (d) 15[sec].

(e) 20[sec]. (f) 25[sec].

Figure 8: *Practical experimental result. Initial state:* $(\theta, \phi, d) = (135[deg], 0[deg], 2.5[m])$

References

[1] M. Sampei, T. Tamura, T. Kobayashi and N. Shibui, "Arbitrary path tracking control of articulated vehicles using nonlinear control theory," *IEEE Trans. on Control Systems Technology*, Vol.1, No.4, pp.587-592, 1995.

[2] D. Nguyen and B. Widrow, "The truck backer-upper: an example of self-learning in neural nerwork," *Proc. of IJCNN'89*, pp.357-363, 1989.

[3] S.G. Kong and B. Kosko, "Adaptive fuzzy-systems for backing-up a truck-and-trailer," *IEEE Trans. on Neural Networks*, Vol.3(2), pp.211-223, 1992.

[4] T. Yamakawa and K. Horio, "Self-organizing relationship (SOR) network," *IEICE Trans. on Fundamentals*, Vol.E82-A, pp.1674-1678, 1999.

[5] T. Koga, K. Horio and T. Yamakawa, "Self-Organizing Relationship (SOR) Network with Fuzzy Inference Based Evaluation and Its Application to Trailer-Truck Back-Up Control," *Proc. of ICONIP 2004*, pp.368-374, 2004.

The Tenth International Symposium on Artificial Life and Robotics 2005(AROB 10th '05),
B-con Plaza, Beppu, Oita, Japan, February 4-6, 2005

Automatic control of an Electric Vehicle using visual information

Koji TOKUDA, Masanori SUGISAKA, MBAITIGA Zacharie
Dept. of Electrical and Electronic Engineering, Oita University
700 Dannoharu Oita 870-1192 Japan
Email : *msugi@cc.oita-u.ac.jp*

Abstract

The aim of this research is to realize automatic control of an Electric Vehicle (EV), which the line ahead of the EV is detected by CCD camera and EV is made to follow the line. In this paper, image processing for line detection and calculation of a steering angle is described. For the method of line detection, edge detection forms the grayscale image. Then, both edges of the line are extracted using Hough transformation.

1. Introduction

In recent years, serious traffic problems, such as traffic accident and traffic congestion, have been encountered by the automotive society. Then, research of ITS (Intelligent Transport Systems) is made to improve and solve the traffic problems. Because of that, the research on automatic operation of a car manage attracts attention. Driver operation support and automatic operation can prevent the accident by artificial control.

Automatic control of a small recognition vehicle has been studied in this laboratory [1][2]. Research of the next stage of automatic operation of a car, the aim of this research is to realize automatic control of an Electric Vehicle (EV), which the line ahead of the EV is detected by CCD camera and EV is made to follow the line.

In this research, image processing for line detection and the compensation for deriving a steering angle is stated.

In this paper, by using EV system composition, image processing for line detection, the EV experiment is described.

2. Overview of the EV

The composition of the EV used in this research is explained. The EV use for our experiment "MINI-SWAY" and is produced by DAIHATSU Company. The "MINI-SWAY" shown in figure 1 is 1,010[mm] of overall width, 2,395[mm] of overall length, and 1,490[mm] of overall height. In order to control from the computer, the EV was improved with accelerator brake and handle by DENKEN. The stepping motor (CSK543AP-TG20, CSK564AP-TG20) are used for an accelerator and a brake. AC servo motor (SGM-01B314) is used for the Steering. The CCD camera is attached to on the top the EV. In order to control the EV, there are two computers located in the EV body particularly in the trunk. The computer for image processing is equipped with the capture card (FDM-PCIIII) and a video frame received form the camera capture card has size of 640×480 pixels which 640 pixels represent the height of the image and 480 pixels represent the width of the image respectively are in RGB format. The computer for driving is equipped with the motor controller board and each motor operation using the data from computer for image processing.

Fig.1 Electric Vehicle

3. Image processing for line recognition

In order for EV to carry out an autonomous travel, the position of EV on the road is recognized and it is required to carry out steering operation using the information. Then, the purpose of the computer for image processing is the target line which it is marked on the road is recognized. Next, the steering is operated based on the recognized line.

3.1 The recognition method

Line recognition was performed using hue and saturation of a HLS table color system. However, the method was not stabilized when disturbance occurred such as light, and has not being able to recognize the target line. In order to be stabilized and to perform line recognition, processing using the edge produced of both edges of the line is performed.

3.2 Reduction of the image and Grayscale image

The input image from the camera is 640×480 pixels. Therefore, an input image is reduced in order to shorten processing time. The input image is scanned at intervals of 2 pixels, and it reduces to 320×240 pixels. Next, in order to perform edge processing, reduced image is converted to a grayscale image as equation (1).

$$Grayscale\_image = (222 \cdot r + 707 \cdot g + 71 \cdot b)/1000 \quad (1)$$

3.3 Edge detection

The white line on a road produces the edges which clarify the edges of the line. The Sobel filter of the transverse direction of primary differentiation is used for edge detection. Using this method, both edges of line can be emphasized and the edge produced in the road is reduced. The detected edge using the Sobel filter is shown in figure 2.

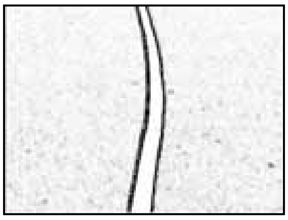

Fig.2 Edge detection result

3.4 Straight line detection

Not only the edge produced to the both edges of the line but the other edge, such as edge produced on the road surface, is remained in the image which had edge detected. In order to extract only the edge produced to both edges of the line, straight line is extracted using Hough transformation. Two straight lines are extracted. Conversion in polar coordinates can be obtained using equation (2). Reverse conversion in rectangular coordinates can be obtained using equation (3).

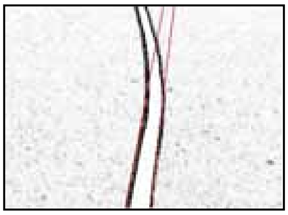

Fig.3 The straight line extraction result using Hough transformation

$$\rho = xi\cos\theta + yi\sin\theta \quad (2)$$

$$y = -\frac{\cos\theta}{\sin\theta}\cdot x + \frac{\rho}{\sin\theta},\; x = -\frac{\sin\theta}{\cos\theta}\cdot x + \frac{\rho}{\cos\theta} \quad (3)$$

When the target line is straight, the both edges of the straight line can be extracted using Hough transformation. However, when the target line has curved, two obtained straight lines using Hough transformation may miss the target. Such a problem is solved by regional division. The straight line extraction result using Hough transformation is shown in figure 3.

3.5 Code area

When extracting the center of gravity coordinates of a line, code area is limited and processed.

The code area in width is made within of 60~89 pixels and 120~149 pixels. The code area in depth depends on center of gravity coordinates in the previous one. For example, when the center of gravity coordinates (x,y) are acquired, next code area in width is immovable and next code area in depth is taken as the range of x-50 and x+50 pixels. This is because the target line is continuity and it does not have a sudden curve. The center of gravity coordinates of a line can be searched by using this method. Moreover, even if strong edge other than a line exists on the road, only the edge of both edges of the line can be extracted. In each code areas, a target line can be regarded as a straight line, when Hough transformation is performed, the straight line of both edges can be obtained correctly.

The same method is used even when there is a target line. The code area is shown in figure 4.

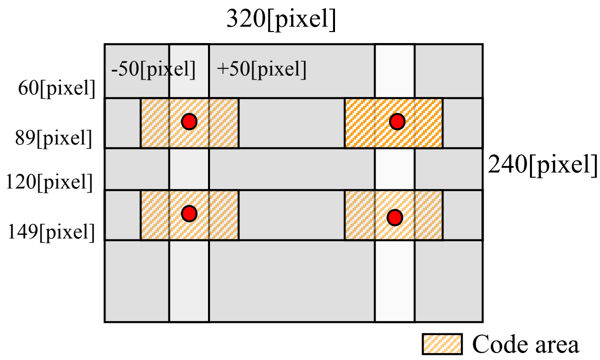

Fig.4 Code area

3.6 Experimental result for the center of gravity coordinates

The extraction result for center of gravity coordinates in case of one target line and two target lines is shown in figure 5 and 6. The center of gravity coordinates can also be acquired by one target line, or two target lines.

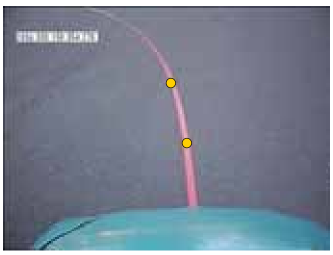

Fig.5 The extraction result for one target line

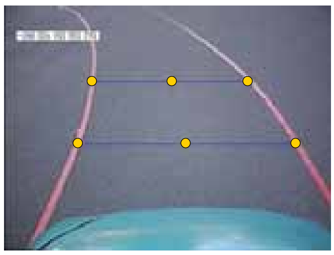

Fig.6 The extraction result for two target line

4. Robust design

Image data tends to be influenced by disturbance. In the steering operation using image data, wrong image processing will cause big accidents. Moreover, since the code area of the inputted image is divided and the target line is extracted. If it fails, it cannot return to the reference code area. Then, the image processing is made robust to disturbance.

4.1 Evaluation algorithm

The center of gravity coordinates for a code area is considered. The Center of gravity coordinates change because the EV moves. Therefore, the next center of gravity coordinates can be expected from the old center of gravity coordinates. In order to calculate a quadratic approximation curve, least-squares method is used. It is based on the old center of gravity coordinates which has being acquired correctly. And, the following center of gravity coordinates are evaluated. The evaluation method configures a certain fixed deviation from the center of gravity coordinates expected.

The x-coordinate (xi) of the center of gravity coordinates acquired from image data is called actual measurement. And, (x_{i_Pre}) from the x-coordinate of the old the center of gravity coordinates is called predictive value. When the actual measurement (x_i,t_i) in Time t is obtained, the predictive value (x_{i_pre},t_{i_Pre}) is calculated on the basis of actual measurement (x_{i-1},t_{i-1})~(x_{i-5},t_{i-5}), and the actual measurement (x_i,t_i) is evaluated. If the acquired coordinates are successful, a quadratic approximation curve is updated, and next the center of gravity coordinates acquired are evaluated. When the actual measurement (x_{i+1},t_{i+1}) in Time t+1 is obtained, the predictive value (x_{i_pre},t_{i_Pre}) is calculated on the basis of actual measurement (x_i,t_i)~(x_{i-4},t_{i-4}), and the actual measurement (x_{i+1},t_{i+1}) is evaluated. If the acquired coordinates are successful, a quadratic approximation curve is updated. The width of an evaluation value is set as −25 pixels~25 pixels and center of gravity coordinates are evaluated. If the acquired coordinates are s fails, a steering angle is calculated from the predictive value. Thus, the evaluation is repeated.

4.2 Return algorithm

A code area is returned using the evaluation method which described the point. If the acquired center of gravity coordinates are over the width of evaluation, center of gravity coordinates may be recognized incorrectly by disturbance. When the next code area is set up from the center of gravity coordinates, the true center of gravity coordinates are no longer acquired. Then, if the acquired center of gravity coordinates exceed the width of evaluation, the next code area is decided from the predictive value. And the code area is set up with ±65 pixels from the prediction value. The algorithm of the return to the code area is shown in figure 7.

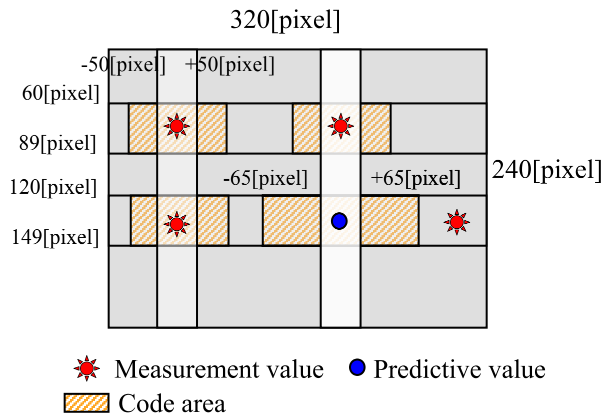

Fig.7 Code area of return algorithm

5. Steering control

5.1 Steering angle

In order to determine a steering angle from image data, the principle of "Method of the move target point following" [4] is used. Coordinates (x_1,y_1) are made into the target point of the EV among the center of gravity coordinates (x_1,y_1) and(x_2,y_2) acquired from the image. At this time, the steering angle δ of the EV is calculated on the basis of the position (x_1,y_1) and the target direction θ of the EV in the position from the move coordinate system.

$$\delta = \arctan 2l(3 \times y_1 - x_1 \times \tan\theta) / x_1^2 \tag{4}$$

It changes into a move coordinate system from the acquired coordinates.

$$X\_real\_coordinate[mm] = \frac{-10.32 \times y_1 + 5733}{640} \times x\_pixel\_length \tag{5}$$

$$Y\_real\_coordinate[mm] = 16.5 \times y\_pixel\_length \tag{6}$$

$$x\_pixel\_length[pixel] = |x_1 - 319| \tag{7}$$

$$y\_pixel\_length[pixel] = |479 - y_1| \tag{8}$$

$$l = 1500[mm]\text{: Wheel base} \tag{9}$$

A steering angle is calculated as the equation (4), and a pulse required for a steering angle is also calculated. The equation (10) changed into a pulse is from experiment data.

$$Pulse = 3360.3 \times steering\_angle(\delta)\ [\mathrm{deg}] \quad (10)$$

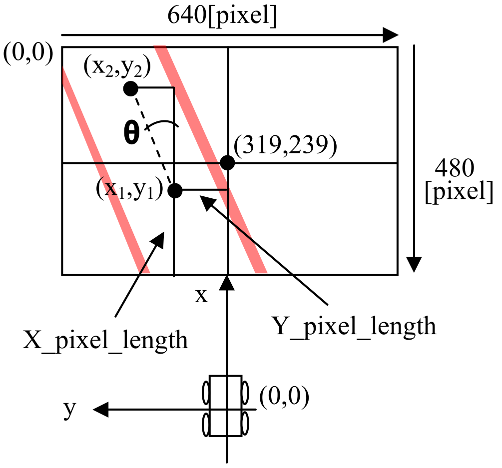

Fig.8 Relation between the EV and the target point

5.2 Steering operation

AC servomotor used for the handle is operated for continuation. And, the rotation direction is determined from the target pulse which is being received from the image data. For example, when the servomotor is carrying out the right rotation, If the target pulse transmitted from the PC for image processing is larger than the present pulse, the rotation direction of the servomotor is maintained, if the target pulse transmitted from the PC for image processing is smaller than the present pulse, the rotation direction of the servomotor is reversed.

6. Run experiment of EV

6.1 Experiment method

The experiment use recognition and steering operation of a target line. In an experiment, A target line is arranged to position forward right of vehicles, the EV is controlled automatically to follow the target line. However, the experiment performed the operation of the accelerator and the brake, and the speed is fixed at low speed. The EV and a target line are shown in figure 7.

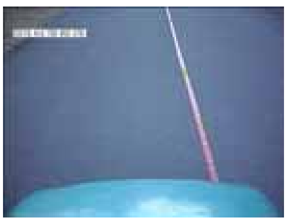

Fig.9 EV and a target line

6.2 Experimental result

As for an initial position, the target line is located at 750 [mm] from the center of the EV. The EV is driven in a zigzag from the start to about 45[s]. The result shows the deviation from the center of the EV is about 50~100[mm]. The line width was 100 [mm], EV is able to run on the line. Even if a target line is in the both ends of a road, the same result can be obtained.

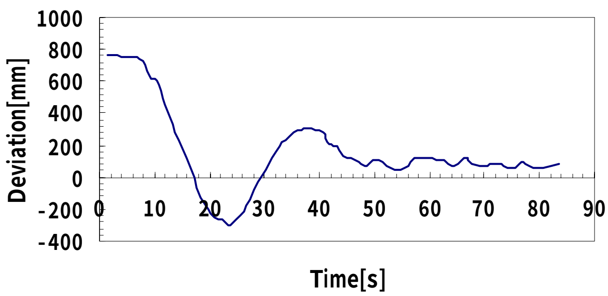

Fig.10 The deviation from the center of the EV

7. Conclusion

The stable the target point can found by replacing the line recognition using color information with the line edge.

In cruise Control, a target line is arranged in the center of a road. Although the deviation from the center of the EV was not 0[mm], it was able to run on the line. But then, the EV is driven in a zigzag until it converges, the cruise control of the EV has been improved.

References

[1]Daisuke Matsumoto, “Run control of a move recognition vehicle”, Oita University Graduate School Master Paper, 1997 (In Japanese)

[2]Osamu TAKADA, “Development of the steering control system of the move recognition vehicle”, Oita University Graduate School Master Paper, 1998 (In Japanese)

[3]Kouichi SAKAI, “A guide to digital image processing”, CQ publication, 2002 (In Japanese)

[4]Hiroaki MORI, Shin KATO, Sadayuki TSUGAWA, “A Lateral Control Algorithm for a Vision-Based Vehicle with a Moving Target in the Field of View”, JOURNAL OF MECHANICAL ENGINEERRING LABORATORY, Vol.53, July 1999, No.4 (In Japanese)

[5]MBAITIGA Zacharie, “IMAGE PROCESSING AND NETWORK COMMUNICATION FOR ELECTRIC VEHICLE”, Oita University Graduate School Master Paper, 2002

The Tenth International Symposium on Artificial Life and Robotics 2005(AROB 10th '05),
B-con Plaza, Beppu, Oita, Japan, February 4-6, 2005

Mobile sensor device in Intelligent Space

H. Isu, T. Sasaki, H.Hashomoto
Institute of Industrial Science, University of Tokyo
Tokyo, 153-8505 (Email: isu@hlab.iis.u-tokyo.ac.jp)

Abstract

In this research, we propose mobile sensor device in Intelligent Space. Intelligent Space, that is our recent research topic, is the system consistituted of distributed sensor devices and robots agents. We focuse on the capabiility of sensor devices which are mainly CCD cameras for acquisition of position information of the object in Intelligent Space.

In this paper, we tried to the estimation of position and posture of mobile distributed sensor device in Intelligent Space. This mobile sensors are for extension of technologies for Intelligent Space in scalability and so on. The estimation method is solving Perspective n Points problem on camera device on the device. Then, we describe the measuring experiments of the objects in Intelligent Space briefly.

Keyword

Intelligent Space, position estimation, camera calibration, Perspective n Points Problem

1 Introduction

This research is about mobile sensors in Intelligent Space[1][2]. Intelligent Space is a kind of platform that serves users through the robots connected the space based on the information from distributed sensor devices. In the recent research, these sensor devices have been realized with general CCD cameras and computers as vision processing system. This is mainly because we assume the services that Intelligent Space will offer are based on the users' and the robots' (received the directions from the space) position information and vision sensors system is very useful and reasonable for this purpose. We note this point, and so purpose mobile sensor device as a technique for acquiring more detailed position information of the objects in Intelligent Space.

To achieve mobile sensor device, first, we will purpose the method of estimation of the position and posture of mobile sensor device. To provide position information of the objects, it is necessary to obtain the sensor's own position and posture information. In this research, in order to construct simple system, we estimate the status of the device by solving Perspective n Points (PnP) problem of camera on the device. This is an appreciate approach is for employing the advantage of Intelligent Space that the information of the space is given as world coordination. In this reserach, we try the methods whose perspective points is 3 and 4. But in this paper, we will describe the metod using P4P problem solution only. Then, we will describe position measurement method of the objects. This is the method in the past researches.

2 Mobile Sensor

As we mentioned above, disributed sensor device in Intelligent Space acts for localization. Since our system uses CCD camera, to provide accurate position information of the object, camera position is necesary. We have researched on evaluation of camera arrangement [2], but we have treated simple environment. To intellectualize more complicated environment, we need to consider more dynamic system. Then, we propose mobile sensor device in Intelligent Space.

The proposal will bring other some merits. For example, since we consider that tracking or trace of the object is basic action of the robots in Intelligent Space, mobility of the sensor will make those task more easily. and, mobile sensor device may make the task which needs more accuracy, such as face or gesture recognition, more easier.

To realize mobile sensor device, we consider the camera self-localization. This is neccesary to cooperate with other distributed sensor device that is basis of Intelligent Space.

The Tenth International Symposium on Artificial Life and Robotics 2005(AROB 10th '05),
B-con Plaza, Beppu, Oita, Japan, February 4-6, 2005

3 Self-position estimation of the mobile sensor using its camera system

3.1 Estimation method

In this research, in order to construct the simplest system, we estimate the status of the device by solving Perspective n Points (PnP) problem of camera on the device by numerical method. PnP problem is the problem to solve the position and posture of camera using the pixel value of n points whose position in world coordinate system.

There are some reasons for using PnP Problem following;

1. The amount and time of computation is stable
2. Estimation error is predictable
3. Easy to realize

1. is fulfilled by taking numerical method and using a small number of landmarks as perspective points. The number of landmarks is related to 3., . The least number for solving PnP Problem is three, but in case using P3P problem the estimation error is too large. Then, in this paper, we abridge the approach using P3P Problem solution and discribe the approach of Perspective 4 Points Problem (P4P Problem). 2. is the one of the merits of this approach.

3.2 P4P Problem of on-board camera

In this paragraph, we describe the simplified P4P problem solution as the sensor device position estimation. To simplify the solution, we assume that;

- Distortion of CCD camera can be ignored.
- Internal parameters of the system (focus length, center of vision, etc) is known.
- Position and posture of sensor device are determined unique if the exteranal camaera paremeters are determined.

The transfer equation from world coordinate system $[x_c\ y_c\ z_c]^T$ to camera coordinate syetem $[x_w\ y_w\ z_w]^T$ is as followed[3](Fig:1);

$$\tilde{c} = M\tilde{w} \tag{1}$$

where M is

$$M = \begin{bmatrix} m_{11} & m_{12} & m_{13} & m_{14} \\ m_{21} & m_{22} & m_{23} & m_{24} \\ m_{31} & m_{32} & m_{33} & m_{34} \\ 0 & 0 & 0 & 1 \end{bmatrix} = \begin{bmatrix} & R & & T \\ 0 & 0 & 0 & 1 \end{bmatrix}$$

where R is 3×3 rotation matrix

$$R = \begin{bmatrix} m_{11} & m_{12} & m_{13} \\ m_{21} & m_{22} & m_{23} \\ m_{31} & m_{32} & m_{33} \end{bmatrix} \tag{2}$$

and T is translation vector

$$T = \begin{bmatrix} m_{14} & m_{24} & m_{34} \end{bmatrix}^T \tag{3}$$

and $\tilde{c}$, $\tilde{w}$

$$\tilde{c} = \begin{bmatrix} x_c & y_c & z_c & 1 \end{bmatrix}^T,\ \tilde{w} = \begin{bmatrix} x_w & y_w & z_w & 1 \end{bmatrix}^T$$

Using orthogonal property of R, the following equation;

$$\sum_{k=1}^{3} m_{km}^2 = 1 \tag{4}$$

$$\sum_{k=1}^{3} m_{km} m_{kn} = 0 \tag{5}$$

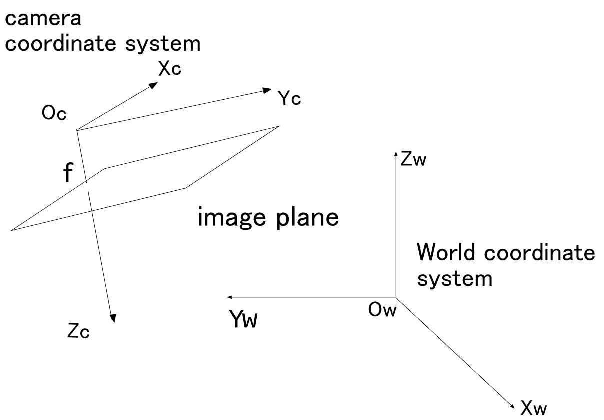

Figure 1: Coordinate system

Transformation from camera coordinate system to vision coordinate system is as followed[3];

$$\begin{bmatrix} x_p \\ y_p \end{bmatrix} = \frac{f}{z_c} \begin{bmatrix} x_c \\ y_c \end{bmatrix} \tag{6}$$

Since we have assumued that the internal parameters of the camera is known, we could easily obtain the transformation from vision coordinate to pixel value in vision. This transformation is depend on the value of internal and external parameters of camera, then landmarks whose position is known in world coordinates system and vision coordinates system will determine the unknown parameters.

Four landmarks used for self position estimation shall arranged on the same plane. At this time, conversion that is made the plane into $z_w = 0$ exitsts, then generality is not lost as $z_w = 0$.

Since equation(1) and equation(6),

$$x_{ip} = f\frac{m_{11}x_{iw} + m_{12}y_{iw} + m_{14}}{m_{31}x_{iw} + m_{32}y_{iw} + m_{34}} \quad (7)$$

normalized with m_{34}, the previous equation is equal to;

$$x_p = fm'_{11}x_w + fm'_{12}y_w + fm'_{14} - m'_{31}x_wx_p - m'_{32}y_wx_p$$

and through the same procrdure about y_p,

$$y_p = fm'_{21}x_w + fm'_{22}y_w + fm'_{24} - m'_{31}x_wy_p - m'_{32}y_wy_p$$

Then, that two equations for four landmarks $[x_{iw}\ y_{iw}\ 0]^T$ $(i = 1, 2, 3, 4)$ are shown as;

$$\begin{bmatrix} x_{1w} & y_{1w} & 1 & 0 & 0 & 0 & -x_{1p}x_{1w} & -x_{1p}y_{1w} \\ x_{2w} & y_{2w} & 1 & 0 & 0 & 0 & -x_{2p}x_{2w} & -x_{2p}y_{2w} \\ x_{3w} & y_{3w} & 1 & 0 & 0 & 0 & -x_{3p}x_{3w} & -x_{3p}y_{3w} \\ x_{4w} & y_{4w} & 1 & 0 & 0 & 0 & -x_{4p}x_{4w} & -x_{4p}y_{4w} \\ 0 & 0 & 0 & x_{1w} & y_{1w} & 1 & -y_{1p}x_{1w} & -y_{1p}y_{1w} \\ 0 & 0 & 0 & x_{2w} & y_{2w} & 1 & -y_{2p}x_{2w} & -y_{2p}y_{2w} \\ 0 & 0 & 0 & x_{3w} & y_{3w} & 1 & -y_{3p}x_{3w} & -y_{3p}y_{3w} \\ 0 & 0 & 0 & x_{4w} & y_{4w} & 1 & -y_{4p}x_{4w} & -y_{4p}y_{4w} \end{bmatrix} \begin{bmatrix} fm'_{11} \\ fm'_{12} \\ fm'_{14} \\ fm'_{21} \\ fm'_{22} \\ fm'_{24} \\ m'_{31} \\ m'_{32} \end{bmatrix}$$
$$= \begin{bmatrix} x_{1p} & x_{2p} & x_{3p} & x_{4p} & y_{1p} & y_{2p} & y_{3p} & y_{4p} \end{bmatrix} \quad (8)$$

Since this equation and focus length f, m'_{11}, m'_{12}, m'_{14}, m'_{21}, m'_{22}, m'_{24}, m'_{31}, m'_{32} can be calulated.

On the other hand, since equation(5),

$$\sum_{k=1}^{3} m'_{km}m'_{kn} = 0 \quad (9)$$

then, m'_{13}, m'_{23}, m'_{33} are determined. Next, Since equation(4), m_{34} can be calculated. Then, the parameter of R and T is determined.

3.3 Computer simulation

We experimented the validity of the approach shown in the previous clause by computer simulation. The procedure of the experimetnt is following. We operated virtual mobile sensor device so that a spiral was drawn in the world coordinate system, and then, we obtained virtual picture from camera model. Next, based on the picture information, we apply the self-position estimation of the camera inthe preceding clauses.

Table1 is landmarks pattern used in this experience.

Table 1: Landmarks Pattern

landmark no.	1	2
position	(0.30 -1.0 0.0)	(-1.0 0.60 0.0)
landmark no.	3	4
position	(0.70 0.40 0.0)	(0.0 0.0 0.0)

The result of the experiment is shown Fig:2. Mean estimation error at eacch step was 10.2 cm.

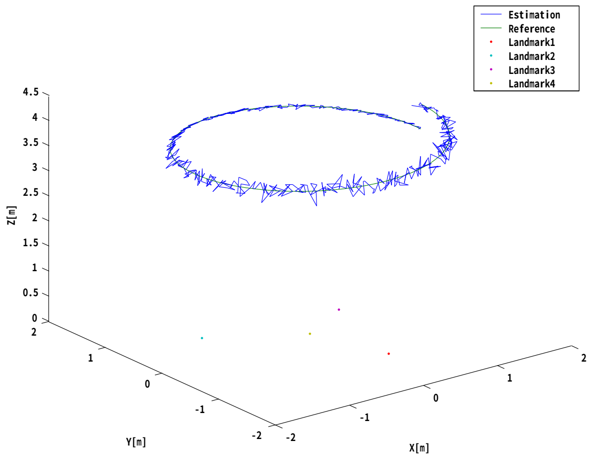

Figure 2: Self position estimation

4 Position mesurement of the object using the mobile sensor

The self-position estimation we described in the previous paragraph is for position measurement of some object (mobile robots or users) in intelligent space. In this paragraph, we show the position measurement experience of the robot whose height is known. Fig:3 is the result of computer simulation based on the self-positionestimation of the sensor in the previous paragraph.

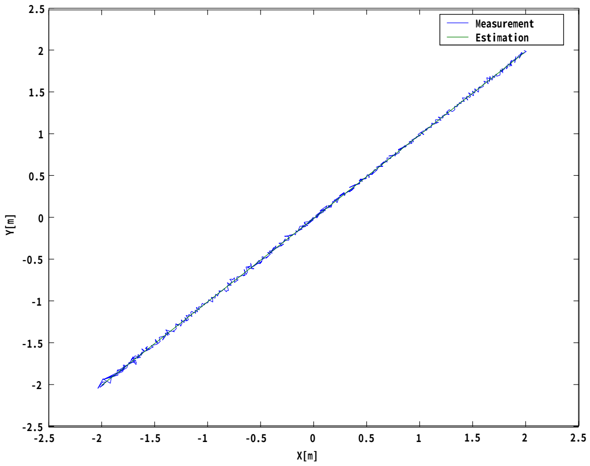

Figure 3: Measurement of the object position

In this case, mean measurement error at each step was 2.44 cm. The figure show this results is sufficient accurate for almost application we consider.

5 Summary

In this paper, we proposed the mobile sensor device in Intelligent Space, and described about self-position estimation of the mobile sensor required for the sensor to measure the position of the object. And we introduced the meaurement experiment of the object in Intelligent Space.

References

[1] J.H Lee, H.Hashimoto, "Intelligent Space - concept and contents," *Advanced Robotics*, Vol.16, No.3, pp.265-280, 2002.

[2] T.Akiyama, J.H.Lee, H.Hashimoto, "Evaluation of CCD Camera Arrangement for Positioning System in Intelligent Space," *Proc. of The seventh Int. Symp. on Artificial Life and Robotics (AROB 7th'02)*, pp.310-315, 2002.

[3] K.Deguchi, *Fundamental of Robot Vision*, CORONA PUBLISHING, 2002.

The Tenth International Symposium on Artificial Life and Robotics 2005(AROB 10th '05),
B-con Plaza, Beppu, Oita, Japan, February 4-6, 2005

Real-time Path Planning For Senor-based Mobile Robot Based On Probabilistic Roadmap Method

Zhiye Li Xiong Chen
Department of Electronic Engineering,
Fudan University, Shanghai, PRC
celletor@hotmail.com, chenxiong@fudan.edu.cn

Abstract

This paper presents a new real-time path planning approach, which is based on the algorithm of probabilistic roadmap, for senor-based mobile robot in unknown environments. The novel idea is that the algorithm changes the on-line navigation problem into off-line one, which makes the work simple. Once the path planning problem becomes finding a way in already known environment, we can use traditional PRM to solve it. Thus, our idea is to guide the robot to make real-time global route planning each step, during the whole planning process, so that the knowledge of the environment is updated gradually. Therefore, the problems of path planning in unknown environments is turned into the problem of that in already known environments in each step. The purpose of the new method is to build a path that not only is relatively the shortest, but also avoids the local minima and other problems effectively. Some experimental results are presented in this paper to strengthen the new proposal.

Key words Probabilistic roadmap, path planning

I, Introduction

There are two main branches dealing with the path planning problem for mobile robot. The first one is about looking for a path in a previously known environment map, in which we can use some fast and effective methods such as the Rapidly Exploring Random Trees (RRT), the Probabilistic Roadmap (PRM)[1,2,3]and the Artificial Potential Field (APF), etc. The second type is for sensor mounted mobile robot to generate a path in an unknown environment, and in this case, methods like Hierarchical Generalized Voronoi Graph (HGVG), BUG and APF have already been used. The problem we are discussing in this work belongs to the latter, that is, a robot equipped with sensors is given a task to move from a set beginning point to a goal, in a completely unknown environment.

To direct the robot to generate an effective path, Lumelsky have done great job on BUG algorithm, which is simple but practical in this problem, so is HGVG, raised by Choset and Burdick, however, both of these two may generate redundant paths. The APF algorithm is also effective in real time avoiding obstacles and planning paths, but it has to face the local minima problem, which may cause the oscillation of the path. Because each approach has its own flaws, therefore new and faster methods are still needed in this case. In [4], Claudio raised a method about using improved PRM to resolve the on line navigation problem, which brought a new way to develop PRM in the path planning field. Although the paths that generated by Claudio's algorithm is not too effective when the environment gets complex, it could help the robot to succeed in many cases. The new method that presented in this paper is also based on PRM to solve this kind of problem, but the difference between it and the Claudio's is that our new proposal still uses the traditional PRM to generate a path in the already known maps, but not the Lazy-DRM or other improved PRM. And the most important discrimination is we use PRM more than once in the whole process, that is to say, the randomly distributed nodes that generated by PRM are not uniform during the task.

The rest of this paper is organized as follows. In section II theories relevant with the new approach are provided. Section III contains a detailed and complete description of our method. In section IV several simulations are provided with which the new approach is evaluated. In the final section we draw the conclusions and the future work are also presented.

II, Probabilistic path planning

In this section we briefly introduce the main theory of the Probabilistic Roadmap method. The framework of PRM planning algorithm consists of two phases: roadmap construction (learning) and query. In the learning phase, the algorithm constructs a probabilistic roadmap by generating random free configurations of the robot and connecting them using a simple, but very fast motion planer, also known as a *local planner.* And then the connected roadmap is stored as a graph whose nodes are the configurations and whose edges are the paths computed by the local planner. In the query phase, a path will be found from the start and goal configurations to two nodes of the roadmap. Then the planner searches the graph to find a sequence of edges connecting those nodes in the roadmap, and finally a feasible path for the robot is generated by concatenating the successive segments. If each segment between its two ending nodes is the shortest one among the segments connecting the same couple nodes, and if between any two nodes in the path, no more effective connection could be found, the path we got is the relatively shortest way from the start to the goal. The following figure gives a simulation result of probabilistic planning in which a feasible path is found quickly by PRM.

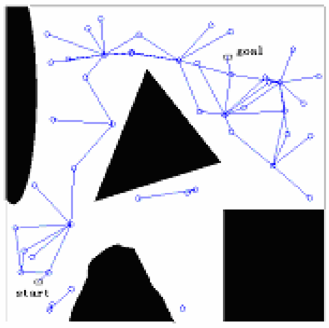

Figure 1 An example of planning result with the method of PRM. In the figure there is a path generated from start to the goal.

The new theory presented in this work is mainly based on the conventional PRM method, and uses it in the case of on-line path planning. In the next section, we will describe the new method in detailed.

III, The Proposed Method

A, The robot

The robot we are using in this paper is car-like mobile robot with sonar sensors all around. All the sensors are regarded as the nearly ideal sensors which can detect well and truly, so that it can *know everything* near it within the detection region. The robot's task is to go to a set target from a given beginning point in an unknown environment. In order to simplify the planning problem, we treat the mobile robot as a represented point in the rest of this paper. We also suppose the robot has self-localization equipment in order that it always knows its own position in the coordinate space of the environment during its motion. In fact self-localization may bring some errors on the positions, which affects the effectiveness of the approach. In this paper we do not consider the error brought by the self-localization, and it is supposed that the robot can get its real time position exactly.

B, The algorithm

Our new proposal is a real-time path planning approach which is based on the method of probabilistic roadmap, and it helps the robot to generate a new and accessible path in the unknown environments. To study it more easily, we call the new method as Real-time PRM. The novel idea of real-time PRM is its combining the problems of route planning both in previously known environment and unknown situation. In each step of the robot's moving, the sensors will collect the new information from the environment, and then an updated map is generated in which there are the circumstances already detected by the robot so far. According to this map, a most effective path from the current configuration to the target could be found with PRM method. Subsequently, the robot goes along the newly built way until it meets new situation, and if so, it means this loop ends and another one just begins, and the renewable map will be updated again. In the algorithm we call this map as built_map. The built_map is a bitmap which is described by a 2 dimension matrix in the database of the robot and it has the same size with the physical environment map. During the task, built_map is generated and updated gradually, which represents the robot's increasing knowledge about the environment. Each time after the renewal of the built_map, the algorithm replans a new path with PRM for the robot to move along. When the robot *sees* new obstacles at point A in the environment, the algorithm firstly calculates the coordinates of A with the knowledge of this path, and then computes the positions of the collision detected.

The real-time PRM can be divided into two steps that are described as follows:

1, The robot arrives at a new point in the environment map; update the built_map with the feedback knowledge of the sensors; go to step 2;

2, In the built_map, find the shortest path from the current point of the robot to the goal with the method of PRM; the robot moves along this path until each of the following things happens:

I, some new obstacles are detected by the sensors, go to step 1.

II, the robot reaches the target, stop.

To generate the shortest path from the current point of the robot to the target with PRM, we need to use the following process:

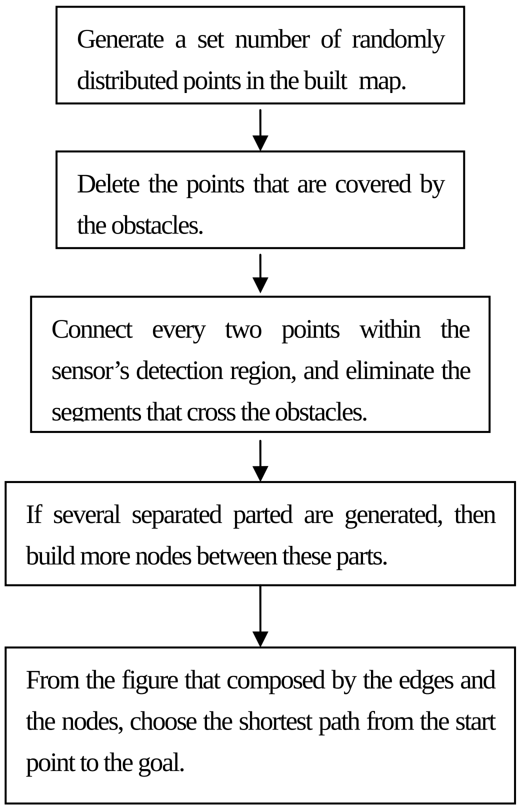

Figure 2

The pseudo-code of the algorithm is given in table 1

Table 1

1, $M \leftarrow \phi$
2, $P_0 \leftarrow$ the start point
3, $P_i \leftarrow$ the current point
4, $P_g \leftarrow$ the goal
5, $i \leftarrow 1$
6, *Loop*
7, If $P_i = P_g$
8, The robot arrives at the goal, and the path is generated.
9, Return
10, Else
11, Obst(i) $\leftarrow$ the obstacles information got by the robot at P_i
12, N $\leftarrow$ M $\cup$ Obst(i)
13, if M! =N
14, M $\leftarrow$ N
15, Path(i) $\leftarrow$ the shortest path built by PRM in M, from current point to Target
16, $P_{i+1} \leftarrow$ the next point after the current in Path(i)
17, else $P_{i+1} \leftarrow$ the next point after the current in Path(i-1)
18, End
19, The robot goes to P_{i+1}, i $\leftarrow i+1$

The number of the random nodes that the algorithm generated is directly relevant to the results, but it the number is too big, then the consuming time will increase dramatically. Therefore the number should be chosen carefully.

IV, Experimental results

In this section the results of some simulations are presented, which show the robustness of the new algorithm. To make our point clearly, we present a complete detailed process of the planning. In these simulations, the environment maps we use are all squares with the size of 50mX50m, and the sensor's maximal detection distance is set as 3m. The number of the probabilistic nodes that generated in each of the robot is set as 200 in experiments. The following experiments are completed on a PC with Pentium IV 2.4G CPU and the algorithm was executed in Matlab. The following figure is the environment map used in the simulation.

Figure 3 The environment map for the simulation. In the figure, the dark areas represent the obstacles.

Figure 5 shows 12 slips of the whole process, each of which is a built_map in the current step. In each slip, the random nodes are regenerated, and the shadow represents the obstacles that are detected by the sensors. More shadow means more information of the environment is got by the robot and the built_map has been updated. The path in each slip is different from each other because it is only built by PRM in that situation. The nodes in the paths that are represented by "o" means the real track passed by the robot in the previous steps, whereas the nodes still described by "*" are the nodes of the new generated route. The path in the last slip is the final path from the start to the goal, which can be seen clearly in figure 4.

Figure 4 The final path.

V, Conclusion and Future work

This paper presents a new motion planning method which develops the trditional PRM on the path planning problems in unknown environments. The main contribution of this work lies in it simplifies the on-line planning to many static computing processes. From the simulation results we can find that the path built by the real time PRM is effective and in built_map a part of the environmental information is stored, which also benifits to map-building work. However, to further evaluate the robutness of the new algorithm, more comparison of the distance and the computing time and other charaters with other methods are necessary, which is work we will do in the future. And the error of the sensors will be considered too in our future work.

Reference

[1] L. E. Kavraki, M. N. Kolountzakis, J-C Latombe, *"Analysis of Probabilistic Roadmaps for Path Planning,"* IEEE TRANSACTIONS on *ROBOTICS AND AUTOMATION*, 1998.
[2] L. E. Kavraki, P. Svestka, J-C Latombe, et al, *"Probabilistic Roadmaps for Path Planning in High-Dimensional Configuration Spaces,"* IEEE TRANSACTIONS on *ROBOTICS AND AUTOMATION*, 1996.
[3] N. M. Amato, O. B. Bayazit, L. K. Dale, C. Jones, D. Vallejo, *"Choosing Good Distance Metrics and Local Planners for Probabilistic Roadmap Methods,"* IEEE Conf. on Robotics & Automation,1998.
[4] C. Lanzoni, A. Sanchez, R. Zapata, *"Sensor-based motion planning for car-like mobile robots in unknown environments,"* IEEE Conf. on Robotics & Automation,2000.

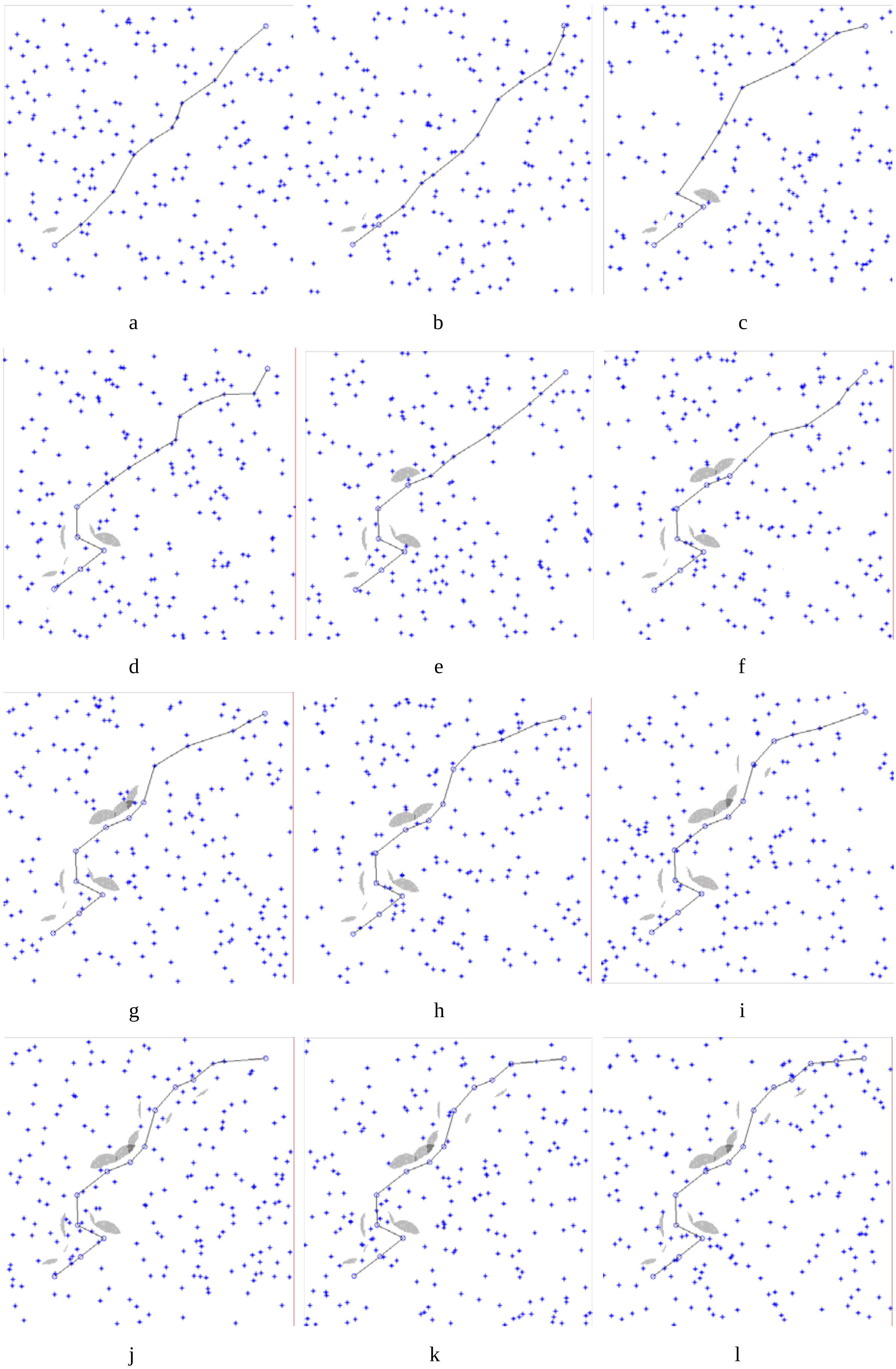

Figure 5

The Tenth International Symposium on Artificial Life and Robotics 2005(AROB 10th '05),
B-con Plaza, Beppu, Oita, Japan, February 4-6, 2005

Gesture Clustering and Imitative Behavior Generation for Partner Robots

Yusuke Nojima
Dept. of Industrial Engineering
Osaka Prefecture University
Gakuen-cho 1-1, Sakai, Osaka 599-8531

Naoyuki Kubota
Dept. of Mechanical Engineering
Tokyo Metropolitan University, PREST
Minami-Osawa 1-1, Hachioji, Tokyo 192-0397

Fumio Kojima
Dept. of Mechanical & Systems Engineering
Kobe University
Rokkodai 1-1, Nada-ku, Kobe, Hyogo 657-8501

Abstract

This paper proposes a method for generating behaviors based on imitation of a partner robot interacting with a human. This method is constructed by a two-step procedure. At first, a gesture clustering is performed to classify a human hand motion. An evolutionary computation is applied for a pattern matching, and then a spiking neural network and a self-organizing map classify the motion as a gesture. Second, the robot take an imitative behavior which follows human hand motion generated by an evolutionary computation using the previous trajectory information identified by the clustered gesture. The goal of this study, by using these learning modules structurally, the robot and its user share various gestures for user friendly communication. Several experimental results show the effect of the proposed method.

1 Introduction

Recently, various partner robots have been developed by many companies and academic groups. Most of these robots can execute a number of given motions to communicate with its user. However their motions are designed based on the expert knowledge of the designer who is not an actual user. Thus, to take suitable actions for the user, the robot should acquire own behaviors through the interaction with the user. Moreover, the robot should accumulate obtained behaviors to reuse them at same situation. To realize the above functions, the robot needs a number of learning modules. In general, since the mechanism of the robot becomes complicated and large increasingly as intelligent capabilities are added gradually to the robot, we should consider the entire structure of intelligence for processing information flow over the hardware and software of the robot, not a single intelligent capability. Accordingly, we have proposed a concept of structured learning which emphasizes the importance of interactive learning of several learning modules through the interaction with its environment. We apply this concept to an imitative behavior learning for generating and accumulating behaviors of the partner robot. For human being, imitation is a powerful tool for gestural interaction with children and for teaching behaviors to children by adults. Partner robots should also obtain various behaviors by using an interactive learning based on the imitation. As the human imitation, there is an advantage that the imitative behavior learning performs without exact human instructions.

In this paper, we propose a method that the robot generates behaviors by imitating the motions of the human hand. Figure 1 shows the total architecture of the proposed method. First of all, the robot detects a series of human hand positions by processing images from CCD camera on the robot. We employ a steady-state genetic algorithm (SSGA) to this image processing in order to cope with environmental noise. We call this SSGA *SSGA-1* in this paper. Next, the motion is recognized as a gesture by using a spiking neural network (SNN), since SNN can learn the spatial and temporal pattern from a series of the human hand positions. Thereafter, a self-organizing map (SOM) is applied for clustering the motion to reuse previous behaviors as the initial trajectories of a SSGA for generating an imitative behavior. We call this SSGA *SSGA-2* in this paper. After generating the behavior, the robot accumulates the behavior by associating

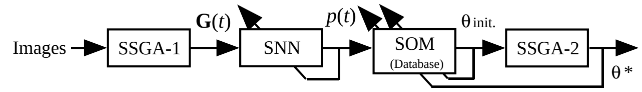

Figure 1: Total architecture for generating and accumulating behaviors.

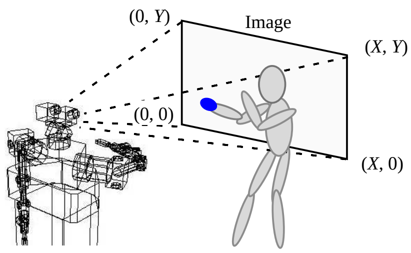

Figure 2: A coordinate system for image processing of a robot.

with the output of SOM. In this way, each learning module (i.e., two SSGAs, SNN, and SOM) relates with one another to achieve the generation and accumulation of imitative behaviors. Experimental results show that the robot can generate imitative behaviors faster by accumulating obtained behaviors.

2 Imitation for Partner Robots

2.1 Human Hand Detection

The robot takes an image from the CCD camera, and extracts a human hand (Fig.2). The human wears a blue glove for performing a gesture. The taken image from CCD camera is transformed into the HSV color space, and the color corresponding to the blue globe is extracted. Next, the blue globe is detected by using SSGA-1 based on template matching. We employ flexible templates to the candidate solutions in SSGA-1, since the robot must identify several hand shapes.

In SSGA-1, only a few existing solutions are replaced by new candidate solutions generated by genetic operators in each generation. The worst candidate solution is eliminated (delete least fitness selection) and replaced with an offspring solution generated by the crossover and mutation. We use elitist crossover and adaptive mutation. Elitist crossover randomly selects one solution and generates an individual by incorporating genetic information from the selected solution and best solution. In the adaptive mutation, the variance of the normal random number

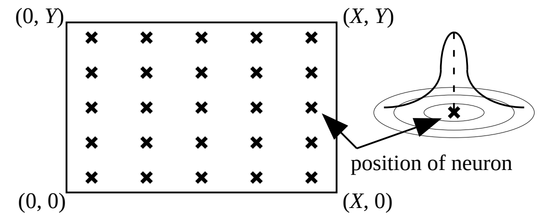

Figure 3: Spiking neurons arranged on the image.

is relatively changed according to the fitness values of the population. A fitness value is calculated by the following equation,

$$f_i = C_{Target} - \eta C_{Other} \tag{1}$$

where η is a coefficient for penalty; C_{Target} and C_{Other} indicate the number of pixels of the color corresponding to a target and other colors, respectively. This problem results in the maximization problem. The robot extracts motion of the human hand from images by using SSGA-1 where the maximum number of images is T. The sequence of the hand positions is represented by $\mathbf{G}(t) = (G_x(t), G_y(t))$ where $t = 1, 2, ..., T$.

2.2 Gesture Recognition and Clustering

We apply a SNN ([1]) for memorizing several motion patterns of a human hand. SNN is often called a pulse neural network and considered as one of the artificial NNs based on the dynamics introduced the ignition phenomenon of a cell, and the propagation mechanism of the pulse between cells.

In this paper, spiking neurons are arranged on a planar grid (Fig.3) and $N = 25$. By using the value of a human hand position, the input to the ith neuron is calculated by the radial basis. The weight parameters are trained based on the Hebbian learning algorithm. Because the adjacent neurons along the trajectory of the human hand position are easily fired by the Hebbian learning, the SNN can memorize the temporally firing patterns of various gestures.

The temporally firing pattern of SNN is used as an input for the clustering by SOM in order to detect a spatial pattern of a human gesture. SOMs is often applied for extracting a relationship among inputs data, since SOMs can learn the hidden topological structure from the learning data. The inputs to our SOM is the sum of pulse outputs from SNN. The output node is selected by comparing the Euclidean distance with each reference vector. Moreover, the reference vectors are updated for classifying several gestures. That is, the

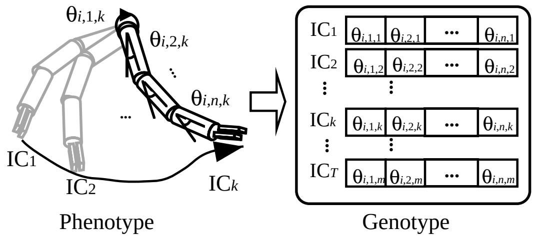

Figure 4: The representation of the ith trajectory candidate composed of m intermediate configurations.

selected output unit means the nearest gesture among the previously learned gestures.

2.3 Trajectory Generation based on Imitation

A trajectory planning problem for a behavior can result in a path planning problem from an initial human hand position to a final human hand position. Here a configuration q is expressed by a set of joint angles, because all joints are revolute,

$$q = (\theta_1, \theta_2, \cdots, \theta_n) \in R^n \tag{2}$$

where n denotes the degree of freedom (DOF) of a robot arm. Because a trajectory can be represented by a series of T intermediate configurations (i.e., IC_k in Fig. 4), the trajectory planning problem is to generate a trajectory combining several intermediate configurations corresponding to $\mathbf{G}(t) = (G_x(t), G_y(t))$, $t = 1, 2, ..., T$. SSGA-2 is applied to generate a trajectory for an imitative behavior corresponding to a human hand motion.

A trajectory candidate is composed of all joint variables of intermediate configurations (Fig.4). Initialization generates an initial population based on the previous best trajectory stored in the knowledge database linked with SOM. The jth joint angle of the kth intermediate configuration in the ith trajectory candidate $q_{i,j,k}$, which is represented as a real number, is generated as follows ($i = 1, 2, ..., gn$),

$$\theta_{i,j,k} \leftarrow \theta^*_{j,k} + \beta^I_j \cdot N(0, 1) \tag{3}$$

where $\theta^*_{j,k}$ is the previous best trajectory referred from the knowledge database; β^I_j is a coefficient for the jth joint angle; $N(0, 1)$ is a Gaussian random variable with mean 0 and standard deviation 1. A fitness value is assigned to each trajectory candidate. The objective is to generate a trajectory realizing the possibly short distance from the initial configuration to the final configuration while realizing good evaluation. To achieve the objectives, we use a following fitness function,

$$f_i = f_p + \mu f_d \tag{4}$$

where μ is a weight coefficient. The first term, f_p, denotes the distance between the human hand position and the position of robot end-effector. The second term, f_d, denotes the sum of squares of the difference between each joint angle between two configurations of t and $t-1$. Therefore, this trajectory planning problem can result in a minimization problem. After SSGA-2, the best trajectory obtained is stored in the knowledge database.

Table 1: Parameters used in SSGA-1 and SSGA-2.

Parameter	SSGA-1	SSGA-2
Chromosome length	10	$4T$
Population size (gn)	120	200
Number of evaluations	300	$1000T$
Crossover rate	0.2	0.2
Mutation rate	1.0	0.2

3 Experiments

This section shows an experimental result using a humanoid-type robot. The size (X, Y) of an image is $(160, 120)$. Here a trial is defined as one cycle from human hand detection by SSGA-1, spatial and temporal pattern generation by SNN, gesture clustering by SOM, and behavior generation by SSGA-2 (Fig. 1). Table 1 show the parameters used in SSGA-1 and SSGA-2. T is the maximum number of human hand positions detected by SSGA-1. According to T, the number of intermediate configurations is changed in this experiment.

Figure 5 shows the history of the selected node in SOM and the history of the gesture pattern displayed to the robot. First of all, the human tried to show various patterns to the robot, because the human wanted to know the reaction of the robot. At the time, various nodes in SOM were selected. After 11 trials, the human tried to teach the hand motions like clockwise and counterclockwise circles. The robot classifies the motions by using the $12th$ and $18th$ nodes mainly. And then, the human tried to show various motion again, in order to search for better motions that the robot can follow them well. Based on this searching process, the human tried to teach the hand motions like a

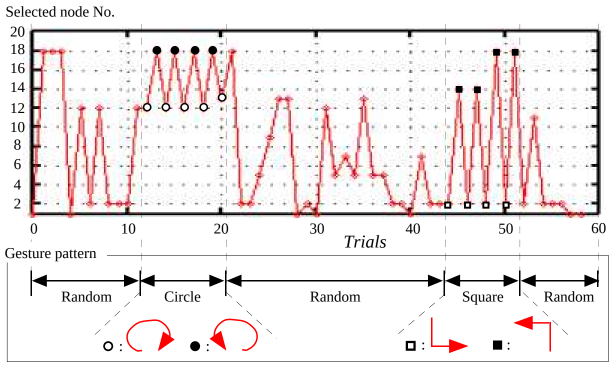

Figure 5: Change of selected nodes in SOM and human motions.

square from $44th$ to $51st$ trial. The robot classifies the motions by using $2nd$, $14th$, and $18th$ nodes mainly. In this way, SOM classifies the human hand motions as specific gestures.

Figure 6 shows the result of image processing at the $51st$ trial. Figures 6 (a), (b), and (c) show the human hand motion, the detected result of the human hand positions, and the outputs of the SNN, respectively. The light and shade of the boxels indicate the time sequence where the lighter boxel indicates the later hand position. Although the detected hand positions were separate, SNN interpolated the detected hand positions and made a sequence as a result of temporal firing. Figure 7 shows the Robot could generate a motion following the human hand motion. That is, it shows that the robot recognized the human hand motion by SNN and SOM, and reproduced the behavior based on imitative behavior generation.

Figure 8 shows the change in fitness value on $2nd$, $14th$, and $18th$ nodes. In each node, the fitness in SSGA-2 decreased trial by trial. This shows the effectiveness of the SOM clustering and the database.

4 Summary

This paper proposed a method for imitative behavior generation of a partner robot. We applied SNN for extracting spatial and temporal patterns of gestures, SOM for clustering gestures, and SSGA for generating trajectory to perform a behavior following to the human hand motion. Experimental results show that the robot learns various motion patterns by imitating human hand motions. Furthermore the robot could reuse obtained trajectories for generating better imitative behaviors at the same situations.

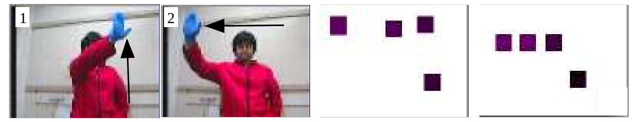

(a) Human motion (b) Detected human hand position (c) SNN Output

Figure 6: The results of image processing at the $51st$ trial.

(a) (b) (c) (d)

Figure 7: The snapshots at the $51st$ trial.

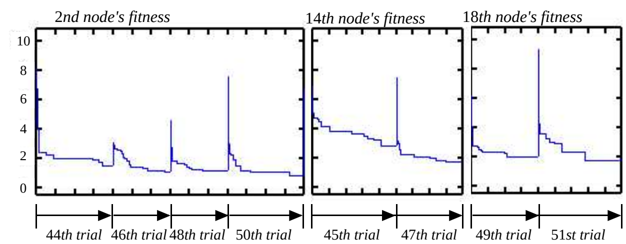

Figure 8: Change in fitness value on $2nd$, $14th$, and $18th$ nodes. A scale interval of the horizontal axis is 1000 iterations.

References

[1] W.Maass, C.M.Bishop, *Pulsed Neural Networks*, MIT Press, 1999.

[2] J.S.R.Jang, C.T.Sun, and E.Mizutani, *Neuro-Fuzzy and Soft Computing*, Prentice-Hall, Inc., 1997.

[3] G.Syswerda, "A Study of Reproduction in Generational and Steady-State Genetic Algorithms," *Foundations of Genetic Algorithms*, San Mateo: Morgan Kaufmann Publishers, Inc., 1991.

[4] T.Kohonen, *Self-Organization and Associative Memory*, Springer, 1984.

[5] A.Billard, "Imitation," *Handbook of Brain Theory and Neural Networks*, MIT Press, pp.566-569, 2002.

[6] N.Kubota, "Intelligent Structured Learning for a Robot Based on Perceiving-Acting Cycle," *Proc. of The Twelfth Yale Workshop on Adaptive and Learning Systems*, pp.199-206, 2003.

The Tenth International Symposium on Artificial Life and Robotics 2005(AROB 10th '05),
B-con Plaza, Beppu, Oita, Japan, February 4-6, 2005

How to make a mobile robot move more reliably?

Jiwu Wang Masanori Sugisaka
Department of Electrical and Electronics Engineering, Oita University, Oita 870-1192, Japan
Email: wangjiwu@cc.oita-u.ac.jp, msugi@cc.oita-u.ac.jp

Abstract When we explore the navigation of a mobile robot, we have to consider how to get necessary data from sensors and how to make good use of those data. Based on present technology, sometimes we can not automatically extract data used for reliable navigation in any environments from those sensors with present algorithms. Even in the structured environments, because of the errors of sensors, the extracted data are not always reliable. In view of above problems, we developed the tele-control subsystem through Internet besides the general control strategy. With the tele-control, the data gotten from sensors, will be sent to the supervisor's computer directly in addition to the robot. And the supervisor can also send the control commands to the robot directly based on human's experience. By this way, the robot may be controlled even in a strange environment.

Key Words Mobile robot, Navigation, Tele-control

1. Introduction

In this paper, we mainly consider how to make a mobile robot move more freely and reliably in structured and unstructured environments. Here the structured environment is the ideal environment with fixed settings. Although the states of some objects in that environment can be changed, but those change do not influence the working state of that robot. On the contrary, it is the unstructured environments. That is, the unstructured environments are more complex. And the practical environment is one of the unstructured environments. Because the change of the environment should be considered when the robot is moving, the control of that robot should be more flexible and reliable.

Navigating freely in the specified environment is the basic and necessary function for a mobile robot. Then the robot can carry out more specified tasks. Here at least two main problems will be considered for the solutions. One is the environment may not always be ideal structured environment. Another is the self-location in the navigation. The ability to solve above problems will determine what kind of jobs the robot can do. Although they seem to be separate problems, they are the necessary components of the navigation subsystem being developed. Here the self-location is mainly explored for the long distance navigation with the errors of sensors and slip at high speed. And the unstructured environment is the structured environment that is changed by some unexpected requirements. Such environment is similar to some practical environments.

In order to solve above problems efficiently, the vision subsystem, voice subsystem, touch screen control subsystem and tele-control subsystem by Internet were developed. Those subsystems shared necessary information from sensors by TCP/IP protocol. For most cases, only one of the subsystems is used. But it will be robust when it works with all the subsystems in some complex environments. All subsystem mainly use the data extracted from the captured images by the CCD video camera to control the driven subsystem. Although the CCD video camera may provide more information than other sensors, we may not develop any corresponding algorithms for any specified applications. That means the robot can not automatically make full use of the information from the CCD video camera. On the other hand, the supervisor may not always follow the robot even if the robot is working. Thus we developed the voice subsystem when the supervisor is not far from the robot, the tele-control subsystem by Internet when the supervisor is far from the robot and the touch screen subsystem when the supervisor is near to the robot. Especially in the tele-control subsystem, the images taken by that CCD video camera will also send to the supervisor's computer at the same time. The supervisor can send the corresponding commands directly to that robot based on some practical requirements. When that robot is confused in a strange environment, with the help of the supervisor by the tele-control through Internet, that robot will complete specified tasks.

On the other hand, making use of as many sensors as possible is another solution to increase the robustness and flexibility of a robot. But it also brings new problems: 1) the cost of sensors; 2) develop algorithms to make good use of the data received from sensors; 3) how to efficiently compound those data received from different sensors etc. At the same time, we have to admit the robot will not have the similar intelligence like a human being till now. The robot can not make good use of all data from all sensors. It is not difficult for us to control a robot to work in a structured environment. But we can not make a robot work in any environments automatically and freely. That is the main purpose that we developed the tele-control through the Internet.

The robot developed in our laboratory is one with the approximate height of 1.7m. All control information is based on the data extract from the CCD video camera. The head is designed with one degree of freedom, which can rotate 360^o. The camera has two degree of freedoms, which can tilt up and down, left and right. Thus the robot can searching specified objects. Just like the common mobile robots, it can move forward and backward for specified distance, and it can rotate for specified angles. Some landmarks, such as triangle and circle, can be recognized. It can also move at a high speed along the double guideline. Moreover, it can perform simple obstacle avoidance. However, with such functions, it can only move freely at structured laboratory. If moving in the more complex environments, the robot will be helped by the voice subsystem or tele-control subsystem base on practical requirements. The corresponding experiments have been done in our laboratory.

2. The realization of the navigation system

The Alife robot prototype, as shown in Figure 1, is a custom built mobile robot which has four wheels: two independently driven wheels located along the central axis, and two auxiliary castor wheels in its front and back. There are six ultra sonic sensors-switches for obstacle detection within a preset range. The robot has two color Charge Coupled Device (CCD) cameras mounted on its head. Each camera is capable of independent pan and tilt movement. The head can be rotated left-right using a stepping motor. Speaker and a microphone are mounted in the body and on the head respectively. A mobile phone may be used instead of the speaker/microphone.

To control the robot, two Personal Computers (PCs) have been built into the body. The PCs are connected to the hardware via controller cards and the serial ports. The PCs also have Ethernet cards, so that network message may be used to carry information (about items seen or heard), from one PC (which has access to the frame grabber/sound card) to another PC (responsible for controlling hardware). If necessary, those information may also be sent to the supervisor's computer.

The integration of the system is shown in figure 2. The figure 3 is the illustration of the implementation process. All of the subsystems were developed separately. It is convenient to later increase any specified based on requirements. In the vision subsystem, the image taken by the CCD video camera, will be processed to extract necessary data for recognition and some signals for navigation. Till now, the sign landmarks, such as circle and triangle etc, and the continuous landmark, the double guideline, have been developed. The voice subsystem can receive Japanese and English commands and translate them to the corresponding signals used for the robot. At the same time, any explanation text will be spoken by this system. The behavior system is responsible for all basic actions of the robot. It can receive specified signals from other subsystems to perform required actions. If necessary, the signals can also be sent to the supervisor's computer by Internet for the tele-control. Based on such system, the robot can satisfy most requirements.

3. Experiments

The experiments on the voice subsystem and image processing subsystem can be found in the reference[1,2]. Here we mainly explain the problems about the tele-control through the Internet. In order to make the tele-control reliable and robust, the communication subsystem must be reliable, and the necessary data should be sent to the supervisor in time. Because the images taken by the CCD video camera will be sent to the supervisor, the volume of the image data and the frequency of the transformation should be controlled in order to make the tele-control system work for all time. On the other hand, the commands sent through Internet should be as simple and short as possible. Most of important, the connection priority between different subsystems should be parallel, and in each system the connection is point to point. Thus the problem produced by one subsystem, will not influence the work of other subsystems. An simple introduction of our system can be seen in figure 4.

4. Conclusions

In order to realize reliable navigation, the robust system, the reliable data extracted from the signals of sensors and the reliable feedback information are necessary. In our system, we make good use of the volume of signals from the CCD video camera. Because we can not deal with all of that information with present algorithms, the tele-control subsystem was developed to realize reliable navigation in the strange environment.

Reference

[1] J. Wang, M. Sugisaka, Study on a color based target detection technique", Proceedings of 7-th international symposium in artificial life and robotics (AROB 7-th'02), B-Con Plaza, Beppu, Oita, Japan, Jan. 16-18 : 532-536

[2] J. Wang, M. Sugisaka, Study on visual-based indoor navigation for an alife mobile robot, ICSEng2002, Las Vegas, USA, 2002, August 6-8 : 390-396.

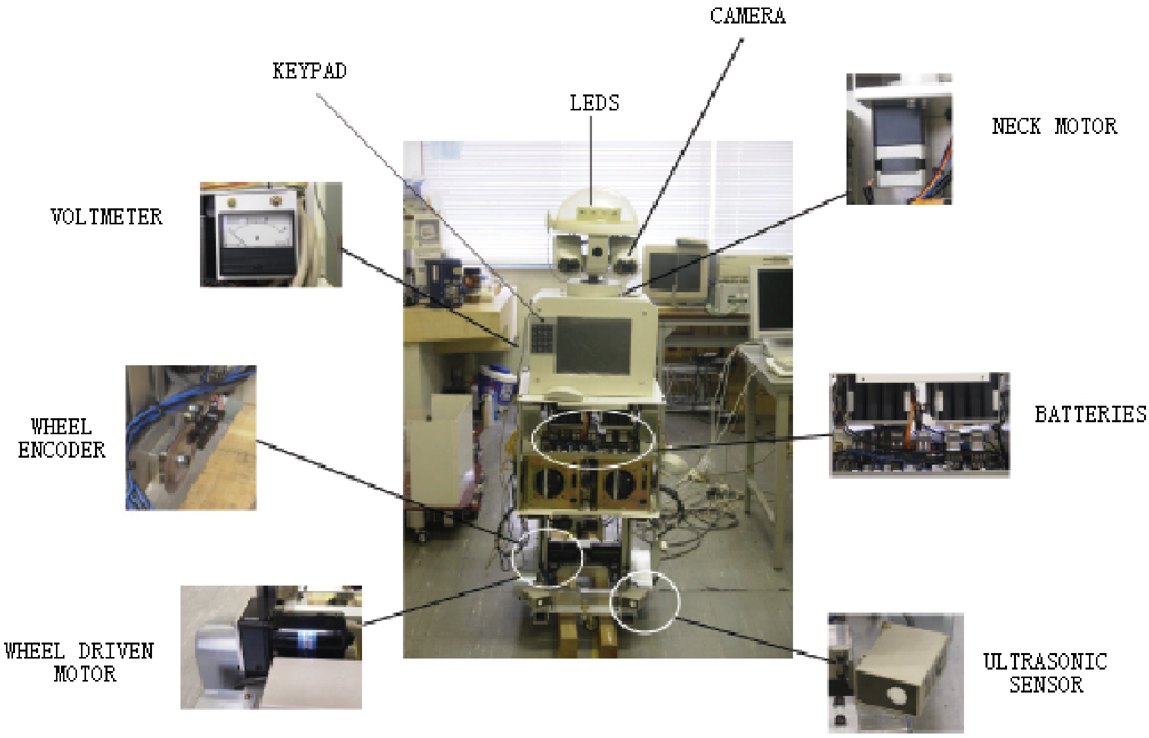

Figure 1. The structure illustration of our mobile robot

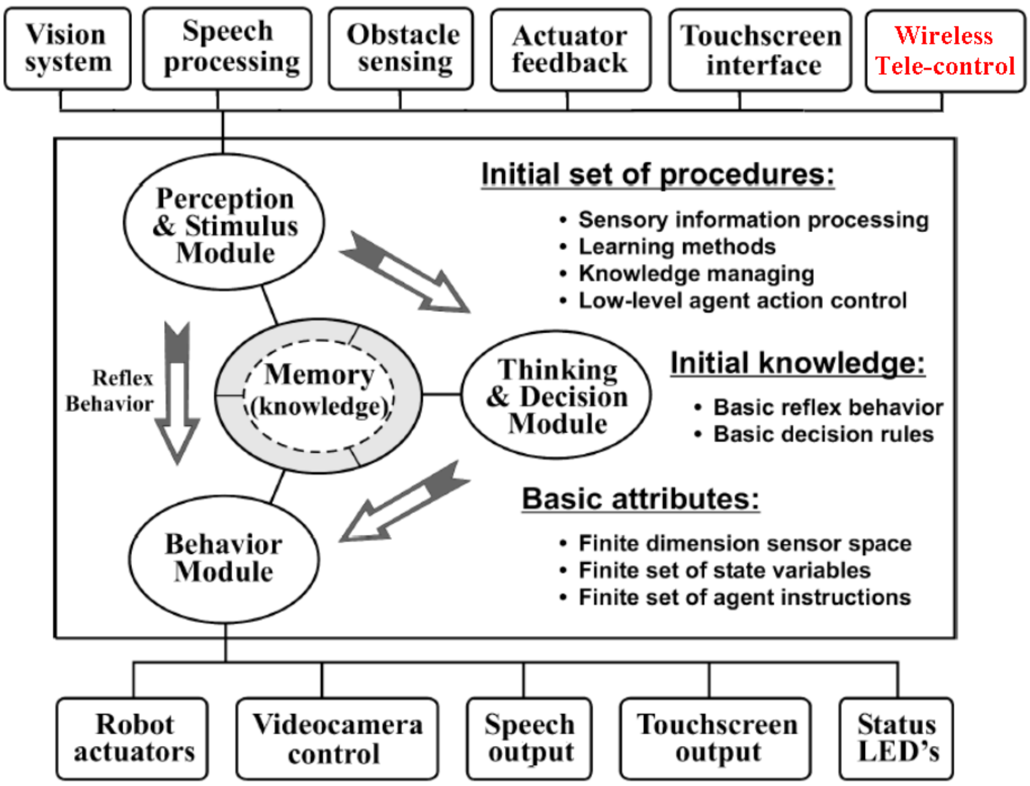

Figure 2 Illustration of the processing of input and output data

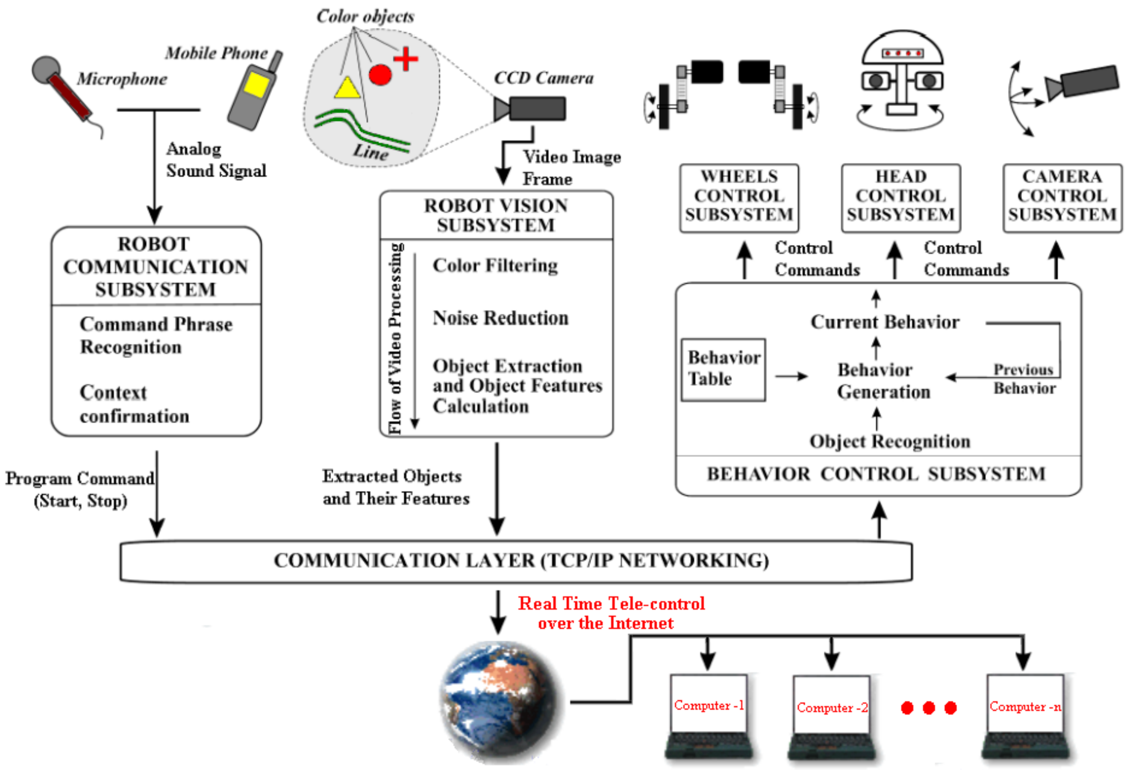

Figure 3 Illustration of the implementation of all subsystems

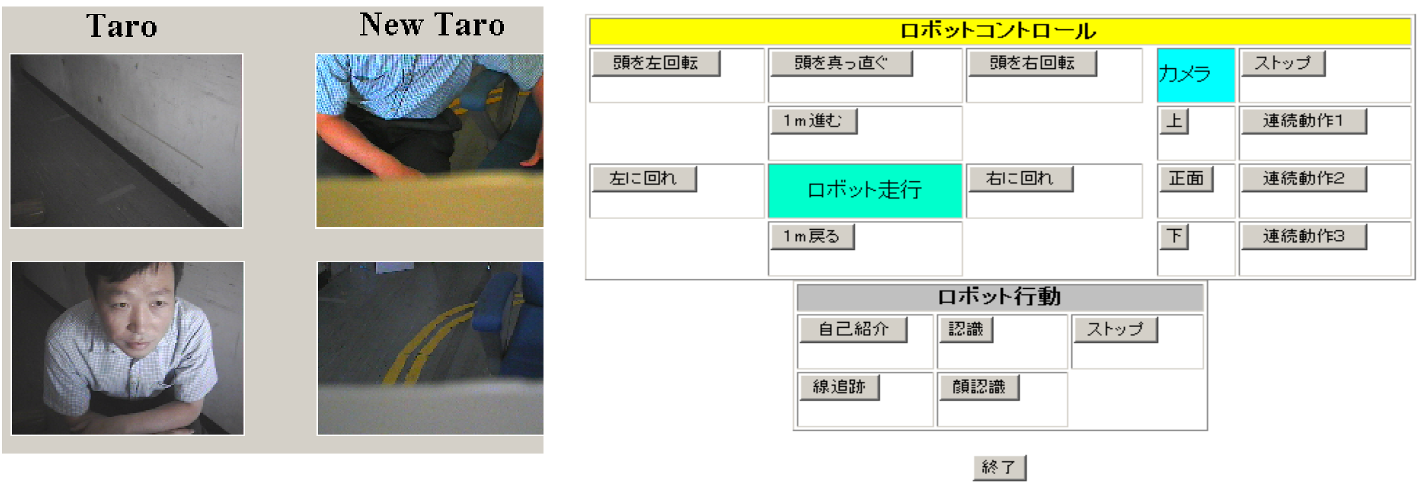

Figure 4 Illustration of the tele-control through Internet

The Tenth International Symposium on Artificial Life and Robotics 2005(AROB 10th '05),
B-con Plaza, Beppu, Oita, Japan, February 4-6, 2005

PID orbit motion controller for indoor blimp robot

Hisao Kadota* Hidenori Kawamura* Masahito Yamamoto*
Toshihiko Takaya** Ohuchi Azuma*

*Graduate School of Information Science and Technology, Hokkaido Univesity
Nishi 9, Kita 14, Kita-ku, Sapporo, Hokkaido, 060-0814, Japan
{kadota, kawamura, masahito, ohuchi}@complex.eng.hokudai.ac.jp

**Ricoh System Kaihatsu Company, Ltd
Nishi 4, Kita 7, Kita-ku, Sapporo, Hokkaido, 060-0807, Japan
takaya@rsk-kitami.grp.ricoh.co.jp

Abstract

A blimp robot is attractive as an indoor robot because a blimp robot can float in the air by buoyancy and realize safe indoor flight with low energy. In our research, we focus on the indoor entertainment blimp robot because a blimp robot can be used the environment where children exist and offer a visual amusingness by combination with animated character-type balloon. Our blimp robot has a wireless camera as a sensor and moves by using the output device that has total of six propellers to produce thrusts for each axis in three dimensional coordinate system. In this paper, we report the circular, square, triangle motion controls of the blimp robot as fundamental motions for entertainment motions.

keywords : indoor blimp robot, entertainment, motion control, camera

1 Introduction

The research on a blimp robot is active area on the various research groups because a blimp robot freely moves in the environment without being influenced by the geographical features, realizes the long time flight by less energy and has high-security for a crash. A blimp robot can be applied to various tasks, e.g., monitoring, climate research, transportation and surveillance [1][2].

In our research, we focus on the indoor entertainment blimp robot such as a dancing blimp robot and an interactive blimp robot. Because a blimp robot can realize safe indoor flight in the environment where children exist and offer the visual amusingness by combination with an animated character-type balloon, a blimp robot is attractive and impressive as a new indoor-type amusement robot. As entertainment flights, a blimp robot can act a synchronized flying motion, a flying exploit, a communication with humans in a show and an event hold in an indoor plaza, gym and theater.

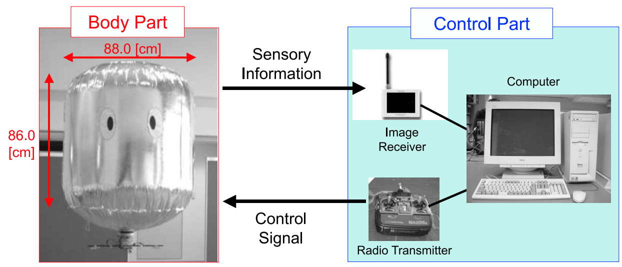

Figure 1: Control System of Our Blimp Robot

Although a blimp robot has various advantages, the control of a blimp robot is difficult compared to a two-dimensional mobile robot. A blimp robot needs the position control in three-dimensional space and the attitude control. Furthermore a blimp robot is influenced by slight air stream and subjected to inertia. In the research groups on a blimp robot, the control is one of the active topics in the problem for a blimp robot.

In this paper, we aim to achieve the circular, square and triangle motions as fundamental motions for a blimp robot. Because a circular motion includes the motion for a basic curve and square and triangle motions include the motions for a basic straight-line and twisting the corner, the realization of the motions can be applied to various motion controls.

2 Control system of our blimp robot

2.1 Pillar-type blimp robot

Figure 1 shows the outline of the control system for our blimp robot. The control system is divided into two parts: the body and the control part. The body

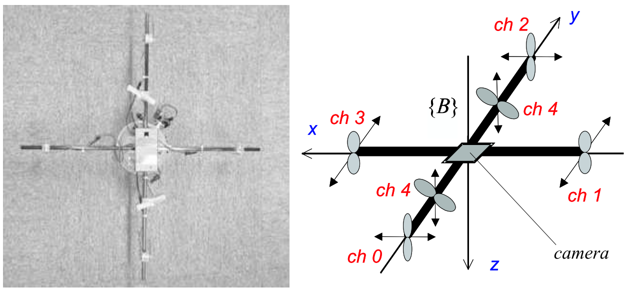

Figure 2: Output Device

part has a pillar-type balloon, an output device and a wireless camera. The control part placed outside has a computer, an image receiver and a radio transmitter.

The diameter of the balloon is 88$[cm]$ and the height is 86.0[cm]. The pillar-type balloon carries a big payload because of the large volume. Furthermore, it realizes the fair air resistance in the horizontal plane.

The output device is attached to the bottom of the balloon. As shown in Figure 2, the output device has total of six propellers. The propellers produce thrusts for each axial direction independently in the coordinate system $\{B\}$ fixed at the blimp robot. The blimp robot moves in the horizontal plane with four propellers, $ch0$-$ch3$, positioned at the tips of a crisscross rod. The propellers $ch0$ and $ch2$ produce thrusts for x-axial movement. The propellers $ch1$ and $ch3$ produce thrusts for y-axial movement and for yaw angular movement. The propellers $ch4$ positioned on the central part of the crisscross rod produce thrusts for z-axial movement.

A wireless camera is attached facing downward on the output device. The blimp robot recognizes the environment and own state about the position and the attitude by using the camera. The image signal is transmitted to the image receiver in the control part, and then it is loaded into the computer through a video capture board. The computer processes the image to decide the operations for each propeller, and then the decisions of the operations for each propeller are transmitted to body part as a control signal through the radio transmitter.

2.2 Positioning system

In the tasks for a monitoring and a surveillance, a blimp robot normally needs to move in the environment by recognizing each local location. However an entertainment blimp robot just recognizes the artificial environment put the prepared landmarks regardless of the locations, e.g., plaza, gym and theater, because the operating environments are comparatively free for an entertainment robots such as RoboCup including an amusing factor.

In our previous work [3], we have developed the simple positioning system in viewpoint of a facile introduction to various places. In the positioning system, M red circles are placed on a gridiron on the floor as shown in Figure 3. Each circle has an identification number $ID_l(l = 1, \ldots, M)$ and two coordinate values P_l and $p_l(t)$. P_l is the value in the absolute coordinate system fixed at the environment $\{U\}$ and $p_l(t)$ is the value in the blimp coordinate system fixed at the blimp robot $\{B\}$. The blimp robot get the own position P_b in $\{U\}$ by recognizing the circles in the image processing and calculating ID_l, P_l and $p_l(t)$ [3].

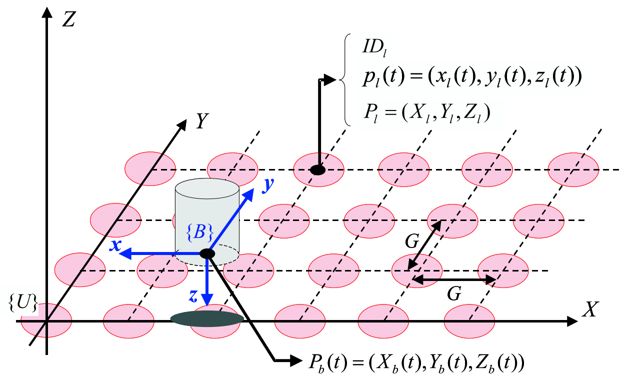

Figure 3: Outline of Positioning System

We can apply the positioning system to various places with facility because we just scatters the landmarks such as red circles in the environment and the blimp robot just recognizes the prepared environment.

2.3 Controller

A blimp robot has complex dynamics because a blimp robot has several nonlinear characteristics, e.g., an inertial influence at a movement, a change of thrusts by burning a battery power and a strain of a balloon form. Therefore PID-controller is applied to the control architecture in the research groups [1][2], because it is difficult to decide the analytical controller for a blimp robot. In PID-controller, we can regulate the controllable parameters with relatively little effort by repeated trial and error.

In our PID-controller, the manipulated variable $m(t)$ is given as the ratio of the rotation time for each propeller in sampling time ΔT. The manipulated variables $m_x(t)$ and $m_z(t)$ corresponding to $ch0$, $ch2$ and $ch4$ are decided by the relative distance from the blimp robot to the target point defined as follow.

$$m_x(t) = K_{px}\left(e_x(t) + \frac{1}{T_{Ix}}\int e_x(t)dt + T_{Dx}\frac{de_x(t)}{dt}\right)$$

$$m_z(t) = K_{pz}\left(e_z(t) + \frac{1}{T_{Iz}}\int e_z(t)dt + T_{Dz}\frac{de_z(t)}{dt}\right)$$

The propellers, $ch1$ and $ch3$, are used to control both the pulsion for y-axis and the attitude for yaw angle

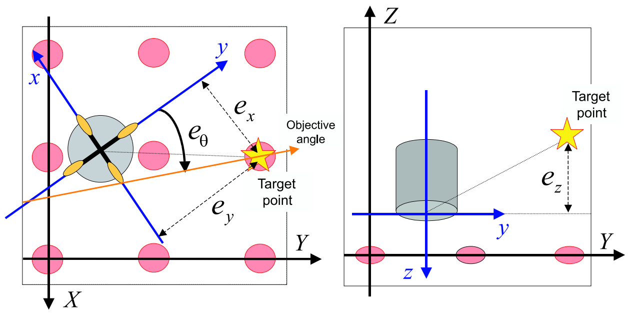

Figure 4: Deviation from the Blimp Robot to the Target Point

as shown in Figure 4. Therefore the manipulated variables $m_{y\_r}(t)$ for $ch1$ and $m_{y\_l}(t)$ for $ch3$ are decided by both the relative distance and the relative angular from the attitude of the blimp robot to the objective attitude defined as follow:

$$m_{y\_r}(t) = m_{y\_d}(t) + m_\theta(t)$$

$$m_{y\_l}(t) = m_{y\_d}(t) - m_\theta(t)$$

where $m_{y\_d}(t)$ is the term of the relative distance for y-axis and $m_\theta(t)$ is the term of the relative angular defined as follow.

$$m_{y\_d}(t) = K_{py}\left(e_y(t) + \frac{1}{T_{Iy}}\int e_y(t)dt + T_{Dy}\frac{de_y(t)}{dt}\right)$$

$$m_\theta(t) = K_{p\theta}\left(e_\theta(t) + \frac{1}{T_{I\theta}}\int e_\theta(t)dt + T_{D\theta}\frac{de_\theta(t)}{dt}\right)$$

3 Experiment

3.1 Experimental setup

In the experiment, we experiment on the control of the blimp robot for circular, square and triangle motions. Because the circular, square and triangle motions includes basic motions for a curve, straight-line and twisting a corner, the achievements of these motions can be applied to various movements. In the circular motion, the blimp robot is controlled to pass 10 target points on the circle with radius 150[cm] in XY-plane. In the square and the triangle motions, the blimp robot is controlled to pass apexes on the square and triangle 250[cm] on a side in XY-plane. The blimp robot is controlled to keep 200[cm] high for Z-axis in all motions. For the attitude control, the blimp robot is controlled to parallelize the line connecting the previous target point and the current target point.

The experimental environment is the space in the building of University as shown in Figure 5. The

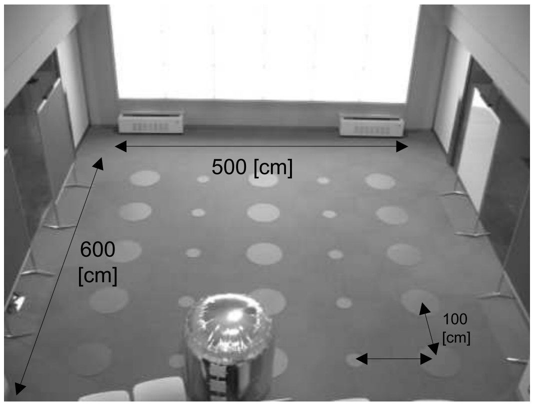

Figure 5: Experimental Environment

width, depth and height are 600, 500 and 500[cm]. 25 red circles are placed on a gridiron on the floor, and the interval is 100[cm]. The controllable parameters K_p, T_I and T_D are manually set by repeated trial and error in the preliminary experiments.

3.2 Result

Figure 6, 7 and 8 show the experimental results for the circular, square and triangle motions. In each figure, the left and right side is the motional orbit in XY-plane and YZ-plane. The solid line shows the motional orbit of the blimp robot and the dashed line shows the objective orbit connecting the target points in turn.

In the circular and square motions, the blimp robot has moved approximately along the objective orbit in XY-plane. In the triangle motion, the blimp robot has got away from the objective orbit after turning the corner compared with the circular and square motions, because the twisting angle for the triangle motion is larger than the angles for the other motions. Moreover, because the blimp robot has turned the corner going in the direction to next target point, the blimp robot has turned the corner without passing over the target points for the corner. However the blimp robot could have modified the own position by the arrival at next target point.

The unstable motional orbits have been caused for Z-axis in all experiments, because the realization of the neutral buoyancy is difficult and the thrusts for x and y-axes in $\{B\}$ have influenced for Z-axial motion by the rocking vibration of the body. The rocking vibration causes the vibrational orbits in Figure 6, 7 and 8, because the motional orbits are measured by the camera attached on the blimp robot. Because the rocking vibration is caused by the high position of the center of the gravity, we consider that we use the horizontally long body as one of the solutions for the rocking vibration.

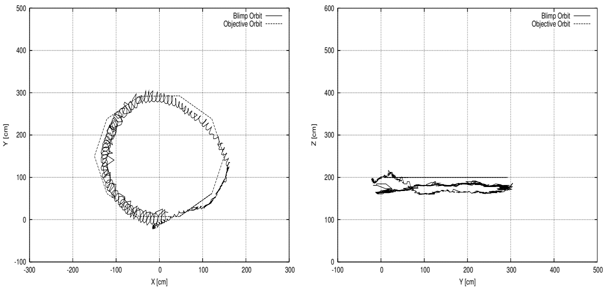

Figure 6: Orbit for Circular Motion

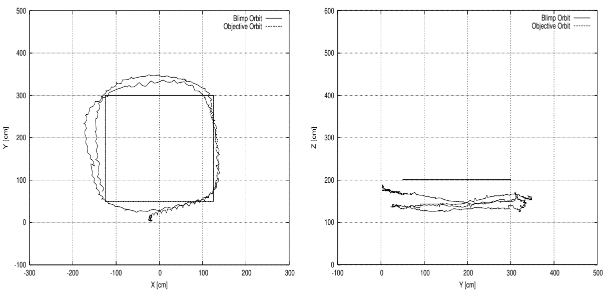

Figure 7: Orbit for Square Motion

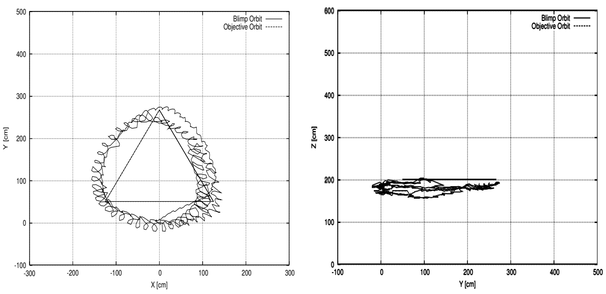

Figure 8: Orbit for Triangle Motion

The attitudinal transition of the blimp for each experiment is shown in Figure 9. Slight over rotation have been caused in the square and triangle motions, because the twisting angles are acute angle. However the blimp robot could have control the attitudes to the objective attitudes in short time.

4 Conclusion

In this paper, we reported the fundamental motion controls of our pillar-type blimp robot for application to an entertainment. In the experiments, we pick up the circular, square and triangle motions as the fundamental motions, because the orbits for the motions have the motions for a basic curving line, straight line and curving a corner. Although we could achieve the fundamental motions to move approximately along the orbits, we need to enhance the control accuracy.

In the future works, we need to achieve the more complex and amusing motions by combination with various motions, e.g., curve line, straight line, twisting

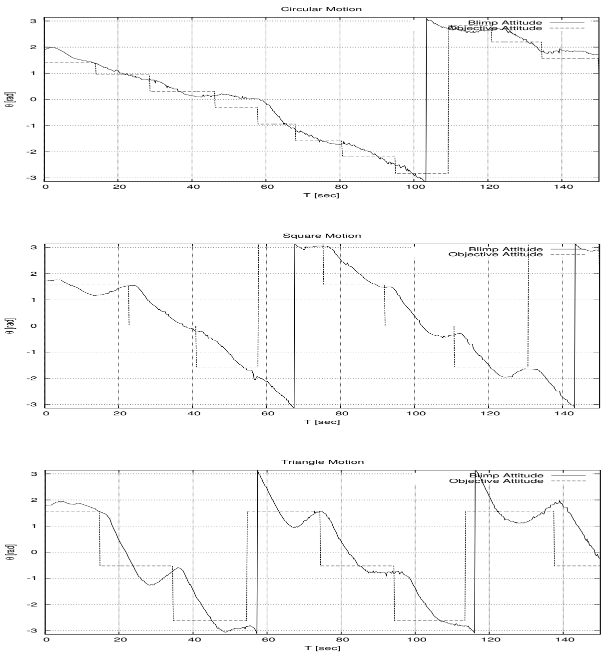

Figure 9: Attitudinal Transition

the corner, rotation on the spot and change of a height. If the blimp robot can execute the sequence of motions given by combinations with the above motions, the blimp robots act the performances and synchronized flight motions as dancing entertainment blimp robots.

Acknowledgment

Our special thanks are due to Mr.Yoshikatsu Henmi, Mr.Hitoshi Murakami and Mr.Yoshihiro Uchimi, Hitachi East Japan Solutions, LTD.; Dr.Dun Wu and Mr.Kenichi Akimoto, North Technology Co., LTD.; Mr.Mikitoshi Amano, TAKARA CO., LTD.; Dr.Keiji Suzuki, Hakodate Future University for considerable cooperation and valuable advice.

References

[1] J. Kobayashi, et al. Flight Control for Blimp Based on CCD Camera Images. Proc. of Int. Symposium on Advanced Control fo Industrial Processes, pp. 269-274, 2002

[2] S. Zwaan, et al. Visual Station Keeping for Floating Robots in Unstructured Environments. Robotics and Autonomous Systems Vol. 39, pp. 145-155, 2002

[3] H. Kadota, et al. Vision-Based Positioning System for Indoor Blimp Robot. Proc. of 5th IFAC/EURON Symposium on Intelligent Autonomous Vehicles, CD-ROM, 2004

Automated Moving Objects Detection with an On-Board Camera for Avoidance of Car Accident

Shohei Sunahara, Yusei Tsuboi, and Osamu Ono

Control Systems Laboratory,

Department of Electric and Electronic Engineering,

Meiji University

1-1-1 Higashimita, Tama-ku, Kawasaki, Kanagawa, JAPAN

(ce33031, tsuboi, ono)@isc.meiji.ac.jp

Abstract

In this paper, we propose a system that detects moving object detection with a CCD camera which captures visual information around a car. The system warns a driver when other vehicles come near to his car, which helps him with avoidance of the car accidents. HSV color space method is employed for the optical flow in the system. In addition, it is possible to find direction of moving objects because the system will be installed on a side door, toward the back of the car. The simulation result indicated some remarks; forty percent of a whole image was cut off by using the HSV color space method; the search time of optical flow was able to be shortened by 50% on the average. As a result, this system could shorten the entire processing time by 60% compared with the case when only the optical flow technique is used.

1 Introduction

Human error occupies a lot of ratios of the cause of traffic accident. This research is support of safe driving, which is one of nine development fields of Intelligent Transport Systems (ITS). Especially, it aims at the avoidance of the contact accident with a vehicle in the next lane at course changes, and a rolling accident with a two-wheeled vehicle at left turn. and driver is warned. In this paper, we propose a system that detects moving object detection with a CCD camera which captures visual information around a car. A CCD camera is attached on the door mirror of the car. The system detects moving objects (car and two wheeled vehicle that approaches the car) from the camera, and warns a driver when they come close to his car. It helps him with avoidance of the car accidents. For constructing the system, we improve the optical flow method by using HSV color space technique.

2 Methodology

In the proposed system, we use an image obtained from the camera on a door mirror. The range of the image obtained from the camera on the door mirror that can be recognized is wider than the door mirror. So, some moving objects within the range that was not able to be recognized only by seeing the door mirror can be recognized. If a wide angle camera is used, more wide-ranging recognition for the moving objects can be done. Moreover, it has the feature that safety is given to the driver only the camera image to be displayed in the monitor.

In this research, it was simulated on PC. The image obtained from the camera on the door mirror is taken into PC by the AVI form, it had divided into the BMP image of full-color, and the image was processed on PC. The size of the image is 320×240, and the 10 frame at a second.

Fig. 1. Image from the camera (upper) and Reflection in a door mirror (below)

2.1 Problem of Optical flow method

When the camera is moving, the background difference method used well for the moving object detection cannot detect the moving body, because the geostationary things of the background are recognized the moving body. Therefore, we use optical flow method that detects the movement of the objects and makes the vector. However, long processing time is generally necessary for the detection of the rate vector of the optical flow method. Then, shortening the processing time is examined in this research.

2.2 HSV color space method

To solve the problem of the optical flow method, we employ the HSV color space method. To decrease the computational complexity that is the problem of the optical flow method, the processing area in the image has been reduced. As the method, the image with RGB color space first input is converted into the image with the HSV color space. And, the saturation(S) of each pixel is measured, and the pixel below the threshold has been reduced. It succeeded in the deletion of the area where the road and the sky so on saturation were low: it succeeded in the deletion of an unnecessary area from 40 to 60% by this processing.

Fig. 2. Original Image (upper) and Conversion Image by HSV color space method (below)

The following equation is a conversion equation from RGB color space to HSV color space.

$$r = \frac{R}{R+G+B} \qquad (1)$$

$$g = \frac{G}{R+G+B} \qquad (2)$$

$$b = \frac{B}{R+G+B} \qquad (3)$$

$$H = \tan^{-1}\left[(g-b)/(2r-g-b)\right] \qquad (4)$$

$$S = \left[(b-r)^2 + (r-g)^2 + (g-b)^2\right]/3 \qquad (5)$$

$$V = (r+g+b) \qquad (6)$$

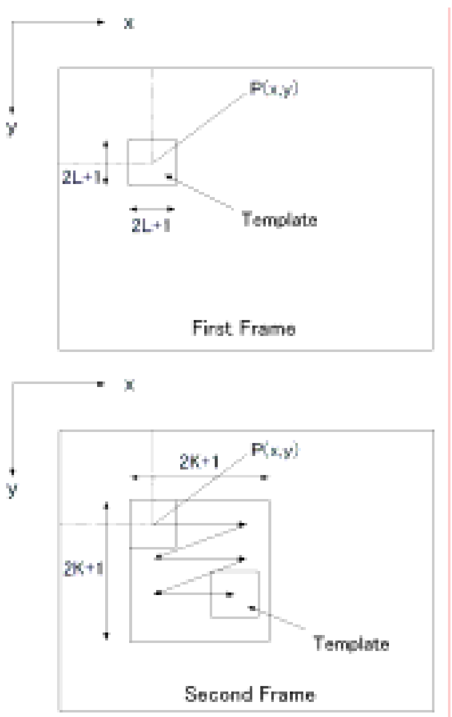

Fig. 3. Illustration of Pattern matching

2.3 Improvement of optical flow method

The pattern matching method is used as a method of requesting optical flow. The template is made in the first frame, and it searches for the place matched from the 2nd frame. It makes the place where the template moved in the matched place. And, the vector is made for the place that moved from former place of the template. It is understood beforehand that the background flows to the back of the screen, and the moving objects moves forward. Then, only the area for lower right one matches the correspondence point from a noteworthy point, a useless calculation is shortened, and the omission processing time can be shortened. The search time of optical flow was able to be shortened by 50% on the average.

Fig. 4. Original Image (upper) and Output Image (below)

3 Simulation result

The technique that has been employed is applied, and the effectiveness is examined. The targeted image is an image that a two-wheeled vehicle approached the car from rear side. The three moving images recorded under each individual place were tested. These moving images have 10 frames per a second. Method of detecting moving objects is that the point with a lot of vectors in the same direction was made a moving object. As a result, this system could shorten the entire processing time by 60% compared with the case when only the optical flow technique is used. However, it is not possible to process in real time. Moreover, a lot of noises occur, and it causes the miss-detection. It is necessary to improve further algorithm to solve this problem. Moreover, we hope further speed up by installing hardware such as DSP.

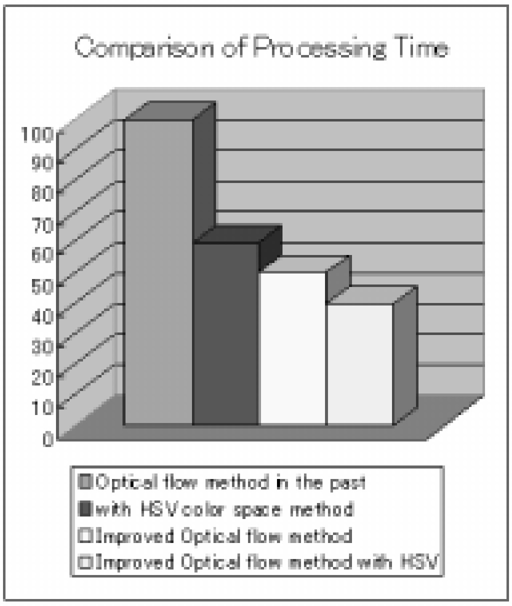

Fig.5. Comparison of Processing Time

4 Summary

In this paper, we have discussed characteristics of the system with the HSV method and the improved optical flow. As a result the system considerably reduced computational time of detection of moving objects. However, the simulation on a normal computer did not realize real-time process. We believe it is able to improve the proposed system in term of computational time. As for that, in future, the computational algorithm of the proposed system will be implemented on DSP.

References

[1] Cucchiara R, et al (2001), Improving shadow suppression in moving object detection with HSV color information. IEEE Intelligent Transportation System Conference Proceedings: 334-339

[2] Prati A, et al (2000), Shadow detection algorithms for traffic flow traffic flow analysis: a Comparative Study. 2001 IEEE Intelligent Transportation Systems Conference Proceedings: 340-345

[4] Honda T, Development of Techniques for Vehicle Maneuvers Recognition with Sequential Images from High Altitude Platforms

[3] Ootani S (2003), Long-range Recognition Method for Moving Objects by Means of Variable Threshold Values on Wide-angle Image Domain. Proceedings of the 22 Japan Simulation Conference: 295-298

[4] Kouzai A (2001), A Detection of Moving Objects by using Image Processing. The Institute of Electrical Engineers of Japan, Electronics, Information and Systems Society

[5] Agui T, Nagano T (2000), Introduction to Image Processing using programming language C, Shoko-Do

The Tenth International Symposium on Artificial Life and Robotics 2005(AROB 10th '05),
B-con Plaza, Beppu, Oita, Japan, February 4-6, 2005

Improving Odometry Accuracy for a Car Using Tire Radii Measurements

Hee Chang Lee
Department of Interdisciplinary Program in Mechatronics
Pusan National University
Busan, 609-735, KOREA

Chang Sup Kim
Department of Mechanical and Intelligent Systems Engineering
Pusan National University,
Busan, 609-735, KOREA

Keum-Shik Hong, Man Hyung Lee
School of Mechanical Engineering,
Pusan National University,
Busan, 609-735, KOREA

Abstract

Odometry is the most widely used method for determining the momentary position of a mobile robot. In most practical applications, odometry provides easily accessible real time positioning information in-between periodic absolute position measurements. Odometry errors are caused by two dominant error sources in vehicles: Systematic errors and nonsystematic errors. Systematic errors stay almost constant over prolonged periods of time and can be calibrated. In most case of mobile robot, unequal wheel diameters are systematic errors. But, they are not systematic errors in case of flexible tires like passenger car case. Radii of flexible tires are always varied by road conditions, rolling of vehicle and etc. So, it is important to measure the variations of tire radii for accurate positioning in odometry navigation of car-like vehicles. The method for measurement of tire radii is described and experimental results are presented in this paper.

1 Introduction

In most positioning system, relative and absolute positioning methods are employed together. Absolute positioning methods usually rely on satellite-based navigation signals (GPS), landmarks or beacons, and map matching. GPS can be used only outdoors and it has poor resolution in a local range (Its errors are about 10m[2]). With a radio station as a compensative reference, differential GPS (DGPS) method has been developed to reduce the errors. GPS suffers from satellite mask occurring in urban environments, under bridges, tunnels or in forests. Moreover, radio frequency-based systems are very expensive. Landmarks or beacons usually require costly installations and maintenance. Map matching methods provide the position and pose of the vehicle. If there were several areas with similar feature, the method would obtain mistake result. In general, absolute positioning methods have the errors that do not accumulate with the movement of the vehicle. Dead reckoning is the representative of relative positioning methods. It has the advantage of cheapness, simplicity, good performance in short term and working in real-time. But its positioning errors accumulated with the traveled distance, and grow without bound. Many cases of relative positioning methods use inertial navigation with accelerometers and gyros. Accelerometer data must be integrated twice to yield position thereby making these sensors exceedingly sensitive to drift. Gyros provide information only on the rate of rotation of vehicle so their data must be integrated once to provide the heading. Besides the deterministic errors contained in accelerometers and gyros measurements, they have also stochastic errors which call for the use of estimation and optimal filtering to correct them. It is common to combine relative positioning with other absolute positioning methods[2][3][4].

Odometry errors are caused by two error sources in vehicles: Systematic errors and nonsystematic errors[1]. Systematic errors (uncertainty of wheelbase, unequal wheel diameters, etc.) stay almost constant over prolonged periods of time and can be calibrated. In most case of mobile robot, unequal wheel diameters are systematic errors. But, they are not systematic errors in case of flexible tires like passenger car. Radii of flexible tires are always varied by road conditions, rolling of vehicle and etc. So, it is important to measure the variations of tire radii for accurate positioning in odometry navigation of car-like vehicles.

Although odometry has several disadvantages, it is important positioning method. Improved odometry can reduce the cost for installations of vehicle systems because it simplifies the fundamental problem of position determination, and the improvement in accuracy of odometry could make high positioning accuracy and robustness by fusing other absolute positioning methods. In modern cars, breaking system is assisted with ABS systems that utilize angular encoders attached to the wheels. In this case, the sensors basically measure the wheel speeds and this measure can be use to estimate travel distances. So, extra encoders to measure wheel rotations are not needed.

This paper reduces such odometry problems with calibration of systematic errors and tire radii measurement. Experiments show the efficiency of consideration of tire radii variation.

2 Odometry Model for a Car

Consider a car-like vehicle. The mobile frame is chosen with its origin P attached to the center of the rear axle. The x-axis is aligned with the longitudinal axis of the car. At time t_k, the vehicle position is represented by the (x_k, y_k) Cartesian coordinates of P in a world frame. The heading angle is denoted θ_k.

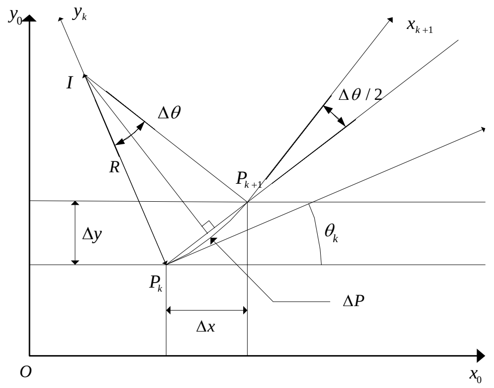

Fig.1 Elementary displacement between two samples

Let P_k and P_{k+1} be two successive positions. Supposing the road is perfectly planar and horizontal, as the motion is locally circular. (Fig.1)

$$\Delta P = R \cdot \Delta\theta \tag{1}$$

where ΔP is the length of the circular arc followed by P, θ, R (the radius of curvature), I (the instantaneous center of rotation)

Supposing the car is moving forward, the variation on the position is expressed as:

$$\begin{aligned} \Delta x &= | P_k P_{k+1} | \cdot \cos(\theta_k + \Delta\theta_k / 2) \\ \Delta y &= | P_k P_{k+1} | \cdot \sin(\theta_k + \Delta\theta_k / 2) \end{aligned} \tag{2}$$

In general, the sampling rate of state is very small compared to their rate of change, so we can approximate $\Delta P \approx | P_k P_{k+1} |$. The integration process is then:

$$\begin{aligned} x_{k+1} &= x_k + \Delta P \cdot \cos(\theta_k + \Delta\theta / 2) \\ y_{k+1} &= y_k + \Delta P \cdot \sin(\theta_k + \Delta\theta / 2) \\ \theta_{k+1} &= \theta_k + \Delta\theta \end{aligned} \tag{3}$$

In Fig.1, the distance traveled, ΔP, and the angle changed, $\Delta\theta$, resulting from the movement P_{k+1} form P_k can be calculated in terms of the incremental changes of the odometric measurements of the right and left wheel motions.

Let us T, ΔP_{RR} , and ΔP_{RL} denote the wheelbase, the covered distances of the right and left rear tires respectively, and we assume that, between two samples, the wheels do not slip and that the distance T is known and constant. Then

$$\begin{aligned} \Delta P_{RR} &= (R + T / 2)\Delta\theta \\ \Delta P_{RL} &= (R - T / 2)\Delta\theta \\ \Delta P &= R \cdot \Delta\theta \end{aligned} \tag{4}$$

Thus, we have

$$\begin{aligned} \Delta P &= (\Delta P_{RR} + \Delta P_{RL}) / 2 \\ \Delta\theta &= (\Delta P_{RR} - \Delta P_{RL}) / T \end{aligned} \tag{5}$$

Equation (5) shows that computation of odometry use left and right traveled distance of tires and wheelbase. That is, ΔP is the average of the right and left traveled distance of rear tires and $\Delta\theta$ is proportional to the difference of the right and left traveled distance of rear tires. Let R_{RR} and R_{RL} be right and left radius of rear tire of a car respectively, ΔP_{RR} and ΔP_{RL} can be expressed as:

$$\Delta P_{RR/RL} = C \cdot R_{RR/RL} \cdot N_{RR/RL} \tag{6}$$

$$C = 2\pi / N_E \tag{7}$$

where $C_{RR/RL}$ are conversion factor that translate encoder pulses into linear displacement of right and left rear tires. N_E, N_{RR} and N_{RL} denote encoder resolution, right and left incremental pulses of rear tires respectively.

3 Tire Radius Measurement Sensor

Tires are attached to axle and they have rotational mechanism, so it is more difficult problem to measure their radius. We suppose that distance between center of tire rotation and the ground which is contacted with tire is approximately same with actual tire radius. From this assumption, the Sharp GP2D12 is used in this paper. It is a short range infrared (IR) proximity sensor. Its output voltage is proportional to the distance between it and an object directly in front of it. It works well in a variety of lighting conditions.

3.1 GP2D12

GP2D12 use triangulation and a small linear CCD array to compute the distance and/or presence of objects in the field of view. The angles vary based on the distance to the object. This method of ranging is almost immune to interference from ambient light and offers amazing indifference to the color of object being detected. Detecting a black wall in full sunlight is possible. Characteristics of the GP2D12 are listed below:

- Output Type : Analog value (0V to ~3V) based on distance measured
- Range : 10cm - 80cm
- Enable Method : Continuous readings ~38ms per reading

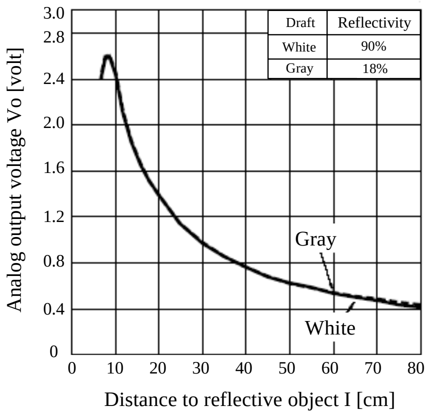

Fig.2 Analog output voltage vs. distance to reflective object (GP2D12)

3.2 Non-linear Outputs and data fitting

Because of some basic trigonometry within the triangle from the emitter to reflection spot to receiver, the output of these detectors is non-linear with respect to the distance being measured. The Fig.2 shows typical output from these detectors. The output of the detectors within the stated range (10 cm - 80 cm) is not linear but rather somewhat logarithmic. This curve will vary slightly from detector to detector so it is a good idea to fit the sensor outputs. In this way, we calibrate each detector and end up with polynomial data that is consistent from detector to detector. Moreover, amplifiers used because of small variation of sensor outputs near nominal tire radius (about 32 cm).

3.3 Sensor implementation

Getting the best results of tire radius measurement with the GP2D12 will require some adjustment. It works best to mount the sensor vertically about 4cm offset from the plane of the tire. Although the sensor has a very narrow beam-width, if the sensor is mounted too close to tire surface it may detect tire itself. Fig.3 shows an implementation of wheel encoder and infrared range finder sensor (GP2D12). Wheel encoder is attached to the center of each tire rotation and a rod is used to prevent case for encoder from rotation. Vertical movement of the rod is supported for suspension system of a car. Infrared range finder is attached to encoder case and it detects the distance between rotation center of a wheel and the ground near a point of the tire contact.

Fig.3 Implementation of wheel encoder and infrared range finder sensor

4 Calibration of Systematic Error

Equation (5) and (6) show that computation of odometry use wheelbase, tire radii and counted pulse of each wheels. In this section, installation uncertainties of infrared range finders and effective wheelbase are considered to calibrate systematic errors.

In case of linear translation, odometry use only information of tires. Therefore, linear translation of specified distance can provide offset of infrared range finder from wheel center.

$$D = \sum \Delta P_{RR/RL} = \sum C \cdot R_{RR/RL} \cdot N_{RR/RL} \qquad (8)$$

where D is specified distance of linear translation for a test car .

If we suppose slow translation, $R_{RR/RL}$ are constants.

$$D = (R_{RR.OFF/RL.OFF} + average(R_{RR.S/RL.S})) \cdot C \sum N_{RR/RL}$$
$$R_{RR.OFF/RL.OFF} = \frac{D}{C\sum N_{RR/RL}} - average(R_{RR.S/RL.S}) \qquad (9)$$

where $R_{RR.OFF/RL.OFF}$ and $R_{RR.S/RL.S}$ are offset of Infrared range finder from wheel center and measurements of tire radii respectively.

We drive the test car along a 10m straight lane for 5 times. From equation (9), the average of $R_{RR.OFF/RL.OFF}$ are calculated. If offsets of range finder sensors are calculated, effective wheelbase T can be calculated form equation (5). The test car is driven along circular path (CW direction and CCW direction) and accumulated heading angle θ is compared with data of electrical compass.

$$T = (\sum(\Delta R_{RR} - \Delta R_{RL})) / \theta_{COMPASS} \qquad (10)$$

where $\theta_{COMPASS}$ denotes heading angle of electrical compass. Initial heading angle of electrical compass is treated as zero degree.

Average of T (for five CW/CCW direction test) is selected as an effective wheelbase.

5 Experimental Results

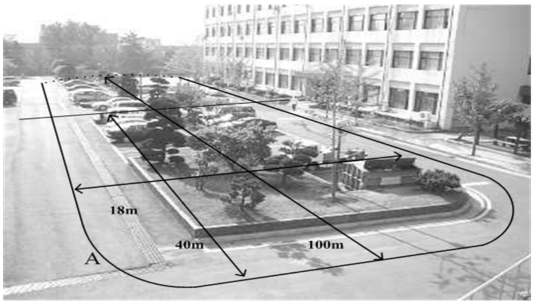

Fig.4 A test Area

Fig. 4 shows a test area. The tested paths are shape of " 8" which can test CW direction and CCW direction together (Fig.5). The car is run twice time for an each test. And other tested paths are also considered for a long distance (Fig.6). Tested road is asphaltic, but it is not flat.

Infrared range finder offset and the effective wheelbase are calculated from the results of section 4. Two rear wheels of the test car are used only. Two cases of results are compared. One case is that the effective wheelbase and initial tire radii (fixed tire radii) are used for odometry computation (dotted line of experimental results). Another case is that the effective wheelbase and unfixed tire radii are used for computation (solid line of experimental results).

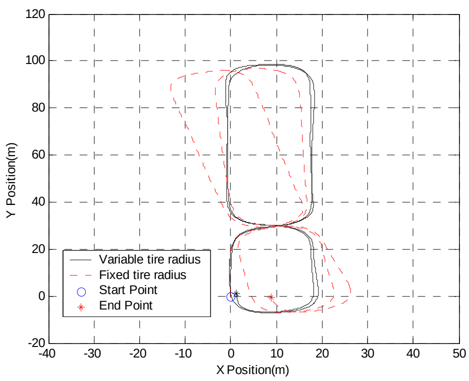

Fig.5 An experimental result (Case 1)

Form Fig.5 and Fig.6, we can see that odometry computation using fixed tire radii has a weak point for roll motion of the car or uneven road surface. Experimental results using information of tire radii show more robust to those situations. The results are meaningful because the positions of the car using odometry are closed for closed reference path. Accumulative error can not be eliminated for odometry computation, but improving odometry accuracy is important for a long navigation which is not available for absolute positioning methods. In a city (especially in a tunnel) or in the forest, many of GPS system can not be available.

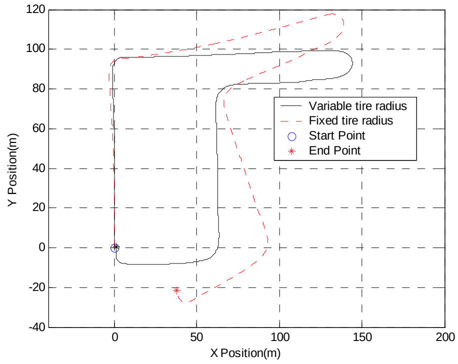

Fig.6 An experimental result (Case 2)

6 Conclusions

This paper presents improving accuracy of odometry for car-like vehicles. Systematic odometry errors are calibrated by straight and circular path navigation. Tire radii are measured by infrared range finders and they are used to reduce nonsystematic odometry errors. Experimental results show that calibration of systematic errors is not sufficient for vehicles which use flexible tires. In case of odometry navigation using information of tire radii, results show good performance without any other sensor fusion.

Acknowledgment

This work was supported by the Ministry of Science and Technology of Korea under a program of the National Research Laboratory, grant number NRL M1-0302-00-0039- 03-J00-00-023-10.

References

[1] Johann Borenstein and Liqiang Feng, " Measurement and Coreection of Systematic Odometry Errors in Mobile Robots," *IEEE Transactions on Robotics and Automation*, vol.12, no.6, December, 1996, pp.869-880.

[2] R. Thrapp, C. Westbrook, D. Subramaian, " Robust localization algorithms for an autonomous campus tour guide," *in Proceedings of the IEEE Conferenceon Robotics and Automation*, 2001, pp.2065-2071.

[3] Ph. Bonnifait, G. Garcia, " Design and experimental validation of an odometric and goniometric localization system for outdoor robot vehicles," *IEEE Transactions on Robotics and Automation*, vol.14, no.4, 1998, pp.541-548.

[4] P. Goel, S. I. Rounmeliotis, and G. S. Sukhatme, " Robust localization using relative and absolute position estimates," *in Proceedings of the IEEE/RSI Conference on Intelligent Robots and Systems*, 1999.

The Tenth International Symposium on Artificial Life and Robotics 2005(AROB 10th '05),
B-con Plaza, Beppu, Oita, Japan, February 4-6, 2005

Improving the Tuning Capability of the Adjusting Neural Network

Yoichi Sugita
Hitachi Research Labolatory
Hitachi Ltd., Japan
6, Kanda-surugadai 4-choume
Chiyoda-ku, Tokyo
101-8010, Japan

Kotaro Hirasawa
Graduate School of
Information, Production and Systems
Waseda University
Hibikino 2-7, Wakamatsu-ku, Kitakyushu-shi
Fukuoka-ken, 808-0135, Japan

Abstract

We have proposed the adjusting neural network (AJNN), which is the extended multi-layered network for control model tuning in the process plant. The AJNN consists of 2 networks (conventional neural network (CNN) and error calculation neural network (ECNN)) and can calculate the accurate tuning value using the ECNN which output the error of the CNN. However, the output of the ECNN does not correspond to the error of the CNN where the input value is large, and decrease the accuracy at this region. In this paper, methodology to improve the accuracy of the AJNN by introducing the procedure to control the ECNN output properly is described and its effectiveness is shown by simulation results.

1 Introduction

In the control system for the plant such as the iron steel plant or chemical plant, which has large dead time and has restricted number of sensors, the model based control is generally applied[1], which predicts appropriate control commands to be inputted to the plant using the model which identifies the plant behavior precisely. In that case, the accuracy of model directly influents the control performance. Therefore, in such control system, model tuning approach is applied and the neural network, which has the high capability to identify the non-linear relationship, is considered to be one of the effective means[2][3].

The neural network establishes the relationship between the error of controlled output ($d\theta$) and the deviation of model parameter to be modified. We have introduced the AJNN in our previous papers [4]~[7], which is extended model of conventional multi layered neural network(CNN) to increase the tuning performance. The AJNN consists of 2 networks which has the same architecture, and one of them calculates the output error of the other network at $d\theta = 0$ (called ECNN; Error Calculation Neural Network). The AJNN generates final output by subtracting the output of ECNN from the others'. The AJNN can calculate the accurate deviation of model parameter in the neighborhood of $d\theta=0$, by eliminating the network error at $d\theta=0$. However, since the ECNN can calculate the network error only at $d\theta=0$ and the AJNN subtracts the output of the ECNN for all region of $d\theta$, accuracy of the output of the AJNN at the region far from $d\theta=0$ may decrease.

In this paper, we discuss the method to increase the AJNN capability where $d\theta$ is large using the non linear function which restrict the output of the ECNN we have proposed before[5]~[7] and describe the optimization of this function.

2 Model Tuning for Reheating Furnace Plant

Reheating furnace plant is one of the typical plant of which the model based control is effecive in the control. The pourpose of this system is to raise the slab temperature to approximetry 1200 centigrate for the rolling process. For this, appropriate furnace temperatures to obtain the target slab temperature are calculated using the control model, which estimate the plant behaivior precicely using the phisical equiations. The accuracy of the model directly effects the control quality, therefore, the model has to be modified corresponding to the plant behaivior change. Fig.1 shows the structure of the model tuning system for the reheating furnace plant. When the slab is extraced, a model tuner modifies one parameter (Φcg) included in the control model and correct the model behaivior using the difference between the detected temperature value and the target one ($d\theta_{out}$), and several state variables such as the furnace temperature. Since the relationship between the deviation of the Φcg ($\Delta\Phi cg$) and $d\theta_{out}$ is basicaly non-linear and the several variables affect this

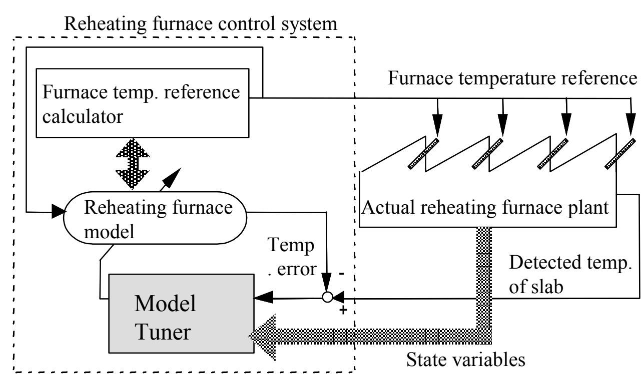

Fig.1. Control system for reheating furnace plant.

relationship, the CNN is considered to be effective to identify this relationship and realizes the model tuner.

3 The Adjusting Neural Network

Let the outputs of the model tuner by given by $F(d\theta_{out}, x_1, \dots, x_n)$, where $x_1, \dots, x_n$ are state variables. Since desired output of the model tuner is obviously zero when $d\theta_{out}$ is equal to zero, the model tuner must always satisfy the following equiation.

$$F(0, x_1, \dots, x_n) = 0 \tag{1}$$

This is a constrain condition for the accurate parameter tuning. However, if the CNN is utilized as the model tuner, it is quite difficult to realize the Eq.1 permanently because of infinite training data and the learning error. The output error at $d\theta_{out}=0$ cause the steady state error when the tuning is converged.

Fig. 2 shows the structure of the AJNN. It has an ECNN(Error Calculation Neural Network) added in parallel to the CNN, which has the same structure of the CNN. The ECNN receive zero instead of $d\theta_{out}$ and calculate the output error of the CNN at $d\theta_{out}$. By subtracting the output of the ECNN from the one of the CNN, an output of the AJNN, $F_{AJNN}(d\theta_{out}, x_1, \dots, x_n)$ is given by

$$F_{AJNN}(d\theta_{out}, x_1, \dots, x_n) = F_{NN}(d\theta_{out}, x_1, \dots, x_n) - F_{NN}(0, x_1, \dots, x_n) \tag{2}$$

Where, $F_{NN}(d\theta_{out}, x_1, \dots, x_n)$ is the output of the CNN and $F_{NN}(0, x_1, \dots, x_n)$ is the one of the ECNN.

When the $d\theta_{out}$ is zero, Eq.2 indicates the following equation, it is obvious the AJNN satisfies the Eq.1 permanently and completes the tuning without the steady state errors.

$$F_{AJNN}(0, x_1, \dots, x_n) = 0 \tag{3}$$

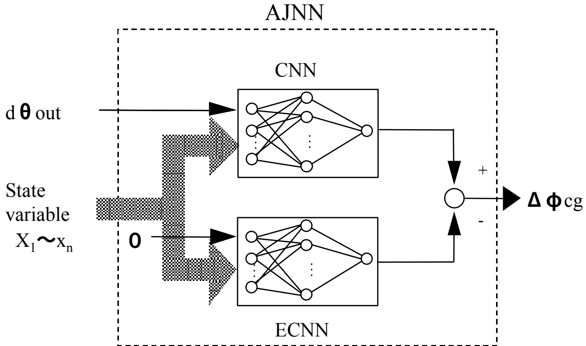

Fig.2. Architecture of AJNN.

4 A Problem of the AJNN

The output of the ECNN directly corresponds to the output error of the CNN at $d\theta_{out}=0$, but not where $d\theta_{out}$ is not equal zero. Therefore, when the $d\theta_{out}$ is large, the output of the AJNN may possibly decrease its accuracy by subtracting the output of the ECNN which does not correspond to the error of the CNN. The problem of the AJNN is the decreasing accuracy where $d\theta_{out}$ is large cause the increase of tuning number compared to the CNN.

5 Non Linear Function

5.1 The AJNN with the Non Linear Function

To solve the problem discussed above, we have introduced the AJNN with the non linear function (see Fig.4). The proposed AJNN has the non linear function, which restrict the output of the ECNN corresponding to the volume of the $d\theta_{out}$, added at the output side of the ECNN and increase the accuracy of output where the $d\theta_{out}$ is large. The output of the AJNN with this function is given by

$$F_{AJNN}(d\theta_{out}, x_1, \dots, x_n) = F_{NN}(d\theta_{out}, x_1, \dots, x_n) - \alpha(d\theta_{out}) \cdot F_{NN}(0, x_1, \dots, x_n) \tag{4}$$

Where $\alpha(d\theta_{out})$ is the non linear function.

The non linear function should have the smooth shape, however, we assume the piecewise function to facilitate the further discussion.

$$\alpha(x) = \begin{cases} 0 & (x < -A/2 - T) \\ \frac{1}{T}(x + A/2 + T) & (-A/2 - T \leqq x < -A/2) \\ 1 & (-A/2 \leqq x \leqq A/2) \\ -\frac{1}{T}(x - A/2 - T) & (A/2 < x < A/2 + T) \\ 0 & (A/2 + T < x) \end{cases} \tag{5}$$

where A is the size of active region and T is the size of transient region.

In the active region, the output of the ECNN is active and in the transient region, the output is decreased gradually. By utilizing this function, the AJNN can calculate the accurate tuning value independently of the volume of $d\theta_{out}$.

5.2 Optimization of the Non Linear Function

To maximize the performance of the AJNN, the non linear

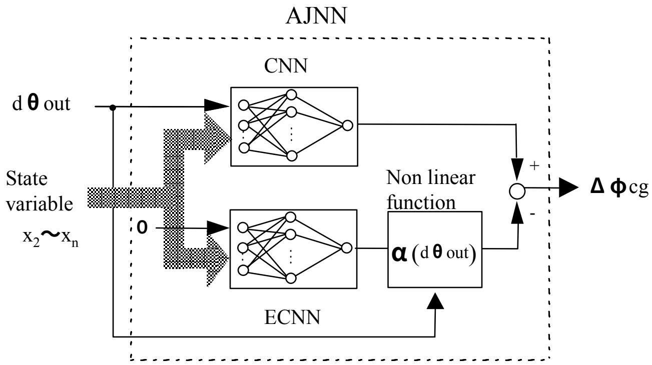

Fig.3. AJNN with a Non-linear Function.

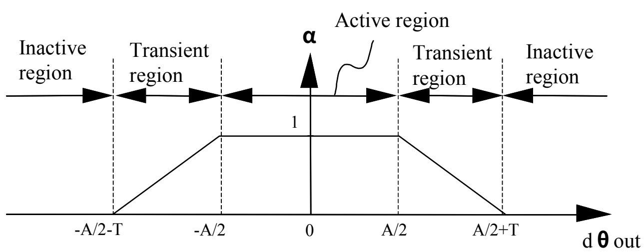

Fig.4. Shape of non-linear function

function has to be optimized, that is, methodology for determination of the size of active region has to be discussed. We propose the methodology to utilize the training data effectively. The determination procedure is described as follows.

Step1; Train the CNN using the training data with BP method.

Step2; Set the initial value(usually 1[℃]) for the size of active region.

Step3;For all training data, evaluate the error between the output of the AJNN with the non linear function and the training data.

Step4; Increment the size of active region by predetermined step width, and find a active region which minimizes the error described at Step 3.

This method is expected to produce the AJNN which minimizes the errors of the training data for all region of $d\theta_{out}$ and even decreases the errors compared to the CNN. That is, the AJNN with the non linear function decided by this procedure can identify the relationship between $d\theta_{out}$ and $\Delta\Phi cg$ described with the training data as much accurately as possible.

6 Simulation Results

6.1 Simulation Conditions

Inputs for the AJNN in this simulation are the current Φcg the control model has, $d\theta_{out}$ and six state variables (the four furnace temperature, an initial slab temperature, thickness of slab). Output of the AJNN in this simulation is the tuning ratio P for the current Φcg. The current Φcg is modified into $(1 + P)\ \Phi cg$ when the slab is extracted from the reheating furnace plant and the output temperature is detected. 672 training data to train the network are prepared by simulation.

6.2 Results and Discussion

Fig.5 shows an example of simulation results. A linear equation, which is a conventional tuning method and identify the relation between $d\theta_{out}$ and P by the linear equation. The linear equation, which can not identify the non linear relation , can not output appropriate tuning value and took 5 times to converge. The CNN can converge quickly but finished the tuning to remain the steady state errors because of the output error at $d\theta_{out}=0$. On the other hand, the AJNN converged by 2 tuning numbers without any steady state error.

Fig.6 indicates the error behavior against the size of active region of the non linear function. The mean error in vertical axis is mean of |training data – output of the CNN|. The size of transient region is fixed at 20[℃]. A size of active region which minimizes the errors is 24[℃], and the error raises gradually corresponding to the increase of the size of active region. Effect of the ECNN is maximized at 24[℃] and after that, the ECNN decrease the accuracy of the output of the CNN gradually. As a result of this examination, 24[℃] is considered to be the best size of active region for the non linear function. Besides, the error at 24[℃] is detected to be lower than the one of the CNN and also the AJNN without the non linear function.

The comparison of tuning performance between the AJNNs which have different size of the non linear function are described in Fig. 7. 30 different conditions which were not used as the training data were applied. A tuning number at 24[℃], which is decided as the size of active region for the non linear function is smallest. Since the $d\theta_{out}$ was less than 200[℃] in this simulation, a tuning number at 200[℃] is exactly equal to the result of the AJNN without the non linear function. The tuning number of the proposed AJNN is obviously lower than the one of the conventional AJNN, and it tells the methodology discussed above can increase the performance of the AJNN and can determine the appropriate the non linear function.

7 Conclusion

We discussed the improvement of the tuning capability of the AJNN, which can modify the control model immediate and accurately for the process control. A methodology to optimize the size of non linear function is introduced, which is a procedure to found the size to minimize the training data error, and its effectiveness is evaluated and found to work effectively to decrease the tuning numbers by simulation result for the reheating furnace plant.

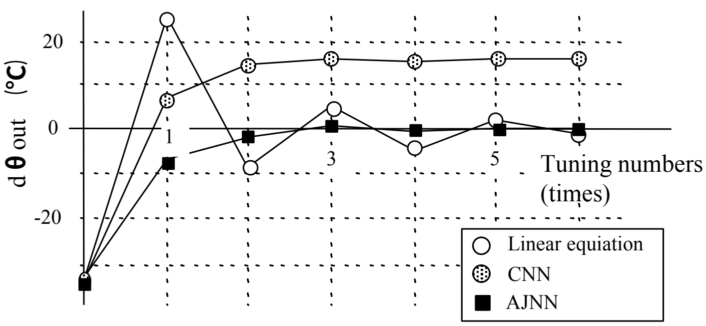

Fig.5. An example of simulation result.

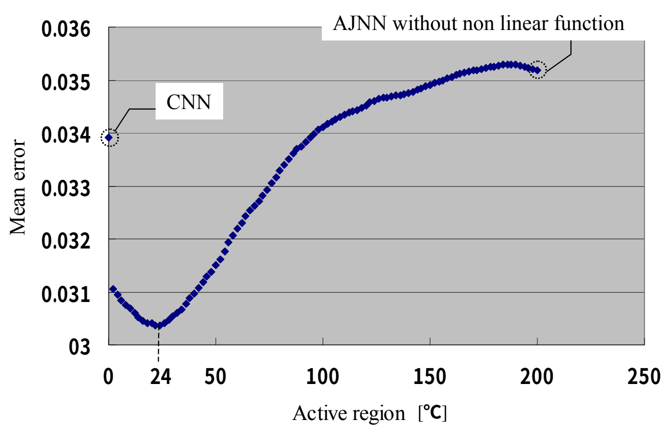

Fig.6. Error behavior against the size of active region

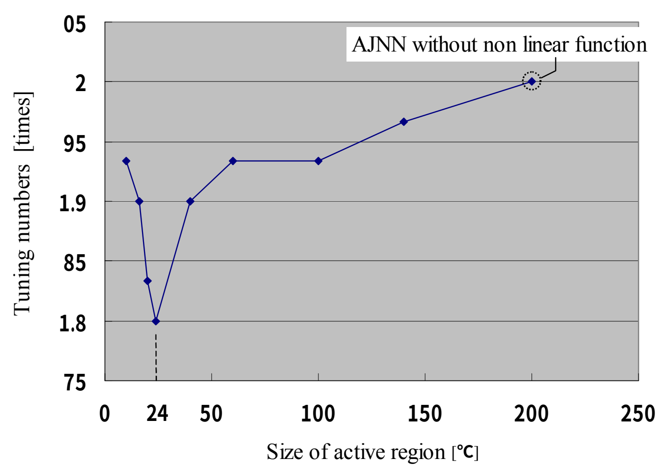

Fig.7. Comparison of tuning performance

References

[1] D.W.Clarke and P.S.Tuffs, "Properties of Generalized Predictive Control", Automatica, Vol.25, pp. 859-875, 1989.

[2] D. Rumelhart et al., "Parallel Distributed Processing", MIT Press, Cambridge, MA, 1986.

[3] W.T. Miller et al., "Neural Networks for Control", MIT Press, Cambridge, MA, 1990.

[3] Y. Sugita et al., "Architecture and Training Algorithm of the Adjusting Neural Network for Accurate Model Tuning", T.IEE of Japan, Vol.115-D,pp461-469, 1995.
Y. Sugita et al., "Extending architecture of the Adjusting Neural Network for Improving Tuning Capability", T.IEE of Japan, Vol.116-C,pp859-866, 1995.

[5] M. Kayama et al, "Adjusting Neural Networks for Accurate Control Model Tuning", FUZZ-IEEE/IFES'95, pp.1995-2000, 2001.

[6] Y. Sugita et al., "Improving Tuning Capability of the Adjusting Neural Network", IEEE IJCNN'97, pp.761-767, 1995.

The Tenth International Symposium on Artificial Life and Robotics 2005(AROB 10th '05),
B-con Plaza, Beppu, Oita, Japan, February 4-6, 2005

Fault Diagnosis for Electro-Mechanical Control System by Neural Networks

Takashi Torigoe, Masami Konishi, Jun Imai, and Tatsushi Nishi
Department of Electrical and Electronic Engineering
Okayama University
3-1-1 Tsushimanaka, Okayama, 700-8530, Japan
konishi@elec.okayama-u.ac.jp

Abstract

In this paper, neuro based intelligent diagnosis methods for electro-mechanical control system are proposed. A self organizing map neural network (SOM) is used to classify measured data of the target system as a qualitative diagnostic method.

Besides of the above procedure, it is expected to attain more efficient maintenance by a quantitative estimation of failure. For the purpose, new method is proposed using a hierarchical neural network (HNN). In the method, classified results by SOM are processed for the quantitative diagnosis. Hierarchical neural network can identify inner structure of the relations between failure causes and its results that enables a quantitative diagnosis.

Keywords : neural network, Self organizing map, fault diagnosis

1 Introduction

When some failure occurs in a mechanical system, diagnosis of the system is to be performed. Then, maintenance or repair action is carried out recovering the system performance to its normal state. As it is impossible to acquire whole internal information of the system, it is usual to analyze output data of the system for the estimation of failure causes.

Traditionally, fault diagnosis is governed by human experts with plenty of experiences and know-how. In these days, mechanical systems are becoming more complex and enlarged in its scale together with its control system. So it becomes necessary to develop new technologies for fault diagnosis not only in a qualitative but also a quantitative manner coping with the needs for automatic diagnosis of complex control systems.

In this paper, SOM[3] method is used for qualitative fault diagnosis in a electro-mechanical control system. Measured data of a system is input to SOM, and classified to particular nodes of SOM. The fault of the system is diagnosed qualitatively from geometrical information of the classified node.

Addition to that, a quantitative diagnosis method using HNN[2, 4] is described. The inputs to HNN are measured data and geometrical information of classification by SOM. The HNN describes correlation between input data and internal fault of the target system. Through learning, the HNN model is updated so as to generate correct value of the internal fault state quantitatively.(Fig. 1)

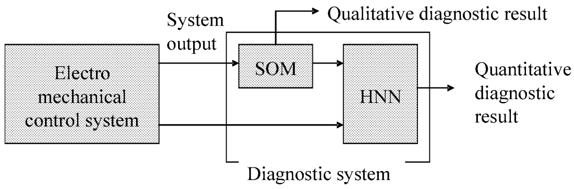

Fig. 1 Diagram of estimation system

First, the looper height control system[1, 5, 6] is selected as a target system of the proposed diagnostic method. After that, diagnosis of an induction motor and that of a robot arm control system are made to verify the versatility of the proposed method.

2 Diagnosis of looper height control system

2.1 The looper height control

The looper height control system consists of looper height detection, PID controller and feedback operation. The block diagram of a looper height control system is shown in Fig. 2.

Here, $G(s)$ represents the transfer function of looper dynamics. There is a time delay in measurement after the output of $G(s)$. This time delay element is a representation of detection delay.

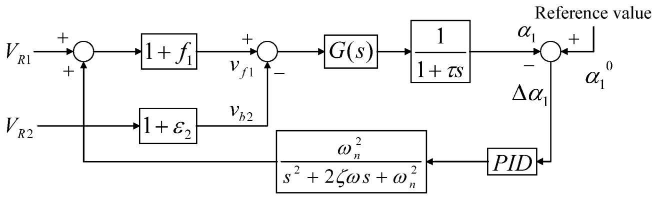

Fig. 2 Block diagram of a looper height control system

Based on detection of the looper height, V_{R1} is manipulated by PID control. There are 2nd order time delay element to manipulate V_{R1}, because of force transmission by torsion.

2.2 Waveform of looper angle

Here, the movement of looper height is simulated when the characteristics of looper height control system in the hot strip mills are changed.

In this paper, 3 factors (K_P, τ, ω_n) are concerned as the characteristics which will be changed.

The looper height is contolled by tuning the proportional gain K_P. The other two elements are internal values of the looper control system. Time delay τ of looper height sensing becomes large with the progression of deterioration in sensing euqipment. Natural angular frequency ω_n becomes small according to fatigue or deterioration in transmission system. These states are abnormal necessary to be found. Where, normal state means that time delay of the element is short time, and abnormal state means that time delay of the element is long time

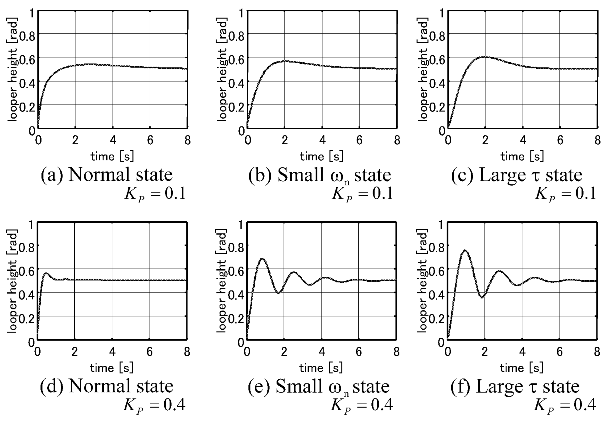

Fig. 3 Waveform of looper angle

The looper height waveforms when the K_P is changed are shown in Fig. 3(a), and Fig. 3(d). There is an overshoot when the K_P is large.

The looper height waveforms when the K_P is changed when ω_n is small are shown in Fig. 3(b), and Fig. 3(e). The oscillation of looper height waveform is enlarged by change of ω_n or τ in comparson with Fig. 3(d). However, By tuning the K_P, oscillation of the waveform is reduced.

3 Classification of looper data

When human get data, it is compared with past data, and result of the comparison leads the conclusion. However, it is difficult to execute those procedure automatically. In this section, the classification method by using SOM neural network is proposed.

3.1 Self Organizing Maps(SOM) N. N.

SOM[3] is a multidimensional scaling method projecting input data space to lower dimentional output space. Typically, output data space is made as 2-dimension. Thus, input data space is visualized into 2-dimensional plane.

Here, the condition in the application of SOM for the classification of looper height waveforms. The looper height waveform is analyzed by wavelet transform, the feature of the waveform is emphasized to wavelet coefficient which is 2-dimentional matrix. The classification method by SOM is applied to the matrix data.

An illustration of the classification is shown in Fig. 4. SOM is trained by a lot of waveforms generated by looper control system in various cases.

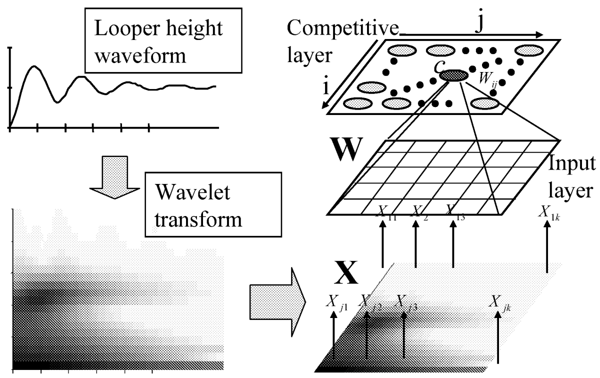

Fig. 4 Qualitative diagnosis by SOM

Where the input waveforms are analyzed by using wavelet transformation as a pre-processing. The number of training times is set to 10000. The number of training data is 250. Where, sampling period is 0.05[s] and sampling time is 5[s]. The size of SOM N. N. in this case is 15×15.

3.2 Classified results (Qualitative diagnosis)

The classified ratio of each nodes in the SOM is described. The failure is considered at small ω_n value and at large τ value. In this case, for failure conditions, $\omega_n < 13$ and $\tau > 0.25$ are considered.

Fig. 5 shows classified results for normal conditions. Lines in Fig. 5 are contour lines corresponding to the ratios with which the data is recognized as normal state. The results in failure state are shown in Figs. 6, 8 respectively.

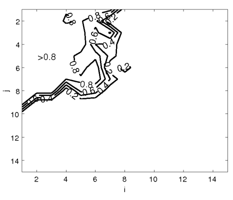

Fig. 5 Classified results of normal state

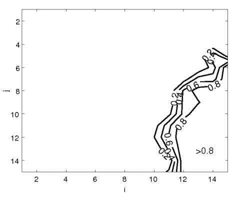

Fig. 6 Classified results of failure state

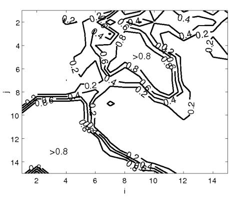

Fig. 7 Classified results of ω_n failure

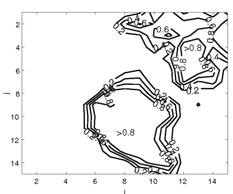

Fig. 8 Classified results of τ failure

These figures show that, data are classified in SOM separately according to the fault.

By classifying the wave form, the data is projected to the 2-dimensional plane. From the position of the plane, it is possible that diagnosis of waveform vibrations or estimation of failure causes qualitatively.

4 Quantitative diagnosis for hot rolling mills

As described above section, the qualitative estimation is made by using SOM. In this section, quantitative estimation method of failure state is described.

4.1 Hierarchical neural network

Neural network is a simplified model of the human brain. It consists of one or more artificial neurons. Therefore, it has the ability to learn and adapt. Also, there are many industrial applications. The hierarchical neural network (HNN) is one of artificial neural networks.[2, 4]

In this paper, the input of HNN is data which contains looper height waveform and classified results described in previous section. And the output of HNN is the parameters in the looper height control system, which provides the fault of the system. Structure of the HNN with the classified results is shown in Fig. 9.

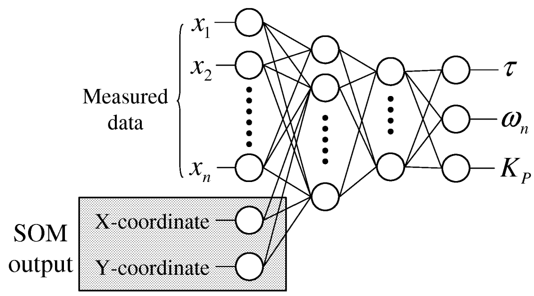

Fig. 9 Quantitative diagnosis by HNN

The HNN model with the classified results (22-40-10-3 4-layer NN) and HNN model without classified results (20-40-10-3 4-layer NN) are trained and compared. These models are trained 5000 times using 500 looper height waveform data which is ramdomly generated. After the training is finished, another 1500 waveform data is applied to these models.

As described above, In this paper, 3 factors are concerned as the characteristics which will be changed. K_P is a configurable parameters by human. Although, parameters to be estimated is τ, ω_n and K_P concerning tuning mistake.

4.2 Estimated results

Table 1 shows RMSE (Root Mean Square Error) of these estimated results. The results of the estimation are shown in Figs. 11, 10. The horizontal axis in these figures is actual parameters of looper height control system, And the vertical axis indicates the estimated parameters. If parameters are estimated with no error, dotted points in these figures are on a straight line.

Table 1 Error comparison

	τ	ω_n	K_P
without som	0.0089	0.50	0.020
with som	0.0044	0.36	0.0072

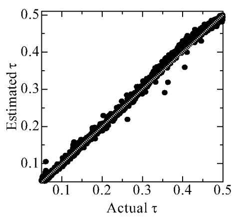

Fig. 10 Estimation result without SOM

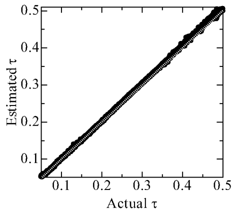

Fig. 11 Estimation result with SOM

Figs. 11, 10 shows that result of estimation using SOM are more accurate. This means that the estimation error is reduced by using SOM.

5 Further applications

5.1 Induction motor

To verify versatility of the proposed diagnostic methods, the estimation system is applied to induction motor. The physical model of induction motor is shown in Fig. 12

The induction motor consists of rotor and stator. In this case, fault of rotor bar is considered to diagnose. This time, the motor has six rotor bars ($R_{B1} \ldots R_{B6}$), and three of them have possibility of fault. When the fault occurs, the electric resistance of the rotor bar is rise. So, it is intended that detection of the rotor bar resistance from angular velocity. Where, the resistance at normal state is $R_{B1} = 33.5[\Omega]$ in this time. Fig. 13 shows angular velocity of the induction motor, when the resistance R_{B1} is changed to $335[\Omega]$, $3350[\Omega]$.

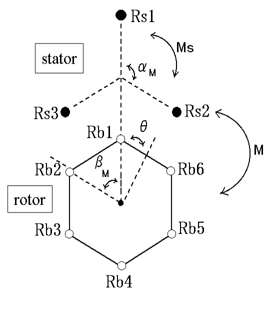

Fig. 12 Physical model of induction motor

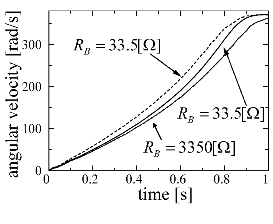

Fig. 13 Angular velocity

The rotor bar resistance is estimated from the angular velocity waveform shown in Fig. 13 using proposed estimation system consists of neural networks. The angular velocity is input to neural network system, and rotor bar resistance is learned as output of the system. Although, the rotor bar resistance is too large to learn as output of neural network, so the neural network learns the resistance as $\log R_{Bn}$. Table 2 shows RMSE of these estimated results. Fig. 14 is the result of R_{B2} estimation using normal neural network. Another estimation result using combined system is shown in Fig. 15.

Table 2 Error comparison

	bar1	bar2	bar3
without som	0.0673	0.0769	0.0670
with som	0.0608	0.0577	0.0597

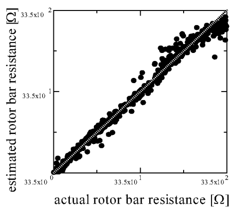

Fig. 14 Resistance of rotor bar #2

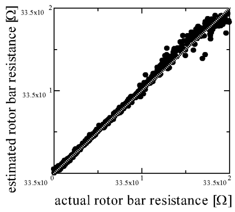

Fig. 15 Resistance of rotor bar #2 with SOM

These results show that estimation error is reduced by neural network combined system, and realized that the neural network system is applicable widely.

5.2 Robot arm

Next, the estimation system is applied to robot arm control system. The robot arm control system is shown in Fig. 16.

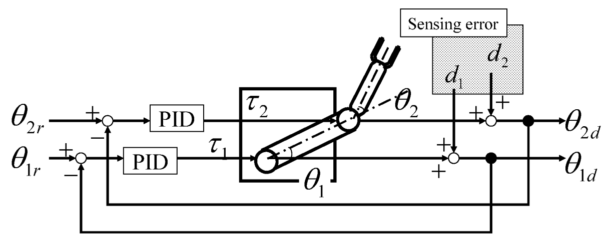

Fig. 16 Robot arm control system

The arm has two motors #1 and #2. The angle θ_n of motor #n are controlled to reference angle θ_{nr} by PID controller. Although, there are sensing error d_n in the part of measuring the θ_n. So, the measured θ_{nd} includes sensing error. Detection of

d_n from θ_{nd} is intended. An example waveform of θ_1, θ_2 are shown in Fig. 17. Sensing error d_1, d_2 are shown in Fig. 18.

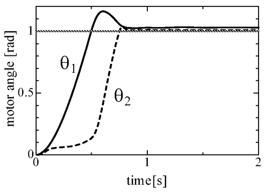

Fig. 17 Angles of arm

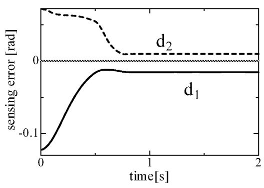

Fig. 18 Disturbances

Two estimation system is applied to θ_{1d} and θ_{2d}, and output the estimated d_1 and d_1 individually.

Figs. 19, 21 shows estimated sensing error by using normal neural network. Figs. 20, 22 are results by using proposed estimation system.

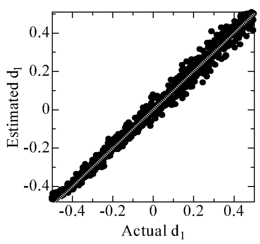

Fig. 19 Estimated d_1

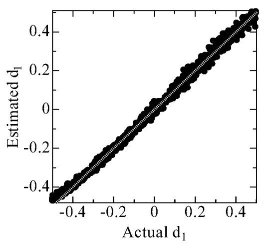

Fig. 20 Estimated d_1 with SOM

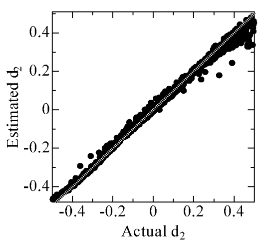

Fig. 21 Estimated d_2

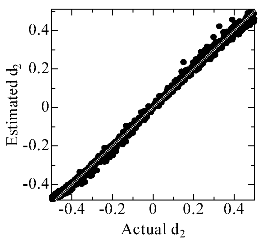

Fig. 22 Estimated d_2 with SOM

Table 3 shows RMSE of these estimated results. It is realized thatThe estimation system using SOM generates better results.

6 Conclusion

In this paper, a quantitative diagnosis method for electro mechanical control system by using SOM neural network is proposed. It is realized that fault of the looper height control system is detected by classifying the system data using SOM neural network model. Using the model, an accurate quantitative estimation of parameters in a looper controller can be made. similarly, effective diagnosis could be carried out for induction motor. Thus, not only detection of failure occurrence but also quantitative analysis of fault causes could be realized.

Table 3 Error comparison

	d_1	d_1
without som	0.029	0.024
with som	0.019	0.017

References

[1] H.Asada et al, "Adaptive and Robust Control Method with Estimation of Rolling Characteristics for Looper Angle Control at Hot Strip Mill", ISIJ International, Vol.43, No.3(2003), pp358-365

[2] I.M.Mujtaba et al, "Application of Neural Networks and Other Learning Technologies in Process Engineering", Imperial College Press, 2001

[3] Lakhmi C.Jain et al, "INDUSTRIAL APPLICATIONS of NEURAL NETWORKS", The CRC Press, 1999

[4] Cihan H. Dagli, "ARTIFICIAL NEURAL NETWORKS for Intelligent Manufacturing", Chapman & Hall, 1994

[5] S.Imajo et al, "Human Model and its Learning for Setting of Looper Control Gain in Threading of Hot Tandem Mills," Proc. of the 46th Annual Conf. of the Institute of Systems, Control and Information Engineers (2002), pp.521-522

[6] S.Imajo et al, "Human Model for Gain Tuning of Looper Control in Hot Strip Rolling," CAMP-ISIJ, Vol.15(2002), p931

The Tenth International Symposium on Artificial Life and Robotics 2005(AROB 10th '05),
B-con Plaza, Beppu, Oita, Japan, February 4-6, 2005

Image processing for GIS applications supported by the use of artificial neural networks*

Tomasz Kubik† Witold Paluszyński†
Adam Iwaniak‡ Przemysław Tymków‡

† Institute of Cybernetics Engineering, Wrocław University of Technology,
Janiszewskiego 11/17, Wrocław 50-372, Poland
E-mail: {tkubik|Witold.Paluszynski}@ict.pwr.wroc.pl
‡ Agricultural University of Wrocław
Norwida 25/27, Wrocław 50-372, Poland
E-mail: iwaniak@ar.wroc.pl, przemyslaw.tymkow@wp.pl

Keywords: image processing, neural networks, GIS

Abstract

This paper presents techniques that can be used as a part of data processing in the remote sensing applications. The techniques proposed employ artificial neural networks for automatic recognition and classification of individual land cover classes, such as forests of some type, buildings, etc. Various quantitative measures have been applied to evaluate the quality of the results. Apart from this a simple Bayesian classifier has been proposed. Presented solutions can be applied for processing of satellite images and aerial images as well.

1 Introduction

A basic problem for any country or region in economic planning, environmental studies, or resource management is availability of accurate, current information. In highly developed countries over 70% of administrative decisions is made on the basis of data related to the earth surface. One significant method for providing current, reliable surface information is remote sensing.

Remote sensing relies on detecting and measuring of electromagnetic energy (usually various spectral fractions of light are measured) emanating from distant objects made of various materials, so that they can identified and categorized by class or type, substance, and spatial distribution. Nowadays this kind of data is mainly acquired in form of satellite images.

Satellite images are an invaluable source of information. Initially providing a resolution of 1x1 km, now commercially available satellite images go down do 60x60 cm. While this is still not as good as the finest resolutions provided by aerial photographs, satellite images can be acquired much faster.

An information system that is designed to work with data referenced by spatial or geographic coordinates is GIS (Geographic Information System). GIS should posses ability of automatic capturing, retrieval, analysis and displaying of spatial data. Because satellite images provide a wealth of information, there is a growing demand for automatic routines that can be applied in GIS. Therefore image processing methods and models targeted at satellite images are being developed.

For uniform areas reflectance measured is enough to perform proper objects classification. However this approach fails for areas with a high heterogeneity of spectral response, such as urban areas. Texture processing algorithms can be applied in this case. These algorithms are usually divided into three major categories: structural, spectral and statistical. Structural methods consider texture as a repetition of basic primitive patterns with a certain rule of placement. Spectral methods analyze the power spectrum. Statistical methods are based mainly on local statistical parameters (entropy, fractal dimension, local variance, variogram, etc. [1, 2, 3, 4, 5, 6, 7, 8, 9].) Other methods make use of artificial neural networks [7, 10, 11, 12].

2 Image processing

The images used in the experiments described in this paper were received from Landsat satellite and produced by the TM (Thematic Mapper) scanner. The TM sensor records reflected electromagnetic energy from the visible to thermal infrared regions of the

*This research was supported in part by the Committee for Scientific Research through grant 5T12E02924

spectrum in 7 bands. The spatial resolution of TM images is 30x30 m for all bands except the thermal, which has 120x120 m resolution. In our case the problem of image processing has been transformed into the problem of classification defined as follows:

Given: 1) a reference image, consisting of points represented by the set of corresponding pixels intensities in n spectral channels, together with a correct points classification into K classes; 2) a test image, consisting of points represented by the set of corresponding pixels intensities in n spectral channels.
Find: correct classification of points in a test image.

The reference images were produced with the aid of CORINE Program (*Coordination of Information on the Environment*) database and an expert knowledge. The CORINE classification consists of twenty-two classes of land use. After conducting some initial experiments, it turned out that this material is insufficient and does not represent correctly physical features, such as: leafy forests, and parks within a city. Therefore, an improved reference classification map was hand-created by an interpreter. The resulting reference map contained only 12 different classes of land use.

3 Neural network based classifier

The design of artificial neural network based classifier involved the following: 1) preparing data sets and patterns from images, 2) building and training a network, 3) processing and visualizing results, 4) estimating the classification error.

The patterns files were usually made up of all Landsat spectral images and one reference image. The reference images was partitioned into two parts: the training set and the testing set, for result evaluation.

We used traditional feed-forward, multi-layer neural networks trained in a supervised mode. The architecture and size of a particular network was dependent on classification problem currently defined.

For classification per pixel an input layer of a neural network consisted of as many neurons as the number of spectral channels used. The output level consisted of the number of classes the neural network was expected to be sensitive for. Thus the training pattern was build from the intensity values of the corresponding pixels in all spectral channels and the reference image (classification results for different architectures are shown in Fig. 2.)

For classification per parcel training patterns were created moving a square mask within a reference image (for which the results of classification were known). The size of the mask was an odd number, the center of the mask was a subject of classification. In this case neural networks were design in that way, that input level of a particular network matched a mask of predefined size, but the output level was made of one neuron. Different neural networks were created for different kinds of objects and different masks.

The results of experiments were evaluated by comparing images segmented by the neural networks with corresponding reference images (see Fig. 1.) For this purpose we involved the measures described in the section 5.

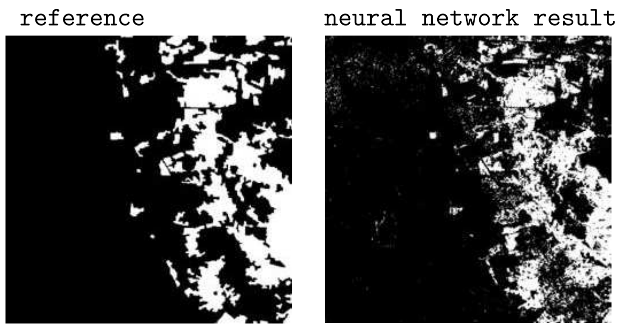

Figure 1: The reference map and the image obtained with a neural network trained to recognize coniferous forests (3 input neurons, 24 hidden neurons, 1 output neuron), $\kappa = 0.945$.

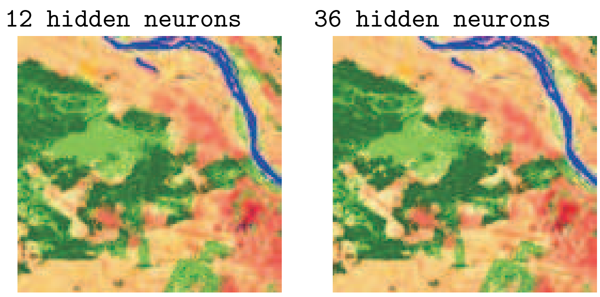

Figure 2: Classification results for different neural network architectures (3 input neurons, 12 output neurons.)

4 Naive Bayes classifier

Naive Bayes classifier combines probability model with a decision rule. Usually the rule is specified as the choice of hypothesis which is the most probable.

This rule is called maximum a posteriori rule. Corresponding classifier is defined by the function $\mathcal{B}$:

$$\mathcal{B}(\bar{x}) = \arg\max_{c_k} P(C=c_k) \prod_{i=1}^{n} P(X_i=x_i|C=c_k) \quad (1)$$

where: $\bar{x} = [x_1, \ldots, x_n]$ – vector of features x_i (in the case of multispectral image these are pixels intensities for one point in n spectral channels); c_k – classes labelled with $k = 1, \ldots, K$; $P(C=c_k)$ – probability, that observed case belongs to the class c_k; $P(X_i = x_i|C = c_k)$ – conditional probablitities (that intensity of a pixel X_i equals given x_i in a channel i, when it is known that corresponding point is of the class c_k).

To build classifier $\mathcal{B}$ at first step the probability $P(C = c_k)$ should be approximated. This can be done as follows:

$$P(C=c_k) = \frac{N_k}{\sum_{k=1}^{n} N_k} \quad (2)$$

N_k - amount of points of the reference image classified to the class k (sum of all N_k equals total number of points of the reference image). Next conditional probabilities should be approximated by the normal distributions:

$$P(X_i=x_i|C=c_k) \cong f(x_{k,i}) = \frac{1}{\sigma_{k,i}\sqrt{2\pi}} e^{\frac{-(x_{k,i}-\mu_{k,i})^2}{2\sigma_{k,i}}} \quad (3)$$

where $x_{k,i}$ - pixel intensity level for class k and for spectral channel i.

Approximation of $\sigma_{k,i}$ can be expressed by the standard deviation of case:

$$S_{N_k-1,i} = \sqrt{\frac{1}{N_k - 1} \sum_{j=1}^{N_k} (x_{k,i,j} - \bar{x}_{k,i})^2} \quad (4)$$

where: $x_{k,i,j}$ - intensity level of pixel j from channel i, for which corresponding point has been assign to class k (according to the provided reference image classification).

Approximation of $\mu_{k,i}$ is given by:

$$\bar{x}_{k,i} = \frac{1}{N_k} \sum_{j=1}^{N_k} x_{k,i,j} \quad (5)$$

5 Quality measures

A number of experiments have been conducted resulting in many classification maps generated. They have been evaluated by human experts and found to be very valuable, readily comparable to the human-processed CORINE map and in some areas more accurate. To quantify the quality of the results in an automatic manner several statistical measures have been considered. For the confusion matrix $A = [a_{ij}]$ where a_{ij} is the number of sample pixels from the jth class that have been classified as belonging to the ith class, the following measures have been proposed[13, 14]:
– the users accuracy of class i: $\frac{a_{ii}}{a_{ri}}$, where $a_{ri} = \sum_i a_{i.}$ (sum of ith row entries);
– the producers accuracy of class i: $\frac{a_{ii}}{a_{ci}}$, where $a_{ci} = \sum_i a_{i.}$ (sum of ith column entries);
– the overall accuracy of the method: $\sum_i a_{ii}/a_t$, where a_t is the total number of pixels;
– simple Kappa coefficient:

$$\hat{\kappa} = \frac{P_o - P_e}{1 - P_e} \quad \text{where} \quad \begin{array}{l} P_o = \sum_i aii/a_t \\ P_e = \sum_i a_{ri}a_{ci}/a_t^2 \end{array} \quad (6)$$

– weighted Kappa coefficient:

$$\hat{\kappa}_w = \frac{P_{ow} - P_{ew}}{1 - P_{ew}} \quad \text{where} \quad \begin{array}{l} P_{ow} = \sum_i \sum_j w_{ij} \frac{a_{ij}}{a_t} \\ P_{ew} = \sum_i \sum_j w_{ij} \frac{a_{i.}a_{.j}}{a_t^2} \end{array} \quad (7)$$

The weights w_{ij} are constructed so that $0 <= w_{ij} < 1$ for all $i \neq j$, $w_{ii} = 1$ for all i, and $w_{ij} = w_{ji}$.

6 Conclusions

Because of the limitations not all of the results obtained had chance to be presented here. Nevertheless the experiments performed proved that satellite images can be processed automatically by supervised learning with a neural network. The best results of classification per-pixel were obtained for areas such as those in the Fig. 1. But sometimes the results for urban areas were only barely acceptable. In such cases the improvements were done by applying per-parcel classification. There information about neighborhood of a pixel (pixels values within moving mask) helped in proper classification. Presented naive Bayesian classifier is an another option (see Fig. 3.) It can be used, as the other techniques discussed, for satellite and aerial image processing.

References

[1] J. R. Carr: Spectral and textural classification of single and multiple band digital images. *Computers and Geosciences*, 22(8):849–865, (1996).

[2] M. Tuceryan and K. Anil: *The handbook of Pattern recognition and computer vision*, chapter 2.1

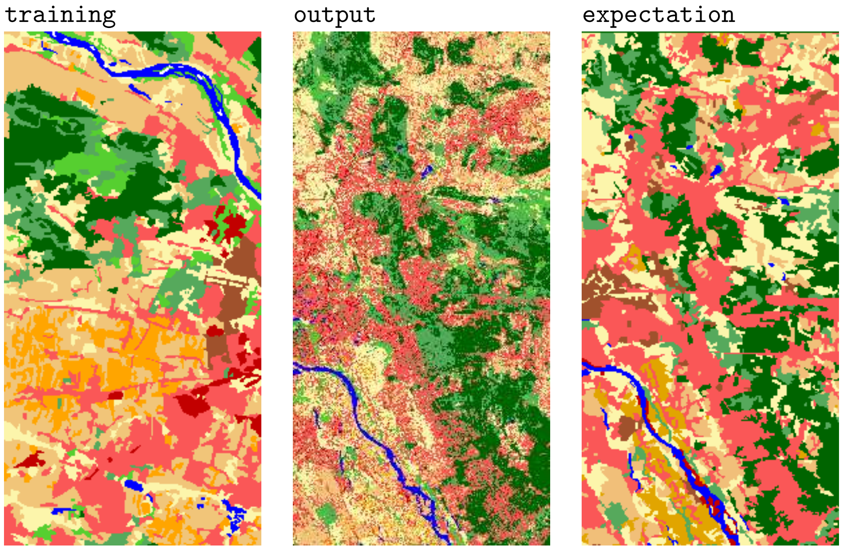

Figure 3: Classification results for naive Bayes classifier build on data coming from three spectral channels (not shown). `training` is a reference image used for classifier building, `output` shows classification results, `expectation` is a reference image showing expected classification results.

Texture Analysis, pp. 207–248 World Scientific Publishing Co., 2nd edition, (1998).

[3] S. Berberoglu, C. Lloyd, P. Atkinson, and P. Curran: The integration of spectral and textural information using neural networks for land cover mapping in the Mediterranean. *Computers and Geosciences*, 26(4):385–396, (2000).

[4] J. Keuchel, S. Naumann, M. Heiler, and A. Siegmund: Automatic land cover analysis for Tenerife by supervised classification using remotely sensed data. *Remote Sensing of Environment*, 86(4):530–541, (2003).

[5] Q. Cheng: Multifractality and spatial statistics. *Computers and Geosciences*, 25(9):949–961, (1999).

[6] M. Chica-Olmo and F. Abarca-Hernndez: Computing geostatistical image texture for remotely sensed data classification. *Computers and Geosciences*, 26(4):373–383, (2000).

[7] X.-H. Liu, A. Skidmore, and H. Van Oosten: Integration of classification methods for improvement of land-cover map accuracy. *ISPRS Journal of Photogrammetry and Remote Sensing*, 56(4):257–268, (2002).

[8] J. Ju, E. D. Kolaczyk, and S. Gopal: Gaussian mixture discriminant analysis and sub-pixel land cover characterization in remote sensing. *Remote Sensing of Environment*, 84(4):550–560, (2003).

[9] G. M. Foody: Estimation of sub-pixel land cover composition in the presence of untrained classes. *Computers and Geosciences*, 26(4):469–478, (2000).

[10] G. W. H. German and M. N. Gahegan: Neural network architectures for the classification of temporal image sequences. *Computers and Geosciences*, 22(9):969–979, (1996).

[11] D. M. Miller, E. J. Kaminsky, and S. Rana: Neural network classification of remote-sensing data. *Computers and Geosciences*, 21(3):377–386, (1995).

[12] J. Ruiz-del Solar: TEXSOM: Texture segmentation using self-organizing maps. *Neurocomputing*, 21:7–18, (1998).

[13] L. Hubert-Moy, A. Cotonnec, L. Le Du, A. Chardin, and P. Perez: A Comparison of Parametric Classification Procedures of Remotely Sensed Data Applied on Different Landscape Units. *Remote Sensing of Environment*, 75(2):174–187, (2001).

[14] G. M. Foody: A Coefficient of Agreement for Nominal Scales. *Educational and Psychological Measurement*, 20:37–46, (1960).

The Tenth International Symposium on Artificial Life and Robotics 2005(AROB 10th '05),
B-con Plaza, Beppu, Oita, Japan, February 4-6, 2005

A supervised learning rule adjusting input-output pulse timing for pulsed neural network

Makoto Motoki
motoki@graduate.chiba-u.jp

Seiichi Koakutsu
koakutsu@faculty.chiba-u.jp

Hironori Hirata
hiro@faculty.chiba-u.jp

Graduate School of Science and Technology
Chiba University
1-33 Yayoi-cho, Inage-ku, Chiba-shi, 263-8522, Japan

Abstract

Some supervised learning rules have been already proposed for pulsed neural network (PNN). Those learning rules use information expression with pulse frequency, however, does not use that with pulse timing. Therefore, the conventional learning rules cannot learn pulse timing, although it is important to adjust input/output (I/O) pulse timing of network. The purpose of this paper is to propose a supervised learning rule adjusting I/O pulse timing for PNN. In the proposed method, pulse timing error and pulse frequency error are corrected by adjusting transmission delay and synaptic weight among neurons. Results of computational experiments indicate that the proposed method enables learning of pulse timing in multi-layered feedforward PNN.

1 Introduction

Pulsed Neural Network (PNN) has been getting attention recently as one of neural network models which is proper for temporal data processing. As for learning for PNN, Hebbian learning has been proposed[1][2]. Hebbian learning is one of unsupervised learning rules, and enables to optimize the internal state of network. However, Hebbian learning cannot construct a network which can represent required input/output (I/O) temporal data mapping. In order to construct a network which can represent required I/O mapping, supervised learning rules are necessary. Some supervised learning rules have been already proposed for PNN[3][4]. Those learning rules use information expression with pulse frequency, however, does not use that with pulse timing. Therefore, the conventional learning rules cannot learn pulse timing, although it is important to adjust I/O pulse timing of network.

The purpose of this paper is to propose a supervised learning rule adjusting I/O pulse timing for PNN. In the proposed method, pulse timing error and pulse frequency error are corrected by adjusting transmission delay and synaptic weight among neurons. We verify the effectiveness of the proposed method by computer simulation. Results of computational experiments indicate that the proposed method enables learning of pulse timing in multi-layered feedforward PNN.

2 Pulsed neural network

This study uses a leaky integrate-and-fire neuron model which is the same model used by Gerstner et al[1]. and Eurich et al[2]., so the behavior of this neuron model is explained briefly.

A presynaptic neuron j and a postsynaptic neuron i is connected with a synaptic weight $w_0^{i,j}$ by synapse. A set of firing time T^j of the neuron j and a set of arrival time $T_{\mathrm{d}}^{i,j}$ at which pulses of the neuron j reach the neuron i are defined as follows:

$$\begin{aligned} T^j &= \{t_\nu^j; 1 \le \nu \le n^j\} = \{t \,|\, y^j(t) = 1\}, && (1) \\ T_{\mathrm{d}}^{i,j} &= \{t_{\mathrm{d},\nu}^{i,j} = t_\nu^j + \tau_{\mathrm{d}}^{i,j}; 1 \le \nu \le n^j\}, && (2) \end{aligned}$$

where n^j is the maximum number of pulses of the neuron j, $y^j(t)$ is the output of the neuron j at time t, and ${}_{\mathrm{d}}^{i,j}$ is transmission delay between the neuron j and i.

When the pulse of the neuron j arrives, the membrane potential $P_{\mathrm{m}}^i(t)$ of the neuron i changes as follows:
in case of $t > t_\mu^i + {}_{\mathrm{r}}^i$,

$$\tau_{\mathrm{m}}^i \frac{dP_{\mathrm{m}}^i(t)}{dt} = -P_{\mathrm{m}}^i(t) + \sum_{j \in J} w_0^{i,j} \sum_{t_{\mathrm{d},\nu}^{i,j} \in T_{\mathrm{d}}^{i,j}} \delta \;\; t - t_{\mathrm{d},\nu}^{i,j} \;\; , \qquad (3)$$

and in case of $t \le t_\mu^i + {}_{\mathrm{r}}^i$,

$$P_{\mathrm{m}}^i(t) = 0, \qquad (4)$$

where ${}_{\mathrm{r}}^i$ is absolute refractory period, ${}_{\mathrm{m}}^i$ is depression time constant, J is a set of presynaptic neurons of the neuron i, $w_0^{i,j}$ is synaptic weight, and $\delta(t)$ is Dirac's delta function. In this paper, synaptic weight $w_0^{i,j}$ is $-1 \le w_0^{i,j} \le 1$.

When $P_{\mathrm{m}}^{i}(t)$ exceeds threshold θ^{i}, the neuron i fires, and the neuron i outputs 1 (eq.(5)). In addition, a set of firing time T^{i} of the neuron i is expressed as follows:

$$y^{i}(t) = \mathcal{H}\ \ P_{\mathrm{m}}^{i}(t) - \theta^{i}\ \ , \quad (5)$$

$$T^{i} = \{t_{\mu}^{i}; 1 \le \mu \le n^{i}\} = \{t \mid y^{i}(t) = 1\}, \quad (6)$$

where $\mathcal{H}(t)$ is Heaviside unit function.

3 Proposed method

In this section, definitions of training set and error function are given, and features and procedures of the proposed method are explained.

3.1 Training set and error function

Definitions of training set and error function are given before explaining the proposed method. Input-time-series data L_{I} and output-time-series data L_{O} of training set are defined as follows:

$$L_{\mathrm{I}} = \{l_{\zeta,p}^{i}; i \in I, 1 \le p \le P, 1 \le \zeta \le N_{p}^{i}\}, \quad (7)$$

$$L_{\mathrm{O}} = \{l_{\xi,p}^{o}; o \in O, 1 \le p \le P, 1 \le \xi \le N_{p}^{o}\}, \quad (8)$$

where I is a set of input layer's neurons, P is the number of learning patterns, and N_{p}^{i} is the number of pulses which input to a input layer's neuron i for a pattern p. And O is a set of output layer's neurons, N_{p}^{o} is the number of pulses which should output from a output layer's neuron o for the pattern p.

The error function which is used in this paper is defined as follows:

$$E_{p} = \sum_{o \in O} \int_{0}^{T_{p}} \left| \sum_{\xi=1}^{N_{p}^{o}} \mathcal{H}\ \ t - l_{\xi,p}^{o}\ \ - \sum_{\nu=1}^{n_{p}^{o}} \mathcal{H}\ \ t - t_{\nu,p}^{o}\ \ \right| dt, \quad (9)$$

$$E = \sum_{p=1}^{P} E_{p}, \quad (10)$$

where T_{p} is the length of pattern p, n_{p}^{o} is n^{o} on pattern p, $t_{\nu,p}^{o}$ is t_{ν}^{o} on pattern p, E_{p} is the errors on pattern p, and E is the total of E_{p} on all patterns.

3.2 Features and procedure

Main features of the proposed method are the following.

a. Pulse timing error between actual output of network and corresponding training signal is back-propagated from output layer to input layer. And pulse timing error is corrected by adjusting transmission delay between a presynaptic neuron and a postsynaptic neuron.

b. Pulse frequency error between actual output of network and corresponding training signal is back-propagated from output layer to input layer. And pulse frequency error is corrected by adjusting synaptic weight between a presynaptic neuron and a postsynaptic neuron.

c. The proposed method is able to apply to multi-layered feedforward PNN.

Procedure of the proposed method is described below.

1. Initialize parameters of PNN.
2. Input all pattern of input-time-series data L_{I} of training set to PNN. And record firing time T^{j} of all neurons on each pattern. T^{j} on each pattern p is expressed by $T_{p}^{j} = \{t_{\nu,p}^{j}; 1 \le \nu \le n_{p}^{j}\}$.
3. Calculate E_{p} on each pattern p.
4. Adjust transmission delay τ_{d} between each pair of neurons.
5. Adjust synaptic weight w_{0} between each pair of neurons.
6. Repeat from 2. to 5. until satisfying given termination condition.

Step 4. and 5. are explained in section 3.3 and 3.4 in detail.

3.3 Transmission delay adjustment

Procedures of adjusting transmission delay which is mentioned at step 4 in section 3.2 are explained in detail. Neuron o, j and k denote a output layer's neuron, a hidden layer's neuron and a hidden or input layer's neuron, respectively. Besides, the neuron k is a presynaptic neuron of the neuron j, and the neuron j is a presynaptic neuron of the neuron o.

First of all, $\tau_{\mathrm{d}}^{o,j}$ which is transmission delay between the hidden layer's neuron j and the output layer's neuron o is updated as follows:

$$\tau_{\mathrm{d}}^{o,j}(c+1) = \tau_{\mathrm{d}}^{o,j}(c) + \alpha_{\tau_{\mathrm{d}}} \sum_{p=1}^{P} E_{p} \sum_{t_{\nu,p}^{j} \in T_{p}^{j}} \Delta\tau_{\mathrm{d},p}^{o,j}(t_{\nu,p}^{j}), \quad (11)$$

$$\Delta\tau_{\mathrm{d},p}^{o,j}(t_{\nu,p}^{j}) = \sum_{l_{\xi,p}^{o} \in F_{p}^{o}(t_{\mathrm{d},\nu,p}^{o,j})} W_{\tau_{\mathrm{d}}}^{j}(l_{\xi,p}^{o} - t_{\mathrm{d},\nu,p}^{o,j}), \quad (12)$$

$$F_{p}^{o}(t_{\mathrm{d},\nu,p}^{o,j}) = \{\ l_{\xi,p}^{o} \mid t_{\nu,p}^{j} < l_{\xi,p}^{o} \le t_{\nu+1,p}^{j}\}, \quad (13)$$

$$W_{\tau_{\mathrm{d}}}^{\nu}(\varphi) = e^{-\varphi^{2}} \sin(\frac{2\pi}{\tau_{\mathrm{r}}^{\nu}}\varphi), \quad (14)$$

where c is learning cycle, $\alpha_{\tau_{\mathrm{d}}}$ is learning rate regarding transmission delay, and $\Delta\tau_{\mathrm{d},p}^{o,j}(t_{\nu,p}^{j})$ is a function of $t_{\nu,p}^{j}$. In addition, $F_{p}^{o}(t_{\mathrm{d},\nu,p}^{o,j})$ is a set of elements which are included in L_{O} on pattern p between $t_{\nu,p}^{j}$ and $t_{\nu+1,p}^{j}$, and $W_{\tau_{\mathrm{d}}}^{j}(\cdot)$ is a window function regarding transmission delay.

$\gamma^j_p(t^j_{\nu,p})$ which is the total of $\Delta\ {}^{o,j}_{\mathrm{d},p}(t^j_{\nu,p})$ of all post-synaptic neurons is calculated for each pulse of the neuron j as follows:

$$\gamma^j_p(t^j_{\nu,p}) \ = \ \sum_{o\in O}\Delta\tau^{o,j}_{\mathrm{d},p}(t^{o,j}_{\nu,p}). \tag{15}$$

Secondly, ${}^{j,k}_{\mathrm{d}}$ which is transmission delay between the hidden layer's neuron j and the other hidden layer's or input layer's neuron k is updated as following:

$$\tau^{j,k}_{\mathrm{d}}(c+1) \ = \ \tau^{j,k}_{\mathrm{d}}(c)+\alpha_{\tau_{\mathrm{d}}}\sum_{p=1}^{P}E_p\sum_{t^k_{\nu,p}\in T_p}\Delta\tau^{j,k}_{\mathrm{d},p}(t^k_{\nu,p}), \tag{16}$$

$$\Delta\tau^{j,k}_{\mathrm{d},p}(t^k_{\nu,p}) = \sum_{t^j_{\mu,p}\in F^j_p(t^{j,k}_{\mathrm{d},\nu,p})} W^k_{\tau_{\mathrm{d}}} \ t^j_{\nu,p}+\beta_{\tau_{\mathrm{d}}}\gamma^j_p(t^j_{\mu,p})-t^{j,k}_{\mathrm{d},\nu,p} \ , \tag{17}$$

$$F^j_p(t^{j,k}_{\mathrm{d},\nu,p}) = \{\, t^j_{\mu,p}\,|\,t^k_{\nu,p}<t^j_{\mu,p}\le t^k_{\mathrm{d},\nu+1,p}\}, \tag{18}$$

where $F^j_p(t^{j,k}_{\mathrm{d},\nu,p})$ is a set of elements which are included in T^j_p on pattern p between $t^k_{\nu,p}$ and $t^k_{\nu+1,p}$, and $\beta\ _{\mathrm{d}}$ is reduction rate regarding transmission delay.

$\beta\ _{\mathrm{d}}$ should be set appropriate value in accordance with time step of the finite difference Δt and transmission delay $\ _d$.

In order to update transmission delay of presynaptic neurons of the neuron k, $\gamma^k_p(t^k_{\nu,p})$ which is the total of $\Delta\ {}^{j,k}_{\mathrm{d},p}(t^k_{\nu,p})$ of all postsynaptic neurons is calculated for each pulse of the neuron k as follows:

$$\gamma^k_p(t^k_{\nu,p}) = \sum_{j\in J}\Delta\tau^{j,k}_{\mathrm{d},p}(t^k_{\nu,p}). \tag{19}$$

Eq.(16)$\sim$(19) is repeated until the presynaptic neuron k becomes the input layer's neuron.

3.4 Synaptic weight adjustment

Procedure of adjusting synaptic weight which is mentioned at step 5 in section 3.2 is explained in detail. Neuron o, j and k is the same as the neurons described in section 3.4.

First of all, $w^{o,j}_0$ which is synaptic weight between the hidden layer's neuron j and the output layer's neuron o is updated as follows:

$$w^{o,j}_0(c+1) \ = \ w^{o,j}_0(c)+\alpha_{w_0}\sum_{p=1}^{P}E_p\Delta w^{o,j}_{0,p}, \tag{20}$$

$$\Delta w^{o,j}_{0,p} \ = \ \sum_{\nu=1}^{n^j}\sum_{g^o_{\mu,p}\in H^o_p(t^{o,j}_{\mathrm{d},\nu,p})} W^j_{w0}(g^o_{\mu,p}-t^{o,j}_{\mathrm{d},\nu,p})\Psi^o_p(g^o_{\mu,p}), \tag{21}$$

$$W^{\mu}_{w_0}(\varphi) = \frac{e^{-2\varphi/\tau^{\mu}_{\mathrm{r}}}}{(1+e^{-2\varphi/\tau^{\mu}_{\mathrm{r}}})^2}, \tag{22}$$

$$H^o_p(t^{o,j}_{\mathrm{d},\nu,p}) \ = \ \{g^o_{\mu,p}\,|\,t^j_{\nu,p}<g^o_{\mu,p}\le t^j_{\nu+1,p}, \quad g^o_{\mu,p}\in G^o_p\}, \tag{23}$$

$$G^o_p \ = \ \{g^o_{\mu,p};1\le\mu\le N^o_{\mathrm{G},p}\}=\{t\,|\,\Psi^o_p(t)\ne 0\}, \tag{24}$$

$$\Psi^o_p(t) \ = \ \sum_{\xi=1}^{n^{\xi}}\int_{t-\Delta t/2}^{t+\Delta t/2}\delta(u-l^o_{\xi,p})du-\sum_{\nu=1}^{n^o}\int_{t-\Delta t/2}^{t+\Delta t/2}\delta(u-t^o_{\nu,p})du, \tag{25}$$

where c is learning cycle, α_{w_0} is learning rate regarding synaptic weight, and $\Delta w^{o,j}_{0,p}$ is update value of weight between the neuron j and o on pattern p. In addition, $W^j_{w_0}(\cdot)$ is a window function regarding synaptic weight, $H^o_p(t^{o,j}_{\mathrm{d},\nu})$ is a set of elements which are included in G^o_p on pattern p between $t^j_{\nu,p}$ and $t^j_{\nu+1,p}$, G^o_p is a set of time when $\Psi^o_p(t)$ is plus or minus value, and $\Psi^o_p(t)$ is a function which denotes the difference between the output of the neuron o and corresponding training signal.

$\Psi^j_p(t)$ which denotes the difference between the output of the neuron j and $\Psi^o_p(t)$ of the postsynaptic neuron o is calculated by eq.(26). G^j_p which denotes a set of time when $\Psi^j_p(t)$ is plus or minus value is defined by eq.(27).

$$\Psi^j_p(t) = \mathrm{Sign}\Bigg(\mathrm{Sign}\ \sum_{o\in O}w^{o,j}_0\Big\{\beta_{w_0}\Psi^o_p(t+\tau^{o,j}_{\mathrm{d}}) + \sum_{t^o_{\nu,p}\in(T^o_p\cap\bar{G}^o_p)}\int_{t-\Delta t/2}^{t+\Delta t/2}\delta(u-t^o_{\nu,p}+\tau^{o,j}_{\mathrm{d}})du\Big\} -\sum_{\nu=1}^{n^j}\int_{t-\Delta t/2}^{t+\Delta t/2}\delta(u-t^j_{\nu,p})du\Bigg), \tag{26}$$

$$G^j_p = \{g^j_{\mu,p};1\le\mu\le N^j_{\mathrm{G},p}\}=\{t\,|\,\Psi^j_p(t)\ne 0\}, \tag{27}$$

$$\mathrm{Sign}(\varphi)=\begin{cases}-1 & \text{for} \quad \varphi<0,\\ \ \ 0 & \text{for} \quad \varphi=0,\\ \ \ 1 & \text{for} \quad \varphi>0,\end{cases} \tag{28}$$

where β_{w_0} is reduction rate for synaptic weight, and $\bar{G}^o_p$ is a complementary set of G^o_p. In other words, $\bar{G}^o_p$ is a set of elements which are not included in G^o_p, but are included in a set of time $\{0,\Delta t,2\Delta t,\cdots,T_p-\Delta t,T_p\}$, where the number of elements of this set is $T_p/\Delta t+1$. Consequently, $(T^o_p\cap\bar{G}^o_p)$ denotes a set of required firing-time of the neuron o on pattern p.

Secondly, $w^{j,k}_0$ which is a synaptic weight between the hidden layer's neuron j and the other hidden layer's or input layer's neuron k is updated as following:

$$w^{j,k}_0(c+1) \ = \ w^{j,k}_0(c)+\alpha_{w_0}\sum_{p=1}^{P}E_p\Delta w^{j,k}_{0,p}, \tag{29}$$

$$\Delta w^{j,k}_{0,p} = \sum_{\nu=1}^{n^k}\sum_{g^j_{\mu,p}\in H^j_p(t^{j,k}_{\mathrm{d},\nu,p})} W^k_{w0}(g^j_{\mu,p}-t^{j,k}_{\mathrm{d},\nu,p})\Psi^j_p(g^j_{\mu,p}), \tag{30}$$

$$H^j_p(t^{j,k}_{\mathrm{d},\nu,p}) \ = \ \{g^j_{\mu,p}\ |\ t^k_{\nu,p}<g^j_{\mu,p}\le t^k_{\nu+1,p}, \quad g^j_{\mu,p}\in G^j_p\}. \tag{31}$$

In order to update synaptic weight of presynaptic neurons of the neuron k, $\Psi_p^k(t)$ which denotes the difference between the output of neuron k and $\Psi_p^j(t)$ of the postsynaptic neuron j is calculated by eq.(32). G_p^k which denotes a set of time when $\Psi_p^k(t)$ is plus or minus value is defined by eq.(33).

$$\Psi_p^k(t) = \mathrm{Sign}\Bigg(\mathrm{Sign}\sum_{j\in J} w_0^{j,k}\Big\{\beta_{w_0}\Psi_p^j(t+\tau_{\mathrm{d}}^{j,k}) + \sum_{t_{\nu,p}^j\in(T_p^j\cap \bar{G}_p^j)} \int_{t-\Delta t/2}^{t+\Delta t/2}\delta(u-t_{\nu,p}^j+\tau_{\mathrm{d}}^{j,k})\Big\}\, du - \sum_{\nu=1}^{n^k}\int_{t-\Delta t/2}^{t+\Delta t/2}\delta(u-t_{\nu,p}^k)du\Bigg), \quad (32)$$

$$G_p^k = \{g_{\mu,p}^k;\, 1\le\mu\le N_{\mathrm{G},p}^k\} = \{t\,|\,\Psi_p^k(t)\neq 0\}. \quad (33)$$

Eq.(29)-(33) is repeated until the presynaptic neuron k becomes the input layer's neuron.

4 Experiments

In this section, results of computational experiments are given in order to demonstrate the advantages of the proposed method.

The network structure of PNN used in the experiments is a multi-layered feedforward network which is one input layer, one output layer, and two hidden layers. The number of the input layer's neurons is two, that of the output layer's neurons is one, and that of the hidden layer's neurons per layer is 3∼15.

The training set used in the experiments is the following. Input-time-series data and output-time-series data are both periodic data.

The termination condition of learning used in the experiments is the following. The learning is stopped as success when error E becomes less than 5.0×10^{-3}, and as failure when the learning cycle c reaches 4,000 epochs without E being less than 5.0×10^{-3}.

In the experiments, convergence rate of learning is observed when the number of hidden layer's neurons is changed from 3 to 15. In addition, difference of convergence rate between synchronized I/O pulse timing case and non-synchronized I/O pulse timing case is compared. The learning is executed 100 times from different initial snaptic weights and transmission delay.

The convergence rate which is the average of 100 trials is showed in Figure 1. In Figure 1, x-axis indicates the number of hidden layer's neurons par layer and y-axis indicates the convergence rate. Figure 1 indicates that the convergence rate becomes large when

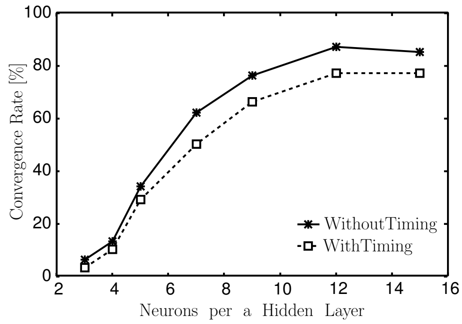

Figure 1: Convergence rate of learning.

the number of hidden layer's neurons increases. However, the rate saturates when the number of neurons becomes 15. In addition, the convergence rate of synchronized I/O pulse timing case is lower than that of non-synchronized one. This result indicates that the proposed method enables PNN to learn pulse timing with only small reduction of the convergence rate.

5 Conclusion

The purpose of this paper was to propose a supervised learning rule adjusting I/O pulse timing for PNN. We verified the effectiveness of the proposed method by computer simulation. Results of computational experiments indicated that the proposed method enables learning of pulse timing in multi-layered feedforward PNN. However, the searching ability of solutions of the proposed method is not enough, since the convergence rate decreases when the number of hidden layer's neurons becomes small. To improve the searching ability of solutions is one of future works.

References

[1] Gerstner W, Kempter R, van Helmmen JL and Wagner H (1996), A neuronal learning rule for sub-millisecond temporal coding. *Nature*, vol.383, pp.76-78

[2] Eurich CW, Cowan JD and Milton JG (1997), Hebbian delay adaptation in a network of integrate-and-fire neurons. *Artificial neural networks* - ICANN'97, pp.157-162

[3] Kuroyanagi S, Iwata A (1998), An Supervised Learning Rule of Puled Neuron Model (in Japanese). *Technical report of IEICE*, NC97-151, pp.95-102

[4] Fatamata N, Kuroyanagi S and Iwata A (2002), An Implementation Method of Pulsed Neuron Model for FPGA Devices (in Japanese). *Technical report of IEICE*, NC2001-211, pp.121-128

[5] Maass W and Bishop CM (2001), Pulsed Neural Networks," *The MIT Press* (2001)

The Tenth International Symposium on Artificial Life and Robotics 2005(AROB 10th '05),
B-con Plaza, Beppu, Oita, Japan, February 4-6, 2005

Remarks on tracking method of neural network weight change for learning type neural network direct controller

Takayuki Yamada
Department of Computer and Information Sciences
Faculty of Engineering
Ibaraki University
4-12-1 Nakanarusawa, Hitachi, Ibaraki, 316-8511, Japan

Abstract

A neural network usually learns so as to minimize a scalar value such as a cost function. This scalar value is useful for a confirmation of neural network learning performance. However, this confirmation may not be correct for neural network controllers because a plant dynamics affects the cost function. This paper proposes a new tracking method of neural network weight change. The proposed tracking method can provide a new confirmation of the neural network learning performance.

1. Introduction

Many studies have been undertaken in order to apply both the flexibility and the learning capability of neural networks to control systems[1][2]. A neural network controller is usually designed so as to minimize the error between a plant output (or neural network output) and a desired output (teaching signal). For this aim, neural network learning rules are designed to change neural network weights whose number reaches into thousands or tens of thousands in some applications. The reason to use these huge number of weights is that a biological neural network has huge number of neurons and it is proved that more neurons realize more accurate nonlinear mapping capability of the neural network. As mentioned above, the essence of neural network learning is nothing but the change of the neural network weights. However, in order to examine the performance of the neural network learning, most researchers use a cost function (squared error between the desired output and the neural network output (or the plant output)). This is because it is not practical to examine the huge number of the neural network weights and the cost function is a scalar value which is easily dealt with. However, the neural network weight change may not be reflected in the cost function. This problem is especially serious in neural network controller applications. This is because the performance of the cost function is affected by dynamics of the plant. This fact leads that more accurate examination of the neural network controller learning performance requires to track the neural network weight change directly.

This paper proposes a new tracking method of the neural network weight change. A leaning type neural network direct controller[3] for a second order discrete time plant is selected in order to examine the proposed tracking method and its simulation results show the usefulness of the proposed method.

2. Tracking method of neural network weight change

This section proposes the tracking method of the neural network weight change and its application to the learning type neural network direct controller. For our tracking method, first, one weight vector is derived from the neural network weights. Next, we calculate an inner product of this weight vector and a standard vector. Any vector, which has same order as that of the weight vector, can be selected as this standard vector, for example, the weight vectors derived from the initial neural network weights, the final neural network weights and so on. We can also calculate an angle between the weight vector and the standard vector. The track of the neural network weight change can be drawn on a 2D plane through the use of these calculated inner product and angle. This track does not show whole neural network weight change, but it is not affect by the plant dynamics and it can show an another characteristic of the neural network learning performance. We can realize the new examination of the neural network learning through the use of the proposed tracking method or its combination with the cost function.

In order to verify the usefulness of the tracking method, we applied it to the learning type direct controller.

A reason of this selection is that the direct controller is simplest. The another reason is that the cost function of the learning type is the sum of the squared error at each sampling time and the plant dynamics less affect it in comparison with an adaptive type. This fact is useful to examine the proposed tracking method effectiveness. We also select a discrete time SISO (single input and single output) plant as an object plant because it is simplest and useful for a practical controller application. When we use above selections, an output layer of the neural network has one neuron, the weights between the output layer and a hidden layer can be expressed as a vector ω and the weights between the hidden layer and an input layer can be expressed as a matrix W. To simplify, the neuron number of the input layer is equal to that of the hidden layer. That is, the weight matrix W is the square matrix.

We can derive a new weight vector Γ from these neural network weight vector and matrix as follows:

$$\Gamma^T = [\omega_1 \cdots \omega_n \; W_{11} \cdots W_{1n} W_{21} \cdots W_{2n} \cdots W_{n1} \cdots W_{nn}] \qquad (1)$$

where n is the neuron number both the input layer and the hidden layer. When we define the standard vector Γ_0 , the track of the neural network weight change on the 2D plane can be expressed as the following equations.

$$X = |\Gamma| \cos\theta, \quad Y = |\Gamma| \sin\theta \qquad (2)$$

$$\theta = \cos^{-1}\left(\frac{<\Gamma_0 \quad \Gamma>}{|\Gamma_0| \; |\Gamma|}\right) \qquad (3)$$

Where $<\Gamma_0 \quad \Gamma>$ is the inner product between the vector Γ_0 and the vector Γ, and $|\Gamma|$ is the norm of the vector Γ. As mentioned above, we can draw a new weight performance on the 2D plane by use of X and Y in equations (2) and (3). The plant dynamics does not affect this weight performance directly.

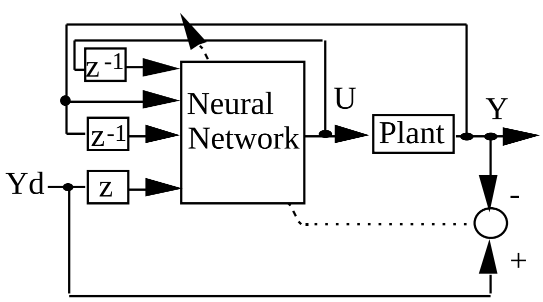

Fig.1 Block diagram of learning type neural network direct controller for second order discrete time plant.

3. Simulation

To verify the usefulness of the proposed tracking method, it is applied to the learning type neural network direct controller for the second order discrete time plant. The simulated plant is follows:

$$Y(k) = -a_1 Y(k-1) - a_2 Y(k-2) + U(k-1) + bU(k-2) - a_3 Y(k-3) + C_{non} Y^2(k-1) \qquad (4)$$

Where Y(k) is the plant output, U(k) is the plant input, k is the sampling number, a_1, a_2 & b are the plant parameters, a_3 is the parasite term and C_{non} is the nonlinear term. For this simulation, a_1=-1.3, a_2=0.3, b=0.7, a_3=-0.03 and C_{non}=0.2 are selected. The rectangular wave is also selected as the desired value Yd. The output error ε and the cost function J(p) of the trial number p are defined as follows:

$$\varepsilon(k) = Yd(k) - Y(k) \qquad (5)$$

$$J(p) = \sum_{k=1}^{\rho} \varepsilon^2(k) \qquad (6)$$

where ρ is the sampling number within one trial period. In this simulation, ρ=300 is selected.

For this simulated plant, the neuron number n in both the input and hidden layers is 4. The neural network input vector I is defined as the following equation.

$$I^T(k) = [Y_d(k+1) \; Y(k) \; Y(k-1) \; U(k-1)] \qquad (7)$$

We select the following sigmoid function f(x) as the input output relation of the hidden layer.

$$f(x) = \frac{X_g\{1 - \exp(-4x/X_g)\}}{2\{1 + \exp(-4x/X_g)\}} \qquad (8)$$

Where Xg is the parameter which defines the sigmoid function shape. The plant input U(k) equals the neural network output composed as follows:

$$U(k) = \omega^T(p) f\{W(p) I(k)\} \qquad (9)$$

The block diagram of the learning type neural network direct controller is shown in fig.1. The learning rule of this neural network controller is shown in the following equations.

$$W_{ij}(p+1) = W_{ij}(p) + \eta \sum_{k=1}^{\rho} [\varepsilon(k)\omega_i(p) I_j(k-1) f'\{\sum_{j=1}^{n} W_{ij}(p) I_j(k-1)\}] \qquad (10)$$

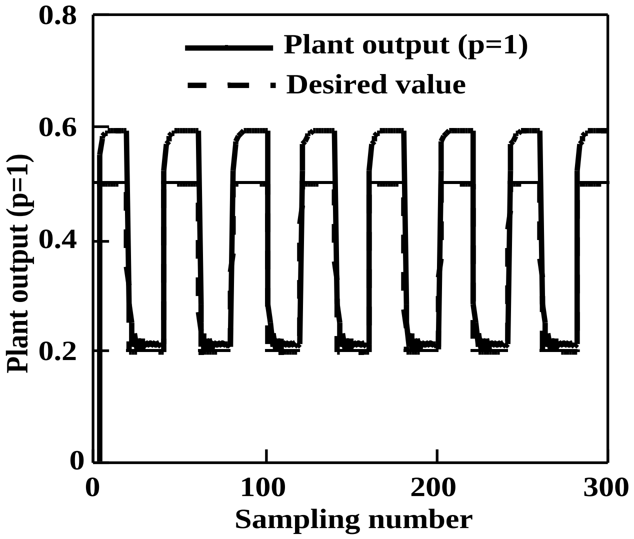

Fig.2 Plant output (p=1).

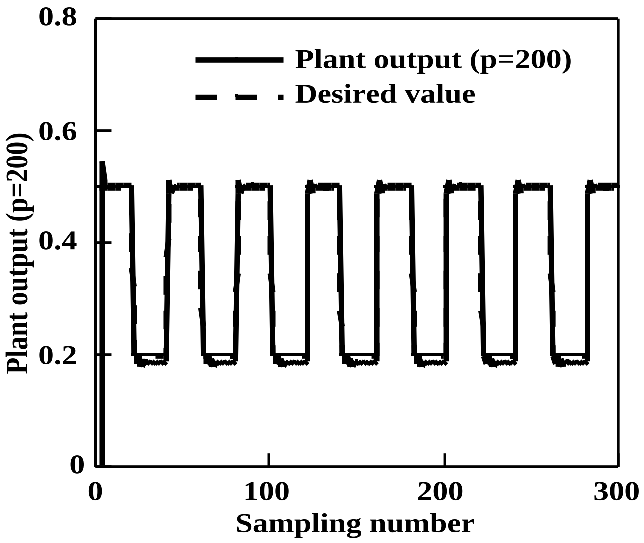

Fig.3 Plant output (p=200).

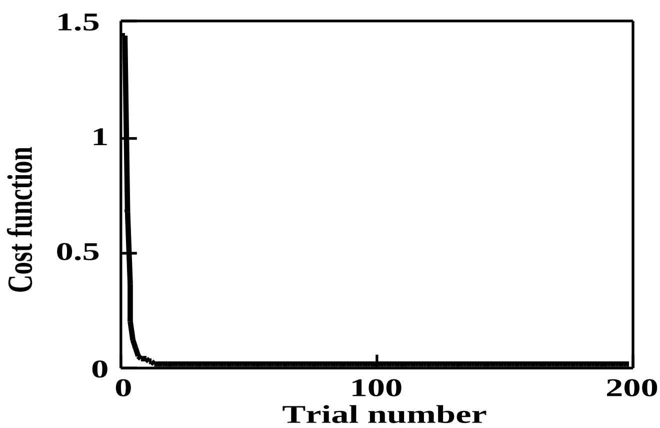

Fig.4 Cost function.

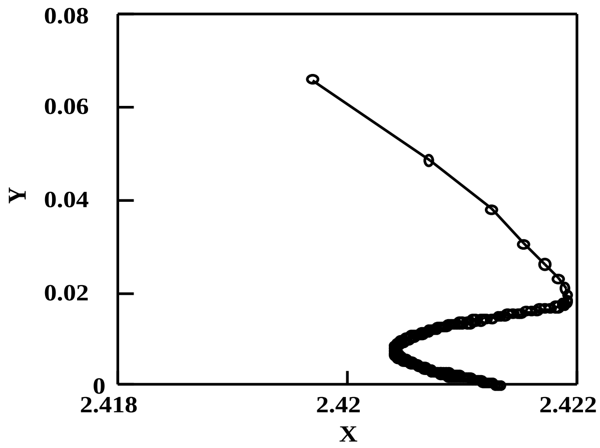

Fig.5 Track of neural network weight change (p=1~200).

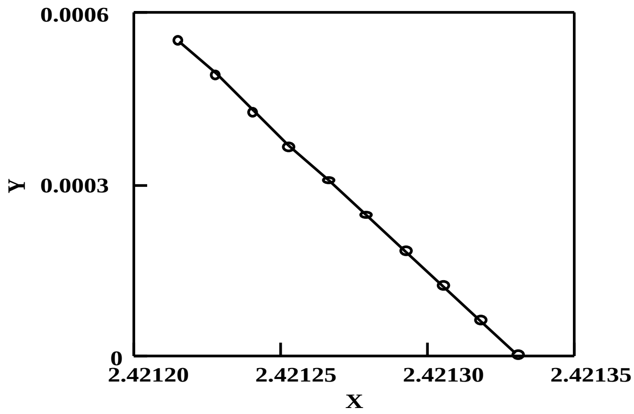

Fig.6 Track of neural network weight change (p=191~200).

$$\omega_i(p+1) = \omega_i(p) + \eta f \left[\sum_{j=1}^{n} \{ W_{ij}(p) \sum_{k=1}^{\rho} (\varepsilon(k) I_j(k-1)) \} \right] \quad (11)$$

Where η is the parameter to determine the neural network convergence speed. We select the weight vector derived from the final neural network weights as the standard vector Γ_0 of the equations (2) and (3)

Figure 2 shows an example of the plant output (p=1) using an initial neural network weight. The solid line and the dotted line show the plant output and the desired value respectively. Figure 3 shows the final plant output (p=200). As shown in these figures, the neural network learning well performs and the plant output converges to the desired value. Figure 4 shows the cost function with regard to the trial number. As shown here, it appears that the neural network weights do not change after several tens of trials and the neural network learning is completely finished. Figure 5 shows the track of the neural network weight change (p=1~200) through the use of the proposed tracking method. As shown in this figure, the neural network weights change relatively large from the first trail p=1 to six trials p=6. After p=6, they change continuously and this change is not finished at p=200. To verify this, figure 6 shows the expansion of fig.5 which is the track of the neural network weight change (p=191~200). As shown here, we confirm that the neural network weights continuously change at p=200. That is, the neural network learning is not finished yet at p=200. This fact can not be observed by use of the cost function shown in fig.4 and the proposed tracking method is useful for the neural network performance examination. Figure 7 shows an another example of the cost function. In this example, it also appears that the neural network learning is finished within tree trials. Figure 8 and 9 shows the track of the neural network weight change (p=1~200) and its expansion (p=191~200) respectively. The neural network weights change continuously and the neural network learning is not finished yet.

As mentioned above, the proposed tracking method is useful to track the neural network weight change on 2D plane. This track shows another feature of the neural network learning performance.

4. Conclusion

This paper proposed the new tracking method of the neural network weight change. It was applied to the learning type neural network direct controller and simulated. The simulation results showed the usefulness of the proposed tracking method and it could be observed that the neural network weights were continuously changed in some cases although the neural network learning appeared to be finished. The combination of the cost function and the proposed tracking method is useful to examine the neural network learning performance more accurately.

Acknowledgment

The author wishes to express his thanks to Mr.Chihiro Kaneko, graduated student, Ibaraki University, for his programming and simulation.

References

[1]K.S.Narendra and K.Parthictsarathy, "Identification and Control of Dynamics System Using Neural Networks", IEEE Transaction on Neural Networks, Vol.1, No.1, pp.4-27, 1990

[2]D.Psaltis, A.Sideris and A.Yamamura, "Neural Network Controller", Proceedings of 1987 IEEE International Conference on Neural Networks, Vol.IV, pp.551-558, San Diego, 1987

[3]Takayuki Yamada and Tetsuro Yabuta, "Nonlinear Neural Network Controller for Dynamic System", Proceedings of IECON'90 (16th Annual Conference of IEEE Industrial Electronics Society), pp.1244-1249(1990)pp.295-302, 1994

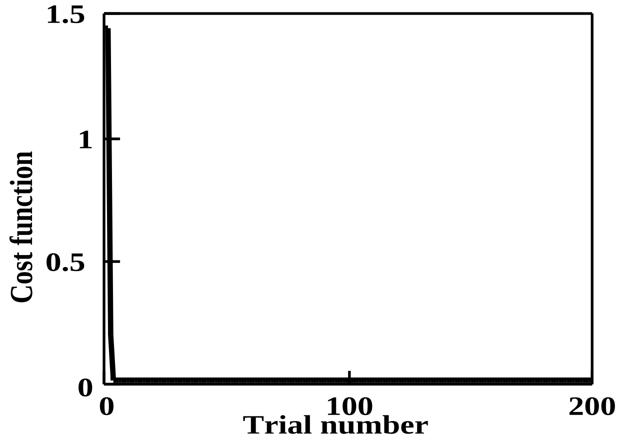

Fig.7 Cost function.

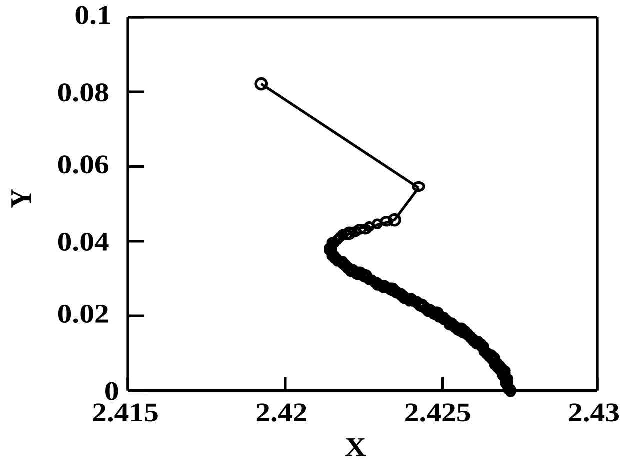

Fig.8 Track of neural network weight change (p=1~200).

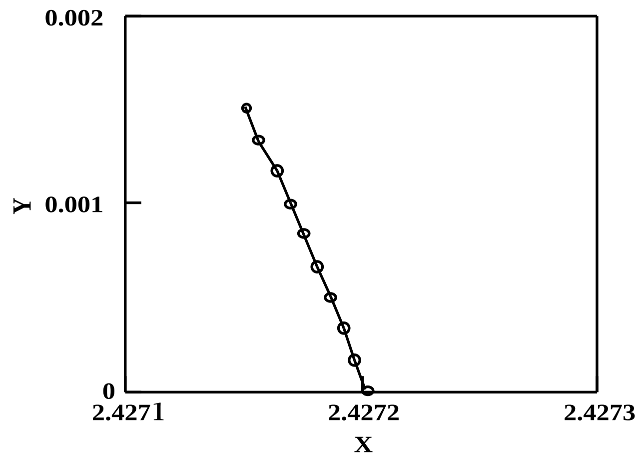

Fig.9 Track of neural network weight change (p=191~200).

The Tenth International Symposium on Artificial Life and Robotics 2005(AROB 10th '05),
B-con Plaza, Beppu, Oita, Japan, February 4-6, 2005

Applying FIFO-Queue ACO Algorithm to Broadcast Problem of Wireless Sensor Networks

Jun Katsuki, Teijiro Isokawa, Naotake Kamiura, and Nobuyuki Matsui
Division of Computer Engineering, University of Hyogo
2167 Shosha, Himeji, 671-2201, Japan
katsuki@comp.eng.himeji-tech.ac.jp, {isokawa, kamiura, matsui}@eng.u-hyogo.ac.jp

Abstract

Minimum-energy Broadcast Problem in wireless sensor networks is categorized as an NP-complete problem in which one sensor node sends packets to all other nodes in network under the condition of minimizing the total power dissipation of all nodes in sending. In this paper, we investigate an application of FIFO-queue Ant Colony Optimization (ACO) algorithm to this problem. Experimental results show that FIFO-queue ACO can find better solutions than other algorithms.

1 Introduction

Wireless Sensor Network (WSN) is a system for dynamic environmental monitoring. A large number of so-called sensor nodes (hereafter, nodes), each of which is responsible for collecting measurements and for interacting with other nodes, form a network in self-organized ways. Communications among nodes are performed cooperatively for relaying measurements obtained by nodes to the host computer at outside of the network as well as for distributing commands from the host computer to nodes; almost all the nodes do not need to communicate to the host computer directly. WSN can be formed easily and rapidly, because there are no wires for communication. For this reason, WSNs are favorable for monitoring dangerous areas, such as disaster areas. Nodes are driven only by their built-in batteries, thereby they determine the lifetime of a WSN.

It is important to reduce the power consumptions of nodes from the viewpoint of the cost-effectiveness for WSNs. The task of broadcasting, i.e., a node (or the host computer) sends commands to all the nodes, is important for operating a WSN and is the most power-consuming task. This task can be formulated to a combinatorial optimization problem, known as Minimum-energy Broadcast Problem (MBP) [1]. MBP is an NP-complete problem where the total power dissipation for all the nodes should be minimized under the condition that all the nodes receive a packet of data from a node.

It is shown that an Ant Colony System (ACS) [2] approach is effective for finding good solutions for MBP [3]. ACS is a particular class of Ant Colony Optimization (ACO) meta-heuristics [4], which are inspired by observations of biological ants' behaviors. On ACS, several agents make candidates of the solution according to the best candidate in the past, choose the best candidate among them, and preserve it. The cycles of 'make candidates'–'evaluate'–'preserve' lead the candidates to gradually improved. However, it is prone to fall into one of local minima in the search space because this strategy utilizes the only one candidate in the past cycles.

In this paper, we propose a method to cope with MBP by applying a FIFO-queue ACO algorithm [5]. FIFO-queue ACO is also a class of ACO meta-heuristics. Several candidates in the past cycles are put in the queue with a certain length that works in a first-in-first-out (FIFO) manner and are available for making candidates. This approach corresponds to a kind of multiple-point search methods and is expected to avoid local minima. We show the effectiveness of our proposed method, by comparing with ACS and Broadcast Incremental Procedure (BIP) that is an approach mainly used for MBP, through computer simulations. The performance is evaluated by the total power dissipations with respect to the number of nodes in the network. Before describing the ACS and FIFO-queue procedure for MBP in sensor networks, first we assume the network model.

2 Minimum-energy Broadcast Problem

We assume a WSN that consists of fixed N-nodes. Any node can be used as a relay node to bring a packet to other nodes in the network. All nodes have omni-directional antennas, so that if the node i transmits to node j, nodes closer to i than j will also receive. The power consumption for node i sending a packet to node j, P_{ij}, is defined as:

$$P_{ij} = [(x_i - x_j)^2 + (y_i - y_j)^2]^{\alpha/2} \tag{1}$$

where (x_i, y_i) $(1 \leq i \leq N)$ are the coordinates of the nodes in the network, and $\alpha (2 \leq \alpha \leq 4)$ is the channel loss exponent. Minimum-energy Broadcast Problem (MBP) is a problem to find the minimum power dissipation for all the nodes when a source node sends a packet to all other nodes in the network. This is categorized as NP-complete because the solution space expands exponentially with respect to linear increase in the number of nodes in the network.

3 Ant Colony Optimization Meta-heuristic

Biological ants can find short paths between their nest and food placed at a distance. This is performed by indirect communications among them by the use of their pheromones. This behavior of ant colonies has motivated the design of Ant Colony Optimization (ACO) Meta-heuristic. The ACO Meta-heuristic has been applied to several combinatorial optimization problem for which the construction of a solution can be described as a path in a decision graph. An ACO Meta-heuristic is an iterative search process where in every iteration each of M (artificial) ants constructs one candidate for the solution by following a path through the decision graph. In their constructions, which edge in a graph should be chosen depends on pheromone information, which is modified by the candidates made by former ants. The pheromone information τ_{ij} represents the effectiveness in sending packets from node i to node j. The pheromone information is stored in a so called pheromone matrix where element τ_{ij}, indicate how good it seems to send packet from node i to node j, for $i, j \in [1 : N] = \{1, ..., N\}$. Ants tend to choose an edge in a graph with relatively high value of pheromone information.

In every generation each of m ants construct one solution that describes a sequence of broadcasting. Starting at a source node an ant selects the next transmission using pheromone information as well as heuristic information. The heuristic information, denoted by η_{ij}, is static information that wouldn't change. The heuristic value is $\eta_{ij} = 1/P_{ij}$.

Let R and NR be a set of nodes that have received data and a set of nodes that have not yet respectively. Each of ants start to make a candidate from $R = \{Source\}, NR = \{\text{other } N-1 \text{ nodes}\}$. An ant makes a transmission to choose a sender node i from R and a receiver node j from NR with probability q_0 so that this transmission maximizes $\tau_{ij} \cdot \eta_{ij}^{\beta}$, where $\beta = \{\beta_A, \beta_B\}$ is a parameter for each ant; otherwise a transmission is determined by choosing nodes i and j according to the probability distribution described as

$$p_{ij} = \frac{\tau_{ij} \cdot \eta_{ij}^{\beta}}{\sum_{k \in R, l \in NR} \tau_{kl} \cdot \eta_{kl}^{\beta}}. \tag{2}$$

It repeats to select a sender and a receiver by these manners until all node have received data, i.e., $NR = \{\phi\}$. A parameter β determines the characteristic of an ant. An Ant with a large β tends to choose transmissions with low power consumptions, while one with a small β may take transmissions that need high power consumptions. In our experiments, each of ants have either β_A or β_B as the value of β where $\beta_A \geq \beta_B$ for enriching the diversity of candidates.

After all the ants make candidates for a solution of MBP, each of these candidates is evaluated by calculating the total power dissipation of it. The pheromone information τ_{ij} is then updated by the quality of these candidates. The τ_{ij} is increased (decreased) when the transmission from node i to node j is included in the candidate with a good(worse) evaluation. After modifications of pheromone information, ants start to make candidates again.

We have shown the general scheme of ACO Meta-heuristic. The updating of pheromone information are most important in ACOs, because the actions of ants deeply depend on these information and irrelevant modifications for them lead ants to one of local minima, not to the global minimum in the search space. For this reason, several scheme for updating pheromone information have been proposed, such as Ant Colony System (ACS)[3] and FIFO-queue ACO[5]. In the following we will describe them with focusing on updating scheme.

3.1 Ant Colony System

In ACS, there are two rules for updating pheromone information τ_{ij}, which represents *evaporation* and *deposit* of pheromone. The rule of evaporation makes the ants not to choose the same transmission as previously selected one, and it is expressed by

$$\tau_{ij} \leftarrow \rho \tau_0 + (1 - \rho) \tau_{ij}, \quad \forall (i, j) \in T_k \tag{3}$$

where $0 < \rho < 1$ is the evaporation constant that determines inheritance of the past transmissions, τ_0 is the initial value of pheromone, and T_k is a set of transmissions made by ant k. This rule is applied at each time of each of ants making a candidate.

After all the ants make candidates and evaluation for them are finished, the deposit rule is applied. Let *best* be the index of the candidate with the best evaluation out of all the candidates in the past, the deposite rule is represented as follows:

$$\tau_{ij} \leftarrow \rho/Y_{best} + (1-\rho)\tau_{ij}, \quad \forall(i,j) \in T_{best} \qquad (4)$$

where Y_{best} and T_{best} are the total power dissipation and the set of transmissions, respectively, for the best candidate. By using this rule, the value of τ_{ij} increases where the transmission from node i to node j is contained in the best candidate, and hence searching the solution is performed around the best candidate in the past.

3.2 FIFO-queue ACO

FIFO-queue ACO algorithm is one of extension from ACS algorithm. The key idea of updating pheromone information is to introduce *queue* that can store several candidates and works First-In-First-Out (FIFO) manner. These candidates are also used for updating τ_{ij}.

Let $T_k(t)$ be the candidate made by ant k and $T_{min}(t)$ be the best candidate at the iteration t. Ants make the candidates $T_k(t)$ for each iteration, $T_{min}(t)$ is chosen so that it has the least power consumption, and it is then put in the queue. This queue has a certain capacity so that up to certain number (say, K) of candidates can be stored, and it is empty at $t = 0$. When it contains K candidates and a new candidate come in the queue, the candidate that was put in at the earliest ($T_{min}(t-K)$) is removed. The updating of τ_{ij} are performed on the addition of new candidate ($T_{min}(t)$) and on the removal of oldest candidate in the queue ($T_{min}(t-K)$), these are defined as follows:

$$\tau_{ij} \leftarrow \tau_{ij} - (1-w_e)(\tau_{max} - \tau_0)/K, \quad \forall(i,j) \in T_{min}(t-K), \qquad (5)$$

$$\tau_{ij} \leftarrow \tau_{ij} + (1-w_e)(\tau_{max} - \tau_0)/K, \quad \forall(i,j) \in T_{min}(t). \qquad (6)$$

These rules mean that the τ_{ij}s of the candidate on the removal from the queue decrease and those on the addition to the queue increase.

The updating rule for the best candidate (deposit rule) is also introduced in FIFO-queue ACO, but it is different from that in ACS. The updating is performed only when the best candidate is changed, while in ACS it is done for each iteration. Let T_{old} be the best candidate for all the candidates until the iteration $t-1$. When $T_{min}(t)$ has the lower power consumption than T_{old}, the following updates of τ_{ij} are applied:

$$\tau_{ij} \leftarrow \tau_0 - w_e(\tau_{max} - \tau_0), \quad \forall(i,j) \in T_{min} \qquad (7)$$

$$\tau_{ij} \leftarrow \tau_0 + w_e(\tau_{max} - \tau_0), \quad \forall(i,j) \in T_k(t) \qquad (8)$$

where $w_e (0 \le w_e \le 1)$ is a parameter that controls the degree of pheromones to be placed at updating $T_{min}(t)$ and τ_{max} is the maximum value of τ_{ij}.

4 Experimental results

In this section we explore the improved performance of our proposed scheme through different scales of MBP. For comparing the performance, we also apply the same task to ACS and Broadcast Incremental Power (BIP) algorithm that is a standard algorithm for solving MBPs.

We prepare the networks with 10, 25, 50, 75, 100 nodes. Nodes are placed randomly at (x_m, y_m) in the network, where $0 \le \{x_m, y_m\} \le 10$ holds. The source node is randomly selected out of these nodes. We generate 20 different configurations for the network with each number of nodes.

We adopt the total power dissipation for a network as the metric for evaluating the performance. To facilitate the comparison of these algorithms over a range of configurations of networks, we introduce *normalized power* for each network configuration. Let $C_i(n)$ be the total power dissipation with respect to the network configuration n and in the case of using the algorithm i, where i takes ACS, BIP, or FIFO-queue, the normalized power $C_i^{/}(n)$ is then defined as

$$C_i^{/}(n) = C_i(n)/C_{best}(n). \qquad (9)$$

where $C_{best}(n)$ denotes the lowest power dissipation for the network configuration n, i.e., $C_{best}(n) = \min(C_{\mathrm{ACS}}(n), C_{\mathrm{BIP}}(n), C_{\mathrm{FIFO-queue}}(n))$. The calculation of $C_i^{/}(n)$ for each configuration is performed by the average for 20 simulations where the random sequences are different each other.

The parameters of ACS algorithm we use in this experiment are shown in Table 1, where T_{MAX} denotes the maximum iteration for this algorithm, and M_A and M_B are the number of ants that take the value of β as β_A and β_B respectively. Note that the parameters β_B and q_0 are modified during the simulation.

For FIFO-queue ACO algorithm, we apply the parameters as $\tau_{MAX} = 1.0$, $K = 1$, and $q_0 = 0.5$, for all the configurations. The initial value of pheromone τ_0 is set to $1/N$. The conditions of T_{MAX}, β_A, and β_B are the same as those in Table.1.

The normalized powers of ACS, BIP, and FIFO-queue ACO with respect to the number of nodes are shown in Fig.1. Figures 1(a), 1(b), and 1(c) are the results in the case that the parameter of propagation loss exponent α are 2, 3, and 4, respectively. This α indicates the difficulty in communications in

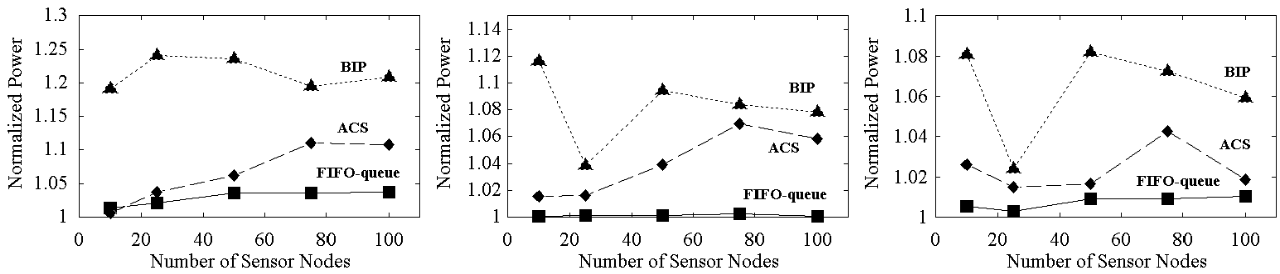

(a) $\alpha = 2$ (b) $\alpha = 3$ (c) $\alpha = 4$

Figure 1: Normalized power with respect to the number of nodes

Table 1: Parameters used in ACS.

	number of nodes				
	10	25	50	75	100
T_{MAX}	50	100	100	100	200
M_A	5	7	13	19	25
M_B	5	6	12	18	25
τ_0	10^{-2}	$5 \cdot 10^{-3}$	$5 \cdot 10^{-3}$	10^{-3}	$5 \cdot 10^{-4}$
ρ	0.2				
β_A	2.0				
β_B	$2/\alpha^2$ for $t \leq 0.5 \cdot T_{MAX}$ $2/\alpha$ for $0.5 \cdot T_{MAX} < t \leq 0.75 \cdot T_{MAX}$ 2 for $0.75 \cdot T_{MAX} < t$				
q_0	0.3 for $t \leq 0.5 \cdot T_{MAX}$ 0.6 for $0.5 \cdot T_{MAX} < t \leq 0.75 \cdot T_{MAX}$ 0.9 for $0.75 \cdot T_{MAX} < t$				

a long range. From the definition of normalized power (Eq.(9)), smaller value of $C_i^{/}(n)$ means more improved performance. From these results we see that FIFO-queue ACO(solid lines) can achieve lower power dissipations than ACS and BIP for almost all cases. The values of $C_{FIFO-queue}^{/}(n)$s are steady with respect to the number of nodes, while those for ACS and BIP change widely. This shows the stability of FIFO-queue ACO algorithm.

5 Conclusion

We propose a method of applying FIFO-queue ACO algorithm to MBP in this paper. In our method, a queue for storing candidates in the past iterations is introduced for enriching the diversity of candidates, in order not to converge the local minima in search space. The improved performance of the proposed method, as compared to the previously proposed algorithms such as ACS and BIP, is also investigated. From the numerical results, we find that our proposed method can aquire better solutions, from the viewpoint of the total power dissipation, than other algorithms.

However, there are two challenging issues for further improvement of our method: the computational time required for our method and the application to the multicast communications rather than broadcast communications. These issues remain for future work.

References

[1] M.Cagalj, J.P.Hubaux, and C.Enz, "Minimum-Energy Broadcast in All-Wireless Networks: NP-completeness and Distribution Issues," in Proc. 8th Ann. Int. Conf. Mobile Computing and Networking, pp.172–182, 2002.

[2] E.Bonabeau, M.Doringo, and G.Theraulaz, "Swarm intelligence : From natural to artificial systems", Oxford University Press, 1999.

[3] A.K.Das, R.J.Marks, M.E-Sharkawi, P.Arabshahi, and A.Gray, "The Minimum Power Broadcast problem in Wireless Networks: An Ant Colony System Approach," in Proc. IEEE CAS Workshop Wireless Communications and Networking, 2002.

[4] M.Doringo and G.D.Caro, "Ant Algorithms for Discrete Optimization," Artificial Life, vol.5, No.3, pp.137–172, 1999.

[5] M.Guntsch, M.Middendorf, "A population based approach for ACO," Lecture Notes in Computer Science, vol.2279, pp.72–81, 2002.

[6] J.E.Wieselthier, G.D.Nguyen, and A.Ephremides, "On the construction of energy-efficient broadcast and multicast trees in wireless networks," in Proc. 19th Ann. J. Conf. IEEE Computer and Communications Societies, pp.585–594, 2000.

Predicting selection of artificial network by cluster coefficient

Shinya Yoshimura, Shinichiro Yoshii
Information Science and Technology
Hokkaido University
Hokkaido, JAPAN

Abstract

In this paper, an artificial network such as A-life is targeted. A predicting method for the selection limit in a heterogeneous system by using a cluster coefficient as an index, which shows small world structure, is proposed.

As evaluation, evolutions of IT infrastructures in an enterprise have been employed for the study as the most typical example. Although IT infrastructures change rapidly and evolution has been continued, the number of a server has been increased. In practical, increase of the total cost of ownership (TCO), including management cost, caused by the increase of servers is the current problem. The relation between the simulation for the evolution and selections in IT infrastructures, and cluster coefficient were observed. The result shows that cluster coefficient and selection predictions are related. In fact, the maturity for a system can be obtained by observing a cluster coefficient for IT infrastructures simply. The number of heterogeneous elements shows the selection limit. The selection limit rate at which the global behavior is not destructed can be obtained from these two measurement values, without performing simulations.

1 Introduction

In information processing based on A-life, information processing which can be realized by employing a group that varies dynamically, maintaining redundancy and diversity, has been argued. In an artificial network, global behaviors always change being accompanied with local interaction fluidly as well. The artificial network for this paper is defined as the one in which the global behavior is determined artificially.

A grid computing [1] which requires common global behavior even in the case where it is distributing locally, Web service [2] which forms a processing system on a common network, and the IT infrastructure [3] of the company which connote a large number of the heterogeneous element are the examples of an artificial network.

In an artificial network, after global behavior, such as evolution and selection, are decided artificially, a local interaction occurs. The quantity of elements mainly becomes a problem in such cases. In most of those problems, the quantity of the capacity that systems possess and elements in the systems are almost equal. In such a case, the system cannot be maintained unless the collective quantity is reduced. For example, too many employees are not necessary because it is not effective. Therefore, the employees are reduced in such a case. Besides, some efficiency improvements can be obtained for production line by reducing employees. This is the top-down emergence [4]. The self-organization criticality [5] resembles it well. In a problem in real issues, the number of the element tends to be reduced after it is expanded.

However, in case that the number has been reduced in the simplicity, individual properties of the element are abandoned and the property of the whole system has consequentially been destroyed. Then, it is required that the number of the element is reduced without changing the property of the system. In the case of the artificial network, the relation of the node for which the persistence node is selected as an evolution is acquired. It can be expressed with the order formation of minimizing the system components as an emergence [6]. The important issue here is, how much of the elements can be reduced without destroying the property of the network. In other words, a prediction method by the simulation is being required. In the case of factory, it is a prediction to determine how many of employees can be reduced without changing their process. However, the selection cannot be predicted simply by the simulation since the simulation becomes even more complicated and difficult as it closes to the realistic.

Therefore, the relationship between cluster coefficient and general behavior of the network in the selection of the system has been investigated. Since selections are predicted only by network behaviors, the time and effort for prediction trial calculation can be reduced. It can be applied to the prediction for the composition result of server consolidation of the IT infrastructure in an enterprise. It is a representative example of the artificial network.

2 Artificial network

The artificial network described in this paper shows the relationship between an element as a center and other elements. It is formed by the top which shows edge and an element which shows the interaction in the simplicity. They are shown in Figure 1.

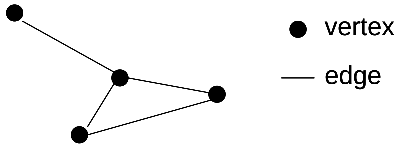

Figure 1. Artificial network

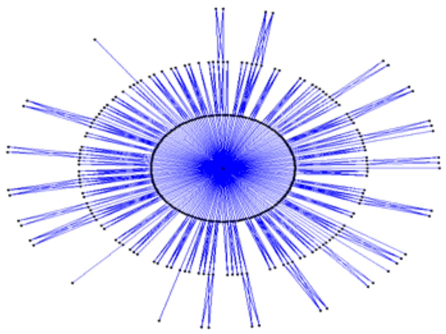

Figure 2. IT infrastructure in the enterprises described by artificial network

Figure 2 shows an enterprise IT infrastructures. The top as a center is client PC, and the relationship between the servers for the treatment is shown in the circumference. Set of vertex and edges indicate the property of the system. The form shown Figure 2 indicates the relationship between the systems. Therefore, the property of the system is destroyed in case that the top is reduced simply. It is necessary to acquire the relation of the node in which the persistence node is selected in order to maintain the property of the system. In other words, the edge re-connects with the peak which substitutes for the neighborhood and is maintained even in case that the number of the peak reduces. It is shown in Fig. 3.

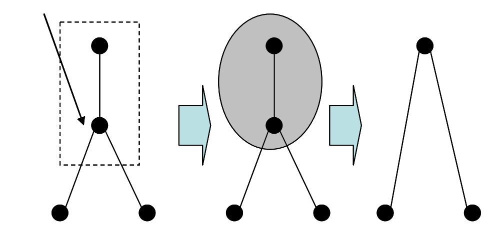

Figure 3. Behavior in the selection

In case where the artificial order in which the element of the system is minimized is given, decrease of the top and reconnection of the edge are repeated as shown in Figure 3 while the element maintains the property of the system. However, this behavior can be obtained only in case where element and substitution element selected are homogeneous relation. It is not possible to obtain this behavior in case that the relation is heterogeneous.

3 Cluster coefficient

The cluster coefficient [7] which shows small world structure as an index is introduced here. Since a cluster coefficient is an index with which the element itself carries out the self reference of the relation with other elements, it is believed to be effective for investigating the relation of an artificial network. In other words, in case where a cluster coefficient is compared to an acquaintance relation, their acquaintances become acquainted and come out and a certain probability is expressed.

The cluster coefficient is obtained from the equation below under the condition that Γ_v is a neighborhood of v , E is a set of Γ_v edges and k_v is the node number of the neighborhood.

$$r_v = \frac{|E(\Gamma_v)|}{\binom{k_v}{2}}$$

Next, an actual artificial network is measured based on the cluster coefficient.

4 The simulation of the selection in the IT infrastructure

The network shown in Figure 4 which imitates the IT infrastructure as a representative example is created, and the simulation of the selection is executed. This resembles the structure of actual IT infrastructure shown in Figure 2, and almost the same form can be expressed.

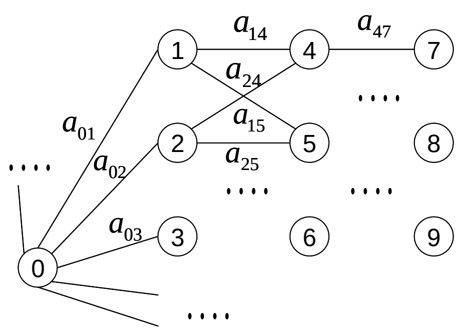

Figure 4. Simulation of artificial network

A random network is generated for each top. The edge is expressed by a_{ij} . The edges and the tops are determined randomly. It is expressed by the equations below.

$$a_{0i} = \hat{a}_{0i}, \quad a_{ij} = a_{0i} \cdot \hat{a}_{ij}, \quad a_{jk} = a_{0i} \cdot a_{ij} \cdot \hat{a}_{jk}$$

$\hat{a}$ is determined as 1 or 0 randomly.

In the equal type (homogeneous), each top possesses the parameter of type and cost and the selection shall be repeated as long as the parameter of the cost permits it. In the other type (heterogeneous), the selection is not generated. This transition is shown in Figure 5.

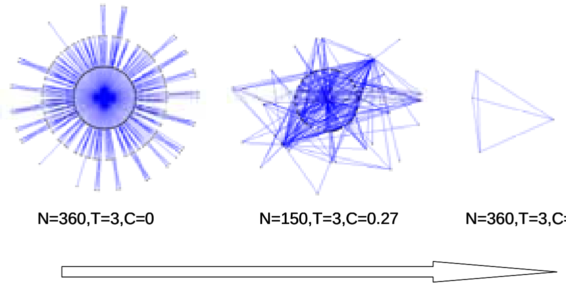

Figure 5. Change of network

N is the number of the vertexes and C is a cluster coefficient. C, at this time, changing from 0 to 1 finally is noticed. Focusing on the selection simulation, the 100, 200, 500, and 1000 peaks and the type parameter were fixed to the cluster coefficient of 0.3, and the simulation was performed 50 times per each. The result is shown in Figure 6.

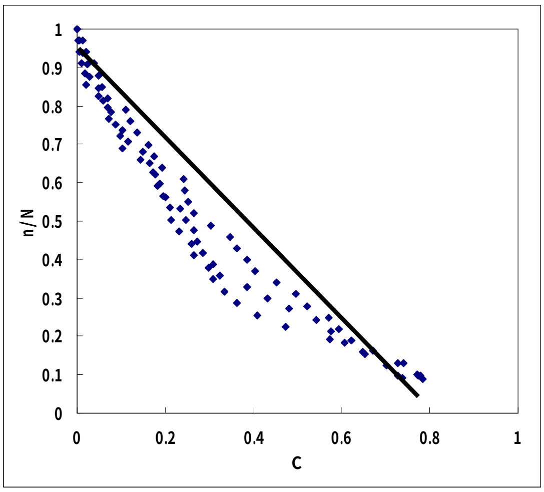

Figure 6. Selection ratio and cluster coefficient

A vertical axis is a selection ratio and a horizontal axis is a cluster coefficient. A cluster coefficient and a selection ratio have the relation of an inverse proportion. Therefore, in the artificial network of IT infrastructure, in case where a cluster coefficient is investigated, a grade of the selectivity can be obtained. For example, a selection ratio is 0.7 supposing Figure 6 to a cluster coefficient is 0.2. Selection will already have been performed about 0.3 from the original element. That is, in IT infrastructure, in case where a cluster coefficient is investigated simply, the degree of a system's maturity is obtained. Then, the parameter of consequences and types shows the selection limit, as the hetero genius element can not be selected. For example, it is clear that 60%of a system can be selected even at the maximum, in the case that 40% of it is the hetero genius. It will be able to estimate the culling rate of the degree in which the system does not collapse by these two measured value without performing the simulation.

5 Conclusion

In this paper, the relationship between the transitions for the selection of the cluster coefficient in an artificial network has been clarified. The relationship between them is almost an inverse proportion. The selection ratio can be estimated regardless the number of the element in case where the cluster coefficient can be measured using the property. The local behavior with the order in which the number of the element in a system had to be minimized has been clarified by the change of the cluster coefficient.

However, the parameter of precision criterion and costs and types are not mentioned this time. These will be one of our targets in the future.

6 Reference

[1] Adrian Li Mow Ching (2002), " Super resource-managment for Grid Computing" , London Communications Symposium.

[2] Haverty, P. M. (2004), " CARRIE web service: automated transcriptional regulatory network inference and interactive analysis" , Nucleic Acids Res 32, W213-W216.

[3] Sherri Smith (2004), " Successful server consolidation: it's all in the preparation", http://h200001.www2.hp.com/bc/docs/support/SupportManual/c00257494/c00257494.pdf , 2004.

[4] kanji ueda (1996), " METHOD ON ARTIFICIAL LIFE" , Kogyo Chosakai Publishing

[5] B. A. Carreras (2002), " Dynamics, Criticality and Self-organization in a Model for Blackouts in Power Transmission Systems" ,Proceedings of the 35th Hawaii International Conference on System Sciences.

[6] Albert-Laszlo Barabasi (1999), " Emergence of Scaling in Random Networks" , SCIENCE VOL 286, pp. 509-512.

[7] D.J. Watts S.H. Strogatz (1998), " Collective dynamics of " small-world" networks." , Nature 393, pp440-442.

The Tenth International Symposium on Artificial Life and Robotics 2005(AROB 10th '05),
B-con Plaza, Beppu, Oita, Japan, February 4-6, 2005

Evolution of Development and Heterochrony in Artificial Neural Networks

Artur Matos Reiji Suzuki Takaya Arita
Graduate School of Information Science, Nagoya University
Furo-cho, Chikusa-ku, Nagoya 461-8601, Japan
amatos@create.human.nagoya-u.ac.jp, {reiji,arita}@nagoya-u.jp

Abstract

Recently, evolutionary algorithms coupled with simulated developmental processes have been used successfully for generating designs ranging from neural networks to artificial creatures. Although several of these models do exist, their evolutionary dynamics, and more specifically how the ontogenic models themselves interact with artificial evolution are still poorly understood. One of these specific interactions, and of particular importance in biological systems is heterochrony — the change in timing and rate of developmental events by evolution. In this paper, we analyze heterochronic change in one artificial developmental model - the cellular encoding model first described by Gruau [1]. For this purpose, we apply the framework and methods defined by Alberch *et al* [2] for biological systems to neural networks evolved for the odd-3-parity problem. Preliminary results show that: 1) All heterochronic changes occur with significant frequency; 2) The combined effects of predisplacement, hypermorphosis, and neoteny was the most common heterochronic change; 3) Pure recapitulation (isomorphosis) is prevalent.

Keywords: Heterochrony, evo-devo, Cellular encoding, Artificial embriogeny, Neural Networks.

1 Introduction

Evolutionary algorithms have been used successfully for generating designs ranging from neural networks, to full artificial creatures with both generated morphology and behavior. One of the reasons for this recent success is due to the integration of simulated developmental processes with evolutionary algorithms. Although several of these models do exist, their evolutionary dynamics, and more specifically how the ontogenic models themselves interact with artificial evolution are still poorly understood.

In biological systems, one of the key concepts in this interaction is known as heterochrony. Heterochrony, as it is usually defined in evolutionary biology, is the change in the rate and timing of developmental events caused by evolution. Heterochrony is prevalent in the evolution of species: some examples include the conservation of juvenile characters in salamanders and the loss of the tadpole stage in toads. Due to this, there is a wide array of studies and data available on heterochrony in biological systems.

For artificial neural networks, previous studies have shown that heterochrony does indeed occur in artificial systems: For instance, Cangelosi [3] evolved neural networks for foraging food in a simulated environment. By comparing the development processes between ancestor and descendant networks, he could observe changes in the timing of developmental events. However, this analysis was only done for a small number of individuals, and it was not extended to a whole phylogenetic tree. Thus, studies focusing on heterochrony in a large scale in artificial systems are still lacking. Specifically, these questions are still largely unanswered: 1) What kind of heterochrony processes are more common in artificial systems? 2) How does the developmental model and the evolutionary parameters affect heterochrony? 3) How does heterochrony in artificial and biological systems relate to each other? These points are the main motivations behind this paper.

In attempting to answer these questions, we applied the framework defined by Alberch *et al* [2] for biological systems to the evolution and development of neural networks. This framework defines a precise terminology for classifying heterochrony. For simulating neural network development, we used the cellular encoding model first described by Gruau [1]. This is one of the earliest models described in the literature, and representative for grammar based models of development. We used this encoding coupled with genetic programming for solving the odd-3-parity problem and then analyzed the resulting growing dynamics on important traits like the number of neurons, their average degree and also how the fitness value itself changes within ontogeny.

2 Alberch *et al*'s framework

The framework by Alberch *et al* for classifying heterochrony is widely used for biological systems. This framework is based on the measurement and comparison of quantitative traits, for instance, body length, width or height. The traits are measured as development unfolds, yielding growth curves. These growth curves can then be compared between related species for understanding the heterochronic change involved.

The basis for comparison lies on three metrics that can be extracted from the growth curves: α — the time when growth starts, β — the time when growth ends, and K — the growth rate. Comparing these values between species yields the outcomes summarized in figure 1. For instance, considering only changes in the K parameter, two outcomes are possible: if the descendant would grow faster than the ancestor (K would be larger), the corresponding

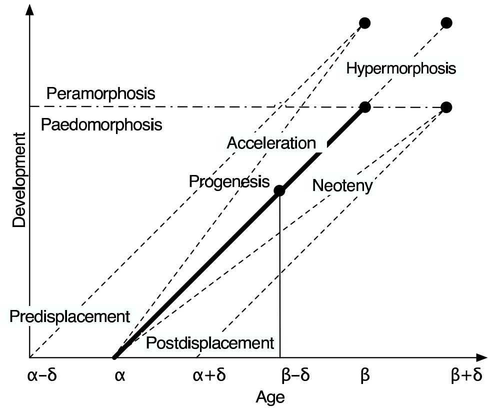

Figure 1: The formalism of Alberch *et al.* A trait measure is plotted against developmental time in the X axis. The solid line plotted from α to β represents the growth curve for the ancestor, while the remaining ones possible heterochronic outcomes for the descendant.

outcome is acceleration. The reverse process — the descendant growing slower than the ancestor — is labeled neoteny. Furthermore, heterochronic changes can be combined on the three parameters, as for instance postdisplacement and hypermorphosis would refer to an increase in both α and K respectively.

3 The model

The phenotypes in this model are simple boolean neural networks: Nodes are simple threshold neurons, with a threshold of either 0 or 1. The connections between neurons can either be -1 or 1. Neurons are activated if the sum of the values on their incoming connections is above their threshold.

For the developmental model, we used the cellular encoding model by Gruau [1]. In this model, the neural network starts as a single neuron and undergoes several developmental events as specified in the genotype. The genotype is represented as a Genetic Programming (GP) tree with nodes as developmental commands such as neuron division, setting the weight and threshold and similar. Each neuron has a pointer to the GP tree representing its current developmental stage. Development occurs in a parallel fashion: in each time step, each neuron executes the command pointed by its register in the tree and moves to the following leaf. The arity of each GP node depends on the command used: for instance, commands for neuron division have two children, representing separate programs for each of the daughter neurons. Development for the network finishes when all the neurons have reached their final leaf node in the tree.

Using this model, we evolved networks for the 3-odd-parity problem, a standard problem for GP. The solution is defined as a neural network with at least 3 inputs, that outputs *true* whenever the number of *true* inputs is odd. A fitness function based on the number of wrong outputs didn't produce a good performance so we used the fitness function used by Gruau in [1]. It is defined by:

$$f(out_{eval}) = 1 - \frac{I(out_{right}, out_{eval})}{H(out_{right})}, \qquad (1)$$

where out_{eval} is the output vector of the evaluated network and out_{right} the expected correct output vector for the problem. $I(X,Y)$ is the mutual information between X and Y:

$$I(X,Y) = \sum_{x=0}^{1}\sum_{y=0}^{1} P_{XY}(x,y) \cdot log_2 \frac{P_{XY}(x,y)}{P_X(x) \cdot P_Y(y)}, \qquad (2)$$

and $H(X)$ is the information entropy of X:

$$H(X) = \sum_{i=0}^{1} P_X(i) \cdot log_2(P_X(i)), \qquad (3)$$

with $P_X(x)$ as the probability of $X = x$, and $P_{XY}(x,y)$ as the joint probability of $X = x$ and $Y = y$. This fitness function is defined in the range $[0,1]$, with 0 as the best fitness. Please note that due to using mutual information, either correct networks or networks that output the inversed expected output will have the same best fitness.

We adopted a GP based system without crossover, and tournament selection was used. Each individual is mutated (addition, deletion, replacement of nodes) with a certain probability, while the others are simply reproduced. The individuals are therefore connected among generations by either reproduction or mutation, forming lineages.

4 Basic results

Using the model and fitness function described in the above section, we evolved networks for analyzing heterochronic change. Population size was 200, and the mutation rate was set at 80%. The fitness graph for a typical run can be seen in figure 2 and the best network in figure 3. All of the results reported on this article are from this run. We can see that the average fitness gradually decreased while the best fitness decreased discontinuously, and this model was able to solve the problem in 314 generations.

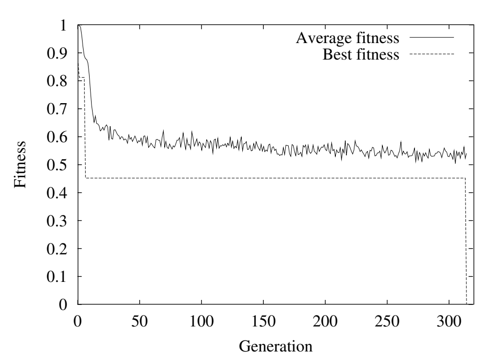

Figure 2: Fitness graph for a typical run.

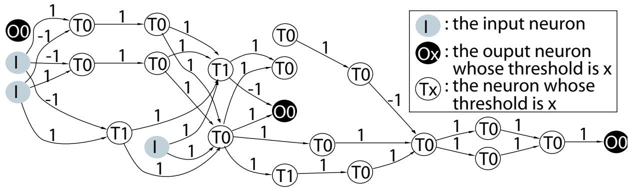

Figure 3: The best neural network for the run. Please note that the cellular encoding model may produce more inputs and outputs then necessary, as it can be seen in this case, although only one output is actually used. The output node in the center is the used one.

Table 1: Summary for the determination coefficient for different growth models, on the number of nodes trait. R^2, the determination coefficient, indicates how well the model fits the data, with 1 being a perfect fit. The value shown is the average R^2 value among all the individuals in the winning lineage (the lineage of the best individual in the last generation).

Model	Average R^2
Linear regression	0.933
Von Bertalanffy	0.968
Sigmoid	0.974

5 Measuring heterochrony

Next, we analyzed the networks for the following traits: number of nodes, average connectivity (taking into account both incoming and outgoing connections) and how the fitness value changes within ontogeny. Sample growth curves for the best individual on each trait can be seen in figure 4.

One significant problem in using the Alberch *et al*'s framework described before is how to extract significant α, β and K parameters from the growth data. This is also an issue in biological systems although they tend to follow more regular patterns. One common approach is to use non-linear regression to fit the data to a growth model and extract the parameters from the fitted model. This, for instance, was applied by Creighton and Strauss [4] to rodent growth data.

This approach works well for biological systems because their growth dynamics tend to follow regular patterns and there are several sensible mathematical models. These models fit well the data and are grounded on experimental evidence. In contrast, our artificial developmental model can generate rather irregular growth curves — with sudden reverting ontogenic polarity as it can be seen in figure 4 (b) or even with sharp discontinuities as in figure 4 (c).

Another possible approach is simply to extract the values directly from the experimental data, for instance K could be defined as the average growth increment during the development period, or estimated by linear regression. An example of this approach can be seen in Pigliucci [5].

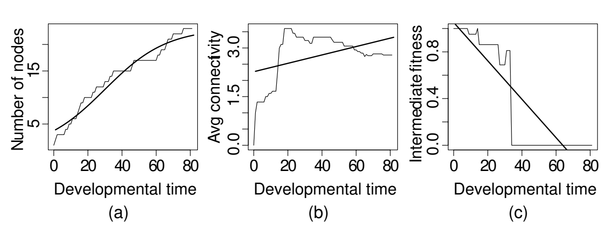

Figure 4: Growth curves for the analyzed traits on the best individual. Both growth data and fitted curves are shown. For the number of nodes, a sigmoidal curve was fitted, while simple linear regression was used for the other traits.

In this paper we decided to use both approaches depending on the trait used. The number of nodes trait seems to follow dynamics similar to biological systems, so we attempted to fit the data to growth models commonly described in the literature. We attempted the Von Bertalanffy's growth function defined as:

$$y = Sa(1 - e^{-k(t-t_0)}), \tag{4}$$

and also the standard sigmoidal function defined as:

$$y = \frac{Sa}{1 + e^{-k(t-t_0)}}. \tag{5}$$

In both functions, Sa stands for the maximum value achieved during growth and k for the speed of growth. We used a Gauss-Newton algorithm for fitting the data, with Sa fixed to the last value reached during development and the other remaining parameters (k, t_0) were initialized to adequate starting values. A summary of the results for the fit can be seen in table 1. The determination coefficient R^2 was the highest on average for the sigmoidal function and therefore we adopted this model . We defined K as the same parameter k in the sigmoidal function, α and β as the period when the model reaches 10% and 90% of the total growth Sa respectively. This approach is coherent with the above mentioned study by Creighton and Strauss [4]. An example of this fitting can be seen in figure 4 (a).

For the other remaining traits, we used simple linear regression and defined K as the slope of the fitted line. This approach was used because the other models assume monotonous increase in the trait while the developmental curves in these traits can decrease. α and β were defined as the period where growth can be observed to effectively start and stop in the data. Examples of these fittings can be seen in figures 4 (b) and 4 (c). This approach cannot be considered completely adequate as the fitting is not sufficient (R^2 is low due to the complexity of the developmental curves in these traits), but nevertheless it allows to have consistent values for the three parameters.

By comparing the parameters between related individuals in the lineage it is therefore possible to classify the heterochrony process involved as depicted in figure 1. Figure 5 shows the transitions of α, β and K for each trait in the winning lineage. In the transitions for the number of nodes trait, we can see the gradual decrease in α and the increase in β with large fluctuations, and that K converged to a small value. We also see transitions similar to the number of nodes in the average degree trait, except for the steady evolution of α, and a quite different evolution of all parameters can be seen for the fitness trait. Figure 6 shows the occurrences of the combined heterochrony processes for the number of nodes trait in the winning lineage. Isomorphosis refers to no change at all in any of the parameters between ancestor and descendant.

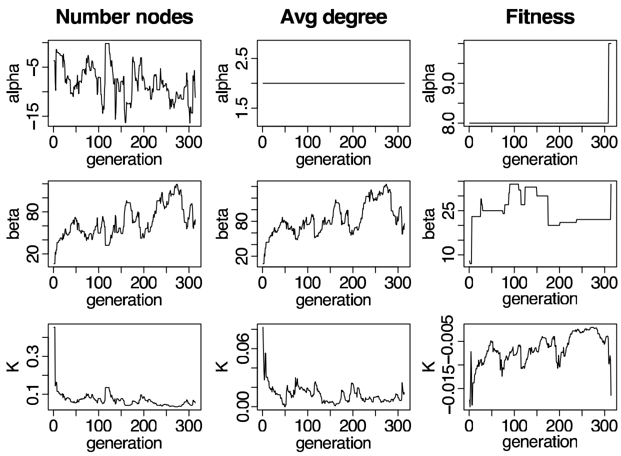

Figure 5: Evolution of the α, β and K parameters for the winning lineage on all traits.

As it can be seen in figure 6, all possible heterochronic changes occur with significant frequencies. One interesting point is that pure recapitulation (isomorphism) seems to be a common heterochronic change in these runs. Even accounting for errors in estimating the parameters, this should be significant considering the low reproduction rate (20%). The fitness function shows sharp discontinuities (as can be seen from figure 2) and therefore it may be exerting selection pressure for either neutral or invalid mutations.

The most frequent heterochronic change is the combination of predisplacement, hypermorphosis and neoteny. The net effect of this combination is that developmental time increases on the descendant. This can also be observed on the gradual increase in the β parameter in figure 5. In the cellular encoding model, developmental time is roughly proportional to the GP tree size; Therefore developmental time is expected to increase, as in GP systems the average tree size gradually increase with evolutionary time (tree bloat).

6 Conclusion

As the use of simulated developmental processes increases, it becomes more important to understand their dynamics. In this paper, we have shown that the framework by Alberch *et al* is a valid method for studying dynamics in artificial systems, by measuring heterochrony in the evolution of neural networks. We successfully observed heterochrony in the number of neurons trait such as the frequent occurrences of the combination of predisplacement, hypermorphosis and neoteny, and also pure recapitulation.

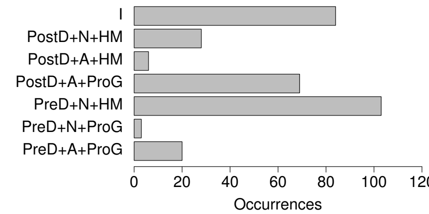

Figure 6: Occurrences of heterochrony for the number of nodes trait on the winning lineage. I - isomorphism; PostD - postdisplacement; PreD - predisplacement; N - neoteny; A - acceleration; HM - hypermorphosis; ProgG - Progenesis.

This framework is particularly well suited for artificial systems because it is solely based on observable quantitative traits and it can be applied regardless of the epigenetic process involved. This should be particularly important when comparing heterochronic change between different developmental models, as for instance, cell chemistry and grammar based models. Future work will therefore continue on extending this analysis for different models and fitness functions.

Acknowledgments

The simulated evolutionary experiments were conducted with the ECJ (Evolutionary Computation in Java) package. I would like to thank both Sean Luke and Gabriel Balan for their helpful assistance with some technical ECJ programming details. This research is funded with a Japanese MEXT scholarship (400000357010989).

References

[1] Frederic Gruau. *Neural Network Synthesis using Cellular Encoding and the Genetic Algorithm.* PhD thesis, Laboratoire de la Informatique du Parallelisme, Ecole Normale Superieure de Lyon, 1994.

[2] Pere Alberch, Stephen Jay Gould, George F. Oster and David B. Wake. Size and shape in ontogeny and phylogeny. *Paleobiology*, 5(3): 296–317, Summer 1979.

[3] Angelo Cangelosi. Heterochrony and adaptation in developing neural networks. In *Proceedings of the Genetic and Evolutionary Computation Conference*, volume 2, pages 1241–1248, Morgan Kaufmann, 1999.

[4] G. K. Creighton and Richard E. Strauss. Comparative patterns of growth and development in cricetine rodents and the evolution of ontogeny. *Evolution*, 40(1): 94–106, January 1986.

[5] Massimo Pigliucci. Ontogenic phenotypic plasticity during the reproductive phase in arabidopsis thaliana (brassicaceae). *American Journal of Botany*, 84(7): 887–895, July 1984.

Multi-Procedure Ozone Concentration Prediction using Fuzzy Clustering and DPNN

Seong-Pyo Cheon, Seng-Tai Lee, and Sungshin Kim

School of Electrical and Computer Engineering, Pusan National University, Busan, Korea

Pusan National University Changjeon-dong, Keumjeong-ku, Busan 609-735, Korea
E-mail: buzz74@pusan.ac.kr, youandi@pusan.ac.kr, sskim@pusan.ac.kr

Abstract

Ozone reaction is a complex mechanism because of its intrinsic complexity and nonlinearity. It is not easy to predict its concentration using traditional numerical and statistical methods. Especially, we found that conventional single model could not get corrected ozone concentrations at high range. We propose a multi-procedure model to overcome the complexity and nonlinearity of ozone concentrations. At first, we suggest fuzzy clustering method to divide high- and low- concentration groups for input ozone data in past two years. Then, we determine proper input data group and its data are used to input data for DPNN models. We divide two groups for input ozone data because the results of the proposed model seriously depend upon their inputs. Preprocessing and postprocessing algorithms are applied to the input data as two steps in order to get more accurate and reliable prediction results of ozone concentrations.

Keywords: Fuzzy clustering, DPNN, multi-procedure model

1 Introduction

One of the emerging major issues about air pollution is the abnormal ozone concentration of the troposphere in summer. High concentration ozone is strong oxidizing material which is responsible for various adverse effects on both human being and foliage. And it frequently appears metropolis in the daytime from June to August in summer. In general, it revealed that the features on ozone distribution and creation are closely related to the photochemical reaction and meteorological factors. So far, there is not enough information about detailed cause and effect of the ozone. In the ozone reaction mechanism around the troposphere, nitric dioxide and hydrocarbon which are components of exhaust fumes act as precursors and ultraviolet radiation, wind speed, and temperature play the role of meteorological materials. Therefore, ozone is a second pollution material. To reduce harms by high concentration ozone, it needs prediction system which forecasts maximum ozone concentration every morning in summer.

There are some conventional methods to predict ozone concentration. For instances, multiple regression model [1] by static methods, a multivariate analyses and artificial neural networks [2] have been developed and applied to predict ozone concentration. However, it does not show a good prediction performance. We analyses major related reasons as follows: First, ozone is a kind of second pollution material. Due to both first pollution ones and other related factors affected on its behavior and concentration, it is impossible to create complete model which was considered all factors. Second, there are not sufficient data when high concentration ozone appeared. Third, we couldn't get ultraviolet ray data directly. So, we couldn't help using solar radiation data that we estimated ultraviolet ray indirectly. Finally, we couldn't be considered that precursors inflow from long distance. As shown in Figure 1, we suggested multi- procedure ozone concentration forecasting system. In this paper, we introduce a multi-procedure model which consists of preprocessing, dynamic polynomial neural networks (DPNN) models, and postprocessing. Fuzzy clustering method as a preprocessing is employed to decide the fuzzy sets of the low and high ozone concentration. After clustering the two fuzzy sets, the different two models are determined by the DPNN. The decision making process as a postprocessing is applied to forecast the ozone concentration by the compensation of the weight factors to the output of the two models.

The proposed forecasting system is adaptively constructed by a successive basic structure of the DPNN. Also, important input variables for the final structure of the forecasting system are selected from the possible input variables by a selection criterion. The historical data that consist of pollution materials and meteorological information are divided into training data and testing data to identify dynamic system and to prevent overfitting. The structure of the final model is compact and the computational speed to produce an output is faster than other modeling methods. The proposed method shows that the prediction of the ozone concentration based upon the DPNN gives us a good performance with ability of superior data approximation and self-organization.

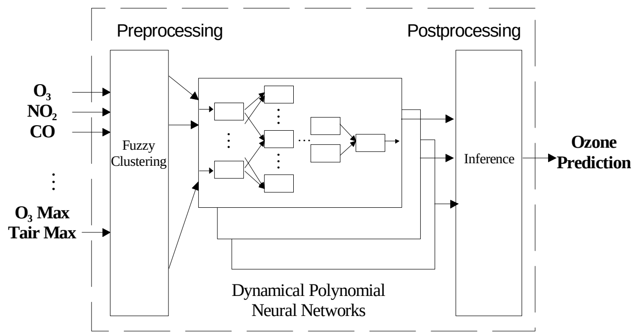

Figure 1. The full structure of the ozone prediction system.

2 Fuzzy Clustering

The fuzzy c-mean algorithm (FCM) generalizes the hard

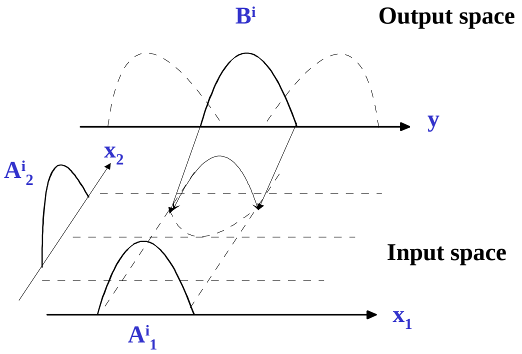

Figure 2. The mapping of input variables into output space

c-mean algorithm to allow a point to partially belong to multiple clusters. Therefore, it produces a soft partition for a given dataset[3]. FCM of Bezdek [4] is normally applied for the fuzzy clustering. In this paper, fuzzy space classification using FCM based on the similar feature of ozone concentration output data is implemented to compute the classified degree of input

variables. Figure 2 illustrates that the output space classified by fuzzy clustering is mapped to input spaces, and then the related features between input variables and output data are determined by fuzzy clusters.

3 Dynamic Polynomial Neural Network

3.1 The Basic Structure of DPNN

DPNN uses GMDH (Group Method Data Handling) method [5] to compose an input/output model based on observed data and variables. This method is widely used for modeling of system, prediction, and artificial intelligent control. As shown in Figure 3, the simple DPNN structure has four inputs and one output at each node. Following polynomial equations between input and output are used at each node in the DPNN. Output y_1 and y_2 at each node are expressed as follows.

$$\begin{aligned} y_1 &= w_{01} + w_{11}x_1 + w_{21}x_2 + w_{31}x_1x_2 + w_{41}x_1^2 + w_{51}x_2^2 \\ y_2 &= w_{02} + w_{12}x_3 + w_{22}x_4 + w_{32}x_3x_4 + w_{42}x_3^2 + w_{52}x_4^2 \end{aligned} \qquad (1)$$

The final output $\hat{y}$ is represented by a polynomial equation.

$$\hat{y} = w_{03} + w_{13}y_1 + w_{23}y_2 + w_{33}y_1y_2 + w_{43}y_1^2 + w_{53}y_2^2 \qquad (2)$$

where, w_{ij} ($i=0,1,2,\ldots,n, j=0,1,2,\ldots,k$) is the coefficient. If input variables of each node are more than three, other combination terms of input variables are added to the above equation. The least square method is employed to estimate the parameters of each node in the DPNN. And it searches the solution of parameters to minimize the objective function formed by error functions between node outputs and actual target values.

$$J = \sum_{k=1}^{\#\text{ of data}} (y(k) - \hat{y}(k))^2 = |y - wA|^2 \qquad (3)$$

$$w = (A^T A)^{-1} A^T y \qquad (4)$$

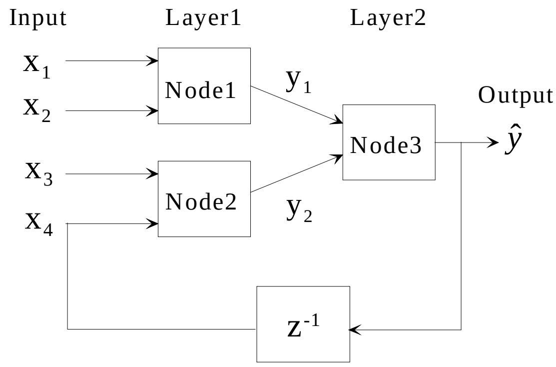

Figure 3. The basic structure of DPNN.

Equation (3) and (4) show the objective function and the coefficient, respectively. Parameters are solved by the least square method and polynomial functions of current node are structured at each of layer. This process is repeated until the criterion is satisfied. Thereafter, we could finally get the best function for the best performance.

3.2 Self-Organization

Another specific characteristic of DPNN is self-organization [6]. The DPNN based on the GMDH method separates data into training data and testing data for modeling [7]. The purposes of this stage are to identify the behavior of the dynamic system and to prevent overfitting problem. The DPNN estimates the parameters of each node and composes the network structure of dynamic system using two-separated data sets. Training data set is used to solve the parameter of function of each node and testing data set is used to evaluate the performance of DPNN. The final network structure is constructed by the relationship of error in training data and testing data. Therefore, the DPNN selects the input of the next node under a performance criterion(PC) that is the relationship between training error and testing error at each node. The final network structure is determined as shown in Figure 4. The PC could be determined by following Equation (5), where is existed in the range of *0 ~1*. The model performances are also evaluated by Equation (5). This performance criterion can be applied for the testing data

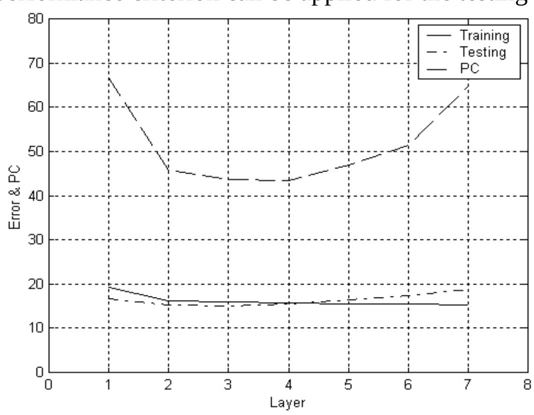

Figure 4. The variation of model performances corresponding to increment of layer.

and the training data. And also it can be used for the unprepared new data.

$$e_1^2 = \sum_{i=1}^{n_A} (y_i^A - f_A(x_i^A))^2 / n_A,$$
$$e_2^2 = \sum_{i=1}^{n_B} (y_i^B - f_B(x_i^B))^2 / n_B, \tag{5}$$
$$PC = e_1^2 + e_2^2 + \eta(e_1^2 - e_2^2)^2$$

where, e_1, e_2, n_A, n_B, and y_i indicate training errors, testing errors, the number of training data, the number of testing data and measured outputs, respectively. And $f_A(x_i^A)$ and $f_B(x_i^B)$ are outputs of training data and testing data separately. Total number of data is $n=n_A + n_B$. From the results, the optimized model structure is constructed at the point of minimized PC.

4 Fuzzy Inference in the Postprocessing

High and low levels are classified based on ozone concentration data in the postprocessing and then ozone concentrations are predicted by DPNN. The predicted results are shown in Figure 5. As shown in Figure 5, the predicted results are represented as Y_L and Y_H. Y_i and Y_j are calculated by the means and variations of two input variables X_i and X_j ($i \neq j$), respectively. In this case, the two input variables have the longest distance between high and low level concentrations. It means that the X_i and X_j affect strongly to ozone concentrations. The outputs of the Y_i and Y_j influenced by the X_i and X_j are computed by the fuzzy inference in the Equation (6).

$$Y_i = \frac{(0.7 \times Y_L) + (0.3 \times Y_H)}{0.7 + 0.3}$$
$$Y_j = \frac{(0.2 \times Y_L) + (0.8 \times Y_H)}{0.2 + 0.8} \tag{6}$$

The final prediction result based upon the decision support system is decided by Equation (7). In this equation, the weights W_{Xi} and W_{Xj} are the relative distances of the input membership functions.

$$\hat{Y} = \frac{(W_{X_i} \times Y_i) + (W_{x_j} \times Y_j)}{W_{x_i} + W_{x_j}} \tag{7}$$

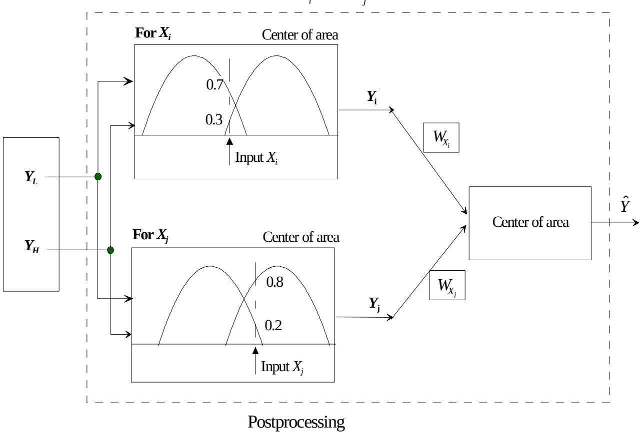

Figure 5. The fuzzy inference in the Postprocessing.

5 Performance Assessment

Ozone, CO, NO_2, SO_2, TSR, wind speed, wind direction, temperature, solar radiation, humidity, and rain fall are used for the parameters of air pollution materials and meteorological materials in ozone prediction systems. Within the data, the amount of rainfall is normally *0mm* at high-level ozone, so it cannot influence the high-level ozone prediction. And TSR and SO_2 are skipped because these values are decreased by the restriction of air pollution material and wind direction is also excluded due to the difficulty of quantification. Therefore, ozone, CO, NO_2, wind speed, temperature, humidity, and solar radiation, maximum O_3 of previous day and maximum atmosphere temperature of previous day are chosen as the possible input variables. Because the daily maximum of ozone concentration is appeared at 2～5 p.m., the prediction of the ozone concentration for this time is the goal of this paper. Within the data, ozone, CO, and NO_2 are extracted from morning data and the other data are selected at 2～5 p.m. These data structure could show as Table 1. In the first simulation, the number of clusters is applied from 2 to 4. Basically, high-level ozone used the highest value and low-level ozone consists of the other set. Figures 6, 7 and 8 show the ozone prediction results of several areas in Seoul, Korea from August 1 to 10, 1997. Total data are constructed by the data from May to September in 1996 and from May to July in 1997. And the training data and testing data are selected from among the total data. When the input variables are applied to predict ozone concentration, those of data are classified by the predicted time and measured time. The upper column point out the input variables and the higher columns of inner cells indicate the time. The left row is a number of data. In this simulation, a model is chosen based on the *RMSE* that is yielded from the selected model. This model is determined after clustering the training data. When the number of the cluster is 4, the lowest training *RMSE* is 27.918 and the prediction *RMSE* is 20.183. The slope and intercept values for *R-square* are displayed in the scatter graphs of ozone observation (*x*-axis) against the predicted

Table 1. Prospective input variables and data structure

		O_3	NO_2	CO	Rh	Sr	Ws	O_3 Max	Tair Max	O_3
980	2	6	6	6	14	14	14	PRE	PRE	14
	4	⋮	⋮	⋮	⋮	⋮	⋮	⋮	⋮	⋮
	5	⋮	⋮	⋮	⋮	⋮	⋮	⋮	⋮	⋮
	2	7	7	7	15	15	15	PRE	PRE	15
	4	⋮	⋮	⋮	⋮	⋮	⋮	⋮	⋮	⋮
	5	⋮	⋮	⋮	⋮	⋮	⋮	⋮	⋮	⋮
	2	8	8	8	16	16	16	PRE	PRE	16
	4	⋮	⋮	⋮	⋮	⋮	⋮	⋮	⋮	⋮
	5	⋮	⋮	⋮	⋮	⋮	⋮	⋮	⋮	⋮
	2	9	9	9	17	17	17	PRE	PRE	17
	4	⋮	⋮	⋮	⋮	⋮	⋮	⋮	⋮	⋮
	5	⋮	⋮	⋮	⋮	⋮	⋮	⋮	⋮	⋮

* Tair : Atmosphere temperature, Rh : Relative humidity, Sr : Solar radiation, Ws : Wind Speed, O_3 Max : The Maximum O_3 of previous day, Tair Max : The Maximum atmosphere temperature of previous day.

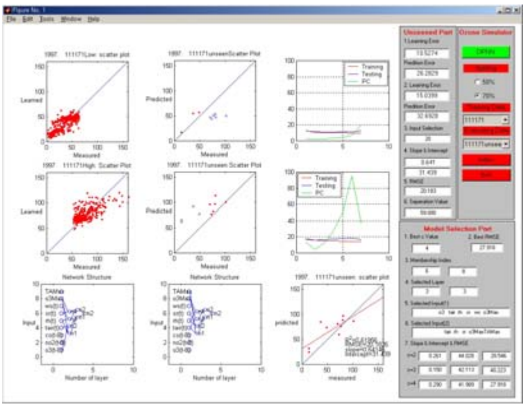

Figure 6. The prediction results for BangHak-Dong.

values (y-axis) for each model. The two diagonal lines in the plots represent the best-fit regression and the perfect correspondence between observations and predictions [8]. In the second simulation, the predicted area is Ssang-Mun-Dong in Seoul, which is high-level ozone area in the summer. The predicted period is from May to July in 1999. The training data and testing data are constituted by the data from May to September in 1996, 1997 and 1998. In this ozone prediction, missing data are interpolated by the spline interpolation method. For the decision support system, a low concentration model and a high concentration model are constructed by the fuzzy clustering method based on the basic training data. In this system, mean values and standard deviations are firstly found with respect to input variables of each model and then required membership functions are selected by the correlative distance of each membership function. The number of clusters is applied from 2 to 4. Basically, the high-level ozone uses the highest value and the low-level ozone consists of the other set. Figure 7 shows the result of the ozone prediction the period from May 20 to July 20 in 1999. When the number of the cluster is 4, the lowest training *RMSE* is 15.634, and the prediction *RMSE* is 18.034. In the decision support system, prediction data are passed through the preprocessor and then the low and high concentration models fulfill the prediction processing. Thereafter, the final outputs are obtained by the outputs,

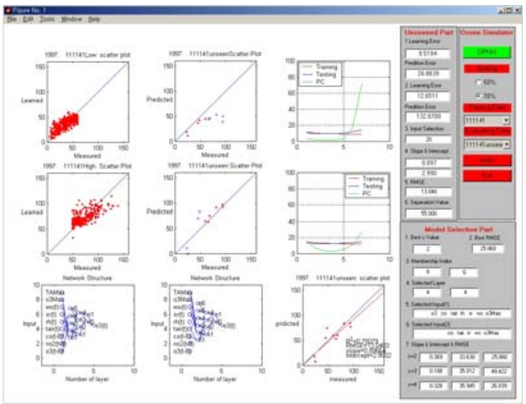

Figure 7. The prediction results for GooEui-Dong.

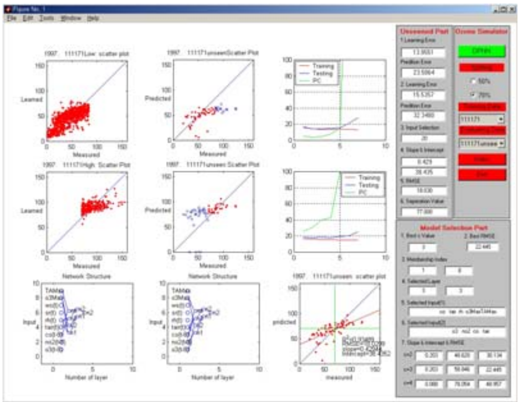

Figure 8. The prediction result for Ssang-Mun-Dong.

which are by the two models at the postprocessing. At the postprocessing, the outputs of the models are handled by membership functions, which are formed by the fuzzy clustering.

6 Conclusion

In this paper, we propose the multi-procedure prediction system using various approaching methods. i.e. Fuzzy clustering method, DPNN, and weighted combining postprocessing. The model designed by DPNN, which includes decision support system, is suitable for the high concentration o zone prediction. When the models are daily updated based on n ew input variables, the prediction performances are getting bet ter than the results by the fixed model. And it is confirmed that the selection of the cluster number in the fuzzy clustering is als o very important for the high-level ozone. Finally, the combini ng over two models, using various input selection and optimizi ng the structure of models will fulfill better performances.

References

[1] Sungi Lee and Chong-Bum Lee, "The development of the AR model to estimate photochemical pollution concentration in Seoul," *Meteorological research paper*, 1991, pp 71-85.

[2] Duc Trung Pham and Liu Xing, *Neural Networks for Identification, Prediction and Control*, Springer-Verlag Inc., 1995.

[3] Sungshin Kim, "A Neuro-Fuzzy Approach to Integration and Control of Industrial Processes: Part I," *KFIS*, 1998, pp 58-69.

[4] James C Bezdek, *Pattern Recognition with Fuzzy Objective Function Algorithms*, Plenum, 1981.

[5] A G Ivakhnenko, "The Group Method of Data Handling in Prediction Problem," *Soviet Automatic Control*, vol 9, no 6, 1976, pp 21-30.

[6] S Farlow, ed., *Self-Organizing Method in Modeling: GMDH-Type Algorithms*, Marcel Deckker Inc., New York, 1984.

[7] A G Ivahnenko, "Polynomial theory of complex system," *IEEE trans. System. Man and Cybernetic*, 1971, pp 364-378.

[8] Greg Spellman, "An application of artificial neural networks to the prediction of surface ozone concentrations in the United Kingdom," *Applied Geography*, 1999, pp 123-136.

The Tenth International Symposium on Artificial Life and Robotics 2005(AROB 10th '05),
B-con Plaza, Beppu, Oita, Japan, February 4-6, 2005

A model of emergence of reward expectancy neurons using reinforcement learning and neural network

Shinya Ishii and Katsunari Shibata, Oita university
Munetaka Shidara, National Institute of Advanced Industrial Science and Technology

Abstract In an experiment of mult-trial task using a monkey in which some successful trials are required until it gets a reward, some neurons that relate to reward expectancy have been observed in the anterior-cingulate in its brain. The reward expectancy neuron is activated in each trial except for the reward trial. Therefore, it is difficult to explain the emergence of the neurons simply by reinforcement learning. In this paper, a model that consists of a recurrent neural network trained based on reinforcement learning is proposed. From the simulation of the model, it is suggested that such neurons can emerge to realize an appropriate value function in the transition period from the single-trial task to the mult-trial task.

Keyword reward expectancy, anterior cingulate, reinforcement learning, recurrent neural network

1 Introduction

It is thought that motivation and reward expectancy must be related to our action learning. Recently, in an experiment of multi-trial task using a monkey in which some successful trials are required until it gets a reward, some neurons that relate to schedule fraction, motivation and reward expectancy has been observed in the Anterior Cinglate and the Ventral Striatum in its brain by Shidara who is one of the authors[1]. These neurons belong to the loop circuit that is working when taking actions in response to important stimulus for emotion or motivation. The Anterior Cinglate is located in the frontal cortex, and has nerve fiber connections with various areas such as prefrontal cortex, supplementary motor area and limbic system, and bears an important role for motivation. On the other, the Ventral Striatum is located in the basal ganglia. It is reported that the basal ganglia relate to action learning based on reward, and some models has been already proposed to explain the reward-related motion generation based on reinforcement learning. It is easy to explain the motivation neurons whose activation becomes large as it approaches the reward. However, it is difficult to explain the reward expectancy neurons which activate in each trial except for the reward trial.

In this paper, a model that consists of a recurrent neural network trained based on the actor-critic type reinforcement learning is proposed, and the reason of emergence of the reward expectancy neurons observed in the physiological experiment is investigated by the analysis of the model during learning. Furthermore, we aim to reinforce the possibility that reinforcement learning is a main principle of learning in the brain.

2 The experiment using a monkey[1]

2.1 Task setting

This chapter explains multi-trial reward schedule task using a monkey. In the first stage, the monkey trains visual color discrimination trial as shown in Fig.1. At first, the monitor is pitch-black, and after 500ms a white bar light called visual cue is presented at the upper edge of the monitor. When the monkey touches a bar, the fixation point presented at the center of the monitor turns red. After the varying waiting period lasting between 400 and 1200ms, the target color becomes green, which instructs the monkey to release the bar. If the bar is released within 1sec after the onset of green target, the target turns blue to signal the monkey that the trial is correct, and the monkey can get juice as a reward after 250∼350ms.

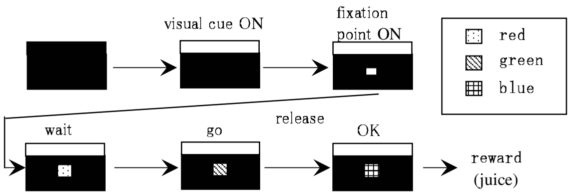

Fig.1 Visual color discrimination trial

After training of this visual color discrimination trial (single-trial task), the task transits to multi-trial reward schedule task (multi-trial task). In the multi-trial task, the reward is given to the monkey when it succeeds in successive 1∼4 trials. The necessary number of trials to get reward is determined at random. For example, the flow of the four-trial schedule is shown in Fig.2. Since the visual cue becomes bright as the monkey approaches the reward trial, it can recognize the number of trials remaining until it can get the reward. The schedule fraction, in other words, the number of trials in schedule is shown by (the number of

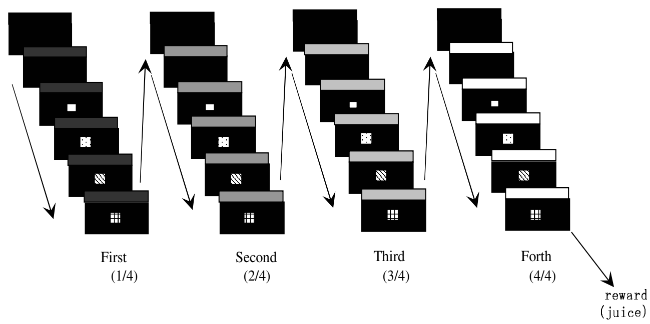

Fig.2 Multi-trial reward schedule task

trials)/(schedule). For example, 1/4 in Fig.2 indicates the first trial in the four-trial schedule. In the control experiment, the cue sequence is random not depending on the schedule so that the cue loses its meaning.

2.2 Experimental result[1]

The activation of the Anterior Cinglate neurons are shown in Fig.3. The neurons A and C in Fig.3(A)(C) generate phasic activations, while B and D in Fig.3(B)(D) keep a tonic activations. As for A and B, the activation decreased before the reward trial, and as for C and D the activation decreased after reward. It is said that A and B express the expectancy for the reward, because they did not activate in the last trial in which the reward is obtained certainly. C and D express the distance to the reward, since the activation becomes the maximum in the trial when the monkey can obtain the reward. The neurons like C and D can be explained easily as the state value(critic) by reinforcement learning. In this paper, the reason of the emergence of such neurons like A and B are investigated. Moreover, the neurons which activate only in the reward trial existing in the Ventral Striatum in the basal ganglia are focused on together with the reward expectancy neurons.

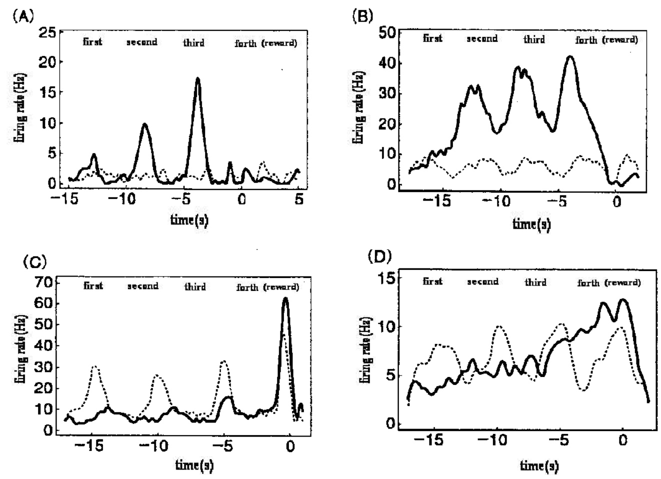

Fig.3 The response of the anterior cingulate neurons (These figures are copied from "Representation of motivational process reward expectancy in the brain", Igakuno ayumi,Vol.202 No.3,p181-p186,2002)

3 Proposed model

3.1 Usefulness of the combination of reinforcement learning and neural network

In the conventional brain research, the main purpose seems to analyze the function of each area in the brain. Also, in robotics research, each functional module such as recognition, action planning, and control was developed, and by integrating such functions, intelligent robots have been developed. In this trend, reinforcement learning has been used as the learning for the function of motion planning, and has been used in the models of the basal ganglia. However, each area in the brain is inseparably connected with each other, and it is thought that learning is done in harmony in the whole brain. One of the authors has been shown that many functions including recognition, memory and so on are acquired in a system constructed seamlessly using a neural network that is trained based on reinforcement learning. Also in each area other than basal ganglia in the brain of living things, we have thought that reinforcement learning can be a main learning principle. In the experiment of hand reaching task using a tool by a monkey, some neurons representing whether the tool is recognized as a part of the body or not are observed in the Interparietal Sulcus. The activation of the neuron representing such high order information can be explained well by the combination[6].

3.2 Proposed model

The architecture of the model proposed in this paper is shown in Fig.4. Actor-critic architecture is employed in this paper. The part called critic generates a state value from a state vector. It playes a role to evaluate the action generated by actor. Temporal difference error (TDerror) $\hat{r}_t$ is expressed by

$$\hat{r}_t = r_{t+1} + \gamma V(\mathbf{x}_{t+1}) - V(\mathbf{x}_t) \tag{1}$$

where, r: reward, $V(\mathbf{x}_t)$: output of the critic, $\mathbf{x}_t$:observed state, and γ: a discount factor. A neural network is used in the proposed model. The neural network is trained by the following training signals that are generated based on reinforcement learning.

$$V_{s,t} = \hat{r}_t + V(\mathbf{x}_t) = r_{t+1} + \gamma V(\mathbf{x}_{t+1}) \tag{2}$$

$$\mathbf{a}_{s,t} = \mathbf{a}(\mathbf{x}_t) + \hat{r}_t \cdot \mathbf{rnd}_t \tag{3}$$

where, $V_{s,t}$: training signal for the critic, $\mathbf{a}_{s,t}$: training signal for the actor, $\mathbf{a}(x_t)$: output of the actor, $\mathbf{rnd}_t$: trial and error factors added to $\mathbf{a}(x_t)$.

In addition, in order to deal with the past information in the neural network, a recurrent structure is introduced.

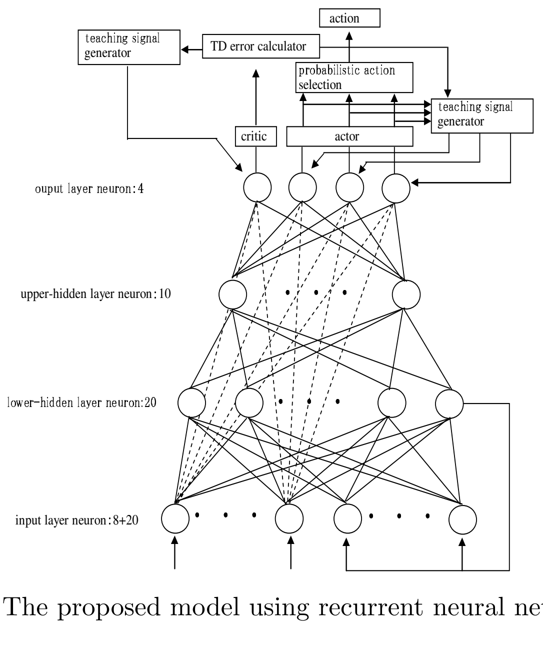

Fig.4 The proposed model using recurrent neural network

The number of layers is four. The number of neurons in each layer is 8 in the input layer, 20 in the lower-hidden layer, 10 in the upper-hidden layer, and 4 in the output layer. The R,G,B signal of the visual cue are inputted into the first 3 neurons in the input layer. Since the visual cue is gray scale from black to white, the values are always the same among the three neurons. The value was 1.0 in the single-trial task. In the multi-trial task, it became large as it approached to the reward such as $0.1 \rightarrow 0.4 \rightarrow 0.7 \rightarrow 1.0$. The R,G,B signals of the target color are inputted into the 4th∼6th neurons in the input layer. The signal to the input neuron 7 represents whether the monkey touched the bar or not. If the bar is touched, the signal is 1, otherwise it is 0. The signal to the input neuron 8 is 1 when the reward is given, otherwise it is 0. In addition, the direct connections from the input layer to the output layer were added. This idea is based on the knowledge that there exist different paths to the basal ganglia. One is through the frontal cortex, and the other is not through the area. It is because the latter is thought to realize an easy linear input-output relation, and the former is thought to complement the latter. Moreover, by considering that the output of each neuron is expressing pulse density, the output function of each neuron is the sigmoid function whose value ranges from 0 to 1.

The output neuron 1 is used as critic output, and the output neurons 2,3 and 4 are used as the actor output vector. One of the three actions, "keep", "touch", or "release", is assigned to each actor neuron. An action is selected statistically by comparing the values after adding a random number *rnd* to each actor output. The random number is in the range of $\pm$ 0.3. BPTT (Back Propagation Through Time) is used as a learning algorithm for the recurrent neural network, and the time to be traced back was set to 80 step. Sampling time, i.e., one step, was set to 100ms. Furthermore, when it transited from the single-trial task to the multi-trial task, the discount factor was changed as $0.96 \rightarrow 0.976$ since the necessary time steps to the reward becomes long. Each initial weight from the input layer to the lower-hidden layer or each from the lower-hidden layer to the upper-hidden layer was set to a small random value. All the weights from the upper-hidden layer to the output layer were set to 0. For this reason, at first, an action is always chosen randomly among the above three actions because the three actor outputs are the same. As for the feedback connections, self-feedback connection weights are set to 4.0, and the others to 0.0. By this setting, the propagated errors by BPTT propagate efficiently without divergence when the learning is traced back in the past, and two stable equilibrium points can be learned easily. The value 4.0 is calculated as the reciprocal of the maximum derivative of the sigmoid function.

4 Simulation rusult

In this simulation, when the learning could be performed almost completely in the single-trial task, it moved to the multi-trial task. Here, the number of trials in the single-trial task was 16500.

4.1 The activation of each neurons

4.1.1 The result after total 20000 trials

First, the activation change of some neurons after 20000 trials, in other words, soon after switching to the multi-trial task is shown in Fig.5. The results are shown for the case when the reward is given after 4 successful trials.

The activation of the critic is shown in Fig.5(a). If the learning is performed ideally, the critic increases exponentially and smoothly toward the time when the reward is given. However, in this case, the upward trend towards the reward can be seen only in the reward trial after 6 second. Henceforth, the upper-hidden neurons 3,4 and 9, which are considered to contribute to the critic greatly by judging from the weight value to the critic, are observed. The activation of them after 20000 trials are shown in Fig.5(b)∼(d), and the change of the weight from each of the neuron to the critic are shown in Fig.6. Here, since the upper-hidden neuron 4 shown in Fig.5(c) has a negative connection to the critic, the output value is observed after turning the value upside down. In this case, the critic is expressed mainly by the upper-hidden neurons 4 and 9 in Fig.5(c),(d) in the last trial. In each trial except for the last one, since the reward cannot be got, a large negative TDerror appears. Therefore, it is thought that the activation was depressed greatly in non-rewarded trials.

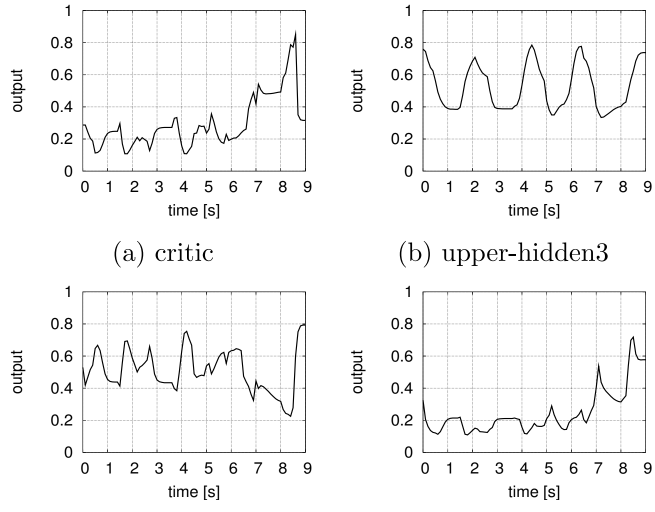

(a) critic (b) upper-hidden3

(c) upper-hidden4 (d) upper-hidden9

Fig.5 The response of some neurons after 20000 trials

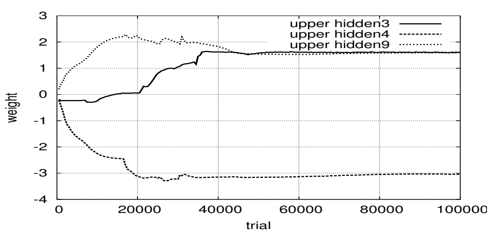

Fig.6 The change of the connection weights from the upper-hidden neuron 3,4,9 to the critic

4.1.2 The result after total 30000 trials

Next, the activation of each neuron after 30000 trials is shown. The activation of critic is shown in Fig.7(a). Comparing with the previous activation curve of the critic shown in Fig.5(a), the critic is increasing even before the last trial. The activation of the upper-hidden neurons are shown in Fig.7(b)∼(d). In this case, the neuron that did not activate in the last trial emerged as shown in Fig.7(b). Since the weight from the upper-hidden neuron 3 to the critic is large around 30000th trial as shown in Fig.6 as well as the upper-hidden neuron 4,9, these neurons are contributing to the critic output. Then the upper-hidden neuron 3 is considered to be equivalent to the reward expectancy neuron in the experiment using a monkey. Then, in order to consider how this reward expectancy neuron is represented, the activation of the lower-hidden neurons contributing the upper-hidden neuron3 are observed. Fig.7(e),(f) show the activations. The upper-hidden neuron3 shown in Fig.7(b) receives a positive connection from the neurons whose activation is depressed in the reward trial as shown in Fig.7(e),(f). Each of the neuron has a negative connection to the neuron which activates only in the reward trial. This means that they are contributing to both the reward expectancy neuron and the neuron which activates only in the reward trial.

4.2 Emergence reason of reward expectancy neuron

From the analysis of the above results, the reason for the emergence of the reward expectancy neuron is summarized as follows.

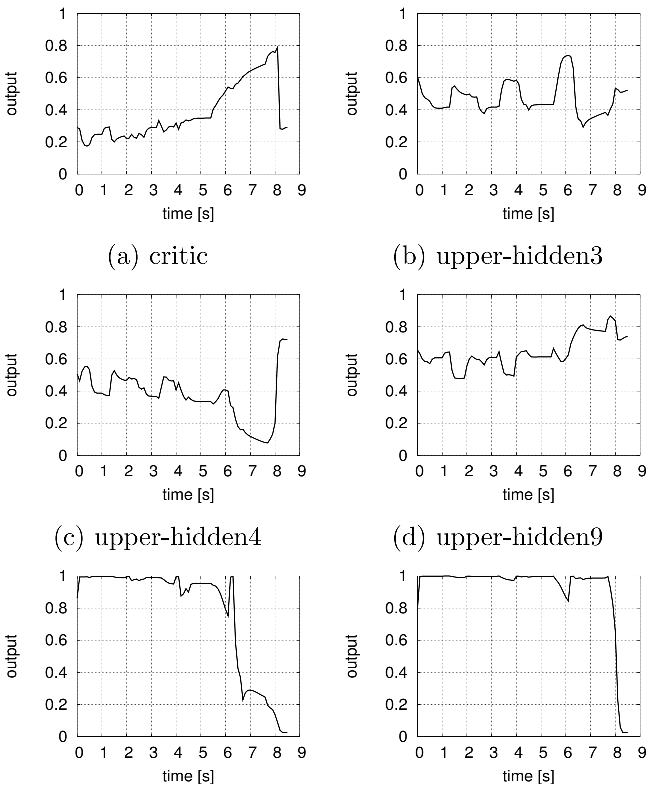

(a) critic (b) upper-hidden3

(c) upper-hidden4 (d) upper-hidden9

(e) lower-hidden15 (f) lower-hidden17

Fig.7 The response of some neurons after 30000 trials

(1) Just after the transition to the multi-trial task, the critic is inhibited by a large negative TDerror appeared in each trial except for the reward trial. The neuron that activate only in the last trial as shown Fig.5(d) emerged.
(2) When the learning progressed to some extent, the critic output was required to increase according to the distance to the goal, and as a result, the reward expectancy neuron emerged to complement the neurons which activate only in the reward trial.

5 Conclusion

In this paper, a model that consists of a recurrent neural network trained based on the actor-critic architecture for reinforcement learning is proposed. From the simulation of the model, a neuron that relates to "reward expectancy" was observed in the hidden-layer. It is suggested that such neurons can emerge to realize an appropriate value function in the transition period from the single-trial task to the mult-trial task. The relation between the reason of emergence and the function of "reward expectancy" should be considered in the future, but we think that the result supports the idea that reinforcement learning is a main principle of learning in the brain.

Acknowledgement

This research was partially supported by the Japan Society for the Promotion of Science, Grants-in-Aid for Scientific Research, 14350227 and 15300064.

Refarence

[1] Shidara,M. : Representation of motivational process reward expectancy in the brain, Igakunoayumi,Vol.202 No.3, p181-p186, 2002

[2] Doya,K. : Complementary roles of basal ganglia and cerebelum in learning and motor control, Curr. Opin. Neurobiol.Vol.10,No.6,pp.732-739, 2000

[3] Barto,A.G., Hauk,C.J., Davis,J.L. and Beiser,D.G. : Adaptive Critics and the Basal ganglia, in Models of Information processing in the basal ganglia eds.MIT Press, 1955

[4] Williams,R.J. and Zipser,D. : Gradient-Based Learning Algorithm for Recurrent Connectioninst Networks, Tech.Report NU-CCS-90-9, Northeastern University, 1990

[5] Shibata,K. :Reinforcement Learning and Rbot Intelligence -Can Intelligence be Realized by Carrot-and-stick? - , The 16th Annual Conference of Japanese Society for Artificial Intelligence, 2002 (In Japanese)

[6] Shibata,K. and Ito,K. : Hidden Representation after Reinforcement Learning of Hand Reaching Movement with Variable Link Length, Proc. of IJCNN, 2003, 1475-674.pdf, pp.2619-2624, 2003

The Tenth International Symposium on Artificial Life and Robotics 2005(AROB 10th '05),
B-con Plaza, Beppu, Oita, Japan, February 4-6, 2005

Shape-recognition using randomly selected pixel-pair neurons

Valerie Rose and Jeffrey Johnson
Department of Design and Innovation
The Open University
Milton Keynes, MK7 6AA, England
j.h.johnson@open.ac.uk and vrose@ukonline.co.uk

Abstract

Designing low level recogniser/filters for vision systems restricts their potential. We show how *retinal neurons* based on pixel-pair sensors can recognise shapes. The next step is evolving optimum retinal neurons to support the evolution of vision systems that can abstract their own higher level constructs.

1. Introduction

Our group is investigating a new vision architecture based on a multilayer representation [1].This architecture is intended to produce machine vision systems that:

- evolve appropriate retinal configurations
- evolve connectivities to represent spatial relationships
- abstract their own higher level constructs
- have levels which are integrated by new relational mathematics

A key feature of the architecture is a *multilevel representation*, with pixels at the lowest level, and objects and scenes at higher levels.

At the lowest layer, configurations of pixels respond to objects and are connected to an hypothetical neuron that fires when activated by appropriate inputs. We call these *retinal configurations*. The outputs of lower level neurons feeds forward through the system, ultimately allowing objects and scenes to be recognised.

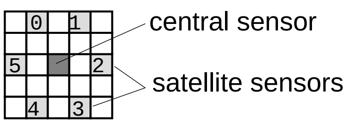

Figure 1. Inputs to a low-level neuron

Elsewhere [1] we have experimented with retinal configurations based on fixed pixel positions, as illustrated in Figure 1. Here there is a central sensor, surrounded by six satellite sensors. The idea is that if the central sensor detects darkness, the neuron is triggered. There are sixty four light-dark responses for the six satellite pixels, (Fig 2 We assume that there are sixty-four associated retina neurons. Once the central neuron is triggered, the neuron fires if the six satellite pixels match the black-white greyscales of the image. Thus, every dark pixel in an image responds to one of these sixty-four retinal neurons, according to the black-white states of its satellite pixels.

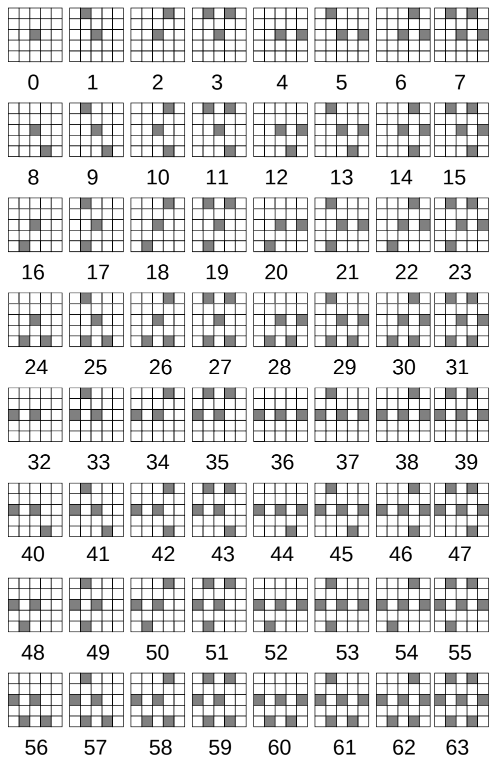

Figure 2. 64 retinal neuron patterns

Figure 3 shows the three shapes used in the experiments reported in this paper. Each shape responds differently to the retinal neurons. For example, the diamond shape has more type-57 responses than the circle or square, because this configuration of the satellite sensors responds well to the sloping edges. For a given shape, the numbers of responses for each retinal neuron can be counted, giving a 64-element *response vector* for each shape.

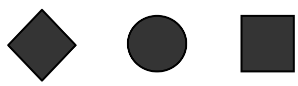

Figure 3. The simple shapes used for our experiments

It has been shown that these vectors contain sufficient information to discriminate the simple shapes, in the context of our hierarchical architecture, which is described in detail in [1].

2. Random Neural Pair Generation

An essential feature of our architecture is that it must be able to *adapt* to changes in objects and scenes. We believe that this pre-empts approaches to machine vision in which programmers *design* a fixed retinal processing architecture. In particular we believe that the approach typified by our designing the sixty four retinal neurons in Figure 2 inevitably leads to vision systems that will be limited in their recognition ability, and incapable of adapting to radically new objects and scenes.

We conclude from this that we need to *generate the retinal neuron configurations at random*. There are many questions associated with this, including:

- compared to one plus six sensors used in Figure 1, how many sensors should be connected together to produce a retinal neuron?
- what should be the maximum or minimum 'diameter' of the neuron?
- how many neurons are required for successful pattern recognition?

To begin our experiments we used pairs of pixel sensors connected to hypothetical neurons, as shown in Figure 4. They can occur at any distance from one another within the image, as shown in Figure 4.

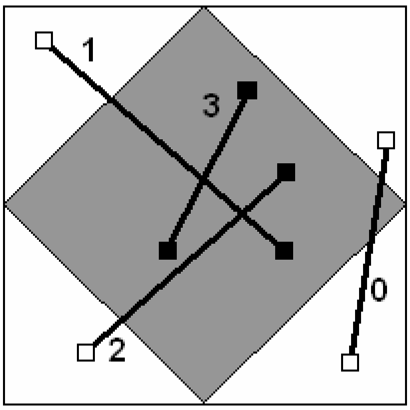

Figure 4. The four pixel-pair configurations
0 - background-background
1 - background-foreground
2 - foreground-background
3 - foreground-foreground

There are four possibilities for the pixel pair: background-background (0) background-foreground (1), 2 - foreground-background (2), and foreground-foreground (3).

For our experiments, we generated sixty pixel pair configurations. These random configuration were fixed and used for training and recognition. The retinal neurons are illustrated in Figure 5.

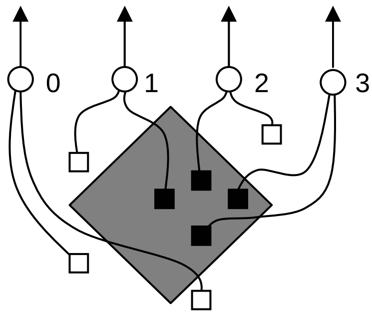

Figure 5. Pixel pair retinal neurons

Three 'template' shapes were generated using one shape of each class shown in Figure 3 as the training set. If the sensor black-white inputs correspond to the fixed black-white input configuration of the neuron, then that neuron fires. For example, if the neuron is of Type 0 and both input pixels are white, the neuron fires.

3. Recognising unseen shapes

For a given set of pixel pairs and a given shape, the neuron response is recorded as a template. These templates are matched against unseen shapes and used to recognise them. Thus each unseen shape gets a score of the number of neurons that were matched and fired. We apply a winner-takes all strategy, and the shape with the highest number of matches is recognised. If two or more shapes have the same score, a non-classification is made.

Circle	Diamond	Square
88/88	87/88	88/88

Table 1. Recognition of the three shapes

For this experiment we used eighty eight examples of each test shape. All the circles, all the squares, and all but one of the diamonds were correctly recognised (Table 1). This result strongly suggests that this approach of matching shapes against randomly generated retinal neurons is viable.

Trial	Circle	Diamond	Square	%
1	88/88	87/88 *	88/88	99%
2	88/88	88/88	88/88	100%
3	88/88	80/88 *	84/88 *	94%
4	88/88	85/88 *	88/88	98%
5	88/88	88/88	88/88	100%
6	88/88	88/88	88/88	100%
7	88/88	88/88	88/88	100%
8	88/88	88/88	88/88	100%
9	87/88 *	88/88	88/88	99%
10	88/88	88/88	88/88	100%

Table 2. Ten recognition trials (60 neurons)

To strengthen this conclusion the experiment was repeated ten times. The results of these experiments are shown in Table 2.

These results support the conclusion that the randomly generated retinal neurons can be used for shape recognition, though they show that errors can occur.

In order to see if these results could be improved, the experiment was repeated using sets of one hundred randomly generated neural pairs. The results in Table 3 suggest that adding extra neurons can improve the pattern recognition performance.

Trial	Circle	Diamond	Square	%
1	88/88	88/88 +	88/88	100%
2	88/88	88/88	88/88	100%
3	88/88	84/88 +	88/88 +	100%
4	88/88	87/88 +	88/88	99%
5	88/88	88/88	88/88	100%
6	88/88	88/88	88/88	100%
7	88/88	88/88	88/88	100%
8	88/88	88/88	88/88	100%
9	88/88 +	88/88	88/88	100%
10	88/88	88/88	88/88	100%

Table 3. Ten further trials with 100 neurons

Not surprisingly, the location as well as the type of configuration of the random pairs affects performance, as does the number of pairs selected.

4. Discrimination by configuration

The next set of experiments is concerned with the relative 'usefulness' of the different configurations.

Table 4 indicates that, as one would expect, considering the relatively large shapes we are using, that the largest proportion of the 60 pairs are of type '3', black-black, for each of the three template shapes.

Trial	Circle	Diamond	Square
1	44	24	56
2	41	19	54
3	40	19	53
4	37	17	53
5	40	19	56
6	34	12	55
7	36	20	55
8	34	14	53
9	38	16	55
10	42	21	54

Table 4. Frequency of Configuration 3

Using just configuration 4 for matching gave an improvement in all the scores over the first set of experiments (Table 2), and no worsening of any score. The performance for diamonds is notably better.

So these black-black pairs are being generated in sufficient quantity to give reasonably good recognition.

Increasing the number of random pixel-pairs to 100 further improves performance

The next set of experiments restricted the permitted configurations to types '1' and '2', white-black and black-white.

This gives some slight improvements with recognition of diamonds in Trial sets 1and 3, but some deterioration in recognition with trial sets 3, 4, 5, 7, 9 and 10.

Another factor which is possibly affecting performance is that the 'not 1 and 2' configurations, '0' and '3', are opposites – background/background versus foreground/foreground, so that grouping them together into one type may reduce discriminatory ability. In other words, it seems that information about 'edges' and 'not edges' without further categorization of the 'not edges' as 'shape' or 'background' is insufficient for reliable recognition.

Again selecting 100 random pairs increases the quantity of type '1' and '2' configurations and performance improves correspondingly.

Increasing to 130 pairs brings further improvement – 100% recognition for all but the diamonds, with one trial giving a marked deterioration . So, in general, even when the number of pairs is increased producing more type '1' and '2' pairs, recognition is not as reliable as for all four configurations or types '3' and 'not 3'.

5. Distance between paired pixels

So far there has been no restriction on the separation of the pixel pairs. In this section we investigate whether restricting the distance affects the results.

It appears that restricting the permitted distance between the pixels in each pair adversely affects performance for a given number of random pairs.

The recognition experiments were repeated with the distance, in both horizontal and vertical directions being reduced to < =10 to < =5 and finally to < =3. For 60 pixel-pairs recognition deteriorates correspondingly.

Increasing to 150 pairs and setting the distance to < =10 pixels gives 100% recognition for all except the diamonds in one of ten trial sets. However, with 150 pairs and any distance, all shapes are correctly classified across all ten random sets, so restricting the distance appears to give no advantage.

One might expect that restricting the distance would provide useful 'local' discriminatory information. Possibly the reason this does not appear to do so is the relatively small number of pixel-pairs, and the lack of redundancy. When more random pairs are generated, there is a better chance of gathering enough useful information to compensate for this.

6. Informal Discussion

These experiments have addressed a number of questions. They have been concerned with how randomness might used as the basis of recognition and what gives useful information in order to develop strategies that able it to repeat successful behaviours.

In order to succeed at this, the system needs to be able to quantify the amount of information is getting from parameters such as distance between pixels, their location, the configurations they form in combination, and so on. It may even be useful to base its evaluations on information theory related to the inputs and outputs on the various connections in some form of hierarchical neural network.

However this raises issues such as how to put a value on the relative quantities of information being conveyed. For example, how would the system differentiate between the amount of information obtained from a pair of pixels of type '3' configuration 10 pixels apart and a type '2' configuration pair 60 pixels apart? The answer to this probably lies in having feedback of some sort about the varying strengths of neuronal responses to the different input patterns as the system learns. Rolls and Deco [2] have recognized the contribution information theory can make to understanding communications among individual neurons and networks of neurons within the brain.

7. Conclusions and the next step

The conclusions from the experiments reported here are that:

- randomly generated retinal neurons using pairs of pixel sensors can be used to recognise shapes
- increasing the number of neurons from 60 to 150 improved performance
- of the four types of neuron, Type-3 appears to give the most information, but this rather inconclusive
- restricting distances between sensor pairs did not appear to improve recognition performance, although the performance improved with the number of neurons.

These conclusions have to be set in the context of the small number of test shapes we have used, and their simple nature.

The results support our belief that we will be able to use randomly generated neurons for recognising shapes and features. In future experiments we intend to use evolutionary methods to select the most appropriate neurons for particular purposes. It is our intention to 'breed' new sets of retinal neurons from those that perform best for a given application.

The result that restricting distance does not appear to improve performance is particularly interesting. Combined with the result that increasing the number of neurons improves performance, this suggest that evolutionary principles can best select the most appropriate distances for any particular application, provided enough neurons are used.

References

[1] Johnson, J.H., Rose, V., 'Autonomous Evolutionary machine vision systems', AROB-10, Beppu, Japan, M. Sugisaka (ed).

[2] E. T. Rolls, G. Deco, 2002, *Computational Neuroscience of Vision*, Oxford.

The Tenth International Symposium on Artificial Life and Robotics 2005(AROB 10th '05),
B-con Plaza, Beppu, Oita, Japan, February 4-6, 2005

Development of an autonomous personal robot "The visual processing system for autonomous driving"

Takuma Umeno **Eiji Hayashi**
Department of Mechanical Information Science and Technology
Faculty of Computer Science and Systems Engineering , Kyushu Institute of Technology
680-4, Kawazu, Iizuka-City, Fukuoka Prefecture, Japan

Abstract

Currently, an autonomous self-driving robot is expected to provide various services within the human living environment. Such robotic technology is already seeing practical use in industry and being used in industrial applications. But the robots for industry only faithfully follow the given motion which human make. We are therefore working to develop an autonomous personal robot with the ability to perform practical tasks in a human living environment by using information derived from sensors and a knowledge database.

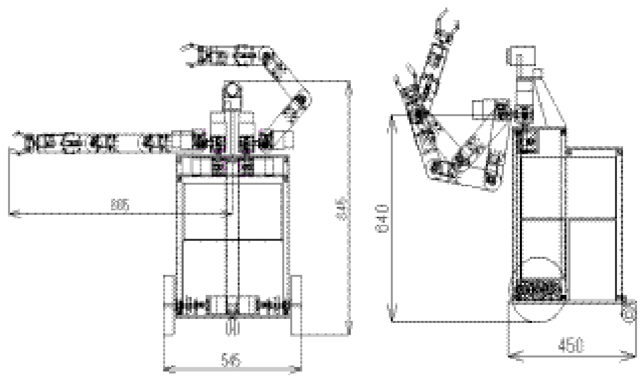

Fig. 1 Robot design

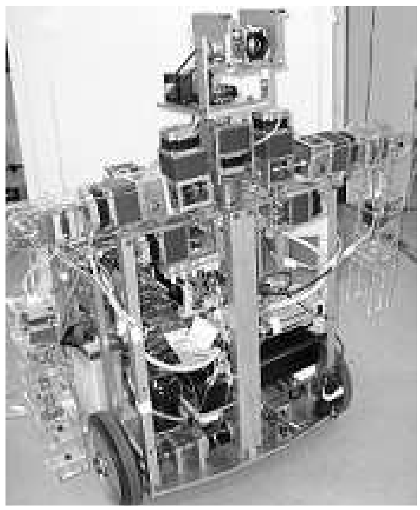

Fig. 2 Robot appearance

1. Introduction

There are many problems to develop autonomous self-driving personal robots which can work like humans instead of us. These problems can be roughly divided into three categories: (1) how to process contextual information regarding the robot's environment; (2) how to form a robot's action plan based on this information; and (3) how to correctly control the robot using the robot's action plan. The purpose of the present study was to develop a way to allow the robot to determine its own position and posture as related to the above-mentioned problems. We have thus developed a visual processing system that enables a self-driven robot to advance in a straight line.

The robot's visual processing system uses only a CCD camera and processes the image information displayed by that camera. We have used the Hough transformation, which is knot to be able to extract straight lines from an image, to extract the features of an image. We define the intersection of vertical lines and horizontal lines as a "characteristic point," and we calculate the errors of position that occur while the robot is moving along a linear path by using the flow of the plotted characteristic points over time. However, the system that we previously developed could not obtain useful data because the rate at which that system acquired the characteristic point was very low. Therefore, in the present research, we have included and have developed an algorithm for extracting straight lines and characteristic points.

We explain herein how the additional image processing and the improvement of the algorithm enhance the stability of the system. In addition, we have experimentally evaluated the visual processing system for autonomous driving.

2. Recognition system and Decision system

The environment for robot activity assumed in this study is a finite space such as a family room, an office, or a hospital room. Our robot has a map showing robot's sphere of activity, and we call this map 'the finite space map'. The finite space map has information including the size of each parameter of the map, the initial position coordinates of the robot, the coordinates of the movement needed to get to the destination, the number of placed objects, and the positions and sizes of those objects. The robot can do autonomous driving based on the finite space map. The finite space map is shown in Fig.3.

In addition, we are developing a recognition system that will allow the robot to recognize the external environment. The recognition system consists of a CCD camera, an optical sensor, and a supersonic wave sensor. The supersonic wave sensor primarily recognizes unknown objects that don't exist on the finite space map. The optical sensor recognizes measurement of an actual distance with an unknown object. The recognition system supports the robot's autonomous action by using information for each device and the finite space map. The composition of the system is shown in Fig.4.

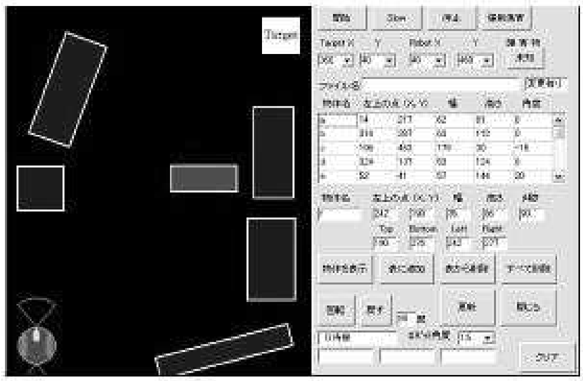

Fig. 3 Map of a finite space

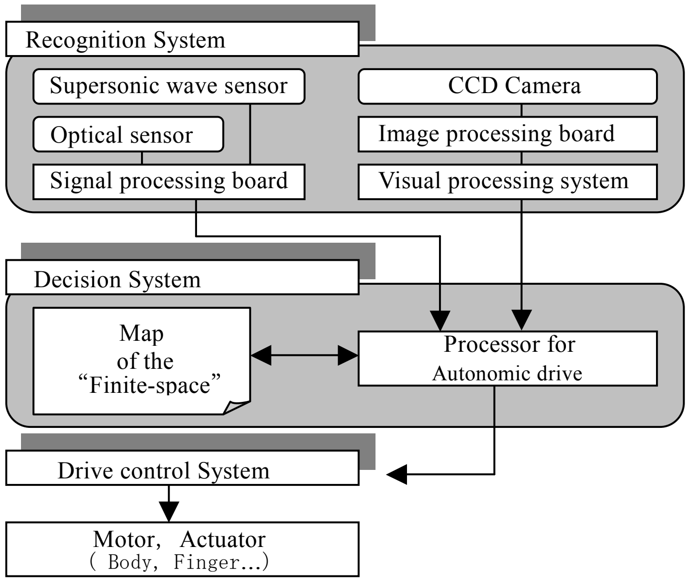

Fig. 4 Processing system for the personal robot.

3. The visual processing system

3.1 Outline of the system

When the robot moves, the positions in the map need to be synchronized with its real position in order to correctly reach the desired destination. Therefore, it is useful to consider a case in which the robot can't correctly drive because of a subtle unevenness in the ground's surface and the resulting slight difference in the rotation of the right and left driving wheels. In addition, we must reduce the error of position produced by this case as much as possible. The purpose of the visual processing system is to enable a self-driven robot to advance in a straight line. The visual processing system captures objects on an image in order to detect errors in the robot's position. Incidentally, this system doesn't consider large amount of error that is produced by disturbances.

3.2 System flow of the system

The system receives an image whenever the robot moves a certain distance. At the same time, the system generates the flow of characteristic points by processing the data obtained from such images. In addition, the system analyzes whether the robot could advance in a straight line. The flow of this system is shown in the following sentences (Ⅰ－Ⅴ).

Ⅰ. Image Acquisition

The image obtained by the CCD camera is read into PC in the robot. The visual processing system uses only form extraction processing, and color information is not needed. Therefore, we only use an 8-bit gray-scale image.

Ⅱ. Edge processing

The system uses Laplacian edge enhancement.
.

Ⅲ. Segmentation processing

To limit the extracted data that are required for form extraction, the system performs Segmentation processing.

Ⅳ. Thinning processing

The edge extracted by the edge processing has line width. In order to decrease the amount of calculation and to stabilize the hough transformation, the system performs thinning processing.

Ⅴ. Hough transformation and Characteristic point

The Hough transformation can extract the straight lines contained in an image. And we define the intersection of vertical lines and horizontal lines as the characteristic point.

3.3 Processing for extraction of straight lines and characteristic points

In this system, the portions of straight lines on an image are extracted using the hough transformation. However, an actual image consists of many straight line portions. By virtue of that, the system produces getting unnecessary data. And in the case of extracting characteristic points, if the system captures a characteristic point that are different from characteristic points of the object currently being pursued, the system causes errors. These problems would directly affect the accuracy and speed of the system. So, in order to avoid these problems, we have improved processing for extraction of straight lines and characteristic point in the visual processing system.

■Processing for extraction of straight lines

When the system extracts straight lines, each of two processings is working in order to raise accuracy and processing speed.

In case of using the hough transformation, it is possible to select the threshold value about the reliability of straight lines on an image. The processing chooses automatically the threshold value until it only extracts the effective data of straight lines. The histogram about selecting the threshold value is shown in Fig.5.

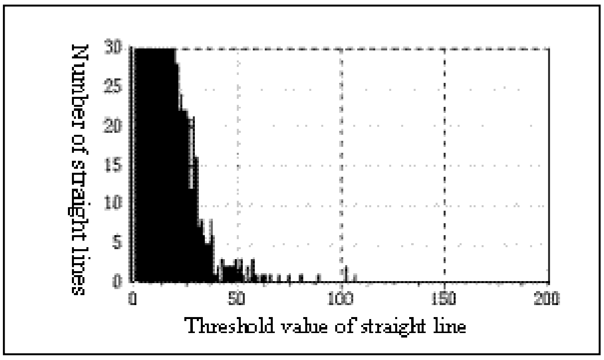

Fig. 5 Histogram for selecting the threshold value

The system is restricted to processing rectangular objects, as the robot environment generally has many rectangular objects.

Figure 6 shows the image taken with the CCD camera, and the image after edge processing. In addition, the bottom part of fig.6 shows the images that have been processed to extract straight lines. In comparing differences between these two images, it can be seen that the one image is normally processed to extract straight lines, while the other is restricted to extract only a rectangular object.

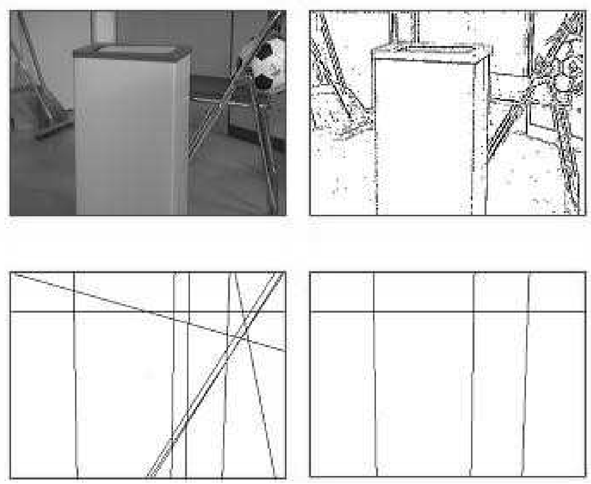

Fig. 6 Processed images to extract straight lines

■Processing for extraction of characteristic points

The data for characteristic points are actually used for detecting errors in the robot's position. It is important in this processing that the characteristic points of the objects being moved by robot's drive be continuously captured. We have therefore developed a processing method that gets the nearest point from the former characteristic point on an image as a new characteristic point.

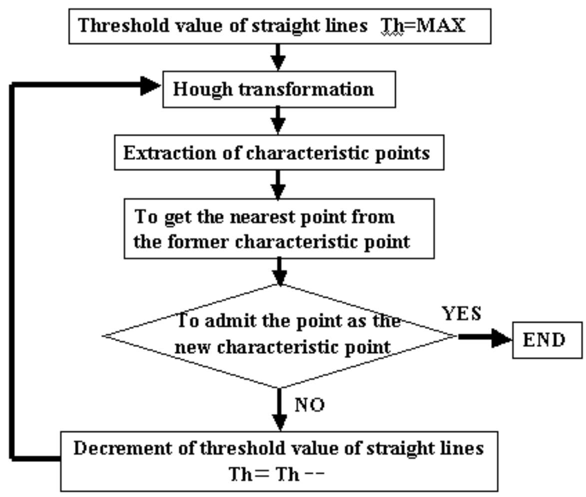

Fig. 7 System flow

3.4 Evaluation of whether the robot is advancing in a straight line

The flow of characteristic points is changed by the state of the robot's driving. Moreover, it is possible to calculate geometrically the flow of characteristic points in the case in which the robot advances normally in a straight line. Therefore, we can evaluate whether the robot advances in a straight by comparing the actual flow with the theoretically calculated flow.

4. Experiment for evaluating the visual processing system

In this experiment, a case in which the robot normally advances in a straight line is compared with a case in which a gap is intentionally produced. The robot has been driven in a flat room using DC motors.

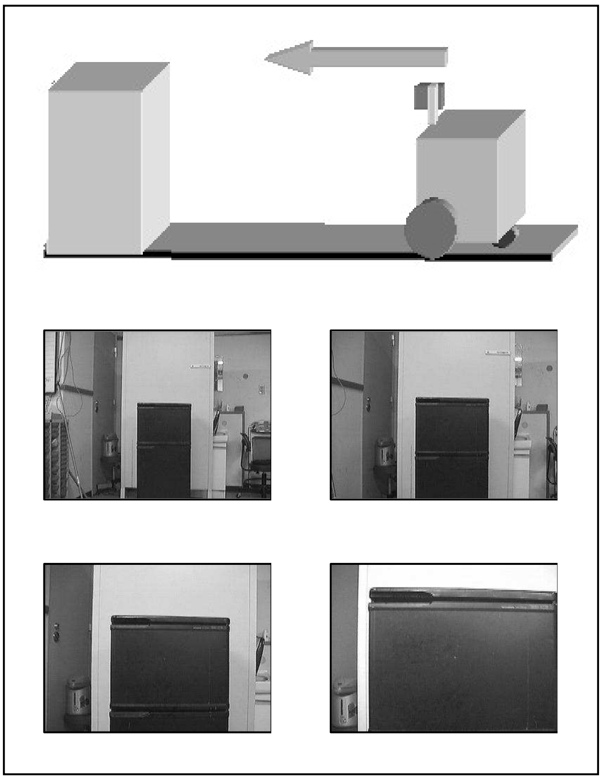

Fig. 8 Situation of experiment

We made the robot go straight toward a rectangular object and used the system to generate the flow of characteristic. The flow of characteristic points in the case where the robot normally goes straight is quite different from that in the case where the robot doesn't go straight (Fig. 9). We have confirmed that the flow of characteristic points drawn by geometrical calculation and such flow drawn by the visual processing system are similar (Fig. 10). As such, we can conclude that the developed system can evaluate whether a robot is advancing in a straight line.

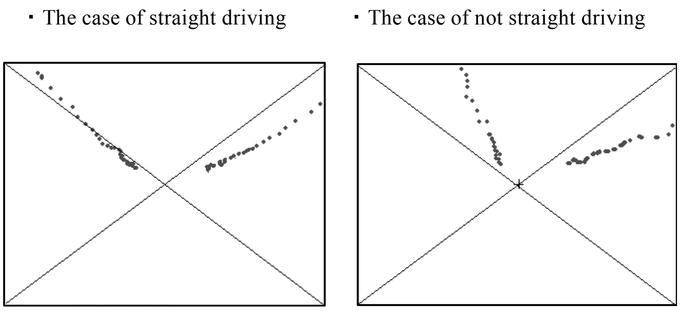

Fig. 9 Flow of characteristic points

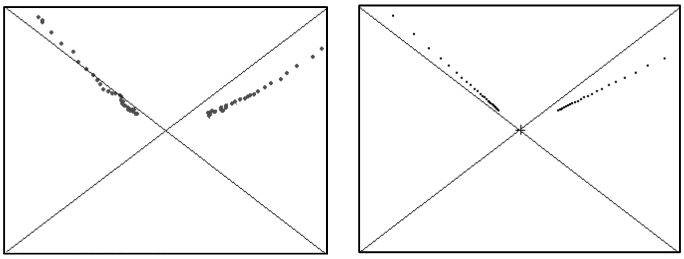

Fig.10 The actual flow and the theoretically calculated flow

5. Conclusions

In this research, we added additional image processing capability to a robot's processing system and developed an algorithm for extracting straight lines and characteristic points. As a result, the system's ability to capture the characteristic points has improved remarkably.

Our results indicate that the system was able to output the flow of the feature point well against the single object. In addition, the system allowed us to evaluate whether the robot is advancing in a straight line.

Our next subject of study for the robot processing system involves calculating actual data regarding errors in the robot's position. In addition, we must develop a system that allows for feedback control of the robot.

References

[1]Funakubo, Process and recognition of the vision pattern, Keigakusyuppan, 1990.

[2]Shinoda, Self-driven robot on the grand, Journal of the Robotics Society of Japan, Vol. 18, No.7, pp.928-932. 2000.

The Tenth International Symposium on Artificial Life and Robotics 2005(AROB 10th '05),
B-con Plaza, Beppu, Oita, Japan, February 4-6, 2005

Development of a system for self-driving by an autonomous robot

Eiji Hayashi and Keisuke Ikeda
Faculty of Computer Science and Systems Engineering,
Kyusyu Institute of Technology
680-4, Kawazu, Iizuka-City, Fukuoka Prefecture, Japan

Abstract

Expanded and advanced functions for a self-driven robot equipped with environment recognition and the ability to learn using a sensor and a camera are being developed. The robot is active in the manufacturing field, the medical field, the welfare field, the public field, and elsewhere, in each case contributing to a higher quality of life. However, it is difficult for the robot to understand the human environment because the environment is always changing.

In this research, we are developing an autonomous robot that can execute simple directions from a human in a particular environment (the home, the office, the sickroom, and so on). The autonomous robot will execute an action while referring to "finite mapping" when moving around in the room. Finite mapping is data about the space in the field of activities of the robot. The robot recognizes known objects that are shown by this mapping and drives, being autonomous.

1. Introduction

In recent years, the rapid development of semiconductor technology has allowed the development of robots that can perform advanced processing in response to complex information input using a sensor, machine vision, etc. Various functions are demanded of the personal robot using such technology in people's various environments (home, office, a sickroom etc.). However, developing a robot that can fill these requests is difficult.

In our laboratory, we are developing an autonomous personal robot that can apprehend the environment and meet the demands of its users. This robot has the known information called "finite mapping". The map has a movable range and the information about an objective position, and the robot drives with reference to the map. However, the position of the map and the robot's actual position do not always correspond. Therefore, the robot has to aim at synchronization between the position of the robot on the map and the actual robot's position.

This paper describes "a system for self-driving by an autonomous robot" which corrects the position error that occurs when the robot moves. This system corrects a self-position using the image information acquired from a CCD camera.

2. Outline of the personal robot

A general view of the robot being developed at our laboratory is shown in Fig 1. The composition of the self-driving system is shown in Fig 2. This paper explains the robot's drive mechanism.

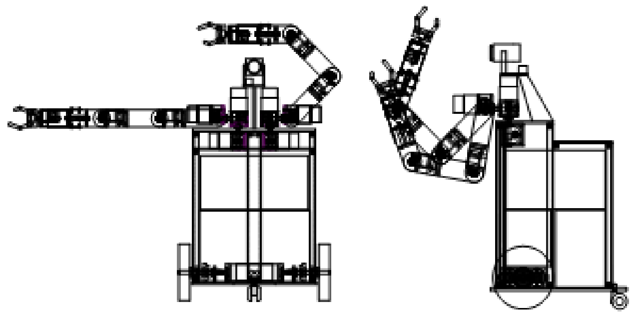

Fig 1. General view of the robot

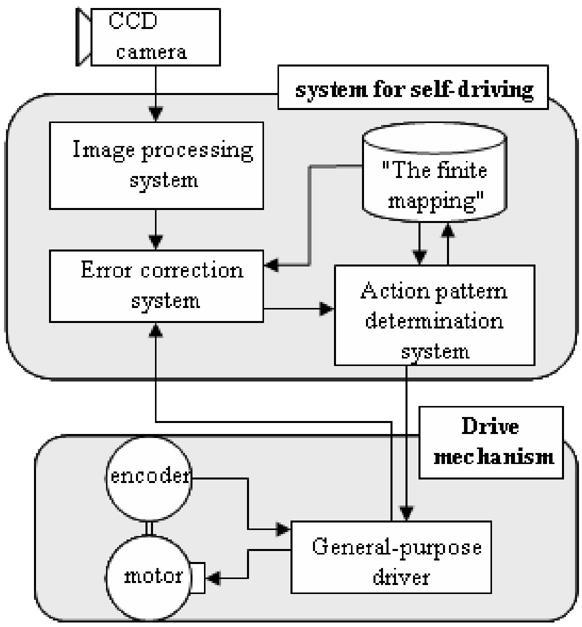

Fig 2.Composition of the self-driving system

2.1 Composition of the drive mechanism

The robot we are developing consists of a drive mechanism of two front wheels and a back wheel, for a total of three wheels. The front wheels are attached to the motor and are independent on either side, and the back wheel is a castor. This method has the advantage of allowing a small turn, compared with the steering system that steers the wheel of a passenger car.

DC servo motors are used for the robot's drive mechanism, and position control and speed control are used for the control system of the drive mechanism. It is possible to determine the amount of movement when the robot drives from one known position to another by using position control. Using speed control, the robot can apply load for a fixed time and can drive it continuously. That is, it is possible to move a load from place to place at the speed specified.

The robot moves based on the specified position and speed.

2.2 System for self-driving

By this self-driving system, in order to perform an operation determined, action patterns are generated. And the system transmits the data for the drive to the drive mechanism. Based on past research, the robot was able to aim at the synchronization of the self-driving system and the drive mechanism.

Now, we have developed an image-processing system and an error correction system. Using the image –processing system, a robot acquires an image using a CCD camera and performs image processing. The error correction system has the job of detecting the position error generated at the time of the robot drive, with reference to the data obtained from the image-processing system.

The finite mapping

The environment assumed by this research is a limited space, such as a home, office, or sickroom, and the given space is the range within which the robot can move.

When objects (furniture, a desk, shelves, etc.) exist in the space where a robot drives, they are described on the map of the limited space as known objects. The robot refers to the map. Evasion course calculation is attained by feed forward. Therefore, the robot's efficiency of autonomous drive processing is raised. The finite mapping has parameters indicating the size of the map and the objects, a robot's initial position condition, target position coordinates, and object arrangement coordinates.

Sample the finite mapping is shown in Fig 3.

Action pattern determination system

When it has a target position specified, the robot has to calculate a course and has to generate an action pattern. By this system, the robot refers to the information on the finite mapping, searches for the course to the target point, and creates a set of data for driving. The robot drives based on this data.

Moreover, in consideration of the position error searched for by the error correction system that we have developed, the robot includes performing feedback control into the calculations. Using this control, the robot should be able to drive in spite of position errors.

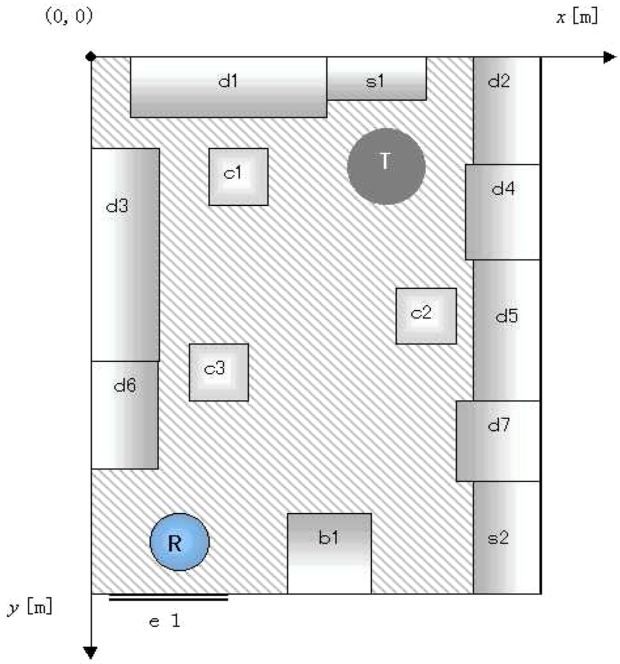

Fig 3. Sample the finite mapping

3. Consideration of position errors

When a robot moves, an error occurs in the mismatch between the position of the robot in the finite mapping and the robot's actual position. When the robot goes from a stopped state to a moving state, the fact that an unstable state is in control of a motor is cited as a cause of this error generation.

The robot at a stopped state needs excessive torque compared with the state where it is moving. Since power is not well transmitted at this time, an error arises in position and speed control of each motor. Then, each motor is converged on the position and speed of the inputted target by feedback control. However, it takes time until each motor converges on the target. Therefore, the robot moves in an unstable state.

Because of this error, the robot performs unstable movement at the time of initial action, and the robot has produced an error in the target value and the actual position.

The moving distance (pulse) of each drive motor and its relationship to timing are shown in Fig 4.

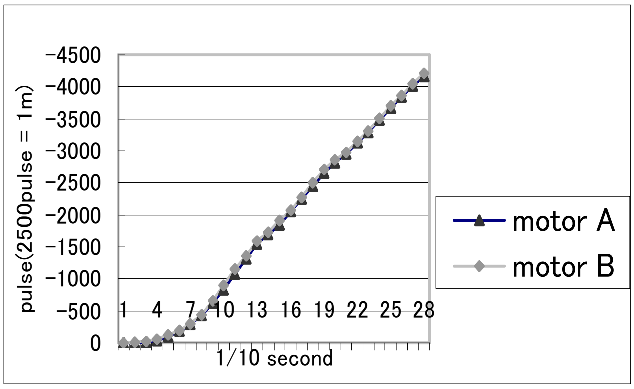

Fig 4 Relation between move distance and time

4. Image-processing system

In order to cope with the problem of error generation described in the preceding paragraph, the robot has to detect its actual position. Therefore, when a robot acquires image data using a CCD camera, the system in which the surrounding environment is recognized can be developed. This system extracts the characteristic point of the target object. And the extraction is repeated and the data flow of the point is created. The characteristic point is defined as the information on the corner of the object obtained from image processing.

The flow of an image-processing system is shown in Fig 5, and the results of processing using the image-processing system are shown in Fig 6. From the image data of the Hough transformation, as shown in figure 6 (d), a linear intersection is calculated. This point is extracted as a characteristic point. At the time of movement, a robot repeats processing of Fig 5 and plots the flow of the characteristic point. The robot recognizes the environment based on the flow.

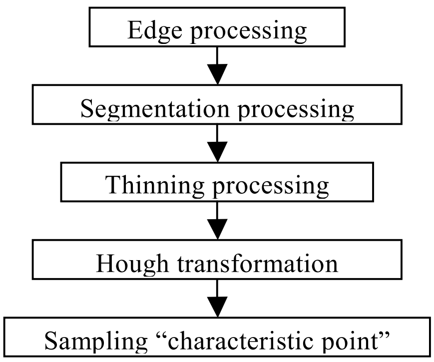

Fig 5. Image-processing system

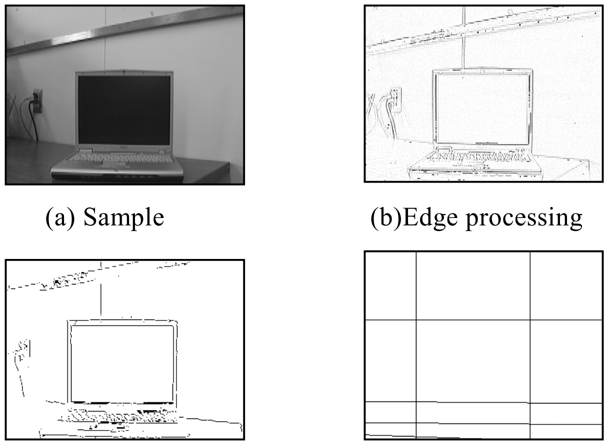

(a) Sample (b)Edge processing

(c)Segmentation processing (d) Hough transformation

Fig 6. Image processing

5. Error correction system

5.1 Geometric calculation for the acquisition of Position information

The error correction system calculates a robot's position from the feature point and a robot's move distance. As shown in Fig 7, let picture coordinates be o-xy coordinates, and let camera coordinates be O-XYZ coordinates. As for camera coordinates and picture coordinates, the following relation is realized:

$$x = f\frac{X}{Z}, y = f\frac{Y}{Z}$$

The x-coordinate of the picture obtained from image processing of an initial state is set to x1. If the x-coordinate of the picture obtained when a robot z advanced is made into x2, the following expression of relations will be realized:

$$x1 = \frac{X}{Z}f, x2 = \frac{X}{Z-\Delta Z}f$$

$$X = \frac{x1 * x2 * \Delta Z}{f(x2 - x1)}, Z = \frac{X}{x1}f$$

Therefore, it turns out that the present robot's position (X, Z) can be predicted.

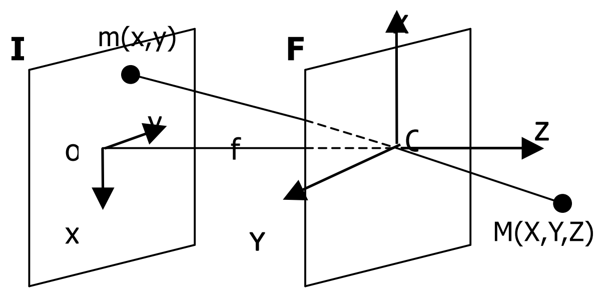

Image plane: I **Focus plane: F**

Fig 7. The relationship between picture coordinates and camera coordinates

A characteristic point flow computed from the relation between a robot and an object is shown in Fig 8. This figure is the flow by which the robot moved as the ideal. By comparing with the flow of an ideal state the flow obtained by image processing, the robot computes the position error.

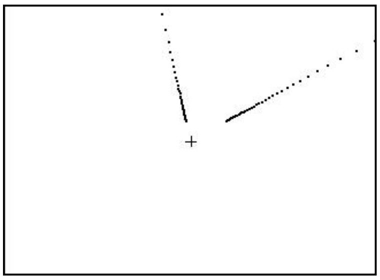

Fig 8. characteristic point flow

5.2 Consideration of error correction

By introducing this system, a robot's position information can be acquired and error compensation can be attained. However, this is during motion, when a robot is stabilized. As shown in Fig 4, gaining stability takes about 1 second. At this time, a robot's driving speed is 0.5 m/second. By the time it goes into a stable state, it has moved at least half a meter.

In areas such as a corridor, this system will have little difficulty. However, error detection is difficult if the robot is moving in a confined space where distances are comparatively short. Therefore, detected errors must be discovered very quickly.

6. Conclusions

When the autonomous drive personal robot moves, a problem arises because coordinates change with respect to objects in the environment. We have proposed an error correction system to solve this problem. This system uses a information on the motion distance acquired from a image data and the drive mechanism, and the system computes an error. However, when a robot's move distance is short, it cannot fully respond. A system to detect position errors immediately is needed.

We have studied the unstable action generated as a cause of the error at the time of initial movement of the robot. In the future, we will analyze the drive parameter at the time of the robot's initial movement and then build a system that can perform action stabilized by the robot.

References

[1]Funakubo, Process and recognition of the vision paturn, Keigakusyuppan, 1990.
[2]Shinoda, Self-driven robot on the grand, Journal of the Robotics Society of Japan, Vol. 18, No.7, pp.928-932. 2000

The Tenth International Symposium on Artificial Life and Robotics 2005(AROB 10th '05),
B-con Plaza, Beppu, Oita, Japan, February 4-6, 2005

Research about ZMP of biped walking robot

Kota Imamura, Masanori Sugisaka

Department of Electrical and Electronic Engineering
Oita University
700 Oaza Dannoharu, Oita, 870-1192, JAPAN
Tel: 097-554-7831
Fax: 097-554-7841
E-mail: s1132005@mail.cc.oita-u.ac.jp

Abstract

In this paper, ZMP (Zero Moment Point) of biped walking robot is explained. OpenHRP2 (AIST) is used for walking pattern simulation. The purpose of this research is to calculate the theoretical value and actual value of ZMP. Firstly, the reference ZMP of the robot is calculated from CoM (Center of Mass) and CoM position. Then, the actual ZMP of the robot is calculated from Force/Torque sensor value. Next, the reference ZMP is compared to the actual ZMP. Finally, the robot walking pattern behavior is controlled by restoring the actual value of ZMP to the theoretical value of ZMP.

1. Introduction

Recently, biped walking robots are widely known and concerned by mass media such as TV or magazines. People are interested in robots such as "ASIMO", "QRIO" and "PINO". Impressively, these robots are expected to be used for transportation device at complex environment such as steps. Therefore, biped walking robots are studied by many research institutions.

Two years ago, research of biped walking robot has been done for the first time in our laboratory. Then, in order to study biped walking robots, a robot composed of microcomputer and servo motors was developed. By assigning the command value of each joint or servo motors, "Static walking" of the biped robot was successfully done.

However, a lot of servo motors were broken because of overload during the experiment. In order to save the coot of servo motors, the robot walking pattern was verified using simulator.

In this research, ZMP concept is applied for "Dynamic walking", so that "Static walking" will be successfully done by the actual robot. For this purpose, the theoretical value and the actual value of ZMP is calculated. Then, the robot walking pattern behavior is controlled by restoring actual ZMP value to theory ZMP value.

2. Simulation environment

2.1 OpenHRP2

OpenHRP2 (AIST) is used for walking pattern simulation. OpenHRP2 is composed of "Dynamics server", "Controller server" and etc. These servers are distributed object system that used CORBA (Common Object Request Broker Architecture). Each server is mounted as CORBA object.

Computer specification is Windows2000 for OS and AMD Athlon™ Processor (1000.04-MHz) for CPU.

2.2 Robot model

Robot model is created by 3D modeling language called VRML (Virtual Reality Modeling Language). Robot model that has been used for walking pattern simulation in this research is shown by Fig.1. One leg has 6 DOFs (Degree of Freedom), and 4 steps forward pattern is used for walking pattern of this robot model. This simple robot model is used for walking pattern simulation, so calculating the ZMP value of the robot is focused in this research.

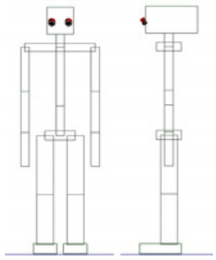

height	0.45[m]
weight	13[kg]
DOF	leg 6×2, arm 7×2, body 3 (total 29)
step	4[steps]

Fig.1 Robot model

3. Reference ZMP

3.1 ZMP simple model

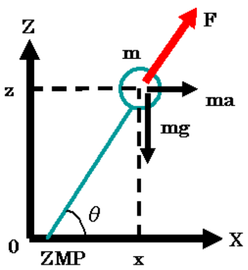

F: force effecting mass point from floor
g: gravity
a: mass point acceleration effecting to direction of resultant of F and g.

Fig.2 Inverted pendulum model on sagittal plane

Inverted pendulum model on sagittal plane is shown as ZMP simple model by Fig.2. Firstly, Eq.1 is obtained from dynamic equation of horizontal and vertical direction about mass point.

$$m\ddot{x} = f_x = |\mathbf{F}|\cos\theta$$
$$m\ddot{z} = f_z - mg = |\mathbf{F}|\sin\theta - mg \qquad (1)$$

Secondly, Eq.2 is given by ZMP definition that total momentum around ZMP is zero.

$$zf_x - (x - ZMP)f_z = 0 \qquad (2)$$

Finally, Eq.3 is derived from Eq.1 and Eq.2.

$$ZMP = \frac{m\{x(\ddot{z}+g)\} - z\ddot{x}\}}{m(\ddot{z}+g)} \qquad (3)$$

By changing x to y, Eq.3 can adapt to lateral plane.

3.2 ZMP robot model

Eq.4 is obtained by expanding Eq.3 to each link of robot.

$$x_{ZMP} = \frac{\sum_{i=1}^{n} m_i\{x_i(\ddot{z}_i + g) - z_i\ddot{x}_i\}}{\sum_{i=1}^{n} m_i(\ddot{z}_i + g)} \qquad (4)$$

where n is total number of piece of robot link. By replacing x with y, Eq.3 can adapt to lateral plane. It is shown as Fig.3 that the reference ZMP on sagittal plane is calculated by running the walking pattern simulation using Eq.4.

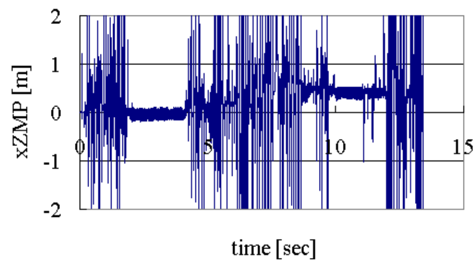

Fig.3 Reference ZMP on sagittal plane (used Eq.4)

It is shown as Fig.4 that the reference ZMP is widely oscillating in walking. It is cited as a factor that solutions are underspecified, so there are two variables (x, z). It is thought that optimization problem is solved. But, in this paper, it is decided that this problem is replaced with pseudo ZMP for simplicity. The following, pseudo ZMP is explained.

3.3 Pseudo ZMP

Eq.5 is given by representing gravity M of the whole robot in Eq.4.

$$x_{zmp} = \frac{M(g+\ddot{z})x - M\ddot{x}z}{M(g+\ddot{z})} \qquad (5)$$

At this moment, attention should be paid to z direction of gravity position of walking pattern. By assuming that z direction of gravity position stays constant, z and $\ddot{z}$ in Eq.5 can be simply transformed into

$z = h_{ref}(const)$ and $\ddot{z} = 0$ in Eq.6.

$$x_{zmp} = \frac{gx - h_{ref}\ddot{x}}{g} \tag{6}$$

By changing x to y, Eq.3 can adapt to lateral plane.

Simulation results using Eq.6 is shown by Fig.4.

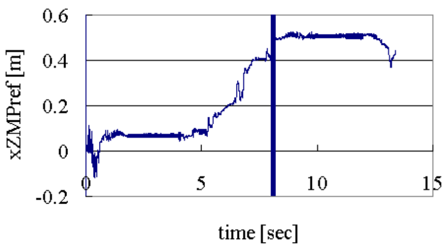

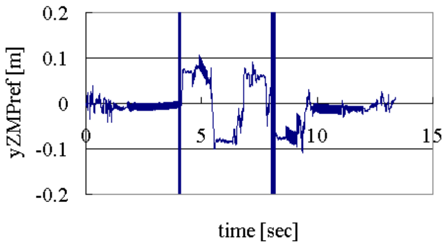

Fig.4 Pseudo ZMP using Eq.6

At x direction and y direction of ZMP, the results are displayed by Fig.4. It is taken that x direction ZMP moves to forward and y direction ZMP is shifting on supporting leg while the robot is walking. We understand that x and y ZMP are greatly amplified at about 4 and 8 seconds. From here, it is obtained that walking pattern of the robot does not go well and the robot movement on the floor taking extra time about 4 and 8 seconds. Therefore, $\ddot{x}$ of Eq.6 amplified widely by moving on the floor.

As described, theory value of ZMP of robot is calculated from gravity position and acceleration. This theory value of ZMP is called the reference ZMP.

4. Actual ZMP

In this topic, the actual ZMP is introduced. By A.Goswami, $ZMP = CoP$ (Center of Pressure) is verified in 1999. Therefore, ZMP is calculated by measuring CoP of sole. And so, it is thought that CoP, or ZMP, is measured from Force/Torque sensor value of sole of the robot.

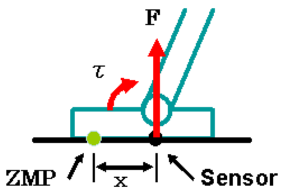

F: vertical component of floor reactive force at sensor position
τ : torque at sensor position
x: distance between sensor and ZMP

Fig.5 Foot model of robot on sagittal plane

Foot model of robot on sagittal plane is shown by Fig.4. Moment of force around ZMP is expressed by Eq.7.

$$Fx - \tau = 0 \tag{7}$$

Eq.7 is rearranged to Eq.8.

$$x = \frac{\tau}{F} \tag{8}$$

The actual ZMP is calculated from x in Eq.8 and sensor position information. By replacing x with y, Eq.8 is able to be used for lateral plane.

Simulation result using Eq.8 is shown by Fig.6.

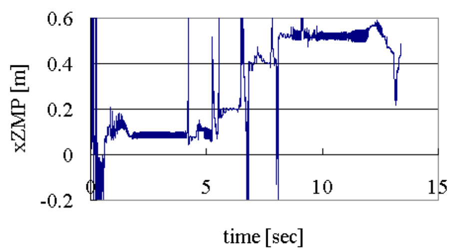

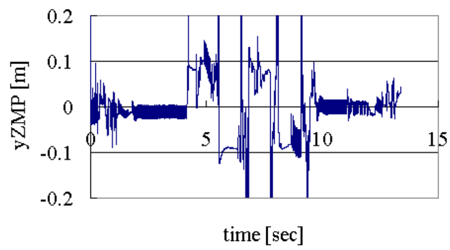

Fig.6 The actual ZMP using Eq.8 and sensor position information

The actual ZMP of x direction and y direction are shown as Fig.6. It is taken that x direction of ZMP moves to forward and y direction of ZMP is shifting on supporting leg while the robot is walking. We understand that x and y ZMP greatly amplified when supporting leg shifts on next leg. This is because F in Eq.8 becomes much lower to almost zero in changing supporting leg. Therefore, x in Eq.8 is made larger became F near to zero.

As described, measuring value of ZMP of the robot is calculated from CoP and sensor position information. This measuring value of ZMP is called the actual ZMP.

5. Comparing the reference ZMP with the actual ZMP

The reference ZMP calculated from Eq.6 is compared with actual ZMP calculated from Eq.8 for walking pattern simulation. Result of the comparison is shown by Fig.7.

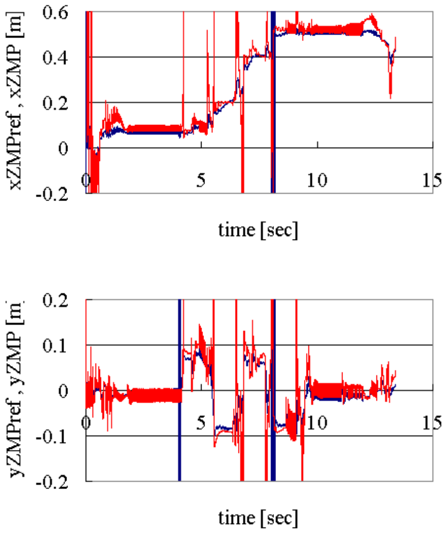

Fig.7 Comparing the reference ZMP with the actual ZMP

x direction and y direction are shown by Fig.7. It is understood that by comparing two graphs, two ZMPs follow the similar track. Comparing two ZMPs in detail, about x direction of ZMP, the actual ZMP when simulation starts and finishes, or in dumping and pumping hip, amplify in comparison with reference ZMP. This indication shows that the upper body of the robot is on the point of falling to back or front. At y direction of ZMP, it is also understood that the actual ZMP gets larger than reference ZMP at one leg supporting period. Also, this indication shows that the upper body of the robot leans to left or right.

6. Conclusion

In this paper, ZMP concept for "Dynamic walking" is observed. Firstly, the reference ZMP of the robot is calculated from CoM (Center of Mass) and CoM position. Next, the actual ZMP of the robot is calculated from Force/Torque sensor value. Finally, the reference ZMP is compared to the actual ZMP.

We understood that the reference ZMP and the actual ZMP used for walking pattern in this research have a slight difference in track. However, more stable walking pattern is obtained by bringing the actual ZMP close to the reference ZMP.

As for the future reference, it is thought that the actual ZMP is brought closer to the reference ZMP by using feed back control. For example, after actual ZMP is obtained around the reference ZMP by accelerating hip position according to error between the actual ZMP and the reference ZMP, walking pattern behavior of the robot is controlled by handling the reference ZMP. Finally, optimization problem should be overcome, too.

Reference

[1]H.Takeutchi (2001) "Real Time Optimal Control for Legged Robot" Transactions of JSCES, Paper No.20010001

[2]A.Masuyama, K.Mitobe and Y.Nasu (1999) "Ankle joint control for walking robots" The 184th Research convention SICE Tohoku 184-3

[3]F.Yamasaki (2003) "Sole sensor and Control" ROBO-ONE Technical Conference

[4]S.Kajita (2002) "ZMP and Walking Control" Journal of the Robotics Society of Japan Vol20 No.3

The Tenth International Symposium on Artificial Life and Robotics 2005(AROB 10th '05),
B-con Plaza, Beppu, Oita, Japan, February 4-6, 2005

Verification of trajectory generation of bipedal walking robot

Naoki Masuda, Masanori Sugisaka
Dept. of Electrical and Electronic Engineering, Oita University
700 Dannoharu Oita 870-1192 Japan.
Email:*msugi@cc.oita-u.ac.jp*

Abstract

A bipedal walking robot and a humanoid robot are developed in various research organizations in recent years, and research towards utilization is done. Under the environment which has irregular ground or various road surface, also the bipedal walking robot and human, working and living together, need to be studied, so that the bipedal walking robot will be able to respond to multiple conditions. By doing so, it was considered that generating the walking orbit which can respond to the walking movement on the irregular ground which is the purpose of this research have been achieved. In this paper, using a simulation, the walk orbit in leveling is generated and it verifies whether it can walk with the level of differences created virtually.

1. Introduction

A bipedal walking robot and a humanoid robot are developed in various research organizations in recent years. Currently, research organization is working toward the utilization of this technology and manage to attract public society. By studying and learning from biological model, in this case human, is the direction of the bipedal walking robot. You may say that the dynamic bipedal walking in reproducible leveling was realized at present although having to be regarded as an actual thing like the directions of bipedal walking robot or humanoid. However, the technical study of bipedal walking robot movement been conquered completely [1][2].

On the other hand under the environment which has irregular ground or various road surface, also the bipedal walking robot and human, working and living together, need to be studied, so that the bipedal walking robot will be able to respond to multiple conditions. There are various methods, [3][4] such as using the linear inverted pendulum mode which fixed ZMP, in orbital generation of the irregular ground, using moment as $N = 0$. However, in order to perform an irregular standpoint line, the orbit control of the center of gravity is indispensable first. And there are some which fix the height of the center of gravity and the height of the ground [5], and are generating the orbit by the research which is carrying out orbit control of the center of gravity. However, I fix the position and the ground of the center of gravity, and think that the walk in the irregular ground is not possible. Then, by paying attention to the center of gravity vibration by the velocity which is one of the fall reason, target velocity was set up and it is considered as controlling, advancing or translation velocity to converge on the target velocity. This is operating ZMP and controlling the center of gravity, and is transposing the problem which determines the orbit of the center of gravity to the problem which determines the orbit of ZMP.

By doing so, it was considered that generating the walking orbit which can respond to the walking movement on the irregular ground which is the purpose of this research have been achieved. In this paper, using a simulation, the walk orbit in leveling is generated and it verifies whether it can walk with the level of differences created virtually.

2. Generation of orbit

2.1 The equation of a strict model [5]

First, gravity and the anti-power of a floor act on a bipedal robot. The anti-power and the moment of a floor can be described using the position of ZMP (Zero Moment Point), the inertia power of the whole body, and the gravity which are defined on floor. Balance of the circumference of the X-axis and Y-axis on the basis of the center of gravity uses the next equation.

$$\begin{aligned} N_y &= m(x_{cg} - x_{ZMP})(\ddot{z}_{cg} + g) - m(z_{cg} - z_{gnd})\ddot{x}_{cg} \\ N_x &= -m(y_{cg} - y_{ZMP})(\ddot{z}_{cg} + g) + m(z_{cg} - z_{gnd})\ddot{y}_{cg} \end{aligned} \quad (1)$$

Here, $N := [N_x, N_y, N_z]^T$ is the moment which acts on the circumference of the center of gravity. And L is the angle quantity of motion of the circumference of the center of gravity. And $[x_{cg}, y_{cg}, z_{cg}]^T$ is a center of gravity position. And $[x_{ZMP}, y_{ZMP}, z_{gnd}]^T$ is in ZMP. m is the mass of the whole body. g is the size of gravity acceleration.

2.2 Assumption

Approximation is taken as assumption conditions is one and it is the moment N of the circumference of the center of gravity produced by change of a posture. The anticipation value $\tilde{N}(t)$ is calculated beforehand.

$$N \cong \tilde{N} \quad (2)$$

Since a moment is not correctly obtained until it determines actual movement, an error is included in an anticipation value. However, if the influence which it has on ZMP of the error is settled in the grade which does not jump out of a support leg, it is thought that the problem by approximation will be produced as a result.

The next equation will be obtained, if the above assumption is applied to the equation (1) of the model.

$$\begin{cases} \ddot{x}_{cg} = a(x_{cg} - x_{ZMP} - \dfrac{\tilde{N}_y}{mg}) \\ \ddot{y}_{cg} = a(y_{cg} - y_{ZMP} + \dfrac{\tilde{N}_x}{mg}) \end{cases} \tag{3}$$

The center of gravity generation is performed based on the equation (3) of an approximation model.

2.3 The formulization in question

The center of gravity orbit is a problem which attains the center of gravity position and center of gravity velocity of the specification with the appointed time, and is expressed with the next equation.

$$\begin{cases} \begin{bmatrix} x_{cg}(t_0+T) \\ \dot{x}_{cg}(t_0+T) \end{bmatrix} = \begin{bmatrix} \overline{x_{cg}} \\ \overline{\dot{x}_{cg}} \end{bmatrix} \\ \begin{bmatrix} y_{cg}(t_0+T) \\ \dot{y}_{cg}(t_0+T) \end{bmatrix} = \begin{bmatrix} \overline{y_{cg}} \\ \overline{\dot{y}_{cg}} \end{bmatrix} \end{cases} \tag{4}$$

Here, $t = t_0$ is the time specification of $t = t_0 + T$ at the present time. For specified center of gravity position $(\overline{x_{cg}}, \overline{y_{cg}})$ and the appointed center of gravity velocity by $(\overline{\dot{x}_{cg}}, \overline{\dot{y}_{cg}})$ above equation will become as shown below.

$$\begin{cases} \begin{bmatrix} \overline{x_{cg}} \\ \overline{\dot{x}_{cg}} \end{bmatrix} = e^{TA} \begin{bmatrix} x_{cg}(t_0) \\ \dot{x}_{cg}(t_0) \end{bmatrix} + \int_0^T a e^{(t-\tau)A} h_x(t_0+\tau)\,d\tau \\ \begin{bmatrix} \overline{y_{cg}} \\ \overline{\dot{y}_{cg}} \end{bmatrix} = e^{TA} \begin{bmatrix} y_{cg}(t_0) \\ \dot{y}_{cg}(t_0) \end{bmatrix} + \int_0^T a e^{(t-\tau)A} h_y(t_0+\tau)\,d\tau \end{cases} \tag{5}$$

Since a center of gravity position and ZMP have the relation of the equation(3), by ZMP operation,it shows that a center of gravity position is controllable. By applying ZMP, center of the gravity orbit can be obtained. However, the range which can operate ZMP with the behavior is limited inside a support leg.

3. Simulations

3.1 Orbit marking

In order to decide the position of a leg, the target orbit of the imagination body is considered. The position of a leg is arranged along this target orbit. A target orbit makes the starting point a position, velocity, a present angle, and present angular velocity. And in order to make it converge on the target speed and target angular velocity which were specified, it is made constant angular acceleration and constant acceleration. And an orbit which becomes uniform angular velocity and uniform velocity from the middle is made.

Moreover, the length of the grounding term one of the both legs and the length of the grounding term of both legs are decided beforehand. It asks for the time of the center of both the leg grounding term according to the schedule. And a landing position is decided near the point in the time on a target orbit.

3.2 Modeling

By aiming at the orbital generation, the simplified model is used. A front is the X-axis, a horizontal axis is the Y-axis and, as for this model, the vertical axis is the Z-axis. A hip joint is 3flexibility, a knee joint is 1flexibility and, as for flexibility, the leg joint has 2flexibility. (Fig.1)

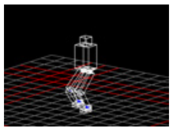

Fig.1 Bipedal walking robot model

3.3 An environmental setup of the irregular ground

An environmental setup of the irregular ground creates the level differences of height (0.1[m] and 0.05[m]) virtually as the first phase. Moreover, sidewall is made leveling.

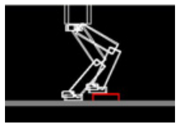

Fig.2 The irregular ground

3.4 Walking conditions of the model

The conditions of the model of the bipedal walking robot are shown below.

- Time in one step＝0.5[s]
- The rate of both legs grounding term in one step＝0.2[s]
- Maximum acceleration＝0.4[m/s^2]
- Maximum angle acceleration＝3.0[rad/s^2]
- Distance from the target orbit to the landing position of a leg ＝0.02[m]

4. Results

4.1 Walking pattern and Advancing translation velocity to target velocity, Velocity of center of gravity

Fig.3 is the walking pattern at the time of leveling. A closed example and Fig.5 show the displacement of center of gravity velocity to Fig.4 for the advancing translation velocity to target velocity.

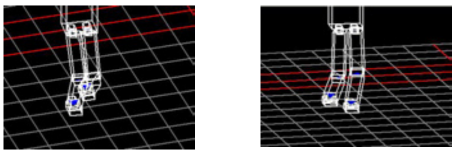

(a) Right leg grounding term (b) Left leg grounding term

Fig.3 Waking pattern (Height of ground = 0.0[m])

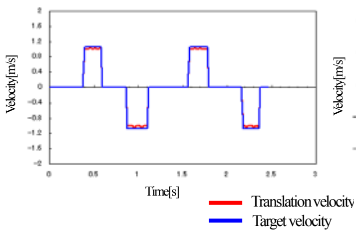

Fig.4 Advancing translation velocity to target velocity

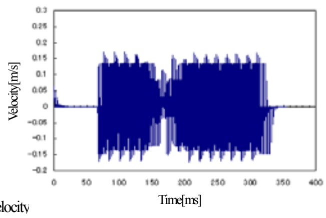

Fig.5 Velocity of center of gravity

The walk pattern was able to obtain the walk stabilized mostly. Although target velocity is not as expected, by referring to Fig.3, it turns out that acquaintance and uniform velocity are mostly maintained at target velocity. Although Fig.4 is a figure showing the velocity of the center of gravity, it turns out that it is walking maintaining a certain fixed center of gravity velocity. Therefore the stabilized walking pattern is studied.

In case the height of the ground goes up, which the level difference is 0.05[m] as shown in Fig.6. And Fig.8 show the displacement of center of gravity velocity to Fig.7 for the advancing translation velocity to target velocity.

(a) from front view (b) from side view

Fig.6 Form of a walk (Height of ground = 0.05[m])

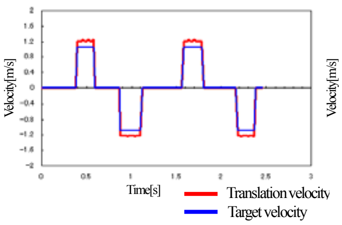

Fig.7 Advancing translation velocity to target velocity

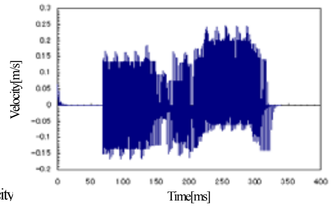

Fig.8 Velocity of center of gravity

Although the walk pattern was shaky, it was maintaining the walk orbit. Since the center of gravity movement was the range which a support leg can bear, the walk orbit which overcomes the level difference of 0.05[m] was generable. By referring to Fig.7, it turns out that advancing translation velocity is over a few to target velocity compared with the walk at the time of leveling. Although center of gravity velocity was carrying out the velocity rise at the moment of going up a level difference, the width is the width of the inside which can be walked and seldom affected the walk pattern. (Fig.8)

Next, walk form in case the height of the ground goes up the level difference which is 0.1[m] is shown in Fig.9. And Fig.11 show the displacement of center of gravity velocity to Fig.10 for the advancing translation velocity to target velocity.

(a) from front view (b) from width view

Fig.9 Form of a walk (Height of ground = 0.1[m])

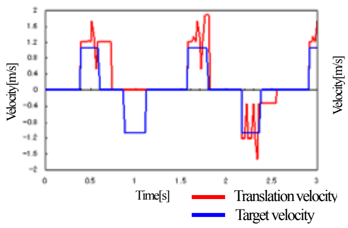

Fig.10 Advancing translation velocity to target velocity

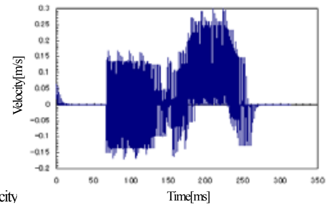

Fig.11 Velocity of center of gravity

For the walking pattern, the model collapse at the beginning, because putting the left leg on the difference level and carrying the right leg. Although it has balancing translation velocity to target velocity, it has balancing translation velocity clearly beyond target velocity. Moreover, center of gravity velocity has generated a double velocity, when rising a level difference as compared with the walk at the time of leveling. Therefore, I think that the rise of this velocity caused a fall. It is observed that this double velocity caused the model to fall.

4.2 Displacement of the center of gravity (Form by each road surface)

The displacement of the center of gravity position in each road surface form is shown in Fig.12.

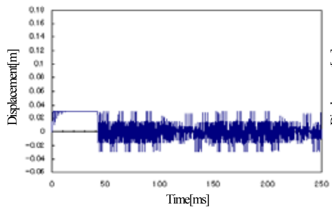

(a) Height of ground = 0.0[m]

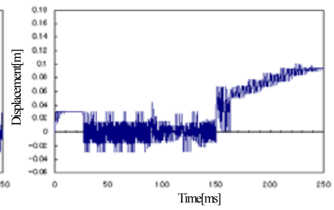

(b) Height of ground = 0.05[m]

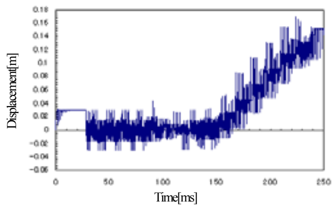

(c) Height of ground = 0.1[m]

Fig.12 Displacement of the center of gravity

The displacement of the center of gravity position in each road surface is compared. Since the displacement of an almost fixed center of gravity position is shown at the time of leveling, as walking pattern, it turns out that it is possible within the limits. Moreover, it is considered that this vibration occurred since the contact power of the sole and the floor in sidewall is vibrating. Next, for 0.05[m] and 0.1[m], when the center of gravity position rises at a level difference in both, the center of gravity position is changed completely. If by comparing these two levels, although change of a center of gravity position may be sharp at the moment of rising level difference at 0.05[m], after that, the change of a center of gravity position will not be much, and it turns out that there is none. However, while rising the level difference of 0.1[m], it can grasp that it is intense in center of gravity movement. Too, the rise of center of gravity velocity led to change of a center of gravity position. And it turns out that a result to reverse was brought.

4.3 Displacement of Moment

The displacement of moment in each road surface form is shown in Fig.13.

It turns out that the moment in the height 0[m] and 0.05[m] of the ground is maintaining fixed width mostly, and there is no influence of center of gravity portion. However, it has generated clearly, and by comparing the moment of the circumference of the center of gravity in 0.1 [m] with 0[m] and 0.05[m], 3 [Nm] it has slight a difference. It is the moment produced since this had advancing translation velocity clearly beyond target velocity, and since the influence which the error has on ZMP has jumped out of the support leg, I think that it is the cause of a fall. You have to control generating of this moment.

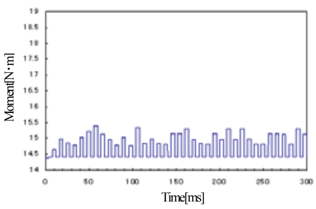

(a) Height of ground = 0.0[m]

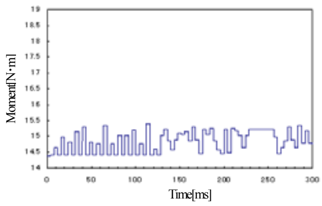

(b) Height of ground = 0.05[m]

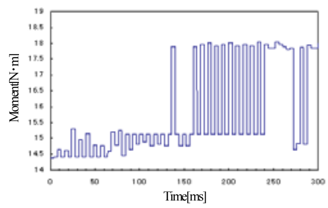

(c) Height of ground = 0.1[m]

Fig.13 Displacement of Moment

4.4 Displacement of Hip Angle

The displacement of the waist angle of Hip Angle in each road surface form is shown in Fig.14.

When the height of the ground is 0[m] as it understands, even if it sees a Fig.14, the difference of the maximum angle is 10[degrees], when it is 0.05[m], it is 20[degrees], and in the case of 0.1[m], it is 40[degrees]. The angle at the time of 0[m] and 0.05[m] is the displacement of the angle within the limits which can maintain a walk pattern. However, at the time of 0.1[m], since the displacement of a center of gravity position had become large as the displacement of the center of gravity position of the foregoing paragraph also showed, displacement of the angle of the waist was enlarged for it as a method of prevention. And it was going to do by force and is going to maintain the walk pattern at an angle of the waist. It is one of the causes of moment generating.

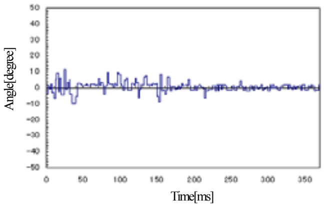

(a) Height of ground = 0.0[m]

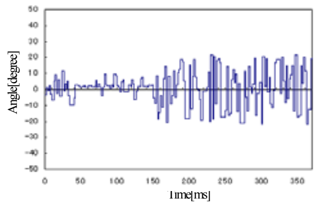

(b) Height of ground = 0.05[m]

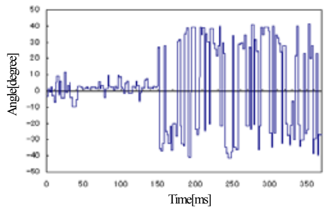

(c) Height of ground = 0.1[m]

Fig.14 Displacement of Hip Angle

5. Conclusions

From this research, it is observed when the height of the ground was 0 [m] and 0.05 [m], the orbit of the walk which follows a target orbit was able to be generated. However, since the moment of the circumference of the center of gravity occurred, 0.1 [m] brought a reverse result. In addition, since the contact power of a sole and a floor occurred, the burden of each joint supporting a robot became large, and a result which affects the vibration and the walk orbit in a center of gravity position was brought. From research observation, for the moment control produced by velocity rise, velocity control is performed and the moment of the circumference of the center of gravity is controlled. Also, you have to consider generation of the orbit which performs an interference check etc to the contact power of a sole and a floor.

Reference

[1]Inoue,H.,Tachi,et.al : "Overview of Humanoid Robotics Project of METI", Proc.Int.Symp.Robotics, pp.1478-1482, 2001.

[2]Nishiwaki,K.,Sugihara,T.,et.al : "Designand Development of Research Platform for Perception-Action Integration in Humanoid Robot:H6", Proc.Int.Conference on Intelligent Robots and Systems, pp1559-1564, 2000.

[3] Kajita, S. and Tani, K., : "Control of Dynamic Biped Locomotion Based on Realtime Sensing of the Ground Profile" , Journal of the Robotics Society of Japan, vol.14, No.7, pp.1062-1069, 1996. (in Japanese)

[4]Kajita,S., : "Real-time Dynamic Walking Control of a Biped Robot Using the Linear Inverted Pendulum Mode" ,Report of Mechanical Engineering Laboratory No.171,1996. (in Japanese)

[5]Shino,et.al : "Real-time orbital generation of a bipedal robot" , Tokyo institude of Techology project newmanoid,2001.(in Japanese)

Run control of the mobile robot using visual information

Masanori Sugisaka , Tetsuro Hashizume
Dept. of Electrical and Electronic Engineering,
Oita University
700 Dannoharu, Oita 870-1192, JAPAN
TEL +81-97-554-7841 FAX +81-97-554-7818
E-MAIL msugi@cc.oita-u.ac.jp , s1132061@mail.cc.oita-u.ac.jp

Abstract

This research aims at capturing a mobile robot the environment information of based on the picture obtained from the CCD camera carried in the mobile robot, and carrying out the stable autonomous run. This paper considers the technique of image processing with the CCD camera for an autonomous run, and the basic experiment of a run.

1.Intoroduction

In the recent years, the introduction of robot was bean considered in various fields. Various functions were bean required and the robot use was expanded. One of the functions requires environmental recognition and avoidance of an obstacle. In order to develop such robot, this laboratory, for some time, has mainly respond to the field of welfare and nursing. A mobile recognition robot has been researched and developed [1][2][3].

This research is aimed at capturing the surrounding each environment information of mobile robot based on the pictures obtained from the CCD camera carried in the mobile robot, and carrying out the stable autonomous run. This paper considers the technique of image processing with the CCD camera for an autonomous run, and the basic experiment of a run.

2. Experiment System

The robot which is being used in this research was manufactured by incorporated company DENKEN in 2000. The figure is shown in Fig.1. It consists of 2 drive 2 caster (2DC2W) systems. The mobile robot is equipped on the right and left with the driving wheel, auxiliary caster rings at the front and back, a driving wheel on either side rotates by DC motor. Equipped with the rotary encoder of resolution 80 (Pulse Per Resolution) beside the driving wheel, and counting the number of pulses, the right-and-left independence can be achieved and a wheel can be controlled. The difference in the rotation speed of a right-and-left driving wheel performs a steering function. The CCD camera (EVI-G20: Sony) is carried by the height of about 130 [mm] at 55 degrees of perpendicular directions at the head. The picture obtained from the camera is taken in by the memory on an image-processing board (FDM-PCI3: FOTORON).

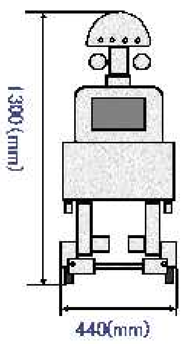

Fig. 1 View of The Mobile robot

3. Model of mobile robot

The mobile robot figure used in this research is shown in Fig.2.[2][4]。 The mobile robot is a system, which drives a driving wheel on either side by another actuator, and is an independent driving wheel type and PWS (Powered Wheel Steering).

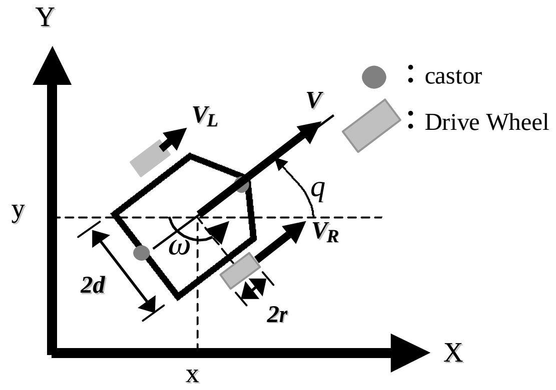

Fig. 2 Model of mobile robot

If the thickness of a wheel is disregarded and sets the distance from a body center to a wheel is d, and the radius of a wheel r, and the grounding speed of a wheel V_R, V_L, and a rotation angle of a wheel ϕ_R, ϕ_L, it can write.

$$f_{R,L} = 2 * PI * count_{R,L} / Encoder\_Slots \tag{1}$$

$$V_R = r\,\dot{f}_R \tag{2}$$

$$V_L = r\,\dot{f}_L \tag{3}$$

Moreover, if the actuator which drives a wheel regards it as the control input of this system as (V,ω) ($\dot{\phi}_R, \dot{\phi}_L$)that by which speed control is carried out, it can express a relation with generalization coordinates in the following forms.

$$\begin{pmatrix} \dot{x} \\ \dot{y} \\ \dot{q} \end{pmatrix} = \begin{pmatrix} \cos q & 0 \\ \sin q & 0 \\ 0 & 1 \end{pmatrix} \begin{pmatrix} V \\ w \end{pmatrix} = \frac{r}{2} \begin{pmatrix} \cos q & \cos q \\ \sin q & \sin q \\ \frac{1}{d} & -\frac{1}{d} \end{pmatrix} \begin{pmatrix} \dot{f}_R \\ \dot{f}_L \end{pmatrix} \tag{4}$$

Moreover, the equation below a equation (4) is obtained and this means the Nonholonomic restraint that a wheel does not sideslip [4].

$$\dot{x} \sin q - \dot{y} \cos q = 0 \tag{5}$$

4. Image Processing

The picture is taken in from a CCD camera, it is a picture expressed with a total of 24 bits of 8 bits each of RGB. It is very hard to treat RGB for correlation to be strong in each and acquire the feature from a picture. Then, in order to treat the feature from a picture independently as much as possible, the following equation performs LHS conversion of lightness, hue, and the saturation.

$$L = 0.299R + 0.587G + 0.144B \tag{6}$$

$$H = \tan^{-1}\left\{\frac{R-L}{B-L}\right\} = \tan\left\{\frac{0.701R - 0.587G - 0.144B}{-0.299R - 0.587G + 0.856B}\right\} \tag{7}$$

$$\begin{aligned} S &= \sqrt{(R-L)^2 + (B-L)^2} \\ &= \sqrt{(0.701R - 0.587G - 0.144B)^2 + (-0.299R - 0.587G + 0.856B)^2} \end{aligned} \tag{8}$$

Also in this, L picture serves as a numerical value mostly proportional to the strength of the brightness which man's eyes feel, and used only this picture also for improvement in the speed of processing.

Edge detection was performed in order to ask the luminosity picture like the point for an objective boundary and an objective outline. First, the difference the operator is using and it asked for the strength of the edge between each pixel. Next, if smaller than the value L with the difference of the strength of edge altogether and it was white and except it, the figure was displayed as Edge Image as black. It turns out that an objective boundary and an objective outline are called for to some extent.

(a) Original Image

(b) Monochrome Image

(c) Edge Image

Fig.3 Image Processing

5. Driving Experiment

In order to run at the rate of following a course linearly and a target, the experiment run on a mobile robot was conducted the following condition.

- Target number of rotations：8（pulse/0.1s）In order to carry out a wheel one revolution in 1 second
- Run a mobile robot only by Proportional control. This is because it is shown that number of rotations reaches to a target value only in Proportional control by research of the past mobile robot [3].

The number of rotations of an actual wheel is shown in Fig4.The equation of speed control of the wheel at this time has become like (11) equation, 0 has become the maximum and 255 has become the minimum. Moreover, the value to which applied the deviation by (9) equation and which applied the proportionality parameter to the deviation by (10) equation is expressed as an amount of operations.

$$\begin{aligned} er &= r\_set - rightcount \\ el &= l\_set - leftcount \end{aligned} \tag{9}$$

$$\begin{aligned} r\_ope &= r\_ope + r\_K_p \times er \\ l\_ope &= l\_ope + l\_K_p \times el \end{aligned} \tag{10}$$

$$\begin{aligned} rightspeed &= 235 - 12.3 \times r\_ope \\ leftspeed &= 235 - 12.3 \times l\_ope \end{aligned} \tag{11}$$

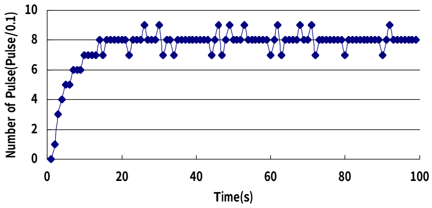

Fig. 4 Right Wheel Rotation Number

Although the value of target number of rotations was mostly detectable, it has checked carrying out amplitude slightly. Therefore, it is necessary to examine the optimal parameter using PI, PID control, and still newer control.

6. Obstacle Avoidance Experiment

The obstacle avoidance experiment was actually conducted in the environment, which is said to the method of the forward left as the 1st obstacle, and is said to the method of the forward right as the 2nd obstacle. At this time, target speed in case there is no obstacle was set to 15.7 [cm/s].

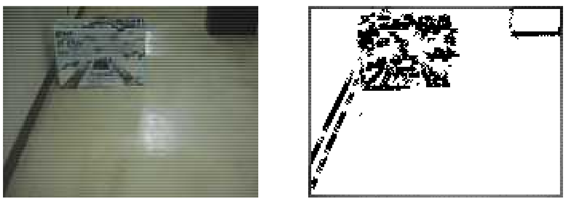

(a)Original Image **(b)Edge Image**

Fig.5 Obstacle Image

Giving imagination repulsive potential between the edge portion of a picture, and a robot's center performs the obstacle avoidance.

Since the picture is using only the left-hand side of the camera carried in the robot, it turns out that the center of a picture and a robot's center have shifted. When the size of a picture serves as width 160 [pixel] and length 120 [pixel], a horizontal axis is set to i and a vertical axis is set to j by making the upper left into the starting point, a robot's center will be located in the position which is i= 93 pixels.

The equation, which gave repulsive potential so that it might become so large that a robot's center and edge portion are near, is shown in (12). At this time repulsive potential in i=93-160[pixel] is made into Uo_r and repulsive potential in i=1-93[pixel] is made into Uo_l.

$$\begin{aligned} Uo\_r &= Uo\_r + 1/\sqrt{(93-i)^2 + 0.5j^2} \\ Uo\_l &= Uo\_l + 1/\sqrt{(93-i)^2 + 0.5j^2} \end{aligned} \tag{12}$$

Since an actual distance in the portion of the bottom of a picture is 240 [cm] at this time, an actual distance in the portions of 126 [cm] and the top is rectifying the horizontal axis using (13) and (14) equation.

$$calibration = 1 + 0.0075 * (120 - j) \tag{13}$$

$$\begin{aligned} &if \quad i > 80 \\ &\quad new\_i = 80 + (i - 80) * calibration \\ &if \quad i < 80 \\ &\quad new\_i = 80 - (80 - i) * calibration \end{aligned} \tag{14}$$

When Uo_r is larger than Uo_l and an obstacle exists in right-hand side, load is given to left_speed, and the left is revolved. Conversely, when Uo_l is larger than Uo_r and an obstacle exists in left-hand side, load is given to right_speed, and the left is revolved. The equation at this time is shown in (16).

$$\begin{aligned} &if \quad Uo\_r < Uo\_l \quad Uo = Uo\_l - Uo\_r \\ &if \quad Uo\_l < Uo\_r \quad Uo = Uo\_r - Uo\_l \end{aligned} \tag{15}$$

$$\begin{aligned} rightspeed &= 235 - 12.3 \times r\_ope + kUo \\ leftspeed &= 235 - 12.3 \times l\_ope + kUo \end{aligned} \tag{16}$$

Thus, change of the number of counts of the encoder when carrying out speed control has become like Fig.6. In about 8 - 13 seconds, it turns out that the left number of counts is larger than the right number of counts, it circled on the right, and the 1st obstacle is avoided. Next, it turns out that the right number of counts became larger than the left number of counts in about 18 - 22 seconds, it circled on the left, and the 2nd obstacle is avoided. Since an obstacle does not exist in a screen, by 4 [pulse / 0.1s], it is stabilized after 23 second and it is carrying out the going-straight run.

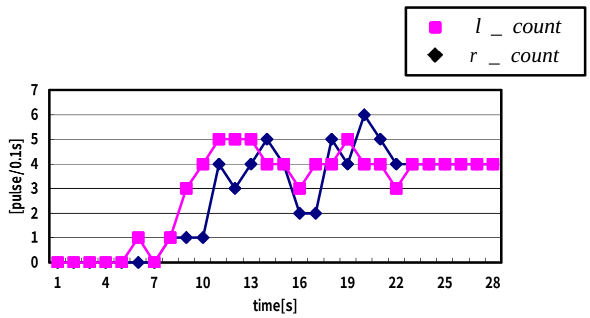

Fig.6 Wheel Rotation Number

7. Conclusions

Imagination repulsive potential was given to the speed of a wheel using the edge information on the picture obtained from the CCD camera, and carrying out speed change performed the obstacle avoidance run on a smooth orbit.

As a problem, after avoiding an obstacle, it will go straight on with an angle as it is. Imagination repulsive potential will receive influence not only in distance and a size with an obstacle but in the pattern and.

I decide a target point from now on, and think that the run stabilized by taking in not only imagination repulsive potential, but also imagination attraction can be performed.

References

[1]Syuiti Otsu, Masanori Sugisaka : Research on the environmental recognition in a mobile robot, Oita University Graduate School Master Paper(2003)

[2]Syohei Kuriyama , Masanori Sugisaka : Development of the mobile robot run system using dead reckoning and vision information, Oita University Graduate School Master Paper(2003)

[3]Toshio Maeyama , Masanori Sugisaka : The obstacle avoidance run in the mobile robot using the CCD camera, Oita University Graduate School Master Paper(2002)

[4]Tsutomu Mita : A guide to nonlinear control - Be lacking driving robot's skill control theory , Syokodo , pp61-63(2000)

[5]Yoshihisa Hiyama , Kenji Murao , Yoshio Yamamoto : Flexible collision avoidance maneuver of wheeled mobile robots , Japan Society of Mechanical Engineers [No.03-4] Robotics and Mechatronics Division lecture meeting collected papers(2003)

The Tenth International Symposium on Artificial Life and Robotics 2005(AROB 10th '05),
B-con Plaza, Beppu, Oita, Japan, February 4-6, 2005

Digital RAC for Underwater Vehicle-Manipulator Systems Considering Singular Configuration

Shinichi Sagara Masakazu Tamura Takashi Yatoh Kenzo Shibuya
Department of Control Engineering, Kyushu Institute of Technology
Tobata, Kitakyushu 804-8550, Japan
E-mail: sagara@cntl.kyutech.ac.jp

Abstract

We have proposed continuous-time and discrete-time resolved acceleration control methods for underwater vehicle-manipulator systems and the effectiveness of the control methods have been shown by experiments. In this paper, we propose a digital control method considering singular configuration of manipulator. Experimental result shows the effectiveness of the proposed method.

1 Introduction

Underwater robots, especially Underwater Vehicle-Manipulator Systems (UVMS), are expected to make important roles in ocean exploration. Many studies about dynamics and control of UVMS have been reported [1–3], however the experimental studies are only a few.

We have proposed continuous-time and discrete-time Resolved Acceleration Control (RAC) methods for UVMS [4–6], and the effectiveness of the RAC methods are demonstrated by using a floating underwater robot with vertical planar 2-link manipulator shown in Fig. 1. There is no discrete-time control method for UVMS except our proposed method. The performances of both control methods are similar, however position and velocity feedback gains of the discrete version cannot set separately. So we have proposed a new discrete-time RAC method whose feedback gains can set individually [7].

Here, in the case of singular configuration of manipulators the control input cannot be generally calculated. So, in this paper, we propose a discrete-time RAC method considering singular configuration of manipulator. To keep away from singular configuration, desired position of the vehicle is modified based on the determinant of the manipulator's Jacobian matrix. The effectiveness of the proposed method is shown by experiment.

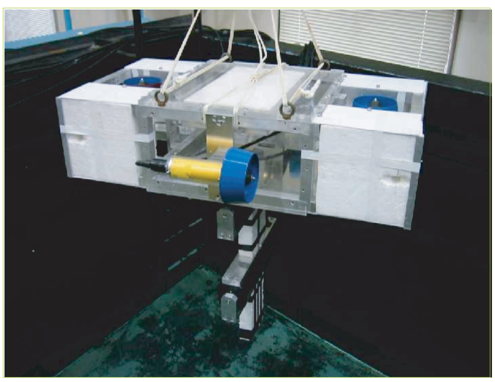

Fig. 1 Floating 2-link underwater robot

2 Modeling [4]

The underwater robot model used in this paper is shown in Fig. 2. It has a robot base (vehicle) and

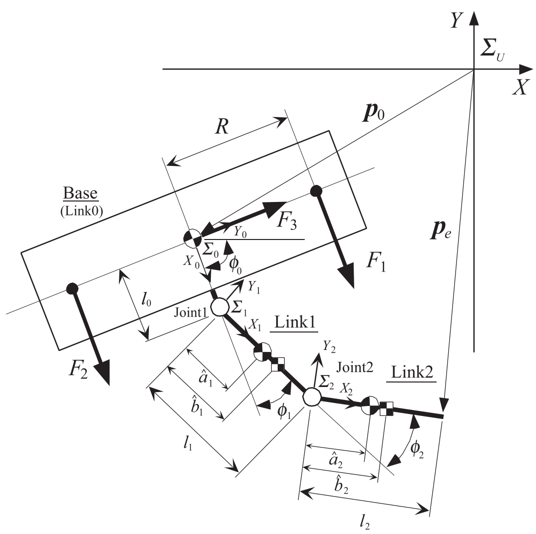

Fig. 2 2-link underwater robot model

2-DOF manipulator that can move in a vertical plane. Thrusters are mounted on the base to provide propulsion for position and attitude control of the base. Symbols used in Fig. 2 as follows:

- Σ_U : inertial coordinate frame
- Σ_i : ith link coordinate frame ($i = 0,\ 1,\ 2$; link 0 means base)
- l_i : length of link i
- ϕ_i : relative joint angle
- $\boldsymbol{p}_0$: position vector of origin of Σ_0 with respect to Σ_U
- $\boldsymbol{p}_e$: position vector of end-tip of manipulator with respect to Σ_U
- $\hat{\boldsymbol{a}}_i$: position vector from joint i to center of gravity of link i with respect to Σ_i
- $\hat{\boldsymbol{b}}_i$: position vector from joint i to center of buoyancy of link i with respect to Σ_i
- F_j : thruster force ($j = 1,\ 2,\ 3$)
- R : length form origin of Σ_0 to thruster

First, from Fig. 2 a time derivative of $\boldsymbol{p}_e$ is

$$\dot{\boldsymbol{p}}_e = \boldsymbol{A}\dot{\boldsymbol{x}}_0 + \boldsymbol{B}\dot{\boldsymbol{\phi}} \tag{1}$$

where $\boldsymbol{x}_0 = [\boldsymbol{p}_0^T,\ \phi_0]^T$ and $\boldsymbol{\phi} = [\phi_1,\ \phi_2]^T$, $\boldsymbol{A} \in R^{2\times 3}$ and $\boldsymbol{B} \in R^{2\times 2}$ are matrices consisting of attitude angle of base and joint angles.

Next, let $\boldsymbol{\eta}$ and $\boldsymbol{\mu}$ be a linear and an angular momentum of the robot including hydrodynamic added mass tensor $\boldsymbol{M}_{a_i}$ and added inertia tensor $\boldsymbol{I}_{a_i}$ of link i. Then

$$\boldsymbol{\eta} = [\eta_1,\ \eta_2,\ 0]^T = \sum_{i=0}^{2} \boldsymbol{N}_i, \tag{2}$$

$$\boldsymbol{\mu} = [0,\ 0,\ \mu_3]^T = \sum_{i=0}^{2} (\boldsymbol{I}_i + \boldsymbol{I}_{a_i})\boldsymbol{\omega}_i + \hat{\boldsymbol{x}}_i \times \boldsymbol{N}_i \tag{3}$$

where $\boldsymbol{N}_i = {}^U\boldsymbol{R}_i(m_i\boldsymbol{E} + \boldsymbol{M}_{a_i})\tilde{\boldsymbol{a}}_i$ and m_i is the mass of link i, ${}^U\boldsymbol{R}_i$ is the coordinate transformation matrix from Σ_i to Σ_U, $\boldsymbol{I}_i$ is the inertia tensor of link i, $\boldsymbol{E}$ is the unit matrix, $\tilde{\boldsymbol{a}}_i = \boldsymbol{v}_i + \boldsymbol{\omega}_i \times \hat{\boldsymbol{a}}_i$, $\boldsymbol{v}_i$ is the velocity vector of link i with respect to Σ_i, $\boldsymbol{\omega}_i = [0,\ 0,\ \dot{\phi}_i]^T$.

From Eqs. (1)-(3) the following equation can be obtained:

$$\boldsymbol{s} = [\eta_1,\ \eta_2,\ \mu_3]^T = \boldsymbol{C}\dot{\boldsymbol{x}}_0 + \boldsymbol{D}\dot{\boldsymbol{\phi}} \tag{4}$$

where $\boldsymbol{C} \in R^{3\times 3}$ and $\boldsymbol{D} \in R^{3\times 2}$ are matrices including the added mass $\boldsymbol{M}_{a_i}$ and the added inertia $\boldsymbol{I}_{a_i}$.

In the meanwhile, the drag force and moment of joint i can be generally represented as follows [8, 9]:

$$\boldsymbol{f}_{d_i} = \frac{\rho}{2} C_{D_i} D_i \int_0^{l_i} ||\boldsymbol{w}_i||\boldsymbol{w}_i d\hat{\boldsymbol{x}}_i, \tag{5}$$

$$t_{d_i} = \frac{\rho}{2} C_{D_i} D_i \int_0^{l_i} \hat{\boldsymbol{x}}_i ||\boldsymbol{w}_i||\boldsymbol{w}_i d\hat{\boldsymbol{x}}_i \tag{6}$$

where $\boldsymbol{w}_i = \boldsymbol{v}_i + \boldsymbol{\omega}_i \times \hat{\boldsymbol{x}}_i$, and ρ is the fluid density, C_{D_i} is the drag coefficient, D_i is the width of link i.

Furthermore, the gravitational and buoyant forces acting link i are described as follows:

$$\boldsymbol{f}_{g_i} = ({}^U\boldsymbol{R}_i)^T(\rho V_i - m_i)\boldsymbol{g}, \tag{7}$$

$$\boldsymbol{t}_{g_i} = ({}^U\boldsymbol{R}_i)^T(\hat{\boldsymbol{b}}_i \times \rho V_i \boldsymbol{g} - \hat{\boldsymbol{a}}_i \times m_i \boldsymbol{g}) \tag{8}$$

where V_i is the volume of link i and $\boldsymbol{g}$ is the gravitational acceleration vector.

3 Control method

In this section, we propose a control method of UVMS considering singular configuration of manipulator.

3.1 Digital RAC [7]

Differentiating Eqs. (1) and (4) with respect to time, the following equation can be obtained:

$$\boldsymbol{W}(t)\boldsymbol{\alpha}(t) = \boldsymbol{\beta}(t) + \boldsymbol{f}(t) - \dot{\boldsymbol{W}}(t)\boldsymbol{v}(t) \tag{9}$$

where

$$\boldsymbol{W} = \begin{bmatrix} \boldsymbol{C}+\boldsymbol{E} & \boldsymbol{D} \\ \boldsymbol{A} & \boldsymbol{B} \end{bmatrix}, \quad \boldsymbol{\alpha} = \begin{bmatrix} \ddot{\boldsymbol{x}}_0 \\ \ddot{\boldsymbol{\phi}} \end{bmatrix},$$

$$\boldsymbol{\beta} = \begin{bmatrix} \ddot{\boldsymbol{x}}_0 \\ \ddot{\boldsymbol{p}}_e \end{bmatrix}, \quad \boldsymbol{f} = \begin{bmatrix} \dot{\boldsymbol{s}} \\ \boldsymbol{0} \end{bmatrix}, \quad \boldsymbol{v} = \begin{bmatrix} \dot{\boldsymbol{x}}_0 \\ \dot{\boldsymbol{\phi}} \end{bmatrix}$$

and $\dot{\boldsymbol{s}}$ is the external force including hydrodynamic force and thrust of the thruster which act on the robot.

Discretizing Eq. (9) by a sampling period T, and applying $\boldsymbol{\beta}(k)$ and $\dot{\boldsymbol{W}}(k)$ to the backward Euler approximation, we have

$$\begin{aligned} \boldsymbol{W}(k)\boldsymbol{\alpha}(k-1) = \frac{1}{T}[&\boldsymbol{\nu}(k) - \boldsymbol{\nu}(k-1) + T\boldsymbol{f}(k) \\ &- \{\boldsymbol{W}(k) - \boldsymbol{W}(k-1)\}\boldsymbol{v}(k)] \end{aligned} \tag{10}$$

where $\boldsymbol{\nu} = \left[\dot{\boldsymbol{x}}_0^T,\ \dot{\boldsymbol{p}}_e^T\right]^T$. Note that computational time delay is introduced to Eq. (10) and the discrete time kT is abbreviated to k.

For Eq. (10) the desired acceleration is defined as

$$\begin{aligned} \boldsymbol{\alpha}_d(k) = \frac{1}{T}\boldsymbol{W}^{-1}(k)\,[&\boldsymbol{\nu}_d(k+1) - \boldsymbol{\nu}_d(k) \\ &+ \boldsymbol{A}\boldsymbol{e}_\nu(k) + T\boldsymbol{f}(k)] \end{aligned} \tag{11}$$

where

$$\boldsymbol{e}_\nu(k) = \boldsymbol{\nu}_d(k) - \boldsymbol{\nu}(k) \tag{12}$$

and $\boldsymbol{\nu}_d(k)$ is the desired value of $\boldsymbol{\nu}(k)$, $\boldsymbol{\Lambda}$=diag$\{\lambda_i\}$ $(i = 1, \cdots, 5)$ is the velocity feedback gain matrix.

From Eqs. (10) and (11) we have

$$\begin{aligned} T\boldsymbol{W}(k)\boldsymbol{e}_\alpha(k-1) &= \boldsymbol{e}_\nu(k) - \boldsymbol{e}_\nu(k-1) + \boldsymbol{\Lambda}\boldsymbol{e}_\nu(k) \\ &- T\{\boldsymbol{f}(k) - \boldsymbol{f}(k-1)\} \\ &+ \{\boldsymbol{W}(k) - \boldsymbol{W}(k-1)\}\boldsymbol{v}(k) \end{aligned} \tag{13}$$

where $\boldsymbol{e}_\alpha(k) = \boldsymbol{\alpha}_d(k) - \boldsymbol{\alpha}(k)$. Assuming $\boldsymbol{W}(k) \approx \boldsymbol{W}(k-1)$ and $\boldsymbol{f}(k) \approx \boldsymbol{f}(k-1)$ for one sampling period, Eq. (13) can be rewritten as follows:

$$T\boldsymbol{W}(k+1)\boldsymbol{e}_\alpha(k) = \{(q-1)\boldsymbol{E} + \boldsymbol{\Lambda}\}\, \boldsymbol{e}_\nu(k) \tag{14}$$

where q is the forward sift operator. From Eq. (14), if λ_i is selected to satisfy $0< \lambda_i <1$, the convergence of $\boldsymbol{e}_\alpha(k)$ to zero as k tends to infinity and all elements of $\boldsymbol{W}(k)$ are bounded, $\boldsymbol{e}_\nu(k)\to\boldsymbol{0}$ $(k\to\infty)$ can be ensured.

Furthermore, the desired velocity is defined as

$$\boldsymbol{\nu}_d(k) = \frac{1}{T}\{\boldsymbol{p}_d(k) - \boldsymbol{p}_d(k-1) + \boldsymbol{\Gamma}\boldsymbol{e}_p(k-1)\} \tag{15}$$

where $\boldsymbol{e}_p(k) = \boldsymbol{p}_d(k) - \boldsymbol{p}(k)$ and $\boldsymbol{p}(k)=[\boldsymbol{x}_0^T(k), \boldsymbol{p}_e^T(k)]^T$, $\boldsymbol{p}_d(k)$ is the desired value of $\boldsymbol{p}(k)$, $\boldsymbol{\Gamma}$=diag$\{\gamma_i\}$ $(i=1, \cdots, 5)$ is the position feedback gain matrix.

From Eq. (12) and (15) the following equation can be obtained:

$$T\boldsymbol{e}_\nu(k) = \left\{\boldsymbol{E} - (\boldsymbol{E} - \boldsymbol{\Gamma})\, q^{-1}\right\} \boldsymbol{e}_p(k) \tag{16}$$

where $\boldsymbol{\nu}(k)$ is applied to the backward Euler approximation. From Eq. (16), if γ_i is selected to satisfy $0< \gamma_i <1$ and the convergence of $\boldsymbol{e}_\nu(k)$ to zero as k tends to infinity, $\boldsymbol{e}_p(k)\to\boldsymbol{0}$ $(k\to\infty)$ can be ensured.

3.2 Avoidance of singular configuration

In many works of UVMS it is considered that the vehicle is keeping the initial state during manipulation. Then, to keep away from singular configuration of manipulator, the desired value of vehicle is modified by using the determinant of Jacobian matrix $J(k)$=det$\boldsymbol{J}(k)$ of manipulator.

The desired linear acceleration of vehicle $\ddot{\boldsymbol{p}}_{0_d} = [\ddot{p}_{0x_d}, \ddot{p}_{0y_d}]^T$ is defined as

$$\ddot{p}_{0*_d} = \begin{cases} \dot{p}_{e*_d}^2/|\dot{p}_{e*_d}| & (k_1 \le k < k_1 + n) \\ 0 & (\text{otherwise}) \\ -\dot{p}_{e*_d}^2/|\dot{p}_{e*_d}| & (k_2 \le k < k_2 + n) \end{cases} \tag{17}$$

where $*$ denotes x or y, and $\dot{p}_{e*_d}$ is the desired value of end-tip of manipulator, k_1T and k_2T are the time at the time when $|J(k)|$ becomes less and greater than the threshold J_s respectively, nT is the acceleration time.

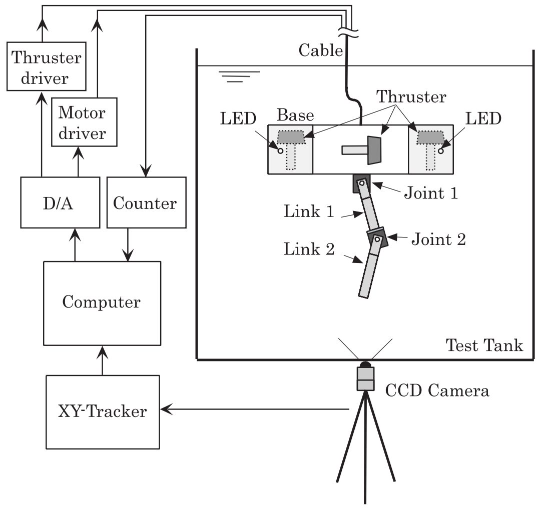

Fig. 3 Configuration of underwater robot system

Table 1 Physical parameters of underwater robot

	Base	Link 1	Link 2
Mass [kg]	26.04	4.25	1.23
Moment of inertia [kg m^2]	1.33	0.19	0.012
Link length (x axis) [m]	0.2	0.25	0.25
Link length (y axis) [m]	0.81	0.04	0.04
Link width [m]	0.42	0.12	0.12
Added mass(x) [kg]	72.7	1.31	0.1
Added mass(y) [kg]	6.28	3.57	2.83
Added moment of inertia [kg m^2]	1.05	0.11	0.06
Drag coefficient(x)	1.2	0	0
Drag coefficient(y)	1.2	1.2	1.2

4 Experiment

In this section, to verify the effectiveness of the proposed control method, the experiment is done.

Fig. 3 shows a configuration of experimental system. Physical parameters of the underwater robot are shown in Table 1. The details of the system, tne dynamic equation of robot and thruster characteristics are shown in [4].

The experiment was carried out under the following condition. The desired end-tip position was set up along a straight path from the initial position to the target. On the other hand, the basic desired position and attitude of vehicle were set up the initial values, and the threshold of the determinant of Jacobian matrix was $J_s = 0.45$. The sampling period was T=1/60[s] and the feedback gains were $\boldsymbol{\Lambda}$ = diag$\{0.6,\ 0.6,\ 0.25,\ 0.25,\ 0.25\}$ and $\boldsymbol{\Gamma}$ =

diag{0.6, 0.6, 0.2, 0.25, 0.25}. Furthermore, the initial relative angles of the robot were $\phi_0 = -\pi/2$[rad], $\phi_1 = \pi/3$[rad] and $\phi_2 = -5\pi/18$[rad].

The typical experimental result is shown in Fig. 4. From Fig. 4 it can be seen that the end-tip of manipulator and base follow the reference trajectories in spite of the influence of the hydrodynamic forces and the tracking errors are very small. The experimental result shows that the control performance can be improved by using the proposed method.

5 Conclusion

In this paper, a digital RAC system for UVMS was proposed. The experimental result showed the effectiveness of the proposed method.

References

[1] T. W. McLain *et al.*, "Experiments in the Coordinated Control of an Underwater Arm/Vehicle System", *Autonomous Robots 3*, Kluwer Academic Publishers, pp. 213 – 232, 1996.

[2] G. Antonelli *et al.*, "Tracking Control for Underwater Vehicle-Manipulator Systems with Velocity Estimation", *IEEE J. Oceanic Eng.*, Vol. 25, No. 3, pp. 399 – 413, 2000.

[3] N. Sarkar and T. K. Podder, "Coordinated Montion Planning and Control of Autonomous Underwater Vehicle-Manipulator Systems Subject to Drag Optimization", *IEEE J. Oceanic Eng.*, Vol. 26, No. 2, pp. 228 – 239, 2001.

[4] S. Yamada and S. Sagara, "Resolved Motion Rate Control of an Underwater Robot with Vertical Planar 2-Link Manipulator", *Proc. of AROB 7th*, pp. 230 – 233, 2002.

[5] S. Sagara, "Digital Control of an Underwater Robot with vertical Planar 2-Link Manipulator", *Proc. of AROB 8th*, pp. 524 – 527, 2003.

[6] S. Sagara, K. Shibuya and M. Tamura, "Experiment of Digital RAC for an Underwater Robot with vertical Planar 2-Link Manipulator", *Proc. of AROB 9th*, pp. 337 – 340, 2004.

[7] S. Sagara, K. Shibuya and M. Tamura, "Digital Resolved Acceleration Control of Underwater Vehicle-Manipulator Systems", *Proc. Int. Symp. Bio-inspired Systems*, Part V: Robotics and Motion Control, pp. 21 – 26, 2004.

[8] B. Lévesque and M. J. Richard, "Dynamic Analysis of a Manipulator in a Fluid Environment", *Int. J. Robot. Res.*, Vol. 13, No. 3, pp. 221 – 231, 1994.

[9] S. McMillan *et al.*, "Efficient Dynamic Simulation of an Underwater Vehicle with a Robotic Manipulator", *IEEE Trans. Syst., Man, Cybern.*, Vol. 25, No. 8, pp. 1194 – 1206, 1995.

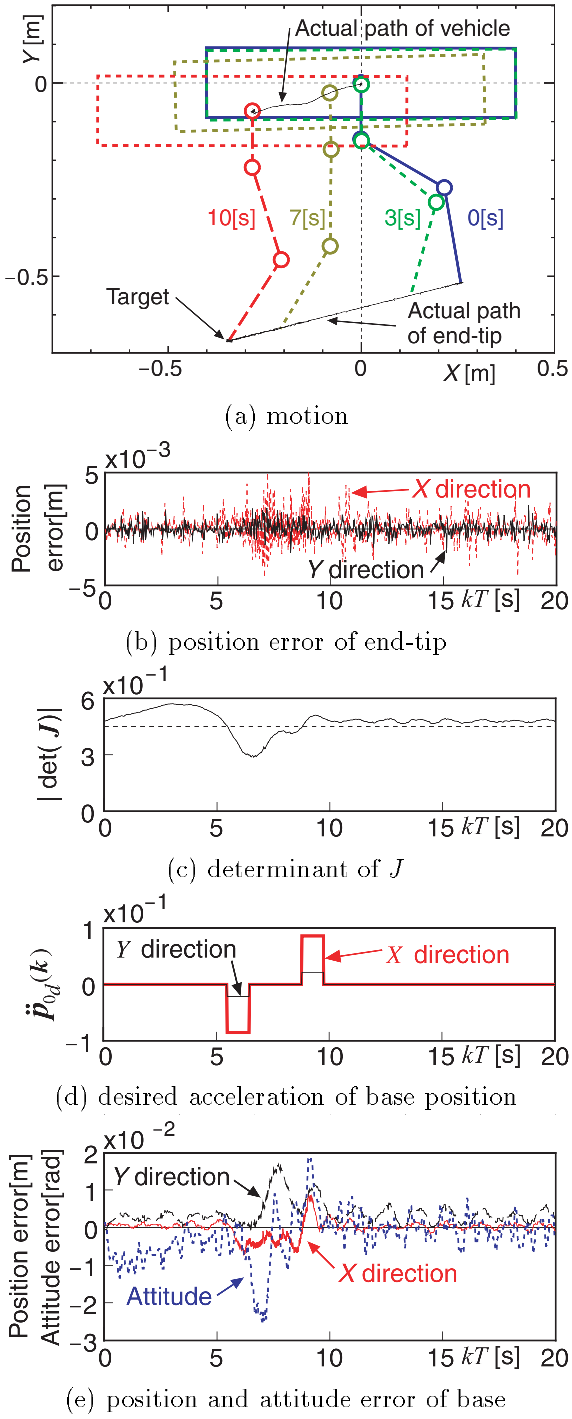

Fig. 4 Experimental result

The Tenth International Symposium on Artificial Life and Robotics 2005(AROB 10th '05),
B-con Plaza, Beppu, Oita, Japan, February 4-6, 2005

Modeling of Pneumatic Artificial Muscle Actuator

Huailin Zhao[*,**,***](zhao_huailin@yahoo.com) Masanori Sugisaka[*] Datai Yu[**]
[*] Department of Electrical and Electronic Engineering, Oita University
[**] School of Information Engineering, University of Science and Technology Beijing
[***] Zhengzhou University, China

Abstract: This paper mainly developed the static model of pneumatic artificial muscles in theoretically. From its physical model, the geometrical model was turned up, and the mathematical model was established. It discussed the contraction ratio, formulated the force output as a function of gas pressure and the structure parameters, and analyzed the stiffness.

Key word: Pneumatic artificial muscles, static model, contraction ratio, force output, stiffness

1. Introduction

In recent years, a new kind of artificial muscles-pneumatic artificial muscle (PAM) has been developed [1][2]. It consists of a rubber tube covered in tough braided fibre mesh, which shortens in length when inflated with compressed gas. Sometimes it is also called as air muscles, because usually the used gas is air. It can generate enough force and maintain proper compliance at the same time-a little like real muscles [3][4]. So, it can be used as the actuator in robots, so that the actuator will inherently behave a little like animals. Sometimes it is just called as pneumatic artificial muscle actuator. Fig. 1 is a photo of a pneumatic artificial muscle actuator made by Robot Shadow Company [4]. Fig. 2 is its enlarged part view.

Based on the possible applications in robots, it is necessary to establish its models. This paper is going to set up its static mathematics model.

Fig. 1 Pneumatic artificial muscle

Fig. 2 Physical structure

2. Geometric model

A piece of pneumatic artificial muscle can be geometrically modeled as a cylinder. Of course the cylinder can change its volume when gas pressure is applied. The non-cylindrical end effects are ignored, and the thickness of the braided mesh is assumed to be zero. The dimensions of this cylinder are the length L, diameter D, and the interweave angle θ. Neither of these dimensions remains constant, because all the three parameters will change when it contracts or extends. Assuming inextensibility of the mesh material, the geometric constants of the system are the mesh thread length b, and n-the number of turns for a single thread. The interweave angle θ is the angle between the thread and the long axis of the cylinder (look at Fig. 3). θ changes as the length of the actuator changes. The relationships between these parameters are shown in Fig. 4.

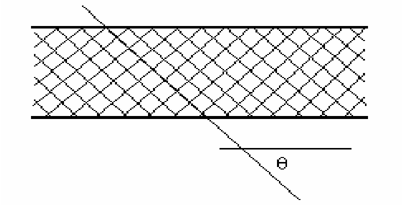

Fig. 3 Geometrical model

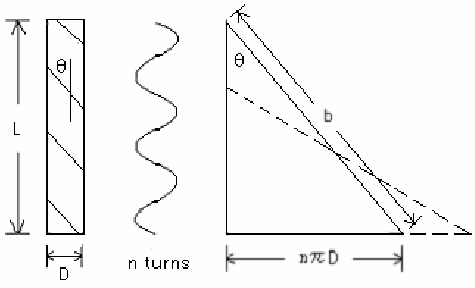

Fig. 4 Structure model

Now let's formulate the relationship between the length L and the angle θ.

$$L=b\cos\theta \quad (1)$$

$$n\pi D=b\sin\theta \quad (2)$$

The cylinder volume $V=\pi D^2L/4$, combining (1) and (2),

$$V=b^3\sin^2\theta\cos\theta/(4\pi n^2) \quad (3)$$

The minimum length (the maximum contracted length) should arise when the actuator's volume gets to its greatest, because this results in the equilibrium of the system. So, at the equilibrium point, there should be:

$$dV/d\theta=0$$

Based on (3),

$$dV/d\theta = (2\sin\theta\cos^2\theta-\sin^3\theta)b^3/(4\pi n^2) = 0$$

Then we get

$$\theta_{max} \approx 54.7°$$

We can say that the cylinder gets to the maximum of its volume when the interweave angle changes to 54.7°, or we say that the actuator gets to the greatest contraction by applied gas.

By now the geometrical model has been established.

Besides, the contraction ratio R_c is one of the most important characteristics. Now we can calculate it:

$$R_c = (L_0-L)/L_0 = (L_0-b\cos\theta_{max})/L_0 \quad (4)$$

Here, L_o is the relaxed length, or called it free length.

To two pieces of the same kind of pneumatic artificial muscles in different lengths, their interweave angle should be same. Therefore,

$$L1_0=b1\cos\theta$$

$$L2_0=b2\cos\theta$$

$$R_{c1}=(L1_0-b1\cos\theta_{max})/L1_0 =1- L1_0/b1\cos\theta_{max} =1- \cos\theta_{max}\cos\theta_0$$

$$R_{c2}=(L2_0-b2\cos\theta_{max})/L2_0 =1- L2_0/b2\cos\theta_{max} =1- \cos\theta_{max}\cos\theta_0$$

Where, θ_0 is the interweave angle corresponding to the relaxed length. So,

$$R_{c1} = R_{c2} =\text{constant}$$

This means that their contraction ratios are same to two actuators with the same structure in different lengths.

3. Static model

Because it is a kind of motion-generating device, we should try to find the force expression as a function of the related factors. Probably the force F has relationship with gas pressure, because the actuator acts when gas pressure is applied. Besides the relationships between the force and the length, interweave angle and so on will be developed too.

Here we use a simple energy analysis. It is assumed that the actuator is a conservative system in which the work in (W_i) is equal to the work out (W_o). The losses will be accounted for later. Work is input to the actuator when gas pressure is applied to the inner bladder surface.

$$dW_i=\int_{S_i} (P_{abs}-P_{atm})dl_i*ds_i =(P_{abs}-P_{atm})\int_{S_i}dl_i*ds_i =P_rdV \quad (5)$$

Where,

P_{abs} = Absolute internal gas pressure

P_{atm} = Atmosphere pressure (a little more than 1 bar)

P_r = relative gas pressure

s_i = Total inner surface

ds_i = Area vector

dl_i = Inner surface displacement

dV = Volume change

The output work arises when the actuator shortens due to the change in volume.

$$dW_o=-FdL \quad (6)$$

Now the ideal system assumption can be applied. The work input to the system should be equal to the work done by the actuator.

$$dW_i= dW_o$$

Combining (5) and (6),

$$P_r dV=-FdL$$

So,

$$\begin{aligned} F&=-P_r dV/dL \\ &=-P_r\,(dV/d\theta)/(dL/d\theta) \\ &=P_r b^2(2\cos^2\theta-\sin^2\theta)/(4\pi n^2) \\ &=P_r b^2(3\cos^2\theta-1)/(4\pi n^2) \quad (7) \end{aligned}$$

When $\theta=54.7°$, $F= P_r b^2(3\cos^2\theta-1)/(4\pi n^2) =0$. So please note that at the maximum interweave angle 54.7° the force output of the actuator is zero. In another word, the force output will be zero at the greatest contraction. Besides, under the condition of P_r is constant, when θ is equal to its minimum $\cos\theta$ gets to its maximum, so F will get to its maximum. We denote the maximum of F as F_{max}, therefore,

$$F_{max} = P_r b^2(3\cos^2\theta_0-1)/(4\pi n^2),$$

θ_0 is the interweave angle when the actuator is relaxed.

Besides, in (7), based on Fig. 4, we can imagine the diameter D will get to its maximum D_{max} when $\theta=90°$. Then

$$b=n\pi D_{max}$$

Take this into (7), it will become:

$$F=\pi D_{max}^2 P_r(3\cos^2\theta-1)/4 \quad (7')$$

The geometric variables used above provide a straightforward calculation, but to use the resulting equations in practice, they need to be modified, because the parameters b and θ are not easy or convenient to be measured. Now let us discuss this. If the cylindrical mesh is opened and laid flat, the weave geometry is easily observed (Fig. 5). The shape of the weave quadrilateral is governed by the interweave angle θ and the quadrilateral side length l.

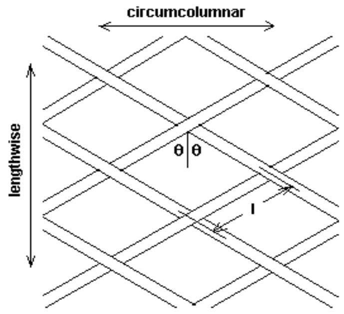

Fig. 5 The weave mesh structure

The cylinder length L and circumference C of the actuator is easy to be formulated by the following formulas:

$$L = 2Al\cos\theta \quad (8)$$

$$C = 2Bl\sin\theta \quad (9)$$

Where:

A = number of lengthwise quadrilaterals

B = number of circumferential quadrilaterals

Since the circumference can also be expressed as πD, so there is:

$$\pi D=2Bl\sin\theta$$

$$D=2Bl\sin\theta/\pi \quad (10)$$

Recall equations (1) and (2),

$$L=b\cos\theta$$

$$D=b\sin\theta/n\pi$$

Comparing (1) and (8), (2) and (10) results in the following:

$$b=2Al \quad (11)$$

$$n=A/B \quad (12)$$

Therefore, to practically characterize an actuator only the quadrilateral size and count are necessary. Now let us try to remove θ from the equations. It is difficult to sense the interweave angle during operation of the actuator. But it is much easier to measure the length. If the equations can be rewritten in terms of force, pressure, and length, then they will be more useful, because these variables can be measured most easily. Recall the triangle from Fig. 4, and note that the length of side opposite to angle θ has been rewritten in terms of b and L.

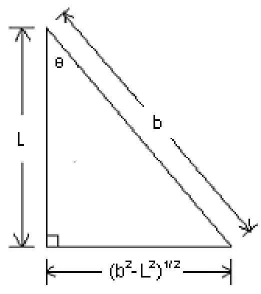

Fig. 6 The triangle relationship

The relationships between θ, L, and b can be expressed as:

$$\cos\theta = L/b \quad (13)$$

$$\sin\theta = (b^2-L^2)^{1/2}/b \quad (14)$$

Substituting these relationships into the volume (3) and force (7) equations,

$$V = L(b^2-L^2)/(4\pi n^2) \quad (15)$$

$$F = P_r b^2(3L^2/b^2-1)/(4\pi n^2) \quad (16)$$

It is easy to imagine that pneumatic artificial muscles act somewhat like springs. We know that the spring has an important parameter-the constant elasticity coefficient. Does the actuator exhibit the same property – the constant stiffness as the spring? According to the concept of stiffness, it is simply a derivative of force with respect to length.

$$K = dF/dL$$

Differentiating (16) with respect to L,

$$K = P_r b^2(3L^2/b^2-1)/(4\pi n^2) dP_r/dL + 3P_r L/(2\pi n^2) \quad (17)$$

The first term (dP_r/dL) is the most difficult to formulate. When the valves are closed, the pressure changes proportionally with volume according to gas laws. As a result, the relationship dV/dL would need to be developed. However, when the gas valves are opened, this relationship (dP_r/dL) is even more difficult to model. But we think that the pressure change as a function of length is small, and can be neglected. Besides, there is some space in the inlet hose, and it can help to cause the pressure change to remain minimal through the actuators' range of motion. In this case we can assume:

$$dP_r/dL \approx 0 \quad (18)$$

So, actuator stiffness is now given by

$$K = 3P_r L/(2\pi n^2) \quad (19)$$

Or solving (16) for P_r and substituting the result into (19),

$$K = 6F/(3L-b^2/L) \quad (20)$$

4. Conclusion

From the above theoretical analysis, we can conclude:

- Pneumatic artificial muscle is a linear motion engine, because the force output is proportional to the stimulating gas pressure (see (7));
- To a constant gas pressure, force output is related with the length. And it will become zero when it gets to the shortest length (see (7));
- The stiffness is not constant. It changes with both the gas pressure and the length;
- To determine actuator state, only two of the parameters are needed: gas pressure, length, force, or stiffness. The other two can be calculated from the above formulas.

Reference

[1] John Iovine, Artificial pneumatic muscle, Poptronics, Nov.2000, p49-65

[2] Graham-Rowe, Duncan, Power dressing, New Scientist, 5/25/2002, Vol. 174, Issue 2344

[3] Bjorn Verrelst, Frank Daerden, Pleated Pneumatic Artificial Muscles for Robotics Applications, 1st Flanders Engineering PhD Symposium about Industry-Ready Innovative Research, Brussels, 11 December 2003

[4] http://www.shadow.org.uk/products. 2004.7.1

The Tenth International Symposium on Artificial Life and Robotics 2005(AROB 10th '05),
B-con Plaza, Beppu, Oita, Japan, February 4-6, 2005

Secure Cooperation in a Distributed Robot System using Active RFIDs

Makoto Obayashi
Dept. of Product Development
Tokyo Metropolitan Industrial Technology Research Institute
115-8586, Nishigaoka 3-13-10,
Kitaku, Tokyo, Japan.

Hiroyuki Nishiyama and Fumio Mizoguchi
Information Media Center
Tokyo University of Science
270-1163, Yamazaki 2669-1,
Noda, Chiba, Japan.

Abstract

In this paper, we developed a distributed robot system that can provide various services in a real environment using ad-hoc networked active radio frequency identifications (RFIDs). These services are derived from a large amount of data from sensors connected to active RFIDs. The primary advantage of this method is that it allows the construction of a real environment monitoring system easily. Moreover, human status and position are easily identified by outfitting active RFIDs to subjects. However, a security system is required for a radio ad-hoc network and cooperation system between active RFIDs. In our research, we developed a multi-robot cooperating system as a multi-agent system and applied it to an active RFID, which has limited resources. We also developed a security system for active RFID communication that can be executed using limited resources. We then integrated the multi-agent system and security system. We also constructed a robotic environment that can provide various services using active RFIDs and then evaluated it.

1 Introduction

In recent years, the significance of developing a ubiquitous computing environment by establishing information terminals in various places has been recognized. This purpose aims to construct a highly developed information society[4] and build a barrier-free society for the elderly and the physically handicapped. Autonomous control of various devices in the real environment enables access to information and various services[2]. For these purposes, active Radio Frequency Identification (RFID) is both important and convenient recognized. Unlike a passive RFID represented by an IC tag, an active RFID has a CPU and a battery and can operate autonomously. It becomes possible to easily build a sensor network by developing the ad-hoc interconnection between active multi-sensor RFIDs. Generally, each active RFID is small and inexpensive. Therefore, it minimizes the risk when applied to outdoor or hazardous areas. Also, since it can attach to a person without incongruity, it is possible to collect varied information using sensor technology and to realize various services. It is also easy to make a home or office adapt to a robotic environment by arranging active RFIDs equipped with actuators (Fig.2). However, there are several problems in operating active RFIDs. First, all communications are carried out by an ad-hoc radio network, and packets are intercepted by neighboring active RFIDs. Second, in order to achieve low power consumption and downsizing, RFIDs have limited computer resources and transmission speed. For this reason, it is impossible to implement the usual security techniques. When developing a robotic environment using active RFIDs, anticrime and disaster prevention must be considered. While communicating is crucial, malicious hackers must be intercepted. In order to build a robot environment, dynamic cooperation between active RFIDs is necessary. Examples of this cooperation include invader authentication and the control of information appliances according to sensors in the real environment. In this case, processing of Cooperation and security are interrelated, making it difficult to deal with these problems. Therefore, we developed a secure dynamic active RFID (Fig.1) cooperation system suitable to limited computer resources. Our system incorporates a multi-robot cooperation system produced in our previous work[3] into an active RFID ad-hoc network system. We also implemented the framework for cryptography and authentication to facilitate dynamic cooperation between active RFIDs. Finally, we discuss the applicability of our system based on the experiments.

2 TinyMRL

We developed the multi-agent language "TinyMRL" to solve the problems described in

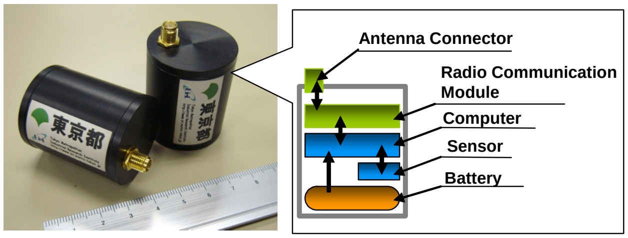

Figure 1: This figure shows active RFIDs in our research: It is small computer which has battery and ad-hoc radio network module. It can get various information using sensors and control actuators.

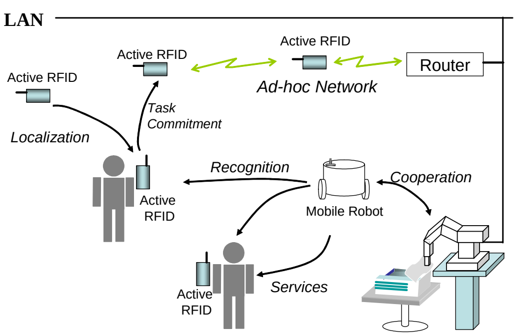

Figure 2: Our model of Communication between devices. Our system detects the position and status of persons by sensors equipped to active RFID.And it realizes various services by cooperating with devices in the environment via ad-hoc network.

the previous section. TinyMRL enables dynamic secure cooperation between active RFIDs. We achieved dynamic cooperation and competitive resolution between robots by developing a multi-agent system "MRL"[3]. When heterogeneous robots cooperate in a real environment, efficient task assignment and competition resolution are required. These are indispensable when multiple robots cooperate in executing a task. MRL allows robot behavior to be defined as a set of rules, where an action is determined by its internal state and environment alteration. Moreover, functions of shared variables and streams enable the simple description of competition resolution between robots. TinyMRL, which we developed in this research, is a multi-agent language and its execution environment. TinyMRL is applied MRL, which is then applied to active RFIDs. TinyMRL is executable on embedded computers, even those with limited resources (including 8-bit CPUs).
Although TinyMRL has a small system, it isn't

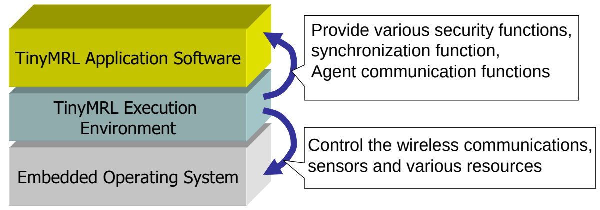

Figure 3: TinyMRL System Configuration

a subset of MRL. MRL is a processing system based on the assumption of parallel computing.
It is designed based on a concurrent logic language,
which enables it to efficiently unify functions and synchronization between parallel processes. It is confirmed by heterogeneous robots executing cooperative tasks[3]. However, the concurrent logic language has several shortcomings. First, it needs a parallel computer and a UNIX OS. This is not necessary for a large-scale robot system, but it is redundant or superfluous equipment to a sensor network and an information appliance network. Second, concurrent logic language is more difficult than procedural language. Operation of an undefined variable and stream make debugging difficult. Third, MRL does not allow some branch and loop instructions ("'if," "for," or "while"), therefore implementation of control calculations is difficult. TinyMRL is implemented using the advantages of MRL to the embedded computer, and is also designed for devices that have a network communication module. Moreover, it functions as a script language for rapid behavior setup of active RFID. Also, TinyMRL can describe an agent state transition as a set of defining rules that inherits the features of MRL. Moreover, in TinyMRL, "for", "while", and "if" sentences can be written in a description of a predicate. These are necessary for implementing data processing. Furthermore, TinyMRL execution environments provide a security system as the system call, so the developer can communicate securely. Figure 3 illustrates the TinyMRL system configuration. The bottom block is an embedded OS, such as μITron. The top block is the agent software, which is defined by TinyMRL syntax. The middle block is the TinyMRL execution environment that interfaces with the OS, ecurity functions, and the cooperation framework between active RFIDs.

3 Implementation

We adopted MOTE developed by the Crossbow Corporation as the active RFID. It has an 8-bit CPU, 128Kbyte ROM and a radio network module that can constitute an ad-hoc network.

The Tenth International Symposium on Artificial Life and Robotics 2005(AROB 10th '05),
B-con Plaza, Beppu, Oita, Japan, February 4-6, 2005

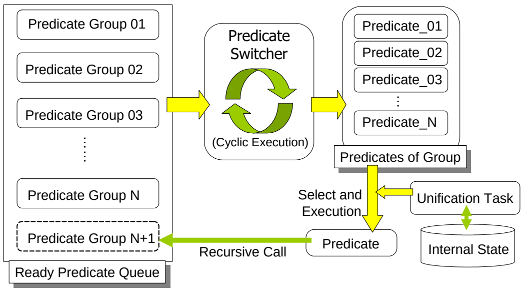

Figure 4: Processing flow of selecting and switching predicates.

3.1 Agent definition using TinyMRL

In TinyMRL syntax, behavior of an active RFID is controlled by a set of predicates. Each predicate consists of a predicate name, condition part, and execution part (the same as a Guarded Horn Clause GHC)). Figure 4 illustrates the TinyMRL execution process diagram. A predicate is classified by its number of arguments. Namely, predicates with the same name and same number of arguments are classified in the same group, and predicates are launched from each predicate group. When a predicate group is launched, only the predicate whose internal state of a definition formula and active RFID in a condition paragraph is called. If several predicates satisfy the launch condition, only one predicate is called according to its priority. In general, a predicate priority is determined by the number of conditions. When two or more predicates have the highest priority, one predicate is chosen at random. Finally, in the predicate execution, a series of processes can be constituted by calling a predicate recursively at the end of the execution paragraph. Hence, TinyMRL syntax easily describes the state transition of agent behavior. A predicate that belongs to the same predicate group expresses a state, and a recursive call means continuing the state. Furthermore, when an agent transitions to another state, it is realized by the predicate definition that corresponds to arbitrary events and calls the other predicate group. The end of a state is also realized by not calling any other predicate. In this case, predicates are not queued into the ready predicate queue, resulting in a simultaneous completion of the series of state transition operations. Figure 5 shows an example of a TinyMRL program.

3.2 Security function of TinyMRL execution environment

This section describes the details of TinyMRL security functions. Generally, an active RFID has poorer

```
start() :- true {      /* Start execution */
  run(1);              /* Launch a predicate */
  run(1,2);            /* Launch a predicate */
}
   /* When the variable a is equal to 1,
      followng predicate is executed */
run(int a) :- a == 1 {
  syscall:dataRequest(Turtle);
  run(2);                /* Recursive Call */
}
   /* When a message is received,
      following predicate is executed */
run(int a) :- a==2 && syscall:receiveMsg(){
  Massage msg = syscall:getMsg();
  run(msg);            /* Recursive Call */
}
```

Figure 5: TinyMRL Example Code

resources than a common computer. It also has low throughput corresponding to low power consumption. The radio signal is therefore weak. This restricts the speed and range of radio communication. μTESLA and SNEP provide techniques for achieving network security with limited resources[1]. We developed the system by fusing these security techniques to TinyMRL. The TinyMRL execution environment has a secure communication framework between active RFIDs and allows developers to construct dynamic secure cooperation without special operations. TinyMRL provides cryptography, packet authentication and semantic security functions. In our system, we assume that all active RFIDs a developer employs are reliable. We also assume that malicious hacking attempts are elicited from participating in the adhoc network by the cracker's active RFID. Also, all active RFIDs a developer initializes have a common secret key. Keys used by data encryption, decryption, and authentication are generated from a secret key, which all reliable active RFIDs possess. When $Agent_a$ tries to communicate with $Agent_b$, $Agent_a$ has to launch the following system call. Its procedure is then changed to the TinyMRL execution environment.

$$\texttt{system:sendMsg(}Agent_b\texttt{, <Message>)} \tag{1}$$

In this case, the communication content processed by TinyMRL between $Agent_a$ and $Agent_b$ is expressed as follows.

$$Agent_a \rightarrow Agent_b : N_a, \texttt{<Message>} \tag{2}$$

$$Agent_b \rightarrow Agent_a : \{\texttt{<Message>}\}_{<K_{ba}>}, \texttt{MAC}(K_{ba}, N_a || E_b) \tag{3}$$

$$E_b = \{\texttt{<Message>}\}_{<K_{ba}>} \tag{4}$$

Table 1: Time required to commitment in contract net protocol

The number of predicates	10	20	30	40
Time required to commition [msec]	2988	3092	3156	3733

N_a in equations 1 and 2 means the nonce is generated by the active RFID defined as $Agent_a$. The TinyMRL execution environment generates a nonce at every communication instance between agents. Nonce is a randomly generated bit array. It is used to maintain the order and novelty of packets. In our system, a 64-bit-long nonce is implemented. When a nonce is generated according to the system call of communication, the TinyMRL execution environment stores the nonce in internal memory. After this procedure, it guarantees the packet order and launches the agent communication process by checking whether the received packet includes its own generated nonce. In this implementation, we use the RC5 algorithm developed by RSA for cryptography. We use the OFB mode in the RC5 algorithm processing. Therefore, one function achieves encryption and decryption. We use the CBCMAC and the RC5 algorithm for generating a Message Authentication Code (MAC). A MAC is generated as the final block of the CBC mode. In our system, a MAC is generated using the received packet nonce and encrypted message, shown as Equation (3).

4 Experiment

We examined the performance of a contract net protocol using several active RFIDs to evaluate our system. A contract net protocol is used as the typical negotiation technique for task assignment. Figure 6 shows agent task behavior when executing a contract net protocol. We use four active RFIDs, and NODE1 serves as the client. The other three NODEs bid for requests from NODE1. USER is a person's process of information terminal. The processing of the contract net protocol begins when indicated by USER. In this experiment, we measured the change of average time required to negotiation by increasing predicate in each active RFID. The experimental results are shown in Table 1. As the shown in the table, even the result of the least predicate number takes about 3 seconds. Therefore, the experiment result shows that our system can't be applied to reactive system. But, our system is available to secure cooperating system of active RFIDs.

5 Conclusion

In this research, we developed a multi-agent language and its execution environment to resolve cooperation problems and negotiation for task assignment of a distributed robot system using active RFIDs. Moreover, we developed the security system to guarantee the secure communication between active RFIDs, which have limited resources. We also developed an active RFID behavior definition system that allows the developer to easily construct an ad-hoc network robot system by fusing these functions. We then evaluated the applicability of our system through experimentation.

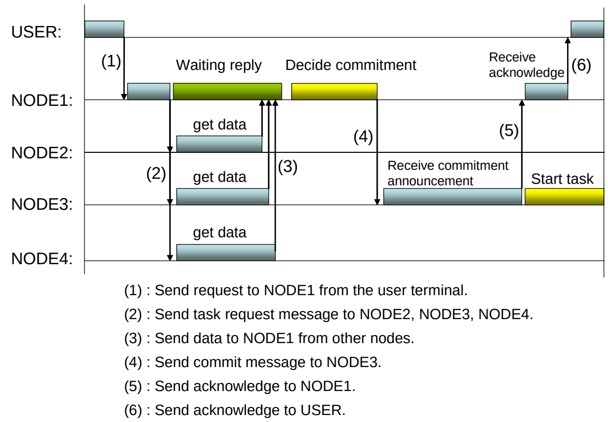

Figure 6: Time line of the execution of contract net protocol between active RFIDs.

References

[1] Adrian Perrig , Robert Szewczyk , Victor Wen , David Culler , J. D. Tygar, "SPINS: security protocols for sensor netowrks," Proceedings of the 7th annual international conference on Mobile computing and networking, pp.189-199, July 2001, Rome, Italy.

[2] F.Mizoguchi, H.Nishiyama, H.Ohwada and H.Hiraishi, "Smart office robot collaboration based of a multi-agent programming," Artificial Intelligence, Vol.114, 1999.

[3] Hiroyuki Nishiyama, Makoto Obayashi, Hayato Ohwada, Fuimo Mizoguchi, "A Concurrent Logic Programming Language for Multiple Robot Cooperation," Journal of the Robotics Society of Japan, vol.19, No.5, pp.620-631, 2001.

[4] Ora Lassila and Mark Adler: "Semantic Gadgets: Ubiquitous Computing Meets the Semantic Web," in: Dieter Fensel et al (eds.): Spinning the Semantic Web, pp.363-376, MIT Press, 2003

The Tenth International Symposium on Artificial Life and Robotics 2005(AROB 10th '05),
B-con Plaza, Beppu, Oita, Japan, February 4-6, 2005

A Soccer Robot Control Design Based on the Immune System

Jungo Ito, Kazunori Sakurama and Kazushi Nakano

Dept. of Electronic Eng., The University of Electro-Communications
1-5-1 Chofu-ga-oka, Chofu, Tokyo 182-8585, Japan

Abstract

This paper proposes a control system design for soccer robots based on the immune system. The immune system is a kind of engineering model imitating the human immunity action. It has some features such as self-optimization by learning, and easiness in dynamic reconfiguration of robots themselves. Thus, the immune system can be effectively applied to robot control in dynamic environments.

The immune system is applied to construct the soccer robot control system for RoboCup. First, applying the immune system to the obstacle avoidance problem of the mobile robot, we demonstrate its validity in simulation. Next, we execute 3 to 3 soccer plays by the soccer robots in simulation. These results show that the immune system is useful for robot control.

Keywords: immune system, dynamic environments, RoboCup

1 Introduction

The problem in development of industrial robots until now is focused mainly on the improvement of accuracy and speed in robot motion, due to the use of robots in static environments such as automated factories. However, for robots which will infiltrate our daily life from now on, it is necessary to cope with dynamic environments which are continually changing around the robots. In addition, it is important to develop the capability of cooperative behavior between robot-robot and between robot-human.

In order to promote research on these problems, we have dealt with RoboCup [1] as an international robot soccer game. And we now try to design a new soccer robot control system by applying the theory of immune system (IS) which imitates the human immunity action. The IS has some features such as self-optimization by learning, and easiness in dynamic reconfiguration of robots themselves. Thus, this system can be effectively applied to robot control in dynamic environments. Kondo, et al. proposed applying the IS to action control of an autonomous mobile robot [2]. However, there are still a few examples of application of the system to continually changing environments in which robots are tasked with a job.

In this paper, we apply the IS to soccer robot control in the RoboCup small league section, and show a possibility of designing a robust robot control system which can flexibly cope with dynamic environments. First, a simulation is performed for obstacle avoidance of a small mobile robot in which the IS is installed as a controller. Furthermore, it is demonstrated to improve the capability of obstacle avoidance via a learning mechanism of the IS. Secondly, the other simulation of 3 to 3 soccer plays is performed, in which the IS is used for both of obstacle avoidance and action selection. Then, we show to improve the performance of soccer play via the learning mechanism of the IS. Finally, we give the conclusions.

2 Immune System

2.1 Summry of Immune System

The IS is a kind of engineering model imitating the human immunity action. The human being has complex immume responses via multiple mechanisms. Here, we pay attention to the immune network, i.e. network between an antigen-antibody and between antibody-antibodies which is based on the idiotypic network hypothesis proposed by Jerne [3]. We will construct the IS based on Jerne's hypothesis.

2.2 Dynamics of Immune System

The model equation which represents the behavior of the immune system is given by Kondo, et al [2]. We modify this in the following form :

$$r_i(t+1) = r_i(t) \quad + \quad \left(\frac{\sum_{j=1}^{N} T_{ij} A_j(t)}{N} + m_i - k_i \right) \cdot A_i(t) \qquad (1)$$

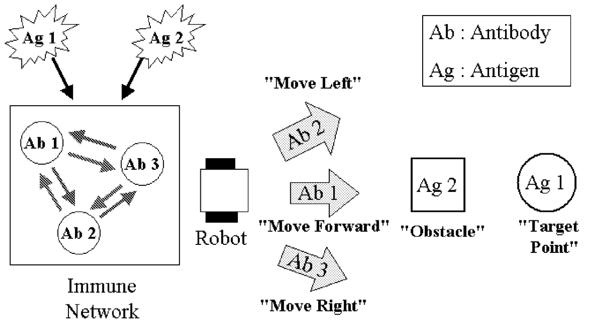

Fig. 1: Application of IS to robot control

$$A_i(t+1) = \frac{1}{1+\exp\{\beta - r_i(t+1)\}} \tag{2}$$

where A_i is the concentration number of antibody i, r_i is the parameter to determine A_i, T_{ij} is the immune network parameter which represents the relationship of stimulation and suppression between antibodies i and j, m_i is the reaction between antibody i and antigen, k_i is the number of natural death, N is the number of antibodies, and β is the threshold value. After being updated by m_i, $\sum_{j=1}^{N} T_{ij}A_j$, and k_i, the concentration number of antibody i is normalized via the sigmoid function in eq.(2).

In our robot control, the IS is used by considering that the antigen is an environmental information such as a target point and an obstacle, and the antibody is the movement direction to be selected by a robot. For example, to antibody 1 (Ab1) we give the following command, "when a target point exists in the forward direction, move forward". On the other hand, to antibody 2 (Ab2) we give the following command, "when an obstacle exists just in front, move left".

Let m_1 be 1(0) in the case that the target point exists (does not exist) in the forward direction. Similarly, let m_2 be 1(0) if the obstacle exists (does not exist) in front of the robot. On this setup, the antibodies concentration is continuously calculated by eqs.(1) and (2) from initial values $A_i(0) = 0, r_i(0) = 0$. This calculation is finished when one of antibodies concentration exceeds the fixed value decided previously. The antibody who has eventually the highest concentration determines the movement direction of the robot.

Unfortunately, it is quite difficult to give suitable network parameters T_{ij} because of a huge number of the combination of T_{ij}. Thus, we need an optimization method of T_{ij} by self-learning, which is discussed in the next subsection.

2.3 Learning Mechanism

An immune network can optimize its parameters by a learning method as shown below. The parameter T_{ij} is updated to improve the adaptation capability of the system by learning from a result of the action selected by the IS. In the simulation shown in Sections 3 and 4, the update rules of T_{ij} are assigned as follows:

[Update Rules]

1. In the case that the robot reaches the target point: For the selected antibody i, if its concentration exceed the fixed value, T_{ij}, which is related to other antibody j, increases based on the following:

$$T_{ij}(k+1) = 0.95 \times T_{ij}(k) + 0.05 \tag{3}$$

2. In the case that the robot collides with the obstacle: For the selected antibody i, if its concentration exceed the fixed value, T_{ij}, which is related to other antibody j, decreases based on the following:

$$T_{ij}(k+1) = 0.95 \times T_{ij}(k) - 0.05 \tag{4}$$

3. In the case that the robot cannot reach the target point in a limit time: For each i and j, T_{ij} changes based on the equation

$$T_{ij}(k+1) = 0.95 \times T_{ij}(k) + d, \tag{5}$$

where d is uniform random number on [-0.5,0.5].

3 Obstacle Avoidance Simulation

3.1 Method of Obstacle Avoidance

In this simulation, the robot can search the field divide into 16 areas (refer to the left figure of **Fig.2**), and move to one of 16 directions (refer to the right figure of Fig.2).

When the number of obstacles is only one, there exist 16 types of the obstacle detection pattern. Then, we can specify the movement direction of the robot according to each pattern in advance. Unfortunately, it becomes difficult to specify the movement direction of the robot in advance as the number of obstacles increases, because the detection pattern increases exponentially as it does. Therefore, we introduce an immune system in the next subsection to achive an easy situation where we need assign only some types of simple behavior of the robot, e.g., when an obstacle exists in the search area 6, move to direction number 15.

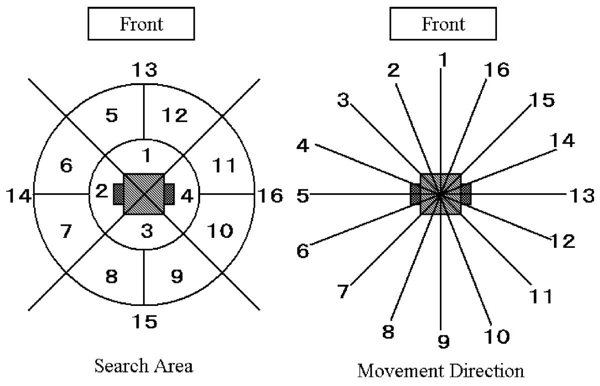

Fig. 2: Search area and movement direction

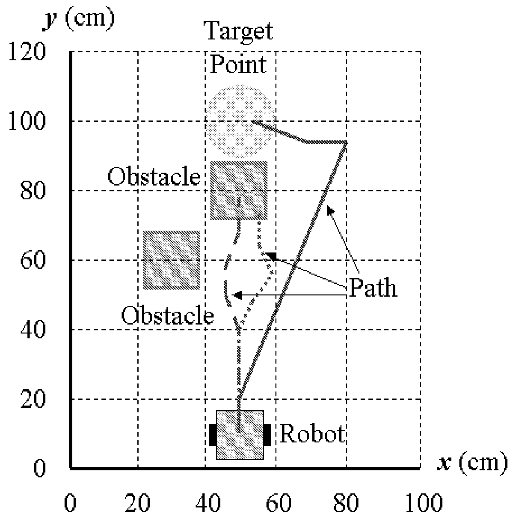

Fig. 3: Obstacle avoidance

3.2 Simulation Result

This subsection shows a result of a simulation where the robot tries to move a target point with avoidance of stationary obstacles. In this example, the target point is in front of the robot while the obstacles exist between the robot and the target point. Let antigens be the position information of the target point and the obstacles, and the antibodies be the movement directions shown in the right figure of Fig.2.

The broken line in **Fig.3** shows the path of the robot in the case that $T_{ij} = 0$ for any i and j. The robot collides an obstacle and cannot reach the target point. On the other hand, the dotted line in Fig.3 depicts the path of the robot whose parameters T_{ij} are updated once using the learning mechanism, which is shown in Section 2.3. Finally, the solid line shows the path after T_{ij} are updated 12 times until the robot reaches the target point. The iteration of the update of T_{ij} enables the robot to reach the target point with avoidance of the obstacles.

4 3 to 3 Soccer Play Simulation

4.1 Soccer Robot Control

Next, we perform a simulation of a soccer game, which continues until one of three player robots shoot a ball to an opponent goal, which is defended by three opponent robots. In this simulation, the antigens are given from the position information of the player robots, the opponent robots and the ball. The antibodies are assigned as robot actions such as a dribble, a pass and a shoot. Each player robot distinguishes 9 types of the field situation from 2 information, that is the ball position and the ball owner. Each robot receives a command according to the situation, e.g., if there exists the ball near the opponent goal and one of player robots has the ball, then this robot receives the command "move to the opponent goal", another does "move to near the opponent goal", and the other does "move to center".

We perform simulations in 10 cases, where one of opponent robots is a goalkeeper the others chase the ball without obstacle avoidance action. The movement velocities of the opponent robots and the player robots are equal.

4.2 Extended Learning Rules

In the simulation of the soccer game, the following are attached to the update rules of T_{ij}.

[Additional rules]

1. If the player robots never score in a limit time, these parameters are updated so that the antibody selected then becomes more difficult to be selected.

2. When the player robots change the role, the following update is performed for each robot according to the action evaluation which is introduced below. If the value of the evaluation is positive, T_{ij} is updated for the antibody selected then to become easier to be selected. If the value is negative, T_{ij} is updated for it to become more difficult to be selected.

[Action Evaluation]

Let $EL_i(t)$ be the distance between the ball and the opponent robot i at the time t:

$$EL_i(t) = \sqrt{(bx(t) - ex_i(t))^2 + (by(t) - ey_i(t))^2}, \quad (6)$$

where $(bx(t), by(t))$ and $(ex_i(t), ey_i(t))$ represent the ball position and the position of the opponent robot i, respectively, and t is the time just after the change of the robots' roles. Similarly, let $GL(t)$ be the distance between the ball and the opponent goal at t:

$$GL(t) = \sqrt{(bx(t) - gx)^2 + (by(t) - gy)^2}. \quad (7)$$

The following is the action evaluation which the additional rule 2. uses.

> The action evaluation is set positive if $P(t) > P(t-1)$, and is negative if $P(t) < P(t-1)$. The parameter T_{ij} is not updated if $P(t) = P(t-1)$.

$$P(t-1) = \sum_{i=1}^{E} \frac{1}{EL_i(t-1)} - \frac{1}{0.5 \times GL(t-1)}, \quad (8)$$

$$P(t) = \sum_{i=1}^{E} \frac{1}{EL_i(t)} - \frac{1}{0.5 \times GL(t)}. \quad (9)$$

4.3 Simulation Results

Fig.4 shows the simulation result with the non-updated T_{ij}. Each player robot cannot pass and dribble well, and an opponent robot take the ball from one in a moment. On the other hand, after the update of T_{ij} using that learning mechanism, the player robots can get a score with suitable actions as shown in **Fig.5**. The player robots can score 7 goals in 10 simulations after learning, while they cannot before learning. This simulation result illustrates clearly the improvement of the ability of the player robots by learning.

5 Conclusions

In this paper, we have constructed the multi-robot control system for RoboCup. This system can flexibly deal with dynamic environments by using the IS. The simulation results show the effectiveness of the IS for robot control.

There remain some problems in developing more efficient learning mechanisms and implementing this IS with real robots.

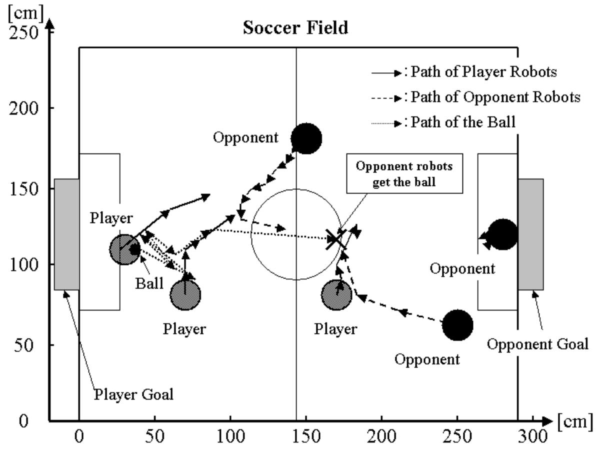

Fig. 4: Simulation result of soccer play before learning

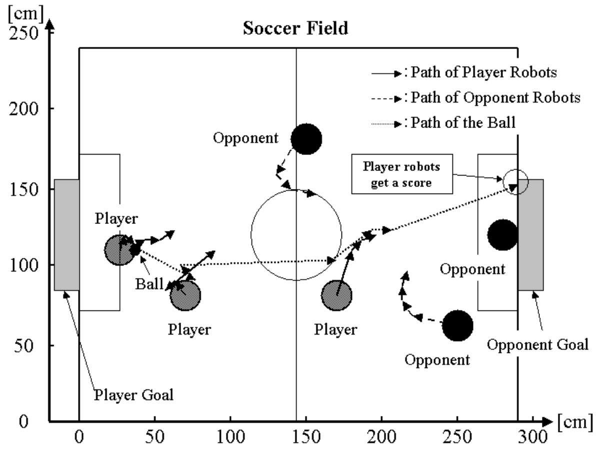

Fig. 5: Simulation result of soccer play after learning

References

[1] RoboCup Official Site
URL : http://www.robocup.org/

[2] T. Kondo, A. Ishiguro, Y. Uchida : "An Emergent Approach to Construct Behavior Arbitration Mechanism for Autonomous Mobile Robot," T.SICE, vol.35, no.2, pp.262-270, 1999.

[3] N. K. Jerne : "Idiotypic Networks and Other Preconceived Ideas," Immunological Reviews, no.79, pp.5-24, 1984.

The Tenth International Symposium on Artificial Life and Robotics 2005(AROB 10th '05),
B-con Plaza, Beppu, Oita, Japan, February 4-6, 2005

Robot's behavior driven by internal tensions regulated by pulsed para-neural networks

Junquan Li
School of Information Engineering
University of Science and Technology Beijing
Haidian Zone, Beijing 100083 China
tq097rr@163.com

Andrzej Buller and Juan Liu
ATR International, Network Informatics Labs,
2-2-2 Hikaridai, Keihanna Science City
Kyoto 619-0288 Japan
{ buller; juanliu } @atr.co.jp

Abstract We tested a psychodynamic controller called PreBrain using a simulated mobile robot. According to our approach, an agent seeks for pleasure that comes from the discharge of selected psychic tensions. The quality of control depends on the pleasure record. Perception may regulate the dynamics of tensions. The discussed version of PreBrain processes three pleasure-related tensions: boredom, interest, and excitement. An object-of-interest appearance discharges the first tension, but results in an increase of the second one. Contact between a toy and the robot's frontal touch sensor discharges tension related to excitement.

There are two kinds of building elements used for PreBrains: tension-accumulation cells (TAC) and pulsed para-neural networks (PPNN). TAC produces spiketrains whose frequency depend on accumulated tension, where increment/decrement of tension levels depend on received spiketrains and spontaneous accumulation or discharge. PPNN is a graph consisting of processing nodes and directed edges representing defined delays.

We tested three kinds of PreBrains. The first one forced the robot to rotate to get an image of an object-of-interest (toy) to the central zone of the visual field and then to go forward full-speed. The second one slowed the appropriate wheel to facilitate a turn when the image of the toy deviated from the center of the visual field. The third one employed a mechanism detecting certain cases of disappearance of the object from visual field and facilitating appropriately fast turn.

1 Introduction

The psychodynamic approach to machine intelligence assumes that an agent is doing something because he seeks for pleasure, where pleasure is nothing but a possibly fast discharge of a psychic tension [1]. Such relationship between tension and pleasure was suggested by Sigmund Freud [2][3]. Although not all Freudian concepts are supported by convincing empirical evidence, some of them seems to be valuable tips for building artificial minds. One of such concepts is continuous battle between conflicting mental forces [4] that, when implemented, resulted in robot's life-like hesitation [5][6].

PreBrain is a simple controller employing basic psychodynamic mechanisms intended to evolve toward a complex neural-like circuitry in which an emergence of communication behaviors and the phenomenon of thinking could take place [7][8]. PreBrain has a highly modular structure. One kind of modules, called tension-accumulation cells (TAC) constitute Tension Accumulator. The second kind of modules, called pulsed para-neural networks (PPNN) constitute Tension Discharger. There is a bi-directional communication between Tension Accumulator and Tension Discharger (Fig. 1). Since not only perception contributes to increase of tension level, PreBrain's "mental life" (resulting in various actions) can take place outside the framework of sensing-action loop.

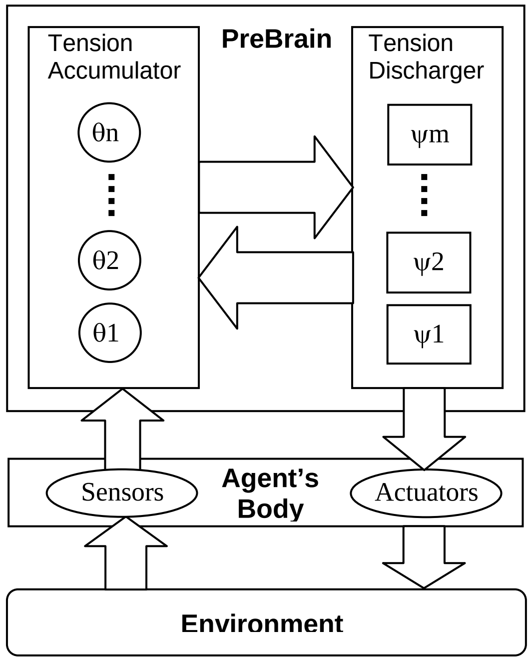

Fig.1. PreBrain structure and its relationship with agent's body and environment. θ1, θ2, …, θn – tension-accumulating cells (TAC); ψ1, ψ1, …, ψm – pulsed para-neural networks.

The PreBrain research contributing to both the Artificial Brain project conducted at the ATR, Kyoto and Intelligent Controller based on Artificial Brain (IC/AB) conducted at the USTB, Beijing [9]. Currently investigated PreBrains still fit to the behavior-based paradigm summarized by Ronald Arkin as sharing an aversion to the use of representational knowledge, emphasis on a tight coupling between sensing and action, and decomposition into behavioral units [10, p. 173]. Rodney Brooks's postulate to reject "cognitive box" [11, p. 36] is treated in PreBrain research only as a ban on handcrafted algorithms manipulating handcrafted symbolic knowledge. Intended development of psychodynamic architecture assumes facilitating emergence of various models of reality (perceived and imagined) [12], which will require a kind of knowledge representation to emerge as a result of social interactions.

2 PreBrain cells

The primary cause for any PreBrain action (related to environment or to itself) is a psychic tension being accumulated in one or more TACs. PPNN is a complementary technique used for purposeful manipulation on spiketrains, which is difficult in the framework of TAC-only networks. Although internal states of TAC are real numbers, whereas internal states of PPNN cells are integers, all of the cells send/receive only spiketrains, i.e. series of pulses of unitary amplitude occurring at discrete moments of time called clocks.

TAC state changes according to the formula:

$$\theta_{t+1} = G\left(\theta_t + \frac{\frac{u}{T_S} + \frac{A_t}{T_A} - \frac{D_t}{T_D}}{f}\right)$$

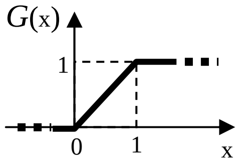

where
t – time (in clocks),
θ_t – accumulated tension,
u – parameter determining direction of uncontrolled change of tension (1 – increase, -1 – decrease),
$A_t = A_{0,t} + A_{1,t} + \dots + A_{15,t}$ – tension-increasing signal,
$D_t = D_{0,t} + D_{1,t} + \dots + D_{15,t}$ – tension-discharging signal,
T_S – uncontrolled increase/discharge time,
T_A – duration of tension change from 0 to 1 when influence of uncontrolled charge/discharge is negligible and the control signal A_t is a spiketrain of 1s only,
T_D – duration of tension change from 1 to 0 when influence of uncontrolled charge/discharge is negligible and the control signal A_t is a spiketrain of 1s only,
f – frequency of clocking (clocks per second).

TAC produces an output spiketrain whose frequency is proportional to current tension level so $f_t^{out} \approx k\, f\, \theta_t$, where $k \in [0;\ 1]$ is a parameter regulating the tension impact. According to psychodynamic assumptions, pleasure is related to the dynamics of tension discharge. The greater tension discharged in a given time, the greater pleasure recorded; the faster discharge of a given tension, the greater pleasure recorded.

PPNN is a graph consisting of processing nodes and directed edges, called axons. The nodes represent functions operating on spiketrains. Axons represent pure delays [13]. To date we used PPNNs in which a given node can be a *mexor* or *paraneuron*. Mexor returns a spike at clock t if it received one and only one pulse at clock $t\text{-}1$. Paraneuron returns a pulse and resets its counter at clock t if the counter was greater than 1 at clock $t\text{-}1$, while counter at clock $t\text{-}1$ is counter at clock $t\text{-}2$ plus the weighted sum of pulses the cell received at clock $t\text{-}2$ (a weight can equal 1 or –1). If axons are strings of one-input mexors and every cell is a 1×1×1 cube whose coordinates are three integers, then such a PPNN is called NeuroMaze. We have developed the NeuroMaze editor/simulator for rapid prototyping of desired PPNNs [14]. It was shown that a PPNN/NeuroMaze can be build for every Boolean function and practically for every manipulation on spiketrains [15].

3 How PreBrain works

Figure 2 shows PreBrain that was a subject to the presented research. The attached mobile robot uses two motors equipped with 2-input frequency-to-voltage converters (FVC). A frequency provided to the left FVC's "positive input" (L+) or the FVC's "negative input" (L-) forces the left wheel to roll forward or backward, respectively. The same applies to the right FVC's inputs (R+ and R-). Hence, equal-frequency spiketrains provided to L+ and R+ results in the robot's moving forward, whereas unequal spiketrains provided to L+ and R- results in the robot's rotation. Spiketrains to FVCs are provided by PPNN labeled Or8x4 (four 8-input OR-gates). The TAC labeled θ0 is related to boredom. Its T_S = 10s and $u = +1$. Its output is connected to the central input of the PPNN labeled PB1. Tension θ0 grows by internal causes and PB1 facilitates discharging via forcing the robot to wander in search for something interesting (spiketrains provided to L+ and R+). When the PreBrain is switched on, we observe the robot start, 1 accelerate for 10s, and then proceed forward at full-speed. Note that this behavior is not caused by any perception.

Although, according to psychodynamic approach, perception does not cause behaviors, it can regulate them. If right or left touch sensor is excited, PB1 (responsible also for obstacle avoidance) redirects one of involved spiketrains (L+ to L- or R+ to R-), which results in robot's rotation. A device labeled V-Green5 processes images from camera and recognizes an object-of-interest (and its direction) and provides signal D_t to θ0 where T_D = 0.1s. Hence, when an object-of-interest is seen, the robot immediately ceases moving.

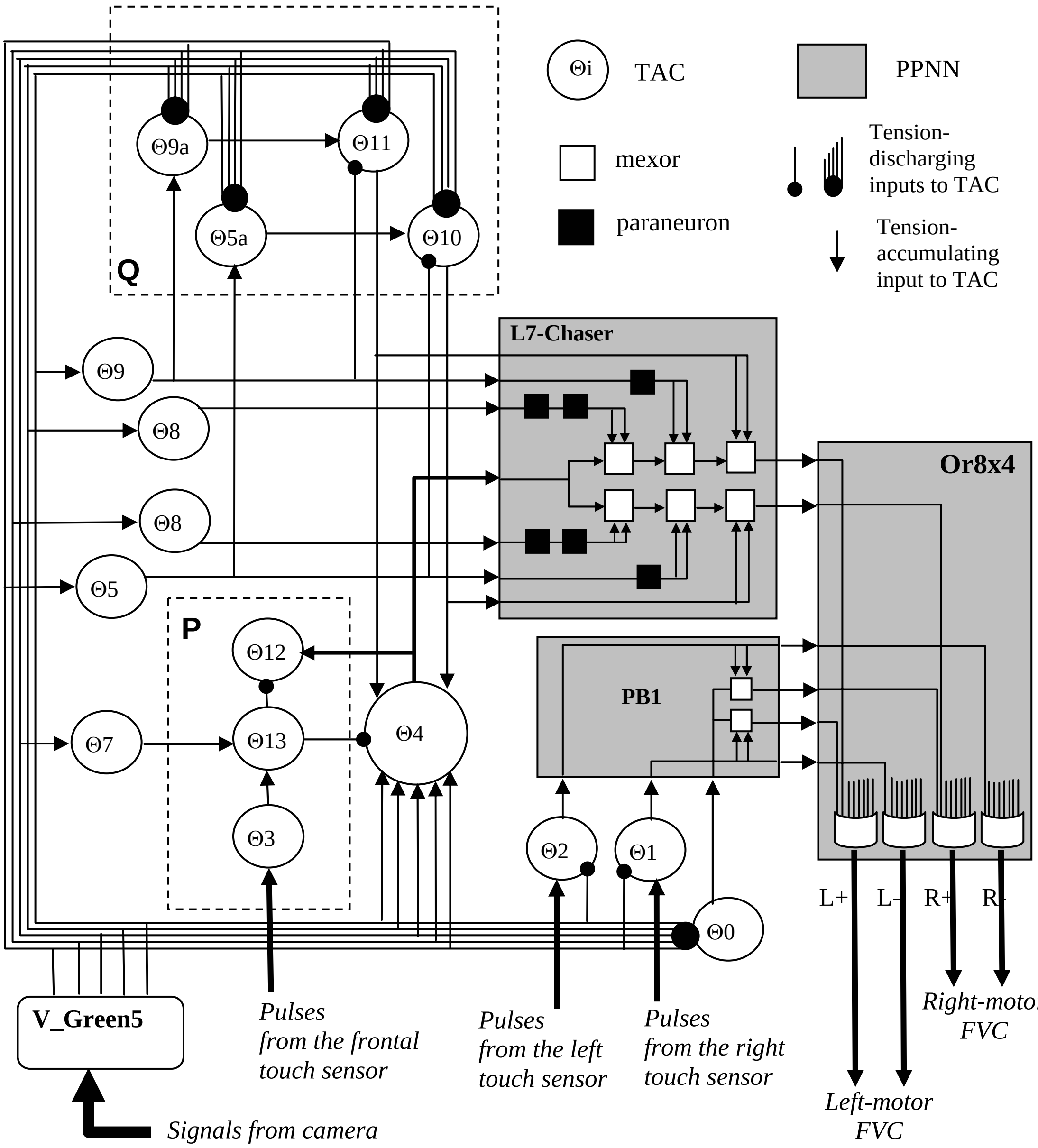

Fig.2. An example of PreBrain. TAC – Tension-Accumulating Cell; PPNN – pulsed para-neural network. **V_Green5** – a device processing signals from camera, recognizing object of interest and determining the direction it is seen at (one of five considered). *FVC* – Frequency-to-Voltage Converter. L+ , L- – positive and negative input to left-motor FVC; R+ , R- – positive and negative input to left-motor FVC (equal-frequency spiketrains provided to L+ and R+ results in the robot's moving forward; spiketrains provided to L+ and R- results in the robot's rotation). **Or8x4** – PPNN substituting four 8-input OR-functions. Θ0 – tension related to "boredom"; Θ1, Θ2 – tensions resulting from touching an obstacle (disabled in case of touching an object-of-interest). **P** – "pleasure" block: Θ3 – tension resulting from stimulation of the frontal touch sensor; if an object-of- interest is being touched and seen in the middle of visual field (Θ3 & Θ7), the tension Θ12 (representing "excitement") gets discharged contributing substantially to the "pleasure record". **PB1** – a PPNN providing signal from Θ5, Θ6 and Θ8...Θ11 to L+ and R+ (via Or8x4) and responsible for collision avoidance (blocking the spiketrain directed to L+ or R+ and providing a spiketrain to L- or R-, respectively, which result in robot's rotation); Θ4 – tension related to action-driving "interest" in a perceived object; it makes the robot going forward (in the course of providing spiketrains to L+ and R+ via Chaser and Or8x4) as well as increase of Θ12 at **P**. Θ5…Θ9 – tensions related to five directions an object can be seen at. **L7-Chaser** – a device providing a spiketrain from Θ4 to both L+ and R+ (via Or8x4) and allowing spiketrains from Θ5, Θ6 and Θ8...Θ11 to lower the frequency of the spiketrain provided to L+ or R+, which results in appropriate distortion of the robot's trajectory facilitating approaching the object-of-interest. **Q** – a device improving efficiency of the Chaser; it detects disappearance an the object of interest seen for the last time in the furthest left or furthest right zone of the visual field and in such case provides a dense spiketrain to appropriate inputs of the Chaser, which results in complete blocking of one of the Chaser's outputs, which results in providing a spiketrain to only one wheel, which results in a quick turn of the robot giving the object a chance to get back to the visual field.

If PreBrain consisted of θ0 and PB1 only, the robot would stay until the object's disappearance. But other tensions are also involved. θ4, representing "interest" (u = -1; T_S = 0.06s; T_A = 0.05s; T_D = 0.1s) gets high when the toy is detected and sends a spiketrain to the central input of L7-Chaser—a PPNN in which the axon carrying the spiketrain from θ4 forks into two branches delivering the spiketrain to both L+ and L- via Or8x4. Spiketrains leaving the Chaser will remain equal only when the toy is seen in the central zone of the visual field. Depending on how far the object deviates from the middle of the visual field more or fewer spikes are cut off the spiketrain passing through a given branch. In this way perceptual signals provided to other inputs of the Chaser regulate chasing behavior. If the object is out of current direction, frequencies of spiketrains provided to L+ and R+ differ, so the robot's trajectory becomes a circle of bigger or smaller radius.

Tension θ4 (to be interpreted as interest) is discharged when at the same time the object of interest is seen in the middle of the visual field (θ7) and being touched by the robot's frontal touch sensor. Necessary Boolean function is implemented as TAC θ13 "&". Related parameters are set so that discharging of θ12 ("excitement") contribute the most to PreBrain's "pleasure record". From the point of view of the "pleasure record", the best control strategy is to chase the toy, but not hurry with touching it.

4 Experiment

PreBrains were implemented using the ParallelBrain v.1.1 – a special client-server platform dedicated to rapid prototyping of very large modular brain-like structures. PreBrain clients were built partially as C++ programs and partially as pulsed para-neural networks (PPNN) synthesized using the NeuroMaze v. 3.0 Pro.

We tested three kinds of PreBrains. The first one used L6-Chaser that forced the robot to rotate to get a perceived image of the object-of-interest in the central zone of the visual field and then go forward full-speed. Such strategy of chasing appeared suitable for approaching motionless object. PreBrain of the second kind employed L7-Chaser, described in the previous section, which slowed down appropriate wheel when the image of the object deviated from the center of the visual field. Such strategy worked in case of chasing objects going with constant speed along straight lines. The third kind of PreBrain employed L7-Chaser together with a structure (labeled Q in Fig. 2) detecting disappearance of the object of interest seen for the last time in the furthest left or furthest right zone of the visual field and then providing a dense spiketrain to the highest or lowest input of L7-Chaser. This results in complete blocking of one of the Chaser's branches, which results in providing a spiketrain to only one wheel, which results in a quick turn giving the object a chance of getting again to the visual field.

Acknowledgements: J. Li's research was supported by NSFC, China, Grant 60374032. A. Buller's and J. Liu's research was supported by National Institute of Information and Communications Technology of Japan (NICT), Grant 13-05.

References

[1] Buller A. (2004) From q-cell to artificial brain, *Artificial Life and Robotics*, *8* (1), pp. 89-94.

[2] Freud S. (1920/1990) *Beyond the Pleasure Principle*, W.W.Norton & Co, pp. 3-4.

[3] Freud S. (1940/1989) *An Outline of Psycho-Analysis*, W.W.Norton & Co, p. 15.

[4] Freud S. (1923/1962) *The Ego and the Id*, W.W.Norton & Co, p. 40-42.

[5] Buller A. & Shimohara K. (2001) On the dynamics of judgment: does the butterfly effect take place in human working memory? *Artificial Life and Robotics*, *5* (2), pp. 88-92.

[6] Liu J. & Buller A. (2004) Tensions and Conflicts: Toward a Pleasure-Seeking Artifact, *The 5th IFAC Symposium on Intelligent Autonomous Vehicles (IAV'2004), July 5-7, Lisbon, Portugal*.

[7] Buller A. (2004) "Artificial Brain and Psychodynamic Mechanisms", In: Yin Yixin and Dong Jie (Eds.) *Proceedings of 2004 Sino-Japan Symposium on KANSEI & Artificial Life, July 3-4, University of Science and Technology, Beijing, China*, pp. 73-78.

[8] Buller A., Hemmi H., Joachimczak M., Liu J., Shimohara K. and Stefanski A. (2004) "ATR Artificial Brain Project: Key Assumptions and Current State", *9th International Symposium on Artificial Life and Robotics (AROB 9th '04), January 28-30, 2004, Beppu, Japan*, pp. 166-169.

[9] Li J. & Yin Y. (2004) Intelligent Controller based on Artificial Brain vs. Psychodynamic Brain, 2004 Sino-Korean Symposium on Intelligent Systems, Pusan, October, pp. P83-87.

[10] Arkin R. (1998) *Behavior-Based Robotics*, MIT Press.

[11] Brooks R. (2002) *Flesh and Machine*, Pantheon Books.

[12] Buller A (2002) Volitron: On a Psychodynamic Robot and Its Four Realities, In: Prince CG, Demiris Y, Maron Y, Kozima H, Balkenius C (Eds.) *Proceedings of the 2nd International Workshop on Epigenetic Robotics: August 10-11, Edinburgh, Scotland, Lund University Cognitive Studies 94*, 17-20.

[13] Buller A. (2002) CAM-Brain Machines and Pulsed Para-Neural Networks: Toward a hardware for future robotic on-board brains, *The Eight International Symposium on Artificial Life and Robotics (AROB 8th '03), January 24-26, Beppu, Japan*, 490-493.

[14] Buller A., Joachimczak M., Liu J. & Stefanski A. (2003) NeuroMazes: 3-Dimensional Spike-train Processors, *2nd WSEAS International Conference on Electronics, Control and Signal Processing (ICECS '03), December 7-9, Singapore*.

[15] Eeckhaut H. & Van Campemhout J. (2003) Handcrafting Pulsed Neural Networks for the CAM-Brain Machine, *The Eight International Symposium on Artificial Life and Robotics (AROB 8th '03), January 24-26, Beppu, Japan*, 494-498.

Robotic-Control Blocks (RCB) for Research and Education

Adam Stefanski and Andrzej Buller
Network Informatics Laboratories
Advanced Telecommunications Research Institute International (ATR)
Kyoto, Japan
{ ajstefan, buller} @atr.jp

Abstract This paper proposes a new hardware platform, called Robotic-Control Blocks (RCB), for robotic research and education. RCBs are being developed to address the requirements specific to Psychodynamic Architecture developed in the framework of the ATR Artificial Brain Project. The presented CPLD-based implementation is an interim solution. RCB-set contains blocks that can be interconnected to create a control system of custom complexity. Some of them are designed to cooperate with certain sensors and/or actuators. At its proof-of-concept state, RCB process three kinds of tensions: "boredom", physical contact with an external object, and being stuck in an endless loop. The basic functionality can be easily scaled using more kinds of blocks (only simulated to date) and additional copies of universal behavior-mixing blocks. Implemented as dedicated chips and enclosed in aesthetic cases, RCBs right now might be used in classroom as an inexpensive aid free of tedious programming.

Keywords- Discrete Control Systems, Modular Robotic Hardware, Mobile Robots, Robotic Education Aids

1 Introduction

Physical blocks covering elementary control functions give children the opportunity to learn principles of robotics without tedious programming. Maybe the most devoted promoter of this approach is Henrik H. Lund of the University of Southern Denmark who, inspired by works of developmental psychologists, elaborated Intelligent Building Blocks (I-Blocks) enclosed in popular LEGO DUPLO® elements. Particular I-Blocks represent several useful sensor/motor functions. Standard I-Blocks for processing and communication are equipped with a PIC16F876 micro-controller. Special I-blocks contain internal sensors, micro-motors, etc. [1]. The solution we propose, called Robotic-Control Blocks (RCB), being developed at the Advanced Telecommunications Research Institute International (ATR), Kyoto, Japan in the framework of the Artificial Brain Project, shares with I-Blocks the program-by-building paradigm, however, some assumptions differ substantially. Our project (albeit still in its infancy) is striving to attain the research frontiers in human-machine communication in quest for emergent communication [2]. While I-Blocks are to serve, first of all, as amusing education aid, the primary issue in RCB is practically unlimited scalability that is indispensable in building intelligent robots, however, small RCB sets also can be used in classrooms. As for other differences, unlike I-Blocks (that contain advanced pre-programmed micro-controllers), each RCB has only as many gates as it is really necessary to accomplish its task. Unlike the I-Block approach (aimed to provide components of both "brains" and movable "bodies"), RCB approach deals only with "brains" to be connected to given commercially available "bodies".

This paper first briefly explains the underlying concepts and theories motivating the development of the Robotic-Control Blocks (RCB). A new hardware test bench for RCBs is also presented and examples of RCB-based control systems are given. This is followed by a detailed explanation of the prototype sets of RCBs that have been developed and tested. Finally, the future research of RCBs is discussed and concluding remarks are also included.

2 Robotic-Control Blocks (RCB)

The idea of RCB emerged in face of various drawbacks, such as expandability, speed, and financial considerations, that arose in 2002 during development of first psychodynamic mobile robot, called Neko-1. The robot used a Parallax Basic Stamp II microprocessor to collect the data from three infrared proximity sensors and an ultrasound sensor and then sent out serial packets containing the data via a radio frequency transmitter. This data was processed by a C++ program running on a PC client which then sent out serial packets back to the robot with speed inputs to the two motors. Although the robot functioned correctly and depicted behaviors of boredom, excitement, and fright, all of the processing was still software based and accomplished using a PC [4]. This robot was not self-contained and mainly re-emphasized the correct functionally of the software simulation since rather than sending the processed data to a graphic user interface, it was now being sent to an actual robot.

RCB set includes various Function Control Blocks (FCB), identical Behavior Mixing Units (BMU), Drivers, Voltage-to-Signal Converters (VTSC) and Signal-to-Voltage Converters (STVC). In the current version of RCB hardware each FCB covers both accumulation of a given tension and a related behavior. BMUs can form a column defining priority when two or more FCBs produce pulse trains. Drivers decode behavior-defining pulse trains and produce pulse trains defining actions of particular motors.

VTSCs convert analog voltage values of taken from attached sensors into standard pulse trains. STCVs convert pulse trains into appropriate analog voltage values controlling attached motors. A system overview of the blocks is shown in Fig. 1. The RCB-based system can be expanded from the bottom-up by adding more various FCBs and from-centre-to-sides by adding more different sensors and actuators. In future versions the functions will be separated, making the set much more flexible. Although the presented BMU-based "working memory" covers only a kind of behavior subsumption, the simulated version includes a block in which tension compete for access to related behavior blocks [3].

The input for each sensor is encoded using a VTSC, processed, and later decoded using a STVC before being connected to the actuator. In order to allow for analog values, all the input signals are quantized and framed as a value between 0 and 255. The VTSC samples the input of the analog sensor and sends out the corresponding amount of pulses during a predetermined time frame. This is similar to duty cycles using pulse width modulation, however, in RCBs the pulses do not have to be sent consecutively and can be sent anytime during the predetermined time frame. The exact location of the sampling frame does not matter, therefore, the individual FCBs do not have to be synchronized.

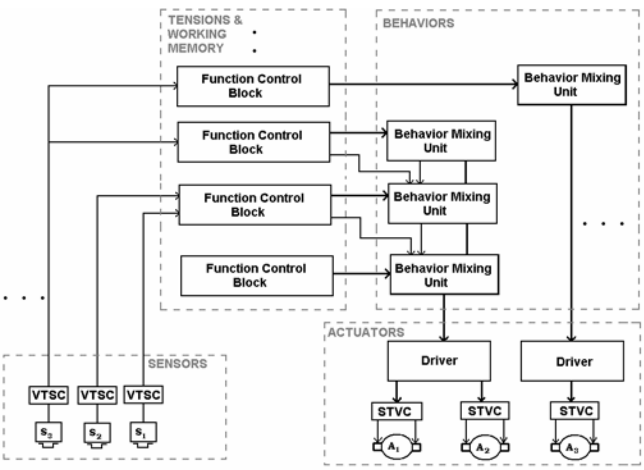

Figure 1. Robotic-Control Blocks Overview

The predetermined time frame was selected to be one millisecond, which corresponds to the approximate pulse of a biological neuron [5]. There is not single 'correct' predetermined time frame since the biological neuron conducting velocity is affected by many factors such as myelin, age of the neuron, etc. Furthermore, an exact time frame is not necessary for simulating PDA concepts in its simplest form. Assuming a one millisecond time frame, the minimum clock frequency required is 256 kHz in order to correctly quantize analog values as discrete neuron pulses.

Complex programmable logic devices (CPLDs) were used to implement each function block. The devices were chosen because they are well suited for combinatorial-intensive logic designs and the devices can be reprogrammed easily using hardware description languages. CPLDs provide a sound economic alternative for developing a prototype in a short period of time. Other options were field programmable gate arrays, which are suited for register-intensive logic designs, and individual digital circuits, which are very time consuming to design and can not be easily altered.

3 Development and testing

The development and testing of RCBs was divided into three distinct tasks in order to prove the functional concept. First, a simple unintelligent robot was created that goes straight ahead at all times. This is the most basic arrangement of RCBs and comprises of only a few blocks and two motors. All other current block sets expand the capabilities of this fundamental robot kit. Next, an obstacle avoidance expansion set was developed. It utilized two touch sensors to detect objects that impede the robots forward motion. A simple emergent phenomenon occurs when using the obstacle avoidance expansion set, which led to the design of the third expansion set, a meta-sensing expansion module [6]. The development of these three RCB sets will be discussed in this section.

A. Prototype Robotic-Control Block

In the future, each RCB will be implemented on a single dedicated IC. However, the current prototypes were designed on 2"x3" through-hole prototype boards. All the blocks, excluding the Power Block and the Clock Block, have ground, V_{DD}, and clock input signals. Furthermore, all blocks also output those same three input signals which allows for easy interconnecting, or daisy-chaining, of the RCBs. Each block also has necessary input and output signals, depending on the function of the block. The Power and the Clock Block are special blocks since they help generate the ground, V_{DD}, and clock signals. A functional diagram of a single regular RCB is shown in Fig. 2.

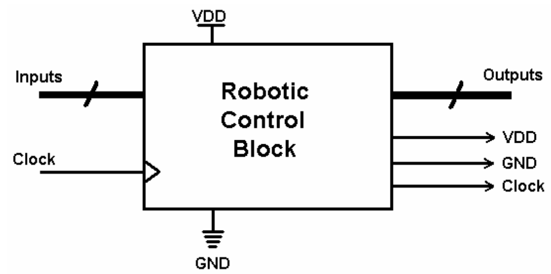

Figure 2. Prototype Robotic-Control Block

B. Basic Robotic-Control Blocks Set

In order to be compatible with the existing pulsed para-neural networks concepts, the fundamental set of RCBs is very primitive since it is supposed to represent instinctive functions. The basic set only includes the blocks necessary to power-up the robot and for the robot to move in a forward direction. It has actuators, two Lego® motors, but no sensors. Table 1 describes the blocks included in the basic RCBs set, while Fig. 3 shows the functional diagram of the robot that can be constructed using the supplied blocks.

TABLE I. BASIC ROBOTIC-CONTROL BLOCKS SET

Block Name	Qty.	Description
Power[1]	1	Outputs a V_{DD} and ground signal
Clock[1]	1	Outputs a clock signal
Forward	1	A Function Control Block that produces pulses so the robot moves forward
Behavior Mixing Unit	1	Selects which behaviors is sent to the Motor Driver
Motor Driver	1	Decodes the behavior and processes the signal for each motor
Signal-to-Voltage Converter	2	Produces a voltage corresponding to the frequency of the pulse train

1. Power and Clock Blocks are not shown in Fig. 3 since their signals are inputted to all blocks

C. Obstacle Avoidance Robotic-Control Blocks Set

The first expansion set of RCBs allows the robot to maneuver around objects that impede its constant forward movement governed by the Forward Block. This expansion set has the blocks necessary to receive the touch sensor inputs and encode them using pulse trains. These pulse trains are then processed by a FCB, the Obstacle Avoidance Unit (OAU). A BMU is also included to allow for further expansion of the system. Table 2 describes the blocks included in the Obstacle Avoidance RCBs set, while Fig. 4 shows the functional diagram of the robot that can be constructed using the supplied blocks.

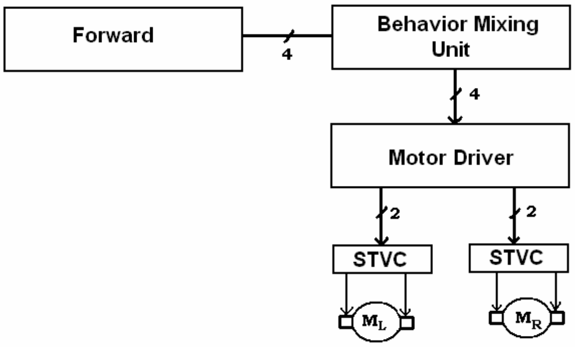

Figure 3. Basic Robotic-Control Blocks Set Schematic

TABLE II. OBSTACLE AVOIDANCE ROBOTIC-CONTROL BLOCKS SET

Block Name	Qty.	Description
Voltage-to-Signal Converter	2	Produces a pulse train corresponding to the analog voltage detected at its inputs
Obstacle Avoidance Unit	1	A Function Control Block that produces pulses so the robot avoid objects impeding forward movement
Behavior Mixing Unit	1	Selects which behaviour is sent to the Motor Driver

D. Meta-Sensing Robotic-Control Blocks Set

One of the problems with the OAU is that the robot would get stuck in endless loops. It would be functioning correctly and still be moving around, however, it would repeat the same action endlessly. This unfavorable phenomenon emerges from the robots basic rule set. It can be eliminated by meta-sensing, i.e. trying to detect the endless loop behavior. The meta-sensing expansion block set utilizes these concepts to avoid being stuck in an endless loop. Table 3 describes the blocks included in the meta-sensing RCBs set, while Fig. 5 shows the functional diagram of the robot that can be constructed. The role of the Meta-Sensing Unit (MSU) is to monitor the activity of the robot, specifically that of the OAU, to make sure it is not operating in an endless loop. Once the MSU detects an endless loop, it takes control of the robot and attempts to force it out of the loop by sending pulses on the correct signal lines.

E. Test Robot

All of the three developed block sets were not only tested for individual functionality but each set was put together and tested using a constructed robot with two Lego® touch sensors and two Lego® 9V motors. The RCBs Robot with all three sets interconnected is shown in Fig. 6. When the robot was powered up with only the basic set attached, it went straight forward as expected. Next, the Obstacle Avoidance Set was attached. The robot managed to rotate when it hit a wall or another obstacle, however, it sometimes got stuck in the corners of the room, which was the reason for implementing the Meta-Sensing Set. Once all the developed RCBs were correctly interconnected, the robot was able to wander around a room with various obstacles on the ground for extended periods of time without any difficulties. It would hit the obstacles, rotate, and continue to move forward.

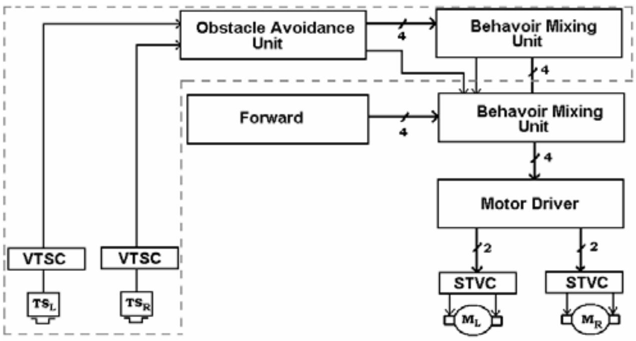

Figure 4. Obstacle Avoidance Robotic-Control Blocks Set Schematic

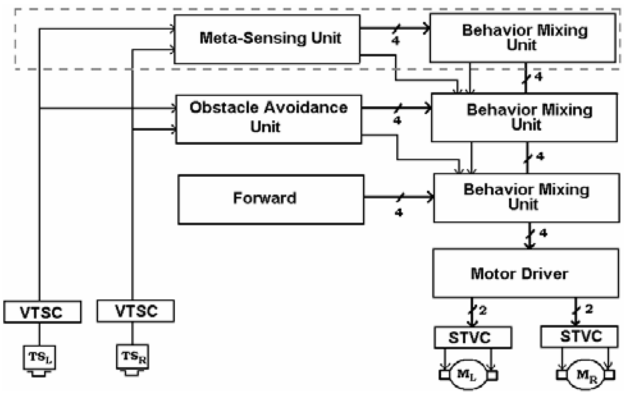

Figure 5. Meta-Sensing Robotic-Control Blocks Set Schematic

F. Future Blocks Sets

There are many different possible blocks sets that can be developed and added the current RCBs. Since the agent is a pleasure seeking creature, the robot needs to have methods to discharge tensions of boredom. One idea for a future block set is to make the robot be excited and chase green objects and be scared and run away from red objects. The escaping action will have a higher priority than the pursuit action. The existing obstacle avoidance and meta-sensing actions would obviously have a higher priority than either of the two new actions. If the robot did not see any green or red objects, it would continue to roam around pseudo-randomly in search of them.

There are many other possible blocks set that can be designed to enrich the repertoire of the robot. It can detect a hungry state, which is equivalent to a battery low sensory signal, and then search for a battery charger station before continuing to roam its environment. Another possible set can be found on simulating concentrated and distracted tensions based on the principles of Piaget's theory how 0-2 year old children perceive new objects of interest [3].

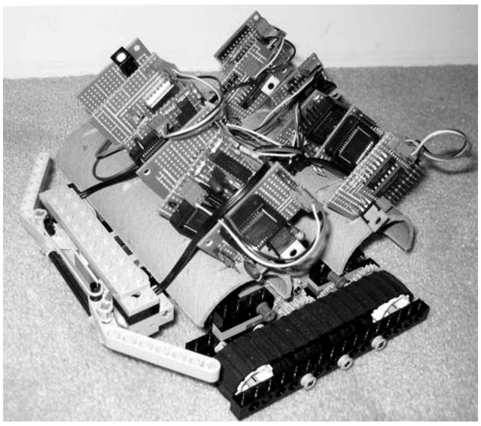

Figure 6. Robotic-Control Blocks Set prototype robot

RCBs can also have advanced behavior-based architectures with the possibility of many complex functions [8]. Different types of learning schema can be implemented such as genetic algorithms and fuzzy behavioral control. The agent can expand to accommodate dozens of different sensors and tensions which can be discharged through various behaviors by means of actuators. These advanced blocks may allow for functions that vary from voice generation and recognition to cognitive learning and evolution. Future advanced blocks will only have basic rules coded into them, so-called instincts, and will evolve over time to into complex functions.

4 Concluding remarks

After the completion of the first prototype set, some changes and future developments to the current block sets became evident and are possible. First of all, since the blocks were developed on through-hole prototype boards and wire connections were used, some of the connections are fragile. The power, ground, and clock headers are designed to be irreversible; however, proper irreversible headers should be added for the signal lines. Using a single voltage to power all devices would also simplify the design. This could be accomplished by using only a 5V or 3.3V power supply and then use charge pumps for higher voltages when necessary. Once the design for each and every block is finalized completely, the RCBs should be transferred to printed circuit boards or a CMOS IC which will make them more durable and aesthetically appealing.

The development and testing of Robotic-Control Blocks (RCB) has been quite successful thus far. Since the blocks adhere to psychodynamic architecture and substitute Pulsed Para-Neural Networks, they are a suitable hardware test bench for ATR Artificial Brain Project. The basic RCBs set worked as expected. By adding the Obstacle Avoidance Set and Meta-Sensing Set on the run, it was shown that a number of new tensions and behaviors can be added. The practically unlimited scalability is the most important virtue of RCB approach. Furthermore, the blocks are self-contained, operate in real-time, and do not require a PC. The development should be considered a step in the correct direction but more research and development in other fields is still necessary before achieving the ultimate goal of emergent thought. When a bigger block set is created and evolution is incorporated into the system, the covered functionalities will deserve to be moved into a future-generation evolvable hardware. Regardless, if implemented as dedicated chips and enclosed in aesthetic cases, RCBs right now may be used in classroom as an inexpensive aid free of tedious programming.

Acknowledgments. This research was a part of the *Research of Human Communications* sponsored by the National Institute of Information and Communications Technology of Japan (NICT). A. Stefanski's work was made possible thanks to the Coop Japan Program. The authors also thank Dr. Marek Syrzycki and Dr. Shahram Payandeh for their invaluable critical review and suggestions.

REFERENCES

[1] Lund H.H. "Intelligent Artefacts", Proceedings of the Eighth International Symposium on Artificial Life and Robotics, Japan, p. I-11-14, 2003.

[2] Buller A., Hemmi H., Joachimczak M. , Liu J., Shimohara K., and Stefanski A. ATR "Artificial Brain Project: Key Assumptions and Current State", Ninth International Symposium on Artificial Life and Robotics (AROB 9th '04), Beppu, Japan, p. 166-169, 2004.

[3] Liu J. and Buller A "Tension and Conflicts: Towards a Pleasure Seeking Artifact", Proceedings, 5th IFAC Symposium on Intelligent Autonomous Vehicles, Lisboa, Portugal, 2004, to appear.

[4] Buller A., Harada Y., Joachimczak M., Lee S.-I., and Tuli T.S., "Tension-driven behaviours of a mobile robot - Early experimental results", Proceedings of the Eighth International Symposium on Artificial Life and Robotics, Japan, p. 510-512, 2003.

[5] Best B., "Basic Neuron Physiology", http://www.benbest.com/science/anatmind/anatmd1.html, Accessed: December 2003.

[6] Martin, F.G. Robotic Explorations: A Hands-on Introduction to Engineering, Prentice Hall, 2001.

[7] Brooks R. Flesh and Machines: How Robots will Change Us, Pantheon Books, 2002.

[8] Arkin, Ronald C. Behavior-Based Robotics, MIT Press, 2000.

The Tenth International Symposium on Artificial Life and Robotics 2005(AROB 10th '05),
B-con Plaza, Beppu, Oita, Japan, February 4-6, 2005

Human-robot communication through a mind model based on the Mental Image Directed Semantic Theory

Masao Yokota — *Fukuoka Institute of Technology* — *yokota@fit.ac.jp*

Masato Shiraishi — *Fukuoka University of Education* — *siraisi@fukuoka-edu.ac.jp*

Genci Capi — *Fukuoka Institute of Technology* — *capi@fit.ac.jp*

Abstract

The Mental Image Directed Semantic Theory (MIDST) has proposed a methodology for integrated multimedia information understanding, for example, cross-media translation. This paper describes a multi-agent model of human mind based on MIDST and its application to human-robot communication.

1. Introduction

On the way to grow up from infant to adult, people would sometimes encounter curious but instantly understandable sentences such as S1-S4. This curiosity perhaps comes from their apparently unscientific contents while such understandability perhaps comes from our everyday perceptive experiences in space and time.

(S1) Time passes swiftly (or slowly).
(S2) It is the longest day.
(S3) The Andes Mountains run south and north.
(S4) The road sinks to (or rises from) the basin.

In near future, this kind of human mental phenomenon may lead to a certain barrier preventing humans and robots from comprehensible communication by natural language. This is because both entities can be equipped with sensors, actuators and brains of different performances and their vocabularies may well be grounded on quite different sensations, physical actions or mental actions. And in turn such a situation may bring inevitably different kinds of semantics to them, so called, "Natural Semantics (NS)" for humans and "Artificial Semantics (AS)" for robots.

The authors have been trying to develop such a methodology that can integrate NS and AS into a certain "Compatible Semantics (CS)" and that ultimately can lead to such a "Compatible Mind Model (CMM)" that is intended to organize CS autonomously [1]. The CMM is one kind of the multi-agent models [2]. Its most distinctively remarkable point is that it works by computing mental phenomena representations so called 'Locus formulas' based on the Mental Image Directed Semantic Theory (MIDST) [3], whose validity has been proven by the successful results of several versions of the intelligent system IMAGES [3], [6], [7], [9].

In this paper are presented a multi-agent model of human mind aimed at CMM, a brief description of MIDST as framework for CMM, several significant postulates for the basis of CS, formalization of communication, and their implementation on the intelligent system IMAGES-M.

2. Multi-agent model of human mind

The authors have proposed a prototype model of human mind consisting of Stimulus, Knowledge, Emotion and Response processing agents as shown in Figure1 [1]. This is a functional model of human central nervous system consisting of the brain and the spine.

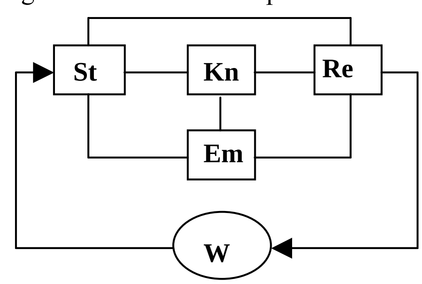

St: Stimulus processing agent.
Kn: Knowledge processing agent.
Em: Emotion processing agent.
Re: Response processing agent.
W: World surrounding human mind, including his/her body.

Figure 1. Multi-agent model of human mind.

The basic performances of the agents are as follows.

(1) Stimulus processing agent (**St**) receives stimuli from **W** and encodes them into mental images (i.e. encoded sensations) such as *"I sensed something oily."* (if verbalized in English.)
(2) Knowledge processing agent (**Kn**) evaluates mental images received from the other agents based on its memory (i.e. knowledge), producing other mental images such as *"It is false that the earth is flat."*
(3) Emotional processing agent (**Em**) evaluates mental images received from the other agents based on its memory (i.e. instincts), producing other mental images such as *"I like the food."*

(4) Response processing agent (**Re**) converts mental images (i.e. encoded physical actions such as *"I'll walk slowly."*) received from the other agents into real physical actions against **W**.

A *performance* ***P*** against a *stimulus X* with a *result Y* at each agent can be formalized as a function by the expression (1).

$$Y=\boldsymbol{P}(X), \quad (1)$$

where

P : a combination of ***atomic performances*** described later,

X : a spatio-temporal distribution of stimuli from **W** to **St** or a mental image for another agent, and

Y : a series of signals to drive an actuator for **Re** or a mental image for another agent.

A performance ***P*** is assumed as a function formed either consciously or unconsciously. In a conscious case, a set of atomic performances are to be chosen and combined according to *X* by a meta-function, so called, '***Performance Selector*** (PS)' assumed as '***Conscience***'. On the contrary, in an unconscious case, such a performance as associated most strongly with *X* is to be applied automatically [8]

3. MIDST as framework for CMM

MIDST has modeled mental images as "Loci in Attribute spaces" [3], [7]. An attribute space corresponds with a certain measuring instrument just like a barometer, a map measurer or so and the loci represent the movements of its indicator. The performance of 'Attribute space' is the model of '***Atomic performance***' introduced in Section 2.

A general locus is to be articulated by "Atomic locus" formalized as the expression (2) in first-order logic, where "L" is a predicate constant.

$$L(x,y,p,q,a,g,k) \quad (2)$$

The expression (2) is called "Atomic locus formula" whose arguments are referred to as 'Event Causer', 'Attribute Carrier', 'Initial Attribute Value', 'Final Attribute Value', 'Attribute Kind', 'Event Kind' and 'Standard Attribute Value', respectively.

The interpretation of (2) is as follows, where "matter" means "object " or "event".

"Matter 'x' causes Attribute 'a' of Matter 'y' to keep (p=q) or change (p ≠ q) its values temporally (g=Gt) or spatially (g =Gs), where the values 'p' and 'q' are relative to the standard 'k'."

When g=Gt and g=Gs, the locus indicates monotonous change or constancy of the attribute in time domain and in space domain, respectively. The former is called 'temporal event' and the latter, 'spatial event'.

For example, the motion of the 'bus' represented by S5 is a temporal event and the ranging or extension of the 'road' by S6 is a spatial event whose meanings or concepts are formalized as expressions (3) and (4), respectively, where the attribute is "physical location" denoted as *A12*. We think that the verb 'run' used in S6 must reflect the motion of the observer's attention [4].

(S5) The bus runs from Tokyo to Osaka.

$$(\exists x,y,k)L(x,y,\mathrm{Tokyo},\mathrm{Osaka},A12,Gt,k)\wedge \mathrm{bus}(y) \quad (3)$$

(S6) The road runs from Tokyo to Osaka.

$$(\exists x,y,k)L(x,y,\mathrm{Tokyo},\mathrm{Osaka},A12,Gs,k)\wedge \mathrm{road}(y) \quad (4)$$

The expression (5) is the conceptual description of the English word "fetch", implying such a temporal event that 'x1' goes for 'x2' and then comes back with it, where 'Π' and '•' are instances of the tempo-logical connectives, 'SAND' and 'CAND', standing for "Simultaneous AND" and "Consecutive AND", respectively.

In general, a series of atomic locus formulas with such connectives is called simply 'Locus formula'.

$$(\exists x1,x2,p1,p2,k)\ L(x1,x1,p1,p2,A12,Gt,k)$$
$$\bullet\ (L(x1,x1,p2,p1,A12,Gt,k)\Pi L(x1,x2,p2,p1,A12,Gt,k))$$
$$\wedge x1\neq x2\ \wedge p1\neq p2 \quad (5)$$

In order for complete representation of temporal relations, we have introduced a concept called 'Empty Event (EE)' and symbolized as 'ε' which stands exclusively for time collapsing. For example, (6) represents 'X_1 during X_2 '.

$$(\varepsilon_1 \bullet X_1 \bullet \varepsilon_2)\ \Pi\ X_2 \quad (6)$$

The image model presented here is also valid for formalizing word concepts (i.e. coding) of actions because any action must be measured with sensors for its formalization. That is, ***grounding words on actions is equivalent to grounding words on sensations of actions***

Sensors and actuators are assumed to collaborate very closely in feedback or feed-forward ways in cybernetics and there is a hypothesis that some kinds of sensations (or perceptions) and actions are encoded in the same way in organisms [5]. If not, real-time coordination of multiple sensors and actuators would be impossible. 'Mimicking' may be a good support for this hypothesis.

As easily imagined, if an attribute space corresponds to one of human senses, then its loci associated with certain words belong to NS, otherwise to AS.

4. Formalization of communication

At first, we formalize a piece of information (***I***) as a set of messages (*m*'s) in the expression (7).

$$\boldsymbol{I}=\{m_1, m_2, \ldots, m_n\} \quad (7)$$

In turn, a message (*m*) is defined in the expression (8), where *D, S, R* and *B* mean the duration, sender(s), receiver(s) and the body of the message, respectively.

$$m=(D, S, R, B) \quad (8)$$

The body (B) consists of the two elements shown in the expression (9), where *E* and *T* mean the event referred to and the task requested or intended by the sender, respectively.

$$B=(E, T) \tag{9}$$

For example, each item of the message m_0: "Fetch me the book from the shelf, Tom" uttered by Jim during the time-interval $[t_1, t_2]$ is as follows:

$m_o=(D_0, S_0, R_0, B_0)$, $B_0=(E_0, T_0)$,

$D_0=[t_1, t_2]$, $S_0=$ *"Jim"*, $R_0=$ *"Tom"*,

$E_0=$ *"Tom FETCH Jim BOOK FROM SHELF"*,

and $T_0=$ *"realization of* E_0*"*.

The authors have found that there are almost unique correspondences between the kinds of tasks (T's) and the types of sentences as shown in Table 1, which are very useful for computation.

Table 1. Sentence types and Tasks.

Sentence type (Examples)	Task (T)
Declarative (It is ten o'clock now.)	To believe E.
Interrogative ([A] Is it ten o'clock now? [B] What time is it now?)	[A] To reply whether E is true or false. [B] To reply what makes E true.
Imperative (Show me your watch.)	To realize E.

5. Human-robot communication

The authors have planned to implement IMAGES-M [6] on real robots as a mind model. One of the most significant works of robots equipped with IMAGES-M is to help people by performing dialogs with them. For example, assume such a scenario as follows:

…***A human 'Masato' and a humanoid robot 'Robbie' encounter at the terrace in front of the room where a Christmas party is going on merrymaking. Masato says "Robbie, please fetch me a colorful sweet soft scentless candy from the noisy room." Robbie replies "OK, Masato."….***

Robbie interprets Masato's statement as the expression (10) that reads "If Robbie fetches Masato the candy (***E1***), then consecutively it makes Masato happier (***E2***)," or as its logical equivalent, the expression (11), reading "It is not the case that Robbie fetches Masato the candy and consecutively it does not make Masato happier." Both the expressions are adopted in MIDST as the canonical conceptual structures of an imperative sentence.

$$\boldsymbol{E1} \rightarrow_c \boldsymbol{E2} \tag{10}$$

$$\sim(\boldsymbol{E1} \bullet \sim \boldsymbol{E2}) \tag{11}$$

where

$\boldsymbol{E1} \Leftrightarrow (\exists x1,x2,k1,\ldots,v,\mathbf{C})$ (L(R,R,M,x2,A12,Gt,k1)$\bullet$
(L(R,R,x2,M,A12,Gt,k1)ΠL(R,x1,x2,M,A12,Gt,k1)))
Π($\underline{\text{L(v,x1,c1,c2,A32,Gs,k2)}\bullet}$
$\underline{\text{L(v,x1,c2,c3,A32,Gs,k2)}}$
$\underline{\bullet\cdot\ldots\bullet\cdot\text{L}(\text{v,x1,}c_{m-1},c_m\text{,A32,Gs,k2})}$)
Π L(v,x1,Sweet,Sweet,A29,Gt,k3)
Π L(v,x1,Soft,Soft,A24,Gt,k4)
Π L(v,x1,/,/,A30,Gt,k5)
ΠL(v,x2,Noisy,Noisy,A31,Gt,k6)
$\wedge$ candy(x1) $\wedge$ room(x2) $\wedge$ $\mathbf{C}$={c1,c2,…,ci} $\wedge$ #($\mathbf{C}$) >1

$\boldsymbol{E2} \Leftrightarrow (\exists e1,e2,k7)$ L($\boldsymbol{E1}$,M,e1,e2,B04,Gt,k7) $\wedge$ e2>e1.

The special symbols and their meanings in the expressions above are:

'X→c Y' ='If *X* then consecutively *Y*', *'R'*='Robbie', *'M'*='Masato', '**C**'='the total set of colors', *'#(**X**)'*='cardinal number of set **X**', *'A29'*='taste', *'A24'*='touch', *'A30'*='smell', *'/'*='absence of value', *'A31'*='sound', *'A32'*= 'color', and *'B04'*= 'happiness (=degree of happiness)'

According to Table1, Robbie's task (T) is only to make ***E1*** come true where each atomic locus formula is associated with his actuators/sensors. By the way, the underlined part of ***E1*** represents the spatial distribution of colors over the candy referred to by the word 'colorful'. Of course, Robbie believes that he will become happier to help Masato, given by expression (12) where 'B03' is 'trueness (=degree of truth)'and 'K_B' is a certain standard of 'believability'. That is to say *emotionally*, Robbie likes Masato. Therefore, this example is also very significant for intentional sensing and action of a robot driven by logical description of its belief.

$$(\exists p)\text{L}(\text{R},\boldsymbol{E},\text{p},\text{p},\text{B03},\text{Gt},K_B) \wedge p>K_B$$
$$\wedge\ \boldsymbol{E} = \boldsymbol{E1} \rightarrow_c \boldsymbol{E2} \tag{12}$$

For constructing a plausible CMM it is most essential to find out functional features of human mind and to formalize them as postulates that rule the performances of CMM and form the basis of CS [1]. APPENDIX shows some of such postulates and examples of dialog processing by IMAGES-M based on them.

6. Discussions and conclusions

The mind model proposed here is much simpler than Minsky's [2] but the locus formula representation can work for representing and computing mental phenomena fairly well as shown in APPENDIX. One of the most important problems to be solved is how to realize the atomic performances corresponding to attribute spaces, including the meta-function '*conscience'*. In order to solve this problem, we will consider the application of soft computing theories such as neural network, genetic algorithm, fuzzy logic, etc. in the future.

References

[1] Yokota, M. & Shiraishi: "A multi-agent mind model for comprehensible communication between humans and robots", Reports of CSL, FIT, 18, pp.1-9, 2004.

[2] Minsky, M: The society of mind, Simon and Schuster, New York, 1986.
[3] Yokota, M. *et al.*: "Mental-image directed semantic theory and its application to natural language understanding systems'', Proc. of NLPRS'91, pp.280-287, 1991.
[4] Rybak, I.A., *et al*: "A model of attention-guided visual perception and recognition", Vision Research, 38, pp.2387-2400, 1998.
[5] Prinz, W.: "A common coding approach to perception and action", In *Relationships between perception and action* (Neumann, O. and Prinz, W. eds.), pp.167-201, Springer-Verlag, 1990.
[6] Hironaka, D., Oda, S., Ryu, K., and Yokota, M.: "Mutual Conversion of Sensory Data and Texts by an Intelligent System IMAGES-M'', Proc. of the 8th International Symposium on Artificial Life and Robotics (AROB '03), pp.141-144, 2003.
[7] Yokota, M. and Hironaka, D.: "Cross-media translation based on Mental Image Directed Semantic Theory toward more comprehensible communication between humans and robots", Proc. of AINA '04 IEEE, Fukuoka, 2004.
[8] Brooks, R. A.: "A robust layered control system for a mobile robot", IEEE Journal of Robotics and Automation, RA-2, pp.14-23, 1986.
[9] Oda, S., Oda, M.and Yokota, M.: "Conceptual Analysis and Description of Words for Color and Lightness for Grounding them on Sensory Data'', Trans. of JSAI, 16-5-E, pp436-444, 2001.

APPENDIX

Examples of postulate-based dialog processing by IMAGES-M, where 'H' and 'S' mean a human's and IMAGES-M's utterance, respectively.

[Dialog 01]
Postulate 01: "Sensation precedes perception in humans."
H: Tom heard Mary sing "Hey, Jude".
H: Did he sense any sounds?
S: Yes, he did.

[Dialog 02]
Postulate 02: "There are sensor-specific pieces of knowledge in humans."
H: Tom knows Mary by sight.
H: Is he familiar with her?
S: No, he isn't.

[Dialog 03]
Postulate 03: "Perceived matters are memorized as facts belonging to knowledge in humans."
H: Tom saw Mary move to Tokyo.
H: What did Tom know about Mary?
S: He knew that she went to Tokyo.

[Dialog 04]
Postulate 04: "Intentional performances are necessarily accompanied by decisions in humans."
H: Tom sold his book to Mary.
H: Did Tom decide to sell his book?
S: Yes, he did.

[Dialog 05]
Postulate 05: " Desire precedes decision in humans."
H: Tom decided to sell his book.
H: What did he want?
S: He wanted someone to buy his book.

[Dialog 06]
Postulate 06: "For humans, a desire for something is a belief of becoming happier with it."
H: Tom wants to go to Tokyo.
H: Does Tom believes to become happier if he goes to Tokyo?
S: Yes, he does.

[Dialog 07]
Postulate 07: "Some emotion can coexist with another in humans."
H: Tom loves Jane.
H: Whom does he like?
S: He likes Jane.

[Dialog 08]
Postulate 08: "A physical object has never two values of an attribute."
H: Tom melted the ice (*into water*) and drank it.
H: Did he drink the ice?
S: No. He drank the water.

[Dialog 09]
Postulate 09: "Communication is not transfer but duplication of information."
H: Tom said to Mary that his mother was sick.
H: Who knew that Tom's mother was sick?
S: Tom and Mary did.

[Dialog 10]
Postulate 10: "A spatial event is reversible."
H: The path sinks to the brook.
H: Does the path rise from the brook?
S: Yes, it does.
H: The roads meet at the city.
H: Do the roads separate at the city?
S: Yes, they do.

The Tenth International Symposium on Artificial Life and Robotics 2005(AROB 10th '05),
B-con Plaza, Beppu, Oita, Japan, February 4-6, 2005

The Case for Radical Epigenetic Robotics

Alexander I. Kovács
Grad. Univ. Advanced Studies
Nat. Inst. of Informatics
2-1-2 Hitotsubashi, Chiyoda-ku
101-8430 Tokyo, Japan
aik@grad.nii.ac.jp

Haruki Ueno
Grad. Univ. Advanced Studies
Nat. Inst. of Informatics
2-1-2 Hitotsubashi, Chiyoda-ku
101-8430 Tokyo, Japan
ueno@nii.ac.jp

Abstract

We propose a way to study cognitive robotics whereby one completely departs from a task-centered methodology. The new approach, "radical epigenetic robotics", tries to chart new territory, likely not explored by task-centered approaches because there one starts with a certain cognitive task for a robot and then tries to come up with suitable "control" mechanisms in order to achieve this specific task. Arguably, this approach has a high risk of making many task-specific assumptions and of leaving unexplored possible mechanisms. To avoid these problems, radical epigenetic robotics starts not with an outside cognitive task, but from the inside, with the "control" mechanism, which we call "cognitive substrate"; the design of this "cognitive network" is the focus of research, resultant cognitive competencies of a robot are tested, ex post facto.

Keywords Epigenetic robotics, cognitive substrate, designer's dilemma

1 Introduction

The aim of this paper is to propose and justify a way of studying the fabrication of cognizers (in the form of robots) that jettisons one of the central assumptions in the field of cognitive robotics, viz., that one has to start from the cognitive competency that one wants to model. Only then, the assumptions goes, can one try to understand what mechanism to use to make progress. We turn things around: we start with the mechanism and then study what cognitive competencies result. We argue here, that this approach—if properly construed—is not at all foolish or blind (that is lacking a tangible goal).

Our approach, tentatively called "radical epigenetic robotics" (to be explained below), completely departs from standard task-centered methodologies. In a task-centered approach one starts with a certain cognitive task for a robot—say, wall-following, map-learning, gesture recognition, playing soccer, six-legged walking, learning of movement by imitation, object perception and learning, etcetera—and then tries to write developmental programs [1], evolve controllers [2], design behaviors [3], formulate knowledge to reason about[4] or somehow come up with suitable sensor-effector-mappings in order to achieve this specific task. While there is nothing wrong with this approach, one could argue that it (a) has a high risk of making many task-specific assumptions and (b) leaves unexplored possible "control" mechanisms.

Radical epigenetic robotics does not try to replace or compete with such task-centered approaches. It is complementary by trying to chart new territory; territory likely not explored by common approaches for reasons (a) and (b). In the next section we elaborate on why (a) and (b) are so common and why they can be problematic. In section 3 we take a quick look at the different flavors of robotics out there to position our approach and loosely define some important terms (such as "radical" and "epigenetic"). In section 4 we outline our proposal and in section 5 we elaborate on cognitive substrates. We conclude the paper with a discussion of some difficulties of our approach.

2 Problems with Task-Centered Approaches

[W]e must admit the likelihood that top-down reverse engineering will simply fail to encounter the right designs in its search of design space [5, p. 258]

Task-centered approaches—i.e. approaches that start with a certain cognitive task to be modelled—to repeat, can be said to (a) have a high risk of making many task-specific assumptions and (b) leave unexplored possible "control" mechanisms. Why is this so and what are the problems?

Regarding (a), there are of course good reason for simplifying assumptions. As Dennett [6, p. 308] puts it, "AI research, like all other varieties of research on this huge topic [understanding how the brain works - AIK], must make drastic oversimplifications in order to make even apparent progress."

However, such assumptions are often implicit and since they are made on a case-by-case basis this leads to many possibly incompatible models. An often voiced critique of artificial intelligence is that it works under the unjustified assumption that all the models in its different subfields will eventually be put together to result in truly intelligent systems that can, say, pass Harnad's Total Turing Test [7]. The critique is based on precisely the fact that many researchers work under different simplifying and implicit assumptions that can lead to utterly incompatible models.

As far as (b) is concerned, one could argue that by having a certain task in mind, one is likely to choose ways of achieving this task by utilizing techniques that will obviously or most likely work. In such a methodology, there are good reasons not to try out many (possibly much simpler) mechanisms for, at first sight, *they may just not look appropriate for the task at hand*; and so, as the epigraph states, one may "simply fail to encounter the right designs."

3 Oh No, Not Yet Another Robotics!

There are now a large number of different approaches to cognitive robotics. One finds (the original) cognitive [4], behavior-based [3], developmental [1], cognitive developmental [8], epigenetic [9], evolutionary [2], and adaptive neuro-robotics [10]. As it stands, the boundaries between them are not clear-cut, but what all these approaches, in one way or another, are addressing is how to get more out of the robots than was (and could have been) designed for; that is to have "control" mechanisms that do more than *just* control (whence the quotes).

The original cognitive robotics [4] was concerned with sense-plan-act style cognition where the planning component was based on logical programming languages, such as Golog. Cognition here was construed as *reasoning about X*, where X could be anything from goals, to perceptions, to actions, and so forth. Logicist cognitive robotics ignores learning and development setting it apart from the other approaches mentioned, which acknowledge that cognitive robots have to be "beneficiary of a longish period of infancy" [11, p. 157] in which certain cognitive structures develop and organize, rather than being fixed by the designer.

Our proposal shares this emphasis on epigenetic development, i.e., the development determined primarily by interaction rather than genes (that is a prior design), in the sense of Piaget [9]. Whatever the name, all approaches just mentioned are task-centered. The point of departure, and novelty, of our approach is that we believe that only by shifting the focus from specific tasks to appropriate, plausible "control" mechanisms (see below) can the the problems associated with task-centered approaches be avoided. This shift of focus to an inside-out approach is what we mean by "radical".

Dennett's quote above continues: "There are many strategies of simplification, of which [...] five, while ubiquitous in all areas of mind / brain research, are particularly popular in AI. [...] Many of the best-known achievements of AI have availed themselves of all five [...] strategies of simplifications [...]. Some critics hostile to any efforts in cognitive science enabled by these strategies, but *there is no point in attempting to 'refute' them a priori* [emphasis added - AIK]. Since they are strategies, not doctrines or laws or principles, their tribunal is 'handsome is as handsome does.'" So, rather than further argue against such simplifications we leave it at having justified our approach via (a) and (b) and take it (again) with Dennett [6, p. 309]: "one might just adopt some rival strategy or strategies, and let posterity decide which are the most fruitful."

4 Radical Epigenetic Robotics

To avoid problems (a) and (b), radical epigenetic robotics proposes to *not* start with a task-specification (outside), but focus on the inside mechanisms first. The five strategies of simplification mentioned above by Dennett are, in short, as follows:

- ignore both learning and development;
- ignore how isolated subcomponent under study might be attached to the larger system;
- hope that scaling-up from toy problem to real domain will be a straightforward extrapolation;
- bridge various gaps in one's model with unrealistic stopgaps; and
- avoid the complexities of real-time, real-world coordination.

Our research program tries to find new mechanisms that precisely don't make any of these assumptions, thats what we mean by *appropriate*. Since we aspires to avoid these simplifications, clearly, *something else has to give*. That something is that we will initially have to make do with the fabrication of rather simple proto-cognition. However, by definition, an appropriate mechanism will, e.g., scale well, make additions of new components easy, not introduce makeshifts whose fixing turns out problematic.

To be *plausible*, the mechanisms we investigate try to avoid as many known problematic assumptions as possible, such as e.g. regarding encodingist representation [12]. So, to be plausible, they must, e.g., be radical constructivist [13], interactivist [12], and there are other criteria. They must also offer a solution to what we call the Designer's Dilemma. Since we are talking about *fabricating* cognizers, qua artifact, there must be something that the engineer *designs*. We now know that neither behaviors nor knowledge are the right level we can design for cognition (this assertion is irrespective of whether we use machine learning or not) because the designer just cannot anticipate (and hence not accommodate) an infinite number of cases. The Designer's Dilemma forces us to focus on a level where we *can* (in principle) have complete knowledge, that is, not the cognitive task but the level of the cognitive substrate, as we call appropriate and plausible mechanisms for the fabrication of veritable cognizers.

5 Cognitive Substrates

We shall call an appropriate and plausible "control" mechanism *cognitive substrate*. By cognitive substrate we mean, roughly: the layer underlying or bringing about cognitive capabilities; so we could call the animal brain a "neurobiological cognitive substrate". The volume in design space of "control" mechanisms that we are specifically targeting is located where one finds what Varela et al. [14] have called "cognitive networks".

It would now be rather foolish to blindly try to find such mechanisms such that if implemented on a target robot architecture would lead to "interesting" behavior or what Beer calls minimally cognitive behavior [15]. We therefore urge to base the development of such cognitive substrates on a solid theoretical foundation, on a "general theory of cognitive systems". Apart from the animal brain, biologist have also for a while been speaking of the immune system as a "biological cognitive network" [16] with—though very much simpler [17]—similar capabilities to the brain (memory, perception, etc.). And if one looks at the literature on so-called complex adaptive systems one cannot help but notice the cognitively laden vocabulary used to talk about these systems. Though these parallels have been noticed and also lead to interesting applications, more general theoretical work is outstanding. We can, nevertheless, already guess at what our cognitive substrate might look like: a self-organizing, synergetic network of loosely-coupled anticipating self-sustained oscillatory elements.

The reader might now object, *How is this different from research into artificial neural networks (ANN); isn't that just such an approach where you start with a mechanism (the inside) and then see what you can do with it (the outside)?* The quip reply to this objection is: maybe, but nobody ever put ANN's in robots just to study "what happens". Besides, ANN's wouldn't be under such heavy fire from workers pointing out what ANN's cannot do to realize *whole* cognizers if they were even a suitable tool.

Whether ANN's (whatever kind you look at) have serious short-comings that rule them out as cognitive substrate (and they do) is besides the point. However, *how* to "hook up" the sensors and effectors of a robot with an ANN (whatever kind) to produce some form of proto-cognition is precisely the point of contention. Of course, you could just as well take ANN's and embark on the research program we propose. This hasn't been done yet and it is an open problem, whether any proto-cognition would be producible. That is, of course, if we start with a network which *hasn't been already trained for a certain task*, for in radical epigenetic robotics, there are no a priori tasks to train an ANN for.

6 Conclusion

> *Is this optimistic prospect an illusion? Is this bottom-up project as hopeless as trying to build a tower to the moon? You can't get there from here, say [...] the skeptics. Don't even try.* [18, p.196]

The radical epigenetic robotics approach proposed could perhaps be express by stating: "Let the robot think what it wants and do what it wants". As thus, the approach has a number of obvious disadvantages compared to other approaches and will likely face difficulties (and because of that, perhaps outright rejection). For example, since we start with a (theoretically motivated) cognitive substrate, and hopefully some predictions made by the theory as to the expected behavior of the system, the question remains how to evaluate resultant behavior of a robot. What counts as proto-cognition and how can it be verified to be veritable, i.e., attributable to the cognitive robot itself, and not some human designer. However, this problem of evaluation is an highly interesting problem by itself. Perhaps what is needed are new sciences of cognitive robot psychology and ethology.

A second problem (though not of the approach as such) is that the "general theory of cognitive systems" on which to base our proposed cognitive substrates doesn't yet exist. However, there are hints in the literature, such as a criterion differentiating cognitive from non-cognitive systems [16, 17]—we might want to call "Hershberg-Efroni-criterion"—which states, that "in a cognitive system the capabilities of the system are not preordained merely by the plan of the system but need interaction with their environment to define them exactly."

We are in an early phase of developing this new approach, but think it is timely to start debate.

Acknowledgements

AIK was supported by the Joint Studies Program of The Graduate University for Advanced Studies and an NII Fellowship Grant provided by Sumitomo Electric Industries, Ltd.

References

[1] J. Weng. Developmental robotics: Theory and experiments. *Int. J. of Humanoid Robotics*, 1(2):199–236, 2004.

[2] S. Nolfi and D. Floreano. *Evolutionary Robotics.* MIT Press, Cambridge, MA, 2000.

[3] R.A. Brooks. Intelligence without reason. A.I. Memo 1293, MIT, AI Lab, April 1991.

[4] R. Reiter. *Knowledge in Action: Logical Foundations for Specifying and Implementing Dynamical Systems.* MIT Press, Cambridge, MA, 2001.

[5] D.C. Dennett. Cognitive science as reverse engineering: Several meanings of "top-down" and "bottom-up". In Dennett [18], chapter 16, pages 249–259.

[6] D.C. Dennett. Cognitive ethology: Hunting for bargains or a wild goose chase. In Dennett [18], chapter 21, pages 307–322.

[7] S. Harnad. Minds, machines and Searle. *Journal of Theoretical and Experimental Artificial Intelligence*, 1:5–25, 1989.

[8] M. Asada, K.F. MacDorman, H. Ishiguro, et al. Cognitive developmental robotics as a new paradigm for the design of humanoid robots. *Robotics and Autonomous System*, 37(1):185–193, 2001.

[9] C. Balkenius, J. Zlatev, C. Brezeal, et al., editors. *Proc. 1st Int. Workshop on Epigenetic Robotics.* Lund, Sweden, 2001.

[10] T. Ziemke. The construction of 'reality' in the robot: Constructivist perspectives on situated artificial intelligence and adaptive robotics. *Foundations of Science*, 6(1):163–233, 2001.

[11] D.C. Dennett. The practical requirements for making a concious robot. In Dennett [18], chapter 9, pages 153–170.

[12] M. H. Bickard and L. Terveen. *Foundational Issues in Artificial Intelligence and Cognitive Science: Impasse and Solution.* Elsevier Science, New York, NY, 1995.

[13] E. von Glaserfeld. *Radical Constructivism: A Way of Knowing and Learning.* Falmer Press, London, 1995.

[14] F. Varela, A. Coutinho, B. Dupire, and N.Vaz. Cognitive networks: Immune, neural, and otherwise. In A. Perelson, editor, *Theoretical Immunology, Part II*, SFI Series on the Science of Complexity, pages 359–375. Addison-Wesley, Redwood City, NJ, 1988.

[15] R. A. Beer. Toward the evolution of dynamical neural networks for minimally cognitive behavior. In P. Maes, M. J. Mataric, J.-A. Meyer, et al., editors, *From Animals to Animats 4: Proc. Fourth Int. Conf. on Simulation of Adaptive Behavior*, pages 73–76, Cambridge, MA, 1996. MIT Press.

[16] U. Hershberg and S. Efoni. The immune system and other cognitive systems. *Complexity*, 6(5):14–21, 2001.

[17] U. Hershberg. Proposing a new focus for the study of natural and artificial cognitive systems. In C.G. Prince, Y. Demiris, Y. Marom, et al., editors, *Proc. 2nd Int. Workshop on Epigenetic Robotics*, Edinburgh, Scotland, 2002.

[18] D. C. Dennett, editor. *Brainchildren: Essays on Designing Minds.* Bradford Books, 1998.

The Tenth International Symposium on Artificial Life and Robotics 2005(AROB 10th '05),
B-con Plaza, Beppu, Oita, Japan, February 4-6, 2005

Development of a robotic surgical manipulator for Minimally Invasive Surgery

Ho-Seok Song
Dept. of Mechanical Engineering
Korea Advanced Institute of Science and Technology,
Taejon, Korea 305-701
hosek@kaist.ac.kr

Jong-Ha Chung
Dept. of Mechanical Engineering
Korea Advanced Institute of Science and Technology,
Taejon, Korea 305-701
jongha@imhp.kaist.ac.kr

Jung-Ju Lee
Dept. of Mechanical Engineering
Korea Advanced Institute of Science and Technology,
Taejon, Korea 305-701
jjlee@mail.kaist.ac.kr

Abstract

Minimally Invasive Surgery (MIS) is surgery of the chest, abdomen, spine and pelvis, done with the aid of a viewing scope, and specially designed instruments. Benefits of minimally invasive surgery are less pain, less need for post-surgical pain medication, less scarring and less likelihood for incisional complications. Since the late 1980's, minimally invasive surgery has gained widespread acceptance because of the such advantages. However there are significant disadvantages which have, to date, limited the applications for these promising techniques. The reasons are limited degree-of-freedom, reduced dexterity and the lack of tactile feeling. To overcome such disadvantages many researchers have endeavored to develop robotic systems. Even though some robot aided systems achieved success and commercialized, there still remain many thing to be improved. In this paper, the robotic system which can mimic whole motions of a human arm by adding additional DOF is presented. The suggested design is expected to provide surgeons with improved dexterity during minimally invasive surgery.

Keywords— minimally invasive surgery, articulated manipulator, and robot aided surgery

1. Introduction

Minimally Invasive Surgery (MIS) is surgery of the chest, abdomen, spine and pelvis, done with the aid of a viewing scope, and specially designed instruments. In these procedures, a slender imaging prove is typically introduced via a puncture incision. The surgical site is viewed through a videoscope equipped with a miniature video camera. A CRT screen displays the resultant camera output. In the abdomen, carbon dioxide is pumped in to create viewing a working room. Tools are fed through additional puncture incisions using trocars. The benefits of minimally invasive surgery are many. Traditional surgery often requires a lengthy hospital stay and weeks of recovery. With minimally invasive surgery, many procedures require one to two days or less in the hospital and recovery time is generally shorter. That usually means that patients can get back to their normal routines quicker. The faster recovery is possible because there are only a few small incisions requiring a stitch or two instead of a large incision through the skin and muscles. Other benefits of minimally invasive surgery are less pain, less need for post-surgical pain medication, less scarring and less likelihood for incisional complications. Since the late 1980's, minimally invasive surgery has gained widespread acceptance because of the such advantages. However there are significant disadvantages which have, to date, limited the applications for these promising techniques [1]-[3]. For example the standard laparoscopic instruments used in many minimally invasive procedures do not provide the surgeon the flexibility of tool placement found in open surgery. As the instrument slide, twist and pivot through the trocar (the point at which instruments enter the body wall), they are four–degree–of-freedom manipulators. Conse- quently the surgeon can reach points within a three-dimensional volume but cannot fully control orientation. Most current laparoscopic tools have rigid shafts, so that manipulation of delicate and sensitive can be difficult while manipulating these long-handled tools from outside the body [3]. Additionally, the fact that the port in the patient's abdomen (trocar) acts as a laterally restrictive pivot point for the body of the positioning apparatus complicates the proper positioning of the surgical tools. Because entry portal (trocar) is embedded in abdominal wall, it cannot be perfectly fixed. This allows the movement of entry portal which acts as a fulcrum and it leads to the lack of dexterity and sensitivity of endoscopic tools [4]. Moreover trocar makes the direction of the surgeon's hand motion reverse at the instrument tip. The video monitor is often located on the far side of the patient, and the difference in orientation between the endoscope and the monitor requires the surgeon to perform a difficult mental transformation between visual and tool coordinate frames. Impaired contact force reception by friction and absence of distributed tactile information also become problems. Although many abdominal operations can be performed laparoscopically at this moment in time, performance of complex minimally invasive surgery is in the hands of a limited number of experts. Therefore, researchers have started to develop new tools for laparoscopic surgery to minimize the unsatisfactory aspects of the process [5]. The launch of robotic telemanipulation system heralds this development.

Reduced dexterity and impaired visual control were considered the major burdens of endoscopic surgery and initial attempts in developing robotic endoscope support systems aimed at enhancing the surgeon's control of the scope. AESOP® (Computer Motion, Inc.) and Endoassist® (Armstrong Healthcare, Inc.) are representative works among laparoscope support systems. While developments in imaging systems clearly progressed, dexterity problems remained a crucial problem. In the early 1990s, the concept of a master-slave tele-manipulator was developed. This concept required the surgeon to control a manipulation system from a master console remote from the patient. A computer uses computing power to support the surgeon's dexterity. The surgeon moves two master devices made to resemble surgical instruments at the console, and each motion is translated to the robotic arm which scale down the movements at the end of the instruments inside the patient's body. The robotic slave arm follows all commands of the master arm in a natural way, comparable to manipulation in open surgery. Many researchers have developed robot aided minimally invasive surgery systems. Among them, da Vinci® (Intuitive Surgical, inc.) and ZeusTM (Computer Motion, Inc.) telemanipulation systems received FDA clearance. The major advantage of these newer master-slave robotic systems is the introduction of extra degrees-of-freedom at the end of the instruments, allowing surgeons to manipulate in a manner similar to that of open surgery. The ZeusTM offers five DOF and da Vinci® offers six DOF by using the Endowrist® system. In addition, the unnatural opposite response of the instruments is corrected by the robotic telemanipulation systems. Tremors and trocar resistance are eradicated by the man-machine interface. The digital processing allows the scaling down of the surgeon's hand movements to a level where micro-vascular procedures are feasible. The ergonomic and reduced fatigue features will be a great advantage [5].

2. Design Concepts

Previously described robotic tele-manipulation systems potentially offer great benefits for minimally invasive surgeries. However there still remain several points to be improved in the aspect of dexterity. In open procedure, the surgeon has unlimited flexibility in positioning his body, elbow, wrist and fingers; the operative field may be approached from various direction. The most up-to-date robotic MIS systems have six-degrees-of-freedom; four at the entry portal and two at the end of tool. These, so to speak, resemble the human arm which just has wrist and shoulder and no elbow. Some researchers reported that if we could develop either mechanical or electromechanical teleoperators which enable surgeons to move a MIS system in a manner analogous to an open instrument, we could potentially reduce the time of current laparoscopic procedures by at least 15% and we could perhaps also enable surgeons to perform procedures which are currently too difficult [6]. This result shows that the robotic system which can mimic whole motions of a human arm by adding additional DOF may have more powerful usages. This is the first and underlying premise of our design. The second premise is that the entry portal, trocar, which acts as a fulcrum is having bad effects on the dexterity and the repeatability of surgery tool. The most serious reason is that the fulcrum does not be firmly fixed. The most movements of conventional tools for minimally invasive surgery depend on that through the trocar and very few movements which are not effected by the motion of the trocar is achieved. Thus the main design concept of this research is to add two DOF rotational joint at the surgery tool so that this added joint function as a human elbow (Fig.1). By adopting this mechanism, the surgery tools can behave like a human arm because the type of degree-of-freedom of the trocar (3-rotations and 1-translation) is exactly same that of a shoulder and the type of degree-of-freedom of tool tip (2-rotations; perpendicular to the longitudinal axis) and added joint (2-rotations; one is perpendicular and the other is parallel to the longitudinal axis) are same that of a wrist and an elbow respectively. Moreover the added joint is not affected by the movement of the trocar because it is placed inside the abdomen during surgery. Thus the space where the surgery tool can move independently to the trocar is enlarged and the dexterity and the repeatability are enhanced**.**

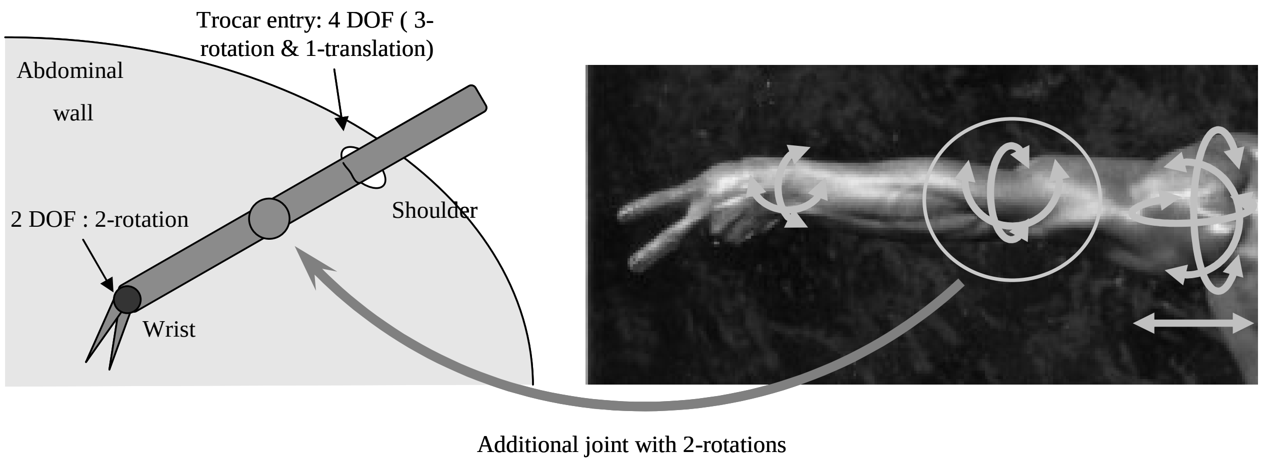

Fig 1. Design Concept

3. Design Requirements

There are several design requirements which should be satisfied for robotic tools to be used at minimally invasive surgery. Typical properties are size, force which can be produced at the tool tip, speed, repeatability, dexterity, workspace, weight, and convenience to operators.

Size : The surgery tool is inserted into the patient's abdomen through a trocar, so that the width of a tool should not exceed the size of conventionally used trocar. The size of currently used trocar is rarely above 10mm. Thus we will design the surgery tool with 10mm diameter.

Force : It is generally known that the amount of force needed for fine motion tasks such as suturing is roughly 10N at the gripper [3]. Thus we set the lower limit of required force as 10N.

Speed : In the aspect of speed we need about 3-5 Hz for the joints to achieve a speed comparable to human fingers.

Repeatability : The human's end repeatability is known about 1mm. In due consideration of practical fabrication process, our design goal for repeatability is under 0.25mm.

Dexterity : The suggested design has more joint and degree-of-freedom than conventional robotic surgery tools, it will inherently shows improved dexterity. Thus design goal is the maximization of the dexterity through whole workspace by rearranging kinematic parameters.

Workspace : As written at dexterity, workspace is also enlarged by adopting the additional joint. Thus maximization of not workspace but dexterous workspace is our design object.

Convenience to operators : Originally this parameter is the most important point to be considered during the design process. Thus the link length of surgery tool is determined by continuous simulation and consultation with surgeons.

4. Design in detail

The main idea of suggested design is to add the additional joint which behaves like an elbow. In human arm, an elbow joint moves with two rotational degrees-of-freedom; one is perpendicular to the longitudinal axis and the other is parallel to the axis. To adopt this type motion, the differential mechanism is used (Fig.2). The differential mechanism is composed of three bevel gears whose axes intersect mutually through a common point at right angle. Two gears are input (gear 1 & 2) and one

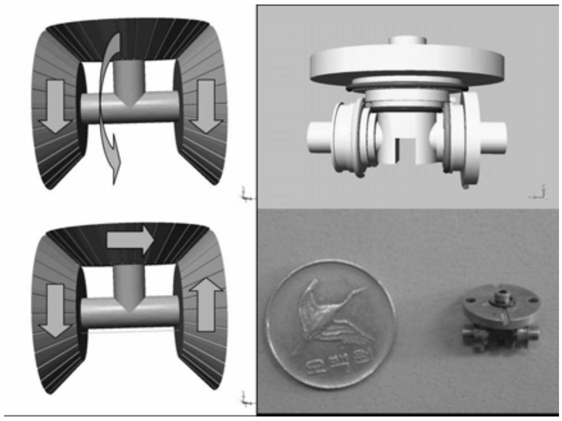

Fig 2. Differential Drive

(gear 3) is output device. When input gears rotate to same direction, the output gear is turned on the axis of input gear. When input gears rotate to opposite directions, the output gear is turned on the longitudinal axis. This is the exactly same motion with a human elbow. The suggested design shows 45-degrees motion range of output gear at each rotational axis. The wrist part should be able to be manipulated with two axes which are perpendicular to longitudinal axis. To this end, the universal joint may be best solution. But universal joint has a intersect axis which looks like a cross and it is very difficult to drive such a part by using a wire. To solve this problem, rotational axes are split apart and are driven separately. But this design needs one more joint than that of universal joint and it makes the manipulator become more complex and pliable. To overcome this drawback, the axis for tool tip rotation and the axis for tool opening are joined together and two parts of a tool tip are driven separately (Fig.3). In this design, the average of two rotations (pulley 1 & 2) represents the change of the orientation of tool end and the difference between two rotations does the tool tip opening angle. Thus the orientation and the tool opening angle can be controlled in one axis.

Because wire-mechanism is only operated when tension-force work on it, wire-driven system requires 2n wires to control n-DOF motion. In our system, we need 6 wires to control 3 DOF motion of tool tip (pitching in wrist, gripping and yawing in hand). However, the space where driving mechanisms are to be installed is restricted by size of trocar, and wires must be passed

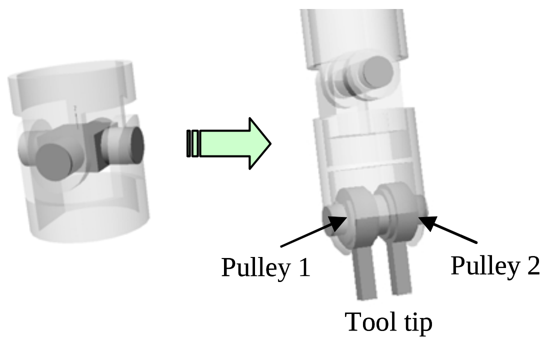

Fig 3. Universal joint and suggested design

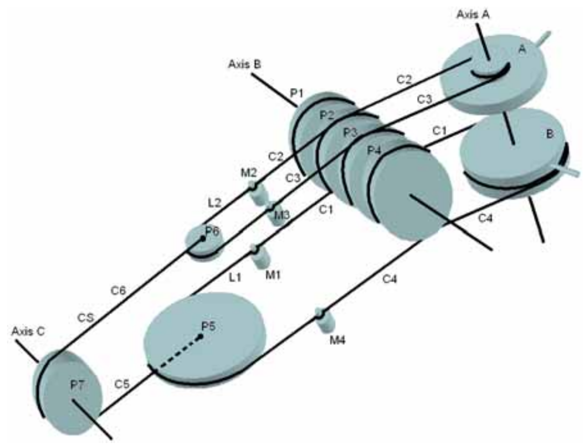

Fig 4. Schematic diagram for cabling

through axle of bevel gear of differential drive. Therefore, technique that can reduce number of wire is required. Consequently, only 4 wires are required to pass through axle of the upper bevel gear by adopting following technique.[7]

As shown in fig.4, this system is composed of 2 capstans, 7 pulleys and 4 motors. Cables C1 and C4 form two sides of a continuous loop L1. Cable C1 of loop L1 engages proximal pulley 5, drive shaft of motor M1, intermediate pulley P1, and driven capstan B. Loop L1 returns from capstan B as cable C4 and engages intermediate pulley P4, drive shaft of motor M4, and proximal pulley P5. The cables C1 and C4 are fixed to capstan A in order to pull it.

In the same manner, Cables C2 and C3 form two sides of a continuous loop L2. Cable C2 of loop L2 engages proximal pulley 6, drive shaft of motor M2, intermediate pulley P2, and driven capstan A. Loop L2 returns from capstan A as cable C3 and engages intermediate pulley P3, drive shaft of motor M3, and proximal pulley P6. The cables C2 and C3 are fixed to capstan B.

Fig 5. overall shape of surgical tool

Cable C5 and C6 form two sides of a single cable CS that engages pulley P7.

The movement of wrist and fingers acts like following. If motors M1 and M4 rotate in opposite direction, capstan A will rotate for gripping and yawing. Likewise if motors M2 and M3 rotate in opposite direction, capstan B will rotate. If motors M1 and M4 rotate in the same direction, motors M2 and M3 rotate in the same direction, but in opposition to M1 and M4, then the wrist will pitch about axis B.

The surgery tool is composed of previously described parts and is shown in Fig.5. It is expected to make the surgery tool be applied more various tasks.

5. Summary

This paper presents the design of the dexterous manipulator for minimally invasive surgery. The capability of the suggested surgery tool is enhanced by adopting additional joint which acts like a human elbow joint. The improved manipulability may contribute to performing complex tasks during surgery and popularization of minimally invasive surgery.

Acknowledgements

We gratefully acknowledge the financial support of the Korea Science and Engineering Foundation (HWRS-ERC).

References

[1] US Patent 006594552, "Grip Strength with Tactile Feedback for Robotic Surgery"

[2] R. Mukherjee, G. Song and R. Satava, "An Articulated Manipulator for Enhanced Dexterity in Minimally Invasive Surgery," Proc. IEEE Eng. Med. Bio., pp.220-222, 1996

[3] S.S. Sastry, M. Cohn and F. Tendick, "Milli-robotics for Remote, Minimally Invasive Surgery," Robotics and Autonomous Systems, Vol. 21, pp.305-316, 1997

[4] R. D. howe and Y. Matsuoka, "Robotics for Surgery," Annu. Rev. Biomed. Eng., pp.211-240, 1999

[5] J. Ruurda, T. Vroonhoven and I. Broeders, "Robot-assisted Surgical Systems: A New Era in Laparoscopic Surgery," Ann. R. Coll. Surg. Engl. Vol. 84, pp. 223-226, 2002

[6] A. J. Hodgson, R. A. Pantazopol, M. D. Visser, S. E. Salcudean and A. G. Nagy, "Assessing Potential Benefits of Enhanced Dexterity in Laparoscopic Surgery," Proc. IEEE/EMBS, pp.1966-1969, Oct. 1997

[7] A. J. Madhani, "Design of Teleoperated Surgical Instruments for Minimally Invasive Surgery," Doctoral Thesis, pp.121-124, Feb. 1998

The Tenth International Symposium on Artificial Life and Robotics 2005(AROB 10th '05),
B-con Plaza, Beppu, Oita, Japan, February 4-6, 2005

Identification of nonlinear mechatronic servo motor system having backlash

Y.TOYOZAWA [1], H. HARADA[2] and H. KASHIWAGI[2]

[1] FANUC Corp., Kyushu Branch Office, Servo Lab, Tsukure 2570-2, Kikuyo-gun, Kumamoto 869-1196, Japan
[2] Faculty of Engineering, Kumamoto University, Kurokami 2-39-1,Kumamoto 860-8555,Japan
(Tel/Fax: +81-96-342-3742)
E-mail: [1]Toyozawa.Yukio@fanuc.co.jp, [2]kashiwa@gpo.kumamoto-u.ac.jp

Abstract- Volterra series representation is a useful method to describe a nonlinear system of single valued function, though the method to identify Volterra kernels are generally difficult. The authors have recently developed a new method for identification of Volterra kernels of nonlinear systems by use of pseudorandom M-sequence and correlation technique. Using this technique and the experimental setup consisiting of AC servo motor and the backlash, this paper makes the feasibilty study that Volterra kernel representation can describe not only single valued but also multi valued nonlinearity. The experimental results show that we can still use Volterra kernel representation for those backlash-type two-valued nonlinear systems.

I. INTRODUCTION

Backlash type nonlinear element exists in a mechanical transmission systems. An interval of transmission is a kind of nonlinear backlash characteristics. When the main tooth wheel makes a change of direction, the following wheel does not change until the interval is used up.

The nonlinear systems with backlash element which has multi-valued function between the input and output are generally thought difficult to be identified. Many researchers have tried to identify this kind of system by various methods. Simpson and Power[3)] have shown that a method of identification developed for a class of system containing a zero-memory nonlinearity is applicable to certain types of nonlinear elements with memory.

The extension of the Weierstrass theorem to the Volterra functionals was made in 1910 by Maurice Fréchet who showed that any continuous functional can be represented by a series of functionals of integer order whose convergence is uniform in all compact sets of continuous functions. Therefore, Volterra kernel expansion method can only be used for those nonlinear systems which are continuous for input-output relation, and single valued, theoretically. The nonlinear systems having backlash type element are multi-valued as far as input-output relationship is concerned, so these nonlinear systems are not suited to Volterra kernel representation.

However, Volterra kernel expression of nonlinear system is one of the most useful method for representing nonlinear systems. So we would like to know what would be the result if we apply Volterra kernel identification method to nonlinear system having backlash element.

In this paper, we apply the method of Volterra kernel identification by use of M-sequences to the identification of a nonlinear system consisting of backlash characteristics. In this method, M-sequences are applied to the nonlinear system and the crosscorrelation function between the input and the output is measured. ¿From the crosscorrelation function ,we can get not only the linear impulse response of the linear part of the system, but also cross-sections of high-order Volterra kernel up to 3rd order of the nonlinear system.[6)]

II. Identification of Volterra Kernels

One of the solutions of the identification ploblem of a nonliear system is based on the measurement of Volterra kernels. Consider the identification of a nonlinear system which can be described as follows,

$$y(t) = \sum_{i=1}^{\infty} \int_0^{\infty} \int_0^{\infty} \cdots \int_0^{\infty} g_i(\tau_1, \tau_2, \cdots \tau_i)$$
$$\times u(t-\tau_1)u(t-\tau_2)\cdots u(t-\tau_i)d\tau_1 d\tau_2 \cdots d\tau_i$$
$$+n(t) \qquad (1)$$

where $u(t)$ is the input, and $y(t)$ is the output of the nonlinear system, and $g_i(\tau_1, \tau_2, ...)$ is called Volterra kernel of i-th order. $n(t)$ is noise. When $i = 1$, Eqn.(1) shows a linear systerm.

In order to get the Volterra kernels $g_i(\tau_1, \tau_2, ...)$, we use an M-sequence as an input to the nonlinear system. The crosscorrelation function $\phi_{uy}(\tau)$ between the input $u(t)$ and the output $y(t)$ can be written as,

$$\phi_{uy}(\tau) = \overline{u(t-\tau)y(t)}$$

The Tenth International Symposium on Artificial Life and Robotics 2005(AROB 10th '05),
B-con Plaza, Beppu, Oita, Japan, February 4-6, 2005

$$= \sum_{i=1}^{\infty} \int_0^{\infty} \int_0^{\infty} \cdots \int_0^{\infty} g_i(\tau_1, \tau_2, \cdots \tau_i) \times \overline{u(t-\tau)u(t-\tau_1)\cdots u(t-\tau_i)} d\tau_1 d\tau_2 \cdots d\tau_i \tag{2}$$

where $\overline{\quad\quad}$ denotes time average. Generally the n-th moment of $u(t)$ is difficult to obtain. But when we use M-sequence, we can get n-th moment of $u(t)$ easily. Namely, the $(i+1)$th moment of the input M-sequence $u(t)$ can be written as

$$\overline{u(t-\tau)u(t-\tau_1)u(t-\tau_2)\cdots u(t-\tau_i)} = \begin{cases} 1 & \text{(for certain } \tau) \\ -1/N & \text{(otherwise)} \end{cases} \tag{3}$$

where N is the period of the M-sequence. When we use the M-sequence with the degree greater than 16, $1/N$ is in the order of 10^{-5}. So Eqn.(3) can be approximated as a set of impulses which appear at certain τ's.

Let us consider the case where we measure up to i-th Volterra kernel. Then for any integer $k_{i1}^{(j)}, k_{i2}^{(j)}, \cdots k_{i,i-1}^{(j)}$ (suppose $k_{i1}^{(j)} < k_{i2}^{(j)} < \cdots, k_{ii-1}^{(j)}$), there exists a unique $k_{ii}^{(j)} (mod\ N)$ such that

$$u(t)u(t+k_{i1}^{(j)})u(t+k_{i2}^{(j)})\cdots u(t+k_{i,i-1}^{(j)}) = u(t+k_{ii}^{(j)}) \tag{4}$$

where j is the number of a group $(k_{i1}, k_{i2}, \cdots, k_{i,i-1})$ for which Eqn.(4) holds. This property is called "shift and add property" of M-sequence. We assume that total number of those groups is m_i(that is, $j = 1, 2, \cdots, m_i$). Then Eqn.(3) becomes unity when

$$\tau_1 = \tau - k_{i1}^{(j)}, \tau_2 = \tau - k_{i2}^{(j)}, \cdots \tau_i = \tau - k_{ii}^{(j)} \tag{5}$$

Therefore Eqn.(2) becomes

$$\phi_{uy}(\tau) \simeq \sum_{i=1}^{\infty} \sum_{j=1}^{m_i} g_i(\tau - k_{i1}^{(j)}, \tau - k_{i2}^{(j)}, \cdots \tau - k_{ii}^{(j)}) \tag{6}$$

Since $g_i(\tau_1, \tau_2, \cdots \tau_i)$ is zero when any of τ_i is smaller than zero, each $g_i(\tau - k_{i1}^{(j)}, \tau - k_{i2}^{(j)}, \cdots \tau - k_{ii}^{(j)})$ in Eqn.(6) appear in the crosscorrelation function $\phi_{uy}(\tau)$ when $\tau > k_{ii}^{(j)}$.

In order to obtain the Volterra kernels from Eqn.(6), $k_{ii}^{(j)}$'s in Eqn.(6) are sufficiently apart from each other. For this to be realized, we have to select suitable M-sequences, which make the appearance of each cross-section of Volterra kernels sufficiently apart from each other. Some of those usable M-sequences are shown in reference (7).

When we measure Volterra kernels up to 3rd order, the crosscorrelation function $\phi_{uy}(\tau)$ becomes,

$$\begin{aligned} \phi_{uy}(\tau) &= \Delta t g_1(\tau) + F(\tau) \\ &+ 2(\Delta t)^2 \sum_{j=1}^{m_2} g_2(\tau - k_{21}^{(j)}, \tau - k_{22}^{(j)}) \\ &+ 6(\Delta t)^3 \sum_{j=1}^{m_3} g_3(\tau - k_{31}^{(j)}, \tau - k_{32}^{(j)}, \tau - k_{33}^{(j)}) \end{aligned} \tag{7}$$

where

$$F(\tau) = (\Delta t)^3 g_3(\tau, \tau, \tau) + 3(\Delta t)^3 \sum_{q=1}^{m_1} g_3(\tau, q, q) \tag{8}$$

In general case, we have,

$$\begin{aligned} \phi_{uy}(\tau) &= \Delta t g_1(\tau) + F(\tau) \\ &+ \sum_{i=2}^{\infty} i!(\Delta t)^i \sum_{j=1}^{m_i} g_i(\tau - k_{i1}^{(j)}, \tau - k_{i2}^{(j)}, \cdots, \tau - k_{ii}^{(j)}) \end{aligned} \tag{9}$$

Here the function $F(\tau)$ is the function of τ and sum of the odd order Volterra kernels when some of its argument are equal. Since $F(\tau)$ appears together with $g_1(\tau)$ in a overlapped manner, $F(\tau)$ must be calculated from the odd order Volterra kernels and be subtracted from the measured $g_1(\tau)$ in order to obtain the accurate $g_1(\tau)$.

III. Simulation

We carried out Volterra kernel identification for the system having backlash type nonlinearity as is shown in **Figure 1**.

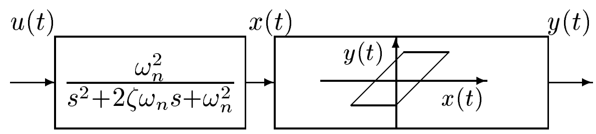

Figure 1: Nonlinear system consisting of backlash nonlinearity

As is well known, when the input to a backlash element is sinusoidal signal,

$$x(t) = X sin\omega t \tag{10}$$

the output of backlash element becomes as follows:

$$y(t) = \begin{cases} k_0(X sin\omega t - a) & 0 < \omega t < \frac{\pi}{2} \\ k_0(X - a) & \frac{\pi}{2} < \omega t < (x - \beta) \\ k_0(X sin\omega t + a) & (x - \beta) < \omega t < \pi \end{cases} \tag{11}$$

where $\beta = arcsin(1 - \frac{2a}{X})$, ρ is the slope of the inclined lines of the backlash characteristic curve and $k_0 = tg\rho$.

The parameters of the simulated system are as follows:

$\zeta = 0.4$
$\omega_n = 1.0$
Backlash width: $W = \mid 2a \mid = 0.8$
$\rho = \pi/4$
Sampling period: $\Delta t = 0.5s$

IV. Results of Simulation

As an input $u(t)$, 12 degree M-sequence with the characteristic polynomial ($f(x) = 15341$ in octal notation) is used. The first, second and third order Volterra kernels of the system are measured by calculating the crosscorrelation between the input and the output.

Figure 2 shows the first order Volterra kernel $g_1(\tau)$ thus measured. As is seen here, the response is not so smooth as the response of single-valued nonlinear system, because of the multi-valued characteristic of the backlash.

Figure 3 shows one of the crosssection of the third Volterra kernel $g_3(\tau_1, \tau_2, \tau_3)$, when $\tau_3 = 1\Delta t$.

Figure 4 shows the result of comparison of the actual output (solid line) and the output (x) calculated by use of first Volterra kernel and the output(+) calculated from up to third order Volterra kernels. From these results of simulation we can say that the use of Volterra kernel indentification method is effective even for backlash type nonlinear system.

V. Experiment for AC servo moter with backlash

An experiment is carried out for AC servo motor system having backlash element. The block diagram of the motor is shown in **Figure 1**. Driven by this motor, a mechanical backlash element is attached, and the rotary encoder of high resolution measures the output. Here the torque constant K_T and the moment of inertia J are given as follows.

$$K_T = 0.03606(Nm/A) \tag{12}$$

$$J = 0.00025(kgm^2) \tag{13}$$

The transfer function of the motor system is as follows,

$$G(s) = \frac{2\zeta\omega_n s + {\omega_n}^2}{s^2 + 2\zeta\omega_n s + {\omega_n}^2} \tag{14}$$

where

$$\omega_n = \sqrt{\frac{K_I K_T}{Jm}} \tag{15}$$

$$\zeta = \frac{K_P}{2}\sqrt{\frac{K_T}{J_m K_I}} \tag{16}$$

The parameters of the experiment are as follows;
Characteristic polynomial of the M-sequence: $f(x) = 40473$ (in octal notation),
Sampling period: $\Delta t = 8ms$,
Width of backlash: $W = 0.72 \quad or \quad 1.5(degrees)$

Figure 5 shows the schematic diagram of experimental setup. The PC commands the velocity command of M-sequence, and the pulse width modulated signal becomes the input voltage on the motor driver. The motor drives the rotary encoder connected through the backlash coupling at opposite side in order to measure the output. The cross-correlation function between the velocity command and output is calculated for extracting the volterra kernels. **Figure 6** shows the control block diagram. **Figure 7** shows the first Volterra kernel extracted from the crosscorrelation function. **Figure 8** shows the second Volterra kernel showing that the second Volterra kernel is very small in this case. **Figure 9** shows a crossection of the third Volterra kernel when $\tau_3 = 1$. **Figure 10** shows the comparison between the actual output of the AC servo motor system having backlash element and the output calculated from the measured Volterra kernels. The dotted line shows the actual output, (+)line shows the comparison when we use up to the third order Volterra kernles. It is seen that when we use up to the third order Volterra kernel, the actual output can be very closely estimated from the measured Volterra kernels.

VI. Conclusion

A method for identification of Voterra kernels using M-sequence was applied to identify a kind of multi valued function, which appeares frequently at the mechatronics field as the backlash. M-sequences are applied to the two-valued nonlinear system and the crosscorrelation function between the input and the output are measured. From the crosscorrelation function, we obtain not only the linear impulse response, but also cross-sections of 3rd order Volterra kernels of backlash element nonlinear system.

After verifying the effect by simple simulation, this method was applied to the actual AC servo motor system having backlash element. The calculated result using up to third order Volterra kernels showed good agreement with the actual output which was driven by M-sequence velocity command through the backlash coupling. ¿From these results , we can say that the method of Volterra kernels is practically useful for indentification of backlash type nonlinear system.

References

1) Barker,H.A. *et al*, "Performance of antisymmetric pseudorandom signal in the measurement of second-order Volterra kernels by crosscorrelation," *Proc. IEE*, vol. 119, no.3, pp.353-362, 1972

2) Simpson,R.J.,"Use of high frequency signals in identification of certain nonlinear systems," *Int. J. Syst. Sci.*, 1973,4,pp.121-127

3) Simpson,R.J. and H.M.Power, "System identification using almost periodic functions - application to nonlinearities with memory," *ibid.* , 1973, 4, pp.261-268

4) Baheti,R.S., R.R.Mohler and H.A.Spang, "A new cross correlation algorithm for Volterra kernel estimation of bilinear systems", *ibid.* , 1979,AC-24,pp.661-664

5) Billings, S.A. and S.Y.Fakhouri, "Identification of Nonlinear Systems Using Correlation Analysis and Pseudorandom Inputs," *Int. J. Systems Sci.*, Vol.11-3, pp.261-279, 1980

6) Kashiwagi, H. and Sun Yeping, "A Method for Identifying Volterra Kernels of Nonlinear System," *Trans. SICE*, vol.31, no.8, pp.1054-1060, 1995

7) Kashiwagi, H., *M-sequence and its application*, Shoukoudo co., 1996

8) Kashiwagi,H., L.Rong, H.Harada and T.Yamaguchi, "Model Predictive Control of Nonlinear Processes by use of 2nd and 3rd Volterra Kernel Model" *Proc. '98KACC held in Pusan, Korea,* pp.451-454, 1998

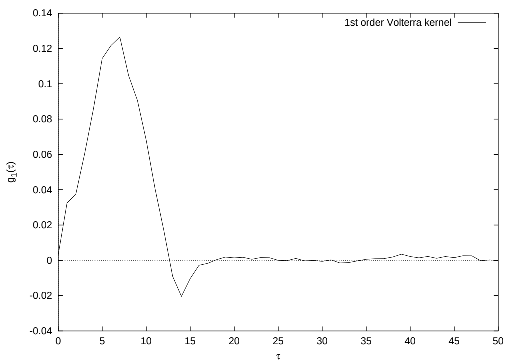

Figure 2: Obtained first Volterra kernel $g_1(\tau_1)$ in the simulation.

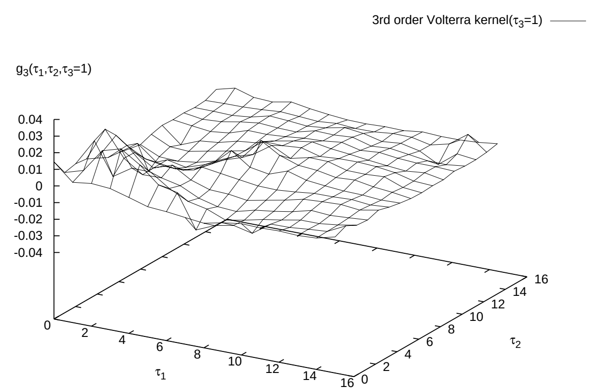

Figure 3: Obtained third Volterra kernel $g_3(\tau_1, \tau_2, \tau_3 = 1)$ in the simulation.

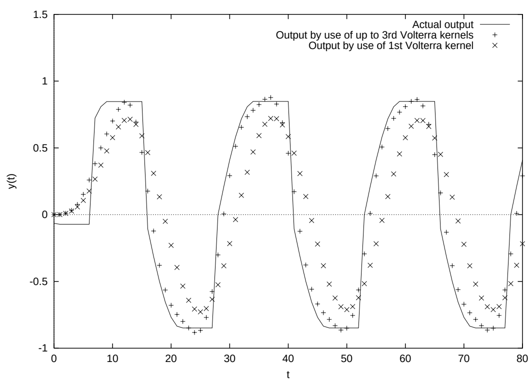

Figure 4: Comparison between actual output with calculated output from Volterra kernels in the simulation.

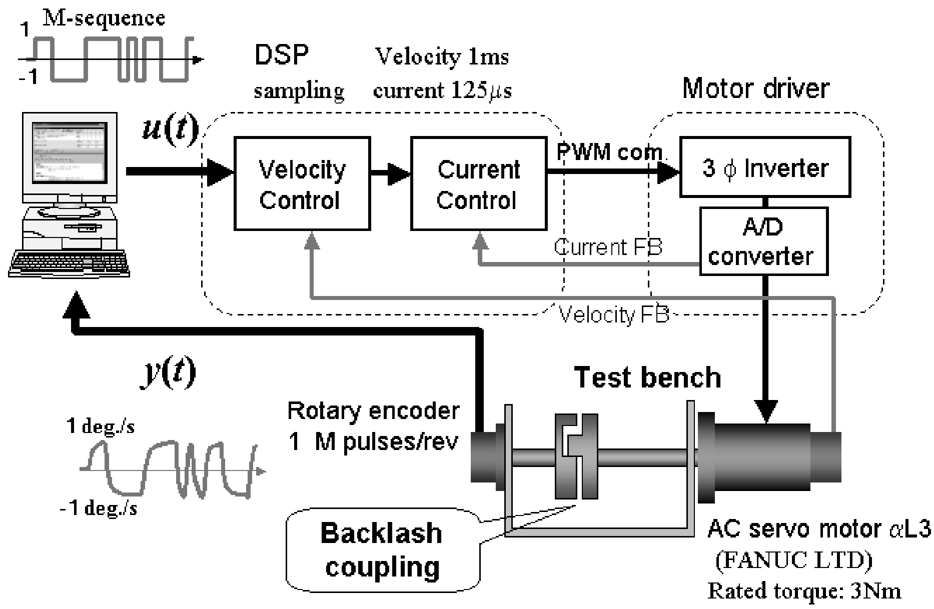

Figure 5: Experiment for AC servo motor with backlash.

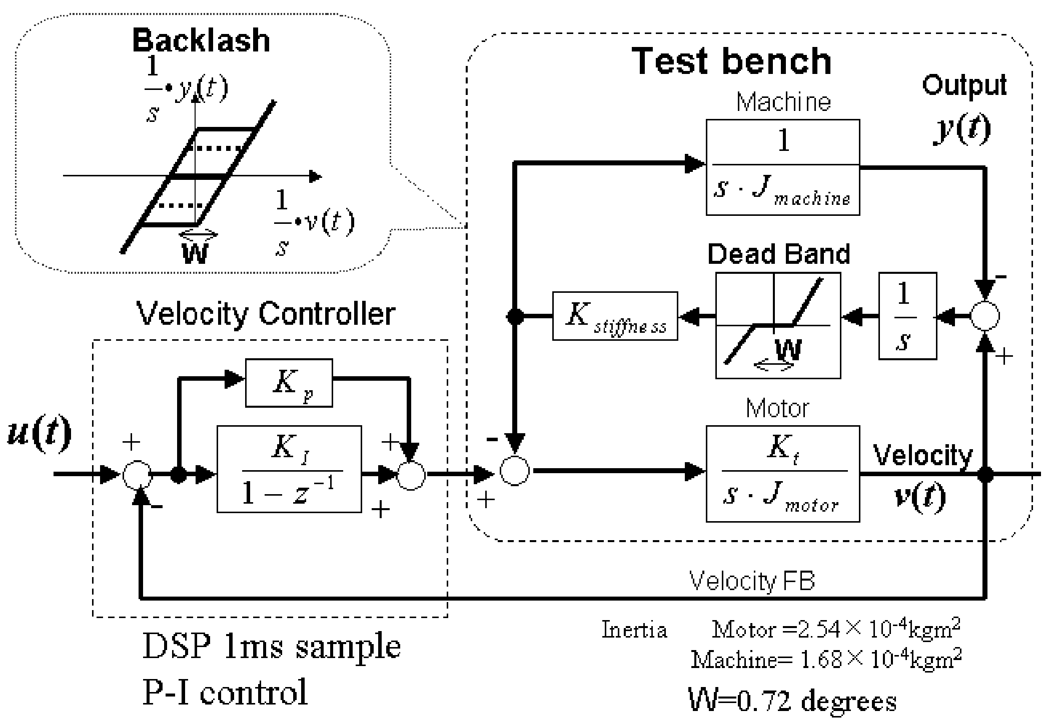

Figure 6: Control system block.

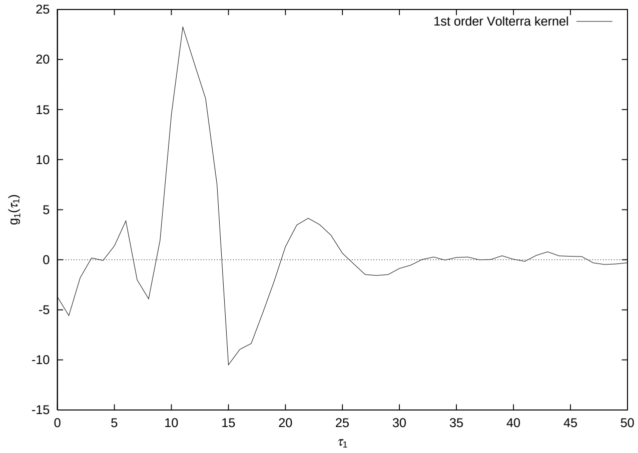

Figure 7: First Volterra kernel $g_1(\tau_1)$ in case of AC servo motor system.

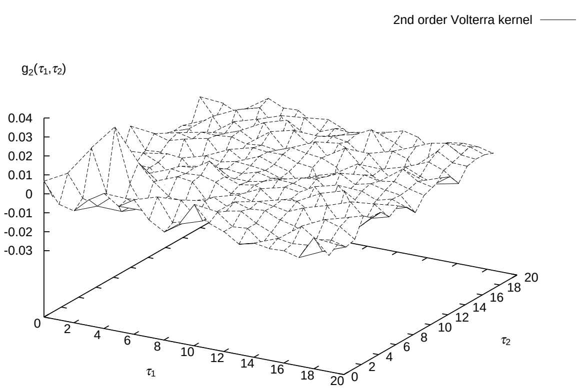

Figure 8: Second Volterra kernel $g_2(\tau_1, \tau_2)$ in case of AC servo motor system.

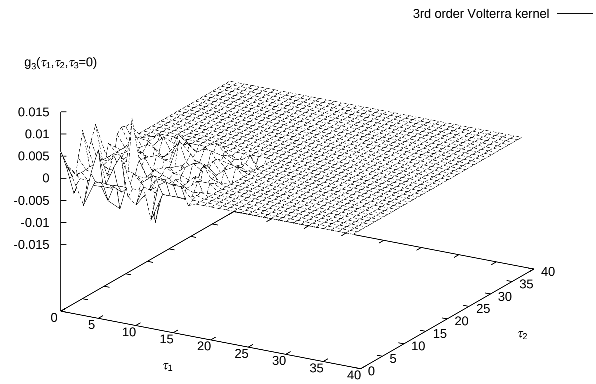

Figure 9: Third Volterra kernel $g_3(\tau_1, \tau_2, \tau_3), \tau_3 = 1)$ in case of AC servo motor system.

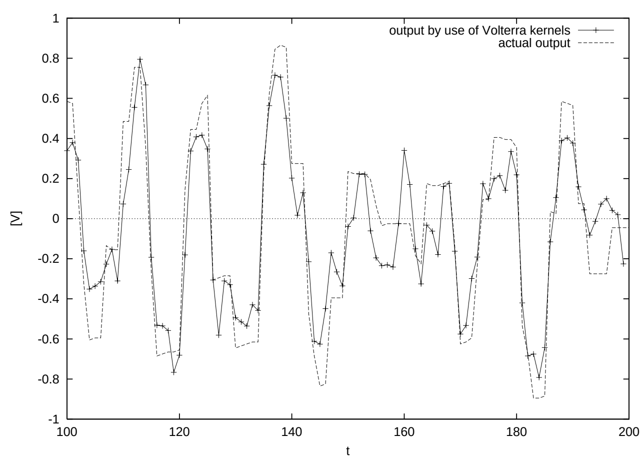

Figure 10: Comparison between the actual output with the output calculated from Volterra kernels in case of AC servo motor system.

The Tenth International Symposium on Artificial Life and Robotics 2005(AROB 10th '05),
B-con Plaza, Beppu, Oita, Japan, February 4-6, 2005

An Optimal Capturing Trajectory Planning for a Moving Object

Byoung-Suck Choi
Dep. of Electronics Engineering
Pusan National University
Busan, Republic of Korea

Jang-Myung Lee
Dep. of Electronics Engineering
Pusan National University
Busan, Republic of Korea

Abstract

An optimal capturing trajectory for a moving object is proposed in this paper based on the observation that a single-curvature path is more accurate than double- or triple-curvature paths. Traveling distance, tracking time, and trajectory error are major factors considered in deciding an optimal path for capturing the moving object. That is, the tracking time and distance are minimized while the trajectory error is maintained as small as possible. The three major factors are compared for the single and the double curvature trajectories to show superiority of the single curvature trajectory. Based upon the single curvature trajectory, a kinematics model of a mobile robot is proposed to follow and capture the moving object, in this paper.

Keywords Single curvature trajectory; Mobile robot; Capturing; Moving object

1 Introduction

From 1970's, 'Robot' has come close to our daily lives. More precise and fast control became possible with the development of integrated circuits, sensors, artificial intelligence, image processing, and computer technologies. As the result, intelligent robots which recognize changes of environment and decide their reactions automatically, appeared in daily lives[1][2].

There are two typical robots: a robotic manipulator and a mobile robot. The robotic manipulators that has a fixed base, have been utilized for precise assembly operations. However their workspace is limited within a small volume. On the contrary, workspace of a mobile robot is not limited to a certain area. However, in the control of the mobile robot, position control accuracy, velocity and acceleration limits, obstacle recognition, and trajectory planning must be considered carefully[3].

Therefore researches on a mobile robot can be globally classified into four categories: mobile robot navigation itself, trajectory planning, position estimation, and driving control. Trajectory planning of a mobile robot aims at providing an optimal path from an initial to a target position. Generally there are three major factors to be considered in the trajectory planning: the driving time, distance, and error. Note that these factors are not independent but closely related to each other. Therefore the trajectory planning aims at the selection of best trajectory in view of all the factors. There are not many researches on the trajectory planning, while many papers on the position estimation and trajectory control are published. The importance of driving trajectory planning which reduces driving distance and time has not been studied closely[4].

This paper proposes a single curvature trajectory for a precise motion of a mobile robot and it is applied for the trajectory of a mobile robot to capture a moving object. Based on the kinematics modeling of a mobile robot, a theoretical driving model is proposed; the driving characteristics of the single curvature trajectory, that is, driving time, distance, and error have been measure and analyzed through the simulations and real experiments. In chapter 2, driving characteristics of a mobile robot have been analyzed through kinematics analysis. The single curvature planning is described in chapter 3 concretely. In chapter 4, the capturing algorithm following the single curvature trajectory is introduced with theoretical formulars. The comparison between a single curvature trajectory and a double curvature trajectory in terms of tracking error, time, and distance has been shown in chapter 5. The real capturing experiments are also demonstrated in the chapter. Chapter 6 concludes this paper.

2 Kinematics Modeling and Moving Characteristics of a Mobile Robot

To form a trajectory for a mobile robot to follow the desired path, kinematics analysis which shows the relation between robot control variables and robot position and velocity needs to be done previously.

2.1 Kinematics analysis of a mobile robot

As shown in Fig. 1-(a), a mobile robot with differential driving mechanism has two wheels on the same axis, and each wheel is controlled by an independent motor. Let us define v_L as the velocity of left wheel, v_R as that of the right wheel, and l as the distance between the two wheels. The robot motion can be determined by the two wheel velocities, v_L and v_R, and the linear and angular velocities of the mobile robot can be described in terms of v_L and v_R as follows[5]:

$$v_1 = \frac{v_R + v_L}{2} \qquad (1)$$

$$v_2 = \frac{2(v_R - v_L)}{l} \qquad (2)$$

Kinematics model of a mobile robot with differential driving mechanism can be described as Fig. 1-(b). On the two dimensional $X-Y$ Cartesian coordinates, position of the mobile robot is described by $x_R(t)$ and $y_R(t)$ while the orientation is represented as $\theta_R(t)$.

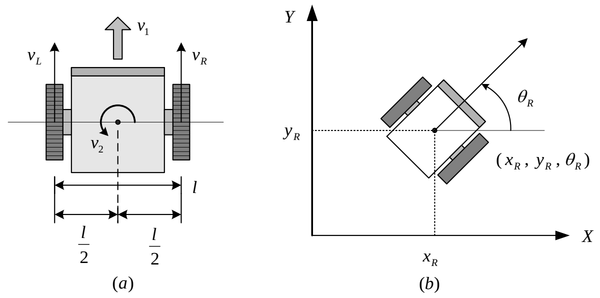

Fig. 1. Kinematics model of a mobile robot.

Then $\dot{x}_R(t)$ and $\dot{y}_R(t)$ represent the linear velocity of a mobile robot while $\dot{\theta}_R(t)$ represents the angular velocity. The velocity vector of the mobile robot is defined as

$$\dot{P} = \begin{bmatrix} \dot{x}_R & \dot{y}_R & \dot{\theta}_R \end{bmatrix}^T \tag{3}$$

where $P = \begin{bmatrix} x_R & y_R & \theta_R \end{bmatrix}^T$.

Now the kinematics model of the mobile robot can be represented as[6]

$$\dot{P} = \begin{bmatrix} \cos\theta_R & 0 \\ \sin\theta_R & 0 \\ 0 & 1 \end{bmatrix} \begin{bmatrix} v_1 \\ v_2 \end{bmatrix}. \tag{4}$$

Kinematics analysis aims at the proper velocity assignment to each wheel to drive the mobile robot to a desired position and orientation[7].

2.2 Driving Principle of a Mobile Robot

Motion states of the mobile robot with differential driving mechanism are changing according to the two wheel velocities. A robot with multiple wheels rotates along a rotation center instantaneously, and this rotation center is defined as ICC (Instantaneous Center of Curvature). As it is shown in Fig. 2-(a), ICC locates on the cross-section point of the extension-lines of the wheel centers. For a mobile robot with differential driving mechanism, as shown in Fig. 2-(b), ICC can be located any point on the wheel axis since the two wheel axes are on the same line[5].

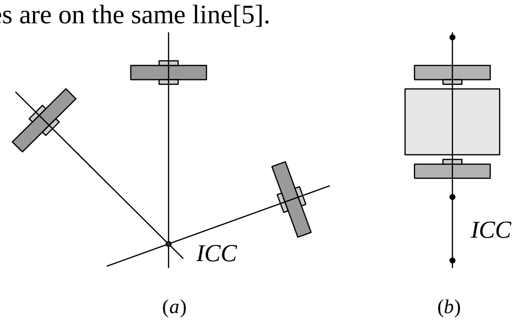

Fig. 2. Center of instantaneous rotation.

In this case, ICC will be determined by the velocity ratio between the two wheels'. Fig. 3 illustrates ICC along with the robot's velocity and position. There exists proportional relationship between the wheel velocity and the distance from the wheel to the ICC, which is represented as

$$v_L : v_R = R - \frac{l}{2} : R + \frac{l}{2} \cdot \tag{5}$$

Equation (5) can be simply represented as

$$R = \frac{l}{2}\left(\frac{v_R + v_L}{v_R - v_L}\right) \cdot \tag{6}$$

Note that the rotation radius of the mobile robot is determined by the values of left and right wheel velocities. When the robot is following a straight line, $R = \infty$ and $v_R = v_L$. When $v_R \neq v_L$, the robot follows a circular trajectory with a certain rotation radius.

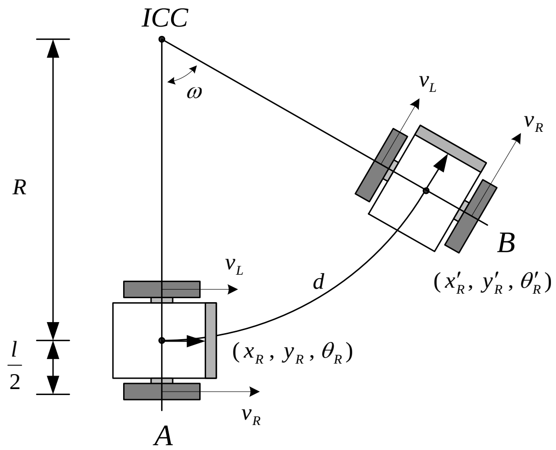

Fig. 3. ICC of a mobile robot

In Fig. 3, when the mobile robot is moving from A where the robot is located on (x_R, y_R, θ_R) at time $= t$ to B where the position is on (x'_R, y'_R, θ'_R) at time $= t + \delta t$, the coordinates of ICC can be determined as

$$ICC = [\, x_R - R\sin(\theta_R),\ \ y_R + R\cos(\theta_R)\,] \tag{7}$$

Also the mobile robot position, (x'_R, y'_R, θ'_R), at time= $t + \delta t$, can be expressed in terms of position of ICC and angular velocity, ω, as follows:

$$\begin{bmatrix} x'_R \\ y'_R \\ \theta'_R \end{bmatrix} = \begin{bmatrix} \cos(\omega\,\delta t) & -\sin(\omega\,\delta t) & 0 \\ \sin(\omega\,\delta t) & \cos(\omega\,\delta t) & 0 \\ 0 & 0 & 1 \end{bmatrix} \begin{bmatrix} x_R - ICC_X \\ y_R - ICC_Y \\ \theta_R \end{bmatrix} + \begin{bmatrix} ICC_X \\ ICC_Y \\ \omega\,\delta t \end{bmatrix} . \tag{8}$$

Now, the total distance, d, and the rotation angle, φ, of the mobile robot movement from location A to B can be obtained as follows:

$$d = \int_t^{t+\delta t} v_1\, dt = \int_t^{t+\delta t} \frac{v_L + v_R}{2}\, dt \tag{9}$$

$$\varphi = \frac{d}{R} = \frac{\int_t^{t+\delta t} (v_L + v_R)\, dt}{l(v_L + v_R)} (v_R - v_L) \tag{10}$$

Using these equations, when the rotation radius, distance of movement, and rotation angle of the mobile robot are planned previously, the desired linear and angular velocities, v_L, v_R, and ω can be obtained when it makes a curved motion[5].

3 Single-Curvature Trajectory

3.1 Curvature

Curvature, k, is defined as ratio of $\Delta\theta$ to Δs, when a mobile robot is rotating from a point, P, to Q as it is illustrated in Fig. 4. The curvature is defined as[8]

$$k = \lim_{\Delta s \to 0} \left|\frac{\Delta\theta}{\Delta s}\right| = \left|\frac{d\theta}{ds}\right| \quad (11)$$

Rotation radius can be defined as the inverse of the curvature as

If $k > 0$, then $\rho = 1/k$. (12)

As it can be clearly recognized from Eq. (11), the total travel distance along the curve, Δs, is the length of the arc and is proportional to the curve radius. Since curvature, k, is inverse proportional to Δs, curvature k is inverse proportional to the radius of the curve. If $k = 0$, then the radius of the curve, in other words, rotation radius becomes infinite. That is, $k = 0$ implies a straight line which is a circle with the infinite radius [5].

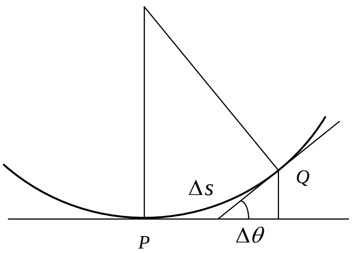

Fig. 4. Curvature.

When the mobile robot is moving along the curved trajectory, the rotation radius affects severely on the driving error. Generally the mobile robot has smaller error along a straight line path $(k = 0)$, than the curved $(k \neq 0)$. Theoretically, the curved trajectory can be calculated with the Eq's (5)~(8) assuming the pure rolling and non-slipping conditions. Practical driving may have some differences from the theoretical values. When the mobile robot is following a curved path, there exist centrifugal and centripetal forces all together. The friction force between the surface and the wheels acts as centripetal force to ICC and keeps the curved motion of the mobile robot. Under the ideal conditions, the driving error becomes zero without the slippage. However, practically, there always exists the driving error caused by the slippage. From the following equation, it can be formulated that the centrifugal force is a function of rotation radius and velocity:

$$F = \frac{mv^2}{r} \quad (13)$$

Fig. 5 illustrates the driving situation of a mobile robot, starting from A and following a circular curved path. In the ideal condition, the estimated position of robot becomes B1. However, practically the robot arrives at B2 by the driving error. So far there are lots of researches to reduce the driving error caused by the rotation radius and driving speed.

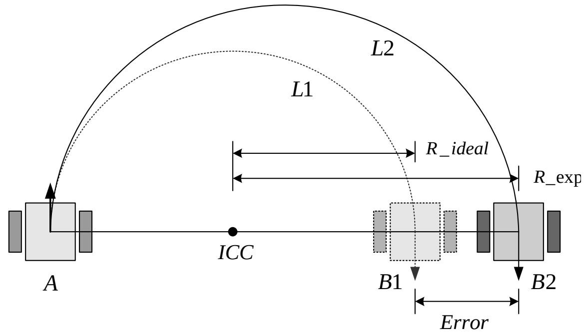

Fig. 5. Driving error of a mobile robot on a curved path.

Fig. 6 shows the error characteristics according to the driving radius and speed with a real mobile robot. The speed of right wheel is kept constant, while that of left wheel was changed to make a curved motion of the mobile robot. With the increase of the left wheel velocity, the driving error is increased as well. Also note that the driving error becomes large with the small rotation radius even though the speed is same. From the analysis of Fig. 6, it can be concluded that the driving error of a mobile robot becomes larger with the smaller rotation radius and with the higher speed while it is driving along the curved path[4].

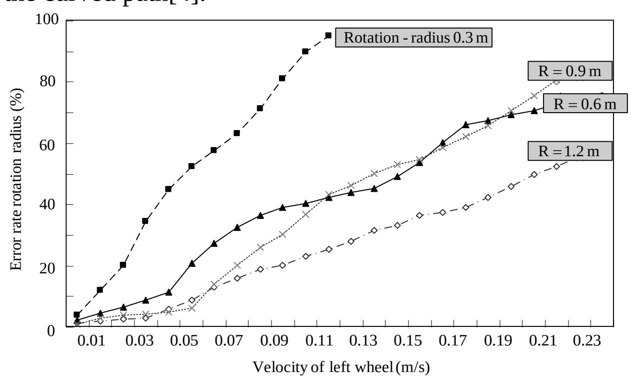

Fig. 6. Driving errors in terms of speed and rotation radius

3.2 Single curvature trajectory

The single curvature trajectory keeps the same curvature while the double curvature trajectory changes the driving direction and curvature at the point of inflection.. That is, the points of inflection exist at several locations. While a mobile robot is moving along the trajectory , the wheel velocities of the mobile robot need to be changed whenever the rotation radius and driving direction are changed according to Eq. (6).

For the same travel distance, the single curvature trajectory has the biggest rotation radius, while the others have varying radius with smaller values. Therefore it can be predicted that when the mobile robot is traveling along the single-curvature trajectory, it may have the least tracking error. To verify the fact, the tracking errors are going to be recorded and analyzed through the real experiments. Before the real experiments, pre-simulations are performed to show the rotation angles, traveling distance, trajectory, etc.

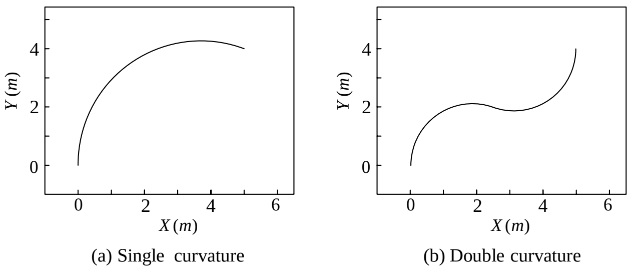

Fig. 7. Single-curvature and double-curvature trajectories.

Table 1. Computed single-curvature and double-curvature trajectories

	Single Curvature	Double Curvature
Initial Position	Pi=(0, 0, 90^o)	Pi=(0, 0, 90^o)
Final Position	Pf=(5, 4, 109.6^o)	Pf=(5, 4, 90^o)
Path Distance(m)	7.18 m	7.18 m
Curve Radius(m)	3.75 m	1.88 m
Rotation Angle(deg)	109.65^o	109.65^o, 109.65^o
ICC Coordinates	(3.75, 0)	(1.87, 0) (3.13, 4)

Simulation results the total travel distance is same for the single-curvature and double-curvature trajectories. However, the rotation radius is double for the single-curvature trajectory. In more detail, the rotation radius for the single-curvature trajectory is 3.75m, while that of double-curvature is 1.875m, which has the point of inflection at (2.5, 2). As the result of close observation of Fig. 6, it can be concluded that the single curvature trajectory has less tracking error than the double-curvature.

4 Capturing Algorithm

When a mobile robot is tracking to capture a moving object, the decision of tracking trajectory is a very important factor for a successful operation. To minimize the tracking error, a single curvature trajectory is selected and the mobile robot is planned to follow the trajectory. Fig 8 shows the mobile robot path to capture a moving object along the single-curvature trajectory. The total path is composed of two single-curvature and a straight-line trajectories. The left-wheel velocity and acceleration of the robot are defined as v_L and a_L, respectively. At the first part of the path, the robot needs to rotate clock-wise along the circular trajectory, the left-wheel velocity is higher than the right-wheel velocity, $v_L > v_R$. The velocities can be related to the accelerations as follows:

$$v_L = \int_0^t a_L(\tau)d\tau = a_L t \quad \text{(14-a)}$$

$$v_R = \int_0^t a_R(\tau)d\tau = a_R t \quad \text{(14-b)}$$

As it can be noted from the relations between the velocities and accelerations, the velocity is proportional to the acceleration, that is, $a_L > a_R$. The second segment is a straight line along which the robot follows from (x_{line1}, y_{line1}) to (x_{line2}, y_{line2}). At the third part of the path, the mobile robot estimates the position, (x_{obj}, y_{obj}), and velocity of the moving object using a CCD camera attached on its body, and follows the single-curvature trajectory to capture the moving object precisely.

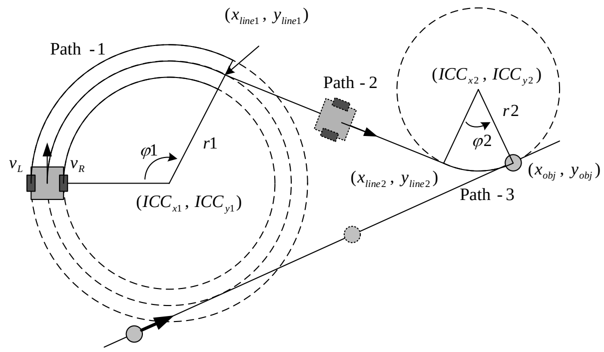

Fig. 8. Capturing trajectory of a moving object

5 Experiments

5.1 Experimental system

Experiments were performed in the research laboratory building. The floor was flat and slippery.

A. Moving object

The moving object does not need any specific characteristics. Therefore it is implemented as a simple and small mobile robot. To estimate the position of the moving object easily, a red color patch is attached on the object. The color information of the patch is obtained by the CCD camera on the mobile robot and is utilized to estimate the position of the moving object.

B. Mobile Robot

The mobile robot utilized for the experiments has a two DOF active vision camera to recognize the objects and surrounding environments. To enable the autonomous navigation, several sensors including rate-gyroscope sensors are used for the mobile robot. The hardware specifications of the mobile robot are summarized in Table 2.

Table 2. Specifications of the mobile robot

Item	Specifications
Size (mm)	660 * 430 * 465 (L*W*H)
Weight (kg)	19.5 kg
Distance between Wheels (mm)	400 mm
Diameter of Wheel	210 mm

5.2 Experimental results and discussions

In the first experiment, the single-curvature and double-curvature trajectories are compared in terms of tracking error, traveling distance, and tracking time with the same mobile robot for a moving object. Figure 9 shows the real experimental environment. The experimental results are summarized in Table 4 and 5. Figure 10 shows tracking error, traveling distance, and tracking time as a graph according to the real experimental values.

Table 3. Computed velocity of the mobile robot for each trajectory

Lists		Single-curvature Trajectory (r=3.75m)		Double-curvature Trajectory (r=1.875*2m)	
v_1 (m/s)	Time(s)	v_L (m/s)	v_R (m/s)	v_L (m/s)	v_R (m/s)
0.1	72.8	0.105	0.095	0.089	0.111
0.2	37.9	0.211	0.189	0.179	0.221
0.3	26.9	0.316	0.284	0.268	0.332
0.4	21.9	0.421	0.379	0.357	0.443
0.5	19.3	0.527	0.473	0.447	0.553

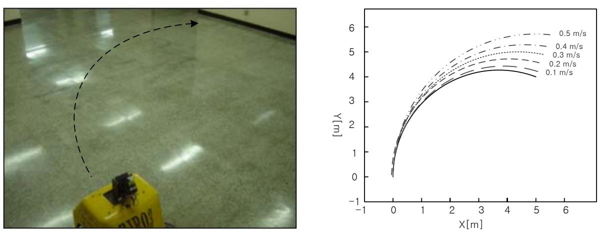

(a) Single Curvature

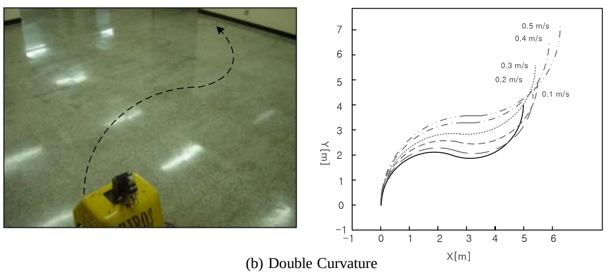

(b) Double Curvature

Fig. 9. Real experiments of the mobile robot Driving

Table 4. Rotation radius, driving error, time, and distance along the single-curvature trajectory

v_1 (m/s)	R_real (m)	Error (m)	Time (s)	Distance (m)
0.1	3.88	0.13	74.0	7.31
0.2	4.13	0.38	39.5	7.54
0.3	4.37	0.62	28.8	7.75
0.4	4.61	0.86	24.0	7.98
0.5	4.98	1.23	21.5	8.32

Table 5. Rotation radius, driving error, time, and distance along the double-curvature trajectory

v_1 (m/s)	R1_real (m)	R2_real (m)	Error (m)	Time (s)	Distance (m)
0.1	2.02	2.06	0.51	77.2	7.67
0.2	2.25	2.25	1.02	41.6	8.08
0.3	2.47	2.38	1.44	32.1	8.12
0.4	2.85	2.89	2.43	28.8	8.80
0.5	3.12	3.15	3.01	26.2	9.33

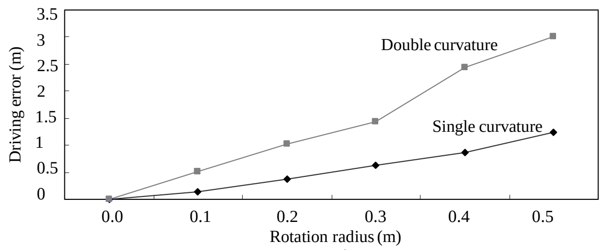

(a) Comparison of driving-error

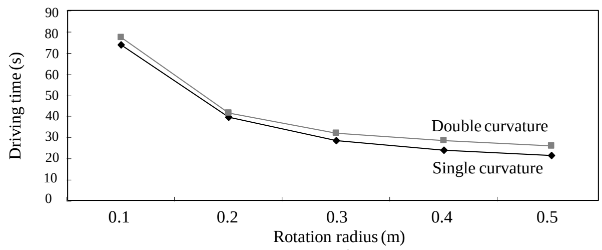

(b) Comparison of driving-time

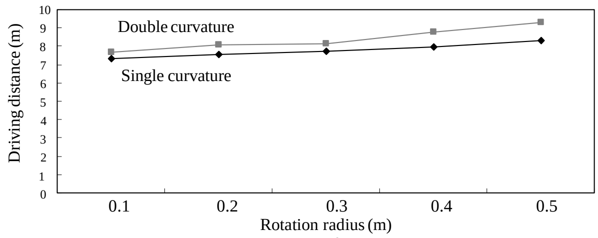

(c) Comparison of driving-distance

Fig. 10. Comparison of single- and double-curvature driving characteristics

The second experiment is performed to show the tracking and capturing of a moving object by the mobile robot. As it is shown in Fig. 8, the mobile robot follows two curved paths and a straight path to capture a moving object. Figures 12 and 13 show the real trajectories followed by the mobile robot. In this experiment, the mobile robot's velocity is 0.1m/s, while the moving object has the velocity of 0.05m/s. To minimize the tracking error of the mobile robot, the maximum allowable acceleration was kept as $0.05m/s^2$. The initial position of the mobile robot was (1, 2, 90^o), and the moving object was initially located at (0, 2, 25.5^o) before the experiment. The first curved path has rotation radius of 1.5m. When the mobile robot followed this path, it had tracking error of 0.6m. Along the second straight line path, the mobile robot moved 2.8m, and by following the third curved path with rotation radius of 1m, the mobile robot hits the moving object to capture. The total traveling distance of the mobile robot was 6.91m, the the tracking error was 1.4m. The total time to capture the moving object was 71.2seconds.

Fig. 11. Capturing operation along the single-curvature trajectory

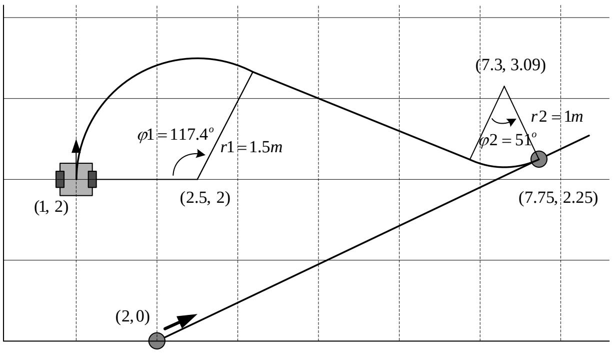

Fig. 12. Tracking and Capturing Trajectory

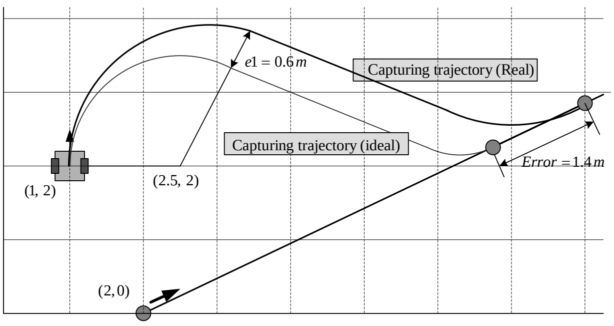

Fig. 13. Tracking error

6 Conclusions

This paper demonstrated optimality of a single curvature trajectory in capturing a moving object by a mobile robot. For the trajectory planning of a mobile robot in a curved path, superiority of the single curvature trajectory is verified based on the experiences and theoretical backgrounds. To practically show the effectiveness of the proposed algorithm, several experiments are performed with other trajectories, for an example, double-curved trajectory. Since the mobile robot using only dead-reckoning sensors aggregates the position estimation error while it is navigating, an error correction algorithm is necessary to support a precise and prompt control performance. Frequent error correction processes degrade the driving performance critically and may cause unstable operations. Providing a trajectory which causes less error for the mobile robot is very effective for the precise and fast curved motion. To improve the driving accuracy of the mobile robot, intelligent position estimation schemes and driving control algorithms are necessary to develop further as future research works.

This work was supported (in part) by the Ministry of Science and Technology, Korea, under the University Region Research Center Project

References

[1] M. W. Spong and M. Vidyasagar, Robot Dynamics and Control, John Wiley & Sons, 1989.

[2] K. Hirai, M. Hirose, Y. Haikawa and T. Takenaka, "The Development of Honda Humanoid Robot," Proc. *IEEE Int. Conf. on Robotics and Automations*, pp. 1321-1326, 1998.

[3] Jong-Woo Moon, "A Study on Kinematic Correction and Trajectory Tracking of Wheeled-Mobile Robots with 2 D.O.F," Department of Electronic Engineering Graduate School of Kyung Hee University, Seoul, Korea, 2000.

[4] Yong-Jun N, "A Study on the reduction of Navigation error for Curvilinear navigation of Mobile Robot using Neural Network," Department of Electronic Engineering Graduate School of Chonnam National University, Kwangju, Korea, 2002.

[5] G. Dudek and M. Jenkin, Computational Principles of Mobile Robotics, Cambridge university press, 2000.

[6] W. E. Dixon, D. M. Dawson, E. Zergeroglu and A. Behal, Nonlinear Control of Wheeled Mobile Robots, Springer, 2003

[7] W. E. Dixon, M. S. de Queiroz, D. M. Dawson, and T. J. Flynn, "Controlling Mobile Robots in Distributed Intelligent Sensor Network," *IEEE Trans. On Control Systems Technology*, vol. 12, no. 1, Jan. 2004.

[8] S. I. Grossman and W. R. Derrick, Advanced engineering mathmatics, HarperCollins Publishers, 2000.

The Tenth International Symposium on Artificial Life and Robotics 2005(AROB 10th '05),
B-con Plaza, Beppu, Oita, Japan, February 4-6, 2005

Proposing a Passive Biometric System for Robotic Vision

M. Masudur Rahman, Seiji Ishikawa
Department of Mechanical and Control Engineering
Kyushu Institute of Technology, Japan
Email: rahman@ss10.cntl.kyutech.ac.jp

Abstract:
We present a passive biometric system to the detection and identification of human faces and ears and develop a multimodal biometric system using eigenfaces and eigenears. A new technique of tracking a human face and an ear from the same image of a particular person is proposed that provides us to use a single camera for developing the proposed biometric system. The proposed system uses the extracted face and ear images to develop the respective feature spaces via the PCA algorithm called eigenfaces and eigenears, respectively. A new face and ear can be characterized by calculating the Euclidean distance between the classes of eigenfaces or eigenears and the new face or ear, respectively. Eighteen persons' faces and ears are employed for developing the databases of the eigenfaces and eigenears, and new faces and ears taken from various sessions of the same persons are employed for the identification. The proposed multimodal biometric system shows promising results than individual face or ear biometrics investigated in the experiments.

1. Introduction

Many of security companies are seeking a suitable biometric system that can create its database and identify targeted person passively. Such a system is especially important for robotic vision where subject's cooperation or direct interaction of human and robot may not always be available. In some cases, a subject's involvement may cause severe threat to the biometric systems especially for identifying a suspect or a terrorist. In addition, an automatic personal identification system based solely on a particular biometric component such as fingerprint or face is often not able to meet the security satisfaction [1]. We need such a system where acquisition of biometric database and its verification could be developed without a subject's concern, and the system performance will satisfy the security requirement. A new multimodal biometric system based on eigenfaces [2] and eigenears [3] is introduced in this paper. We develop a passive multimodal biometric system where subject's concern is not necessary. The proposed system can be implemented for developing a passive identification system employing a humanoid robot and it can be of a suitable application to an airport security system.

In the past, various studies have been done in biometric systems. However, the area of passive and/or multimodal biometric systems is quite new in biometric research. We have seen some of studies where face and ear have been chosen individually as the biometric components [4, 6]. However, the present study merges the eigenfaces and eigenears for developing a passive multimodal biometric system where face and ear are the biometric component.

In this paper, we propose and develop a prototype passive biometric system using eigenears and eigenfaces. The images of the ears and faces are collected from a single image of a particular person, and the databases of eigenears and eigenfaces via the PCA algorithm are produced. New type of biometric data (ear or face) is verified using the databases, and personal verifications are done judging the match-record. Since the proposed study extracts face and ear from the same image, the system does not require the application of multiple cameras. Or, we can also employ a ceiling camera for extracting such images. To the best of our knowledge, this is a new method in the biometric systems.

We have presented a brief formulation of the proposed biometric system. In the experiment, we have presented three different results for comparing the face, ear and multimodal biometrics. A discussion and concluding remarks are also placed at the end of this study.

2. Eigenfaces and Eigenears

PCA is a very powerful technique for selecting appropriate features or to reduce the dimension in which variation in the dataset is preserved. Thus the

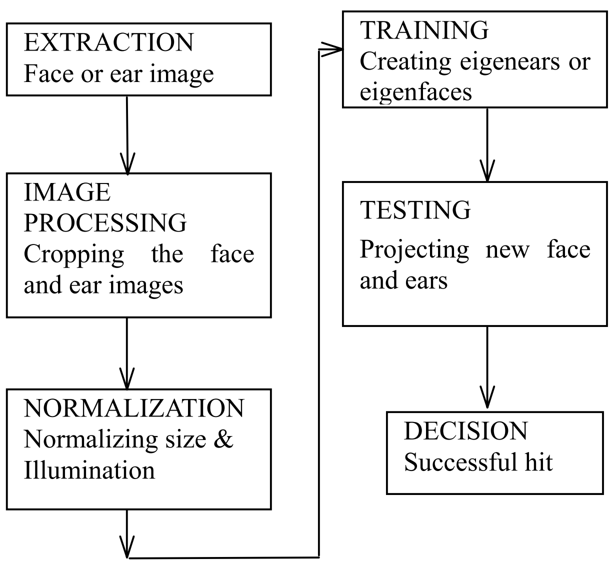

Figure 1: Flow chart of the system's algorithm.

classification is done in a lower dimensional space called the eigenspace, which is just the space defined by the principal components or the eigenvectors of the data set.

In case of face or ear images, the principal components are called eigenfaces or eigenears, respectively. The proposed system performs various procedures that are shown in **Figure 1**. In the extraction stage, acquired training face and ear images are cropped to a specified size from the same image of a particular subject. Image processing step includes geometric normalization and masking. Different masks can be used to avoid the unnecessary parts of the images. In the verification stage, it consists of two stages; training stage and testing stage. In the training phase, the eigenears and eigenfaces are developed choosing the appropriate eigenvectors. In the testing phase, the decision of the identification is taken based on the Euclidean distance between the classes of eigenfaces or eigenears and new faces or ears, respectively.

2.1 Calculating Eigenfaces or Eigenears

Let a face or ear image *I*(x,y) be a two dimensional *N* by *N* array of intensity or a vector dimension N^2. Let the training set of face or ear images be

$$\boldsymbol{x}_1, \boldsymbol{x}_2, \boldsymbol{x}_3, \ldots \boldsymbol{x}_M \tag{1}$$

The average face or ear of the set is defined by

$$\boldsymbol{\psi} = \frac{1}{M}\sum_{n=1}^{M} \boldsymbol{x}_n \tag{2}$$

Each face or ear differs from the average by the vector $\boldsymbol{\varphi}_i = \boldsymbol{x}_\mathrm{i} - \psi$. A covariance matrix can be obtained by

$$\begin{aligned} C &= \frac{1}{M}\sum_{i=1}^{n} \boldsymbol{\varphi}_i \boldsymbol{\varphi}_i^\mathrm{T} \\ &= \mathbf{X}_n \mathbf{X}_n^T \end{aligned} \tag{3}$$

where, X is the new image set obtained by the subtraction result between each image and φ_i. This set of very large vectors is then subject to principal component analysis that seeks a set of *k* orthogonal vectors or the principal components $\boldsymbol{e}_i$ and their associated eigenvalues λ_i which best describes the distribution of data. The vectors $\boldsymbol{e}_k$ and scalars λ_k are the eigenvectors and eigenvalues, respectively, of the covariance matrix. The *N* dimensional space defined by all the eigenvectors of *C* is reduced via the principal component analysis [8]. One may find a simple method to select the eigenvectors proposed by Turk and Pentland [2]. As a result, the chosen *K* ($1 \le k << N^2$) eigenvalues $\boldsymbol{\lambda}_k$ (*k*=1,2,…,*K*) and corresponding eigenvectors $\boldsymbol{e}_k$ are obtained. The *k*-dimensional vector defined by the eigenvectors $\boldsymbol{e}_k$ is called an eigenface or eigenear. Because these vectors are the eigenvectors of the covariance matrix corresponding to the original face or ear images and they are faces or ears like their appearances.

2.2 Classifying new Faces or Ears using Eigenfaces or Eigenears

After creating the eigenfaces or eigenears, classification of new images becomes a pattern recognition matter. A new face or ear image (**x**) is transformed into its eigenface or eigenear component projected onto the eigenfaces or eigenears by the following way,

$$w_k = \boldsymbol{e}_k^T(\mathbf{x} - \psi) \tag{4}$$

for $k = 1, 2, \ldots, k'$. This describes a set of point-by-point image multiplication and summations. The weight from the vectors $\boldsymbol{\Omega}^\mathrm{T} = [w_1, w_1, \ldots, w_{k'}]$ that describes the contribution of each eigenface or eigenear in representing the input face or ear image treating the eigenfaces or eigenears as a basis set of face or ear images [4]. Calculating an Euclidian distance is the simplest way to classify the new face or ear class as follows,

$$d_k = \left\|(\Omega - \Omega_k)\right\| \tag{5}$$

where Ω_k is a vector describing the *k*th face or ear class. A face is classified as belonging to class *k* when the minimum d_k is in the defined threshold limit of ε_k. Otherwise, the new face or ear is defined as 'unknown'. The unknown face or ear can be used for developing further database.

3. Experimental Results

Three different issues are considered for performing this study. We have initially developed two individual biometrics using face and ear separately. Finally, a multimodal biometric system is developed merging the face and ear biometrics.

As we have described in the Section 2 and Figure 1, there are three main steps involved in developing the proposed system: (a) extraction of images, pre-processing and normalization, (b) creating eigen databases for ears and faces, and (c) verification. We have employed the databases of university of Notre Dame [9] which is composed of five different sessions and imaging conditions. The database contains five different variations based on the sessions collected in the database. We employ one set for creating the databases of eigenears and eigenfaces, and four other variations are used for the verification. In the preprocessing step, we have used only the side faced-images for obtaining the (right) ears and faces together. **Fig. 2** shows 5 person's images out of total 18 employed in this study. Some of image samples used in the experiments are shown in **Fig. 3** along with extraction procedures of the ear and face

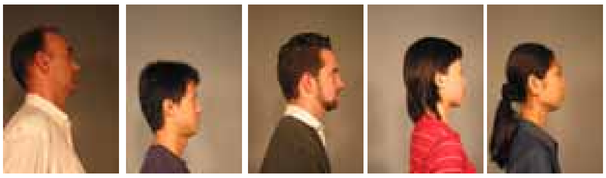

Figure 2: Some of models employed in the experiment out of total 18.

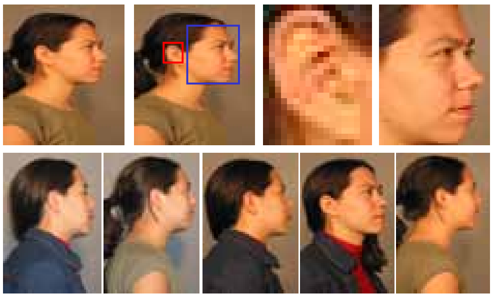

Fig. 3. Procedures of extracting ear and face images (upper), and image variations used in the experiments (lower).

area (upper row). In the Fig. 3 (lower row), 5 images of a particular subject taken from 5 different sessions are shown. The extraction of faces and ears are yet not automatic, as we need some manual interruption for selecting the exact size of the ear and face. The images are cropped to a specific size with just containing the face and ear. Finally, the original size of the cropped images is reduced to a size of 32x32 pixels for the sake of efficiency. Now, the images are normalized for minimizing the lighting effect.

We have developed the databases of eigenears and eigenfaces of 18 subjects as described in the section 2. Performance of the verifications is obtained based on successful hits by calculating the distance within the prescribed threshold. In case of multimodal biometric system, if the system recognizes any one of the ear or face of a particular person successfully, we consider the correct identification of the subject. Detail of experimental dataset is placed in **Table 1.** We have also obtained the classification results on various issues that are placed in **Fig. 4, Fig., 5, Fig. 6** and **Fig. 7**. Performance based on eigenvectors, eigenvector vs. CPU time, and performance based on day variations are shown in Fig 4, Fig. 5 and Fig. 6, respectively. Fig. 7 shows the performance of the proposed multimodal system based on required eigenvectors. It has shown that multimodal biometrics has better performance over individual face and ear biometrics. In comparison between face and ear biometrics, face biometrics has shown better performance than ear biometrics. However, ear biometrics has shown better performances in case of CPU time and day variations. Ear biometrics has absolutely no effect on day variations. We have obtained the best recognition rate of 94.44% by multimodal biometric system on 40 eigenvectors. The best performances of each system are also placed in Table 1.

4. Discussion

The present study has aimed to develop a multimodal biometric system for personal identification that can also work passively. Experimental results have shown that the concept of tracking the ear and face from the same image of a person has received better performances over the many available methods [4-7]. Although there was no intention to make any recommendation in favor of any particular biometric systems, it is observed that face biometrics has performed better than ear biometrics. The

Table 1: Experimental setup

Biometrics	Total images	Test Variations	Best Perform.
Face	5x18=90	4	88.88 %
Ear	5x18=90	4	77.77%
Multimodal	2x5x18=180	4	94.44%

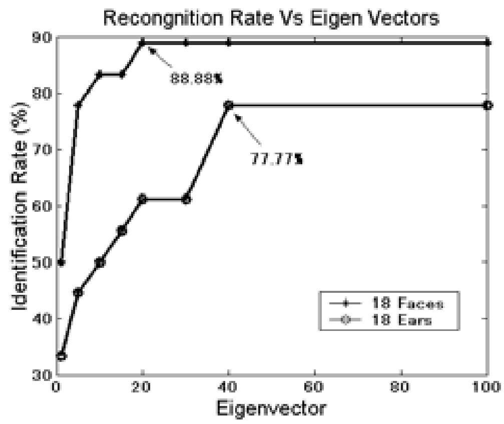

Figure 4: Experimental results on eigenvectors vs. recognition rates.

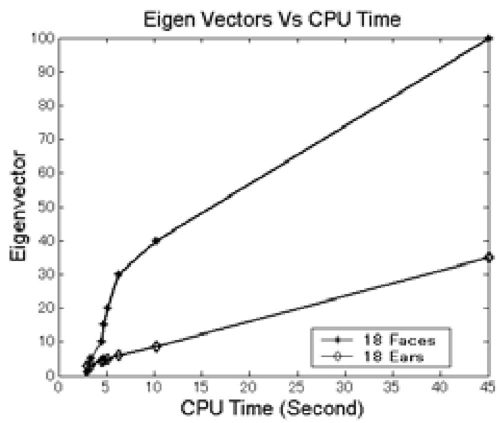

Figure 5: Experimental results on CPU time vs. eigenvectors.

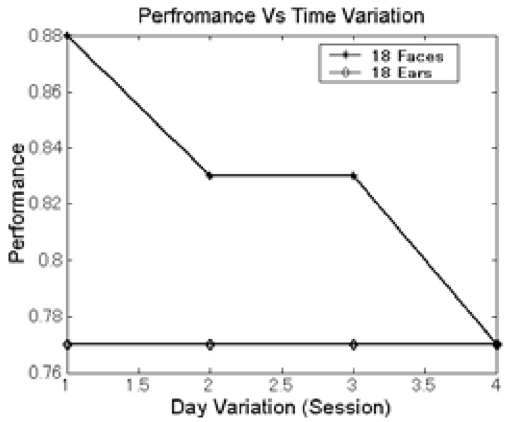

Figure 6: Experimental results on recognition rate vs. day variations.

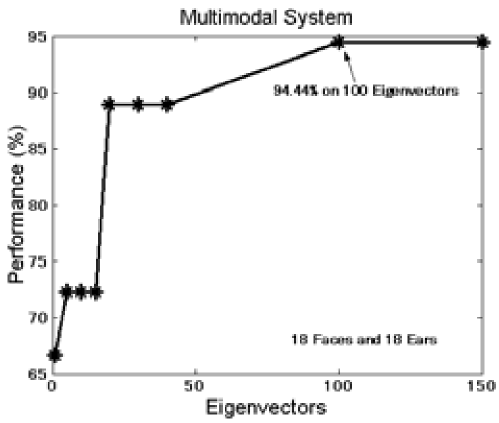

Figure 7: Multimodal biometric system. Experimental results on eigenvectors vs. recognition rate.

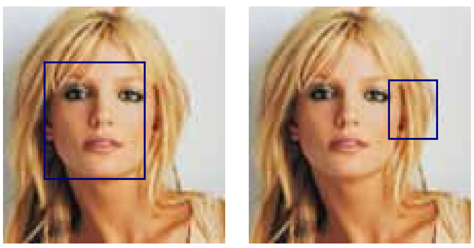

(a) (b)

Figure 8. Occlusion problems in extracting face and ear images. Extraction of (a) face is possible but (b) ear is not possible due to long hair. *Images of Britney Spears collected from the Internet*

results presented in this paper differ slightly with the paper by Burge and Burger [7] where they have showed ear-based biometrics better than face biometrics. Variations on the ears and faces may give us different results as described by Chang and Bower [3]. Our results, on the other hand, do support the conclusion that a multimodal biometric using eigenfaces and eigenears can perform better than either one alone. We have seen the same results in case of using face and fingerprint or face and voice [1]. However, use of face and ear has the best combination for developing a passive biometric system. This research may open up some new multimodal biometric systems with merging two or more biometric systems such as face and gait or face, ear and gait.

Since the proposed biometric system can detect and identify human face and ear passively, it can be of a suitable application in a robotic vision field. A robot can be a part of security systems in an airport for security checking.

The present study has some limitations on several factors, e.g., occlusion, use of appropriate mask, etc. The occlusion may sometimes greatly influence to the proposed system. **Fig. 8** shows a simple example where occlusion problem makes impossible to use the ear as a biometric component. Although face biometric can be implemented in this particular case, a multimodal system cannot be developed due to absence of ear image. There are some extensive works on extracting face and ear images using different masking. Although use of such masks needs some manual work, better results can be obtained in different imaging conditions [3,9]. We need some further studies with considering the mentioned factors such as occlusion by facial hair or partially covered ear by long hair, and different masking.

5. References

1. L. Hong and A. Jain: "Integrating Faces and Fingerprints for Personal Identification", *IEEE Trans. on PAMI*, Vol. 20, No. 12, pp. 1295-1307 (1998).
2. M. Turk and A. Pentland: "Eigenfaces for Recognition", *J. of Cognitive Neuroscience*, Vol. 3, No. 1, pp. 71-86 (1991).
3. K. Chang and K. W. Bowyer: "Comparison and Combination of Ear and Face Images in Appearance-Based Biometrics", *IEEE Trans. on PAMI*, Vol. 25, No. 9, pp. 1160-1165(2003).
4. M. Turk and A. Pentland: Face recognition Using Eigenfaces, *Proceedings of the CVPR*, pp. 586-591(1991).
5. L. Sirovich and M. Kirby: "Low Dimensional Procedure for Character of Human Faces", *J. of Opt. Society of America*, Vol. 4, No. 3, pp. 519-524(1987).
6. B. Victor, K. Bower and S. Sarkar: "An Evaluation of Face and Ear Biometrics", *Proceedings of the ICPR* CDROM Version (2002).
7. M. Burge and W. Burger: "Ear Biometrics in Computer Vision", *Proc. of the Int'l Conf. on Pattern Recognition*, CD ROM (2002).
8. R. C. Gonzalez and P. Wintz: *Digital Image Processing*, Addison-Wesley Publishing Company, Inc. (1992).
9. P. J. Flynn, K. W. Bowyer, and P. J. Phillips: "Assessment of time dependency in face recognition: An initial study," *Audio and Video-Based Biometric Person Authentication*, pp.44-51 (2003).

The Tenth International Symposium on Artificial Life and Robotics 2005(AROB 10th '05),
B-con Plaza, Beppu, Oita, Japan, February 4-6, 2005

Human Motion Recovery by Mobile Stereoscopic Cameras

Tan, J. K.*, Yamaguchi, I.*, Ishikawa, S.*, Naito, T.**, Yokota, M.**

*Department of Control Engineering, Kyushu Institute of Technology
Sensuicho 1-1, Tobata, Kitakyushu 804-8550, Japan
Email: {etheltan, ishikawa}@cntl.kyutech.ac.jp

**Department of Periodontology and Endodontology, Kyushu Dental College
Manazuru 2-6-1, Kokurakita, Kitakyushu 803-8580, Japan

Abstract

A method is described for reconstructing 3-D object models, particularly human models, based on multiple calibration-free mobile cameras and a computer. Existing optical 3-D modeling systems must employ calibrated cameras that are set at fixed positions. This inevitably gives constraints to the range of movement with object motions. In the proposed method, multiple mobile cameras take images of an object moving widely and its 3-D model is reconstructed from the obtained video image streams. Advantages of the proposed method include that the employed cameras are calibration-free and that the method claims at least two cameras, stereoscopic cameras, to be employed, which offers a simple system. The theory is described and the performance is shown by the experiment on 3-D human motion modeling. Precision of the 3-D model is also shown with discussion.

Keywords: Stereoscopic cameras, mobile cameras, motion capture, motion recovery, computer vision.

1. Introduction

Three-dimensional shape recovery techniques of deformable objects have attracted researcher especially in a computer vision community over the last decade. Particularly human motion recovery has become popular, since it has various potential applications such as creating a human model in video games or in a virtual reality space, motion analysis in various sports, traditional dances or skills preserving in an electronic museum, *etc*. Stereoscopic vision is, as is well known, a popular technique for performing such 3-D shape recovery. But it is not very convenient particularly for outdoor use because of camera calibration. Alternatively motion recovery employing magnetic sensors is also a common technique. It restricts motion range of the subject, however. Optical measurements with non-contact techniques that can capture wide range motions are obviously better for wide spread of the technique.

We have already proposed a shape recovery technique of 3-D non-rigid objects based on multiple calibration-free cameras [2,3]. It employs a factorization method [1] with an extended measurement matrix [2] that contains spatiotemporal information on the object's deformation. Since the technique necessitates cameras to be fixed around the object concerned, it can only deal with the motions/ movements in a limited space. This disadvantage can be overcome by the employment of multiple mobile cameras with much more flexibility in image taking.

The idea of our approach is to devise a way of creating a measurement matrix that should be a full matrix whose entries are all known. Once a full measurement matrix is given, it can be factorized into a camera orientation matrix and a shape matrix [1]. The shape matrix gives information on a 3-D shape/motion of the object concerned. This paper proposes a multiple mobile cameras system as a most convenient way of taking images of an object moving in a wide range. The method is described and some experimental results are shown. Precision of the created 3-D model is as well explained and discussion is given.

2. A measurement matrix for mobile cameras

The measurement system proposed in [2,3] places cameras at fixed positions like existent 3-D measurement systems commercially available. This inevitably restricts the motion of a person whose 3-D model is the present concern. An efficient way of taking images of such a moving object is to let cameras move along with the object. The idea of moving a camera is normally employed when static objects are concerned for 3-D shape recovery [1]. The technique presented in this paper allows camera motion to widely moving non-rigid as well as rigid objects.

We suppose that F cameras take images of an object by changing their locations L times. If we denote a measurement matrix of the F cameras at location l (l=1,2,…,L) by W_l, a general form of an overall measurement matrix W is given by the following;

$$W = \begin{pmatrix} W_1 & \mathbf{0} & \mathbf{0} & \mathbf{0} \\ \mathbf{0} & W_2 & \mathbf{0} & \mathbf{0} \\ \mathbf{0} & \mathbf{0} & \ddots & \mathbf{0} \\ \mathbf{0} & \mathbf{0} & \mathbf{0} & W_L \end{pmatrix}. \quad (1)$$

Here matrices W_l (l=1,2,…,L) are placed at the diagonal positions of W and the remaining entries are all vacant. The matrix having this form cannot be further processed in terms of factorization [1].

It should as well be noted that cameras cannot be calibrated in this technique because of their mobility.

3. Mobile cameras system I

Ncan be done in the context of factorization method. To go further, we proposed a mobile frame system [5] in which cameras are placed fixed on a mobile frame. We placed the world coordinate system on the mobile cameras, instead of placing it on the ground where the mobile cameras move. Then the circumstance is equivalent to that the world moves around the cameras in place of the cameras moving in the world. This means that all the sub-matrices W_l (l=1,2,…,L) can be aligned in the same rows as follows;

$$W' = \begin{pmatrix} W_1 & W_2 & \cdots & W_L \end{pmatrix}. \quad (2)$$

Equation (2) provides a full measurement matrix and it can be factorized according to [2,3], and finally obtained shape matrix S giving 3-D coordinates of the motion of the object relative to the cameras.

4. Mobile cameras system II

In this section, we describe a technique [6] how to take images and recover shape of a widely moving object, employing independently moving cameras. In the technique, the camera orientations are all different through the camera movement from location l=1 to l=L. Therefore the cameras need calibration to obtain 3-D information of the object. But unlike existent 3-D recovery techniques that perform camera calibration using 3-D tools, the proposed technique doesn't employ such tools for the calibration. Instead, it employs rigid points that are observed in the captured image streams. The proposed procedure is described in the following.

At the position l (l=1,2,…,L), the cameras are required to observe common feature points on static objects (referred to as *static feature points* hereafter) other than the feature points on non-rigid objects (referred to as *moving feature points* hereafter). Let the sub-matrix containing static feature points be denoted by W_l^{R} and the sub-matrix containing moving feature points be denoted by W_l^{N}. Then the sub-matrix W_l at position l in Eq.(1) can be written as

$$W_l = \begin{pmatrix} W_l^{\mathrm{R}} & W_l^{\mathrm{N}} \end{pmatrix}. \quad (3)$$

Since matrix W_l^{R} (l=1,2,…,L) only contains common static feature points, they are collected into a single matrix W^{R} by

$$W^{\mathrm{R}} = \begin{pmatrix} W_1^{\mathrm{R}} \\ W_2^{\mathrm{R}} \\ \vdots \\ W_L^{\mathrm{R}} \end{pmatrix}. \quad (4)$$

Applying factorization to the above full matrix W^{R}, we have

$$W^{\mathrm{R}} = M \cdot S^{\mathrm{R}}, \quad (5)$$

where matrix S^{R} contains the 3-D coordinates of all the chosen static feature points. Camera orientations at location l (l=1,2,…,L) are also obtained by matrix M. Let us denote the camera orientation matrix M by

$$M = \begin{pmatrix} M_1 & M_2 & \cdots & M_L \end{pmatrix}^{\mathrm{T}}. \quad (6)$$

Then the 3-D coordinates of moving feature points are then calculated by

$$S^{\mathrm{N}} = M^{+} \cdot W^{\mathrm{N}}. \quad (7)$$

Here S^{N} is a matrix composed of S_l^{N} , M^+ is a matrix whose diagonal elements are M_l^+, and W^{N} is a matrix whose diagonal elements are W_l^{N}.

In this way, the measurement matrix of Eq.(1) can be decomposed as

$$W = M \cdot S \quad (8)$$

and all the feature points registered in matrix W recover their 3-D positions. They are given by

$$S = (S^{\mathrm{R}} \mid S^{\mathrm{N}}). \quad (9)$$

Precision of recovered 3-D shape is evaluated by projecting the obtained 3-D shape back onto the original video images [2]. We multiply the derived matrices M and S to obtain 2-D positions of recovered feature points on each image plane. Let us denote the result of the multiplication by $\hat{W}$, i.e.,

$$\hat{W} = M \cdot S. \quad (10)$$

The precision is then computed by evaluating the difference between W and $\hat{W}$.

5. Experimental results

In the performed experiment, a subject moved around in the yard and its motion was taken images by two mobile cameras, denoted by C_L and C_R, respectively. The cameras were connected to video transmitters and the video images were sent via the transmitter and the receivers to two PCs in a distant room. Sampling interval was 0.1 second and 100 images were sampled. Thus 10 seconds motion was processed for recovery. The chosen feature points are 24 for static feature points and 17 for moving feature points. In this particular experiment, the subject's motion was controlled so that the two cameras could observe the 24 static feature points during all the observation time.

Video images, obtained from cameras C_L and C_R, of the subject's motion are partly shown in **Fig.1**. The result of 3-D recovery is given in **Fig.2**. In both figures, the time proceeds as indicated by arrows. The precision of the recovery was computed and the recovery error was 1.75% for static feature points and 1.71% for moving feature points with respect to the left camera, and 1.72% for static feature points and 2.12% for moving feature points with respect to the right camera. Thus we have 1.8% of the average recovery error. **Figure 3** is the illustration of the precision of the experiment. The recovered images shown by broken lines are superposed onto the original image shown by solid lines. As we have achieved very small recovery errors, it is actually not easy to see the difference between them.

6. Conclusions

We have shown a technique for 3-D human motion recovery employing mobile cameras. In this technique, at least two cameras are used for the recovery. Therefore it can be called mobile stereoscopic vision by mobile stereoscopic cameras. Camera calibration is done using some representative points observed in images. This is completely different from existent techniques that use 3-D tools for the calibration. In this sense, our technique is easier to use especially for those who are not very familiar with shape/motion recovery.

The precision of the recovery or the recovery error was satisfactorily small, 1.8%, in the performed experiment, which is comparable to existent techniques based on fixed stereo cameras. At the moment, we employ orthographic projection as a lens model. Changing the model to week perspective projection, e.g., may result in better precision. This remains for the next step of the study.

Since the proposed mobile cameras system does not need ordinary camera calibration, it can be employed in remote places of interest where time compensation by tedious camera calibration may cause loosing important shots of the event of interest. In the proposed system, one only have to bring two cameras or more to such a place and just start taking images of the event there. If one sends the taken images back to the lab by a video transmitter or even internet, for example, the event can be modeled in a 3-D way in the lab. This means that a dynamic event at any distant place can be modeled in a 3-D way by the proposed technique. This pattern of employment of the technique may have various applications in future.

This study was partly supported by JSPS KAKENHI (14580450), which is greatly acknowledged.

References

[1] C. Tomasi, T. Kanade, "Shape and motion from image streams under orthography: A factorization method", *Int. J. Computer Vision*, Vol.9, No.2, pp.137-154, 1992.

[2] J. K. Tan, S. Ishikawa, "Human motion recovery by the factorization based on a spatio-temporal measurement matrix", *Computer Vision and Image Understanding*, Vol.82, No.2, pp.101-109, 2001.

[3] J. K. Tan, S. Ishikawa, "Recovering 3-D motion of team sports employing uncalibrated video cameras", *IEICE Trans. on Information and Systems*, Vol. E84-D, No.12, pp.1728-1732, 2001.

[4] Y. Chen, G. Mediomi, "Object modeling by registration of multiple range images", *Image and Vision Computing*, Vol.10, No.3, pp.145-155, 1992.

[5] T. Tabusa, J. K. Tan, S. Ishikawa, "Recovering human motions by mobile video cameras and factorization", *Proc. of Asian Conf. on Computer Vision*, 2002.

[6] J. K. Tan, I. Yamaguchi, T. Tabusa, S. Ishikawa, S. Hirokawa, "Various image taking strategies for 3-D object modeling based on multiple cameras", *Proc. of Int. Conf. on Image Processing,* 2487-2490, 2004.

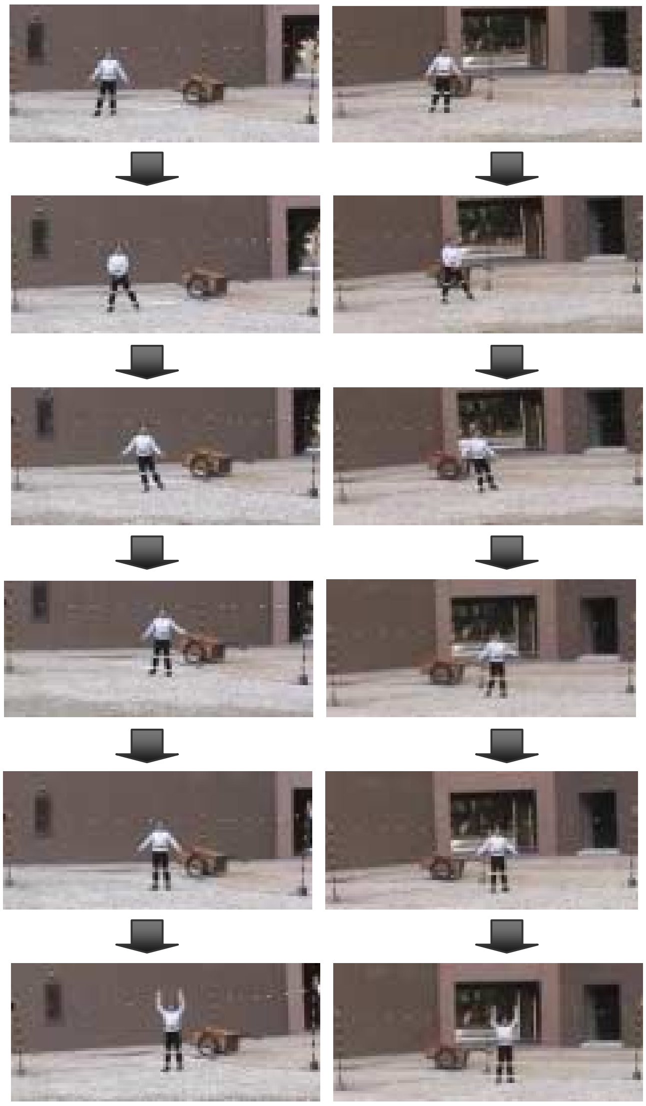

(a) (b)

Fig. 1. Video images of a human in motion: (a) C_R, and (b) C_L .

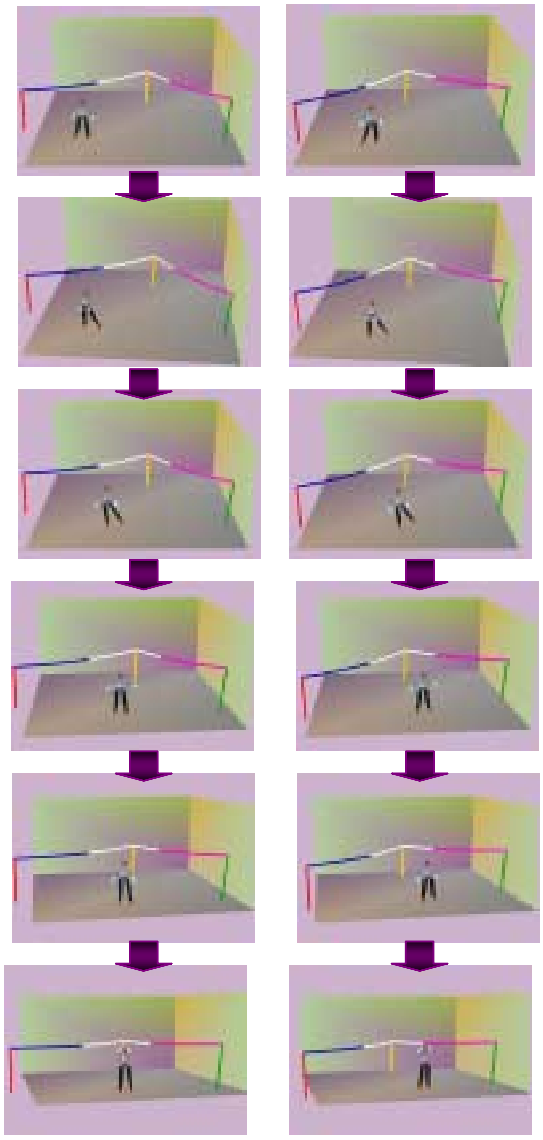

(a) (b)

Fig. 2. Recovered 3-D motion: (a) C_R, and (b) C_L.

C_R

C_L

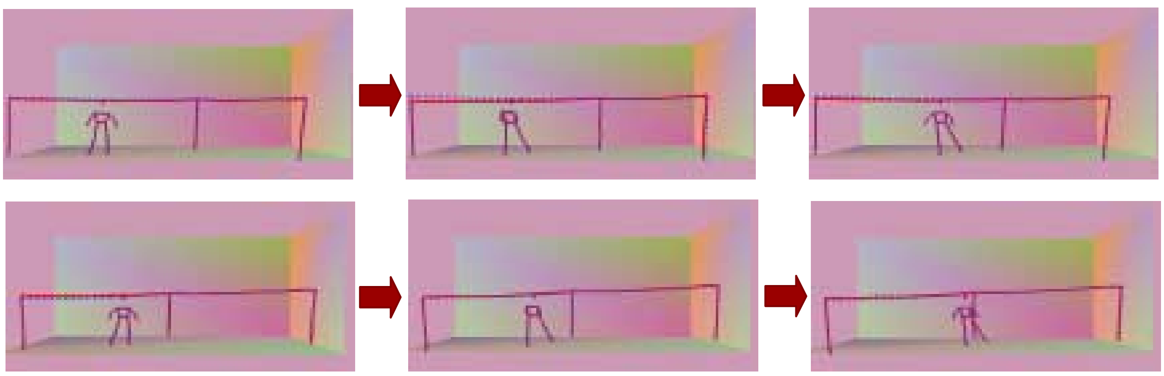

Fig. 3. Precision of the recovered 3-D model.

The Tenth International Symposium on Artificial Life and Robotics 2005(AROB 10th '05),
B-con Plaza, Beppu, Oita, Japan, February 4-6, 2005

A High-speed Human Motion Recovery Based on Back Projection

M. Uchinoumi*, J. K. Tan*, S. Ishikawa*, T. Naito**, M. Yokota**

*Department of Control Engineering, Kyushu Institute of Technology
Sensuicho 1-1, Tobata, Kitakyushu 804-8550, Japan
Email: {etheltan, ishikawa}@cntl.kyutech.ac.jp

**Department of Periodontology and Endodontology, Kyushu Dental College
Manazuru 2-6-1, Kokurakita, Kitakyushu 803-8580, Japan

Abstract

This paper describes a novel technique for high-speed human motion recovery. For a 3-D human motion recovery, stereoscopic vision is a normal technique as well as the employment of the magnetic field. But they cannot escape from the difficulty of marker tracking. In this paper, a novel motion recovery technique is proposed based on back projection of silhouette images. This technique has some advantages over others that it does not employ markers and that it has a simple architecture. In the performed experiment, the proposed motion recovery technique is implemented on a system containing a LAN, a host computer and four pairs of a camera and a computer and it achieves high-speed human motion recovery.

Keywords: Motion recovery, human motion, back projection, silhouette, real-time.

1. Introduction

Three-dimensional human motion recovery is an attractive field of study and recently it has gained much attention among various communities related to digital image processing. It is, for example, employed for producing 3-D characters in video games. Evaluating 3-D motions in sports or in rehabilitation is as well an important application field.

An optical motion recovery is a technique that captures images by cameras and recovers 3-D motion sequences of a human by a computer. Existent major motion recovery techniques are divided into two categories; one with marker tracking [1,2] and the other without markers [3]. In the former, 3-D positions of the markers attached on a human body recover by geometric computation. But automatic marker tracking remains a bottleneck of the technique. On the other hand, motion recovery without markers has an advantage over the former in its high-speed nature in processing. But it still suffers from heavy computational load, resulting in expensive products. These drawbacks prevent the existent motion recovery techniques from being popular among various users who need motion recovery for their familiar subjects such as evaluation of the effect of exercises in rehabilitation.

In this paper, a novel technique is presented for 3-D human motion recovery based on back projection of silhouette images. It contains some accelerated computational techniques that contribute to high-speed motion recovery. They include (1) simple architecture by the employment of a server-client system for computation of back projected images, (2) use of a look up table to realize quick search for the voxels within the object concerned, and (3) use of difference images for volume recovery. Experiments are performed employing the proposed technique. The implemented system contains a host computer as a server and four camera-computer units as clients mutually connected via a LAN. Some results are shown on the recovery. The achievement of this study and further issues to be challenged are finally discussed.

2. Shape recovery by back projection

The idea of back projection is simple. Suppose one takes an image of an object by a camera. Subtraction of a background image from the acquired image yields a mask image of the object after some steps of image processing. The mask image is equivalent to a silhouette of the object from the camera orientation. Then one is able to imagine a cone defined by connecting the center of the camera lens and every point on the contour of the silhouette on the image plane, i.e., an image hull. Clearly the object exists within the cone. If one takes many images of the object from different orientations, each image defines a cone and the original object is obtained from the intersection of all the cones. This is the idea of back projection. See **Fig.1** for intuitive explanation of back projection. It is obvious that concave portions of the object concerned are lost in this recovery technique, since they cannot be observed on the silhouette from any orientations.

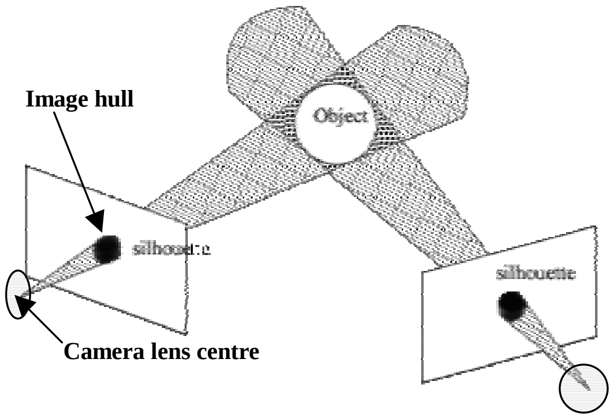

Fig. 1. Explanation of back projection.

At sample time t (t=1,2,…,T), a silhouette image $I_i(t)$ (i=1,2,…,n) of a human in motion is made from the image frame $\hat{I}_i(t)$ by subtracting the background image I_i^{B}, i.e.,

$$I_i(t) = \hat{I}_i(t) - I_i^{\mathrm{B}} \tag{1}$$

Image $I_i(t)$ contains a figure part and a ground. It then receives binarization. The resultant image is again denoted by $I_i(t)$ in which a human region denoted by $R_i(t)$ remains as a figure with the value 1. The ground is given the value 0. The region $R_i(t)$ is then projected back into the 3-D space to yield a volumetric region (or a cone) $V_i(t)$. These cones $V_i(t)$ (i=1,2, …,n) are collected and intersected to obtain a common region by

$$V(t) = \bigcap_{i=1,\dots,n} V_i(t) \tag{2}$$

The idea of the intersection is explained in **Fig.2** as a 2-D case, in which (a-c) three camera-client pairs produce cones and (d) their common part is extracted.

This procedure is repeated for t=1,2,…,T to obtain the set $\{V(t) \mid t = 1,2,...,T\}$, which gives the recovered 3-D motion sequence.

In order to use this technique, all the observing cameras must be calibrated in advance, since the back projection is performed employing direct linear transformation [4].

3. Strategies for high-speed computation

In order to realize high-speed shape recovery, some ideas are employed in the computation of back projection:

(1) Use of a server-client system to distribute computational load to client computers;

(2) Use of a look up table (LUT) to realize quick search for those voxels in the 3-D space whose projection onto a camera image plane is a single pixel within the silhouette in the image plane;

(3) Use of difference images for successive volume recovery, *i.e.*, the 3-D area at sample time t is produced by the back projection of those pixels in the region that received displacement between the image frame at t-1 and the image frame at t.

3.1 Distributing computational load by parallel architecture

In the back projection technique, a larger number of image taking cameras can realize higher precision of recovered motion. To speed up the computation, a server-client system is employed, when implementing the technique. Cones $V_i(t)$ (i=1,2,…,n) are produced at client computers i (i=1,2,…,n), respectively, and they are transferred through a LAN to a server, where the intersection by Eq.(2) is performed to yield $V(t)$.

One of the advantages of a server-client system is that it is a distributed computation system. If one needs to get more precise shape of the object concerned, one only has to connect more number of camera and client pairs to the system. This doesn't increase the overall computational load much, as the computation is done in parallel. Too many clients, however, cause the increase in data transfer time in the LAN, which may give negative influence on high-speed computation.

3.2 Listing correspondence between pixels and voxels

In the back projection method, the camera system employed must be done calibration in advance. Suppose that a voxel $\boldsymbol{X}_k \equiv (X_k, Y_k, Z_k)$ in the XYZ world coordinate system be projected onto the pixel $\boldsymbol{x}_{ij} \equiv (x_{ij}, y_{ij})$ of the ith camera's image plane. Then, as their relation, we have $x_{ij} \equiv x_{ij}(X_k, Y_k, Z_k)$

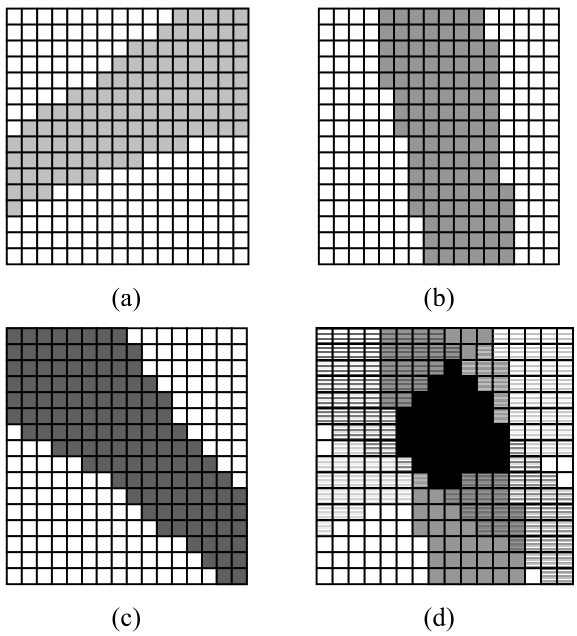

Fig. 2. The idea of back projection and intersection.

and $y_{ij} \equiv y_{ij}(X_k, Y_k, Z_k)$ by direct linear transformation method [4].

Employing these relations, every voxel in the *XYZ*-coordinate system is projected onto the corresponding single pixel on the image plane. It is obvious that, given a pixel $\boldsymbol{x}_{ij}$ on an image plane, the voxels on the line L_{ij} passing through the point $\boldsymbol{x}_{ij}$ and the lens center of the *i*th camera are all projected onto the pixel $\boldsymbol{x}_{ij}$. So this is normally many–to-one correspondence.

Let us denote the set of voxels on the above line L_{ij} by

$$S_{ij} = \{\boldsymbol{X}_k \equiv (X_k, Y_k, Z_k) \mid k = 1,2,..., K_{ij}\}. \quad (3)$$

Then the pairs $\{\boldsymbol{x}_{ij}, S_{ij}\}$ (*i*=1,2,…,*n*; *j*=1,2,…,*m*) are stored into a table called a LUT. Here *m* is the number of the pixels in the image plane of camera *i* (*i*=1,2,…,*n*). The elements of the set S_{ij} are calculated in advance, given the *XYZ* world coordinate system.

Once a silhouette image $I_i(t)$ is given, those pixels within the figure region $R_i(t)$ are found by scan on the image plane. Since the voxels corresponding to the pixels in $R_i(t)$ are known from the LUT, these voxels are marked 1 in the 3-D space yielding the volumetric region $V_i(t)$. The regions $V_i(t)$ (*i*=1,2,…,*n*) are all sent to the server to receive the procedure given by Eq.(2).

3.3 Employment of difference images

If the human motion concerned is not acted very fast, the difference of volumetric regions $V_i(t)$ and $V_i(t-1)$, and hence the difference of silhouette images $I_i(t)$ and $I_i(t-1)$, is not very large. Then creation of $V_i(t)$ can be done by creating only the different part between the silhouette images $I_i(t)$ and $I_i(t-1)$. If the motion is fast, this strategy may not be very effective and $V_i(t)$ had better be made directly. Selection of the strategies depends on the magnitude of the difference.

Let us denote $V_i(t)$ by $V_i(\boldsymbol{X}, t)$ and $R_i(t)$ by $R_i(\boldsymbol{x}, t)$ in order to emphasize the voxels and pixels in them, respectively. Let us also denote a difference image by $I_i^{\mathrm{d}}(t) \equiv I_i^{\mathrm{d}}(\boldsymbol{x}, t)$, i.e.,

$$I_i^{\mathrm{d}}(\boldsymbol{x}, t) = I_i(\boldsymbol{x}, t) - I_i(\boldsymbol{x}, t-1). \quad (4)$$

We further define the following two sets of pixels;

$$S_i^{\mathrm{d}}(t) = \{\boldsymbol{x} \mid I_i^{\mathrm{d}}(\boldsymbol{x}, t) = \pm 1\} \quad (5)$$

$$S_i(t) = \{\boldsymbol{x} \mid I_i(\boldsymbol{x}, t) = 1\} \quad (6)$$

Then the following three cases are applied to create successive cones. Here the number of the elements in the set *A* is denoted by n(*A*).

***Case* 0:** $t=1$:

For all $\boldsymbol{x}_{ij}$ such that $\boldsymbol{x}_{ij}$ is an element of $R_i(\boldsymbol{x}, t)$, and for all $\boldsymbol{X}$ such that $\boldsymbol{X}$ is an element of S_{ij}, let $V_i(\boldsymbol{X}, t) = 1$.

***Case* 1:** $n(S_i^{\mathrm{d}}(t)) < n(S_i(t))$ for *t*=2,3,…,*T*:

Let $V_i(\boldsymbol{X}, t) \equiv V_i(\boldsymbol{X}, t-1)$.

For all $\boldsymbol{x}_{ij}$ such that $I_i^d(\boldsymbol{x}_{ij}, t) = -1$, and for all $\boldsymbol{X}$ such that $\boldsymbol{X}$ is an element of S_{ij}, let $V_i(\boldsymbol{X}, t) = 0$.

For all $\boldsymbol{x}_{ij}$ such that $I_i^d(\boldsymbol{x}_{ij}, t) = 1$, and for all $\boldsymbol{X}$ such that $\boldsymbol{X}$ is an element of S_{ij}, let $V_i(\boldsymbol{X}, t) = 1$.

***Case* 2:** $n(S_i^{\mathrm{d}}(t)) \geq n(S_i(t))$ for *t*=2,3,…,*T*:

For all $\boldsymbol{x}_{ij}$ such that $\boldsymbol{x}_{ij}$ is an element of $R_i(\boldsymbol{x}, t)$, and for all $\boldsymbol{X}$ such that $\boldsymbol{X}$ is an element of S_{ij}, let $V_i(\boldsymbol{X}, t) = 1$.

Case 0 is the initial situation, i.e., *t*=1, and the region $V_i(1)$ is created directly from a silhouette image $I_i(1)$. There are two strategies for *t*=2,3,…,*T*. In case 1, the difference is smaller than the silhouette itself. The voxels are deleted from $V_i(t-1)$ that correspond to the pixels whose gray value is –1, and the voxels are added to $V_i(t-1)$ that correspond to the pixels whose gray value is 1, yielding $V_i(t)$. In case 2, the difference is larger than the silhouette itself and $V_i(t)$ is created directly from a silhouette image $I_i(t)$.

In this way, the region $V_i(t)$ is created. Once $V_i(t)$ (*i*=1,2,…,*n*) are collected at the server, the entire volumetric region $V(t)$ is computed and the entire motion is given as the set $\{V(t) : t = 1,2,..., T\}$.

4. Experimental Results

We have implemented the proposed technique in a system, which consists of four PCs and a single PC (CPU: Pentium, 1.7-3.2GHz) employed as clients and a server, respectively, and a 100Mbps LAN combining them each other. The clients are connected to respective digital cameras settled in a room. The cameras are calibrated in advance employing the DLT method. A 2m×2m×2m space in front of the cameras are digitized into 80×80×80 voxels in this particular experiment. A person acts various motions within the cubic space. The motions recover in a 3-D way by the proposed technique and the recovered motion is shown in the PC display.

In this paper, the result of a batting motion is shown. The experimental environment is shown in **Fig.3** and the recovered 3-D motion is given in **Fig.4**.

The process time for the recovery with each sample time was approximately 91 *msec* in average. It includes the time for the recovery calculation at the clients, the time for data transfer between the clients and the server, and the time for the intersection calculation and displaying the result at the server. This signifies that video images were processed every three frames. In this

Fig. 3. Experimental environment.

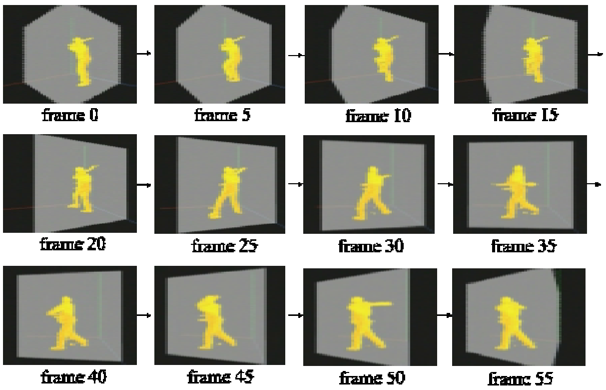

Fig. 4. Recovered batting motion.

way, high-speed human motion recovery has been realized.

5. Conclusions

A technique was proposed to perform high-speed 3-D human motion recovery based on back projection of silhouette images provided from multiple cameras. In order to speed up the computation, (i) distributed computation architecture was employed in order to build a volumetric region (a cone) in a parallel way, (ii) lists of correspondence between voxels in the world coordinate system and pixels in image planes was prepared for high-speed back projection, and (iii) difference images between successive frames were effectively used for less computational load of back projection. Performance of the proposed technique was experimentally shown.

The presented technique has an advantage over those existent techniques based on markers tracking in that it doesn't have to use markers. This makes the technique much simpler than such existent techniques, since markers tracking problem is still an issue of difficulty. Instead, the present technique cannot escape from camera calibration like other shape/motion recovery techniques, except for [2]. Ideally a technique that employs neither markers nor camera calibration for the recovery is desirable for wide spread of a motion recovery technique to various users who don't have much related knowledge. Such a technique still remains unknown.

References

[1] R. C. Gonzalez and P. Wintz, *Digital Image Processing*, Addison-Wesley, 1987.

[2] J. K. Tan, and S. Ishikawa, "Deformable shape recovery by factorization based on a spatiotemporal measurement matrix", *Computer Vision and Image Understanding*, Vol 82, No. 2, pp. 101-109, May, 2001.

[3] K. Tomiyama, et al., "A dynamic 3D object-generating algorithm from multiple viewpoints using the volume intersection and stereo matching methods", *The Journal of the Institute of Image Information and Television Engineers*, Vol 58, No. 6, pp. 797-806, 2004. (in Japanese)

[4] R. Shapiro, "Direct linear transformation for three-dimensional cinematography", Res. Quart., Vol. 49, pp. 197-205, 1978.

The Tenth International Symposium on Artificial Life and Robotics 2005(AROB 10th '05),
B-con Plaza, Beppu, Oita, Japan, February 4-6, 2005

Auto-Correlation Probabilistic Relaxation Matching Method

Xin Wang[1], Masanori Sugisaka[2], Jin Wang[3]

[1]Graduate School of Engineering,
The University of Tokushima, Tokushima 770-8506, Japan

[2]Department of Electrical and Electronic Engineering,
Oita University, Oita 870-1192 Japan

[3]College of Textile and Garments,
Hebei University of Science and Technology, Shijiazhuang 050031 China

Abstract

The statistics of the neighborhood gradients in an image can yield useful descriptions of target features. This paper presents a new approach, which is iterative and begins with the detection of all potential correspondence pairs, on auto-correlation relaxation algorithm by using those features to match image clips. Each pair of matching points is assigned a number representing the probability of its correspondence. The probabilities are iteratively recomputed to get global optimum sets of pairwise relations. This algorithm could be found wide applications of matching video frames, industrial detection recognition and so on.

1. Introduction

Image matching is the problem of finding correspondence points in two or more images of the same scene, traditionally. Recently, many researches also show their interest in image stream, which is large amount of information for 3-D image reconstruction from 2-D images.

Two image points p and p' match if they result from the projection of the same physical point P in the scene, a property that is often approximated by a similarity constraint requiring, for example, p and p' to have similar intensity or color. The desired output of an image correspondence algorithm is a disparity map, specifying the relative displacement of matching points between images. The image correspondence problem is inherently under constrained and further complicated in image stream and also by the fact that the images typically contain noise. Traditional approaches thus either try to only recover a subset of matches, or make additional assumptions.

The feature based matching problem can generally be fall into three categories: matching points, curves, and areas. Point based matching is, for a location in one image, to find the displacement that aligns this location with a matching location in the other image [5][7][12]; curve-based matching is by analysis of the similarity and compatibility between curves in different images [2][3][4]; area based method yield a dense disparity map by matching small image patches as whole with respect to geometry, textures [6][8][10][11]. Theoretically, point correspondences, which matches points with a certain amount of local information, are the robust way. Traditional point based approaches, however, have two foundational difficulties when applied to more general scenes. First, they usually assumed known camera geometries for stereo matching, so less point's relation in one image considered. Second, the similarity constrains are seriously required.

We depict the attributes of a target by its significant energy points. Our idea to understand a target is from its points of this target to its lines, from its points to its lines and areas. This is related to manipulate our knowledge database in our further works. If the proposed auto-correlation approach is used alone, it also gives very satisfied results [14].

2. Auto-correlation model

Let $I(X)$(also denoted as I), $X=\{x_i|_{x_i\in X}, X\subset\mathcal{R}^n\}$, be the image function in an image frame. Given the shift of X as ΔX, the auto-correlation function is defined as:

$$f(X) = \sum_w \big(I(X) - I(X+\Delta X)\big)^2 \qquad (1)$$

where X presents the global position in the working window w . According to the Taylor expansion, in the case of $X \subset \mathcal{R}^2$, we rewrite the elements in X as x, y, the item $I(X+\Delta X)$ has:

$$\begin{aligned} &I(X+\Delta X)\\ &\quad = I(X) + I_x(X)\Delta x + I_y(X)\Delta y +, \cdots\\ &\quad \approx I(X) + \nabla I(X)(\Delta X)^t \end{aligned} \tag{2}$$

where $I_x = \partial I(X)/\partial x$, $I_y = \partial I(X)/\partial y$. Substituting the above approximation (2) into Eq.(1), then

$$\begin{aligned} &f(X)\\ &= \sum_w \left(\nabla I(X)(\Delta X)^t\right)^2\\ &= \sum_w (\Delta X)\begin{pmatrix} I_x^2 & I_x I_y\\ I_x I_y & I_y^2 \end{pmatrix}(\Delta X)^t\\ &= (\Delta X)\left(\sum_w \begin{pmatrix} I_x^2 & I_x I_y\\ I_x I_y & I_y^2 \end{pmatrix}\right)(\Delta X)^t && (3)\\ &= (\Delta X)\big(\mathcal{Q}(X)\big)(\Delta X)^t && (4) \end{aligned}$$

$I(X)$ is smoothed as $\mathcal{I}(X)$ by a Gaussian G. Then we write $\mathcal{Q}(X)$ as $\nabla I(\nabla I)^t$, build up a transform relation $\mathcal{H}(X)$ in a local window about X.

$$\begin{aligned} \mathcal{H}(X) &= \mathcal{T}(X) * \sum \left\{\nabla I(\nabla I)^t\right\}\\ &= \mathcal{T}(X) * \sum \begin{Bmatrix} (G_x * \mathcal{I})^2 & (G_x * \mathcal{I})(G_y * \mathcal{I})\\ (G_x * \mathcal{I})(G_y * \mathcal{I}) & (G_y * \mathcal{I})^2 \end{Bmatrix} \end{aligned} \tag{5}$$

where G is with standard deviation one, $G_x = \partial G/\partial x$, $G_y = \partial G/\partial y$. $\mathcal{T}(X)$ is a weight mask to weight the derivatives over the window. In (5), $\mathcal{I}=\mathcal{I}$(X), there are relations $\partial I/\partial x = \partial/\partial x * I$, $\partial/\partial x * (G * \mathcal{I}) = (\partial/\partial x * G) * \mathcal{I} = \partial G/\partial x * \mathcal{I}$. $\mathcal{H}(X)$ captures the local structure. The eigenvectors of this matrix are the principal curvatures of the auto-correlation function. We consider a cost function $\mathcal{M}$(X) :

$$\mathcal{M}(X) \propto \mathcal{H}_\infty + \mathcal{H}_\in \tag{6}$$

where $\mathcal{H}_\infty$, $\mathcal{H}_\in$ are the determinant and trace of $\mathcal{H}(X)$ respectively. We can get some image energy points, called interest points, by (5) and (6). An example of $\mathcal{M}(X)$ is illustrated in Fig.1 and Fig.2.

3. Probabilistic relaxation algorithm

Assume that there be two local windows $A'_m \subset I(X)$ and $A'_n \subset I(X+\Delta X)$. Let $A_m = \{\mathbf{x}_m\}$ be the set of all interest points in the first starting image that is input state space, and $A_n = \{\mathbf{y}_n\}$ the interest points in the second image that is output state space. Let $\mathbf{c}_{mn}$ be a vector connecting points $\mathbf{x}_m$ and $\mathbf{y}_n$ (thus $\mathbf{y}_n = \mathbf{x}_m + \mathbf{c}_{mn}$). Let the probability of correspondences of two points $\mathbf{x}_m$ and $\mathbf{y}_n$ be P_{mn}. Two

Fig.1: An original image.

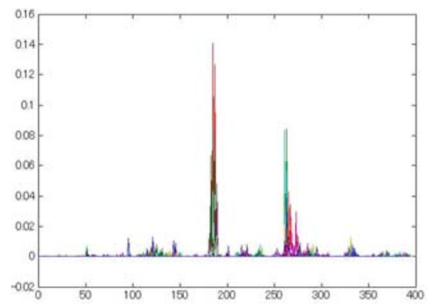

Fig.2: Distribution of the global correlation about Fig.1.

points $\mathbf{x}_m$ and $\mathbf{y}_n$ can be considered potentially corresponding if their distance satisfies the assumption of maximum velocity,

$$|\mathbf{x}_m - \mathbf{y}_n| \le D_{max} \tag{7}$$

where D_{max} is the maximum distance a point may move in the time interval between two consecutive images. Two correspondences of points $\mathbf{x}_m\mathbf{y}_n$ and $\mathbf{x}_k\mathbf{y}_l$ are termed consistent of

$$|\mathbf{c}_{mn} - \mathbf{c}_{kl}| \le D_{dif} \tag{8}$$

where D_{dif} is a pixel distance deviation. Consistency of corresponding point pairs will increases the probability that a correspondence pair is correct. We Determine the sets of interest points $A_m \subset A'_m \subset I_i(\mathbf{x})$, $A_n \subset A'_n \subset I_j(\mathbf{x})$, and construct a data structure as follows:

$$[\mathbf{x}_m, (\mathbf{c}_{m_1}, P_{m_1}), (\mathbf{c}_{m_2}, P_{m_2}), \ldots, (NoV^*, NoP^*)]$$

where P_{mn} is the probability of correspondence of points $\mathbf{x}_m$ and $\mathbf{y}_n$, NoV^*, and NoP^* are special symbols indicating that no potential correspondence was found.

We initialize the probabilities $P_{mn}^{(0)}$ of correspondence based on local similarity –if two points correspond, their neighborhood should correspond as well:

$$P_{mn}^{(0)} = \frac{1}{1 + k_p \omega_{mn}}\left(1 - P^{(0)}_{(NoV^*, NoP^*)}\right) \tag{9}$$

where $P^{(0)}_{(NoV^*,NoP^*)}$ is the initialized probability of no correspondence, k_p is a constant and

$$\omega_{mn} = \sum_{\mathbf{\Delta x}} [I_m(\mathbf{x}_m \pm \mathbf{\Delta x}) - I_n(\mathbf{y}_n \pm \mathbf{\Delta x})]^2 \tag{10}$$

$\mathbf{\Delta x}$ defines a neighborhood for image match testing – a neighborhood consists of all points $(\mathbf{x} + \mathbf{\Delta x})$, where $\mathbf{\Delta x}$ is defined as a symmetric neighborhood around $\mathbf{x}$.

We iteratively determine the probability of correspondence of a point $\mathbf{x}_m$ with all potential points $\mathbf{y}_n$ as a weighted sum of probabilities of correspondence of all consistent pairs $\mathbf{x}_k\mathbf{y}_l$, $\mathbf{x}_k$ are neighbors of $\mathbf{x}_m$ and the consistency of $\mathbf{x}_k\mathbf{y}_l$ is evaluated according to $\mathbf{x}_m, \mathbf{y}_n$. A quality q_{mn} of the correspondence pair is defined as

$$q^{(s-1)}_{mn} = \sum_k \sum_l P^{(s-1)}_{kl} \tag{11}$$

where s denotes an iteration step, k refers to all points $\mathbf{x}_k$ that are neighbors of $\mathbf{x}_m$, and l refers to all points $\mathbf{y}_l \subset A_n$ that form pairs $\mathbf{x}_k\mathbf{y}_l$ consistent with the pair $\mathbf{x}_m\mathbf{y}_n$.

The probabilities of correspondence are updated for each point pair $\mathbf{x}_m$, $\mathbf{y}_n$.

$$\hat{P}^{(s)}_{mn} = P^{(s-1)}_{mn}(k_a + k_b q^{(s-1)}_{mn}) \tag{12}$$

where k_a and k_b are preset constants. They deal with the convergent speed of P_{mn}. Normalize

$$P^{(s)}_{mn} = \frac{\hat{P}^{(s)}_{mn}}{\sum_j \hat{P}^{(s)}_{mj}} \tag{13}$$

Those interest points that hold high probabilities that obviously differ from those interest points without correspondences. Repeat (11) (12) and (13) until the $P^{(s)}_{mn} > P_{thr}$ (threshold) is found for all points $\mathbf{x}_m$, $\mathbf{y}_n$.

4. Experiments and discussions

To show availability of the presented approach, experiments are executed by matching image stream. A starting image is given in Fig.3. To illustrate the method easily, we have made an 11-points-based contour model as shown in Fig.3. Details how to make this contour can be found in [7][15][16], but beyond scope of this paper. As shown in Fig.4, one small window is selected in our experiment. Because the experiment is to match image stream, the second frame for matching should take into account this displacement with the respect to time t, and

Fig.3: Stating clip from image stream.

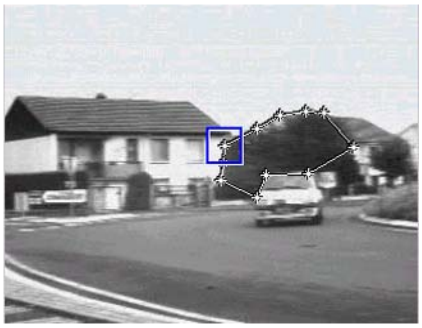

Fig.4: Local window selected.

this is the reason why Fig.6 gives the larger window in it. The frames should be referred to the same center. Comparing Fig.5 and Fig.6, we can find 8 pairwise relations are detected from A'_m and A'_n. Fig.7 and Fig.8, the images zoomed in, show us surprising good results.

From Fig.3 to Fig.8, the entire experimental images are in the form of gray. In the case of color image, color images can bring us more detail image energy distribution and less similarity than gray ones. So this method is also recommended to the color case.

5. Conclusions

This paper presents a new matching approach without camera calibrations. The matching principle is based on the probabilistic relaxation under local image energy constraints. This algorithm can find contributions to image classification [14] and object tracking [7][15][16]. We also recommend this technique to visual based intelligent navigation.

Acknowledgements

Part of this research was done while Xin Wang was at the Department of Electronics, Oita Institute of Technology.

Fig.5: Matching results of Fig.4.

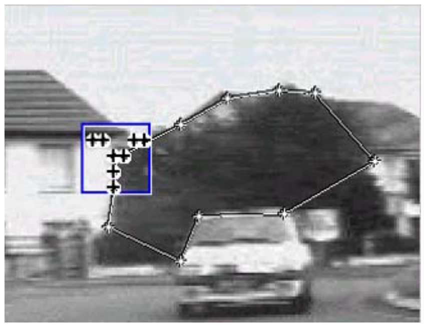

Fig.7: Fig.5 is zoomed in.

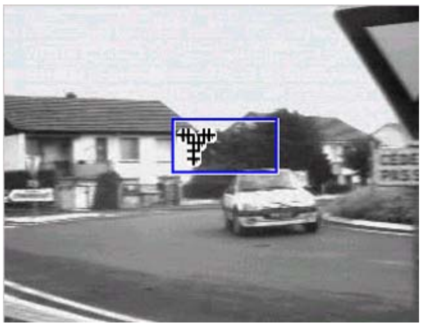

Fig.6: Matching results of the clip following Fig.4.

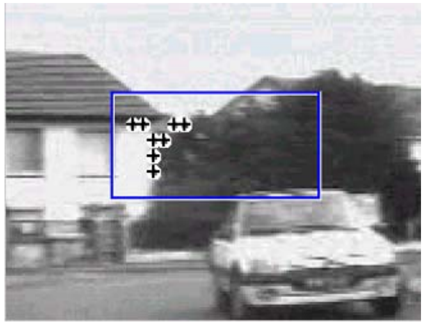

Fig.8: Fig.6 is zoomed in.

References

[1] D. Scharstien, "Stereo Matching with Nonlinear Diffusion," *International Journal of Computer Vision*, vol.28, no.2, pp. 155-174, 1998.

[2] S. B., Pollard, J. Mayhew, and J. P. Frisby, "Implementation details of the PMF stereo algorithm," *3D Model Recognition from Stereoscopic Cues, MIT Press, Cambridge*, MA, pp. 33-41, 1991.

[3] L. Robert, and O. Faugeras, "Curve-based ster -eo: Figural continuity and curvature," *Proc. CVPR'91*, pp. 57-62, 1991.

[4] A. Kumar, A. Tannenbaum, and G. Balas, "Optical flow: a curve evolution approach," *IEEE Trans. Image Processing*, vol.5, no.5, pp. 598-610, 1996.

[5] R. Green, D. Gray, and J. Powers, *Artificial Vision*, Academic Press, London, 1997.

[6] W. Yu, K. Daniilidis, and G. Sommer, "Approximate orientation steer ability based on angular Gaussians," *IEEE Trans. Image Processing*, vol. 10, no. 2, pp. 193-205, 2001.

[7] X. Wang, M. Sugisaka, W. Xu, "Active contour model based tracking analysis" *Proc. of the 12th Int. Conference of Systems Engineering, UK,* vol, 3, pp. 347-352, 2003.

[8] D. A. Forsyth, J. Ponce, *Computer Vision*, Prentice Hill, USA, 2003.

[9] B. Jähne, *Image processing for scientific applications*, CRC Press, New York, 1997.

[10] M. Brown, D. Terzopoulos, *Real time computer vision*, Cambridge University Press, 1994.

[11] H. Zhang, S. Roth, it Camera aided robot calibration, CRC Press, Boca Raton, 1996.

[12] L. Torresani, C. Bregler, "Space-time tracking," *Computer Vision - ECCV 2002, Part I*, pp. 801-812, 2002.

[13] W. Kropatsch, R. Klette, F. Solina, and R. Albrecht, *Theoretical foundations of computer vision*, Springer Wien, New York, 1996.

[14] X. Wang, M. Sugisaka, W. Xu, "Recognizing static target in video frames taken from moving platform" *Proc. of the Int. Conference on Control, Automation, and System,* Korea, pp. 223-227, 2003.

[15] X. Wang, M. Sugisaka, W. Xu, "Image energy pilot, FA soil-salt recognition Approach," *The 4th Int. Conference on Advanced Mechatronics Toward Evolutionary Fusion of IT and Mechatronics*, pp. 373-376, 2004.

[16] X. Wang, M. Sugisaka, W. Xu, "Model based recognition for artificial brain," *Proc. of the 9th Int. Symposium on Artificial Life and Robotics,* vol, 2, pp. 605-609, 2004.

Segmentation and Object Recognition for Robot Bin Picking Systems

R. Nagarajan[+], Sazali Yaacob*, Paulraj Pandiyan[+], Hema C.R.[+], Shamsudin Amin[++], Marzuki Khalid[++], M. Rizon*

[+]*Artificial Intelligence Group*
School of Engineering and Information Technology
Universiti Malaysia Sabah, 88999 Kota Kinabalu, Sabah, Malaysia
[++]*Center for Artificial Intelligence and Robotics*
Faculty of Electrical Engineering
Universiti Teknologi Malaysia Kuala Lumpur, Malaysia
**School of Mechatronic Engineering*
Northern Malaysia University College of Engineering
01000 Kangar, Perlis, Malaysia
E-mail: rizon@kukum.edu.my

Abstract

This paper presents a vision based segmentation and object recognition system for bin picking applications. Objects in the bin are usually placed in a disorganized manner inside the bin. A method to segment the topmost object from the bin image is presented using threshold derived from the histogram of the bin image. Once the object is segmented its singular value features are extracted for object recognition. Object recognition is accomplished using a simple feed forward neural network. The proposed method is capable of segmenting occluded object as well as recognizing complex objects.

Keywords: Bin Picking, Object Recognition, Occluded Object Segmentation, Singular Value Decomposition.

1 Introduction

In bin picking robot systems, objects to be picked are placed inside a bin in an unorganized pile. Any vision system attached to a bin picking robot must be able to analyze the image of the bin and be able to locate all the parts seen as well as identify them correctly. Research on bin picking systems had started in the 80s’ but most bin picking publications consider only non-occluded objects. Some researches pick up an object and analyse the object for pose determination and recognition using database of the object images, while others rely on sensors other than the vision sensors[1],[2],[3]. We present here a vision based system to isolate and recognise the object to be picked. If all the parts are separated from each other, then identifying the parts is relatively easy. However when the parts are partially occluded more than one object will be merged into a single blob making it difficult to identify each one of them.

The image segmentation that divides the image into meaningful sub regions is an indispensable step in image analysis. One approach of solving the problem of identifying objects is by detecting and measuring all segments belonging to the object border and all internal angles [4]. A regional growth is a technique that starts at the known pixel points and extends to all neighbouring pixels that are similar in gray level, colour texture, or other properties in order to form a complete region. Using the difference chain code in contour encoding is another way of recognizing partially occluded object. An object shape is identified by the system through the detection of selected discrete feature segments in the contour code instead of attempting to search for a complete boundary [5]. Image segmentation can be considered as a clustering process in which the pixels are classified to specific regions based on their gray-level values and spatial connectivity.

We propose a vision based segmentation and object recognition method for occluded objects using thresholding, singular value decomposition and Neural Networks. Section 2 briefly introduces singular value decomposition. Section 3 describes the methodology of segmentation that includes feature extraction and a neural network architecture for object recognition. The experimental results and conclusion derived from this work are given in section 3 and 4 respectively.

2 Singular Value Decomposition

The Singular Value Decomposition [SVD] is a widely used technique to decompose a matrix into several component matrices, exposing many of the useful and interesting properties of the original matrix [6]. Any ‘m x n’ matrix **a** ($m >= n$) can be written as the product of a ‘m x m’ column-orthogonal matrix **u**, an ‘m x n’ diagonal matrix **w** with positive or zero elements, and the transpose of an ‘n x n’ orthogonal matrix **v** [7]:

$$a = u\, w\, v^t \qquad \dots (1)$$

where

$$\mathbf{w} = \begin{bmatrix} w_1 & 0 & . & 0 & 0 \\ & w_1 & . & 0 & 0 \\ . & . & . & . & . \\ 0 & 0 & . & w_{n-1} & 0 \\ 0 & 0 & . & 0 & w_n \end{bmatrix} \tag{2}$$

and

$$u^t u = vv^t = I \tag{3}$$

where

$w_1, w_2, ..., w_{n-1} w_n \geq 0$,

and 't' is the transpose.

The diagonal elements of matrix '**w**' are the singular values of matrix '**a**' which are non-negative numbers. The singular values obtained by the SVD of an image matrix is an algebraic feature of an image which represents the intrinsic attributes of an image[6].

3 Methodology

Images of the occluded objects in the bin are captured using a Pulnix TM 6702 CCD machine vision camera. Direct bin lighting of the bin is avoided to reduce brightness and albedo effects. The captured images are of size 640 x 480 pixels and are monochromatic. To minimise the processing time and to improve the efficiency of the system without significant loss of information of the objects, the images are resized to 128 x 96 pixels. The resized images have to be further processed using filtering techniques to identify the borders of the objects and to smooth the intensity of the object region. First the image is filtered using a regional filter and a mask. This masked filter filters the data in the image with the 2-D linear Gaussian filter and a mask the same size as the original image for filtering. This filter returns an image that consists of filtered values for pixels in locations where the mask contains 1's, and unfiltered values for pixels in locations where the mask contains 0's. The above process smoothens the intensity of the image around the objects. The resultant image is passed through a median filter which defines the object edges. The median filter performs median filtering of the image matrix in two dimensions. Each output pixel contains the median value in the M-by-N neighbourhood around the corresponding pixel in the input image. The filter pads the image with zeros on the edges, so that the median values for the points within [M N]/2 of the edges may appear distorted. The M-by- N is chosen according to the dimensions of the object. In our experiment, a 4 x 4 matrix was chosen. The resulting filtered image is then subjected to segmenting techniques as detailed in the following section.

3.1 Bin Image Segmentation

Bin image segmentation involves identifying the top most object from the cluster of objects in the bin for picking up. Since all the objects are partially occluded except the topmost object, separating the topmost object can be done using the grey value of the object. A histogram of the bin images displays the grey levels of the image. Pixels of grey levels higher than a threshold value relate to the topmost object. The threshold value is determined by taking log of the magnitudes using equation (4) for 40 maximum values.

T = [log10 (COUNTS a)] i (4)

where

'T' is the threshold

'i' is the Gray scale value

'COUNTS a' is the Gray value count

The maximum value is chosen experimentally to get satisfactory results for all images. The grey images are converted to binary images by applying the threshold derived from the histogram using equation (4). The Figure 1 shows the bin images before and after segmentation.

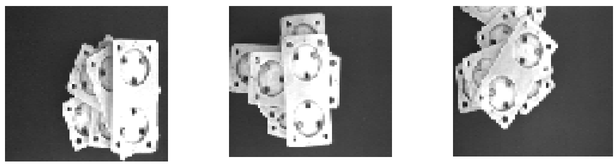

(a) Bin images

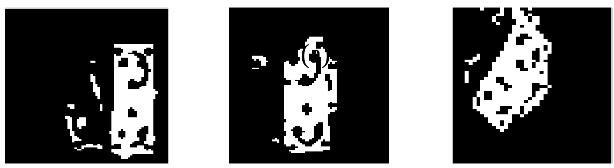

(b) Segmented images showing the top most object

Figure 1 Bin Image Segmentation

3.2 Object Feature Extraction

The topmost object extracted from the segmentation process varies in orientation and pose as the objects in the bin are not placed in an organised pile. It now becomes essential to recognise the object irrespective of its orientation. To recognise the object, features of the object in various poses and orientation are extracted to train a neural network to recognise the object. In the feature extraction process the edge images of the segmented object is extracted using a canny edge detector. The edge image matrix is decomposed using singular value decomposition to extract the singular value. Edge features minimise the computational time and pocess optimum information of the object for recognition. Figure 2 shows the edge images of object with different orientation and pose.

Figure 2 Edge images of object

The singular value features extracted from the edge images are the object features; singular values below 1 are ignored since they h are sometimes due to noise in the image and do not relate to the object under consideration. Twenty five such significant features of the object is fed to a neural network to train the network for object recognition.

3.3 Neural Network Architecture

The Neural Network architecture shown in Figure 3 consists of three layers. 25 singular values are fed to the network as input data. The hidden layer is chosen to have 13 neurons and the output consists of 2 neurons which represent the two objects to be recognised. The hidden and input neurons have a bias value of 1.0 and are activated by binary sigmoid activation function. The choice of initial weight will influence whether the network reaches a global minimum of the error and if so how quickly it converges. It is important that the initial weights must not be large in order to avoid the initial input signals to each hidden or output unit falling in the saturation region. On the other hand, if the initial weights are too small, the net input to a hidden or output unit will be close to zero which also causes extremely slow learning [8]. Hence the initial weights for the above Network are randomized between
-0.5 and 0.5 and normalized. The initial weights that are connected to any of the hidden or output neuron are normalized in such a way that the sum of the squared weight values connected to a neuron is one. This normalization is carried out using equation (5) which is used to implement the weight updating.

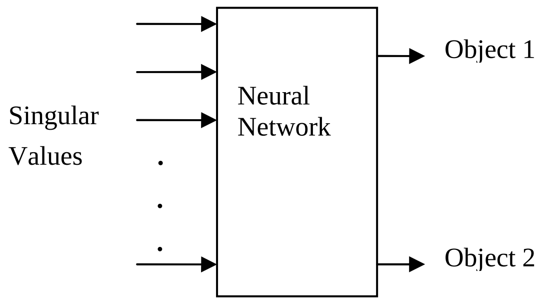

Figure 3 A Feed Forward Neural Networks for Object Recognition

$$w_{1j}(new) = \frac{w_{1j}(old)}{\sqrt{w_{1j}^2 + w_{2j}^2 + \ldots + w_{nj}^2}} \text{ , j=1,2,3,…,p} \quad (5)$$

where n - number of input units

p - number of hidden units

A sum squared error criteria as defined by equation (6) is used as a stopping criteria while training the network. The sum squared tolerance defined in equation (6) is fixed as 0.01. The network is trained by the conventional back propagation procedure. The cumulative error versus epoch plot of the trained neural network is shown in Figure 4. The cumulative error is the sum squared error for each epoch and is given by:-

$$\text{Sum squared error} = \sum_{p=1}^{p}\sum_{k=1}^{m}(t_k - y_k)^2 \quad (6)$$

where

t_k is the expected output value for the kth neuron,

y_k is the actual output value for the kth neuron,

m is the total number of output neurons, and

p is the total number of input neurons.

4 Experimental Results

In the experimental study two sets of bin images are acquired for two different objects. Only similar objects are placed in the bin at a time. The neural network is trained with 60 percent of the data and tested with 116 image data. Table I lists the training parameters of the Neural Network. The proposed method is found to successfully classify 93 % of the tested images. Figure 4 shows the Cumulative error versus epoch plot of the neural network. At each iteration, an objective function is minimized to find the best location for the clusters.

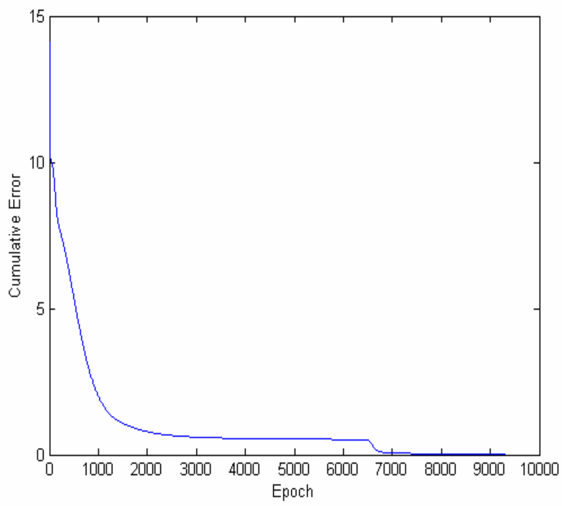

Figure 4 Cumulative error versus Epoch Plot

Table I – Training Parameters of NN

Parameters	Values
No. of input neurons	25
No. of Output neurons	2
No. of hidden neurons	13
Bias value	1.0
Tolerance	0.01
Percentage Classification	93%
Maximum Epoch	9331

4 Conclusion

A vision based segmentation and object recognition method is presented. The method is experimentally verified and results presented are satisfactory. The proposed method however was found to be ineffective for object images with albedo effects and over brightness. Optimal lighting is essential to derive satisfactory results. The proposed method has successfully segmented partially occluded objects. Methods to improve the segmentation results are under study.

Acknowledgement

The authors thankfully acknowledge the funding [Code. No. 04-02-10-0024-PR001] received from IRPA through UTM and UMS.

References

[1]Ayako Takenouchi, Naoyoshi Kanamaru and Makoto Mizukawa, Hough-space-based Object Recognition Tightly Coupled with path planning for Robust and fast Bin-picking, *Proceedings of International Conference on Intelligent Robots and Systems*, Canada, October 1998, pp 1222 – 1229.

[2]Kohtaro Ohba, Katsushi Ikeuchi, Recognition of the Multi Specularity Objects for Bin-picking Task, *Proceedings IROS*, IEEE October 1996 pp 1440 – 1447.

[3]Yoshimasa YANAGIHARA, Toshiro KITA, Parts Picking in Disordered Environment, IEEE International Workshop on Intelligent Robots and Systems 1991, Osaka , Japan pp 517-522.

[4] Paulo Lopes, Eugenio Oliveira. Identification of Partially Occluded Objects Using Object Chain Code. *Proceedings of IEEE/RSJ International Conference on Intelligent Robots and Systems Yokohama*, Japan 1829-1834 July 1993

[5]Peter W.M. Tsang, P.C.Yuen. Recognition of Partially Occluded Objects. *IEEE Transactions on Systems, Man and Cybernetic*s Vol. 23, No.1 January February 1993

[6]Zi-Quan Hong, Algebraic Feature Extraction of Image for Recognition *IEEE Transactions on Pattern Recognition* Vol. 24 No. 3 pp 211-219, 1991.

[7] David S. Watkins, *Fundamentals of Matrix Computations*. John Wiley & Sons 2001.

[8]S.N. Sivanandam, M.Paulraj, *Introduction to Artificial Neural Networks* Vikas Publishing House, India. 2003

[9] Laurene Fausett, *Fundamentals of Neural Network Architecture and Applications*, Prentice Hall, USA. 1990

Stereo Camera based Artificial Vision for Blind through Hearing

G.Balakrishnan+ G.Sainarayanan+ R. Nagarajan+ Sazali Yaacob* M. Rizon*
+AI Research Group, School of Engineering and Information Technology
Universiti Malaysia Sabah, Locked Bag No. 2073, 88999, Malaysia
**School of Mechatronic Engineering*
Northern Malaysia University College of Engineering
01000 Kangar, Perlis, Malaysia
E-mail: rizon@kukum.edu.my

Abstract

In this paper, a design of real time methodology for object identification and image sonification applied to vision substitution for the blind is presented. The proposed methodology includes intelligent image processing, stereopsis and image sonification modules. The hardware system consists of stereo digital video cameras as vision sensors, stereo headphone and a laptop computer. The images captured from stereo cameras are processed to obtain isolated object image. The stereopsis module performs area based stereo correspondence over the object image and calculates the disparity. The object is given a preference based on its distance and position using fuzzy rule base for collision free navigation by blind user. Finally the information is conveyed to the blind through stereo sound in the form of musical tones. In the proposed algorithm distance information of the object is determined with less computation compared to conventional area based stereo correspondence method. Experiments were conducted in an indoor environment, and the results obtained are promising.

Keywords:

Vision substitution, Fuzzy inference system, Stereopsis, Blind navigation

1 Introduction

Human navigation consists of two distinct components: sensing the immediate environment for impediments to travel (e.g., obstacles and hazards) and navigating to remote destinations beyond the immediately perceptible environment. Informations about way finding are passed to humans through the most sophisticated sensory system, the vision system. The visually impaired are at a considerable disadvantage, as they often lack the needed information for bypassing obstacles and hazards. According to World Health Organization census, around 180 million people worldwide are visually disabled, of those 40 to 45 million are totally blind [7]. This population is expected to double by the year 2020.

During the past three decades, several researchers have introduced devices called *Electronic Travel Aids* (ETAs) [6], that use sensor technology to assist and improve the blind users mobility in terms of safety and speed. In early type of ETAs, the users had to scan the environment constantly and continuously. Locating an obstacle in the path was time consuming and similar to having a long cane. But in recent years, due to advancement in the development of high-speed computers and sensory devices, attempts to design sophisticated equipment for the vision substitution are in progress.

The concept of using video camera as vision sensor had been introduced in Peter Meijer's portable system, the vOICe [4]. The image captured is scanned from left to right direction for sonification or sound generation. The top portion of the image is converted into high frequency tones and the bottom portion into low frequency tones. The loudness of sound depends on the brightness of the pixel. In Peter Meijer's work, image-processing efforts to enhance the object properties are not undertaken. The sound produced from the unprocessed image will contain more information of the background rather than object. This may be the reason for the blind user having difficulties to distinguish the object and the background through sound from earphones.

Navigational Assistance for Visually Impaired (NAVI) [5] makes use of single camera and the captured image is resized to 32 X 32 and the gray scale of the image is reduced to 4 levels. The image is differentiated into objects and background. The objects are assigned high intensity and the background is suppressed. Here the processed image is converted into stereo sound where the amplitude of the sound is directly proportional to intensity of image pixels, and the frequency of sound is inversely proportional to vertical orientation of pixels. Both in vOICe and NAVI the distance between the user and the obstacle cannot be obtained directly by the users. The distance is one of the important aspects for collision free navigation for blinds. In order to incorporate the distance information, stereo cameras are used in this work. The manner in which human beings use their two eyes to see and perceive the three-dimensional world has inspired the use of two cameras to model the world in three dimensions.

2 Experimental Setup

A prototype system is designed for this work. The hardware model constructed for this vision substitution system has a sunglass fitted with two mini video cameras, stereo earphone and a laptop computer. The two cameras are displaced from each other by a distance of 5 cm. Both the cameras are adjusted to same focus by experimentations. Figure 1 shows the experimental setup used in this work. When the sunglass is worned by the blind user, the stereo cameras capture the scene infront of the user.

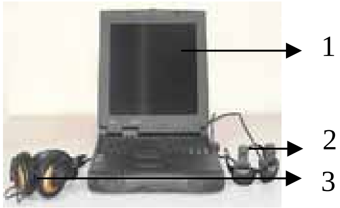

(a)

1 – Laptop Computer
2 – Sunglass fitted with stereo camera
3 – Stereo headphone

Figure 1: Prototype system

3 Image Processing Methodology

In this paper, objects or obstacles are identified and are assigned preference based on their position and distance. The first step in this methodology is the image acquisition, in which scene in front of blind is captured using both cameras simultaneously. The image captured from camera is a color image of size 352 x 288. Processing the image with original size will increase computation time. This work involves real time computation. So the computation time is critical and has to be minimized. Therefore pre-processing is undertaken to reduce the computation time, where both the left and right stereo images are converted to gray scale intensity image and resized to 64 x 64. Figure 2 shows the preprocessed left and right image. The main task involved here is to identify and assign preference to the objects. In this work, the objects in both the left and right camera images are identified by locating its edges.

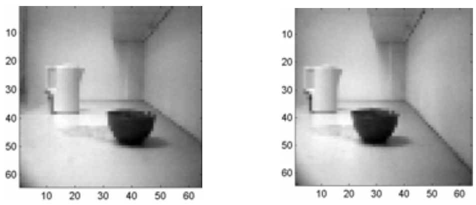

(a) (b)

Figure 2: Resized Gray Scale Intensity Image
(a) left image (b) right image

3.1 Image Post Processing

Edge detection is one of the important human vision properties as it has the ability to recognize the object boundaries. The goal of edge extraction is to provide useful structural information about object boundaries. Canny edge detector is used for edge detection because this method uses two thresholds to detect strong and weak edges, and includes the weak edges in the output only if they are connected to strong edges. Canny edge detector is an optimum edge detector [2]. Figure 3 shows the edge features of the right camera image extracted using canny edge detector. Similar processing is undertaken for left camera image also.

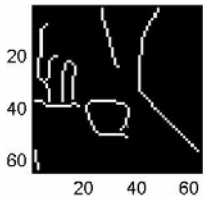

Figure 3: Edge Image of Right Stereo Image

In this work a region enclosed within edges is considered as an object. It is realized that edge detection alone is not enough to extract the closed boundary of an object from the image. Therefore further processing is undertaken to connect the edges to form a meaningful object. Edge linking process is required to assemble these edges into meaningful edges. Morphological operation using dilation [1] is proposed to link the broken edges. The region within the closed boundary is considered as an object. The intensity of pixels in the region is enhanced to higher level using flood fill operation. Each object in the image is labeled. It is found that some of the extraneous edges still exist after flood fill operation. Hence noise removal operation is performed to remove extraneous edges present in the image without eliminating the desired objects. Erosion and dilation operations are undertaken to smooth the objects [1]. Thus image with only objects will be obtained. Figure 4 shows the image obtained after flood fill and noise removal method.

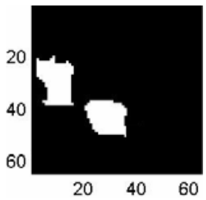

Figure 4: Right Image with only objects

3.2 Image Object Isolation

Binary images of both left and right camera image with only objects are derived from the previous section. This binary image is mapped with the resized gray scale intensity image and new gray scale intensity image with only objects is derived. These processes are preformed for both left and right camera images to obtain two gray scale images with only objects. Figure 5 shows the left and right images with only objects.

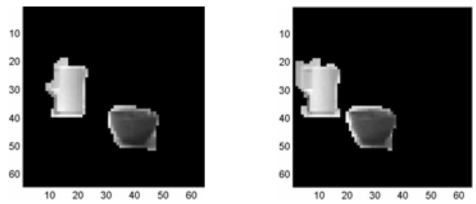

Figure 5: Grayscale Image with Only Objects of Left and Right Camera Images

4 Stereo Vision Methodology

After obtaining the isolated object image, the disparity has to be determined in order to calculate the distance between the blind user and the obstacle. The concept of stereopsis is employed here. Given two camera images, if it is possible to identify the image locations that correspond to the same physical point in space from both the camera images, then it is possible to determine its three-dimensional location. In order to calculate the disparity correspondence or matching of two images has to be done. In this work, area based correspondence method is applied over two isolated object images. To decrease the total computation time, the maximum disparity is bounded to a certain range and thus avoids examining an entire row for each pixel. Since only the isolated object images are used for correspondence, the mismatch error is less and also the computation time is reduced when compared to conventional area based and feature based techniques.

From the disparity map obtained, it is observed that in some areas, the disparity value within the object varies due to some mismatch. For uniform disparity value in an object, histogram is used. In a histogram, disparity value that occurs most within the object is found and that particular value is assigned to all pixels within the object Figure 6 shows the disparity map obtained after assigning uniform value.

Figure 6: Disparity Map

5 Object Preference

A Real time environment contains more than one object. If all objects are given same preference, then the blind user finds it difficult to identify those objects, which are obstacles in their path for navigation. So each object has to be assigned some priority for collision free navigation. In this work objects are given preference based on two important conditions. One is the distance of the object from the user and another one is the position of the object. In human vision system, the eyes mostly concentrate on a particular object rather than the background, which gets less focus. The object of interest will be usually at the center of the sight. In this paper, the center of the image is considered as the center of sight. Any object that is located in the central region with high disparity will be considered for high preference and objects located outside the central region with low disparity will be less preferred.

In order to check whether the object is located in the central region, object characteristics such as size and centroid have to be determined. Based on these characteristics, the ratio of the object area lying within the central region can be calculated. But with these inputs, devising an algorithm to compute object preference is very difficult. In order to overcome this uncertainty fuzzy logic is applied. Four main characteristics are measured for object preference assignment. They are size of an object, Euclidean distance between the object centroid and image centroid, ratio of objects lying within the center of an image and the distance through disparity of an object [1]. These characteristics are applied as input to fuzzy logic algorithm. Each characteristic is expressed using three membership functions namely low, medium and high. Membership functions are expressed using a trapezoidal curve. The output is object preference, which has four trapezoid curve memberships. The defuzzification is performed using centroid method. 81 rules are formed based on four inputs.

From the fuzzy output the objects are given different intensity values based on their preference. The object with very high preference is symbolized by white intensity and the object with least preference is symbolized with very dark gray intensity. The object preference based on fuzzy rule based system is shown in Figure 7.

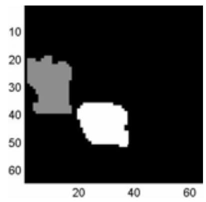

Figure 7: Object Preference Based on Fuzzy Output

The fuzzy output image is then converted to stereo sound using the following sonification methodology.

6 Image Sonification

The effective audible frequency range extends from about 20 Hz to around ten thousand hertz, although it depends entirely on the individual. The audible range is divided into octaves. An octave is really a frequency range from a frequency f1 to f2 such that f2 is twice that of f1 in terms of cycles or hertz. The human ear is logarithmic and is sensitive to frequency octaves. The audible frequency is then comprised of many octaves. The f1 can be any number but f2 is double the f1. Even a frequency range from 20 Hz to 40 Hz is defined as an octave [3].

In most of the western musical instruments the frequencies are arranged in such a manner that they are in a geometric series. That is, the frequency deviation between any key and the key immediately to its left is a constant, the constant being equal to the twelfth root of two or 1.059. Even though there is a degree of freedom for selecting the range of an octave (whether it is from 240 to 480 Hz or 254 to 508 Hz etc.), the western music defines a standard octave called the Middle A octave starting from 440 Hz.

With the help of the above concept, musical tones can be incorporated for image sonification. By experimentation it is found that octave frequency of 440 Hz to 880 Hz produce pleasing music. In the developed method, this octave frequency of 440 Hz to 880 Hz is selected. With this octave, 12 musical notes are developed. Let f (1,..,12) be the 12 octave frequencies.

The music pattern generated is given by

$$M(j) = \sin(2\pi f(j)t) \qquad j=1,2,\ldots,12 \qquad (1)$$

where

M(j) is the musical note generated for f(j) frequency and 't' varies from zero to desired total duration of the acoustic information.

Different musical tones are generated with the combination of these notes. In this work three notes are combined to form musical tones. Four half steps between first and second note and three half steps between second and third note define major chords. Here eight tones including some major chords are generated using these notes. The image to be sonified is resized to 32 X 32 for reducing the computation time. Musical tones are assigned in such a way that high frequency tones occupies the top portion of the image and low frequency tones are assigned to lower portion of the image. So each pixel in an image is assigned with samples of musical tones based on their position in the image.

The conversion of image into sound involves taking one column at a time starting from left most one and generating sound pattern for that column. The sound pattern generated is given by

$$S(i) = \sum_{j=1}^{32} I(i,j)M(i,j) \qquad i = 1,2,..,32 \qquad (2)$$

where S(i) is the sound pattern for column i of the image I(i,j) is the intensity value of (i,j)th element, M(i,j) is the samples of musical tone for (i,j)th pixel.

The sound pattern from each column is appended to construct the sound for the entire image. The scanning of picture is performed in such a way that stereo sound is produced. In this stereo type scanning, the sound patterns created from the left half side of the image is given to left earphone and sound patterns of right half side to right earphone simultaneously. The scanning is performed from leftmost column towards the centre and from right most column towards the centre.

Since the sound produced are differentiated into left and part, objects that lie to the left of the user will produce sound only in the left earphone and the object that lies to the right will be heard only in the right earphone. Different tones are produced for different shapes. Hence the sound pattern generated by this sonification method is able to differentiate objects based on its position, shape and distance. The most advantage of this method is that since musical tones are used, the sound generated will be pleasing to the user and continuous use will not fashion loss of interest. Prototype has been designed to minimize the hardware and using the system in outdoor environment also. Figure 8 shows the design of future prototype.

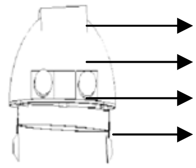

Figure 8: Future Wearable Prototype

7 Conclusions

Distance information is one of the most important criteria for blind navigation. In this work stereo cameras are used to find the distance information and the information is conveyed to the blind user through musical tones. Experiments were conducted in an indoor environment, and the results obtained are promising. The computation time of this method is also fast compared to conventional area based methods. There are some errors due to stereo mismatching. In the near future, the work will be continued towards achieving higher accuracy, minimizing the hardwares and testing the system with the blind people.

Acknowledgment: Authors wish to thank Ministry of Science, Technology and Innovation, Malaysia for funding the research through Universiti Malaysia Sabah under IRPA code: 03-02-10-0043/EA0041.

Reference

[1] Balakrishnan G, Sainarayanan G, Nagarajan R, Yaacob S, "Blind Navigation Using Stereopsis With Fuzzy Rule Base", *International Conference on Artificial Intelligence in Engineering and Technology*, Malaysia, pp. 232-237, 2004.

[2] Canny J, "A Computational Approach to Edge Detection", *IEEE Trans. Pattern Analysis and Machine Intelligence*, Vol. 6, pp. 721-741, 1984.

[3] Elliott R, "Fundamentals of music", New Jersey: Prentice-Hall.

[4] Meijer P, "An Experimental System for Auditory Image Representations", *IEEE Transactions on Biomedical Engineering*, Vol 39, pp 112-121, 1991.

[5] Sainarayanan G, "On Intelligent Image Processing Methodologies Applied to Navigation Assistance for Visually Impaired", *Ph. D. Thesis*, University Malaysia Sabah, 2002.

[6] Wong F, Nagarajan R, Yaacob S, Chekima A, "Electronic travel aids for visually impaired – A guided tour", *Proceedings of Conference in Engineering in Sarawak*, Malaysia, pp 377-382, 2000.

[7] World Health Organization, Internet site address: http://www.who.int//mipfiles/2400/AllenFoster.pdf

AUTHORS INDEX

Notation of session name:

PT: Plenary Talk; SS: Special Session; GS: General Session; IS: Invited Session or Organized Session